Franco Pirajno

The Geology and Tectonic Settings of China's Mineral Deposits

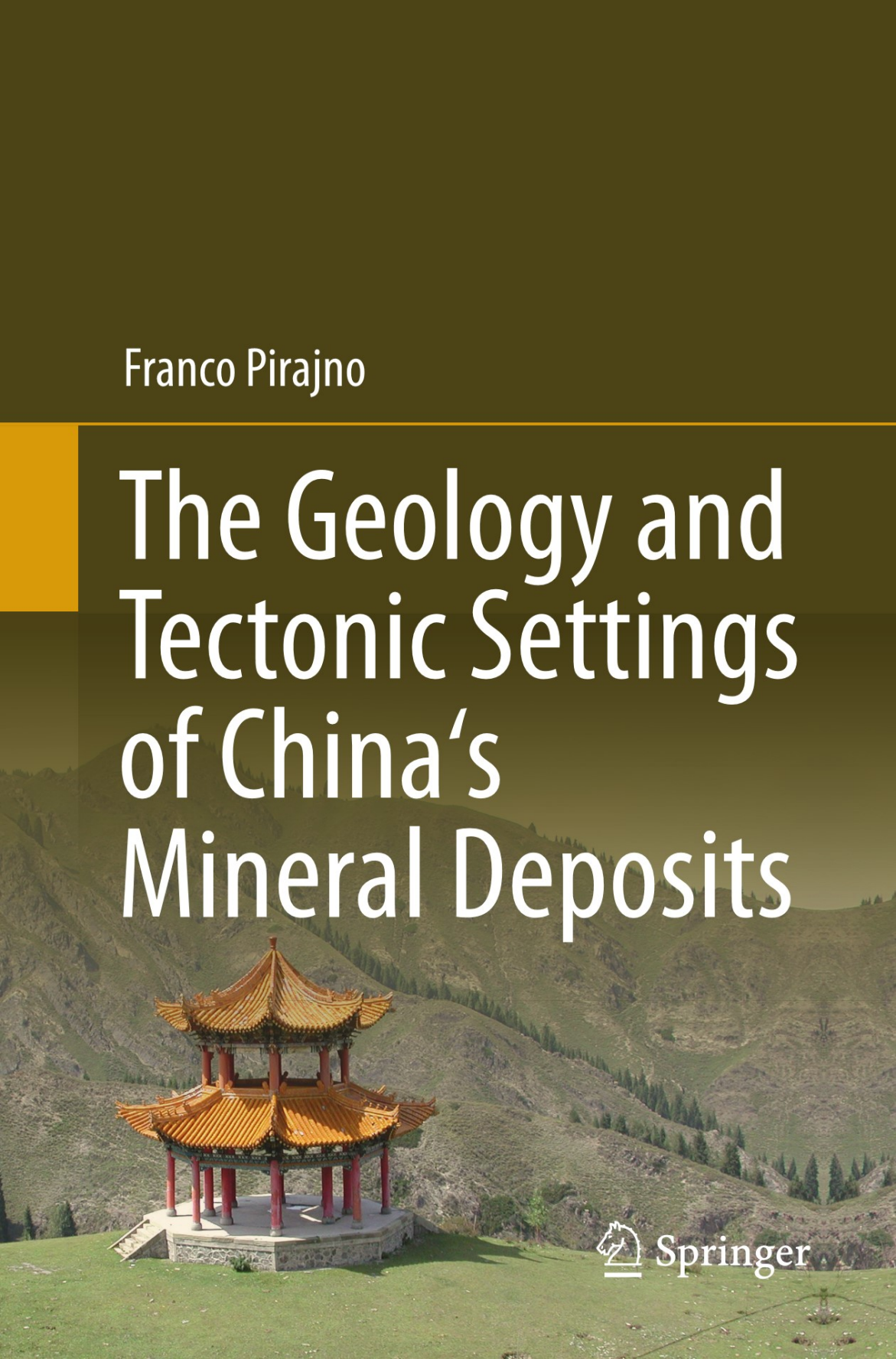

Springer

The Geology and Tectonic Settings of China's Mineral Deposits

Franco Pirajno

The Geology and Tectonic Settings of China's Mineral Deposits

Springer

Franco Pirajno
Geological Survey of Western Australia
Centre for Exploration Targeting
The University of Western Australia
Perth, Western Australia
Australia

ISBN 978-94-007-4443-1 ISBN 978-94-007-4444-8 (eBook)
DOI 10.1007/978-94-007-4444-8
Springer Dordrecht Heidelberg London New York

Library of Congress Control Number: 2012938367

Printed on acid-free paper

Springer is part of Springer Science+Business Media (www.springer.com)

献给中国人民

to the people of China

Foreword

China is an emerging superpower, with a huge demand for raw materials and mineral resources that are being used to increase the standard of living conditions for its residents and bolster its surge forward in the global economy. To enable this rapid growth, China is also undertaking an education revolution with the help of experts from around the world in many different fields of endeavour.

This authoritative book—encyclopaedic in scope—fits very nicely into that frame by presenting a comprehensive account of China's mineral deposits and how they relate to the geological history of that vast country by one of the world's leading experts on mineral systems from Australia, Dr. Franco Pirajno.

Dr. Pirajno is eminently qualified to present this work, having had a diverse career in industry, government and academia that includes 19 years in mineral exploration with the Anglo-American Corporation of South Africa, a stint as Chair of Economic Geology at Rhodes University, South Africa, and 20 years with the Geological Survey of Western Australia. He has held visiting professorships at Peking University and China University of Geosciences and currently has honorary appointments at the Institute of Mineral Resources (Chinese Academy of Geological Sciences), Beijing, the University of Western Australia, Perth, the Centre for Russian and Central EurAsian Mineral Studies (CERCAMS, Natural History Museum, London) and the Australian Centre for Astrobiology, University of New South Wales, Sydney. This is his fourth book on mineral deposits. His first three are "Hydrothermal Mineral Deposits—Principles and fundamental concepts for the Exploration Geologist" (Springer-Verlag 1992), "Ore Deposits and Mantle Plumes" (Kluwer Academic Publishers 2000), and "Hydrothermal processes and mineral systems" (Springer 2009).

More importantly, Dr. Pirajno has travelled extensively through China and visited a variety of that country's mineral deposits, providing the reader with first-hand accounts of critical observations.

The understated title of the book should not fool anyone: this richly illustrated and comprehensively referenced book achieves two remarkable, never previously attempted (at least in English), feats:

1) It describes and interprets the entire, 3.2 *billion* years, of geological history of China;

and

2) It provides detailed accounts of a wonderfully diverse range of mineral systems and places their genesis in the context of that long and complex history.

These achievements are no mean feat, given that the People's Republic of China is the third largest country in the world, with a land area of about 9.6 million sq km.

The book is divided into seven chapters. An introductory *Chap. 1* presents historical notes on mining and geology in China, time scales and definitions used in the book. *Chapter 2* provides a welcome overview of China's tectonic framework in the global context, together with tectono-thermal events that have formed the various mineral systems. This chapter provides the backdrop to the six chapters that follow, which focus on specific periods of China's geological history. *Chapter 3* describes the Archaean and Palaeoproterozoic geology of the North China and Tarim cratonic blocks, including the Phanerozoic mineral systems found in these areas. In *Chap. 4*, the geology of the Yangtze Craton and Cathaysia are described, together with their Mesoproterozoic through Early Palaeozoic amalgamation to form the South China Block. *Chapter 5* reviews the Phanerozoic South China Fold Belt, and the Qinling-Dabie-Sulu, Qilian and Hinggan orogens. *Chapter 6* presents the geology of the Tianshan, Junggar and Altay orogenic belts in northwest China (Xinjiang), part of the huge Central Asian Orogenic Belt that extends from the Uralides in the west to the Pacific Ocean margin of eastern Asia. The Alpine-Himalayan fold belts (Tethyan orogens), and Kunlun and Songpan-Ganzi terranes are also described in this chapter. *Chapter 7* is devoted to an overview of the Large Igneous Provinces (LIPs) of China, which range in age from Paleoproterozoic through to the Jurassic, and the widespread Yanshanian (Mesozoic) tectono-thermal event. Lastly, *Chap. 8* describes the volcano-sedimentary and sedimentary basins and grabens that cover much of China and are important due to their hydrocarbon resources.

However, the real strength of the book lies in the diversity of mineral systems investigated and the detailed descriptions of their occurrence, including well-known volcanogenic massive sulphide (VMS) deposits, epithermal and orogenic lode Au-Ag deposits, and orthomagmatic Ni-Cu and porphyry-style mineralisation, to less well known rare earth element (REE) deposits, Cu-Fe-Au skarns, rare metal pegmatites, and phosphorite and uranium deposits.

In summary, The Geology and Tectonic Setting of China's Mineral Deposits by Dr. Franco Pirajno represents a remarkable contribution in the understanding of China's rich and diverse mineral resource that will significantly enhance the success of commodity exploration in that country and its ability to sustain its growth well into the future.

Martin J. Van Kranendonk
Professor of Geology
University of New South Wales
Sydney, Australia

Foreword

The study of ore genesis is to understand how different mineral commodities, essential for the well-being of human beings, were formed. Such studies serve two purposes. First, they help to satisfy our curiosities about the world we live in. More practically, a good understanding of how the various mineral deposits were formed gives us the predictive power of defining where to look for new deposits.

I was almost totally ignorant about ore genesis during the early days of my career, partly because of my lack of opportunity to learn about it, partly because I was scared by the jargon such as VMS, MVT, SEDEX etc. Later on through my tectonic work in Jiaodong, eastern China where about a quarter of China's gold production comes from, and through running a research project on the tectonic evolution and iron ore genesis in the Hamersley Province of the southern Pilbara craton in Western Australia, of course also through attending talks by people working in the field, I gradually learnt that ore genesis is just part of the geological process that most of us can relate our research to. In other words, mineral deposits are no more than rocks (or sands in the case of mineral sand deposits) with special concentration of certain minerals or elements that are of economical value to society.

Economic geology is no doubt a field that requires specific knowledge, and has some unique approaches in conducting research. There are many excellent studies which approach ore genesis from the angle of Earth processes, linking mineralisation systems to broader geotectonic processes and events. Nonetheless, I noticed that there are also many studies that appear to stop at classifying mineral deposits into certain known categories, thus producing little new understanding about ore genesis and limiting the potential of having real predictive power of such studies to mineral exploration.

The Chinese continental crust is a mosaic of small cratons or terranes that had diverse origins, complex amalgamation histories, and often multiple post-amalgamation modifications. As such, it exhibits a full range of geotectonic environments and provinces fertile for a wide spectrum of mineral deposits. To fully understand the genesis of major mineralisation systems, be it related to continental rifting, mantle plume events, subduction systems, continental collision, terrane accretion, delamination, etc. etc., it is important to examine such mineralisation systems (not just individual deposits) in the context of the regional geotectonic

environments. Much excellent work has been done in the past, dominantly by Chinese researchers on Chinese ore genesis. A good such example is the study of the V-Fe-Ti-PGE and Ni-Cu-PGE deposits related to the Permian Emeishan mantle plume event. Nonetheless, because of the complex tectonic histories experienced by the Chinese continental blocks and orogenic belts, either between these blocks or within individual blocks, our past understanding of many of the mineral systems has been hampered by our limited knowledge of the tectonic evolution of the region, such as the nature of each major orogenic or magmatic event and how such events influenced the major mineralisation systems and provinces.

All these started to change rapidly in the past decade or so, thanks to the wide availability of modern analytical tools such as LA-ICPMS and SIMS among others, and the introduction of modern research approaches and scientific concepts into the Chinese geoscience community. For instance, we are now able to link discrete gold mineralisation events in Jiaodong to precisely dated tectono-thermal events; we can now link the major pulses of magmatic events and related mineralisation systems in south China to possible plume events, orogenic collapses, slab delamination events, and so on. Nonetheless, this renaissance of geoscience research in China has only just started, with many new hypotheses still hotly debated, and many orogenic and magmatic events still poorly understood.

It is from this point of view that Professor Franco Pirajno's new book on "Geology and tectonic settings of China's mineral deposits" is very timely. Franco has a distinguished scientific career specialising on tectonics and mineral systems in Africa, Australia and many other parts of the world. He previously published three books on tectonics and mineral deposits: Hydrothermal Mineral Deposits (Springer-Verlag 1992), Ore Deposits and Mantle Plumes (Kluwer Academic Publishers 2000) and Hydrothermal Processes and Mineral Systems (Springer 2009). His interest turned to China about 15 years ago, leading to many high-impact scientific papers with Chinese colleagues. In the current book, he offers his views, as a western-based researcher, on Chinese tectonics and mineral deposits.

Following an Introduction (Chap. 1), the book is structured in such a way that readers will first get a general picture of the tectonic evolution of the Chinese continent in general (Chap. 2), and that of particular cratons or orogenic belts concerned by each chapter (Chaps. 3 to 6), followed by detailed accounts of all major mineral deposits in geological province concerned. Large Igneous Provinces in China are given special emphasis in a standalone Chap. 7, whereas Chap. 8 is devoted to volcano-sedimentary basins. In such a way individual deposits are no longer being treated in isolation. Instead, they are all part of various mineral systems/provinces lined to particular tectonic events.

During his years of interactions with China-based researchers, Franco has visited many parts of China and numerous deposits. The personal insights gained during such close collaborations are no doubt reflected in the many chapters. Of course, any book of such comprehensive nature would unavoidably involve much literature review and data compilation, including traditional views. In some instances Franco's preferred interpretations differ from mine, but this merely reflects the rapidly evolving nature of our understanding of the region.

This book will thus serve as an invaluable starting point for researchers from both outside and inside China to gain a general knowledge of a specific region or mineral commodity that they are interested in. I look forward to having a printed copy in hand.

Prof. Zheng-Xiang Li
Palaeomagnetism and Tectonics
Department of Applied Geology
Curtin University of Technology,
Perth, Western Australia

Acknowledgements

I consider myself lucky to be part of a "sans frontierès" geoscience community, which has allowed me to visit and study numerous geological sites and mineral deposits and to share ideas and knowledge with colleagues from China, Australia, New Zealand, Russia, the United Kingdom, South Africa, Kyrgystan, the USA and Canada. They have all been a source of inspiration. Since my early visits and field experiences in China, I witnessed over the years, what can be labelled as an unprecedented surge and achievements by the Chinese in scientific, social and humanistic endeavours, perhaps never before experienced in the history of humanity .

In the writing of this book, I thank the reviewers who have taken precious time to read a selection of chapters: Remair Seltmann (Chap. 1), Nacho González-Álvarez (Chap. 3), Hugo de Boorder (Chap. 4), Peng Peng (Chap. 6) and Leon Bagas (Chap. 7). Rick Rogerson and Don Flint of the Geological Survey of Western Australia (GSWA) are thanked for their understanding (mostly behind the scenes) to let me wander and allowing time to write this book and to use the GSWA technical resources. Murray Jones, Michael Prause, Dellys Sutton and Joyce Peng (all at GSWA) drafted the figures, and gave their time even when under pressure for other jobs. Nell Stoyanoff (GSWA secretary) typed most of the tables. Librarians Brian Knyn and Eunice Cheung are thanked for never failing in their help in tracking down papers and books. I extend my gratitude to my Chinese friends and colleagues for their hospitality and generous support in numerous field trips in China, in no special order they include: Mao Jingwen (Institute of Mineral Resources, Chinese Academy of Geological Sciences), Chen Yanjing (Peking University), Zhou Taofa (Hefei University of Technology), Zhang Shihong, Han Higuy and Cheng Yanbo (China University of Geosciences, Beijing), Xiao Long (China University of Geosciences, Wuhan), Zhang Lianchang, Xiao Wenjiao, Peng Peng and Wu Huaying (Chinese Academy of Sciences, Beijing).

I take full responsibility for the contents of this book. If I have misrepresented some of the concepts or ideas obtained from the literature, this was unintentional and in no way reflects a disregard for the original author(s)' work.

Last, but not least, I thank my wife and lifelong companion for not giving up on me.

Contents

Chapter 1
Introduction

Abstract In this introductory chapter an overview of the status of the P. R. China in terms of mineral resources is briefly reviewed, based on published data from the USGS Mineral Year Book, from which it is of great interest to note that China has become the world's largest gold producer for the first time overtaking South Africa. This is followed by historical notes on metal mining, which can be traced with certainty as far back as 8000 years before present. Geological time scales providing local names and usage of terms (e.g. Indosinian, Yanshanian, Sinian, Variscan), commonly used by Chinese geologists. The topics treated in the next seven chapter are also outlined, ending with an explanation of definitions and terms used in this book.

1.1 Introductory Statement and Overview of Mineral Resources in P. R. China, Past and Present

Chinese civilisation and cultural influence reached Turkic, Mongolian, eastern and southeastern Asian peoples. Indeed, China led most of the world in the northern hemisphere in the arts and sciences for hundreds of years. Then in the nineteenth century, China experienced civil unrest, significant food shortages, military defeats, and foreign occupation. With the end of World War II, the Communists under the leadership of Mao Zedong established a dictatorship which, while ensuring China's independence, imposed strict controls on everyday life. After 1978, his successor Deng Xiaoping gradually introduced market-oriented reforms and decentralized economic decision-making. Today, while political controls still remain, more and more economic controls continue to be relaxed. China's economy is booming and its influence is growing worldwide.

China is endowed with several world-class metallic mineral deposits, and became first in the world, since 2003, for total metal production of copper, aluminium, zinc, nickel, tin, magnesium, mercury, antimony and titanium (Mining Journal, August 13th, 2004). At the time of writing, the latest statistics for China's mineral production can be found in USGS Minerals Year Book 2008, 2010 (Tse 2009, 2010; Table 1.1). In 2008 China was the leading producer of aluminium, antimony, barite, bismuth, coal, fluorspar, gold, graphite, lead, rare earths, tin, tungsten and zinc, as well as the leading exporter of antimony, barite, coal, fluorspar, rare earths and tungsten (Tse 2009; USGS Minerals Year Book 2008). Mineral

F. Pirajno, *The Geology and Tectonic Settings of China's Mineral Deposits,*
DOI 10.1007/978-94-007-4444-8_1, © Springer Science+Business Media Dordrecht 2013

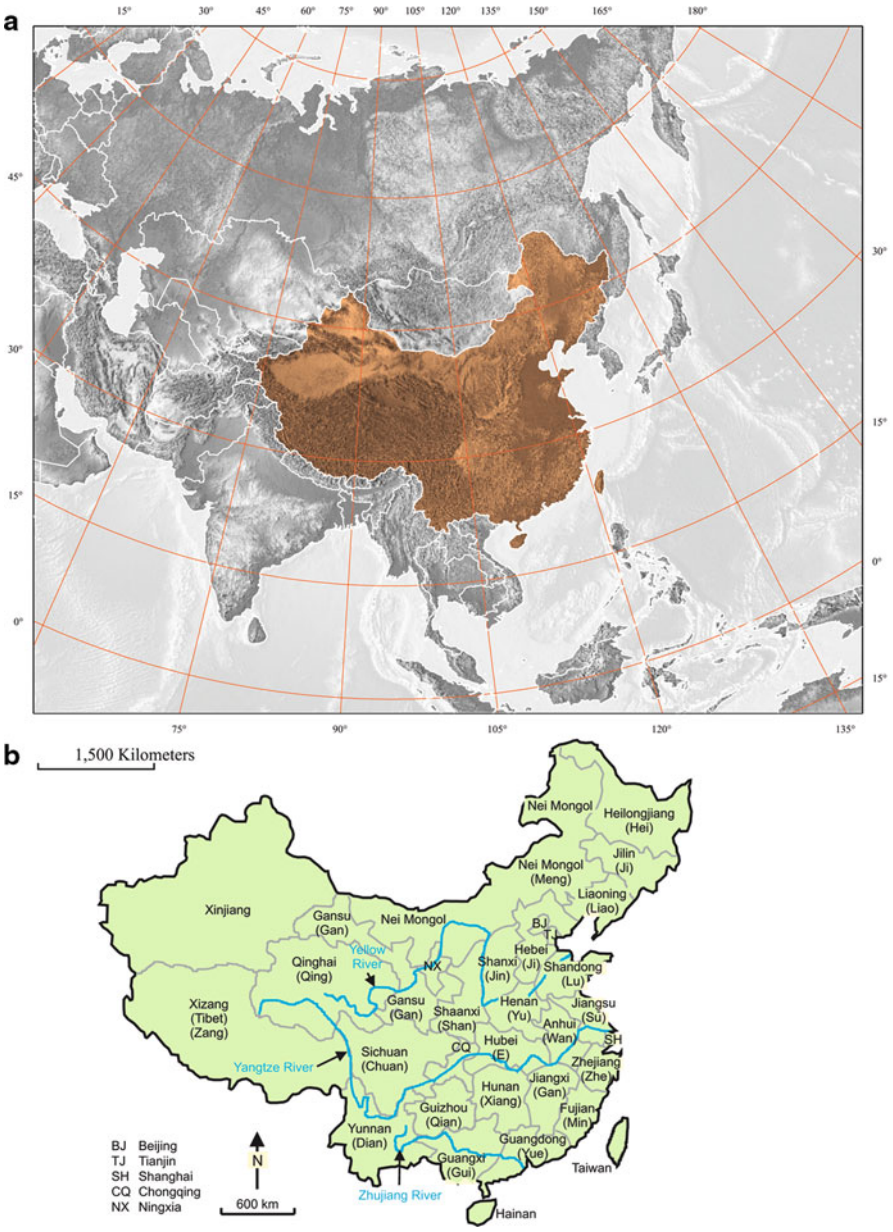

Fig. 1.1 **a** Position and extent of the People's Republic of China in Asia; **b** Administrative and provincial divisions of China

Table 1.1 Reserves of major metal commodities in China. (Source: Tse 2009; USGS Mineral Yearbook 2008, 2010)

Metal	Reserves in thousand tonnes or million tonnes (Mt)
Antimony	950
Chromite ore	5,800
Copper	30,000
Cobalt	80,000
Gold	1,900
Iron ore	23,000 (iron content 7,200)
Lead	13,000
Manganese ore	220 (metal content 44,000)
Mercury	21,000
Molybdenum	4,300
Nickel	3
Rare earths	55
Silver	43
Tin	1.5
Tungsten (WO_3)	2,400
Vanadium (V_2O_3)	13,000
Zinc	42,000

deposits in east Asia are listed in an excel spreadsheet, available at http://www.gsj.jp/Map/EN/docs/overseas_doc/DataSheet.xls (last accessed in February 2012), which includes 2,326 deposits from eastern China. The reader, however, is cautioned that this listing is by no means complete.

In the last 20 years a great deal of knowledge of the geology and tectonics of China has been gained, enhanced by a vigorous cooperation between Chinese and western geologists. Extracts from a press release by the Xinhua News Agency (October 23rd, 2008) stated: "*Chinese geologists have discovered 1,202 mineral fields, which could greatly reduce the country's dependence on imported minerals, nationwide since the start of 2008..... Reserves of badly needed minerals have been largely expanded, including iron, copper and bauxite, among others..... More than 100 million tons of iron ore was discovered in Gongchanling iron mine, in the northeastern Liaoning province. With a reserve of 62.3 million tons, it has become the largest iron mine in China..... In the Tibet Autonomous Region, a huge reserve of more than 10 million tons of copper had been found in Qulong.....*"

Gold mining has recently made that country the world's largest gold producer. For the year 2007, gold output rose 12 % from 2006 to 276 tonnes (or 9.7 million ounces) to become the world's largest for the first time overtaking South Africa, which produced 272 tonnes. Gold output in China has risen by 70 % for the past decade. China produced nearly 300 tonnes of gold in 2008 (http://en.wikipedia.org/wiki/Gold_mining_in_China).

Here, I provide references and/or books that are worthy of mention for students of Chinese geology and mineral deposits. The list is probably not comprehensive, but it does cover most of what has been published in English in the last 25 years or so. The geology of China has been described in English language books by Yang et al. (1986) and Cheng (2000). Books that deal with the tectonic evolution of China include those by Chen (1988) and Ren et al. (1987). A five volume tome describes in

detail some of China's individual mineral deposits (Editorial Committee of Mineral Deposits of China 1990, 1992, 1995, 1996a, b). A comprehensive atlas of China, comprising geological and geophysical maps as well as data on igneous systems can be found in Ma (2002). A book published in Chinese and English provides information on selected mineral deposits (Li 1992). Tectonics and mineral resources have been reviewed by Wang and Ma (1995), Chen and Tao (1995) and Zhai and Deng (1996). Ren et al. (1987) published a book on the tectonic units and evolution of China, whereas English language papers arising from the 30th International Geological Congress (IGC), held in Beijing, are published in a monograph (Liu 1996), and from the 31st IGC and 32nd IGC in special issues of Acta Geologica Sinica (2000a, b, 2004a, b, respectively). Also from the 30th International Geological Congress is a collection of papers on uranium mineralisation (Chen et al. 1996). Other works that review mineral deposits in China include: Zhou et al. (2002b, c) and Tang et al. (2006) on magmatic sulphide deposits; Wu (1993) on Sb deposits; Feng and Zhang (2004) on Co deposits; Nie (1997) on Au deposits and Chen et al. (1996) on U deposits. A special issue of Mineralium Deposita provides a comprehensive and authoritative collection of papers on the tectonics and gold metallogeny of China (Zhou et al. 2002a). Special issues of Ore Geology Reviews have been devoted to Tibetan metallogeny (Hou and Cook 2009) and Mesozoic mineral systems of eastern China (Mao et al. 2011). It is also worth mentioning the Explanatory Notes for the 1:2,500,000 scale geological map of China, in which a series of sketches shows the distribution of key units and magmatic systems, such as ophiolites, granitic plutons and batholiths from Archaean to Mesozoic (China Geological Survey 2004). Although not exclusively dealing with China, excellent key publications that describe in some detail various geological aspects of Asia, include Hendrix and Davis (2001) and Yin and Harrison (1996). In the latter volume is the outstanding contribution of Sengör and Natal'in (1996) in which the geodynamic evolution of China within the framework of the Asian continent is discussed. Special volumes of the Geological Society (London) addressing the thinning of the sub-continental lithosphere and "de-cratonisation" of eastern North China Craton (Zhai et al. 2007) and Malpas et al. (2004) on the tectonic evolution of China from the Precambrian to Present.

A book providing a comprehensive database of China's metallic and non-metallic mineral resources, as well as energy resources (Zhu 2007), was compiled in 1998, first published in English in 2002 and subsequently redistributed by Elsevier in 2007. More recently, a two-volume compilation of formal names of Chinese lithostratigraphic formations (from 1866 to 2000) by Zhang (2009) is a massive compilation that is a must for everyone engaged in geological work in China. This is especially important, because of common confusion, due to different spellings and names for the same unit, only too often used and published both by Chinese and non-Chinese researchers.

In addition to the above cited works, the reader should be aware of a number of geological and metallogenic maps (usually at scales from 1:2,500,000 to 1:5,000,000) that have been published in the last 30 years or so. These are not readily available but, if not out of print, some can be obtained from the Geological Publishing House, Beijing. Worthy of note, in my opinion, are the following:

- Geological map of China, 1:4,000,000 scale with Explanatory Notes, 2nd edition, 2004, compiled by the Institute of Geology, Chinese Academy of Geological Sciences (ISBN 7-116-03916-3)
- Metallogenic map of endogenic ore deposits of China, 1:4,000,000 scale, 1987, compiled by the Institute of Geology, Chinese Academy of Geological Sciences (ISBN 7-5031-0000-1)
- Geological map of Central Asia and adjacent areas; comprising nine sheets at 1:2,500,000 scale, Chief Editor Geng Shufang, 2008, Geological Publishing House, Beijing (ISBN 978-7-116-05482-0)
- Geological map of igneous rocks of China, 1:5,000,000, compiled by the Institute of Geology, Chinese Academy of Geological Sciences, 1997, Geological Publishing House, Beijing (ISBN 7-116-02245-7)
- Gold resources map in volcanic regions of China, 1:5,000,000, compiled by the Institute of Geology, Chinese Academy of Geological Sciences, 1997, Geological Publishing House, Beijing (ISBN 7-116-02425-5)
- Geological map of China, 1:12,000,000, compiled by Ma et al. (1996), Geological Publishing House, Beijing (ISBN 7-116-02250-3)
- Geological map of the People's Republic of China, 1:2,500,000, with Explanatory Notes, compiled by China Geological Survey, 2004, SinoMaps Press (ISBN-7-5031-3374-0/K 1769)

1.2 Historical Notes on Mining

Copper implements in China date back to about 4,000 years before present (B. P.), bronze and iron wares were made about 3,600 years B. P. and descriptions of mineral species and metallic ores were written since about 2,500 years B. P. (Yang et al. 1986). A mining site, discovered in the 1980s in the Tonglu mountains (Hubei Province) and dating back to about 3,000 years B. P. revealed metallurgical equipment estimated to have treated 1–1.5 tonnes/day (Yang et al. 1986). Notwithstanding earlier times, from about 2,300 years B. P., the Chinese mining industry thrived under the Han dynasty. State monopoly of iron and salt was instituted about 2,120 years B. P., when some 48 foundries were established, each employing up to a thousand workers (Gernet 1999). However, it was not until 2,500 B. P. that the first descriptions of mining operations were made. While cast iron was used mainly for agricultural tools and weapons, steel weapons replaced bronze weapons as early as the 2,100 B. P.

Pliny the Elder (2,033–2,089 B. P.) praised the quality of iron produced by the Seres (name for the inhabitants of the northwestern part of modern China, people of the "land where silk comes from", the country of the Seres was called Serica; http://en.wikipedia.org/wiki/Seres). The estimated distribution of the iron industry under the Han emperors is shown in Fig. 1.2. More recently, new and exiciting archeological discovery delightfully discussed in a News Focus article in Science (Lawler 2009), have traced very ancient cultures back to 8,000 B. P. (Yangshao culture) and 6,000 B. P. (Hongshan culture) and metal-utilising (bronze) in the Erlitou,

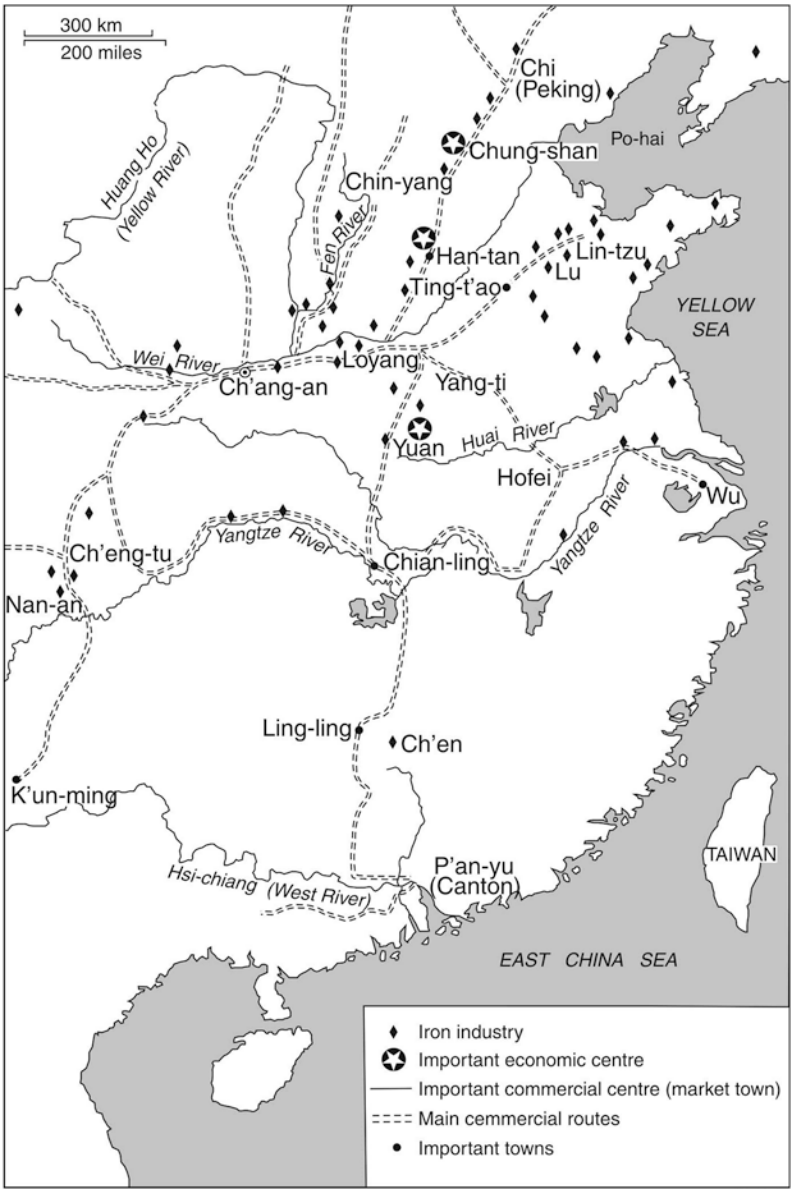

Fig. 1.2 Distribution of iron mines and industries in China during the Han emperors (ca. 2,300 B. P.). (After Gernet 1999)

Erligang and Sanxingdui cultures, dating back to 4,000 B. P. Erlitou, east of the ancient capital Xi'an, in the Yellow River valley, was a civilisation that may have flourished between 4,000 and 3,600 B. P., in which many bronze and gold artifacts have been found. North of the city of Chengdu (Sichuan Province), abundant metal artifacts have been unearthed, such as massive bronze statues (e.g. a 4 m-high representation of a tree) and gold masks, dating to about 3,200 B. P. and part of the Sanxingdui culture (Lawler 2009). Between the eleventh and thirteenth centuries there was a great economic expansion in both agriculture, manufacture and mining. In the eleventh century, explosives were first employed in the mines and in 1,078 CE (current era) the production of cast iron exceeded 114,000 tonnes, while in 1788 CE in England reached only 68,000 tonnes (Gernet 1999). In southeastern China, copper and gold deposits were exploited during the Sui and Tang Dynasties (605–908 CE) and the Song Dynasty (1,279–960 CE); these deposits represent a range of porphyry-epithermal systems and are still being explored and mined and are discussed in this book. The web site http://www-chaos.umd.edu/history/toc.html (last accessed in February 2012) provides a good overview of history of China, as well as numerous references. Hu et al. (2011) published a frank political and technological discourse on the mineral resources, their development and requirements of the Peoples Republic of China. This edited book, directed at potential investors, provides a "road map" to 2,050 for predictive discoveries, exploration and utilisation of mineral resources.

1.3 Historical Notes on Geology in China

Modern geology in China is considered to have started with the translation in 1873 of Charles Lyell's Principles of Geology by Hua Hengfang. Yang et al. (1986) briefly reviewed the history of modern Chinese geology and described two periods: 1912–1949 and 1949–1980s. The 1949–1980s time span is one of reconstruction and the institution of organisations, such as the Ministry of Geology and Mineral Resources and the Chinese Academy of Science (Academia Sinica), leading to an upsurge of State run mineral exploration and discoveries of mineral deposits. During this time, Chinese geoscience was largely inspired by Soviet Russia and this is still noticeable today, although there has been since the 1990s a concerted effort by Chinese geoscientists to adopt Western methodologies and usage, in order to enter the international arena. The remarkable vitality of Chinese geoscience is testified by the ever escalating number of Chinese authors in international journals, as well as Chinese publication of journals in English (e.g. Acta Geologica Sinica; Science in China, series D, Geoscience Frontiers). Indeed, the ever-increasing publications on China's geology and mineral deposits, makes it quite challenging to keep up with the latest developments. Furthermore, Western geoscientists, both from academia and mining concerns routinely work in many cooperative projects with Chinese colleagues.

1.4 Chinese Language and Styles

Trumbull et al. (1992) in their Preface warned the readers on the problems encountered by non-Chinese about Chinese language and styles. These authors considered this to be an important aspect and I concur, because only too often there is confusion from both sides of the cultural and linguistic platforms.

Chinese is the most widely spoken language in the world, albeit with a series of dialects that can be quite different. Mandarin Chinese is the unifying official idiom or lingua franca. Mandarin Chinese is commonly referred to by the Chinese themselves as Hanyu, the language of the Han, the dominant ethnic group. Cantonese and Fujianese are languages in their own right, widely spoken in the Hong Kong region and by Chinese communities in South East Asia. In all cases, Mandarin and dialects come together in the Chinese script. No matter how different dialects may sound when spoken, once written in Chinese characters, they will become comprehensible to the Chinese reader. Chinese characters are complex to non-Chinese and during the Shang dynasty (about 3,600–3,100 B. P.) there were thousands of these characters (according to some sources, up to 56,000), although most are considered obsolete and only about 2,500 are needed to read a text or a newspaper. In the seventeenth century, Mei Yingtsu, a philologist, was the first to classify Chinese characters, producing a dictionary in 1615, in which 33,179 characters were recorded (Gernet 1999). Chinese characters are pictograms designed to represent a concept, an idea similar to that of numerals (1 is one, 2 is two, etc.). A good overview for the uninitiated can be found in the continuously updated Lonely Planet books on China (e.g. Harper et al. 2002).

The important point that non-Chinese have to bear in mind is that Chinese languages are **tonal**. This means that the pronunciation of a word needs to have not only the correct sound, but also the correct tone. Mandarin Chinese has 4 tones: high, rising, falling-rising and falling. For this reason the Latin alphabet is totally inadequate for the Chinese linguistic tones. This leads to many different spellings for the same name, causing considerable confusion with both Chinese and non-Chinese (the Kalatongke Ni-Cu deposit in Xinjiang is also spelt Karatongkh, Karatongk, Kalatunge; the major northwest-trending Irtysh Fault, is in many instances also spelled Ertix, Yrtish, Erqis). While on this topic, Chinese locality names are always written as one word (e.g. Shanghuangqi, Tianshan and not Tien Shan or Tian Shan).

In the 1950s the **pinyin** system was deviced in order to use the Latin alphabet, with accents being used to represent the 4 tones. The pinyin system is useful for non-Chinese, particularly Westerners, because the letters and accents do provide many of the sounds and tones, but not all by any means. Thus, the pinyin system writes Mao Tsetung and Deng Xiaoping. Another system in use is the **Wade-Giles**, in which Mao Tsetung becomes Mao Zedong and Deng Xiaoping becomes Teng Hsiao-p'ing. The latter system is now more commonly used, but is perhaps less user-friendly for speakers of Western languages.

The above discussion takes us to persons' names. In the Chinese tradition family names come first (Smith John), although it must be remembered that many

well-educated Chinese use the Western style out of a sense of hospitality and kindness towards foreigners. This may also be a cause of confusion. In many English language papers we see Qiu Y-M, or Qiu Y. M., meaning Qiu Yu-min, which can also be Qiu Yumin or Qiu Yu Min. In the same volume one may encounter an authorship like: Rui-Zhong H., Wen-Chao S. etc., which in fact should be Hui R. Z. or R-Z. and Su W-C or W. C. Also, and interestingly, Chinese family names are comparatively few, so that there are quite literally millions of Zhang, Zhou, Chen, Mao, Han, Li etc., whereas first names are almost unique for each person (Yan-jing; Jing-wen, Yu-min etc.). This is the opposite of European names, in which first names are commonest (John, William, Franco, Frank, Franz, Nikolai, Jacques etc.), whereas surnames generally are the identifier of a person.

1.5 Geological Time Scales

Inevitably, as elsewhere in the world, the Chinese geological literature has local names and usage of terms, such as Indosinian, Yanshanian, Sinian, Variscan, that are either not used or not commonly used by non-Chinese geologists. For this reason, I believe that it useful to make the reader aware of some of these terms, particularly those used in the geological time scales. As will be noted, the samples of geological time scales shown below from various sources, use different names for the same event.

Wang and Mo (1995) and Cheng (2000) provided tables of the main geological events in China within the IUGS time scale. Zhou et al. (2002a) gave a list of tectonic and tectonothermal events in China, using a nomenclature that is commonly used in Chinese literature and this is reproduced in Table 1.2, with minor modifications, traditional subdivision of the Precambrian in China are shown in Table 1.3 (Wilde et al. 2004), whereas another compilation of the time scale from Wang et al. (2005) is shown in Table 1.4.

1.6 This Book

In this book I discuss the general geology and the geodynamic evolution of China's major tectonic domains and corresponding mineral districts and/or individual deposits, whose choice and geographic provinciality is based partly on personal experience and/or knowledge of the deposit(s) in question. I have drawn heavily from published literature and from publications and special issues of journals in which I have participated with Chinese colleagues.

Following this introductory chapter, this book comprises seven chapters, whose topics and their ordering at first may appear somewhat confusing to the newcomer. However, this will become clear in the pages that follow. Overprinting tectonothermal events from the Archaean to Recent have affected almost all tectonic domains

Table 1.2 Main tectonic events in China. (After Zhou et al. 2002a)

Eon	Era (Ma)	Period (Ma)	Orogenic epochs and geological events
PHANEROZOIC	Cenozoic	Himalayan	Upheaval of Qinghai–Tibet Plateau Himalayan Orogeny
		90	Foreland basin, rift basins and marginal basin **Yanshanian tectono-thermal events**
	Mesozoic	Yanshanian	Formation of the Circum–Pacific magmatic belt
		208	**Indosinian Orogeny**
		Indosinian	Collision of North–South China
		270	**Late Variscan Orogeny**
			Collision of North China Angara
	Palaeozoic	Variscan	**Early Variscan Orogeny**
		405	**Late Caledonian Orogeny**
		Caledonian	Merging of North China and Tarim
			Early Caledonian Orogeny
PROTEROZOIC	Late Proterozoic	Sinian	Opening of Qilian and Qinling Oceans
		800	**Late Jinningian Orogeny**
		Jinningian	**Early Jinningian Orogeny**
	Middle		Aulacogens, rifts
			Luliangian Orogeny
	Early Proterozoic	Luliangian	Protoplatforms Protoaulacogens
			Wutaian Orogeny
ARCHAEAN	Late Proterozoic	Wutaian	
		2800	**Fupingian Orogeny**
		Fupingian	Continental nuclei
	Early Archaean	3200	
		Qianxian	

Table 1.3 Precambrian orogenies in China. (From Wilde et al. 2004)

Eon	Ga	Group/System	Orogeny
Palaeoproterozoic	1.8	Guojiazhai	Lüliang
	2.4–2.3	Hutuo	Wutaian
	2.6–2.5	Wutai	Fupingian
Archaean	3.0–2.9	Fuping Qianxi	Qianxian

Table 1.4 Main stages and events in China. (After Wang et al. 2005)

Geologic time scale (Ma)			Tectonic stage		Tectonic and magmatic events
Eon	Era	Period / Q	Mega stage	Stage (Ma)	
Phanerozoic	Cenozoic	Neogene	Intracontinent	– 20 Hm2 Orogeny	– Intracontinental collision in Qinghai Tibet
		Paleogene		– 40 Hm1 Orogeny	– Openingof South China Sea basalt in NE china & SKP
	Mesozoic	Cretaceous		Hm Himalayan	Crustal and Lithospheric thickening in Qinghai-Tibet and thinning in E China
		Jurassic		– 100 Yanshanian Orogeny	– Rift Basins in N & NE China & Mongolia
				Yanshanian	Intracontinental collision granites and Calc-alkali extrusives in E China J Continental margin magmatism in CTA
		Triassic	Pangaea and supercontinent	– 210 Indosinian Orogeny	– 220 Dable-Sulu UHP zone
	Palaeozoic	Permian			– Pangaea (250) and Laurasia Supercontinent –
		Carboniferous			CFB in W YZP
		Devonian		Hercynian-Indosinian	Basalt in W Yannan
		Silurian		– 400 Qilianian Orogeny	Felsic and intermediate extrusives in N – Tianshan
		Ordovician		Caledonian *sensu stricto*	Intermediate extrusives in N & S Qilian
		Cambrian		– 510 Salairian Orogeny	– Platform cover sequence Predominant
Proterozoic	Neoproterozoic	Sinian		Salairianar	
		Nanhuan			
		Qingbalkouan	Platform	– 830 Jinningian Orogeny	– Pangaea (850)-(Rodinia) Partial convergence of YZP & CTA Approach between SKP & YZP Accretion of W & E Kunlun to TAP & QD
	PM Meso-proterozoic	Jixianian		Jinningian	Possible convergence of Cathaysiana Supercontinent Alkali-basalts in SW YZP & NW CTA
		Changchenglan			
	Palaeoproterozoic		Proto-platform	– 1850 Lullangian Orogeny	– Aulacogens in SKP Cratonization of SKP
				Lullanglan	Amalgamation in S TAP & N CTA United basement in SKP
Archaean	Neoarchaean				Nuclear aggregation in NSKP & NE TAP
	Mesoachaean		Continental nuclei	2800	
	Palaeoarchaean			Nuclei formation	
	Eoarchaean				
Hadean					

and/or lithotectonic units, resulting in a wide range of diverse mineral systems that are best discussed for each tectonic domain, even though their inception may be through a superimposed event. For example, many of the Au lode deposits and porphyry systems of Mesozoic or Late Palaeozoic ages occur in Precambrian rocks of the North China Craton and in fold belts along its margins. Each chapter of this book can be considered on a stand-alone basis, although where appropriate reference is made to other chapters and/or their figures. The reader interested in a specific topic or part of China can select the relevant chapter. For this reason, some concepts and descriptions of certain tectono-magmatic events are repeated in individual chapters.

I begin with a brief account in **Chap. 2** of China's tectonic framework in the global context, the various geodynamic events that resulted in the present day lithotectonic domains, including overlying volcano-sedimentary basins. **Chapter 3** deals with the North China Craton (NCC) and the Tarim cratonic block, which were finally amalgamated during the Phanerozoic. On present-day coordinates, these cratons form a nearly continuous east-west trending domain. The NCC extends to the Korean peninsula, hence the commonly used term of Sino-Korean Craton. For the NCC, following a summary of its geodynamic and magmatic evolution and its final assembly as a stable cratonic block, I describe Archaean and Palaeoproterozoic mineral systems, such as magmatic deposits in mafic-ultramafic rocks, volcanogenic massive sulphides (VMS), iron-formations and the rift-related giant REE deposit of Bayan Obo, alone accounting for a large proportion of the rare earth resources in the world. As mentioned above, precious metal lode deposits, porphyry and porphyry-skarn polymetallic deposits occur within the North China Craton or along its margins have ages ranging from Permian to Late Cretaceous. The Precambrian rocks that make the Tarim Craton are poorly exposed mostly along its margins and overprinted by several later tectonic and tectono-thermal events, which make it difficult to gain a suitable insight into the geological history of this cratonic block.

In **Chap. 4**, I describe the main features of the Yangzte Craton and Cathaysia, which together are commonly referred to as South China Block. These tectonic domains host, perhaps the widest and diverse series of mineral systems in China: stratabound-stratiform sedimentary-rock hosted massive sulphides, Carlin-style Au deposits, Mississippi Valley Type (MVT), porphyry and lode deposits. The Middle-Lower Yangtze River Valley metallogenic belt, at the northern margin of the Yangtze Craton, comprises porphyry-skarn and Kiruna-style mineral systems that have been and still are the subject of many studies (e.g. Mao et al. 2011). The Cathaysia Block and border regions with the Yangtze Craton contain the world-class Gejiu Sn-Cu deposits, linked to ca. 80 Ma granitic cupolas that intruded sedimentary and basaltic rocks, resulting in greisen-related Sn deposit, skarns and replacement mineral systems. The unusual metalliferous shale horizon probably hosting Mo-Ni-V-PGE along a transitional shelf zone, from platform sedimentation in the northwest to a deeper foreland setting in black shales in Cathaysia. Uranium deposits in rift basins and granite-related U and REE mineralisation are also recorded in the Cathaysia Block. In Chap. 4, the reader will appreciate the complexity of the tectonic settings of mineral systems that are present in the Yangtze-Cathaysia terranes.

For **Chap. 5**, I have chosen to discuss three orogenic (fold) belts: South China Fold Belt, Qinling-Dabie-Sulu and Hinggan. The South China Fold Belt is superimposed on the Cathaysia Block and is linked to a complex geodynamic evolution, for which the consensus is a subduction-related tectonic and magmatic belt formed along the Palaeopacific Asian continental margin. In detail however, models range from steep to shallow subducting slabs, breakoff of the slab in more advanced stages and upwelling asthenospheric melts, resulting in partial melting of the lower crust and emplacement of I- and A-type granitic rocks, with which porphyry-epithermal systems are temporally and genetically associated. The Qinling-Dabie-Sulu (Central China Orogen) orogens, effectively extend across mainland China, suturing the North China and Tarim cratons in the north with the Tibet-Himalayan belts and South China Block. A combination of accessibility and the fact that those parts of the Qinling-Dabie-Sulu orogenic belts host world-class deposits along the collision zone between the Yangtze and North China Craton and along the Tanlu (Tangcheng-Lujiang; abbreviated as Tanlu) fault, have attracted and still do, at least in my opinion, an inordinate amount of research at the expense of other regions. For example, most of the western parts of the Qinling orogens, along the southern and southwestern margins of the Tarim (see Fig. 2.3) remain little investigated. In China's northeast is the Xinggan orogen, which is the eastern part of the Central Asian Orogenic Belt (CAOB). The Xinggan belt contains porphyry and epithermal deposits, orthomagmatic Ni-Cu deposits, again of different ages and associated with multiphase tectonic features, some linked to the closure of the Okhotsk ocean (Solonker suture), between the Siberian-Mongolian plate and the NCC, others associated with the Mesozoic Yanshanian tectono-thermal event.

Porphyry, porphyry-skarn deposits, described in Chap. 4 and 5 are not related to calc-alkaline magmatism linked to subduction systems, such as those of the southwest Pacific island arcs, or the continental margins of the Americas (e.g. Sillitoe 1997; Cooke et al. 2005). The Chinese porphyry deposits and associated skarns, where carbonate rocks are abundant, in the Yangtze and Qinling provinces are intracontinental and associated with potassic calc-alkaline, alkaline or magmas of shoshonitic affinities, as indeed well documented by many Chinese authors. Although these mineral systems share many similarities with the classic, calc-alkaline, subduction-related porphyry deposits, their tectonic and metallogenic settings are remarkably different. One of the distinguishing features, for example, are that the ore-fluids that typically form these intracontinental porphyry systems are rich in CO_2 and fluorine. As described in Chap. 4 and 5, these porphyry systems were formed during Indosinian and Yanshanian times and controlled by major trans-lithospheric breaks, particularly those around the margins and boundaries of the NCC and the South China Block (see Figs. 2.1 and 2.3), temporally associated with lithospheric thinning or cratonic keel removal beneath the Eastern Block of the NCC.

In **Chap. 6**, I describe those sectors of the CAOB that are in northwest China, the Tianshan and Altay (Altai) orogens and the Alpine-Himalayan fold belts in southwest China and Tibet (Tethyan orogens or Tethysides), the Qunlun and Songpan-Ganzi terranes to the north. As with the central and eastern Qinling, the Tianshan and Altay orogens in Xinjiang Province (northwest China) have attracted much attention

from Chinese and non-Chinese geoscientists, partly because of the importance of the CAOB for the geological history of central Asia and partly because of the rich endowment of mineral resources. Needless to say that controversy is ripe in attempting to resolve the evolution of these orogenic belts, particularly the timing of subduction, terrane docking, suturing, post-collision extension and collapse, intraplate magmatism and the role of strike-slip structures, why and which caused the inception of mineral systems, ranging from porphyry and epithermal, lode deposits, rare metal pegmatites, VMS deposits and Ni-Cu in mafic-ultramafic intrusions. Xinjiang, apart from its geology, is a culturally fascinating region, where the historically famous silk route passed through and at the cross-road of several central Asian countries. Equally fascinating is the part of the Alpine-Himalayan orogenic belts (Tethysides) that are present in China. These are exposed in Tibetan plateau (Xizang Zizhiqu) and Yunnan provinces, where sutures, reactivated time and again as strike-slip faults and thrusts abound (e.g. Red River fault), mostly related to the on-going India-Eurasia collision. Porphyry and rare earths in carbonatites are common and reasonably well studied (e.g. Hou and Cook 2009). In southwest China (Yunnan province), later events (Emeishan large igneous province) and the eastward and southeastward directed lateral push (escape tectonics) created by the India-Eurasian collision, resulted in multiphase deformation and hydrothermal remobilisation of ore minerals along these faults. Chapter 6 ends with an overview of the Kunlun and Songpan-Ganzi terranes and contained mineral systems (porphyry, MVT, VMS).

Large igneous provinces (LIPs) and the Yanshanian tectono-thermal event are discussed in **Chap. 7**. Here, I describe LIPs from oldest (ca. 1.8 Ga Xiong'er) to youngest (260 Ma Emeishan). The Yanshanian event takes special place, principally because of its role in the removal of the eastern part of the cratonic keel of the NCC, because of what exactly caused it, thermal erosion, removal of dense lithospheric mantle, detachment or delamination, subduction of the Palaeopacific (Izanagi) plate, eastward slab retreat and breakoff, far-field push from the rise of mantle plumes in the Pacific Ocean, flat-slab and dehydration of mantle wedges above the slab. The presence of ultra-high pressure (UHP) metamorphic rocks along major fault zones (Tanlu fault) testify to rapid uplift due to breakoff or removal of the crustal roots. Lamprophyres, gabbros, carbonatites, dolerite, diorites and A-type granites are part of the Yanshanian "giant igneous event" in an extensional setting due to lithospheric removal, associated with metamorphic core complexes, in combination with the northward continental subduction of the Yangtze Craton beneath the NCC (Windley et al. 2010).

This delamination has been attributed to the Kula-Pacific plate subduction (or Izanagi plate), which according to Mao et al. (2010, 2011), changed direction from orthogonal to oblique to the Asian margin, corresponding to differences in magmatism before and after 135 Ma. Interesting also to note that Windley et al. (2010) suggested that the Kula-Pacific plate subduction may have been enhanced by superplume activity in the Pacific Ocean (oceanic plateaux, which would have pushed the plate to subduction; equivalent to ridge push, but much stronger). Indeed, early Cretaceous plume activity occurred in both Indian and Pacific oceans (Kerguelen and Ontong-Java-Hikurangi oceanic plateaux).

These magmatic and tectonic events, concentrated along terrane boundaries and faults that may reach into the lithospheric mantle. Singly or in combination these were the extensive causative effects that formed varied mineral systems that are superimposed on much older tectonic terranes. This is the reason of the apparently erratic discussion of the enormous range and variety of mineral systems in different chapters, but all linked to this tectono-thermal episode.

Chapter 8 concludes the book with an overview on volcano-sedimentary basins in China, many of which host important oil, gas and coal resources, as well as sandstone-hosted (roll-front) U mineralisation.

1.7 Some Useful Definitions Used in this Book

The terms mineral deposit, ore deposit, mineral occurrence, prospect, mine, reserves and resources are familiar, but more rigorous definitions are often needed for scientific accuracy and/or legal requirements.

Cox and Singer (1986) defined **mineral deposits** as occurrences of a valuable commodity (e.g. copper) or mineral (e.g. barite) that are of sufficient size and concentration (grade) that they might, under favourable circumstances, be considered to have potential for economic exploitation. An **ore deposit** is a mineral deposit that has been tested and discovered to be of sufficient size, grade and accessability to allow it to be extracted at a profit. **Mineral deposit** carries no necessary profitability implications and usually, but not necessarily, denotes subeconomic or incompletely evaluated occurrences of ore minerals. **Mineral occurrences** or ore-mineral occurrences are uneconomic, but still anomalous concentrations of minerals that may form ores elsewhere.

Reserves include orebodies in production, or known by drilling or other specific measurements, to exist. Reserves are subdivided into measured, indicated and inferred (in Australia these are strictly defined regulations set out by the JORC Code 2004). **Resources** include reserves and all other potentially viable mineral deposits that are either unknown or uneconomic at present, but can still be reasonably expected to exist. The reader needs to be aware that many of the above definitions remain somewhat fuzzy or contradictory in Chinese literature, commonly varying from province to province and from author to author. In addition, terms such as large, superlarge, giant ore deposit are not formally defined. Although, recently there have been efforts to formalise these definitions, for example in the case of gold deposits, small is < 5 t Au metal; medium is 5–20 t Au and large 20–100 t Au.

In every day practice, and in the majority of recent publications, the general term **ore deposit** is used a broader sense to include both economic and non-economic mineral deposits. **Mineral system** or **ore system** are terms used interchangeably in this book. The concept of a mineral (ore) system is analogous to that of a petroleum system, but owing to the nature of ore deposits and host rocks, a mineral system is far more diverse and complex. The formation of an ore deposit requires a source of metals, a mode of transport (usually a hydrothermal fluid, but also can be a magma)

and a site of deposition or accumulation, where commodities become concentrated to enable economically viable extraction during a given period. A mineral system includes all geological and geodynamic factors, at all scales, that control the inception, evolution and preservation of ore deposits, *sensu lato*. Thus, the study of a mineral (ore) system(s) should comprise:

- Local studies of known deposits
- Tectonic controls
- Space-time distribution
- Physico-chemical processes
- Evolution of fluids, magmas and other energy sources
- Regional context

A mineral deposit can be classified:

- According to host rock(s) → e.g. sedimentary-hosted
- Preferred or perceived genetic model → e.g. orogenic
- Metal association → e.g. iron oxide-copper-gold
- Comparison with a prototype → e.g. Carlin-style

1.8 Additional Notes

Spelling is English Australia (Moore 2000), except in references where original spelling is maintained. Unless otherwise explained, the abbreviations and symbols used in this book (such as, t for tones, Mt for million tonnes, Bt for billion tones; element symbols, such as Cu for copper, Ag for silver and so forth; ca. for circa, wt% for weight percent, ppm for part per million, g/t grams per tonne, kbar for kilobar etc.) should be familiar to all geoscientists. Here I use dolerite instead of diabase, normally used in Chinese literature and Cenozoic instead of Tertiary. The reader must also note that the information and data listed in tables in some instances may not be accurate, although I have tried my best in attempting to keep the data presented as reliable as possible.

References

Acta Geologica Sinica Special Issue I (2000a) Papers on geology of China for the 31st IGC, Rio de Janeiro, 2000, 74(2)

Acta Geologica Sinica Special Issue II (2000b) Papers on geology of China for the 31st IGC, Rio de Janeiro, 2000, 74(3)

Acta Geologica Sinica Special Issue I (2004a) Papers on geology of China for the 32nd IGC, Florence, Italy, 2004, 78(1)

Acta Geologica Sinica Special Issue II (2004b) Papers on geology of China for the 32nd IGC, Florence, Italy, 2004, 78(2)

Brock RW (1928) China and its mineral resources. Econ Geol 23:209–213

Chen G (1988) Tectonics of China. Pergamon Press, Oxford, p 250
Chen YC, Tao WP (1995) Metallic and nonmetallic minerals in China. Episodes 18:17–20
Chen ZB, Zhang WX, Liu XH, Zhao FM, Du LT, Huang SJ, Chen ZY, Jiang YY (1996) Galaxy of research achievements of uranium geology of China, Volume Dedicated to the 30th International Geological Congress, Bureau of Geology, China National Nuclear Corporation, Beijing Research Institute of Uranium Geology, Open laboratory of Nuclear Energy Resource Research, Uranium geology Branch of China Nuclear Society, p 393
Cheng YQ (2000) Concise regional geology of China. Geological Publishing House, Beijing, p 430
China Geological Survey (2004) Geological map of the People's Republic of China—1:2,500,00 explanatory notes. SinoMaps Press, Beijing, p 198
Cooke DR, Hollings P, Walshe JL (2005) A special issue devoted to giant porphyry deposits. Econ Geol 100(5):801–818
Cox D, Singer DA (eds) (1986) Mineral deposits models. US Geol Surv Bull 1693, p 379
Editorial Committee of the mineral deposits of China (1990) Mineral deposits of China, vol 1. Geological Publishing House, Beijing, p 355
Editorial Committee of the mineral deposits of China (1992) Mineral deposits of China, vol 2. Geological Publishing House, Beijing, p 349
Editorial Committee of the mineral deposits of China (1995) Mineral deposits of China, vol 3. Geological Publishing House, Beijing, p 343
Editorial Committee of the mineral deposits of China (1996a) Mineral deposits of China, vol 4. Geological Publishing House, Beijing, p 288
Editorial Committee of the mineral deposits of China (1996b) Mineral deposits of China, vol 5. Geological Publishing House, Beijing, p 228
Feng CY, Zhang DQ (2004) Cobalt deposits of China: classification, distribution and major advances. Acta Geol Sin 78:352–357
Gernet J (1999) A history of Chinese civilization. Cambridge University Press, Cambridge, p 801
Harper D, Cambon M, Mayhew B, Gaskell K, Miller K, Huhti T, Org M (2002) China. Lonely Planet, Melbourne, p 974
Hendrix MS, Davis GA (eds) (2001) Palaeozoic and Mesozoic tectonic evolution of central Asia: from continental assembly to intracontinental deformation. Geol Soc Am Mem 194:447
Hou ZQ, Cook NJ (2009) Metallogenesis of the Tibetan collisional orogen: a review and introduction to the special issue. Ore Geol Rev 36:2–24
Hu RZ, Liu JM, Zhai MG (eds) (2011) Mineral resources science in China: a roadmap to 2050. Science Press, Springer, Beijing, p 93
JORC Code (2004) Australasia code for reporting of exploration results, mineral resources and ore reserves. Austral Inst Min Metall, Aust Inst Geosci, Min Council Aust, p 17
Lawler A (2009) Beyond the yellow river: how China became China. Science 325:930–943
Li YW (ed) (1992) Mineral resources of China. China Building Materials Industrial Press, China, p 390
Liu YK (1996) Geology and mineral resources. In: Proceedings of Ministry of Metallurgical Industry, International Academic Publishers, Beijing, p 297
Ma L, Ding XH, Fan BX (1996) Geological map of China. Geological Publishing House, Beijing.
Ma L (2002) Geological Atlas of China. Geological Publishing House, Beijing, p 348
Malpas J, Fletcher CJN, Ali JR, Aitchison JC (2004) Aspects of the tectonic evolution of China. Geological Society, London, Sp Publ 226, p 362
Mao JW, Xie GQ, Pirajno F, Ye HS, Wang YB, Li YF, Xiang JF, Zhao HJ (2010) Late Jurassic-Early Cretaceous granitoid magmatism in Eastern Qinling, central-eastern China: SHRIMP zircon U-Pb ages and tectonic implications. Aust J Earth Sci 57(1):51–78
Mao JW, Pirajno F, Cook N (eds) (2011) Mesozoic metallogeny in East China and corresponding geodynamic settings—an introduction to the special issue. Ore Geol Rev 43(1):1–7
Moore B (ed) (2000) The Australian Oxford dictionary. Oxford Univ Press, Oxford
Nie FJ (1997) An overview of the gold resources of China. Int Geol Rev 39:55–81
Ren JS, Jiang CF, Zhang ZK, Qin D (1987) Geotectonic evolution of China. Science Press, Beijing, Springer, Berlin, p 203

Sengör AMC, Natal'in BA (1996) Paleotectonics of Asia: fragments of synthesis. In: Yin A, Harrison TM (eds) The tectonic evolution of Asia. Cambridge University Press, Cambridge, pp 486–640
Sillitoe RH (1997) Characteristics and controls of the largest porphyry copper-gold and epithermal gold deposits in the circum-Pacific region. Aust J Earth Sci 44:373–388
Tang Z, Yan H, Jiao J, Li X (2006) Classification of magmatic sulphide desposits in China and mineralization of small intrusions. Acta Geol Sin 80:412–419
Trumbull RB, Morteani G, Li ZL, Bai HS (1992) Gold metallogeny in the Sino-Korean platform. Springer, Berlin, p 202
Tse PK (2009) The mineral industry of China. In: USGS 2008 Minerals Yearbook, China Advance Release, US Dept Int, p 9.1–9.26
Tse PK (2010) The mineral industry of China. In: USGS 2010 Minerals Yearbook, China Advance Release, US Dept Int, Revised Feb 2012, p 9.1–9.29
Wang YP, Mo XY (1995) Basic characteristics of active tectonics in China. Episodes 18:73–82
Wang H, Zhang SH, He GQ (2005) China and Mongolia. In: Selley RC, Cocks LRM, Plimer IR (eds) Encyclopedia of geology. Elsevier, Amsterdam, pp 345–358
Wilde SA, Cawood PA, Wang KY, Nemchin A, Zhao GC (2004) Determining Precambrian crustal evolution in China: a case-study from Wutaishan, Shanxi Province, demonstrating the application of precise SHRIMP U-Pb geochronology. Geological Society, London, Spec Publ 226, pp 5–25
Windley BF, Maruyama, S, Xiao WJ (2010) Delamination/thinning of subcontinental lithospheric mantle under eastern China: the role of water and multiple subduction. Am J Sci 310:1250–1293
Wu J (1993) Antimony vein deposits of China. Ore Geol Rev 8:213–232
Yang ZY, Cheng YQ, Wang HZ (1986) The geology of China. Clarendon Press, Oxford, p 303
Yin A, Harrison M (eds) (1996) The tectonic evolution of Asia. Cambridge University Press, Cambridge, p 666
Zhai Y, Deng J (1996) Outline of the mineral resources of China and their tectonic setting. Aust J Earth Sci 43:673–685
Zhai MG, Windley BF, Kusky TM, Meng QR (eds) (2007) Mesozoic sub-continental lihtospheric thinning under eastern Asia. Geological Society, London, Sp Publ 290, p 352
Zhang SX (2009) Geological formation names of China (1866–2000), vol 1 and 2. Springer, Dordrecht, p 1537
Zhou TH, Goldfarb RJ, Phillips GN (2002a) Tectonics and distribution of gold deposits in China—an overview. Miner Depos 37:249–282
Zhou MF, Yang ZX, Song XY, Keays RR, Lesher CM (2002b) Magmatic Ni-Cu-(PGE) sulphide deposits in China. In: Cabri LJ (ed) The geology, geochemistry, mineralogy and mineral beneficiation of platinum-group elements, Volume Can Inst Min Metall Pet, Montreal Special Volume 54. pp 619–636
Zhou MF, Yang ZX, Song XY, Keays RR, Lesher CM (2002c) Magmatic Ni-Cu-PGE sulphide deposits in China. Chem Geol 209:233–257
Zhu X (ed) (2007) Mineral facts of China. Elsevier, Amsterdam, p 776

Chapter 2
China's Tectonic Framework in the Global Context

Abstract The tectonic framework of China within the wider Asian context, together with tectono-thermal events that have formed the various mineral systems are presented in this chapter. The geological configuration of present-day China is characterised by terranes and provinces that comprise the North China Craton and Tarim Craton amalgamated during the Archaean and Palaeoproterozoic between 3.2 and 1.8 Ga. The east-west aligned (present day coordinates) North China Craton and Tarim cratonic block are framed to the north by orogens of the Central Asian Orogenic Belt (CAOB), which in China include the Tianshan and Altay in the northwest and the Hinggan fold belt to the east. The CAOB terranes are the result of accretionary events, which attained their main configuration following the closure of oceanic seaways, such as the Mongol-Okhotsk ocean. In east-central and southern China are the Yangtze Craton and Cathaysia Block, bordered to the west and southwest by the Himalayan fold belts of the Tibetan region. These terranes were largely affected by a series of tectono-thermal events and strike-slip structures, in the Mesozoic and continuing to present day. A figure showing an overview of the distribution of Phaneorozoic mineral systems associated to these events is presented in this chapter. Large and small rift basins, containing important hydrocarbon resources and sandstone-hosted U deposits, are superimposed on the older terranes.

2.1 Introduction

Mineral systems are the result of metallogenic processes associated with the geodynamic evolution of tectonic plates, and their eventual amalgamation. An understanding of the complexities of the geology of China is continuously improving, while at the same time providing new challenges. China occupies a large portion of the southeastern and eastern Asian continent and the study of its tectonic history needs to be considered within the wider Asian continent tectonic framework. The principal geotectonic provinces of China comprise the North China Craton (part of the larger Sino-Korean craton), the Tarim Craton, the Yangtze Craton, the Cathaysia Block (Yangtze and Cathaysia together form the South China Block), the Altay-Tianshan-Hinggan orogens (part of the great Central Asian Orogenic Belt, CAOB, also known as the Altaids), the Kunlung-Qinling fold belt (or Central China Orogen), the South China Fold Belt, the Himalayan, Gandise and Qingai-Yunnan fold belts. In addition, volcano-sedimentary and sedimentary basins occupy large areas across China and are

F. Pirajno, *The Geology and Tectonic Settings of China's Mineral Deposits,*
DOI 10.1007/978-94-007-4444-8_2,

superimposed on existing tectonic units. These tectonic elements represent a complex geological history spanning more than 3,000 million years. Important mineral deposits in these provinces include gold, silver, copper, molybdenum, tin, antimony, nickel, platinum group elements, iron, uranium, lead and zinc. Ore forming processes for these deposits relate to the tectonic evolution and associated magmatic events of the region. The geodynamic evolution of China was subdivided by Wang et al. (2005) in five stages: (1) formation of continental nuclei (ca. 2.8–2.7 Ga); (2) formation of protoplatforms between ca. 1.9 and 1.8 Ga; (3) platform formation (ca. 0.85–0.8 Ga); (4) amalgamation of tectonic units in the assembly of Laurasia and Pangea supercontinents; (5) intercontinental development (tectono-thermal events, ca. 210 Ma to present). A modified tectonic map of Asia (Wang et al. 2005) is shown in Fig. 2.1a. This figure shows the present-day position of the main cratonic blocks, Siberian, Tarim-Sino-Korean, Yangtze and India, fragments of ancient amalgamated microcontinents, such as those that border the Siberian Craton, Kazakhstan, Qaidam, Qiantang, Gangdise and Cathaysia. These units are all surrounded by Phanerozoic orogenic belts. To tectonic complexity of the Asia region is further highlighted by different interpretations of the various tectono-orogenic collages, as shown in Fig. 2.1b, modified and somewhat simplified from Şengör and Natal'in (1996).

In a more schematic representative view, the principal tectonic domains of mainland China and surrounding orogenic belts are shown in Fig. 2.2a, whereas a present-day generalised tectonic map of southeastern Asia is shown in Fig. 2.2b. The purpose of these figures is to show the reader, who may be unfamiliar with the region, in a diagrammatic fashion the tectonic architecture of that part of the Asian continent, which includes mainland China. Figure 2.3a is yet another schematic illustration of China's tectonic units, modified from Ma et al. (1996), whereas Fig. 2.3b is more detailed and shows tectonic subdivisions, bearing in mind that commonly different names are used for the same tectonic unit, by different authors; for example in the original Fig. 2.3b, Cathaysia is shown as Huanan Orogen (see Chap. 4). It is important to note that continental fragments rifted from Gondwana, moved northward to become accreted with the Asian continental margin, before the main India-Asia collision event, about 66–50 Myrs ago. The rifting of continental fragments from Gondwana, resulted in the opening of oceanic arms or seaways, between a given fragment and Gondwana, at the same time oceanic corridors north of these continental fragments were closed by subduction. One of these oceanic arms is the Palaeo-Tethys Ocean. These oceanic closures and subduction systems ended up as major suture zones bounding the remnants of the rifted continental fragments (Fig. 2.2a, b).

The schematic cartoon of Fig. 2.2a, shows the tectonic units and the sequence of geodynamic events that led to the amalgamation of the units between the Late Palaeozoic, Early Jurassic ca. 180 Ma, to Cretaceous and the Cenozoic. This sequence of events is as follows (Chen et al. 2007): Opening, spreading and northward subduction of the Palaeo-Tethys Ocean (Late Palaeozoic to Triassic) resulting in development of the Qilianshan-North Qinling-Dabie orogens (Central China Orogen) and breakup of the Southern Qinling and Aba blocks from the Yangtze Craton. The Paleo-Tethys sea closed when the Qiangtang-Indochina and Huanan (South China

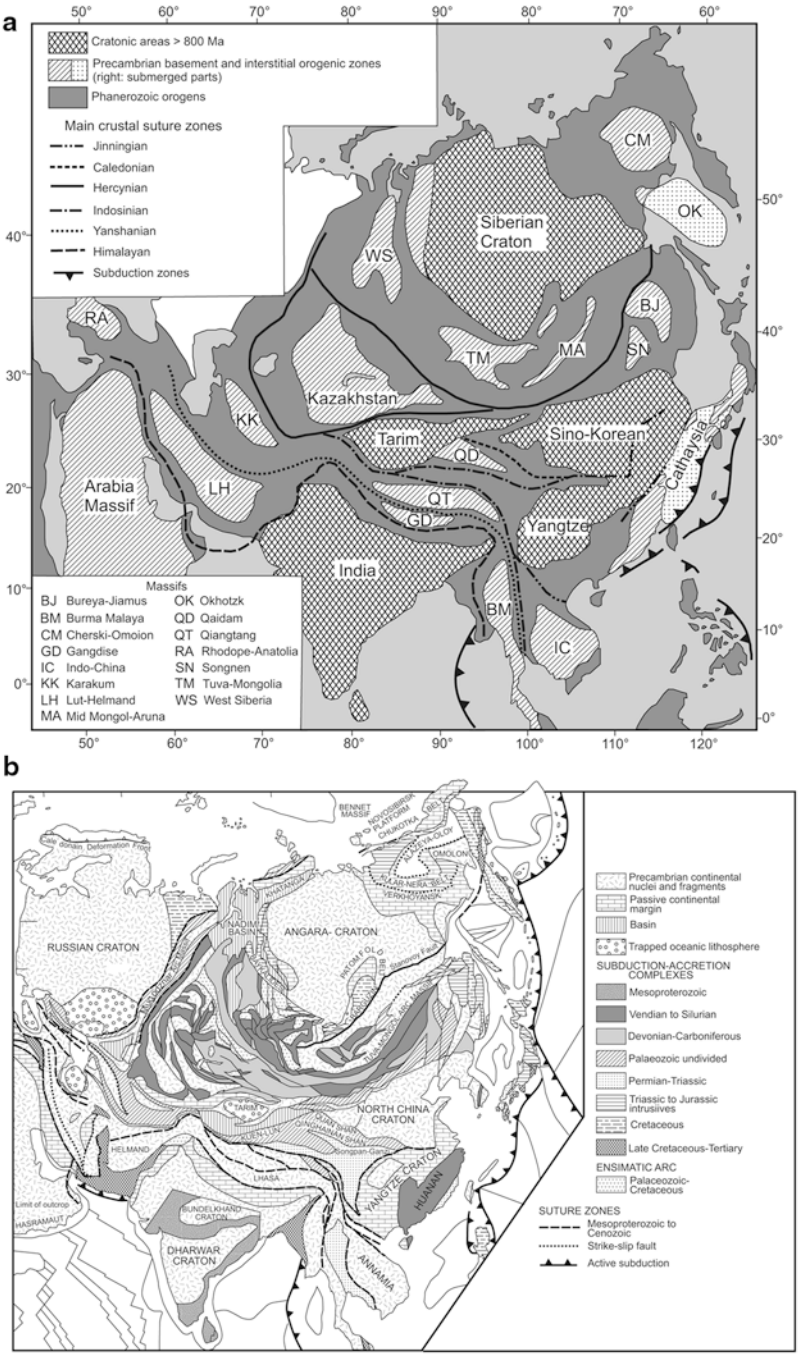

Fig. 2.1 **a** Simplified tectonic map of Asia (modified from Wang et al. 2005); **b** Tectonic map of Asia (according to Şengör and Natal'in 1996), note that Kuen-Lun corresponds to Kunlun and Quan Shan and Qinghainanshan correspond to the Qaidam terranes (Chap. 6)

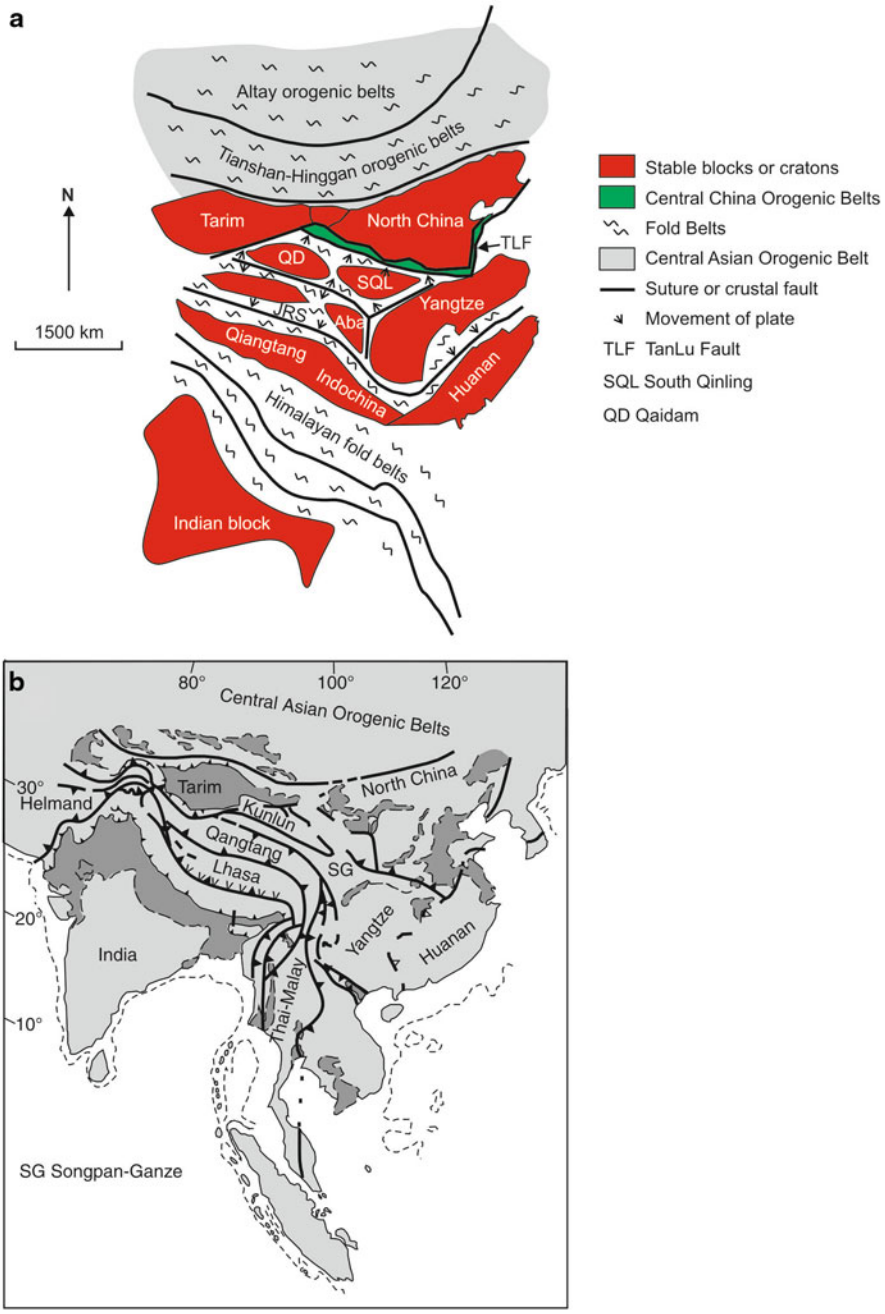

Fig. 2.2 **a** Sketch showing the stable and/or cratonic blocks of China and intervening accreted terranes, now forming fold or orogenic belts; **b** shows major southeast Asian fragments accreted during the Late Palaeozoic, Mesozoic and Cenozoic. Sutures between the Qangtanga and Songpan-Ganze represent the closure of the Palaeotethys in the Mesozoic; sutures bordering the India block (Indus-Tsango) to the north represent the closure of the Neo-Tethys (India-Asia collision); sutures to the north of the Tarim-North China cratonic block represent Palaeozoic oceanic closures associated with the geodynamic evolution of the Central Asian Orogenic Belt. Details in text for both **a** and **b**

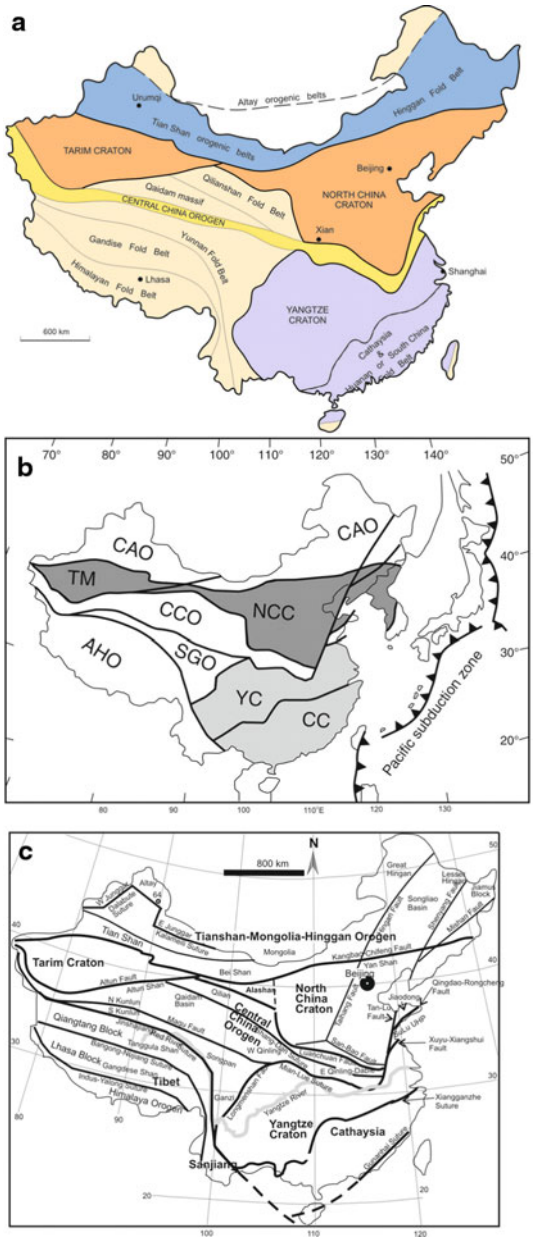

Fig. 2.3 Three versions of the main tectonic units of China; **a** schematic (modified from Ma et al. 1996); **b** according to Zhai et al. (2010), CAO, Central Asia orogen, TM, Tarim craton; NCC, North China craton; CCO, Central China orogen; SGO, Songpan–Ganze orogen; AHO, Alpine–Himalayan orogen; YC, Yangtze craton; CC, Cathaysia craton; **c** more detailed and showing major faults and subdivisions of the main tectonic domains (modified from Chen et al. 2007)

Fold Belt) blocks collided northwards with the Kunlun Terrane, the Aba Block and the Yangtze Craton at the end of Triassic, resulting in collision orogenies in central, southern and southeastern China areas. The development of the Huanan Orogen (South China Fold Belt), resulting in shortening and sinistral strike-slip in East China;

the northeastwards subduction of the Bangong-Nujiang Ocean (Meso-Tethyan Sea) produced back-arc extension. Northwestward subduction of the Palaeo-Pacific plate resulted in the inception of the Nipponides orogeny and subsequent orogenic overprinting of the Tethysides in southeastern China. The Lhasa Block collided with Qiangtang-Indochina Block, the Meso-Tethyan Sea closed, and back-arc extension ended in the whole of China. During 66–50 Ma, the India Craton and the Eurasia Continent sutured, resulting in a progressive eastward closure of the Neo-Tethyan Sea (Indus-Yalong Ocean) and clockwise rotation and strike-slip escape of the Lhasa and Qiangtang blocks. India is underthrust beneath the Eurasia Continent, resulting in crustal shortening and uplift of the Tibet-Sanjiang orogenic area, and causing extensive far-field uplifts of the western and northwestern regions of China (e.g. Tianshan, Kunlun).

However, it must be pointed out that the recognition and definition of the accreted continental fragments, subduction-related systems and remnants of oceanic crust (ophiolites) caught in between, remains an arduous and on-going task. Furthermore, the stable cratonic blocks (Tarim-North China, Yangtze cratons), themselves show rifting and accretion processes that occurred in the Precambrian (e.g. the Trans North China orogen that separates an eastern block from a western block of the North China Craton, as discussed in Chap. 3). North of the Tarim-North China cratonic areas is the above-mentioned CAOB (discussed in Chap. 6), itself a collage of subduction-related terranes, continental fragments and sutures representing fragments of oceanic crust, all accreted at various stages in the Phanerozoic on cratonic land masses, such as the Siberian and East European cratons (Fig. 2.4).

In the pages ahead, brief descriptions of main tectonic units or domains, as well as volcano-sedimentary and sedimentary basins are provided, but individual units or domains are taken up again in more detail in the relevant chapters, in which their link with metallogenesis is discussed.

2.2 Outline of the Tectonic Framework and Geodynamic Evolution of China and Its Mineral Systems

Wang and Mo (1995), Wang et al. (2005) and more recently Wan (2010) reviewed the tectonic evolution of China and a simplified map showing the principal tectonic domains of China with superimposed basins and igneous events is shown in Fig. 2.5. A special issue of Gondwana Research was devoted to the tectonic evolution of China, with a collection of papers directed at specific topics in the North China Craton, South China Block and the CAOB (Zhai et al. 2007). Pan et al. (2009) reviewed the tectonic subdivision of China. The nomenclature and the boundaries between tectonic domains are far from being well established. Different names are commonly used for the same fold belt or orogenic zone, by different authors at different times and a coherent consensus is yet to be reached. For example, the Tianshan-Hinggan orogenic belt is also called Tianshan-Inner Mongolia-Great Hinggan fold belt, which in its eastern parts is also known as Inner Mongolia-Daxinganling Orogenic Belt (Miao

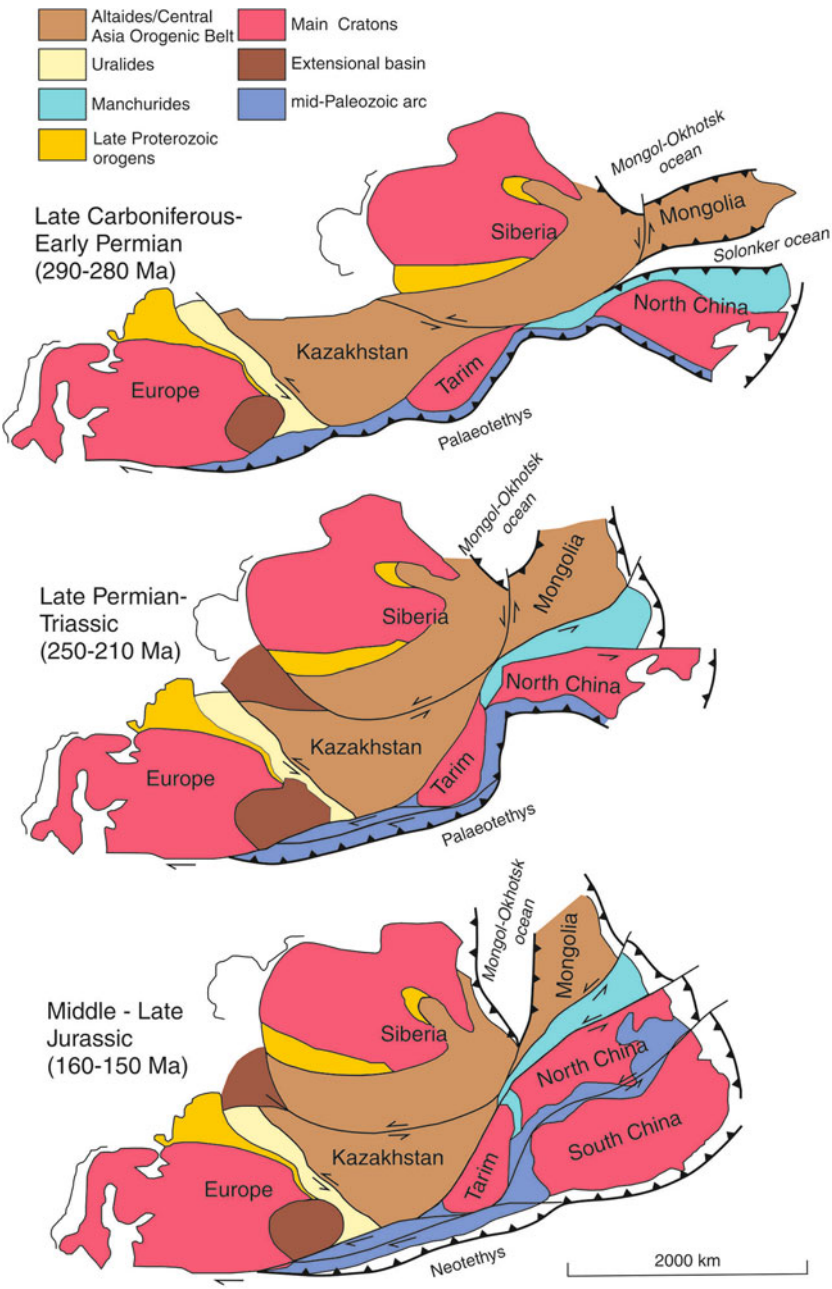

Fig. 2.4 Late Carboniferous-Early Permian, Late Permian-Triassic and Mid-Late Jurassic palaeotectonic reconstruction of Eurasia, sinistral transpressions between the converging Siberia and Eastern Europe cratonic blocks. (Modified from Metelkin et al. 2010; and references therein)

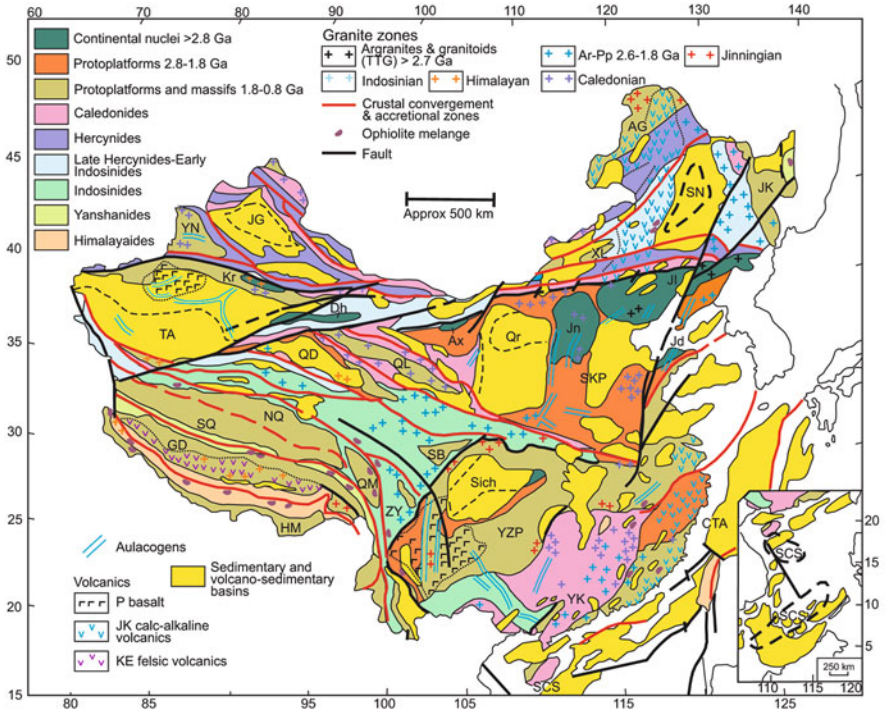

Fig. 2.5 Simplified geology map of China (modified from Wang et al. 2005); (*alternative names in parenthesis)*; *AG* Arguna, Sich Sichuan basin, *CTA* Cathaysia, *Dh* Dunhuang, *GD* Gandise, *HM* Himalayan belt, *QD* Qaidam, *JG* Junggar, *NQ* North Qiangtang, *Or* Ordos basin, *QM* Qamdo massif, *SKP* Sino-Korean platform (*Sino-Korean cratonic block*), *SN* Songnen (*Songliao basin*), *JK* Jamus-Xingai (*Hinggan*), *TA* Tarim basin (*Tarim Block*), *Kr* Kuruktagh nucleus (*Tianshan belt*), *SB* Songpan-Bikou massif, *SCS* South China Sea massif, *SQ* South Qiangtan, *YZP* Yangtze platform, *ZY* Zhongza-Yidua massif, *YK* Yangtze craton, *YN* Yining massif (*Yili Block*); also note that Yanshanian granites are not shown to avoid cluttering the figure

et al. 2007); the South China Fold Belt is also the Huanan Fold Belt. The names of the various tectonic domains or units used in this work are therefore "somewhat flexible" and by no means part of an established nomenclature, as will become apparent in the chapters that follow. There are a number of English-language books and publications with overviews of the geology and tectonic evolution of China, cited in Chap. 1, to which here I add Zhang et al. (1984). However, some of these works are largely superseded, as a wealth of geochronological data is continuously published in both Chinese and English geoscience literature. A more recent and authoritative collection of papers can be found in Malpas et al. (2004). More recently, a special issue of Gondwana Research (Zhao et al. 2012) deals with aspects of plate tectonics of Asia in general, with particular emphasis the geodynamic evolution of the Tibetan Plateau, the North and South China blocks, the Central Asian Orogenic Belt (CAOB).

As mentioned above, the key tectonic elements of domains of China are the Tarim Craton, the North China Craton (part of the larger Sino-Korean cratonic ensemble) and the Yangtze Craton (part of the greater South China Block). On the northern margin of the Tarim-North China cratonic block are the Tianshan-Hinggan orogenic belts and the Altay orogenic fold belts, both part of the greater Central Asian Orogenic Belt (CAOB; Jahn 2004). On the southern margin are fold belts of the Central China Orogen, a complex collage of Palaeozoic fold belts, which mark various collision sutures with tectonic terranes to the south. The Qinling Orogen (Qinling-Dabie), in the eastern part of the Central China Orogen, marks the tectonic boundary between the North China Craton and the Yangtze Craton. The latter is in tectonic contact with the South China Fold Belt to the southeast and the Yunnan Fold Belt along its western margin. The South China Fold Belt together with the Yangtze Craton are commonly referred to as South China Block. The Yunnan belt, together with the Gandise and Himalayan fold belts are part of the larger Tethysides, as defined by Şengör and Natal'in (1996).

The tectonic evolution of China, as reviewed by Zhou et al. (2002), is summarised here (see also Table 1.2 in Chap. 1). The North China, Tarim and Yangtze cratons experienced three Archaean orogenic events: 3.2 Ga Qianxian, 2.8 Ga Fuping and the 2.5 Ga Wutai orogenies, which resulted in extensive magmatism and widespread metamorphism from greenschist to granulite facies. At about 1.8 Ga the Lüliang orogenic movements occurred mainly along cratonic margins with folding and uplifting. At 1.78 Ga rifting affected the central parts of the North China Craton, resulting in extensive magmatism and the formation of a large igneous province (Xion'ger igneous event, discussed in Chap. 7). According to Wang and Mo (1995), the three cratons were possibly geographically close during the assembly of the Rodinia supercontinent by about 1.0 Ga. The 1.0–0.85 Ga Jinning orogeny, correlates with the Grenvillian event and involved the closure of an oceanic arm, resulting in the formation of the Jiangnan orogenic belt (or suture), between the North China and Yangtze cratons (Chap. 4). At about the same time, deformation events affected the margins of the Tarim Craton, which was amalgamated with the Qaidam block to the southeast. These events are exhibited by the Kunlun (also spelt Qunlun) orogenic belt, which may be considered as the western extension of the Qinling-Dabie orogenic belt, together forming the Central China Orogen (Figs. 2.2 and 2.3). During the Jinning orogeny the Yangtze Craton collided with the Cathaysia Block, forming the South China Block. The breakup of Rodinia led to the Sinian rifting events at about 850–820 Ma, perhaps induced by the rise of mantle plumes and associated extensive magmatic activity (Chap. 7), and linked to the breakup of the Rodinia supercontinent (Li et al. 2008).

The Caledonian orogeny spans the period from 600 to 400 Ma, when the China cratonic blocks may have been close to the Australian cratons. In the Mid-Ordovician to Late Silurian there was subduction of an oceanic plate from the north. At the same time, an oceanic arm separating the North China Craton from the Yangtze Craton, was being subducted northward under the southern margin of the North China Craton, resulting in the formation of the Qinling-Dabie orogen, referred to above. These subduction events led to uplift of the North China Craton. To the north

and northwest (present day coordinates) subduction was occurring along the margins of the Palaeo-Tethys Ocean, resulting in magmatic arcs and island arcs that were later to amalgamate to form the Central Asian Orogenic Belt (CAOB), within which are the Tianshan and Altay orogenic belts. In southern China, the Yangtze Craton and Cathaysia were rifted apart during Sinian times, collided again to reform the South China Block.

The period from about 405 to 270 Ma (Variscan) was characterised by collision of Tarim Craton to the Yili Block and the Junggar Block, while at the same time the South Tianshan orogenic belt was formed. Back arc oceans that existed between the Yili and Junggar blocks, closed and formed the North Tianshan orogenic belt, and the Tarim, Yili and Junggar were amalgamated. These collision events migrated eastward, with the amalgamation of the Tarim and North China Craton, and the collision of the latter with the Siberia-Mongolia plate, which formed the wider Tianshan-Hinggan fold belt (Chap. 5 and 6).

The Indosinian event occurred between 270 and 210 Ma (refer to Tables 1.2 and 1.4 in Chap. 1), with the Yangtze Craton moving northward and the eruption of flood basalts along its southwestern margin, resulting in the emplacement of the 260 Ma Emeishan large igneous province (Chap. 7). The collision between the North China Craton and the South China Block was diachronous, with the Jiadong province forming first, followed in the Late Triassic by deformation along the Qinling-Dabie orogenic belt and the development of the Tanlu Fault system, along the eastern margin of China. The Qinling-Dabie belt represents the final suture between the North China Craton and the South China Block.

The Indosinian continued with the great Yanshanian tectono-thermal event from the Jurassic onward to about 90 Ma. The Yanshanian was a complex large scale phenomenon associated with collision and extensional tectonics on the northern and southern margins of the North China Craton, asthenospheric upwellings and the oblique subduction of the Izanagi-Pacific plate under the eastern margin of Asia (Mao et al. 2010 and references therein). Eastern China was subjected to intense magmatic activity, which can be subdivided into three main periods (Yi et al. 1992): (1) Late Jurassic-Early Cretaceous; (2) Mid-Late Cretaceous; and (3) Cenozoic to present-day. The Yanshanian event resulted in extensive magmatic belts, rifting,metamorphic core complexes, basin formation and the development of a wide range of mineral systems.

Zhou et al. (2002) examined the distribution of Au deposits in China within the framework of the main tectonic events that occurred between the Variscan (Devonian) and the Jurassic-Cretaceous periods. These authors noted that most Au deposits, and for that matter most of hydrothermal systems, are sited along the margins of cratonic and major suture zones that border tectonic terrane units or blocks (see Figs. 2.2 and 2.3). On the basis of this observation, Zhou et al. (2002) recognized the following metallogenic provinces: (1) Jiadong (east Shandong); (2) Northern China; (3) Qinling and Xiao Qinling provinces, situated along the southern margin of the North China Craton and the Qinling Orogen; (4) Yangtze River Valley province along the northeastern margin of the Yangtze Craton, where most of the mineralisation is associated with skarns and porphyry-skarn systems; (5) Southeast

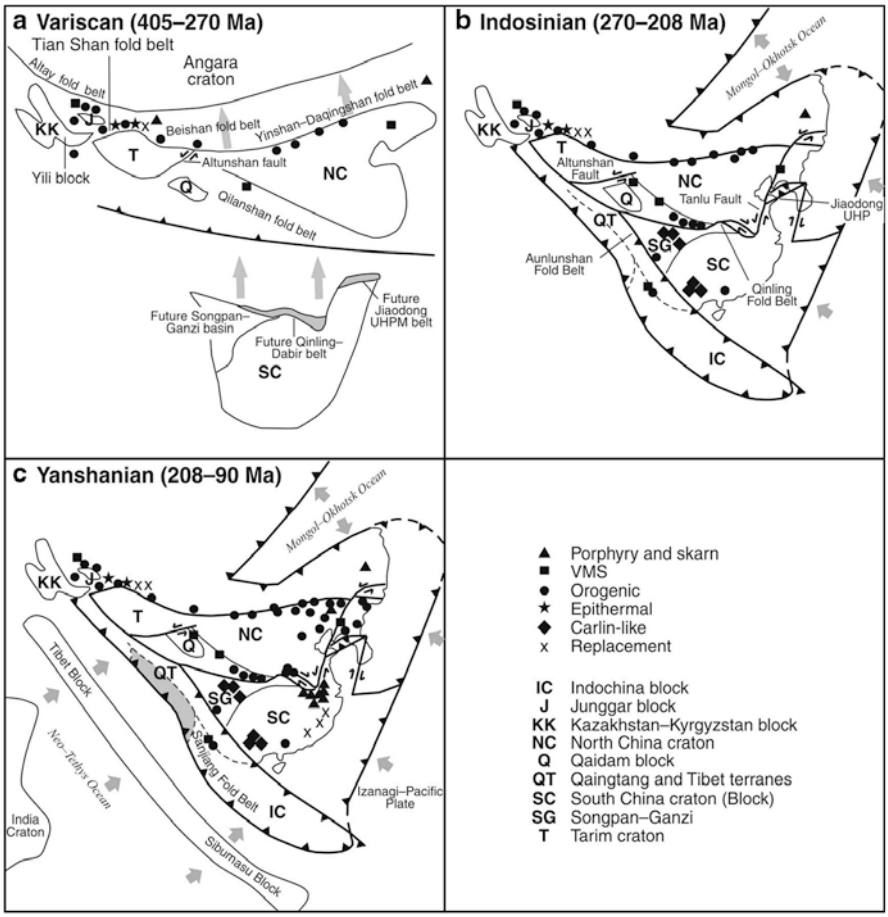

Fig. 2.6 Distribution of ore systems in China and their relationship to the geodynamic evolution of the China terranes between the Variscan (405 Ma) and the Yanshanian (208–90 Ma). (Modified after Zhou et al. 2002)

China, where lode porphyry and epithermal systems are present; (6) Dian-Gui-Qian province, along the southwestern margin of the Yangtze Craton, where both Carlin style and epithermal systems are found; (7) Chuan-Shaan-Gan province, along the northwestern margin of the Yangtze Craton; (8) the Altay and Tianshan orogenic belts, with epithermal, porphyry and volcanogenic massive sulphide (VMS) ore systems.

The distribution of these Phanerozoic mineral systems in relation to the main tectonic events is shown in Fig. 2.6.

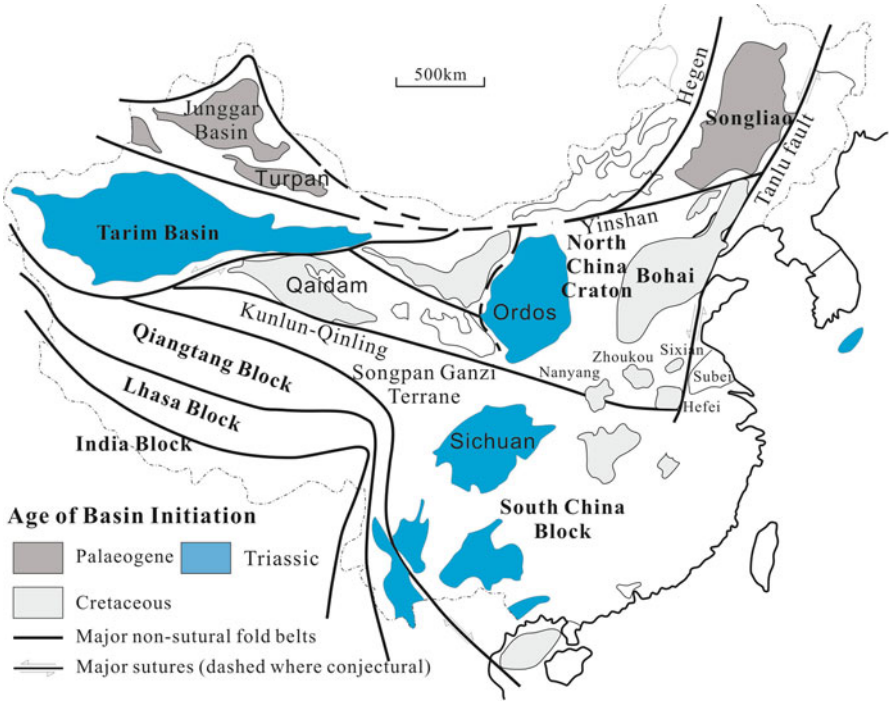

Fig. 2.7 Basin structures in China. (Modified after Watson et al. 1987; Menzies and Xu 1998)

2.3 Volcano-sedimentary and Sedimentary Basins

The widespread Yanshanian tectono-thermal event was responsible for a wide range of geodynamic, magmatic and ore-forming processes that affected eastern and south-eastern China (Chap. 7). The inception of grabens, rift basins and diffuse volcanism, as well the formation of coal seams and hydrocarbons, are linked with these processes and are discussed in Chap. 8. In the northwest, southwest and central regions of China large basins were formed as a result of tectonic processes unrelated to the Yanshanian movements. The best known, for their hydrocarbon resources, are the Junggar, Turpan and Tarim basins. They are also discussed in Chap. 8. A schematic distribution of China's major basins is shown in Fig. 2.7.

Ma and Wu (1987), Gilder et al. (1991), Tian et al. (1992), Ren and Xiao (2002) and Ren et al. (2002) discussed the formation of rift structures and associated basins in mainland China. Gilder et al. (1991) and Yi et al. (1992) provided an overview of the temporal and spatial distribution of rift structures in mainland China. Ren et al. (2002) gave an excellent account of the evolution of the Mesozoic to Cenozoic rift systems in eastern China. Most rift basins of eastern China contain two lithological successions: syn-rift and post-rift.

Many large and small Mesozoic and Cenozoic rift basins cover parts of the North China Craton and beyond. These rift basins were formed between the Jurassic and Cretaceous and from the Cretaceous to Quaternary. The north-northeast trending Shanxi graben system in the centre of the North China Craton (Fig. 2.6), the Hebuai basin, in the south at the boundary with the Yangtze Craton, the Bohai and Songliao basins are the prime examples. There is general agreement that the formation of these basins is related to extensional stress fields associated with lithospheric thinning and asthenospheric upwelling, detailed in Chap. 7. Some researchers contend that lithospheric thinning and extensional tectonics are related to subduction processes (Kula plate and Izanagi-Pacific plate) beneath the eastern margin of Asia (e.g. Griffin et al. 1998). Geophysical data show that the thinner lithosphere corresponds to the deepest Cenozoic basins, such as the Songliao Basin. The Shanxi and the Yinchuang-Hetao graben systems surrounding the Ordos block in the western North China Craton were initiated in the Cenozoic with the Shanxi grabens being the youngest at ca. 6 Ma, its opening occurring with northward propagation (Xu and Ma 1992; Kusky et al. 2007).

Watson et al. (1987) classified the basins in China into two types: flexural basins and rift basins. The former are formed by subsidence due to downwarping of the lithosphere in response to compressional tectonics. Rift basins are formed as a result of extensional thinning of the lithosphere, followed by thermal subsidence. Rift basins of eastern China are generally of the western USA Basin-and-Range style and are associated with core complexes (Li et al. 2007; Cope and Graham 2007). Yanshanian core complexes are especially common in the eastern Liaoning peninsula and are described by Lin et al. (2007). Economically important for hydrocarbon resources and sandstone-hosted U deposits are the Junggar and Tarim basins in Xinjiang Province, the Qaidam Basin to the southeast of Tarim, Ordos and Sichuan basins in central China and the Songliao and Bohai basins in eastern China (Fig. 2.6).

2.4 Concluding Remarks

The main scope of this chapter is to provide a brief introduction of the main tectonic elements of China within the Asian continent geodynamic framework. The tectonic elements considered are shown in Figs. 2.1–2.7, which illustrate the positions of Central Asian Orogenic Belt (CAOB), Tarim craton, North China Craton, Central China (Qinling) Orogen; Songpan–Ganze Orogen; Alpine-Himalayan Orogen, Yangtze and Cathaysia cratons (South China Block), according to various authors. An overview of the metallogenesis and ditribution of key hydrothermal mineral systems that characterise the Variscan (405–270 Ma), the Indosinian (270–208 Ma) and the Yanshanian (208–90 Ma) orogenic and magmatic events is shown in Fig. 2.6. Volcano-sedimentary and sedimentary basins occupy large areas covering the older tectonic units, are important elements for hydrocarbon and uranium mineral resources.

References

Chen YJ, Chen HY, Zaw K, Pirajno F, Zhang ZJ (2007) Geodynamic settings and tectonic model of skarn gold deposits in China: an overview. Ore Geol Rev 31:139–169

Cope TD, Graham SA (2007) Upper-crustal response to Mesozoic tectonism in Western Liaoning, North China, and implications for lithospheric delamination. Geological Society, London, Sp Publ 280, pp 201–222

Gilder SA, Keller GR, Luo M, Goodell PC (1991) Timing and spatial distribution of rifting in China. Tectonophysics 197:225–243

Griffin WL, Andi Z, O'Reilly SY, Ryan CG (1998) Phanerozoic evolution of the lithosphere beneath the Sino-Korean Craton. In: Flower M, Chung SL, Lo CH, Lee T (eds) Mantle dynamics and plate interactions in East Asia, Geodynamic Ser 27, American Geophysical Union, pp 107–126

Jahn BM (2004) The Central Asian Orogenic Belt and growth of the continental crust in the Phanerozoic. Geological Society, London, Spec Publ 226, pp 73–100

Kusky TM, Windley BF, Zhai MG (2007) Tectonic evolution of the North China Block: from orogen to craton to orogen. Geological Society, London, Sp Publ 280, pp 1–34

Li Z, Li Y, Zheng JP, Han D (2007) Late Mesozoic tectonic transition of the eastern North China Craton: evidence from basin-fill record. Geological Society, London, Sp Publ 280, pp 239–266

Li ZX, Bogdanova SV, Collins AS, Davidson A, De Waele B, Ernst RE, Fitzsimons ICW, Fuck RA, Gladkochub DP, Jacobs J, Karlstrom KE, Lu S, Natapov LM, Pease V, Pisarevsky SA, Thrane K, Vernikovsky V (2008) Assembly, configuration, and break-up history of Rodinia: a synthesis. Precambrian Res 160:179–210

Lin W, Faure M, Monie P, Wang QC (2007) Polyphase Mesozoic tectonics in the eastern part of the North China Block: insights from the eastern Liaoning peninsula massif (NE China). Geological Society, London, Sp Publ 280, pp 53–170

Ma XY, Wu DN (1987) Cenozoic extensional tectonics in China. Tectonophysics 133:243–255

Ma LF, Ding XZ, Fan BX (1996) Geological map of China, 1:12,000,000. Geological Publishing House, Beijing

Malpas J, Fletcher CJN, Ali JR, Aitchison JC (2004) Aspects of the tectonic evolution of China. Geological Society, London, Spec Publ 226, p 362

Mao JW, Xie GQ, Pirajno F, Ye HS, Wang YB, Li YF, Xiang JF, Zhao HJ (2010) Late Jurassic-Early Creatceous granitoid magmatism in Eastern Qinling, central-eastern China: SHRIMP zircon U-Pb ages and tectonic implications. Aust J Earth Sci 57:51–78

Menzies MA, Xu YG (1998) Geodynamics of the North China Craton. In: Flower MEL, Chung SL, Lo CH, Lee TY (eds) Mantle dynamics and plate interactions in East Asia, Geodynamic Ser 27, American Geophysical Union, pp 155–165

Miao L, Zhang F, Fan WM, Liu D (2007) Phanerozoic evolution of the inner Mongolia-Daxinganling orogenic belt in North China. Constraints from geochronology of ophiolites and associated formations. Geological Society, London, Spec Publ 280, pp 223–237

Pan GT, Xiao QH, Lu SN, Deng JF, Zhang KX, Zhang ZY, Wang FG, Xing GF, Feng YF (2009) Subdivision of tectonic units in China. Geol China 36:1–28 (in Chinese with English abstract)

Ren JS, Xiao LW (2002) Tectonic settings of petroliferous basins in continental China. Episodes 25:227–235

Ren JY, Tamaki K, Li ST, Zhang JX (2002) Late Mesozoic and Cenozoic rifting and its dynamic setting in eastern China and adjacent areas. Tectonophysics 344:175–205

Şengör AMC, Natal'in B (1996) Paleotectonics of Asia: fragments of a synthesis. In: Yin A, Harrison M (eds) The tectonic evolution of Asia. Cambridge University Press, Cambridge, pp 486–640

Tian ZY, Han P, Xu KD (1992) The Mesozoic-Cenozoic East China rift system. Tectonophysics 208:341–363

Wan TF (2010) The tectonics of China. Springer, Heidelberg, High Education Press, Beijing, pp 501

Wang YP, Mo XY (1995) Basic characteristics of active tectonics in China. Episodes 18:73–82

Wang HS, Zhang SH, He GQ (2005) China and Mongolia. In: Selley RC, Cocks LRM, Plimer IR (eds) Encyclopedia of geology. Elsevier, Amsterdam, pp 345–358

Watson MP, Hayward AB, Parkinson DN, Zhang ZM (1987) Plate tectonic history, basin development and petroleum source rock deposition onshore China. Mar Pet Geol 4:205–225

Xu XW, Ma XY (1992) Geodynamics of the Shanxi rift system, China. Tectonophysics 208:325–340

Yi TZ, Ping H, Xu KD (1992) The Mesozoic-Cenozoic east China rift system. Tectonophysics 208:341–363

Zhai MG, Xiao WJ, Kusky T, Santosh M (2007) Tectonic evolution of China and adjacent crustal fragments. Gondwana Res 12:1–3

Zhang ZH, Liou JG, Coleman RG (1984) An outline of the plate tectonics of China. Geol Soc Am Bull 95:295–312

Zhao XX, Xiao WJ, Hebert R, Wang CS (2012) Plate tectonics of Asia: geological and geophysical constraints. Gondwana Res. doi:10.1016/j/gr.2012.01.002

Zhou TH, Goldfarb RJ, Phillips GN (2002) Tectonics and distribution of gold deposits in China—an overview. Miner Depos 37:249–282

Chapter 3
North China and Tarim Cratonic Blocks

Abstract In this chapter the Archaean and Palaeoproteroic geology and geodynamic evolution of the North China Craton and the Tarim Craton are described, from published literature. The North China Craton consists of a Western Block and an Eastern Block, separated by the north-trending Trans-North China Orogen, which developed through a series of subduction-related systems that were eventually accreted onto the Western and Eastern Blocks, resulting in the final amalgamation of the North China Craton at about 1.8 Ga. There are still conflicting ideas regarding the geological history of the Trans-North China Orogen. Dyke swarms, anorogenic magmatism and rifting processes are also recorded from about 2.5 Ga. Mineral systems that occur in the North China Craton can be divided into those that formed during the geological history of the Craton, such as podiform chromite and Fe-Ti-V deposits in mafic-ultramafic rocks and massif-type anorthosite intrusions, banded iron-formation (BIF) hosted Fe deposits and volcanogenic massive sulphide deposits (VMS). BIF include both Algoma-type and Superior type. Various types of mineral deposits were formed during Palaeoproterozoic rifting processes and igneous activity that affected the Craton. One of these is the giant Bayan Obo rare earth deposit in Inner Mongolia, developed in a Palaeoproterozoic rift, but through a series of multistage episodes involving carbonatite magmas. To the same period also belong unusual and somewhat enigmatis massive sulphide deposits, considered as transitional submarine to Irish-type. A wide range of hydrothermal deposits, including the Jiaodong lode Au deposits, porphyry and porphyry-skarn were formed during phases of collision tectonic between the North China Craton and the Mongolia-Siberian plate in the Permian-Triassic and during the widespread Mesozoic Yanshanian tectonothermal event. The Yanshanian event is probably the most productive in terms of mineral systems and is considered by most authors to be related to delamination of the lithospheric mantle, resulting in magmatic underplating, crustal melting and the development of A- and I-type granitic magmas and volcanism along the east Asian margin in rift structures. Giant and world-class mineral systems, all formed during the Yanshanian in eastern China.

The Tarim Craton, commonly called Block or Basin, regardless of whether the topic in question is basement or cover rocks, is poorly known, mainly due to its extensive cover of Phanerozoic sedimentary and volcanic successions. The Tarim Craton was amalgamated with the North China and Yangtze Cratons during the Phanerozoic, probably following the the assembly of Pangea and the closure of the Palaeo-Tethys Ocean. Most of the cratonic lithostratigraphy is known from deep

F. Pirajno, *The Geology and Tectonic Settings of China's Mineral Deposits,*
DOI 10.1007/978-94-007-4444-8_3,

drilling and from exposures along its margins. Mineralisation that can be ascribed to the Tarim Craton include Ni-Cu sulphides and the potential exists for carbonatite-hosted rare earth deposits.

3.1 Introduction

The North China (Sino-Korean craton) and the Tarim cratonic blocks consist of Archaean to Palaeo- and Mesoproterozoic lithotectonic units that are largely covered by Meso-Neoproterozoic platform successions and Mesozoic-Cenozoic sedimentary basins. On present-day coordinates, these two cratonic blocks are approximately east-west trending and line up eastward with the Kazakhstan-Kyrgyzstan Precambrian block (see Figs. 3.1 and 3.6). The boundary between the North China Craton and the Tarim Craton is somewhat poorly defined, although most publications show these two cratonic blocks joining along a comparatively narrow zone (e.g. Zhao et al. 2005; Fig. 3.3). The North China Craton and the Tarim Craton in the south and the Siberian Craton in the north "wedge-in" the central and eastern sectors of the Central Asian Orogenic Belt (CAOB, discussed in Chap. 5). To the south of the North China Craton, lie the Yangtze and Cathaysia cratonic blocks, discussed in Chap. 4. Collision orogens (fold belts) mark the tectonic boundaries between the NCC, Tarim, Yangtze and Cathaysia cratonic blocks.

In this chapter, the North China and Tarim Cratons are described, together with a selection of mineral systems that are temporally and spatially linked with these tectonic domains.

3.2 North China Craton

The North China Craton (NCC) is the largest cratonic block in China, with an area of 1.5×10^6 km^2 (Wilde et al. 2002) and extending as far as the northern half of the Korean peninsula, forming the Sino-Korean Craton (Figs. 2.1 and 3.1). Works that deal with the complex tectonic evolution of the NCC, include Zhao et al. (2001, 2005), Wilde et al. (2002), Zhai and Liu (2003), Kusky and Li (2003), Zhai (2004), Zhai et al. (2005, 2010), Santosh (2010) and Kusky (2011). In the south, the NCC is separated from the Yangtze Craton by the Qinling orogenic belt and the Dabieshan-Sulu high pressure metamorphic belt. In the north the NCC is bound by the Chifeng-Bayan Obo Fault (also called Kangbao-Chifeng Fault), which separates it from a complex collage of arc and accretionary terranes that are part of the Tianshan-Hinggan orogenic belts at the eastern end of the CAOB (see Fig. 2.2); also called Tianshan-Inner Mongolia-Daxinganling or Tianshan-Mongolia-Hinggan orogenic belts, or Manchurides in the terminology of Şengör and Natal'in (1996). These accretionary terranes collided following the closure of the Palaeo-Asian ocean, which is now marked by the Solonker suture belt, characterised by ophiolites, dismembered terrane units and post-collision

magmatism (Chap. 5). To the east, the NCC is bounded by the Tanlu fault. The NCC is extensively covered by Proterozoic platform cover rocks and Phanerozoic lithotectonic units, including volcano-sedimentary rift basins (Chap. 8). The Precambrian rocks of the NCC include high-pressure granulites, ultrahigh-temperature metamorphic rocks, greenstone belts and mafic-ultramafic rocks (Fig. 3.4a). Rocks of the NCC have been traditionally grouped into the >3.0 Ga Qianxi, the 3.0–2.5 Ga Fuping, the 2.5–2.4 Ga Wutai and the 2.4–1.8 Ga Lüliang orogenies (Tables 1.2 and 1.3 in Chap. 1). However, Zhao et al. (2005) stated that these subdivisions and tectonic events are not entirely valid, because they were established on misconceptions, such as the fact that deformed and high-grade metamorphic rocks were considered to be older basement. Archaean rocks include 3.8–2.5 Ga gneiss, tonalite-trondhjemite-granodiorite (TTG), granites, migmatites, various schist, marbles, graphite- and sillimanite-bearing gneiss (referred to as khondalites in Chinese literature; Lu et al. 1995 and see below) and banded iron-formations. Palaeoarchean continental nuclei of the NCC include the 3.5–3.3 Ga Huai'an Complex, the 3.1–2.97 Ga Yishui Complex, 3.1–3.0 Ga Xingyang and Longgang complexes (Zhai et al. 2010 and references therein). Supracrustal rocks are well represented in eastern Hebei with the 3.3–3.0 Ga Caozhuang Group that includes amphibolite, marble, fuchsitic (chromian mica) quartzite, BIF and gneissic rocks, metamorphosed at 2.5 and 1.89 Ga (Zhai et al. 2010; Fig. 3.4a). The 2.5 Ga Shuichang Complex, mostly comprises migmatite and gneissic rocks, diorite and granodiorite, forming the Qian'an dome. The Neoarchaean Zunhua Complex, a metamorphosed greenstone belt consisting of amphibolite and granulite facies units, such as orthogneiss, metagabbroic rocks, amphibolite, two-pyroxene granulites, intermediate-felsic granulite and BIF. Zhai et al. (2010) considered the eastern Hebei Archaean terranes as remnants of oceanic crust or island arc. The 2.9–2.7 Ga Yanlingguan greenstone belt has bimodal volcanic and sedimentary rocks metamorphosed to amphibolite facies. Also present are pyroxenite and hornblendite, which Zhai et al. (2010) claimed that these rocks may have a chemical signature similar to komatiites. The metasedimentary rocks comprise pelite, marble and banded iron-formations (BIF). The BIF rocks are locally exploited for iron ore. Other greenstone rocks, such as the Wuitashan greenstone belt are characterised by calc-alkaline volcanic rocks, interpreted to represent an island arc association (Zhai et al. 2010).

The Palaeo-Mesoproterozoic rocks overlie the Archaean units and comprise, 1.85–1.4 Ga quartzite, sandstone, conglomerate, shales and carbonates, whereas the 2.4–1.9 Ga Palaeoproterozoic rocks are more rare and only preserved within grabens in the central parts of the NCC. Greenstone belts and mafic-ultramafic rocks characterise the 3.5–3.0 Ga Qianxian period (Tables 1.2 and 1.3 in Chap. 1), during which palaeocratonic nuclei were formed and amalgamated into larger protocontinents during the Fupingian epoch (3.0–2.8 Ga) (Sengör and Natal'in 1996). The Late Archaean is represented by Wutaian epoch, when continental shelf sequences were developed. It is interesting to note that Sengör and Natal'in (1996) stated that the NCC does not deserve the status of craton, in spite of its Archaean-Proterozoic basement sequences. This is because, the NCC was extensively deformed and repeatedly affected by magmatic systems from the Mesoproterozoic to the Cenozoic. Mostly,

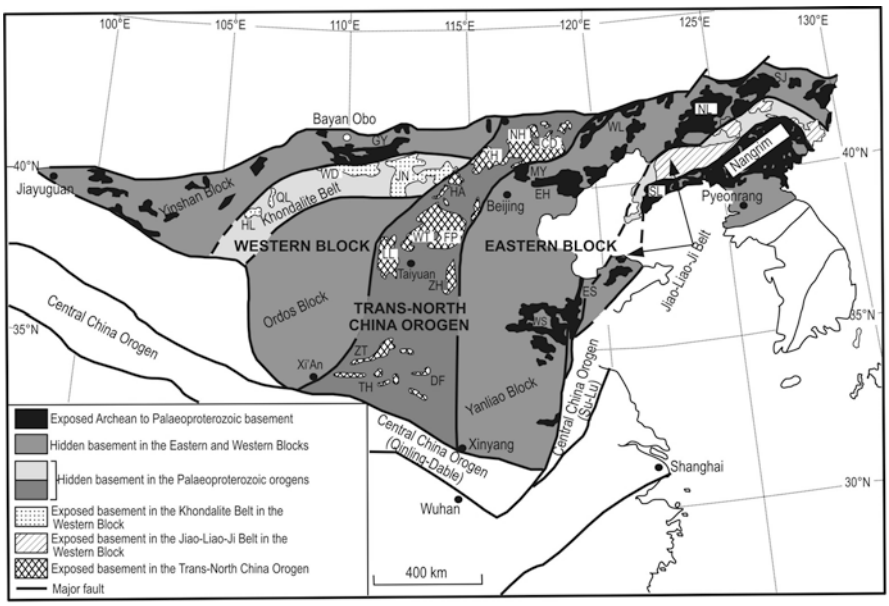

Fig. 3.1 Tectonic subdivisions of the North China Craton (after Zhao et al. 2005); *CD* Chengde, *DF* Dengfeng, *EH* Eastern Hebei, *ES* Eastern Shandong, *GY* Guyang, *DF* Dengfeng, *HA* Huaian, *LL* Lüliang, *JN* Jining, *MY* Miyun, *NH* Northern Hebei, *NL* Northern Liaoning, *QL* Qianlishan, *FP* Fuping, *SL* Southern Liaoning, *TH* Taihua, *WD* Wulashan-Daqingshan, *WT* Wutai, *WS* Western Shandong, *XH* Xuanhua, *ZH* Zanuang, *ZT* Zhongtiao

the Precambrian sequences were uplifted along the northern and southern margins of the NCC, during Phanerozoic collision and accretionary processes (Zhou et al. 2002).

3.2.1 Eastern and Western Blocks

The North China Craton (NCC) is subdivided into an Eastern Block and a Western Block, separated by the north-trending Trans-North China Orogen (Fig. 3.1) (or Central Orogenic Belt; Santosh 2010). Zhao et al. (2004, 2005), Kusky et al. (2007) and Kusky (2011) gave reviews of the Precambrian tectonic evolution of these cratonic subdomains and the following is summarised from these authors. Zhao et al. (2005) built their model of the tectonic evolution of the NCC, largely on the basis of isotope systematics (Nd, Re-Os, U-Pb and Hf). For example, they stressed the following: Nd model age peaks of 3.0–2.6 and 3.6–3.2 Ga for the Eastern Block, only one Nd model age peak of 2.8–2.4 for the Trans-North China Orogen; wide range of Nd model ages for the Western Block from 3.2 to 2.4 Ga with a peak at 2.8–2.6 Ga. Re-Os data support the concept that the lithosphere of the Trans-North

China Orogen was replaced at about 1.9 Ga, due to collision between the Eastern and Western Blocks, whereas Re-Os data showing that the lithosphere in the Eastern Block was not replaced till about 220 Ma, following collision of the Yangtze and NCC cratons. U-Pb dating of felsic granulite xenoliths found in Mesozoic volcanic rocks, show that ca. 3.6 Ga crust is confined to the Eastern Block. The Eastern and Western Blocks contain Palaeoproterozoic linear structural and/or metamorphic belts, such as the northeastern-trending Jiao-Liao-Ji belt in the Eastern Block and the Khondalite belt in the Western Block, representing fold belts, which led to the amalgamation of the various blocks, resulting in the final assembly of the NCC. The Jiao-Liao-Ji belt consist of greenschist to amphibolite facies volcanic and sedimentary rocks of Palaeoproterozoic age. The Khondalite belt consists by graphite-bearing sillimanite-garnet schist, garnet quartzite, paragneiss, calc-silicates, marbles and minor mafic granulites, charnockite and S-type granites (Zhao et al. 2005). However, 2.3 Ga khondalite series rocks have been recognised in several other localities and, according to Zhao et al. (2010), occur in the Fengzhen Formation in the Jinning block (JN), in the Lüliang Formation in the Fuping Block (FP), Fengishan Formation in the Jiaoliao Block (JL), the Huoshan and Lushan formations in the Xuchang Block (XCH) and the Louzishan Formation in the Qianhuai Block (QH) (Fig. 3.4b).

The Eastern Block consists of rather poorly exposed Archaean and Paleoproterozoic rocks, overlain by younger platform and basin successions. The Early and Mid Archaean (>3.4 Ga; 3.4–2.9 Ga) rocks are very limited and represented by ca. 3.8 Ga trondhjemitic gneisses and 3.4–3.2 Ga supracrustal rocks, whose original extent is not known and variably overprinted by 2.5 Ga tectono-thermal events. The Late Archaean (2.9–2.5 Ga) represents more than 80 % of the total exposed Archaean in the Eastern Block and consists of tonalite-trondhjiemite-granodiorite (TTG) gneisses with minor supracrustal rocks, intruded by syntectonic granites and exhibiting greenschist to granulite facies metamorphism at about 2.5 Ga. The Palaeoproterozoic of the Eastern Block is characterised by I- and A-type granites, bimodal volcanic rocks and sedimentary rocks, interpreted as having formed in intracontinental rift basins (see references in Zhao et al. 2004). Wu et al. (2011) working on enclaves of mafic granulites in the TTG gneisses of the Yishui Group (Western Shandong Complex), modelled the P-T conditions of the metamorphic minerals of the mafic granulites. These researchers concluded that the P-T anticlock-wise path involving isobaric cooling that characterizes the mafic enclaves is linked to continental rift magmatism, possibly associated with a mantle plume. Wu et al. (2011) concluded that the mantle plume activity produced three phases of metamorphism: (M1) initial heating of the overlying crust by a relatively cooler mantle plume head, resulting in amphibolites facies prograde metamorphism (730–660 °C at <6.6 kbar with the corresponding assemblage of hornblende-plagioclase-quartz-ilmenite-magnetite); (M2) a hotter mantle plume tail further heated the crust, producing granulite-facies metamorphism (820–800 °C at 8.0–8.5 kbar with the corresponding assemblage of orthopyroxene-clinopyroxene-plagioclase-garnet-hornblende-quartz-ilmenite-magnetite); (M3) isobaric cooling followed producing post-peak metamorphic assemblages (710–686 °C at 8.6–7.6 kbar and the corresponding garnet-quartz- and garnet-ilmenite/magnetite symplectite).

A peculiarity of the Eastern Block has made the NCC internationally famous. In fact, unlike all other Precambrian cratons, the Eastern Block is the site of earthquake activity, high heat flow, a thin lithosphere and Mesozoic to present-day volcanism. These features prompted Kusky et al. (2007) to label the evolution of the NCC: *from orogen to craton to orogen*. I return to discuss this aspect in Chap. 7. This phenomenon of "de-cratonisation" is unique to the NCC and is of enormous importance, not just for academic studies, but also because of its link with magmatism and the development of a wide range of hydrothermal mineral systems, including epithermal, porphyry, skarn and lode deposits, as is elaborated in the next section and the relevant chapters in this book.

The Western Block is dissected by the approximately east-west-trending Khondalite belt (see below), separating the Ordos Block to the south from the Yinshan Block to the north (Cope and Graham 2007; Santosh 2010; Santosh et al. 2011; Kusky 2011). The Archaean-Palaeoproterozoic rocks of the Western Block are also poorly exposed, due to the overlying Mesozoic and Cenozoic basins (see Fig. 2.5). Exposures in the Yishan Block consist of greenschist to granulite facies metamorphosed TTG gneisses and supracrustal rocks, similar to those of the Eastern Belt. The Palaeoproterozoic, however, is quite different and is largely represented by the graphite-bearing, sillimanite-garnet gneiss (Khondalite Belt), calc-silicates and marbles, interpreted to have been deposited in a stable continental margin. In contrast to the Eastern Block, the Western Block is a stable cratonic region, with no post-Precambrian deformation and is overlain by Mesozoic and Cenozoic sedimentary basins (Fig. 2.5), with most cratonic exposures confined to the northern parts. Basement rocks and supracrustals are metamorphosed to greenschist to granulite facies (Zhao et al. 2004, 2005), covered by a thick platform sedimentary cover and intruded by a belt of 2.55–2.5 Ga continental magmatic arc plutons along its eastern margin (Kusky et al. 2007). The exposed Palaeoarchaean basement rocks of the Western Block consist of granite-greenstone and high-grade metamorphic rocks, mostly in the northern sectors of the Block, whereas Neoarchaean units comprise low-grade granite-greenstones and high-grade TTG gneiss and granulites.

According to some recent views (Santosh 2010 and references therein) the Western Block is the result of Palaeoproterozoic collision events at 1.95–1.92 Ga and at ca. 1.85 Ga. Between 1.95–1.92 Ga, collision of the Yinshan Block in the north with the Ordos Block in the south formed the Khondalite Belt, which amalgamated these two blocks to form the wider Western Block. Thus, the Western Block would consist of the Ordos sub-Block and the Yinshan sub-Block, welded along a suture zone, named Inner Mongolia Suture Zone (IMSZ; Santosh et al. 2010). The collision of the Ordos and Yinshan sub-blocks along the above mentioned suture, resulted in the formation not only of the khondalites but also UHT (ultra-high temperature) granulites. The Khondalite Belt contains remnants of oceanic rocks (ocean plate stratigraphy, OPS), included in an accretionary complex and recording mid-ocean ridge successions that were subsequently subducted at an oceanic trench (Kusky and Santosh 2009; Santosh 2010; Santosh et al. 2011). The Khondalite Belt in the IMSZ comprises quartzite and metacarbonates associated with amphibolite and metagabbro, interpreted to represent oceanic crust (OPS), later incorporated within an accretionary prism (Santosh

et al. 2010). Aspects of the Khondalite belt are discussed in some detail by Wan et al. (2009), who recognised the following tectono-thermal events (Daqingshan area): 2.6–2.5 Ga, related to subduction and emplacement of TTG rocks; 2.45–2.37 Ga, further subdivided into three stages, namely 2.45 Ga high-grade metamorphism, 2.40 Ga anatexis and 2.37 Ga magmatism, all associated with extension, uplift and mantle underplating; 2.3–2.0 Ga, perhaps related to an island arc; 1.95–1.85 Ga representing the time of a major tectono-thermal event as well as metamorphism, which could be related to continent-continent collision. Ultra-high temperature (UHT) metamorphism is considered to be the result of large scale magmatic under- or intraplating due to upwelling mantle material and in the Khondalite Belt this is evidenced by the presence of sapphirine granulites, with a metamorphic peak of 980–910 °C and 12–9.2 kbar (Wan et al. 2009 and references therein).

In summary, the lithological packages of the IMSZ are indicative, according to the Santosh and co-workers, of subduction of hydrated oceanic crust (mafic rocks and pelagic sediments, or oceanic plate stratigraphy, OPS), which in the accretionary wedge are associated with remnants of island arc, oceanic plateau, passive margin sediments and fragments of Archaean lithologies of the Yinshan sub-block, mentioned above. Also within the Khondalite Belt are TTG rocks (tonalite-trondhjemite-granodiorite), charnockite and calc-alkaline granitic rocks, which may relate to a subduction system. Santosh (2010) and Kusky and Santosh (2009), suggested that subduction was south-directed towards the Ordos Block. Furthermore, Santosh (2010) proposed a model of "double subduction" of the Western Block (Yanliao) towards the west under the Trans-North China Orogen and of the Yinshan Block southward under the IMSZ, contributing to the amalgamation of the NCC continental components.

3.2.2 Trans-North China Orogen

At about 1.85 Ga the Western and Eastern Blocks collided to form the Trans-North China Orogen (or Central orogenic belt). Santosh (2010) pointed out that these collision events were associated with other global-scale collisions that led to the assembly of the Columbia Supercontinent (see also Kusky and Santosh 2009). As briefly introduced above, the Eastern Block (Yanliao) is that portion of the NCC in which thermal destruction (or de-cratonisition) of the sub-continental lithospheric mantle took place between the Ordovician and the Cenozoic, as well demonstrated by Griffin et al. (1998) through the study of xenoliths carried by basalts and kimberlites. Recent research suggests that this thermal erosion of the lithospheric mantle may be related to upwelling of asthenospheric mantle linked to subduction of the Pacific Izanagi plate from the east (Mao et al. 2010). I return to discuss this unusual phenomenon, which has important implication for the generation of hydrothermal mineral systems.

The Trans-North China Orogen (TNCO), which Santosh and co-workers prefer to call Central Orogenic Belt, because they pointed out that it is not a single

orogen, but a Palaeoproterozoic suture zone containing several and diverse fragments (including Archaean rocks) and amalgamating the Eastern and Western Blocks through a complex series of subduction-accretion-collision processes (Santosh, written communication 2010). Thus, as a whole, the Central Orogenic Belt (hereinafter TNCO) is a north-trending 1,200 km long and 100–300 km wide fault bounded zone (Fig. 3.1) comprising the following lithotectonic elements: (1) dominant Late Archaean-Palaeoproterozoic crust; (2) strike-slip ductile shear zones, large scale thrusts and folds; (3) high-pressure granulites and retrograde eclogite; (4) ophiolitic rocks; (5) syn- to post-tectonic granites; and (6) mafic dyke swarms. Zhao et al. (2004) pointed out that whereas the first five elements are related to collisional events, the mafic dyke swarms are indicative of extensional tectonics. Zhao et al. (2004) studied the Hengshan-Wutai Complex, interpreted as the remnant of an island arc, formed between 2.55 and 2.45 Ga and now situated in the central part of the TNCO. These authors suggested that the Hengshan-Wutai complex is evidence of east-directed subduction beneath the Eastern Block, resulting in the formation of a magmatic arc. Closure of the intervening ocean, led to continent (Western Block)-arc-continent (Eastern Block) collision between 1,880 and 1,820 Ma, resulting in the amalgamation of the two Blocks and the formation of the intervening fold belt of the TNCO. More recently, Zhang et al. (2011c) further examined the deformational history and structures of the Wutai Complex and recognized three stages, namely: (D_1) northeast-trending fabrics and linear structures associated with initial collision prograde metamorphism; (D_2) north-northeast-trending ductile shear zones and Z-shaped fold that overprinted the D_1 structures, resulting in fan-shaped thrust patterns (top-to-the NW and opposite top-to-the SE), the D_2 event also resulted in thicknening of the crust with peak metamorphism; (D_3) overprinted all previous fabrics, characterized by decompression and retrograde metamorphism. Zhang et al. (2011c) stressed the importance of the fan-shaped orogenic belt (D_2) with opposite senses of thrust (a kind of flower-structure) which, they suggested, support the model of eastward subduction and final collision of the Western and Eastern blocks to form the TNCO at ca. 1.85 Ga.

Trap et al. (2009) further contributed to the studies of the geodynamic evolution of the TNCO with their detailed structural and geochronological work on the 2,100 Ma Lüliang Massif (or Lüliang Complex of Liu et al. 2011) in the western-central part of the orogen. The Lüliang Massif consists of a series of lithotectonic units that from northwest to southeast comprise: (1) TTG gneissic and Al-rich metasedimentary rocks; (2) basalt, gabbro, quartz-green schist and metapelites (Lüliang Group), considered to have formed in an oceanic rift setting; (3) orthogneiss and metavolcanic and amphibolite units, whose protoliths may have been basalt and felsic volcanics. These lithotectonic units sit on a basement composed of TTG gneiss and migmatites and are unconformably overlain by greenschist facies metaclastic and carbonates of the Yejishan Group, now outcropping in a narrow northeast-trending strip. All these units are intruded by undeformed porphyritic granitic rocks formimg a batholitic complex. Trap et al. (2009), on the basis of their structural analysis and geochronological work, interpreted the Lüliang Massif as a part of a southeast-verging nappe, with its lithotectonic units forming a series of thrust sheets over basement gneissic

rocks. The nappe event is dated at 1,890–1,870 Ma. Trap et al. (2009) and in a later publication Trap et al. (2011) proposed that the Lüliang Massif and its correlatives, Fuping, Wutaishan, and Hengshan massifs, are the result of west-directed subduction of the Eastern Block and subsequent closure of an oceanic basin. On the other hand, Liu et al. (2011), on the basis of U-Pb dating of zircons from metavolcanic rocks of the Yeijshan and Lüliang groups, suggested that volcanism occurred at $2{,}210 \pm 13$ and $2{,}213 \pm 47$ Ma, respectively for these lithotectonic units, followed by metamorphism at ca. 1,832 Ma, leading these authors to conclude that the Lüliang Complex was part of a magmatic arc system at a continental margin.

Huang et al. (2010) working on the 2.7 Ga Lushan-Taihua Complex (Lushan amphibolite, gneiss and TTG rocks mainly) in the southern part of the TNCO, determined that TTG-like gneiss suite of the Complex, resulted from the interaction of mantle melt with partial melting of subducted oceanic crust. Using trace element geochemistry, these authors proposed a model for the geodynamic evolution of this part of the TNCO involving: (1) creation of oceanic crust (amphibolite) at 3.0 Ga, followed by; (2) either obduction of oceanic crust or accretion of oceanic plateau material; (3) flat subduction of the oceanic slab at 2.77 Ga, producing TTG melts (partial melting of the oceanic crust), which interacted with melts of peridotite in a thin mantle wedge, the TTG melts then intruded the overlying oceanic lithosphere; (4) at 2.72 Ga oceanic plateau accretion and intraoceanic plate stacking led to crustal thickening, followed by its partial melting, resulting in the formation of the Lushan TTG. Huang et al. (2010) concluded that the Lushan-Taihua Complex records accretion of Archaean crust, from oceanic crust to flat subduction to crustal thickening, leading to the establishment of a protocontinent.

The NCC was finally cratonised at ca. 1.8 Ga. Zhai et al. (2004) described the ca. 1.8 Ga tectono-thermal events that led to the final establishment of the NCC and recognised two main events: (1) 1.9–1.8 Ga orogeny and metamorphism and (2) rifting. The former is characterised by high-pressure regional metamorphism at 1,890–1,830 Ma and resulted in granulite facies rocks. The latter consist of a volcano-sedimentary succession and is associated with the 1.78 Ga Xiong'er volcanic province and dyke swarms, discussed in more detail in Chap. 7. The Xiong'er volcanic province is part of the Xiong'er Terrane on the southern margin of the NCC, which includes the Palaeoproterozoic Taihua Group (also called Complex, Supergroup and by some authors Formation), consisting of medium-high grade metamorphic rocks, ranging in age from 3.0 to 2.1 Ga (TH in Fig. 3.1; Zhang 1989; Chen and Zhao 1997). The Taihua Group is divided into three lithostratigraphic units: Beizi, Dangzehe and Shuidigou. The Beizi Formation comprises amphibolite and gneissic rocks with a Sm-Nd isochron age of ca. 2.77 Ga (Xue et al. 1995). The ca. 2.5–2.3 Ga Dangzehe Formation consists of amphibolite and biotite gneiss (Xu et al. 2009), whereas the ca. 2.3 Ga Shuidigou Formation comprises rocks of a khondalite-like lithological package including sillimanite-garnet gneiss, graphitic gneiss, marble, banded iron-formation (Chen and Zhao 1997). The geodynamic evolution of the NCC, according to a model by Kusky and Santosh (2009) and Santosh et al. (2010) is shown in Fig. 3.2.

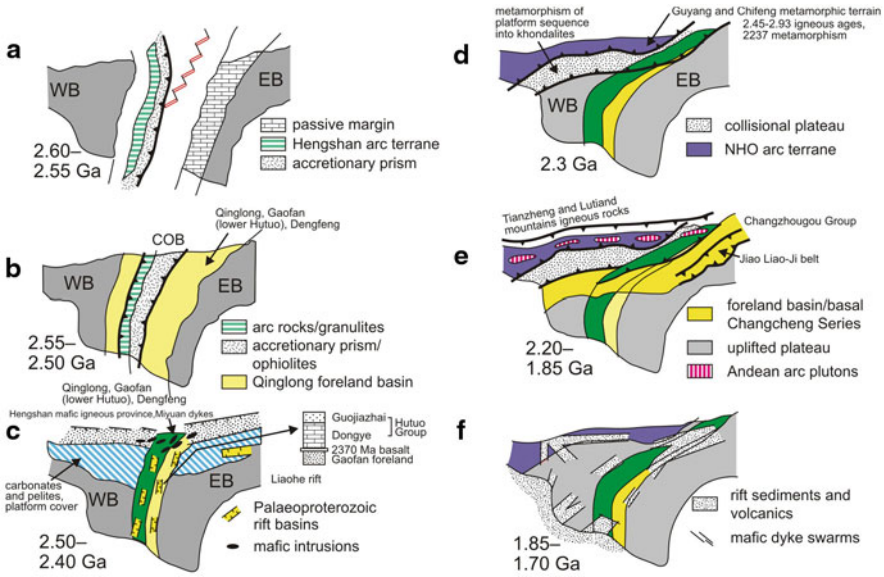

Fig. 3.2 Sketch illustrating the geodynamic evolution of the North China Craton, between 2.60 and 1.70 Ga (according to Kusky and Santosh 2009). Between 2.60 and 2.55 Ga, a west-directed subduction-related arc terrane was developing along the margin of the Western Block, while a passive margin was present along the Eastern Block, separated by an intervening ocean (**a**); the Eastern and Western Blocks collided to form the Central Orogneic Belt with the formation of accretionary prism, ophiolitic belts and granulte facies rocks as well as development of foreland basins at about 2.55 and 2.50 Ga (**b**); between 2.50 and 2.40 Ga a series of rift structures were formed and a passive margin on the northern margin of the amalgamated cratonic block (Western, Eastern and Centrak Orogenic belts) (**c**); subduction-related arc terranes developed to the north at about 2.3 Ga, forming the North Hebei Orogen, followed by arc collisions (2.20–1.9 Ga) resulting in the development of the UHP Khondalite belt; these collisions were temporally associated with the amalgamation of the Columbia Supercontinent (**d** and **e**); the last stages, between 1.85 and 1.70 Ga, are characterised by the formation of large rift systems and associated magmatism, such as that of the Xiong'er volcanic province, discussed in Chap. 7 (**f**)

Much of the evidence for models of the tectonic evolution of the NCC, rests with the nature of mafic-ultramafic intrusions that occur within it. These rock bodies are not only important for a clearer understanding of the geodynamic settings in which they formed, but also for the inherent mineral systems that are or may be associated with them (see below). One of these is the Yanmenguan intrusion in the Trans-North China Orogen, recently investigated by Wang et al. (2010). Another important mafic-ultramafic intrusion is the Dongwanzi Complex in the Eastern Block, studied by Zhao et al. (2005, 2007a). Both these mafic-ultramafic complexes are briefly discussed here.

The ca. 2.2 Ga Yanmenguan mafic-ultramafic intrusion is considered to be an Alaskan-type complex (see definition in Chap. 5). The Yanmenguan complex is one of many in the Hengshan-Wutai-Fuping and Lüliang terranes, where they are associated with amphibolite facies rocks consisting of mafic, pelitic and lesser ultramafic

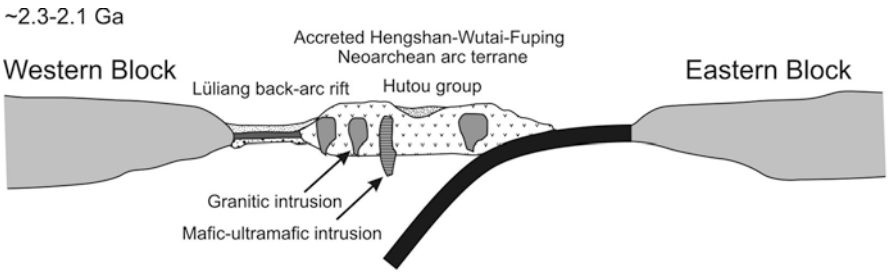

Fig. 3.3 This schematic illustration shows an inferred arc terrane in the Trans-North China Orogen and associated granitic and mafic-ultramafic Alaskan-type intrusions. (After Wang et al. 2010)

rocks, all intruded by tonalitic granitic rocks (Wang et al. 2010). The study of the Yanmenguan mafic-ultramafic intrusion, led Wang et al. (2010) to propose a new model for the geodynamic evolution of the TNCO between the Neoarchaean and the Palaeoproterozoic, schematically shown in Fig. 3.3. These authors considered that at ca. 2.5 Ga and intraoceanic arc-back-arc basin system was present and accreted at the end of the Neoarchaean. This was followed by a hiatus in magmatic activity between ca. 2.5 and 2.3 Ga; followed by magmatism at ca. 2.3 and ca. 2.1 Ga in the Hengshan-Wutai-Fuping arc terranes and the Lüliang terrane. Collision occurred at ca. 2.1 Ga with the closure of the Lüliang back-arc basin and accretion of the Hengshan-Wutai-Fuping arc terranes to the Western Block. As mentioned above, final collision between the Western and Eastern Blocks and subsequent amalgamation took place at around 1.85 Ga.

The Dongwanzi mafic-ultramafic complex, about 200 km northeast of Beijing, has been debated whether it is an Archaean ophiolite or a Phanerozoic intrusion. Kusky et al. (2001, 2004) interpreted the Dongwanzi complex as a 2.5 Ga ophiolite, consisting of pillow lavas, sheeted dykes, gabbro, pyroxenite, harzburgite and peridotite, metamorphosed to amphibolite facies. Zhao et al. (2005, 2007a) disputed this interpretation, first on the basis that the complex does not exhibit pillow lavas, which instead may be structural features and that the sheeted dykes do not provide hard evidence of an oceanic setting. Eventually, the evidence from U-Pb SHRIMP dating of euhedral zircons with sharp oscillatory zoning by Zhao et al. (2007a) effectively ended the controversy and established that the Dongwanzi complex is not an ophiolite. The Dongwanzi complex, which consists of gabbro, pyroxenite, hornblendite and associated mafic dykes, has U-Pb SHRIMP ages of about 300 Ma (306 ± 6 Ma mafic dyke; 308 ± 4 Ma pyroxenite), which also happen to coincide with similar ages for dioritic and granitic rocks in the general area (Zhang et al. 2007). The Dongwanzi mafic-ultramafic complex intrudes unmetamorphosed Mesoproterozoic rocks (Changcheng-Jixian System in Chinese literature). As mentioned above, the correct identification and age of mafic-ultramafic complexes have important implications, not only for constraining the tectonic setting and hence geodynamic evolution of the NCC, but also for the assessment of the mineral potential of these rocks. The distribution of known Archaean and Proterozoic rocks is shown in Fig. 3.4.

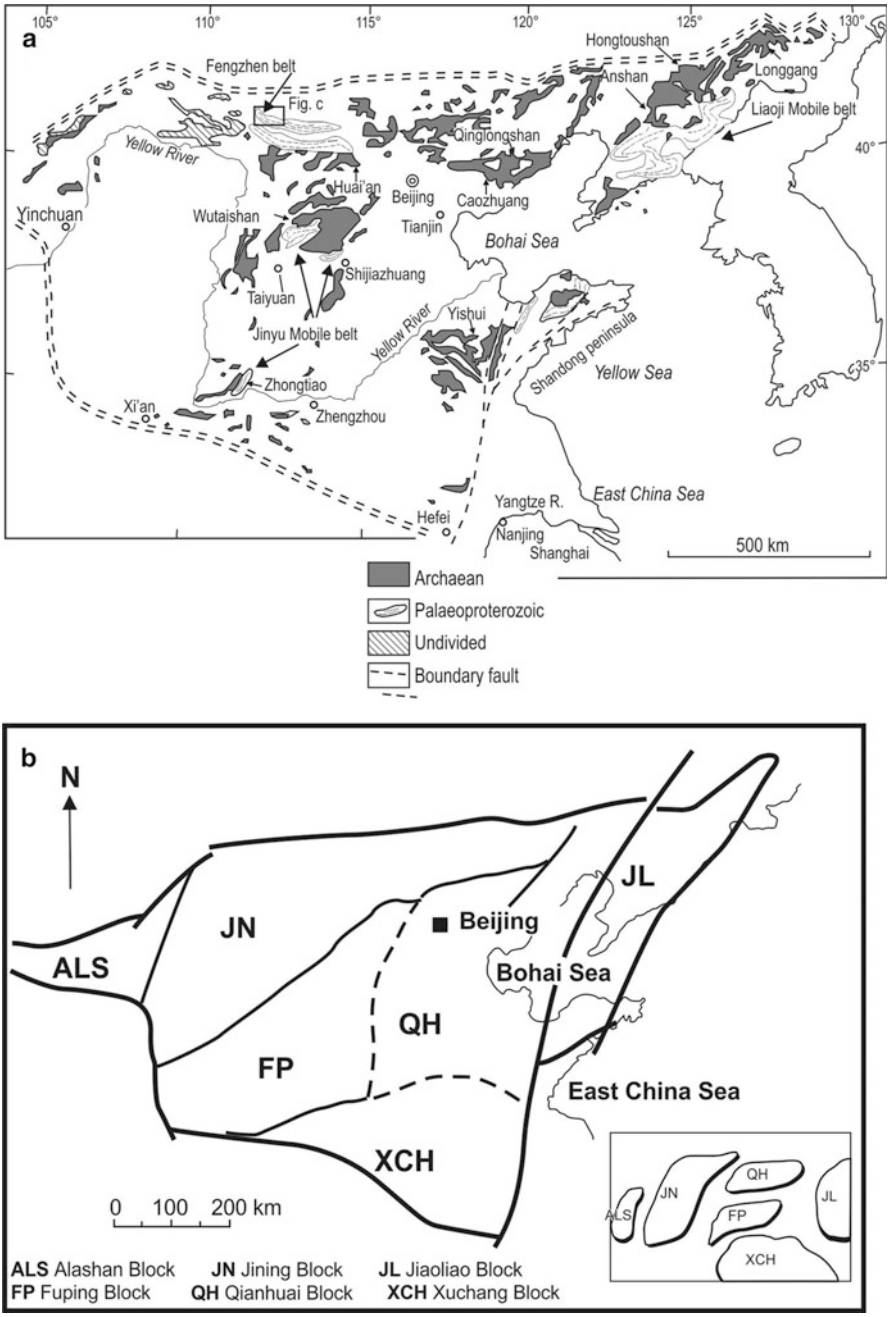

Fig. 3.4 **a** Distribution of Archaean rocks in the North China Craton; **b** subdivision of the Craton into Neoarchaean blocks in the interpretation of Zhai (2004 and references therein); more recent subdivisions by Zhai et al. (2010), show yet again different boundaries and an unlikely craton-wide northeast-trending 2.5 Ga greenstone belt; **c** geodynamic evolution of the Halaqin volcano-sedimetary succession (according to Peng et al. 2011), who kindly provided this figure

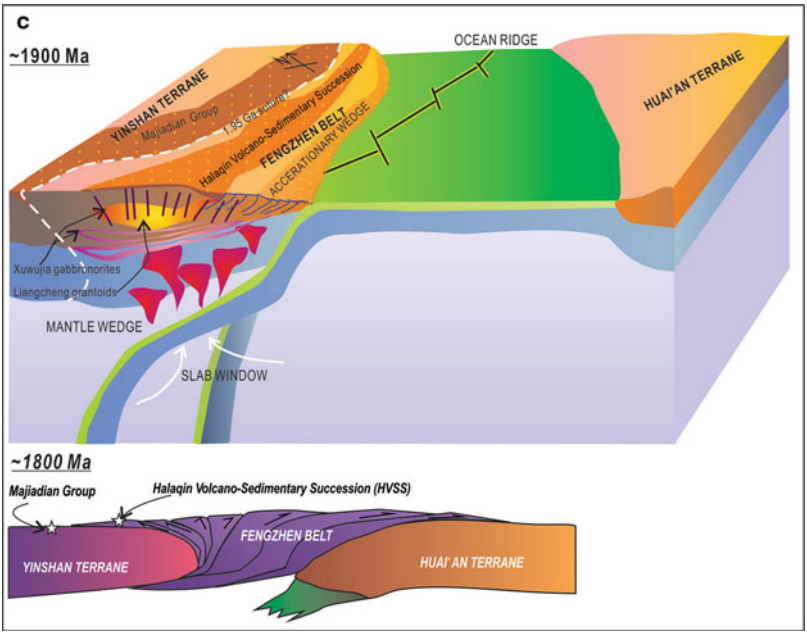

Fig. 3.4 (continued)

Before concluding this section, it is opportune to also outline other views regarding the geological history and evolution of the NCC. Zhai (2004), Zhai et al. (2005, 2010) and Li et al. (2010) tectonically divided the NCC into six micro-continental blocks or ancient continental "massifs", from west to east, as follows: Alashan, Jining, Fuping, Xuchang and Qianhuai, roughly in the centre, and Jiaoliao to the east, which amalgamated to form the NCC (Fig. 3.4b). A northeast-trending belt of 2.5 Ga greenstone rocks borders the Jining, Fuping and Qianhuai blocks, whereas a 2.67–2.70 Ga greenstone belts cut across the eastern NCC, bordering the Xuchang, Qianhuai and Jiaoliao blocks. These subdivisions are doubtful and not based on clear evidence (Zhao et al. 2005). Zhai MG's work (2004) did not mention, however, the presence of a Trans-North China Orogen or a Central Orogenic Belt, advocated by other authors (e.g. Zhao et al. 2004, 2005; Kusky et al. 2007; Kusky and Santosh 2009; Santosh et al. 2010 and others). Figure 3.4b shows the subdivisions of the NCC in the interpretation of Zhai (2004).

3.2.3 Palaeoproterozoic Fold Belts and Rifting in the NCC

Zhai et al. (2010) also recognise major metamorphic (1.9–1.8 Ga), rifting and widespread anorogenic magmatism, including the emplacement of mafic dyke swarms (1.8–1.65 Ga). As previously mentioned, Zhai (2004) supported the idea of a ca. 1.8 Ga mantle plume and subsequent north-northeast-trending rifting across the NCC, within which the Xiong'er magmatism occurred (Chap. 7), an event that

could have been associated with the breakup of the Columbia Supercontinent and later amalgamated into the Rodinia Supercontinent.

The NCC was probably cratonised by ca. 2.5 Ga. The next tectono-thermal events took place in the Palaeoproterozoic, beginning at ca. 2.3 Ga. Palaeoproterozoic fold (or mobile) belts in the NCC formed around 2.35–1.9 Ga in rift systems, passive continental margins and foreland basins. The following is extracted from Zhai et al. (2010). At least three Palaeoproterozoic mobile belts are present in the northeast (Fengshen mobile belt), northwest (Liaoji mobile belt). and southern (Jinyuy mobile belt (Fig. 3.4). The Liaoji mobile belt, trending northeast in the Liaoning Province along the North Korean border (Liaohe Group) and to the south in the Shandong peninsula (Fenzishan Group) has been interpreted to have originated in a continental rift basin. The Liaoji belt comprises volcano-sedimentary rocks metamorphosed to greenschist, amphibolite and granulite facies. The volcanic rocks are of bimodal composition (tholeiitic and Na-rich felsic volcanics). Zhai et al. (2010) also reported that these Na-rich felsic volcanic rocks are locally extensively tourmalinised, but did not provide details (boron metasomatism may be linked to alkaline magmatic systems and mineralisation; Pirajno 2009). The sedimentary rocks comprise argillaceous schist, metasiltstone, graphitic marble and detrital carbonates with magnesite deposits. The Jinyuy (also spelt Jinyü) mobile belt in the southern part of the NCC contains sedimentary and volcanic rocks that, although with similar features, have been grouped into three lithostratigraphic units (Hutuo, Lüliang and Zhongtiao). The Hutuo Group consists of conglomerate, sandstone, shale, mafic volcanic and volcaniclastic rocks as well as mafic dykes. The latter have SHRIMP U-Pb ages ranging from 2.45 to 1.8 Ga (Zhai et al. 2010 and references therein). The Zhongtiao Group comprises clastic rocks, shale, carbonate and mafic to felsic volcanic rocks, interpreted as calc-alkaline related to an island arc. Copper mineralisation is vaguely reported in Zhai MG and co-workers' paper, but again no details given.

Peng et al. (2011) reported on a 1.9 Ga volcano-sedimentary terrane in Inner Mongolia, which they called Halaqin, and consisting of quartzite, marble, amphibolites derived from protoliths of sandstone, limestone and volcanic rocks. The Halaqin volcano-sedimentary terrane sits on top of the Neoarchaean-Palaeoproterozoic Yinshan Block, referred to above. The Halaqin volcanic rocks comprise basalt, andesite and dacite-rhyolite, correspondingtheYinshan Block to the northwest to gabbronorite and granitic intrusions that underlie the Fengzhen belt to the southeast (Fig. 3.4c). Peng et al. (2011) proposed a model of ridge subduction at ca. 1.9 Ga below a continental margin comprising the Yinshan and Fengzhen terranes or belts, all of which later (at ca. 1.8 Ga) collided to form the Fengzhen fold-and-thrust belt, between the Yinshan Block to the northwest and the Huai'an terrane to the southeast (Fig. 3.4c).

The east-west-trending Fengzhen mobile belt on the northwestern margion of the NCC, just above the major bend of the Yellow River, comprises a thick sequence of granulite facies metasedimentary rocks. These rocks can be divided into a lower sequence and upper sequence. The former, comprises quartzite, graphitic gneiss, mica-quartz schist, garnet-sillimanite gneiss, (khondalite sequences). The upper sequence comprises marble, mica-schist and calc-silicate rocks. The khondalite sequence also contains garnet-granites with zircon U-Pb ages of ca. 1.9 Ga.

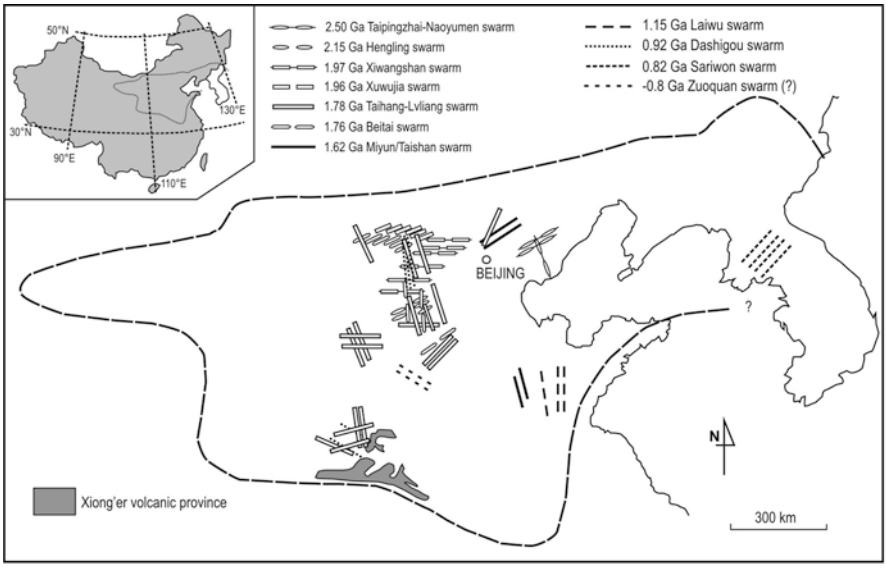

Fig. 3.5 Distribution of Palaeoproterozoic mafic dykes and sills in the NCC. (After Peng 2010)

However, it transpires from Zhai et al. (2010) that the age of the Fengshen mobile belt rocks is by no means well constrained, with some workers suggesting that the Fengshen khondalites are of Archaean age (see references in Zhai MG et al's paper).

The presence of Palaeoproterozoic mafic dyke swarms in the NCC clearly demonstrate that extension tectonics and rifting took place. One of these is the 1.7 Ga giant Taihang-Lüliang dyke swarms (Peng 2010), linked to the Xiong'er volcanic province and triple rift junction, discussed in some detail in Chap. 7. Other dyke swarms include the 2.5 Ga Taipingzhai-Naoyumen, 2.15 Ga Hengling, 1.97 Ga Xiwangshan, 1.96 Ga Xuwujia, 1.76 Ga Beitai, 1.62 Ga Miyun-Taishan, 1.15 Ga, 1.15 Ga Laiwu, 0.92 Ga Dashigou, 0.82–0.8 Ga Sarlwion-Zuoquan swarms (Peng 2010). Most and largest swarns are concentrated within the Trans-North China Orogen and along the northern part of the NCC (Fig. 3.5).

The emplacement of dyke swarms is commonly associated with rifting processes. In the NCC two important rifting events are the Xiong'er, Yanshan and Bayan Obo (see below and Fig. 3.16). The Xiong'er rift system, associated with the homonymous volcanic province, forms an aulacogen that extends to north, east and west in the southern margin of the NCC. The Xiong'er volcanic rocks are intercalated with clastic sedimentary rocks and have U-Pb SHRIMP ages of zircons ranging from 1.8 to 1.75 Ga. The geochemical signature of the Xiong'er volcanic rocks is the cause of controversy, because of their apparent island arc affinity, but as elaborated in Chap. 7, the consensus of opinion is that the Xiong'er Group is related to an intracontinental rift system and is part of a large igneous province (Pirajno and Chen 2005). Furthermore, it has been suggested that the Xiong'er rift and associated volcanic activity may be

linked with the breakup of the Columbia supercontinent (Kusky and Santosh 2009). As pointed out in Zhai et al. (2010) and more recently by Cui et al. (2011), 1.78 Ga dioritic intrusions mark the end of the Xiong'er magmatism and of the rift tectonics.

The Yanshan northeast-trending rift system, northwest of Beijing and merging into the Taihang Mountains, contains a volcano-sedimentary succession, which is part of the Changcheng Formation/Group (also known as Changcheng System or Changcheng Quartzite, but these terms should be considered obsolete; see Zhang 2009). The Changcheng Formation (or Changcheng Group, according to Meng et al. 2011) comprises conglomerate, sandstone, greywacke, mudstone, shale and carbonate rocks, associated with a continental bimodal volcanic series, with U-Pb zircon ages of ca. 1.72–1.62 Ga (Lu et al. 2002). Meng et al. (2011) in their study of the Changcheng and Nankou volcano-sedimentary successions proposed two stages of "rift to drift" evolution (syn-rift and post-rift) for the northern margin of the NCC, during which the NCC separated from the Indian Craton at ca. 1.6 Ga in the general breakup of the Columbia sueprcontinent, but in a different reconstruction from that shown in Fig. 3.16. It is important to note that the initial rifting at ca. 1.8 Ga led to the inception of the Yanshan-Lioaxi rift and the Bayan Obo rift system. The latter is highly significant for its contained world-class carbonatite-hosted mineralisation, as discussed below (Fig. 3.15). From about 1.6 Ga, during the post-rift stage of continental breakup and drifting, in the interpretation of Meng QR and co-workers the northern margin of the NCC became a passive margin.

3.2.4 Mineral Systems

Mineral systems within the NCC and in its superimposed tectonic units (e.g. rift basins) and Phanerozoic magmatic systems can be divided into:

- those that were formed during the formation of the NCC and that are part of the assembled cratonic block,
- those that were formed during Palaeoproterozoic rifting and igneous activity (e.g. Xiong'er large igneous province) and
- those that were formed in later times (e.g. Indosinian and/or Yanshanian tectonothermal events of Mesozoic age) and which may be either hosted in rocks of the NCC, or in Palaeoproterozoic lithotectonic units, or in superimposed rift basins, or in accreted magmatic arcs.

3.2.4.1 Archaean and Palaeoproterozoic Mineral Systems of the NCC

In the first group of the above list, are chromite deposits interpreted to be of the podiform type associated with ocean floor hydrothermal activity, Fe-Ti-V in anorthosite massifs, and volcanogenic massive sulphide and banded iron-formations.

The mineral systems of Precambrian age that are hosted in mafic-ultramafic rocks which, as discussed above, occur within the TNCO (Fig. 3.1). The mafic-ultramafic

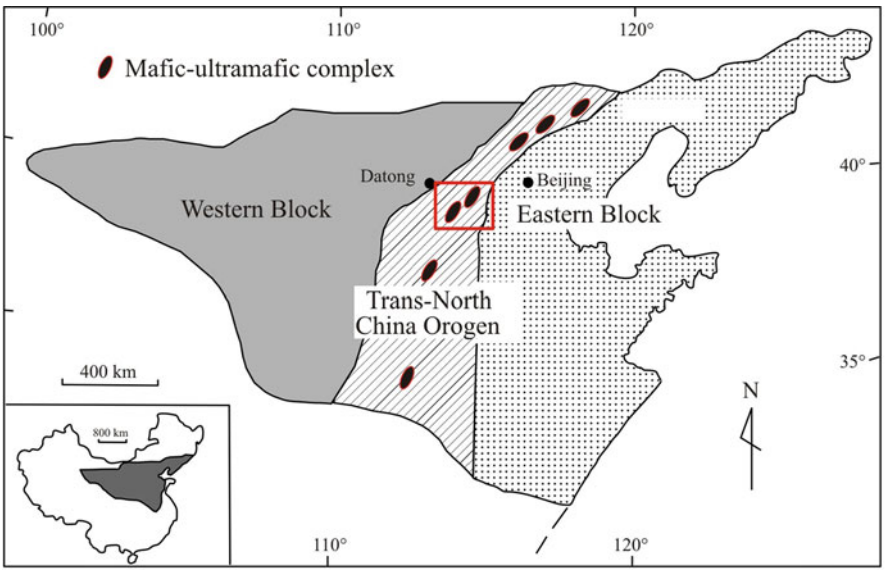

Fig. 3.6 Distribution of mafic-ultramafic complexes in the Trans-North China Orogen. (Li et al. 2004)

complexes in the TNCO are located at Dongwanzi, Zunhua (Liaoning Province), North Taihang Mountain and at Wutai Mountain in the central parts of the Orogen, where dismembered units are associated with high-grade metamorphosed greenstone belts, intruded by 2.6–2.5 Ga tonalite-trondhjemite gneissic rocks. For details of these mafic-ultramafic complexes the reader is referred to Kusky (2004). The distribution of mafic-ultramafic complexes in the TNCO is shown in Fig. 3.6.

Chromite Deposits

Zhou and Bai (1992) reviewed chromite deposits in China and listed six occurrences in layered intrusions in the NCC: Gaosi (Gaositao), Maojia, Pinding, Tongyu, Shangnan and Xiasong (Fig. 3.7). These authors listed these deposits as stratiform type, mostly occurring in dunitic rocks forming dismembered fragments of intrusions within Archaean rocks. The Gaositao and Maojia mafic-ultramafic zoned intrusions are of the Alaskan type and of Early Permian age and are introduced in Chap. 5. Chromite occurs in the Tongyu anorthosite complex, intruded into the Archaean Fuping Group. Zhou and Bai (1992) compared the Tongyu intrusion to Fiskenaesset intrusion in West Greenland.

Chromite is hosted in serpentinised harzburgite surrounded by dunite in the Zunhua greenstone belt, about 60 km southwest of the Dongwanzi complex. The shape and size of the orebodies are highly variable with lenses generally ranging from 1 to 20 m long, 0.5–2 m thick and 10–30 deep. Larger chromite orebodies can be

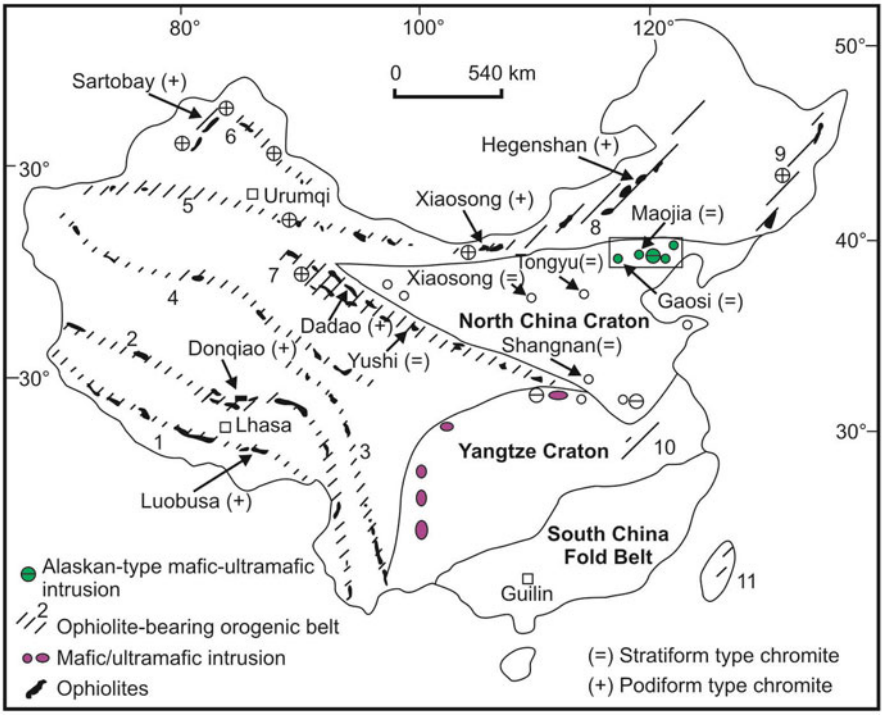

Fig. 3.7 Distribution of mafic-ultramafic rocks, ophiolite belts and types of chromite deposits in China; ophiolite belts shown are *1* Yarlungzangbo; *2* Bongong-Nujiang; *3* Jinsha-Ailao; *4* Kunlun; *5* Tianshan; *6* Junggar; *7* Qilian-Qinling; *8* Solonker suture zone; *9* Nadanhada; *10* Jiangshan; *11* Eastern Taiwan (After Zhou and Bai 1992). It must be noted that some of the mafic-ultramafic intrusions are not ophiolites, but Alaskan-type zoned intrusions; for example the Gaosi (Gaositai) complex and others along the east-west-trending fault zone on the northern margin of the North China Craton, have ages of about 280 Ma and were emplaced during southward subduction of the Palaeoasian ocean (Chen et al. 2004; see Chap. 5)

up to 100 m long, 10 m thick and tens of metres deep (Huang et al. 2004). These chromite ores, have been considered as typical Alpine-type podiform chromitites associated with ophiolites (Li et al. 2002) and described in detail by Huang et al. (2004). The ores comprise disseminated chromite grains, network veinlets, antinodular, nodular and orbicular textures. Chromite, with disseminated textures consists of randomly oriented rounded subhedral crystals scattered in dunitic rocks. Network veinlets consist of euhedral crystals that form, as the name implies, net-like veins. Antinodular chromite forms a net-mesh-like texture of round olivines within which are fine-grained chromites. Orbicular chromite is typically represented by ball- and elliptical-shaped chromite masses that themselves include several individual balls. Nodular chromite consists of nodule shapes in an olivine matrix. Flow, banded, mylonitic and fold structures of these chromites led Huang et al. (2004) to suggest that the chromites were associated with vertical magmatic accretion formed in an

active and fast spreading mid-ocean ridge. The ophiolitic association is again disputed by Zhao et al. (2005), who pointed out; first that Alpine-type ophiolite-hosted podiform chromites are restricted to Neoproterozoic and Phanerozoic orogenic belts and second that the high Fe and Ti and low Cr, Al, Mg abundances in the Zunhua chromites are not typical of ophiolitic podiform chromitites. Rather, these authors argued, the chromitite occurrences of the Zunhua mafic-ultramafic complex were formed in a continental intrusion. As a point of note, the reader may be interested that other authors considered 3.8 Ga sheeted dyke complex in the Isua greenstone belt in Greenland to be part of Earth's oldest ophiolite (Furnes et al. 2007).

Fe-Ti-P Mineralisation in Massif-type Anorthosites Intrusions

Massif-type anorthosite and nelsonite (dominantly apatite and ilmenite) rocks with ages ranging from 2.1 to 1.74 Ga are known from the northern part of the Eastern Block of the NCC (Zhao et al. 2009, 2010). Here, the Damiao Fe-Ti-P oxide deposit consists of irregular lenses, pods and veins that have sharp contacts with the host anorthosite rocks (Zhao et al. 2010; see also Zhao and Zhou 2009). The ores contain apatite, and Fe-Ti oxides, which Zhao et al. (2010) interpreted to be mixtures of cumulus minerals and trapped liquid. The Damiao Fe-Ti-P orthomagmatic deposit is described in some detail by Cheng et al. (1995). The Damiao complex is a north-south-trending body about 40 km long and 2–9 km wide that mainly consists of anorthosite, gabbro-norite, with minor peridotite, pyroxenite and hornblendite rocks. Zhao et al. (2009), however, recognised that the complex consists of 85 % anorthosite, 10 % norite, 4 % mangerite and <1 % troctolite. Anorthosite is therefore the main lithology and is characterised by a number of intrusions. Anorthosite is coarse-grained with plagioclase crystals ranging in size from 3 to 5 mm and representing 80–90 % by vol of the rock. This plagioclase is generally altered (saussuritised) and is andesine in composition (An_{35-50}), but this composition may not be primary and may only reflect alteration. Accessory minerals are titano-magnetite, apatite, chlorite, and locally rutile and leucoxene. The norite-gabbro rocks include gabbro, monzogabbro, hypersthene gabbro, noritic pegmatite. The anorthosite and gabbro-norite are reported as being co-magmatic. Hornblendite intrudes gabbro-norite and consists of hornblende with lesser pyroxene, biotite, titano-magnetite, ilmenite and apatite. Also present are late dioritic, lamprophyre and dolerite dykes. An emplacement sequence from anorthosite, norite to Fe-Ti-P oxide ores to mangerite is advocated by Zhao et al. (2009). U-Pb zircon dating of mangerite and norite, yielded ages of $1{,}739 \pm 4$ Ma (MSWD = 1.4) and $1{,}742 \pm 17$ Ma (MSWD = 0.39), respectively, whereas Nd model ages (T_{DM}) range from 2.46 to 2.77 Ga (Zhao et al. 2009). Similarly, initial Hf istopic ratios for zircons show a regular distribution with $\varepsilon_{Hf}(t)$ negative values (−4.7 and −5.9, averages for mangerite and norite, with Hf model ages of 2.71 and 2.79 Ga, respectively; Zhao et al. 2009). The Nd and Hf isotope systematics, confirm that the Damiao complex is a massif-type anorthosite-norite-magerite suite, for which Zhao and co-workers proposed a model, suggesting that crustal rocks were dragged into the upper mantle during collision of the Western and

Eastern Blocks to form the NCC. The ambient temperature of the upper mantle was greater than 1,271 °C resulting in widespread melting and producing a deep-seated magma chamber, from which anorthosite was formed and injected to mid-crustal levels.

The Fe-Ti-P mineralisation is distributed along the southern margin of the eastern part of the anorthosite intrusion and along its contact with gabbro rocks. According to the information reported by Cheng et al. (1995), 40 orebodies (southern, middle and northern) were defined, which although forming separate outcrops, they are linked below the surface as one body. The orebody is northeast trending and dips 70° to the southeast, extending for up to 500 m along strike and 500 m downdip, with variable thicknesses ranging from tens of metres to about 100 m. In the Heishan district the mineralisation is developed in gabbro rocks. There are two types of ores: injection- or vein-type and disseminated. "*Injection-type orebodies*", form lenses and veins in fractures within anorthosite and gabbro units. Injection ores are massive, enclosing clasts of anorthosite and principally consist of titano-magnetite, accompanied by lesser ilmenite, pyrite, chalcopyrite and rutile. Gangue minerals are plagioclase, chlorite, hornblende and small amounts of apatite. The ore grades for the injection- or vein-type orebodies are up to 32–34 % Fe, but generally in the range of 5–15 %, V_2O_5 range from 0.005 to 0.17 % and P_2O_5 about 0.07 %. Disseminated titano-magnetite, ilmenite, apatite, rutile and sulphides are hosted in gabbro or along the contacts with anorthosite. Here the P_2O_5 content is from 0.59 to 0.93 %, with Fe grades of about or less than 20 %. Following Zhao et al. (2009), the ores occur as dykes, veins or irregular sheets as disseminated and massive. Massive ores are divided into Fe-Ti oxide grading upward into Fe-Ti-P oxide types, with increasing abundance of silicate minerals.

Volcanogenic Massive Sulphides (VMS)

At Wutai Mountain, volcanogenic massive sulphide (VMS) deposits form small lenses, sheets and tabular bodies of massive, layered and disseminated sulphides, distributed along 7 km of strike (Li et al. 2004). The VMS are within an ophiolitic mélange that can be traced for about 40 km and comprising pillow lavas, amphibolite, sheeted dykes, dunite, serpentinite and harzburgite, intercalated with layers of banded iron-formation (BIF). The mélange lies at the tectonic boundary between an ancient island arc complex and a foreland fold-and-thrust belt. The Wutai deposit consists of stacked lenses and concordant sheets of massive sulphides hosted in amphibolite, rhyolite, BIF and metasedimentary rocks; the BIF are the dominant host and are interpreted as an exhalative sequence associated with the sulphides (Li et al. 2002, 2004). Massive sulphide bodies range from 100 to 1,000 m in strike length, with thicknesses ranging from 50 to 60 m, down to only 0.3 m in the distal parts. The depth extension is highly variable, from 20 to 500 m. Li et al. (2004) reported relics of chimney structures, associated with clastic sulphides, silica exhalites and stockwork zones of pyrite and chalcopyrite, forming pipe-like bodies (probably feeders). The massive sulphides have pyrite as the dominant ore mineral, followed by

variable quantities of pyrrhotite, bornite, marcasite, chalcopyrite, sphalerite, galena, magnetite, barite, anhydrite and siderite. Alteration mineral phases include quartz, calcite, chlorite, sericite and epidote. The ores can be massive lenses, banded (pyrite interleaved with BIF) and clastics. The latter forms layers on the flanks of the massive lenses, interpreted as talus surrounding the original chimneys. Exhalite material consists of fine-grained laminations of silica and/or carbonate with disseminated pyrite that are interpreted as vent complexes. Li et al. (2004) suggested that the Wutai VMS is comparable to Cyprus-type sulphide mineralisation, formed in a suprasubdcution zone setting.

In the Liaoji metallogenic belt in the NE of the NCC (Liaoning province) there are more than 100 VMS deposits and occurrences, as well as iron deposits (BIF-hosted, see below) and a shear-zone hosted Au deposit (Nanlongwangmiao) with a Rb-Sr isochron age of 2.41 Ga (Li et al. 1995), located in the Archaean Hunbei granite-greenstone terrane (Fig. 3.8). Of these, the economically most important is the Hongtoushan VMS (Zn-Pb-Cu), which was recently studied by Gu et al. (2007). The reserves of this deposit are about 0.5 Mt grading 1.72 % Cu, and 0.7 Mt grading 3.04 % Zn, 20 t of Au at 0.5–0.8 g/t and 1,000 t of Ag at 20–60 g/t (Gu et al. 2007; Nokleberg 2010). The following is summarised from the work of Gu et al. (2007).

The Hunbei granite-greenstone terrane consists of Early Archaean gneisses and amphibolites of Qingyuan Group. The gneissed have tonalitic, trondhjemitic and granodioritic composition and the amphibolites are part of supracrustal rocks. The Hunbei terrane is in fault contact with other granite-greenstone terranes to the south (Longgang terrane) and to the northeast (Jingjiagou). The Qingyuan Group is subdivided into the Jinfengling and Hongtoushan Formations, consisting of several hundred metres of biotite and quartz-feldspar geniss, anthophyllite- and sillimanite-bearing biotite and quartz-feldspar gneiss, a roughly 100 m thick succession, referred to as "*rhythmical member*" and containing the massive sulphides. Quartz-magnetite rocks (banded iron-formation, BIF) overlie the *rhythmical member*. The precursor rocks of the Qing Yuan Group are 3.0 Ga mafic, intermediate to felsic volcanic rocks of tholeiitic to calc-alkaline affinity and metamorphosed to upper amphibolite facies between 2.9 and 2.8 Ga, with a calculated peak metamorphic temperature of 600–650 °C. Post-orogenic granitic intrusions first dated at ca. 2.55 Ga and metamorphosed to gneiss, but subsequently shown to be of Mesozoic age (ca. 160 Ma; Gu et al. 2007) are present in the area. However, post-ore mafic dykes have zircon U-Pb ages of about 2.54 Ga. The sulphide orebodies are stratiform, but extensively deformed and, as mentioned above, hosted within the "*rhythmical member*" which, from base to top, is made up of five submembers, namely: (1) 20 m of biotite gneiss, quartz-feldspar gneiss, intercalated with amphibolite, (2) 20 m of amphibolite intercalated with gneisses, (3) 25 m of interbedded hornblende gneiss, biotite- and quartz-feldspar gneisses, (4) 25 m of garnet-sillimanite-anthophyllite gneisses, (5) 12 m of quartz-feldspar gneiss interbedded with hornblende and biotite gneiss. The sulphide zones are usually within the fourth submember. At least three deformation events are recognised (D_1, D_2, D_3), which occurred between 2.8 and 2.5 Ga and characterised by axial foliations (D_1), steeply dipping or vertically plunging folds and north-northeast-trending lineations (D_2), followed by north-south-trending vertical

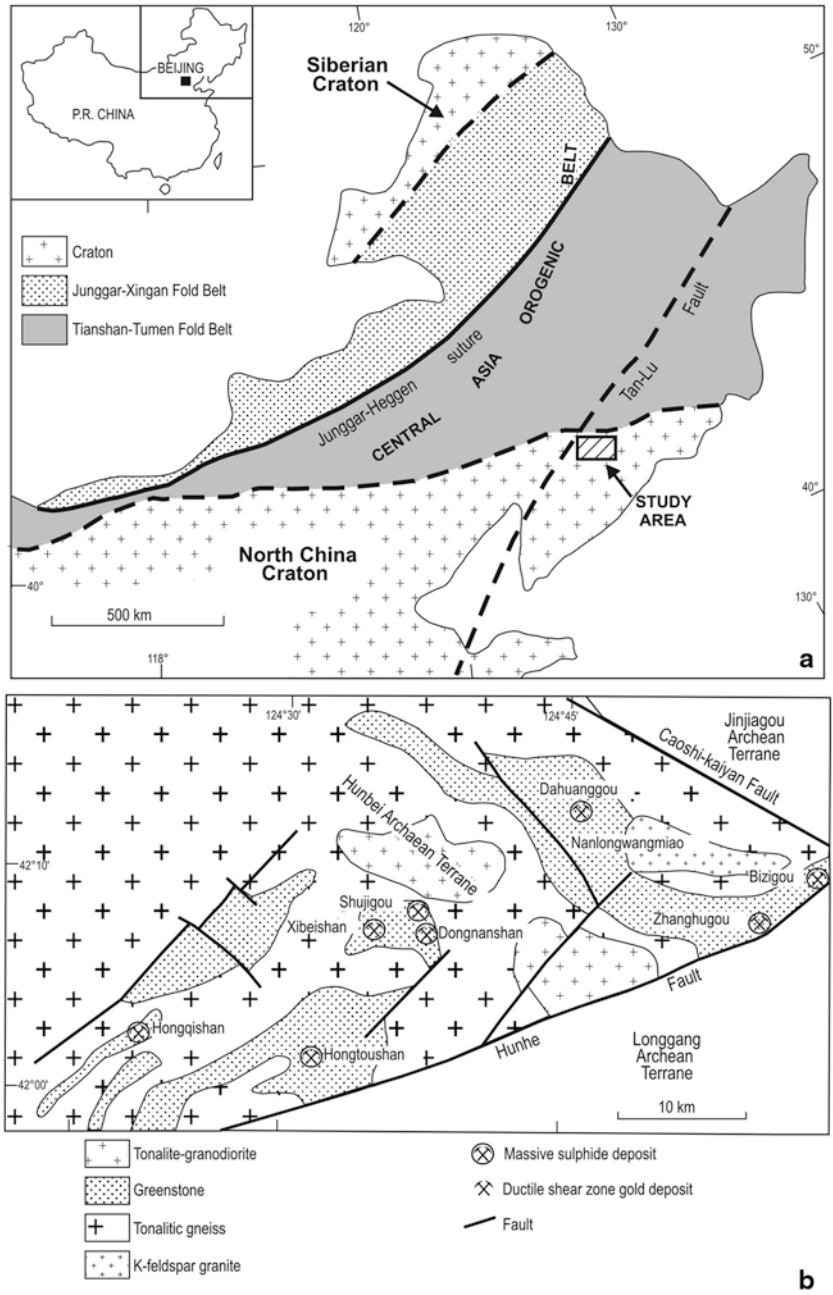

Fig. 3.8 **a** Position of Hunbei granite-greenstone region in the northeast of the North China Craton, close to the Tan-Lu Fault; **b** distribution of VMS deposits in the Hunbey belt. (After Gu et al. 2007)

to slightly inclined folds (D_3). As a result the sulphide zones form vertically plunging synformal folds, with a vertical hinge at the junction of a three-arm (Y shape) orebody. The sulphide ores are massive, locally banded with alternating folded sulphide and gneiss layers. Gu et al. (2007) reported that stringer or feeder zones had not been identified for the submarine exhalation responsible for the deposition of sulphide lenses, although disseminated sulphides are present in the surrounding rocks. The massive sulphide layers can be more than 100 m long and tens of metres thick, mostly with uneconomic grades, but enclosing economic ore zones. In addition, ore shoots with mylonitic textures, ranging in size from 2 to 30 m long and 0.1–1.5 m wide and 2–30 m deep, are also enclosed in the massive sulphide layers and account for 10 % of the ore reserves. The ore minerals are pyrite, pyrrhotite, chalcopyrite, sphalerite, associated with lesser amounts of cubanite, electrum, chalcocite and magnetite. Gangue mineral are quartz, plagioclase, garnet, hornblende, actinolite, biotite, muscovite and gahnite. The presence of garnet and gahnite, associated with high temperature metamorphism, would also suggest that perhaps some degree of sulphide melting occurred, with the possibility that melt segregations from the original sulphide lenses may have resulted in the physical separation of the economic from the uneconomic ores (see Frost et al. 2002 for more information on sulphide melting). Sulphides have $\delta^{34}S$ values ranging from -1.2 to $+5.6$ ‰ (relative to Canon Diablo Troilite; CDT), suggesting magmatic derivation. The ores are also characterised by millimetre-size veins and irregularly-shaped centimetre-size vugs with pyrite, chalcopyrite, pyrrhotite and sphalerite. Pyrite has porphyroblastic textures, whereas gangue minerals in the sulphide ores are characterised by globular textures, ranging in size from 2 to 10 mm. The reader is referred to Gu et al. (2007) for a detailed account of the mineralogical and textural features of the sulphide minerals in the Hongtoushan VMS deposit.

Ductile deformation textures characterise the Hongtoushan sulphide ores. Mylonitic ores exhibit ductile shear deformation, with the more brittle pyrite showing cataclastic minute fragments. Ductile foliation results in gneissic-type layering of pyrrhotite and sphalerite. Some minerals, such as plagioclase, hornblende, epidote, magnetite and pyrite, exhibit dominant cataclastic textures, commonly resulting in the formation of porphryroclasts (e.g. pyrite) aligned along shear directions. Other minerals, such as biotite, quartz, chalcopyrite, pyrrhotite and sphalerite, are more prone to plastic deformation and do not form porphyroclasts. The more ductile chalcopyrite is remobilised, forming anostomosing cross-cutting veinlets or filling cracks of pyrite porphyroclasts. By contrast hydrothermal alteration minerals, hornblende, actinolite, epidote, clinozoisite, biotite, albite, carbonate and quartz, appear undeformed, occurring as veinlets and patches replacing the deformed minerals.

Gu et al. (2007) proposed that the Hongtoushan intesely deformed and metamorphosed massive sulphide layers were originally formed by submarine exhalations on the sea floor. As mentioned above, and based on biotite-garnet geothermometry and presence of gahnite, probable peak metamorphic temperatures of 650–600 °C are likely. The high-temperature metamorphism effectively destroyed the original depositional ore textures, with present textures reflecting peak and post-peak

metamorphism. Both physical and chemical remobilisation occurred, the latter represented by the presence of undeformed sulphide-quartz veins, interpreted as channels for post-metamorphism fluid flow. It is of interest to note that Gu et al. (2007), suggested that Au and Cu abundances were especially enhanced in ductile shear zones and ore mylonites. The sequence that led from the sea floor sulphide mounds to the mylonitic and Cu-Au enriched ore shoots is portrayed in Fig. 3.9. Similar conditions have been recorded for the VMS ore systems in the Matchless Amphibolite Belt in Namibia (see Pirajno 2009 for an overview).

The Hongtoushan deposit, provides a good example not only of an Archaean VMS in the NCC, but also of the effects of metamorphism and deformation on sulphide layers, formed by hydrothermal exhalations on the sea floor.

Banded Iron-formations

Banded iron-formation (BIF) hosted Fe deposits are present in Archaean and Palaeoproterozoic rocks of the NCC and are listed in Table 3.1. The isotopic ages of these BIF range from ca. 3.5 to 2.5 Ga and are interpreted to be of the Algoma-type, formed in back-arc basin or island arc settings (for an overview of types of BIF, see Clout and Simonson 2005; Trendall and Blockley 2004; Bekker et al. 2010). Superior-type BIF deposits are also present in the NCC and these are discussed in Section "Superior-type BIF".

The main BIF-hosted Fe deposits in the NCC occur in the Jidong, Liaoji, Wutai, Jiliaojiao, Luliangshan and Qinglong metallogenic belts (Table 3.1), described in the comprehensive and monumental volume edited by Nokleberg (2010), in which it is reported that the above mentioned metallogenic belts also contain shear zone-hosted Au deposits. However, the origin of these lode deposits, although within the NCC, may be related to the Indosinian and Yanshanian tectono-thermal events (see below). One of these Au lode deposits is Hadamengou described below in Section "Hadamengou", which is spatially associated with metamorphosed BIF. The following short review of Algoma-type BIF in the NCC is taken from the work of Nokleberg (2010).

The Jidong metallogenic belt (eastern Hebei Province) was developed in Archaean-Proterozoic rocks, extends for about 300 km and is 50 km wide and is related to volcanic and sedimentary processes in small volcano-sedimentary basin. Supracrastal rocks of the Qianxi Group and Dantazi Group were metamorphosed to granulite and amphibolite facies, folded and with thrust structures. The BIF deposits of this belt include: Shuichang, Miyun, Shirengou and Sijianying. The Shuichang BIF deposits (e.g. Qian'an Fe ore mine) consist of layers and lenses of iron ore with an average thickness of 10 m and from 170 to 300 m long. Reserves are about 100 Mt with 25–35 % Fe. Ore minerals are coarse-grained magnetite associated with minor pyroxene and garnet. Host rocks, with Rb-Sr ages of more than 3.5 Ga, are biotite gneiss, sillimanite gneiss, thought to be derived from volcanic rocks, felsic volcanogenic greywacke and siltstone. The Sijiaying BIF belt is about 25 km long, trending N-S, the main deposit consists of multiple layers hosted in biotite gneiss,

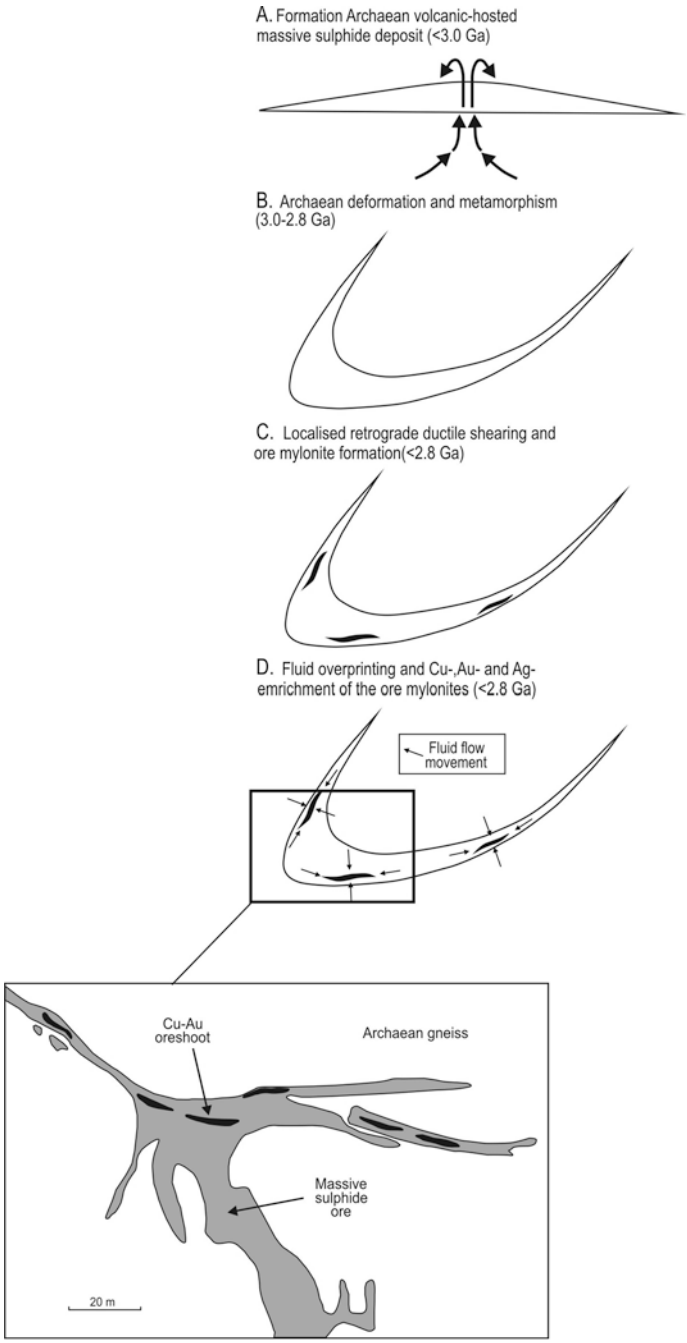

Fig. 3.9 Sequence of (<2.8 Ga) deformation events that affected a VMS ore lenses into mylonitic Cu-Au enriched ore shoots. (After Gu et al. 2007)

Table 3.1 Selected Archaean and Palaeo-Mesoproterozoic BIF deposits in the North China Craton. (Modified after Nokleberg 2010)

Name	Mineral deposit types (major deposits)	Unit or structure related to origin of belt	Age range	Tectonic event for origin of metallogenic belt
Major BIF Belts—Archaean (> 2.5 Ga)				
Jidong metallogenic belt	Banded iron formation (Shuichang (Fig. 3.11), Sijiaying)	West Liaoning-Hebei-Shanxi granulite-orthogneiss terrane	U-Pb isotopic age, 2.5 Ga	Banded iron formation (Algoma-type) deposits are interpreted as having formed in a back-arc basin
Liaoji metallogenic belt	Banded iron formation (Gongchangling); Volcanogenic Zn-Pb-Cu massive sulphide	Jilin-Liaoning-East Shandong terrane	Late Archaean. Metamorphic age of the Anshan Group hosting the banded iron formation deposits is 2.5–2.6 Ga. Isotopic age of the banded iron formation deposits units is probably older than 2.8 Ga. U-Pb zircon isotopic age for trondhjemite (mylonite) is 3.8 Ga	Host greenstone belt in the Northern Liaoning (Hubei) area interpreted as having formed in an active continental margin whereas the greenstone belts in the Anshan-Benxi and Jiapigou areas are interpreted as having formed in oceanic rifts along a continental margin
Wutai	Banded iron formation (Baizhiyan)	West Liaoning-Hebei-Shanxi terrane (granulite-orthogneiss)	Archaean. Isotopic ages of <2.5 Ga	Wutai greenstone belt and contained banded iron formation deposits interpreted to have formed in an island arc
Major BIF Belts, Palaeoproterozoic (2.5–1.6 Ga)				
Jiliaojiao	Banded iron formation (Dalizi)	East Shandong-East Liaoning-East Jilin rift basin overlying the NCC	Late Palaeoproterozoic. Metamorphism and intense deformation at 1.9 Ga. Palaeoproterozoic Dashiqiao Formation has isotopic ages of 1.7–1.5 Ga. Marble in the Proterozoic Liaohe group has isotopic age of 1.8 Ga	Passive continental margin, possibly as part of the Paleoproterozoic East Shandong-East Liaoning-east Jilin rift
Luliangshan	Banded iron formation (Yuanjiachun)	Hutuo rift basin or foreland basin	Early Palaeoproterozoic. Pb-Pb isotopic age of 2.23 Ga. U-Pb zircon isotopic age of 2.37 Ga	Banded iron formation deposits iron and shear zone Au deposits are interpreted as having formed in a Paleoproterozoic Hutuo Basin that was superposed on the Archean Northern China craton
Qinglong	Banded iron formation (Zhalanzhangzhi)	West Liaoning-Hebei-Shanxi terrane	Palaeoproterozoic	Banded iron formation deposits hosted in marine volcaniclastic and clastic sedimentary rocks with minor conglomerate, metamorphosed to amphibolite and greenschist facies. Belt is interpreted as having formed in a passive continental margin or aulacogen

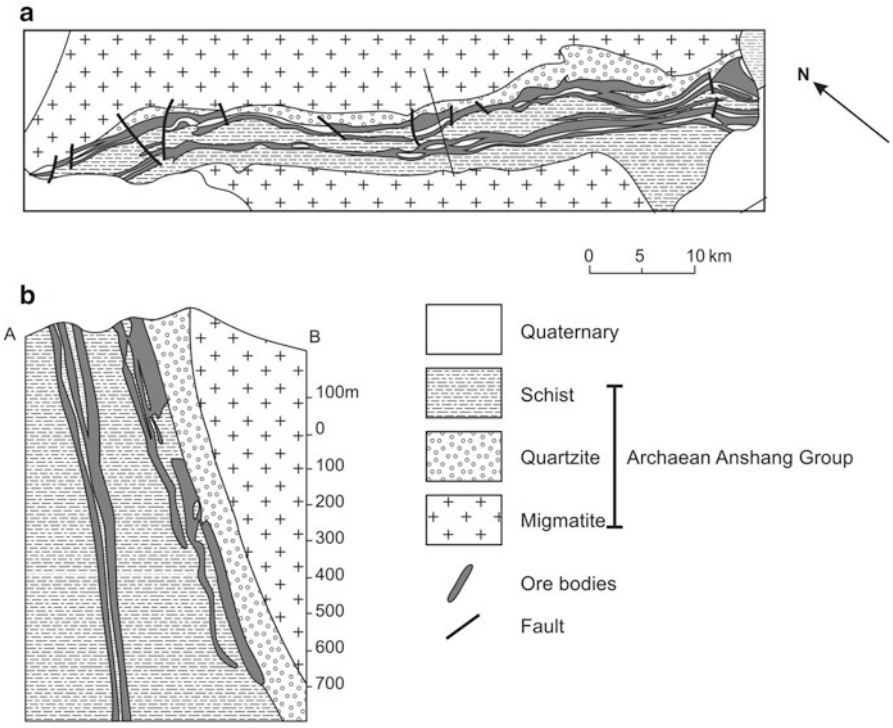

Fig. 3.10 Algoma-type BIF Gongchangling iron deposit in the Liaoji belt; simplified geology (**a**) and cross-section (**b**). (After Nokleberg 2010)

K-feldspar gneiss, amphibolite, quartzite and marble. The deposit contains reserves of 2.2 billion tonnes (Bt), grading 30–50 % Fe. The ores consists of magnetite and quartz, and locally of hematite, with minor actinolite, tremolite, amphibole and some sulphides.

The Liaoji BIF belt comprises several deposits hosted in amphibolite facies supracraustal rocks of the Anshan, Qingyaun and Longgang Groups, represented by mafic, intermediate and felsic metavolcanic and metaclastic rocks deposited in basin structures formed in a continental margin setting. One of the main iron deposit is Gongchangling (Liaoning province), hosted in the ca. 2.65–2.5 Ga Anshan Group (also known as Tagushan Group; Zhang 2009; Fig. 3.10). This deposit has reserves of some 760 Mt grading 32.8 % Fe. Individual stratiform orebodies are several metres to several tens of metres thick and up to 1 km long. The ore minerals are magnetite, maghemite, with lesser amounts of pyrite and pyrrhotite, accompanied by various amounts of graphite, quartz, garnet, cummingtonite. The development of these BIF-hosted Fe ores is thought to be the result of either enrichment of primary siderite during high-grade regional metamorphism, or hydrothermal reworking. The latter hypothesis is supported by the fact that the Anshan Group was intruded by

two periods of granitic intrusions at 2.3–2.1 Ga and 1.9–1.7 Ga, during which hydrothermal enrichement of the BIF may have occurred, perhaps in the combination of hypogene-supergene model advocated by Thorne et al. (2004), or the hypogene alteration proposed by Lobato et al. (2008).

In the Wutaishan area (western Shanxi province) BIF units extend along a belt 200 km long and up to 20 km wide, where iron deposits are hosted in the Wutai Group (Baizhiyuan and Jinganku Formations) with poorly constrained istopic ages of >2.5 Ga. Rocks of the Wutai Group are mainly mafic and felsic volcanic rocks and sedimentary rocks in a greenschist facies greenstone belt. The main deposit is Baizhiyan, which consists of BIF layers 30–50 m thick and 3–5 km long, totalling reserves of about 180 Mt grading 33 % Fe. The ores consist of an oxide facies with magnetite and quartz, a silicate facies with magnetite, quartz and grunerite and a carbonate facies with siderite and ferrodolomite.

Metamorphosed BIF occurs in the Archaean Daqingshan granulite belt (Inner Mongolia) on the northwestern margin of the NCC where, as mentioned above, it is associated with the Hadamengou lode Au deposit. This BIF consists of magnetite-quartz-granulite and magnetite-garne-plagioclase-quartz gneiss (Gan et al. 1994).

A well-studied Algoma-type BIF deposit is the ca. 2.5 Ga Shuichang iron deposit in eastern Hebei province, one of the largest in the region (Zhang et al. 2011b). Other Algoma-type BIF-hosted Fe deposits in the region are Shirengou, Xingshan, Mengjiagou, Sijiaying and Zhaianzhangi. The age of the Shuichang BIF is likely to be $2{,}516 \pm 5$ Ma, by SIMS U-Pb dating of zircons from the hosting plagioclase-hornblende gneissic rocks. The Shuichang BIF is within in deformed (Shuichang-Beitun fold belt) high-grade metamorphic rocks of the Neoarchaean Qianxi Group, which consists of hypersthene granulite, biotite-plagioclase gneiss, pyroxene-plagioclase gneiss, plagioclase-hornblende gneiss, biotite migmatitic gneiss, hypersthene migmatitic gneiss, pyroxene-garnet granulite and magnetite quartzite. The Shuichang BIF extends for about 3,200 m in a northeast direction and in the mine area a synclinal structure contains three ore lenses (Fig. 3.11a, b). Magnetite quartzite is the principal ore, accounting for 95 % of the total (Fig. 3.12). Martite quartzite is also present as an weathered product of magnetite and therefore is found only at and near the surface. Zhang et al. (2011b) classified the magnetite quartzite ore into four types, based on the width and continuity of individual bands, as follows: (1) Finely laminated magnetite quartzite, with laminations less than 1 mm thick; (2) magnetite quartzite with laminations from 1 to 3 mm wide; this is the most common and economically important ore with good lateral continuity, the quartz laminations are slightly wider than the magnetite and the boundaries between the two are sharp; (3) coarsely-laminated magnetite quartzite, with laminae from 3 to 5 mm wide; and (4) banded magnetite quartzite, in which the bands are wider than 5 mm and with good continuity and with the quartz bands being wider than the magnetite ones.

Zhang et al. (2011b) used zircon U-Pb dating, Hf isotopic and geochemical data of the host lithologies to determine the nature of the protolith and constrain the age and type of the Shuichang BIF. Major and trace element geochemistry of these

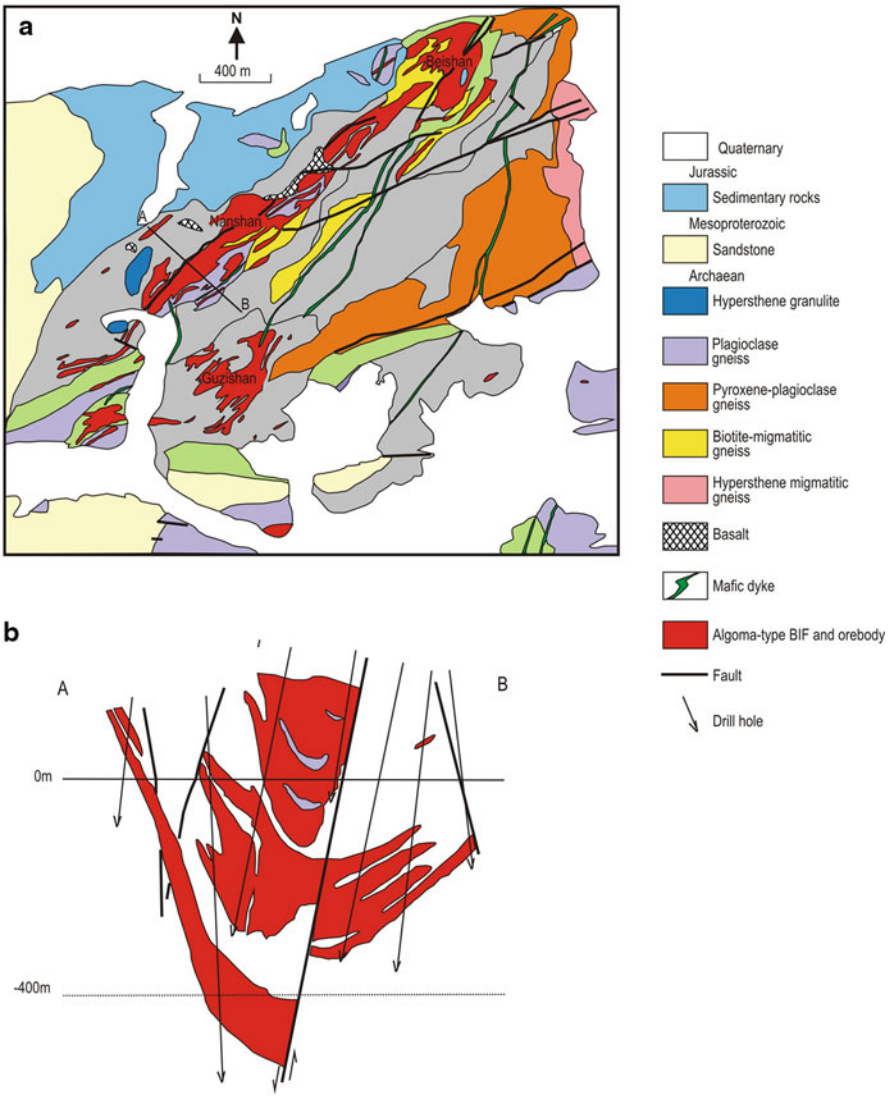

Fig. 3.11 **a** Simplified geologic map of the Shuichang area and distribution of the Algoma-type BIF; **b** cross-section of the Shuichang iron deposit. (After Zhang et al. 2011b)

rocks is consistent with volcanic protoliths of a back-arc tectonic setting ((al + fm)-(c + alk) and Al_2O_3 vs ($Na_2O + K_2O$) discrimination diagrams). Trace element geochemistry and chondrite-normalized REE patterns of individual magnetite and chert bands are suggestive of hydrothermal Fe and Si. For example, positive La anomalies with $La/La^*_{PAAS} = 1.05 - 1.35$ are recorded for the magnetite bands and

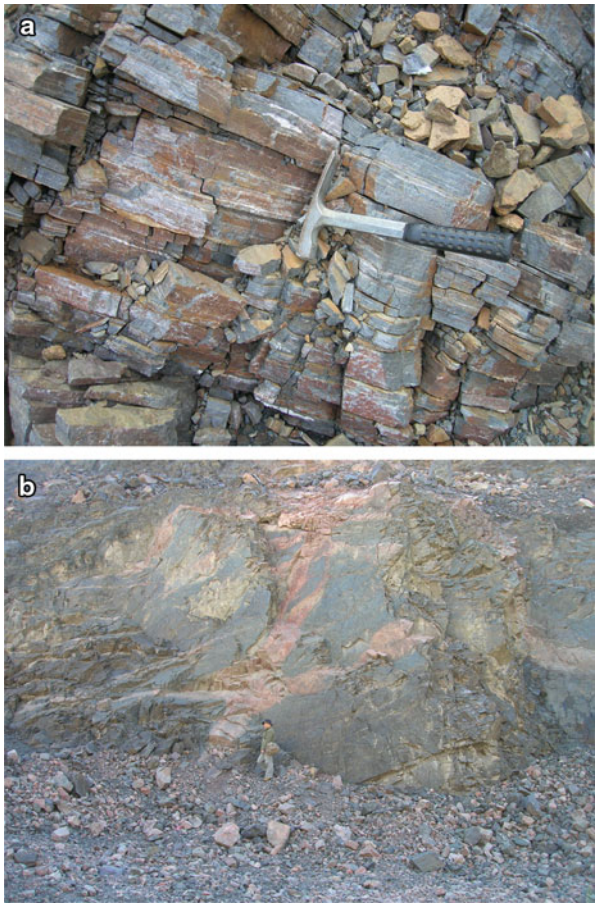

Fig. 3.12 Field photographs of Shuichang Algoma-type BIF, **a** typical ore; **b** syenite (possibly of Yanshanian age) intruding the Shuichang BIF

1.07–1.35 for the chert bands, with all bands showing Eu enriched characteristics with Eu/Eu* of 1.86–3.23. Generally, Algoma-type BIFs are related to volcanic activity, resulting in these rocks having relatively high Eu/Eu^*_{PAAS} ratio (>1.8), whereas Superior-type BIFs are not related to volcanism and therefore they display relative low Eu/Eu^*_{PAAS} ratios (<1.8) (Huston and Logan 2004). The Eu anomalies of the samples from Shuichang, show that the BIF ore formed by submarine exhalative hydrothermal processes, and confirm that the Shuichang BIF fits the Algoma-type definition. Submarine hydrothermal effluents associated with volcanic activity, may have supplied the iron and silica of the Shuichang BIF.

Also in eastern Hebei is the 2.5 Ga Shirengou Algoma-type BIF-hosted iron deposit, about 70 km west of Shuichang. The iron deposit, studied by Zhang et al. (2011a), is hosted in metamoprhic rocks of the Neoarchean Malanzhuang Formation in the Qianxi Group. The metamorphic rocks the Qianxi Group consist of hornblende plagiogneiss, plagioclase amphibolites, granitic migmatite and magnetite quartzite.

The protolith of the host rocks, plagioclase amphibolite and plagiogneiss, are interpreted as basaltic andesite, and dacite, respectively. Zhang et al. (2011a) assessed their geochemical signatures on the basis of trace elements discrimination diagrams, which exhibited enrichment in large ion lithophile elements (LILE), Rb, K, The and Sr, and depleted in heavy rare earth (HREE), Yb, high field strength elements (HFSE), Nb, Ta, and Ti. These authors concluded that the volcanic rocks originated in an island-arc or back-arc basin. The zircons contained in these metavolcanic rocks provided the ideal means to constrain the age of the Shirengou Algoma-type BIF, as was the case for the Shuichang BIF. U-Pb ages of igneous zircons from amphibolite and gneiss, yielded of $2{,}541 \pm 21$ and $2{,}553 \pm 31$ Ma (Neoarchaean), whereas metamorphic overgrowths yielded $2{,}512 \pm 13$ and $2{,}510 \pm 10$ Ma, respectively and relating to a later metamorphic event.

The total Fe_2O_3 in the Shirengou BIF-hosted Fe deposit ranges from 26.93 to 52.02 %. The iron deposit comprises three parallel orebodies, referred to as I, II and III. The No. I is the main orebody, is 4,200 m long and 9–40 m thick (averaging 25 m), east-west trending and dipping west at angles of 50–75°. The orebodies extend to depths of more than 600 m. The ore consist of alternating quartz-rich (metachert) and magnetite-rich bands or laminae in hand specimen. These BIF are locally micro-banded, with quartz, magnetite and, occasionally, grunerite micro-laminae. The banding is well preserved in spite of the high-grade metamorphism. Magnetite ranges from 0.05 to 1.2 mm in size, with the majority falling within a range of 0.25–1.0 mm. Zhang et al. (2011a) concluded that the Shiregou BIF was formed during periods of quiescent volcanic activity by submarine exhalative processes.

3.2.4.2 Metallogenesis in Palaeo-Mesoproterozoic Rift Basins

Between 1.8 and 1.4 Ga, some rift basins were formed subparallel to the zone of collision between the Siberian Craton and the NCC, whereas others are north-northeast trending (Xiong'er rift; see Chap. 7) on the southern margin of the NCC. In places, this rifting was accompanied by subalkaline and alkaline magmatism. The major rifts superimposing on the NCC, include (Nokleberg 2010): the Hutuo rift, the Shandong-East Liaoning-East Jilin rift, the Zhangbei-Bayan Obo-Langshan rift and the Hebei-Liaoning basin. The rifting and formation of passive continental margins were probably the result of the onset of the breakup of a Paleoproterozoic supercontinent. In this section, the metallogeny associated with rift structures that were formed during Palaeo- and Mesoproterozoic times are reviewed. Prominent amongst these is the giant, world-class, polygenetic Bayan Obo REE-Nb-Fe deposit, which is discussed below, and interpreted as being related to a carbonatite magma and associated hydrothermal activity. The Paleoproterozoic and Mesoproterozoic Zhangbei-Bayan Obo-Langshan rift basin and related metasedimentary and metavolcanic units formed along the passive continental margin of the NCC. The Yanliao belt contains chemical-sedimentary Mn (Wafangzi) and sedimentary exhalative Pb-Zn (SEDEX) deposits in the Jixian Group that are interpreted as having formed in a shallow marine basin

on the NCC. Superior-type BIF, listed in Table 3.1, are associated with passive continental margins, developed along the northern margin of the NCC, characterised by intermediate to felsic volcanic rocks and thick successions of clastic and carbonate rocks. At a later stage, greenschist to amphibolite facies metamorphism, transformed these rocks into biotite-, hornblende- or diopside-bearing gneiss, intercalated with graphite-bearing biotite gneiss, amphibolite, marbles, calc-silicate rocks, phyllite, muscovite-biotite schist and dolomitic marbles (Nokleberg 2010).

Superior-type BIF

The Palaeo-Mesoproterozoic Qinlong and Jiliaojiao composite metallogenic belts contain several mineral systems, including Superior-type BIF deposits (Table 3.1). The Qinlong belt in the western Liaoning-Hebei-Shanxi terrane comprises Superior-type as well as Algoma-type BIF, formed in a passive continental margin and a rift setting, respectively. The Jiliaojiao belt is in the northeastern part of the NCC, is about 800 km long and 50–100 km wide, within a rift basin overlying the Archaean rocks of the NCC from the Liaodong peninsula to the Shandong peninsula. The BIF-hosted Fe deposits in the belt are associated with a thick volcano-sedimentary succession of the Laoling, Laohe, Jingshan and Fenzishan Groups. Little is known about the BIF deposits of the Qinlong and Jiliaojiao belts in both Chinese and English literature.

The Palaeoproterozoic Luliangshan belt of Superior-type BIF is hosted in the Hutuo basin and is more than 200 km long and 40–60 km wide. The BIF deposits are associated with greenschist facies metamorphosed clastic and marble rocks of the Hutuo Group. In this belt, Yuanjiachun is the main iron deposit with reserves of about 895 Mt at 32.4 % Fe. The Fe ore units extend along strike for up to 10 km and attain thicknesses of 300 m. Ore minerals include hematite, magnetite and specularite, accompanied by cummingtonite and stilpnomelane. The BIF was possibly in a cratonic passive margin.

The Qinlong BIF belt is in the northern part of the NCC within the volcano-sedimentary basins in eastern Hebei province. The belt is 80 km long and up to 30 km wide and the BIF are in amphibolite facies metaclastic rocks of the Qinglonghe Group, in which the main deposit is Zhalanzzhangzi. The ore zones of this deposit are 2 km long and 10–30 m wide with total estimated reserves of about 200 Mt but with low grades. Magnetite is the principal ore mineral, associated with quartz, actinolite, tremolite, cummingtonite, calcite, garnet, biotite and pyrite. The Qinlong BIF is thought to have formed along a passive continental margin, or within an aulocogen.

Bayan Obo REE-Nb-Fe Polygenetic-polychronous Deposit (Inner Mongolia)

The Bayan Obo REE-Nb-Fe deposit in Inner Mongolia contains a resource of 57.4 Mt with grades ranging from 5.17 to 6.19 % REE_2O_3, Nb reserves estimated at about 2.2 Mt with average grades from 0.126 to 0.141 % Nb_2O_3 and 1.5 Bt of Fe at an average grade of 35 % (Drew et al. 1990; Fan et al. 2005). Bayan Obo constitutes

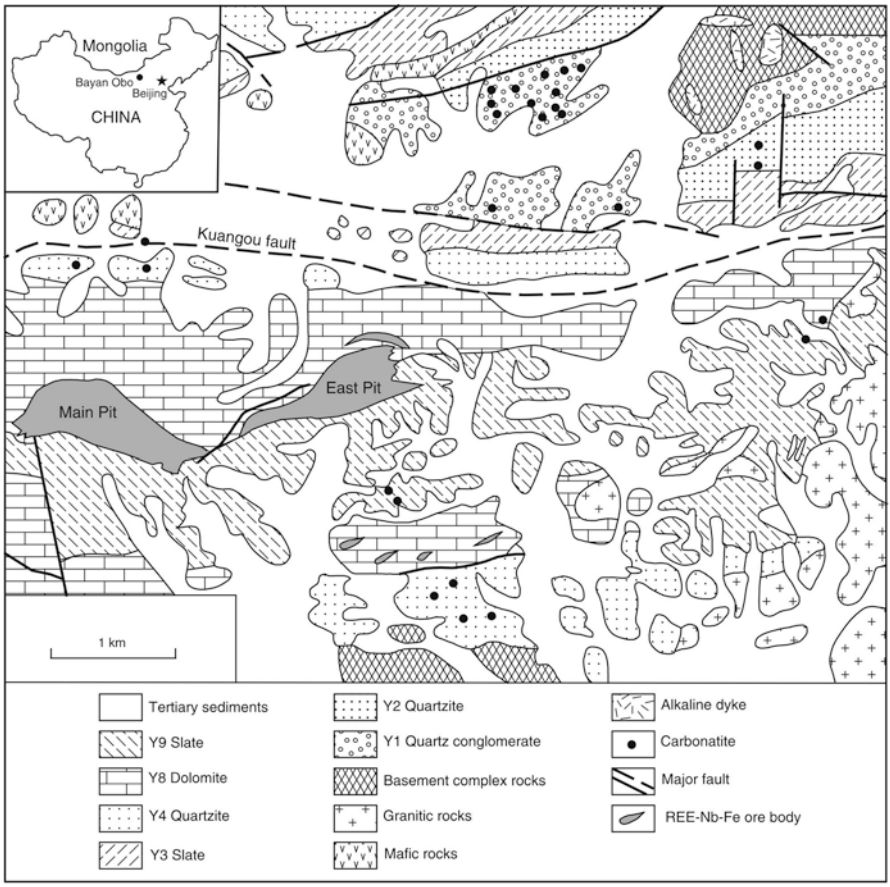

Fig. 3.13 Simplified geological map the Bayan Obo area, distribution of ore zones and carbonatite dykes, shown as dots because their length (ca. <60 m) is too small to be represented at this scale. (After Fan et al. 2004b)

the largest rare earth element (REE) resource so far discovered, representing about 95 % of China's total REE resources (Zhu 2007) and about 70 % of the world's total. This unusual deposit was discovered in 1927 by one Ding Daoheng and has been, and still is, the object of numerous studies of which, in addition to the above, I cite those of Chao et al. (1997), Smith and Henderson (2000), Smith et al. (2000), Yang and Le Bas (2004), Fan et al. (2004a, 2004b), Smith (2007) and Yang et al. (2011a, 2011b). I have drawn from these works for the account that follows.

Bayan Obo, located on the northern margin of the North China Craton (NCC), is an extremely complex, hydrothermal, stratabound mineral system hosted in carbonate rocks of the Mesoproterozoic Bayan Obo Group (Fig. 3.13). This Group is a ca. 1,850 m thick package of clastic and carbonate rocks deposited in graben structures that formed in the Archaean basement (Fig. 3.14). The Bayan Obo Group is deformed

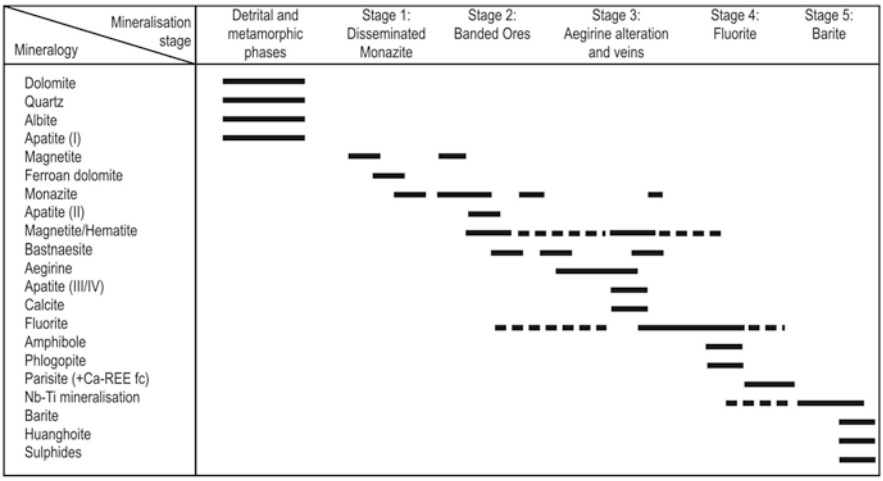

Fig. 3.14 Simplified paragenesis and mineralisation stages at Bayan Obo. (After Smith et al. 2000)

as a series of northwest-dipping thrust slices and duplex structures. Granitic rocks of Carboniferous-Permian age intruded into the basement and the sedimentary rocks and comprise diorite, granodiorite, biotite granite and leucogranite. Gold-bearing quartz veins are associated with some of these granites. Importantly, as further discussed below, is that other igneous rocks in the area include at least two suites of carbonatite dykes, with fenitised (Na-amphibole-albite-phlogopite) country rocks.

The Bayan Obo Group consists of a number of sedimentary units, variably labelled Y, H or Hb in the literature (here I use Y). These consists of a basal conglomerate and sandstone (Y1 unit), overlain by a succession of carbonaceous shale, arkosic sandstone and quartzite (Y2 to Y7 units), followed by limestone and dolomite beds (Y8 unit hosting the mineralisation), black shale (Y9), capped by white and grey limestone (Y14 to Y18 units). Drew et al. (1990) emphasised that the palaeoenvironmental setting of the base of Y8 is very important for the understanding of the origin of the Bayan Obo system, interpreted as representing a barrier island sequence with numerous tidal channels, from 1 to 3 m across and 0.5–1 m deep, filled with clastic sediments. This sequence was disrupted by thrust faulting resulting in misinterpretations that suggested that the chaotic nature of the sedimentary beds were due to stoping by carbonatitic magma. The 350 m-thick Y9 shale is conformable on the Y8 unit and it probably acted as a seal to the hydrothermal fluids. This shale is extensively brecciated and altered by potassic metasomatism in the core of the syncline where the orebodies are located. Volcanic rocks, possibly of Carboniferous age, within a fault-bounded tectonic slice comprise rhyolitic flows, domes, breccia and pyroclastics, hosting a volcanogenic massive sulphide deposit of the Kuroko style. As mentioned above, the structural setting of the Bayan Obo area is very complex and this complexity has hindered a clearer understanding of the mineral system. The

complex deformation is the result of collisional processes that affected the northern margin of the North China Craton, with tectonic transport from northwest to southeast. According to Drew et al. (1990), the entire deformed package is now a giant roof pendant (6–8 km across) in the Carboniferous-Permian granitic rocks, which were emplaced during the collision event.

There are three main orebodies: Main, East and West, all characterised by an Fe-rich zone, dolomite, aegirine, riebeckite, biotite and fluorite zones. The ore material is hosted by fine- and coarse-grained dolomitic marble of the Y8 unit, which is banded and consists of recrystallised dolomite, apatite, magnetite, with minor pyrochlore and Na-amphibole. Le Bas et al. (2007) suggested that the ore-hosting dolomitic marble is a carbonatite pluton that intruded the sedimentary rocks of the Bayan Obo Group. Ore minerals include monazite [(Ce,La,Nd)PO_4], bastnaesite [(Ce,La,Nd)(CO_3)F], huanghoite [Ba(Ce,La,Nd) $(CO_3)_2$F], parasite [(Ce,La,Nd)$_2$-$(CaCO_3)_3F_2$], cebaite [$Ba_2Ce_2(CO_3)_5F_2$] for the REE ores, columbite ($FeNb_2O_6$), pyrochlore [$(Ca,Na)_2Nb_2O_6(OH,F)$], fergusonite ($YNbO_4$), aeschynite [(Ce,Ca,Fe, Th)$(TiNb)_2$(O, OH)$_6$] for the Nb ores and magnetite, hematite, ilmenite, martite and goethite for the Fe ores. Barite, fluorite, apatite, cerianite, aegirine, arfvesdsonite, riebeckite, albite and microcline are common gangue minerals. Carbonate minerals, apart from dolomite, include benstonite [$(Ca,Sr)_6Ba_6Mg(CO_3)_{13}$], norsethite [$BaMg(CO_3)_2$], barytocalcite [$BaCa(CO_3)_{27}$] and strontianite ($SrCO_3$). Sulphide gangue minerals are pyrite, pyrrhotite, sphalerite, galena and chalcopyrite. The hydrothermal system that formed Bayan Obo is responsible for widespread alteration over an area of ca. 50 km^2 in both Archaean migmatites and sedimentary rocks. Drew et al. (1990) distinguished footwall and hanging wall alteration. Calcite-barite-magnetite-albite-monazite veins, up to 3 m wide, cut the footwall migmatite rocks forming alteration haloes containing aegirine, Na amphibole, albite and K-feldspar. Thinner veins and stockworks cut the Y7 and Y6 units and have the same mineralogy as those that cut the migmatites. The Y8 unit is pervasively altered as the clastic rocks and migmatites described above. Sodic amphibole, micas (annite, biotite and phlogopite) and Fe oxides are the dominant minerals. Magnetite and hematite are disseminated in the host carbonate rocks, locally forming lenses up to 20 cm thick along bedding planes in economically viable concentrations. In the hanging wall, the Y9 shale acted as an impermeable cap rock focusing the fluids derived from the reactions that replaced the Y8 dolomite, along the contact between Y8 and Y9, resulting in the emplacemet of the REE-Nb-Fe orebodies. The base of the Y9 shale is brecciated and cut by small veins and stockworks, which exhibit a zonation of alteration minerals, outward from fluorite to biotite to K-feldspar. K-feldspar is dominant alteration phase in the matrix of the brecciated material. The paragenesis of the Bayan Obo ore is also complex with 11 stages proposed by Chao et al. (1997), from deposition to metamorphism and mineralisation, to granite intrusions. This was simplified by Smith and Henderson (2000) and Smith et al. (2000), with a paragenetic sequence, shown in Fig. 3.14, comprising five stages of mineral deposition.

Age Data, Ore Genesis and Tectonic Setting

The age of the Bayan Obo mineralisation is controversial and uncertain. The K-Ar and $^{39}Ar/^{40}Ar$ isotopic systems provide a range of ages from 1,290, 900–800, 555–474, 430–420 Ma (Chao et al. 1997) to 311–306 Ma for early stage granites (mainly granodiorite) and 258–234 Ma for late stage biotite K-feldspar granites (Fan et al. 2004a and references therein). Whole-rock Sm-Nd isochron ages from the carbonatite dykes in the Bayan Obo area yield an age of $1{,}354 \pm 59$ Ma, comparable to the whole-rock Sm-Nd isochron ages of the ore-hosting dolomitic marble of $1{,}341 \pm 160$ Ma, by Yang et al. (2011b). Chao et al. (1997) distinguished three periods of regional metamorphism and metasomatism: (1) 890 Ma, with recrystallisation of the Y8 carbonate to marble; (2) 425–395 which would have formed metasomatic-metamorphic sodic amphibole; (3) Hercynian event at ca. 300 Ma. Dating of monazite, using ^{232}Th-^{208}Pb chronology, yielded ages ranging from 555 to 420 Ma, with peaks at 430–420 Ma (Wang et al. 2004). Given the wide range of ages it is likely that the Bayan Obo mineral system is polychronous and polygenic, that is the product of multiple tectono-thermal events, beginning at ca. 1,800 Ma, that successively overprinted later ones. Moreover, the variability of the age data led Yang et al. (2011b) to suggest that different types of carbonatites were emplaced sequentially, accounting for the large errors in the age determinations.

Fan et al. (2004a, 2005) working on fluid inclusions found three types: two-phase aqueous liquid-vapour (L-V), two to three-phase, almost pure, CO_2 (C) and three-phase liquid-vapour-solid (L-V-S). In the latter, daughter minerals are REE-carbonates (cebaite and bastnaesite), halite, sylvite, barite and calcite, identified by SEM and EDX analyses. Homogenisation temperatures of 480–420 and 250–220 °C were obtained from heating-cooling experiments on the L-V-S inclusion fluids. Salinities ranging from 1 to 15 wt% NaCl equivalent were obtained by Smith and Henderson (2000). In another paper, Fan et al. (2004b) reported on fluid inclusions from the contact zone between the Y8 dolomite and granitic rocks and referred to this zone as a skarn. The Y8 dolomite was subjected to strong metasomatism with the formation of typical skarn minerals, such as diopside, tremolite, garnet, humite, phlogopite, quartz, fluorite and magnetite. The fluid inclusions from this skarn are of three types too: two-phase primary CH_4-rich, three-phase L-V-S and two-phase aqueous. Microthermometric measurements on the CH_4-rich inclusions revealed homogenisation temperatures ranging from 344 to 280 °C; L-V-S from 280 to 200 °C, whereas aqueous inclusions showed a range from 180 to 140 °C. Fan and co-authors suggested that the CH_4-rich inclusion fluids were derived by interaction of magmatic fluids with graphitic country rocks (black shales).

Thus, the genesis of the Bayan Obo mineral system, like its age, remains controversial. Ore genesis models included synsedimentary and exhalative deposition or epigenetic hydrothermal linked to granite magmatism or A-type alkaline magmatism and/or carbonatite magma. The main question hinges on the origin of the ore-hosting Y8 dolomitic marble, with ideas ranging from sedimentary, hydrothermal, skarn to carbonatite-related. The skarn hypothesis has problems because of the age gap between the granitic rocks (ca. 311–306 and 258–234 Ma) and the age of the monazite

(555–420 Ma; Wang et al. 1994). The presence of carbonatite and albitite dykes that cut the sedimentary package a few km north and south of the orebodies and the composition of the dolomite support the carbonatite hypothesis. Yang and Le Bas (2004) showed that the Y8 dolomitic marble in the ore zone has a geochemical composition (MnO and SrO contents higher than 0.15 wt%) similar to that of the carbonatite dykes. Therefore, the ore-hosting dolomitic marble has carbonatitic affinities and is not part of the Y8 sedimentary carbonate sequence (Yang and Le Bas 2004). As mentioned above, Le Bas et al. (2007), largely on the basis of REE abundances and major elements data, proposed that the various carbonate dykes and ore-hosting dolomitic rocks, represent intrusive carbonatite (carbonatite, ferrocarbonatite and magnesiocarbonatite), which are indisputable different from sedimentary carbonate rocks.

Thus, the carbonatite model seems feasible and could be considered within the framework of intraplate A-type magmatism, linked to a mantle plume. Considering the regional context, the Bayan Obo sedimentary package, the rift setting, subsequent collision and extensional events that affected the NCC and the accompanying magmatism, it is possible that some of these magmas could have been linked to the mantle plume that originated the rifts and caused the continental volcanism and dyke swarms in the NCC at ca. 1,800 Ma. The complex paragenesis of the ores, the wide range of ages could be interpreted to reflect overprinting of the subsequent thermal, tectonic and metamorphic events.

As mentioned above and shown in Fig. 3.15, the Bayan Obo mineral system is located on the rifted margin of the NCC. The NCC was subjected to rifting events that affected both its northern and southern margins, beginning about 1,800 Ma. Rift systems were formed within the Trans-North China Orogenic Belt, which separates the Eastern and Western blocks of the NCC (Zhao et al. 2004, 2005; Kusky and Li 2003). There is reasonable evidence that this rifting was associated with the emplacement of continental flood basalts and giant dyke swarms (Peng et al. 2005, 2008). In the north, the Taihang Mountains mafic dyke swarm and the Xiong'er Volcanic Province belong to this 1,800 Ma thermal event that affected the NCC and have been linked to the breakup of the Columbia supercontinent (Wang et al. 2004; Peng et al. 2005). Peng et al. (2005) working on the geochronology of dyke swarms in the NCC, identified four dyke suites with SHRIMP U-Pb ages of $2{,}147 \pm 5$, $1{,}929 \pm 8$, $1{,}834 \pm 5$ and $1{,}778 \pm 3$ Ma. On the basis of this geochronology, Peng et al. (2005) suggested that the older group of dyke suites could relate to the amalgamation of the NCC to the Columbia supercontinent, whereas the younger suites are related to the breakup of Columbia and a mantle plume event at 1,830–1,750 Ma. This mantle plume would have been implicated in a triple-junction rifting at the southern margin of the NCC at ca. 1.78 Ga, leading to its breakup from the Dharwar Craton in India (Peng et al. 2005; Fig. 3.16). In this scenario, the Bayan Obo Group was deposited in a rift system with graben structures on the northern margin of the NCC (Fig. 3.15), estimated to have occurred between 1,800 and 1,350 Ma. Carbonatite and mafic dykes in the Bayan Obo region, have Sm-Nd isochron ages of $1{,}354 \pm 59$ and $1{,}227 \pm 60$ Ma, respectively, confirming mid-late Neoproterozoic rifting processes within the NCC and have been linked to a mantle plume that led to the breakpup of the Columbia supercontinent (Yang et al. 2011a; see also Chap. 7).

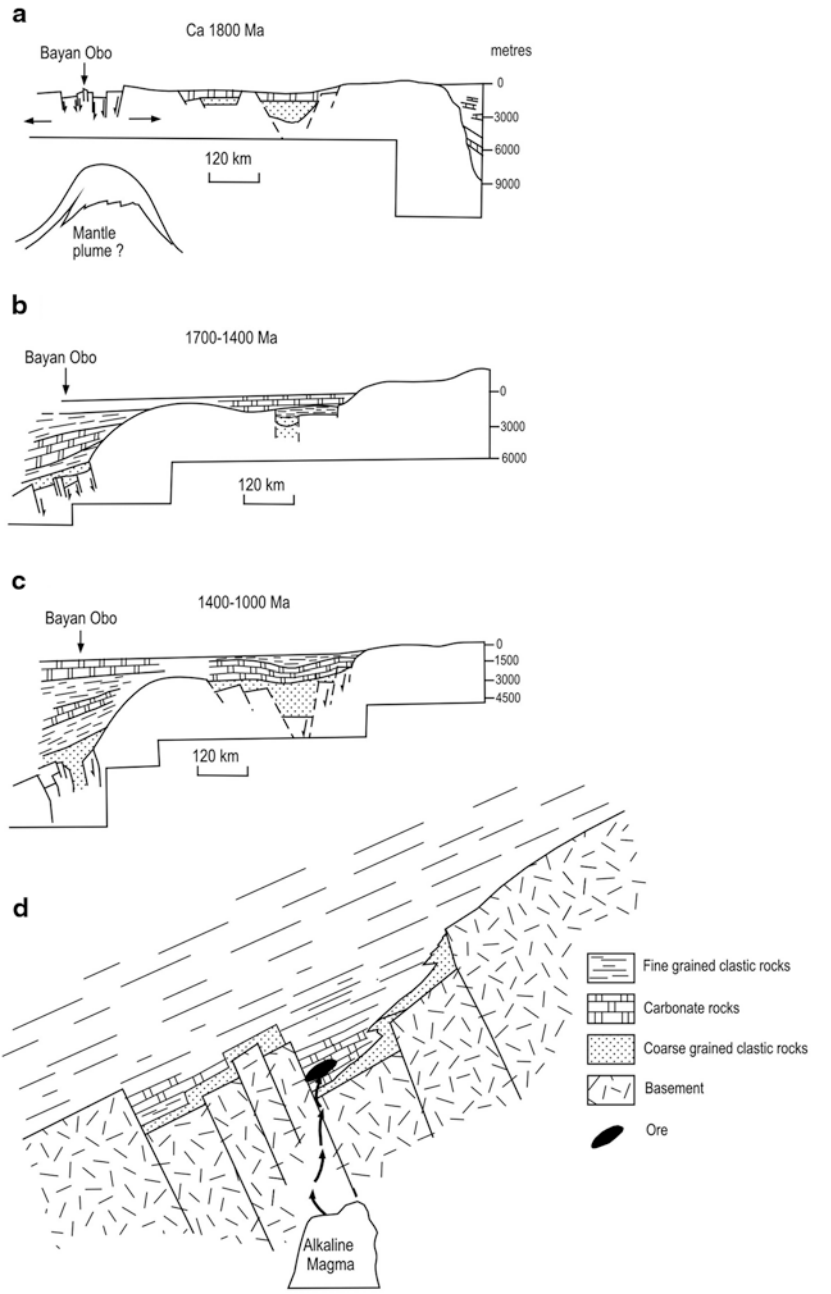

Fig. 3.15 Evolution of the Bayan Obo rift, between ca. 1,800 and ca. 1,000 Ma on the northern margin of the North China Craton (according to Drew et al. 1990). At 1,800 Ma a major thermal event occurred in the region, possibly due to a mantle plume; details in text

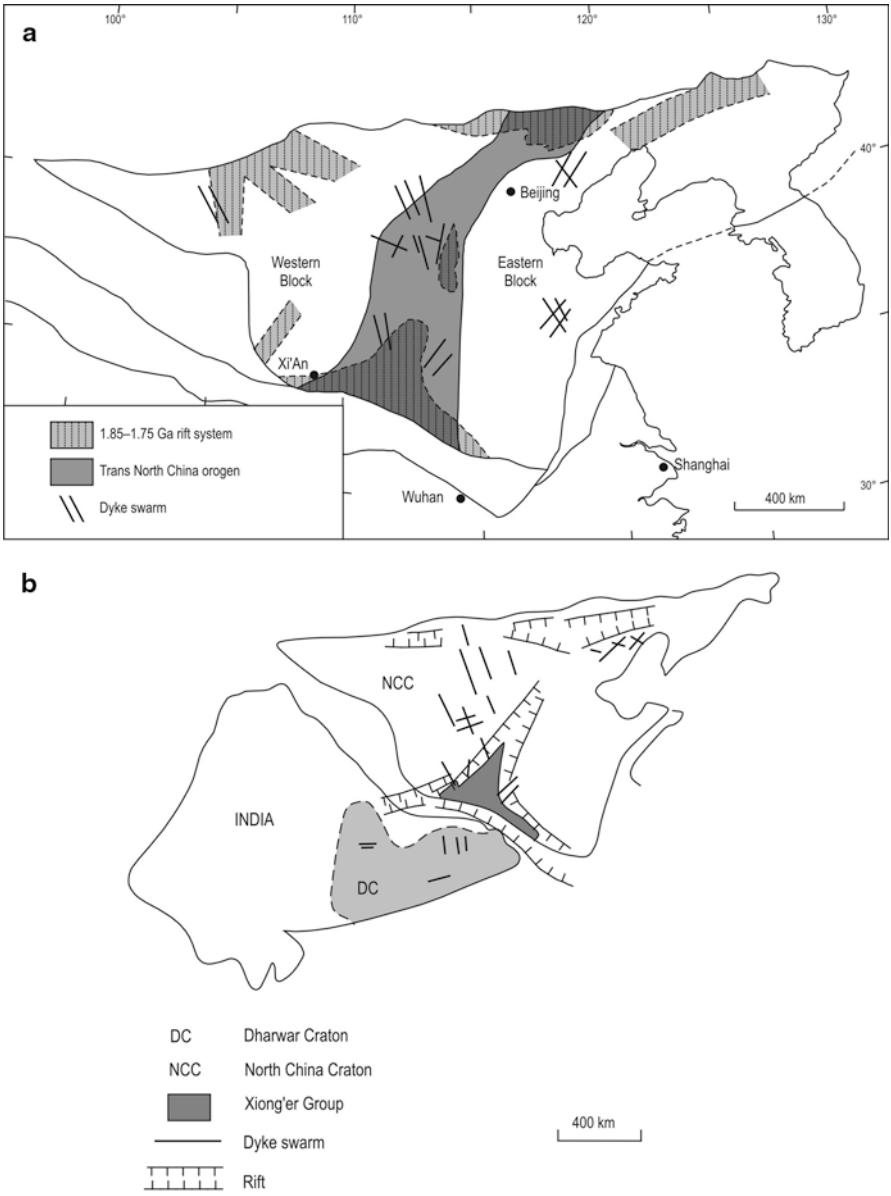

Fig. 3.16 **a** The rift system in the northern margin of the North China Craton is where Bayan Obo is located. The Xiong'er Group is represented by continental flood lavas of bimodal composition, dyke swarms occur north of the Xiong'er rift and are of the same age (ca. 1,800 Ma), which led Peng et al. (2005) to postulate the activity of a mantle plume; **b** possible join between the Dharwar Craton (India) and the North China Craton prior to breakup and postulated three-arm Xiong'er rift system. (After Peng et al. 2005)

A Transitional Submarine (Irish-type) to SEDEX Mineralisation in the North China Craton

Li and Kusky (2007) reported the occurrence of 1.43–1.48 Ga black smoker chimneys, sulphide mounds and fossil microbialites from the Gaobanhe Pb-Zn deposit, located in the northeast-trending Yanliao graben structure in the northern part of the NCC, some 150 km north of Beijing. Nokleberg (2010) listed the Gaobanhe Pb-Zn deposit as a SEDEX type, hosted in Mn shale and dolomite of the late Proterozoic Gaoyuzhuang Formation. Li and Kusky (2007) showed the sulphide deposits sitting above the manganiferous sediments in their cross-section (Fig. 2 of their paper), whereas in their Fig. 10, the sulphide mounds are shown to be spatially associated with the manganiferous sediments, a more likely scenario. Ore minerals of the Gaobanhe Pb-Zn deposit, are sphalerite, galena, and pyrite, and the ore varies from massive to banded. Framboidal, colloform, and pelletoidal pyrite are common (see below). Li and Kusky (2007) provided good evidence for chimney-like and associated microbial structures for this deposit. These authors recognised four morphological types of structures, interpreted as remnants of chimneys. Large columnar structures, represented by 5–50 cm wide fragments, which were interpreted as fragments of originally vertical chimneys. Concentric mineralogical and textural arrangements are revealed by alternating layers of sulphides, mud, carbonate and barite, associated with microbialites. The core parts of the chimneys are usually composed of pyrite and the axial conduits filled with pyrite and sphalerite. Conical chimneys, showing well-preserved orifices and axial conduits are the most common type. These structures are 3–15 cm high and 3–10 cm in diameter, exhibiting colloform pyrite and marcasite, radiating pyrite and sphalerite and networks of carbonate and silica. The conical chimneys are enveloped by layered sulphides and underlain by sulphide mounds. Li and Kusky (2007) also described layers of fine-grained sphalerite and pyrite pellets or framboids, usually ate the top of the conical structures. Small columnar chimneys are 2–5 cm high and 0.5–1 cm wide, forming clusters at the top of sulphide mounds, and containing pyrite, sphalerite and galena showing banding and colloform textures. The fourth type is represented by bulbous to round chimneys, locally with well developed orifices. Sulphides are pyrite, sphalerite and galena with laminated and colloform textures. The microbialites include layered dome-like features that clearly resemble stromatolites, which may have been part of microbial communities developed around the hydrothermal vents on the sea floor. Vertical sections of these putative stromatolites do display millimetre-scale laminae of pyrite and dark organic-rich material, forming individual columns 1–2 cm high and 3 mm to 1 cm in diameter, overlain by several cm-thick pyrite laminae. Further investigations carried out by Li and Kusky (2007) using SEM (scanning electron microscopy) revealed the presence of abundant filament and spheroidal microtextures coated with pyrite and carbonates, commonly ascribed to fossil bacteria. Figure 3.17 shows possible chimney structures of the Gaobanhe seafloor mineralisation.

Li and Kusky (2007) considered the Gaobanhe sulphide deposit as having formed in a continental graben setting, comparable to the Lake Baikal region or perhaps the Red Sea. However, the Gaobanhe Pb-Zn deposit is probably best described

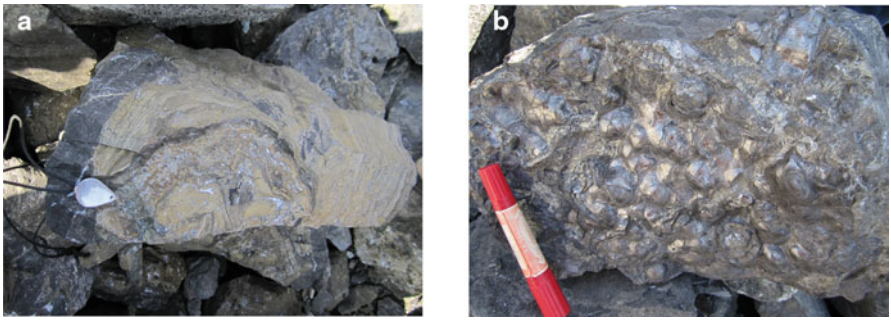

Fig. 3.17 Field photographs of the Gaobanhe sulphide deposit possible chimneys; **a** section through a round chimney; **b** columnar chimneys; photos taken by Dr Wu Huaying (Chinese Academy of Sciences)

as a transitional ore system between Irish-type, where fossil chimneys have been recognised (e.g. Boyce et al. 2003) and SEDEX mineral system. The rift setting for the Gaobanhe submarine sulphide deposit is one of several 1.8 to 1.4 Ga rift structures that are superimposed on the Archaean-Palaeoproteroic basement of the NCC, which include the major rift at the northern margin of the Craton, where the world-class Bayan Obo REE deposit (discussed in the previous section).

3.2.4.3 Gold and Mo Mineralisation in High-grade Metamorphic Rocks of the NCC

In the NCC there are several lode-style Au deposits hosted in Archaean high-grade metamorphic rocks. In this section, I describe two lode gold deposits, both on the northern margin of the NCC, one of these, in the west, is the Hademengou deposit (Inner Mongolia; Fig. 3.18, metallogenic district IX), located in the east-west-trending Daqingshan granulite belt, the other is Jiapigou in southern Jilin province, in the northeasternmost corner of the NCC (Fig. 3.18, metallogenic district V).

Hadamengou

The Hadamengou Au deposit on the northern margin of the NCC, hosted in the Alashan granulite-paragneiss terrane of Nokleberg (2010). A Chinese language paper on the deposit is by Zhou (1995). English language details on this deposit can be found in Gan et al. (1994), from whom the following is extracted.

The age of the Hadamengou Au mineralisation is poorly constrained, with Pb-mixing ages ranging from 227 to 170 Ma, and Pb model ages of ore material and granite ranging from 704 to 605 Ma. An undeformed dolerite dyke that post-dates vein formation gave a K-Ar age of 412 Ma. Gan et al. (1994) concluded that the Au mineralisation formed in the Neoproterozoic.

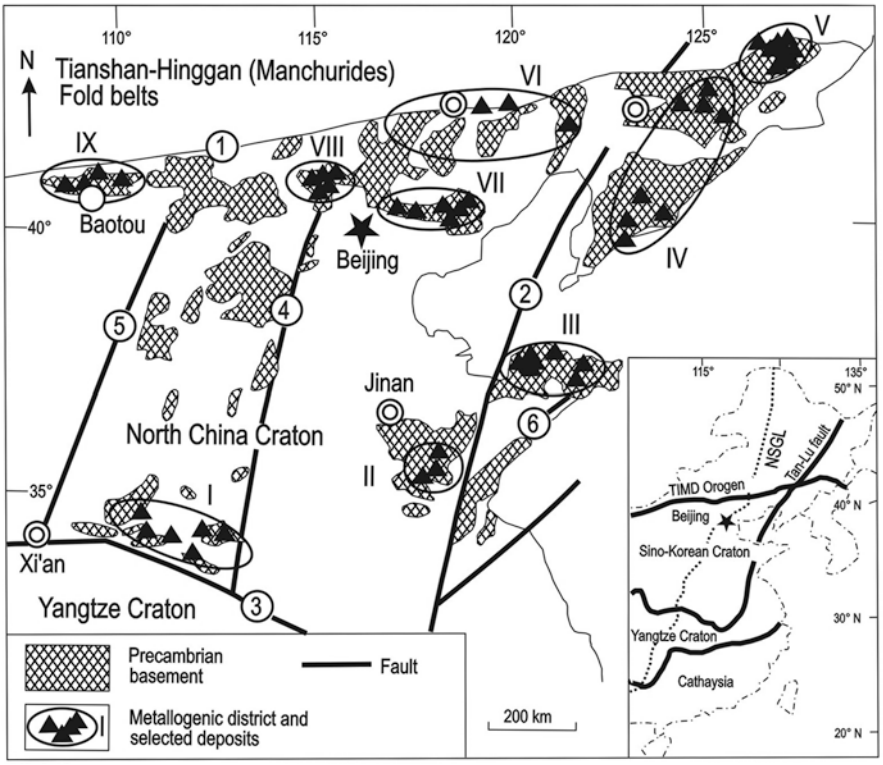

Fig. 3.18 Distribution of Mesozoic (Yanshanian) lode Au deposits in the North China Craton (after Yang et al. 2003). *I* Xiaoqinling (see Chap. 5), *II* Western Shandong, *III* Jiaodong, *IV* eastern Liaoling, *V* southern Jilin, *VI* Chifeng-Chaoyang, *VII* eastern Hebei-western Liaoling, *VIII* Zhang-Xuan, *IX* Baotou-Daqingshan; Faults *1* Chifeng, *2* Tan-Lu, *3* Xiaotian-Mozirtan, *4* Xingyang-Kaifeng, *5* Huashan-Lishi-Datong, *6* Wulian-Mishan. *Inset* shows position of the NCC, North-South Gravity lineament and Tanlu (Tan-Lu) Fault

The host rocks belong to the Archaean Wulashan Group, metamorphosed to granulite facies and comprising various types of gneisses and metamorphosed BIF. Gneissic rocks in the Hadamengou mine area include, biotite-gneiss, biotite-garnet gneiss, biotite-feldspar gneiss, amphibole-gneiss. Metamorphosed BIF include hornblende-magnetite-quartz and magnetite-quartz-garnet-plagioclase gneisses. Granitic rocks are present to the west of the deposit and form a biotite-granite pluton about 6×8 km, intruding the gneissic rocks of the Wulalshan Group. According to Gan et al. (1994), the granulite facies metamorphism of the Wulashan Group rocks occurred during the Neoarchaean, typically with ortho- and clinopyroxene, biotite, hornblende and garnet-bearing assemblages, and with augen-gneiss mylonitic textures. The gneissic rocks were later overprinted by retrograde metamorphism in the Neoproterozoic, typically with mineral assemblages consisting of biotite, epidote, actinolite, chlorite and quartz.

At Hadamengou there are 80 quartz-K-feldspar veins, of which 50 carry gold. Three styles of Au mineralisation are: (1) Au-bearing quartz-K-feldspar veins; (2) Au-bearing quartz veins and (3) Au-bearing altered rocks with sulphides. The first style forms veins up to 3 km long, but mostly from 500 to 200 m long and 1–3 m wide, traceable to depths of 400 m. These veins are hosted in brittle-ductile shear zones. The veins contain coarse K-feldspar, whereas the quartz is fine-grained and are cut by late quartz veins and stockworks. Fluid inclusion studies on feldspar and quartz, showed crystallisation temperatures of 300–500 and 150–400 °C, respectively. These quartz-K-feldspar veins also contain about 5–15 vol % of sulphides (pyrite, chalcopyrite, galena); magnetite is also present. The Au-bearing quartz veins, consist of quartz only, locally with a small amount of sulphides, but the Au content is uneconomic. These quartz veins are of several generations filling fractures and faults in the metamorphic rocks and are later than the quartz-K-feldspar veins. The auriferous quartz veins are locally displaced by late shear zones. The wall rocks exhibit K-feldspar and silica alteration, accompanied by fine-grained sulphide disseminations, extending for tens of metres and locally up to 100 m from the veins. This alteration is closely associated with the Au mineralisation and is considered the result of alkaline fluids interaction with the wall rocks, producing K-feldspar along fractures and veins. Fluid inclusion studies on quartz revealed single-phase $H_2O + CO_2$ vapour inclusions and two-phase $H_2O + CO_2$ liquid + vapour inclusions. The vapour contains small amounts of CH_4, N_2, H_2 and CO; K+ and Na+ are the main cations, whereas F^-, SiO_4^{2-} and Cl^- the main anions. Homogenisation temperatures mostly fall between 200 and 450 °C; calculated pressures correspond to depths of 2–3 km. Measurement of pH and Eh from fluid inclusions, show values of 8.33–9.55 and 226.9–299.2 mV, respectively, with the pH of about 8 being associated with the highest Au grades, suggesting weak alkaline and oxidising conditions for the mineralising event.

The genesis of the Hadamengou mineralisation remains unresolved. Gan et al. (1994), suggested a relationship to a Neoproterozoic tectono-thermal event that affected the NCC, with the gold being sourced from the granulite facies rocks during a deep-seated metamorphism and the activity of CO_2-rich mantle fluids. The retrograde metamorphism, mentioned above, would have been related to the Neoproterozoic tectono-thermal event, which also introduced brittle-ductile deformation, resulting in E-W-trending fractures, faults and foliation. This retrograde event liberated the gold from the high-grade metamorphic rocks, but Gan et al. (1994) do not exclude the possibility that the granite pluton west of the deposit may have provided heat energy and additional hydrothermal activity in the system, with re-distribution of the gold and other ore minerals.

Jiapigou District

The northeastern region of the NCC (Fig. 3.18, area V) is well endowed with Au mineralisation, estimated to have more than 100 t of gold reserves, whilst in the 1960s it produced almost half of China's gold (Miao et al. 2005). The Jiapigou district is in

the Jilin Province, where Au deposits are shear-zone hosted in Archaean greenstone rocks, has been the focus of many studies, resulting in a number of conflicting models for the origin of the ores and their timing. Miao et al. (2005) addressed these issues and constrained the timing of the mineralisation event at between 220 and 204 Ma (Indosinian), as elaborated below.

In the Jiapigou gold district, within the Archaean Longgang high-grade metamorphic terrane, there are several Au deposits, Jiapigou, Erdagou, Baijiazi, Sandaocha, Erdaocha, Caicangzi, Miaoling, Laoniugou, Xiaobeigou, Haigou, Erdaodianzi and Banmiaozi. Gold grades in these deposit range from 5 to 27 g/t and metal contents from about 10 to >45 tonnes. The Archaean Longgang terrane consists of biotite-plagioclase gneiss, amphibole-biotite-plagioclase gneiss, which represent the amphibolite to granulite facies metamorphosed product of tonalite-trondhjemite-granodiorite (TTG) intrusives. The age of these gnessic rocks is reported at between 2.57 and 2.49 Ga, and as old as 3.81 Ga (SHRIMP U-Pb on zircons). Supracrustal rocks of the Jiapigou Group occur as enclaves within the gneisses along a northwest-trending shear zone and a shear zone that bounds the high-grade terrane to the northeast. The Jiapigou Group consists of chlorite-actinolite amphibolite, hornblende-plagioclase gneiss, biotite-quartz schist and BIF. Although disputed, the Jiapigou Group has been considered as a typical Archaean greenstone belt, which together with the gneissic basement has undergone ductile deformation and retrograde metamorphism to greenschist facies. These gneissic and greenstone rocks are intruded by a massive, locally weakly deformed, K-feldspar granite with an age of ca. 2.5 Ga. Finally, these ancient rocks are in places covered by Mesozoic and Cenozoic sedimentary and volcanic rocks and affected by Palaeozoic and Cretaceous granitic intrusions.

All the deposits in the Jiaopigou district are confined within a 40 km long and 4–10 km wide corridor, which is in fact a ductile shear zone (Jiapigou Shear Zone) at the boundary between the Archaean rocks and the Mesozoic granites. There are Au-bearing quartz veins and disseminated ores, with the former accounting for 85 % of the total resources. These quartz veins can extend up to 1 km along strike, with widths of a few centimetre to a few metres and known to extend about 500 m down dip. Most of the quartz veins are massive, locally banded and with comb textures. Disseminated ores surround the quartz veins and are characterised by sulphides and quartz-sulphide stockworks. The ore minerals make up less than 10 % by volume of the ore material and include pyrite, minor chalcopyrite, galena, pyrrhotite, magnetite, scheelite, wolframite, argentite, bismuthinite. Gold ore is represented by native Au, electrum and calaverite, generally hosted within microcracks in pyrite and quartz. Gangue minerals are quartz, sericite, chlorite, calcite, ankerite and barite. Hydrothermal alteration includes sericitisation, chloritisation, sulphidation and silicification, mainly confined to the ductile shear zones. The paragenetic sequence reported by Miao et al. (2005) is from (early to late) quartz-magnetite → quartz-pyrite-native gold → quartz-sulphides → quartz-calcite-pyrite.

The Jiapigou deposit, controlled by northeast and east-northeast shear zones in Archaean amphibolite and gneiss, consist of more than 20 quartz veins, several are

not exposed at the surface and are all concentrated in three sub-parallel east-northeast trending shear zones. The middle one is the largest and is about 5 km long and 100–300 m wide. The ores show a broad mineral zonation from an eastern Au-Cu ± W zone to a central Au-Cu-Pb ± W to a western Pb-Au-Cu ± W zone. The latter has high Pb grades of up to 10.3 %.

Isotope systematics and fluid inclusion studies on the Jiapigou Au deposits have been summarised by Miao et al. (2005). Sulphur isotopic ($\delta^{34}S$ on pyrite) values, ranging from 1.5 to 12.6 ‰ (CDT), suggest a fairly restricted range sulphur source. Similarly, narrow ranges of $\delta^{18}O$ and $\delta^{13}C$, from 5 to 12 ‰ and −4.2 to 5.0 ‰, respectively, and δD values of −70 to −94 ‰ (relative to standard mean ocean water; SMOW), are recorded. These values are consistent with both orogenic lodes and intrusion-related Au deposits. Fluid inclusion in quartz are of three types: CO_2-rich, mixed H_2O-CO_2 and aqueous. Homogenisation temperatures range from 150 to 350 °C, with low salinity (0.7–6.5 wt% NaCl equiv). Miao et al. (2005), performed zircon U-Pb SHRIMP and Ar-Ar age determinations on gneiss samples. $^{207}Pb/^{206}Pb$ ages of 2,457 ± 11 and 2,544 ± 13 Ma were obtained and interpreted as the age of the protolith of the gneissic rock. A granodiorite dyke, considered to be coeval with or pre-mineralisation, gave a U-Pb SHRIMP zircon age of 223 ± 2 Ma. A pre-Au mineralisation quartz syenite dyke yielded zircon SHRIMP ages from 241 ± 4 to 218 ± 6 Ma, with the latter interpreted as the age of the dyke emplacement. A granite batholith (Huangnihe Granite), east of the Jiapigou district and locally hosting Au mineralisation gave a U-Pb SHRIMP age of 166 ± 2 Ma. Dating of sericite from the Bajaizi deposit by the $^{39}Ar/^{40}Ar$ method gave a well-defined plateau age of 203.6 ± 0.4 Ma. Miao et al. (2005) acknowledged that the timing of the Jiapigou Au deposits is controversial. Some researchers considered the Jiapigou lodes to be of Archaean age and of typical greenstone orogenic type. However, Miao and co-authors believed that the zircons of Archaean age in the quartz veins are inherited from the host rocks. The ages of the quartz syenite and granodorite dykes (223 and 218 Ma), which are spatially associated with the ore veins, may in fact represent the maximum age of the mineralisation, which occurred during the Indosinian. The 166 Ma of the Huangnihe granite makes it of Yanshanian age. Similarly, sericite from the Haigou Au deposit yielded Ar-Ar ages of between 144 and 120 Ma. Miao et al. (2005) concluded that the Jiapigou Au mineralidsation formed in two stages: Indosinian (220–204 Ma) and Yanshanian (144–120 Ma).

The Jiapigou district lends itself well for the on-going debate whether Au deposits in metamorphic and deformed terranes are orogenic, how much orogenic, or intrusion-related, or a combination thereof. Miao et al. (2005), aptly discussed the issue in their paper, as follows. The Jiapigou district is located at the northeastern margin of the NCC (Fig. 3.18), indeed several other metallogenic belts are located along the northern boundary of the NCC, along the Tanlu Fault and the southern margin (Qinling Orogen). The northern margin of the NCC was subjected to at least two major tectonic events. The first, is related to the Mesozoic collision of the Siberian (Angara) craton and the NCC, with closure of the intervening ocean that resulted in the Solonker suture and ophiolite belt and accretion of magmatic arcs, proba-

bly completed at about 240 Ma and forming the Tianshan-Hinggan orogenic belt (or Manchurides, or Tianshan-Inner Mongolia-Daxinganling orogenic belt(s)). This major collision was followed by intense post-orogenic magmatism at about 215 Ma with the intrusion of A-type granites, alkaline, high-K calc-alkaline intrusives, as well as mafic-ultramafic complexes, some of which hosting Ni-Cu sulphides (Wu et al. 2004). The second, is the widespread Yanshanian tectono-magmatic event of Late Jurassic-Cretaceous-Cenozoic, related to the oblique subduction of the Pacific plate beneath the eastern Asia continental margin.

Thus, the geochronological data on the Jiapigou Au mineralisation, indicate two peaks (220–204 and 166–120 Ma) of Au mineralisation, The 220–204 Ma (Triassic; Indosinian) Au mineralisation event is coeval with the above-mentioned post-orogenic magmatism, associated with the Siberian Craton-NNC collision. This post-orogenic magmatism seems to be temporally associated with parts of the metallogenic belts along the norther margin of the NCC. The west-directed oblique subduction of the Pacific plate is generally considered the principal far-field cause of the Yanshanian tectono-thermal event, all along the eastern margin of Asia, with widespread plutonism, volcanism, formation of rift basins and of numerous mineral systems, mostly concentrated along zones of weakness, provided by the NCC boundaries and major strike-slip faults, such as the Tanlu Fault. In the Jiapigou district the Yanshanian-related Au mineralisation occurred between 140 and 120 Ma, which is more or less coeval with that of Jiadong province (see below) and other metallogenic belts in the NCC. The Yanshanian event has been variably attributed to lithospheric thinning and upwelling of asthenospheric mantle or slab breakoff of the subducting Pacific plate, or a combination of both. As mentioned previously, I return to discuss this topic again in Chap. 7.

The Longmendian Ag- and Mo-bearing Veins

Li et al. (2011) recently reported a ca. 1.85 Ga Re-Os age of molybdenite from quartz vein systems in the Ag Longmendian deposit in the Neoarchaean-Palaeoporoteozoic Taihua Group and Xiong'er group rocks of the Xiong'er Terrane on the southern margin of the NCC (see Fig. 5.8). Silver-bearing quartz veins trend northeast and north-northeast, extending along strike for up to 2.5 km and up to 8 m thick. The silver lodes are surrounded by hydrothermal alteration (silica, sericite and more distally chlorite-sericite). The Ag-bearing minerals are native Ag, fahlore, proustite, electrum and minor amounts of pyrite, galena, sphalerite, chalcopyrite and magnetite. Gangue minerals include quartz, feldspar, fluorite and sericite. The Mo-bearing veins are effectively confined to the Taihua Group, where molybdenite occurs as isolated veins or lenses that cross-cut the Ag-bearing quartz veins, or in places as brecciated Mo-bearing veins in the Ag lodes. Li et al. (2011), noted that the molybdenite is associated with veinlets or stockworks of quartz-microcline-perthite and lesser tourmaline, suggesting a link with melts generated during high-grade metamorphism and migmatitisation. These migmatites typically consist of leuco- and melanosome (biotite-rich) bands with apatite, zircon and titanite as accessory minerals (mostly in

the leucosome). According to Li et al. (2011), some of the melanosome bands, up to 2 cm wide, contain more than 80 vol% tourmaline, with lesser amounts of epidote, quartz and carbonate. Amphibolite units that carry leucosomes are also extensively altered and mineralised, with the amphiboles being altered to actinolite-tremolite, epidote, chlorite, carbonate and titanite. The high content of tourmaline is suggestive, in my opinion, of boron metasomatism (see Slack 1996; Pirajno 2009).

The ore minerals of the Mo-bearing veins are molybdenite, pyrite, chalcopyrite, pyrrhotite and magnetite. Molybdenite occurs as coarse aggregates in the leucosome and altered amphibolite, as well as in the cleavage lines of amphiboles. Gangue minerals are microcline, Perthite, quartz, carbonate, amphibole, epidote, chlorite and tourmaline. Dating of pyrite and molybdenite, using the Re-Os system, gave isochron ages of $1{,}855 \pm 29$ and $1{,}853 \pm 36$ Ma, respectively.

The genesis of the Longmendian Mo mineralisation remains poorly understood. Li et al. (2011), suggested that because is hosted in migmatite and amphibolite rocks, the mineral system could be regarded as a migmatitic hydrothermal deposit. Their conclusion is based on the fact that there are no intrusions and related alteration patterns, that the mineralisation is associated with leucosome, melanosome and amphibolite and perhaps more importantly, the Re-Os ages indicate that the mineralisation is coeval with regional metamorphism of the Taihua Group at 1.87–1.84 Ga. The high Re content of the Longmendian molybdenite (ca. 500–1,130 ppm) is explained by injection of anatectic melts into amphibolite rocks, with the breakdown of amphibole and tourmaline supplying both Re and Mo to metamorphism-generated fluids. There was widespread anatectic melting and re-working of basement rocks at ca. 1.85 Ga in the NCC. These events are thought to be related to the collision of the Western and Eastern blocks and final consolidation of the NCC. Clearly, however, more work is required to better understand the genesis of the Longmendian Mo mineralisation and associated boron metasomatism.

3.2.4.4 Mineral Systems in the North China Craton (NCC) Related to the Mesozoic Yanshanian Event

The Mesozoic mineral systems that occur in the NCC are of great economic value and their distribution is shown in Fig. 3.18. These include porphyry, porphyry-skarn and lode Au deposits, all of which were formed during various episodes of the Yanshanian tectono-thermal event (ca. 208–90 Ma). As can be seen from Fig. 3.18, these mineral systems are largely confined to major structures or crustal/lithospheric breaks and at the northern and southern margins of the cratonic block. There are at least three important metallogenic provinces: (1) Jiadong lode Au, (2) Liaoning porphyry, skarns and epithermal belt and (3) Qinling polymetallic belt, with porphyry, skarns and lode Au-Ag systems. Here, I focus on the first two; whereas the Qinling polymetallic belt is dealt with in Chap. 5.

The Yanshanian tectono-thermal event occurred between the Middle Jurassic and Cretaceous, when magmatic belts and several types of mineral systems were formed

in a zone extending for about 5,000 km along the eastern margin of the Asia continent. The eastern margin of Asia is typically characterised by widespread intraplate magmatism, for which various lines of evidence show that it can be attributed to tectono-thermal events beginning in the Early Mesozoic (ca. 208 Ma) and probably continuing to present day (Pirajno et al. 2009). These events are particularly well-studied in the NCC, where a north-northeast-trending gravity lineament marks the boundary between thick lithosphere to the west and thin lithosphere to the east (see also Chap. 7). To the east of the gravity lineament, the crust and lithosphere are thinner, there is high heat flow and the Bouguer anomalies are from zero to slightly positive. This region is also seismically active and there are low-velocity and high-conductivity anomalies, which have been interpreted to be associated with fluids. Xenoliths carried by Ordovician kimberlites, lamproites and Cenozoic basalts, provide valuable information on depths of crust-mantle boundary and the thermal structure of the lithosphere to a depth of up to 250 km (O'Reilly et al. 2001). Thus, to the west of the gravity lineament the Archaean lithospheric keel is about 200 km thick with low heat flow, whereas to the east high heat flow is associated with a lithosphere that is only 55–120 km thick. Clearly, there was substantial and rapid removal or erosion of the lithospheric keel. This phenomenon is manifested by widespread magmatic activity, encompassing a wide range of granitic and mafic-ultramafic intrusions, bimodal volcanism, rifting and basin formation hosting world-class mineral systems as well as major gas and hydrocarbon resources.

Lode Au Deposits in the Jiadong Province

The Jiaodong gold province in the Jiaodong peninsula (Figs. 3.18, area III and 3.19), on the eastern margin of the North China Craton, is an important gold-producing region, with several world-class gold deposits (>100 t gold) accounting for about 25 % of China's reserves (Fan et al. 2003). Total measured Au reserves are in excess of 1,000 t and annual production is more than 30 t (Mao et al. 2008), with seven world-class deposits (>100 t), eight large deposits (20–100 t) and about 100 medium to small size deposits (<20 t) (Fan et al. 2007). The Jiadong province has been, and still is, intensively studied (Zhou et al. 2002, 2003; Qiu et al. 2002; Chen et al. 2005; Mao et al. 2008). Yang and Lü (1996) published a Chinese language book on the Jiadong geology and mineralisation. The following is mostly based on the work of Zhou et al. (2002), Chen et al. (2005), Fan et al. (2007) and Mao et al. (2008).

The province is bounded by the Tanlu fault to west, the Qingdao-Rong fault to east, the Jiao-Lai basin to south, and Longkou-Penglai fault and the Bohai Sea to north (Fig. 3.19). The main lithological units are rocks of the Late Archaean Jiaodong Group, the Palaeoproterozoic Jingshan Group, Jurassic and Cretaceous granites, Cretaceous shoshonite-like volcanic rocks and ultra-high pressure metamorphic (UHP) rocks. The UHP rocks are intruded by Yanshanian granites, and are present only east of the Wulian-Jimo fault (Fig. 3.19). Cenozoic basalts outcrop on the northwest coast of the Jiaodong peninsula and are associated with the Longkou-Penglai fault. The Jiaodong province was affected by two major tectono-thermal events, related to

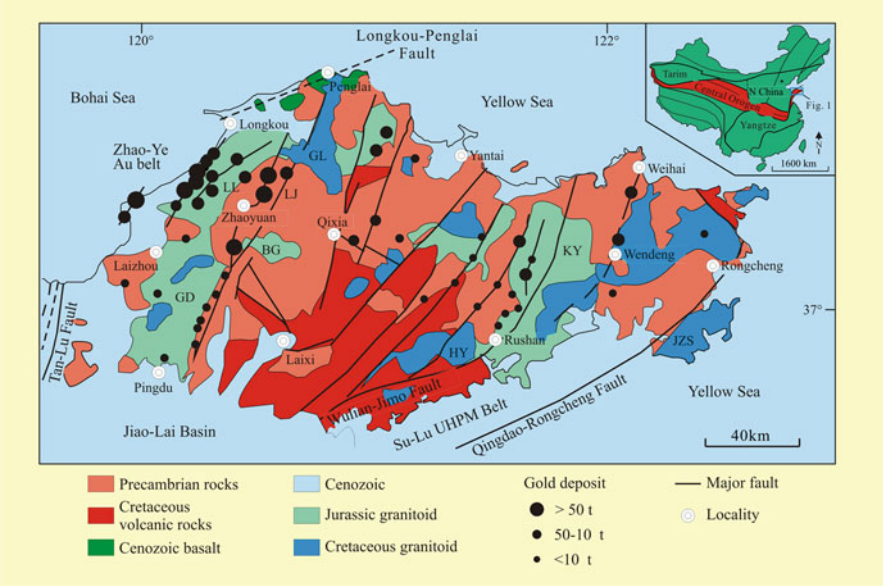

Fig. 3.19 Simplified geology and distribution of lode gold deposits in the Jiadong peninsula. (After Fan et al. 2007; Chen et al. 2005)

the collision between the Yangtze Craton and the North China Craton during the Indosinian (250–208 Ma) and the subduction of the Pacific plate beneath the Eurasian plate (Yanshanian event, 208–90 Ma) (Zhou et al. 2002).

Evidence from geochronological data has led most researchers to conclude that most, if not all, the gold deposits were formed between 130 and 110 Ma. Mao et al. (2003) proposed that three episodes of gold mineralisation occurred in the time spans of 250–180, 170–140 and 130–100 Ma. The complexity and multiplicity of the metal source has been argued by the above-cited workers. Some of the more popular views are: (1) the crust or combination of granite-greenstone terranes and high grade metasedimentary rocks rocks; (2) the mantle; (3) Yanshanian granites; (4) mixture of mantle and crust; and (5) lamprophyre dykes. Regarding the source of ore-forming fluids, key interpretations include: (1) mantle fluids; (2) magmatic fluids; (3) meteoric water; and (4) syncollisional metamorphic fluids; and combinations thereof in various proportions.

Published isotopic ages of ores and host rocks show that a peak in gold metallogenesis occurred in the period of 130–110 Ma, more or less coincident with granitic intrusions (Fig. 3.20). This metallogeny was facilitated by far-field interactions between the Pacific and Eurasian plates, accompanied by lithospheric thinning and an overall regime of extensional stress field in eastern China and adjacent regions (e.g. Mongolia; southern Siberia between the NCC and the Siberia Craton; Ren et al. 2002).

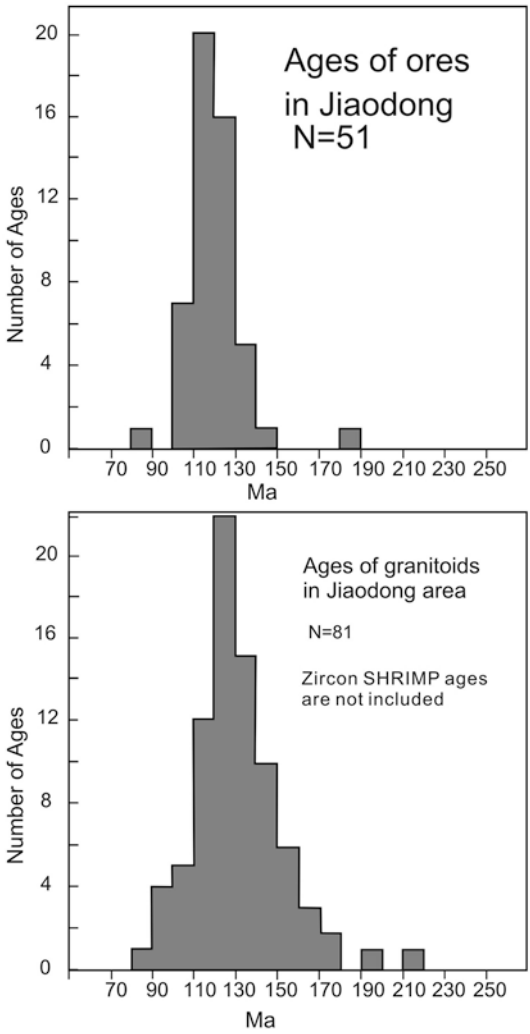

Fig. 3.20 Histograms of isotope ages for the Jiaodong gold province and for granitoids in the region. (After Chen et al. 2005)

In addition to numerous occurrences and prospects, the major deposits in the Jiaodong province are: Sanshandao, Jiaojia, Xincheng, Linglong, Fushan, Taishang and Daingezhuang (Zhou et al. 2002). The gold deposits of the Jiaodong province are all controlled by north-northeast-trending fault zones (Fig. 3.19), possibly a subsidiary set to the major crustal structure of the Tanlu Fault. The gold lodes are predominantly hosted in Mesozoic granitic intrusions (metaluminous biotite-granite, hornblende-bearing granodiorite and monzonite), intruded by numerous lamprophyre, basaltic, and felsic dykes. In one classification (Zhou et al. 2002), the gold lodes are of two types: (1) stockworks and disseminated ores, and (2) massive quartz vein type. The former is best represented by the Jiaojia-Xincheng ore field and the latter by the Linglong ore field. The Jiaojia-Xincheng ore field in-

cludes the Wungershan, Hedong and Hexi deposits, apart from Jiaojia and Xincheng. These deposits are controlled by north-northeast- and northeast-trending faults and brittle-ductile shear zones in the contact zone between the Linglong and Guojialing granites and Archaean greenstone rocks. Mao et al. (2008) classified the Jiadong lode Au deposits into: (1) quartz-vein type, as exemplified by the Linglong gold deposit; (2) altered-fracture type, as in the Jiaojia deposit, and (3) breccia-type as shown by the Pengjiakuang and Fayunkuang deposits. The quartz-vein type gold deposits, including Linglong, Dongfeng, Dayigezhuang, Denggezhuang, Jinqingding and Sanjia, are sited along the Zhaoyuan-Pingdu, Jinniushan, and Jinqingding faults; whereas the altered-fracture type gold deposits, comprising Sanshandao, Cangshang, Xincheng, Wang'ershan, Hongbu, Matang, Dongji, and Taishang, are situated along the Sanshandao, Cangshang, and Zhaoping faults in the western part of the Jiaobei basin. The breccia-type gold deposits, comprising Pengjiakuang, Fayunkuang, Guocheng, and Dazhuangzi, are located in the detachment faults at the north margin of the Jiaolai basin. By and large, orebodies are from 2 to 4 m thick, with strike lengths of 1 km or more, and extending to depths of 850 m.

As mentioned above, the mineralisation is mostly stockworks and veinlets, or disseminated in altered wall rocks. The ore minerals include pyrite, pyrrhotite, electrum, native gold, chalcopyrite, galena, sphalerite and locally arsenopyrite. Alteration and gangue minerals are sericite, K-feldspar, chlorite, epidote, Fe carbonates, forming broad haloes extending tens of metres from the hosting structures. The Linglong ore field comprises, apart from Linglong, Dongfeng, Jiuqyu, Daikaitou, Shuangding, Dongshan and Vein-108 deposits. The Au mineralisation occurs in large quartz veins that cut through the Linglong and Guojialing granites and is localised at the intersection of north-northeast-, northeast- and east-northeast-trending shear zones. Zhou et al. (2002) reported that about 540 major Au-bearing veins have been located, with strike lengths ranging from 100 m to 5.8 km, 1–10 m wide and extending downdip for up to 700 m.

Timing of Au Metallogeny in the Jiadong Province and Implications for Ore Genesis

As shown in Fig. 3.20, most isotopic ages fall between the Late Jurassic and Cretaceous, i.e., 190–65 Ma (Yanshanian), recording an important and widespread metallogenic event. More specifically, the timing of gold metallogeny in the province peaked in the period of 130–110 Ma (Cretaceous; Fig. 3.20).

Mesozoic granites are widespread in the Jiadong province, and are spatially associated with the gold mineralisation. Because of this, isotopic dating, geological and geochemical characteristics of the granites have been well studied (e.g. Mao et al. 2008), mainly in pursuit of a possible genetic link with the mineralisation. A multistage evolution of granite complexes is revealed by zircon SHRIMP ages, shown in Table 3.2 (Chen et al. 2005). Isotopic ages of ore deposits and associated altered wallrocks are listed in Table 3.3 (Chen et al. 2005 and references therein).

The Linglong and the Luanjiahe granitic intrusions formed in the period of 150–170 Ma, the Guojialing granite intruded during 126–130 Ma, whereas a post-ore granitic dyke intruded at ca. 120 Ma. Recent $^{40}Ar/^{39}Ar$ dating of magmatic biotites

Table 3.2 Selected SHRIMP U-Pb zircon ages of granitic rocks from the Jiadong peninsula; number in parenthesis represents total number of data. (After Chen et al. 2005)

Lithology	Peak age (Ma)	Ages of inherited zircon grains, and/or ages of Pb-loss zircon grains (Ma)
Porphyric granodiorite, Linglong complex	153 ± 4 (19)	Inherited zircon: 206 ± 7–294 ± 9; Pb-loss zircon: 131 ± 3
Loushan garnet-bearing granite, Linglong complex	158 ± 4 (13)	175 ± 4–305 ± 9; core of zircon: 3,446 ± 2, growth rim: 152 ± 2; 2 grains with Pb-loss
Jiumoushan body, Linglong-like granite	160 ± 3 (23)	Zircon core: 658 ± 11, rim: 154 ± 3; core: 783 ± 13, rim: 201 ± 3, 165 ± 3; core: 210 ± 4, rim: 162 ± 3
Moushan body, Linglong complex	158 ± 3 (7)	176 ± 4–239 ± 7; core: 226 ± 6, edge: 146 ± 3, for a grain without core-rim texture
Guojiadian coarse-grained granite, Luanjiahe complex	–	139–2,875, cluster at 200–300
Luanjiahe body, Luanjiahe complex	157 ± 5 (12) or 154 ± 4 (9)	181 ± 5–386 ± 9
Biguo two-mica granite, Luanjiahe complex	152 ± 10 (5)	188 ± 5–224 ± 6; core: 224 ± 6, edge: 142 ± 4, for one grain without core-rim texture
Sanshandao, Guojialing porphyric granodiorite	128 ± 2 (19)	155 ± 3; two grains yield concordant ages of 1,934 ± 48 and 2,708 ± 65, respectively
Jiehe, Guojialing porphyric granodiorite	126 ± 2 (19)	Core: 2,530 ± 11, edge: 2,483 ± 21, for one idiomorphic grain; core: 225 ± 4, edge: 159 ± 3 for one idiomorphic grain with ring texture
Guojialing granite complex	130 ± 3 (14)	1,860 ± 15 (1); 230 ± 5
Guojialing granite complex	129 ± 3 (5)	116 ± 3; 155 ± 5
Guojialing granite complex	128 ± 6 (9)	
Linglong gold mine, posture K-feldspar porphyry dyke	120 ± 2 (21)	Pb-loss: 110; inherited zircon: (150–3,100), mostly cluster at 150–300, minor of 2,300–3,100
Footwall granodiorite of the Cangshang gold deposit	166 ± 4 (10)	181 ± 5, 188 ± 4, 202 ± 4, 244 ± 11, 378–805, 1,800–2,105, 2,542 ± 8
Intensively altered granitic breccia within orebody, Cangshang gold mine	154 ± 5 (6)	291 ± 4, 598 ± 13, 771 ± 10, 2,158 ± 61, 2,292 ± 21, 2,517 ± 8
Plagioclase amphibolite of hanging wall, Cangshang gold mine	2,530 ± 17 (7)	Metamorphic zircon: (2,391–2,482, 2,013–2,321), 1,852 ± 37, 1,125 ± 809, 1,336 ± 638

from these granites (Linglong and Guojialing) yielded ages of around 124 Ma (Li et al. 2003b). The development of these granites is generally contemporaneous with or slightly predates the timing of gold mineralisation. It is important to note that younger granites always contain inherited zircon grains with similar ages to older granites, which provide insights as to the thermal history of the region. The majority of zircon grains from altered granitic breccias in the Cangshang gold mine have isotopic ages of 154 Ma, whereas zircon grains from the footwall granodiorite were dated at 166 Ma. SHRIMP ages of inherited zircons from Yanshanian granites cluster into two groups of 180–300 Ma and >1,800 Ma, suggesting that several thermal events occurred in the Jiaodong metallogenic province before 180 Ma. The 180–300 Ma magmatic events

Table 3.3 List of selected isotope ages for ore deposits and associated altered rocks in the Jiaodong gold province. (From Chen et al. 2005 and references therein)

Mine/ orefield	Host rock	Analysed sample	Method	Ages[a] (Ma) and I_{Sr}
Dongji	Altered tectonite	K-feldspar of altered rocks	Ar/Ar	116.1 ± 0.3 (P), 116.3 ± 0.8 (I)
Dongji	Altered tectonite	Ore-bearing quartz vein	Ar/Ar	115.2 ± 0.2 (P), 114.4 ± 0.2 (I)
Linglong	Quartz vein	Pyrite of ores	Rb-Sr	123 ± 4, 123 ± 3, 122 ± 11
Linglong	Quartz vein	Pyrite of ores	Rb-Sr	121.6 ± 8.1 ($I_{Sr} = 0.7094 \pm 0.0019$)
Linglong	Quartz vein	Ore and its pyrite	Rb-Sr	121.8 ± 3.5 ($I_{Sr} = 0.7102 \pm 0.0001$)
Linglong	Quartz vein	Ore and its pyrite	Rb-Sr	120 ± 29 ($I_{Sr} = 0.7113 \pm 0.0048$)
Linglong	Quartz vein	Five samples of ores	Rb-Sr	110.6 ± 2.4 ($I_{Sr} = 0.7121 \pm 0.0002$)
Xishan, Linglong	Quartz vein	Sericite of Vein 108	Rb-Sr	101 ± 4 ($I_{Sr} = 0.7120 \pm 0.0002$)
Dongshan, Linglong	Quartz vein	Sericite quartzite and its alteration minerals such as chlorite	Rb-Sr	111.4 ± 2.8 ($I_{Sr} = 0.7121 \pm 0.0001$)
Xishan, Linglong	Quartz vein	Fluid inclusions in quart	Rb-Sr	126.6 ± 7.5 ($I_{Sr} = 0.7111 \pm 0.0002$)
Xishan, Linglong	Quartz vein	Altered rocks	Rb-Sr	112 ± 2 (I_{Sr} un-reported)
Xishan, Linglong	Quartz vein	Altered rocks	K-Ar	111 ± 2
Jiehe, Jiao-Xin belt	Altered tectonite	Altered rocks, K-feldspar, clay mineral	Rb-Sr	46.5 ± 2.3 ($I_{Sr} = 0.7120 \pm 0.0001$)
Jiaojia	Altered tectonite	Fluid inclusions in quartz	Rb-Sr	134 ± 8 ($I_{Sr} = 0.7104 \pm 0.0001$)
Jiaojia	Altered tectonite	L-stage sericite	Rb-Sr	88.1 ± 0.1 ($I_{Sr} = 0.71161 \pm 0.00018$)
Jiao-Xin belt	Altered tectonite	Muscovite of altered rocks	Rb-Sr	105 ± 7 (I_{Sr} un-reported)
Jiao-Xin belt	Altered tectonite	Muscovite of altered rocks	K-Ar	106 ± 2
Cangshang	Altered tectonite	Fluid inclusions in quartz vein	Rb-Sr	113.5 ± 0.6 (I_{Sr} un-reported)
Cangshang	Altered tectonite	Fluid inclusions in quartz vein	Ar/Ar	121.3 ± 0.2 (P); 121.1 ± 0.5 (I)
Lingshangou	Altered tectonite	K-feldspar, fuchsite in ores	Rb-Sr	188.9 ± 4.2 ($I_{Sr} = 0.7111$)
Lingshangou	Altered tectonite	Altered rock	Rb-Sr	115 ± 5 (I_{Sr} un-reported)
Qixia	Quartz vein	Pyrite-sericite-quartz assemblage	Rb-Sr	125.8 ± 1.7 ($I_{Sr} = 0.7168 \pm 2$)

Table 3.3 (continued)

Mine/ orefield	Host rock	Analysed sample	Method	Ages[a] (Ma) and I_{Sr}
Majiayao	Quartz vein	Fluid inclusions in quartz	Rb-Sr	137.6 ± 7.1 (I_{Sr} = 0.7163 ± 0.0001)
Majiayao	Quartz vein	Sericite of ores	Rb-Sr	135.1 ± 5.2
Majiayao	Quartz vein	chlorite, siderite, sericite quartzite	Rb-Sr	106 ± 5 (I_{Sr} = 0.7152 ± 0.0001)
Majiayao	Quartz vein	Sericite	Rb-Sr	135.1 ± 5.2 (I_{Sr} = 0.7215 ± 0.0025)
Majiayao	Quartz vein	Sericite	K-Ar	120 ± 2
Denggezhuang	Quartz vein	Sericite quartzite	Rb-Sr	118 ± 9 (I_{Sr} = 0.71015 ± 0.00019)
Jinqingding	Quartz vein	Pyrite-sericite-quartz assemblage	Rb-Sr	104.8 ± 1.5 (I_{Sr} = 0.7131 ± 0.0001)
Jinqingding	Quartz vein	Alteration minerals and rocks	Rb-Sr	101.8 ± 3.4 (I_{Sr} = 0.7106 ± 0.0004)
Xiayucun	Quartz vein	Sericite	K-Ar	124.6 ± 2.5
Pengjiakuan	Altered tectonite	M-stage quartz	Ar/Ar	118.42 ± 0.25 (P), 117.03 ± 0.13 (I)
Pengjiakuang	Altered tectonite	M-stage quartz	Ar/Ar	120.53 ± 0.49 (P), 117.33 ± 0.15 (I)
Pengjiakuang	Altered tectonite	Sericite of ore	K-Ar	100.59 ± 1.96
Dazhuangzi	Altered tectonite	M-stage quartz	Ar/Ar	117.39 ± 0.64 (P), 115.62 ± 1.01(I)
Fayunkuang	Altered tectonite	Pyrite of ores	Rb-Sr	128.2 ± 7.2 (I_{Sr} = 0.7128 ± 0.0001)

[a]I and P in brackets stand for isochron and plateau ages, respectively; data underlined are used in histograms (Fig. 3.20).

can be interpreted as being related to the northward subduction of the Qinling-Dabie-SuLu oceanic plate and the subsequent collision between the South and North China continents (Indosinian orogeny, 250–200 Ma), which formed the Central Orogen (or Qinling Orogen) (see inset of Fig. 3.8). The >1,800 Ma granitic episode is coeval with amalgamation or collision between the Eastern and Western blocks of the NCC. Thus, granitic magmatism in the span of 1,800–180 Ma may be interpreted as being related to a series of subduction-accretion and rifting episodes at the southern margin of the North China craton (Kusky and Li 2003; Lu et al. 2002). Preservation of inherited zircons in young granites shows that earlier granite or crust were formed by partial melting of crustal materials and/or remelting of earlier granites, or that these late granitic magmas were strongly contaminated by the older granites or crust. Chen et al. (2005) concluded that the Yanshanian granites in the Jiaodong area could not have evolved from juvenile mantle magma, nor could they have been sourced from partial melting of subducted slabs or an enriched mantle wedge, rather they must have been sourced from the crust by partial melting or remelting.

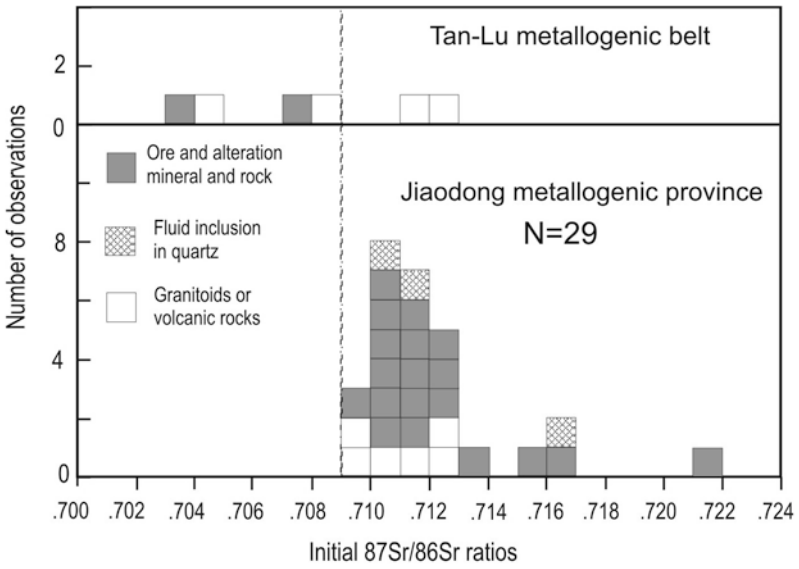

Fig. 3.21 Histograms showing the distribution of I_{Sr} values for ore deposits and granitoids in the Jiaodong gold province and the Tan-Lu metallogenic bel. (After Chen et al. 2005)

Strontium isotope ratios (I_{Sr}) are good indicators of source materials. In general, igneous rocks with $I_{Sr} < 0.705$ are inferred to have been sourced from the mantle; $I_{Sr} > 0.709$ values are indicative of crustal sources, and those between 0.705 and 0.709 probably indicate mixtures of mantle and crustal sources (Faure 1986). Igneous rocks of the same type may have different I_{Sr} values due to their contrasting ages, source region of different composition, and/or regionally geochemical inhomogeneity. For example, in the NCC granitic rocks sourced from continental crust commonly have I_{Sr} values lower than 0.710 (Hu et al. 1997; Chen et al. 2000). Hence the I_{Sr} criteria need to be used with some caution to distinguish the genetic types of geological bodies from different regions.

In the Jiaodong area, all the Yanshanian granites have $I_{Sr} > 0.7095$, whereas $I_{Sr} > 0.710$ are obtained from altered rocks, mineral separates from the ores, and from fluid inclusions and are slightly higher than the associated Yanshanian granites (Fig. 3.21). These I_{Sr} values are higher than those of the Mesozoic collision-type or S-type granites in the southern margin of the NCC (Chen et al. 2000), confirming that the granitic intrusions in the Jiaodong district were sourced from the crust. This conclusion was also reached by several other workers (e.g. Hu et al. 1997; Zhou and Lu 2000; Qiu et al. 2002) and is supported by the Sr-Nd-Pb isotope systematics (Yang et al. 2003). It can be concluded that the ore fluids and metals must have been dominantly sourced from the crust, and it is possible that the Archaean rocks in the region were the main source by partial melting for the Yanshanian granites.

The large-scale Yanshanian gold metallogenesis is believed to have taken place during or following the transition regime from compression to extension (e.g. Hu

et al. 1997; Qiu et al. 2002; Yang et al. 2003; Mao et al. 2003a, 2008). However, there is disagreement as to what caused this transition from a tectonic regime of compression to one of extension. Four views have been proposed: (1) tectonism along the Tanlu fault, (2) mantle plume activity, (3) subduction of the Pacific plate; and (4) post-collision tectonics, extensional collapse and lithospheric delamination. These viewpoints are briefly discussed below.

The Tanlu Fault, with a total displacement estimated at about 500 km, is a major strike-slip crustal structure with a complex history of both sinistral and dextral movements between the Late Jurassic and Early Cretaceous (Xu and Zhu 1994; Ren et al. 2002; Zhu et al. 2010). Li et al. (2003b), on the basis of $^{40}Ar/^{39}Ar$ data envisaged that gold mineralisation and mafic magmatism (e.g. lamprophyre dykes and volcanism) were controlled by transtentional movements along the Tanlu Fault in the period 132–120 Ma. However, most Au deposits and Yanshanian granitic intrusions cluster on the eastern side of the fault, namely the Jiaodong area. In addition, metallogeny and magmatism in the Jiaodong area should be comparable with those in the Tanlu fault belt; but this is not supported by I_{Sr} values of igneous rocks and ore deposits (Fig. 3.21). A small number of I_{Sr} values for the Tanlu fault belt shows a wide variation from <0.705 to >0.710, implying a greater complexity of the ore- and the rock-forming materials, including mantle, crust and mantle-crust mixtures. This variability contrasts with the singularity of gold lodes (gold-only province) in the Jiadong area, thereby indicating a different type of control and tectonic setting. The magmatism and metallogenesis in the Jiaodong province should also occur on both sides of, as well as along, the Tanlu fault, but so far, except for the Tanlu fault-controlled magmatic belt, no gold deposit and only few granitic intrusions have been found in the northern Jiangsu, southern and western Shandong, the northern Anhui and the southern Hebei. It can be concluded that the Tanlu fault was not a dominant factor for the Jiadong gold metallogenesis, although the Tanlu fault remains one of the main controlling structure for the granitic magmatism and gold mineralisation within and along the Tanlu fault belt (Fig. 3.22).

Some authors have argued that the Jiaodong gold province is the result of mantle plume activity (e.g. Wang et al. 1998). However, there is a lack of surface manifestations indicative of mantle plume activity, such as continental flood basalts. Plume-related basalts are sourced from the mantle by decompression melting and in the Jiaodong area, parts of northeastern China and Mongolia vast amounts of basalts are present in rift-basins that might reflect mantle upwelling were emplaced in the Cenozoic (Ren et al. 2002; Barry et al. 2003), whereas lode gold mineralisation is essentially confined to the 130–110 Ma period. East China is adjacent to the Circum-Pacific Rim, and mainly for this reason, the Yanshanian metallogenesis in East China, including the Jiadong province, has been interpreted as the result of back-arc extension during subduction of the Paleo-Pacific plate (Kula or Izanagi) under the Eurasian plate. A number of researchers (e.g. Mao et al. 2003a, 2010; Yang et al. 2003) proposed the Pacific oceanic subduction beneath the Eurasia continent, as the main controlling mechanism for the tectonics, metallogenesis and magmatism in East China. These, in turn, may have been the result of far-field effects may be linked with mantle superplume activity at about 130 Ma, responsible for the

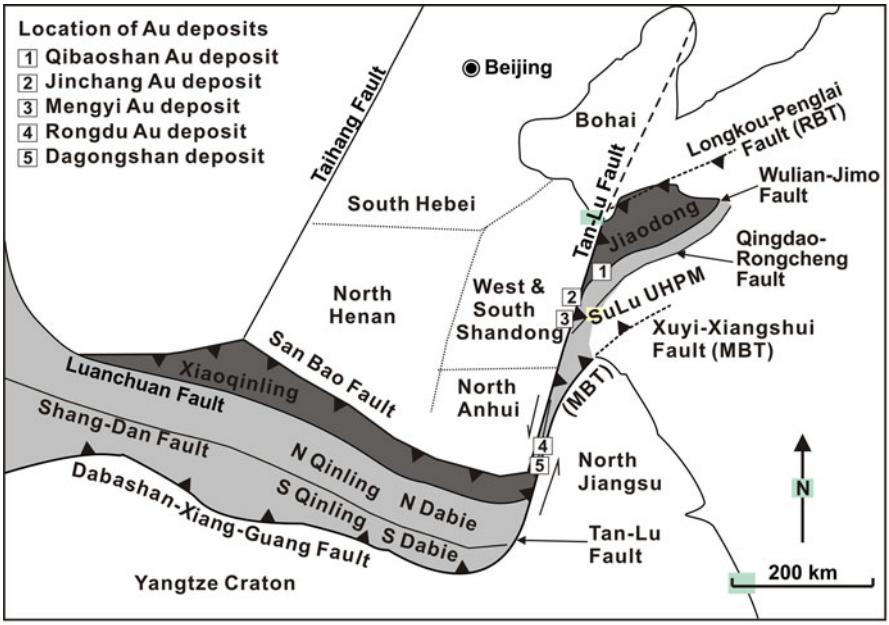

Fig. 3.22 Gold deposits controlled by the Tan-Lu Fault zone; note that Sr_i ratios for these deposits are plotted in Fig. 3.21. (After Chen et al. 2005)

emplacement of the Ontong Java-Manihiki-Hikurangi oceanic plateaux, which could have promoted or enhanced subduction as a result of tectonic push due to the growth of oceanic plateaux on the sea floor.

Mao et al. (2008) on the basis of stable isotope systematics, and the close spatial association with lamprophyre dykes, suggested that the Jiadong mineralisation was the result of lithospheric thinning, asthenospheric upwelling and mantle degassing, ruling out a direct link with granitic magmatism. From these authors the following is summarises. Dykes are common in the Jiaodong area, especially in the Linglong gold field, where the average density is up to 10 dykes/km^2. There are several types of dykes, including minette, kersantite, dolerite, diorite, porphyritic diorite, granite porphyry, aplite and pegmatite. The dykes were emplaced in several stages, which preceded and postdated the gold mineralisation event. Dyke emplacement shows a temporal trend from early lamprophyre to later intermediate-felsic dykes. Zircon SHRIMP U-Pb age of 120 ± 2 Ma for granite porphyry dykes in the Oujiakuang gold deposit, ^{40}Ar-^{39}Ar ages of 103–123 Ma for lamprophyre and dolerite dykes and K-Ar ages of 123.5–122.6 Ma for mafic dykes that are spatially associated with mineralized veins are quoted in Mao et al. (2008 and references therein). The age histograms shown in Fig. 3.20 (see also Table 3.1), indicate that the mineralisation in Jiaodong occurred in a relatively short span of time. Generally, the Jiaodong gold mineralisation is later than the 160–150 Ma age of biotite granites (Linglong, Kunyunshan, and Luanjiahe) and for this reason Mao et al. (2008)

proposed that the 29–46 m.y. time gap rules out a relationship between mineralisation and granite intrusions. The Guojialing granodiorites crop out in a small area, and is seldom exposed in underground workings and drill core. SHRIMP zircon U-Pb ages of the granodiorite are 130–126 Ma (Wang et al. 1998), and the biotite ^{40}Ar–^{39}Ar ages are of 124.5 ± 0.4–124.0 ± 0.4 Ma (Li et al. 2003b), which are nearer the timing of mineralisation, leading most workers to propose a relationship between the granodiorite and the mineralisation. However, the ages of the granodiorite are still 16–4 Ma older than the gold mineralisation. Furthermore, the granodiorite is characterized by albite alteration, whereas the mineralisation is associated with K-feldspar and pyrite-sericite-quartz alteration. In addition, the differences in hydrogen isotope compositions (Table 3.4) also indicate that the granodiorite is unlikely to be related to the gold-bearing hydrothermal fluids. By contrast, the gold mineralisation is temporally and spatially associated with lamprophyre dykes. Lamprophyre and mafic-intermediate dykes are common in the Jiaodong gold fields, and their ages (103–123 Ma) overlap those of the ore-formation. All dykes are enriched in large ion elements (e.g. Ba, Sr, Rb, K) and LREE, strongly depleted in Cr and Ni, and relatively depleted in high field strength elements (e.g. Th, Nb, Ti, and Y), suggesting that their source is the enriched mantle. Lamprophyres are also characterised by biotite alteration, which is similar to the K-feldspar alteration developed during the metallogenic processes. The multi-stage emplacement of lamprophyre and felsic dykes not only indicates strong crust-mantle interaction during the mineralisation, but also implies that the faults occupied by the dykes are the conduits for the ore-forming fluids. The $\delta^{18}O_{SMOW}$ and $\delta^{13}C_{PDB}$ values of calcite in the quartz-vein and fracture-altered types gold ores and those of calcite in the lamprophyre and dolerite dykes are quite similar (see Table 3.4). The strong K-feldspar alteration developed in the dykes and their wallrocks, carbonate veins and CO_2—rich fluid inclusions all point to a source that is the same as that of the ore-forming fluids. A spatial-temporal link with lamprophyres for Archean orogenic gold deposits was first suggested by Rock et al. (1989).

Mao et al.'s (2008, 2010) Geodynamic and Metallogenic Model

As outlined in the preceding section, Chen et al. (2005) proposed that gold mineralisation occurred during periods of transition from compression to extension during the collision of the Yangtze and North China Cratons. The view of a post-collisional tectonic setting, suggested by Wang et al. (1998) and Luo et al. (2003) is similar to that of Chen et al. (2005). Mao et al. (2003, 2008, 2010) reported that large-scale Mesozoic mineralisation in the NCC and adjacent areas occurred during three main periods: 200–160, ca. 140, and 130–110 Ma, which correspond to geodynamic settings of post-collisional extension in the North China and Yangtze cratons, with transfer of the principal stress-field from north-south to east-west directions, and east-west lithospheric extension caused by subduction of the Palaeo-Pacific plate. Although there are differences between these four views, all agree that the large-scale mineralisation in the Jiaodong region was developed in an environment of extension and/or lithosphere thinning.

Table 3.4 Selected sulphur, oxygen and hydrogen isotope values of ores, granites and metamorphic rocks in Eastern Shandong peninsula. (After Mao et al. 2008)

Samples	Sample locations	Measured minerals	$\delta^{34}S_{CDT}$ (‰)	$\delta D_{min-SMOW}$ (‰)	$\delta^{18}O_{min-SMOW}$ (‰)	Th (°C)	$\delta^{18}O_{water-SMOW}$ (‰)
Altered fracture-type ore							
Ore	Sanshandao	Ser, Pyr	12.0	−52	10.7	250	7.55
Ore	Sanshandao	Ser, Pyr	12.0	−48	11.7	250	8.55
Ore	Cangshang	Ser, Pyr	11.7	−56	10.9	250	7.75
Ore	Cangshang	Ser, Pyr	12.4	−52	10.0	250	6.85
Ore	Cangshang	Ser, Pyr	11.3	−51	12.8	250	9.65
Ore	Jiaojia	K-feld, Pyr	11.4	−86	10.2	300	4.37
Ore	Jiaojia	K-feld, Pyr	11.5	−85	10.0	300	4.17
Ore	Wang'ershan	Ser, Pyr	8.7	−57	9.1	250	5.95
Ore	Wang'ershan	Ser, Pyr	8.9	−52	8.7	250	5.55
Quartz vein-type ore							
Ore	Dayigezhuang	Ser, Pyr	7.5	−52	8.8	250	5.65
Ore	Dayigezhuang	Ser, Pyr	7.5	−58	9.2	250	6.05
Ore	Dayigezhuang	Ser, Pyr	7.2	−60	9.3	250	6.15
Ore	Denggezhuang	K-feld		−75	9.6	300	3.77
Breccia-type ore							
Ore	Pengjiakuang	Ser		−58	4.3	250	1.15
Ore	Pengjiakuang	Ser		−59	5.1	250	1.95
Ore	Pengjiakuang	Ser		−64	5.3	250	2.15
Granitic rocks							
Granodiorite	Guojialing	Bio		−117	6.8	550	9.4
Granodiorite	Guojialing	Bio		−87	6.7	500	9.3
Granodiorite	Guojialing	K-feld		−73	10.0	500	8.5
Granodiorite	Guojialing	K-feld		−73	10.2	500	8.7
Granodiorite	Guojialing	K-feld		−76	10.1	500	8.6
Granodiorite	Guojialing	K-feld		−109	10.8	500	9.3
Granodiorite	Guojialing	K-feld		−70	7.4	500	5.7
Biot granite	Linglong	K-feld		−73	9.2	500	7.7
Biot granite	Linglong	K-feld		−79	9.0	500	7.5
Biot granite	Linglong	K-feld, Pyr	7.9	−79	8.7	500	7.2
Biot granite	Wang'ershan	K-feld, Pyr	8.6	−82	10.8	500	9.3
Biot granite	Wang'ershan	K-feld		−79	8.9	500	7.4

Formulae used to calculate the oxygen isotope of water from the corresponding silicates: $1{,}000\ln\alpha_{muscovite-water} = 4.13 \times 10^6/T^2 - 7.41 \times 10^3/T + 2.22$ (0–1,200 °C); $1{,}000\ln\alpha_{alkali\ feldspar-water} = -3.70 + 3.13(10^6/T^2)$; $1{,}000\ln\alpha_{biotite-water} = 0.03(10^6/T^2) - 2.59$. Details and references in Mao et al. (2008).

Bio Biotite; *K-feld* K-feldspar; *min* mineral; *Mus* Muscovite; *Pyr* Pyrite; *Ser* Sericite; *Th* Homogenization temperature

As already mentioned, studies on Palaeozoic kimberlite intrusion in the Jiaodong and Liaodong peninsulas indicate that eastern China had a very thick lithosphere in the Palaeozoic. Griffin et al. (1998) inferred that the lithospheric root was at least 180 km-thick in eastern China in the Palaeozoic, in accordance with the stability field of diamond-bearing peridotite. Zhang and Hou (1991) studied diamond-bearing kimberlites, and suggested that lithosphere thickness in the Palaeozoic could have been 150–200 km in the west, and 180–200 km in the east. Therefore, it is assumed that the lithosphere of eastern China, thinned by about 100 km from the Palaeozoic to the Cenozoic (Griffin et al. 1998; Chen et al. 2001). Hu et al. (2006) argued that the NCC was affected by the impingement of a mantle plume in the Mesozoic, and that the core of the plume was located in the Bohai Sea, while mantle plume branches were active in the Jiaodong and Luxi areas (western Shandong province). The alkali ring complexes in the Luxi area, and a SHRIMP zircon U-Pb age of 177 Ma recorded for the granodiorite in the alkaline complexes (Hu et al. 2005), are indicative that mantle activity and/or lithospheric thinning began in the Mid-Jurassic. Several carbonatite dykes in Badou and Xueye, Luxi area, with K-Ar ages of 122.9 ± 0.7 and 122.5 ± 0.7 Ma, are coeval with those of lamprophyre dykes, felsic dykes, and Guojialing-type granodiorite (Mao et al. 2008). Therefore 135–115 Ma is clearly an important period for thermal events which are temporally associated with the large-scale gold mineralisation in the Jiaodong province.

The similar trace-element patterns of Mesozoic basalts to that of ocean island basalt (OIB), and the depleted Sr and Nd isotopic compositions, imply that basalts were sourced from the asthenosphere (Barry and Kent 1998). Volcanism in the Cenozoic basins, such as the Bohai basin, gravity and magnetic anomalies, seismic profiling and hydrothermal activity, all reflect a shallow Moho depth (Xiao et al. 2001). In addition, the Bohai basin shows early Cenozoic radiating and annular fault systems, from the center of the Bozhong depression (Mao et al. 2008). The emplacement of granitic magmas also suggests lithospheric thinning in the Jiaodong province during Late Mesozoic to Early Cenozoic. The intrusions of the Linglong, Kunyushan, and Luanjiahe biotite granites, of crustal derivation, in the Late Jurassic indicate that the crust was thick at that time. Between 160 and 150 Ma large areas were intruded by peraluminous granites in the South China block, whose differentiation resulted in the formation of tungsten and tin deposits (Mao et al. 2004). In fact, the large-scale emplacement of granites in this period is an important event in the Mesozoic of eastern China. The geodynamic model envisaged by Mao et al. (2008, 2010), which attempts to explain the Yanshanian magmatism and associated ore systems in eastern China, is reproduced in Fig. 3.23.

In the southern and northern margins of the NCC, and the middle-lower reaches of the Yangtze River valley, metallogenic belts are characterized by porphyry—skarn type Cu-Mo-Au, Mo-W, and Mo deposits (Fig. 3.23b), related to ca. 140 Ma I-type granites, whereas there is no mineralisation in the Jiaodong area at this time. At ca. 120 Ma, lithospheric thinning, abundant lamprophyre dykes, emplaced along a group of paralleling north-northeast-trending faults, imply that the mantle magmas and fluids continuously advected into the crust (Fig. 3.23c). Most of gold deposits

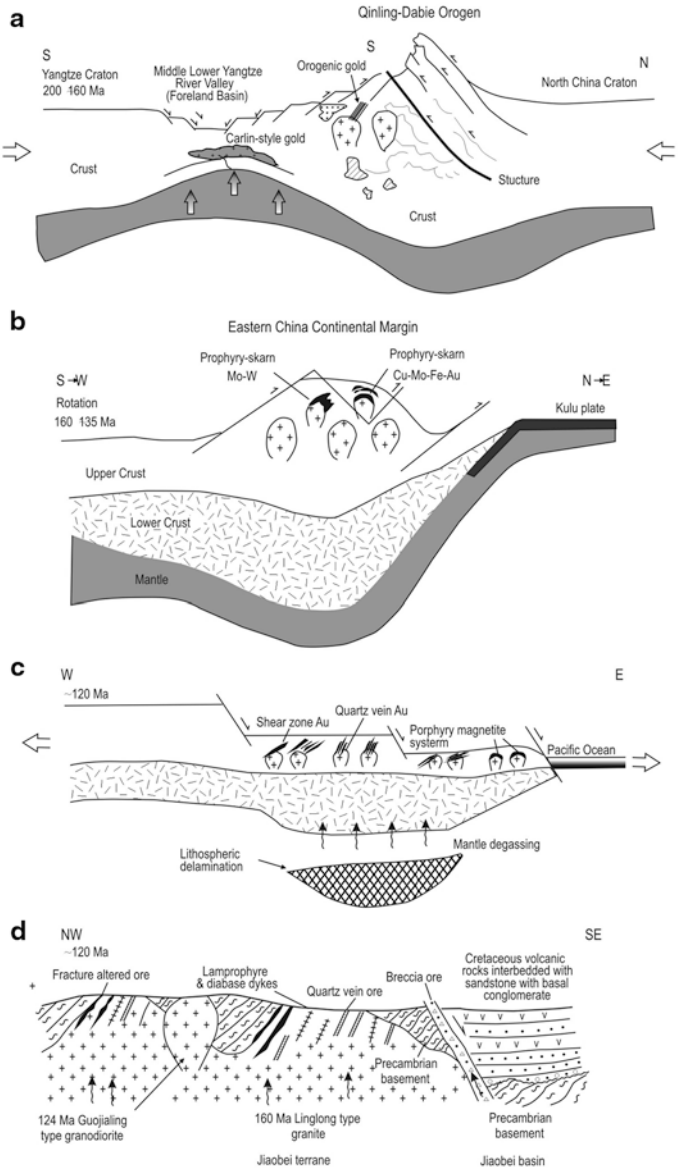

Fig. 3.23 Geodynamic model of ore formation in Eastern China (according to Mao et al. 2008). **a** Qinling-Dabie collisional orogenic belt, with mantle underplating, granite emplacement and associated Carlin-like and lode gold mineralisation during post-collision extensional tectonics (220–160 Ma); **b** transitional period of regional principal stress field from N-S- to near E-W-trending (160–135 Ma), possibly caused by subduction of the Paleo-Pacific or Kula plate, which was accompanied by intrusion of I-type granitoids at shallow crustal levels and related porphyry-skarn Mo-W mineralisation (around 140 Ma); **c** lithospheric thinning event during the Cretaceous possibly caused by delamination, accompanied by A-type magmatism and related magnetite porphyry and gold mineralisation, and mantle degassing (ca. 120 Ma); **d** Quartz vein, fracture altered and breccia type gold deposits in the Jiaodong area formed at ca. 120 Ma, hosted by various rocks and fracture systems; their ore-forming materials probably derived from mantle fluids, which ascended together with lamprophyre and diabase dykes, and interacted with crustal fluids and host rocks

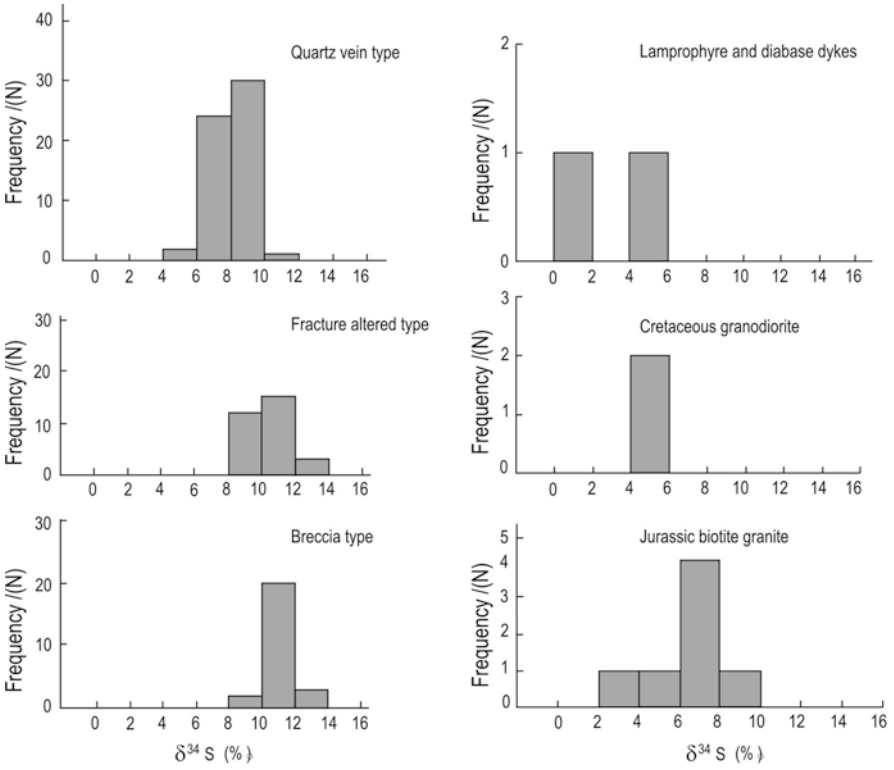

Fig. 3.24 Histograms of sulphur isotope composition of pyrite from quartz vein type, fracture-altered type and breccia type in Jiaodong, compared with lamprophyre, granodiorite and biotite granite; the $\delta^{34}S$ values tend to become higher from quartz vein type to fracture and breccia types (see text). (After Mao et al. 2008)

in both Jiaodong and Eastern Qinling, and porphyry-magnetite system along the Middle-Lower Yangtze belt occurred in this period (Chap. 4).

The carbon, oxygen, hydrogen, and sulphur isotopes systematics of the gold ores in the Jiaodong area (Mao et al. 2008; Table 3.4), show that they were formed from water-rock interaction and mixing of fluids derived from the same reservoir. The metallogenic conditions of quartz vein-type and fracture altered-type ores are similar, with the only difference being the different locales in the fault system (Fig. 3.23d). The breccia-hosted gold deposits occur in the detachment zone at the north margin of the Jiaolai basin (Fig. 3.23d), with fluid mixing and water-rock interaction, led to more crustal fluids with greater input of carbon and sulphur from the crust in the ore fluids. The data show high $\delta^{34}S$ values and hydrogen and oxygen isotopic shift towards meteoric water, and the fluid mixing nature of magmatic or mantle fluids with CO_2-bearing meteoric fluids possibly derived by leaching of Precambrian carbonates. The sulphur isotopic composition of pyrites from the three types of Jiadong lode deposits, compared with associated igneous rocks is shown in Fig. 3.24.

Lode Gold Deposits in the Yanshan-Liaoning (Yan-Liao) Metallogenic Belt

On the northern margin of the NCC, about 100 km from the faulted boundary of the Craton, are the Dongping, Zhongshangou and Xiaoyinpan lode Au deposits, hosted in rocks of the Shuiquangou complex, which consists of aegirine-augite syenite and monzonite intruding Archaean high-grade metamorphic rocks of the Sanggan Group (Miller et al. 1998). The area of these lode deposits is part of the Yanshan-Liaoning (also abbreviated Yan-Liao) porphyry metallogenic belt, discussed below, as well as the type area for the Yanshanian magmatism. Research on the lode Au deposits of this belt include the works of Hart et al. (2002), Mao et al. (2003b) and Cook et al. (2009), which I have perused for the following overview.

The Dongping lode Au deposit (Hebei Province; Figs. 3.18, area VII and 3.25), occurs where Precambrian basement is intruded by alkaline igneous rocks of Mid-Palaeozoic age, such as the above-mentioned Shuiquangou complex, and Mesozoic felsic-intermediate rocks. Isotopic age determinations, using the K-Ar and Ar-Ar systems, have a range of ages from ca. 177 to ca. 150 Ma for the Dongping Au deposit. This age range is coeval with the main Yanshanian event.

The 390 Ma Shuiquangou alkaline complex extends for about 55 km in an easterly direction and is 5–8 km wide and has on its southern margin along an east-west-trending fault a number of Au deposits (Hougou cluster), whereas further to the west and within syenitic rocks of the alkaline Shuiquangou complex and Archaean basement rocks is the Dongping Au deposit (Mao et al. 2003b). The orebodies form a series of sub-parallel quartz veins and altered wall rocks, striking northeast and steeply dipping to the northwest. Of these two vein systems contain about 80 % of the approximately 70 t of Au resources, with individual veins about a few kilometres long, up to 8 m wide and extending downdip for 200–600 m. The wall rocks surrounding the veins are typically characterised by K-feldspar reddish coloured alteration, forming haloes from about few tens of centimetres to 20 m wide (Fig. 3.25); with more distal sericite, chlorite and carbonate alteration. The altered wall rocks also carry gold and where this is of ore grade the vein + altered wall rocks may constitute an orebody. Native gold, electrum, calaverite are the main ore minerals, accompanied by minor amounts (<3 vol%) of galena, chalcopyrite, pyrite, pyrrhotite, sphalerite and Fe oxides. Five stages of vein + ore mineralogy have been described in previous works (see Cook et al. 2009): (1) white quartz-K-feldspar-pyrite; (2) quartz-gold-hematite; (3) gold-sulphides-telluride-quartz; (4) chalcedonic quartz-pyrite; and (5) carbonate-barite. However, these stages have been reconsidered in favour of a single stage, later overprinted by carbonate-barite.

Cook et al. (2009) examined the composition of pyrite from Dongping and other deposits in the same cluster. These authors showed that a remarkable correspondence exists between high Au values and three key features, namely: telluride inclusions, microfracturing and brecciation, pyrite recrystallisation. Furthermore, Cook et al. (2009) also demonstrated that As-free pyrite can contain significant amounts of Au, both as particles or in the lattice and the role of Te (tellurides) in concentrating Au.

Mao et al. (2003b) carried out a fluid inclusion study on Dongping Au-bearing quartz and identified both primary and pseudosecondary inclusions of two types:

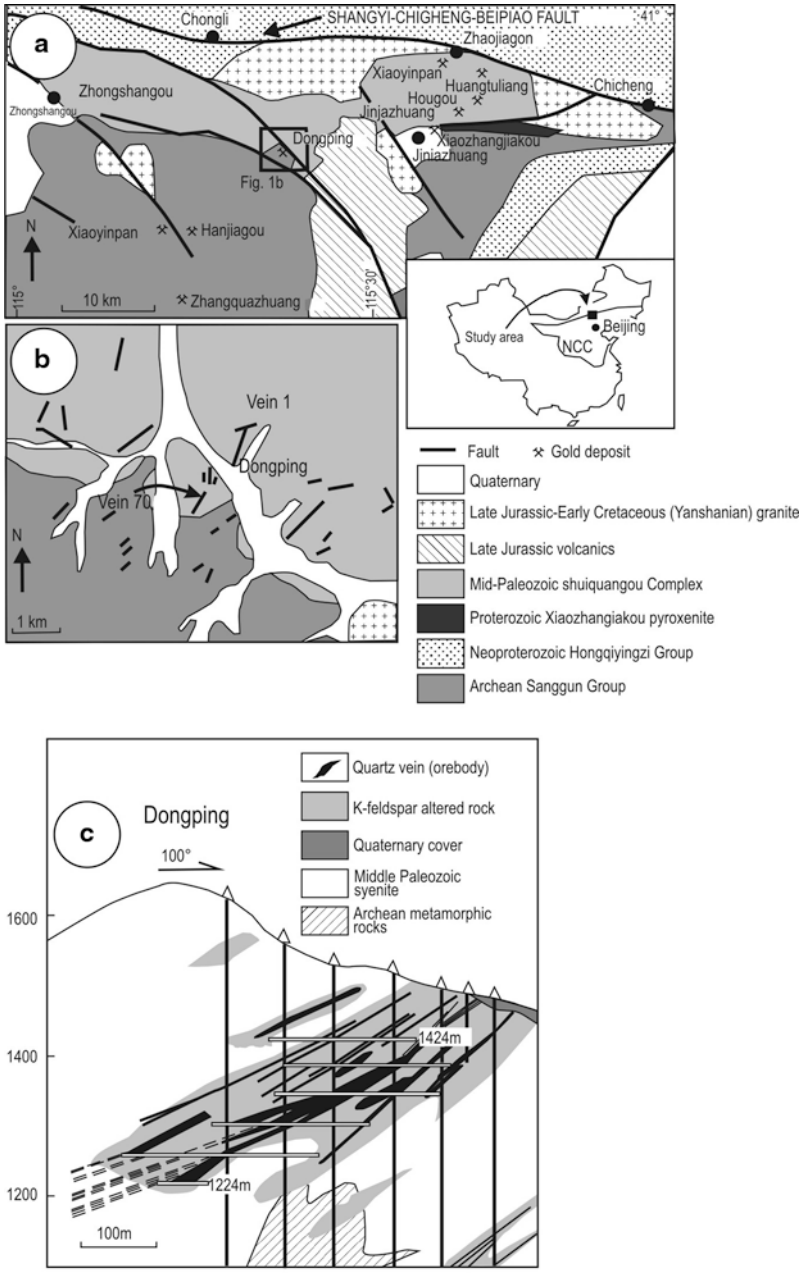

Fig. 3.25 **a** Simplified geology of Northern Hebei and location of the Dongping and other Au deposits; **b** simplified geological map of the Dongping deposit; **c** cross-section of the Dongping orebodies and associated haloes of potassic alteration. (After Cook et al. 2009 and references therein)

CO_2-rich and H_2O-rich. The CO_2-rich fluid inclusions at room temperature appear as three-, two- and one-phase, with the first comprising vapour, LCO_2 and LH_2O being the most common. The H_2O-rich inclusions have daughter minerals. Microthermometric measurements showed that CO_2-type fluid inclusions have homogenisation temperatures ranging from 372 to 247 °C, whereas aqueous inclusions have vapour-liquid homogenisation temperatures from 430 to 160 °C, with a well defined bimodal distribution from 380 to 250 °C and from 250 to 160 °C, the latter being secondary inclusions trapped after the ore-forming event. Salinities of the inclusion fluids range from 5 to 7 wt% NaCl equivalent. Results of Raman spectroscopy confirm that CO_2 and H_2O are the main volatiles, accompanied by small amountsb of N_2, H_2S, CH_4 C_2H_2 and CO. Mao et al. (2003b) also carried out noble gas isotopic determination on fluid inclusions in pyrite, which is considered as a suitable trap for noble gases. The range of values of $^3He/^4He$ is from 0.3 to 5.2 Ra (Ra being the atmospheric ratio of 1.0) which, according to the authors would suggest that the ore fluids had components showing mixing of crustal and mantle He.

The CO_2-enriched, low salinity and $^3He/^4He$ data do not resolve the origin of the source of ore fluids, because they equally fit, mantle, magmatic or orogenic or a combination of both for the fluid source(s). Similarly, geological constraints cannot rule out magmatic, orogenic or mantle sources. However, Mao et al. (2003b) pointed out that Dongping and other deposits in the area are all situated over the 100 km wide north-south gravity lineament that demarkates the boundary of the eastern sector of the NCC (inset of Fig. 3.18), which corresponds to thinned crust and shallow asthenosphere and high heat flow, discussed more fully in Chap. 7, lending some support to the idea of a dominant component of mantle source for the mineralising fluids. Although Dongping and other deposits exhibit features of both intrusion-related and orogenic (metamorphic devolitisation) Au mineral systems, the well documented upwelling of asthenospheric mantle beneath the eastern sector of the NCC (e.g. Zhao et al. 2007b; Griffin et al. 1998), adds to the distinct possibility of a mantle involvement perhaps, as suggested by Mao et al. (2003b), by advection of heat and release of volatiles (e.g. CO_2, He, H_2S) into the lower crust. The impressive halo of K metasomatism that surrounds the ore veins at Dongping (Fig. 3.25), however, could be more an effect of the fluids interacting with alkaline rocks (Shuiquangou alkaline complex) rather than a direct derivation form mantle sources, or devolitisation of the Pacific plate subducted slab beneath the thinned eastern NCC, as also suggested by Mao et al. (2003b).

Porphyry-skarn and Porphyry Mo-Cu Systems in the Yanshan-Liaoning (Yan-Liao) Metallogenic Belt

The Late Jurassic to early Cretaceous Yanshan-Liaoning (Yan-Liao) metallogenic belt is endowed a large number of porphyry-skarn, porphyry, lode gold, polymetallic and epithermal systems. The metallogenic belt extends for more than 700 km from northern Hebei, across into Inner Mongolia, from the northern margin of the NCC, across the Chifeng-Bayan Obo Fault into the Tianshan-Hinggan fold belt (or Manchurides;

Figs. 3.2, 3.3 and 3.18). To the west, in Inner Mongolia, is the Bainaimiao ore field, which comprises a porphyry Cu-Mo system and lode Au deposits (Li et al. 2012). A detailed description of a number of the porphyry deposits in the Yan-Liao belt can be found in vol. 1 of Mineral Deposits of China (Huang et al. 1990). The mineral systems (e.g. Xilamulun deposit) that are located outboard of the NCC, in the Tianshan-Hinggan fold belt, are reviewed in Chap. 5. Here, I focus on two reasonably well-studied deposits: Xiaojiayingzi porphyry-skarn and Lanjiagou porphyry Mo. The distribution of the porphyry systems in the Yanshan-Liaoning metallogenic belt, northern Hebei, is shown in Fig. 3.26 and a list of selected porphyry and porphyry-skarn deposits given in Table 3.5.

The Xiaojiayingzi porphyry-skarn deposit (Liaoning administrative province) is related to an igneous mafic-intermediate body (Xiaojiayingzi igneous complex) intruded into a sequence of Neoproterozoic carbonate rocks (Wumishan Formation). The latter formed skarns along the contacts with the igneous complex. Dai et al. (2009) studied and dated, using the Re-Os system on molybdenite, a number of porphyry Mo deposits in western Yan-Liao metallogenic belt, focusing their work on the Xiaojiayingzi porphyry-skarn Mo(Fe) deposit, detail of which are summarised below.

Basement rocks of the Archaean Jianping Formation, comprising biotite-plagioclase-gneiss, amphibolite and gneissic quartz-mica-feldspar hornfels (called leptynite by Chinese authors), are distributed in north and west of the ore district. Cambrian, Ordovician and Carboniferous marine carbonate rocks and marine-terrigenous facies rocks are exposed in the southern part, and show an unconformable relationship with Mesozoic volcanic rocks. In the eastern part, the Mesoproterozoic Wumishan Formation (Jixian Group; ca. 1.4–1.0 Ga) is composed of dolomite or dolomite with chert nodules. Brecciated, oolite and dolomite form intercalations in the dolomite. The Wumishan Formation is the main host rock in the district, trending northeast. The Xiaojiayingzi igneous complex was emplaced at the intersection of north-northeast-trending and west-northwest-trending faults and has a close spatial relationship with the Mo (Fe) orebody.

Mesozoic magmatic activity in the Yan-Liao area (Yanshan-western Liaoning) is represented by both volcanic and intrusive rocks. Volcanic rocks include basalt, andesite, rhyolite, dacite and associated pyroclastics of the Lanqi and Tiaojishan Formations (western Liaoning province). Intrusive rocks are gabbro, quartz diorite and intermediate-felsic granites. Most granitic plutons occur as stocks or dykes and have aerial extents of less than 10 km^2, with a few being of nearly batholithic dimensions. The Xiaojiayingzi igneous complex consists of 177 Ma (K-Ar) gray-green fine-grained gabbro, composed of plagioclase (65–70 %), biotite (15–20 %), pyroxene (5–10 %), olivine (0–5 %), amphibole (2–3 %) and orthoclase (2–3 %). A younger intrusion with a whole-rock K-Ar age of ca. 113 Ma, consists of medium- to fine-grained diorite. This diorite is composed of plagioclase (60–70 %), orthoclase (10–15 %), biotite (10–15 %), amphibole (3–8 %) with minor quartz and clinopyroxene. Both gabbro and diorite contain accessory zircon, apatite and sphene, which show that they belong to the same magmatic source in the lower crust. Trachytic dykes occur as a radiating swarm around the Xiaojiayingzi complex. At the eastern

Table 3.5 Selected list of porphyry and porphyry-skarn (bold type) systems in the Yan-Liao metallogenic belt. (Modified after Nie et al. 2007; Han et al. 2009; Liu et al. 2010)

Deposit	Metal(s)	Host rocks	Related-intrusion	Alteration minerals	Sulphide assemblage	Approximate age in Ma, isochron or model; (method; mineral)	Mo metal reserve (Mt) and grades (%)
Yangjiazhangzi	Mo	Cambrian-Ordovician limestone, shale an skarn	Porphyritic granite	Silica, pyrite, chlorite, carbonate	mo, py, cpy, gn, sph	191, 187 (Re-Os, mo); 189 (K-Ar; mica)	2.62; 0.14
Lanjiagou	Mo	Dolomitic limestone, Cretaceous volcaniclastics	Porphyritic granite	K-feldspar, greisen, silica, pyrite, chlorite, carbonate	mo, py, cpy, gn, ar, mg	181 (Re-Os, mo); 178–186 (K-Ar, mica)	2.17; 0.13
Xiaojiayingzi	Mo-Fe	Dolomitic limestone, chert-dolomite	Porphyritic diorite	Skarn, K-feldspar, pyrite, carbonate, sericite, chlorite	mo, py, cpy, gn, mg, sph	165.5, 177 (Re-Os, mo)	1.05; 0.28
Dazhuangke	Mo	Carbonates	Monzodiorite	K-feldspar, silica, pyrite, sericite, chlorite	mo, py, cpy, ilm, sph	147, 144.7 (Re-Os, mo)	1.0; 0.08
Dawan	Mo-Cu-Zn-Ag	Dolomitic limestone	Rhyolite porphyry	K-feldspar; silica; skarn; serpentines, carbonate	mo, py, cpy, gn, po, sph	144.4 (Re-Os, mo)	2.6; 0.12
Xiaopigou	Mo-Cu	Dolomitic limestone, chert-carbonate	Granodiorite	K-feldspar, skarn, pyrite, sericite, serpentine	cpy, cc, py, mo, bn, tet	Not available	6; 0.09; 1.9 Cu at 0.74
Shouwangfen	Cu-Mo-Fe	Dolomitic limestone, chert-carbonate	Granodiorite	Skarn, chlorite, sericite, silica, serpentine	cpy, bn, mo, mg, sph, gn	148.0 (Re-Os, mo)	0.22; 0.31; 1.6 Cu at 0.72
Chehugou	Cu-Mo	Syenite porphyry	Not known	Quartz, sericite, chlorite, epidote, carbonate	py, cpy, mo	257.5 (Re-Os, mo)	Not known

Table 3.5 (continued)

Deposit	Metal(s)	Host rocks	Related-intrusion	Alteration minerals	Sulphide assemblage	Approximate age in Ma, isochron or model; (method; mineral)	Mo metal reserve (Mt) and grades (%)
Yuanbaoshan	Mo	Quartz-monzonite	Quartz-monzonite	Not reported	py, mo	248.0 (Re-Os, mo)	Not known
Xiaoshigou	Cu-Mo	Carbonate rocks	Granite porphyry	Not reported	mo	134.0 (Re-Os, mo)	Not known
Xiaodonggou	Mo	Granite porphyry	Granite porphyry	K-feldspar, quartz, sericite, chlorite, epidote	py, cpy, mo, po, sch	135.5 (Re-Os, mo)	Not known
Nianzigou	Mo	Not available	Not available	K-feldspar		154.3 (Re-Os, mo)	Not known

Mineral abbreviations: *mo* molybdenite; *py* pyrite; *cpy* chalcopyrite; *gn* galena; *sph* sphalerite; *arg* argentite; *mg* magnetite; *ilm* ilmenite; *tet* tetrahedrite; *cc* chalcocite; *po* pyrrhotite; *sch* scheelite; *bn* bornite

margin of the fine-grained diorite, a skarn zone occurs in the contact zone between the diorite and chert-banded dolomite, where more than 80 ore veins are located.

The Mo (Fe) orebody forms veins, stockworks, lenses and stratiform bodies in the skarn rocks. The stratiform orebody has a strike length of 100–800 m, a depth extent of 100–600 m and thicknesses ranging from 4 to 21 m; with grades of 0.1–0.3 % Mo and 35–50 % Fe. The stockwork orebody has a strike length of 400 m, a depth extent of 570 m and thicknesses of 10–30 m, with grades of 0.03–0.1 % Mo. A well defined zoning is developed from the diorite to dolomite, as follows: diorite → garnet skarn → garnet-diopside skarn → diopside-forsterite skarn → chondrodite-phlogopite skarn → skarn dolomite → dolomite. The molybdenite mineralisation is present mainly in the garnet skarn and garnet-diopside skarn zones, whereas the Fe ore, represented by magnetite, occurs mainly in the chondrodite-phlogopite skarn zone. Ore minerals are mainly molybdenite and magnetite, with minor pyrite, chalcopyrite, galena, sphalerite, pyrrhotite and bornite, scheelite, marcasite and native silver. Native tellurium and native bismuth have also been reported, in addition to a huge variety of secondary minerals (e.g. ferromolybdite, powellite, tenorite, smithsonite, covellite, etc.; Huang et al. 1990). The gangue minerals are predominantly garnet (andradite and grossular), diopside, tremolite and calcite with minor vesuvianite, wollastonite, chondrodite, phlogopite, K-feldspar and quartz. Mineralisation styles consist of disseminations, stockworks and massive ore.

In the same metallogenic belt (Fig. 3.26) is the Lanjiagou Mo-Cu porphyry deposit, studied and dated, also with the Re-Os isotopic system in molybdenite, by Han et al. (2009) and also described in Huang et al. (1990). The Lanjiagou deposit is associated with a Late Jurassic coarse-grained and fine-grained granitic intrusions (Lanjiagou intrusion), outcropping over an irregular area of about 20 km^2, but showing in a vertical cross-section veins and dyke shapes. These granitic rocks, in turn, intruded a larger (200 km^2) coarse-grained K-feldspar granite, with K-Ar isotopic ages ranging from 186 to 178 Ma. The Lanjiagou intrusion consists of a yellow-pink fine-grained to porphyrytic granite composed of orthoclase, albite, quartz and biotite, for which a K-Ar isotopic age of 154 Ma and initial $^{87}Sr/^{86}Sr$ value of 0.7031 were determined.

The deposit is subdivided into upper, lower and middle section with a total of 101 mineralised bodies, trending northwest and north-south and mostly located in the middle section. Individual orebodies vary from about 80 to 1,300 m in length and from about 3 to 32 m in thickness, extending down dip for up to 400 m below the surface. There are large (up to 3 m wide, but mostly between 0.1 and 0.5 m wide) quartz-molybdenite veins and molybdenite-quartz fine stockworks (<5 mm wide). Hydrothermal alteration is mainly controlled by northeast-trending fractures and typified by K-feldspar, greisen (quartz-muscovite), silicification, illite, Fe-Mn carbonates and chlorite. Greisen and silification are commonly developed around the ore veins.

The main ore minerals are molybdenite and pyrite with minor amounts of sphalerite, chalcopyrite, galena, magnetite and electrum. Gangue minerals consist of K-feldspar, plagioclase, quartz, calcite, muscovite and chlorite, whereas minerals of wall rock alteration include quartz-muscovite (greisen), sericite, carbonate, chlorite and K-feldspar. Cross-cutting relationships of the ore veins and mineral assemblages

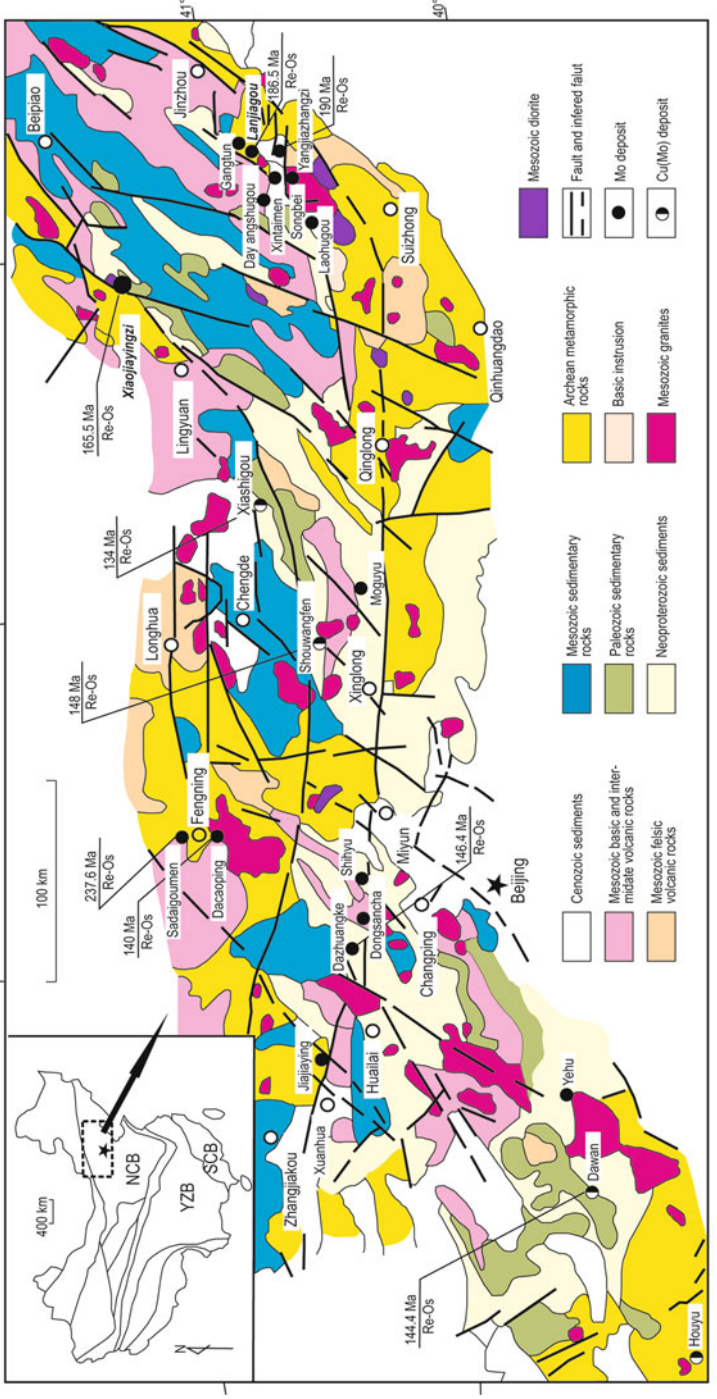

Fig. 3.26 Distribution of Mo (Cu) deposits and their mineralisation ages in the Yanshan-Liaoning metallogenic belt; *NCB* North China Block; *YZB* Yangtze Block; *SCB* South China Block (after Dai et al. 2009); Lanjiagou and Xiaojiayingzi are highlighted

suggest five mineralisation-alteration stages: (1) K-feldspar and greisen type alteration; (2) quartz-sericite-pyrite (phyllic) alteration; (3) main mineralisation stage represented by veins containing quartz-molybdenite-pyrite-sphalerite; (4) disseminations of molybdenite-pyrite-sphalerite associated with barren calcite-quartz veins; and (5) carbonate-chlorite and minor sulphides.

Results of Re-Os dating of molybdenite by Han et al. (2009) gave ages ranging from ca. 184 Ma (model age), ca. 183 Ma (weighted mean) to ca. 181 Ma (isochron). Previous published ages of the host granitic rocks include ca. 186 to ca. 178 Ma (K-Ar) and a Rb-Sr isochron age of ca. 154 Ma for the fine-grained granite.

Han et al. (2009) concluded that the formation of the Lanjiagou porphyry Mo-Cu deposit can be related to subduction of the Pacific (Izanagi) plate and partial melting of the lower crust beneath the eastern sector of the NCC.

Links of the Yanshan-Liaoning Porphyry Systems with Geodynamic Events

The Xiaojiayingzi porphyry-skarn Mo (Fe) deposit is considered different from other Mo (Cu) deposits (e.g. Yangjiazhangzi, Lanjiagou and Sadaigoumen deposits in the Yan-Liao area) in both magma sources and metallogenic ages. The Xiaojiayingzi deposit is associated with intermediate-mafic intrusive rocks, whereas the other Mo (Cu) deposits are related to intermediate-felsic rocks. For instance, the Lanjiagou quartz vein-type Mo and the Yangjiazhangzi skarn Mo deposit in the western Liaoning province are temporally and spatially associated with fine-grained granite and their Re-Os ages are 186.5 and 190 Ma, respectively. The Sadaigoumen porphyry Mo and Dawan porphyry-skarn Cu (Mo) deposits in Hebei province are associated with monzogranite and rhyolite porphyry, respectively. The molybdenite Re-Os age is 237 Ma for the Sadaigoumen deposit and 144 Ma for the Dawan deposit. All Re-Os ages of these Mo deposits, range from 134 to 237 Ma with two peaks of 185 and 145 Ma (Dai et al. 2009). These precise molybdenite Re-Os ages show that the Mo (Cu) mineralisation event in the Yan-Liao area occurred in the Early Jurassic and Late Jurassic, The magmatism in the Yan-Liao belt and the associated Mo (Cu) ore systems were probably linked to the combined effects of post-collision of the Siberian-Mongolian block with the NCC, and the subduction of the Palaeo-Pacific plate (Izanagi) beneath the eastern margin of the NCC. However, the Re-Os ages reported, show that the Xiaojiayingzi deposit was formed in the Middle Jurassic, different from the predominantly Triassic to Jurassic ages of other Mo deposits in the Yan-Liao area.

The Mid-Jurassic was one of the main stages of the Yanshanian tectono-thermal event, when tectonic and magmatic activity developed strongly in the Yanshan region which, as mentioned above, is in fact the type area for this tectono-thermal event (first recognised by Wong 1927). Volcanic rocks are mainly the Jurassic Tiaojishan Formation in the northern Hebei province and of the Lanqi Formation in the western Liaoning province and are the product of central eruptions. These volcanic rocks comprise andesite, trachyte and dacite, with minor basalt and rhyolite, belonging to the calc-alkaline to high-K calc-alkaline series. Intrusive rocks are mainly syntectonic and form stocks, sills or dykes, and include gabbro, diorite, quartz monzonite, syenite

and granite. The intrusive rocks probably belong to a magmatic series that resulted from asthenosphere-lithosphere interactions, perhaps associated with compressive movements in the Yan-Liao area.

In the Mesozoic, the tectonic deformation in the Yanshan region began at about 160 Ma (Zhao et al. 2004), recorded by the nappe thrusts, folding upllift and erosion. Although several studies suggest that the collision between the Siberian craton and the North China-Mongolia Block might have been ongoing until the closure of the Mongolia-Okhotsk Ocean in the Late Jurassic, up to 1,000 km from the North China Craton, the subduction of the Paleo-Pacific Ocean beneath to the East Asian margin began during the Middle Jurassic (ca. 180 Ma) reached a peak of activity during the Late Jurassic to Early Cretaceous period. Large scale volcanic activity (e.g. the Tiaojishan and Lanqi Fromations) occurred at ca. 160 Ma in the Yan-liao area and the geochemistry of the volcanic rocks shows that they have the geochemical character of adakite, indicating that they were derived from partial melting of basaltic rocks in the lower crust and related to underplating of basaltic magma. Thus, the tectonism and magmatic activity associated with the 160 Ma episode, according to Dai et al. (2009), are the result of the subduction of the Paleo-Pacific Ocean beneath to the North China Craton, as shown in Fig. 3.27.

Permian-Triassic Cu-Mo Porphyry Deposits in the North China Craton

Liu et al. (2010) reported on Permian-Triassic porphyry type mineralisation on the Yan-Liao metallogenic belt. The Chehugou porphyry Cu-Mo and the Yuanbaoshan Mo deposits are located 55 km northwest of the town of Chifeng (Inner Mongolia) and close to the east-west trending Chifeng-Bayan Obo fault (Fig. 3.18, area VI), which marks the tectonic contact with an accretionary fold belt (Bainaimiao arc) on the northern margin of the NCC.

The Chehugou porphyry Cu-Mo orebodies are hosted by the Chehugou pluton, composed of syenite and muscovite plagiogranite, and form northeast-striking lodes or lenses. These lenses range from 300 to 450 m long and from 1 to 11 m thick and are associated with extensive hydrothermal alteration, characterised by varying amounts of quartz, sericite, chlorite, epidote and carbonate, with lesser K-feldspar alteration along the edges of the ore lenses. The Yuanbaoshan Mo occurrence, 6–8 km east of Chehugou, is associated with a quartz-monzonite that has an elliptical shape with an area of about 35 km^2. Here, the Mo mineralisation is controlled by a northwest-trending fracture zone and with a simple ore assemblage of molybdenite and pyrite. The molybdenite occurs as disseminations or films within fractures in the host granite.

Re-Os dating of molybdenite was carried out by Liu et al. (2010) for both Chehugou and Yuanbaoshan. The Re-Os ages for the former range from 243.3 ± 2.5 to 269.5 ± 2.7 Ma, yielding an isochron age of 257.5 ± 2.5 Ma (Late Permian-Early Triassic). Interestingly, the authors stated that this age is 118 Ma younger than the host syenite, for which a zircon U-Pb age of 376 Ma was obtained, effectively excluding a genetic relationship between the syenite and the Mo mineralisation. Re-Os

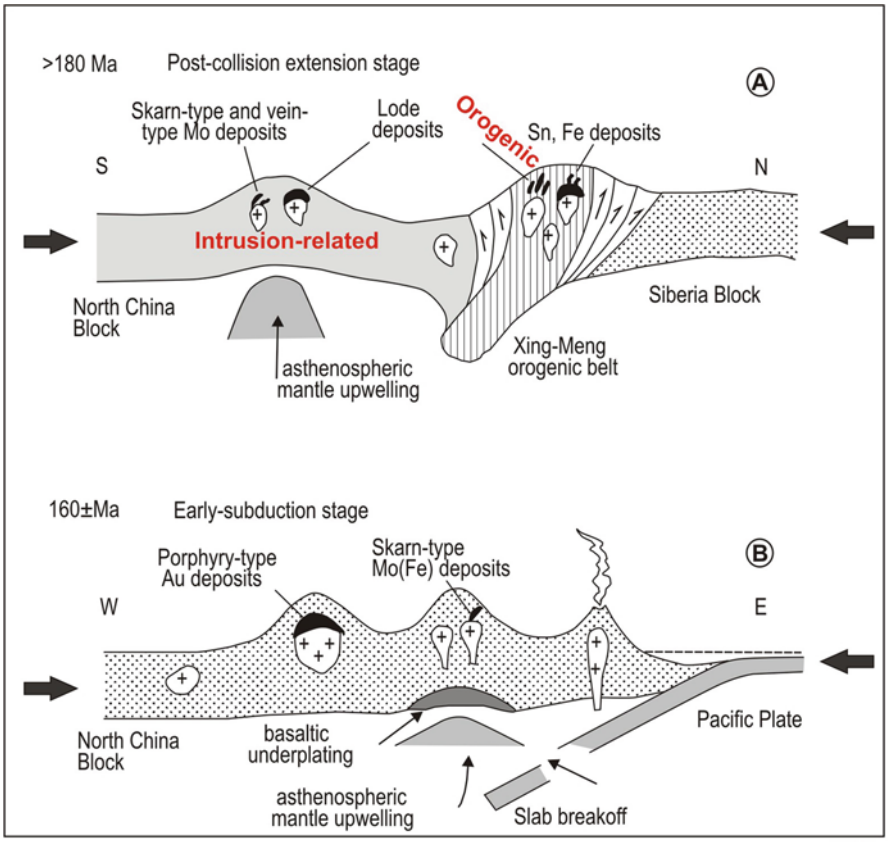

Fig. 3.27 Sketch of Jurassic tectonic evolution, early subduction and post-orogenic metallogeny in the northern margin of North China Craton (according to Dai et al. 2009); note that intrusion-related lode deposits can evolve into orogenic lodes in a fold belt

dating of molybdenite from the Yuanbaoshan Mo occurrence, yielded a model age of 248.0 ± 2.6 Ma, whereas a U-Pb age of 269 ± 3 Ma (Late Permian) was obtained from the host quartz monzonite. In this case, the Mo mineralisation, 21 Ma younger than the host rocks, could be related to post-magmatic hydrothermal fluids that flowed along fracture zones. Whether this hydrothermal activity is actually related to post-magmatic exsolution from the Yuanbashan pluton, is not clear.

Taken together with other age determinations (Table 3.5 and other published ages, e.g. Mao et al. 2010), there are several groups or age peaks, during which mineral systems from porphyry, porphyry-skarn to polymetallic veins and Au lodes, were formed. These peaks, 130–112, 130–150, 185–165 and 250–260 Ma, with the recent work by Liu et al. (2010), indicate several phases of magmatism and associated mineralisation in the structurally-controlled metallogenic belts of the NCC (northern and southern margins, Tanlu fault and associated splays). These phases are all

linked to a combination of lithospheric thinning, asthenospheric mantle upwellings, delamination tectonics, related to Indosinian and Yanshanian tectono-thermal events which are, in turn, related to a geodynamic of collisions between the NCC and the Yangtze Craton in the south and the Mongolia-Siberian blocks in the north. However, the 250–260 (Permian-Triassic) ages of the Chehugou and Yuanbaoshan Mo mineralisation, introduces a new age span, which happens to coincide with mantle plume activity and associated large igneous provinces (e.g. Emeishan and Siberian). But, as mentioned time and again, these events, which are of the utmost importance in unravelling the development of mineral systems in the reactivated parts of the NCC, will be taken up in more detail in Chap. 7.

3.3 Tarim Craton

The Tarim Craton (also variably referred to in the literature as Block or Basin, regardless of whether the topic in question is basement or cover rocks), entirely situated in Xinjiang Autonomous Region and covering an area of about 600,000 km^2, is poorly known, mainly because most of it is covered by Phanerozoic sedimentary and volcanic successions that in this book I refer to as Tarim Basin (Fig. 3.28; Chap. 8). The Tarim Craton (hereinafter referred to as Tarim) was amalgamated with the North China and Yangtze Cratons during the Phanerozoic, probably following the assembly of Pangea and the closure of the Palaeo-Tethys Ocean (Wang et al. 2005). The Tarim effectively acted as a rigid block during Palaeozoic, Mesozoic and Cenozoic collision and accretionary events, almost like a giant clast wrapped around by fold belts. Tectonic movements, such as those related to the India-Asia collision, resulted in a continuing jostling of the Tarim and reactivation of strike-slip faults in the surrounding fold belts, sometimes resulting in catastrophic earthquakes. The interpretation of a recent reflection seismic transect from the middle Tianshan across to the western Tarim, suggests that the Tarim is underthrust beneath the Tianshan (Makarov et al. 2010).

The nature of the basement rocks underlying the younger successions is still controversial, with hypotheses including a Palaeozoic oceanic basin, trapped in Palaeo-Tethys suture zone (Hsü 1988), a Neoproterozoic failed rift (Jia et al. 1991, cited in Guo 2005) and an oceanic plateau (Sengör et al. 1996). In addition, a broad east-trending magnetic anomaly extends right across the central part of the Tarim and interpreted to be Archaean crystalline basement (Guo et al. 2005).

The oldest rocks of the Tarim are exposed along the margins and comprise 3.2 and 2.8–2.6 Ga amphibolites in the northeast and TTG rocks intruded by ca. 2.53 Ga granitoids (Zhang et al. 2012). Amphibolite rocks of the Tuoge Complex in the northeast show a Sm-Nd isochron age of ca. 3.3 Ga, with (Long et al. 2010 and references therein). Orthogneiss rocks in the Kuluketage area, northeasterrn Tarim have U-Pb zircon weighted mean $^{207}Pb/^{206}Pb$ ages of ca. 2.5 Ga with a geochemical signature suggesting that their protolith may have been high silica adakites, derived from a subducted slab (Long et al. 2010). Small blocks of 2.5 Ga high-grade metamorphic rocks in the Altayshan and Beishan regions may have been part of the Tarim

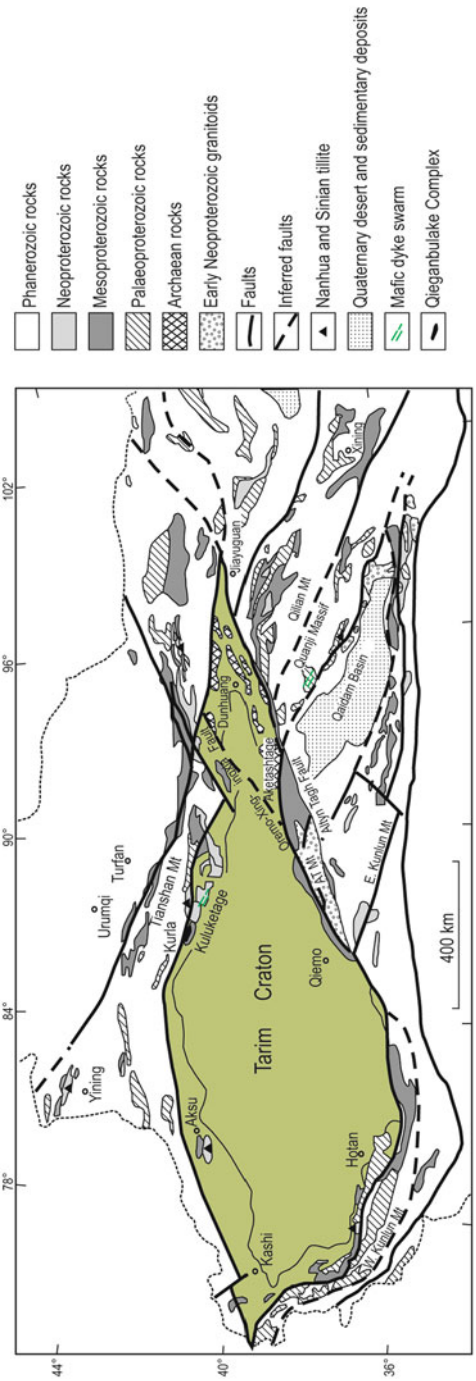

Fig. 3.28 Simplified geology of the Tarim Craton, bordering major structures and surrounding areas. (After Lu et al. 2008)

(Zhou et al. 2002). The Tarim was cratonised at the end of the Jinning orogeny at about 850 Ma, when it became the basement for an inland Late Carboniferous-Early Permian basin (Zhou et al. 2002), but recent geochronological and Hf isotopic studies of Neoarchaen basement rocks, while confirming that the Tarim was cratonised later than the NCC and the Yangtze Craton, show that this may have occurred in the late Neoarchaean (Long et al. 2010).

Zhang et al. (2007a) recorded Palaeoproterozoic magmatism between ca. 2.41 and ca. 2.34 Ga in the southwestern part of the Tarim that resulted in the emplacement of post-orogenic A-type granitic rocks. The 2.41 Ga event refers to the emplacement of the Akazi pluton, which is a granodiorite-adamellite suite, whereas the 2.34 Ga event is represented by the Xuxugou pluton with a more complex petrological make up (foliated potassic granite, granodiorite with gabbroic and dioritic enclaves, suggestive of magma mingling) and geochemically comprising both A-type and S-type granitic rocks. In addition, alkaline mafic dykes dated at ca. 2.34–2.36 Ga intruded TTG Archaean rocks in the eastern Tarim. The above mentioned suites have similar Sm-Nd isotopic compositions, with εNd(t) values for the Akazi pluton ranging from −3.22 to −4.71 and Nd model ages (T_{2DM}) from 3.07 to 3.05 Ga, whereas the Xuxugou pluton has εNd(t) values from −0.41 to −2.18 and model ages (T_{2DM}; two-stage Nd model age) from 2.91 to 2.76 Ga.

On the basis of their geochronological, geochemical and isotopic data, Zhang et al. (2007a) proposed that the Precambrian basement of the Tarim underwent three stages of geodynamic evolution, as follows: formation of a ca. 2.5 Ga TTG-like protocrust was followed by the above mentioned thermal events at ca. 2.41 and ca. 2.34 Ga, then a ca. 1.9 Ga episode of high-grade metamorphism, which finally resulted in the consolidation of the Tarim Precambrian basement. According to Zhang and co-authors, the emplacement of these igneous suites is indicative of basaltic magma underplating or intraplating, leading to partial melting of the mafic crust and of metasedimentary rocks to produce A-type and S-type granitic rocks of the Xuxugou pluton. These events would reflect continental rifting after the formation of the TTG protocrust (Zhang et al. 2012). The 1.9 Ga metamorphism, recorded in zircons of the Akazi pluton, is also recorded in the northern and southeastern parts of the Tarim, suggesting a widespread 1.9 Ga orogenic event in the Tarim which, Zhang et al. (2007a) pointed out is broadly coeval with other Palaeoproterozoic orogenies that may have led to the assembly of the Columbia supercontinent (Rogers and Santosh 2004).

The evolution of the Tarim is also discussed by Lu et al. (2008), who subdivided the lithostratigraphic sequence into an older pre-Mesoproterozoic (pre-Nanhuan) metamorphic basement and a younger sedimentary cover, called Nanhua System (part of the Sinian (Upper Neoproterozoic; see Tables 1.2 and 1.4 in Chap. 1)). Archaean basement rocks are exposed in the Altyn Tagh mountains in the southeastern margin of the Tarim, where they mainly consist of granitic gneiss, granulites and metasedimentary units. SHRIMP U-Pb zircon dating from orthogneiss and tonalite gneiss yield ages from ca. 2.67 to ca. 2.60 Ga, respectively, whereas monzonitic gneiss in the Altyn Tagh yield zircon ages of about 2.83 Ga (Lu et al. 2008). The Palaeoproterozoic in the Tarim comprises events of magmatism, metamorphism and

partial melting and emplacement of mafic dyke swarms and rapakivi granites. In the early Palaeoproterozoic (ca. 2.45 and ca. 2.35 Ga) orthogneisses were predominantly derived from tonalite, granodiorite and monzonite, many containing mafic enclaves. These rocks are found along the southern margin of the Craton and the eastern Altyn Tagh. Granulite and amphibolite facies metamorphism and partial melting occurred between 1.98 and 1.91 Ga, resulting in the formation of migmatites. Mafic dyke swarms, trending northwest, are present in the Quanji Massif, in the northern margin of the Craton, which also contains rapakivi granites. The dyke swarms and rapakivi spatial association is suggestive of an extensional environment (Lu et al. 2008). The ages of these rocks range from 1.85 to 1.77 Ga, slightly older to nearly contemporaneous than the extensional event that affected the North China Craton. Palaeoproterozoic high-grade metamorphic (1.79 Ga amphibolite to granulite facies) supracrustal rocks are also exposed in the Quanji Massif thought to have been derived from a pelitic protolith. The Mesoproterozoic rocks in the Tarim comprise stromatolitic carbonates, clastic sediments along the northern margin, sedimentary, bimodal and calc-alkaline volcanic rocks on the southern margin, and high-pressure and ultrahigh-pressure metamorphic rocks (coesite-bearing eclogites, garnet schist and marbles) that are enclosed in the Phanerozoic orogenic belts that border the Craton. The Mesoproterozoic is marked by the Tarimian Orogeny (1.05–0.90 Ga), which Lu et al. (2008) correlated with the Jinningian Orogeny of the Yangtze Craton, suggesting that these two cratons may have been geographically close. The Neoproterozoic (820–740 Ma) of the Tarim is characterised by rifting events, which are documented by the presence of mafic dyke swarms (e.g. 821 Ma Yifeng swarm), mafic-ultramafic intrusions (e.g. 818–802 Ma Qieganbulake intrusion; see below), alkaline granites and bimodal volcanic rocks (Lu et al. 2008). One of the bimodal volcanic sequences is represented by the 755 Ma Biyixi Formation, reported by Xu et al. (2005), who suggested that this type of rift-related volcanism may have been part of a global event that affected the Rodinia supercontinent. Indeed, Lu et al. (2008) suggested that the Tarimian Orogeny was linked to the assembly of Rodinia and that the subsequent Neoproterozoic rifting events, at about 820 Ma, were related to the breakup of the supercontinent. These rifting events may have been associated with the impingement of a mantle plume that could have been formed a triple junction between Australia, the Yangtze Craton and the Tarim, resulting in radiating dyke swarms and mafic-ultramafic intrusions. This 820 Ma mantle plume event is likely to have produced the Jinchuan mafic-ultramafic intrusion and associated Ni-Cu-PGE sulphide mineralisation (see Chap. 7). The Meso-Neoproetrozoic lithostratigraphy, according to Zhou et al. (2001), of the Tarim is shown below (Tab. 3.6).

On the southwestern edge of the Tarim, a Neoproterozoic bimodal intrusive complex, Kudi complex, was investigated by Zhang et al. (2006). The Kudi igneous complex, located in Yecheng County south from the town of Kashi (Fig. 3.28), consists of mingled gabbro and granitic rocks with gneissic textures, previously interpreted as part of an ophiolitic complex. The Kudi complex is dated at ca. 783 Ma (SHRIMP U-Pb) and was subsequently intruded by Palaeozoic (ca. 405 Ma) and Indosinian (ca. 224 Ma) granites. Sm/Nd isotope systematics revealed εNd(t) values ranging from 0 to + 6.0 and a Nd model ages (T_{2DM}) of the 1.3 Ga granitic rocks.

Table 3.6 Meso-Neoproterozoic lithostratigraphy of the Tarim Craton. (modified after Zhou et al. 2001)

		Tarim Craton			
		Aksu Region (NW Tarim)		***Kuruk Tagh Region (NE Tarim)***	
Post-Sinian Cover		Xiacertulake Fm (Lower Cambrian)	Dolomites, asphalitic dolomites, cherty phosphate rocks. Bearing trilobites, brachiopods, hyolithes, ostracods, and sponge spicules	Xishanbulake (Lower Cambrian)	Gray, gray-black thin-bedded limestone and chert. Local andesitic porphyrite. Cherty phosphorate at the base
Age	**System**				
600 Ma	**Sinian**	Upper Sinian	**Qigebulake Group:** shelfal dolomite and siliciclastic rocks -150 m **Sugaitebulake Group:** nommarine to paralic siliciclastic arenite, and shelfal carbonate and siliciclatic arenite, with top bearing glauconite. -200–900 m	Kuluketage Group	Upper part: predominant siliciclastic rocks, minor chert and carbonate. Many are thought to be glacial deposits. Lower part: intermediate to acid volcaniclastics and lava flow. several thousands of metres
800			**Youermeinake Group:** red and green conglomerates and pebbly sandstone and arenite. -50 m (probably of glacial origin)		Angular Unconformity?
	Qingbaikou	Aksu Group **metamorphosed**	**Qiacenbulake Group:** gray-green colored coarse-medium lithic arkoses, fine sandstone, and muddy and calcareous siltstones; -500–1500 m	Paerganglage Group **metamorphosed**	Upper part (614 m): stromatolitic carbonates (marbles and dolomite). Lower part (<140 m): schist and quartzite.
1000			Angular Unconformity		contact not clear?
	Jixian		-700 Ma metamorphic age Psammitic, pelitic, and mafic schist and minor quartzite, meta-ironstone, and metachert of low-grade green-schist facies and Greenschist-blueschist transitional facies	Erigan Group	Marble, schist, quartzite, iron bearing quartzite, and minor conglomerate
1400					Angular Unconformity?
1800	**Changcheng**	Lower age limit unknown		Xingdilage Group	Metamorphosed clastic and carbonate rocks.

The positive εNd(t) values, led the authors to interpret the Kudi complex as being related to partial melting of volcanic arc-type lower crust rocks, due to a heat source linked to underplated mafic melts derived from the periphery of a mantle plume.

Guo et al. (2005) studied core from a >7,000 m deep well (TC-1), drilled in central part of the Tarim and penetrating about 35 m into the Precambrian basement. Here, the rock intersected was an undeformed diorite with $^{40}Ar/^{39}Ar$ ages ranging from ca. 790 to ca. 744 Ma and with geochemical signatures consistent with those of an arc setting. Guo et al. (2005) suggested that this diorite pluton may be part of a Proterozoic subduction system, which could correlate with similar belts of rocks with similar ages in the southern Tianshan (Aksu Blueschist) and the eastern Altyn Tagh. On this basis, these authors postulated the existence of east to northwest-trending and north dipping subduction zone, which produced a 970–800 Ma magmatic arc, extending from Aksu (Fig. 3.28) in the north to the eastern Altyn Tagh in the southeast. This would have been followed by a collision event at 800–750 Ma, between the northern part of the Tarim with the southern block (south of the subduction), forming a suture zone. An extensional event followed at 750–700 Ma forming an east-west-trending

rift and deposition of a passive margin shallow-marine sequence, after 700 Ma, which cover most of the older Precambrian arc rocks.

A ca. 800 Ma ring complex and nearly coeval granitic intrusions occur on the northeastern margin of the Tarim (Zhang et al. 2007b), which seem to confirm a continental rifting environment at that time in the Tarim. The Qiganbulake (also spelled Qieganbulake and not to be confused with the Qingbulake intrusion in the west Tianshan; discussed in Chap. 5) is a ring complex conprising five mafic-ultramafic stocks, carbonatite and associated dykes. Gravity and aeromagnetic data indicate that many more similar stocks and dykes may be concealed below the surface, making the complex a much larger system than that shown in outcrop. The mafic-ultramafic rocks comprise mainly dunite, apatite-bearing pyroxenite, pyroxenite. The dunite is mostly serpentinised and contains vermiculite (see below) and minor magnetite, diopside and phlogopite. Pyroxenite forms the outer parts of the ring complex and includes, apatite-bearing pyroxenite, phlogopite-bearing pyroxenite, K-feldspar-apatite pyroxenite, megacrystic pyroxenite and magnetite-bearing pyroxenite. A rock, which Zhang et al. (2007b) named phlogopitelite, consists almost entirely of coarse-grained phlogopite, from 10 mm up to 1 cm in size. The carbonatite occurs within the dunite as veins and pods, about 0.5–20 × 2.5–40 m in size and consists of calcite, dolomite, titanomagnetite and apatite, as well as accessory rutile, monazite, phlogopite and baddeleyite. Dating of baddelyite, using the U-Pb TIMS method, yielded a weighted mean age of 810 ± 10 Ma, almost identical with a SHRIMP U-Pb zircon age of a pyroxenite sample (818 ± 11 Ma) and a $^{39}Ar/^{40}Ar$ 812 ± 1.2 Ma of a phlogopite sample. Granitic rocks of about the same age as the ring complex form the Xingdi granodiorite plutons (820 ± 10 Ma, zircons $^{207}Pb/^{206}Pb$) and the Taiyangdsao granitic pluton (795 ± 10 Ma, zircons $^{207}Pb/^{206}Pb$). Sm-Nd isotopic data show fairly consistent $\varepsilon Nd(t)$ values (0.51–0.73) for the ring complex rocks. Zhang et al. (2007b) suggested that the Qiganbulake ring complex and associated granitic rocks are part of widespread 820–800 Ma bimodal magmatism that affected the Tarim and adjacent regions (Aksu mafic dykes, 825–830 Ma Bachu layered mafic-ultramafic intrusion in western Tarim; Pirajno et al. 2009 and references therein). These Tarim intraplate igneous rocks are also coeval with intraplate magmatism in other parts of China, such as the above-mnetioned Jinchuan mafic-ultramafic complex, hosting a world class Ni-Cu-PGE sulphide deposit (discussed in Chap. 7), mafic and ultramafic rocks in Hannan, in the northern margin of the Yangtze Craton and the Tongde-Gaojiashna mafic-ultramafic complex on the western part of the Yangtze Craton (Chap. 4). An interesting implication of these correlations is that they may be related to a Neoproterozoic mantle plume that impinged the Rodinia supercontinent, as proposed by Li et al. (2003a), causing rifting and its break up. It has been proposed, on the basis of palaeomagnetic data and palaeogeographic reconstructions, that the Tarim was connected to the Kimberley Block of Western Australia (Li and Powell 2001). In this hypothesis, the Tarim would have been separated from northwestern Australia in the Neoproterozoic.

In the Aksu area, northwest Tarim, a mafic dyke swarm is dated by SHRIMP U-Pb at 807 ± 12 Ma and comprises a series of dykes that extend for about 5–10 km and intruded the Aksu Group (Chen et al. 2004). Palaeomagnetic work by Chen

et al. (2004) also supports a possible connection between the Tarim and northwestern Australia. About 50 km east of the Qiengbulake intrusion, in the Quruqtagh area is another Neoproterozoic mafic-ultramafic intrusion, dated at 760 ± 6 Ma (SHRIMP U-Pb zircon), coeval with a mafic dyke swarm and bimodal volcanic rocks in the same area (Zhang et al. 2010). Zhang et al. (2010) reported on this intrusion, which they called N2MC, because it is one of six in the northeastern Tarim, including Qiengbulake. N2MC intruded amphibolite facies metasedimentary rocks of a Xingditage Group (not listed in Zhang 2009) and the rock types of this intrusive body, which has a funnel shape, are lherzolite, pyroxenite, gabbro and diorite. These rocks were emplaced in three phases: (1) early ultramafic unit (lherzolite); (2) layered mafic-ultramafic-intermediate unit (pyroxenite and gabbro); (3) late mafic unit (gabbro and diorite). εNd (t = 760) of the N2MC rocks show fairly consistent values from −7.6 to −2.8 and initial $^{87}Sr/^{86}Sr$ values from 0.7067 to 0.71167.

The above discussed mafic-ultramafic intrusions and dyke swarm were emplaced at ca. 820, ca. 807 and ca. 760 Ma, all exhibiting geochemical signatures of continental rift-related igneous rocks, derived from a metasomatised sub-continental lithospheric mantle source (SCLM) (e.g. Zhang et al. 2010) and perhaps all related to pulses of Rodinian mantle plume (or superplume?) activity. These pulses would have led to the fragmentation of Rodinia, separation of Greater India from Australia and the Tarim. The separation of the Tarim from Australia resulted in a series of intervening rift basins, with dyke swarms and mafic-ultramafic intrusions being emplaced along the basins faulted margins.

Turner (2010) studied in detail a sedimentary succession in the northwest Tarim, near Aksu and Wushi, providing evidence of an early phase of Neoproterozoic rifting. The succession, which is 600–900 m thick and unconformably overlies high-grade metamorphic basement rocks of the Aksu Group, comprises two formations: older non-marine Sugaitebulake and the overlying marine Qegebulake. The older Sugaitebulake Formation, consisting of interbedded clastic and volcanic rocks is well represented in the Aksu section. Here a 10 m thick red conglomerate, containing clasts of basement rocks, at the base of the Formation is followed upward by fluvial sandstones concordantly intercalated with three, 15–20 m thick basalts, which can be traced laterally for long distances. At Wushi the succession consists of a coarse-grained red sandstone unconformably overlying basement chlorite schist and interpreted as representing a braided fluvial system. This sandstone is followed upward by finer grained sandstone and siltstone, deposited in a lacustine setting. Here too are basalt horizons, but these are less extensive than those of the Aksu succession. The younger Qegebulake Formation characterised by sandstone and siltstone, overlain by a coarse and sand-rich limestone passing upward to a micritic dolomite with abundant stromatolites. The latter are up to 1 m wide and 0.5 m high, decreasing in size upward in the succession. The age of these stromatolites has been determined as Late Neoproterozoic. The stromatolite-bearing carbonate units are followed by thick-bedded micritic dolomite. The Qegebulake Formation is interpreted to represent a transgression to lacustrine and/or shallow marine environment. The above described Neoproterozoic successions are capped by Lower Cambrian black shales and organic-rich carbonate beds. The black shales are temporally correlated with

phosphorite-bearing black shales in Siberia, Australia and India, suggesting that they were all deposited during a period of anoxia and at low latitudes (McKerrow et al. 1992). On the basis of field studies and sedimentological character of the Sugaitebulake and Qegebulake Formations, Turner (2010) suggested that the Tarim was subjected to a period of rifting, with four stages: (1) rift initiation, as reflected by the basal coarse clastic units (conglomerate and sandstone), perhaps deposited in a number of small fault-bounded sub-basins, which coalesced during the deposition of subsequent stages, ending with a major marine transgression; (2) a stage of rift deepening was associated with a fluvial and lacustrine depositional system, linked to progressive growth faults, further substantiated by intrusion of mafic dykes and eruption of basaltic lavas; (3) this is a stage of rifting climax together with the deposition of marine facies carbonates, due to a marine incursion, which also marks the cessation of volcanic activity; (4) post-rift subsidence brought in the depositon of the Cambrian carbonate and shale beds. Turner (2010) speculated that the Tarim sedimentary and volcano-sedimentary successions again could be correlated with the Neoproterozoic basins of the Kimberley region of Western Australia, where the Neoproterozoic rocks are overlain by the 510 Ma Kalkarindji continental flood basalts (Glass and Phillips 2006). These flood basalts, Turner argued, could represent a widespread extensional event that began at ca. 600 Ma and could have led to the rifting of the Tarim from the Kimberley region.

Zhang et al. (2010), using geochemistry, Nd-isotopes and U-Pb zircon geochronology, were able to trace the evolution of the Precambrian basement of the Tarim. These authors, integrating theirs and published data, proposed a three-stage Precambrian geodynamic evolution of the Tarim, as follows: (1) Archaean stage (2.8–2.5 Ga), characterised by emplacement of tonalite-trondhjemite-granodiorite (TTG) and gabbro intrusions, with arc geochemical signatures, followed by the intrusion of 2.53 Ga alkaline (potassic) granites, marking the development of a proto-continental crust of the Tarim; (2) tectono-thermal events took place at around 1.9–1.8 Ga along the northern margin of the Tarim Craton, which may be related to the assembly of the Palaeoproterozoic Columbia supercontinent and the cratonisation of the Tarim; (3) in the Aksu region, rocks of the Aksu Group represent a late Mesoproterozoic to earliest Neoproterozoic active margin, along the northern margin of the Tarim and possibly related to its amalgamation with Australia at ca. 900 Ma; also part of this stage is a 1.1–0.9 Ga tectono-thermal event, recorded in the Xinditage Group in Quruqtag and possible related to the assembly of the Rodinia supercontinent. Furthermore, Zhang et al. (2010) commented that the Neoproterozoic igneous and sedimentary activities along the northern margin of the Tarim Craton, are comparable with those in South China and other Rodinian continental blocks and these may be related to superplume activity and the breakup of Rodinia (Li et al. 2008). A fairly detailed and interesting study of tectonic unconformities and palaeouplifts of the Tarim Basin can be found in Lin et al. (2012).

As mentioned above, the Tarim is covered by Cenozoic sediments forming a very thick succession (up to 7.5 km) that unconformably overlie a Cretaceous succession of dominantly clastic rocks. Yin and Nie (1996) recognised two foredeeps, Kuche in the central-north and Hotan in the southwestern part. Sediments that accumulated in

these foredeeps comprise various sequences containing conglomerates, sandstones, mudstones and evaporites. The sedimentary rocks are rich in fossils that include mainly ostracods and foraminifera (Yin and Nie 1996). Furthermore, these sedimentary successions host oil and gas fields (see Li et al. 1996; Ren and Xiao 2002, and Chap. 8 for more details).

3.3.1 Mineral Systems

No economic mineralisation is as yet known from the Archaean-Proterozoic rocks that border the Tarim. The above mentioned ca. 820 Ma mantle plume event resulted in the emplacement of dyke swarms, bimodal volcanic rocks and mafic-ultramafic intrusions in the Yangtze Craton, the Tarim as well as Australia. This event, discussed more fully in Chap. 7, resulted in the emplacement of alkaline intrusions, such as Kudi Complex and the above-mentioned Qinganbulake mafic-ultramafic-carbonatite complex, in the northeastern margin of the Tarim can be considered prospective for Ni-Cu, Ti-V and rare earths mineralisation. The Kudi Complex is a bimodal alkaline intrusion consisting of A-type granite and gabbro with an age of ca. 783 Ma (Zhang et al. 2006). The 818 Ma Qeganbulake ring complex is more or less coeval with the Yifeng 821 Ma mafic dyke swarm (Lu et al. 2008) and is host to the second largest vermiculite deposit in the world (Zhang et al. 2007b). Of nearly the same age is the above mentioned Jinchuan layered mafic-ultramafic intrusion, hosting world-class Ni-Cu-PGE mineralisation (Chap. 7), perhaps consolidating the hypothesis of a Neoproterozoic mantle plume. Sulphides are present in the N2CM funnel shaped mafic-ultramafic intrusion, where they form zones at the boundaries between lherzolite and pyroxenite or between pyroxenite and gabbro. The ore zones have grades from 0.2–0.8 % Cu, 0.1–0.6 % Ni and 0.01–0.05 % Co and is at the time of writing reported as being mined (Zhang et al. 2010). Of the six mafic-ultramafic bodies in the same area two others also host Ni-Cu sulphides, but at this stage no information is available.

The rapakivi granites, dated at ca. 1.77 Ga, in the Quanji Massif (Lu et al. 2008 and references therein) can be considered prospective for iron oxide copper gold systems (IOCG).

3.4 Concluding Remarks

In this Chapter, I have attempted to review the geology and mineral systems of the North China Craton (NCC) and the Tarim Craton, two very important tectonic units both for the understanding of the wider geodynamic evolution of China and for mineral systems, known and potentially existing. The reader will have noticed that sometimes one is faced with contradictory data and hypotheses. This is largely because of lack of adequate field constraints that need to be taken into consideration

when interpreting, equally vital, laboratory and geochronological data. The tectonic evolution and the timing of the final amalgamation of the North China Craton is still controversial. At the time of writing, yet another model was published, based on the interpretation of seismic profiles (Kusky 2011), which envisaged double-polarity Andean-style subduction under the Eastern and Western blocks, respectively, at about 2.5 Ga, followed by collision tectonics at about 2.3 Ga and a final docking to the north of the NCC with the Columbia supercontinent. However, in this model, the discredited Dongwanzi ophiolite is part of the scenario, casting doubt on the validity of Kusky's model. Contradictory hypotheses continue their journey: claims are made for east-directed subduction of the Western Block to form a Hengshan-Wutai-Fuping magmatic arc under the Eastern Block at ca. 2.5 Ga, which finally collide in at ca. 1.8 to 1.79 Ga to end up in a "flower-structure" style orogenic belt (Zhang et al. 2011c). In another scenario Trap et al. (2011) suggested westward-directed subduction under a Wutai arc-Fuping block, which is separated by a Lüliang oceanic arm from the Western Block between ca. 2.3 and 2.15 Ga, to finally collide at 1.9–1.8 Ga with dominantly east-directed thrusting. In contrast, Liu et al. (2011) proposed that the Lüliang Complex in the Trans-North China orogen was part of a continental margin magmatic arc. In the latest analysis by Kusky (2011), the geodynamic evolution of the Trans-North China Orogen between 2.55 and 1.8 Ga involved first west-directed subduction, resulting in he Wutai island arc and the Hengshan continental arc in the Western Block (2.55–2.5 Ga), followed by double subduction (west- and east-directed; 2.5–2.4 Ga) and finally collision events leading accretionary orogens of the Trans-North China Orogen.

A clearer picture emerges for the NCC as far as post-Precambrian magmatism and associated mineral systems. The NCC is indeed unusual in that its eastern part was affected by intensive Mesozoic tectonic, thermal and mineralisation events. These resulted in the development of a vast range of mineral systems from porphyry, porphyry-skarn, porphyry-epithermal, hydrothermal veins, precious metal lodes, mostly concentrated in belts or provinces controlled by major structures or zones of weakness around the northern and southern margins of the NCC. It must be noted that the porphyry deposits that adorn the northern margins of the NCC (and the southern margins, Qinling orogen, see Chap. 5), are intracontinental and quite different from those of continental margins, such as the Andean belt. These porphyry systems have distinct features, namely low-H_2O alteration minerals (K-feldspar, epidote), CO_2-enriched ore fluids and abundant fluorite, amongst others. I return to this particular aspect in Chap. 5. The tectonic and magmatic reactivation of the eastern NCC is now well documented and is related to the erosion of the subcontinental lithospheric mantle (SCLM) beneath the Craton, due to a number of combined factors that include subduction of the Izanagi plate, delamination and upwelling asthenospheric mantle. These resulted in the well known Yanshanian, which I mentioned several times in this Chapter and am compelled to return to it in subsequent Chapters, because of its wide ranging effects in the eastern parts of China and the rest of Asia. The Yanshanian occurred in the Mesozoic, albeit with peaks of activity. One of these is well manifested in the Jiaodong province, host to a large number of lode Au deposits and one of the most important gold producing regions of China. These lode deposits, first labelled

as orogenic type because hosted in Archaean rocks, turn out to be solely related to the Yanshanian tectono-thermal processes, casting doubt as to the orogenic origin of these mineral deposits. A point not lost by Goldfarb et al. (2007), who suggested that the Cretaceous mantle plume in the southern Pacific (manifested in the Ontong Java oceanic plateau) may have been the cause of enhanced subduction and tectonism at continental margins, including eastern Asia. Consequently fluid flow would have focussed along major lithospheric and crustal breaks and core complexes, ultimately to form lode deposits. A promising model, but one wonders if other so-called orogenic lodes, hosted in Archaean greenstone belts (e.g. Yilgarn Craton in Western Australia), could not have formed by a similar process, only later to be deformed by collision tectonics and strike-slip movements.

Finally, Precambrian rocks of the Tarim cratonic block, largely covered by Phanerozoic sedimentary successions that host oil and gas fields, are only exposed along its margins and occasionally intersected by deep oil wells. The tectonic significance and mineral potential of these rocks remain unresolved and tantalising.

References

Barry TL, Kent RW (1998) Cenozoic magmatism in Mongolia and the origin of central and East Asian basalts. Geodynamics 27:347–364

Barry TL, Saunders AD, Kempton PD, Windley BF, Pringle MS, Dorjnamjiaa D, Saandar S (2003) Petrogenesis of Cenozoic basalts from Mongolia: evidence for the role of asthenopsheric versus metasomatised lithospheric mantle sources. J Pet 44:55–91

Bekker A, Slack JF, Planavsky N, Krapez B, Hofmann A, Konhauser KO, Rouxe, OJ (2010) Iron formation: the sedimentary product of a complex interplay among mantle, tectonic, oceanic, and biosphere processes. Econ Geol 105:467–508

Boyce AJ, Little CTS, Russell MJ (2003) A new fossil vent biota in the Ballynoe barite deposit, Silvermines, Ireland: evidence for intracratonic sea-floor hydrothermal activity about 352 Ma. Econ Geol 98:649–656

Chao ECT, Back JM, Minkin JA, Tatsumoto M, Wang JW, Conrad JE, McKee EH, Hou ZL, Meng QR, Huang SG (1997) The sedimentary carbonate-hosted giant Bayan Obo REE-Fe-Nb ore deposit of Inner Mongolia, China: a cornerstone example for giant polymetallic ore deposits of hydrothermal origin. USGS Bull 2143

Chen YJ, Zhao YC (1997) Geochemical characteristics and evolution of REE in the early Precambrian sediments: evidence from the southern margin of the North China Craton. Episodes 20:109–116

Chen YJ, Li C, Zhang J, Li Z, Wang HH (2000) Sr and O isotopic characteristics of porphyries in the Qinling molybdenum deposit belt and their implication to genetic mechanism and type. Sci China Ser D 43(Suppl):82–94

Chen S, O'Reilly SY, Zhou XH, Griffin WL, Zhang G, Sun M, Feng J, Zhang M (2001) Thermal and petrological structure of the lithosphere beneath Hannuoba, Sino-Korean Craton, China: evidence from exnoliths. Lithos 56:267–301

Chen Y, Xu B, Zhan C, Li Y (2004) First mid-Neoproterozoic palaeomagnetic results from the Tarim Basin (NW China) and their geodynamic implications. Precambrian Res 133:271–281

Chen YJ, Pirajno F, Qi JP (2005) Origin of gold metallogeny and sources of ore-forming fluids, Jiadong Province, eastern China. Int Geol Rev 47:530–549

Cheng YQ, Zhao YM, Li WW (1995) Iron deposits of China, in mineral deposits of China, Editorial Committee of Mineral Deposits, China, vol 2. Geol Publ House, Beijing, pp 28–36

Cook NJ, Ciobanu CL, Mao JW (2009) Textural control on gold distribution in As-free pyrite from the Dongping, Huangtuliang and Hougou gold deposits, North China Craton (Hebei Province, China). Chem Geol 264:101–121

Clout JMF, Simonson BM (2005) Preacambrian iron formations and iron formation-hosted iron ore deposits. Econ Geol 100th Anniv Vol:643–649

Cope TD, Graham SA (2007) Upper-crustal response to Mesozoic tectonism in Western Liaoning, North China, and implications for lithospheric delamination. Geological Society, London, Sp Publ 280,pp 201–222

Cui ML, Zhang BL, Zhang LC (2011) Baddeleyite/Zircon U-Pb dating for the Shizhaigou diorite in Southern margin of North China Craton: constrains on the timing and tectonic setting of the Paleoproterozoic Xiong'er group. Gondwana Res 20(1):184–193

Dai JZ, Mao JW, Xie GQ, Yang FQ, Wang YT, Zhao CS (2009) U-Pb, Re-Os dating and geodynamic setting of the Xiaojiayingzi Mo (Fe) deposit, western Liaoning province, China. Ore Geol Rev 35:235–244

Drew LJ, Meng Q, Sun W (1990) The Bayan Obo iron-rare earth-niobium deposits, Inner Mongolia, China. Lithos 26:43–65

Fan HR, Zhai MG, Xie YH, Yang JH (2003) Ore-forming fluids associated with granite-hosted gold mineralisation at the Sanshandao deposit, Jiaodong gold province. Miner Depos 38:739–750

Fan HR, Xie YH, Wang KY, Tao KJ, Wilde SA (2004a) REE daughter minerals trapped in fluid inclusions in the giant Bayan Obo REE-Nb-Fe deposit, Inner Mongolia, China. Int Geol Rev 46:638–645

Fan HR, Xie YH, Wang KY, Wilde SA (2004b) Methane-rich fluid inclusions in skarn near the giant REE-Nb-Fe deposit at Bayan Obo, northern China. Ore Geol Rev 25:301–309

Fan HR, Hu FF, Xie YH (2005) Aqueous-carbonic-REE fluids in the giant Bayan Obo deposit, China: implications for REE mineralization. In: Mao JW, Bierlein FP (eds) Mineral Deposit Research: meeting the global challenge, Proceedings of the Eigth Bienn SGA Meeting, Beijing China, 2:945–948

Fan HR, Hu FF, Yang JH, Zha MG (2007) Fluid association and large-scale gold metallogeny during Mesozoic tectonic transition in the Jiadong peninsula, eastern China. Geol Soc, London, Sp Publ 280:303–316

Faure G (1986) Principles of isotope geology, 2nd edn. Wiley, New York, p 589

Frost BR, Mavrogenes JA, Tomkins AG (2002) Partial melting of sulfide ore deposits during medium- and high-grade metamorphism. Can Miner 40:1–18

Furnes H, Witt M de, Staudigel H, Rosing M, Muehlenbachs K (2007) A vestige of Earth's oldest ophiolite. Science 315:1704–1707

Gan SF, Qiu YM, Yang HY, Reenen DD van (1994) The Hadamengou Mine: a typical gold deposit in the Archean Granulite Facies Terrane of the North China Craton. Inter Geol Rev 36:850–866

Glass L, Phillips D (2006) The Kalkarindji continental flood basalt province: a new Cambrian large igneous province in Australia, with possible links to faunal extinction. Geology 34:461–446

Goldfarb RJ, Hart C, Davis G, Groves DI (2007) East Asian gold: deciphering the anomaly of Phanerozoic gold in Precambrian Cratons. Econ Geol 102:341–345

Griffin WL, Andi Z, O'Reilly SY, Ryan CG (1998) Phanerozoic evolution of the lithosphere beneath the Sino-Korean Craton. In: Flower M, Chung SL, Lo CH, Lee TY (eds) Mantle dynamics and plate interactions in East Asia. American Geophysical Union, Monogr 27, pp 107–126

Gu LX, Zheng YC, Tang XQ, Zaw K, Della-Pasque F, Wu CZ, Tian Z, Lu JJ, Ni P, Li X, Yang FT, Wang XW (2007) Copper, gold and silver enrichment in ore mylonites within massive sulphide orebodies at Hongtoushan VHMS deposit, N. E. China. Ore Geol Rev 30:1–29

Guo ZJ, Yin A, Robinson A, Jia CZ (2005) Geochronology and geochemistry of deep-drill core samples from the basement of the central Tarim Basin. J Asian Earth Sci 25:45–56

Han CM, Xiao WJ, Zhao GC, Sun M, Qu WJ, Du AD (2009) A Re-Os study of molybdenites from the Lanjiagou Mo deposit of North China Craton and its geological significance. Gondwana Res 16:264–271

Hart CJR, Goldfarb RJ, Qiu YM, Snee L, Miller LD, Miller ML (2002) Gold deposits of the northern margin of the North China Craton: multiple late Paleozoic-Mesozoic mineralizing events. Miner Depos 37:326–351

Hsü KJ (1988) Relict back-arc basins: principles of recognition and possible new examples from China. In: Kleinspehn KL, Paola C (eds) New perspectives in basin analysis. Springer, New York, pp 245–263

Hu SX, Zhao YY, Xu B, Lu B, Ji HZ, Ye Y (1997) Evidence for the Jiangsu-Shandong ultra-high-pressure metamorphic belt returns from the upper mantle to the earth surface in the Mesozoic-Cenozoic. Acta Geol Sin 71:245–253 (in Chinese with English abstract)

Hu HB, Mao JW, Liu DY, Niu SY, Wang YB, Li YF, Shi RR (2005) SHRIMP zircon U-Pb dating of the Tongshi magmatic complex in western Shandong and its implication. Acta Geol Sin 79:401–406

Hu HB, Mao JW, Niu SY, Li YF, Li MW (2006) Geology and geochemistry of telluride-bearing Au deposits in the Pingui area, Western Shadong, China. Miner Pet 87:209–240

Huang DH, Dong QY, Gan ZX (1990) Molybdenum deposits of China, in mineral deposits of China, Editorial Committee of Mineral Deposits, China, vol 1. Geol Publ House, Beijing, pp 288–355

Huang XN, Li JH, Kusky TM, Chen Z (2004) Microstructures of the Zunhua 2.50 Ga podiform chromite, North China Craton and implications for the deformation and rheology of the Archean oceanic lithospheric mantle. In: Kusky TM (ed) Precambrian ophiolites and related rocks, vol 13. Elsevier, Amsterdam, pp 321–337

Huang XL, Niu YL, Xu YG, Yang QJ, Zhong JW (2010) Geochemistry of TTG and TTG-like gneisses from Lushan-Taihua complex in the southern North China Craton: implications for late Archean crustal accretion. Precambrian Res 182(1–2):43–56

Huston DL, Logan GA (2004) Barite, BIFs and bugs: evidence for the evolution of the Earth's early hydrosphere. Earth Planet Sci Lett 220:41–55

Jia CZ, Yao H, Wei G, Li L (1991) Plate tectonic evolution and characteristics of major tectonic units of the Tarim Basin. In: Tong X, Liang D (eds) The Tarim Basin. Xinjiang Scientific Publishing House, Urumqi, pp 207–225 (in Chinese)

Kusky TM (ed) (2004) Precambrian ophiolites and related rocks. Developments in Precambrian geology, vol 13. Elsevier, Amsterdam, p 727

Kusky TM (2011) Geophysical and geological tectonic models of the North China Craton. Gondwana Res 20:26–35

Kusky TM, Li JH (2003) Paleoproterozoic tectonic evolution of the North China Craton. J Asian Earth Sci 22:383–397

Kusky TM, Santosh M (2009) The Columbia connection in North China. Geological Society, London, Sp Publ 323, pp 49–71

Kusky TM, Li JH, Tucker RD (2001) The Archean Dongwanzi ophiolite complex, North China Craton: 2.505 billion-year-old oceanic crust and mantle. Science 292:1142–1145

Kusky TM, Li JH, Glass A, Huang XN (2004) Origin and emaplacement of Archean ophiolites of the Central Orogenic Belt, North China Craton. In: Kusky TM (ed) Precambrian ophiolites and related rocks, vol 13: developments in Precambrian geology. Amsterdam, Elsevier, pp 223–274

Kusky TM, Windley BF, Zhai MG (2007) Tectonic evolution of the North China Block: from orogen to craton to orogen. Geological Society, London, Sp Publ 280, pp 1–34

Le Bas MJ, Yang XM, Taylor RN, Spiro B, Milton JA, Peishan Z (2007) New evidence from a calcite-dolomite carbonatite dyke for the magmatic origin of the massive Bayan Obo ore-bearing dolomite marble, Inner Mongolia, China. Miner Pet 91:281–307

Li JH, Kusky TM (2007) World's largest known Precambrian fossil black smoker chimneys and associated microbial vent communities, North China: implications for early life. Gondwana Res 12:84–100

Li ZX, Powell CMcA (2001) An outline of the paleogeographic evolution of the Australasian region since the beginning of the Neoproterozoic. Earth Sci Rev 53:237–277

Li JJ, Shen BF, Li SB, Mao DB (1995) The geology and gold mineralisation of the greenstone belts in Qingyuan-Jiaopigou region, China. Tianjin Science and Technology Press, Tianjin, p 132

Li DS, Liang DG, Jia CZ, Wang G, Wu QH, He DF (1996) Hydrocarbon accumulations in the Tarim Basin, China. AAPG Bull 80:1587–1603

Li JH, Kusky TM, Huang XN (2002) Archean podiform chromitites and mantle tectonites in ophiolitic melange, North China Craton: a record of early oceanic mantle processes. GSA Today 12:4–11

Li ZX, Li XH, Kinny PD, Wang J, Zhang S, Zhou H (2003a) Geochronology of Neoproterozoic syn-rift magmatims in the Yangtze Craton, South China and correlation with other continents: evidence for a mantle superplume that broke up Rodinia. Precambrian Res 122:85–109

Li JW, Vasconcelos PM, Zhang J, Zhou MF, Zhang XJ, Yang FH (2003b) $^{40}Ar/^{39}Ar$ constraints on a temporal link between gold mineralization, magmatism and continental margin transtension in the Jiadong gold province, Eastern China. J Geol 111:741–751

Li JH, Kusky TM, Niu XL, Jun F, Polat A (2004) Neoarchean massive sulfide of Wutai mountain, North China: a black smoker chimney and mound complex within 2.50 Ga old oceanic crust. In: Kusky TM (ed) Precambrian ophiolites and related rocks, vol 13, Developments in Precambrian geology. Elsevier, Amsterdam, pp 339–362

Li ZX, Bogdanova SV, Collins AS, Davidson A, De Waele B, Ernst RE, Fitzsimons ICW, Fuck RA, Gladkochub DP, Jacobs J, Karlstrom KE, Lu S, Natapov LM, Pease V, Pisarevsky SA, Thrane K, Vernikovskiy V (2008) Assembly, configuration, and break-up history of Rodinia: A synthesis. Precambr Res 160:179–210

Li TS, Zhai MG, Peng P, Chen L, Guo JG (2010) Ca. 2.5 billion year old coeval ultramafic-mafic and syenitic dykes in eastern Hebei: implications for cratonization of the North China Craton. Precambrian Res 180(3–4):143–155

Li N, Chen YJ, Santosh M, Yao JM, Sun YL, Li J (2011) Recognition of 1.85 Ga molybdenum mineralization in the Xiong'er terrane, China: re-Os ages and implications for metallogeny associated with Columbia Supercontinent assembly. Precambrian Res 186(1–4):220–232

Li WB, Zhong R, Xu C, Song B, Qu WJ (2012) U-Pb, Re-Os geochronology of the Bainaimiao Cu-Mo-Au deposit in the North China Craton, Central Asia Orogenic Belt: implications for ore genesis and geodynamic setting. Ore Geol Rev doi:10.1016/j.oregeorev.2012.03.001

Lin CS, Yang HJ, Liu JY, Rui ZF, Cai ZZ, Zhu YF (2012) Distribution and erosion of the Paleozoic tectonic unconformities in the Tarim Basin, Northwest China: significance for the evolution of paleo-uplifts and tectonic geography during deformation. J Asian Earth Sci 46:1–19

Liu JM, Zhao Y, Sun YL, Li DP, Liu J, Chen BL, Zhang SH, Sun WD (2010) Recognition of the latest Permian to early Triassic Cu-Mo mineralization on the northern margin of the North China block and its geological significance. Gondwana Res 17:125–134

Liu SW, Zhang J, Li Q, Zhang L, Wang W, Yang PT (2011) Geochemistry and U-Pb zircon ages of metamorphic volcanic rocks of the Paleoproterozoic Luliang Complex and constraints on the evolution of the Trans-North China Orogen, North China Craton. Precambrian Res. doi:10.1016/j.precamres.2011.07.006

Lobato LM, Figueredo e Silva RC, Hagemann S, Thorne W, Zucchetti M (2008) Hypogene alteration associated with high-grade banded iron formation-related iron ore. Soc Econ Geol Rev 15:107–128

Long XP, Yuan C, Sun M, Zhao GC, Xiao WJ, Wang YJ, Yang YH, Hu AQ (2010) Archean crustal evolution of the northern Tarim Craton, NW China: Zircon U-Pb and Hf isotopic constraints. Precambrian Res 180:272–284

Lu LZ, Xu XC, Liu FL (1995) The Precambrian khondalite series in northern China. Changchun Publishing House, Changchun, p 99

Lu SN, Yang CL, Li HK, Li H (2002) A group of rifting events in the terminal Paleoproterozoic in the North China Craton. Gondwana Res 5:123–131

Lu SN, Li HK, Zhang CL, Niu GH (2008) Geological and geochronological evidence for the Precambrian evolution of the Tarim Craton and surrounding continental fragments. Precambrian Res 160:94–107

Luo ZK, Guan K, Yu HY, Li YM (2003) The key factors for formation of large-superlarge gold deposits in Zhaolai area, Jiaodong region. J Geol Expl 18:95–102 (in Chinese with English abstract)

Makarov VI, Alekseev DV, Batalev VYu, Bataleva EA, Belyaev IV, Bragin VD, Dergunov NZ, Efimova NN, Leonov MG, Munirova LM, Pavlenkin AD, Roecker S, Roslov YuV, Rybin AK, Shchelochkov GG (2010) Underthrusting of Tarim beneath the Tien Shan and deep structure of their junction zone: main results of seismic experiment along MANAS profile Kashgar-Song-Kol. Geotectonics 44:102–126

Mao JW, Wang YT, Zhang ZH, Yu JJ, Niu BG (2003a) Geodynamic settings of Mesozoic large-scale mineralization in North China and adjacent areas—implication from the highly precise and accurate ages of metal deposits. Sci China Ser D 46:838–851

Mao JW, Li YQ, Godlfarb RJ, He Y, Zaw K (2003b) Fluid inclusion and noble gas studies of the Dongping gold deposit, Hebei Province, China: a mantle connection for mineralization? Econ Geol 98:517–534

Mao JW, Xie GQ, Li XF, Zhang CQ, Mei YX (2004) Mesozoic large scale mineralisation and multiple lithospheric extension in South China. Earth Sci Front (China University of Geosciences, Beijing) 11:45–55 (in Chinese with English abstract)

Mao JW, Wang YT, Li HM, Pirajno F, Zhang CJ, Wang RT (2008) The relationship of mantle-derived fluids to gold metallogenesis in the Jiadong peninsula: evidence from D-O-C-S isotope systematics. Ore Geol Rev 33:361–381

Mao JW, Xie GQ, Pirajno F, Ye HS, Wang YB, Li YF, Xiang JF, Zhao HJ (2010) Late Jurassic-early Cretaceous granitoid magmatism in Eastern Qinling, central-eastern China: SHRIMP zircon U-Pb ages and tectonic implications. Aust J Earth Sci 57:51–78

McKerrow WS, Scotese CR, Brasier MD (1992) Early Cambrian continental reconstructions. J Geol Soc Lond 149:599–606

Meng QR, Wei HH, Qu YQ, Ma SX (2011) Stratigraphic and sedimentary records of the rift to drift evolution of the northern China Craton at the Paleo- to Mesoproterozoic transition. Gondwana Res 20:205–218

Miao LC, Qiu YM, Fan WM, Zhang FQ, Zhai MG (2005) Geology, geochronology and tectonic setting of the Jiaopigou gold deposits, southern Jilin Province, China. Ore Geol Rev 26:137–165

Miller LD, Goldfarb RJ, Nie FJ, Hart CJR, Miller ML, Yang YQ, Liu YQ (1998) North China Gold—a product of multiple orogens. SEG Newsl 33:1–12

Nie FJ, Zhang WY, Du AD, Jiang SH, Liu Y (2007) Re-Os isotopic dating on molybdenite separates from the Xiaodonggou porphyry Mo deposit, Hexigten Qi, Inner Mongolia. Acta Geol Sin 81:898–905 (in Chinese with English Abstract)

Nokleberg WJ (ed) (2010) Metallogenesis and tectonics of northeast Asia. USGS Profess Paper 1765

O'Reilly SY, Griffin WL, Djoman, YHP, Morgan P (2001) Are lithospheres forever? Tracking changes in subcontinental lithospheric mantle through time. GSA Today 11:4–10

Peng P (2010) Reconstruction and interpretation of giant mafic dyke swarms: a case study of 1.78 Ga magmatism in the North China Craton. Geological Society, London, Sp Publ 338, pp 163–178

Peng P, Zhai M, Zhang HF, Guo JH (2005) Geochronological constraints on the Paleoproterozoic evolution of the North China Craton: SHRIMP zircon ages of different types of mafic dikes. Int Geol Rev 47:492–508

Peng P, Zhai MG, Guo JH, Zhao TP, Liu F, Hu B (2008) A 1.78 Ga large igneous province consisting of the North China dyke swarm and Xiong'er Volcanic Province. Lithos 101:260–280

Peng P, Guo JH, Windley BF, Li XH (2011) Halaqin volcano-sedimentary succession in the central-northern margin of the North China Craton: products of late Paleoproterozoic ridge subduction. Precambrian Res 187(1–3):165–180

Pirajno F (2009) Hydrothermal processes and mineral systems. Springer, Berlin, p 1250

Pirajno F, Chen YJ (2005) The Xiong'er Group: a 1.76 Ga large igneous province in east-central China? http://www.largeigneousprovinces.org

Pirajno F, Ernst RE, Borisenko AS, Fedoseev G, Naumov EA (2009) Intraplate magmatism in central Asia and China and associated metallogeny. Ore Geol Rev 35:114–136

Qiu YM, Groves DI, McNaughton NJ, Wang LG, Zhou TH (2002) Nature, age and tectonic setting of granitoid-hosted, orogenic gold deposits of the Jiaodong Peninsula, eastern North China Craton, China. Miner Depos 37:283–305

Ren JS, Xiao LW (2002) Tectonic settings of petroliferous basins in continental China. Episodes 25:227–235
Ren JY, Tamaki K, Li ST, Zhang JX (2002) Late Mesozoic and Cenozoic rifting and its dynamic setting in eastern China and adjacent areas. Tectonophysics 344:175–205
Rock NMS, Groves D, Perring CS, Golding SD (1989) Gold, lamprophyres, and porphyries: what does their association mean? Econ Geol Monogr 6:609–625
Rogers JJW, Santosh M (2004) Continents and supercontinents. Oxford University Press, New York, p 289
Santosh M (2010) Assembling North China Craton within the Columbia supercontinent: the role of double-sided subduction. Precambrian Res 178:149–167
Santosh M, Zhao D, Kusky T (2010) Mantle dynamics of the Paleoproterozoic North China Craton: a perspective based on seismic tomography. J Geodyn 49:39–53
Santosh M, Liu SJ, Tsunogae T, Li JH (2011) Paleoproterozoic ultrahigh-temperature granulites in the North China Craton: implications for tectonic models on extreme crustal metamorphism. Precambrian Res. doi:10.1016/j.precamres.2011.05.003
Sengör AMC, Natal'in B (1996) Paleotectonics of Asia: fragments of a synthesis. In: Yin A, Harrison M (eds) The tectonic evolution of Asia. Cambridge University Press, Cambridge, pp 486–640
Sengör AMC, Graham SA, Biddle KT (1996) Is the Tarim Basin underlain by a Neoproterozoic oceanic plateau? Geol Soc Am Abs Programs 28:67
Slack JF (1996) Tourmaline associations with hydrothermal ore deposits. Rev Mineral 33:559–641
Smith MP (2007) Metasomatic silicate chemistry at the Bayan Obo Fe-REE-Nb deposit, Inner Mongolia, China: contrasting chemistry and evolution of fenitising and mineralising fluids. Lithos 93:126–148
Smith MP, Henderson P (2000) Preliminary fluid inclusion constraints on fluid evolution in the Bayan Obo Fe-REE-Nb deposit, Inner Mongolia, China. Econ Geol 95:1371–1388
Smith MP, Henderson P, Campbell LS (2000) Fractionation of the REE during hydrothermal processes: constraints from the Bayan Obo Fe-REE-Nb deposit, Inner Mongolia, China. Geochim Cosmochim Acta 64:3141–3160
Thorne WS, Hagemann SG, Barley ME (2004) Petrographic and geochemical evidence for the hydrothermal evolution of the North deposit, Mt Tom Price, Western Australia. Miner Depos 39:766–783
Trap P, Faure M, Lin W, Meffre S (2009) The Luliang Massif: a key area for the understanding of the Palaeoproterozoic Trans-North China Belt, North China Craton. Geological Society, London, Sp Publ 323, pp 99–125
Trap P, Faure M, Lin W, Le Breton N, Monie P (2011) Paleoproterozoic tectonic evolution of the Trans-North China Orogen: toward a comprehensive model. Precambrian Res. doi:10.1016/j.precamres.2011.09.008
Trendall AF, Blockley JG (2004) Precambrian iron formation. In: Erikson PG, Altermann W, Nelson DR, Muller WU, Catuneau O (eds) The Precambrian earth: tempos and events. Elsevier, Amsterdam, pp 403–421
Turner SA (2010) Sedimentary record of late Neoproterozoic rifting in the NW Tarim Basin, China. Precambrian Res 181(1–4):85–96
Wan YS, Liu DY, Dong CY, Xu ZY, Wang ZJ, Wilde SA, Yang YS, Liu ZH, Zhou HY (2009) The Precambrian khondalite belt in the Daqingshan area, North China Craton: evidence for multiple metamorphic events in the Palaeoproterozoic era. Geological Society, London, Spl Publ 323, pp 75–97
Wang J, Tatsumoto M, Li X, Premo WR, Chao ECT (1994) A precise ^{232}Th-^{208}Pb chronology of fine grained monazite: age of the Bayan Obo REE-Fe-Nb ore deposit, China. Geochim Cosmochim Acta 58:3155–3169
Wang LG, Qiu YM, McNaughton NJ, Groves DI, Luo ZK, Huang JZ (1998) Constraints on crustal evolution and gold metallogeny in the northwestern Jiaodong Peninsula, China, from SHRIMP U–Pb zircon studies of granitoids. Ore Geol Rev 13:275–291

Wang YJ, Fan WM, Zhang YH, Guo F, Zhang HF, Peng TP (2004) Geochemical, $^{40}Ar/^{39}Ar$ geochronological and Sr-Nd isotopic constraints on the origin of Paleoproterozoic mafic dikes from the southern Taihang Mountains and implications for the ca. 1800 Ma event of the North China Craton. Precambrian Res 135:55–47

Wang HS, Zhang SH, He GQ (2005) China and Mongolia. In: Selley R, Cocks LRM, Plimer IR (eds) Encyclopedia of geology. Elsevier, Amsterdam, pp 345–358

Wang ZH, Wilde SA, Wan JL (2010) Tectonic setting and significance of 2.3–2.1 Ga magmatic events in the Trans-North China orogen: new constraints from the Yanmenguan mafic-ultramafic intrusion in the Hengshan-Wutai-Fuping area. Precambrian Res 178(1–4):27–42

Wilde SA, Zhao GC, Sun M (2002) Development of the North China Craton during the late Archaean and its final Amalgamation at 1.8 Ga: some speculations on its position within a global Palaeoproterozoic Supercontinent. Gondwana Res 5:85–94

Wong WH (1927) Crsutal movements and igneous activities in eastern China, since Mesozoic time. Bull Geol Soc China 6:9–37

Wu FY, Wilde SA, Zhang GL, Sun DY (2004) Geochronology and petrogenesis of the post-orogenic Cu-Ni sulfide-bearing mafic-ultramafic complexes in Jilin Province, NE China. J Asian Earth Sci 23:781–797

Wu M, Zhao G, Sun M, Yin C, Li S, Tam PY (2011) Petrology and P-T path of the Yishui mafic granulites: implications for tectonothermal evolution of the western Shandong Complex in the Eastern Block of the North China Craton. Precambrian Res. doi:10.1016/j.precamres.2011.08.008

Xiao XY, Wang LS, Li H, Li C, Wang GQ, Cai DS, Luo YH (2001) Geotemperature field in Bohai Sea. China Off Shore Oil Gas (Geol) 15:105–110 (in Chinese with English abstract)

Xu JW, Zhu G (1994) Tectonics Models of the Tan-Lu Fault Zone, Eastern China. Int Geol Rev 36:771–784

Xu B, Jian P, Zheng HF, Zou H, Zhang LF, Liu DY (2005) U-Pb zircon geochronology and geochemistry of Neoproterozoic volcanic rocks in the Tarim Block of northwest China: implications for the breakup of Rodinia supercontinent and Neoproterozoic glaciations. Precambrian Res 136:107–123

Xu XS, Griffin WL, Ma X, O'Reilly SY, He ZY, Zhang CL (2009) The Taihua group on the southern margin of the North China Craton: further insights from U-Pb ages and Hf isotope composition of zircons. Miner Pet 97:43–59

Xue LW, Yuan ZL, Zhanmg YS (1995) The Sm-Nd siotope age of Taihua group in Lushan area and their implications. Geochimica 24(Suppl):92–97

Yang MZ, Lu GX (1996) The geology-geochemistry of gold deposits of the greenstone belt in Jiaodong district, China. Geol Publ House Beijing (in Chinese), p 200

Yang XM, Le Bas MJ (2004) Chemical composition of carbonate minerals from Bayan Obo, Inner Mongolia, China: implications for petrogenesis. Lithos 72:97–116

Yang JH, Wu FY, Wilde SA (2003) A review of the geodynamic setting of large scale late Mesozoic gold mineralization in the North China Craton: an association with lithospheric thinning. Ore Geol Rev 23:125–152

Yang KF, Fan HR, Santosh M, Hu FF, Wang KY (2011a) Mesoproterozoic mafic and carbonatitic dykes from the northern margin of the North China Craton: implications for the final breakup of Columbia supercontinent. Tectonophysics 498:1–10

Yang KF, Fan HR, Santosh M, Hu FF, Wang KY (2011b) Mesoproterozoic carbonatitic magmatism in the Bayan Obo deposit, Inner Mongolia, North China: constraints for the mechanism of superaccumulation of rare earth elements. Ore Geol Rev 40:122–131

Yin A, Nie SY (1996) A Phanerozoic palinspastic reconstruction of China and its neighboring regions. In: Yin A, Harrison TM (eds) The tectonic evolution of Asia. Cambridge University Press, Cambridge, pp 442–485

Zhai MG (2004) Precambrian tectonic evolution of the North China Craton. Geological Society, London, Sp Publ 226, pp 57–72

Zhai MG, Liu WJ (2003) Palaeoproterozoic tectonic history of the North China Craton: a review. Precambrian Res 122:183–199

Zhai MG, Guo JH, Liu WJ (2005) Neoarchean to Palaeoproterozoic continental evolution and tectonic history of the North China Craton: a review. J Asian Earth Sci 24:547–561

Zhai MG, Li TS, Peng P, Hu B, Liu F, Zhang YB (2010) Precambrian key tectonic events and evolution of the North China Craton. Geological Society, London, Sp Publ 338, pp 235–262

Zhang GW (1989) Formation and evolution of the Qinling Orogen. Northwest University Press, Xia'n, p 199 (in Chinese)

Zhang SX (2009) Geological formation names of China (1866–2000), vol 1 and 2. Springer, Dordrecht, p 1537

Zhang P, Hou S (1991) Metallogenic model of kimberlite in North China craton, China. Proceedings of the Fifth Kimberlite Conference, CPRM Sp Publ 92:466–469

Zhang CL, Li ZX, Li XH, Ye HM, Wang A, Guo KY (2006) Neoproterozoic bimodal intrusive complex in the southwestern Tarim Block, Northwest China: age, geochemistry and implications for the rifting of Rodinia. Int Geol Rev 48:112–128

Zhang CL, Li ZX, Li XH, Yu HF, Ye HM (2007a) An early Paleoproterozoic high-K intrusive complex in southwestern Tarim Block, NW China: age, geochemistry and tectonic implications. Gondwana Res 12:101–112

Zhang CL, Li XH, Li ZX, Lu SN, Ye HM, Li HM (2007b) Neoproterozoic ultramafic-mafic-carbonatite complex and granitoids in Qurutagh of northeastern Tarin Block, western China: geochronology, geochemistry and tectonic implications. Precambrian Res 152:149–169

Zhang CL, Yang DS, Wang HY, Takahashi Y, Ye HM (2010) Neoproterozoic mafic-ultramafic layered intrusion in Quruqtagh of northeastern Tarim Block, NW China: two phases of mafic igneous activity with different mantle sources. Gondwana Res 19(1):177–190

Zhang LC, Zhai MG, Zhang XJ, Xiang P, Dai YP, Wang C, Pirajno F (2011a) Formation age and tectonic setting of the Shirengou Neoarchean banded iron deposit in eastern Hebei Province: constraints from geochemistry and SIMS zircon U-Pb dating. Precambrian Res. doi:10.1016/j.precamres.2011.09.007

Zhang XJ, Zhang LC, Xiang P, Bo W, Pirajno F (2011b) Zircon U-Pb age, Hf isotopes and geochemistry of Shuichang Algoma-type banded iron-formation, North China Craton: constraints on the ore-forming age and tectonic setting. Gondwana Res 20(1):137–148

Zhang J, Zhao GC, Li SZ, Sun M, Chan LS, Shen WL, Liu SW (2011c) Structural pattern of the Wutai Complex and its constraints on the tectonic framework of the Trans-North China Orogen. Precambrian Res. doi:10.1016/j.precamres.2011.08.009

Zhang CL, Li HK, Santosh M, Li ZX, Zou HB, Wang HY, Ye HM (2012) Precambrian evolution and cratonization of the Tarim Block, NW China: petrology, geochemistry, Nd-isotopes and U-Pb zircon geochronology from Archaean gabbro-TTG-potassic granite suite and Paleoproterozoic metamorphic belt. J Asian Earth Sci.47:5–20

Zhao TP, Zhou MF (2009) Geochemical constraints on the tectonic setting of Paleoproterozoic A-type granites in the southern margin of the North China Craton. J Asian Earth Sci 36:183–195

Zhao GC, Wilde SA, Cawood PA, Sun M (2001) Archean blocks and their boundaries in the North China Craton: lithological, geochemical, structural and P-T path constraints and tectonic evolution. Precambrian Res 107:45–73

Zhao GC, Sun M, Wilde SA, Guo J (2004) Late Archaean to Palaeoproterozoic evolution of the Trans-North China Orogen: insights from synthesis of existing data of the Hengshan-Wutai-Fuping belt. Geological Society, London, Sp Publ 226, pp 27–56

Zhao GC, Min S, Wilde SA, Li SZ (2005) Late Archean to Paleoproterozoic evolution of the North China Craton: key issues revisited. Precambrian Res 136:177–202

Zhao GC, Wilde SA, Li SZ, Sun M, Grantr ML, Li XP (2007a) U-Pb zircon age constraints on the Dongwanzi ultramafic-mafic body, North China, confirm it is not an Archean ophiolite. Earth Planet Sci Lett 255:85–93

Zhao DP, Maruyama S, Omori S (2007b) Mantle dynamics of Western Pacific and East Asia: insight from seismic tomography and mineral physics. Gondwana Res 11:120–131

Zhao TP, Chen W, Zhou MF (2009) Geochemical and Nd-Hf isotopic constraints on the origin of the ~ 1.74 Ga Damiao anorthosite complex, North China Craton. Lithos 113:673–690

Zhao TP, Chen W, Lu B (2010) Characteristic and origin of the Fe-Ti-P oxide deposits associated with Proterozoic massif-type anorthosite. Earth Sci Front 17(2):106–117 (in Chinese, with English abstract)

Zhou K (1995) Geological features and origin of the Hadamengou gold deposit, Inner Mongolia. Gold 16(10):5–8 (in Chinese)

Zhou MF, Bai WJ (1992) Chromite deposits in China and their origin. Miner Depos 27:192–199

Zhou TH, Lü GX (2000) Tectonics, granitoids and Mesozoic gold deposits in East Shandong, China. Ore Geol Rev 16:71–90

Zhou D, Graham SA, Chang EZ, Wang BY, Hacker B (2001) Paleozoic tectonic amalgamation of the Chinese Tian Shan: evidence from a transect along the Dushanzi-Kuqa highway. Geol Soc Am Mem 194:23–46

Zhou TH, Goldfarb RJ, Phillips GN (2002) Tectonics and distribution of gold deposits in China—an overview. Miner Depos 37:249–282

Zhou XH, Yang JH, Zhang LC (2003) Metallogenesis of the superlarge gold deposits in the Jiaodng region and deep processes of subcontinental lithosphere beneath North China Craton in Mesozoic. Sci China (Ser D) 46:14–25

Zhu X (ed) (2007) Mineral facts of China. Elsevier, Amsterdam, p 776

Zhu G, Niu ML, Xie CL, Wang YS (2010) Sinistral to normal faulting along the Tan-Lu fault zone: evidence for geodynamic switching of the East China continental margin. J Geol 118:277–293

Chapter 4
Yangtze Craton, Cathaysia and the South China Block

Abstract The Yangzte Craton and Cathaysia were amalgamated, along a northeast-southwest trending fold belt or tectonic zone (Jiangshan-Shaoxing suture; Jiangnan orogen), following north-directed subduction between the Mesoproterozoic and Early Palaeozoic. Together they form the South China Block, separated from the North China Craton by the Qinling-Dabie orogenic belt, a major Late Triassic collision zone that resulted from the closure of a Palaeo-Tethys oceanic arm. The Yangtze Craton contains Archaean and Palaeproterozoic rocks, overlain by sedimentary succession of the Yangtze platform. However, exposures of Archaean rocks are scarce. The Archaean is largely represented by the 3.1–2.5 Ga Dabie Group that is unconformably overlain by the Proterozoic Hongan Group in the Huaiyang region in Hubei Province. The Dabie Group is a 15 km-thick succession comprising hornblende-plagioclase gneiss, biotite-plagioclase gneiss, amphibolite, granulites, marbles and banded iron- formation (BIF). Unconformably overlying the Dabie Group is the Palaeoproterozoic Susong Group, which contains mainly marble units. Along the upper reaches of the Yangtze River, is the Wudang Group with a total thickness estimated at about 15 km, consisting of quartzite, mica schist, slates and metavolcanic rocks with a possible age of about 2.0 Ga. In the Yangtze River gorges in Hubei Province, the Sandouping Group contains biotite-plagioclase gneiss, amphibolite, quartz schist, marble with a total thickness of about 3 km. The northern part of the Yangtze Craton is the Kongling microcontintal block, which participated in the final amalgamation of the Craton. The Cathaysia Block consists of Palaeo- and Mesoproterozoic rocks, represented by 1.8 Ga granites and volcanic rocks of the Badu Complex and the 1.43 Ga granites of the Baoban Complex in Hainan Island, with superimposed Mesozoic volcanic rocks and granitic intrusions (South China Fold Belt). The Precambrian basement of Cathaysia is exposed in the northeast (Zhejiang and Fujan provinces), where two metamorphic sequences occur between the Jiangshan-Shaoxing and Lishui-Haifeng fault zones. The basement of the Cathaysia Block remains largely unknown, although it is generally assumed that the Block is underlain by Palaeo- to Mesoproterozoic continental crust. In the western parts of Cathaysia, crustal material is of Meso-Neoproterozoic age, with some Archaean components, all extensively reworked at various stages during Caledonian (450 Ma), Indosinian (240 Ma) and early Yanshanian (160 Ma) thermal events. In the Neoproterozoic the Cathaysia Block underwent a rifting stage in the period of 857–837 Ma, corresponding with the breakup of the Rodinia supercontinent. The coastal region of Cathaysia is characterised by widespread intrusive and volcanic rocks of Yanshanian

F. Pirajno, *The Geology and Tectonic Settings of China's Mineral Deposits,*
DOI 10.1007/978-94-007-4444-8_4, © Springer Science+Business Media Dordrecht 2013

age (Mesozoic), forming a magmatic belt extending for more than 400 km from Hainan island to Zhejiang Province to the northeast.

The Yangtze Craton and Cathaysia host a multitude of ore systems, with several falling in the world class category. Mineral systems discussed in this chapter include sedimentary rock-hosted of the Lower Yangtze River region, which include the Dachang polymetallic mineralisation, mostly comprising Sn and other metals, such as Zn, In, Sb, Cu and Ag. Mississippi Valley Type (MVT) deposits are discussed next, with the example of the Huize district, containing a total of about 5 Mt of Pb+Zn reserves. Carlin-type and Carlin-style Au deposits are numerous and are mostly located along the northern margin of the Yangzte Craton; examples discussed are the Shuiyindong and Yata deposits. Porphyry systems in the Cathaysia Block include Dabaoshan, which is part of a larger polymetallic ore system, located along the major Wuchuan-Sihui northeast trending fault zone and comprising a porphyry Mo deposit, stratiform Cu-Pb-Zn ore and Mo-W skarn ore, all associated with felsic intrusions and subvolcanic intrusions. The Dexing porphyry Cu-Mo district, one of the largest in China, is located in the Jiangxi province, in the Dele Jurassic basin.

The Middle-Lower Yangzte River Valley metallogenic province contains a wide range of mineral systems from porphyry, porphyry-skarn, epithermal veins, to Kiruna-style Fe-P. The deposits are generally associated with volcano-sedimentary rift basins and have isotopic ages ranging from 160 to 120 Ma. The Yangzte River Valley mineral deposits are mostly related to phases of Yanshanian magmatism, dominated by I-type high K-calc-alkaline granitic rocks, Na-rich calc-alkaline dioritic intrusions and A-type granites. This magmatism in the region mainly developed in two stages, at 160–135 Ma with I-type intrusions and a later phase at about 120 Ma dominantly with A-type granites. These intruded into above-mentioned thick carbonate sucessions of various ages, resulting in the widespread formation of skarn systems. In this chapter, I describe the Tongshankou porphyry-skarn Cu-Mo, Tonglushan Cu-Fe-Au skarn, the Longqiao Fe skarn, Tongliujing Cu-Au-Mo veins deposit (Yueshan district), the Kiruna-style Zhongu ore field and the Dalongshan U deposit. The section on the Yangzte River Valley metallogenic belt ends with a review of the geodynamic evolution, which was responsible for the development of the mineral systems.

Brief reviews of the Jinshan orogenic Au deposits and the Sn-Cu Gejiu mineral districts in Yunnan Province (SW China) follow. The Geju mineral district is a fascinating region, where ca. 83 Ma granitic cupolas intruded the local lithologies resulting in a complex scenario of greisen-stype Sn deposits to proximal and distal skarns to massive sulphides (Cu-Sn) replacing mafic lavas that are intercalated with the sedimentary beds.

The Lower Cambrian black shales in the Yangzte platform sedimentary succession are enriched in Mo, Ni, PGE, Au, Ag, Zn, V and As. This is a metalliferous shales horizon, which includes phosphorite and stone coal, extends along a belt 1,600 km long, from Yunan Province in the south-southwest to Zhejiang Province in the east-northeast. Several genetic models that have been proposed to explain this metal enrichement in the black shales are discussed in this chapter.

The Cathaysia Block (including the South China Fold Belt) is characterised by numerous northeast-trending continental rift basin of Mesozoic age, referred to as the Cathaysian rift system. In South China there are economically significant U

deposits including granite-related, volcanic-type; black shale-related, also referred to as carbonate-siliceous-pelite (C-Si-pelite). The granite-related Guidong, Xiaozhuang and Zhuhuang U ore fields are described, followed by the volcanic-related U deposits of the Gang-Hang belt in southeast China.

The chapter concludes with brief overviews of two unusual mineral systems: a REE-Nb-Ga in coal seams and the polygenetic Shilu Fe deposit in Hainan Island. The former could open up an entirely new field, in terms of new conceptual models and for future prospects in REE mineral resources, a commodity which is in much demand in the twenty-first century.

4.1 Introduction

In this Chapter, I discuss complex tectonic domains that have interacted since the Proterozoic, again producing an assortment of mineral systems, mostly along their respective margins and/or along major faults, as already noted for the North China Craton (NCC). Indeed, important metallogenic belts are concentrated along the collision zones between the Yangtze and NCC and between the Yangtze and the Cathaysia block, as is elaborated below.

The eastern and southeastern parts of China contain the 3.1–1.8 Ga Yangtze Craton, the 1.8–1.4 Ga Cathaysia Block and the Phanerozoic South China Fold Belt (also called Huanan fold belt; discussed in Chap. 5), which together make up the South China Block (Figs. 2.2, 2.3 and 2.5). An overview of the South China Block can be found in Li et al. (2003a, b) and a schematic tectonic framework from these authors is shown in Fig. 4.1. The Yangtze Craton is in contact with the Cathaysia Block along a tectonically complex zone (Jiangshan-Shaoxing Fault) interpreted as a crustal suture, which contains an ophiolitic-type mélange and high-pressure metamorphic rocks (Sengör and Natal'in 1996). The amalgamation of the Yangtze Craton with the Cathaysia Block, may have first occurred during the 1.0–0.85 Ga Jinning Orogeny. This was followed by a rifting episode around 800 Ma during the Sinian, and a second collision event during the Caledonian (Zhou et al. 2002). However, Wang et al. (2007), on the basis of detrital zircon U-Pb ages, suggested that the amalgamation of the Yangzte Craton and the Cathaysia Block took place during the Jinning Orogeny at about 860–800 Ma. Wang et al.'s tectonic model, shown in Fig. 4.2, proposed that the Yangzte and Cathaysia, were separated by an oceanic arm and an intraoceanic island arc between about 1,000 and 870 Ma; this was followed by closure of the oceanic arm, approach of Cathaysia to the island arc and final collision between these tectonic domains at 860–800 Ma, resulting the in Jiangnan orogenic belt (see also below), which is part of the wider Jinning Orogeny (Chap. 2).

The NCC and South China Block are separated by the Qinling-Dabie orogenic belt (Li 1994; Xue et al. 1996), a major Late Triassic collision zone that resulted from the closure of a Palaeo-Tethys oceanic arm. Details of the tectonic evolution of the South China Block are complex and still largely unresolved, although various lines of evidence (e.g. Li 1998) suggest that it formed through a series of continent-continent collisions with closure of intervening segments of oceanic crust since Proterozoic

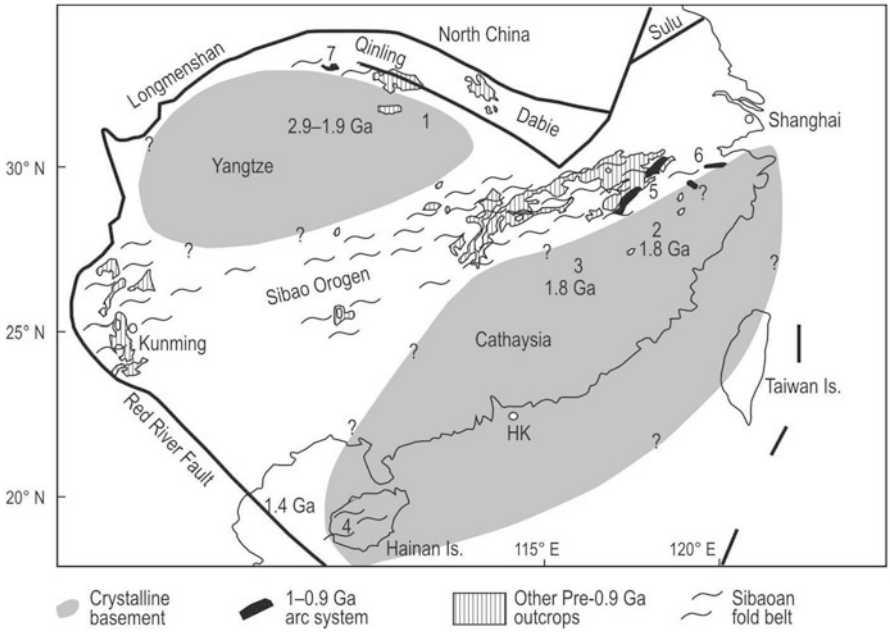

Fig. 4.1 Schematic tectonic framework of the South China Block. (After Li et al. 2003b)

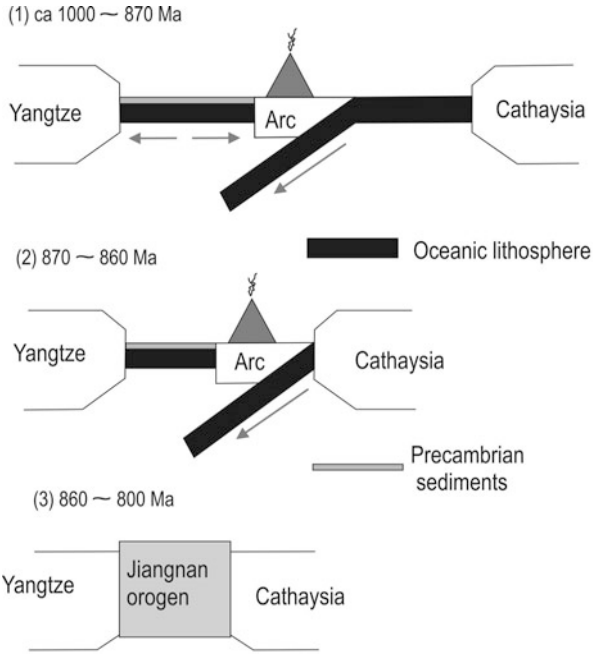

Fig. 4.2 Simplified model of the geodynamic evolution of the Jiangan orogen (details in text). (After Wang et al. 2007)

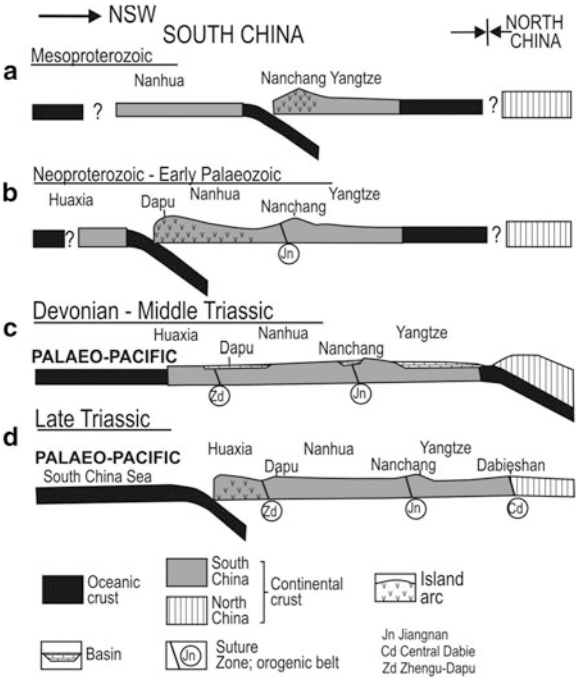

Fig. 4.3 Simplified model of the geodynamic evolution of the South China Block (Yangtze Craton and Cathaysia), details in text. (After Gu et al. 2007)

time (e.g., Li et al. 1997; Ye et al. 1998). Other authors (e.g. Charvet et al. 1996) proposed that the Jiangnan orogenic belt records a series of Neoproterozoic events, which involved the collision of Huaiyu terrane of the Cathaysia Block in the southeast with the Jiuling terrane of the Yangtze Block in the northwest. The Jiuling terrane is largely composed of continent-derived turbidites and littoral facies sedimentary rocks of Meso- to Neoproterozoic age. The Huaiyu terrane contains Meso- to Neoproterozoic ophiolitic rocks, metavolcanics and turbidites. The ophiolitic mélange units were caused by the collision of the two terranes in the Neoproterozoic, also resulting in intensive ductile shearing and deformation (Li et al. 2010d). Although it is not clear, from the English language literature, if the Huaiyu and Jiuling terranes, correspond to Huaxia (or Huanan) and Nanhua terranes of Gu et al. (2007), discussed below, I suspect that this is a case of different names, used for the same geological entity.

Gu et al. (2007 and references therein), came up with a more detailed model for the Mesoproterozoic to Triassic geodynamic evolution of the Yangtze Craton-South China and relationship to the North China Craton. The salient points of the model, shown in Fig. 4.3, are as follows. South China is characterised by continental fragments (mostly Palaeo- to Mesopropterozic metamorphic terranes; see discussion below), rift basins and fold belts, which were formed between the Mesoproterozoic and the Late Triassic. The Yangtze Craton, Nanhua and Huaxia (also called Huanan; see Fig. 2.3) terrane (together forming Cathaysia), from the northwest to southeast

are the main tectonic domains that make up South China (Fig. 4.3a). The Huaxia terrane is thought to have a basement of Archaean-Palaeoproterozoic age and to have been a passive margin from the Mesoproterozoic to the Neoproterozoic (Fig. 4.3a, b). The Yangtze is separated from Cathaysia by the Jiangnan suture (or orogenic belt), with its southeastern margin comprising the Mesoproterozoic Qianyang-Leping island arc, whereas the Nanhua terrane with a Precambrian basement is covered by Neoproterozoic-Early Palaeozoic island arc and back arc systems (Fig. 4.3b). The collision of these terranes results in the formation of orogenic belts (e.g. Jiangnan) and the final amalgamation at the end of the Early Palaeozoic of the South China Block (Fig. 4.3c). The Late Palaeozoic follows with the formation of marine basins; particularly important are the passive continental margin environments that at this time developed along the southern edge of the Yangtze Craton (Fig. 4.3c), prior to its Middle-Late Triassic collision with the NCC, along the Dabieshan suture zone (Fig. 4.3d). The lithofacies that were formed in the passive margin depositional setting, largely consisted of carbonate rocks, which provided the ideal fertile rock type for the formation of skarns and Carlin-style ore systems, some of which overprint pre-existing ores, as discussed in the sections ahead.

4.2 Yangtze Craton

The Yangtze Craton is bound to the north by the Qinling-Dabie orogenic belt with its southeastern margin defined by the Sibao Orogen (Li et al. 2003b), which corresponds to the above-mentioned Jiangnan Orogen of Wang et al. (2004c, 2007), to the southwest is the Red River Fault zone, which marks the boundary with the Himalayan fold belts to the west (see figures in Chap. 2). In the west, the Xianshuihe Fault separates the Songpan-Ganzi terrane from the Yangtze Craton. A well defined tectonic boundary in the southeast between the Yangtze Craton and Cathaysia is the above mentioned Jiangshan-Shaoxing Fault. To the east along and on the north side of this fault bodies of ophiolitic rocks are tectonically emplaced within volcano-sedimentary rocks of the Banxi Group (see below) that are also spatially associated with syntectonic S-type peraluminous granites. The two main ophiolites are the Jiangxi and the South Anhui ophiolitic suites, investigated by Li et al. (1997), who suggested that the former represents oceanic crust of an inter-arc basin at ca. 1.0 Ga, whereas the latter represents oceanic crust formed in a marginal basin behind a continental magmatic arc at about 0.9–0.8 Ga. Li et al.'s model also suggest the presence of a subduction-related continental margin in the southeastern part of the Yangtze Craton. The ophiolites were then formed following the collision between the Yangtze Craton, the intervening continental and oceanic arc with the Cathaysia Block in the Neoproterozoic (Li et al. 1997).

The Yangtze Craton contains Archaean and Palaeproterozoic rocks, overlain by sedimentary succession of the Yangtze platform. However, exposures of Archaean rocks are scarce, although there have been various attempts, using U-Pb and Hf isotope systematics on xenocrystic zircons from lamproites and detrital zircons in sedimentary rocks, to identify Archaean crustal materials (Zheng et al. 2006; Wang

et al. 2010a). In this way, xenocrystic zircon population ages of 2.9–2.8 Ga and 2.6–2.5 Ga with Hf model ages from 2.6 to 3.5 Ga have been recognised (Zheng et al. 2006). More recently, Wang et al. (2010a) detected a 4.3 Ga source in the Hf model ages of the oldest detrital zircons, in addition to zircon ages ranging from 2.5–2.4, 2.0–1.7 to 0.85–0.8 Ga, with other contributions of juvenile crust at 1.6–1.4, 0.95–0.85 and 0.78–0.74 Ga. These age data indicate the presence of ancient basement beneath the exposed Proterozoic cover in the detrital minerals contained in the sedimentary rocks deposited in a 0.8 Ga rift basin in the Yangzte Craton. In the northern part of the Yangtze Craton are few outcrops of 3.2 Ga gneiss, 2.95–2.9 Ga migmatites and granitic rocks (Jiao et al. 2009). These works hint at a complex crustal evolution, spanning the Archaean to the Neoproterozoic.

4.2.1 Archaean and Proterozoic Lithostratigraphy

Yang et al. (1986) described in detail the lithostratigraphy of the Yangtze Craton and most of the following is taken from these authors. The Archaean is largely represented by the Dabie Group that is unconformably overlain by the Proterozoic Hongan Group in the Huaiyang region in Hubei Province. The Dabie Group is a 15 km-thick succession comprising hornblende-plagioclase gneiss, biotite-plagioclase gneiss, amphibolite, granulites, marbles and banded iron- formation (BIF). These rocks are thought to be derived from mafic volcanics, siltstone, greywacke, carbonate beds and arkose. U-Pb zircon ages range from 3.1 to 2.5 Ga. Unconformably overlying the Dabie Group is the Palaeoproterozoic Susong Group, which contains mainly marble units. Along the upper reaches of the Yangtze River, rocks of the Wudang Group with a total thickness estimated at about 15 km, consist of quartzite, mica schist, slates and metavolcanic rocks with a possible age of about 2.0 Ga. In the Yangtze River gorges in Hubei Province, the Sandouping Group is exposed, forming an anticlinorium that is overlain by rocks of the Sinian System. The Sandouping Group contains biotite-plagioclase gneiss, amphibolite, quartz schist, marble with a total thickness of about 3 km. In the northern part of the Yangtze Craton, the ca. 1.85 Ga Quanqitang A-type granitic pluton, was part of a microcontinental block and was emplaced in a post-collisional tectonic settings (Peng et al. 2012). This microcontintal block, named Kongling by Peng M and co-authors, participated in the final amalgamation of the Yangtze Craton.

Near the Red River Fault, in the southwest, the Palaeoproterozoic Dahongshan Group is well exposed and comprises a succession of alternating metasedimentary and alkaline volcanic rocks with isotopic ages ranging from 1.9 to 1.75 Ga. Possible correlatives of this formation are found in northeast Yunnan Province and southwest Sichuan Province, where the Hekou Formation has similar lithologies. Both the Dahongshan Group and the Hekou Formation are overlain by Mesoproterozoic rocks of the Kunyang Group and the Huili Group. Detrital zircon age determinations indicate at least three Palaeoproterozoic events in the Yangtze Craton at 1.75, 1.85 and 2.05 Ga (Wang et al. 2010a).

Neoproterozoic cover rocks are part of the Yangtze platform succession and are exposed in western Hubei (Shennojia Group), the Kham-Yunnan region in the southwestern margin of the South China Block, and the Jiangnan region, where these rocks form a 1,500 km-long belt (Jinning Group). The Shennojia Group consists of an unmetamorphosed carbonate sequence (passive margin?) that is about 6 km thick. In the Kham-Yunnan region are the above-mentioned Kunyang and the Huili Groups that contain metamorphic basement rocks. The Kunyang Group consists of slate, siliceous dolomite, sandstone, siltstone, andesitic and basaltic tuffs, unconformably overlain by volcano-sedimentary deposits. Stromatolites are present in some of the carbonate units and isotopic age determinations yield ages ranging from 1.76 to 0.78 Ga. The Jiangnan region contains two metamorphic sequences separated by an unconformity that marks the boundary between the Meso- and Neoproterozoic. The Meso-Neoproterozoic Fanjingshan Group consists of thick sequences of metasedimentary and metavolcanic rocks that include mafic and ultramafic rocks and amygdaloidal alkaline basalts and pillow lavas with a total thickness of 3,000 m. The Fanjingshan Group, in the central part of the Yangtze Craton (Guizhou Province), is subdivided into five formations, which from the base upward include: Yujiagou, Xiaojiahe, Huixiangping, Waxi and Duyantang (Wang et al. 2010a). The Fanjingshan Group rocks are unconformably overlain by dominantly sandstone beds of the Xiajiang Group, which comprises six formations (from base to top: Jialu, Wuye, Zhangjiaba, Qingshuijiang, Liangjiehe, Datangpo and Nantuo). The Jialu Formation comprises conglomerate and sandstone, conformably overlain by purple slate and siltstone of the Wuye Formation, in turn overlain by coarse-grained sandstone and grey-green siltstone of the Zhangjiaba Formation. The Qingshuijiang Formation consist of tuffaceous sandstone and slate, overlain by the Datangpo Formation characterised by black shales, thin-bedded black Mn-bearing sediments, grey and black shales. The Nantuo Formation is represented by diamictites, up to 51 m thick (Wang et al. 2010a).

The Neoproterozoic Banxi Group, which locally reaches 10 km in thickness, consists of sandstone, arkose, siltstone, slate, red and green sandstone, tuffs and felsic volcanics (keratophyres), basaltic rocks and ignimbrites. Continental rifting on the southern and northern margins of the Yangtze Craton, controlled the platform Neoproterozoic to Cambrian carbonate-dominated depositional systems of the Craton (Wang et al. 2005). Oceanward, the platform developed a series of deep basins, which were filled with organic-rich sediments. These constitute the vast black shale province that borders the northern and southern margins of the Yangtze Craton, covering about 10^6 km^2 (Emsbo et al. 2005). This black shale province hosts polymetallic deposits, discussed in Sect. 4.4.8.

Li et al. (2003a) dated the Neoproterozoic anorogenic granites and mafic-ultramafic intrusions that were emplaced in rift structures. Radiometric dating indicates two episodes: (1) from ca. 830 to ca. 795 Ma; and (2) ca. 780–745 Ma. Li et al. (2003a) recognised two groups from two rift structures: Kangdian Rift and Nanhua Rift in western margin and centre of the South China Block, respectively (see Fig. 7.6). The Kangdian Rift is north-south-trending and contains granite, granodiorite, tonalite, gabbro, mafic dykes and some ultramafic rocks, most of which intrude

the rift sedimentary succession. Platform sedimentary rocks unconformably overlie the Kangdian rift succession. The Nanhua Rift is northeast-trending and contains thick rift sedimentary successions (at least >4 km thick in places), which consists of conglomerate, sandstone, siltstone and volcanic rocks. One of the Nanhua successions is the Doushantuo Formation consisting of shallow and deep-water clastic, carbonate and phosphatic sedimentary rocks, which were deposited after the Neoproterozoic Marinoan global glaciation (Li et al. 2010c). It is of interest to note that Li et al. (2010c) provided evidence from rocks of the Doushantuo Formation, of a stratified ocean in the Ediacarian period, with a wedge of sulphidic waters between oxic surface waters and anoxic and Fe^{2+}-rich waters at the bottom. This evidence has important implications for understanding the depositional mechanism of iron formations, redox conditions and the role of microorganisms in the oxygenation of the atmosphere (see also Poulton et al. 2010). It is also of interest to note that rocks of the Yangtze platform include important Ediacaran (Late Neoproterozoic) successions, well studied by Zhu et al. (2007). These authors carried out detailed sedimentary facies analysis of the upper parts of the Doushantuo Formation and the overlying Dengying Formation and concluded that the sequence boundaries, with strong negative $\delta^{13}C$ excursion at 560–555 Ma, coincide with the end of the Neoproterozoic glaciations and first appearance of animals.

Li et al. (2003a) interpreted the geochronological results to represent episodes of mantle plume activity (bimodal magmatism), suggesting that the ca 830–795 Ma episode correlates with the ca. 827 Ma Gairdner Dyke Swarm in Australia (see Figs. 7.7 and 7.8). The second episode (780–745 Ma) correlates with the Mundine Well Dyke Swarm in Western Australia and the Franklin igneous event in North America (Laurentia). Finally, Li et al. (2003a) proposed that a 6,000-km diameter superplume impacted the Rodinia supercontinent causing its breakup, doming and extensive crustal melting and the formation of rift systems (Adelaide Rift), Bikou-Hannan rift and the Nanhua rift, referred to above (Wang et al. 2010b). Zhao et al. (2008) reported on the association of Neoproterozoic (ca. 860–740 Ma) A- and I-type granites along the northern margins of the Yangtze Craton. These authors provided details of the geochemical character of these granitic rocks and suggested that I-type plutons were formed by dehydration melting of tonalite-trondhjiemite-granodiorite (TTG) rocks by underplating of mafic melts. Heating and dehydration of the rocks above the I-type magmas occurred, converting them to charnockites which, in turn, underwent partial melting to produce A-type granites. The important aspect of Zhao et al's model is that the mafic underplating was likely the result of large-scale crustal extension and asthenospheric upwelling in a back-arc setting, or perhaps as a result of a mantle plume. The back-arc option suggests the presence of an active continental margin in the western Yangtze Block in the Neoproterozoic. More information on a possible Rodinia connection was advanced by Wu et al. (2006), who dated (LA-ICPMS zircon U-Pb dating) granodiorites at the southeastern margin of the Yangtze Craton and obtained two groups of ages at 824 ± 6 and 882 ± 16 Ma. Integrating the geochronological data with trace element and stable isotope systematics (D, O), Wu et al. (2006) suggested that the granitic rocks have a peraluminous composition and were formed in an arc-continent collision setting, which was part of

continental growth that contributed to the assembly of Rodinia. In their paper, Wu et al. (2006) proposed a model for the Neoproterozoic geodynamic evolution that amalgamated the Yangtze and Cathaysia tectonic domains. In this model, which is not too different from that of Wang et al. (2007) (Fig. 4.2), Wu et al. (2006) also envisaged subduction of oceanic crust and the development of an island arc at about 1.1–0.9 Ga, in a seaway between the Yangtze Craton and the Cathaysia Block; this was followed by collision of the arc with the southern margin of the Yangtze Craton at 0.92–0.88 Ga and the final collision and amalgamation of the two blocks, with development of syn-post-collision S-type granitic magmatgism at about 0.83–0.82 Ga.

The Jiangnan (Jiang-nan, means south—nan—of the Yangtze River) orogenic belt (or Sibao Orogen; Fig. 4.1), likely resulted from the collision between the Yangtze Craton, the intervening Jiuling island arc and Cathaysia Block during the Neoproterozoic (870–820 Ma; Wang et al. 2004c). According to Wang et al. (2004c), this collision was followed by the breakoff of a subducted oceanic slab, followed by upwelling asthenospheric mantle, which resulted in the emplacement of S-type, post-collisional granites. Lithospheric extension under the southern margin of the Yangtze Craton, then led to rifting and the eruption of within-plate basalts. On this basis, Wang et al. (2004c), disputed the mantle plume hypothesis put forward by Li et al. (2003a, b). Similarly, Zhao et al. (2011), on the basis of U-Pb ages of detrital and igneous zircons, proposed that the timing of the amalgamation of the Yangtze and Cathaysia blocks occurred at about 830 Ma, with a southeast-directed subduction and back-arc extension model. According to these authors, the Nanhua basin was a back-arc basin, with rift-related magmatism due to asthenospheric upwelling and flat subduction.

The Precambrian rocks of the Yangtze Craton are overlain by a cover of thick carbonate and clastic successions of Cambrian to Triassic ages. These successions largely consist of limestone, dolomite, siltstone, sandstone and shale of continental shallow-water platform to deep water facies in rift basins. These rocks were deformed during the Yanshanian, resulting in the formation of fold-and-thrust belts, but locally only gently folded or domed (Su et al. 2009). The Yanshanian event is also responsible for the emplacement of granitic and felsic volcanic rocks in the Craton. The 260 Ma Emeishan continental flood basalts occur southwestern margin of the Yangtze Craton (Chap. 7).

4.3 Cathaysia

The Cathaysia Block (Figs. 4.1 and 4.4) consists of Palaeo- and Mesoproterozoic rocks, which outcrop mostly in the northeast and southwest and represented by 1.8 Ga granites and volcanic rocks of the Badu Complex and the 1.43 Ga granites of the Baoban Complex in Hainan Island, with superimposed Mesozoic volcanic rocks and granitic intrusions (South China Fold Belt). The Cathaysia Block is covered by platform sedimentary rocks (mainly carbonate, siliciclastics). The Precambrian basement of Cathaysia is exposed in the northeast (Zhejiang and Fujan provinces), where

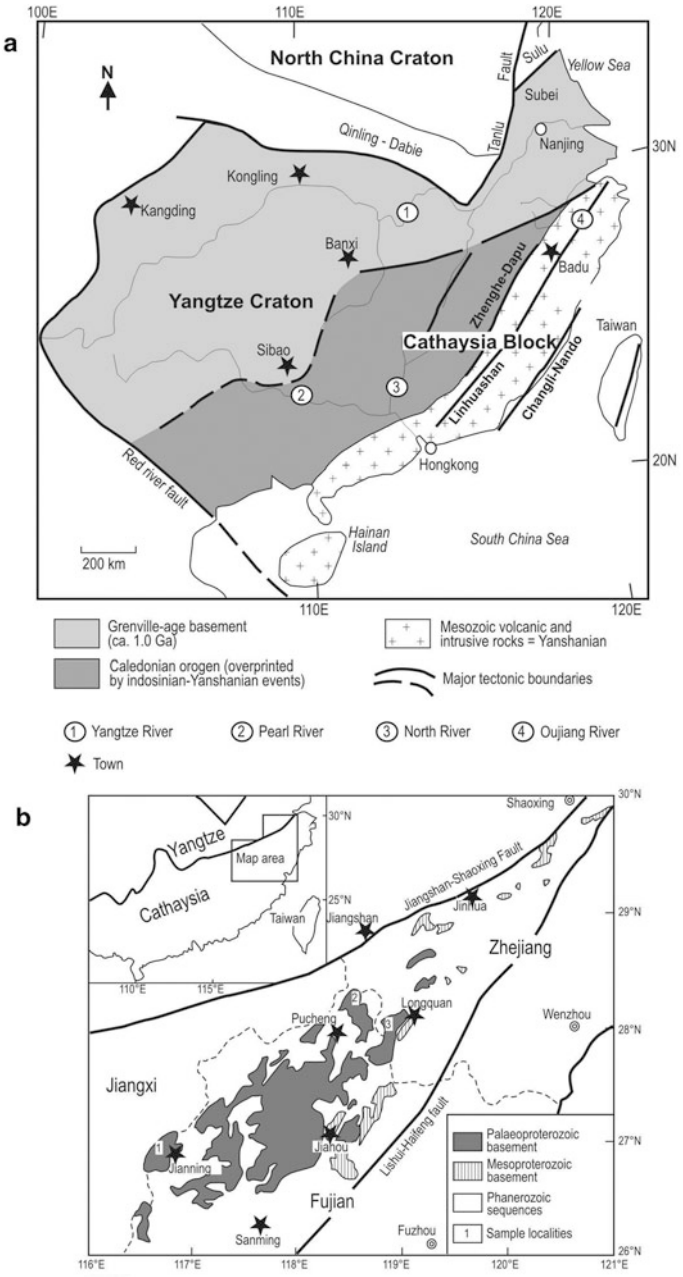

Fig. 4.4 **a** Yangtze Craton and Cathaysia Block and major fault zones (after Xu et al. 2007), Taiwan geology not shown; **b** Precambrian basement in northeastern Cathaysia (Zhejiang Province) (after Li et al. 1997)

two metamorphic sequences occur between the Jiangshan-Shaoxing and Lishui-Haifeng fault zones (Fig. 4.4) (Li 1997). The lower metamorphic sequence is about 3.6 km thick, called Badu Group in Zhejiang and Mayuan Group in Fujian, consists of gneissic granites, amphibolites and leptynites (a term referring to a quartzo-feldspathic rock forming bands alternating with metabasic rocks; Fettes and Desmond 2007). The upper metamorphic sequence, about 2 km thick, called Longquan Group in Zhejiang and Mamianshan Group in Fujian, consist of schist, metavolcanics, marble and Fe-rich quartzite. Li (1997) reported U-Pb zircon ages of ca. 1.76 Ga from the Tianjinping amphibolites in the Mayuan Group. Other ages (Sm-Nd and U-Pb) range from ca. 2.7–2.01 to 1.9–1.6 Ga but, as pointed out by Xu et al. (2007), these are unreliable ages due to discordant zircons. The basement of the Cathaysia Block remains largely unknown, although it is generally assumed that the Block is underlain by an amalgamation of Achaean and Palaeo- to Mesoproterozoic continental crust (Fletcher et al. 2004 and references therein). Furthermore, several authors have suggested that Cathaysia is made up of accreted microcontinental fragments. Xu et al. (2007) used U-Pb dating and Hf isotope systematics from detrital zircons to investigate the basement rocks of the Cathaysia Block and reported Palaeoproterozoic ages of 1.87–1.85 Ga and 2.4–2.1 Ga in the eastern parts of the Block. However, this Palaeoproterozoic basement was extensively reworked by the Yanshanian magmatism in the Mesozoic. In the western parts of Cathaysia, crustal material is of Meso-Neoproterozoic age, with some Archaean components, all extensively reworked at various stages during Caledonian (450 Ma), Indosinian (240 Ma) and early Yanshanian (160 Ma) thermal events. Nd isotopic constraints indicate that in eastern Cathaysia basement rocks are ca. 1.4 Ga, whereas in the western part are ca. 1.7 Ga However, these Nd model ages do not reflect actual thermal events but rather a mixing of juvenile magmas and remelting of the Proterozoic basement, thereby suggesting a complex crustal evolutionary history (Xu et al. 2007). Xu et al. (2007), on the basis of their work and a survey of previous work, suggested that Cathaysia may consist of two distinct terranes, as indicated by the absence of Caledonian and Indosinian events in the eastern parts of the Block. Furthermore, these two terranes would only have amalgamated during the Yanshanian event (common to both eastern and western parts). More recently, Yu et al. (2010), using U-Pb and Lu-Hf isotopic analyses (LAM-ICPMS and LAM-MC-ICPMS) of zircons from basement rocks in southern Cathaysia, attempted to reconstruct the growth history of the Cathaysia Block. From the work of Xu et al. (2007) and Yu et al. (2010), the Cathaysia crystalline basement is confirmed to comprise two distinct terranes with a complex geological history: Wuyishan in the northeast and Nanling-Yunkai in the southwest, separated by an approximately east-west boundary. The Wuyishan terrane consists of metasedimentary and metavolcanic rocks, with zircon isotopic analyses by Yu et al. (2010) showing mainly 1.85 Ga igneous rocks, overprinted by strong Neoproterozoic and early Palaeozoic tectonothermal events. The zircon data further indicate that the terrane was affected by five episodes of juvenile crust generation at 3.6, 2.8, 2.6–2.4, 1.85 and 0.8–0.7 Ga, with a dominant thermal event at 1.85 Ga in the northern part of the terrane and at 0.8–0.7 Ga in the central and southern parts. The Nanling-Yunkai terrane, consists of metasedimentary rocks comprising mica

schist, phyllite, slate and metaclastic rocks. The zircon isotopic data, on the other hand, show that growth of juvenile crust occurred at 3.6, 3.3, 2.6–2.5 Ga (Neoarchaean), 1.6, 1.0 (Grenvillian) and 0.8–0.7 Ga (Neoproterozoic), with the last three involving recycling of older crustal material. In addition, the zircon U-Pb data show that at least three orogenic and metamorphic events affected Cathaysia: Caledonian (470–410 Ma), late Palaeozoic (280–270 Ma) and Indosinian (ca. 230 Ma). Yu et al. (2010) concluded that the Cathaysia Block consists of the two Wuiyshan and Nanling-Yunkay terranes, each with distinct crustal evolutionary history, not only from each other but also from the Yangzte Craton to the north. In addition, it is suggested that the Nanling-Yunkai terrane is thought to have an evolutionary history similar to East India-Antarctica, with the strong possibility that the terrane may have been linked with northern Gondwana (Yu et al. 2008, 2010). The boundary between the Wuiyshan and the Nanling-Yunkai terranes trends from east-west to west-northwest and is reasonably defined by seismic and gravity anomalies, in addition to a concentration of Yanshanian gabbro-syenite, A-type granite and bimodal volcanics within this boundary zone. Shu et al. (2011) dated mafic rocks (gabbros) by SHRIMP U-Pb on zircons, which yielded ages ranging from ca. 857 to 837 Ma with εHf(t) values of +10.5 to +4.1, indicating derivation from a depleted mantle source and showing geochemical signatures of continental rift mafic rocks. By contrast felsic volcanic rocks (rhyolites) in Cathaysia have ages of ca. 970 M and are of arc-affinity. Shu et al. (2011) suggested the in the Neoproterozoic the Cathaysia Block underwent a rifting stage in the period of 857–837 Ma, corresponding with the breakup of the Rodinia supercontinent of which Cathaysia was part.

The Cathaysia Block is widely covered by Palaeozoic platform facies sedimentary rocks, locally with windows of Neoproterozoic metasedimentary rocks. The coastal region of Cathaysia (Figs. 4.1 and 4.4) is characterised by widespread intrusive and volcanic rocks of Yanshanian age (Mesozoic), forming a magmatic belt extending for more than 400 km from Hainan island to Zhejiang Province to the northeast. These Yanshanian igneous rocks are part of the larger magmatic belt of eastern Asia, discussed in more detail in Chap. 7. In Cathaysia this belt largely consists of volcanic and associated volcaniclastic rocks, accompanied by shallow-level (subvolcanic) granitic intrusions. Porphyry and epithermal mineral systems associated with the Yanshanian igneous rocks in Cathaysia are treated in Chap. 5. The dominant structures in the Cathaysia Block are northeast-trending fault zones, namely: Changle-Nanao Fault and Lianhuashan Fault (Fig. 4.4). Importantly, these faults are considered to be the surface expression of deep-seated basement structures that controlled the Yanshanian igneous activity.

4.4 Mineral Systems of the Yangtze Craton and Cathaysia

The Yangtze Craton and Cathaysia host a great variety and abundance of ore systems, some of which are world class. Zaw et al. (2007) reviewed the deposits of the South China region, which effectively encompasses the Yangtze, Cathaysia and South China Fold belt. The latter is discussed in Chap. 5. A list of the deposits discussed by

Zaw et al. (2007) is presented in Table 4.1. In the sections ahead, I review the following ore systems: sediment-hosted massive sulphides (SEDEX), Mississippi Valley Type (MVT), Carlin-style, porphyry-skarn, porphyry-epithermal, skarns and Kiruna style, metalliferous black shales, tin-tungsten, antimony and basin-hosted uranium.

4.4.1 Stratabound and/or Stratiform Massive Sulphides Deposits

Important stratabound and/or stratiform deposits in South China include Dongchuan, Dabaoshan, Fankou, Wushan, Chengmenshan, Dongguashan, Woxi and Qixiashan (Table 4.1). The salient features of these deposits, reviewed and referenced by Zaw et al. (2007) and Gu et al. (2007), are provided here. Those that occur in the Lower Yangtze River Valley region are treated in Sect. 4.4.4.

In Yunnan Province, the poorly documented Dongchuan deposits are hosted in marine and continental red bed sedimentary rocks, deposited in the Kangdian rift. Dongchuan, located about 80 km north of the city of Kunming, is the third largest Cu mining area in China, hosted by the Palaeoproterozoic rocks of the Kunyang and Dongchuan groups, in which the mineralisation consists of stratabound disseminations of chalcocite-chalcopyrite and bornite in algal dolomites (see Zhao et al. 2012). During deformation events the Dongchuan Cu sulphide disseminations were locally redistributed to form hydrothermal vein systems (Ran 1989; Qiu et al. 2002). The Fankou and Dabaoshan deposits are some of the economically most important in South China. The ores are hosted in Devonian to Carboniferous limestone, sandstone and siltstone, which are thought to have accumulated, either in an intra-arc trough or intracontinental rift basin, with the latter perhaps more likely (Gu et al. 2007). At Fankou, the sulphide mineralisation is distributed along a steeply dipping syn-sedimentary fault that clearly acted as the conduit for the hydrothermal fluids. The ore minerals in the Fankou deposit include sphalerite, galena, pyrite, chalcopyrite with lesser scheelite and stibinite. There is both a vertical and lateral zonation, showing a general metal upward trend from Fe → Cu → Cu-W → Pb → Zn → Fe→ Mn-carbonates and laterally from Cu → W → Pb → Zn → Ag-Fe → Mn. Fankou is described in some detail by Tu (1990). The SEDEX-type Woxi W-Sb-Au deposit (Table 4.1) is characterised by fine banding or laminae of stibnite and scheelite ores, underlain by a stringer (feeder) system of quartz-pyrite-Au-scheelite (Gu et al. 2012). The Qixiashan deposit is a SEDEX system with a skarn overprint related to Yanshanian magmatism. The ore is hosted in Carboniferous limestone, dolomite, shale and sandstone. Similarly, the Carboniferous Dongguashan Cu-Au SEDEX deposit was overprinted by skarn-related hydrothermal fluids in the Jurassic.

The Dahongshan Fe-Cu deposit (Table 4.1) hosted in rocks of the Dahongshan Group, located about 200 km south-southwest of Kunming, is characterised by Fe oxides (magnetite and hematite) chalcopyrite-bornite disseminations, veins and massive ores, associated with brecciated host rocks (Zhao and Zhou 2011). Furthermore, the ore zones exhibit extensive sodic (albite) and potassic alteration, overprinted by

Table 4.1 List of selected mineral deposits in South China. (After Zaw et al. 2007)

Deposit name	Province	Lat N/ Long E	Deposit type	Commodity	Tonnage	Grade	Host rocks
Gacun	Sichuan	31°11′/99°32′	VHMS	Zn-Pb-Cu-Ag-Au	4 Mt (metal); combined (Cu + Zn + Pb + Ag + Au)	0.44 % Cu, 5.4 % Zn, 3.7 % Pb, 160 g/t Ag, 0.3 g/t Au	Felsic and mafic volcanic rocks (bimodal)
Liwu	Sichuan	28°36′/101°48′	VHMS	Cu-Zn	0.26 Mt (metal); Cu 0.13 Mt (metal); Zn	2.5 % Cu, 0.6 % Zn	Metavolcanic rocks
Lalachang	Sichuan	26°06′/101°54′	VHMS	Cu-Fe	0.6 Mt (metal); Cu	0.9 % Cu	Spilite-keratophyre
Dahongshan	Yunnan	24°06′/101°41′	IOCG?	Cu-Fe-Ce	0.8 Mt (metal); Cu	0.64 % Cu	Volcanic rocks
Dapingzhang	Yunnan	22°47′/100°31′	VHMS	Cu-Pb-Zn	0.30 Mt (metal); Cu 0.15 Mt (metal); Pb 0.15 Mt (metal); Zn 0.6 Mt (ore); Ag, Au	1.9–6.1 % Cu, 0.2–1.1 % Pb, 0.4–1.8 % Zn, 110 g/t Ag, 3.5 g/t Au	Felsic volcanic rocks
Laochang	Yunnan	22°45′/99°44′	VHMS	Pb-Zn-Ag	0.5 Mt (metal); Pb 0.16 Mt (metal); Zn >500 t (metal); Ag	1.2–8.9 % Pb, 2.9–5.1 % Zn, 57–195 g/t Ag	Trachybasalt—andesite and associated volcanoclastic rocks
Tongchangjie	Yunnan	24°20′/99°45′	VHMS	Cu-Zn	0.2 Mt (metal); Cu No data for Zn	1.54 % cu, 0.4 % Zn	Mafic volcanic rocks
Jinding	Yunnan	26°24′/99°25′	Probable SEDEX	Zn-Pb-Ag	200 Mt (ore)	6.08 % Zn, 1.29 % Pb, 1–20 g/t Ag	Sandstone, siltstone, limestone
Dongchuan	Yunnan	26°13′/102°56′	Stratabound veins	Cu (Fe)	No data	No data	Sandstone, shale, dolomite
Daliangzi	Sichuan	26°38′/102°52′	MVT	Zn-Pb-Ag	24 Mt (ore)	10.4 % Zn, 0.8 % Pb, 43 g/t Ag	Dolomite
Dayinchang	Sichuan	26°37′/102°45′	MVT	Zn-Pb	5.6 Mt (ore)	3 % Zn + Pb	Dolomite
Tianbaoshan	Sichuan	26°58′/102°15′	MVT	Zn-P:b-Ag	11 Mt (ore)	10.1 % Zn, 1.5 % Pb, 93.6 g/t Ag	Dolomite
Tuanbaoshan	Sichuan	29°27′/102°51′	MVT	Zn-Pb-Ag	No data	No data	Dolomite

Table 4.1 (continued)

Deposit name	Province	Lat N/ Long E	Deposit type	Commodity	Tonnage	Grade	Host rocks
Qilingchang and Kuangshan-chang (Huize district)	Yunnan	26°38′/103°44′	MVT	Zn-Pb-Ag	5 Mt (metal)	Combined Zn-Pb >25 % Ag credits	Dolomite
Dexing (district)	Jiangxi	29°01′/117°44′	Porphyry	Cu-Mo-Au-Ag	1,500 Mt (ore)	0.43 % Cu, 0.02 % Mo, 0.16 g/t Au, 1.9 g/t Au	Granodiorite porphyry
Yinshan	Jiangxi	25°00′/120°00′	Porphyry-epithermal	Cu-Pb-Zn-Ag-Au	120 Mt (ore): Cu 5.2 Mt (ore): Zn 5 Mt (ore): Pb 125 Mt (ore): Au 127 Mt (ore): Ag	0.54 % Cu, 2.3 % Zn, 1.8 % Pb, 0.63 g/t Au, 11 g/t Ag	Intermediate to Felsic porphyries
Shaxi	Anhui	31°07′/117°12′	Porphyry	Cu	0.5 Mt (ore)	>0.2 % Cu	Quartz diorite porphyry
Beiya (district)	Yunnan	26°09′/100°12′	Porphyry	Cu-Au	No data	0.1–5 % Cu 0.02–3.3 g/t Au	Alkali-rich porphyry
Xuejiping	Yunnan	27°56′/99°53′	Porphyry	Cu-au-Mo	5.4 Mt (ore)	No data	Syenite porphyry
Machangqing	Yunnan	25°40′/100°30′	Porphyry	Cu-Mo	16 Mt (ore): Cu 56 Mt (ore): Mo	0.5 % Cu, 0.08 % Mo	Felsic porphyry, monzonite porphyry
JinJinzui	Hubei	Not provided	Porphyry	Au-(Cu-Ag)	ca 78 Mt (ore)	9 g/t Au, 0.2 % Cu, 30 g/t Ag	Diorite porphyry
Xinqiao (district)	Anhui	30°55′/118°00′	SEDEX/Skarn overprint	Au-Cu-Fe	116 t (metal): Au 0.23 Mt (metal): Cu no data for Fe	6.90 g/t Au, 0.89 % Cu No data for Fe	Carbonates, volcaniclastics Quartz diorite
Funishan	Jiangsu	32°06′/119°03′	Skarn	Au-Cu	9.3 t (metal): Au No data for cu	0.85 g/t Au No data for Cu	Carbonates/ granodiorite porphyry intrusions
Jinlongshan	Hubei	29°48′/115°25′	Skarn	Au-Cu	15 t (metal): Au No data for Cu	4.0 g/t Au No data for cu	Carbonates/ granodiorite porphyry intrusions

Table 4.1 (continued)

Deposit name	Province	Lat N/ Long E	Deposit type	Commodity	Tonnage	Grade	Host rocks
Changmenshan	Jiangxi	29°41′/115°50′	SEDEX/Skarn overprint	Cu-Mo-Au	1.8 Mt (metal): Cu 6 t (metal): Au No data for Mo	0.75 % Cu, 0.24 g/t au, 0.047 % Mo	Carbonates/ granodiorite porphyry intrusions
Tonglushan	Hubei	30°07′/114°52′	Skarn	Cu-Au	1.0 Mt (metal): Cu 69 t (metal): Au	1.8 % Cu, 1.15 g/t Au	Shale/granodiorite porphyry intrusions
Huangshaping	Hunan	25°42′/112°41′	Skarn	Pb-Zn-Cu	0.8 Mt (metal): Pb 0.8 Mt (metal): Zn 0.3 Mt (metal): Cu	5.9 % Pb, 5.8 % Zn, 0.5 % Cu	Granite porphyry
Kangiawan (Shuikoushan district)	Hunan	26°36′/112°33′	Skarn	Au-Ag-Pb-Zn	30 t (metal): Au 150 t (metal): Ag 0.5 Mt (metal): Pb 0.5 Mt (metal): Zn	3.65 g/t Au 86.8 g/t Au 3.9 % Pb, 4.5 % Zn	Silicified limestone
Tongshankou	Hubei	30°39′/114°53′	Skarn	Cu-Mo	0.5 Mt (metal): Cu 0.01 Mt (metal): Mo	0.94 % Cu, 0.04 % Mo	Granodiorite porphyry
Yueshan district	Anhui	30°01′/116°52′	Skarn	Cu-Au	0.4 Mt (metal) Cu 10 t (metal): Au	Au	Diorite
Jinfeng (Lannigou)	Guizhou	25°10′/105°51′	Carlin-like	Au	107.1 t (metal): Au	5.1 g/t Au	Carbonaceous siltstone, claystone
Zimudang	Guizhou	25°34′/105°28′	Carlin-like	Au	6 t (metal): Au	6 g/t Au	Siltstone, claystone, silty limestone
Getang	Guizhou	25°17′/105°18′	Carlin-like	Au	22 t (metal): Au	6.2 g/t Au	Silicified limestone
Yata	Guizhou	24°56′/105°39′	Carlin-like	Au	15 t (metal): Au	5 g/t Au	Carbonaceous siltstone, sandstone
Banqi	Guizhou	24°46′/105°38′	Carlin-like	Au	10 t (metal): Au	5 g/t Au	Claystone, pelitic siltstone
Jinya	Guangxi	24°33′/106°53′	Carlin-like	Au	30 t (metal): Au	5.3 g/t Au	Silty dolomite, dolomitic siltstone

Table 4.1 (continued)

Deposit name	Province	Lat N/ Long E	Deposit type	Commodity	Tonnage	Grade	Host rocks
Gaolong	Guangxi	24°14′/106°38′	Carlin-like	Au	25 t (metal): Au	4 g/t Au	Calcareous argillite, calcareous siltstone
Mingshan	Guangxi	24°24′/106°51′	Carlin-like	Au	10 t (metal): Au	4.5 g/t Au	Argillite, siltstone, sandstone
Tangshang	Yunnan	122°57′/04°49′	Carlin-like	Au	>21 t (metal): Au	1–3 g/t Au	Argillite, siltstone, sandstone, tuffaceous rocks
Kuzhubao (Gedang)	Yunnan	23°36′/105°31′	Carlin-like	Au-Sb	7 t (metal): Au	5.3 g/t Au	Carbonaceous siltstone, argillite
Bashishan (Piaosi)	Yunnan	23°40′/105°38′	Carlin-like	Au	No data	3 g/t Au	Carbonaceous mudstone
Dongbeizhai	Sichuan	32°47′/105°33′	Carlin-like	Au	>50 t (metal): Au	6.2 g/t Au	Calcareous siltstone, carbonaceous slate
Manaoke	Sichuan	33°39′/104°04′	Carlin-like	Au	20 t (metal): Au	5.0 g/t Au	Siltstone, silty limestone
Qioaqiaoshang	Sichuan	32°44′/103°40′	Carlin-like	Au	15 t (metal) Au	4.0 g/t Au	Carbonaceous slate, pelitic siltstone, sandstone
Dashuigou	Sichuan	29°10′/102°11′	Epithermal	Te-Au	ca. 100 t (metal): Te No data for Au	ca 0.2–25 % Te, ca 3–15 g/t Au	Marble, slate, metabasalt
Zhilingtou (Yinkengshan)	Zhejiang	28°37′/119°25′	Epithermal	Au-Ag	18 t (metal): Au 306 t (metal): Ag	12 g/t Au, 494 g/t Ag	Orthogneiss, paragneiss, felsic volcanics
Zijinshan (district)	Fujian	25°05′/116°40′	Epithermal	Au-Ag-Cu	15 t (metal): Au 619 t (metal): Ag 1.6 Mt (metal): Cu	0.14 g/t Au 6.2 g/t Ag, 1.1 % Cu	Volcanic rocks/granodiorite porphyry
Changkeng	Guangdong	23°01′/112°40′	Epithermal	Au	32 t (metal): Au	7 g/t Au	Siltstone, limestone, brecciated quartzite

Table 4.1 (continued)

Deposit name	Province	Lat N/ Long E	Deposit type	Commodity	Tonnage	Grade	Host rocks
Fuwang	Guangdong	23°00′/112°40′	Epithermal	Ag	6,000 t (metal): Ag	268 g/t Ag	Siltstone, limestone, brecciated quartzite
Ailoashan Belt (Laowangzhai and Daping districts)	Yunnan	22°51′ to 23°54′/101°27′ to 102°59′	Orogenic	Au	150 t Au (combined metal resource)	1–55 g/t Au	Basaltic tuff, mafic-ultramafic rocks, sandstone, limestone
Gaocun and Yunxi (Hetai district)	Guangdong	23°15′/112°16′	Orogenic	Au	30.7 t (metal): Au	3 g/t Au	Mica schist, feldspar schist, mica gneiss
Cangshang	Shandong	37°20′/119°54′	Orogenic	Au	60 t (metal): Au	4 g/t Au	Granitoid
Donggerzhang	Shandong	37°10′/121°367′	Orogenic	Au	20 t (metal): Au	11 g/t Au	Granitoid
Jiaojia	Shandong	37°24′/120°07′	Orogenic	Au	>60 t (metal): Au	7 g/t Au	Granitoid
Jingqingding (Rushan)	Shandong	37°06′/121°40′	Orogenic	Au	25 t (metal): Au	9 g/t Au	Granitoid
Xincheng	Shandong	37°26′/120°10′	Orogenic	Au	>60 t (metal): Au	8 g/t Au	Granitoid
Lingdong	Shandong	37°26′/120°32′	Orogenic	Au	>100 t (metal): Au	3–30 g/t Au	Granitoid
Sanshandao	Shandong	37°21′/119°56′	Orogenic	Au	>60 t (metal): Au	7 g/t Au	Granitoid
Wangershang	Shandong	37°23′/120°09′	Orogenic	Au	45 t (metal): Au	7 g/t Au	Granitoid
Yangliuping	Sichuan	30°40′/102°00′	Noril'sk-type	Ni-Cu-Co-PGE	0.27 Mt (metal): Ni 0.1 Mt (metal): Cu 10,200 t (metal): Co 35 t (metal): PGE's	0.45 % Ni, 0.16 % Cu, 0.016 % Co, 0.55 g/t PGE	Emeishan continental flood basalt sequence (ECFB): mafic-ultramafic sills
Lengshuiqing	Sichuan	26°48′/101°33′	Proterozoic ultramafic-hosted Ni	Ni-Cu-PGE	2.5 Mt (ore)	0.9 % Ni, 0.5 % Cu, 1 g/t PGE	Ultramafic intrusion

Table 4.1 (continued)

Deposit name	Province	Lat N/ Long E	Deposit type	Commodity	Tonnage	Grade	Host rocks
Limahe	Sichuan	26°19′/102°05′	Proterozoic ultramafic-hosted Ni	Ni-Cu-PGE	1.5 Mt (ore)	1.0 % Ni, 0.5 % Cu, 1 g/t PGE	Ultramafic intrusion
Baimazhai	Yunnan	22°50′/102°58′	Noril'sk-type	Ni-Cu-PGE	0.6 Mt (metal): Ni 1.2 Mt (metal): P Cu	>4.0 % Ni, 0.3–4.0 % Cu	ECFB: mafic-ultramafic intrusion
Jinbaoshan	Yunnan	25°03′/100°52′	Noril'sk-type	Ni-Cu-Pt-Pd	13 Mt (ore)	0.19 % Ni, 0.19 % Cu, 0.65 g/t Pt, 1.1 g/t Pd	ECFB: mafic-ultramafic sill
Deze	Yunnan	25°53′/103°37′	Sedimentary-type	Ni-Mo	No data	No data	Black shale
Shizhuyuan (district)	Hunan	25°47′/113°10′	Vein-greisen-skarn	Sn-W-Bi-Mo	0.75 Mt (metal): WO_3 0.49 Mt (metal): Sn 0.30 Mt (metal): Bi 0.13 Mt (metal): Mo	Combined W-Sn-Bi-Mo, 1–5 % with an average 2 %	Dolomitic limestone and porphyritic biotite granite
Xihuashan	Jiangxi	25°22′/114°23′	Vein	W	No data	Average 1.08 % WO_3	Biotite granite
Dachang	Guangxi	124°51′/07°34′	Stratiform, vein	Sn-Pb-Zn-Sb	Combined 100 Mt (ore)	1 % Sn, 3–5 % combined Cu, Pb, Zn and Sb, 100–300 g/t Ag	Limestone, dolomite, shale and siliceous rock
Xikuangshan	Hunan	27°47′/111°29′	Stratabound, vein	Sb	>0.2 Mt (metal): Sb	3.5–4.5 % Sb	Carbonates, shale and sandstone
Woxi	Hunan	28°32′/111°54′	Stratabound	Sb-Au-W	1.67 Mt (metal): Sb 0.25 Mt (metal): WO_3 42 t (metal): Au	2–6 % Sb, 0.2–0.8 % WO_3, 5–10 g/t Au	Siltstone, sandy slate, slate

quartz, carbonate, scapolite, amphibole, chlorite and sericite. The ore-hosting rocks have a zircon U-Pb age of 1,681 ± 13 Ma, whereas a dolerite dyke cutting the Fe-oxide orebodies has an age of 1,659 ± 16 Ma, thereby constraining the maximum and minimum ages of the mineralisation. These features have led Zhao and Zhou (2011) to suggest that the Dahongshan Fe-Cu deposit may represent an iron-oxide-copper gold (IOCG) type. Sulphides from the Dahongshan ores have $\delta^{34}S$ values mostly in the range of +2 to +6 ‰, which Zhao and Zhou (2011) interpreted as a mix of several sources due to large-scale leaching of the rocks containing evaporites. However, this interpretation is at odds with an evaporite source, which should have $\delta^{34}S$ values greater than +6 ‰. If an IOCG mineral system, is considered more likely, it would not require the involvement of evaporite sources.

4.4.1.1 Sedimentary Rock-hosted Massive Sulphide Deposits of the Lower Yangtze River Valley Region

Gu et al. (2007) discussed base metal massive sulphide deposits that formed in a passive continental margin in Late Palaeozoic basins that overlie the Yangtze Craton. The authors also provided a catalogue of 24 of these deposits, listed in Table 4.2 and their distribution in the Yangzte and Cathaysia blocks, presented in Fig. 4.5.

Gu et al. (2007) described these deposits as stratabound and Sullivan-type (Goodfellow and Lydon 2007) and suggest that these were originally formed by "submarine sedimentation" (probably meaning exhalative or SEDEX type) and later modified by hydrothermal fluids associated with Mesozoic granitic intrusions. The authors include for example in this category skarn type deposits, such as Dachang[1], described below. Gu et al. (2007) list the following in support of their claim: (1) the orebodies are dominated by massive sulphides; (2) are stratabound; (3) are associated with mafic and felsic volcanic rocks; (4) contain colloform and framboidal pyrite, locally interlayered with "siliceous" layers (chemical sediments?; banded cherts?) that are associated with tourmaline and adularia-bearing layers (hence the suggestion of a similarity with Sullivan type) mineralisation and with the tourmaline being of exhalative origin; (5) in some deposits the massive sulphides are stratiform. The ore-hosting rocks comprise sandstone, siltstone, shale, limestone and dolostone and the ore horizons occur at the transition from marine clastics to carbonates. The timing of ore formation is diachronous, ranging from Devonian to Mid-Carboniferous. Metal zonations have also been reported for some of these massive sulphide deposits, with a general trend from Fe → Cu → Cu-W → Pb-Zn → Fe carbonates → Fe and Mn oxides, as exemplified by the Dongxiang mine (Table 4.2). The Fe-Mn ores typically have strong enrichement in Pb, Zn, Sb, Au and Ag, a feature that is considered characteristic of sedimentary exhalative deposits. In some deposits, scheelite occurs as impregnations and veinlets and wolframite as disseminations (e.g. Dongxiang, Yongping).

[1] Not to be confused with the Dachang Au deposit in Qinghai Province, Kunlun orogen, western China.

Table 4.2 Geological features of principal massive sulphide deposits in South China. (After Gu et al. 2007)

Name/number in Fig. 4.5	County/ province	Lat N/ Long S	Metals	Tonnage	Grade	Host rock	Alteration minerals	Ore minerals (in order of abundance)
Qixiashan (1)	Nanjing, Jiangsu	32°09′30″ 118°58′00″	Pb-Zn-Mn with skarn overprint	0.42 Mt Pb 0.79 Mt Zn 042 Mt Mn	2.6 % Pb 4.9 % Zn 17.2 % Mn	Lower-Middle Carboniferous dolostone, limestone, shale, siltstone, sandstone	Silica, carbonate	Sphalerite, galena, pyrite, rhodochrosite, colloidal pyrite, tetrahedrite, chalcopyrite
Magushan (East Tongshan) (2)	Xuancheng Anhui	30°59′30″ 118°54′30″	Cu-Pb-Mo-Au	0.1 Mt Cu 0.03 Mt Pb 0.06 Mt Zn 0.01 Mt Mo 2.82 t Au	1.02 % Cu 0.15 % Pb 0.27 % Zn 0.14 % Mo 0.15 t/g Au	Middle Carboniferous dolostone and limestone; granodiorite porphyry	Silica, sericite, carbonate, calc-silicates (skarn)	Pyrite, chalcopyrite, bornite, molybdenite, ludwigite
Xingqiao (3)	Tongling, Anhui	30°54′30″ 117°59′30″	Cu-Au	0.23 Mt Cu 116 t Au	9 % Cu 0.78 g/t Au	Middle Carboniferous dolostone and limestone	Silica, sericite, carbonate, skarn	Pyrite, pyrrhotite, chalcopyrite, bornite, colloidal pyrite, gold
Tongguanshan (4)	Tongling, Anhui	30°55′00″ 117°48′00″	Cu-Au	0.26 Mt Cu Gold: no data	0.60 % Cu Gold: no data	Middle Carboniferous dolostone and limestone	Silica, sericite, carbonate, skarn	Pyrite, pyrrhotite, colloidal, pyrite, chalcopyrite, magnetite, bornite, gold
Dongguashan (5)	Tongling, Anhui	30°55′00″ 117°49′00″	Cu-Au with skarn overprint	0.94 Mt Cu 22 t Au	1.0 % Cu 0.24 g/t Au	Middle Carboniferous dolostone and limestone and limestone with intercalated anhydrite	Silica, sericite, carbonate, skarn	Pyrite, pyrrhotite, chalcopyrite, colloidal pyrite, gold

Table 4.2 (continued)

Name/number in Fig. 4.5	County/ province	Lat N/ Long S	Metals	Tonnage	Grade	Host rock	Alteration minerals	Ore minerals (in order of abundance)
Mashan (6)	Tongling, Anhui	30°54′20″ 117°47′00″	Au-Cu	13 t Au	9.6 g/t Au 0.1–0.3 % Cu	Middle Carboniferous dolostone and limestone	Silica, sericite, carbonate, skarn	Pyrrhotite, pyrite, colloidal, pyrite, arsenopyrite, sphalerite, galena, gold
West Tongshan (7)	Guichi, Anhui	30°26′30″ 117°17′00″	Cu-Au	0.16 Mt Cu 1.7 t Au	1.86 Cu 0.5 g/t Au	Middle Carboniferous dolostone and limestone; Lower Permian limestone	Silica, sericite, carbonate, skarn	Pyrite, chalcopyrite, marcasite, sphalerite, galena
Chengmenshan (8)	Jiujiang, Jiangxi	29°41′30″ 115°47′30″	Cu-Mo-Au	1.80 Mt Cu 43.6 t Au Mo: no data	0.75 % Cu 0.24 g/t Au 0.047 % Mo	Middle Carboniferous dolostone and limestone; Late Jurassic granodiorite porphyry	Silica, carbonate, sericite, potassic, skarn	Pyrite, pyrrhotite, chalcopyrite, sphalerite, chalcocite, pyrite, gold
Wushan (9)	Ruichang, Jiangxi	29°46′10″ 115°32′30″	Cu-Au with skarn overprint	1.45 Mt Cu 67.1 t Au	1.06–1.69 % Cu 0.27–0.72 g/t Au	Middle Carboniferous dolostone and limestone with intercalated dacitic lava; Permian limestone	Silica, sericite, carbonate, kaolinite, skarn	Pyrite, pyrrhotite, chalcopyrite, tetrahedrite, sphalerite, galena, gold
Yinshan (10)	Yanxin, Hubei	29°54′00″ 115°08′40″	Pb-Zn-Ag	Middle size	1.23 % Pb 1.82 % Zn 57.19 g/t Ag	Middle Carboniferous dolostone	Silica, carbonate, pyrite	Pyrite, sphalerite, galena, chalcopyrite

Table 4.2 (continued)

Name/number in Fig. 4.5	County/ province	Lat N/ Long S	Metals	Tonnage	Grade	Host rock	Alteration minerals	Ore minerals (in order of abundance)
Linghou (11)	Jiande, Zhe-jiang	29°29′30″ 119°11′45″	Cu-Zn-Pb-Au	0.05 Mt Cu 0.04 Mt Zn 0.005 Mt Pb Au: no data	1.54 % Cu 2–4 % Zn 1.96 % Pb	Middle Carboniferous dolostone	Silica, sericite, carbonate, skarn	Pyrite, chalcopyrite, bornite, sphalerite, galena, gold
Yongping (12)	Dongxiang, Jiangxi	28°12′00″ 117°45′30″	Cu-W	1.22 Mt Cu 0.16 Mt WO_3	0.77 % Cu 0.13 % WO_3	Lower to Middle Carboniferous sandstone, siltstone, shale, dolostone and limestone	Silica, sericite, carbonate, skarn	Pyrite, chalcopyrite, scheelite, sphalerite, galena
Dongxiang (13)	Dongxiang, Jiangxi	28°17′20″ 116°38′45″	Cu-W	0.31 Mt Cu 0.05 Mt WO_3	1.2 % Cu 0.36 % WO_3	Lower to Middle Caroniferous sandstone, siltstone, shale, dolostone and limestone	Silica, carbonate, pyrite	Pyrite, colloidal pyrite, chalcopyrite, bornite, chalcocite, hematite, ferberite, hübnerite
Lehua (14)	Leping, Jiangxi	28°50′10″ 117°18′00″	Mn-Pb-Zn	19 Mt Mn 0.19 Mt Pb 0.29 Mt Zn	20–28 % Mn 1.3 % Pb 1.9 % Zn	Middle Carboniferous exhalative manganese with underlying Pb-Zn veins cutting the Precambrian	Chlorite, epidote, silica, carbonate	Psilomelane, pyrolusite, rhodochrosite, hematite, limonite, siderite, sphalerite, galena

Table 4.2 (continued)

Name/number in Fig. 4.5	County/ province	Lat N/ Long S	Metals	Tonnage	Grade	Host rock	Alteration minerals	Ore minerals (in order of abundance)
Qibaoshan (15)	Shanggao, Jiangxi	28°10′28″ 114°53′30″	Pb-Zn-Co	0.1 Mt Pb 0.2 Mt Zn 3,669 t Co	1.48 % Pb 3.03 % Zn 0.053 % Co	Middle Carboniferous dolostone	Silica, carbonate	Pyrite, sphalerite, galena, glaucodote, danaite, cobaltite; chalcopyrite, chalcocite
Longfengchang (16)	Datian, Fujian	25°56′ 117°49′	S-Pb-Zn-Cu	2.67 Mt ore S 0.012 Mt Pb 0.04 Mt Zn 1,914 t Cu	21.9 % S 1.9 % Pb 2.8 % Zn 0.8 % Cu	Carboniferous sandstone, siltstone, limestone and dolostone with intercalations of tuffaceous rocks	Silica, chlorite, skarn	Pyrite, pyrrhotite, chalcopyrite, sphalerite, galena
Yushui (17)	Meixian, Guang-dong	24°25′00″ 116°10′45″	Cu-Pb-Ag	0.1 Mt Cu 0.18 Mt Pb 333 t Ag	3.25 % Cu 4.25 % Pb 77.4 g/t Ag	Lower and Middle Carboniferous sandstone, siltstone, shale, dolostone, limestone, siliceous rock	Silica, sericite, carbonate	Pyrite, chalcopyrite, galena, sphalerite, bornite
Fankou (18)	Renhua, Guang-dong	25°07′00″ 113°37′00″	Pb-Zn	1.7 Mt Pb 3.4 Mt Zn	5.1 % Pb 12.0 % Zn	Middle Devonian to Lower Carboniferous carbonates, siltstone and shale	Silica, carbonate, pyritic	Pyrite, sphalerite, galena, stibnite

Table 4.2 (continued)

Name/number in Fig. 4.5	County/ province	Lat N/ Long S	Metals	Tonnage	Grade	Host rock	Alteration minerals	Ore minerals (in order of abundance)
Dabaoshan (19)	Quejiang, Guang-dong	24°33′15″ 113°43′20″	Cu-Pb-Zn-WO_3	0.86 Mt Cu 0.31 Mt Pb 0.85 Mt Zn 0.11 Mt WO_3	0.86 % Cu 177 % Pb 4.44 % Zn 0.12 % WO_3	Middle Devonian limestone, shale, dacite and tuffaceous rock	Silica, sericite	Pyrite, pyrrhotite, chalcopyrite, sphalerite, galena, scheelite
Yangliutang (20)	Lechang, Guang-long	25°07′30″ 113°23′00″	Pb-Zn	Middle size	No data	Lower Carboniferous limestone	Silica, carbonate, sericite	Pyrite, sphalerite, galena
Xiniu (21)	Yingde, Guang-dong	24°08′00″ 114°01′40″	S-Tl	26 Mt ore	20.5 % S 0.004 % Tl	Middle Devonian dolostone, limestone, shale, siltstone, sandstone	Carbonate, chlorite, sericite	Pyrite with minor sphalerite, galena, and chalcopyrite
Hongyan (22)	Yingde, Guang-dong	24°16′00″ 109°31′10″	S-Tl-Ag	0.01 Mt ore	26.1 % S 2–61 g/t Tl 2.4–27.5 g/t Ag	Middle Devonian dolostone and limestone	Silica, sericite	Pyrite with minor sphalerite and galena
Shiding (23)	Yongxian Guangxi	25°03′10″ 109°31′10″	Pb-Zn	0.34 Mt Pb 0.02 Mt Zn	0.3–10 % Pb 0.5–10 % Zn	Middle and Upper Devonian limestone and dolostone	Silica, carbonate	Pyrite, sphalerite, galena
Dachang (24)	Nandan, Guangxi	24°50′20″ 107°34′25″	Zn, Pb-Zn-Sb	1 Mt Sn; no data for other metals	0.71 % Sn; no data for other metals	Upper Devonian limestone, dolomite, shale and siliceous rock	Silica, carbonate, skarn, greisen (quartz-mica)	Pyrite, pyrrhotite, cassiterite, sphalerite, galena, jamesonite, chalcopyrite, arsenopyrite

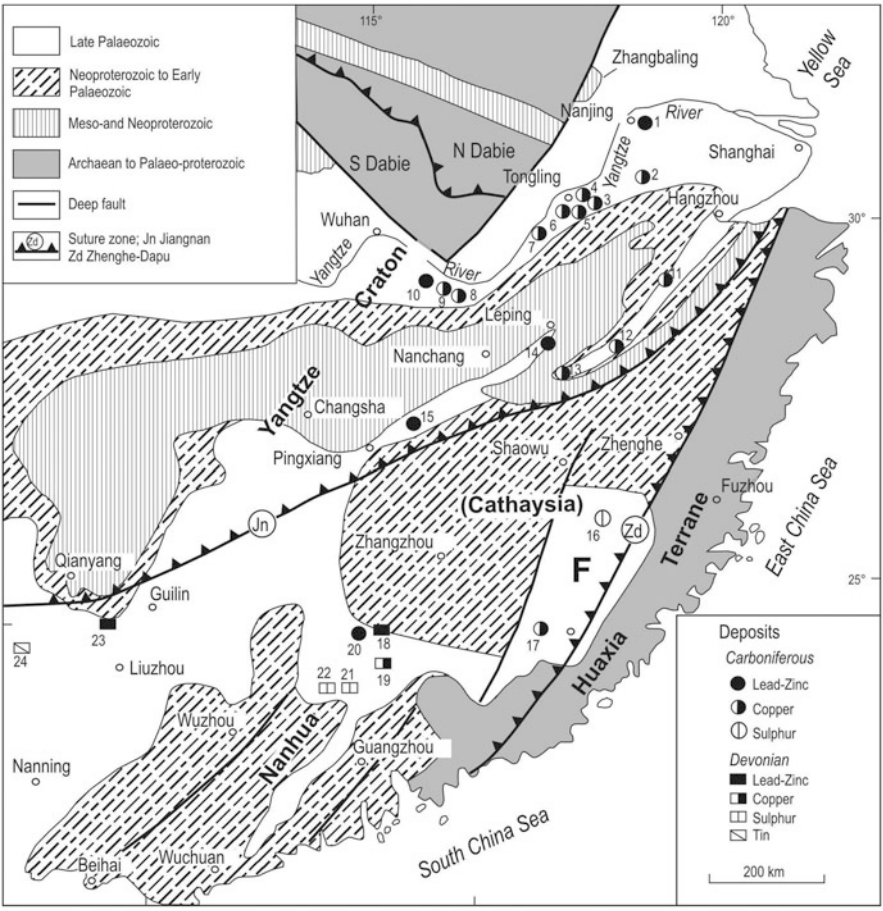

Fig. 4.5 Distribution of the main stratabound massive sulphide deposits in South China (after Gu et al. 2007); deposit numbers correspond to the list presented in Table 4.4 (note that deposits 1–10 occur in the Lower Yangtze River Valley, discussed in Sect. 4.4.4)

A cross-section of the Yongping massive sulphide deposit is shown in Fig. 4.6. The Yongping massive sulphide ore lenses are hosted in Carboniferous sandstone and shale and Late Carboniferous limestone, typically underlain by stringer sulphides, quartz and carbonate veins (feeder zone). Hydrothermal alteration is dominated by chlorite, silica and carbonate minerals. The Fe and Mn oxides are stratiform and considered as the last and/or distal mineralising phase. In the Dabaoshan deposit, pyritised fossils (brachiopoda) have been recognised. The massive sulphide Cu deposit consist of stratiform lenses hosted in sandstone, shale and limestone, underlain by quartz-carbonate-sulphide veins that are interpreted as a stringer feder zone. At Dongxiang, a breccia pipe hosted in clastic sedimentary rocks is present. Gu et al. (2007) contended that these South China massive sulphides are somewhat different

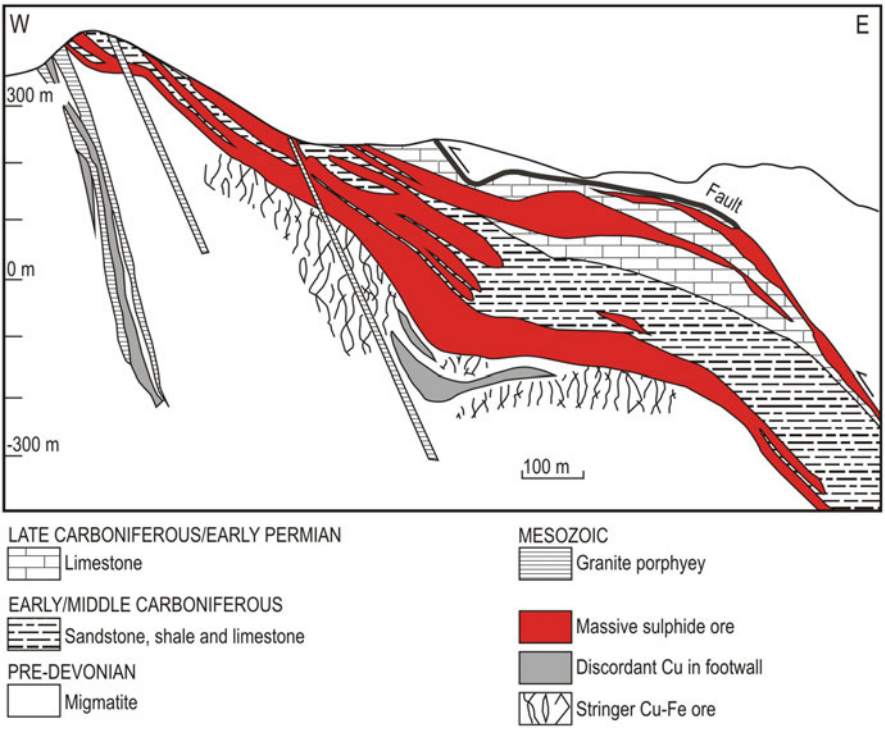

Fig. 4.6 Cross-section of the Yongping massive sulphide ore lenses and stringer ore (feeder pipe). (After Gu et al. 2007)

from typical sediment-hosted mineral systems in that they are commonly spatially associated with mafic and felsic volcanic rocks, as is the case for the Dongxiang deposit. According to Gu et al. (2007), the intrusion of the Mesozoic (Yanshanian) granites in the region, resulted in wholesale modification and recrystallisation of the sulphides, changing for example colloform textures to porphyroblastic textures, converting sedimentary pyrite to pyrrhotite and magnetite, and where carbonate beds are present, resulting in the formation of skarns. The authors also suggested that in some cases the magmas may have supplied additional or further metals to the mineral systems.

Sulphur isotopic values for barite range from +10 to +27 ‰ $\delta^{34}S_{CDT}$ and from −0.2 to +35 ‰ for sulphides, indicative of a predominant involvement of sea water. Homogenisation temperatures of fluid inclusions in barite, range from 105 to 276 °C, contrasting with those from depositsb in the Lower Yangtze River Valley, which show higher homogenisation temperatures and salinities (see below).

The tectonic settings, proposed by Gu et al. (2007), of the South China stratabound massive sulphides are presented in Fig. 4.7, in which the two principal ore-hosting sedimemtary basins are shown, underlain by different basements. The difference in the nature of the basement rocks, has a bearing on the composition and nature of

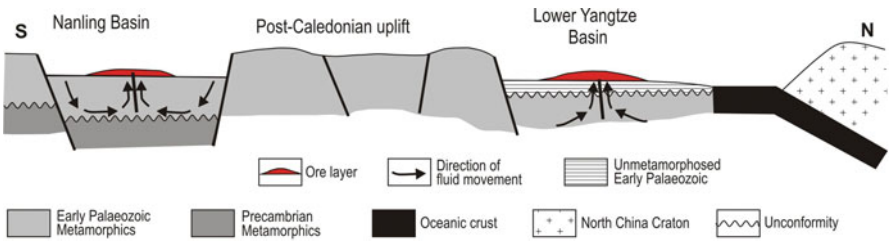

Fig. 4.7 Tectonic settings of stratabound massive sulphide ore systems in South China. (After Gu et al. 2007)

the massive sulphide ores. Thus, the predominantly mafic basement of the Yangtze Valley would produce Cu-, Au- and Co-rich ores, whereas ores that are dominantly enriched in Pb, Zn, U, Ag, Bi, Sb, Hg, Ba, F and B would come from felsic-dominated basement rocks below the Nanling Basin.

The paper by Gu et al. (2007) on the "sedimentary" massive sulphides of the South China Block, highlights the uncertainties that are inherent to a region that was subjected to a number of tectono-thermal events in its geological history. Indeed, this is an interesting case that suggests that mineral systems may be subjected to multiphase ore-making processes that result in highly complex ores. The Yangtze Craton and parts of the South China Fold Belt (Chap. 5), have in fact been subjected to protracted geodynamic evolutionary processes, culminated with the great Yanshanian tectono-thermal event, which added the last, and perhaps economically important, touch to the mineral systems of these regions.

Dachang Polymetallic Ore Field

The Dachang Sn (cassiterite-stannite)-sulphides ore field, Guanxi Province, is one of the largest in the world and located in the Yangtze platform near the boundary with the Cathaysia Block (Cai et al. 2007). The region where the Dachang ore field is located, includes a series of ore clusters in the Nandan-Hechi fold-and-thrust belt, which include Mayang (Hg), Mangchang (polymetallic Sn), Dachang (polymetallic Sn), Beixiang (polymetallic Sn) and Wuxu (polymetallic Pb-Zn) (Fig. 4.8a). These deposits are hosted in Devonian to Triassic platform sedimentary successions that were intruded by Yanshanian (Late Mesozoic) granites. Several lines of evidence show that the Dachang ore field is spatially and genetically associated with a granitic pluton, with the ore zones lying in the thermally metamorphosed sedimentary rocks above the roof of the pluton (Lattanzi et al. 1989). English-language accounts of the Dachang ore field can be found in Lattanzi et al. (1989), Fu et al. (1991, 1993) and Li et al. (1992); recent works are by Gu et al. (2007) and Cai et al. (2007).

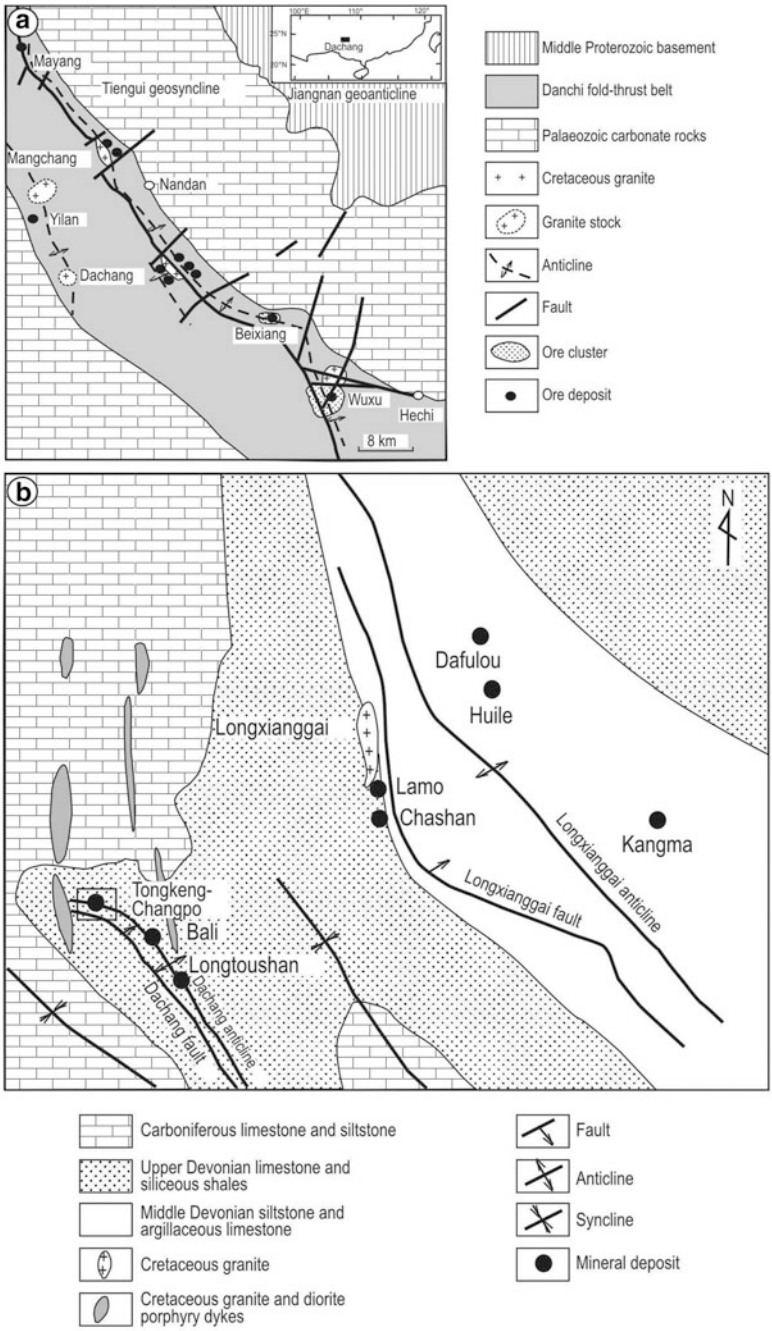

Fig. 4.8 **a** Distribution of ore fields in the Youjiang fold belt on the northern margin of the Yangtze platform; **b** Dachang ore field. (After Cai et al. 2007)

The Dachang ore field (Fig. 4.8b) is endowed with more than 1 Mt Sn metal, averaging 0.71–1 % Sn, with 3–5 % of other metals, such as Zn, In, Sb, Cu and Ag. An exhalative syn-sedimentary origin was proposed, mainly on the basis of the following (Gu et al. 2007 and references therein): (1) stratiform massive orebodies; (2) presence of exhalites, such as tourmalinite and cherts intercalated with sulphides layers; (3) conversion of syngenetic pyrite to pyrrhotite by heat and fluids related to granitic intrusions; (4) presence of hexagonal pyrrhotite in the stratiform orebodies, thought to be induced by contact metamorphism by Yanshanian granites; (5) cassiterite in the stratiform ores and association with tourmalinite are strikingly similar to the Sullivan deposit (British Columbia, Canada: see Goodfellow and Lydon 2007); (6) REE patterns show negative Ce anomalies, indicative of interaction with sea water; (7) stockworks and veins above the orebodies, thought to be related to remobilisation due to deformation. On the other hand, Li et al. (1992) suggested that ore fluids were largely generated by Yanshanian granite porphyry intrusions, which formed the cassiterite-sulphide ores, partly remobilised from pre-existing stratiform sulphides. Figure 4.9 shows a cross-section through the Tongkeng-Changpo Sn deposit, described below. The Longxianggai granite is situated in the central part of the Dachang tin field, near the axis of the Longxianggai anticline, covering an area of ca. 0.5 km^2 (Fig. 4.8b). It consists predominantly of biotite granite with subordinate porphyritic granite, and probably belongs to the S-type granite category as defined by Chappell and White (1974), resulted from partial melting of continental crust. The Lamo skarn Cu-Zn ore deposit, northeast from Tongkeng-Changpo, is at the contact zone between Upper Devonian limestone and the granite. The Tongkeng-Changpo, Bali, Longtoushan, Dafulou, Huile and Kangma polymetallic tin deposits are sited along the eastern and western margins of the granite stock. At the east and west sides of the Tongkeng-Changpo deposit, there occur N-S-trending granite porphyry dyke (Eastern Dyke) and a diorite porphyry dyke (Western Dyke) at the same trend. The SHRIMP U-Pb method was used to determine the ages of the Longxianggai granite stock, granite and diorite dykes (Cai et al. 2006a). The biotite granite was dated at 93 ± 1 Ma, the porphyritic granite, the granite porphyry dyke, and the diorite porphyry dyke all yielded ages of about 91 Ma.

The Tongkeng-Changpo Sn deposit lies about 4 km southwest from the Longxianggai Granite pluton and is one of the economically important in the ore field. As mentioned above and shown in Fig. 4.9, the Tongkeng-Changpo mineralisation essentially consists of a series of lenses and stockwork veins. As mentioned above, these different ore styles have been explained with genetic models, ranging from exhalative to granite-related skarns or combinations thereof. The Tongkeng-Changpo deposit is spatially associated with the Dachang anticline, Dachang fault and a series of detachment fault developed along lithological contacts (Fig. 4.8). The Dachang Fault is in the southwest limb of Dachang anticline, and is parallel with the axis of the anticline (Fig. 4.8b). The detachment fault and subsidiary faults are the main sites for the mineralisation.

The orebodies of the Tongkeng-Changpo deposit can be classified into three major types: veins, stockworks, and stratiform (Fig. 4.9). Vein-style ores include: (1) single, cross-cutting veins and (2) bedding-parallel veins. The cross-cutting veins are at the

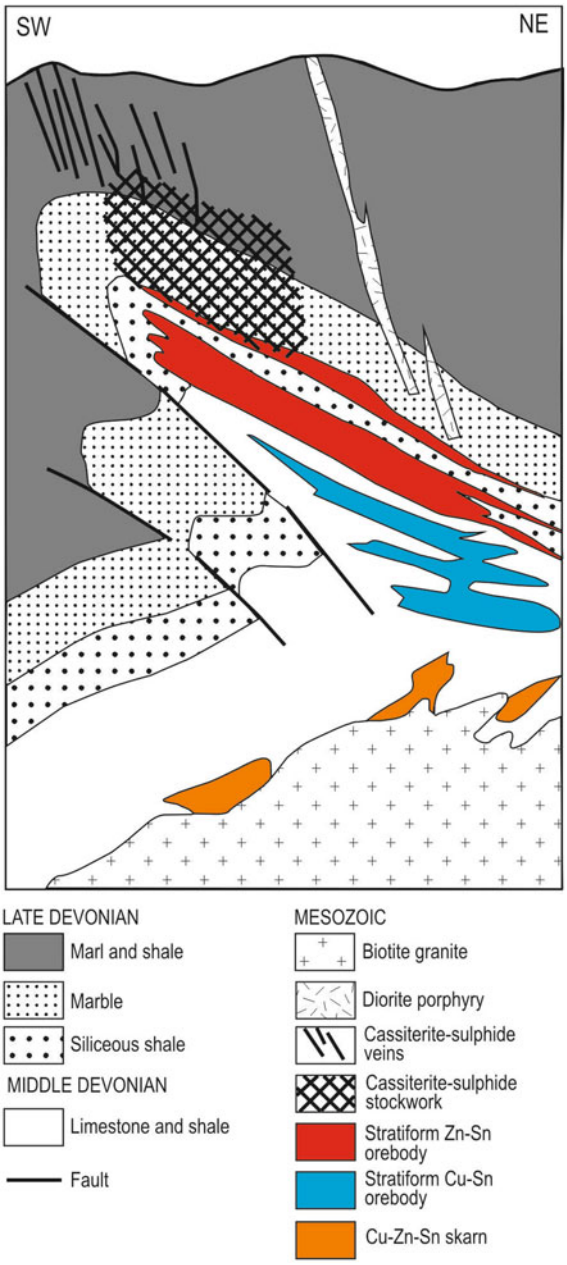

Fig. 4.9 Cross-section through Tongkeng-Changpo Sn deposit. (After Gu et al. 2007)

top of the deposit, and are mainly located near the axis of the Dachang anticline. They are commonly 0.2–1.5 m thick, 50–200 m long and extend to depths of 100–300 m. More than 200 veins have been discovered in the Tongkeng-Changpo deposit. Bedding-parallel veins occur along the detachment fault, they are commonly 0.2–3.5 m thick, 50–300 m long, and extend to depths of 100–250 m. The vein ores contain an average of 7.4 % Zn and 2.1 % Sn. Stockworks occur in the flat northeast limb of the Dachang anticline, and hosted by thick bedded limestones. The orebodies have Sn and Zn grades of 1.1 and 2.7 %, respectively and consist of numerous fine veins, about 0.5–1 cm. Stratiform ores are mainly in the northeast limb of Dachang anticline, and developed along detachment fault. The No. 91 orebody, is hosted by the Devonian laminated siliceous limestone of the Wuzhishan Group, is 1,030 m long, with an average thickness of 16 m. The orebody consists of small crosscutting, bedding-plane veins and disseminations, characterized by high content of sulphide (30 % by volume), and high grades of Sn (1.3 %) and Zn (4 %). The No. 92 orebody, hosted by the Devonian siliceous shale and argillite with calcareous nodules of the Liujiang Group, is 1,130 m long, with an average thickness of 26 m. The orebody consists of stockworks as well as disseminations and is characterized by lower grades of Sn (0.8 %) and Zn (2.1 %). The vein, stockwork, and stratiform orebodies have the same mineral assemblage and paragenetic sequence, which can be divided into three stages (Fig. 4.10), although there is much variation with sulphides abundance and grain size. Stage I consists of pyrrhotite, pyrite, sphalerite, with rare cassiterite, stannite, tourmaline, quartz, and arsenopyrite, and characterized by euhedral quartz and cassiterite crystals. Stage II consists of sphalerite, various sulphosalts, pyrite, pyrrhotite, quartz, and rare cassiterite, marcasite, and calcite. Cassiterite is anhedral and light yellowish in colour. Stage III represents the last mineralisation event in the Tongkeng-Changpo deposit, consisting of calcite and rare quartz, cassiterite, pyrite, marcasite and minor sulphosalts. Stage I and II are the most important mineralisation stages in the deposit.

Fluid inclusions studies of both vein and stratiform ores revealed that primary and pseudosecondary fluid inclusions in quartz can be classified as CO_2-type and NaCl-H_2O type (Cai et al. 2007). The former is further subdivided into A-1 subtype (three-phase consisting of V_{CO2}, LCO_2 and L_{H2O}) and less common A-2 subtype consisting of L_{CO2} and L_{H2O}. The NaCl-H_2O fluid inclusions are subdivided into one (B-1-type), two- (B-2-type), or multiphase (B-3-type) inclusions. The B-1 single phase fluid inclusions of L_{H2O} mainly occur in quartz formed during paragentic stage III (Fig. 4.10). The two-phase B-2 fluid inclusions are the most common and usually coexist with the CO_2-type inclusions. They are either liquid-rich (L_{H2O}) or vapor-rich (V_{H2O}), and contain vapor bubbles up to 10–80 % by volume. B-3 type multiphase daughter (probably halite) mineral-bearing inclusions are high-salinity aqueous inclusion fluids. These are rare, and have a random distribution. Microthermometric measurements of the CO_2-type fluid inclusions from both vein and stratiform orebodies homogenised to H_2O-rich liquid at a temperature of 210–370 °C, with a frequency peak ranging from 275 to 365 °C, and homogenized to CO_2-rich vapor at temperatures ranging from 280 to 365 °C. Both H_2O-rich and CO_2-rich group of inclusions have a similar range of homogenisation temperatures, indicating

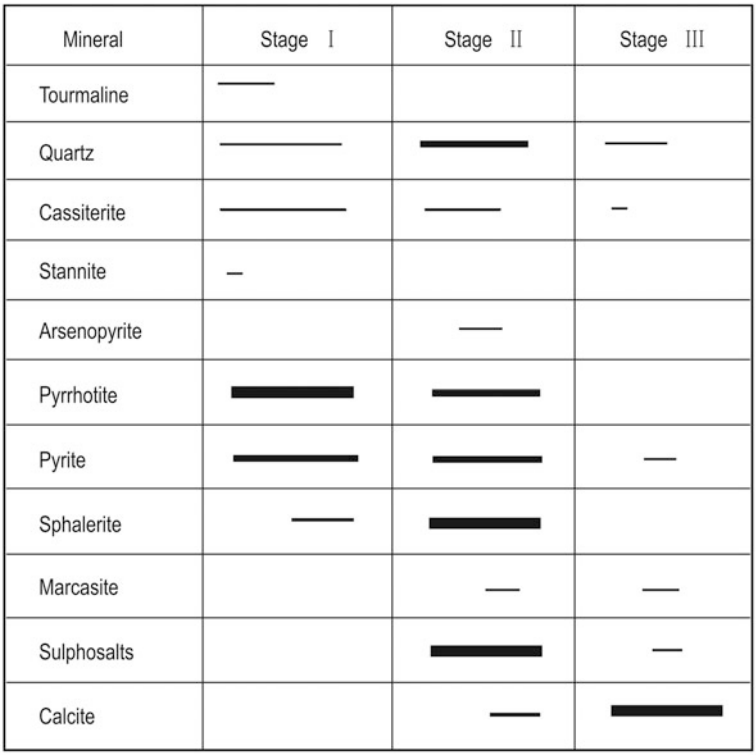

Fig. 4.10 Paragenetic sequence of the main ore and gangue minerals in the Tongkeng-Changpo deposit. (After Cai et al. 2007)

that these fluid inclusions were trapped under similar temperature conditions during ore formation.

Thirty two-phase NaCl-H_2O-type fluid inclusions and five daughter-bearing multiphase NaCl-H_2O-type fluid inclusions were studied in detail. The temperature of fluid inclusions that homogenized to liquid is in a range of 130–360 °C, while for those that homogenized to vapor in a range of 225–320 °C. The salinity of two-phase NaCl-H_2O inclusions ranges from 2.90 to 11.34 wt % NaCl equivalent, with the majority between 3 and 10 wt % NaCl equivalent, which corresponds well to the salinity of CO_2-type inclusions. The salinity of daughter-bearing multiphase inclusions ranges from 29.66 to 35.99 wt % NaCl equivalent. The measured homogenisation temperatures can be divided into three groups of high, medium and low temperature values, ranging from 270 to 365, 210–240, 140–190 °C, respectively, which correspond to above mentioned three ore-forming stages (I, II, III). There are two types of fluid inclusions at the high and middle temperature stages (CO_2– and NaCl-H_2O), whereas the fluid inclusions at low temperature stage are only of the NaCl-H_2O-type.

Cai et al. (2007) also measured He isotope compositions of the inclusion fluids in pyrite, pointing out that the pyrite analysed were euhedral with no evidence of subsequent deformation and show a paragenesis with sphalerite, sulphosalts cassiterite, pyrrhotite, arsenopyrite, and quartz. As compared with air (1.4×10^{-6}, Ra), $^{3}He/^{4}He$ values for pyrite of the Tongkeng-Changpo deposit are within the range of 1.2–2.9, 1.2–1.6 and 1.6–2.5 Ra for veins, stockworks, and stratiform orebodies, respectively. There is not significant difference in the content of typical radiogenic ^{4}He and $^{3}He/^{4}He$ between them which, according to these authors, is indicative that the different types of orebodies have the same fluids source.

Experimental data from inclusion fluids have shown that the composition of mantle derived fluids is mainly constrained by fo_2. When fo_2 approaches the QFM (quartz-fayalite-magnetite) buffer conditions, the composition of upper mantle fluids may be dominated by CO_2 and H_2O (Rui et al. 2003). According to Fu et al. (1993), the mineralisation of the Tongkeng-Changpo ore deposit took place within a field in which fo_2 is near QFM buffer. Furthermore, the inclusions of the early stage at Tongkeng-Changpo are dominated by CO_2 and H_2O, suggesting a composition similar or close to that of upper mantle fluids. At Tongkeng-Changpo, the molar fraction of CO_2 (x_{CO2}) ranges from 9 to 51 % which, Cai et al. (2007) pointed out, is different from the same type of inclusions at another skarn-type Zn-Cu deposit in the Dachang ore field (Fig. 4.8b; Lamo), where x_{CO2} of ore-forming fluids, is demonstrated to have derived from the S-type granite stock, is generally lower than 10 %. The study by Fu et al. (1993) also indicated that the ore-forming fluids related to skarn-type Zn-Cu mineralisation are characterized by minor CO_2; whereas, the fluids in the Tongkeng-Changpo ore deposit are dominated by CO_2. The above data suggest that the CO_2-rich fluids may generate from the mantle, or from a mixture of mantle fluids and magmatic fluids.

As was suggested by Giggenbach (1986), isotopes of noble gases may be valuable discriminators between fluids of mantle versus crustal versus meteoric origins. Therefore, He isotope composition is a useful tool for tracing the source of fluids. In geological materials it has three end-member compositions (Simmons et al. 1987; Stuart et al. 1995; Burnard et al. 1999): (1) saturated meteoric water, the ratio of $^{3}He/^{4}He$ is about 1.4×10^{-6} (Ra); (2) mantle fluids, characterized by high content of ^{3}He with ratio of $^{3}He/^{4}He$ usually in a range of 6–9 Ra; and (3) radioactive He from the crust, with ratios of $^{3}He/^{4}He \leq 0.1$ Ra, a peak of 0.01 and 0.05 Ra. The ratios of $^{3}He/^{4}He$ in the case of Tongkeng-Changpo are lower than mantle values, but much higher than continental crust, indicating that He in the ore-forming fluids is not only from the crust, but also from the mantle. According to Mao et al. (2002b), the proportion of mantle-source He in ore-forming fluids ranges from 19.9 to 48.2 %.

The characteristics of inclusion fluids and He isotope systematics of vein-type and stratiform orebodies are similar, and indicate the vein-type and stratiform orebodies of Tongkeng-Changpo deposit share the same source and processes of ore genesis. Wang et al. (2004a) reported $^{40}Ar/^{39}Ar$ isotopic geochronological data on quartz from the stratiform ores, giving a plateau age of 94.52 ± 0.33 Ma. The Rb-Sr isochron dating of fluid inclusions of quartz of No. 92 orebody is 93.4 ± 1.3 Ma (Cai et al. 2006b). These ages are in accordance with the SHRIMP U-Pb age data of the biotite

granite of Longxianggai, mentioned above (Cai et al. 2006a), showing that there is a close temporal relationship between the mineralisation and the granite. The $^{3}He/^{4}He$ ratios range of between 1.2 and 2.9 Ra, i, e, notably higher than crustal fluids, together with CO_2-rich fluids, point to mantle fluids being involved in the process of ore formation in the Tongkeng-Changpo polymetallic tin deposit. The northwestern-striking Dachang fault may reach into the lower crust or upper mantle and this would provide a favorable geological environment for the mantle fluids to take part in mineralisation.

4.4.2 MVT Deposits

In South China a number of mineral deposits that can be considered as Mississippi Valley Type (MVT) are present. These include the Qilinchang deposit, hosted in dolomitic rocks of Early Carboniferous age and containing about 3.32 Mt of ore, grading 17.5 % Zn and 6.6 % Pb. Typical ore minerals are sphalerite, galena and pyrite in a gangue of quartz and carbonate. In Sichuan Province, MVT deposits include Daliangzi with 24 Mt of ore, grading 10.4 % Zn, 0.8 % Pb and 43 g/t Ag, Tianbaoshan with 11 Mt of ore grading 10.1 % Zn, 1.5 % Pb, 93.6 g/t Ag and Dayinchang with 5.6 Mt of ore at a combined Zn + Pb grade of 3 %. Zaw et al. (2007) compared the South China MVT deposits with those of the Lennard Shelf in northwestern Australia (Pirajno 2009). In Sichuan, the MVT ores are hosted in the Dengying Formation, consisting of algal dolomitic rocks that sit unconformably on a Proterozoic basement of phyllite and schist and overlain by Cambrian black shales and sandstone, in turn overlain by Permian limestone and basalt. Zaw et al. (2007) pointed out that the Cambrian rocks and the Dengying Formation are important for localising epigenetic mineralisation, which occurs in fault-related breccias and in joint, karst and solution collapse structures. Ore minerals are sphalerite, galena, pyrite, barite, with minor chalcopyrite and fluorite.

4.4.2.1 Huize District MVT Deposits

A large Zn-Pb(Ag) metallogenic province (Huize district) straddles the border regions between Sichuan, Guizhou and Yunnan provinces, on the southern margin of the Yangtze Craton. Here are high grade Zn-Pb deposits, whose features fit the carbonate-hosted MVT ore system. Han et al. (2007) reported on the Huize mineralisation and the following is summarised from these authors.

The Huize district contains a number of deposits, Qilinchang, Dashuijing, Kuangshanchang and Yinchangpo, spatially associated with northeast-trending faults and containing a total of about 5 Mt of Pb + Zn reserves. Other faults in the region trend northwest, north-south and east-west, all having undergone at least five episodes of movement. The lithostratigraphy of the Huize district is characterised (bottom to top)

by black shale, sandy mudstone and evaporate beds (Cambrian, Qiongzhushi Formation), overlain by siltstone black shale, dolomite and limestone beds hosting some of the Pb-Zn ores (Devonian, Haikou and Zalpe Formations), followed by coarse crystalline dolomite, which is the main ore host, oolitic and pisolitic limestone beds, brecciated limestone (Carboniferous, Baizuo, Weining and Maping Formations), carbonaceous sandstone, intercalated with coal seams, shale, limestone, dolomite (Permian, LiangshanQixia-Maokou Formations). The Maokou Formation is capped by Permian amygdaloidal basalts of the Emeishan Large Igneous Province (Chap. 7), some of which are mineralised with native copper. Emeishan mafic rocks (sills and dykes) in the region exhibit hydrothermal alteration (silica, epidote) along their contacts and may contain base metal mineralisation. The Carboniferous is the key geological time, resulting in the formation of the marine Baizuo Formation in a restricted basin, characterised by carbonate deposition of lagoonal and tidal facies. Han et al. (2007) considered that the late Permian was the main period of ore formation in the district, associated with extensional tectonics and the outpouring of basaltic lavas. The main ore-controlling structures are the Qilinchang, Kuangshanchang and Yinchangpo faults, typically exhibiting intense hydrothermal alteration (dolomite, silica, pyrite, chlorite, epidote and calcite). The fault breccias contain anomalous abundances of Pb (67–6,725 ppm), Zn (141–1,845 ppm), Fe (up to 18.8 %), Ge (0.3–35 ppm), As (10.6–269 ppm), Ag (6–22.4 ppm) and Tl (0.1–1.5 ppm) (Hans et al. 2007).

At least 50 orebodies have been identified in the Qilinchang, Dashuijing, Kuangshanchang and Yinchangpo deposits, with 42 making up the Kuangshanchang deposit. The orebodies are stratabound and have lenticular shapes. The ore minerals include sphalerite, galena, pyrite and locally chalcopyrite. Barite, hematite, gypsum, tertrahedrite, freibergite, native silver and boulangerite may also be present in varying quantities. The Qilingchang ore zone is 800 m long and is up to 40 m thick, with a depth extension of 1,200 m and has metal reserves of 2 Mt with combined Zn + Pb grades of 36.5 %, 34.6 % and 25.8 %. Kuangshanchang contains 1.8 Mt metal reserves, grading 30.6 % combined Zn + Pb. Silver contents in these orebodies range from 61 ppm to 310 ppm; this metal is contained in galena and in sphalerite. In addition to silver, trace amounts of Cd, Ge, In, Ga and Tl are also recorded. Ore styles are massive and disseminated, locally oxidised in the upper levels. Han et al. (2007) suggested that the mineralising processes can be divided into a diagenetic stage (calcite, dolomite, pyrite), a hydrothermal main ore-forming stage (sphalerite, galena, chalcopyrite) and an epigenetic stage with deposition of gypsum, limonite and hopeite (a Zn phosphate). Wall rock alteration is comparatively simple and is dominated by extensive dolomitisation, with lesser silica, pyrite and clay minerals. Dolomite is coarse-grained, white, grey, cream-yellow or pink in colour and occurs as massive zones associated with the orebodies. Dolomitisation increases with depth and with the thickness of the orebodies. The orebodies also exhibit a mineral zonation from footwall to hanging wall, as follows: coarse pyrite + marmatite → sphalerite + galena + pyrite → fine, crystalline pyrite and carbonate minerals.

Sulphur isotope systematics conducted on sulphides and barite, with values ranging from 15 to 20 ‰, show similarities with Carboniferous seawater sulphate. Carbon

and oxygen isotopic composition of gangue calcite ($\delta^{13}C_{pdb}$ from 1.2 to 3.3 ‰; $\delta^{18}O_{smow}$ from 11.31 to 20.89 ‰) is quite different from the ore-hosting dolomite ($\delta^{13}C_{pdb}$ from 3.35 to 0.85 ‰; $\delta^{18}O_{smow}$ from 11.31 to 16.95 ‰). This difference is interpreted as due to a deep source region for the gangue calcite. Fluid inclusion studies revealed low to moderate homogenisation temperatures, ranging from 165 to 220 °C and salinities of 6–12 % NaCl equivalent. Gas components of the inclusions are H_2O, CO_2, CO, CH_4 and H_2; high concentrations of Na+, Ca2+, F− Cl−, were detected. Han et al. (2007) interpreted that the ore-forming fluids were metal-bearing Na-Cl-Ca brines, possibly derived from overlying evaporitic beds.

Sinistral strike-slip movements along the Xiaojiang and Zhaotong-Qujing fault zones, caused compression and the formation of the northeast-trending folds, followed by tensional structures. These tectonic movements, may have been the main cause of fluid circulation, which locally mixed with evaporites in both basement and the overlying beds, and becoming metal-brines carrying S, Zn, Pb and other metals. The above mentioned tectonic zones were also spatially associated with the Emeishan magmatism in the region, which may have provided a heat source for re-circulation of hydrothermal fluids and the local re-distribution of ores.

4.4.3 Carlin-style Au Deposits

Since its discovery in the 1960s the Carlin deposit in Nevada (western USA) has lent its name to a type of fine-grained disseminated Au-Ag hydrothermal mineralisation hosted in carbonate rocks. The discovery of similar deposits in the region and elsewhere, made it clear that Carlin is most probably the end member of a group of deposits that exhibit considerable variations in their geological, mineralogical, element association and geochemical features. Hence, the commonly used terms of Carlin-type and Carlin-style. China is well endowed with a large number of carbonate-hosted Au deposits that have been variably referred to as Carlin-type or Carlin-style. Most occur in the Qinling Orogen and in the southwest of the Yangtze Craton (Dian-Qian-Gui area) and the middle-lower Yangtze River Valley, where platform facies carbonate rocks are common (see also Figs. 5.20 and 5.21). In this section, I briefly describe the Carlin-type ore systems of the Dian-Qian-Gui district; Table 4.3 shows a comparison of the main characteristic of Carlin-type ore deposits in the USA and China.

In Guizhou (Dian-Gui-Qian area), on the southwest margin of the Yangtze Craton, there are a number of Carlin-type deposits (Table 4.3) that are spatially associated with coal-bearing strata, barite and with a Sb-As-Tl-Hg element association (Peters et al. 2007). The Guizhou deposits are hosted in stratabound breccias, unconformity surfaces and brittle-ductile fault zones. The ores are hosted in impure carbonate and carbonaceous rocks with disseminations of pyrite, marcasites, arsenopyrite and μm-size Au particles. Realgar, orpiment, stibnite, cinnabar, Tl-bearing sulphide minerals, Hg-bearing minerals, some Ni sulphides and PGE minerals are present

Table 4.3 Comparison of Carlin-type deposits in USA and Carlin-like and -type deposits in China. (After Zhang and Zhang 2003)

	Carlin type in Nevada, USA	Carlin- and Carlin-like type in south Qinling	Carlin-type in Yunnan-Guizhou-Guangxi gold triangle area
Tectonic back-ground and basin type	North American Cordillera orogenic belt, basin and range, intracontinental rift basin	Qinling orogenic belt, South Qinling epicontinental area of Tangtze passive foreland basin, fault basin and rift basin	Youjiang rift between southwestern edge of the Yangtze continent and the South China fold belt, intracontinental rift basin
Age of host rocks	Silurian-Devonian	Cambrian, Devonian-Triassic	Permian-Triassic
Metallogenic age	Cenozoic	Indosinian-Yanshanian	Yanshanian
Ore minerals	Native gold, As-bearing pyrite, pyrrhotite, pyrite, marcasite, arsenopyrite, stibnite, cinnabar, realgar, orpiment, arsenic, lorandite, Carlin ore	Native gold, As-bearing pyrite, arsenopyrite, pyrite, tennantite, stibnite, chalcopyrite, gersdorffite, tellurobismuthite, galena, sphalerite	Native gold, As-bearing pyrite, arsenopyrite, pyrite, marcasite, pyrrhotite, stibnite, realgar, orpiment, cinnabar
Vein mineral assemblage	Quartz, ankerite, calcite, barite, fluorite, gypsum, dickite	Quartz, ankerite, calcite, barite, albite, sericite, dickite	Quartz, ankerite, calcite, hydromuscovite, kaolinite
Gold occurrence (primary ore)	Gold occurring in As-bearing minerals, carbonaceous and clay minerals as submicroscopic gold. Microscopic gold occurs as inclusion gold, fracture gold, intergranular gold	Gold occurring in As-bearing minerals as submicroscopic gold; microscopic and visible gold occurring as inclusion gold, fracture gold, and intergranular gold	Gold occurring in As-bearing minerals as submicroscopic gold; some microscopic gold as inclusion gold, micro-fracture gold, and intergranular gold
Metals	Au-As-Sb-Hg-Tl-Ba, Au-As-Cu-Co-Ni-Ba	Au-As-Sb-Hg-Ba, Au-As-Cu-Co-Ni-Ba, Au-Ag-Pb-Zn-Cu-As-Sb-Bi-Te	Au-As-Sb-Hg-Tl
Deposit series	Au-Hg-Sb deposit	Au-Hg-Sb deposit, Au-Pb-Zn deposit	Au-Hg-Sb deposit
Examples	Carlin, Ketezi, Keteqie'er	Jinlongshan, Ertaizi, Bauamiao, Liba, Dashui	Lannigou, Yata, Getang, Zimudang, Banqi

and are of late paragenesis. Base metal sulphides (galena, sphalerite, chalcopyrite) and Pb-As-Sb-sulphosalts are also present.

Hydrothermal alteration is local and represented by silicification and sericite-clay minerals (Peters et al. 2007). An important aspects, pointed out by Peters et al. (2007), is that the Guizhou Carlin-type ore systems are not spatially associated with

igneous rocks and therefore unlikely to be related to magmatic fluids. Fluid inclusion studies indicate temperatures ranging from 200 to 160 °C in late stage Hg-Sb ores, whereas interpretation of stable isotopic data suggest that the hydrothermal fluids responsible for the Guizhou deposits may have originated from the deep crust or from distal magmas (Peters et al. 2007 and references therein). The age of the Guizhou Carlin-type deposits remains largely unresolved. The host rocks are Early Palaeozoic and ore-hosting faults and structures were formed during the Yanshanian period (187–67 Ma), but radiometric dating (Ar-Ar and U-Pb) yielded ages ranging from >300 Ma to as young as 15 Ma (Peters et al. 2007 and references therein).

4.4.3.1 Shuiyindong and Yata Carlin-style Au Deposits (Guizhou)

Su et al. (2009) studied in some detail, focussing on petrography and fluid inclusions, two Au deposits in the Guizhou region on the southwestern margin of the Yangtze Craton, namely: Shuiyindong and Yata (Fig. 4.11), with the former being stratabound and the latter structurally controlled. In southwestern Guizhou, Shuiyindong (not listed in Table 4.4), one of a cluster of deposits, has Au reserves of 55 tonnes of Au with grades ranging from 7 to 18 g/t, with most of the gold residing in arsenian pyrite and arsenopyrite, as further discussed below. The ores are generally hosted in bioclastic limestone, argillite intercalated with bioclastic limestone and calcareous siltstone (Longtan Formation). There are three main orebodies (referred to as IIIa, IIIb, IIIc), which are from 100 to 400 m in length, 50–350 m wide and from 1.7 to 1.9 m thick. Interestingly, Su et al. (2009) suggested that an unconformity may have been a conduit for the ore fluids. Wall rock alteration is characterised by decarbonation, silicification, dolomitisation and sulphidation. Ore minerals are arsenian pyrite, pyrite, arsenopyrite, marcasite, and lesser orpiment, realgar and stibnite. Gold occurs as <50 μm grains, generally contained in arsenian pyrite, arsenopyrite and in the core of porous pyrite, reaching amounts of up to 3,800 ppm. Gold is positively correlated with other elements (in decreasing order), such as A, Sb, Tl, Cu, Pb, Co and Ni.

The Yata deposit (Table 4.4), first mined for As (realgar), is hosted in rocks of the Mid-Triassic Xuman Formation (siltstone, sandstone, argillaceous limestone and shale). More specifically, the ore-hosting is Member 2 of the Xuman Formation consists of sandstone, siltstone and mudstone. The mineralisation is structurally controlled, along a high-angle strike-slip shear zone, where at least 40 orebodies are located. The M1 orebody is 1,500 m long, 40–60 m wide and 200 m thick, grading 1–3 g/t Au; lenses, stockworks and veins surround the M1 orebody. Wallrock alteration at Yata extends well beyond the controlling structures, into the reactive and/or permeable clastic rocks and is characterised by decarbonation, silicification and jasperoidal quartz; the porosity that results from carbonate dissolution hosts orpiment and/or realgar. Ore minerals are arsenian pyrite, arsenopyrite, marcasite, stibnite, orpiment, realgar with trace amounts of sphalerite, galena and chalcopyrite. Pyrite may contain up to 83 ppm Au, whereas arsenian pyrite has 540 ppm Au and 11 % As. Su et al. (2009) recognised three stages of mineralisation for bothdeposits:

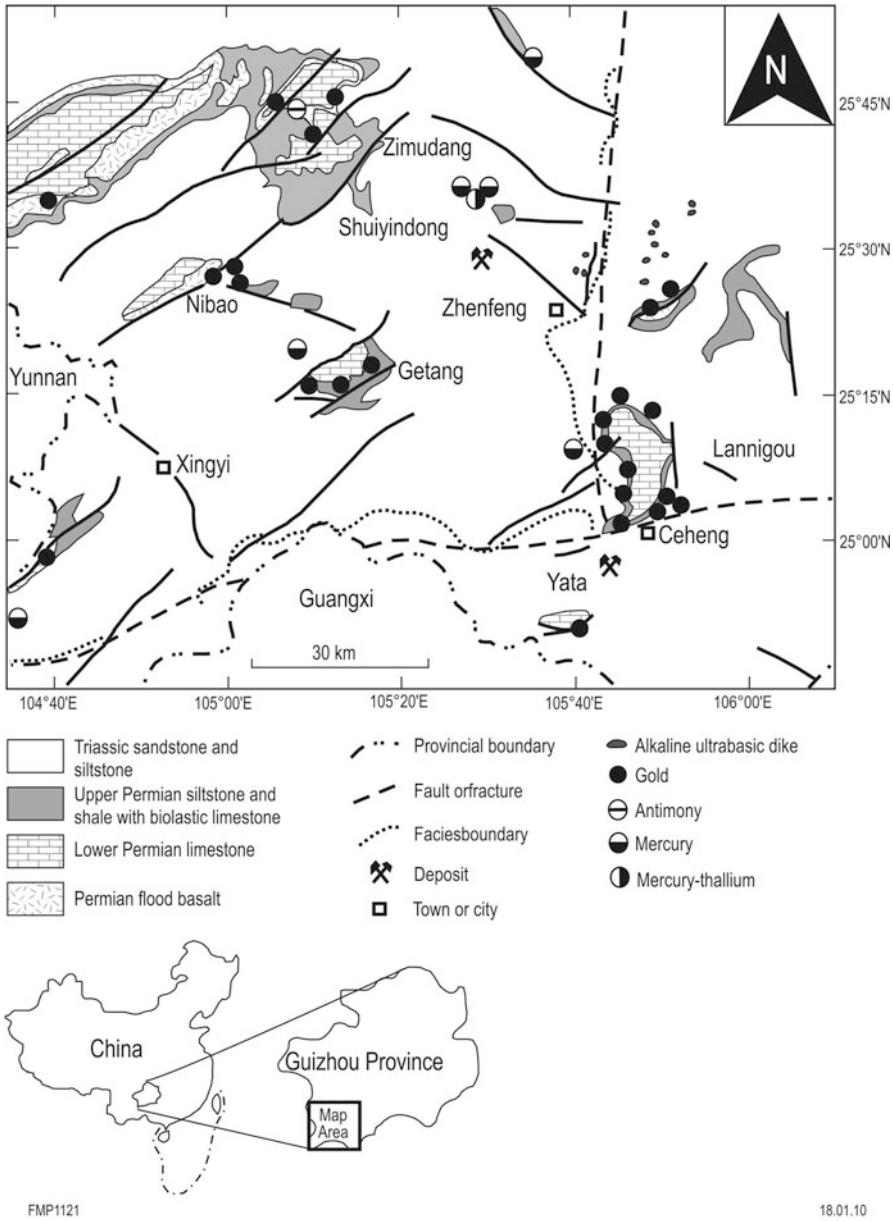

Fig. 4.11 Simplified geology of southwestern Guizhou and distribution of the main Carlin-type Au, Sb and Hg deposits. (After Su et al. 2009)

Table 4.4 Carlin-type and Carlin-like Au deposits in the Yangzte Craton. (After Peters et al. 2007; Mao et al. 2002b)

Deposit	Province	County	Lat N/ Long E	Commodities	Au grade, where available (g/t)	Host rocks age
Badu	Guangxi	Tianlin	20 30′/105 52′	Au		Triassic
Baihe	Guangxi	Hengxian	22 29′/109 28′	Au		Cambrian(?)
Caijaping	Guangxi	Fengshan	24 29′/106 52′	Au		M. Triassic
Damingshan	Guangxi	Lingyun	24 23′/106 52′	Au		M. Triassic
Gaolong	Guangxi	Tianlin	24 14′/105 38′	Au As Sb		M. Triassic
Gengxin	Guangxi	Tianlin	24 40′/106 50′	Au		?
Guohua	Guangxi	Pingguo	23 26′/107 23′	Au		Carboniferous
Hengxian	Guangxi	Hengxian	22 47′/109 05′	Au		M. Cretaceous
Jiaoman	Guangxi	Fengshan	23 42′/106 49′	Au		Carboniferous
Jinya	Guangxi	Fengshan	24 33′/106 53′	Au As Ag Cu Pb Zn Sb		M. Triassic
Jinzhudong	Guangxi	Leye	24 55′/106 24′	Au		M. Triassic
Langquan	Guangxi	Leye	24 50′/106 19′	Au		M. Triassic
Longchuan	Guangxi	Baise	24 04′/106 48′	Au		Triassic
Longhuo	Guangxi	Longlin	24 35′/105 33′	Au		Carboniferous(?)
Longzhen	Guangxi	Tanyang	23 38′/106 42′	Placer Au(?)		?
Luolou	Guangxi	Lingyun	24 23′/106 51′	Au		Carboniferous
Maxiong	Guangxi	Longlin	24 39″/105 25′	Au, As		L. Devonian
Mingshan	Guangxi	Lingyun	24 02′/106 51′	Au		Carboniferous
Nabi	Guangxi	Tianlin	24 04′/105 55′	Au		Triassic
Peyian	Guangxi	Longlin	24 38′/105 26′	Au As		L. Devonian
Pingshan	Guangxi	Yianlin	24 34′/106 11′	Au		M. Triassic
Pingtang	Guangxi	Yianlin	24 31′/105 40′	Au		Carboniferous
Pingwang	Guangxi	Yianlin	24 16′/106 16′	Au		M. Triassic
Posang	Guangxi	Bama	23 57′/107 20′	Au		M. Triassic
Sanhua	Guangxi	Guigang	23 15′/109 32′	Au		Devonian(?)
Shangshi	Guangxi	Pingxiang	22 07′/106 50′	Au		M. Triassic
Tianwan	Guangxi	Xiling	24 40′/104 38′	Au		M. Triassic
Zheyi	Guangxi	Longlin	24 40′/105 25′	Au Sb		L. Devonian
Baidi	Guizhou	Ceheng	24 44′/106 08′	Au		M. Triassic
Bannian	Guizhou	Ceheng	25 10′/105 29′	Au(?)		L. Triassic
Banqi	Guizhou	Ceheng	24 46′/105 38′	Au Hg Sb		L. Triassic, L. Permian
Baqiao	Guizhou	Sandu	25 26′/107 52′	Au		E. Carboniferous
Beiyinpo	Guizhou	Ceheng	25 37′/105 36′	Au Hg		M. Triassic
Ceyang	Guizhou	Minxian	24 59′/105 45′	Au		M. Triassic
Dachang	Guizhou	(?)	25 36′/105 12′	Au Sb As Hg		L. Permian
Daguan	Guizhou	Wangmo	25 01′/106 05′	Au As Sb		L. Triassic
Dayakou	Guizhou	Xingren	25 18′/105 06′	Au (Sb)		L. Permian
Douyajing	Guizhou	Wongmo	25 09′/105 13′	Au		Triassic
Getang	Guizhou	Along	25 17′/105 18′	Au		U. Permian
Jiaoguan	Guizhou	Zhenfeng	25 23′/105 52′	Au(?)		L. Permian
Lannigou	Guizhou	Zhengfeng	25 10′/105 50′	Au As Hg		M. Triassic
Longna	Guizhou	Xingyi	24 40′/104 37′	Au(?)		M. Devonian
Loudong	Guizhou	Zhengfeng	25 21′/105 33′	Au As Sb		M. Triassic
Miaolong	Guizhou	Sandu	26 04′/107 53′	Au As Sb		E. Cambrian(?)

Table 4.4 (continued)

Deposit	Province	County	Lat N/ Long E	Commodities	Au grade, where available (g/t)	Host rocks age
Nibao	Guizhou	Puan	25 25′/104 54′	Au		L. Permian
Pegao	Guizhou	Zhengfeng	25 20′/105 33′	Au		M. Triassic
Puzilong	Guizhou	(?)	25 73′/105 36′	Au Hg		L. Triassic
Qingping	Guizhou	Ceheng	25 18′/105 32′	Au		L. Triassic
Sanchahe	Guizhou	Zhengfeng	25 31′/105 37′	Au		U. Permian, L. Triassic
Shaziling	Guizhou	Qinglong	25 47′/104 57′	Au As		L. Triassic
Sixiangchang	Guizhou	Puan	25 55′/105 00′	Hg Au		L. Cambrian
Tangxinzhai	Guizhou	Zhengfeng	25 20′/105 32′	Au		L. Triassic
Weihuai	Guizhou	Ceheng	25 24′/105 31′	Au As		M. Triassic
Xiongwu	Guizhou	Xingyi	24 56′/104 42′	Au Sb As Hg		L. Permian
Yangyou	Guizhou	Ceheng	25 00′/105 46′	Au		L. Permian
Yata	Guizhou	Ceheng	24 56′/105 39′	Au		M. Triassic
Zimudang	Guizhou	Xingren	25 34′/105 28′	Au Hg Tl		Permian, Triassic
Gedang	Yunnan	Funning	23 35′/105 32′	Au Sb		L. Devonian
Jinba	Yunnan	Funning	23 46′/105 48′	Au		M. Permian
Lubuge	Yunnan	Xingyi	25 10′/104 40′	Au As		M. Triassic
Tangshang	Yunnan	Guannan	24 25′/104 47′	Au		Triassic
Dingping	Gansu	Hequ	34 00/102 48′	Au Hg	5.2	Mid Devonian
Juiyuan	Gansu	Zhouqu	33 51′/104 16′	Au Zn	8.5	Mid Devonian
Luoda	Gansu	Diebu	33 54′/103 56′	Au Hg	5	Silurian
Chabu	Gansu	Diebu	34 03′/103 48′	Au	4	Carboniferous
La'erma	Gansu	Luqu	34 00′/102 19′	Au Sb Hg	1.5–5.6	Cambrian-Ordovician
Dashui	Gansu	Maqu	35 05′/101 59′	Au Fe	5–60	Triassic-Jurassic
Zhongku	Gansu	Muqu	34 10′/101 58.5′	Au	7.6	Mid Triassic
Gongbei	Gansu	Maqu	34 00′/102 12.5′	Au Sb	2–6	Mid Triassic
Shijiba	Gansu	Wenxian	33 00′/104 35′	Au	5.8–8.1	Early-Mid Devonian
Dongbeizhai	Sichuan	Songpan	32 18′/102 45.3′	Au Sb Hg W	5.5	Mid Triassic
Manaoke	Sichuan	Jiuzhaigou	32 18′/103 24′	Au Sb W	3.2	Triassic
Jinmuda	Sichuan	Rangtang	32 22′/101 06′	Au Sb Zn	1.6–2.6	Triassic
Weiguan	Sichuan	Litang	31 29.5′/103 05′	Au Sb Zn Pb Cu	2.9–5.4	Mesozoic?
Yinchang	Sichuan	Pingwu	31 58′/103 21′	Au Hg Sb Fe	3.8	Triassic
Qiongme	Sichuan	Ruo'ergai	32 24.5′/102 29′	Au Sb Zn Cu	3.8	Cambrian
Lianhecun	Sichuan	Nanping	33 02′/104 28′	Au	4	Early Devonian
Qiaoqaio-shang	Sichuan	Songpan	32 44′/103 38′	Au Hg	4	Mid Triassic
Zheboshan	Sichuan	Songpan	32 53′/103 18.25	Au Zn Cu	5	Mid Triassic
Jindonggu	Sichuan	Pingwu	32 10′/103 45.6	Au	5.9	Silurian
Jianchaling	Shanxi	Lueyang	N/A	Au Ag Ni	5	Neoproterozoic
Donggouba	Shanxi	Lueyang	33 14′/106 20.4′	Au Zn Pb Cu	2	Mesoproterozoic

(1) early stage milky quartz with pyrite and arsenopyrite veins; (2) main stage vein and replacement-style quartz-dolomite with arsenian pyrite, pyrite and arsenopyrite; and (3) late stage quartz, calcite, dolomite with stibnite orpiment and realgar.

Su et al. (2009) showed that there are three types of primary and secondary fluid inclusions. Type Ia are two-phase liquid-rich aqueaous, Type Ib are two to three-phase aqueous-carbonic (vapour + CO_2 liquid); Type II are two-phase aqueous carbonic and Type III are monophase carbonic inclusions. On the basis of petrography relationships, the authors suggested that Type Ia fluids can be related to the formation of the early ore minerals in veins, predating the precipitation of the main mineralisation event of disseminated auriferous arsenian pyrite and arsenopyrite, which are related to Type Ib fluids. Type II and III, fluids are instead associated with the waning stages of the mineralisation event. Microthermometric Raman spectroscopy showed the following. Type Ia primary inclusions have salinities ranging from 5 to 6.9 wt % NaCl equivalent, with homogenisation temperatures from 190 to 258 °C. Type Ia secondary inclusions have salinities from 2.1 to 7.2 wt % NaCl equivalent and homogenisation temperatures of about 190 °C. Type Ib primary inclusions have salinities of 1.6–3.3 wt % NaCl equivalent, whereas secondary inclusions gave values of 0.4–1.2 wt % NaCl equivalent. Homogenisation temperatures for both primary and secondary range from 19 to 220 °C. Raman spectroscopy showed CO_2 as the dominant volatile species, with minor CH_4. Type II aqueous-carbonic inclusions have salinities ranging from nil to 8.9 wt % NaCl equivalent, with homogenisation temperatures not reliably obtained, as all inclusions decrepiated when heated above 200 °C. Type III carbonic inclusions also gave unreliable results. Su et al. (2009) estimated that the pressure-temperature conditions of fluid inclusion entrapment corresponded to depths of 1.7–4.3 km, whereas in other cases reported in the literature for other deposits (e g. Lannigou; see Fig. 4.11) CO_2-bearing inclusions indicate depths of 2.2–6.3 km under lithostatic conditions. LA-ICP-MS microanalyses of the fluid inclusions revealed variable amounts of B, Na, K, Sr, Cs, As, Sb and Au abundances from 3.8 to 5.7 ppm.

Stable isotope systematics (D, O) show values that plot near the metamorphic water box. The main ore quartz from Shuiyindong has a narrow range of $\delta^{18}O$ values from 20.9 to 26.1 ‰, whereas at Yata these values range from 9.9 to 15.1 ‰, with δD_{H2O} extracted from fluid inclusions range from −51.1 to −78.8 ‰, which are higher than local meteoric water in the Jurassic-Cretaceous. The authors concluded that no meteoric water was involved in the ore-forming process, instead metamorphic fluids were more likely involved, but not to the exclusion of magmatic fluids.

Su et al. (2009) proposed that the Fe of sulphides derived from the dissolution of the Fe carbonates of the host rocks, leading to sulphidation by H_2S-rich fluids carrying Au complexes, such as $Au(HS)_{-2}$, as well as As complexes, perhaps according to the type of reaction below:

$$2FeCO_3 + 2H_3AsO_3(aq) + H_2S_{(aq)} + 2Au(HS)_{-2} + H_{2(g)} \rightarrow Fe(S, As)_2\, Au_2S^0 + FeS_2 + CO^{-2}{}_{3(aq)} + CO_{2(g)} + 7H_2O$$

In conclusion, the genetic model that best explain these Carlin-style Au deposits in the Guizhou region involves interaction of the ore forming fluids with chemically reactive C-rich and Fe carbonate rocks at pressure and temperatures consistent with

regional metamorphic gradients. Su et al. (2009) contended that the Guizhou deposits might be an end member of orogenic systems formed from fluids generated by metamorphic dehydration and/or magmatism.

4.4.4 Porphyry and Quartz-vein W Ore Systems

Not many porphyry type mineral deposits are known in the South China Block, outside the Yangtze River Valley metallogenic province, discussed below, and the South China Fold Belt, discussed in Chap. 5. Here, I review porphyry style mineral systems, which include the polymetallic Dabaoshan and the Dexing ore districts, as well as an important tungsten producer, the Taoxikeng quartz-vein W deposit.

4.4.4.1 Dabaoshan

Dabaoshan, is part of a larger polymetallic ore system, located along the major Wuchuan-Sihui northeast trending fault zone in the Cathaysia Block. The Dabaoshan mineral systems comprise a porphyry Mo deposit, stratiform Cu-Pb-Zn ore and Mo-W skarn ore, all associated with felsic intrusions and subvolcanic intrusions. The presence of some 400 old workings and widespread remnants of slags, indicate that mining in the area had been carried out during the Tang (61–890 current era; C.E.) and the Song (960–1270s C.E.) dynasties (Ge et al. 1990). Dabaoshan was "re-discovered" in the 1950s through examination of gossan outcrops. The gossan is quite extensive and according to a figure shown in Ge et al. (1990, Fig. 1.38, p. 65), it extends for about 2 km, with a north-northwest strike and is referred to as iron orebody. Although no information is available in English-language publications, it is possible that the extensive gossan may represent a non-sulphide orebody in its own right (see Hitzman et al. 2003). Wang et al. (2011) studied the Dabaoshan porphyry Mo deposit and reported on Re-Os dating of the molybdenite, table (S, D, O) and Pb isotopic systematics. The following is extracted from these authors.

Dabaoshan is a large polymetallic ore system, including stratiform Cu-Pb-Zn ore, porphyry-type Mo, skarn-type Mo-W and stratiform siderite ore bodies. The Mo-W mineralisation is spatially associated with granodiorite porphyry and occurs along the contacts of the porphyry, whereas the Cu-Pb-Zn mineralisation is closely related to dacite porphyry. The metal endowment of the deposit consists of 152,000 t of Mo metal with an average grade of 0.076 wt %, 45,000 t of WO_3 with an average grade of 0.3 wt %, 313,000 t of Cu with an average grade of 0.86 wt %, 20,000 t of Pb with an average grade of 1.77 wt %, 52,000 t of Zn with an average grade of 4.44 wt %, and 11 Mt of Fe with an average grade of 48.21 wt %.

The geological setting of the Nanling region, where the ore system occurs, is dominated by Cambrian, Devonian and Lower Jurassic sedimentary rocks. Cambrian rocks, distributed in the north and west part of the area, consist of graywackes, siltstones, and slate intercalations. Devonian rocks, exposed in the southern and

eastern part of the ore district, unconformably overlying the Cambrian sedimentary rocks, are divided into the Lower-Middle Devonian Guitou Formation (quartz sandstone, feldspar sandstone, siltstone, shale, and conglomerate at the base), Middle Devonian Donggangling Formation (dolomite, dolomitic limestone, and neritic facies limestone, with a total thickness of more than 500 m), and Upper Devonian Tianziling Formation (micritic limestone intercalated with thin-layered, micritic, silty limestone and massive chert-bearing limestone and dolomitic limestone). The lower Jurassic sedimentary rocks occur in the northern part of the ore district and consists of graywackes and shales intercalated with thin marl. The Palaeozoic sedimentary rocks have been folded, forming a broad syncline that is cut by north-south and east-northeast-striking faults, which also acted as the main structural controls for the intrusive porphyries.

The main igneous intrusions include a dacite porphyry and a granodiorite porphyry stock. The dacite porphyry extends over an area of about 1.5 km^2 and its eastern and western margins are fault bounded. The dacite porphyry strikes north-south and dips to the east at 60–65°. Previous age determinations for the granodiorite porphyry are 101–97 Ma (K-Ar) a Rb-Sr whole rock isochron age of 155.5 ± 23 Ma. U-Pb dating of the granodiorite rock by Wang et al. (2011) of magmatic zircons yielded a weighted average of 175.4 ± 1.6 Ma.

In the Dabaoshan ore district, the Cu-Pb-Zn stratiform lenses and ore veins occur in the Dongdangling Formation. Ore minerals are chalcopyrite, pyrite, galena, sphalerite and siderite. Mao et al. (2004) reported a molybdenite Re-Os model age of 164.7 ± 3 Ma for these stratiform Cu-Pb-Zn orebodies. The porphyry-type or quartz-vein-type Mo and skarn-type Mo-W ore bodies occur along the contact zones between the granodiorite porphyry and sedimentary wall-rocks. Here the ore minerals are molybdenite, scheelite, bismuthinite and pyrite. Wall-rocks locally exhibit greisen type alteration (quartz-muscovite), with more widespread alteration minerals that include K-feldspar, garnet, diopside, actinolite, tremolite, chlorite, sericite and epidote. Re-Os dating of molybdenite yielded a weighted average age of 164.0 ± 2.5 Ma, which matches well with the above mentioned Re-Os age of Mao et al. (2004). A cross-section of the Dabaoshan orebodies is shown in Fig. 4.12.

Wang et al. (2011) suggested that the age determinations show that the porphyry Mo and stratiform Cu-Pb-Zn deposits resulted from the same mineralisation event. This is different from previous studies in which Devonian exhalative processes would have been overprinted during mineralisation stages of Yanshanian age.

The $\delta^{34}S$ values of galena, sphalerite, pyrrhotite, chalcopyrite, pyrite and molybdenite from the Dabaoshan polymetallic ores range from -3.7 to $+4.9$ ‰ with most of the $\delta^{34}S$ values from -2 to 3 ‰, which are close to magmatic sulphur. Lead isotopic compositions of galena, sphalerite, pyrrhotite, chalcopyrite and pyrite from the Dabaoshan deposits plot along the supracrustal lead evolution curve, part of which are close to the orogenic curve and the mantle field, suggesting that the Pb was derived mostly from the upper crust, with some mantle or lower crustal component. Wang et al. (2011) concluded that sulphur and Pb isotope systematics and the Re content of molybdenite support a genetic relationship between the Dabaoshan deposit and

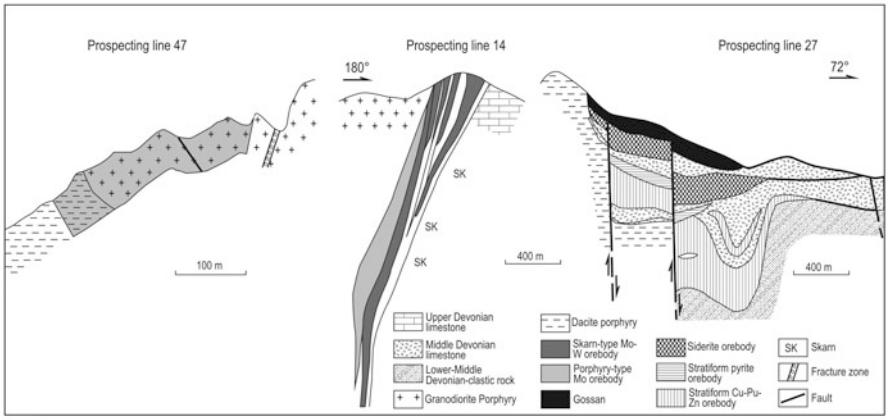

Fig. 4.12 Cross-section along prospecting lines no. 47, 14 and 27 in the Dabaoshan polymetallic ore system (after Wang et al. 2011); section on prospecting line 27 is from Editorial Committee of Mineral Deposits of China (1990, Fig. 1.40)

the granodiorite porphyry and dacite porphyry, and that the Mo mineralisation is related to the granodiorite porphyry Mao et al. (2010) proposed that Mesozoic metallic mineralisation in South China can be grouped into main three pulses, namely: Late Triassic (230–210 Ma), Mid-Late Jurassic (170–150 Ma) and Early-Middle Cretaceous (134–80 Ma). The age of the Dabaoshan Mo mineralisation corresponds to the second episode of Mesozoic metallogenesis in South China.

4.4.4.2 Dexing and Yinshan

The Dexing porphyry Cu-Mo district, one of the largest in China, is located in the Jiangxi province, in the Dele Jurassic basin, in the eastern Jiangnan orogenic belt (Table 4.1 and Fig. 4.13). The district contains about 1,500 Mt of ore, grading 0.43 % Cu, 0.02 % Mo, 0.16 g/t Au (Zaw et al. 2007). Mining in this region was begun during the Sui and Tang dynasties in about 600–900 current era. The Dexing porphyry deposits are discussed by Zhu et al. (1983), Ge et al. (1990) and Zhang et al. (1996b). To the south of Dexing is the Jinshan Au deposit, as a world-class orogenic system, hosted in a ductile shear zone, briefly discussed below.

More recent works that deal with mineral systems in the Dexing area, include Rui et al. (2005), Li and Sasaki (2007) and Mao et al. (2011a). The Jiangnan orogenic belt was intruded by late Permian-Triassic peraluminous granite, syenite, Jurassic-Cretaceous S-type granite and gabbroic rocks that intruded slate and phyllite of the Mesoproterozoic Shuanqiaoshan Group and can be attributed to the Yanshanian event. Rui et al. (2005) listed five stages of Yanshanian magmatic activity in the Dexing region, they are: (1) 193–190 Ma ultramafic and mafic intrusions along the Gandongbei fracture zone; (2) 186–172 Ma granodiorite, diorite, quartz diorite and granite porphyries, associated with the Cu-Mo mineralisation; (3) peak of magmatic

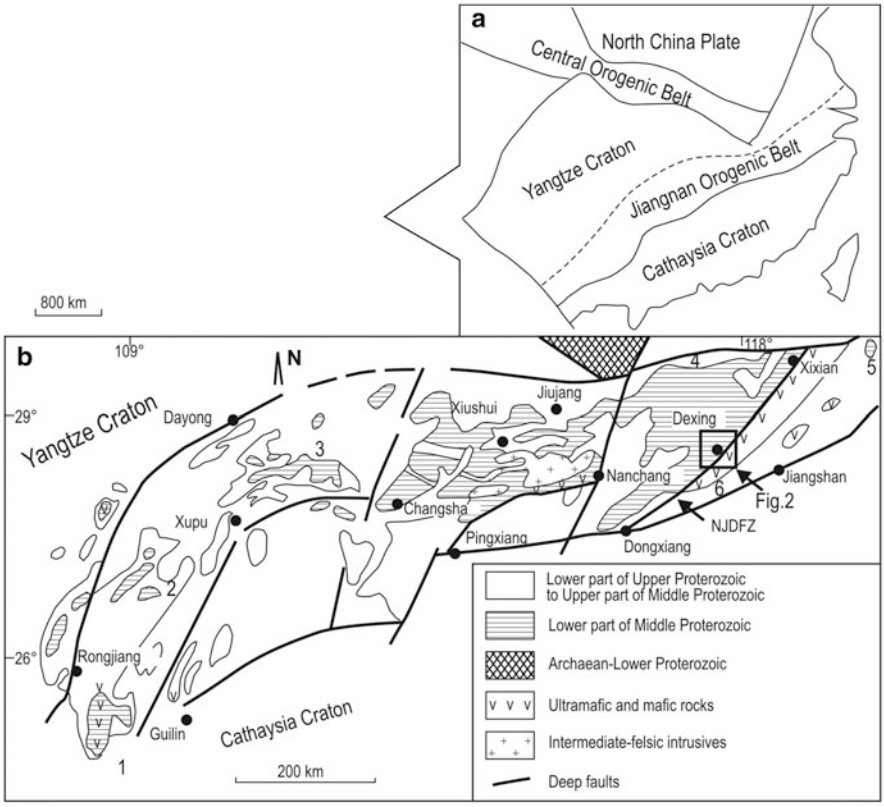

Fig. 4.13 **a** The Jianang orogenic belt in South China (inset) and simplified geology of part of the Jiangnan orogenic belt and position of Dexing district; **b** simplified geology of the Dexing district and position of Zhushaohong, Tongchang and Fujawu porphyry systems. (After Li et al. 2010d and references therein)

activity at 145–125 Ma, represented by dacitic volcanism and pyroclastic forming a 1,660–400 m thick sequence, subvolcanic rocks (dacite porphyry, trachy-andesite porphyry, quartz syenite porphyry), best developed in the Yinshan area and hosting polymetallic mineralisation; (4) 127–103 Ma with intermediate to felsic volcanism, locally with basalt, pyroxenite, gabbro, diorite and quartz diorite porphyries; and (5) 100–96 Ma including post-mineralisation granite, granite, quartz porphyry and quartz-diorite porphyry.

The Dexing district is within a major east-northeast trending shear zone and is characterised by numerous of diverse hydrothermal mineral systems (Li and Sasaki 2007). The Dexing district comprises three porphyry Cu-Mo deposits, namely: Zhushahong, Tongchang and Fujaiwu. There is common confusion in the literature, with some authors describing Dexing as one porphyry deposit comprising three orebodies (Zhushahong, Tongchang and Fujaiwu; Zaw et al. 2007). In fact, and as

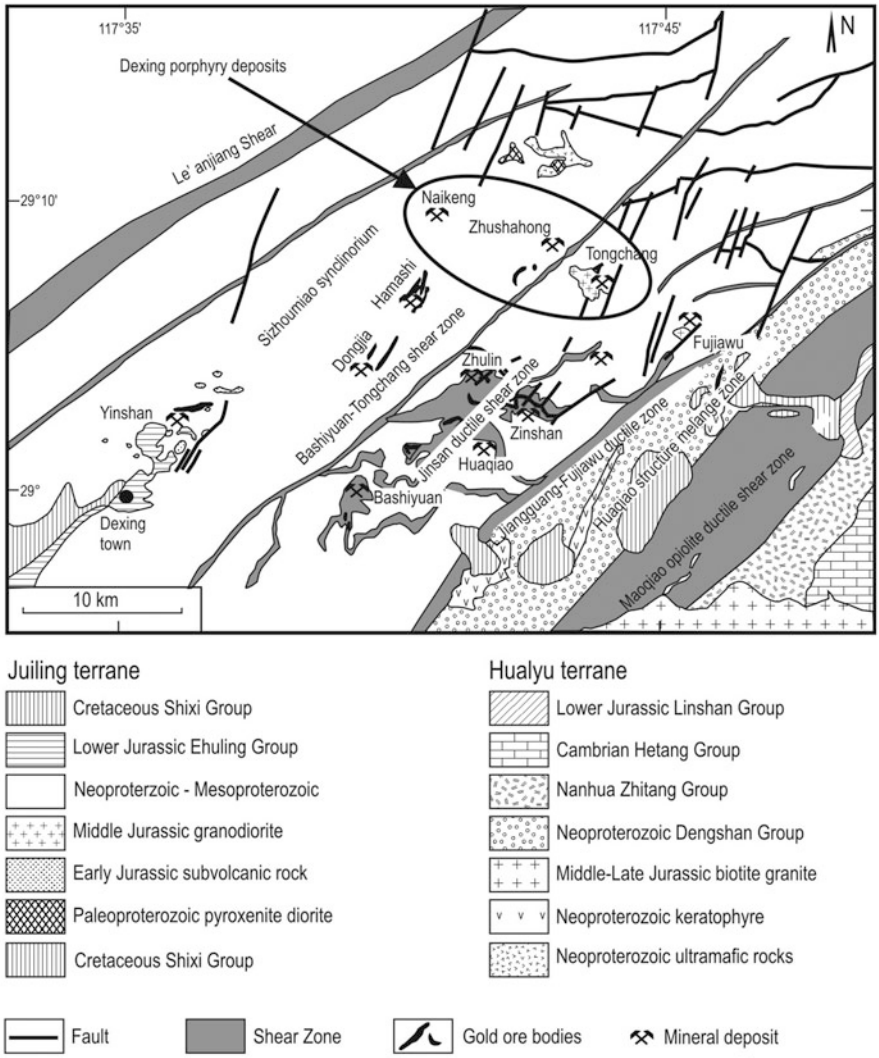

Fig. 4.13 (continued)

shown in Fig. 4.13b, these seem to be three distinct porphyry deposits. The three orebodies, Tongchang, Fujiawu and Zhushahong have a pipe-like shape and circular in plan, with the largest, Tongchang, being 0.7 km in diameter. The contact zone between the porphyry and the host rocks are thermally metamorphosed to hornfels.

The three porphyry deposits are associated with three small granodiorite and quartz diorite stocks and dykes that were emplaced at the intersection of west-northwest and northeast trending faults. The granodiorite is mineralised, whereas

the dioritic rocks are post-mineralisation (Mao et al. 2011a). Re-Os dating of molybdenite yielded 170.4 ± 1.8 Ma (Lu et al. 2005), consistent with SHRIMP, U-Pb dating of zircons in the granodiorite porphyry, which yielded an age of 171 ± 3 Ma (Wang et al. 2004b). The orebodies, as described in Mao et al. (2011a), consist of stockworks and disseminated sulphides, both affecting the granodiorite porphyry and the country rocks, referred to by Chinese authors as endo-contact and exo-contact zones, respectively. About 75 % of the ores are in the exo-contact zones. Tongchang is the largest of the three deposits, it has an oval shape with the a northwest-striking 2.5 km long axis and with a 700 × 400 m barren core. The ore minerals are pyrite, chalcopyrite, molybdenite, tennantite, bornite and minor electrum, chalcocite, galena, sphalerite, bismuthinite, cubanite, pyrrhotite, arsenopyrite, carollite, bravoite, millerite and gersfordite. Gangue minerals are quartz, illite, chlorite and anhydrite. In addition to Cu and Mo, other metals recovered as by-products are Ag, Re, Se, Te and Co.

Rui et al. (2005) recognised three main alteration zones that envelop the granodiorite porphyry: (1) quartz-sericite; (2) chlorite (epidote)-sericite, also comprising carbonate, quartz and anhydrite minerals; (3) chlorite-epidote-illite with variable amounts of albite, carbonate and anhydrite. Rui et al. (2005) stated that early high-temperature potassic alteration is poorly developed, as in the Fujiawu granodiorite porphyry, where secondary K-feldspar and biotite are present. However, their Fig. 4 shows a cap or zone of K-feldspar-anhydrite-sulphide above the granodiorite porphyry, followed upward by a quartz-sericite-sulphide zone and a carbonate-sulphide zone. The country rocks around the porphyry intrusions are thermally metamorphosed up to 400 m from the contacts, with phyllite and slate converted to biotite and andalusite-biotite hornfels.

Li and Sasaki (2007) recognised four types of vein systems: (1) granular quartz—K-feldspar-sulphides or K-feldspar veins; (2) quartz—molybdenite—chalcopyrite veins; (3) sulphides-quartz veins; and (4) carbonate-sulphate-oxide veins. The sulphides-quartz veins are the most important for the mineralisation in the Dexing porphyry deposits. Primary fluid inclusions in these veins include liquid-rich, vapor-rich and halite-bearing ones. Thermometric measurements of fluid inclusions and stable isotope systematics suggest that the temperatures of mineralisation of sulphide-quartz veins are between 115 and 430 °C, and the pressure ranges from $20 - 400 \times 10^5$ Pa (Li and Sasaki 2007).

The hydrothermal fluids responsible for muscovite in the sulphide-quartz vein have an isotopic composition ($\delta^{18}O$ = 3.6–5.4 ‰, δD = −49 to −46 ‰), similar to that considered typical of magmatic fluids ($\delta^{18}O$ values of 4.6 and −87 ‰ and δD values of 7.1–8.9 ‰) (Hedenquist and Richards 1998). Carbon and oxygen isotope values for hydrothermal calcite in H veins are −4.8 to −6.2 ‰ and 6.8–18.8 ‰, respectively. The $\delta^{34}S$ of pyrite in sulphide-quartz veins ranges from −0.1 to 3 ‰, whereas $\delta^{34}S$ for chalcopyrite in carbonate-sulphide-oxide veins ranges from 4 to 5 ‰, suggesting a magmatic origin for sulphur. The O, Nd and Sr isotopic compositions of different altered rocks in the Tongchang show that there are three types of hydrothermal fluids: (1) magmatic, (2) deep- seated non-magmatic and (3) meteoric water (Mao et al. 2011a; Jin et al. 2002). Isotopic data therefore indicate

that magmatic fluids played a predominant role in the ore-forming process. Jin et al. (2002) also explained that strontium isotope ($^{87}Sr/^{86}Sr)_i$ values increase regularly from the interior of a porphyry body towards the contact with country rocks (0.705 → 0.711), possibly indicating that the hydrothermal fluids carrying the ore-forming metals from the interior of the porphyry to the discharge zone along the contacts with country rocks.

To the southwest of Dexing is an epithermal precious and base metal deposit, Yinshan (Fig. 4.13b), according to Li and Sasaki (2007) containing some 83 Mt of ore, grading 0.52 % Cu and 0.8 g/t Au. According to Zaw et al. (2007) and Zhang et al. (2007), Yinshan is an Au-rich polymetallic (Cu, Pb, Mo, Zn, Ag; Table 4.1) porphyry-epithermal deposit, with reserves of 120 Mt of Cu ore at 0.54 %, 5 Mt of Pb ore at 1.8 % Pb, 5.2 Mt of Zn ore at 2.3 % Zn, 125.4 Mt of Au ore at 0.63 g/t Au and 127 Mt of Ag ore at 11 g/t Ag. The deposit is located in an area characterised by low grade metamorphic rocks of the Middle Proterozoic Shuangiaoshan Group and the overlying rhyolitic to dacitic volcanic rocks of the Late Jurassic Ehuling Formation and continental clastic rocks of the Early Cretaceous Shixi Formation. This sequence was intruded by Mesozoic (Yanshanian) intermediate to felsic porphyries (Zaw et al. 2007). The deposit displays a zonal arrangement of mineralisation with Cu–Au in the center, Cu–Zn–Pb in the middle, and Pb–Zn–Ag at the periphery of the deposit (Zaw et al. 2007).

The Yinshan polymetallic (Cu, Pb, Mo, Zn, Ag) deposit (Table 4.1; Fig. 4.13), mentioned above, has been reported and investigated by Zaw et al. (2007), Zhang et al. (2007 and references therein), Mao et al. (2011a). Three cycles of volcanism in the area have been identified (Mao et al. 2011a): (1) rhyolitic and dacitic lavas, subvolcanic quartz porphyry forming east-west trending dykes; (2) dacite porphyry dated at 181 ± 3 Ma (SHRIMP, U-Pb on zircons) and subearial felsic volcanism, resulting in a caldera volcanic edifice; (3) andesitic lavas erupted within the caldera edifice. More recently, Wang et al. (2012) reported Mi-Jurassic ages (176–166 Ma) for the Yishan volcanic rocks, suggesting an adakitic composition. The major structures in the Yinshan deposit area include northeast-trending faults that controlled volcanic activity; north-northeast, northeast, east-west and north-northwest faults that controlled the mineralisation. More specifically, the quartz porphryry associated with the mineralisation was emplaced at the intersection of northeast- and east-west-trending faults.

The Yinshan deposit is divided into five ore sections: Nanshan, Yinshan proper, Jiulogshangtian, Xishan and Beishan, which represent a series of Pb-Zn-Ag-bearing veins that link to a porphyry Cu-Au system laterally and at depth (>1,000 m). A cross-section of the Yinshan ore system is shown in Fig. 4.14. The Pb-Zn-Ag-bearing veins are 600–300 m long and 1–15 m wide and containing native Ag, galena, sphalerite, siderite as the main ore minerals, with lesser amounts of pyrite, arsenopyrite, and Pb-Sb-Ag sulphosalts. The porphyry orebody is made up of stringer veins, stockworks and sulphide disseminations, hosted in quartz porphyry, andesitic volcanic rocks, a breccia pipe and some roof pendants. The ore minerals are pyrite, chalcopyrite, tennantite, enargite, tetrahedrite, galena and sphalerite. At least two mineralisation events are recognised (Li et al. 2007b): an early porphyry Cu-Au, followed

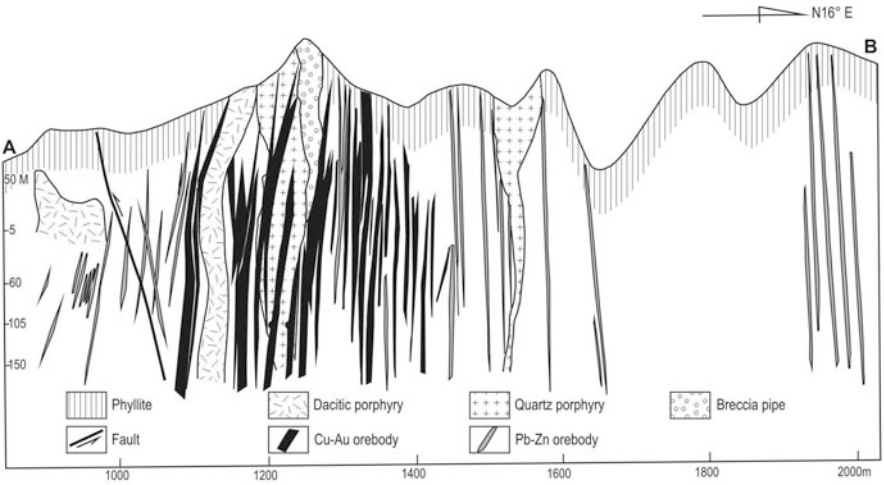

Fig. 4.14 Schematic cross-section of the Yinshan mineral system. (After Zhang et al. 2007)

by Pb-Zn-Ag vein mineralisation, for which Ar-Ar dating on muscovite yielded 178.2 ± 1 and 175.4 ± 1.2 Ma, respectively. These authors also recognised four paragenetic stages: (1) barren quartz; (2) pyrite-quartz; (3) pyrite-chalcopyrite-quartz; and (4) pyrite-sphalerite-galena. Hydrothermal alteration and associated metal zoning outwards from the quartz and dacite porphyries, as follows: sericite-pyrite, pyrite-sericite-chlorite-carbonate, chlrorite-carbonate with a metal zoning from the porphyry outwards of Cu → Cu-Pb-Zn → Pb-Zn → Pb(Ag).

Fluid inclusion studies by Zhang et al. (2007) revealed three major types of fluids: type I vapor-rich, type II liquid-rich (accounts for more than 90 % of total) and type III halite-bearing inclusions within the H_2O–NaCl system. Type I inclusions represent early dilute (low salinity) and hot fluids (homogenisation temperatures of around 440 °C and 260 bars) exsolved from silicate melts. Such a dilute hot fluid is considered responsible for the development of early barren and possibly some pyrite-bearing quartz veins. Type II inclusions showed homogenisation temperatures ranging from 390 to 270 °C and 260 bars, whereas type III inclusions were trapped at pressures above 900 bars and >500 °C. Type III high-salinity fluids resulted from continued crystallisation of saline fluids also exsolved from the crystallising magmas, under high pressure conditions (>900 bars). Collapse of the overpressured system through implosion and accompanied by introduction of meteoric water resulted in the generation of Type II low to moderate salinity fluid inclusions.

Zhang et al. (1997) obtained $\delta^{18}O$ values of fluids from 6.6 to 9.5 ‰ and δD values of inclusion fluids from −48 to −34 ‰ with calculated temperatures from 390 to 270 °C. Zhang et al. (1996a) proposed that the isotope compositions of the late mineralisation fluids related to galena and calcite, are characteristics of meteoric waters ($\delta^{18}O_{H2O} = 0.5$ ‰ and $\delta D_{H2O} = -70$ ‰).

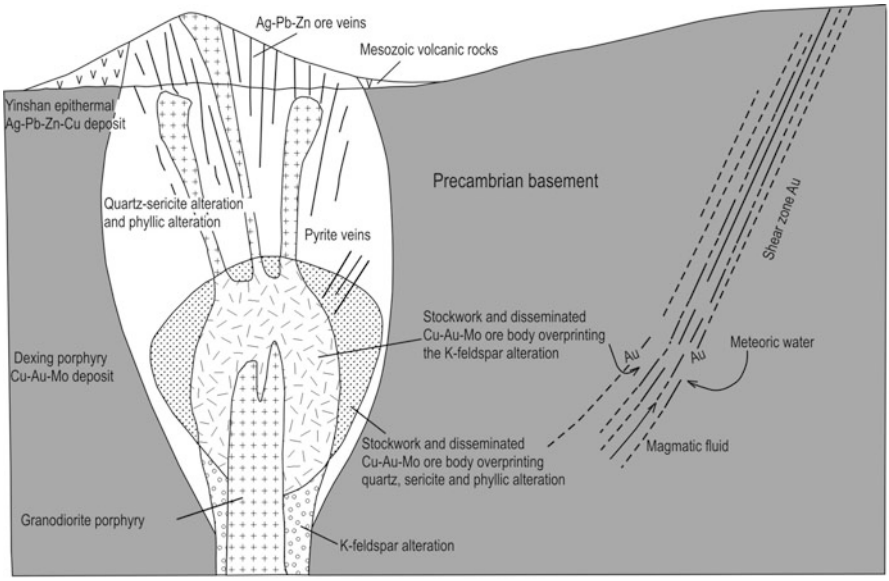

Fig. 4.15 Metallogenic model that schematically illustrates the spatial and genetic relationship of the Dexing porphyry system, the Yinshan porphyry-epithermal veins and allegedly the Jinshan shear zone-hosted lode Au veins; not to scale. (After Mao et al. 2011a)

Metallogenic Model and Geodynamic Setting for Dexing and Yinshan Mineral Systems

Dexing is a typical porphyry Cu-Au-Mo deposit in which both ore-forming fluid and metals are derived from the granite porphyry. The Yinshan deposit consists of a porphyry copper ore located in the cupola of a quartz porphyry stock in the lower part and Ag-Pb-Zn ore veins, laterally and in the upper parts. Mao et al. (2011a), proposed that the spatial arrangement of these deposits from porphyry Cu, to epithermal Ag-Pb-Zn to a distal Au mineral system, represented by Jinshan, which is discussed below and considered by other authors as a typical orogenic lode gold. Mao et al. (2011a) suggested that because they share spatial, temporal and genetic relationships and therefore belong to the same metallogenic system, in a model schematically shown in Fig. 4.15. These deposits were formed in a back-arc setting in a Middle Jurassic active continental margin, with magmas derived from the subducted slab.

From the Middle Jurassic onward, South China was mainly influenced by Palaeo-Pacific plate subduction and related back-arc extensions, influenced and controlled by pre-existing deep structures, north-northeast-trending faults and basin-and-range style rift basins. Li and Li (2007) proposed that South China experienced flat subduction during 250–190 Ma affecting a large area with a width of 1,300 km. This was followed by slab break off at 180–155 Ma, triggering large scale magmatism. This hypothesis is evidenced by ca. 500 km long of 178–173 Ma volcanic belt, extending

from southern Hunan Province, through southern Jiangxi belt to the southwest Fujian Province (Li et al. 2003c; Zhou et al. 2006). The belt includes bimodal volcanic rocks (alkali basalt, tholeiitic basalt, rhyolite and a small amount of andesite). This was followed by the intrusion of Jurassic high differentiation I-type granites (Li et al. 2007a).

Studies on the metallogenic setting for the porphyry copper—epithermal polymetallic—distal hydrothermal gold deposits in Dexing area are commonly contradictory (see Sect. 4.4.6 on Jinshan Au deposit). The Dexing porphyry deposit occurs 50 km north of the Shi-Hang rift zone (Wang et al. 2006), whereas the Yongping Middle-Late Jurassic skarn-type copper deposit occurs about 30 km south of Dexing (see Sect. 4.4.5). Mao et al. (2011a and references therein) suggested that a northeast-trending metallogenic province extending for more than 1,000 km long, in which the Dexing porphyry Cu-Mo, Yinshan porphyry-epithermal system, Jinshan lode gold, as well as other deposits including Lengshuikeng epithermal Ag-Pb-Zn, Yongping skarn-type Cu, Dongxiang Cu, Jiaoli skarn-type Pb-Zn, Qibaoshan porphyry Cu, Baoshan porphyry Cu, Shuikoushan vein Pb-Zn, Tongshan porphyry Cu and Dabeishan skarn Cu deposits are all located inboard of the South China continental margin. The deposits in this metallogenic belt have ages ranging from 180 to 165 Ma and are spatially, temporally and genetically associated with high oxidation magnetite-series granodiorite and diorite, as defined by Ishihara (1977). The metal associations, typically evolve from Cu-Au-Mo → Cu-Ag-Pb-Zn → Pb-Zn-Ag. The 1,000 km long northeast-trending metallogenic belt of porphyry-skarn and porphyry, porphyry-epithermal deposits and related magmatic rocks is almost parallel to the subduction of the Izanagi plate (or Palaeo-pacific plate). Whereas the 500 km long belt of 178–173 Ma bimodal volcanic rocks from southern Hunan Province, through southern Jiangxi Province to the southwest Fujian Province mentioned above, is nearly perpendicular to the line of subduction. Thus, unlike these bimodal volcanic rocks the magmatic rocks in the polymetallic ore belt are possibly the product of partial re-melting of the subducted slab or underplating mantle in an active continental margin. When the magma derived from the mantle rises to a shallow level in the crust, porphyry Cu-Au-Mo deposits are formed. After more contamination with the crust these magmas will form porphyry Cu-Au-Mo to epithermal Ag-Pb-Zn deposits, and locally skarn-vein Ag-Pb-Zn deposits. Where Precambrian metamorphic rocks are present, leachable gold is extracted and precipitated in suitable fractures, such as existing ductile-brittle shear zones.

4.4.4.3 Taoxikeng: Greisen-related Wolframite Deposit

China is one of the largest producer of tungsten metal in the world, accounting for about 75 % of the total production (USGS 2009). About 90 % of China's W resources are in the Nanling region in the Cathaysia Block, where some 78 Sn-W and W deposits occur (Guo et al. 2011). Here, a brief account of the Taoxikeng greisen-related wolframite-bearing quartz vein deposit is given, taken from a recent publication by Guo et al. (2011).

The Taoxikeng deposit has been known since the 1930s, but only coming into production in 1970, contains a WO_3 resource of 120,627 tonnes with an average grade of 1.5 %, with Sn, Cu, Pb and Zn recovered as by-products. The ore is hosted in the ca. 158 Ma Taoxikeng granite, which intrudes rocks of the Sinian-Ordovician basement and Devonian-Permian cover clastic sequence. The ore zones consist of northwest-trending wolframite-bearing quartz veins, located within greisenised parts of the host granite at a depth of 600 m, but also extend into Sinian basement rocks and roof pendants. There are four vein systems: Baoshan, Xishan, Langenzi and Fenglinkeng with lengths ranging from 1,600 to 300 m and up to 2 m wide. The ore minerals comprise wolframite, cassiterite, molybdenite, scheelite, chalcopyrite, sphalerite, arsenopyrite, pyrite and bismuthinite. Gangue minerals, in order of abundance, comprise quartz, calcite, muscovite, sericite, fluorite, chlorite, lithionite, topaz and tourmaline. Guo et al. (2011) determined a Re-Os age of 154.4 ± 3.8 Ma for the molybdenite and Ar-Ar ages of 153.4 ± 1.3 and 152.7 ± 1.5 Ma for the muscovite in the greisen, which led the authors to conclude that the mineralisation is genetically related to the host granite.

The Taoxikeng W deposit is clearly part of a greisen system (Guo et al. 2011), which typically refers to a coarse-grained assemblage of quartz-muscovite with varying amounts of topaz, tourmaline, fluorite, oxides (cassiterite, hematite), wolframite, scheelite, and sulphides of Fe, Cu, Mo, Bi, and Cu-Bi-Pb sulphosalts. The peraluminous granites that usually form greisens are generated during post-collisional processes (see Fig. 3.23).

4.4.5 The Middle-lower Yangtze River Valley Metallogenic Province

In the Middle-Lower Yangtze (Chiangjiang) River Valley (henceforth Yangtze River Valley), East China, there are numerous stratabound pyrite- and magnetite-rich and polymetallic skarns, porphyry and Kiruna-style magnetite deposits as well as the massive sulphide deposits, discussed in Sect. 4.4.1, in Late Palaeozoic basins, all together constituting a vast metallogenic belt. The Yangzte River Valley porphyry, porphyry-skarn and Kiruna style Fe deposits in this metallogenic belt, were described by Zhai et al. (1996), Pan and Dong (1999), Mao et al. (2006) and more recently in a special issue of Ore Geology Reviews (Mao et al. 2011b). The polymetallic skarn deposits can be considered as Fe-dominated, Au-dominated and Cu-Mo skarns (Fig. 4.16). The Yangzte River Valley metallogenic belt is situated on the northern margin of the Yangtze Craton (Fig. 4.16), where Palaeozoic lithostratigraphic successions overlie a metamorphic basement and comprise Cambrian and Ordovician siltstone, shale and dolomitic limestone, in turn overlain by clastic and dolomite rocks of Sinian and Silurian ages. During the Late Silurian and Devonian, uplift occurred with deposition of terrestrial thick successions including sandstone, conglomerate, coal and hematite-rich clastic rocks. The Carboniferous and Permian are characterised by a succession of littoral to shallow marine carbonate, with various intercalations of

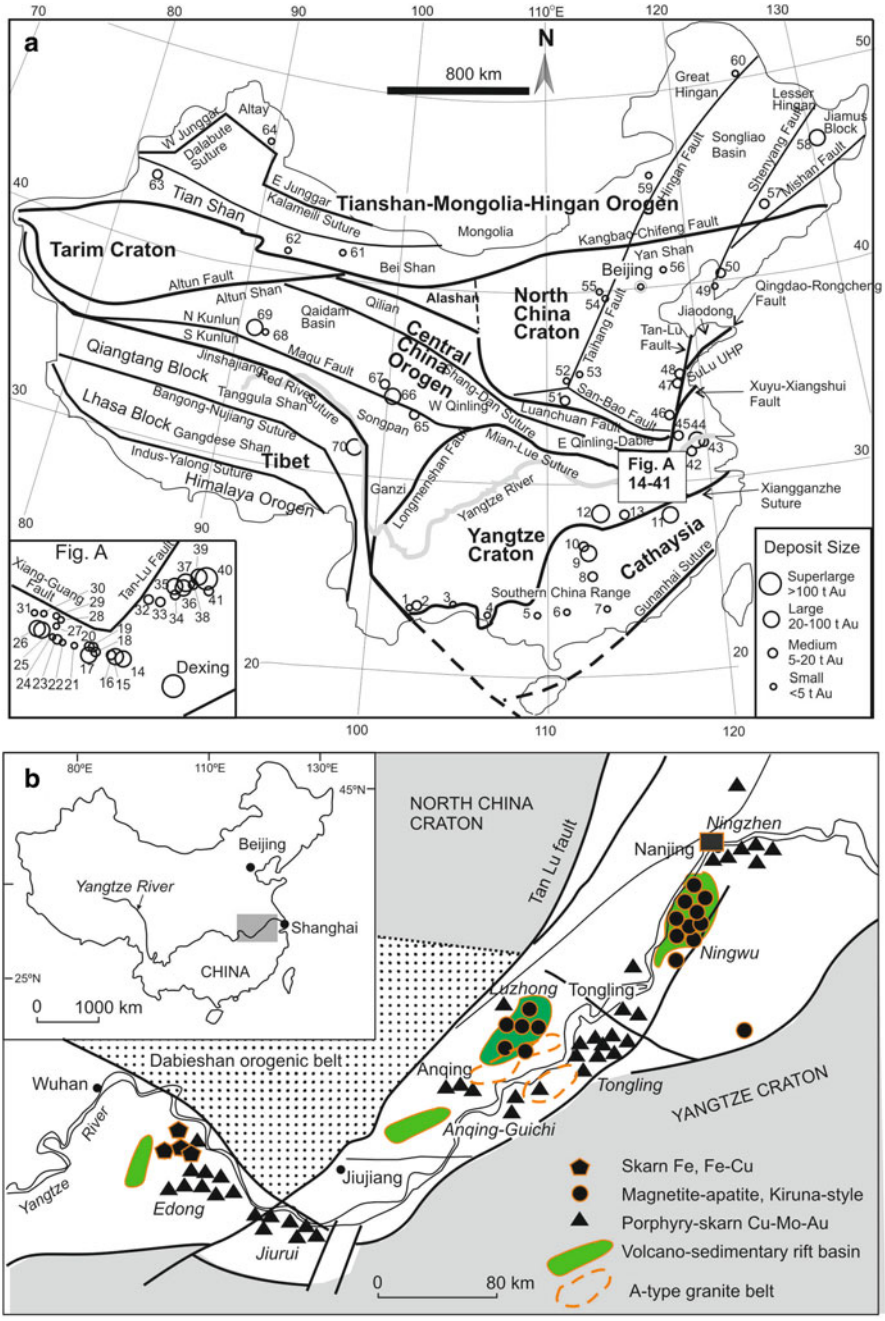

Fig. 4.16 **a** Distribution of skarn systems in China, deposit numbers correspond to those in Table 4.5 (after Chen et al. 2007); **b** distribution of porphyry and porphyry-skarn and Kiruna-type mineral systems in the Yangtze River Valley metallogenic belt (modified after Pan and Dong 1999; Mao et al. 2011a, b, c); see also Fig. 4.22

shales and clastic rocks (Mao et al. 2006). During the Lower-Mid Triassic, shallow marine to littoral carbonate beds and minor evaporites were again deposited, culminating with the deposition of terrestrial sandstone and coal seams. During the Triassic collision between the North China and the Yangzte cratons a foreland basin was formed. A series of fault-bound basins were then formed in the Jurassic-Cretaceous heralding a regime of extensional tectonics throughout the Lower-Mid Yangtze River Valley, with lake- and swamp-facies sandstone, siltstone and shales, followed by volcanic and volcaniclastic rocks. This volcanism produced andesite, rhyolite, shoshonite and alkali basalt (Mao et al. 2006). In the upper Cretaceous and Neogene red bed clastic rocks with volcanic and evaporitic intercalations complete the local extension-dominated geological history. As is the case for the Au skarns, the Yangzte River Valley skarns are also related to phases of Yanshanian magmatism, dominated by I-type high K-calc-alkaline granitic rocks (gabbro, diorite, granodiorite), Na-rich calc-alkaline dioritic intrusions and A-type granites (Mao et al. 2006 and references therein). This magmatism in the region mainly developed in two stages, at 160–135 Ma with I-type intrusions and a later phase at about 120 Ma dominantly with A-type granites. These intrusions were emplaced during stages of extension and upwellings of asthenospheric material, which resulted in the emplacement first of the I-type and later A-type granites. These intruded into above-mentioned thick carbonate sucessions of various ages, resulting in the widespread formation of skarn systems.

Pan and Dong (1999) noted an apparent increase in alkalinity eastward, because large calc-alkaline granitic intrusions (Edong, Jiurui, Anqing-Guichi and Tongling) give way to sub-alkaline to alkaline volcanic and sub-volcanic complexes (Luzhong, Ningwu, Ningzhen) (Fig. 4.16), probably reflecting different levels of exposure. Chen et al. (2007) reviewed 70 skarn deposits from across mainland China, which account for about 20 % of the gold resources. Table 4.5 presents a list of China's major skarn deposits, including those of the Yangtze River Valley.

Skarns are rocks dominated by calc-silicate minerals formed by replacement of carbonate lithologies either during regional metamorphism or by contact metasomatic processes related to igneous intrusions. The terminology and classification of skarns has been reviewed and refined by Meinert and co-workers in several of their works (see Meinert et al. 2000, 2005 and references therein). Skarn mineralogy and metal endownment can be quite complex, generally with Cu, Fe, S, Pb-Zn, Au, Ag and W being the more common metals. Gu et al. (2011), also make a distinction from classical skarn formed by contact metasomatism and considered what they called "magmatic skarn", in which skarn minerals can be formed by direct crystallisation from a low-viscosity water-rich magma. This magma may have been derived by differentiation and carbonate assimilation of a parental quartz monzodiorite magma.

Many porphyry stocks may be sited below stratovolcanoes, and the uppermost sectors of the porphyry intrusions are transitional upward to epithermal mineralisation and laterally to skarn deposits, where carbonate rocks are present. A general sequence of events of skarn genesis in a porphyry-related system is as follows (Pirajno 2009). Firstly, the intrusion of a pluton results in contact metamorphism of the carbonate wall rocks. This stage involves decarbonation and dehydration reactions

Table 4.5 List of major skarn deposits in China, see Fig. 4.15a for position of numbered deposits. (After Chen et al. 2007)

No	Deposit/County/ Province	Lat N/ Long E	Main commodity	Size	Total tons	Ore grade (first comm)	Ore minerals	Major alteration	Ore-related intrusion	Host rock
01	Jinping/Jinping/ Yunnan	22°52′56″ 103°00′06″	Cu, Mo, Au	S	0.67	0.20	Cpy, Py, Apy, St, Mo, Au, El, Sp, Bn, Mt	sk, si, srp, carb, chl, ser, agl	Diorite, granite porphyry	Carb shale
02	Laochang/Gejiu/ Yunnan	23°17′53″ 103°12′38″	Sn, Cu	M	5.0	0.8	Cas, Cpy, Py, Apy, Po, Mo	sk, si, srp, carb, chl, ser, agl	Granite porphyry	Carb
03	Dulong/Maguan/ Yunnan	22°59′22″ 104°29′30″	Sn, Zn, Au	S	0.72	0.18	Py, Po, Cpy, St, Cas, Bi, Bs, Mo, Sp, Apy, Bn, Gl, Au	sk, si, ka, carb, ser, ep, chl, agl		Carb shale
04	Qinjia/Debao/ Guangxi	23°10′48″ 106°39′31″	Cu, Sn, Au	S	4.3	0.50	Py, Po, Cpy, St, Cas, Bi, Bs, Mo, Sp, Apy, Bn, Gl, Au	sk, si, ka, carb, ser, ep, chl, agl	Granite porphyry	Carb shale
05	Liuhe/Hengxian/ Guangxi	22°53′10″ 109°17′34″	Au	S	>1.0	5.00	Py, Cpy, Bi, Bs, Mo, Sp, Apy, Gl, Au	sk, phy, ka, carb, ep, chl, agl		Carb shale
06	Fuzichong/Cenxi/ Guangxi	23°02′42″ 111°11′54″	Cu, Au, Pb, Zn	S	1.5	0.30	Py, Po, Cpy, Gl, Sp, Apy, Bn, Au	sk, phy, pp, carb, agl		Carb clast
07	Dabaoshan/Qujiang/ Guangdong	24°34′05″ 113°33′00″	Cu, Au, Pb, Zn	S	2.0	0.51	Py, Cpy, Gl, Sp, Apy, Po, Bn, Au	sk, phy, pp, carb, agl	Granite porphyry	Carb clast
08	Baoshan/Guiyang/ Hunan	25°44′44″ 112°42′00″	Pb, Au, Zn	M	6.8	0.80	Apy, Py, Sp, Gl, Cpy, Po, Au, El	sk, si, ser, chl, ep, agl, carb	Grano-diorite	Carb shale
09	Kangjiawan/ Changning/Hunan	26°32′44″ 112°36′00″	Au, Pb, Zn	L	34.0	3.65	Apy, Py, Gl, Sp, Cpy, Po, Au, El	sk, si, ser, chl, ep, agl, carb	Dacitic porphyry	Carb shale
10	Yagongtang/ Changning/Hunan	26°33′00″ 112°35′12″	Au, Pb, Ag	M	7.4	2.00	Apy, Py, Gl, Sp, Cpy, Po, Au, El, Ag	sk, si, ser, chl, ep, agl, carb	Grano-diorite	Carb shale
11	Tianpaishan/ Qianshan/Jiangxi	28°12′00″ 117°46′15″	Cu, Au	L	22.3	0.12	Cpy, Apy, Py, Bn, Tth, Sp, Gl	sk, si, ser, chl, ep, agl, carb,	Granite porphyry	Carb shale
12	Qibaoshan/Liuyang/ Hunan	28°17′27″ 113°56′15″	Cu, Pb, Au	L	32	<2.7	Apy, Py, Mt, Hm Gl, Sp, Cpy	sk, si, ser, chl, ep, agl, carb	Granite Porphyry	Carb clast
13	Cunqian/Gao'an/ Jiangxi	28°12′00″ 115°07′30″	Au, Cu	M	14.8	1.00	Cpy, Py, Mt, Apy, Bn, Tth Sp, Gl, Po, Au	sk, si, ser, chl, ep, agl, carb, fl	Grano-diorite	Carb shale

Table 4.5 (continued)

No	Deposit/County/ Province	Lat N/ Long E	Main commodity	Size	Total tons	Ore grade (first comm)	Ore minerals	Major alteration	Ore-related intrusion	Host rock
14	Chengmen-shan/ Jiujiang/Jiangxi	29°40′41″ 115°50′00″	Cu, Au	L	69.7	0.43	Py, Cpy, Sp, Gl, Po, Mt, Sd, Tth, Mo, Bn, Cc, Mr	sk, si, carb, chl, ep, agl	Grano-diorite porphyry	Carb shale
15	Wushan/Ruichang/ Jiangxi	29°45′49″ 115°39′00″	Cu, Au	L	67.1	0.5±	Py, Cpy, Mr, Sp, Gl, Cc, Sd, Tth, Bn, Apy, Mo, Mt	sk, si, carb, chl, ep, ser	Grano-diorite porphyry	Carb shale
16	Wujia/Ruichang/ Jiangxi	29°46′49″ 115°38′45″	Au	M	5.2	4.92	Py, Cpy, Hm, Sp, Gl, Cc, Tth, Bn, Apy, Mo, Mt	sk, si, ka, carb, chl, ep, ser	Grano-diorite porphyry	Carb shale
17	Jilongshan/Yangxin/ Hubei	29°48′00″ 115°25′00″	Au, Cu	L	30.0	4.04	Cpy, Py, Bn, Au, El, Gl, Sp, Mt, Hm, Mr, Rea, Orp, Tth, Mo, Cc, Po, Rds, Smi	sk, carb, si, chl, ep, ser, fl, phl, srp, agl	Grano-diorite porphyry	Carb shale
18	Fengshan-dong/Yangxin/ Hubei	29°48′33″ 115°26′53″	Cu, Au	M	16.1	0.38	Cpy, Bn, Mt, Py, Cc, Mo, Gl, Sp	sk, si, carb, cl, ep	Grano-diorite porphyry	Carb shale evap
19	Banshan/Yangxin/ Hubei	29°49′05″ 115°26′15″	Au, Cu	M	5.0	5.97	Cpy, Py, Mo, Bn, Cc, Tth, El, Au	sk, ka, si, ser, carb, chl	Grano-diorite porphyry	Carb shale evap
20	Lijiawan/Yangxin/ Hubei	29°51′16″ 115°25′00″	Cu, Au	M	5.62	0.82	Cpy, Py, Mo, Bn, Cc, Po, Gl, Sp, Hm, Tth, Pe, El, Wi	sk, alk, si, ser, carb, chl	Grano-diorite porphyry	Carb evap shale
21	Yinshan/Yangxin/ Hubei	29°54′33″ 115°12′30″	Pb, Zn, Au	S	3.4	0.40	Py, Apy, Cpy, Gl, Sp, Au, Ag, El	sk, si, ser, chl, ep, carb, srp	Grano-diorite porphyry	Carb evap shale
22	Fentou/Daye/ Hubei	29°59′30″ 115°00′05″	Au	S	1.75	9.54	Mt, Po, Py, Cpy, Hm, Sp, Au, El, Ag, Mr	sk, ka, si, chl, srp, carb, ser	Quartz diorite	Carb shale

Table 4.5 (continued)

No	Deposit/County/ Province	Lat N/ Long E	Main commodity	Size	Total tons	Ore grade (first comm)	Ore minerals	Major alteration	Ore-related intrusion	Host rock
23	Shitouzui/Daye/ Hubei	30°03′16″ 114°58′08″	Cu, Fe, Au	M	19	0.51	Cpy, Bn, Py, Mt, Hm, Ml, Cc, Cu, Mo, Sp, Sd, Au	sk, alk, carb, phl, si, srp, ep, chl	Granite porphyry	Carb shale
24	Dabaoshan/Daye/ Hubei	30°05′27″ 114°55′00″	Au	S	2.0	8.00	Cpy, Py, Mt, Hm, Gl, Sp, Mo, Bn, Au	sk, ka, carb, si, srp, ep, chl	Granite porphyry	Carb shale
25	Jiguanzui/Daye/ Hubei	30°06′00″ 114°54′23″	Au, Cu	L	42.5	3.80	Cpy, Py, Mt, Bn, Cc, Au, El, Ttd, Tb, Um, Bl	sk, ka, chl, srp, carb, si	Granite porphyry, diorite	Carb shale
26	Tonglushan/Daye/ Hubei	30°06′33″ 114°52′30″	Cu, Au, Fe	L	69	1.15	Cpy, Bn, Py, Mt, Hm, Ml, Cc, Cu, Mo, Sp, Mr, Sd	sk, alk, carb, phl, si, srp, ep, chl	Grano-diorite porphyry	Carb shale
27	Houtoushan/Daye/ Hubei	30°07′38″ 114°56′15″	Mo, Cu, Au	S	0.62	0.49	Cpy, Py, Mo, Ml, Mt, Cc, Cu, Gl, Sp, Sd	sk, ka, carb, phl, si, srp, ep, chl	Granite porphyry	Carb shale
28	Xiaojiapu/Huangshi/ Hubei	30°12′33″ 115°00′15″	Au	S	2.0	4.60	Cpy, Py, Mt, Hm, Ml, Cc, Cu, Mo, Sp, Sd, Bn, Au, El	sk, carb, si, srp, ep, chl	Granite porphyry	Carb shale
29	Xiangzikou/Ezhou/ Hubei	30°15′16″ 114°58′45″	FeS_2, Au	S	0.67	0.17	Cpy, Py, Mt, Hm, Ml, Cc, Cu, Mo, Sp, Sd, Bn, Au, El	sk, carb, si, srp, ep, chl	Granite porphyry	Carb shale
30	Tongkeng/Ezhou/ Hubei	30°16′22″ 114°57′30″	Cu, Fe, Au	S	0.64	0.22	Cpy, Py, Mt, Hm, Ml, Cc, Cu, Mo, Sp, Sd, Bn, Au, El	sk, carb, si, srp, ep, chl	Granite porphyry	Carb shale
31	Chensheng/Ezhou/ Hubei	30°17′27″ 114°52′30″	Cu, Fe, Au	S	1.2	0.37	Cpy, Py, Mt, Hm, Ml, Cc, Cu, Mo, Sp, Sd, Bn, Au, El	sk, carb, si, srp, ep, chl	Granite porphyry	Carb shale
32	Anqing/Huaining/ Anhui	30°34′17″ 116°57′30″	Cu, Au	M	7.4	0.16	Cpy, Py, Mt, Po, Bn, Tth, Mr, Gl, Ml, Sp, Au	sk, alk, carb, si, ser, ep, chl, agl	Diorite	Carb shale evap

Table 4.5 (continued)

No	Deposit/County/Province	Lat N/Long E	Main commodity	Size	Total tons	Ore grade (first comm)	Ore minerals	Major alteration	Ore-related intrusion	Host rock
33	Tongshan/Guichi/Anhui	30°52′30″ 117°17′09″	Cu, Au, Mo	M	6.3	0.48	Cpy, Py, Mt, Po, Au	sk, si, ep, srp, carb	Grano-diorite porphyry	Carb shale evap
34	Huangshilao/Tongling/Anhui	30°52′30″ 117°50′45″	Au, Cu	M	13.5	5.79	Cpy, Py, Mt, Po, Bn, Tth, Mr, Gl, Sp, Au	sk, alk, carb, si, ser, ep, chl	Diorite	Carb evap shale
35	Tongguan-shan/Tong-ling/Anhui	30°55′38″ 117°51′15″	Cu, Au	L	33.0	1.44	Py, Cpy, Mt, Po, Mo, Sp, Gl, Tth, Apy, Au	sk, si, chl, ep, srp, carb, ser	Quartz diorite	Carb shale evap
36	Mashan/Tongling/Anhui	30°54′47″ 117°52′11″	Au, Cu	L	32.8	6.45	Po, Cpy, Py, Apy, Sd, Au, El, Sp, Mr, Mt, Mo, Bi, Cub, Tb	sk, si, srp, carb, chl, ser, tal	Quartz diorite	Carb shale evap
37	Shizishan/Tongling/Anhui	30°55′40″ 117°53′08″	Cu, Au	L	46.3	0.30	Cpy, Py, Po, Mt, Apy, Sd, Sp, Gl, Mr, Cub, Au	sk, alk, si, srp, carb, ser, chl, ep	Quartz diorite	Carb evap shale
38	Baocun/Tongling/Anhui	30°55′40″ 117°55′25″	Au, Cu	M	5.0	7.00	Mt, Py, Po, Cpy, Bi, Bs, Mo, Sp, Apy, Bn, Gl, Au, El	sk, alk, si, carb, ser, ep, chl	Grano-diorite	Carb evap shale
39	Xinqiao-A/Tongling/Anhui	30°55′44″ 117°59′40″	Au, Cu, Fe, S	L	20.9	6.20	Py, Cpy, Apy, Mt, Gl, Sp, Po, Ttd, Wi, Bs, Bn, Tth, Au, El	sk, si, ser, carb, srp, ep, chl, ka	Quartz diorite	Carb evap volc
40	Xinqiao-B/Tongling/Anhui	30°55′44″ 118°00′00″	Fe, Au, Cu	SL	105	?	Bn, Tth, Ml, Tn, Hm, Gt, Ps, Py, Po, Cpy, Mt, Gl, Sp, Au	sk, si, ser, carb, srp, ep, chl, gp, agl	Quartz diorite	Carb evap volc
41	Fenghuang-shan/Tong-ling/Anhui	30°52′30″ 118°01′40″	Cu, Au	M	18.4	0.68	Cpy, Py, Mt, Po, Bn, Tth, Mr, Gl, Sp, Au	sk, alk, carb, si, ser, ep, chl	Grano-diorite porphyry	Carb evap shale

Table 4.5 (continued)

No	Deposit/County/ Province	Lat N/ Long E	Main commodity	Size	Total tons	Ore grade (first comm)	Ore minerals	Major alteration	Ore-related intrusion	Host rock
42	Longqiao	31°46′04″ 117°27.941	Fe	M	100	44.4	Mt, Py, Cpy	ka, phl	Syenite	Carb
43	Tongjing/Jiangning/ Jiangsu	31°07.606″ 11°35′00″	Au, Cu	M	5.5	1.97	Mt, Py, Cpy, Bn, Au, Apy, Mr, Hm, Gl, Sp	sk, ka, na, srp, si, ser, chl, agl	Syenite diatreme	Carb shale
44	Funiushan/Jiangning/ Jiangsu	32°06′00″ 119°02′45″	Cu, Au, Fe	M	9.3	0.85	Mt, Py, Cpy, Bn, Au, Apy, Mr, Hm, Gl, Sp	sk, ka, na, srp, si, ser, chl, agl	Grano-diorite porphyry	Carb shale evap
45	Qixiashan/Nanjing/ Jiangsu	32°10′43″ 118°56′15″	Pb, Zn, Au, Ag	L	28.4	0.95	Gl, Sp, Py, Cpy, Apy, Ps Rds, Mr, Tth, Po, Arg, Bn	si, sk, carb, chl, ep, fl, srp, sf	Diorite	Carb shale evap
46	Langyeshan/Chuxian/ Anhui	32°17′09″ 118°17′30″	Cu, Au	M	8.29	0.66	Py, Cpy, Bn, Apy, Mt, Au, Hm, Gl, Sp	sk, ka, srp, si, ser, chl, agl	Grano-diorite	Carb evap shale
47	Qianchang/Suixi/ Anhui	33°41′49″ 116°52′10″	Fe, Au, Cu	L	23.4	2.38	Mt, Py, Cpy, Bn, Au, Bi, Apy, El, Ku, Mr, Po, Hm, Crk, Ld, Um, Ln	sk, ka, srp, si, ser, chl, agl	Quartz diorite-granite porphyry	Carb shale evap
48	Guilaizhuang/Pingyi/ Shandong	35°22′55″ 117°46′40″	Au	L	>20.0	4.00	Py, Mt, Cpy, Gl, Sp, Apy, Bn, Sd, Cu	sk, si, carb, ka, ser, ep, chl, agl	Granite-syenite porphyry	Carb shale
49	Yinan/Shandong	35°38′11″ 118°26′40″	Au	M	6.8	12.5	Py, Mt, Cpy, Bn, Bi, Cu	sk, si, carb, ka, ser, ep, chl	Diorite-granite porphyry	Carb shale
50	Wangbaoshan/ Wafangdian/ Liaoning	39°40′22″ 122°43′04″	Au, Pb, Zn	S	2.8	2.37	Cpy, Mt, Po, Py, Mo, Au, Bn, Tth, Ml	sk, alk, si, ser, chl, ep, carb, agl	Rhyolitic porphyry	Carb evap shale
51	Huatong/Wafangdian/ Liaoning	40°02′11″ 122°54′21″	Cu, Au	M	>5	3.00	Cpy, Mt, Po, Py, Mo, Au, Bn, Tth, Ml	sk, alk, si, ser, chl, ep, carb, agl	Granite	Carb evap shale

Table 4.5 (continued)

No	Deposit/County/ Province	Lat N/ Long E	Main commodity	Size	Total tons	Ore grade (first comm)	Ore minerals	Major alteration	Ore-related intrusion	Host rock
52	Yinjiagou/Lingbao/ Henan	34°12′03″ 110°48′27″	Au, Fe, S, Mo	M	7.5	13.5	Py, Gl, Sp, Mt, Cpy, Apy, Mo, Bn, Au	sk, ka, si, carb, ser, ep, chl, agl	Granite porphyry	Carb shale
53	Fenghuangzui/Pinglu/ Shanxi	34°45′ 111°10′	Au, Fe	S		>1.0	Py, Mt, Cpy, Gl, Sp	sk, alk, agl, chl, ep, ser	Diorite	Clast carb
54	Sijiawan/Xiangfen/ Shanxi	35°51′16″ 111°40′00″	Au, Cu	S	3.2	2.86	Py, Mt, Cpy, Gl, Sp	sk, alk, agl, chl, ep, ser.	Mon-zonite porphyry	Carb clast
55	Diaoquan/Lingqiu/ Shanxi	39°25′ 114°14′	Cu, Au	S	4.9	0.62	Cpy, Mt, Po, Py, Mr, Mo, Tn, Au, Bn, Ml, Tth	sk, alk, si, ser, chl, ep, carb, agl	Granite porphyry	Carb shale
56	Tainashui/Lingqiu/ Shanxi	39°37′05″ 114°12′42″	Au, Fe	S	2.8	7.45	Py, Mt, Cpy, Gl, Sp	sk, alk, agl, chl, ep, ser	Dacitic porphyry	Carb shale
57	Shouwangfen/ Chengde/Hebei	40°45′ 118°30′	Cu, Mo, Au	S			Cpy, Mt, Po, Py, Mr, Mo, Tn, Bn, Ml, Tth	sk, ka, si, ser, chl, ep, carb, agl	Grano-diorite	Carb shale
58	Lanjia/Shuangyang/ Jilin	43°30′ 126°10′	Fe, Au, Cu	M	18.5	11.0	Py, Mt, Cpy, Gl, Sp, Au, El	sk, ka, si, chl, ep, ser, agl, carb	Granite, granitic porphyry	Carb
59	Laozhashan/Qitaihe/ Heilongjiang	46°09′32″ 131°27′16″	Au, Cu	L	20.4	7.38	Py, Mt, Cpy, Gl, Sp, Mo, Bn, Tth, Au, El	sk, ka, agl, si, chl, ep, ser, carb	Diorite porphyry	Carb evap shale
60	Chaobuleng/ Dongwuqi/ Inner Mongol	46°28′47″ 118°40′00″	Zn, Fe, Bi, Au	S	>1.7	0.25	Py, Sp, Mt, Cpy, Hm, Gl, Mo, Au, Bn	sk, ka, si, chl, ep, ser, carb, agl, fl	Mon-zonite porphyry	Carb shale
61	Sankuanggou/ Nenjiang/ Heilongjiang	50°20′37″ 125°33′40″	Cu, Au	S	1.4	0.39	Py, Mt, Cpy, Gl, Sp	sk, alk, agl, chl, ep, ser	Grano-diorite	Carb shale
62	Heihushan/Anxi/ Gansu	42°20′ 96°50′	Au, Cu, Ag	S			Py, Mt, Cpy, Hm, Gl	sk, ser, chl, carb, si		Carb vols
63	Liujiaquan/Hami/ Xinjiang	41°50′ 92°20′	Au, Fe	S	1.5		Py, Mt, Cpy, Hm, Gl	sk, ser, chl, carb, si	Syenite porphyry	Carb

Table 4.5 (continued)

No	Deposit/County/ Province	Lat N/ Long E	Main commodity	Size	Total tons	Ore grade (first comm)	Ore minerals	Major alteration	Ore-related intrusion	Host rock
64	Ashale/Nileke/ Xinjiang	44°11′00″ 82°50′54″	Au, Cu	M	11	5.5	Py, Cpy, Mt, Gl, Sp, Hm, Au, El, Ml, Bn, Tth, Cc, Az, Cv	sk, si, ep, chl, ser, ka, carb, agl	Biotite granite	Carb shale
65	Qiaoxiahala/Fuyun/ Xinjiang	46°50′53″ 89°42′47″	Au, Cu, Fe			0.35–2.40	Mt, Py, Hm, Spe, Cpy, Bn, Cv, Az, Ml, Cc, Au	sk, ep., chl, carb, ka, si	Quartz Diorite porphyry	Carbclast volc
66	Baxi (Axi)/Ruoergai/ Sichuan	33°43′30″ 103°05′00″	Au	M	6.4	4.0	Py, Apy, Cpy, Gl, Sp, Stb	sk, si, ser, ep, chl, agl	Quartz diorite porphyry	Carb shale
67	Deerni/Maqin/ Qinghai	34°23′42″ 100°07′51″	Cu, Au, Co	L	29.3	0.53	Py, Po, Cpy, Sp, Mt, Mo, Au, Rt	sk, carb, mg, si, chl, ep, ser, fl	Biotite granite	Carb shale
68	Saishitang/Xinghai/ Qinghai	35°18′11″ 99°50′14″	Cu, Au	M	17.1	0.31	Py, Mt, Hm, Ml, Cpy, Bn, Tth, Gl, Sp	sk, si, ka, chl, ep, ser, carb	Biotite granite	Carb shale
69	Yemaquan/Golmd/ Qinghai	37°00′00″ 91°58′41″	Cu, Au	S			Py, Mt, Hm, Ml, Cpy, Bn, Tth, Gl, Sp	sk, si, ka, chl, ep, ser, carb	Grano-diorite	Carb shale
70	Kendekeke/Golmd/ Qinghai	37°01′08″ 91°46′15″	Au, Co, Bi, Cu	L	31.2	1.5–38.2	Py, Apy, Bs, Tb, Mt, Cpy, Ml, Tth, Gl, Sp	sk, si, ser, carb, chl, ep, ka	Mon-zonite porphyry	Carb chert shale
71	Yulong/Jamda/ Tibet	31°37′33″ 97°47′44″	Cu, Au	L	28.6	0.17	Cpy, Mo, Py, Tth, Sph, Bn, Gl, Cub, Au	sk, agl, ka, pp, phl, ep, carb, chl	Granite porphyry	Carb clast

Size abbreviations: S small (<5 t Au); *M* medium (5–20 t Au); *L* large (20–100 t Au); *SL* super-large (>100 t Au).
Ore mineral: Ag native silver; *Apy* arsenopyrite; *Au* native gold; *Az* azurite; *Bi* Native bismuth; *Bl* bellidoite; *Bn* bornite; *Bs* bismuthinite; *Cas* cassiterite; *Cc* chalcocite; *Cpy* Chalcopyrite; *Crk* crookesite; *Cu* native copper; *Cub* cubanite; *Cv* covellite; *El* electrum; *Gl* galena; *Gt* goethite; *Hm* hematite; *Ku* kusttelite; *Ld* ludwigite; *Ln* linnaeite; *Ml* malachite; *Mo* molybdenite; *Mr* marcasite; *Mt* magnetite; *Orp* orpiment; *Pe* petzite; *Po* pyrrhotite; *Ps* psilomelane; *Py* pyrite; *Py-c* colloidal pyrite; *Rds* rhodochrosite; *Rea* realgar; *Rt* rutile; *Sd* siderite; *Smi* smithsonite; *Sp* sphalerite; *Spe* specularite; *St* stannite; *Stb* Stibnite; *Tb* tellurbismuthite; *Tn* tenorite; *Ttd* tetradymite; *Tth* tetrahedrite; *Um* umangite; *Wi* wittichenite.
Alteration: agl argillic; *alk* alkali alteration; *carb* carbonatisation; *chl* chloritic; *ep* epidotisation; *fl* fluoritic; *gp* gypsum; *ka* K-alteration; *mg* magnesite; *na* Na-alteration; *phl* phlogopitic; *phy* phyllic alteration; *pp* propylitic; *ser* sericitic; *si* silicification; *sk* skarn; *srp* serpentinisation; *tal* talc alteration.

to form diopside and wollastonite skarns. The timing of this stage would correspond with the crystallisation of the pluton's margins following the intrusion of the melt phase into the sedimentary lithologies. The temperature range is from 900 to 500 °C. Fluids, which are released from the partially solidified intrusion, infiltrate into and along fractures of pluton and country rocks. This is the stage of potassic alteration and disseminated chalcopyrite mineralisation in the plutonic rocks. This stage corresponds to the movement of the fluids outward into the structural breaks of the country rocks (fractures, contacts, permeable horizons) to form early skarn facies generally comprising andradite, magnetite and sulphides. The temperature range is from approximately 600–400 °C.

The Yangtze River Valley metallogenic belt comprises more than 200 mineral deposits that can be grouped into seven main clusters, which from west to east include: Edong, Jiujiang_Ruichang (JiuRui), Anqing-Guichi, Tongling, Lujiang-Zongyang, Nanjing-Wuhu and Nanjing-Zhenjiang (Fig. 4.16). The mineral deposits of these clusters are found within Yanshanian granitic rocks as porphyry systems, as skarns along the contacts with carbonate rocks and as stratiform massive sulphides in Late Palaeozoic-Early Mesozoic sedimentary units, treated in Sect. 4.4.1.

The skarn systems of the Yangzte River Valley exhibit a range of ore styles, from disseminated to stratabound massive sulphides and magnetite. The Longgiao Fe deposit is a stratabound and stratiform magnetite skarn with a resource of approximately 100 Mt grading 44 % Fe (mine staff pers. comm. 2007). The ore zone extends for 2,200 m, is associated with a 131 Ma syenitic intrusion and consists of pyroxene-magnetite ± epidote ± calcite skarns and magnetite bands replacing a calcareous sandstone (personal field observations 2007). The Jiurui district (Figs. 4.5 and 4.16) contains 13 Cu-Mo and Au skarn deposits all associated with stocks and dykes of granodiorite porphyry, diorite, quartz-porphyry and monzogranite. The diorite and granodiorite porphyry have K-Ar ages of 135–205 Ma (early Yanshanian), whereas the quartz porphyries are younger with ages ranging from 120 to 98 Ma (Pan and Dong 1999). The ore systems in the Juirui district include porphyry, stratabound ores and skarns. The latter are developed at the contact between the intrusions and Carbonifeorus-Triassic carbonate successions. The skarn ores contain chalcopyrite, pyrite, marcasites, bornite, magnetite, molybdenite, chalcocite, native Au, galena and sphalerite. The skarn rocks exhibit a well-developed zonation from endoskarn in the causative intrusion to exoskarns with andradite garnet, diopside, actinolite-tremolite, wollastonite, calcite, epidote, talc and serpentine and silicified marble outward from the intrusion. In the Anqing-Guichi Cu-Fe-Au-Mo district (Fig. 4.16) are small stocks of diorite, granodiorite and alkali-rich granite with K-Ar ages ranging from 118 to 138 Ma (Pan and Dong 1999). Here the main deposits are stratabound massive sulphides hosted in Carboniferous carbonate rocks. The Tongling Cu-Au district contains 45 deposits. One of these is the interesting ore system at Dongguashan, where skarn-hosted magnetite and sulphides (pyrite + chalcopyrite + pyrrhotite) almost entirely surround and cap a dioritic cupola. These skarns formed in Carboniferous and Devonian dolomites and limestones, which along the Carboniferous-Devonian boundary developed retrograde wriggly-type skarns (Mao pers. comm. 2007; Fig. 4.17). An alternative view is that a

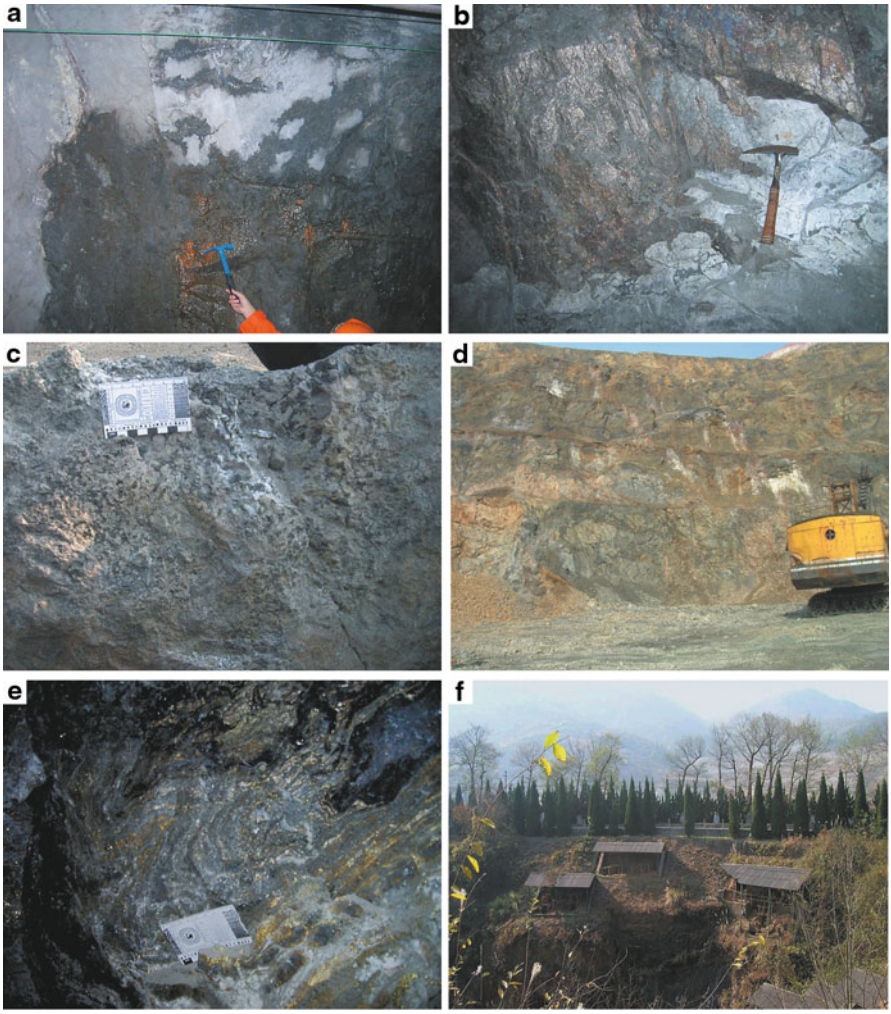

Fig. 4.17 **a** Longqiao Fe mine, underground (Level—370 m) exposure, of limestone and massive magnetite ore (dark material); **b** Dongguashan Cu mine, marble breccia and massive sulphide ore; **c** apatite and magnetite ore at Washan open pit mine (Kiruna-type Fe deposit); **d** breccia zone (possibly a very large breccia pipe); **e** Dongguanshan Cu Mine, contorted sulphide ore, possibly a "wrigglite" skarn in the terminology of Kwak and Askins (1981), or folded sulphide bands of a SEDEX-style massive sulphides (see Table 4.4); **f** ancient mining (ca. 3,000 years BP) in the Yangtze River Valley in the Feng Huang Shan Cu mine area

pre-existing sediment-hosted massive sulphides, were overprinted by a skarn system, related to the intrusion of granites in the Yanshanian period (Gu et al. 2007).

The Ningwu Fe ore district occurs along northeast and northeast-trending volcano-sedimentary basin structures. Volcanic and sub-volcanic rocks are present and consist of alkaline basalt, andesite, trachytes, dacite and phonolite, gabbro-diorite, gabbro,

Table 4.6 Selected fluid inclusion data of Yangtze River Valley deposits. (After Gu et al. 2011)

Deposit	Mineral	Th range (°C)	Th avg (°C)	Salinity wt % (NaCl eq)
Shizishan Cu breccia pipe skarn	Garnet	467–422 (V); 472–443 (L)		45.1–38 (V); 10.7–10.2 (L)
Ditto	Calcite	439–337 (L)	390	30–3
Ditto	Quartz	336–158 (L)	265	40.4–2.1
Shaxi porphyry Cu	Quartz	520–460 (L)	460	58–52
Ditto	Quartz	420–280 (L)	370	52–41
Ditto	Late stage quartz	260–110 (D)	170	24–8
Tongniujing Cu-Au vein	Quartz	450–300 (L)		48–30

Homogenistation temperature (Th); vapour-rich (V); liquid-rich (L); daughter-bearing (D)

diorite, monzonite all with well developed porphyritic textures and with K-Ar ages ranging from 137 to 90 Ma (Pan and Dong 1999). The Ningwu Fe district has recently attracted considerable attention (Yan et al. 2009; Hou et al. 2011; Yu et al. 2011). The Fe ores are sited in the middle to upper parts of sub-volcanic gabbro-diorite intrusions and the skarn ores consist of massive, banded and brecciated to disseminated magnetite, siderite, hematite, pholgopite, actinolite, apatite, albite, chlorite, quartz and carbonate. Other Fe ores (magnetite-hematite) are located in fractures and faults in the aureoles of the intrusions. Hydrothermal alteration is extensive and mainly represented by scapolite and albite. Alteration zoning is characterised by albite-pyroxene-sericite-pyrite-titanite in the lower parts of the subvolcanic intrusion to a middle zone of diopside-garnet-apatite-scapolite-magnetite to an upper zone of argillic and propylitic alteration. The Fe skarns are lenticular and located at the contact between the sub-vocanic intrusions and Triassic calcareous shale and gypsum-bearing carbonates.

Pan and Dong (1999) compiled an extensive dataset of stable isotope analyses (S, O, C). Sulphur isotopic compositions show $\delta^{34}S$ values of −0.9–8.7 ‰ in sulphides from the Yanshanian intrusive rocks and from −1.0 to 8 ‰ in sulphides from the skarn ores, indistinguishable from the host intrusions and indicating a dominantly magmatic sulphur in the orebodies. The $\delta^{34}S$ values of pyrite from individual deposits show systematic variations from proximal (2.3–4.1 ‰) to distal (9.9 ‰) skarns and up to 16 ‰ in the stratabound massive sulphide ores. Strongly negative $\delta^{34}S$ values (−35 to −15 ‰) are recorded from the Mesozoic sedimentary rocks. Thermometric measurements on fluid inclusions from a number of porphyry and skarn deposits, conducted by Gu et al. (2011) show a range of homogenisation temperatures and salinities of vapour- and liquid-rich inclusion fluids, largely indicative of a magmatic source (Table 4.6).

In the sections ahead I describe, what I would consider as key mineral systems, such as porphyry, porphyry-skarn and Kiruna-type, taken from recently published English-language literature (cited in the relevant sections). Some field and thin section aspects of skarn and Kiruna-style ore systems are presented in Figs. 4.17 and 4.18.

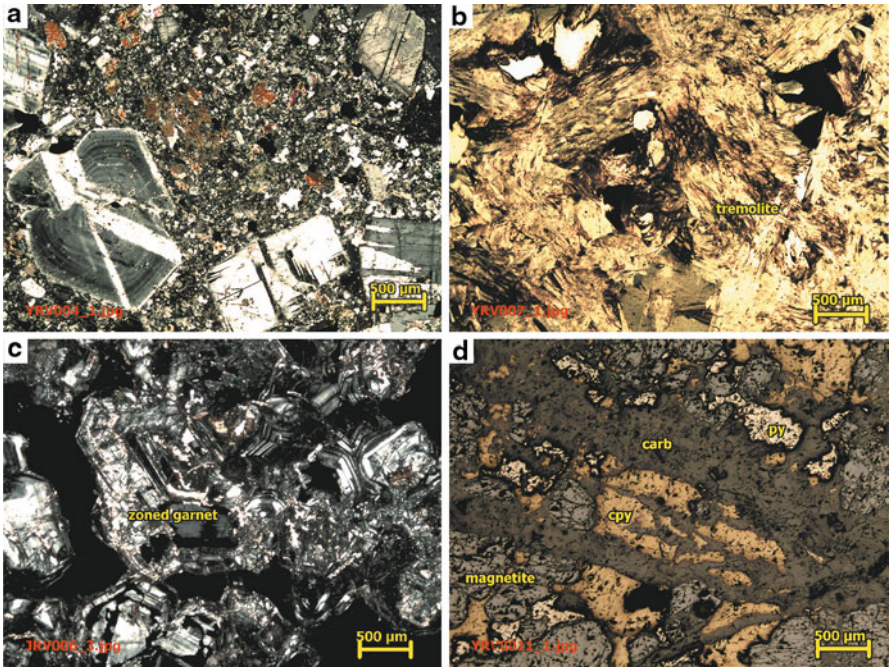

Fig. 4.18 Photomicrographs of samples from the Dongguanshan Cu mine; **a** dacite porphyry, crossed polars; **b** tremolite skarn, plane polarised light; **c** anisotropic, zoned garnet showing dodecahedral twinning, usually found in exocontact zones; Feng Huang Shen Cu mine; **d** magnetite-chalcopyrite ore, cut by late calcite veinlets, reflected light

4.4.5.1 Porphyry-skarn and Kiruna-style Mineral Systems

Yanshanian granitic intrusions in South China and the Yangzte Craton are widespread and commonly associated with mineral deposits (Fig. 4.19). Of these granitic rocks, Li et al. (2010b) considered two main series: a Yangtze River series represented by metalluminoaus granitic rocks (mainly granodiorite and diorite with geochemical affinities to continental adakitic rocks, formed by partial melting of thickened or delaminated lower crust), associated with Cu-Fe-Mo-Au-Pb-Zn mineral systems and a Nanling series, represented by evolved, peraluminous granites, associated with W-Sn-Mo-Bi-Be-Nb-Ta mineral systems. Age determinations of the granites in the Yangzte River Valley, range from 152 to 120 Ma, with peaks at 144–132 M and 128–123 Ma. Li et al. (2010b) carried out more age determinations on zircons (precise SIMS U-Pb) from diorites and granodiorites, yielding ages ranging from ca. 141 to ca. 146 Ma, showing two distinct magmatic events, one synchronous with mineralisation (ca. 140 Ma) and one of barren granites (ca. 145–146 Ma). Li et al. (2010b) referred to the possibility of a tectonic switch in eastern China at the Jurassic-Cretaceous boundary (Zhu et al. 2010) may have been coeval with a magmatic hiatus, marking a change from compressional to extensional tectonics in

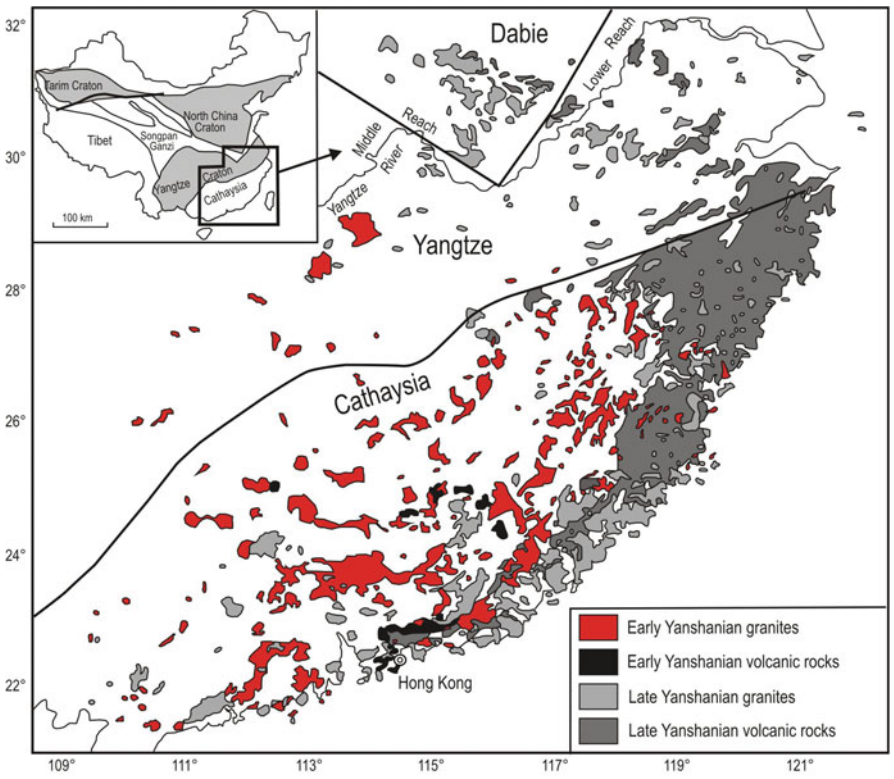

Fig. 4.19 Distribution of Jurassic–Cretaceous (Yanshanian) granitic and volcanic rocks in South China. (After Li 2010)

the Early Cretaceous, which would have caused granitic magmatism in the Yangtze River Valley and associated mineralisation.

In this section, I discuss a selection of porphyry, porphyry-skarn and skarn deposits associated with the granitic intrusions of the Yangtze River Valley metallogenic province. These deposits include: Tongshankou, Tonglushan, Longqiao, Yueshan and Zhonggu.

Tongshankou Porphyry-skarn Cu-Mo

The Tongshankou porphyry skarn Cu-Mo deposit is located in the Edong cluster (Fig. 4.16), more specifically in the Daye district, which also comprises numerous Fe, Fe-Cu-Au, Cu, W-Cu-Mo, Cu-Mo ore deposits. Li et al. (2008) described the Tongshankou deposit and the following is taken from their work.

The main lithologies of the Daye district comprise, from oldest to youngest, 1,000 m of Ordovician-Silurian impure limestone, calcareous mudstone, siltstone;

Devonian conglomerate and sandstone; Carboniferous limestone and dolomite, overlain by 600 m of Permian shale, chert, coal beds and limestone. These Palaeozoic rocks are deformed as a result of the collision between the North China and Yangtze Cratons in the Triassic. The Lower Triassic Daye Formation comprises up to 1,200 m thick limestone and dolomite, which locally host skarn mineral systems. Dioritic, granodioritic and granitic intrusions were emplaced in pre-Jurassic sedimentary rocks between 151 and 132 Ma with, as mentioned above, peak activity at 144–132 and 128–123 Ma. Continental volcanism occurred in the Early Cretaceous, during which time about 2,000 m of bimodal volcanic and pyroclastic rocks accumulated in a tift basin. The volcanic rocks include dacite, rhyolite, basalt mainly with a SHRIMP U-Pb age of ca. 128 Ma obtained from dacite.

The Tongshankou Cu-Mo deposit has resources of about 0.5 Mt Cu and 2,000 t of Mo and consists of porphyry and skarn ores, associated with the Tongshankou granodiorite of adakitic affinity, which intruded limestone and dolomite of the Daye Formation. Re-Os age determinations on molybdenite yielded ca. 144 Ma for the mineralising event. Part of the Tongshankou granodiorite are two small stocks, typically with a porphyritic textures and unusually abundant accessory minerals, such as magnetite, apatite and titanite. At least six orebodies are identified, all related to the same hydrothermal system activated by the granodioritic stocks, resulting in porphyry ore within the intrusion, skarn ore along the contact zones with carbonate rocks and, more distally from the causative intrusion, stratabound ore in the carbonate beds (Carlin-style?). The No. III porphyry Mo and Cu-Mo orebody has grades ranging from 0.4 to 0.6 % Cu and 0.02–0.07 % Mo. The mineralisation consists of stockworks, veinlets and disseminations of chalcopyrite and molybdenite with lesser quantities of bornite and tetrahedrite. The No. IV orebody is a skarn formed along the contacts between one of the granodiorite stocks (Shizishan) and Triassic carbonate beds. Grades were reported at greater than 1.2 % Cu. The No IV orebody is about 500 m long, 10–60 m thick and extends for 140 m down dip. The No. I orebody is also a skarn, is one of the largest in the Tongshankou ore system. This orebody is 2,100 m long, 10–80 m thick and 600 m in depth extension, with ore grades of up to 3.1 % Cu. Chalcopyrite is the main ore mineral, accompanied by minor amounts of pyrite, magnetite, bornite, sphalerite, tetrahedrite and molybdenite. Stratabound orebodies are usually small in size (80–300 m long and 5–16 m thick) and located along fracture zones developed between carbonate strata. The ore minerals are chalcopyrite, pyrite, marcasite, sphalerite, chalcocite and tetrahedrite.

Hydrothermal alteration is well developed around all these orebodies. Potassic and phyllic alteration are typically found in the porphyry mineralisation, with potassic alteration forming K-feldspar veins and envelopes around the stockwork zones. Biotite and magnetite are also present. The phyllic alteration (quartz-sericite-pyrite) is more extensive and is associated with veins and disseminated sulphides. Alteration associated with skarns is dependant on the composition of the carbonate rocks affected. Calcic skarns consist of garnet, scapolite and epidote, with two paragenetic stages of garnet formation. An early fine-grained garnet is associated with the mineralisation and a late stage garnet, generally further away from the contacts, is not associated with the mineralisation. Magnesian skarn is developed in dolomitic

rocks and consist of diopside, phlogopite, actinolite-tremolite and serpentine mainly. Here two paragenetic stages of phlogopite are recognised: an early stage represented by fine-grained aggregates and small veins, associated with magnetite, hematite and chalcopyrite; a late stage phlogopite is massive and coarse-grained and lacking mineralisation.

Age determinations carried out by Li et al. (2008) included Re-Os on molybdenite and Ar-Ar on phlogopite, yielding 143.8 ± 2.6 Ma and 143.0 ± 0.3 Ma, respectively. These data demonstrated that the porphyry and skarn mineralisation were contemporaneous and related to the granodiorite stocks. Sr-Nd-Hf isotope systematics, also by Li et al. (2010a), in conjunction with the lack of inherited zircons, led these authors to the conclusion that the Tongshankou granodiorite was derived from partial melting of an enriched lithospheric mantle and not from partial melting of the lower crust or other basement rocks. Furthermore and as mentioned previously, the granodiorite has geochemical features similar to adakite (enriched in Sr and LREE, low in Y, Yb, Sc, no Eu anomalies and high La/Yb and SR/Y ratios). The Tongshankou adakitic rocks are potassic with unusually high K_2O abundances (3.3–5.8 %), which would indicate that their origin by partial melting of subcontinental lithospheric mantle, modified by slab-derived fluids (Li et al. 2010a).

Tonglushan Cu-Fe-Au Skarn Deposit

The Tonglushan Cu-Fe-Au skarn deposit is located in the central part of the Edong cluster (Fig. 4.15) and one of the largest in the area, endowed with 1.1 Mt of Cu metal, 60 Mt of Fe and 70 t of Au in 12 orebodies (Li et al. 2010b). The mineralisation is in the northwestern margin of the Yangxin granite pluton and its quartz diorite and quartz monzodiorite components, intruded into the Daye Formation carbonate rocks. In addition, lamprophyre, andesitic porphyry and albitite dykes are present, with the latter cutting through the Yangxin pluton. The orebodies are generally lenticular in shape and occur along the contact zones in limestone and in carbonate xenoilts within the quartz monzodiorite porphyry (Pan and Dong 1999). The ca. 138 Ma Yangxin pluton is about 240 km^2 in areal extent and the largest in the Edong district, surrounded by haloes of contact metasomatism, with carbonate, potassic, siliceous and greisen alteration. Recent geochronology on zircon (SHRIMP U-Pb), molybdenite (Re-Os), phlogopite (Ar-Ar) and titanite (ICP-MS U-The-Pb) indicate that the host granites and the skarn mineralisation formed between 140 and 136 Ma (Xie et al. 2011; Li et al. 2010a).

The Tonglushan skarn orebodies trend northeast and are approximately 2,100 m long and up to 600 m wide. Recent discoveries have revealed the presence of north-northwest-trending breccia type ores (Xie et al. 2011). The ore minerals are chalcopyrite, magnetite, bornite, hematite, with minor quantities of chalcocite, cuprite, molybdenite, sphalerite, tetrahedrite, marcasite and native gold and electrum. In the oxidised environment, minerals such as malachite, azurite, goethite are present. Gangue and skarn minerals include calcite, dolomite, quartz, diopside, garnet, phlogopite. wollastonite, tremolite-actinolite and kaolinite. As in other skarn

deposits in the region (e.g. Tongshuankou), calcic and magnesian skarns occur depending on the composition of the carbonate rocks (limestone or dolomite). Here too, two types of garnets represent two stages in the mineralising system: the older coarser garnet (grossular and andradite-grossular), accompanied by abundant phlogopite and diopside is associated with magnetite and chalcopyrite, whereas the younger garnet forming veins, but not associated with ore minerals. Fluid inclusion data reported in Xie et al. (2011), suggest four stages of mineralisation: (1) skarn stage with homogenisation temperatures ranging from 740 to 426 °C; (2) magnetite stage with temperatures from 506 to 340 °C; (3) quartz-sulphide from 360 to 240 °C; and (4) carbonate stage from 250 to 150 °C.

The Tonglushan deposit is characterized by massive exoskarn that typically consists of an early prograde and a late retrograde skarn assemblages. The prograde skarn assemblage consists of andradite, grossular, diopside, hedenbergite, and scapolite, whereas the retrograde assemblage consists of epidote, actinolite, pargasite, phlogopite, chlorite, fluorite, and quartz. These assemblages are overprinted by disseminations of calcite, serpentine, and pyrite. Calcite-dominated and phlogopite monomineralic veins locally cross-cut the skarn and associated ores. On the basis of their geochronological work, Li et al. (2010a) recognised two magmatic pulses and hydrothermal events in Tonglushan. These authors dated titanite (ICP-MS, U-The-Pb) from an albitite dyke that cross-cuts the Yangxin pluton, giving an age of 120.6 ± 2.3 Ma, thereby indicating a second magmatic pulse. Similarly, calcite-hosted hydrothermal titanite, formed during carbonate veining, gave an age of 120.9 ± 1.9 Ma, which is indistinguishable from that of the albitite and close to the 117 Ma Ar-Ar age of a phlogopite vein. Thus, the Tonglushan skarn mineralisation, associated with the Yangxin pluton, was formed in a 140–136 Ma magmatic and hydrothermal event, whereas the second event at ca. 121 Ma post-dates the main skarn system, but is almost coeval with the Kiruna-style magnetite-apatite (Fe-P) mineral deposits (see below).

Longqiao Fe Skarn Mineral System

Stratiform and/or stratabound magnetite skarn and vein type deposits are located in the Luzhong (also spelt Luzong or Lu-zong) Basin (Luzhong cluster; Fig. 4.16), containing approximately 100 Mt of ore, grading 44.4 % Fe (mine geologists and Zhou pers. comm. 2007). The Luzhong volcano-sedimentary basin has a basement of Silurian to Permian sedimentary rocks comprising conglomerate, sandstone, siltstone, greywacke, shale, limestone and dolomite. Permian coal beds are intercalated with shale, sandstone and siltstone. Volcanic rocks are of Early Cretaceous age (see also Section "Zhonggu Ore Field; Kiruna-style Fe Mineral Systems") that overlie continental Jurassic and Triassic limestone, dolomite, shale and sandstone strata. The volcanic rocks are lithostratigraphically assembled into four groups: Longmenyuan, Zhuanqiao, Shuangmiao and Fushan, each representing an eruptive cycle that began with explosive activity, followed by the eruption of trachytic, trachybasaltic and andesitic lavas and related volcaniclastics, resulting in a total accumulation of

more than 2,500 m thick. Geophysical and satellite imagery reveal the presence of ring structures, which can be interpreted as calderas or anorogenic ring complexes associated with the basin's volcanic activity. Each of the volcanic cycle was accompanied by diorite, monzonite and syenite intrusions through the basement and overlying sedimentary and volcanic rocks. This intrusive activity took place during mid- to late-Yanshanian (135–128 Ma). Geochemical and isotope systematics carried out on apatites of the Luzhong volcanic rocks by Tang et al. (2012) have been interpreted to indicate that these volcanic rocks were generated by Yanshanian partial melting of a lithospheric mantle that contained fragments of Neoproterozoic subduced slabs.

Economically significant skarn Fe deposits in the basin include Longqiao, discussed below, Luohe, Nihe and Xiaoling. Other mineral systems in the cluster are the Yueshan polymetallic deposit and Cu-Au vein deposits (see below), as well as sandstone-hosted U occurrences (Dahlkamp 2009).

The Longqiao stratiform Fe orebody is hosted in laminated calcareous sandstone and consists of several bands or layers. The ore-bearing sedimentary layers lie above a 131 Ma syenite intrusion, with which they are temporally and genetically related (see below). The ores consist of magnetite and pyrite with lesser quantities of chalcopyrite, surrounded by zones of phlogopitic alteration (Fig. 4.17). The magnetite has low contents of V and Ti (about 100s of ppm; Zhang et al. 2008). Fluid inclusion studies by Zhang et al. (2008), revealed two peaks of homogenisation temperatures, 390–360 and 450–410 °C. It is of interest to note that above the ore-hosting strata, in the Luzhong Basin, are continental basaltic rocks, exhibiting strong epidote alteration and containing chalcopyrite in the amygdaloidal tops of lava flows (pers. field observation 2007).

Zhou et al. (2011) worked on stable isotopic systematics (C-O-D- and S) and K-Ar dating on the host rocks and ores of Longqiao Fe deposit. The stratiform and stratabound orebody, hosted in siltstone and carbonate rocks of the Dongma'anshan Formation and to a lesser degree in trachyandesite porphyry of the Longmenyuan Formation, is from 20 to 40 m thick and up to 400 m long. The Triassic Dongma'anshan Formation consists of evaporites and carbonates beds, with the main minerals comprising calcite, ankerite, gypsum (anhydrite), siderite, quartz, hematite and pyrite. The siderite has a lamellar texture locally constituting lamellar sideritic ore. These lamellar ores are enclosed, penetrated and replaced by massive magnetite. The laminated structure is characterized by black bands alternating with white bands. The width of the bands ranges from 5 to 30 mm. The white bands are composed of siderite, magnetite, quartz, pyrite, diopside and phlogopite. Dark bands are composed of magnetite with residual siderite grains.

Magnetite is by far the main ore mineral, locally with relic siderite bands, Cu, Pb and Zn sulphides. The causative syenite intrusion, just below the orebody, exhibits potassic, chloritic and magnetite alteration. The magnetite ore is massive, disseminated and in places laminated, locally with brecciated textures. The ore has a range of textures, from granular to xenomorphic-granular, to skeletal, to poilkilitic. Magnetite tends to replace skarn minerals and is in turn replaced by pyrite and chalcopyrite. Skarn (wall rock) alteration minerals are diopside, garnet, K-feldspar,

phlogopite, chlorite, quartz, anhydrite, tremolite-actinolite, tourmaline, pyrite and kaolinite. Skarn alteration is developed both in volcanic rocks and in the sedimentary rocks. Zones of skarn alteration that have been recognised, from top (lower temperature and late) to bottom (higher temperature and early, are): (1) hydromica-quartz-kaolinite; (2) K-feldspar-kaolinite-chlorite; (3) K-feldspar-tourmaline; (4) K-feldspar-diopside-chlorite; (5) thermally metamorphosed wall rocks (hornfels and marble). The paragenetic sequence of the skarn-magnetite mineralisation comprise four stages: (1) skarn with diopside-garnet-tourmaline-K-feldspar ± magnetite; (2) magnetite with K-feldspar-phlogopite-tourmaline-talc-serpentine-actinolite-epidote; (3) sulphide stage with pyrite-chalcopyrite-galena-sphalerite-anhydrite; and (4) carbonate-oxide stage with siderite-ankerite-calcite-hydromica-hematite-kaolinite. Sulphur isotopic compositions of pyrite from Longqiao show values $\delta^{34}S$ ranging from 15.5 to 7.9 ‰ (avg 11.5 ‰), higher than the syenite (6.25 ‰) and lower than anhydrite in the orebody (24.4 ‰). Zhou et al. (2011) concluded the S from the Longqiao deposit is a probably a mixture of magmatic and sedimentary sulphur from the Triassic evaporite-bearing layers. Ar-Ar dating of phlogopite yielded and isochron age of ca. 132 Ma, which is slightly later than the ca. 131 Ma U-Pb zircon age of the syenite, but both falling within the age span of the volcanic cycles in the Luzhong Basin and corresponding to a trend of extensional tectonic regime.

On the basis of their isotopic and age determinations, the geometry of the deposit is controlled by the sedimentary beds of Middle Triassic Dongma'anshan Formation (Zhou et al. 2011). The laminar siderite occurs at the margins of the orebody, or is found as remnant enclaves within the massive magnetite ore. Geological and electron microprobe data of siderite samples confirm that the siderite is of sedimentary (evaporite) origin. Late hydrothermal fluids replaced part of the sedimentary siderite and deposited magnetite. The skarn ore was formed by contact metasomatism, between a syenitic intrusion and wall rock carbonate rocks. The Longqiao iron deposit consists of sedimentary siderite (lamellar ore), derived from evaporitic beds, later overprinted or replaced by magnetite, associated with skarn-type metasomatic processes, related to the emplacement of a syenite pluton. This model is well supported by radiogenic and stable isotopes systematic, as presented in the preceding pages. The ore-forming age of the Longqiao iron deposit is 130.5 ± 1.1 Ma and the age of the Longqiao syenite beneath the orebody and intruded into the Dongma'anshan Formation is 131.1 ± 1.5 Ma. Thus the age of the mineralisation is nearly coincident with the age of the Longqiao syenite intrusion, implying that the formation of the Longqiao iron ore is temporally and genetically associated with the intrusion and that the ore-forming hydrothermal fluids were exsolved from cooling of the magma. The interaction of hydrothermal fluids with Triassic carbonate-evaporite beds must have played a major role in the genesis of the Longqiao iron deposit. The hydrothermal fluid-rock interaction between siderite and the hematite-bearing, evaporite-bearing or calcareous beds influenced the evolution of the ore-forming hydrothermal system and provided part of the ore metals for the iron deposit. The evaporite layers are especially reactive when interacting with magmatic-hydrothermal fluids, thereby becoming a good host for the deposition of magnetite, ultimately resulting in the formation of stratabound and stratiform orebodies.

Cu-Au Deposits in the Yueshan District

Several polymetallic skarn and vein type deposits occur in the Yueshan district (Anqing cluster; Fig. 4.16), generally concentrated around the ca. 138 Ma Yueshan diorite intrusion. Deposits in the Yueshan district total a resource of 400,000 t of Cu metal with grades greater than 2 % and 10 t of Au metal, with grades ranging from 0.2 to 2.0 g/t (Table 4.1). An English language publication on the mineral deposits of this district is by Zhou et al. (2007), which is perused in the overview that follows. In addition, the interested reader is also referred to a paper by Liu et al. (2012) who carried out 3D computer modelling of the Yueshan intrusion to reconstruct the controlling mechamisms for the formation of the ore zones at the contact of the intrusion with carbonate rocks. These authors concluded that the ore zones tend to be located in concave-shaped high dilation zones, where different fluids are focused. A similar conclusion was reached for other mineral deposits in the region (Anqing and Tongshan); Liu et al. (2010b).

In the Yueshan mineral district there are three main lithostratigraphic sequences. The ca. 1.9 Ga basement rocks included in the Dongling Formation, comprising feldspathic gneiss and plagioclase-amphibole schist. These are unconformably overlain by Cambrian to Triassic shallow-marine carbonate rocks, sandstone and shale, followed by Jurassic to Cretaceous continental clastic rocks, red beds and volcanic rocks. The most important host rocks hosting the Cu-Au deposits are dolomite and limestone of the Triassic Yueshan and Lanlinghu formations, overlain by sandstone of the Tongtoujian Formation. Major regional faults trend northeast and east-west and controlled the emplacement of I-type intermediate to mafic intrusions and associated mineralisation. The Yueshan diorite, Zongpu quartz-diorite and Wuhen monzodiorite have Ar-Ar and Rb-Sr ages ranging from ca. 136 to ca. 131 Ma; a U-Pb zircon age for the Yueshan diorite of ca. 138.7 Ma was reported by Zhang et al. (2008). As mentioned above, the Yueshan diorite hosts most of the orebodies in the district, but some deposits also occur associated with the other two intrusions. In the Yueshan district there are two types of Cu-Au mineral systems: (1) Cu-Au-(Fe) skarns and (2) Cu-Mo-Au-(Pb-Zn) hydrothermal vein type. In the first group are the Anqing and Longmenshan skarn deposits and in the second the Tongliujing vein deposit. Figure 4.19 shows cross-sections of the Anqing skarn deposit and the Tongliujing vein deposit.

The skarn mineralisation of the Anqing and Longmenshan skarn deposits, is typically found within the contact zones between the diorites and the Lower Triassic sedimentary rocks of the Yueshan and Lanlinghu formations and in xenoliths within the diorite intrusions. The orebodies have different shapes, largely controlled by the nature of the contact zones (Fig. 4.20a). The ore minerals of the skarn deposits are magnetite, chalcopyrite, pyrrhotite, pyrite, molybdenite and minor amounts of galena, sphalerite, bornite and native gold. The accompanying skarn minerals are garnet, pyroxene, wollastonite, albite, actinolite-tremolite, muscovite, chlorite, epidote, sericite, quartz and calcite. These skarn minerals constitute the alteration haloes that surround the orebodies. A five-stage paragenetic sequence is as follows: early skarn development with (1) garnet-diopside, wollastonite and quartz; (2) magnetite and

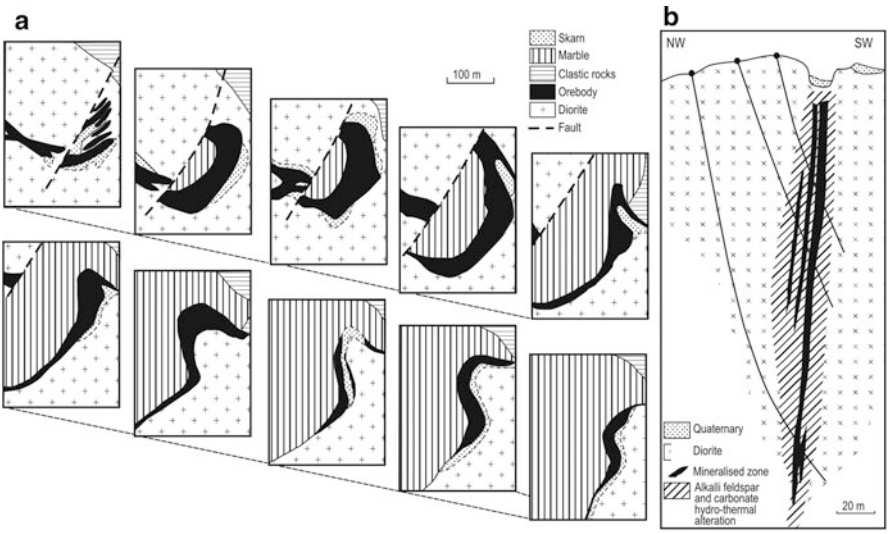

Fig. 4.20 Cross-sections of **a** Anqing Cu skarn orebody, illustrating its different shapes related to the nature of the contact zones; **b** No. 5 orebody of the Tongliujing vein system (after Zhou et al. 2007); position of the Anqing (and Tongliujing) district, see Fig. 4.22

hematite; (3) late vein stage characterised by garnet, diopside, actinolite-tremolite, muscovite and quartz. This was followed by (4) a quartz-sulphide stage, and (5) a late quartz-carbonate stage.

The Tongliujing Cu-Au-Mo deposit consists of veins located in fracture zones within a diorite intrusion, surrounded by a halo of K-feldspar and carbonate alteration (Fig. 4.20b). Ore minerals include chalcopyrite, molybdenite, bornite, gold, with minor amounts of pyrite, chalcocite, hematite, magnetite. A paragenetic sequence comprises three stages: (1) oxide; (2) quartz-sulphide (chalcopyrite-molybdenite); (3) quartz-carbonate (dolomite), accompanied by chalcopyrite, pyrite, hematite, chlorite and sericite.

Fluid inclusions work conducted by Zhou et al. (2007) showed that there are three types of primary fluid inclusions in quartz and carbonate minerals, whereas pseudosecondary inclusions occur in skarn minerals (garnet and actinolite). The three types of primary inclusions are: (1) liquid-rich (liquid 70 %); (2) vapour-rich (vapour 70 %) and (3) fluid inclusions with daughter crystals (generally halite). Homogenisation temperatures showed a range of values for the skarn mineral system and allowed the recognition of the following stages: (1) early garnet-diopside with temperatures ranging from 650 to 440 °C (avg 532 °C); (2) magnetite stage with temperatures from 585 to 380 °C (avg 480 °C); (3) late skarn stage with temperatures from 430 to 364 °C (avg 412 °C); (4) early quartz-sulphide with temperatures from 375 to 220 °C (avg 324 °C) and (5) late quartz-sulphide stage with temperatures from 310 to 200 °C (avg 275 °C). Homogenisation temperatures for the vein deposits are: (1) oxide stage, 430–300 °C (avg 385 °C); (2) sulphide stage, 350–180 °C (avg

325 °C) and (3) quartz carbonate stage, 200–130 °C (avg 172 °C). Fluid salinities show an interesting trend. Fluids that are related to the Yueshan diorite have higher salinities (avg 38.5 % NaCl equivalent) than those associated with the Zongpu intrusion (avg 10.2 % NaCl equivalent) and with the Wuhen intrusion (avg 12.6 % NaCl equivalent). The Zongpu and Wuhen intrusions are associated with minor vein and skarn deposits, whereas most of the larger deposits are related to the Yueshan intrusion.

Results of stable isotope systematics (D, O, S) show that δO_{H2O} values tend to decrease from the early to the late ore-forming stages. Sulphur isotope compositions are quite different for skarns and vein deposits, as follows: for the skarn mineral deposits, $\delta^{34}S$ values range from +19.24 to −11.25 ‰, with a variation of 30.49 ‰; for the vein-type deposits $\delta^{34}S$ values are all positive and with smaller variations +10.0 to +4.2 ‰. The detailed studies on isotope systematics by Zhou et al. (2007), led the authors to conclude that the various stages of skarn mineralisation involved magmatic water with variable degrees of mixing with meteoric water, whereas vein-type deposits, such as Tongliujing, magmatic water was predominant, mixing with only small amounts of meteoric water.

Zhonggu Ore Field; Kiruna-style Fe Mineral Systems

The Zhonggu ore field is located in the eastern part of the Yangtze River Valley metallogenic belt (Ningwu cluster and Ningwu Basin; Fig. 4.16). In the Zhonggu area three diorite porphyry stocks are associated with Kiruna-style stratiform magnetite ores (from Kiruna magnetite-apatite ores in the Fennoscandian Shield, Sweden; see Cliff et al. 1990; Nyström and Enríquez 1994; Naslund et al. 2002), containing a total Fe resource of about 400 Mt grading >45 % (Hou et al. 2010). The northeast-trending volcano-sedimentary Ningwu Basin extends for about 80 km on the northern margin of the Yangtze Craton, from Meishan (Jiangsu Province) in the north to the Zhonggu ore field (Anhui Province) in the south. The Ningwu Basin is filled with Triassic-Jurassic to Lower Cretaceous continental volcanic and sedimentary rocks, intruded by ca. 125 Ma subvolcanic and plutonic intrusions (Yan et al. 2009). The volcanic rocks lithostratigraphy comprises four formations: Longwangshan, Dawangshan, Gushan and Niangnianshan. The volcanic rocks, with U-Pb SHRIMP ages of ca. 130–131 Ma, mostly consist of alkaline basalt, basaltic andesite, trachyte, andesite, dacite, phonolite and related pyroclastic units, grouped into the Niangnianshan Formation (Yan et al. 2009). The suite of associated intrusive rocks comprise gabbro, gabbro-diorite porphyry, diorite, quartz-monzonite and granite. The Triassic to Jurassic sedimentary rocks include dolomitic limestone with gypsum beds, sandstone and shale (Zhouchongcun and Huangmaqing formations).

In the Zhonggu ore field, magnetite-apatite mineralisation is always associated with subvolcanic dioritic intrusions with ages ranging from 128 to 115 Ma (Hou et al. 2010). The ore field comprises a number of deposits, such as Zhongjiu, Gushan, Hemushan, Baixiangshan and Diaoyushan. The magnetite-apatite ores form massive

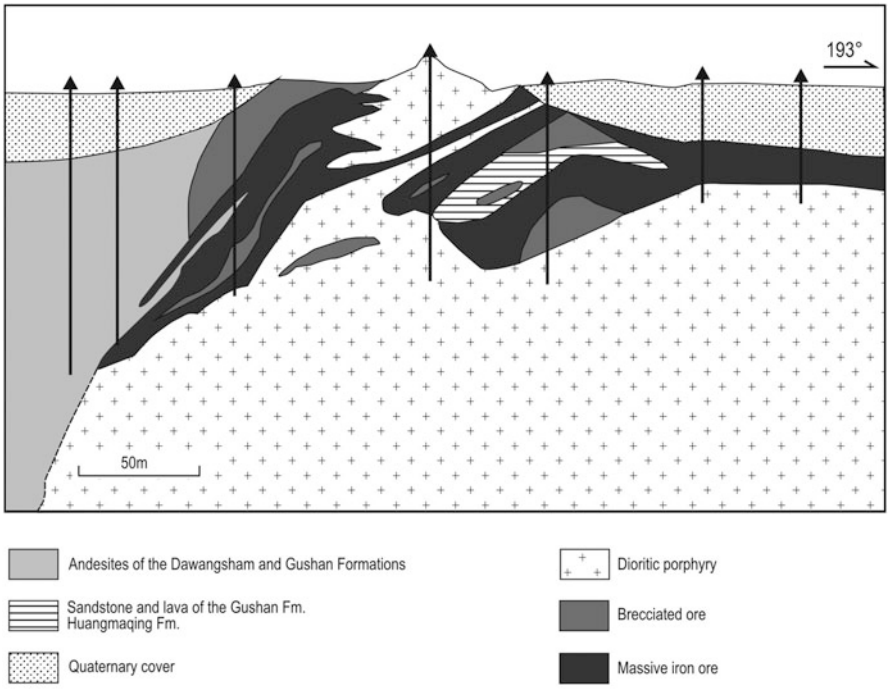

Fig. 4.21 Cross-section showing the relationships between dioritic porphyry, wall-rocks and magnetite orebodies at Gushan, Zhongu ore field. (After Hou et al. 2010)

stratabound lenses, veins, disseminations and breccia pipes, with higher grades usually confined to the latter, which cut through the dioritic stocks and surrounding wall rocks. Hou et al. (2009, 2010) described the main features of the Gushan, Hemushan and Baixiangshan deposits and the following is abridged from these authors.

The Gushan magnetite ± hematite-apatite deposit is characterised by massive and brecciated lenticular orebodies distributed along the contacts between a dome-shaped dioritic porphyry stock and sedimentary country rocks (Fig. 4.21). The sedimentary country rocks comprise Upper Triassic sandstone and shale of the Huangmaqing Formation, Jurassic sandstone of the Xiangshan Group, overlain by Cretaceous andesitic rocks. The sedimentary rocks are intruded by ca. 130 Ma dioritic porphyries, with εNd(T) values of −5.7 to −5.8, which are interpreted as derived from the upper mantle.

The ores predominantly consist of magnetite and martite with minor amounts of apatite and titanite. Ore styles are massive and brecciated, forming lenses or veins, generally grading about 45 % Fe. Disseminations, stockworks and banded ores are locally present, but of minor economic importance (<45 % Fe). Massive orebodies have sharp contacts with the dioritic rocks and grade into brecciated ores. Miarolitic, tubes and amygdaloidal-like structures are present towards the top of ore lenses and filled with calcite and quartz; these structures are absent from their base. Magmatic

flow structures in the massive ores are commonly present as also observed in the classic Kiruna deposits in Sweden (e.g. Nyström and Enríquez 1994). Decrepitation temperatures of inclusion fluids in magnetite and martite range from 350 to 1,040 °C. Hou et al. (2009, 2011) recognised four stages of mineralisation: (1) magmatic, represented by magnetite and co-existing apatite and hematite; (2) hydrothermal stage I, characterised by extensive martite replacement of magnetite and hematite, along grain boundaries, microfractures, associated with calcite, apatite and quartz, veins of coarse-grained magnetite may belong to this stage; (3) hydrothermal stage II, characterised by apatite-magnetite-hematite-quartz mineral assemblage; (4) supergene stage, represented by kaolinite replacing silicate minerals. Wall rock alteration at Gushan is generally weak in the sedimentary rocks and confined to fracture zones, which are filled with kaolinite and quartz. On the other hand the diorite porphyry is extensively altered with quartz, kaolinite, chlorite and carbonate. Hou et al. (2009, 2011) proposed that the Gushan massive, brecciated and banded ores are of magmatic origin, whereas the stockworks are hydrothermal. These authors cite high Ce_2O_3, La_2O_3 and Y_2O_3 contents in apatite as indicating a high temperature environment. Furthermore, chondrite-normalised REE patterns of apatite and diorite are similar, suggesting that they were derived from the same parental magma. By contrast, the stockwork ores form irregular vein networks that emanate from the massive ore into fractures developed above the diorite intrusion, resulting from the rupture of the country rocks due to boiling and decompression of the rising magma.

The orebodies of the Baixiangshan deposit occur at the top of the cupola-like porphyritic diorite intrusion and along the contact with overlying calcareous siltstone, which in the ore zone exhibits a typical skarn assemblage of actinolite, diopside, magnetite and phlogopite. The ores are massive, disseminated and banded and composed of magnetite, apatite and pyrite. Melt inclusions in apatite have homogenisation temperatures of >700 °C. The porphyritic diorite also shows hydrothermal alteration with clinopyroxene altered to hornblende along the margins and the groundmass commonly altered to carbonate and chlorite. The porphyritc diorite has titanite, apatite and magnetites as accessory minerals. The Hemushan deposit also contains massive, disseminated and banded ores, forming lenses at the top of a porphyritic diorite stock and overlying dolomitic limestone. The causative and host porphyritic diorite also has an altered groundmass with minerals, such as kaolinite, carbonate, pyrite, magnetite, apatite, titanite and actinolite.

The Zhonggu dioritic porphyries define a relatively small range of age-corrected εNd(t) (t = 125 Ma) values from −5.2 to −6.8. Values of initial $^{87}Sr/^{86}Sr$ ratios vary from 0.70564 to 0.70926. Previous studies show that the Gushan dioritic porphyry has moderately radiogenic Sr ($^{87}Sr/^{86}Sr$)I (0.7065). For comparison, Mesozoic mafic rocks, such as Jiangmiao and Yanghutang gabbro complexes, have εNd(t) values (∼0) and ($^{87}Sr/^{86}Sr$)t ratios (∼0.704) close to primitive mantle, whereas the Cenozoic basalts in the Yangtze River Valley region are characterized by low $^{87}Sr/^{86}Sr$(t), (0.7032–0.7035) and high εNd(t) values (+5.8 to +6.5).

According to Hou et al. (2010), the origin of the Zhonggu massive magnetite-apatite ores is linked to processes of liquid immiscibility in an Fe-rich parental magmas, which originated by partial melting of an enriched lithospheric mantle. Fe-

and P-rich immiscible melts can separate from the parental magma, providing complexing agents (P, F, Cl) are available in the system. Hou et al. (2010) also suggested that some of the P may have derived by interaction of the magmas with phosphorite layers and nodules in sedimentary rocks. Ultimately, the parental magmas may be represented by deep-seated layered intrusions, which evolve towards Fe-rich melts and saturation of Fe-Ti-P oxides.

4.4.5.2 Dalongshan U Deposit

Zhao et al. (2004) reported on high-grade U mineralisation associated with alkaline granites at Dalongshan in the Luzhong volcano-sedimentary basin in the Yangtze River Valley, intruded by a number of small syenitic and granitic stocks. The alkaline granites consist of quartz-syenite and alkali-feldspar granite (Dalongshan pluton) with U-Pb isochron ages of 1,329 ± 2.2 and 114.7 ± 2.1 Ma, respectively. K-Ar ages of 126 ± 2, 118 ± 3, 105 ± 5 and 94 ± 4 Ma from hornblende, biotite, whole rock and feldspar were also obtained from the quartz-syenite. U-Pb dating of pitchblende samples, yielded a concordia with an age of 106.4 ± 2.9 Ma, clearly post-dating the time of the quartz-syenite crystallisation. The quartz syenite has U contents ranging from 6 to 10 ppm and Th contents from 21 to 24 ppm, with Th/U ratios of 3.7–3.9. The Dalongshan pluton intruded sandstone rocks, which exhibit hydrothermal alteration (silicification, tourmaline, albite, K-feldspar, carbonate, pyrite, hematite) along the contacts with the pluton. The U mineralisation, discovered by an airborne radiometric survey, is hydrothermal and confined to these contact zones. The main ore minerals is pitchblende, accompanied by lesser amounts of metabernite, uraninite and autunite. Other metallic minerals are pyrite, sphalerite, galena, molybdenite, chalcopyrite, marcasite, magnetite, niccolite and millerite. Gangue minerals are fluorite, dolomite, calcite and quartz. Average grade at Dalongshan is 0.805 % U, with the highest grade reported to be 34.22 % U (Dahlkamp 2009).

Fluid inclusion studies reported in the Chinese literature and cited by Zhao et al. (2004), indicated homogenisation temperatures from quartz of 300–250 °C. Oxygen and Sr isotope systematics show whole rock $\delta^{18}O$ values ranging from 11.35 to 9.85 ‰ and initial $^{87}Sr/^{86}Sr$ ratios of 0.7071–0.7082, interpreted to represent a crustal source, possibly from the Proterozoic basement. Zhao et al. (2004), on the basis of the data, summarised above, suggested that magmatic fluids exsolving from the cooling Dalonghan pluton, migrated along fractures in the sedimentary country rocks, with which uranyl complexes carroed by the fluids reacted, resulting in the precipitationof uranium ore.

4.4.5.3 Geodynamic Setting of Metallogenesis in the Yangtze River Valley and Adjacent Regions

Mesozoic-Cenozoic intraplate tectonism and magmatism affected much of the eastern margin of mainland Asia, extending from Far East Russia, through the Baikal

and Mongolia regions, to north-eastern and eastern China (see Pirajno et al. 2009 for an overview). These phenomena are broadly linked with a complex series of events, involving subduction, collision, post-collision collapse and rifting. The Mesozoic (and Cenozoic) extensional tectonics of mainland China and the rest of eastern Asia are the surface expressions of shallow mantle dynamics in the region (Zhao et al. 2010). These may relate to asthenospheric upwellings linked to lithospheric delamination in response to a sequence of rifting following collision between Siberia and Mongolia-North China (Jurassic-Cretaceous) and subduction systems in the western Pacific (Meszoic-Cenozoic) (Barry and Kent 1998). In eastern China this is the extensive and dominantly Cretaceous Yanshanian tectono-thermal event that affected a large region extending for about 1,000 km inland from the coastal areas. This event produced vast amounts of granitic intrusions that invaded Palaeozoic shallow-water dolomitic and limestone strata and resulting in widespread porphyry, porphyry-skarn, Kiruna-style magnetite deposits, epithermal and lode Au systems. A model proposed to explain the range of mineral systems in the Yangtze River Valley and the relationship of the porphyry-skarn-stratabound Cu-Au-Mo-Fe deposits (145 Ma; Late Jurassic) and Kiruna-style magnetite—apatite deposits (ca. 130–125 Ma; Early Cretaceous) is shown in Fig. 4.22, after Mao et al. (2011c). The different ages of the two mineral systems may reflect the "tectonic switch" advocated by Li et al. (2010b), from a Late Jurassic transpressive to Early Cretaceous extensional regimes. This change in tectonic regime affected the whole of eastern China and is considered to be related to the change from oblique, shallow subduction of the Izanagi Plate to orthogonal, steep subduction of the Pacific Plate (see also Zhu et al. 2010, who applied the concept to the Tanlu fault).

In northwestern China, the Palaeo-Asian Ocean closed at the end of the Early Carboniferous (>322.8 Ma), and was followed by collision between the Siberian (or Angara Craton) and Tarim-North China Plates. According to Jahn et al. (2000) and Zhang et al. (2003), peraluminous granites are intruded by K-rich granites, with ages clustering between 300 and 260 Ma, followed by A-type granites of ca. 260 Ma. These K-rich granites and shoshonitic volcanic rocks were developed in a regime of decompression and increasing geothermal gradient; with the A-type granites marking the end of collision, because they are overlain by Late Permian basalts and coal-bearing strata (Zhang et al. 2003). Hence, the magmatism and associated skarn Au deposits in northwestern China probably formed in a regime of decompression and increasing geothermal gradients, during the transition from collisional shortening to extension.

In the western portion of the Central China Orogen (Kunlun-West Qinling orogenic belts), skarn deposits are hosted in Triassic strata deposited in a foreland basin, on south side of the north-dipping Mian-Lue Fault (Chap. 5), interpreted as the suture derived from the closure of an oceanic tract. Li (2001) suggested that from Sinian (Neopreterozoic) to Early Triassic the Middle-Lower Yangtze River Valley was a passive continental margin on the north side of the Yangtze Craton, later to become a foreland basin, located south of the Dabie Orogen, between Middle Triassic to Middle Jurassic. The Middle Triassic rocks are distributed in an elongate valley and fault-controlled basin, along the Yangtze River, comprising dolostone, gypsum-bearing

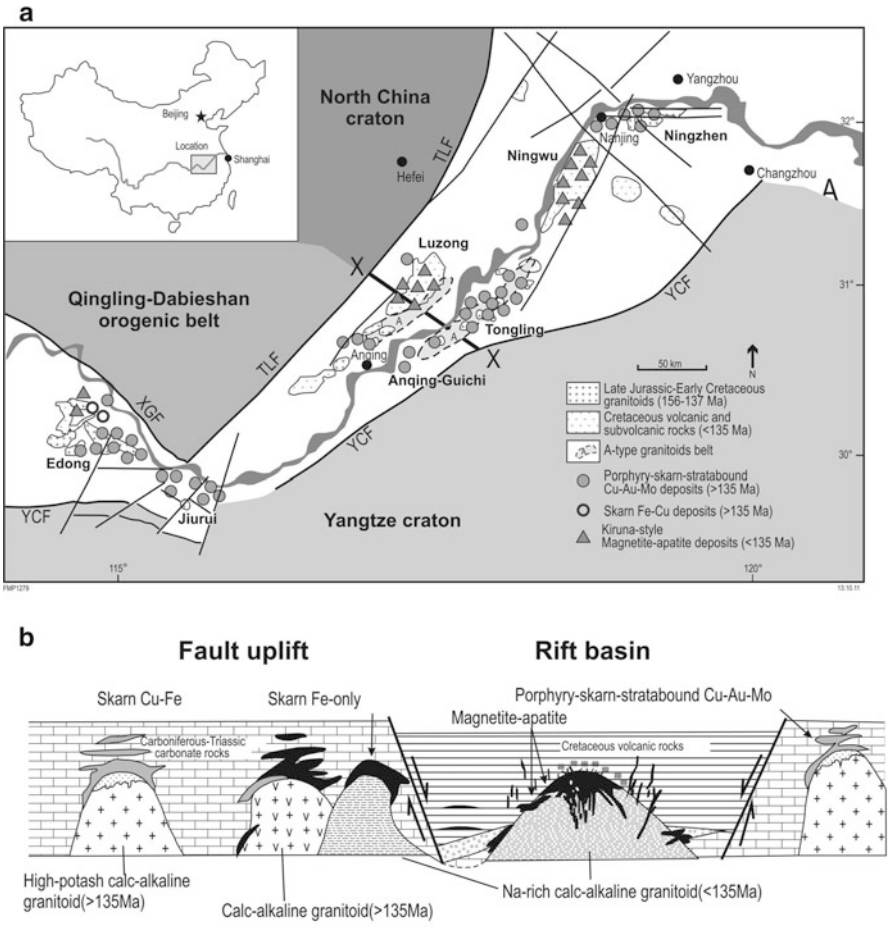

Fig. 4.22 **a** Simplified geology of the Middle-Lower-Yangtze River Valley metallogenic province showing distribution and types of mineral deposits slightly modified version of Fig. 4.16; **b** cross-section showing tectonic settings (not-on-scale, but *line X-X* in **a** shows approximate position) of ca. 145 Ma magnetite-apatite (Kiruna-style) and skarn Cu-Fe deposits in sedimentary rocks of the Yangtze platform (uplift), ca. 130–125 Ma porphyry-skarn deposits in volcano-sedimentary rift basin. (After Mao et al. 2011c)

dolomitic limestone in the lower part, clastic rocks intercalated with limestone and dolostone in the middle part, and clastic rocks in the upper levels, reflecting the intercalation of marine and terrigenous facies rocks (Mao et al. 2011b). Late Triassic and Early to Middle Jurassic terrigenous clastic rocks are distributed in several fault basins, along the Yangtze River Valley The passive margin platform carbonate rocks, provided a fertile lithological entity for granitic intrusions to form skarn mineral systems in the Yangtze River Valley.

As the southeastern portion of Eurasia continent, East China was affected by the Eurasia-Pacific interaction, this has led many geologists (Quan et al. 1992; Zhao et al.

1999) to consider that East China is part of the Circum-Pacific metallogenic belt, and consequently the Mesozoic magmatism and metallogenesis of the East China region may be associated with the northwestward subduction of the Pacific (Izanagi) plate beneath the Eurasia plate (Mao et al. 2010). Important metallogenic provinces, such as the Yanshan, Lower Yangtze River region, southern China, East and West Qinling (Mo, Au, Ag etc. Chap. 5) and Jiaodong (Au) (Chen et al. 2004), all trend perpendicular, and not parallel to the Mesozoic and present-day trenches. All of these features confirm that the Yanshanian granitic magmatism and related metallogenesis in East China probably occurred in a geodynamic regime of post-orogenic extension. The continental collisions in East China began in Permo-Triassic times with North China Craton and Siberian-Mongolian block along the Solonker suture, followed by Triassic continental collisions (North China Craton and Yangtze Craton) to the south. During this sequence of collisional events, the whole of East China was subjected to strong compression, which resulted in the development of peraluminous granites. In the West Qinling, for example, peralunminous granitic intrusions, associated with porphyry Mo mineralisation occurred at 217–215 Ma (Triassic), during the collision between the Yangtze Craton and the North China Craton, which resulted in the formation of the Qinling-Dabie orogenic belt (Zhu et al. 2011).

In the subsequent period from 145 Ma to 98 Ma, no significant collisions occurred and the geodynamic conditions involved a change to an extensional regime. Fluid generation and hydrothermal metallogeny, including porphyry and skarn-type mineralisation, occurred between 145 and 98 Ma, and peaked around 120–130 Ma (Chen et al. 2004; Mao et al. 2010; Zhu et al. 2011).

A model that could explain the post-orogenic extensional metallogenesis of the Mesozoic skarn systems in China is lithospheric delamination and asthenospheric upwelling. The thermo-tectonic evolution of the lithospheric mantle beneath eastern China between the Ordovician and present day is envisaged to have resulted from lithospheric extension, delamination and asthenospheric upwelling, with the possibility of deep mantle plumes being ruled out, given the nature of the volcanism (scattered and alkaline) in the region as well as the lack of continental flood basalts. The onset of this lithospheric extension can be linked to the Triassic collision between the North China Craton and the Yangzte Craton, forming the Qinling orogenic belt (Xu 2001) and the collision of the North China Craton in the Jurassic-Cretaceous with the Siberian Craton (Wang et al. 2006). Lithospheric thermal weakening and erosion proceed as a result of conductive heating by the upwelling asthenosphere. Importantly, this asthenospheric upwelling was most likely affected by the existing lithospheric and lower crustal heterogeneities, with the result that the flow of hot mantle was preferentially channelled along major discontinuities and lithospheric breaks, such as the Tanlu fault and other tectonic boundaries or zones of crustal weakness, such as the Qinling orogenic belt, between the North China Craton and the Yangtze Craton (Fig. 4.23). Indeed, the latter is an important crustal break, which is where an abundance of porphyry, skarn and lode systems are present, thus explaining the perpendicularity of Mesozoic-Cenozoic magmatic products and ore systems in relation to the subducting plates of the Pacific Ocean beneath the east Asian margins. The 210–90 Ma Yanshanian tectono-thermal event is part of and a manifestation

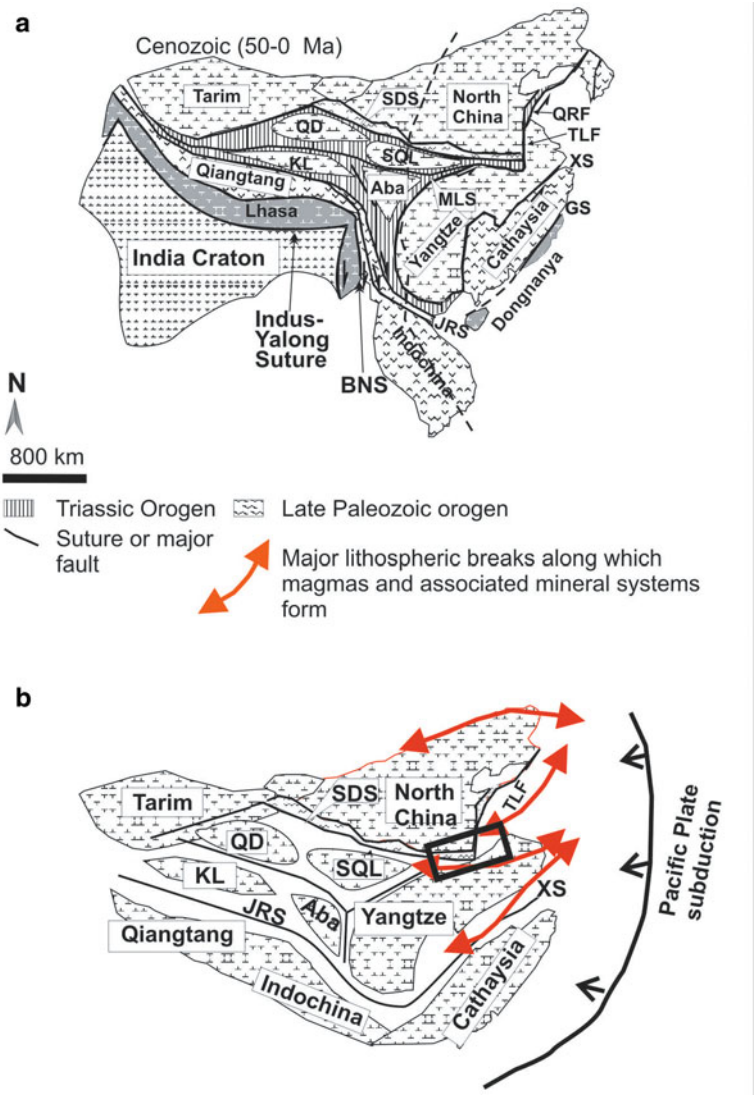

Fig. 4.23 **a** Cartoon schematically depicting the major tectonic units of mainland China (after Chen et al. 2007); **b** shows exaggerated breaks between the various tectonic units and the structural breaks provided by the boundaries between the tectonic units along which magmatism and related mineral systems formed; *BNS* Bangong-Nujiang suture, *GS* Gunanhai suture, *JRS* Jinshanjiang-Red River fault, *KL* Kunlun terrane, *MLS* Mian-Lue suture, *QD* Qiadam Block, *SDS* Shang-Dan suture, *SQL*, Southern Qinling terrane, *TLF* Tan-Lu fault, *XS* Xiangganzhe suture; *rectangle* indicates approximate position of the Qinling and Yangtze River Valley regions

of the above-mentioned intraplate geodynamic evolution and is characterised by a range of intrusives from gabbro to granitic rocks, including A-type alkaline rocks and Basin-and-Range style rifting with volcano-sedimentary basins (Shanxi Rift System; Chap. 8). Volcanic rocks are bimodal in composition but dominated by alkali basalt. Intrusive activity particularly affected regions along major zones of weakness, such as the above-mentioned boundaries between the North and Yangtze Cratons and the North China and Siberian Cratons, and the crustal-scale north-northeast-trending Tan Lu Fault (Fig. 4.23).

Wang et al. (2006) linked the nature of Mesozoic magmatism in northeastern China (Great Xing'an range) with a geodynamic scenario spanning the Jurassic-Cretaceous, a topic further taken up in Chap. 6. They recorded an age progression from 160–140, 130–120, 100–80 Ma, from the northeast China interior towards Japan and attribute it to retreat and delamination of the subducting slab, with upwelling of asthenospheric mantle under each window created by each slab retreat. It may be that metallogenesis, both for porphyry and skarn systems, was related to this regime of delamination tectonics and mantle upwelling and extension, during which magmatism and large scale flow of hydrothermal fluids occurred. The geodynamics of mantle upwelling and lithospheric extension created a favourable environment for the development of granitic magmas and the generation of hydrothermal fluids.

4.4.6 Orogenic Gold Deposit: Jinshan

The Jinshan world-class Au deposit (Jiangxi Province, Dexing district) is situated in the eastern part of the Jiangnan orogenic belt, 20 km south of the Dexing porphyry deposits (Fig. 4.13). The Jinshan orebodies consist of mylonite and/or laminated quartz veins with pyrite, with grades ranging from 3 to 10 g/t Au, locally reaching values as high as 1,600 g/t Au (Li et al. 2010d). As mentioned above (Sect. 4.4.4.2), the Jinshan mineralisation is considered to be part of a larger mineral system that includes porphyry and epithermal deposits. Other quartz vein-type gold deposit in the region, include Hamashi, Dongjia, Shangluo, Naikeng also within northeast-trending shear zones, to the northeast of Yinshan Ag-Cu-Pb-Zn-Au deposit and southwest of Zhushahong porphyry Cu deposit (Fig. 4.13).

The Jinshan lode Au is located in the 715–730 Ma Jinshan ductile shear zone, which is part of a set of northeast-trending shear zones in the region (Fig. 4.13) that resulted from the collision of the Yangtze and Cathaysia blocks and named Northeast Jiangxi Deep Fault (NJDF; Li et al. 2009, 2010d). This ductile shear zone was studied in detail by Li and co-authors, who identified several second- and third-order shear zones, which host quartz vein Au deposits that are considered to be of the orogenic type (e.g. Groves et al. 1998, 2003). The mineralisation occurs in quartz veins hosted and cross-cutting altered (silica, pyrite and ankerite) and Au-bearing mylonite and ultramylonite. The mylonitic units are within carbonaceous phyllite and tuffaceous phyllite (Li et al. 2003d). The orebodies are parallel to the shear zone and consist of pyritic mylonite and laminated quartz veins, with the latter containing most of

the Au resource. According to Li et al. (2009, 2010d), the quartz veins were formed in the early stages of ductile deformation, associated with pressure solution. Gold grades range from 3 to 10 g/t in the mylonite and from 5 to 20 g/t in the quartz veins, with high grade pockets assaying up to 1,600 g/t Au. Native Au is present as dendrites, veinlets and films and, locally, as grains that can be seen in hand specimens. Native Au is also found in fragmented pyrite and quartz grains (Li et al. 2010d). Ore minerals are mainly pyrite, subordinate magnetite, hematite, arsenopyrite, sphalerite, chalcopyrite and galena. Gangue minerals are quartz, subordinate sericite, albite, ankerite and chlorite. Pyrite is the most important gold-bearing mineral with a Au content of at 1.17–1.28 %. Native gold has a fineness of 953.6 ~ 969.4.

Quartz, albite, pyrite, sericite, chlorite and carbonate constitute the alteration minerals of country rocks, with silicification and pyritisation being closely associated with the Au mineralisation. Based on the metamorphism and deformation of the rocks and mineral paragenesis, Li et al. (2010d) identified three alteration zones, from the center of the shear zone outward, as follows: (1) quartz-albite-ankerite-pyrite, occurring around the main shear zone with the highest strain and a vertical thickness of several metres to tens of metres, but generally less than 50 m, and containing highest gold grades; (2) quartz-sericite-ankerite, developed on both sides of the first alteration zone with vertical thickness of ca. 100 m; (3) chlorite-calcite-sericite, occurring in the outermost parts of the shear zone but not extendign beyond it.

Zhang and Tan (1998) recognised four types of fluid inclusions: (1) gas-liquid brine inclusions, which make up 80–85 % of total inclusions; (2) pure hydrocarbon inclusions, which account for 10–15 % of inclusion types; (3) saline daughter minerals-bearing polyphase inclusions that constitute about 1 %; and (4) pure CO_2 inclusions (as well as liquid CO_2-bearing three-phase inclusions) that make up less than 1 %. Zhang and Tan (1998) also proposed that high contents of organic matter in the fluids are important for Au transportation and precipitation.

According to the characteristics of fluid inclusions, Li et al. (2009) suggested that the mineralisation in the above-mentioned Hamashi Au deposit can be divided into three stages: (1) quartz—pyrite stage, comprising dominant quartz and a small amount of pyrite and native gold; (2) sulphide stage, characterized by massive sulphide (pyrite, arsenopyrite, chalcopyrite, minor galena and sphalerite); and (3) carbonate—sulphide or sulphate—sulphide stage, with abundant calcite, siderite and ankerite. These would correspond to three stages of homogenisation temperatures from fluid inclusions: (1) quartz-pyrite, with trapping temperatures ranging from 250 to 215 °C; (2) quartz- sulphide, with homogenisation temperatures ranging from 225 to 190 °C; (3) carbonate, with homogenisation temperatures ranging from 190 to 160 °C. Salinities of 12.3–14.5 wt % NaCl equivalent were determined for medium and low temperature fluids.

The origin and age of the Jinshan lode Au mineralisation remain controversial. Fan and Li (1992) and Zhang and Tan (1998) suggested the mineralisation in the Jinshan gold deposit is related to a granitic intrusion at depth. He/Ar isotopic systematics by Li et al. (2009) indicate that the ore-forming fluids are mainly derived from the crust, but with involvement of a small amount of mantle fluids. Hydrogen and oxygen isotope systematics have led researchers to propose several different

and contradictory sources of ore-forming fluids, such as mixtures of magmatic and meteoric waters, mixture of magmatic and metamorphic water, metamorphic waters, mixtures of metamorphic and meteoric water, mixtures of magmatic water, metamorphic water and meteoric water.

Li et al. (2010d) also investigated noble gases (He and Ar), carbon and stable isotope systematics of the Jinshan quartz veins and ankerite, in order to constrain the source of the mineralising fluids. The $^{3}He/^{4}He$ ratios range from 0.13 to 0.24 Ra (atmospheric ratio Ra is 1.4×10^{-6}). The $^{40}Ar/^{36}Ar$ ratios range from 575 to 1,090, with two samples giving 2,838 and 3,060. The $\delta^{18}O$ values in quartz range from 12.4 to 15.3 ‰ and δD of water from fluid inclusions shows values ranging from −73 to −62 ‰. Ankerite samples returned $\delta^{18}O_{SMOW}$ values ranging from 4.4 to 8.0 ‰ and $\delta^{13}C_{PDB}$ values from −5.0 to −4.2 ‰. The $\delta^{18}O$ values of the auriferous quartz veins are close to those of metamorphic quartz (14.5–15.2 ‰) and the δD values of fluid inclusions in auriferous quartz overlap the range of −80 to −40 ‰, considered typical of magmatic and/or metamorphic fluids (Rollinson 1993, cited in Li et al. 2010d). Similarly, the carbon isotopic data appear to fall within the range of lode Au deposits of all ages (−23 to +2 ‰).

In the view of Li et al. (2010d), the Jinshan Au mineralisation was formed during the Jinning Orogeny, with structural relationships suggesting that the main phase of mineralisation occurred after the peak of regional metamorphism with metamorphic fluids originating from the deeper levels in the crust, although these authors do not exclude a contribution during pressure solution in the ductile shear zone. As such, the Jinshan deposit would be a typical orogenic mineral system (Groves et al. 1998, 2003).

4.4.7 Gejiu Sn-Cu District, SW Cathaysia

The Gejiu Sn-Cu mineral district (Yunnan Province), located about 300 km south of the city of Kunming, is on the southwestern margin of the Cathaysia Block and contains one of the largest tin resources in the world, with an estimated yearly production of 40,000 tonnes of tin and with Sn + Cu resources greater than 300 Mt locally with W, Bi, and Mo recovered as by-products (Mo Guopei of Yunnan Tin Company pers. comm. 2010). Tin mining in the Gejiu district, which currently accounts for 50 % of China's tin production, has been known for more than 2,000 years, since the Han Dynasty, when between 2,000 and 3,000 tonnes of tin were produced (Mo Guopei of Yunnan Tin Company pers. comm. 2010). The deposits are all associated with the thermal aureoles of ca. 83 Ma highly fractionated granitic cupolas that emanate from a larger biotite granite intrusion. The ores are distributed within and around the granitic cupolas in the country rocks. The Gejiu mineral district is described in some detail in Li et al. (1992) and Zhuang et al. (1996).

The district is mostly underlain by the Middle Triassic Gejiu Formation, consisting of more than 3,000 m of carbonate (limestone and dolomite mainly) and the 1,800 to 2,800 m thick Falang Formation fine-grained clastic and carbonate rocks, with

the intercalated mafic lavas. The district was affected by deformation (folding and faulting), resulting in north-south and east-west oriented structures, as well as second and third order northeast- and northwest-trending faults. Numerous faults in the Gejiu area, include the north-northeast-trending Longchahe fault, Jiaodingshan fault, Yangjiatian fault, northeast-trending Baishachong fault, and the north-south-trending Gejiu Fault. The Gejiu Fault divides the district into a western zone with large areas of outcropping granitic rocks and an eastern, poorly exposed, but richly mineralised zone, characterised by east-west trending faults and anticlinal structures associated with mineral deposits (Fig. 4.24). Late Cretaceous magmatism in the Gejiu region, was intensive and represented by: (1) Longchahe porphyritic granite; (2) Songshujiao porphyritic granite; (3) Laochang porphyritic granite; (4) Shenxianshui equigranular granite; (5) Baishachong equigranular granite; (6) Laochang equigranular granite; (7) Xinshan equigranular granite; (8) Jiasha gabbro; (9) Jiasha mafic microgranular enclaves; (10) Baiyunshan alkaline rocks (syenite); and (11) Laochang mafic dykes. These rocks, part of the 450 km^2 Gejiu granite batholith which, as mentioned above, are well exposed in the western part of Gejiu district (west of the Gejiu Fault), whereas in the eastern part they are below the surface (Fig. 4.24).

The mineral systems in the Gejiu district are related to Late Cretaceous granitic intrusions, for which recent precise age determinations by zircon SHRIMP and LA-ICP-MS methods include the following (Cheng et al. in press; Cheng Yanbo pers. comm. 2011): Longchahe (83.2 Ma), Songshujiao (82.8 Ma), Laochang porphyritic granites (83.3 Ma), Shenxianshui (83.0 Ma), Beipaotai (79.0 Ma), Laochang (85.5 Ma), and Xinshan (83.1 Ma) equigranular granites.

A variety of mineral systems in the district are controlled by first- (north-trending), second- (north-trending), third- (east-west-trending) and fourth-order (northeast-trending) faults and their intersections. Mineral systems include endo- and exoskarns, greisen, stratabound and/or stratiform ores, fracture-controlled veins and lenses. All stratiform and/or stratabound mineral deposits are hosted in dolomitic and limestone beds of the Gejiu Formation, except for the Kafang Cu deposit, which is hosted in mafic lava. The associated granitic rocks form cupola bodies intruded into the carbonate rocks. The granitic cupolas are leucogranite with locally developed greisen, associated with skarn ores and lenses of disseminated sulphides, fluorite and cassiterite. Skarn orebodies are developed along the contacts with carbonate rocks. There is a regional metal zoning, both laterally and vertically outward from the granite cupola: Cu-Sn → Sn-pyrrhotite-arsenopyrite → Pb-Zn-Sn → Pb-Zn. A great variety of primary ore minerals include, cassiterite, chalcopyrite, pyrrhotite, arsenopyrite, pyrite, scheelite, bismuthinite, molybdenite, magnetite. Fluorite is common in wall rocks and in the surrounding altered granitic rocks. Ore minerals in oxidised ores are: hematite, limonite, goethite, chalcocite, malachite, covellite, cerusiite, hemimorphite, scorodite. The main ore deposits, exploited at the time of writing, are: Laochang, Dadoushan, Kafang and Songshujiao (positions shown in Figs. 4.24 and 4.25).

The Laochang Sn-Cu deposit is a typical skarn formed in marble rocks at the contact with a granite cupola. The ore extends to more than 300 m of depth, with the first 100 m being oxidised. The ore mainly consist of cassiterite and chalcopyrite,

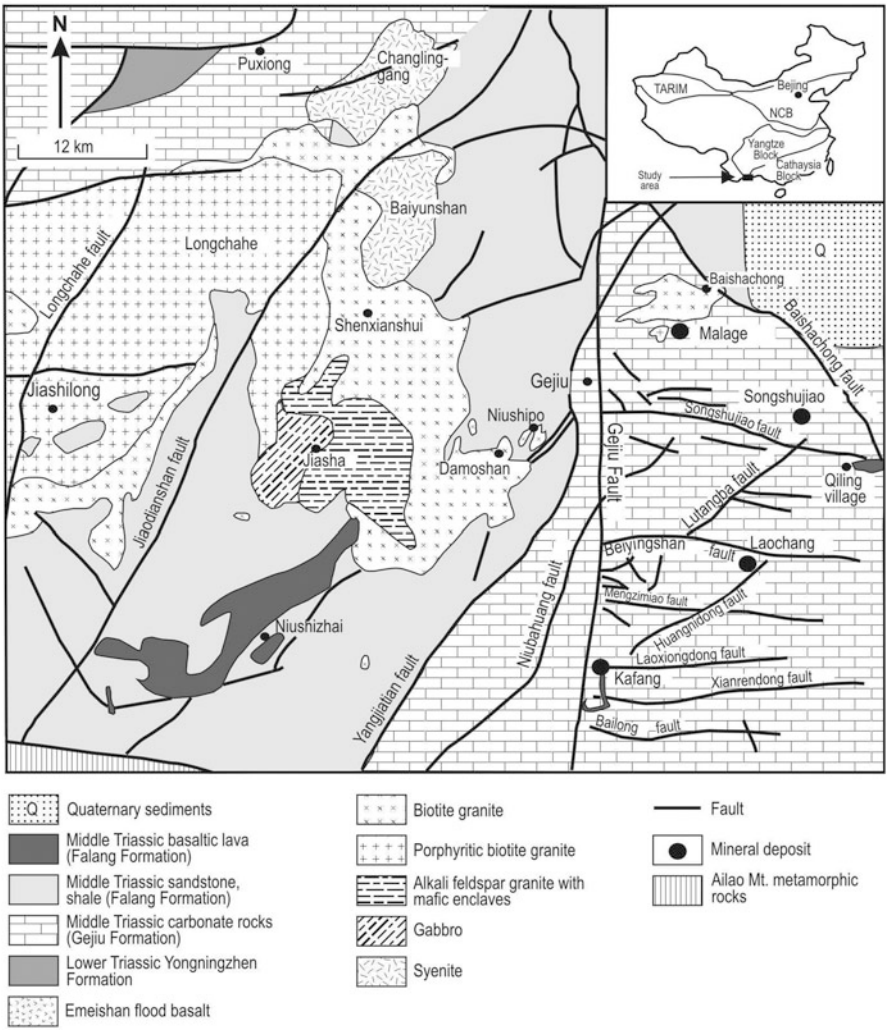

Fig. 4.24 Gejiu Sn-Cu mineral district in Yunnan province and location of deposits discussed in text. (Modified after Cheng YB et al. in press and written comm. 2010)

with grades greater than 1 % Sn (see also Table 4.5). The Dadoushan tourmaline-cassiterite stockwork is mined from an open pit and consist of vein stockworks of quartz, tourmaline and skarn minerals (garnet, wollastonite, biotite), containing cassiterite. The ore zone, with grades of about 0.3 % Sn, is developed within a layer of impure limestone, in contrast to limestone layers above and below, which are not mineralised (see Fig. 4.25).

The Kafang Cu-Sn deposit is unusual in that it is almost entirely hosted in an alkali basalt lava interlayered with carbonate layers of the Gejiu Formation (Cheng

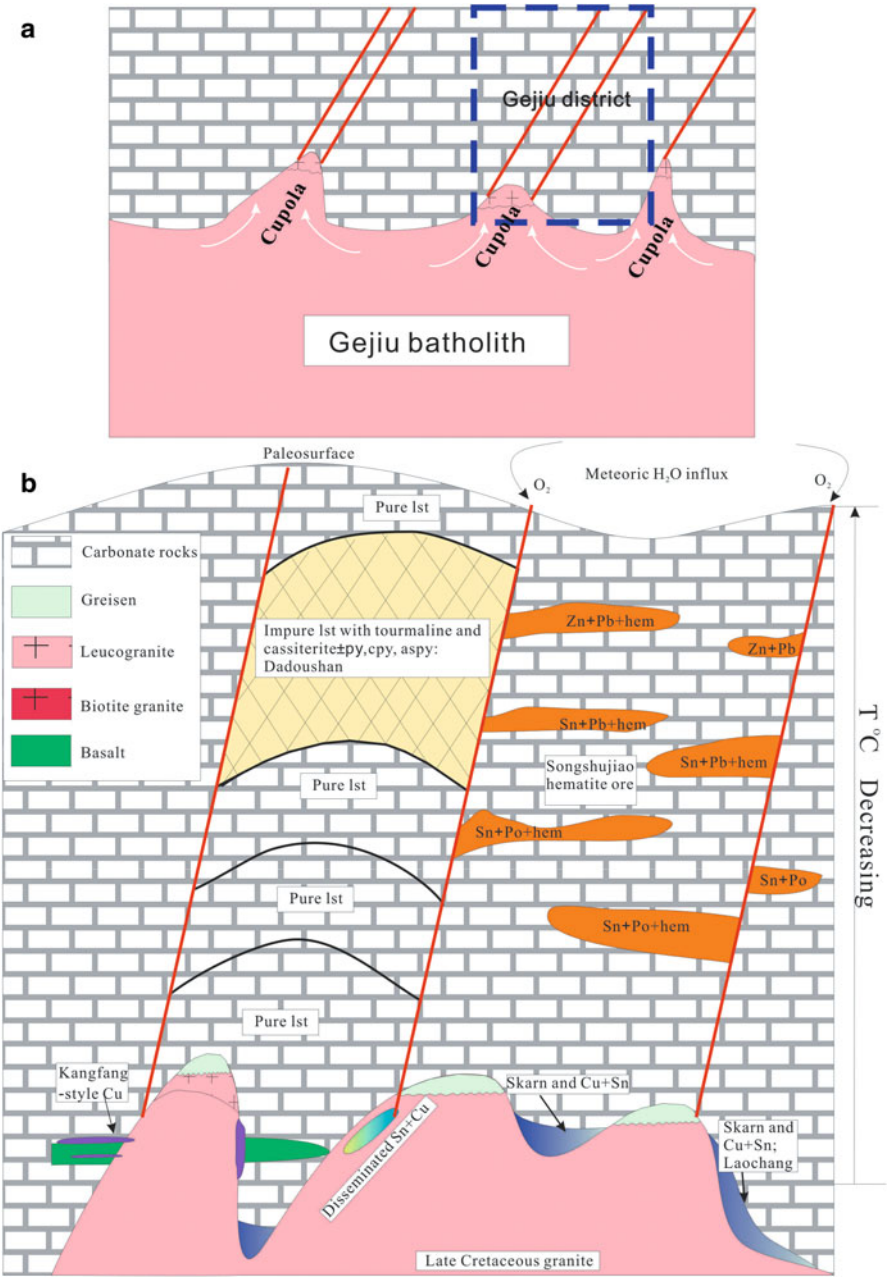

Fig. 4.25 **a** Genetic model showing cupolas of highly fractionated granite emanating from the main biotite-grannite batholith; the cupolas are locally greisenised and are associated with endoskarns (within the greisen) and exoskarns developed in the carbonate country rocks, as well as vein systems and replacement ores; **b** shows the formation of hematite-cassiterite ores from meteoric fluids that descend along fault zones. (Figure courtesy of Cheng Yangbo, Institute of Mineral Resources, Beijing)

et al. in press). The ore is massive to disseminated and consist of cassiterite, chalcopyrite, pyrrhotite, arsenopyrite and pyrite mainly and extends laterally for about 400 m. Scheelite is also present (about 50,000 t of WO_3). Gangue minerals (altered basalt) are actinolite-tremolite, phlogopite, chlorite and epidote. In addition, fluorite veins cut through the basaltic rock. Away from the basalt-hosted ore zone, sulphide lenses occur in the greisenised granite. The position of the Kafang orebody in relation to the granite cupola is shown in Fig. 4.25. The Kafang deposit is located between two east-west-trending faults that abut against the major north-trending Gejiu Fault (Fig. 4.24). The host basalt unit is 100–60 m thick, which is intercalated with limestone and dolomite beds of the Gejiu Formation. The surrounding, footwall and hangingwall carbonate rocks are altered to skarn, comprising actinolite-tremolite and phlogopite. Sulphur isotopic compositions of pyrite, chalcopyrite and pyrrhotite show $\delta^{34}S$ values ranging from −0.86 to 3.3 ‰ (Cheng YB unpublished data), suggesting a magmatic source. The origin of the basalt-hosted Kafang massive sulphides is not clear, although it is reasonable to infer that the highly fractionated granitic cupola(s) would have played an important role. Fluids emanating from these cupolas could selectively replaced the basaltic lavas closest to the intrusion, as shown in Fig. 4.25. Research work is on-going for the unusual Kafang Cu-Sn deposit.

The Songshujiao deposit is one of several stratiform hematite-cassiterite ores in the region, which consist of almost entirely hematite and goethite replacing sulphides with cassiterite as a residual mineral. Ore grades are in the range of 2 % Sn (Mo Guopei of Yunnan Tin Company pers. comm. 2010). Lenses of relic massive sulphides (pyrrhotite, pyrite and arsenopyrite) are locally preserved. The host rock is dolomitic limestone and there is no visible skarn nearby and the nearest granite cupola is about 500 m below the ore zone. The origin of these hematitic-cassiterite ore zone is poorly understood, but a possible model, shown here in Fig. 4.25, suggests that meteoric water may have percolated along major faults, resulting in the near-pervasive oxidation of massive sulphide lenses in dolomitic limestone layers.

A genetic model for the Sn-Cu ores in the Gejiu district (Fig. 4.25a, b). proposes that fractionated cupolas emanate from the Gejiu batholith, mostly guided by existing faults or fractures in the verlying carbonate beds of the Gejiu Formation. It is also of interest to note that multivariate statistics (Principal Component Analysis, PCA) have been used to identify possible locations of buried granitic cupolas in the Gejiu district (Cheng et al. 2011). These authors managed to identify areas of felsic intrusions within the Gejiu Formation, beyond those already mapped.

4.4.8 Metalliferous Black Shales in the Yangtze Platform

Black shales are sediments rich in organic carbon that accumulate under anoxic conditions. It must be emphasised that these anoxic conditions are created through oxygen consumption of decaying organic matter, so anoxia is not necessarily a deep-water condition, as is commonly perceived, except for density-stratified silled basins, such as the Black Sea (Wignall 1994). Black shales are economically very important,

not only because they are the source of hydrocarbons, but also because they are commonly enriched in several trace metals (Zn, Cu, Pb, Mo, Ag, Au, V, Ni, PGE, Mn, U and REE). Black shales also host a range of exhalative type mineral systems, as for example black shale-hosted Cu and Cu-Pb-Zn deposits, such as those of the Copperbelt and the Kupferschiefer, in which the ores are hosted in reduced black mudstone, dolomite or sandstone, typically associated with red bed successions in rift basins (Pirajno 2009). There is abundant literature on metalliferous black shales, which are defined as "*a black shale that is enriched in any given metal by a factor of two (except for Be, Co, Mo and U, for which 1X is sufficient) relative to the U. S. Geological Survey Standard SDO-1*" (Huyck 1990; Schultz 1991; Pašava 1996).

The reason for the metal enrichment of black shales is not entirely clear. An interesting possibility, advanced by Coffin and Eldholm (1994), is that the deposition of black shales may be correlated with mantle plumes and associated emplacement of large igneous provinces (oceanic plateau and continental flood basalt eruptions). The implication arises that black shales may owe their anomalous metal content to these vast volcanic eruptions. The important factor of this relationship is the reduction of the O_2 content in bottom waters. There are at least two possible reasons for this. One is the release of CO_2 in the atmosphere, caused by the eruptions of continental flood basalts, which induces global warming and reduces the amount of O_2 in bottom waters. This, in turn, contributes to anoxic conditions and the deposition of black shales. The near-contemporaneous emplacement of the Ontong Java Plateau and the deposition of black shales lend support to the idea (Coffin and Eldhom 1994). The second reason may be that oceanic plateau volcanism causes global anoxia due to increased hydrothermal venting on the seafloor, which results in a reduction of the O_2 content of bottom waters (Sinton and Duncan 1997). Coveney et al. (1992, 1994), Murowchick et al. (1994), Lott et al. (1999), Orbeger et al. (2007), Jiang et al. (2007), have studied various aspects of Phanerozoic black shale-hosted ore deposits from southern China. Geoscientists working on the polymetallic black shales of southern China, consider two main models: submarine hydrothermal discharge (exhalative type) and synsedimentary deposition in euxinic basin (seawater precipitation). The two models have been the topic of interesting debates (Coveney 2003; Lehmann et al. 2003). In southern China, polymetallic black shales locally have metal concentrations that are amenable to exploitation, as discussed below.

4.4.8.1 Mo-Ni-V-PGE-Au in Black Shales, Southern China

The lower Cambrian black shales in the Yangzte platform sedimentary succession are enriched in Mo, Ni, PGE, Au, Ag, Zn, V and As and were first reported by Fan et al. (1973). Continental rifting on the southern and northern margins of the Yangzte Craton, controlled the platform Neoproterozoic to Cambrian carbonate-dominated depositional systems of the Craton (Wang et al. 2005). Oceanward, the platform developed a series of deep basins, which were filled with organic-rich sediments. These constitute the extensive black shale province that borders the northern and southern margins of the Yangzte Craton, covering about 10^6 km^2 (Emsbo et al.

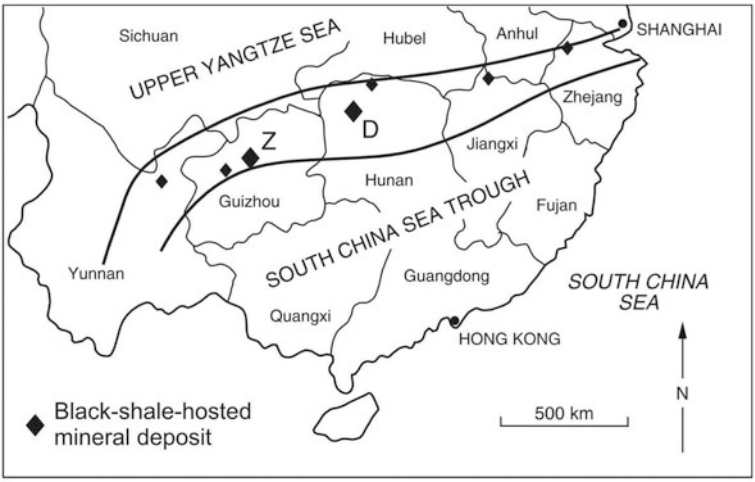

Fig. 4.26 Distribution of major black-shale hosted Ni-Mo-Au-PGE deposits in south China; the *larger symbols* marked *Z* and *D*, indicate deposits near Zunyi and Dayong, respectively. (After Coveney et al. 1992, 1994)

2005). The metalliferous shales horizon, which includes phosphorite and stone coal, extends along a belt 1,600 km long, from Yunan Province in the south-southwest to Zhejiang Province in the east-northeast (Fig. 4.26). The shale sequence is part of the Niutitang Formation (Mao et al. 2002c). The Niutitang Formation is underlain by the Neoproterozoic carbonate succession of the Dengying Formation, which in turn is underlain by a succession of black shale, locally hosting V-Ag mineralisation, chert and dolomite rocks of the Doushantau Formation. The latter rests on the 590–575 Ma tillites of the Nantuo Formation, correlated with the global Marinoan glaciation (Mao et al. 2002c and references therein). The entire sedimentary package was deposited in a sedimentary shelf environment, built on the Precambrian basement of the Yangzte Craton. Rocks of the Niutitang Formation, from older to younger, consists of:

- 0–0.3 m discontinuous lenses of Fe-Mn palaeoweathering crust, resting on undulating palaeosurface of the Duoshatau Formation;
- 0.5 m U-rich phosphorite;
- 0.5–2.5 m organic C-rich shale with lenses of phosphorite, containing collophane with 200–300 ppm U and locally economic concentrations of Mo, Ni, V, Y and light REE;
- 5 cm to 2 m Ni-Mo-PGE-Au ore unit, continuous for several kilometres, locally with flat-pebble conglomerate, colloidal Ni-Mo sulphides with nodular textures;
- Mo-V-Ni-bearing stone coal layer, consisting of organic C-rich hydromica claystone-shale with up to 35 % C_{org}, 0.3 % Mo, 0.2 % Ni and 0.9 % V;
- 100 m carbonaceous hydromica claystone-shale. The ore nodules, mentioned above, are 1–3 mm long and consist of microcrystalline Fe, Mo and Ni sulphides,

Table 4.7 Concentration (ppm) of selected elements in black shale (a) and sulphidic material (b) from the Niutitang Formation, Zunyi, Guizhou Province. (After Jiang et al. 2006)

(a) Element	1	2	3	4	3	4	5	6	Mean value
V	538	1,629	8,232	3,168	8,603	11,339	15,652	16,515	8,209.5
Cr	218	1,234	397	1,591	5,157	5,686	2,455	3,153	2,486.4
Co	0.21	1.8	0.26	0.83	3.53	4.03	5.96	4.89	2.689
Ni	26.1	186	42.6	124	254	308	399	337	209.6
Cu	140	524	731	379	434	1,392	312	187	512.4
Zn	114	259	443	357	774	1,490	3,189	2,318	1,118
Mo	41.9	70.2	53.9	74.4	80.5	132	315	261	128.6
Ba	5,231	13,686	11,384	4,804	5,276	5,919	7,163	6,497	7,495
Pb	23.3	32.2	21.3	27.5	30.4	36.1	44.3	51.8	33.36
U	41.2	31.6	80.9	57.1	81	71.5	66.7	80.9	63.86
(b) Element	1	2	2	3	4	5	6	7	Mean value
V	52.8	14.9	358	149	25.4	10.4	152	102	108.06
Cr	22.9	6.73	39.7	17.6	13.1	6.5	23.2	16.8	18.32
Co	9.62	0.45	42.6	3.52	8.49	0.57	41.8	3.66	13.84
Ni	9,237	615	7,381	595	8,789	751	9,792	688	4,731
Cu	814	68.7	248	24	429	74.9	451	40.4	268.7
Zn	1,284	204	390	39.7	1,739	194	374	39.7	533.05
Mo	2,027	552	26,973	1,407	1,203	490	19,677	10,107	7,804.5
Ba	27	66.6	40.3	128	40	25	8.64	119	56.82
Pb	61.4	5.75	137	8.05	55.7	9.79	86.8	6.46	46.37
U	57.2	16.6	90.6	5.72	61.9	34.2	123	6.8	49.5

a colloidal Mo-S-C phase, mixed with organic debris, quartz, carbonate, clay minerals and apatite.

The colloidal material has a composition that can be approximated by the formula (Mo, Fe, Ni) $(S, As)_2C_2$ (jordisite), a mineral phase with a layered structure that pseudomorphoses fossil bacteria and is thought to have replaced sedimentary organic material (Kao et al. 2001).

This metalliferous shale horizon probably represents a change, along a transitional shelf zone, from platform sedimentation in the northwest to a deeper foreland setting in the southeast (Murowchick et al. 1994). These metalliferous shale beds are stratigraphically correlated with apropelic alginate or combustible shale with organic C in excess of 30 %, barite and phosphorate deposits and V- and U-rich shales (Lehmann et al. 2007; Coveney et al. 1994). The sulphidic rocks are characterised by unusual textures, including polymictic mm-size pebbles, sulphide clasts or nodules in a siliceous-carbonaceous matrix and microlaminated sulphidic sediments (Lehmann et al. 2007). The sulphide nodules consist of micron-size globular aggregates. The sulphur isotopic composition of the nodular sulphides has a wide range of $\delta^{34}S$ values, from +30 to −30 ‰ (Lehmann et al. 2007). The concentrations of selected elements (Ni, Cu, Zn, Mo, Ba) of black shales and associated ores are shown in Table 4.7.

At Zunyi (Guizhou Province; Fig. 4.26), the ores average 4 % Mo and contain up to 7 % Ni, 2 % Zn, 2 % As, 2 % V, 1.4 ppm PGE + Au and 50 ppm Ag (Coveney et al. 1992, 1994). In the Hubei Province, black shales are enriched in Ag and V and are associated with intraclastic phosphorite, illitic shale and dolostone, at the same stratigraphic horizon as the Zunyi shales. Vanadium is contained in the illite, whereas Ag is present as sulphide, selenide and native metal (Fan et al. 1992). The ores consist of sulphides and phosphates that form laminae and nodules up to 10 mm across. The principal sulphides are pyrite, vaesite (NiS_2), gersdorffite (NiAsS) and jordisite, associated with fluorapatite, dolomite, calcite, fluorite and sulphates (barite and gypsum) (Murowchick et al. 1994; Coveney et al. 1994). The Ni-Mo-(PGE-Au) ores of the Huangjaiwan mine (Guizhou province) are characterised by a complex assemblage of sulphides and sulpharsenides, together with gersdorffite, millerite, polydymite, pyrite, sphalerite, chalcopyrite, galean and calusthalite (Belkin and Luo 2007). The paragenetically late assemblages gersdorffite-millerite-ploydymite and millerite-gersdorffite indicate temperatures of 200–300 °C, which Belkin and Luo (2007) interpreted as having precipitated from hydrothermal fluids.

Re-Os isotope systematics indicate ages for the sulphide material ranging from 541 ± 16 Ma (Mao et al. 2002c), whereas Pb-Pb isochrons yielded ages of 531 ± 24 and 521 ± 54 Ma (Jiang et al. 2006). More recently, Xu et al. (2011), reported a composite Re-Os isochron age of sulphides of 521 ± 5 Ma, from several mine sites, several hundred kilometres apart. Fluid inclusion studies (Lott et al. 1999) of quartz and fluorite in black shale ores in Guizhou and Hunan provinces, indicate that the minimum temperature of deposition was between 65 and 187 °C. Lott et al's study also revealed that there are negative correlations between homogenisation temperature and salinity upward in the stratigraphy, suggesting boiling of fluids. This led the authors to argue for a sedimentary exhalative origin for the Chinese black shale ores. The presence of quartz veining and stockworks in the underlying dolomite units was cited in support of the model.

4.4.8.2 Genesis of Metalliferous Black Shales in China

Mao et al. (2002c) and Lehmann et al. (2007) suggested a model involving precipitation from seawater enriched in metals. According to these authors, localised euxinic basins developed in the Yangzte carbonate platform, had stagnant water that was episodically replenished by upwelling oxidised sea water. The upwelling oxidised sea water deposited phosphorites along the raised edges of these basins, where oxidised conditions prevailed, while synsedimentary polymetallic sulphides were deposited at the bottom of the euxinic basins. Lehmann et al. (2007) used the Mo isotopic composition of sulphides from the Huangjiawan mine to monitor the isotopic signature of seawater at the time these sulphides were precipitated. The $\delta^{98//95}Mo_{MOMO}$ values (relative to modern ocean water, MOMO = mean ocean molybdenum) have a narrow range, averaging −1.24 ‰, quite different from that of modern oxic oceans (about −3.0 to −2.5 ‰). This average value of the $\delta^{98/95}Mo_{MOMO}$ in the Early Cambrian sulphides is indicative that the ocean Mo sinks were predominantly anoxic. The

model calls for a seawater column similar to that of present-day Black Sea, where metal-rich sediments are in contact with a metal-depleted water column. Bacterial sulphate reduction produces H_2S, which in the specific case of the Chinese black shales, resulted in the sulphidation of a MoO_4^{2-} ligand (Mao et al. 2002c). The role of organic matter, principally cyanobacterial and algal mats, was emphasised by Murowchick et al. (1994). Bacterial decomposition of the organic debris may have caused deposition of metal sulphide and phosphorite beds, through replacement processes. The metals would have been introduced by hydrothermal fluids discharging into the basin either through vents or by diffuse seepage (Murowchick et al. 1994). Coveney (2003), citing Lott et al. (1999), pointed out the presence of quartz stockworks and fluid inclusions with homogenisation temperatures of up to 290 °C, below the ore beds at Daping (Hunan), to suggest a hydrothermal origin for the mineralisation. Jiang et al. (2006) used REE geochemistry and the positive Eu anomaly in the sulphide ores, to infer a submarine hydrothermal origin. Their genetic model proposes venting of Ni-Mo-PGE-bearing hydrothermal fluids in a euxinic basin filled with organic-rich sediments. In this setting a hydrothermal plume rises above the vent, precipitating and adding the metals to the organic-rich muds. Polymetallic sulphides could have formed by the action of anaerobic bacteria by sulphate reduction producing H_2S that interacted with the metallic elements in the organic-rich muds.

More recently Pašava et al. (2010) suggested that anomalously high PGE concentrations in felsic tuff horizons, stratigraphically below the black shales, may have provided the PGE source and may have played an important role in the formation of the polymetallic ores in the black shales. The felsic tuff rocks, interbedded with phosphorites of the Kunyang phosphate deposit, have whole-rock abundances of 434 ppb Pt, 142 ppb Pd, 58 ppb Rh (Pašava et al. 2010). Xu et al. (2011, 2012) suggested that, given similar $^{187}Os/^{188}Os$ values in the sulphides of the polymetallic ores and black shales (ca. 0.87 and 0.80, respectively), the metals may have originated directly from seawater.

4.5 South China; Basins in Cathaysia and Uranium Mineralisation

South China is one of the major U mineral provinces of China, in addition to Junggar-Tianshan (northwest China; Chap. 5), Yinshan-Liaohe province (northeast China), Qilian-Qinling (central China; see Sect. 4.4.5.2 on Dalongshan U deposit, U in the Ordos Basin in Chap. 8) and West Yunnan (southwest China). A review of China's U mineral systems is provided in Dalhkamp (2009). In South China the main types of economically significant U deposits are, in order of importance: granite-related, volcanic-type; black shale-related, also referred to as carbonate-siliceous-pelite (C-Si-pelite).

The Cathaysia Block (including the South China Fold Belt; Chap. 5) is characterised by numerous northeast-trending continental rift basin of Mesozoic age, referred to as the Cathaysian rift system (Fig. 4.27; Hu et al. 2008), which is part of

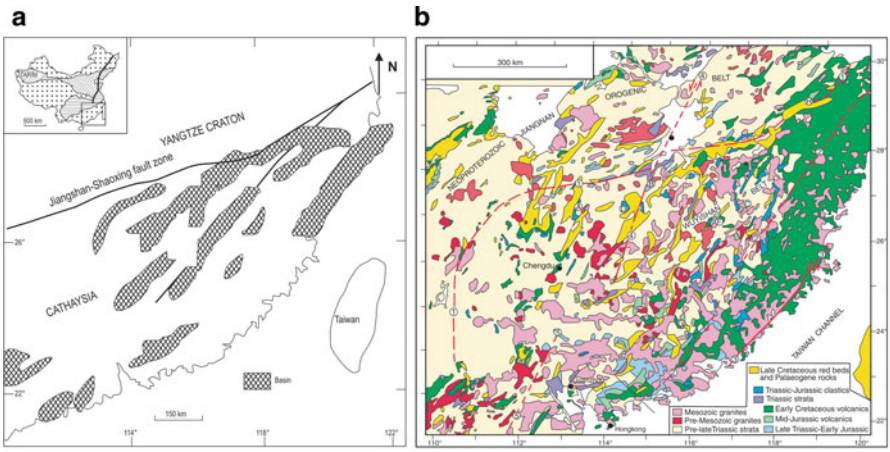

Fig. 4.27 Schematic representation of the distribution of Mesozoic-Cenozoic basin structures in southeastern China (Cathaysia); **a** (after Xie et al. 2006a, b); **b** a more detailed map of basins and distribution of igneous rocks in the same region. (After Shu et al. 2009; see also Wang and Shu 2012)

the greater eastern China rift systems, described in Chap. 8. In this region two types of basins have been recognised: post-orogenic basins, grabens and half-grabens (Shu et al. 2009). The latter were formed during Mid-Jurassic-Early Cretaceous (Yanshanian events) and are characterised by I- and A-type granitic intrusions, mafic dykes (dolerite and lamprophyre) and sills, bimodal volcanism and continental red beds (Fig. 4.27b). Volcanic rocks are represented by basalts and rhyolites, with minor andesite and dacite (Wang and Shu 2012). In the Taihe Basin in central Jiangxi province, northern part of the Cathaysia block (Fig. 4.27a), there are gabbroic intrusions and mafic dykes, emplaced in Late Cretaceous siltstone, sandstone, mudstone and conglomerate of the Guangxi and Gangzhou Groups.

The mafic intrusions of these basins were emplaced in three stages: 147–139, 118–78 and 65–50 Ma (Xie et al. 2006a, b). In the southern Jiangxi province mafic dykes are dominantly sub-alkaline and have LILE (large ion litholphile elements; e.g. Rb, Ba, Sr) enriched and variably depleted in HFSE (high field strength elements; e.g. Nb, Ta, Ti). Xie et al. (2006a) considered the 147–139 and 118–78 Ma dykes to have originated from lithospheric mantle and asthenospheric mantle, associated with lithospheric thinning. Similarly, the Palaeocene (60–50 Ma) mafic dykes show geochemical characteristics similar to ocean island basalt (OIB), such as strong LILE enrichment, high REE and a range of $\varepsilon Nd(t)$ values from +0.8 to +6.2, clearly suggesting mantle sources (Xie et al. 2006b). The geochemical features of mafic rocks in the South China basins are transitional between Late Cretaceous and Palaeocene, which are interpreted by Xie et al. (2006b) as the result of increasing involvement of asthenospheric mantle from the late Mesozoic to the Cenozoic. This, in turn, would reflect lithospheric and crustal extension and decompression melting of the upwelling asthenosphere in Palaeocene time. Gravity data from one of the

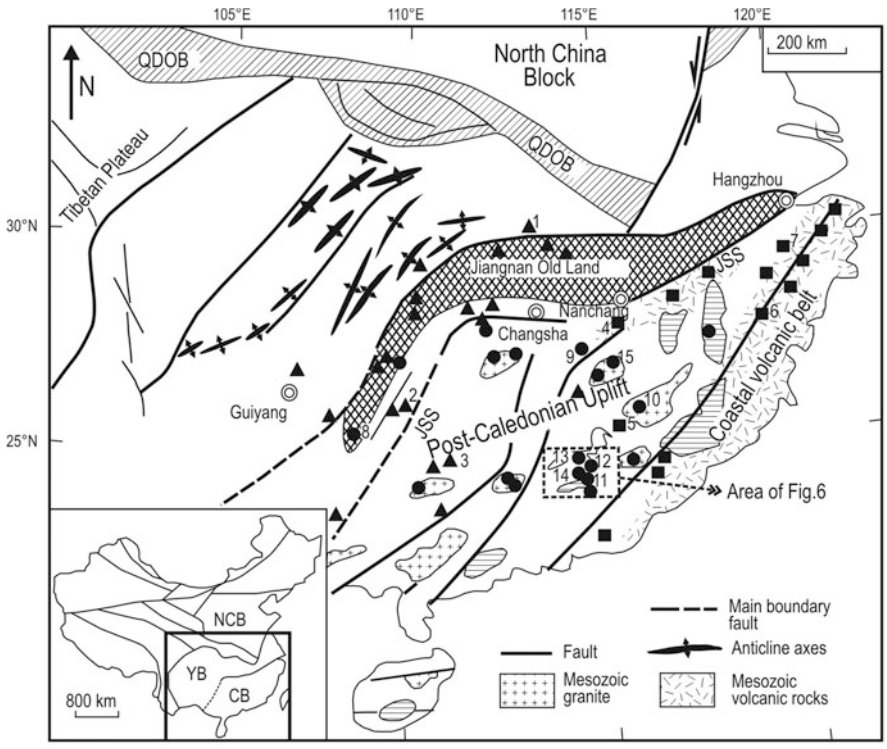

Fig. 4.28 Distribution of three main types of uranium mineral systems in Cathaysia (South China); carbonaceous-siliceous-pelitic, *1* Yaobasi, *2* Sanyaoylin, *3* Xujiadong, granite-related, *4* Xiamgshan, *5* Caotobei, *8* Sanqisi, *9* Liueryaoqi, *10* Hecaokeng, *12* Sanliuyao, *13* Sanliner, *14* Sanerer, *15* Qierlin, volcanic-related, *6* Liubayao, *7* Wuqilin. (After Hu et al. 2008)

fault basins (Gan-Hang) clearly indicate a large positive anomaly suggesting that the Moho discontinuity lies at a shallow depth (Hu et al. 2008), thereby confirming the view of an upwelling asthenospheric mantle. The response of the overlying crust to this upwelling of asthenospheric mantle is extension, which is accompanied by mantle magmatism. These phenomena were instrumental in generating U mineralisation in the region. Hu et al. (2008) classified the U deposits of South China into three types: (1) carbonaceous, siliceous and pelitic rock-hosted, referred to as C-Si-pelite in Dahlkamp (2009); (2) volcanic-hosted and (3) granite-hosted. Most of these deposits occur in veins. Their distribution is shown in Fig. 4.28. The vein-type U granite-related deposits in South China described by Hu et al. (2008), are summarised here. The main deposits and their characteristics are shown in Table 4.8. The six deposits studied by Hu et al. (2008) contain combined resources of 29,000–80,000 tonnes.

The hydrothermal vein deposits are hosted in two-mica S-type granitic rocks of Jurassic-Triassic age, felsic volcanic rocks and carbonaceous and pelitic sedimentary rocks, ranging in age from Precambrian to Jurassic, which shows that the U mineralisation is not related to a particular rock type. Age determinations, reported in Chinese

literature, show a wide range of U forming mineralisation events, namely: 135, 120–115, 90–85, 70–65, 50–45, and 25 Ma. These ages indicate that mantle-derived magmatism, crustal extension and U mineralisation are temporally associated. Silica, hematite, sericite, carbonate, illite and kaolinite constitute the main phases of hydrothermal alteration of the host rocks, which extends for only tens of centimetres along the faults and fractures that contain the mineralisation. The ore mineralogy is relatively simple and consists mostly of pitchblende, brannerite, broggerite, fluorite and molybdenite (Table 4.8). Minor amounts of sulphides, such as marcasite, pyrite, galena, sphalerite and chalcopyrite, may be present. The host quartz veins are formed in the early stages and consist of coarse-grained and microcrystalline quartz. Paragenetic studies indicate three alteration-mineralisation stages: quartz-pyrite-magnetite-sericite (early stage) → sericite-pitchblende-hematite-calcite-fluorite-galena-marcasite-illite (main stage) → quartz-pyrite-calcite-fluorite-illite-kaolinite (late stage). Fluid inclusion studies give variable homogenisation temperatures, ranging from 350–250 °C in the early stages, to 250–150 °C in the main stages and 175–125 °C in the late stages. Salinities range from 3.9 to 1.3 % NaCl equivalent. There are two main types of fluid inclusions: H_2O-rich and H_2O-CO_2-rich. Stable isotope systematics ($\delta^{18}O_{H2O} = -13$ to $+4$ ‰, $\delta D = -85$ to -50 ‰) show that the ore-forming fluids were of meteoric origin. The genetic model envisaged by Hu et al. (2008) postulates a genetic link with mafic magmatism in the region. Cretaceous to Cenozoic extension facilitated the intrusion of mafic dykes and the upward flow of mantle-derived CO_2. This CO_2 was incorporated in the groundwater in fault systems that cut through U-enriched rocks, resulting the mobilisation of U as soluble $UO_2(CO_3)_2^{-2}$ and $UO_2(CO_3)_4^{-3}$ (uranyl carbonate complexes). These uranyl carbonates lost CO_2, due to pressure release, resulting in strong outgassing and release of U-rich hydrothermal fluids.

In the sections that follow, I summarise from Dahlkamp (2009, Chap. 2) a selection of granite-related and volcanic-related U ore fields from South China.

4.5.1 Granite-related U Ore Fields

Granite-related U ore fields are numerous and all have U mineralisation hosted in quartz veins that are both within granitic rocks (intragranitic), or are distributed around the S-type granitic intrusions, commonly referred to as massif. In other cases the ore-bearing quartz veins are in fractures that cut through mafic dykes. Dahlkamp (2009) described the following granite-related U ore fields or deposits: Xiazhuang, Zhuguang, Lujing, Juiyishan, Xiangcao, Mao'ershan, Ziyuan, Motianling, Ma'andu, SL and Dabu. Min (1999, 2005) carried out studies of granite-related U deposits in southeast China.

4.5.1.1 Guidong Granite and Xiaozhuang U Ore Field

In Guandong Province, the Xiaozhuang ore field occupies an area of about 320 km^2, containing granitic rocks, mafic dykes and red beds. At least 15 deposits and occur-

Table 4.8 Uranium vein deposits in southeast China. (After Hu et al. 2008)

Deposit Name	Reserves (t U)	Grades (% U)	Mineral assemblage	Host rocks	Alteration	Ages (Ma)
Xiazhuang	3,000–10,000	0.1–0.3	Pit + Py + Qtz + Cal + Flu	Jurassic two-mica granite and biotite granite	Quartz, hydromica, hematite, calcite	(1) ca. 87 (2) ca. 71
Hechaokeng	1,500–5,000	0.1–0.3	Pit + Py + Qtz + Cal + Flu	Triassic-Jurassic two-mica granite and biotite granite	Quartz, hydromica, hematite, calcite	(1) 90 ± 3 (2) ca. 66 (3) 47 ± 5
Xiangshan	20,000–50,000	0.1–0.3	Pit + Bra + Bro + Py + Mol + Qtz + Cal + Flu + Ap + Gra	Jurassic felsic volcanic rock and granite porphyry	Quartz, hydromica, albite, calcite	(1) 119 ± 1 (2) 99 ± 2
Wuqilin	1,500–5,000	0.1–0.3	Pit + Py + Mol + Qtz + Cal + Flu	Jurassic felsic volcanic rock	Quartz, hydromica, hematite, calcite	89 ± 3
Sanyaoyilin	1,500–5,000	0.1–0.3	Pit + Py + Qtz + Cal + Flu	Cambrian siliceous rock and limestone	Quartz, hematite, calcite	(1) 72 ± 10 (2) 43 ± 7
Yaobasi	1,500–5,000	0.1–0.3	Pit + Py + Qtz + Cal + Flu	Late Proterozoic pelitic rocks and dolomite	Quartz, hematite, calcite	27 ± 1

Pit pitchblende, Py pyrite, Qtz quartz, Cal calcite, Flu fluorite, Mol molybdenite, Ap apatite, Bra brannerite, Bro broggerite, Gra graphite

rences are known from this field with the first discoveries dating back to the 1950s. The Jurassic Guidong granitic massif comprises medium- to fine-grained two-mica granite, hornblende-biotite granite, porphyritic biotote granite, intruded by east-west trending dolerite dykes. Quartz veins trend north-northeast and many host U mineralisation. The Guidong granitic rocks contain uraninite as intergranular grains and the U content of the granite ranges from 6 to 10 ppm. A Cretaceous subvolcanic dacite belt occurs on the northern margin of the massif. Three stages have been recognised in the mineralisation process: (1) pre-ore, brecciated, fine-grained quartz with 1–10 ppm U; (2) syn-ore with red or black microcrystalline quartz-pitchblende, coffinite, fluorite and some sulphides; (3) post-ore quartz-carbonate-fluorite. Pitchblende is the main ore mineral, occurring as disseminations and massive aggregates. The orebodies are veins, lenticular or columnar in shape, mostly intragranitic, others are hosted in quartz veins that cut through mafic dykes (Fig. 4.29). Average grades range from 0.1 to 0.5 % U. Hydrothermal alteration of wall rocks consists of potassic, sodic (albite), silica, muscovite, hematite, argillic and pyritic. Figure 4.29 shows the main features of a quartz vein U deposit in the Xiaozhuang ore field.

Published fluid inclusion studies are somewhat limited. Pre-ore stage quartz contains CO_2 as the dominant gas phase (40–70 vol %). Daughter minerals, mostly calcite, halite and sylvite are also present. Homogenisation temperatures are 280–150 °C for pre-ore quartz, 300–160 °C for syn-ore quartz and 80 °C for post-ore inclusions fluids. Salinities range from 19 to 16 wt % NaCl equivalent and for inclusions with daughter-minerals, salinity values of up to 30–20 wt % NaCl equivalent have been determined. Pre-ore quartz has $\delta^{18}O$ values of between +8.5 and 1.52 ‰, with an average of +7.2 ‰; ore-stage quartz yields an average $\delta^{18}O$ value of 11.99 ‰. The average $\delta D_{(H2O)}$ in the liquid phase of inclusion fluids of pre-ore quartz is −82 ‰, ore-stage fluorite is −65 ‰ and post-ore fluorite −74.5 ‰. These values are transitional from magmatic to meteoric, suggesting that pre-ore to post-ore fluids were of mixed magmatic and meteoric origin.

4.5.1.2 Zhuguang Granite and Related U Ore Fields

The Zhuguang (also called Zhuguangshan) granitic massif is 6,140 km^2 in areal extent (Guandong Province), seems to be a "sack name" for a variety of plutons of widely different ages (Hercynian, Caledonian, Indosinian and Yanshanian) and compositions (adamellite, granodiorite, mignatitic granite). Some of these are referred to as core complexes (Longhuashan heterogeousc complex, Lanhe-Fuzhu migmatite, Waliangang complex). There is clearly some confusion, caused by use of inappropriate terminology, lack of basic geological, geochronological and geochemical data, prompting Dahlkamp (2009) to use the term heterogeneous for the Zhuguang massif. An important granitic complex that is part of the Zhuguang massif is the Longhuashan complex, mostly a coarse-grained porphyritic biotite adamellite, about 18 km long in a west-northwest direction, about 10 km wide and covering an area of 200 km^2. Isotopic dating of parts of this complex yielded a U-Pb age of ca. 205 Ma and a K-Ar age of ca. 182 Ma. There are four main U ore fields associated with this heterogeneous granite complex: Baishun, Chengjiang, Chengkou

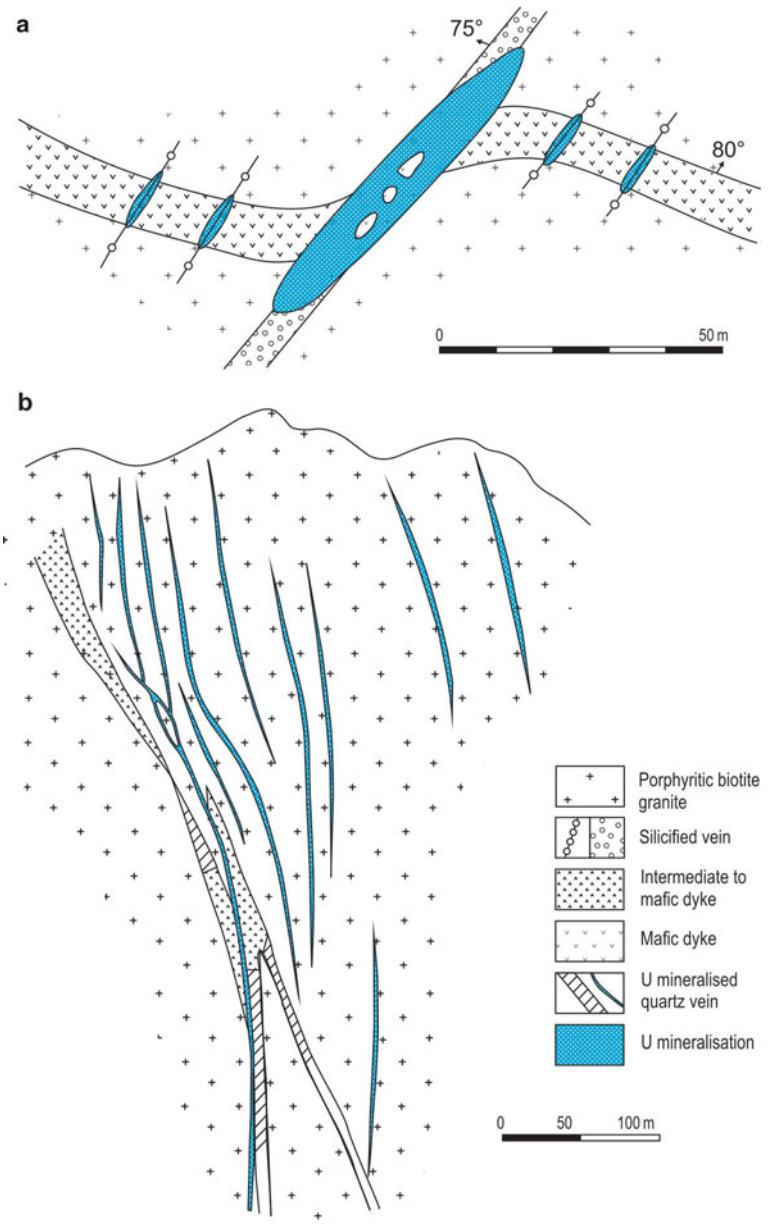

Fig. 4.29 Aspects of U mineral systems in the Xiaozhuang ore field; **a** Uraniferous quartz veins emplaced within a dolerite dyke; **b** cross-section of the granite-related uranifeorus quartz veins in the Zhushnaxia deposit. (After Dahlkamp 2009)

and Lujing. Average grades of the ore veins range from 0.3 to 0.5 % U. Dalhkamp (2009) mentioned from Chinese literature two types of U mineralisation, namely: red and black ore, with the former being more common. Red ore forms veins of microcrystalline quartz containing pitchblende, hematite and locally pyrite. Red ore, from wall rocks to centre of the vein consist of white comb quartz, pitchblende, red microcrystalline quartz with minor pyrite, hematite and pitchblende. Black ore consists of dark microcrystalline quartz containing fluorite, pyrite, marcasite and pitchblende. The black ore veins characteristically exhibit, face-controlled growth of quartz crystals perpendicular to cavity or wall rocks, zoning inward from the wall rocks with: comb quartz + pitchblende, microcrystalline quartz with fragments of pitchblende, pyrite and marcasite, coarse-grained comb quartz and white calcite. These comb-structured ore veins are north-south-trending and hosted in adamellite and biotite granie of Yanshanian age. At the Dongkeng deposit, the ore veins are in the footwall of a northeast-trending mylonitic fault zone at the contact between alkali altered porphyritic biotite granite and Palaeogene red beds.

The Huangao U deposit (Jiangxi Province; Fig. 4.28, No. 14), hosted by the Sanerer pluton of the Zhuguang batholith, is briefly reviewed below (Min et al. 1999). The main host rock type of the mineralisation is a medium- to coarse-grained porphyritc biotite granite with a Rb-Sr isochron age of 215 ± 6 Ma (Indosinian) and initial $^{87}Sr/^{86}Sr$ ratio of 0.7229. Small stocks of fine-grained porphyritic biotite granite with whole-rock Rb-Sr isochron age of 155.7 ± 6.4 Ma (Yanshanian) and $^{87}Sr/^{86}Sr$ ratio of 0.7233 and a variety of dykes, lamprophyre, dolerite, quartz porphyry, are also present in the area. The Huangao U mineralisation is controlled by prominent north and north-northeast fault zones, which are also associated with extensive alkali metasomatism. Indeed, the host granitic rocks of the Huangao deposit exhibit varying degrees of albitic and K-feldspar alteration, which has been attributed to the Yanshanian granitic stocks. Whole rock samples of alkali metasomatised granitic material have returned a Rb-Sr isochron age of 132.1 ± 5.8 Ma, which likely represent the age of the alkali metasomatism event. Apart from this metasomatism, the U mineralised veins are surrounded by chlorite, pyrite, hematite, quartz, damourite (hydro-mica) and carbonate alteration. Most prominent is the hematitic alteration, which imparts a distinct reddish colouration to the altered rocks; furthermore the intensity of this hematitic alteration is directly proportional to high ore grades. Interestingly, Min et al. (2005) pointed out that the host rock hematitic alteration (involving oxidation of Fe^{2+} to Fe^{3+}) can be attributed to radiation-induced oxidants. These authors quote their experimental results, which showed that strong gamma irradiation of simulated ground water produces H_2, O_2, OH, H_2O_2, etc, with amounts increasing with the absorbed dose of gamma rays. This phenomenon is due to radiolytic decomposition of the ground water with Fe^{3+} eventually precipitating as post-mineralisation Fe oxyhydroxides. K-Ar dating of alteration illite yielded ages of 123.5 ± 3.1 and 109.9 ± 3.3 Ma, which are older than the earliest stage mineralisation (U-Pb isochron on pitchblende, 103–47 Ma). Fluid inclusions and stable isotope systematics reported by Min et al. (1999) are summarised as follows.

Homogenisation temperatures of primary fluid inclusions from ore-stage fluorite returned values ranging from 247 to 120 °C and from post-ore calcite values ranging

from 140 to 100 °C. Salinities in ore-stage fluorite range from 21.6 to 11.7 wt % NaCl equivalent, whereas for post-ore calcite salinity is from 5.8 to 0.7 wt % NaCl equivalent. These results were interpreted by Min et al. (1999) as due to mixing of magmatic fluids with meteoric water. Oxygen and deuterium isotopic compositions of the mineralising fluids obtained from fluid inclusions in quartz show $\delta^{18}O$ values of 15.6 to 11.3 ‰, with calculated $\delta^{18}O_{H2O}$ values, based on homogenisation temperatures, of −4.0 to 3.6 ‰. This range of $\delta^{18}O_{H2O}$ values is explained by exchange of meteoric waters with fluids derived from the host granite. The range of $\delta^{34}S$ for pyrite is −6/7–0.4 ‰ (avg −1.3 ‰), which are not too dissimilar from the $\delta^{34}S$ values of −12.4–4.3 ‰ (avg −2.0 ‰) for the host granite, suggesting that the granitic rocks were likely the source of the mineralising fluids.

The paragenetic sequence for the Huangao U mineralisation began with a stage of veinlets and disseminations of pyrite, sphalerite, galena and chalcopyrite. This was followed by a stage 2 characterised by 0.1–1 cm wide dark-green chlorite veinlets associated with pyrite, pitchblende, galena and chalcopyrite. Min et al. (1999) were able to distinguish three generation of chlorite for stage 2. The first is spherulitic aggregates of penninite in fractures or as isolated rosettes; ripidolite is of the second generation and forms vermicular aggregates in microfractures; the third generation occurs as replacement of biotite and is not associated with the mineralisation. The third mineralisation stage consists of black microcrystalline to chalcedonic quartz, pyrite and red microcrystalline hematite. Pitchblende that is part of this stage occurs in the microcrystalline quartz or surrounds sulphides. Fluorite veins up to 30 cm wide and associated with pitchblende, pyrite and minor galena disseminations forms the fourth mineralising stage. Lastly, the fifth stage has comb quartz and carbonate veins. Post-ore minerals formed by wearthering and oxidation include torbanite, uranophane and autunite.

A somewhat unusual granite-related U mineralisation occurs in the Liuerylin district (Jiangxi Province), studied by Min et al. (2005). The ore district comprises at least nine deposits of which the Liuerylin deposit has the largest tonnage and is hosted by a 1,000 km^2 composite granite batholith (Taoshan granitic complex) made up of ten plutons of Indosinian (U-Pb zircon age of 193 Ma) and Yanshanian timing (U-Pb zircon ages of 144–75 Ma). The Taoshan granites intrude a 7 km-thick sequence of Cambrian schist and gneiss and Triassic migmatites. Also in the area are Cretaceous to Tertiaty conglomerate, sandstone and shale that fill rift basins that unconformably overlie the basement metamorphic rocks. The Liuerylin U deposit is hosted by the Daguzhai pluton of Early Cretaceous age (Rb-Sr 136.9 ± 29 Ma), which is a porphyritic two-mica granite characterised, apart from the usual rock-forming silicates (quartz, feldspars, biotite and muscovite), by having trace amounts of zircon, apatite, monazite, sphene, uraninite, allanite, fluorite, magnetite and ilmenite. The mineralisation consists of a south-dipping fracture-controlled sheeted vein system, associated with chlorite, damourite, hematite, pyrite, clay, fluorite and carbonate hydrothermal alteration minerals. The main U minerals are uraninite and coffinite, accompanied by varying amounts of clausthalite (PbSe), galena, sphalerite, bornite and chalcopyrite. These ore minerals fill fractures and exhibit colloform textures. A single ore vein is from 50 to 150 m long and 5–15 m wide.

Most granite-related U mineral systems in South China are associated with U-enriched granitic rocks. In the case of the Sanerer granite pluton, the average U abundance is 9 ppm, about double that of the average 4–5 ppm for granites. Most of these South China U mineral systems are located along fractures near or at contact zones between granites of different ages (e.g. Indosinian and Yanshanian). The mineralisation events begin with what Min et al. (1999) called "deuteric metasomatism or green alteration", involving the replacement of biotite and other rock-forming minerals (K-feldspar, etc) by chlorite and clay minerals. This alteration would have resulted in the liberation of U and other metallic elements from the rock-forming minerals. The hot and dry climatic conditions in Cretaceous to Cenozoic times, favoured the dissolution of uraninite and pitchblende, with leaching and transport of U from the uplifted and weathered U-enriched granites and carbonaceous shales from rift basins. Uranium-bearing oxidised meteoric waters flowed along faults and fractures. These waters were subsequently heated by regional tectonics and radioactive decay of U, The and K in the granites, resulting in the hydrothermal transport and enrichement of U in the fluids. These late phases in the timing of the U mineralisation is supported by the U-Pb isochron ages of pitchblende that range from 103 to 47 Ma. The mineralising fluids were carbonate-rich, suggesting that U was transported as a uranyl carbonate complex, with concomitant depositon of carbonate and pitchblende, resulting from CO_2 effervescence from the mineralising fluids. Min et al. (1999) concluded that the key elements in the formation granite-related U deposits were: (1) A U-enriched and weathered granite source; (2) regional tectonism, which created fractures, faults and enhanced geothermal gradients; (3) hot and dry palaeoclimate; (4) deuteric alteration processes, which liberated U from rock-forming minerals; and (5) contact zones between granites of different ages.

4.5.2 Volcanic-related U Ore Fields

Volcanic-related U deposits occur in a wide region from Zhejiang Province, through Fujian to eastern Guandong (see Fig. 1.1 in Chap. 1), accounting for most of the U deposits in South China. Mesozoic volcanism and formation of volcano-sedimentary basins in South China occurred during Late Jurassic to Late Cretaceous and can be considered as part of the great Yanshanian tectono-thermal event (Fig. 4.19). This volcanism produced calderas, stratovolcanoes and breccia pipes, as discussed in more detail in Chap. 5. Many U deposits are associated with silicic volcanic complexes, dominated by ignimbrite, rhyolite and dacite with lesser andesite, trachyte and basalt. Uranium mineralisation is commonly hosted in calderas, particularly along peripheral ring faults. Other U deposits, generally stratiform, are hosted in sedimentary-volcanic basins, where the mineralisation occurs between layers of impermeable beds, or is associated with breccia pipes and small volcanic edifices. Uranium ores are structurally controlled by deformed margins of volcanic depressions, faults and ring and arcuate structures. A schematic representation of volcanic-related U mineral systems in South China is shown in Fig. 4.30. By and

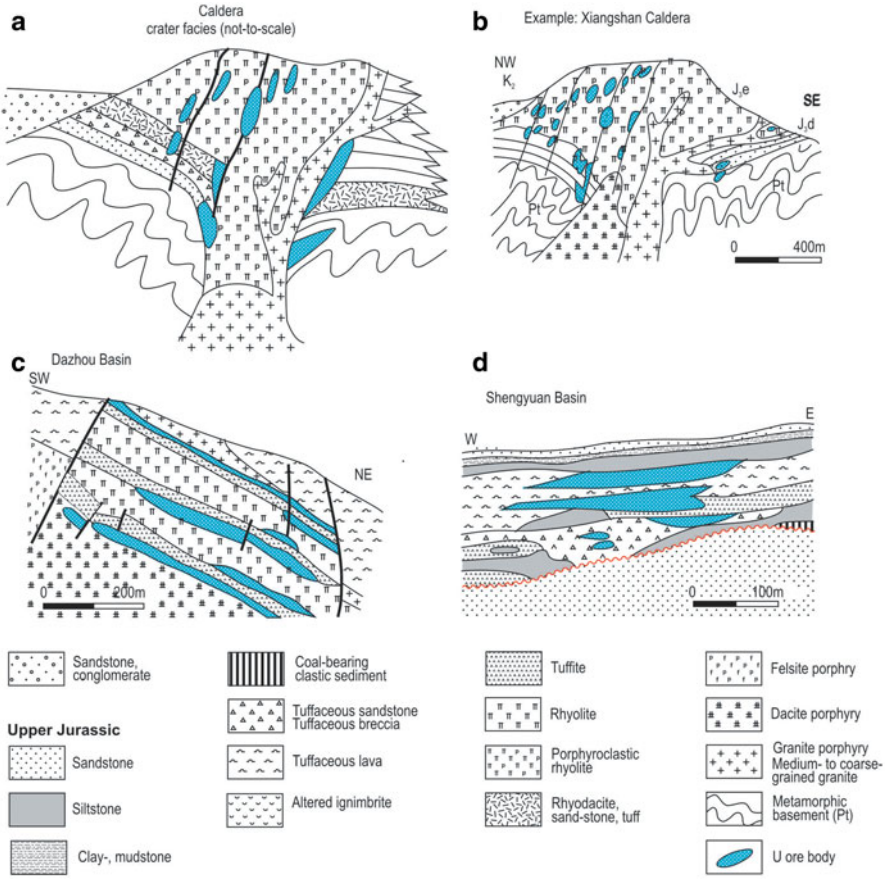

Fig. 4.30 Schematic representation of settings of volcanic-related U mineral systems in South China. (After Dahlkamp 2009)

large the main ore minerals are pitchblende, brannerite, coffinite and uranothorite, accompanied by zones of albitic or illitic alteration, varying amounts of pyrite, fluorite, alunite, apatite, chlorite and carbonates. Potential sources of U may be basement rocks as well as the volcanic units. Uranium abundances in metamorphic rocks in the South China Fold Belt (Chap. 5) average about 5 ppm in Proterozoic rocks and up to 30 ppm in Cambrian carbonaceous slate. Uranium and Th abundances in Jurassic felsic volcanic rocks range from 3 to 26 ppm and 20 to 32 ppm, respectively (cited in Dahlkamp 2009). It is of interest to note that some 40 deposits, accounting for 97 % of the total U resources, are in volcanic rocks that overlie Proterzoic metamorphic basement.

4.5.2.1 Gang-Hang Volcanic Belt and Associated U Deposits

The Jiangxi-Hangzhou, shortened to Gang-Hang, volcanic belt extends for about 600 km from Shaoxing in the northeast to Yuhuashan in the southwest and is from 80 to 50 km wide. The Gang-Hang volcanic belt is one the largest and economically important belts of uranium deposits in China, with a U resource of at least 30,000 t (Dahlkamp 2009). Dahlkamp (2009) in his review (numerous sources are provided in his book), names three ore fields, from northeast to southwest: Xiaoqiuyuan (or Dazhou; Zhejiang Province), Shengyuan (or Shuyan or Yingtan) and Xiangshan in Jiangxi Province. Of these, Xiangshan is the most important (see Table 4.8).

The Gang-Hang volcanic belt was formed in a zone that was repeatedly uplifted and downfaulted between the Carboniferous and Permian. At least five cycles of volcanism have been identified, three in the Jurassic and two in the Cretaceous, resulting in a complex array of volcanic structures, collapsed calderas, downfaulted or downwarped basins and post-collapse subvolcanic intrusions. Mineralisation is usually hosted in Upper Jurassic to Lower Cretaceous felsic lavas and pyroclastics that fill calderas and basins, with only a few lodes hosted in subvolcanic intrusions. there are two types of U mineralisation: (1) structurally controlled and (2) stratabound and/or stratiform. The former, is usually found in caldera structures and constitutes rich and large orebodies that persist to depths of 900 m and consist of veins and stockworks, in which U ore minerals are disseminated. In some cases, as at Xiangshan deposit, the veins form clusters. The controlling structures are ring faults, collapse and crater structures and breccia pipes. Host rocks include subvolcanic microgranite, quartz porphyry, rhyolitic and dacitic lavas. Stratabound/stratiform U mineralisation occurs in volcanic basins, in which the ores are within fractures zones confined to horizons, such as lithogical contacts and unconformities. Host rocks are ignimbrite, volcaniclastic beds, sandstone and rhyolitic lava flows. The orebodies have lenticular shapes from tens to several hundred meters long and from 1 to several metres thick.

The Xiangshan U ore field (also called Fuzhou ore field) is contained within the above-mentioned Xiangshan caldera, which is 300 km^2 in areal extent and hosts some 20 deposits and occurrences with complex metal associations, such as U-Th-Mo-P-REE, U-REE, U-P, U-Pb-Zn-Ag and U-Mo, totalling U resources of around 20,000–50,000 t grading 0.1–0.3 % (Table 4.8). The Xiangshan caldera was formed by two volcanic cycles. The first cycle comprises 169–158 Ma rhyolitic tuff, ignimbrite, rhyodacite lavas, intercalated with tuffaceous sandstone and sandstone beds. The second cycle (150–140 Ma) followed the caldera collapse with the eruption of rhyolitic ignimbrite intercalated with sediments and rhyolite lavas forming dome edifices in the central parts of the caldera. At ca. 135–114 Ma, intrusion of subvolcanic stocks and dykes occurred. The mineralised areas are extensively altered, mostly with albite, micas, kaolinite, dickite, montmorillonite and quartz during the pre-ore phases. Syn-ore alteration is dominated by hematite at the ore lodes, changing progressively outward to carbonate, chlorite and albite. Two are ore assemblages are present: Th-free with U-REE-U-Mo, U-Pb-Zn-Ag and U-P mineral assemblages and U-Th group with U-Th-Mo-P-REE mineral assemblages. Pitchblende from the Th-free group was dated using the SHRIMP U-Pb method to 115 ± 0.5 Ma.

The Shengyaun U ore field (Jiangxi Province) is situated in a volcanic basin covering an area of 300 km^2 and containing three deposits. The area is characterised by Upper Jurassic rhyolitic ignimbrite and other pyroclastics alternating with fluvial sandstone. These rocks overlie a metamorphic basement and Early Palaeozoic granitic stocks. Cretaceous red bed units cover much of the central parts of the volcanic basin. Orebodies have tabular to lenticular shapes, are from 300 to 20 m long, 7–1 m thick and hosted in ignimbrite and tuffaceous sandstone. The ore minerals are pitchblende, coffinite and brannerite, associated with abundant fluorite and jordisite (amorphous molybdenite). Wall rock alteration consists of silicification, dickite, illite and topaz.

In the western part of the Shengyuan volcanic basin is the Guixi U deposit with a resource of 1,500 t grading from 0.1 to 0.3 % U. Here too the mineralisation consists of pitchblende, coffinite and brannerite, associated with variable amounts of fluorite, sulphides, apatite, dickite, hematite. The pitchblend gave a U-Pb age of 90 Ma.

4.6 REE, Nb, Ga (Rare Metal) Mineralisation in a Coal-bearing Sedimentary Succession

In Yunnan Province, southwestern China, Late Permian Yanshan coalfield, developed along the western margin of the South China Block (Dai et al. 2008), hosts Nb(Ta)-Zr(Hf)-REE-Ga mineralisation, discovered during routine well logging. Late Permian coal series are widely present in southern China, particularly in the western part of Guizhoum southern Sichuan and eastern Yunnan provinces.

In northwestern Guizhou is one of the largest coalfields of southern China with reserves probably exceeding 60 Bt (see Li et al. 1995, for an overview).

Dai et al. (2010) reported on the unusual occurrence in a coal-bearing succession, where intra-coalbed alkalic tonstein bands (kaolinite and altered volcanic ash, associated with organic material, typically forming thin bands in coal seams; Neuendorf et al. 2005) are enriched in Nb(Ta)-Zr(Hf)-REE-Ga. Nine rare metals ore beds are in the Xuanwei Formation and range in thickness from 1 to 10 m, but mostly around 2–5 m. The Xuanwei Formation consists of sandstone, siltstone and mudstone with intercalated coal seams, overlying basaltic rocks of the Xuanwuyan Formation. The concentrations of Nb, Ta, Zr, REE, Ga are much higher than industrial grade Nb(Ta), typically 80–200 ppm, whereas Zr, Hf, REE and Ga in the coalfield tonsteins are up to industrial standards (Dai et al. 2010). REO values reported by these authors range from 2,789 to 184 ppm and Ga from 106 to 32 ppm. The common Nb-, Zr-, REE- and Ga-bearing minerals, such as columbite, pyrochlore, zircon, etc., have not been observed in these ore beds by either XRD or optical microscopy, leading Dai et al. (2010) to suggest that these elements occur as absorbed ions in the alkalic tonsteins, which show pervasive alteration from pyroclastic material to kaolinite and mixed layer illite-smectite. The presence of high-temperature euhedral quartz (β-quartz) confirm the pyroclastic nature of the tonstein units. Four types of ore beds have been recognised: (1) clay-altered volcanic ash; (2) tuffaceous clay; (3) tuff, all composed

of quartz, albite, illite-smectite and berthierine; the fourth type of ore bed is a pyroclastic unit with particles larger than 2 mm. The rare metals were likely derived from the pyroclastic unit (Dai et al. 2010).

It is also of interest to note that the coal beds of the Yanshan coalfield are enriched in S, F, V, Cr, Ni, Mo and U, mostly associated with organic matter with these elements ultimately originating from mafic magmas and submarine exhalations (Dai et al. 2008).

4.7 Shilu Fe (Cu-Co) Deposit (Hainan Province); A Polygenetic Mineral System

The Shilu Fe(Cu-Co) deposit, located in the western part of Hainan Island (Hainan Province), has been mined for more than 50 years and is currently producing 5 Mt year of Fe ore at an average grade of 43 % TFe, with Cu and Co as by-products (Chen FX of Hainan Mining Co. Ltd pers. comm. 2011). Hainan Island is situated at the southwestern end of the South China Block (South China Fold Belt) (see Figs. 2.5 and 4.1), with the southern two thirds of the Island underlain by granitic plutons and bimodal volcanic rocks of Mesozoic age (Indosinian and Yanshanian), representing the extension from the South China Block. This area is separated by an east-west-trending fault from the remaining one third to the north, characterised by recent alkali basalt volcanoes. The granitic plutons intruded Neoproterozoic and Palaeozoic (Carboniferous-Permian) rocks, which occur as northeast-trending inliers, entirely surrounded by the Mesozoic igneous rocks. The inliers are part of the Cathaysia Block to the northeast and are metamorphosed to greenschist to amphibolite facies.

The Shilu Fe (Cu-Co) deposit is listed as a medium size (<1 Bt) by Zhu (2007) in a table cataloguing 106 Fe deposits in China. In spite of its size (reserves estimated at ca. 460 Mt of Fe ore), this deposit has received little attention and not much is known about it in English language literature. Mine geologists considered that the Fe ore is BIF-hosted (Lake Superior type?) and is hosted by calc-silicate (skarn) rocks of the Shilu Group. Calc-silicate minerals mainly include tremolite, diopside, garnet and epidote. The ore is dominantly hematite, with lesser quantities of hematite-magnetite and hematite-magnetite-sulphide ore. Barite veins are also present (Yu and Lu 1988). Some tens of metres below the BIF units, are Co-Cu sulphide (cobaltiferous pyrite and chalcopyrite) lenses or beds, allowing Co and Cu to be recovered as by-products. The overlying Fe ores are in places cut by cobaltiferous pyrite and chalcopyrite veinlets, forming the above mentioned hematite-magnetite-sulphide assemblage. The Fe oxides orebodies are generally conformable with the calc-silicate banding, but in places have irregular and cross-cutting contacts with the host lithologies. The lithologies above the Shilu Group, contain Fe-Mn oxides lenses or beds. The BIF units are part of the metamorphosed Shilu Group, comprising six units (formations?), which include quartz schist, crystalline limestone and dolomite, phyllite, metapelite and quartzite with the BIF units located at the top in the sixth unit, intercalated with banded calc-silicates (skarn-altered dolomite?) and

jaspilitic rocks. In plan view the ore lenses have a northwest trend and are folded within a regional synclinorium structure, about 4–5 km across. The Shilu synclinorium is entirely surrounded by younger granitic intrusions and it is possible that the metasedimentary rocks of the synclinorium are a giant roof pendant. On the west side of the synclinorium, is a northeast-trending brittle-ductile shear zone within which are lode Au (orogenic?) deposits. One of these is the Baolun deposit, hosted by sericite-quartz schist, carbonaceous phyllite and slate overlying a basement of high-grade metamorphic rocks (migmatite gneiss and schist). The Baolun deposit has resources of about 73 Mt of ore, grading about 10 g/t Au (Ding et al. 2005).

The precise age of the Shilu Fe ore is not clear, apart from the Neoproterozoic age of the Shilu Group which is constrained by algal fossils found in the uppermost unit 6 (*Chuaria-Tawuia* assemblage; Zhang et al. 1990). Similarly, the origin of the mineralisation and the calc-silicate host rocks, is not known. Fluid inclusion studies by Yu and Lu (1988) showed two populations of decrepitation temperatures: 502–484 °C and 361–344 °C, which they interpreted as relating to regional metamorphism and representing hydrothermal fluids, respectively. However, given that the succession, from base to top, consists of sulphides, Fe oxides, barite and Fe-Mn oxides, it is possible that the Shilu mineralisation may have initially formed as a result of submarine exhalations in a rift setting. These sedimentary-hosted sulphide-Fe oxides were later subjected to regional greenschist to amphibolite facies metamorphism, resulting in the formation of regional calc-silicate skarns and partial re-distribution of the Fe oxides. Following the intrusion of Indosinian granites, contact metamorphism ensued with the localised formation of magnetite. In this scenario, the Shilu Fe (Co-Cu) deposit can be considered as a polygenetic ore system. The deposit is currently the focus of research by the Institute of Mineral Resources (Academy of Geological Sciences, Beijing).

4.8 Concluding Remarks

In this Chapter mineral systems, spanning ages from the Archaean to Cretaceous have been briefly described, mostly from published literature. These mineral systems occur in the Yangtze Craton and the Cathaysia Block, which together with the South China Fold Belt, form the South China Block. As mentioned above, these tectonic domains host mineral systems spanning almost 3,000 million years of geological time, which means that they are not necessarily related to the making of the actual host domain but, as also observed for the North China Craton, most of the known mineralisation is the result of a number of tectonic and magmatic events that affected Yangtze and Cathaysia after they were established as cratonic domains. Although there are some controversial issues, some of which may be related to lack of adequate field observations and/or isotopic data, the general consensus is that in most cases, such as the porphyry, skarns and Kiruna-style deposits of the Yangtze River Valley, were formed during the Yanshanian tectono-thermal event, between ca. 200 and 90 Ma. The Yanshanian Fe-P deposits in the Ningwu basin of the Yangtze River Valley belt are

still debated, whether an origin by magmatic or hydrothermal processes can account for this type of mineralisation (e.g. Gushan magnetite-apatite; Hou et al. 2010, 2011). In the Luzhong basin, magnetite-apatite deposits (e.g. Longqiao) are more clearly linked to skarns and as such are considered as hydrothermal in origin. While the conundrum remains unresolved, it is interesting to note that Charlier et al. (2011) examined Fe-rich and Si-rich melt inclusions in the gabbros of the ca. 564 Ma Sept Iles layered intrusion and concluded that the typically bimodal distribution (Galy gap) occurs when during differentiation the melt splits into Fe-rich and Si-rich liquids. Importantly, Charlier et al. (2011) also pointed out that the granitic rocks at the top of the layered intrusion do not show evidence of liquid immiscibility, therefore they must be derived from fractional crystallisation of the tholeiitic parental magma.

On a more speculative note, it is possible that the Longqiao Fe skarn deposit (Section "Cu-Au Deposits in the Yueshan District") and its association with the evaporite sedimentary beds may be comparable to the Cenozoic hypogene stratabound and fault-bound Fe-P deposits that occur in northwest Jordan, in the intracontinental rift setting of the Dead Sea transform fault (Dill et al. 2010). This possibility is intriguing and worthy of further investigation, because the intracontinental volcano-sedimentary basins of the Yangtze River Valley and associated Fe and Fe-P deposits bear remarkable similarities in both tectonics (basin-and-range style), variety of styles and depositional environments to the Fe-P mineralisation in northwest Jordan.

The causes of the widespread Yanshanian event are also a matter of dispute, but the evidence now seems to point to effects of subduction of the Izanagi plate beneath the east Asia continental margin. This subduction progressed in different steps and orientations (vertical to oblique towards the eastern Asia continental margin), resulting in episodes of slab break off and upwelling asthenspheric mantle, which in turn produced a series of magmatic events that were linked with the generation of the mineral systems described in this Chapter. The same applies to the North China Craton and the fold belts that adorn the margins of these cratonic domains. In the latter case (fold belts), to discriminate between ore systems related to subduction-related magmatic arcs, collision tectonics and the late superimposition or overprinting of the Yanshanian, remains a challenge. For example, the role of adakitic magmas has only recently been examined in an attempt to clarify tectonic settings in central and eastern China. Liu et al. (2010a) investigated two groups of Yanshanian high-Mg adakites, namely those that are associated with porphyry deposits in the Lower Yangtze River Valley and those that are barren of mineralisation aligned the Tanlu fault. They found that different geochemical signatures relate to a water-rich basaltic source for ore-bearing adakites and to a dry basaltic source of the ore-barren ones. More specifically, the former are characterised by lower K_2O, MgO, Cr, Ni, K_2O/Na_2O, $(La/Yb)_N$, Mg#, higher Al_2O_3, Sr/Y and substantially lower εNd(t) (−12.1 to −3.4) compared to the ore-barren adakites (e.g. εNd(t) ranging from −11.4 to −26.5). Liu et al. (2010a), contrary to popular ideas, go as far as to suggest that the ore-bearing adakites are associated with melting of a wet oceanic slab and therefore models calling on delamination or partial melting of lower continental crust are not viable. The ore-barren high Mg-adakites have a younger age range (135–125 Ma) than the ore-bearing adakites in the Lower Yangtze River Valley (143–134 Ma).

Geochronology, major and trace element geochemistry and isotope systematics offer the best solution, providing that these data are supported by good field observations. Work continues with many enthusiastic young and not-so-young geoscientists eagerly and continuously supplying new data in English-language papers. This relatively new effort is solving old problems and, as normal in scientific endevours, opens new ones.

The few paragraphs in this chapter devoted to the world-class Geju mineral district contains Sn (polymetallic) deposits, could not possibly do justice to the fascinating variety of mineral systems in the region, ranging from greisen-hosted, skarns to replacement-style. The metal zoning at both local (near granite contacts) and regional (distal) of the Gejiu district is a remarkable text book case. Research on the Geju deposits is on-going and at the time of writing a number of papers have been submitted for publication in international journals.

Uranium deposits in the volcano-sedimentary basins of South China are poorly represented in the international literature but again, as is the case for the Geju mineral district, more publications are making their way in specialist journals. Rare metal and REE-bearing coal-bearing succession (tonstein bands) of the Yanshan coalfield, opens up new possibilities that could provide new exploration targets of REE in the near future.

References

Barry TL, Kent RW (1998) Cenozoic magmatism in Mongolia and the origin of central and east Asian basalts, Geodyn Ser 27, American Geophysical Union, pp 347–364

Belkin HE, Luo K (2007) Late-stage sulfides and sulfarsenides in Lower Cambrian black shale (stone coal) from the Huangjiawan mine, Guizhou Province, People's Republic of China. Miner Pet 92:321–340

Burnard PG, Hu RZ, Turner G, Bi XW (1999) Mantle, crustal and atmospheric noble gases in Ailaoshan Gold deposits, Yunnan Province, China. Geochim Cosmochim Acta 63:1595–1604

Cai MH, He LQ, Liu GQ, Wu DC, Huang HM (2006a) SHRIMP zircon U-Pb dating of the intrusive rocks in the Dachang tin-polymetallic ore field, Guangxi and their geological significance. Geol Rev 3:407–414 (in Chinese with English abstract)

Cai MH, Liang T, Wei KL, Huang HM, Liu GQ (2006b) Rb-Sr dating of the No. 92 orebody of the Tongkeng-Changpo deposit in the Dachang tin-polymetallic ore field, Guangxi, and its significance. Geol Miner Resour South China 2:35–42 (in Chinese with English abstract)

Cai MG, Mao JW, Ting L, Pirajno F, Huang HL (2007) The Origin of the Tongkemg-Changpo tin deposit, Dachang metal district, Guangxi, China: clues from fluid inclusions and He isotope systematics. Miner Depos 42:613–626

Chappell BW, White AJR (1974) Two contracting granite types. Pac Geol 8:173–174

Charlier B, Namur O, Toplis M, Schiano P, Cluzel N, Higgins MD, Auwera JV (2011) Large-scale silicate liquid immiscibility during differentiation of tholeiitic basalt to granite and the origin of the Daly gap. Geology 39(10):907–910

Charvet J, Shu LS, Shi YS, Guo LZ, Faure M (1996) The building of South China: collision of Yangtze and Cathaysia blocks, problems and tenative answers. J Asian Earth Sci 13:223–225

Chen YJ, Pirajno F, Sui YH (2004) Isotope geochemistry of the Tieluping silver-lead deposit, Henan, China: a case study of orogenic silver-dominated deposits and related tectonic setting. Miner Depos 39:560–575

Chen YJ, Chen HY, Zaw K, Pirajno F, Zhang ZJ (2007) Geodynamic settings and tectonic model of skarn gold deposits in China: an overview. Ore Geol Rev 31:139–169

Cheng QM, Bonham-Carter G, Wang WL, Zhang SY, Li WC, Xia QL (2011) A spatially weighted principal component analysis for multi-element geochemical data for mapping locations of felsic intrusions in the Gejiu mineral district of Yunnan, China. Comput Geosci 37:662–669

Cheng YB, Mao JW, Yang ZX, Rusk BG (in press) Geology and genesis of Kafang Cu-Sn deposit, Gejiu district SW China. Ore Geol Rev

Cliff RA, Rickard D, Blake K (1990) Isotope systematics of the Kiruna magnetite ores, Sweden: Part 1, age of the ore. Econ Geol 85:1770–1776

Coffin MF, Eldhom O (1994) Large igneous provinces: crustal structure, dimensions and external consequences. American Geophysical Union, Rev Geophys 32:1–36

Coveney RM (2003) Re-Os dating of polymetallic Ni-Mo-PGE-Au mineralization in Lower Cambrian black shales of South China and its geological significance—a discussion. Econ Geol 98:661–665

Coveney RM, Murowchick JB, Grauch RI, Chen NS, Glascock MD (1992) Field relations, origins, and resource implications for platiniferous molybdenum-nickel ores in black shales of south China. Explor Min Geol 1:21–28

Coveney RM, Grauch RI, Murowchick JB (1994) Metals, phosphate and stone coal in the Proterozoic and Cambrian of China: the geologic setting of precious metal-bearing Ni-Mo ore beds. SEG Newsl 18:1–11

Dai SF, Ren DY, Zhou YP, Chou CL, Wang XB, Zhao L, Zhu XW (2008) Mineralogy and geochemistry of a superhigh-organic-sulfur coal, Yanshan Coalfield, Yunnan, China: evidence for a volcanci ash component and influence by submarine exhalation. Chem Geol 255:182–194

Dai SF, Zhou YP, Zhang MQ, Wang XB, Wang JM, Song XL, Jiang YF, Luo YB, Song ZT, Yang Z, Ren D (2010) A new type of Nb (Ta)-Zr(Hf)-REE-Ga polymetallic deposit in the Late Permian coal-bearing strata, eastern Yunnan, southwestern China: possible economic significance and genetic implications. Int J Coal Geol 83:55–63

Dalhkamp FJ (2009) Uranium deposits of the world, vol 4. Springer, Berlin

Dill HG, Botz R, Berner Z, Abu Hamad AMB (2010) The origin of pre- and syn-rift, hypogene Fe-P mineralization during the Cenozoic along the Dead Sea Transform Fault, Northwest Jordan. Econ Geol 105:1301–1319

Ding SJ, Fu YR, Zhou TH, Dong GY (2005) The high-grade Baolun gold deposit, Hainan Island, China. In: Mao JW, Bierlein FP (eds) Mineral deposit research: meeting the global challenge. Proceedings of the Eigth Bienn SGA Meeting, Beijing, China, vol 2, pp 1521–1522

Emsbo P, Hofstra AH, Johnson CA, Koenig A, Grauch R, Zhang XC, Hu RZ, Su WC, Pi DH (2005) Lower Cambrian metallogenesis of south China: interplay between diverse basinal hydrothermal fluids and marine chemistry. In: Mao JW, Bierlein FP (eds) Mineral Deposit Research: meeting the global challenge. Proceedings of the Eighth Bienn SGA Meeting, Springer, Beijing, pp 115–118

Fan HR, Li ZL (1992) Geological characteristics, physico-chemical conditions and source materials for mineralization of the Jinshan Gold Deposit. Sci Geol Sin 17(Suppl):147–160 (in Chinese with English abstract)

Fan TL, Yang HC, Wang FL, Chen NC (1973) Petrologic and geochemical characteristics of a nickel-molybdenum-multi-element-bearing lower Cambrian black shale from a certain district in south China. Geochimica 9:143–164 (in Chinese)

Fan D, Ye J, Lui TB (1992) Black shale series-hosted silver-vanadium deposits of the upper Sinian Doushantuo Formation, western Hubei province, China. Explor Min Geol 1:29–38

Fettes D, Desmons J (eds) (2007) Metamorphic rocks—a classification and glossary of terms. Cambridge University Press, Cambridge, p 244

Fletcher CJN, Chan LS, Sewell RJ, Campbell SDG, Davis DW, Zhu JH (2004) Basement heterogeneity in the Cathaysia crustal block, southeast China. Geological Society, London, Sp Publ 226, pp 145–155

Fu M, Changkakoti A, Krouse HR, Gray J, Kwak TAP (1991) An oxygen, hydrogen, sulfur, and carbon isotope study of carbonate-replacement (skarn) tin deposit of the Dachang tin field, China. Econ Geol 86:1683–1703

Fu M, Kwak TAP, Mernagh TP (1993) Fluid inclusion studies of zoning in the Dachang tin-polymetallic ore field, People's Republic of China. Econ Geol 88:283–300

Ge CH, Sun HT, Zhou THE (1990) Copper deposits of China, in Mineral Deposits of China, Editorial Committee of Mineral Deposits, China. Geological Publishing House, Beijing, pp 1–106

Giggenbach WF (1986) The use of gas geochemistry in delineating the origin of fluid discharges over the Taupo volcanic zone: a reviews: 5th International Volcanological Congress, Volcanism, Hydrothermal Systems, and Related Mineralization, Hamilton, Newland, February 1986, Proceedings, pp 47–50

Goodfellow WD, Lydon JW (2007) Sedimentary exhalative (SEDEX) deposits. Geological Association of Canada, Sp Publ 5, pp 163–183

Groves DI, Goldfarb RJ, Gebre-Mariam M, Hagemann SG, Robert F (1998) Orogenic gold deposits: a proposed classification in the context of their crustal distribution and relationship to other gold deposit types. Ore Geol Rev 13:7–27

Groves DI, Goldfarb RJ, Robert F, Hart CJR (2003) Gold deposits in metamorphic belts: overview of current understanding, outstanding problems, future research, and exploration significance. Econ Geol 98:1–29

Gu LX, Zaw K, Hu WX, Zhang KJ, Ni P, He JX, Xu YT, Lu JJ, Lin CM (2007) Distinctive features of Late Palaeozoic massive sulphide deposits in South China. Ore Geol Rev 31:107–138

Gu LX, Wu CZ, Ni P, Chen PR, Pirajno F, Xiao XJ, Zhang ZH (2011) Comparative study of reforming fluids of hydrothermal copper-gold deposits in the Lower Yangtze River Valley, China. Int Geol Rev 53:477–498

Gu XX, Zhang YM, Schulz O, Vavtar F, Liu JM, Zheng MH, Zheng L (2012) The Woxi W-Sb-Au deposit in Hunan, South China: An example of Late Proterozoic sedimentary exhalative (SEDEX) mineralization. J Asian Earth Sci doi:10.1016/j.jseaes.2012.06.006.

Guo CL, Mao JW, Bierlein F, Chen ZH, Chen YC, Li CB, Zeng ZL (2011) SHRIMP U-Pb (zircon), Ar-Ar (muscovite) and Re-Os (molybdenite) isotopic dating of the Taoxikeng tungsten deposit, South China Block. Ore Geol Rev 43(1):26–39

Han RS, Liu CQ, Huang ZL, Chen J, Ma DY, Lei L, Ma GS (2007) Geological features and origin of the Huize carbonate-hosted Zn-Pb-(Ag) district, South China. Ore Geol Rev 31:360–383

Hedenquist JW, Richards JP (1998) The influence of geochemical techniques on the development of genetic models for porphyry copper deposits. Rev Econ Geol 10:235–256

Hitzman MW, Reynolds NA, Sangster DF, Allen CR, Carman CE (2003) Classification, genesis and exploration guides for nonsulphide zinc deposits. Econ Geol 98:685–714

Hou T, Zhang ZC, Du YG, Li ST (2009) Geology of the Gushan iron oxide deposit associated with dioritic porphyry, eastern Yangtze Craton, SE China. Int Geol Rev 51:520–541

Hou T, Zhang ZC, Encarnacion J, Du YS (2010) Geochemistry of Late Mesozoic dioritic porphyries associated with Kiruna-style and stratabound carbonate-hosted Zhonggu iron ores, Middle-Lower Yangtze Valley, eastern China: constraints on petrogenesis and iron resources. Lithos 119(3–4):330–344

Hou T, Zhang ZC, Kusky T (2011) Gushan magnetite-apatite deposit in the Ningwu basin, Lower Yangtze River Valley, SE China: hydrothermal or Kiruna-type? Ore Geol Rev 43(1):333–346

Hu RZ, Bi XW, Zhou MF, Peng JT, Su WC, Liu S, Qi HW (2008) Uranium metallogenesis in South China and its relationship to crustal extension during the Cretaceous to Tertiary. Econ Geol 103:583–598

Huyck HLO (1990) Proposed definition of "black shale" and "metalliferous black shale" for IGCP # 254. Eighth IAGOD Symposium, Geological Survey of Canada, pp A183–A184

Ishihara S (1977) The magnetite-series and ilmenite-series granitic rocks. Min Geol 27:293–305

Jahn B, Wu F, Chen B (2000) Massive granitoid generation in Central Asia: Nd isotope evidence and implication for continental growth in the Phanerozoic. Episodes 23:82–92

Jiao WF, Wu YB, Yang SH, Peng M, Wang J (2009) The oldest basement rock in the Yangtze Craton revealed by zircon U-Pb age and Hf isotope composition. Sci China Ser D52:1393–1399

Jiang SY, Chen YQ, Ling HF, Yang JH, Feng HZ, Ni P (2006) Trace- and rare-earth element geochemistry and Pb-Pb dating of black shales and intercalated Ni-Mo-PGE-Au sulfide ores in Lower Cambrian strata, Yangzte Platform, South China. Miner Depos 41:453–467

Jiang SY, Yang JH, Ling HF, Chen YQ, Feng HZ, Zhao KD, Ni P (2007) Extreme enrichment of polymetallic Ni-Mo-PGE-Au in lower Cambrian black shales of South China: an Os isotope and PGE geochemical investigation. Palaeogeogr Palaeoclimatol Palaeoecol 254:217–228

Jin ZD, Zhu JC, Li FC (2002) O, Sr and Nd isotopic tracing of ore-forming process in dexing porphyry copper deposit, Jiangxi Province. Miner Depos 21:341–349 (in Chinese with English abstract)

Kao LS, Peacor DR, Coveney RM, Zhao G, Dungey KE, Curtis MD, Penner-Hahn JE (2001) A C/MoS, mixed-layer phase (MoSC) occurring in metalliferous black shales from southern China, and new data on jordisite. Am Miner 86:852–861

Kwak TAP, Askins PW (1981) Geology and genesis of the F-Sn-W (Be-Zn) skarn (wrigglite) at Moina, Tasmania. Econ Geol 76:439–467

Lattanzi P, Corazza M, Corsini F, Tanelli G (1989) Sulfide mineralogy in the polymetallic cassiterite deposits of Dachang, P. R. China. Miner Depos 24:141–147

Lehmann B, Mao JW, Li SG, Zhang GD, Zeng MG (2003) Re-Os dating of polymetallic Ni-Mo-PGE-Au mineralization in Lower Cambrian black shales of South China and its geological significance—a reply. Econ Geol 98:661–665

Lehmann B, Nägler TF, Holland HD, Wille M, Mao JW, Pan JY, Ma DS, Dulski P (2007) Highly metalliferous carbonaceous shale and Early Cambrian. Geology 35:403–406

Li ZX (1994) Collision between the North and South China blocks: a crustal-detachment model for suturing in the region east of the Tanlu fault. Geology 22:739–742

Li XH (1997) Timing of the Cathaysia Block formation: constraints from SHRIMP U-Pb zircon geochronology. Episodes 20:188–192

Li ZX (1998) Tectonic history of the major East Asian lithospheric blocks since the mid-Proterozoic—a synthesis, Mantle Dynamics and plate interactions in East Asia. American Geophysical Union, Washington, DC, pp 221–243

Li JY (2001) Timing and pattern of collision of the Sino-Korea and Yangtze cratons: the evolution of the Sinian-Jurassic sedimentary environment in the Middle-Lower Reaches of Yangtze River. Acta Geol Sin 75:25–34 (in Chinese with English abstract)

Li ZX, Li XH (2007) Formation of the 1300-km-wide intracontinental orogen and postorogenic magmatic province in Mesozoic South China: a flat-slab subduction model. Geology 35:179–182

Li XF, Sasaki M (2007) Hydrothermal alteration and mineralization of Middle Jurassic dexing porphyry Cu-Mo deposit, Southeast China. Resour Geol 57:409–426

Li XJ, Yang Z, Shi L, Shi JX (1992) Tin deposits of China, in mineral deposits of China, Editorial Committee of Mineral Deposits, China, vol 2. Geological Publishing House, Beijing, pp 150–222

Li ST, Mao BZ, Lin CS (1995) Coal resources and coal geology in China. Episodes 18:26–30

Li XH, Zhao JX, McCulloch MT, Zhou GQ, Xing FM (1997) Geochemical and Sm-Nd isotopic study of Neoproterozoic ophiolites from southeastern China: petrogenesis and tectonic implication. Precambrian Res 81:129–144

Li ZX, Li XH, Kinny PD, Wang J, Zhang S, Zhou H (2003a) Geochronology of Neoproterozoic syn-rift magmatism in the Yangtze Craton, South China and correlation with other continents: evidence for a mantle superplume that broke up Rodinia. Precambrian Res 122:85–109

Li ZX, Li XH, Wang J, Zhang SH (2003b) A tectonic overview of the South China Block. In: Li ZX, Li XH, Wang J, Zhang SH (eds) From Sibao orogenesis to Nanhua rifting: late Precambrian tectonic history of eastern South China—an overview and field guide, IGCP 440. Geological Publishing House, Beijing, pp 1–13

Li XH, Chen ZG, Liu DY, Li WX (2003c) Jurassic gabbro-syenite suites from southern Jiangxi province, SE China: age, origin, and tectonic significance. Int Geol Rev 45:898–921

Li XF, Hua RM, Mao JW, Ji JF, Wang CZ (2003d) A study of illite Kubler indexes and chlorite "crystallities" with respect to shear deformation and alterations, Jinshan gold deposit, east China. Resour Geol 53(4):283–292

Li XH, Li ZX, Li WX, Liu Y, Yuan C, Wei GJ, Qi CS (2007a) U–Pb zircon, geochemical and Sr–Nd–Hf isotopic constraints on age and origin of Jurassic I- and A-type granites from central Guangdong, SE China: a major igneous event in response to foundering of a subducted flat-slab? Lithos 96:186–204

Li XF, Watanabe Y, Mao JW, Liu SX, Yi XK (2007b) Sensitive high-resolution ion microprobe U-Pb Zircon and ^{40}Ar-^{39}Ar muscovite ages of the Yinshan deposit in the Northeast Jiangxi Province, South China. Resour Geol 57:325–337

Li JW, Zhao XF, Zhou MF, Vasconcelos P, Ma CQ, Deng XD, Souza ZS de, Zhao YX, Wu G (2008) Origin of the Tongshankou porphyry-skarn Cu-Mo deposit, eastern Yangtze Craton, eastern China: geochronological, geochemical and Sr-Nd-Hf isotopic constraints. Miner Depos 43:315–336

Li XF, Yi XK, Zhu HP (2009) Source of ore-forming fluids in Jinshan gold deposit of Dexing County: constraints from microstructures and stable isotope. Miner Depos 28:42–52 (in Chinese with English abstract)

Li JW, Deng XD, Zhou MF, Liu YS, Zhao XF, Guo JL (2010a) Laser ablation ICP-MS titanite U-Th-Pb dating of hydrothermal ore deposits: a case study of the Tonglushan Cu-Fe-Au skarn deposit, SE Hubei province, China. Chem Geol 270:56–67

Li XH, Li WX, Wang XC, Li QL, Liu Y, Tang GQ, Gao YY, Wu FY (2010b) SIMS U–Pb zircon geochronology of porphyry Cu–Au–(Mo) deposits in the Yangtze River Metallogenic Belt, eastern China: magmatic response to early Cretaceous lithospheric extension. Lithos 119(3–4):427–438

Li C, Love GD, Lyons TW, Fike DA, Sessions AL, Chu XL (2010c) A stratified redox model for the Ediacaran ocean. Science 328:80–83

Li XF, Wang CZ, Hua RM, Wei XL (2010d) Fluid origin and structural enhancement during mineralization of the Jinshan orogenic gold deposit. Miner Depos 45:583–597

Liu SA, Li SG, He YS, Huang F (2010a) Gecohemical contrasts between early Cretaceous otre-bearing and ore-barren high-Mg adakites in central-eastern China: implications for petrogenesis and Cu-Au mineralisation. Geochim Cosmochim Acta 74(24):7160–7178

Liu LM, Zhao YL, Zhao CB (2010b) Coupled geodynamics in the formation of Cu skarn deposits in the Tongling-Anqing district, China: computational modeling and implications for exploration. J Geochem Explor 106:146–155

Liu LM, Zhao YL, Sun T (2012) 3D computational shape- and cooling process-modeling of magmatic intrusion and its implication for genesis and exploration of intrusion-related ore deposits: an example from the Yueshan intrusion in Anqing, China Tectonophysics. 526–529:110–123

Lott DA, Coveney RM, Murowchick JB, Grauch RI (1999) Sedimentary exhalative nickel-molybdenum ores in south China. Econ Geol 94:1051–1066

Lu JJ, Hua RM, Yao CL (2005) Re-Os age for molybdenite from the Dexing porphyry Cu-Au deposit in Jiangxi province, China. Geochim Cosmochim Acta 69(Suppl):A882

Mao JW, Robert K, Li HY, Li YH (2002a) High ^{3}He/^{4}He ratios in the Wangu gold deposit, Hunan Province, China: implications for mantle fluids along the Tanlu deep fault zone. Geochem J 3:197–208

Mao JW, Godlfarb RJ, Zhang ZW, Xu WY, Qiu YM, Deng J (2002b) Gold deposits in the Xiaoqinling-Xiong'ershan region, Qinling Mountains, central China. Miner Depos 37:306–325

Mao JW, Lehmann B, Du AD, Zhang GD, Ma DS, Wang YT, Zeng MG, Kerrich R (2002c) Re-Os dating of polymetallic Ni-Mo-PGE-Au mineralization in Lower Cambrian black shales of South China and its geologic significance. Econ Geol 97:1051–1061

Mao JW, Xie GQ, Li XF, Zhang CQ, Mei YX (2004) Mesozoic large scale mineralization and multiple lithospheric extension in south China. Earth Sci Front 11:45–55 (in Chinese with English abstract)

Mao JW, Wang YT, Lehmann B, Yu JJ, Du A, Me YX, Li YF, Zang WS, Stein HJ (2006) Molybdenite Re-Os and albite $^{40}Ar/^{39}Ar$ dating of Cu-Au-Mo and magnetite porphyry systems in the Yangzte River valley and metallogenic implications. Ore Geol Rev 29:307–324

Mao JW, Xie GQ, Pirajno F, Ye HS, Wang YB, Li YF, Xiang JF, Zhao HJ (2010) Late Jurassic-Early Cretaceous granitoid magmatism in Eastern Qinling, central-eastern China: SHRIMP zircon U-Pb ages and tectonic implications. Aust J Earth Sci 57:51–78

Mao JW, Zhang JD, Pirajno F, Ishiyama D, Su HM, Guo CL, Chen YC (2011a) Porphyry Cu-Au-Mo–epithermal Ag-Pb-Zn–distal hydrothermal Au deposits in the Dexing area, Jiangxi province, East China: a linked ore system. Ore Geol Rev 43(1):203–216

Mao JW, Pirajno F, Cook NJ (eds) (2011b) Mesozoic metallogeny in East China and corresponding geodynamic settings—an introduction to the special issue. Ore Geol Rev 43(1):1–7

Mao JW, Xie GQ, Chao D, Pirajno F, Ishiyama D, Chen YC (2011c) A tectono-genetic model for porphyry Cu-Au-Mo-Fe and magnetite-apatite deposits along the Middle-Lower Yangtze River Valley, eastern China. Ore Geol Rev 43(1):294–314

Meinert LD, Lentz DR, Newberry RJ (eds) (2000) A special issue devoted to skarn deposits. Econ Geol 95(6):1183–1370

Meinert LD, Dipple GM, Nicolescu S (2005) World skarn deposits. Econ Geol 100th Ann Vol: 299–336

Min MZ, Luo XZ, Du GS, He BA, Campbell AR (1999) Mineralogical and geochemical constraints on the genesis of the granite-hosted Huangao uranium deposit, SE China. Ore Geol Rev 14:105–127

Min MZ, Fang CQ, Fayek M (2005) Petrography and genetic history of coffinite and uraninite from the Liueryqi granite-hosted uranium deposit, SE China. Ore Geol Rev 26:187–197

Murowchick JB, Coveney RM, Grauch RI, Eldridge CS, Shelton KL (1994) Cyclic variations of sulphur isotopes in Cambrian stratabounds Ni-Mo-(PGE-Au) ores of southern China. Geochim Cosmochim Acta 58:1813–1823

Naslund HR, Henríquez F, Nyström JO, Vivallo W, Dobbs FM (2002) Magmatic iron ores and associated mineralisation: example from the Chilean High Andes and Coastal Cordillera. In: Porter TM (ed) Hydrothermal iron oxide copper-gold & related deposits: a global perspective, vol 2. PGC Publishing, Adelaide, pp 207–226

Neuendorf KKE, Mehl JP, Jackson JA (2005) Glossary of geology, 5th edn. American Geological Institute, Alexandria, p 779

Nyström JO, Enríquez F (1994) Magmatic features of iron ores of the Kiruna type in Chile and Sweden: ore textures and magnetite geochemistry. Econ Geol 89:820–839

Orbeger B, Vymazalova A, Wagner C, Fialin M, Galline JP, Wirth R, Pasava J, Momtagnac G (2007) Biogenic origin of intergrown Mo-sulphide- and carbonaceous matter in Lower Cambrian black shales (Zunyi Formation, southern China). Chem Geol 238:213–231

Pan YM, Dong P (1999) The Lower Chiangjiang (Yangzi/Yangzte River) metallogenic belt, east central China: intrusion- and wall rock-hosted Cu-Fe-Au, Mo, Zn, Pb, Ag deposits. Ore Geol Rev 15:177–242

Pašava J (ed) (1996) A group of papers devoted to the metallogeny of black shales: preface. Econ Geol 91(1):1–3

Pašava J, Frimmel H, Luo TY, Koubova M, Martinek K (2010) Extreme PGE concentrations in Lower Cambrian acid tuff layer from the Kunyang phosphate deposit, Yunnan Province, South China—possible PGE source for Lower Cambrian Mo-Ni-polyelement ore beds. Econ Geol 105:1047–1056

Peng M, Wu YB, Gao S, Zhang HF, Wang J, Liu XC, Gong HJ, Zhou L, Hu ZC, Liu YS, Yuan HL (2012) Geochemistry, zircon U-Pb age and Hf isotope compositions of Paleoproterozoic aluminous A-type granites from the Kongling terrain, Yangtze Block: constraints on petrogenesis and geologic implications. Gondwana Res 526–529:110–123

Peters SG, Huang JZ, Li ZP, Jing CG (2007) Sedimentary rock-hosted Au deposits of the Dian-Qian-Gui area, Guizhou, and Yunnan Provinces, and Guangxi district, China. Ore Geol Rev 31:170–204

Pirajno F (2009) Hydrothermal processes and mineral systems. Springer, Berlin, p 1256
Pirajno F, Ernst RE, Borisenko AS, Fedoseev G, Naumov EA (2009) Intraplate magmatism in central Asia and China and associated metallogeny. Ore Geol Rev 35:114–136
Poulton SW, Fralick PW, Canfield DE (2010) Spatial variability in oceanic redox structure 1.8 billion years ago. Nat Geosci 3:486–490
Qiu HN, Zhu BQ, Sun DZ (2002) Age significance interpreted from $^{40}Ar/^{39}Ar$ dating of quartz samples from the Dongchuan copper deposits, Yunnan, SW China, by crushing and heating. Geochem J 36:475–491
Quan H, Han QY, Ai YF, Lin YC, Wei JY (1992) The features and prospects of metallogenesis of polymetals, gold and silver in Yan-Liao area of China. Geological Publishing House, Beijing, p 134 (in Chinese)
Ran CY (1989) Dongchuan-type stratabound copper deposits, China: a genetic model. Geological Association of Canada, Sp Pap 36, pp 667–678
Rollinson HR (1993) Using geochemical data: evaluation, presentation, interpretation. Longman Scientific and Technical, Harlow, p 352
Rui ZY, Li YQ, Wang LS (2003) Approach to ore forming conditions of ore fluid inclusions. Miner Depos 22:13–23 (in Chinese with English abstract)
Rui ZY, Zhang LS, Wu CY, Wang LS, Sun XY (2005) Dexing porphyry copper deposits in Jiangxi, China. In: Porter TM (ed) Super porphyry copper and gold deposits: a global perspective, vol 2. PGC Publishing, Adelaide, pp 409–421
Schultz RB (1991) Metalliferous black shales: accumulation of carbon and metals in cratonic basins. Rev Econ Geol 5:171–176
Sengör AMC, Natal'in B (1996) Paleotectonics of Asia: fragments of a synthesis. In: Yin A, Harrison M (eds) The tectonic evolution of Asia. Cambridge University Press, Cambridge, pp 486–640
Shu LS, Zhou XM, Deng P, Wang B, Jiang JH, Yu JH, Zhao XX (2009) Mesozoic tectonic evolution of the Southeast China Block: new insights from basin analysis. J Asian Earth Sci 34:376–391
Shu LS, Faure M, Yu JH, Jahn BM (2011) Geochronological and geochemical features of the Cathaysia Block (South China): new evidence for the Neoproterozoic breakup of Rodinia. Precambrian Res 187(3–4):263–276
Simmons SF, Sawkins FJ, Schulutter DJ (1987) Mantle-derived heliumin two Peruvian hydrothermal ore deposits. Nature 329:429–432
Sinton CW, Duncan RA (1997) Potential links between ocean plateau anoxia at the Cenomanian-Turonian boundary. Econ Geol 92:836–842
Stuart FM, Burnard P, Taylor RP, Turner G (1995) Resolving mantle and crustal contributions to ancient hydrothermal fluid: He-Ar isotopes in fluid inclusions from Dae Hwa W-Mo mineralisation, South Korea. Geochim Cosmochim Acta 59:4663–4673
Su WC, Heinrich CA, Pettke T, Zhang XC, Hu RZ, Xia B (2009) Sediment-hosted gold deposits in Guizhou, China: products of wall-rock sulfidation by deep crustal fluids. Econ Geol 104:73–94
Tang M, Wang XL, Xu XS, Zhu C, Cheng T, Yu Y (2012) Neoproterozoic subducted materials in the generation of Mesozoic Luzong volcanic rocks: evidence from apatite geochemistry and Hf-Nd isotopic decoupling. Gondwana Res 21(1):266–280
Tu GC (1990) Lead-zinc deposits of China, in Mineral Deposits of China, Editorial Committee of Mineral Deposits, China, vol 1. Geological Publishing House, Beijing, pp 107–208
USGS (United States Geological Survey) (2009) Mineral commodities summaries. U. S. Govt Printing Office, Washington, DC, p 179
Wang D, Shu LS (2012) Late Mesozoic basin and range tectonics and related magmatism in Southeast China. Geosci Front 3(2):109–124
Wang DH, Chen YC, Chen W, Sang HQ, Li HQ, Lu YH, Chen KL, Lin ZM (2004a) Dating of the Dachang superlarge tin polymetallic deposit in Guangxi and its implication for the genesis of the No. 100 orebody. Acta Geol Sin 78:452–458 (English edition)
Wang Q, Zhao ZH, Jian P, Xu JF, Bao ZW, Ma JL (2004b) SHRIMP zircon geochronology and Nd-Sr isotopic geochemistry of the Dexing granodiorite porphyries. Acta Pet Sin 20:315–324 (in Chinese with English abstract)

Wang XL, Zhou JC, Qiu JS, Gao JF (2004c) Geochemistry of the Meso- to Neoproterozoic basic-acid rocks from Hunan Province, South China: implications for the evolution of the western Jiangnan orogen. Precambrian Res 135:79–103

Wang H, Zhang SH, He GQ (2005) China and Mongolia. In: Selley RC, Robin L, Cocks M, Plimer IR (eds) Encyclopedia of geology, vol 1. Elsevier, Oxford, pp 345–358

Wang F, Zhou XH, Zhang LC, Ying JF, Zhang YT, Wu FY, Zhu RX (2006) Late Mesozoic volcanism in the Great Xing'an Range (NE China): timing and implications for the dynamic setting of NE Asia. Earth Planet Sci Lett 251:179–198

Wang XL, Zhou JC, Griffin WL, Wang RC, Qiu JS, O'Reilly SY, Xu XS, Liu XM, Zhang GL (2007) Detrital zircon geochronology of Precambrian basement sequences in the Jiangnan Orogen: dating the assembly of the Yangtze and Cathaysa blocks. Precambrian Res 159:117–131

Wang LJ, Griffin WL, Yu JH, O'Reilly SY (2010a) Precambrian crustal evolution of the Yangtze Block tracked by detrital zircons from Neoproterozoic sedimentary rocks. Precambrian Res 177:131–144

Wang XC, Li XH, Li ZX, Liu Y, Yang YH (2010b) The Willouran basic province of South Australia: its relation to the Guibei large igneous province in South China and the breakup of Rodinia. Lithos 119:569–584

Wang L, Hu MG, Yang Z, Qu WJ, Xia JL, Chen KX (2011) U-Pb and Re-Os geochronology and geodynamic setting of the Dabaoshan polymetallic molybdenum deposit, northern Guandong Province, South China. Ore Geol Rev 43(1):40–49

Wang GG, Ni P, Zhao KD, Wang XL, Liu JQ, Jiang SY, Chen J (2012) Petrogenesis of the Middle Jurassic Yinshan volcanic-intrusive complex, SE China: Implications for tectonic evolution and Cu-Au mineralization. Lithos, doi: 10.1016/j.lithos.2012.05.030

Wignall PB (1994) Black shales. Clerendon Press, Oxford, p 124

Wu RX, Zheng YF, Wu YB, Zhao ZF, Zhang SB, Liu XM, Wu FY (2006) Reworking of juvenile crust: element and isotope evidence from Neoproterozoic granodiorite in South China. Precambrian Res 146:179–212

Xie GQ, Hu RZ, Mao JW, Pirajno F, Li RL, Cao JJ, Jiang GH, Zhao JH (2006a) K-Ar dating, geochemical, and Sr-Nd-Pb isotopic systematics of Late Mesozoic mafic dikes, southern Jiangxi Province, south east China: petrogenesis and tectonic implications. Int Geol Rev 48:1023–1051

Xie GQ, Mao JW, Hu RH, Pirajno F, Li RL, Cao JJ (2006b) K-Ar dating, geochemical and Sr-Nd-Pb isotopic systematics of Paleocene mafic rocks in central Jiangxi, SE China: evidence for lithosphere replacement. Geochem J 40:485–500

Xie GQ, Mao JW, Zhao HJ, Wei KT, Jin SG, Pan HJ, Ke YF (2011) Timing of skarn Cu-Au-Fe deposits from the Tonglushan ore district, southeast Hubei, Middle-Lower Yangtze River belt and its implication. Ore Geol Rev 43(1):62–77

Xu YG (2001) Thermo-tectonic destruction of the Archaean lithospheric keel beneath the Sino-Korean Craton in China: evidence, timing and mechanism. Phys Chem Earth 26:747–757

Xu XS, O'Reilly SY, Griffin WL, Wang XL, Pearson NJ, He ZY (2007) The crust of Cathasya: age, assembly and reworking of two terranes. Precambrian Res 158:51–78

Xu LG, Lehmann B, Mao JW, Qu WJ, Du AD (2011) Re-Os age of polymetallic Ni-Mo-PGE-Au mineralization in early Cambrian black shales of South China—a reassessment. Econ Geol 106:511–522

Xu LG, Lehmann B, Mao JW (2012) Seawater contribution to polymetallic Ni-Mo-PGE-Au mineralization in Early Cambrian black shales of South China: Evidence from Mo isotope, PGE, trace element, and REE geochemistry. Ore Geol Rev doi:10.1016/j.oregeorev.2012.06.003

Xue F, Krökner A, Reischmann T, Lerch F (1996) Palaeozoic pre- and post-collision calc-alkaline magmatism in the Qinling orogenic belt, central China, as documented by zirocn ages on granitoid rocks. J Geol Soc Lond 153:409–417

Yan J, Liu HQ, Song CZ, Xu XS, An YJ, Dai LQ (2009) Zircon U-Pb geochronology of the volcanic rocks from Nanchang-Ningwu volcanic basins in the Lower Yangtze region and its geological implications. Chin Sci Bull 54:2895–2904

Yang ZY, Cheng YQ, Wang HZ (1986) The geology of China. Clarendon Press, Oxford, p 303

Ye Y, Shimakazi H, Simizu M, Hu S (1998) Tectono-magmatic evolution and metallogenesis along the Northeast Jiangxi Deep Fault, China. Resour Geol 48:43–50

Yu CB, Lu HZ (1988) An investigation into the genesis of the Shilu iron deposit with special reference to its fluid inclusions. Geochemistry 2(2):127–141

Yu JH, Griffin WL, Wang LJ, O'Reilly SY, Zhang M, Wang RC, Jiang SY (2008) Where was South China in the Rodinia supercontinent? Evidence from U-Pb ages and Hf isotopes of detrital zircons. Precambrian Res 164:1–15

Yu JH, O'Reilly SY, Wang L, Griffin WL, Zhou MF, Zhang M, Shu L (2010) Components and episodic growth of Precambrian crust in the Cathaysia Block, South China: evidence from U-Pb ages and Hf isotopes of zircons in Neoproterozoic sediments: Precambrian Res 181(1–4):97–114

Yu JJ, Chen YC, Mao JW, Pirajno F, Duan C (2011) Review of geology, alteration and origin of iron oxide-apatite deposits in the Cretaceous Ningwu basin, Lower Yangtze River Valley, eastern China: implications for ore genesis and geodynamic setting. Ore Geol Rev 43(1):170–181

Zaw K, Peters SG, Cromie P, Burrett C, Hou Z (2007) Nature, diversity of deposit types and metallogenic relations of South China. Ore Geol Rev 31:3–47

Zhai YS, Xiong YL, Yao SZ, Lin XD (1996) Metallogeny of copper and iron deposits in the Eastern Yangtse Craton, east-central China. Ore Geol Rev 11:229–248

Zhang WH, Tan TL (1998) Relationship between organic fluids and gold mineralization in the Jinshan gold deposit, Jiangxi Province. Miner Depos 17:15–24 (in Chinese with English abstract)

Zhang FX, Zhang J (2003) Geological-geochemical characteristics of Carlin- and Carlin-like-type gold deposits in South Qinling mountains. Chin J Geochem 22:11–22

Zhang RJ, Feng SN, Xu GH, Yang DL, Jiang DH, Wu W (1990) Discovery of Chuaria-Tawuia assemblage in Shilu group, Hainan Island and its significance. Sci China Ser B Chem 33(2):211–220 (in Chinese with English abstract)

Zhang L, Liu J, Yu G, Chen Z (1996a) Hydrogen and oxygen isotopes of the water-rock interaction in the Yinshan Cu-Pb-Zn-Ag deposit, Jiangxi Province. Acta Geol Sin 9:274–289 (English Edition)

Zhang LG, Liu JX, Chen ZS, Yu GX (1996b) The isotopic evolution of water/rock system in Tongchang porphyry deposit, Dexing, Jiangxi province. Sci Geol Sin 31:250–263

Zhang DH, Yu C, Bao Z, Tang Z (1997) Ore zoning and the dynamics of ore-forming processes in the Yinshan polymetallic deposit, Jiangxi. Chin J Geochem 16:123–132

Zhang ZJ, Chen YJ, Chen HY, Bao JX, Liu YL (2003) The petrochemical characteristics of the Hercynian granitoids in Tianshan and its geodynamic implications. J Miner Pet 23:15–24 (in Chinese with English abstract)

Zhang DH, Xu GJ, Zhang WH, Golding SD (2007) High salinity fluid inclusions in the Yinshan polymetallic deposit from the Le-De metallogenic belt in Jiangxi province, China: their origin and implications for ore genesis. Ore Geol Rev 31:247–260

Zhang LJ, Zhou TF, Yuan F, Duan C (2008) SHRIMP U-Pb zircon dating of Yueshan intrusion in the Yueshan ore field, Anhui, and its significance. Acta Pet Sin 24(8):1725–1732 (in Chinese)

Zhao XF, Zhou MF (2011) Fe–Cu deposits in the Kangdian region, SW China: a Proterozoic IOCG (iron-oxide–copper–gold) metallogenic province. Miner Depos 46:731–747

Zhao YM, Zhang YN, Bi CS (1999) Geology of gold-bearing skarn deposits in the middle and lower Yangtze River Valley and adjacent regions. Ore Geol Rev 14:227–249

Zhao ZF, Zheng YF, Wei CS, Gong B (2004) Temporal relationship between granite cooling and hydrothermal uranium mineralization at Dalongshan in China: a combined radiometric and oxygen isotopic study. Ore Geol Rev 25:221–236

Zhao XF, Zhou MF, Li JW, Wu FY (2008) Association of Neoproterozoic A- and I-type granites in South China: implications for generation of A-type granites in a subduction-related environment. Chem Geol 257(1–2):1–15

Zhao DP, Pirajno F, Dobretsov NL, Liu L (2010) Mantle structure and dynamics under East Russia and adjacent regions. Russ Geol Geophys 51:901–914

Zhao JH, Zhou MF, Yan DP, Zheng JP, Li JW (2011) Reappraisal of the ages of Neoproterozoic strata in South China: no connection with the Grenvillian orogeny. Geology 39:299–302

Zhao XF, Zhou MF, Hitzman MW, Li JW, Bennett M, Meighan C, Anderson E (2012) Late Paleoproterozoic to Early Mesoproterozoic Tangdan sedimentary rock-hosted strata-bound copper deposits, Yunnan Province, southwest China. Econ Geol 107:357–375

Zheng JP, Griffin WL, O'Reilly SY, Zhang M, Pearson N, Pan YM (2006) Widespread Archean basement beneath the Yangtze Craton. Geology 34:417–420

Zhou TH, Goldfarb RJ, Phillips GN (2002) Tectonics and distribution of gold deposits in China—an overview. Miner Depos 37:249–282

Zhou XM, Sun T, Shen WZ, Shu LS, Niu YL (2006) Petrogenesis of Mesozoic granitoids and volcanic rocks in South China: a response to tectonic evolution. Episodes 29:26–33

Zhou TF, Yuan F, Yue SC, Liu XD, Zhang X, Fan Y (2007) Geochemistry and evolution of ore-forming fluids of the Yueshan Cu-Au skarn and vein type deposits, Anhui Province, South China. Ore Geol Rev 31:279–303

Zhou TF, Wu MG, Yu F, Chao D, Feng Y, Zhang LJ, Jun L, Bing Q, Pirajno F, Cooke DR (2011) Geological, geochemical characteristics and isotope systematics of the Longqiao iron deposit in the Lu-Zong volcano-sedimentary basin, Middle-Lower Yangtze (Changjiang) River Valley, Eastern China. Ore Geol Rev 43(1):154–169

Zhu X (ed) (2007) Mineral facts of China. Elsevier, Amsterdam, p 776

Zhu X, Huang CK, Rui ZY (1983) Dexing porphyry copper deposit. Geological Publishing House, Beijing, p 336

Zhu MY, Zhang JM, Yang AH (2007) Integrated Ediacaran (Sinian) chronostratigraphy of South China. Palaeogeogr Palaeoclimatol Palaeoecol 254:7–61

Zhu G, Niu ML, Xie CL, Wang YS (2010) Sinistral to normal faulting along the Tan-Lu fault zone: evidence for geodynamic switching of the East China continental margin. J Geol 118:277–293

Zhu LM, Zhang GW, Chen YJ, Ding, ZJ, Guo B, Gong HJ, Wang, F, Lee B (2011) Zircon U-Pb ages and geochemistry of the Wenquan Mo-bearing granitoids in West Qinling, China: constraints on the geodynamic setting for the newly discovered Wenquan Mo deposit. Ore Geol Rev 39:46–62

Zhuang Y, Wang R, Yang S, Yi J (1996) Geology of Gejiu tin-copper polymetallic deposit. Earthquake Publishing House, Beijing, p 189

Chapter 5
Orogenic belts: South China, Central China and Qinling-Dabie, Hinggan

Abstract The South China Fold Belt, Qinling-Dabie-Sulu, Qilian and Hinggan orogens are reviewed in this chapter. The South China Fold Belt is the coastal part of the Cathaysia Block, which was directly influenced by subduction-related calc-alkaline magmatism in the Jurassic-Cretaceous. During this time mineral deposits of Sn, W, Mo, Pb-Zn, Cu, Sb, hydrothermal vein-type, porphyry Cu-Au, skarns, and precious metal epithermal were formed. The Zhilingtou and Huangshan epithermal deposits are reviewed, followed by Au-Cu high-sulphidation epithermal mineralisation in the Zijinshan mining district (Fujian Province) and the polymetallic Ag-rich and low-sulphidation veins and/or stockworks of the Coastal Volcanic Belt. Chinkuashih is the youngest (1 Ma) epithermal system in the northern tip of Taiwan and part of the western extension of the active Ryukyu volcanic arc.

The Qinling-Dabie-Sulu orogen is the eastern part of the Central China Orogen and was formed by continental subduction and collision between the Yangtze Craton and the North China Craton. The orogen extends northward along the major Tanlu fault zone (Sulu orogen). An understanding of the geodynamicevolution and associated magmatism of the Qinling-Dabie-Sulu orogen is pivotal for the genetic modelling of related mineral systems. Although tectonic models are debated, unifying factors include the Mesozoic Indosinian and Yanshanian tectono-thermal events, dominated by granitic magmatism, and the northward subduction of crustal materials beneath the North China Craton. Partial melting of the Proterozoic lithologies was instrumental in the delivery of CO_2- and F-rich fluids as well as metals, resulting in the formation of porphyry deposits, auriferous breccia pipes and lode deposits. In the Xiaoqinling-Xiong'ershan region of the Qinling mountains there are more than 100 lode Au-Ag, with an estimated total resource greater than 550 tonnes. Tieluping and Shanggong are examples described in this chapter. The East Qinling porphyry, porphyry-skarn systems have a total resource of Mo metal of about 2.7 Mt In addition, the Sandaozhuang deposit also contains 502,465 tonnes of W metal. A review of the salient features of a number of these porphyry deposits is provided. The Qiyugou auriferous breccia pipe is discussed in some detail and linked to a wider hydrothermal system, characterised by volatile-rich fluids derived from subducted Proterozoic lithologies. The unusual Huanglongpu Mo-Pb mineralisation associated with carbonatite dykes is briefly described. There are numerous sediment-hosted Au deposits in the Qinling region. These all share some similarities with the classic Carlin deposits of the western USA, such as jasperoidal alteration and metal assemblages (Au, Hg, Sb, Ag, Tl). Some of the Carlin-type or style deposits have local features with metals such as W and U. The Qilian orogen is the western extension of

F. Pirajno, *The Geology and Tectonic Settings of China's Mineral Deposits,*
DOI 10.1007/978-94-007-4444-8_5,

the Qinling-Dabie orogenic belt, striking west-northwest from Gansu Province, to Qinghai, Shaanxi and Henan provinces. In southeastern Gansu Province, the Qilian orogen hosts numerous VMS deposits in a submarine 600–520 Ma bimodal volcanic belt, about 1,200 km long and 50 km wide, at the southeast margin of the Tarim Craton.

The closure of the Palaeo-Asian Ocean separating the North China Craton from the Siberian plate resulted in the formation of the Altai and Tianshan-Hinggan orogenic belts, which are part of the Central Asian Orogenic Belt. In northeast China, the Hinggan orogenic belt evolved by accretion of volcanic arc systems, oceanic crust and microcontinental blocks, eventually sutured along the Solonker zone and the Kangbao-Chifeng fault that separates the terranes of the Altaids from the northern margin of the North China Craton. Indosinian to Yanshanian intraplate magmatism, comprising calc-alkaline to high-K calc-alkaline volcanic rocks and subvolcanic intrusions, overprinted the Hinggan orogen. The Hinggan mineral deposits can be geographically grouped into four districts: the northern Great Hinggan Range, the southern Great Hinggan Range, the Lesser Hinggan Range and Changbaishan. In the Great Hinggan Range are low-sulphide Au (Ag) epithermal systems characterised by quartz veins, with low contents of sulphides, as exemplified by the Shabaosi, Sandaowanzi, Dong'an, Ciweigou and Tuanjiegou deposits. High-sulphide Au (Cu, Zn) systems, are less common and exemplified by Jinchang Au deposit, Daba Au (Cu), Naozhi Au (Cu) and Naoniushan Cu (Au) deposits. Silver-rich polymetallic deposits and occurrences are mainly found in the Manzhouli Basin and Erguna Massif, exemplified by the Jiawula, Chaganbulagen and E'rentaolegai deposits. The Jiwula, Chaganbulagen, Xijinuo Shan and Erdaohezi deposits have atypical epithermal features, as shown by the absence of diagnostic minerals (adularia or enargite) and are considered as hydrothermal vein deposits. In the southern Manzhouli basin is a porphyry-epithermal district, where porphyry Cu-Mo mineralisation is associated with skarns and high-level epithermal systems. The Dong'an is a low-sulphidation (adularia-sericite) epithermal Au deposit, characterised by at least 14 orebodies, surrounded by quartz- and sericite-dominated alteration zones. In general, the country rocks and Au orebodies have distinct boundaries which are characterized by alteration zones along faults.

The east-west-trending Xilamunum metallologenic belt, is within the Hinggan orogenic belt and is known to contain at least 20 porphyry Mo deposits as well as vein-type and epithermal deposits. Some of the economically most important are: Chehugou, Kulitou, Daiheshan, Xiaodonggou and Jiguanshan porphyry Mo, Nianzigou and Xinjing vein-type Mo and Hongshanzi Mo-U epithermal deposit. The time of the Mo mineralisation and host porphyry rocks between 156 and 154 Ma.

Within the Hinggan fold belt there are also about 1,000 mafic-ultramafic complexes. In the Hongqiling area, there is a series of northwest-trending mafic-ultramafic intrusions and dykes, some of which host orthomagmatic Ni-Cu disseminated and massive sulphide mineralisation. In the Hongqiling district at least five intrusions are known to have Ni-Cu sulphide mineralisation. The No. 7 Fujia intrusion has ore reserves estimated at 88.9 Mt grading 2.3 % Ni, 0.63 % Cu and 0.05 %

Co. Re-Os dating of pyrrhotite from Ni-Cu sulphide ore in the Fuja (No. 1) intrusion, gave an age of 208 ± 21 Ma (Lü et al. 2011). These ages are coincident with A-type post-orogenic granitic magmatism in northeast China. Chromitite lenses are present in 280 Ma zoned mafic-ultramafic intrusions (Alaskan type), intruded during south-directed subduction beneath the northern margin of the North China Craton.

5.1 Introduction

In this Chapter, and the one that follows, I review what I consider to be important orogenic belts (or fold belts), not only because they are key tectonic elements in the assembly and amalgamation of continental China, but also because of their considerable metallogenic endowment and potential for future discoveries. The South China, Central China, Qinling-Dabie and Hinggan orogenic belts are reviewed and examined for the known mineral systems. Figures 2.2, 2.3b, 2.4 and 2.5 provide the necessary graphic background for this Chapter. The formation of the Central China-Qinling-Dabie and Songpan-Ganzi (Chap. 6) belts between Late Carboniferous and Jurassic, resulted in the suturing of the Tarim, North China and Yangtze cratonic and stable blocks, with the closure of the Palaeo-Tethys and Neo-Tethys oceanic arms (Fig. 2.4). The South China Fold Belt in the southeastern part of Cathaysia, formed as a result of subduction of the Pacific plate, as explained below. The development of these orogenic belts and associated suturing processes, was accompanied by the establishment of mineral systems, related to subduction, collision and post-collision tectonics. These orogenic belts also acted as zones of weakness and easy access for magmas and fluids during the widespread igneous activity related to the Mesozoic Yanshanian tectono-thermal events, which led to the generation of new mineral systems and the overprinting of existing ones.

5.2 South China Fold Belt

The South China Fold Belt (or Huanan Orogen; see Figs. 2.3a and 4.4) is part of the South China Block (Chap. 4), which is the result of multiple tectonic and magmatic events that formed a collage of accreted Proterozoic and Phanerozoic terranes. The Jurassic to early Cretaceous Yanshanian event (ca. 208–90 Ma), a time of major tectono-thermal events that affected much of eastern and southeastern China, is of great metallogenic importance in the fold belt. This period is linked to subduction of the Pacific plate beneath the Eurasian continent, and is manifested by voluminous volcano-plutonic activity of predominantly calc-alkaline and alkaline affinity.

The South China Fold Belt (SCFB) is well endowed with numerous resources of Sn, W, Mo, Pb-Zn, Cu, Sb, mostly hydrothermal vein-type, porphyry Cu-Au, skarns as well as Au and Au-Ag epithermal mineral deposits all related to stages of Yanshanian magmatism (Table 5.1). In this section I focus on the porphyry and epithermal

Table 5.1 Main mineral deposits in SE China. (After Pirajno and Bagas 2002)

Deposits	Tectonic setting	Location and administrative province		Approximate reserves (kg; t = tonnes)		Grade Au g/t
				Remaining	Total	
Huangshan	Chencai-Suichang uplift	Zhuj Zhejiang	E120°18′41″ N29°34′27″	990	3,317	9.00
Zangao	Chencai-Suichang uplift	Shaoxing, Zhejiang	E120°36′32″ N29°55′40″	607	1,271	11.40
Miao Xia Fan	Chencai-Suichang uplift	Zhuj, Zhejiang	E120°17′40″ N29°31′40″	1,483	2,158	12.49
Qicun	Chencai-Suichang uplift	Zhuj, Zhejiang	E120°15′30″ N29°33′36″	1,310	1,345	5.79
Gaocun	Yunkai uplift	Gaoyao, Guangdong	E112°17′44″ N23°17′58″	26,047	27,827	6.84
Hetai	Yunkai uplift	Gaoyao, Guangdong	E112°17′44″ N23°17′58	30,224	32,004	?
Yunxi	Yunkai uplift	Gaoyao, Guangdong	E112°16′00″ N23°19′00″	16,753	18,200	8.35
Taipingding	Yunkai uplift	Gaoyao, Guangdon	E112°17′17″ N23°18′23″	2,043	2,044	10.30
Shantai	Yunkai uplift	Gaoyao, Guangdon	E112°17′47 N23°17′06″	1,714	1,796	5.99
Xinzyhou	Yunkai uplift	Gaoyao, Guangdon	E112°56′16″ N24°02′30″	3,557	8,234	11.33
Dagaogu	Yunkai uplift	Yingde, Guangdon	E112°55′30″ N24°03′30″	4,090	5,263	5.31
Dongkeng	Yunkai uplift	Xinyi, Guangdong	E110°20′19″ N22°21′28″	6,664	6,664	5.75
Banti	Yunkai uplift	Fungkai, Guangdong	E111°54′00″ N123°49′10″	2,364	3,107	66.84
Hejiang	Yunkai uplift	Luoding, Guangdong	E111°10′18″ N22°43′39″	1,538	1,538	12.01
Babaoshan	Costal volcanic belt	Longquan Zhejiang	E118°56′45″ N27°54′54	875	1,309	4.63 Ag 212 t
Zhilingtou	Chencai-Suichang uplift	Shuishang, Zhejiang	E119°25′30″ N28°37′28″	2,400 Ag 612 t	18,547 Ag 494 t	12.10 Ag 306 t
Zijinshan gold deposit	Coastal volcanic belt	Shanghang, Fujian	E116°24′41″ N25°10′42″	4,275	5,451	4.24
Zijinshan gold-copper deposit	Coastal volcanic belt	Shanghang, Fujian	E116°24′41″ N25°10′42″	13,800	13,800	0.13
Shuang-quishan	Coastal volcanic belt	Dehua Fujian	E118°11′27″ N25°54′5″	4,715	4,715	7.19
Hebaoshan	Coastal volcanic belt	Taining Fujian	E117°10′51″ N26°55′49″	3,355	3,355	8.45
Ancun	Coastal volcanic belt	Dehua Fujian	E118°11′27 N25°52′27″	3,192	3,192	8.11

metallogeny in the SCFB, mostly taken from Pirajno et al. (1997), Pirajno and Bagas (2002), Pirajno (2009) and updated here. The gold resources of the SCFB are estimated at around 2–3 % of the total gold resources of China (about 4,500 t according to Zhou et al. 2002a, and 3,832 t according to Nie 1997) and undoubtedly these figures will since have changed. Mineralizing events in the SCFB occurred during the Neoproterozoic through to the late Mesozoic. In this long span of geological time, precious metal deposits were formed and re-worked during lithospheric plate movements and microcontinent collisions.

The southeastern part of China is formed by the Yangtze Craton, and the ca. 1.8–1.4 Ga Cathaysia Block (Figs. 4.1 and 4.4), which are in contact along a tectonically complex zone interpreted as a crustal suture, containing an ophiolitic-type mélange and high-pressure metamorphic rocks (Şengör and Natal'in 1996). The amalgamation of the Yangtze Craton with Cathaysia, first occurred during the 1.0–0.85 Ga Jinning Orogeny. This was followed by a rifting episode around 800 Ma during the Sinian, and a second collision event during the Caledonian (Zhou et al. 2002a). Details of the tectonic evolution of the South China region are complex and still largely unresolved, although various lines of evidence (e.g. Li 1998) suggest that it formed through a series of continent-continent collisions with closure of intervening segments of oceanic crust since Proterozoic time (Ye et al. 1998). Li and Li (2007) proposed a flat-subduction model for the geodynamic evolution of the SCFB between 250 and 190 Ma, with subsequent roll-back, slab breakoff and its foundering.

The SCFB is exposed along the southeastern side of mainland China (Zhejiang, Fujian, Jiangxi, Guandong, Hunan provinces), on Taiwan, on Hainan Island, and is that part of the South China Block that was affected by Yanshanian deformation and magmatism (Wu et al. 1998; Wang et al. 2005b). Several northeast-trending fault zones traverse the SCFB, including the Jiangshan-Shaoxing Fault Zone and the Yuao-Macao fault zone, both of which constitute major crustal-scale structures. The Jiangshan-Shaoxing and Yuao-Macao fault zones delineate two structural and tectonostratigraphic domains (A and B in Fig. 5.1). These domains are also broadly defined by the distribution of initial $^{87}Sr/^{86}Sr$ ratios (Sr_i) of volcanic and plutonic rocks (Pei and Hong 1995), which increase from less than 0.708 in the coastal areas (domain B, Fig. 5.1) to between 0.708 and 0.724 in the interior (domain A, Fig. 5.1). The domains identified by the Sr_i values also coincide with the regional distribution of granitic rocks, from dominantly I-type along the coast in domain B (Zhejiang-Fujian-Guandong coastal belt; <0.708 Sr_i) to dominantly S-type in the interior belt in domain A (Hunan-Jiangxi-Guandong transitional belt and Hunan-Guangxi intracontinental belt; $0.708 < Sr_i > 0.724$). The distribution of initial $^{87}Sr/^{86}Sr$ ratios and the nature of the associated magmatism (I-type, magnetite-series versus S-type, ilmenite-series) may be explained by lithospheric domains, from mantle-dominated (I-type; domain B) to accreted crustal rocks (S-type; domain A). This in turn would

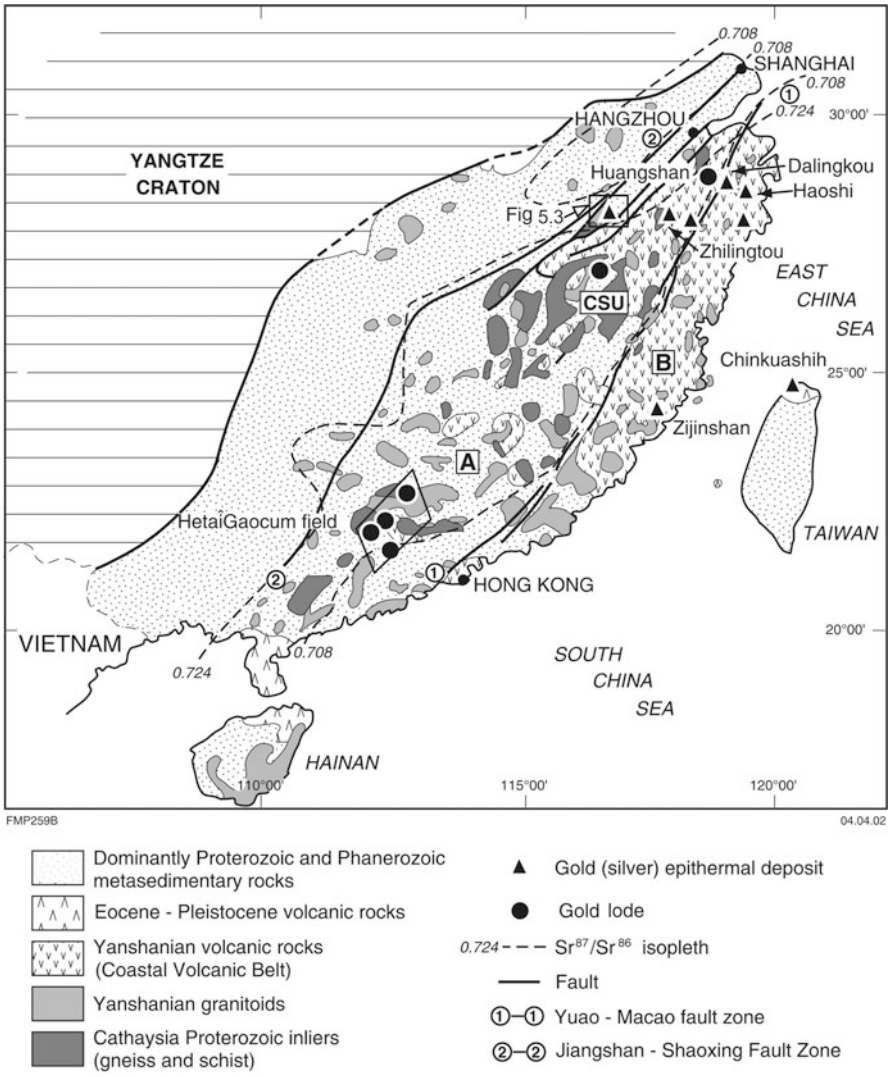

Fig. 5.1 Simplified geological map of the South China Fold Belt and distribution of selected epithermal Au-Ag deposits, east of the Jiangshan-Shaoxing Fault; $^{87}Sr/^{86}Sr$ contours are taken from Pei and Hong (1995). The Yuao-Macaoo and Jiangshan-Shaoxing faults delimit two structural and tectonostratigraphic domains, *A* and *B*. *A* represents structural uplifts and tectonic windows (inliers) of older rocks (Cathaysia), between the Yuao-Macao and Jiangshan-Shaoxing faults; *B* represents the Cretaceous Coastal Volcanic Belt east of the Yuao-Macao fault

reflect in the nature of the associated mineralisation. Indeed, Pei and Hong (1995) defined a regional metal zonation, from a dominant Pb-Zn-Ag-Au metal association in domain B to an Au-Mo-Cu metal association in domain A.

The structural and tectonostratigraphic region between the Jiangshan-Shaoxing and Yuao-Macao fault zones (domain A), is characterized by the presence of Proterozoic inliers of orthogneiss and paragneiss that are exposed through Yanshanian cover sequences of felsic-intermediate volcanic, volcaniclastic and plutonic rocks (Fig. 5.1). The inliers consist of rocks metamorphosed to the greenschist to upper amphibolite facies, which are considered part of the Cathaysia Block. The rocks of the inliers formed part of the Neoproterozoic Shuangxiwu and Chencai island-arcs or back-arcs and are interpreted to be remnants of microcontinental fragments that were first accreted to the Yangtze Craton during the Neoproterozoic. The Jiangshan–Shaoxing Fault marks the suture between these ancient arcs (Xu et al. 1994b) that collided and together were accreted onto the eastern margin of the Yangtze Craton between 950 and 800 Ma (Jinning Orogeny; Zhou et al. 2002a). The exposure of the Cathaysia inliers is the result of orogenic uplift, which is related to convergence tectonics that occurred in the Yanshanian, along the western Pacific margin. One of these uplifted areas in the Zhejiang Province is termed the Chencai-Suichang Uplift (CSU); others occur further to the southwest in Fujian and Guandong Provinces. These uplifted blocks and associated inliers are economically important because they host significant Au-Ag deposits, such as the Zhilingtou, Huangshan and the Hetai deposits in the Zhejiang and Guandong Provinces (Fig. 5.1), discussed in this section.

Although the SCFB was affected by the early Palaeozoic (Caledonian), late Palaeozoic (Hercynian) and early Mesozoic (Indosinian) orogenies, as mentioned above by far the most common tectono-thermal imprint in the belt are the Yanshanian events that resulted in the establishment of a broad magmatic zone, as much as 1,000 km wide and 3,000 km long, along the entire eastern margin of China (see Chap. 7). The Yanshanian period in its various manifestations is ultimately linked to the oblique subduction of the Pacific plate under the Eurasian plate, affecting the continental margin of eastern Asia (Şengör et al. 1993; Mao et al. 2010). In southeastern China, the Yanshanian magmatic zone is subparallel to and overlaps in space with magmatic belts of Caledonian-Variscan and Indosinian ages. This overlapping pattern has been attributed to successive phases of oceanic crust subduction beneath an active continental margin (Jahn et al. 1990), or to the flat subduction of Li and Li (2007).

The main phases of Yanshanian tectono-magmatic activity began in the mid-Jurassic between ca. 180 and 140 Ma and peaked with extensive I-type plutonism in the Cretaceous between ca. 120 and 90 Ma (Jahn et al. 1990; Chen et al. 2000b). Chen et al. (2000b) and Zhou and Li (2000) noted the presence of Cretaceous A-type plutonic rocks with the extensive high-level I-type plutonic rocks. They related this plutonism to a geothermal gradient greater than 40 °C/km, large-scale underplating of basaltic magma, and a high exhumation rate. Zhou and Li (2000) further suggested that the slab-dip angle of the early Pacific oceanic plate subduction beneath southeastern China increased from a low angle to a moderate angle between 180 and 80 Ma. The consequence of this change in angle was that magmatic activity migrated some 800 km southeast towards the coastal regions of the Zhejiang and Fujian

provinces. The flat subduction model proposed by Li and Li (2007) provides a good explanation for these migrating magmatic events that occurred between approximately 250 and 155 Ma. Post-orogenic A-, I-type granites and rift-related syenites, show a coastward younging trend suggesting both extensional and subduction-related magmatic arc environments. According to Li and Li (2007), the uplift of the coastal region in southeast China is associated with the Mid-Permian North China-South China collision. These authors interpreted the anorogenic I- and A-type magmatism to reflect the beginning of slab breakoff and asthenospheric upwelling, resulting in a Basin-and-Range topography. The younging of this magmatism towards the coast is interpreted as due to successive phases of slab roll-back that produced a combination of arc-related and bimodal rift-related volcanism. Work by Meng et al. (2012) on basaltic rocks in the central area of the SCFB using geochemical, Sr-Nd data and high precision Ar-Ar geochronology, revealed three stages of mafic volcanism as follows: (1) 195–160 Ma basalts inland of the SCFB, with low initial $^{87}Sr/^{86}Sr$ ratios ranging from 0.7038 to 0.7078, εNd(t) values from −1.5 to 6.0 and geochemical signatures of ocean island basalt (OIB); (2) 160–110 Ma basalts from the same general area, with $^{87}Sr/^{86}Sr$ ratios ranging from 0.7053 to 0.7102, εNd(t) values from −6.0 to 5.0 and low La/Nb ratios from 0.9 to 1.8, interpreted by the authors as relating to asthenosphere-lithosphere interaction; (3) 110- to ≤80 Ma basalts, subdivided into: one group along the coast characterized by arc isotopic and geochemical arc signatures (εNd(t) values from −8.1 to 3.7 and high La/Nb ratios of up to 4.8) and an inland group characterized by high εNd(t) values from −1.9 to 6.8 and low La/Nb ratios from 0.6 to 1.2. Meng et al. (2012) interpreted these three stages of basaltic volcanism to correspond to three evolutionary stages: (1) flat slab subduction (195–160 Ma) and its initial breakup with the first generation of basaltic rocks as well as A-type magmatism in the inland part of the SCFB; (2) collapse of the flat-slab between 160 and 110 Ma, resulting in strong asthenospheric mantle upwelling, which resulted in partial melting of the continental lithospheric mantle, basaltic volcanism as well as I- and A-type granitic magmatism; (3) during this stage between 110 and ≤80 Ma, basaltic volcanism with strong arc signatures mostly affected the coastal region, interpreted as the final stage indicating normal continental margin subduction.

Yet, another interpretation of Yanshanian magmatism in southeast China was presented by He and Xu (2011), who focused their work on syenitic and gabbroic rocks. On the basis of zircon U-Pb dating and Sr-Nd isotopic compositions two age groups were recognized: 141–118 Ma and a late stage at 98–86 Ma. The early stage syenitic and gabbroic rocks are associated with rhyolitic and dacitic volcanism, whose parental magmas derived from metasomatised subcontinental lithospheric mantle enriched by subduction dehydration. The 98–86 Ma syenitic rocks, on the other hand, are accompanied by silicic volcanic calderas and alkaline volcanic ring complexes, mostly concentrated in the northeast (Zhejiang province; Coastal Volcanic Belt) of the SCFB, along or close to the coast line, where the Dalingkou and Haoshi mineral deposits are located (see below and Fig. 5.1). The parental magmas of these late stage syenites and associated silicic-alkaline volcanics would have been derived from mixing of depleted asthenospheric mantle and subduction-related melts. He and Xu

(2011) interpreted the two-stage volcano-plutonic magmatic activity as due to a progressive roll back of the Palaeopacific subducting slab, leading to a corresponding change from compressional to extensional setting.

Although both these interpretations of the magmatic evolution of the SCFB are different from the subduction scenario presented in Fig. 5.4, the second model proposed by He and Xu (2011), is somewhat closer and perhaps best explains the magmatic-mineral systems of the Coastal Volcanic Belt of the SCFB, described below.

Basaltic underplating and magma fractionation resulted in the release of magmatic fluids and the possible introduction of metals such as Sn, Mo and W (Zhou and Li 2000). The magmatic activity continued, however, through to the Early Neogene (Himalayan Orogeny) along the entire continental margin of eastern Asia (Şengör et al. 1993; Hou et al. 2011). East of the Yuao-Macao fault zone (domain B; Fig. 5.1), Yanshanian volcanic and plutonic rocks that form the Coastal Volcanic Belt (CVB) extend for approximately 1,200 km from northern Zhejiang Province, across Fujian Province and through to southwest Guandong Province. The CVB volcanic and plutonic rocks consist predominantly of rhyolite, dacite, andesite and cogenetic granites (Pei and Hong 1995). The volcanic rocks that outcrop on the islands of Hainan and the western side of Taiwan are of Eocene and Pleistocene age, and belong to the Himalayan Orogeny (<90 Ma), and it is worthy of mention that the important 1 Ma dacite-hosted Chinkuashih epithermal gold deposit on the northern tip of Taiwan (Fig. 5.1) is one of the largest epithermal deposit in southeastern China.

In southeastern China, most gold deposits in the Cathaysia Block inliers, and all of the hydrothermal Au, Ag, Sn, W, Sb, Pb, Zn, and Cu deposits in the CVB (Fig. 5.1), are spatially associated with Yanshanian volcanic structures, granitic dykes and subvolcanic intrusions. There are two distinct metallogenic provinces, corresponding to the structural and tectonostratigraphic A and B domains, referred to previously (Fig. 5.1). These are the areas in which the Cathaysian inliers are exposed (e.g. CSU, and other scattered uplifts to the southwest shown in Fig. 5.1), and where Yanshanian volcano-plutonic rocks define the CVB. Gold, silver and polymetallic deposits, hosted in Cathaysian inliers, are typically localised along shear zones. The deposits have a range of styles and types that include mesothermal and epithermal replacement lodes, veins and stockworks. A large number (>200) of Au, Ag, fluorite or polymetallic (mainly Pb-Zn ± Au ± Ag, Cu-Mo) dominated occurrences are present in the coastal areas of the Zhejiang Province. From the descriptions given in the available literature (Pirajno et al. 1997; Pirajno and Bagas 2002 and references therein), all of these deposits represent epithermal and/or porphyry systems.

5.2.1 *Zhilingtou and Huangshan Epithermal Systems, Chencai-Suichang Uplift, Zhejiang Province*

Zhilingtou is a low-sulphidation epithermal Au-Ag deposit, and is the largest and economically most important in Zhejiang Province (Fig. 5.1). The deposit located in the CSU, had in the 1990s an *in situ* resource of approximately 2 Mt grading 12 g/t

Au and 306 g/t Ag. Quartz-dominated veins and stockworks in the mineralised zone are sulphide-rich and can be classified as Au-Ag, Pb-Zn, or Cu-Pb-Zn-Ag types. Precious metal-bearing phases include electrum, native and sulphide-hosted gold, acanthite, hessite and calaverite. Other ore minerals are pyrite, sphalerite, galena, chalcopyrite, pyrrhotite and tellurobismuthite. Gangue minerals include adularia, rhodochrosite, rhodonite and colloform quartz. Hydrothermal alteration zones surrounding the vein system include sericite, epidote, chlorite, and Mn-carbonates. The orebodies occur as veins and stockworks, veins with open-space filling textures and locally replacement zones. A 900-m drill hole intersected propylitically-altered felsic and intermediate igneous rocks and zones of quartz stockworks with molybdenite in silicified and sericitized quartz-porphyry rocks. These features led Pirajno et al. (1997) to suggest that the Zhilingtou deposit could be spatially and genetically related to a porphyry system at depth. Zheng and Liu (1987) and Xu et al. (1995b) carried out studies of fluid inclusions of mineralised quartz-vein material at Zhilingtou and measured homogenisation temperatures ranging from 160 to 400 °C, with the main hydrothermal stage at about 270 °C. Calculated salinities are from 5 to 8 wt % NaCl equivalent; no CO_2-rich inclusion were found. These temperature and salinity values are consistent with those that are considered typical for the circum-Pacific epithermal systems (White et al. 1995).

Xu (1988) showed that the Zhilingtou "early" ore veins have narrow ranges of δD and $\delta^{18}O$ (−62 to −53 ‰ and +1.0 to +4.7 ‰ respectively). On this basis he concluded that the early ore-forming fluids originated from "syngenetic metamorphic water", perhaps hinting at a mineralising event not related to Yanshanian magmatism, but inherited from pre-existing Proterozoic basement mineralisation. Late ore-veins at Zhilingtou have a wider spread of δD and $\delta^{18}O$ values (−73 to −58 ‰ and −4.9 to −2.1 ‰ respectively) (Fig. 5.2). Other researchers (cited in Xu et al. 1995b), using O, H and Si isotope systematics concluded that an earlier stage of mineralisation resulted from fluids of metamorphic origin at Zhilingtou. It has also been suggested that this early mineralisation may be related to the second collision event between the Yangtze Craton and the Cathaysia Block forming the South China Block during the Caledonian (Zhou et al. 2002a). Sulphur isotopic determinations on sulphides (Xu et al. 1994a, 1995a) indicate that most of the δS^{34} values at Zhilingtou cluster around +4 to +6 ‰ (Fig. 5.2b) and overlap those of the Mesozoic volcanic rocks, which range between −1 and +5 ‰.

Evidence from K-Ar and Rb-Sr isochron dating on the auriferous quartz veins in the Zhilingtou mine confirms that epithermal vein formation was formed during three distinct gold-mineralising events at ca. 227, 164–152 and 107–82 Ma. Furthermore, the high $^{87}Sr/^{86}Sr_i$ ratio of 0.72496 for the 160 Ma date and the high $^{87}Sr/^{86}Sr_i$ ratio of 0.72889 for the 127 Ma date indicate a crustal source for the mineralisation (Chen and Xu 1997).

The Huangshan deposit (Figs. 5.1 and 5.3) consists of a lode about 400 m long and up to 9 m wide, with an average grade of 8.8 g/t Au. The ore minerals are native gold, petzite, calaverite, pyrite, chalcopyrite and galena, hosted by vein-quartz lenses within strongly sheared quartz-diorite. Hydrothermal alteration

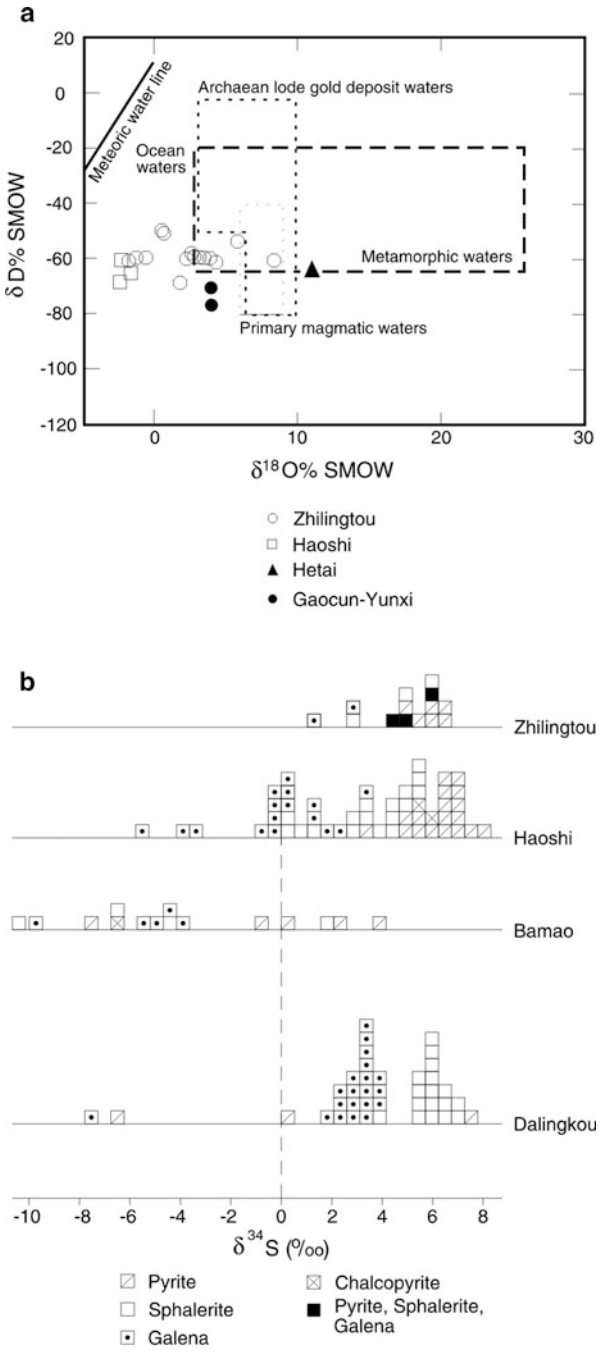

Fig. 5.2 **a** δ^{18}O-δD plot for the Zhilingtou, Hetai, Gaocun, Yunxi and Haoshi mineral deposits; Hetai is an orogenic lode deposit and its O-D composition plots close to the metamorphic water box (Wang et al. 1997); Zhilingtou exhibits a rebd from metamorphic to porphyry-epithermal, whereas Haoshi forms a cluster within the epithermal range. The magmatic and metamorphic boxes are from Sheppard (1986). **b** Histogram of δ^{34}S values for Zhilingtou, Dalingkou and Haoshi (data from Xu et al. 1994a, 1995a); the S isotopic data suggest mixing of magmatic (near 0 ‰) and crustal sources (heavier δ^{34}S values). (After Pirajno and Bagas 2002 and references therein)

assemblages surrounding the lode consist of quartz-carbonate-sericite, and quartz-albite-muscovite-carbonate-chlorite. Tourmaline, carbonate, pyrite and galena are in cleavage planes parallel to the regional foliated fabric of the mylonite zone, and gold fills late dendritic fractures in the pyrite. Rubidium-Sr isochron dating of auriferous quartz yielded an age of 397 ± 34.5 Ma, with $^{87}Sr/^{86}Sr_i$ ranging from 0.7042 to 0.7053 (Chen and Xu 1997). Other operating gold mines in the area include Miaoxifan, Mali, Xipai and Xingsheng (Fig. 5.3), all hosted in strongly sheared mafic rocks (Pirajno et al. 1997).

The distribution of the mineral deposits and occurrences in the Huangshan district indicates a strong structural and iron-rich lithological control. There are approximately 30 gold deposits and occurrences, most of which are found in the ca. 808 Ma Huangshan Complex, with a few in Mesozoic volcanic rocks (Fig. 5.3). The Huangshan Complex is an intermediate-mafic-ultramafic layered intrusion about 34 km long and 4 km wide, emplaced within the Jiangshan-Shaoxing Fault Zone. Copper, Pb-Zn and Cu-Pb-Zn occurrences are also present in the basement and Mesozoic volcanic rocks in addition to Au (Fig. 5.3). An important and major feature in the Huangshan area is the Fuyongshan volcanic complex, which is approximately 14 km in diameter and is possibly a caldera (Fig. 5.3). Small Au, Cu and epithermal fluorite occurrences are present within and around the volcanic complex.

5.2.2 Fujian Province's Epithermal-porphyry Systems

The Fujian Province contains Au-Cu high-sulphidation epithermal mineralisation in the Zijinshan mining district (Fig. 5.1), and at least five other Au-Cu prospects in the district ranging from epithermal to porphyry styles. Mao et al. (2006) reported on the age of plutonic rocks in Fujian Province. The Sifang pluton consists of porphyritic granodiorite with and outcrop area of 10 km^2, and is the main host of epithermal Au and Cu mineralisation. The Sifang granodiorite porphyry has a zircon U-Pb age of 107.8 ± 1.2 Ma and a Ar-Ar plateau age on hornblende of 104.8 ± 8.0 Ma. The Sifang pluton intrudes into Cambrian, Devonian-Carboniferous clastic sedimentary rocks and into the Zijinshan pluton as well. The Zijinshan pluton has an outcrop area of 20 km^2 and intrudes Cambrian and Devonian clastic sedimentary rocks, which also host Cu mineralisation in the area. The Zijinshan pluton is medium- to coarse-grained biotite granite. Zircon U-Pb age of the pluton is 157 ± 9 Ma, whereas whole-rock Rb-Sr age determination yielded an age of 145 ± 12 Ma. Other plutons in the region, also investigated by Mao et al. (2006) are: the 130 km^2 granodiorite Tangquan with U-Pb ages ranging from ca. 187 to 179 Ma, the 2.5 km^2 monzonite Caixi pluton (U-Pb age of 133 ± 8 Ma) that also intruded into the Zijinshan pluton and the 10 km^2.

The early Mesozoic granites, such as the Tangquan pluton, characteristically host porphyry Cu-Mo deposits (e.g. Matoushan), hydrothermal polymetallic deposits (e.g. Cu, Pb-Zn in vein systems) and skarns. The latter consist of stratabound polymetallic Fe, Cu, Pb-Zn deposits along the contact zones between the Tangquan granodiorite pluton and carbonate rocks. Late Mesozoic intrusions, such as the Sifang granodiorite

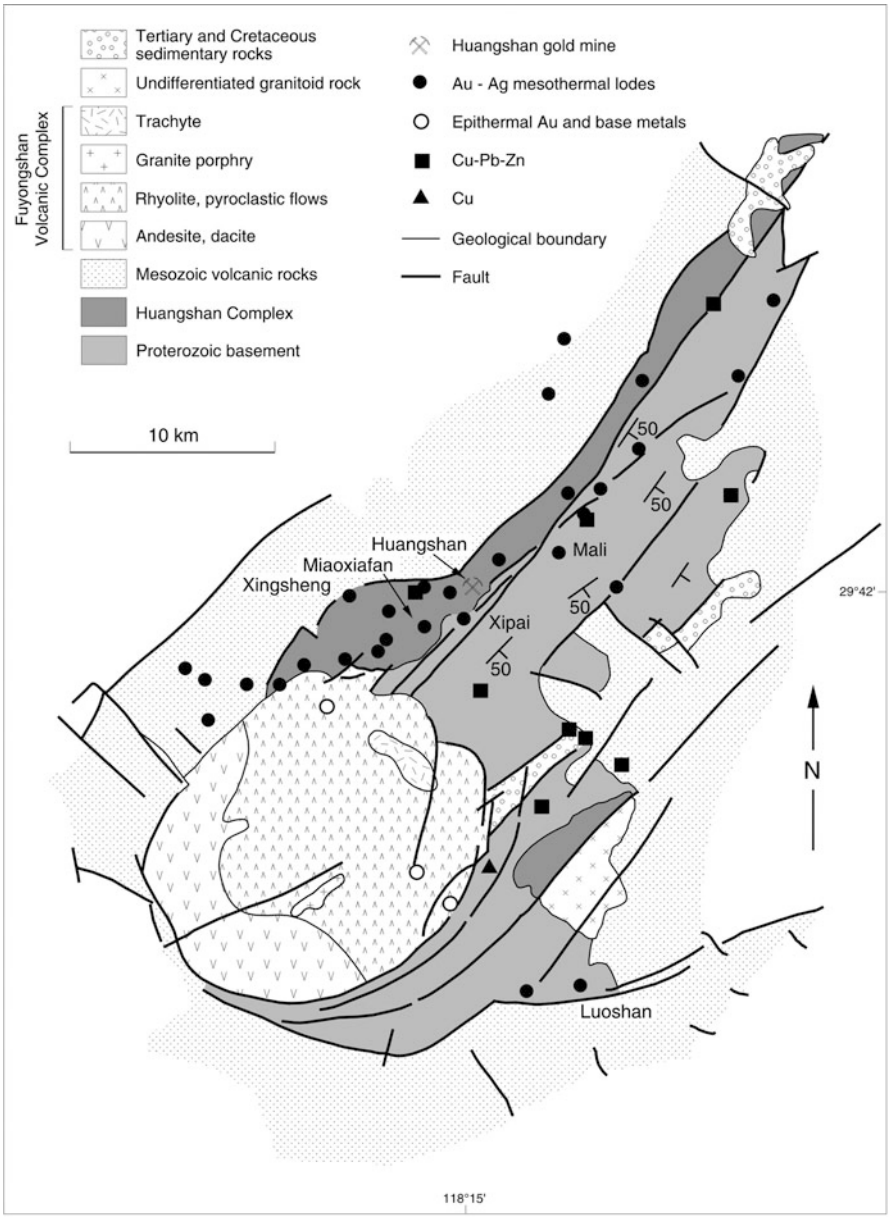

Fig. 5.3 Simplified geology of the Huangshan area and distribution of precious metal deposits, which are lithologically (Fe-rich), structurally controlled and spatially associated with the Fuyongshan volcanic complex. (After Pirajno and Bagas 2002)

subvolcanic porphyries are typically associated with the well-known Zijinshan Au-Cu ore field. Mao et al. (2006) suggested an evolutionary trend of igneous rocks from granodiorite to granodiorite porphyry, to intermediate-felsic volcanism to dacite porphyry. In addition to the Zijinshan ore field briefly discussed below, other mineral systems that belong to this magmatic phase are Cu, Au, Ag vein deposits and porphyry Cu-Mo deposits.

The Zijinshan epithermal-porphyry deposits was reported to have a resource of about 17 t with an average grade of 4.2 g/t Au and 1 Mt with an average grade of 1 % Cu (So et al. 1998). So et al. (1998) described in detail the hydrothermal alteration and mineralisation of the Zijinshan area and the brief account that follows is taken from these authors. The Zijinshan ore is characterised by northwest-trending breccia bodies and veins within a Cretaceous (105–100 Ma) volcanic pipe of dacitic composition. Hydrothermal alteration and mineralisation are typically zoned, with quartz-sericite-pyrite in the deeper part of the system, to dickite-quartz-pyrite-zunyite in the middle levels, to alunite-quartz-pyrite between 350 and 1,200 m from the surface. At levels shallower than 350 m, intense silicification dominates and is associated with Au-Ag mineralisation. Metal zoning within the alunite and silica zones is from Cu-Pb-Zn to Au-Ag-As near the surface. Fluid inclusion studies indicate mineralising temperatures of 300–380 °C in the deeper porphyry sector of the system, 320–250 °C in the alunite zone, and 100–180 °C in the shallow silica—gold zone (epithermal sector). So et al. (1998) suggested that the zone of alteration with dominant alunite was formed by mixing of high salinity fluids (10–22 wt % NaCl equivalent) with groundwater, whereas the near surface silica-rich auriferous zone was formed from low salinity acidic gas condensates (<2 wt % NaCl equivalent).

Mao et al. (2006) also discussed the possible source and tectonic setting of the Fujian Province granitic rocks and associated mineral systems. These authors, based on Sm-Nd and Sr isotopic systematics of granitic rocks, suggested that the magmatic systems in east China are mainly of adakitic affinity and related to partial melting of lower crust or underplated basalt. Bimodal volcanic rocks, alkaline and A-type granites of early-mid Jurassic age are common in some regions of southeast China (Nanling Mountains and southeast Henan). It is possible that this mantle-sourced magmatism may be linked with extensional tectonics, following the arc-continent subduction collision at 180 Ma. Mao et al. (2006) postulated that the underplated basaltic magma provided the heat source for the development of granites in the Fujan region. With further extension and crustal thinning in the early Cretaceous more granites were formed with the emplacement of the Tangquan and Sifang plutons.

5.2.3 Mineralisation in the Coastal Volcanic Belt

Epithermal systems in the Coastal Volcanic belt (CVB) include polymetallic Ag-rich and low-sulphidation veins and/or stockworks. (e.g., Haoshi, Dalingkou in Zhejiang Province), and high-sulphidation Cu-Au deposits (e.g., above-mentioned Zijinshan

in Fujian Province) hosted by Late Jurassic to Early Cretaceous dacite and rhyolite (domain B in Fig. 5.1).

The Haoshi and Dalingkou deposits are associated with the late stage (98–86 Ma) caldera type silicic volcanism, referred to above (He and Xu 2011). The Haoshi and Dalingkou polymetallic low-sulphidation epithermal veins are sulphide-rich, with pyrite, sphalerite, galena and chalcopyrite. Precious metal-bearing ore minerals include freibergite, electrum, argentite, pyrargite and stephanite. The silver-rich mineralisation is present as veinlets or disseminations in vein-quartz and dacitic dykes that are hosted by north- and east-trending faults associated with the Yuao-Macao fault zone. No reliable data are available for the metal resources at Haoshi and Dalingkou, but Wu et al. (1993) reported ore grades for Dalingkou of about 112 g/t Ag and 0.3–4.8 g/t Au, with Pb and Zn credits. The mineralisation is accompanied by silicic, pyritic, chloritic and sericitic wallrock alteration. The main hydrothermal alteration phases are quartz, chalcedony, sericite, rhodochrosite, muscovite and kaolinite (Wu et al. 1993). Fluid inclusion studies on the Haoshi deposit reveal a range of homogenisation temperatures from 70 to 300 °C in gas-liquid inclusions, hosted by quartz, sphalerite, calcite and fluorite (Xu et al. 1995a). These authors identified: (1) a quartz-pyrite mineralising stage at 300–230 °C; (2) a quartz-carbonate-sulphide mineralising stage at 220–200 °C; and (3) a quartz-fluorite-carbonate-sulphate mineralising stage at 70–180 °C. The gaseous and liquid composition of the inclusions in quartz and sphalerite include H_2O, Na^+, K^+, Ca^2+ and Cl^{2-}, but little or no CO_2. Whole-rock Rb-Sr and K-Ar dating of sericite from altered wallrock at Haoshi and Dalingkou yields ages ranging from 130 to 95 Ma (Li et al. 1993). The $^{87}Sr/^{86}Sr_i$ of 0.711 for the mineralised quartz suggests that the mineralising fluid was probably of a mixed crustal-mantle source derived from the Mesozoic volcanic rocks in the region (Chen and Xu 1997). Sulphur isotope compositions of pyrite, sphalerite, galena and chalcopyrite from Haoshi and Dalingkou range from −7 to +7 ‰ δS^{34}, which is similar to those from Zhilingtou (−1 to +5 ‰ δS^{34}) from the CSU.

5.2.3.1 Ore Genesis in the South China Fold Belt

A conceptual model of multiple stages of ore-forming events related to the Jinning, Caledonian and Indosinian-Yanshanian tectono-thermal activities is shown in Fig. 5.4. In this model, Pirajno and Bagas (2002) envisaged that during tectonic events of Neoproterozoic (Jinning, ca. 850–900 Ma), Late Caledonian (ca. 400 Ma) and Indosinian (ca. 200 Ma) ages, island-arcs collided and were accreted to the eastern margin of the Yangtze Craton. These events were characterized by an active continental margin, subduction of oceanic crust and accretion of trench sediments. It is possible that during deformation and metamorphism, related to compression along the active margin, structurally controlled orogenic lode gold deposits were formed. In the SCFB, examples of mineralisation related to these events are the lode gold deposits of possible Caledonian age (ca. 400 Ma) hosted by the Huangshan Complex. The Caledonian event records the final amalgamation of the Yangtze Craton with the Cathaysia Block. The mylonite-hosted orogenic lode gold deposits of the

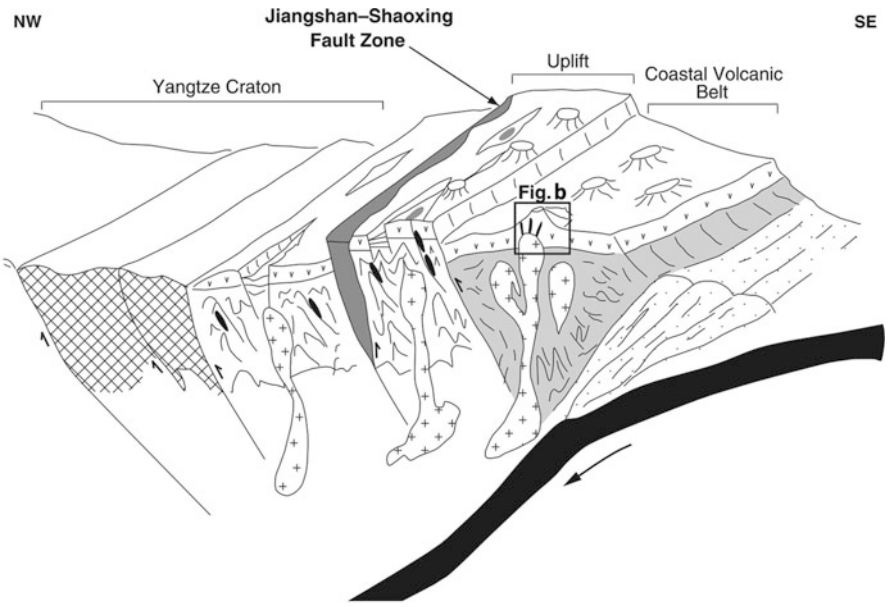
NW
Jiangshan–Shaoxing
Fault Zone
SE
Uplift
Yangtze Craton
Coastal Volcanic
Belt
Fig. b
Accretionary prism
Ophiolitic belt
Yanshanian volcanic - plutonic belt
Cathaysia Proterozoic rocks
Cathaysia basement windows
Structurally - controlled orogenic
gold lodes
Porphyry - epithermal system
and granitoid rocks
Yangtze Craton

a

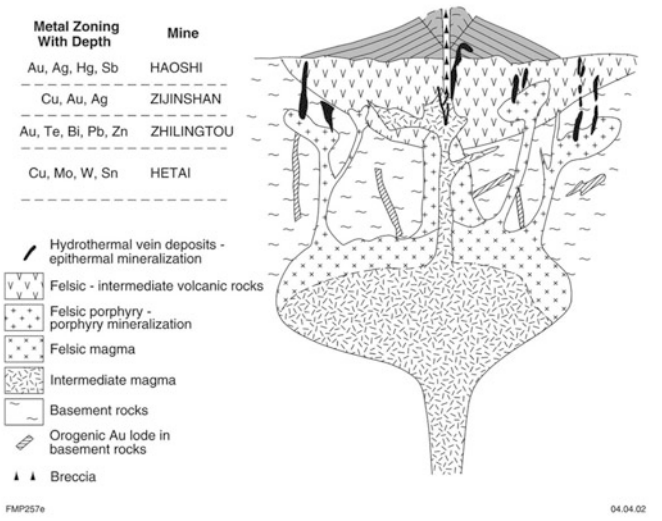
Metal Zoning
With Depth
Mine
Au, Ag, Hg, Sb
HAOSHI
Cu, Au, Ag
ZIJINSHAN
Au, Te, Bi, Pb, Zn
ZHILINGTOU
Cu, Mo, W, Sn
HETAI
Hydrothermal vein deposits -
epithermal mineralization
Felsic - intermediate volcanic rocks
Felsic porphyry -
porphyry mineralization
Felsic magma
Intermediate magma
Basement rocks
Orogenic Au lode in
basement rocks
Breccia
FMP257e
04.04.02

b

Hetai-Gaocun field (Fig. 5.4) are considered to have an age of ca. 200 Ma. If this age is correct, the Hetai mesothermal lodes may be linked to Indosinian tectonic events and the collision of the North and South China Blocks along the Qinling-Dabie orogen (Wang et al. 1997). In a later ore-forming event, a continental margin was again active, during the latter part of the Indosinian and the Yanshanian tectono-thermal events, with the formation of the magmatic arc of the CVB, perhaps as a result of the flat-subduction, proposed by Li and Li (2007). The volcanic-hosted epithermal Au-Ag (e.g., Haoshi, Dalingkou, Zijinshan) and associated porphyry mineralisation was probably formed at this time.

The spatial relationship of Au-Ag mineralisation with uplifted basement rocks has also been noted in other parts of China that were affected by the Yanshanian magmatism (Miller et al. 1998). The uplifts probably formed because of compressional tectonics related to subduction and collision along the eastern continental margin of southeastern China. Hydrothermal circulation associated with Yanshanian magmatism resulted in epithermal-style deposits in Cathaysian basement rocks and within and around the overlying volcanic edifices. Stable isotope systematics from Zhilingtou show O- and H-isotopic compositions within the trends of low-salinity magmatic vapour and of neutral-pH geothermal waters, as defined in Hedenquist and Lowenstern (1994). However, the range of $\delta^{18}O$ and δD provide some evidence of pre-existing lodes in Cathaysian basement rocks, formed during earlier (Neoproterozoic and Caledonian) mineralising events. If this concept is correct, modification and reconcentration of precious metals at the site of the pre-existing orogenic lodes would have occurred as a result of the input of thermal energy during the Yanshanian magmatism. This may have been the case for the Zhilingtou field and perhaps in parts of the Huangshan field.

To conclude, in the model proposed in Pirajno and Bagas (2002), although different from that of He and Xu (2011), is valid to explain that the Au and Ag metallogeny of the SCFB is the consequence of multiple ore-forming events. These events are linked to a series of tectono-thermal events spanning about 700 Ma and responsible for the collision and amalgamation of the Yangtze Craton, Cathaysia Block, followed by subduction of the Pacific Plate under the South China margin.

Fig. 5.4 **a** Conceptual model of geodynamic setting for the South China Fold Belt (SCFB) and associated metalogeny; in this model Yanshanian subduction beneath a continental margin (Cathaysia) builds a magmatic arc, within which regional scale hydrothermal systems are activated due to magmatic heat and forming porphyry and epithermal systems. Compression along the arc causes uplift of basement blocks, such as the Chengai-Suichang Uplift (SCU) and exposed the ophiolitic rocks of the Huangshan Complex. Earlier collision events, such as the accretion of the Cathaysia Block against the Yangzte Craton, would have produced orogenic lode deposits, some of which were modified during the Cretaceous Yanshanian magmatic event, and some Au of epithermal systems, such as Zhilingtou, could have been sourced from pre-existing lodes (after Pirajno and Bagas 2002); an alternative model for the geodynamic evolution and subduction-related magmatism of the SCFB was proposed by Meng et al. (2011). **b** Idealised representation of a Yanshanian volcano-plutonic complex in the South China Fold Belt, with associated porphyry-epithermal mineral systems (e.g. Zhilingtou and Zijinshan) and depth-related metal zoning, older orogenic lodes are in the basement rocks; see text for details

More recently, another model of the geodynamic evolution and ore genesis for south China, including parts of Cathaysia (excluded from my definition of the SCFB) was presented by Wang et al. (2011b). These authors envisaged an east-west magmatic-metallogenic regional zoning, almost perpendicular to the coast line and from oldest (160–150 Ma; W-Sn) to middle (150–140 Ma; Pb-Zn-Ag) to youngest (140–125 Ma; porphyry Cu-Au), from west to east, respectively. Each approximately corresponding to different stages and nature of granitic magmatism. The older igneous rocks (160–150 Ma) are interpreted to have formed in an intracontinental rift settings. The magmatic events that followed mainly consisted of I- and S-type granites as well as A-type granites. Wang et al. (2010) stressed that A-type magmatism in southeast China was probably more common than previously realised, indicative of lithospheric extension and accompanied by bimodal volcanic suites. Wang et al. (2011b) compared the metallogenic zoning and associated magmatism of southeast China to the Andean continental margin. In their model, the magmatic-metallogenic zoning is related to the Palaeopacific plate subduction from northeast to southwest, almost parallel to the coast line. This, however, is in contradiction with the spatial arrangement of intrusive and extrusive rocks in the region, which clearly parallels the coast line (see above and Li and Li 2007). Wang et al. (2011b) proposed the southwest oblique subduction of the Palaeopacific plate, which although applicable to the eastern Asian continental margin (Mao et al. 2010), the subduction front in the southeastern part of China was almost perpendicular to the continental margin and not oblique. Wang et al. (2011b), however did suggest a plausible mechanism of slab roll-back of the Palaeopacific plate, which would have begun from the far end, gradually moving towards the subduction front, resulting in a change of granitic magmatism and associated mineral systems, from Sn-W to Pb-Zn-Ag to Cu-Au deposits, respectively.

5.2.4 Chinkuashih Epithermal Systems in Taiwan

The island of Taiwan and adjacent islets are the only part of China situated on the western extension of the Ryukyu volcanic arc formed by the active oblique subduction of the Philippine Sea Plate beneath the Eurasian plate (Ho 1986). In the northern tip of the island is the Chinquashih district (Fig. 5.1), where high- and low-sulphidation epithermal occurrences and deposits of Pleistocene age are located. English-language publications on the Chinquashih epithermal systems include Tan (1991), Wang et al. (1999) and Wang (2010). The following is summarised from these papers.

The Chinquashih district is underlain by sedimentary rocks of Miocene age and calc-alkaline subvolcanic and volcanic rocks of Pleistocene age. The volcanic rocks were first labelled as dacite, but in the most recent work these are recognised as hornblende andesite (Wang 2010). Since the discovery of these deposits in 1894 about 94 t of Au metal, 120,000 t of Cu and 180 t of Ag were mined from 20 Mt of ore. Copper resources are not mentioned in these resource assessments. The mineralisation in the district is characterised by Au-Cu veins and breccia pipes that cut through the Miocene sedimentary rocks or are hosted by andesite. The veins have northwest to

northerly trends and as such are controlled by north-trending regional faults, which provided the conduits for hydrothermal fluids in the region. The Chinquashih district contains high-sulphidation epithermal deposits (Penshan, Tsushishan and Chanjien) and low-sulphidation deposits (Chiufen and Wutanshan). The economically more significant veins are those of the Penshan deposit, which consists of the Main Vein, continuing southward as the Shumei (also spelled Hsumei) vein system, have been traced from 1.6 to 2.3 km along strike and vertically for about 700 m. As a whole, the Main Vein has inferred resources of about 2 Mt at 1.05 g/t Au and 7.5 g/t Ag, whereas the Shumei veins contain 2.4 Mt at 0.84 g/t Au and 1.63 g/t Ag. The Main Vein is hosted by andesite, whereas the Shumei veins are hosted by fossiliferous calcareous sandstone and grey mudstone of the Nankang Formation. K-Ar and Ar-Ar dating of alunite gave ages ranging from 1.4 to 1.1 Ma. The ore minerals of the Penshan veins include native gold, electrum, enargite, luzonite and auriferous pyrite. Hydrothermal alteration is typically associated with acid-sulphate fluids and consists of silicification (vuggy silica), argillic and advanced argillic alteration, which in the lower and higher temperature levels include dickite, nacrite, pyrophyllite, enargite and luzonite as well as pyrite octahedrons. Closer to the surface the veins are surrounded by an alteration halo comprising kaolinite, alunite, diaspore, cinnabar, barite, electrum, enargite and pyrite cubes. Fluid inclusion studies of quartz in vuggy silica from the Penshan Main Vein showed the ubiquitous presence of a liquid phase (I) and a vapour phase (II) at room temperature. Microthermometric measurements on primary type Ia inclusions gave homogenisation temperatures (Th) ranging from 298 to 238 °C, with salinities of 0.9–2.5 wt % NaCl eqv. The Th of secondary fluid inclusions range from 282 to 162 °C and salinities ranging from 1.2 to 4.0 wt % NaCl eqv. Bulk analyses (average of all inclusions) of vapour phase (type II) inclusions, probably derived from boiling fluids, showed that the gases mainly consist of H_2O and CO_2.

East of the Penshan high-sulphidation epithermal veins are a number of diatreme breccias (e.g. Tsushishan and Chanjen), possibly due to phreatic or phreato-magmatic eruptions, which cut through the Miocene sedimentary rocks. The funnel shaped diatreme breccias have diameters ranging from 10 to 40 m and extend to depths of 200–700 m. Ore minerals, mostly Au and barite, are in fractures and cavities of the silicified breccia material, suggesting that ore deposition was of a late stage. The Au grades of these breccia pipes can be very high (100–10,000 g/t). The pipes are also surrounded by lower grades (3–4 g/t Au) and disseminated mineralisation, preferentially hosted in calcareous sandstone and beds of alternating carbonaceous shale and laminated sandstone. Wang (2010) pointed out the importance of the physical and chemical composition of the host rocks in determining ore grades. The Chinquashih deposits are not currently in production.

5.3 Qinling-Dabie-SuLu Orogenic Belt

The approximately E-W-trending Kunlun/Qilian-Qinling-Dabie-SuLu orogenic belts, together form the Central China Orogen, which stretches across the entire China mainland, from Jiaodong peninsula in the east to the southwestern margin

of the Tarim Block in the west (see Fig. 2.3). The Central China Orogen marks a series of collision events, during Late Palaeozoic and Mesozoic, between the North China Craton and the Yangtze Craton, the Tibetan fold belts and the southern margin of the Tarim. The effects of these collisions can be traced eastward to the Korean collision belt, across to the Korean peninsula and perhaps even Japan (Kwon et al. 2009). The Central China Orogen contains two giant sutures, which resulted from the closure, during the Late Palaeozoic and Triassic, respectively, of the Qilian-North Qinling and the Kunlun-South Qinling oceans (Fig. 2.3). The Qinling-Dabie orogen (also called Qinling-Tongbai-Dabie) refers to that part of the Central China Orogen, which is the 2,000 km long collision boundary between the North China and Yangtze Cratons, displaced northward at its eastern end along the Tanlu fault, where it is called Sulu orogen (Fig. 5.5) and is characterised by high-pressure rocks that extend to the northern part of the Korean peninsula (Kwon et al. 2009). The Qinling-Dabie orogen is divided into three tectonic units, bound by thrust faults: South Qinling, North Qinling and Xiaoqinling. The North Qinling is separated from the North China Craton (NCC) by the Luanchan Fault (Fig. 5.5). North of the Luanchan Fault is the Xiaoqinling orogenic belt, which is on the southern margin of the NCC and is bound to the north by the San Bao Fault. Another important tectonic boundary between the NCC and the Qinling-Dabie orogenic belt is marked by the Machaoying Fault (Fig. 5.5; Han et al. 2009). This fault was reactivated time and again since the Mesoproterozoic through to the Cretaceous, when it was intruded by granites associated with Mo mineralisation (Han et al. 2009).

The Qinling-Dabie and Sulu orogenic belts are world famous for their ultra-high pressure metamorphic rocks (UHP), which contain diamond and/or coesite, recording temperatures of 800 °C and pressures of nearly 4 GPa (Hacker et al. 1996; Liou et al. 1996). These metamorphic rocks record subduction of continental crust to depths greater than 200 km and are represented by diamond-bearing eclogites in marble and calc-silicate units in the Dabieshan and coesite-bearing eclogite in the Sulu region. The bulk of the Qinling-Dabie orogen contains successions of metasedimentary, paragneiss and orthogneissic rocks of amphibolites, eclogite and granulite grades. Indeed, UHP rocks are also found further to the west of the Qinling-Dabie orogen in the Alpine-Himalayan-type orogens in the Altun-Qaidam-Qilian mountains (Fig. 2.3; Yang et al. 2001, 2005). To the east and along side the Tanlu strike-slip fault, which displaces the Sulu orogen to the northeast (see Figs. 2.3 and 5.5), UHP rocks record movements along the Tanlu fault. Wang et al. (2011a) investigated these movements by a using a proxy provided by zircon growth phases in the Jingshan monzogranite, which showed that the last zircon phase (III) is associated with leucosome in migmatites with an age of 156 Ma, interpreted to represent the peak activity of the Tanlu fault.

The Qilian-North Qinling Ocean is recorded by ophiolitic associations along the boundary fault belts between the Qaidam block and Qilian mountains (Yin and Nie 1996), the Shang-Dan suture between the northern and the southern Qinling orogenic belts (Hacker et al. 1996; Zhang et al. 1996), the Guishan-Meishan fault separating the southern and northern Tongbai belts, the Xiaotian-Mozitan fault between the southern and northern Dabie Shan (Liou et al. 1996), and the Qingdao-Rongcheng

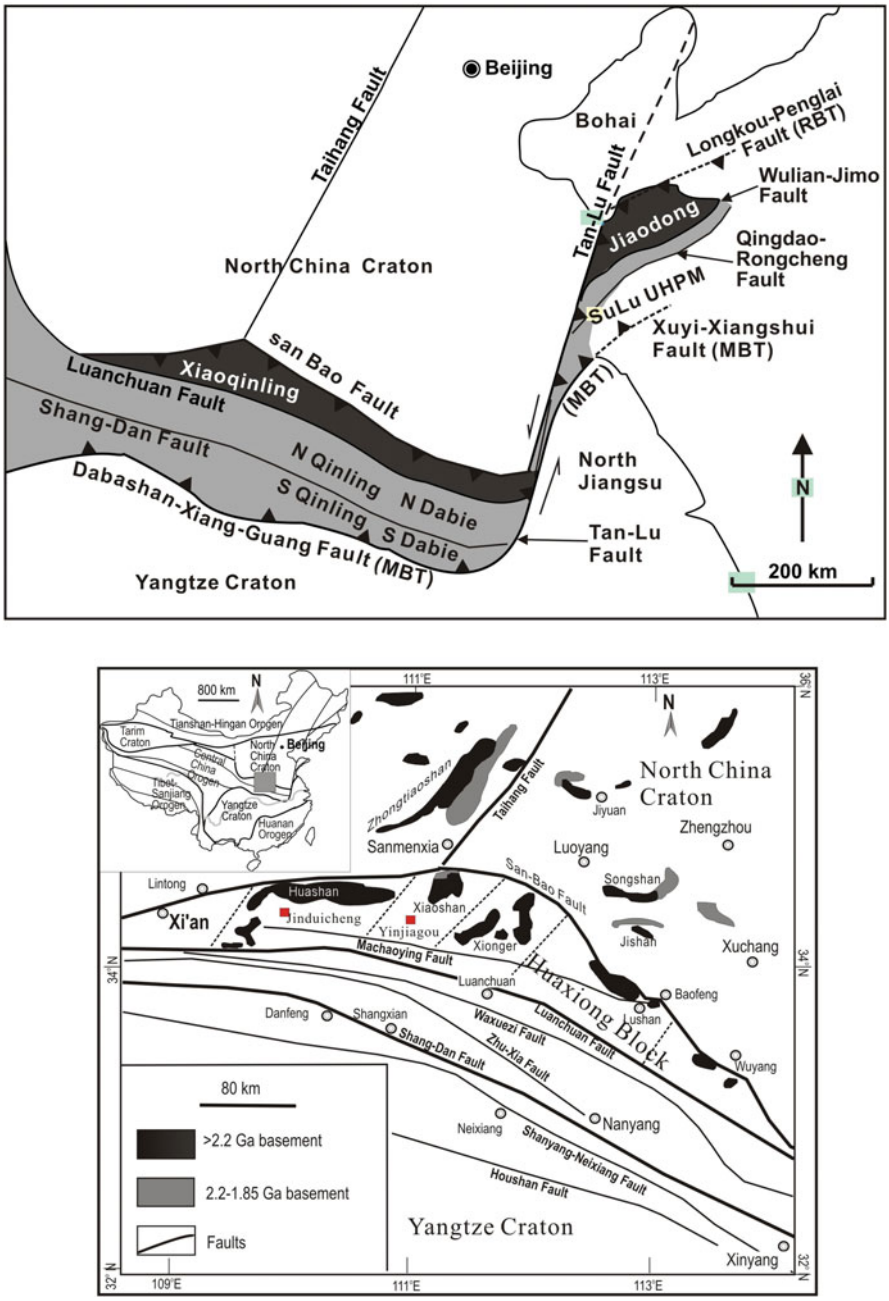

Fig. 5.5 **Top** Main tectonic subdivisions of the Qinling-Dabie-Sulu orogen; the *light grey* shade marks the accretionary terranes that suture the North China Craton and the Yangtze Craton, the Xiaoqinling is the zone of deformed Qinling on the southern margin of the North China Craton and bound by the Main Boundary Thrust (MBT). Note that this figure is about the same as Fig. 3.18 in which the position of lode gold deposits along the Tanlu Fault are shown; **Bottom** simplified map of part of the Qinling-Dabie showing the main structural elements and basement rocks on the southern margin of the North China Craton. (After Chen et al. 2006; 2008a)

fault in eastern Shandong (Yin and Nie 1996). Orogenesis related to these sutures is largely masked by the later Triassic events linked to closure of the Kunlun-South Qinling Ocean. The Kunlun-South Qinling Ocean is now represented, from west to east, by the boundary of the northern Kunlun and central Kunlun terranes, the boundary of the western Qinling and Songpan-Ganzi complex (Zhou and Graham 1996), the Mianxian-Lueyang (or Mian-Lue) ophiolite belt (Lai et al. 2000; Xu et al. 2008b), the Xiangfan-Guangji fault (Liou et al. 1996), and the Xuyi-Xiangshui fault (Yin and Nie 1996). The Mian-Lue suture zone has widths of 1–5 km and contains a mélange of tectonic blocks and fragments of mafic rocks, volcanic rocks, radiolarian cherts and limestones (Xu et al. 2008b). The Mian-Lue ophiolites are concentrated in two main blocks, Anzishan in the eastern part of the suture zone and the Hunshuiguan-Zuangke (HZ) in the western part. The Mian-Lue ophiolites consist of amphibolite, metabasalts, gabbro and ultramafic cumulates, which typically show MORB geochemical compositions (Xu et al. 2008b). In the Anzishan block the ophiolitic rocks consist of serpentinised harzburgite, dunite and listvenites forming an ultramafic core, surrounded by amphibolites derived from mafic volcanic and intrusive rocks. Listvenite or listwänite is a fuchsite-quartz-carbonate (ankerite, magnesite) rock, derived from metasomatic alteration of ultramafic rocks. It is important to note that listvenites can be locally associated with lode Au mineralisation and less commonly with Au-Sb, Co, Sb, Cu (Pirajno in press).

The destruction of oceanic lithosphere is also recorded by the Jinshajiang-Red River fault zones (Şengör and Natal'in 1996; Yin and Nie 1996), the Songpan-Ganzi fold belt (Zhou and Graham 1996), the Xiangganzhe and the Gunanhai suture (Şengör and Natal'in 1996), followed by Triassic collisions between the Kunlun Terrane, Qiangtang-Indochina Block, Yangtze Craton and the South China Fold Belt. These collisions, which induced extreme crustal shortening and thickening over most of mainland China, were defined as the Indosinian Orogeny (Huang and Hsu 1936; Zhao 1986 and references therein). The Lower Yangtze River Valley district is regarded as the foreland fold-and-thrust belt of the Qinling-Dabie Mountains (Hacker et al. 1996). In the Cretaceous (ca. 98 Ma), closure of the Bangong-Nujiang Ocean (Li and Xiao 1996; Yin and Nie 1996) caused orogenesis and development of a new subduction zone. Subsequently (98–66 Ma), the India microcontinent collided with the Eurasia continent along the Indus-Yarlung Zangbo suture, thereby closing the Neo-Tethyan sea (see Figs. 2.2 and 2.4). This resulted in mountain-building of the Himalayan orogenic belts, uplift of the Tibet Plateau and various styles of Cenozoic deformation, such as the eastward escape tectonics, in southwestern China.

The eastern parts of the Qinling-Dabie orogenic belt comprise a Early-Late Archaean (ca. 3.0–2.55; 2.6–2.9 Ga) crystalline basement composed of gneiss, granulite and migmatite of the Taihua Group (Zhang et al. 2001b). The Mesoproterozoic Xiong'er Group (ca. 1.78 Ga), covering an area of ca. 60,000 km^2 and considered as part of a large igneous province (Chap. 7; Peng et al. 2008) or continental margin volcanic rocks (He et al. 2008), overlies the Archaean crystalline basement and is, in turn, overlain by Mesoproterozoic metasedimentary rocks and Neoproterozoic littoral carbonate rocks. Cambrian and Lower Ordovician clastic and carbonate rocks are extensively developed, but Upper Ordovician to Lower Carboniferous strata are

absent in the region. Middle-Upper Carboniferous terrigenous clastic rocks, intercalated with marine carbonate rocks and coal seams, overlie discordantly the Cambrian and Lower Ordovician clastic and carbonate rocks. They are in turn overlain by Permian coal-bearing terrigenous clastic rocks. Locally, Triassic alluvial and fluvial deposits, Jurassic continental sediments, and Cretaceous volcano-sedimentary (lacustrine) rocks accumulated in graben-style basins, which are part of the wider rift system that extends all along the eastern continental margin of China (see Fig. 8.2) Andesitic sub-volcanic rocks in the Cretaceous basins have been dated at ca. 131.8–117 Ma, using SHRIMP zircon U-Pb and K-Ar methods (Wang et al. 2002a; Xie et al. 2007a, b).

The western parts of the Qinling-Dabie orogenic belt are bounded by the Linxia–Zhangxian–Wushan fault (westward extension of the Shangdan suture) to the north, and by the Mian-Lue suture to the south. The Phanerozoic lithostratigraphic sequence in the area is a continuum from Cambrian to Triassic, but with mostly developed Devonian-Cretaceous sedimentary rocks. Granitic rocks are mainly distributed between the Shangdan and Mian-Lue sutures in an approximately east-west trending belt, nearly parallel to the faults mentioned above. Most of the granites in this sector of the Qinling-Dabie formed in the Triassic, with individual outcrop areas varying from $<1\ km^2$ to $>500\ km^2$ (Li et al. 2003b; Zhang et al. 2007a). In the eastern sector, however, widespread granitic magmatism occurred and is described below.

5.3.1 Mesozoic Granitic Magmatism

Mao et al. (2008a, b) recognised six major episodes of granitic magmatism in the Qinling-Dabie orogenic belt: (1) Neoarchaean (2.9–2.5 Ga); (2) Palaeoproterozoic (2.0–1.6 Ga) with emplacement of A-type granites; (3) Neoproterozoic (1.1–0.8 Ga); (4) Early Palaeozoic with subduction, collision and post-collision magmatism; (5) Mesozoic granitic magmatism at 230–190 Ma and (6) at 170–80 Ma. The last two are the most important in terms of metallogenesis. Indeed, there is good evidence of the 160–115 Ma magmatism all along the southern margin of the NCC and its boundary with the Qinling-Dabie orogenic belt. This has been documented by Han et al. (2007) for the Xiong'ershan-Waifagshan region (Henan Province). Here, these authors reported on the nature and ages of Mesozoic granitic plutons, such as Wuzhangshan, Huashani, Heyu and Taishanmiao, which are locally associated with Mo porphyry systems, breccia pipes and lode deposits, as detailed in Sect. 5.3.3. The Wenyu and Niangniangshan granitic plutons in the Xiaoqinling region were emplaced at 138.4 ± 2.5 and 141.7 ± 2.5 Ma, respectively, and the SHRIMP U-Pb zircon dating of granitic porphyries in the Xiong'ershan region yielded 136.2 ± 1.5 Ma for Leimengou, 158.2 ± 3.1 Ma for Nannihu and 157.6 ± 2.7 Ma for Shangfanggou (Mao et al. 2005). More recent U-Pb zircon geochronology for the Wenyu and Niangniangshan granitic plutons, yield slightly younger ages of 131 ± 1 and 134 ± 1 Ma, respectively (Zhao et al. 2012). Zhao et al. (2012) considered these granitic plutons to have tonalite-trondhjemite-granodiorite (TTG) and adakitic affinity, as suggested by their

major (enriched in Si, K; depleted in Mg), trace (depleted in Nb, Ta, P, Ni, V and Y) elements relative to primitive mantle. The Wenyu and Niangniangshan plutons have negative εNd(t) of −15.0 to −10.1 and −18.5 to −12.2, respectively.

Han et al. (2007), by integrating geochemical and age data, recognised three pulses of Jurassic-Cretaceous granitic magmatism: (1) ca. 160 Ma, I-type granites; (2) ca. 130 Ma I-type granites and (3) ca. 115 Ma A-type granites. The I-type granites could be linked to delamination of subducted lithosphere of the Qinling-Dabie orogenic belt, whereas the A-type granites formed during post-collision extensional processes. These are factors that are crucial for the understanding of associated mineral systems.

Geochemical features of REE and trace elements of these granites can be summarized as follows: (1) Early-stage high-Ba-Sr I-type granite: Wuzhangshan pluton, which displays significantly high Sr and Ba contents relative to other plutons: Sr 1,150 ppm, Ba 2,300 ppm and Sr/Y ratio 70. The pluton has slightly positive Eu anomaly, relatively high K/Rb ratios (ca. 300) and low Y contents (ca. 17.0), coincident with features of typical high-Ba-Sr granites (Fowler et al. 2001) and the high Sr granites in the Dabieshan region and on the northern margin of the NCC (Ma et al. 2004). The chondrite-normalized REE patterns are LREE enriched and HREE flat. High field strength elements (HFSEs) such as Nb, Ta, P and Ti are more depleted than the Huashani and Heyu plutons. (2) Middle-stage I-type granite: Huashani and Heyu plutons. These two plutons have more enriched LREE and similar HREE contents relative to the Wuzhangshan pluton. The negative Eu anomaly and concave-upward REE patterns indicate that amphibole and feldspar played a dominant role during magma segregation. On the primitive mantle-nomalized spiderdiagram, the middle-stage granites show depletion of Ba, Nb, Ta, P and Ti and obviously low Sr than the Wuzhangshan pluton. The Wuzhangshan and Huashani plutons have lower to medium initial $^{87}Sr/^{86}Sr$ ratios (0.7075−0.7077) and $\delta^{18}O$ values between 6.06−9.19, which are similar to I-type granites in the Lachlan fold belt in Australia (Chappell and White 1974), implying a relatively low crustal origin and some mantle contributions (Faure 1986). The Sr and O isotopic ratios of the Heyu granite are relatively high (initial $^{87}Sr/^{86}Sr$ 0.7100; $\delta^{18}O$ 9.11−9.84), and this may be due to crustal contamination during magma ascending (Faure 1986). (3) Late-stage A-type granite (A-type denoting anoroghenic and/or anhydrous granites emplaced in rift zones), represented by the Taishanmiao pluton and related porphyries. The Taishanmiao pluton is different from highly fractionated I-type granites because of its relatively high Y, La, Nb, Ce contents and Ga/Al ratios. The Taishanmiao granite has very low Ca, Sr and Ba contents, relatively high Nb, Ga and Y contents, seagull-shaped REE patterns with pronounced negative Eu anomaly ($Eu/Eu^* = 0.04 - 0.43$) and strong depletion of Ba, Sr, Eu and Ti. This chemistry is typical of A-type granites (Whalen et al. 1987). The HREE contents of the Taishanmiao granite are higher than other granitic plutons in the study area. The 10,000 × Ga/Al-FeOt/MgO and 10,000 × Ga/Al-Ce diagrams confirm that the Taishanmiao granite belongs to the A type. Moreover, on the basis of the Nb-Y-3 × Ga plots, the Taishanmioa granite can be classified as A1 granite, supporting an anorogenic tectonic environment (Eby 1992). Recent investigations have revealed that the Donggou granitic porphyry, with a SHRIMP U-Pb zircon age

of 112 ± 1 Ma (Ye et al. 2006), in the Wangfangshan region has similar geochemical characteristics to the Taishanmiao granite, and is also an A-type granite.

Han et al. (2007) concluded that the emplacement of these granites in three separate stages reflects a tectonic transition from post-collisional to intraplate anorogenic on the southern margin of the NCC between 160 and 115 Ma. The extensive 160–130 Ma post-collisional granite magmatism may be linked to delamination of the lower crust in the Qinling orogenic belt, whereas the 115 Ma A-type granites indicate the end of the continental collision and extensional tectonics.

5.3.1.1 Granitic Plutons

Mao et al. (2010) studied and dated a number of granitic intrusion in the East Qinling orogen, which occur as numerous plutons and stocks with limited areal extents ranging from few tens of square kilometres to less than 10 km^2. Granitic stocks (<10 km^2) are spatially and temporally associated with porphyry-skarn Mo-W and vein type polymetallic mineralisation, whereas the larger plutons are commonly unmineralised. As mentioned above, Triassic alkaline stocks and dykes (223–194 Ma) and rapakivi-type granite stocks (213–217 Ma), emplaced in a post-collisional setting (Wang et al. 2007a), are common in the western part of the Eastern Qinling. Late Jurassic to Cretaceous magmatism in the eastern Qinling region, resulted in the emplacement of granitic intrusions such as the Huashan, Laoniushan, Jinduicheng, Wenyu, Niangniangshan, Wuzhangshan, Huashani, Nannihu, Shangfanggou, Leimengou, Heyu, Donggou, Haopinggou, Huangluding and Taishanmiao intrusions (Fig. 5.6). There are also small syenite stocks, dolerite, diorite and granitic dykes. The Huashan, Laoniushan, Jinduicheng, Wenyu and Niangniangshan granites are located in the Xiaoqinling area, whereas others are located in the above mentioned Xiong'ershan area, east of the Xiaoqinling area (Fig. 5.6). Shallow-emplaced granite porphyries are closely related to porphyry-skarn Mo and Mo-W deposits, forming the largest Mo metallogenic belt in China. Many Ag-Pb-Zn vein-type deposits have also been recognized within the porphyry Mo ore districts. These vein systems are located distally from the contacts of the granite Mo and Mo-W mineralised porphyries and may represent the distal expression of the porphyry mineral systems (Mao et al. 2010, 2011).

The Wenyu and Niangniangshan plutons have similar mineral and chemical compositions (Li et al. 1993), exposed in an area of 71 and 31 km^2, respectively, and intrude gneiss and migmatite of the Archaean Taihua Group. They are located along a regional east-west-striking fault at the north margin of the Xiaoqinling metamorphic core complexes. Biotite monzogranite is the main rock type. The northwest-trending Wuzhangshan pluton lies near the contact zone between the Taihua Group and the Xiong'er Group in the central part of the Xiong'ershan area (Fig. 5.6). It consists of massive, medium-coarse-grained, pale grey porphyritic monzogranite and granodiorite, with rare mafic enclaves. The Wuzhangshan intrusion is intruded by the Haoping pluton in the north. The Huashani and Haoping plutons, located in the north of the Xiong'ershan area, are part of the same intrusion with a total area extent of

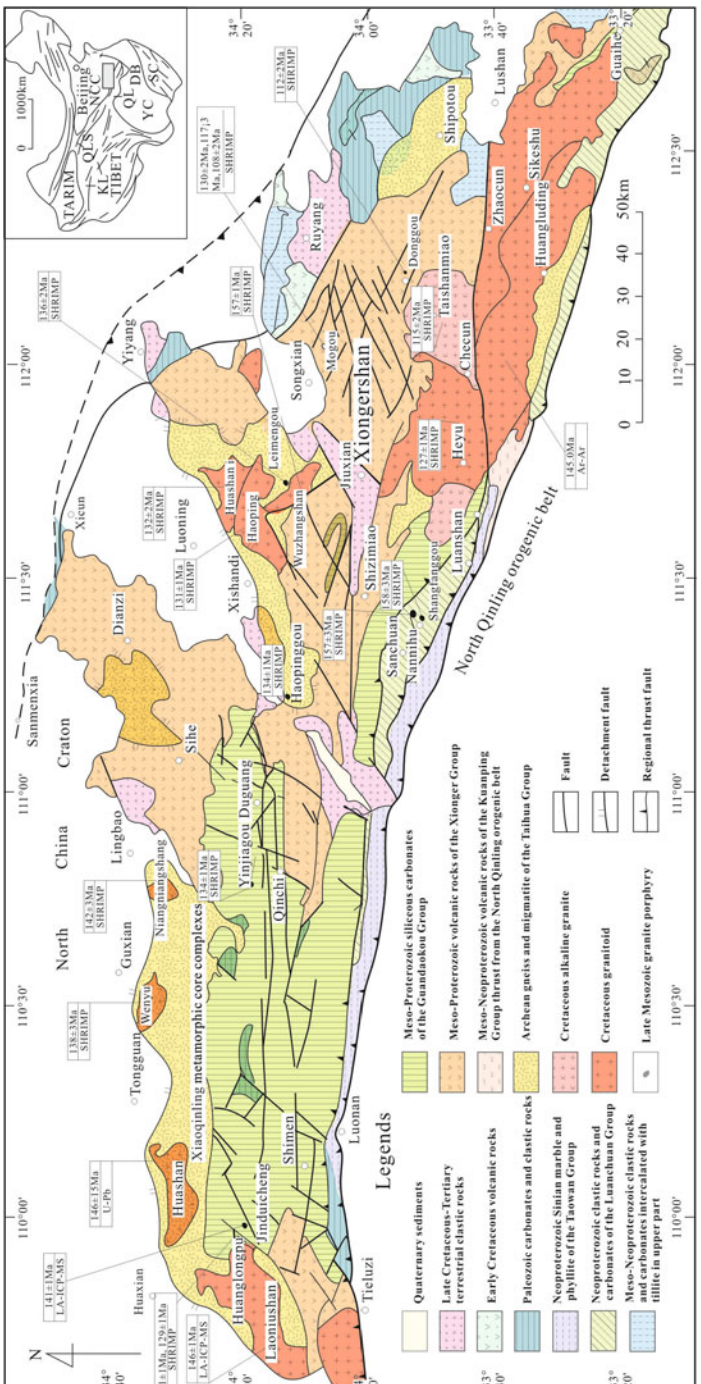

Fig. 5.6 Simplified geology of the East Qinling region and age data and methods. *Inset* shows the position of the East Qinling and other tectonic units in China: *YC* Yangtze Craton, *NCC* North China Craton. *KL* Kunlun orogenic belt, *DB* Dabie orogenic belt, *QL* Qinling orogenic belt, *SC* South China (Cathaysia Block). (After Mao et al. 2010)

ca. 128 km^2, but formed in two stages. Field observations show that the Haoping pluton intrudes the Huashani pluton. Both plutons intruded the metamorphic rocks of Taihua Supergroup and locally the metavolcanic rocks of the Xiong'er Group (Fig. 5.6). The Heyu intrusion covers an area of 784 km^2 and is one of the largest granitic intrusion in the Eastern Qinling region. It intrudes gneiss of the Taihua Group, metavolcanic rocks of the Xiong'er Group and Meso-Neoproterozoic sedimentary rocks, and consists of massive reddish megacrystic biotite monzogranite with rare mafic enclaves. The Heyu granitic intrusion is surrounded by an extensive thermal aureole and intruded by abundant aplite and pegmatite dykes. The Taishanmiao intrusion, covering an area of 290 km^2, intrudes both metavolcanic rocks of the Xiong'er Group and the Heyu biotite granite, and forms a composite batholith (Fig. 5.6). It consists of medium- and coarse-grained syenogranite, fine- and medium-grained syenogranite, and alkali-feldspar granite porphyry. Miarolitic cavities are common, suggesting that these intrusions were volatile rich and emplaced at a relatively shallow level. As mentioned previously, in addition to the large granitic intrusions there are several small stocks emplaced at shallow levels. These include the Nannihu, Shangfanggou, Leimengou, Donggou and Haopinggou stocks (Fig. 5.6), which are spatially and temporally associated with Mo and/or vein type Ag-Pb-Zn mineralisation surrounding the porphyry or porphyry-skarn Mo (W) deposits. The Nannihu and Shangfanggou granitic stocks in the Nannihu Mo ore district, intruded the carbonate and clastic rocks of the Mesoproterozoic Guandaokou Formation, and host the Nannihu-Sandaozhuang skarn-porphyry Mo-W and the Shangfanggou porphyry Mo deposits, respectively. The Nannihu stock consists of biotite monzonite and porphyritic biotite granodiorite, with an exposed area of ca. 0.12 km^2, whereas the Shangfanggou stock consists of biotite monzonite and K-feldspar granite porphyry, with an exposed area of ca. 0.05 km^2. Drilling programs carried out during mineral exploration have revealed that these two granite porphyries merge at depth into a single pluton. The Leimengou granite porphyry, also associated with Mo mineralisation and covering an area of 0.77 km^2, intrudes gneiss of the Archaean Taihua Group. Compositional zoning is evident, with granite porphyry in the centre and monzonitic granite porphyry in the peripheral zones. The 0.01 km^2 Donggou granite porphyry crops out in the east of the Taishanmiao granite (Fig. 5.6). Mineral exploration revealed that the porphyry at depth is 1,550 m long and 850 m wide. The rocks are reddish in color and have a massive structure and a porphyritic texture. The general characteristics of the Donggou granite are similar to those of the Taishanmiao aluminous A-type granite. Regional gravity and magnetic geophysical interpretations indicate that the Taishanmiao intrusion plunges to the north as a tongue extending in a north-northeast direction, of which the Donggou porphyry is an apophysis. The Haopinggou granite porphyry is located in the Haopinggou–Shagou vein type Ag-Pb-Zn ore district. It intrudes Archaean gneiss of the Taihua Group and has an outcrop area of ca. 0.8 km^2. The Mogou syenite pluton covers an area of 15 km^2 and intrudes metavolcanic rocks of the Xiong'er Group. It is a composite pluton consisting of a northwest-trending, 9 km^2, syenite stock in the south, intruded by granitic and diorite dykes and a northeast-trending, 6 km^2, aegirine syenite stock in the north. The syenite stock yielded a SHRIMP zircon U-Pb age of 194 $\pm$ 4 Ma. Granite porphyry

and dolerite dykes are present in the northeast of Huanglongpu Mo deposit, eastern end of the Xiaoqinling area. They intrude quartz sandstone of the Neoproterozoic Gaoshanhe Formation.

In terms of mineral endowment, the Late Jurassic–Early Cretaceous granites of the Eastern Qinling can be divided into Mo (W) mineralised and Mo barren (Mao et al. 2008a), although no obvious geochemical differences exist between these two. Their initial $^{87}Sr/^{86}Sr$ ratios are 0.7061–0.7089 (Chen et al. 2000a) and 0.7064–0.7100 (Ye 2006), respectively, suggesting mixed mantle and crustal sources or derivation from partial melting of lower crust. The Early Cretaceous magmatic rocks in Eastern Qinling are more complex. Rock types, comprise Mo-mineralised A- and I-type granites (Mao et al. 2008a), crust-sourced granites (e.g. Heyu and Haopinggou), aegirine syenite stocks, dolerite, diorite and granitic dykes. The widespread dolerite dykes in the Xiaoqingling gold district have emplacement ages of 128.6–116.9 Ma (Wang et al. 2008). Similar rock types occur in the Dabie orogen, east of the East Qinling area, where crust-sourced and mantle-crustal sourced granites (partly Mo-mineralised) and adakitic rocks were emplaced in the 130–127 Ma time interval (Zi et al. 2007), whereas mafic dykes (dolerite, lamprophyre and anorthosite) and basaltic to andesitic volcanic rocks formed between 129–116 Ma (Wang et al. 2005b; Xie et al. 2007a), respectively.

5.3.1.2 Geodynamic Processes Involved in the Late Mesozoic Granitic Magmatism in Eastern Qinling

As previously mentioned, a vast area of East China, and perhaps the whole East Eurasian continental margin, was affected by major magmatic events in the late Jurassic to Early Cretaceous, interpreted to result from the westward subduction of the Palaeo-Pacific plate (Mao et al. 2010 and references therein). The intensity of these magmatic events seems to decreases westward (Ratschbacher et al. 2003), perhaps indicating a gradually diminishing interaction between the Palaeo-Pacific plate and Eurasian continental margin. The belts of granitic intrusions in the Qinling-Dabie, Yanliao, Middle-Lower Yangtze River Valley and the Nanling Range, in the central part of the Cathaysia Block are generally east-west oriented, reflecting major zones of lithospheric weakness and associated fold belts, formed by a series of collisions of the NCC with the South China block in the south and with the Mongolian-Siberian plate and the closure of the Mongol-Okhotsk Ocean in the north (see Figs. 2.2, 4.19 and 4.23; Yin and Nie 1996; Xiao et al. 2003). The Mongol-Okhotsk suture is about 1,800 km north of the Yanliao belt, and Davis et al. (2001) argued that the granitic intrusions in the Yanliao belt may have been related to the closure of the Mongol-Okhotsk Ocean. Precise geochrolonogical data show that the high-aluminous Indosinian granites (250–215 Ma) in the East Eurasian continent margin were related to late-collisional and post-collisional processes that involved the Indo-China plate, South China plate, North China–Mongolian plate and the Siberian plate. However, the northeast and north-northeast orientation of the Late Mesozoic-Cenozoic magmatism in East China continent is prominent, and

strongly overprints previous geological events. The northeasterly Mesozoic tectonics (Qi et al. 2000; Wan 2004) parallel to the Daxing'anling–Taihangshan or North–South Gravity Lineament (NSGL) (Fig. 7.30) are reflected by regional topography and parallels the Pacific margin magmatic belt (Xu 1990). Moreover, even in the east-west trending belts, the individual Mesozoic granite plutons were emplaced along north-northeast-trending fractures, especially at the intersections of north-northeast- and east-west-trending structures. Xiang (2009) reported that the Mogou syenite stock, spatially associated with the Mogou aegirine syenite and diorite dykes in East Qinling, formed at 194 ± 4 Ma (SHRIMP zircon U-Pb method). Zhou et al. (2006) mentioned a magmatically quiescent period during the Early Jurassic (205–180 Ma) in South China. In fact, there was no granitic magmatism in the Early Jurassic throughout the major part of the East China continental margin, including South China, Middle-Lower Yangtze River Valley, Qinling–Dabie, and eastern Shandong peninsula. The Yanliao belt contains some Early Jurassic granites, possibly a response to the interaction between the North China-Mongolian plate and the Mongol-Okhotsk oceanic plate. The amagmatic period in this extensive region of East China could represent a tectonic quiescence after the assembly of the NCC, South China block and Indo-China block along the Dabie and the Songma-Mojiang sutures, respectively. The Izanagi plate commenced subduction beneath the eastern Eurasian continental margin from the Middle Jurassic (Maruyama et al. 1997). Prior to ca. 135 Ma, the now extinct Izanagi plate was being subducted and undergoing orthogonal convergence with the Eurasian continental margin (Maruyama et al. 1997; Wan 2004; Goldfarb et al. 2007). Maruyama et al. (1997) and Li and Li (2007) suggested that the Izanagi plate subducted at a shallow angle or flat-slab, explaining the extensive occurrence of granitic intrusions in the interior of the continent. The Middle Jurassic–Early Cretaceous granites (180–135 Ma) were emplaced in back-arc extensional zones, developed parallel to the continental margin (Ratschbacher et al. 2003). After 135 Ma, the Izanagi plate motion changed and became oblique to the continental margin (Goldfarb et al. 2007). In the period of 135–108 Ma, a series of north-northeast-trending strike-slip faults, including the 2,500 km long Tancheng-Lujiang (or Tan-Lu or Tanlu) fault (Fig. 7.30), extending from the Yangtze Craton to the Sikhote-Alin, Far East Russia, were active with a sinistral shear sense (Zhu et al. 2005), although a new $^{40}Ar/^{39}Ar$ age of 161 ± 3 Ma (Sun et al. 2008) indicates that the northern segment of the Tanlu Fault may have been acitivated in Late Jurassic. The tectono-thermal Yanshanian events of late Mesozoic age along the East China continental margin include widespread volcanism, the intrusion of I-, S-, and A-types of granites, the development of rift basins and metamorphic core complexes in the NCC and adjacent regions (e.g. Qinling-Dabie belt, Middle-Lower Yangtze River Valley), ranging in age from 135 to 108 Ma and with a peak at 120–115 Ma. In the Yangtze and Cathaysia blocks these tectono-thermal events occurred between 120 and 80 Ma (Mao et al. 2008b). There are two prevailing models to explain these geological phenomena: (1) thermal erosion and metasomatism of subcontinental lithospheric mantle beneath the eastern China continent (Menzies and Xu 1998; Griffin et al. 1998), and (2) lithospheric delamination (Gao et al. 2002, 2004; Deng et al. 2004; 2007). Both models envisage upwelling of asthenospheric mantle into a

metasomatised lithosphere and the lower crust. Wu et al. (2005a) further proposed that the rising of the Cretaceous mid-Pacific superplume may have increased subduction rates along the outer margins of the western Pacific Ocean, which in turn may have assisted lithospheric delamination. These suggestions are essentially similar and all point to the intensive magmatism caused by lithospheric thinning processes. This in turn resulted in the asthenosphere rising into the lower, and perhaps even the upper crust with strong magmatic underplating and crust remelting. This would also account for a range of sources for igneous rocks, comprising I-, S-, and A-types of granites, syenite and dolerite in the same period (Mao et al. 2010).

5.3.2 *Geodynamic Evolution Model for the Qinling-Dabie Orogenic Belt*

An understanding of the geodynamic evolution of the Qinling-Dabie orogenic belt is an essential prerequisite in order to gain insights into regional and local metallogenesis. Details of the geodynamic evolution of the Qinling-Dabie Orogen can be found in Zhang et al. (1995), Meng and Zhang (2000), Ratschbacher et al. (2003) and more recently Zhu et al. (2011a) who used detrital zircon U-Pb ages and Hf systematic to propose that interesting hypothesis that the North Qinling terrane was a separate microcontinent that was eventually accreted onto the southern margin of the NCC at about 640 Ma. A model showing the key tectonic processes that formed the Qinling-Dabie Orogen, slightly modified from Chen et al. (2004a) and Dong et al. (2010), is schematically illustrated in Fig. 5.7 and described below. Although applicable to a restricted region, these models have general validity, at least along the suture boundary between the North China and the Yangtze Cratons.

Between 1.85 and 1.5 Ga the Huaxiong Block, bounded by the Luanchuan fault to the south and the San Bao fault to the north (Fig. 5.5) formed a crystalline basement comprising the ca. 2.5–2.2 Ga Taihua Group, which was sutured at about 1.85 Ga with the Songji Block along the San-Bao fault (Fig. 5.7a). The Huaxiong Block, which contains the volcanic rocks of the Xiong'er Group, experienced a number of tectonic events, briefly summarized as follows. The first event took place with a northward subduction of the Kuanping palaeo-Ocean along the Luanchuan fault. Although the precise timing is not well constrained, at 1.78 Ga there was rifting with the emplacement of dyke swarms and continental volcanic rocks of the Xiong'er Group, forming a large igneous province, as detailed in Chap. 7. At about 1.45–1.3 Ga, the Central Qinling Terrane collided with the NCC, ending the continental-arc regime (Fig. 5.7b). Between 1.3 and 1.05 Ga, post-collisional extension resulted in deposition of the fore-arc carbonate-shale-chert sequence of the Guandaokou Group along the Luanchuan fault and the back-arc sedimentary assemblage of the Ruyang Group along the San-Bao fault, respectively (Fig. 5.7c). From 1.05 to >0.5 Ga, an arc-back-arc system was formed above a northward subduction of the Shan-Dan palaeo-ocean, and an extensional passive continental margin was formed (Fig. 5.7d). At the southern margin of the Huaxiong Block, the sedimentary rocks of the Luanchan Group and

its overlying Sinian-Early Palaeozoic strata, including glacial tillites, accumulated upon the Guandaokou Group. Meanwhile, the Luoyu Group, Sinian glacial tillites and a Cambrian-Middle Ordovician carbonate-shale succession developed along the San-Bao fault, inboard of the Songji Block. With the closure of the back-arc sea at about 0.45 Ga, the Huaxiong Block was uplifted and eroded (Fig. 5.7e). Finally, during 0.4–0.25 Ga, the opening of the Mian-Lue Ocean and re-opening of the Shang-Dan (or Shangdan) Ocean and their northward subduction led to the development of the Devonian-Middle Triassic tectonostratigraphic unit in the southern and northern areas of the Huaxiong Block (Fig. 5.7e).

Because Middle-Lower Triassic turbidites are common in the southern and western parts of the Qinling Orogen, and are also locally found in the eastern Qinling Orogen, the final stages of the continental collision between the South and North China plates would have occurred later than 230 Ma. As localised collisions might have occurred from about 250 Ma, this age may be the best estimate for the beginning of this continental collision and is in accordance with radiometric ages (Zhang et al. 1995). This continental collision is part of the Indosinian orogeny, which effectively involved the closure of a Palaeo-Tethys oceanic seaway. During these final stages of collision, a stack of underthrust slabs formed within the Qinling Orogen (Fig. 5.7e). For instance, the Machaoying fault within the Huaxiong Block became a north-dipping thrust zone (Han et al. 2007). The Shang-Dan, Longmenshan-Dabashan and San-Bao faults served as a main central thrust (MCT), the southern main boundary thrust (MBT) and the northern reverse boundary fault (RBT), respectively (Fig. 5.7e). The tectonic regime changed from Triassic-Early Jurassic compression (Indosinian Orogeny), through Late Jurassic-Early Cretaceous transpressive compression (or transition from compression to extension), to Late Cretaceous extension (Yanshanian event), with continental collision ending during the Late Cretaceous. It is during this collision, that large-scale fluid circulation, granitic magmatism and ore formation took place in the Qinling Orogen. Metallogenic provinces that formed at this time include the Carlin-like Shan-Gan-Chuan Au belt, the Xiaoqinling-Xiong'ershan Au belt, and the Jinduicheng-Luanchuan Mo porphyry belt, discussed in the sections ahead. The closure of the Shang-Dan Ocean is represented by an ophiolitic mélange zones (Shang-Dan) composed of oceanic mafic and ultramafic rocks and subduction-related igneous rocks, which have been interpreted to also include magmatic arc basalts, in addition to mid-ocean ridge rocks (Dong et al. 2010). Dong et al. (2010) determined a U-Pb zircon age of 517.8 ± 2.8 Ma, obtained from a gabbro in the Shang-Dan mélange. According to these authors, another ophiolitic mélange, called Erlangping is present to the north of Shang-Dan and consist, in addition to mafic and ultramafic rocks, of andesites and rhyolites, possibly related to a continental margin. Thus, a geodynamic model, shown in Fig. 5.7h, as proposed by Dong YP and co-workers, envisages two subduction systems under a North Qinling continent, with a Shang-Dan oceanic arm north of the South China Block and a back-arc basin between the North Qinling terrane and the NCC. Collision between these tectonic units between 460 and 400 Ma, resulted in the formation of the Shang-Dan and Erlangping sutures.

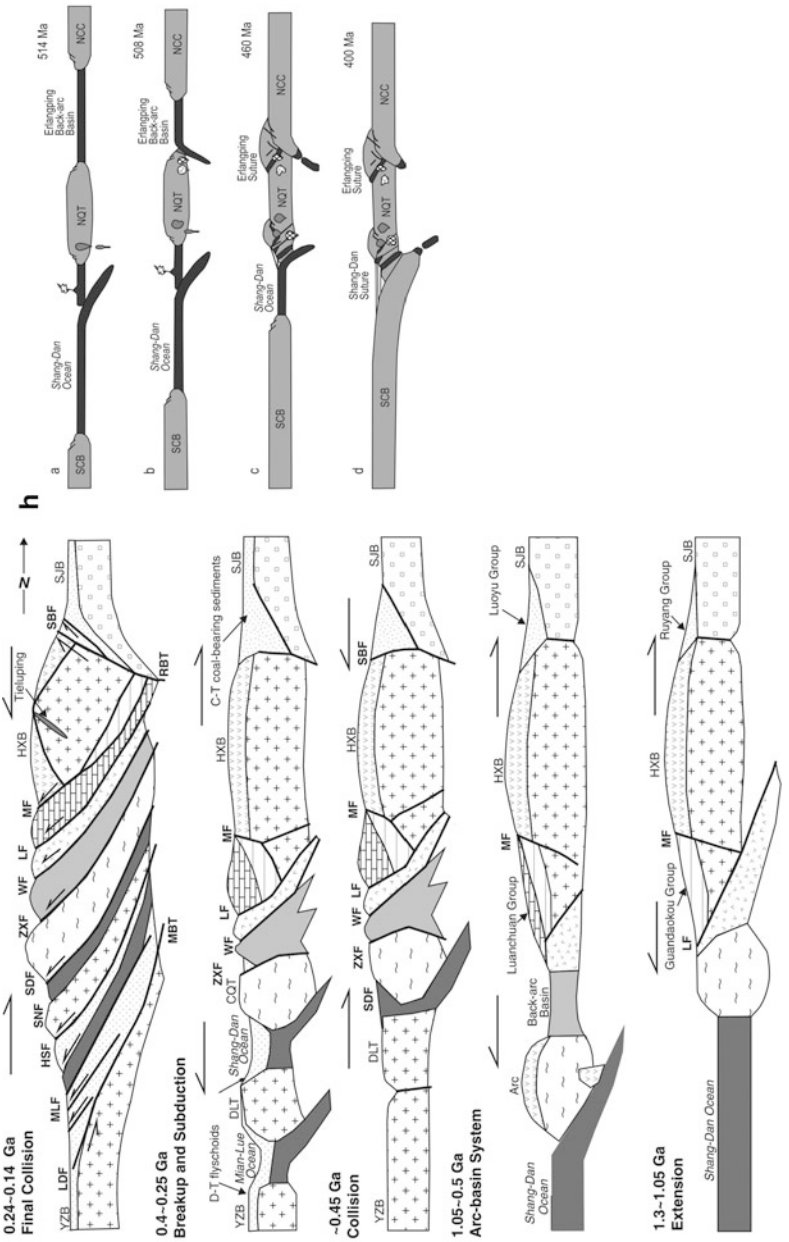
h
a
b
c
d
514 Ma
508 Ma
460 Ma
400 Ma
Erlangping Back-arc Basin
Erlangping Suture
Shang-Dan Ocean
Shang-Dan Suture
NQT
SCB
NCC
e 0.24~0.14 Ga Final Collision
d 0.4~0.25 Ga Breakup and Subduction
c ~0.45 Ga Collision
b 1.05~0.5 Ga Arc-basin System
a 1.3~1.05 Ga Extension
YZB
LDF
MLF
HSF
SNF
SDF
ZXF
WF
LF
MF
HXB
SBF
RBT
MBT
SJB
Tieluping
D-T flyschoids
Mian-Lue Ocean
DLT
COT
C-T coal-bearing sediments
Arc
Back-arc Basin
Luanchuan Group
Luoyu Group
Ruyang Group
Guandaokou Group
Shang-Dan Ocean

Fig. 5.7 Tectonic evolution of the Qinling Orogen (after Chen et al. 2004a); **a** post-collision extension of the southern margin of North China Craton and development of the Guandaokou Group in a fore-arc basin and the Ruyang Group in a back-arc basin (Ruyang Basin) along the San-Bao fault. **b** Opening of the Erlangping Sea back arc and deposition of the Luanchuan Group along the passive continental margin and the Luoyu Group in the Ruyang Basin, while the Shang-Dan Ocean is subducted beneath the Central Qinling Terrane. **c** The Shang-Dan Ocean closes and the Yangtze Craton collides with the Central Qinling Terrane; the Erlangping Sea closes and Central Qinling Terrane collides with the North China Craton. **d** Opening of the Mian-Lue Ocean and partial re-opening of the Shang-Dan Ocean; Devonian-Middle Triassic flysch and volcanic rocks widely develop in areas of the Shang-Dan fault, and Late Carboniferous-Late Triassic coal-bearing sediments extensively develop in the area north of the San-Bao fault. **e** Final closure of oceans and full-scale collision between the Yangtze and North China continents between Triassic and Jurassic time; intense intracontinental subduction (slab stacking) and crustal shortening and thickening. **h** shows the model proposed by Dong et al. (2010), for the geodynamic evolution of the oceanic arms and subduction systems, between the South China Block and the North China Craton. Abbreviations: *SJB* Songji Block, *HXB* Huaxing Block, *CQT* Central Qinling Terrane, *DLT* Douling Terrane, *YZB* Yangtze Block, *SBF* San-Bao fault, *MF* Machaoying fault, *LF* Luanchuan fault, *WF* Waxuezi fault, *ZXF* Zhu-Xia fault, *SDF* Shang-Dan fault, *SNF* Shanyang-Neixiang fault, *HSF* Houshan fault, *MLF* Mian-Lue fault, *LDF* Longmenshan-Dabashan fault, *MBT* Main boundary thrust, *RBT* Reverse boundary thrust, *NCC* North China Craton, *SCB* South China Block, *NQT* North Qinling Terrane

5.3.3 *Mineral Systems of the Qinling-Dabie Orogenic Belt*

A variety of hydrothermal ore deposits including precious metal lodes, porphyry Mo, breccia pipes containing Au and Mo, and base metal skarns are present in the Qinling-Dabie orogenic belt. Geochronological data, structural and geological constraints show that all these deposits, although hosted in rocks of Archaean to Palaeo-Mesoproterozoic age, are Mesozoic in age and their genesis is related to post-collisional and extensional tectonics during the Indosinian and Yanshanian times (250–90 Ma). Before proceeding with the topic of this section, it may be opportune to highlight some of the key aspects of the Qinling-Dabie orogenic belt.

Continental collisions between the South and the North China continents can be considered in terms of a three-stage evolution: (1) early compression (Triassic to middle Jurassic); (2) transition from compression to extension (late Jurassic to early Cretaceous) and (3) late extension tectonics (Cretaceous). The evolution of the Qinling-Dabie orogenic belt and related mineral systems involved the following: (1) Palaeo-Tethys ocean closed in the Triassic forming the Mian-Lue ophiolite belt; (2) In southern Qinling, middle Triassic turbidites are widespread, confirming final ocean closure in late Triassic, possibly at ca. 213 Ma (Yin and Nie 1996); (3) widespread distribution of Cretaceous intramontane molasses intercalated with felsic volcanics (Chen and Fu 1992) suggesting uplift in Jurassic, followed by extension in the Cretaceous; (4) isotopic ages for metamorphic rocks including UHP eclogites (235–190 Ma) and blueschists (220–200 Ma) are indicative of collision starting from middle-late Triassic (Hacker et al. 1996); (5) isotopic ages of shows that syncollisional granites started to develop at from 250–205 Ma (Indosinian), followed by granitic magmatism in the Jurassic and Cretaceous (Yanshanian), when it reached a peak at about 130 Ma; (6) Geophysical data, including palaeomagnetic and seismic reflection, indicate that crustal uplift and mountain-building mainly occurred in the period from late Triassic to early Cretaceous; (7) Isotopic ages of most hydrothermal ore systems range from Jurrassic to early Cretaceous, coeval with granite emplacement.

The Mesozoic collision events in the Qinling-Dabie resulted in north-dipping underthrusting/continental subduction (Fig. 5.7). This created an architecture characterised by a stacking of crustal slabs by underthrusting, and intensive crustal thickening (Fig. 5.7). The north-dipping underthrusting was terminated by the south-dipping San-Bao fault, which reaches deeper than the Moho discontinuity, and acts as the reverse boundary thrust (RBT; Fig. 5.7). This geodynamic setting makes all the hydrothermal ore systems, such as Au, Mo-W, Pb-Zn, Ag and Cu in the Qinling-Dabie, lie south of the San-Bao fault. North of the San-Bao fault, no significant hydrothermal deposit has been found. Ore fields are usually located in areas of enhanced crustal thickness, indicating that collisional tectonics must have been important. For example, the major Au district is present in the Xiaoqinling area, which is where crustal thickness is larger than the other areas of the Huaxiong block. Similarly, the Jinduicheng-Luanchuan porphyry Mo belt is located along contour lines of high crustal thickness. Most mineral deposits in the Qinling region, formed in the Mesozoic (Yanshanian; Jurassic and Cretaeous).

5.3.3.1 Precious Metal Lode Deposits

Precious metal lode deposits are one of the most important sources of Au and Ag. Lode deposits mostly occur in accretionary and metamorphic terranes and typically consist of precious-metal-bearing quartz veins, locally with variable amounts of sulphide disseminations and/or stockworks, with pyrite and arsenopyrite as the main sulphides and locally tellurides and base metal sulphides. In the eastern part of the orogen is the Xiaoqinling-Xiong'ershan region of the Qinling mountains, in eastern Sanxi and western Henan provinces, where more than 100 lode Au-Ag deposits have been recorded (Table 5.2), with an estimated total resource plus production of greater than 550 tonnes (Mao et al. 2002a). These lode deposits are characterised by quartz vein systems and disseminations in basement and cover rocks. Hydrothermal alteration is dominated by quartz, sericite, pyrite and carbonates. Radiometric ages range from about 172–100 Ma, corresponding with the emplacement of granitic rocks emplaced during the final collision and/or post-collison stages between the NCC and the Yangtze Craton.

Good examples of lode deposits in the Xiaoqinling district are the Ag-dominated Tieluping and the Au-dominated Shanggong (Fig. 5.8). Chen et al. (2004a, 2006, 2008a) studied these two lode deposits in the eastern Qinling orogen which, together with other lode systems and the Yinjiagou gold skarn belt in the Xiong'er Terrane, the Jinduicheng porphyry Mo and the Qiyugou Au-Mo breccia pipes are all controlled by northeast-trending structures (Fig. 5.8). Other examples of well-known lode deposits include Dongchuan, Wnyu, Qiangma, Tonggou and Yangzhaiyu (Table 5.2). The latter deposit has reserves of about 50 t of Au distributed in tens of quartz veins emplaced within amphibolites facies metamorphic rocks of the Taihua Group (Bi et al. 2011).

The Xiaoqinling regional setting is dominated by the Xiong'er Terrane (Fig. 5.8), which is a northeast-trending, roughly wedge-shaped area, containing two main lithostratigraphic units: the Neoarchaean-Palaeoproterozoic Taihua Group and the overlying Palaeoproterozoic Xiong'er Group. To the south and in contact with the Machaoying Fault are the sedimentary successions of the Guandakou and Luanchuan Groups. Subsidiary fault-splays of the Maochaoying fault are common in the Xiong'er Terrane, which served as major conduits for both granitic intrusions and hydrothermal fluids. The east-west-trending Machaoying fault (Fig. 5.8), with a strike length of over 200 km and inferred depth of 34–38 km, has been interpreted as the trace of a major north-dipping thrust, formed during the continental collision that in the Triassic sutured the North China and the Yangzte Cratons, resulting in the Qinling-Dabie orogenic belt (Han et al. 2009). The Taihua Group is a high-grade metamorphic sequence of amphibolite to granulite facies rocks (2.55–2.3 Ga Beizi Group Dangzehe greenstone belts) and a passive margin succession of graphite schist, marble and iron-formation rocks (2.3–2.2 Ga Shuidigou Group). The Xiong'er Group, is up to 7,600 m thick (Zhao et al. 2002), and is a well preserved unmetamorphosed and only slightly deformed predominantly bimodal volcanic sequence with well-constrained ages of $1{,}826 \pm 32$ Ma to $1{,}840 \pm 14$ Ma (Peng et al. 2005) that unconformably overlies the metamorphic basement (TaihuaSupergroup) and is overlain by Mesoproterozoic carbonate rocks. The origin of the Xiong'er volcanic

Table 5.2 List of selected gold deposits in the Xiaoqinling-Xiong'ershan region. (After Mao et al. 2002b)

Name of deposit	Longitude, Latitude (from – to)	Host rocks	Ore minerals	Alteration minerals	Metals	Estimated Au reserve (t)/ grade (g/t)
Dongchuang	110°26′35″–110°28′25″E, 34°24′15″–34°25′11′N	Late Archean Lujiayu Formation	Pyrite, galena, pyrrhotite, chalcopyrite, chalcocite, bornite, scheelite, wolframite, calaverite, petzite	Quartz, chlorimmte, sericite, biotite, carbonate, pyrite, epidote	Au, Ag, Pb, W, Te	27.6/8.2
Wenyu	111°26′15″E, 34°25′38″N	Late Archean Lujiayu Formation	Pyrite, galena, chalcopyrite, calaverite	Pyrite, sericite, quartz, K-feldspar, biotite, chlorite, epidote, carbonate	Au, Pb, Cu, Ag, Te	32.7/7
Tonggou	110°34′16″–110°34′52″E, 34°25′21″–34°25′41″N	Late Archean Qiangmayu Formation	Pyrite, galena, chalcopyrite, sphalerite, pyrrhotite, scheelite, magnetite, molybdenite, calaverite, petzite, hessite, altaite, tellurobismuthite	Quartz, calcite, plagioclase, microcline, biotite, muscovite, sericite, chlorite, carbonate, pyrite	Au, Pb, Cu, Ag, W, Mo, Te, Bi	1.5/20.3
Huanchiyu	110°33′29″E, 34°28′01″N	Late Archean Huanchiyu Formation and the Lujiayu Formation	Pyrite, magnetite, sphalerite, molybdenite, chalcopyrite	Quartz, sericite, epidote, microcline, carbonate, serpentine, pyrite	Au, Cu, Mo	1.2/6.7
Dahu	110°36′29″E, 34°23′50″–34°27′35″N	Late Archean Lujiayu Formation	Pyrite, chalcopyrite, galena, sphalerite, pyyrhotite, bornite, molybdenite, covellite, bismuthinite, arsenopyrite, magnetite	Quartz, microcline, plagioclase, calcite, sericite, biotite, sphene, apatite	Au, Ag, Cu, Mo, Pb	38/6.8
Linghu	110°38′31″E, 34°23′50″–34°23′40′N	Late Archean Lujiayu Formation	Pyrite, chalcopyrite, galena, sphalerite, pyrrhotite, bornite, covellite, bismuthinite, arsenopyrite, magnetite	Quartz, K-feldspar, plagioclase, calcite, sericite, sphene, apatite	Au, Ag, Cu, Mo, Pb	20/5.6

Table 5.2 (continued)

Name of deposit	Longitude, Latitude (from – to)	Host rocks	Ore minerals	Alteration minerals	Metals	Estimated Au reserve (t)/ grade (g/t)
Yangzhaiyu	110°31′40″–110°33′07″E, 34°23′45″–34°24′35″N	Late Archean Lujiayu Formation	Pyrite, galena, chalcopyrite, sphalerite, magnetite, scheelite, wolframite, silver, pyrrhotite, ilmenite, tellurobismuthite	Quartz, sericite, microcline, biotite, ankerite, calcite, zircon, rutile, kaolinite, pyrite, K-feldspar	Au, Pb, Ag, Cu, W, Te, Bi	34.4/11.4
Qiangma	110°31′19″E, 34°24′00″N	Late Archean Lujiayu Formation	Pyrite, chalcopyrite, sphalerite, galena, magnetite, pyrrhotite, bornite, scheelite, siderite, ilmenite	Quartz, ankerite, calcite, sericite, pyrite	Au, Pb, Cu, Zn, W	8.6/8.9
Jingtongcha	110°38′18″, 110°31′52″E, 34°24′51″–34°25′06″N	Late Archean Lujiayu Formation and the Guanyintang Formation	Pyrite, sphalerite, galena, chalcopyrite, magnetite, wolframite, bornite, specularite, siderite, silver	Quartz, calcite, ankerite, dolomite, rutile, sphene, barite, pyrite	Au, Ag, Cu, Pb, Zn, W	12.4/7.7
Shanggong	111°32′33″–111°34′14″E, 34°10′24″–34°11′25″N	Middle Proterozoic Jidanping Formation of the Xiong'er Group	Pyrite, galena, sphalerite, chalcopyrite, tetrahedrite, scheelite, calaverite	Sericite, quartz, chlorite, ankerite, fluorite, barite, calcite, pyrite, fluorite	Au, Ag, Pb, Zn, Te	29.1/6.9
Qiyugou	111°57′00″E, 34°13′30″N	Middle Proterozoic Xiong'er Group; Mesozoic porphyries and breccia	Pyrite, chalcopyrite, galena, bismuthinite, native gold, chalcocite	Quartz, sericite, K-feldspar, chlorite, calcite, hastingsite, taramite, pyrite	Au, Ag, Pb, Cu	40/7.4
Yaogou	111°54′36″ 111°55′35″E, 34°05′51″–34°06′44″N	Middle Proterozoic dacite, andesite and agglomerate lava of the Jidanping Formation of the Xiong'er Group	Pyrite, specularite, limonite, chalcopyrite, galena, sphalerite, molybdenite, malachite, hematite	Quartz, sericite, calcite, ankerite, chlorite, barite, fluorite, K-feldspar, epidote, pyrite	Au, Ag, Cu, Fe	2/8.9

Table 5.2 (continued)

Name of deposit	Longitude, Latitude (from – to)	Host rocks	Ore minerals	Alteration minerals	Metals	Estimated Au reserve (t)/ grade (g/t)
Beiling Tantou	111°44′24″–11°46′09″E, 34°03′28″–34°04′07″N	Middle Proterozoic andesite and rhyolite rocks of the Xiong'er Group	Pyrite, marcasite, galena, sphalerite, arsenopyrite, telluride minerals	Quartz, plagioclase, K-feldspar, chlorite, sericite, kaolinite, ankerite, barite	Au, Ag, Te	44/8
Qianhe	111°51′45″–111°52′36″E, 33°59′31″–33°59′58″N	Middle Proterozoic andesite and rhyolite rocks of the Xiong'er Group	Pyrite, marcasite, galena, siderite, hessite, altaite, calaverite, krennerite	Quartz, plagioclase, K-feldspar, sericite, kaolinite, pyrite, fluorite	Au, Ag, Te	22/8.7–13.9
Kangshan-Xingxingyin	111°20′40″–111°22′30″E, 34°03′00″–34°04′00″N	Middle Proterozoic andesitic volcanic rock series of the Xiong'er Group	Pyrite, galena, sphalerite, chalcopyrite, limonite	K-feldspar, quartz, sericite, carbonate, chlorite, epidote, pyrite	Au, Pb, Zn	13.7/6
Shenjiayao	111°14′10″E–34°32′30″N	Late Proterozoic Xiaoshan Group	Pyrite, arsenopyrite, marmatite, sphalerite, galena, chalcopyrite, chalcocite	Quartz, sericite, siderite, dolomite, calcite, chlorite, barite, kaolinite	Au, Ag, Pb, Zn	3.8/5.1
Tongyu (a)	110°18′00″E, 34°24′51″N	Late Archean Guanyingtang Formation	Pyrite, chalcopyrite, galena, sphalerite, magnetite, specularite, silver	Quartz, ankerite, sericite, chlorite, pyrite	Au, Ag, W, Cu, Pb, Sb	9.9/5.7–8.9
Tongyu (b)	110°19′48″E, 34°24′24″N	Late Archean Lujiayu Formation and the Guanyintang Formation	Pyrite, magnetite, chalcopyrite, galena, siderite, wolframite, scheelite, sphalerite, chalcocite, pyrrhotite, specularite, bismusthinite	Quartz, calcite, sericite, barite, epidote, chlorite, biotite, muscovite, zircon, sphene, pyrite	Au, Cu, Pb, W, Bi	21.3/7.8–20

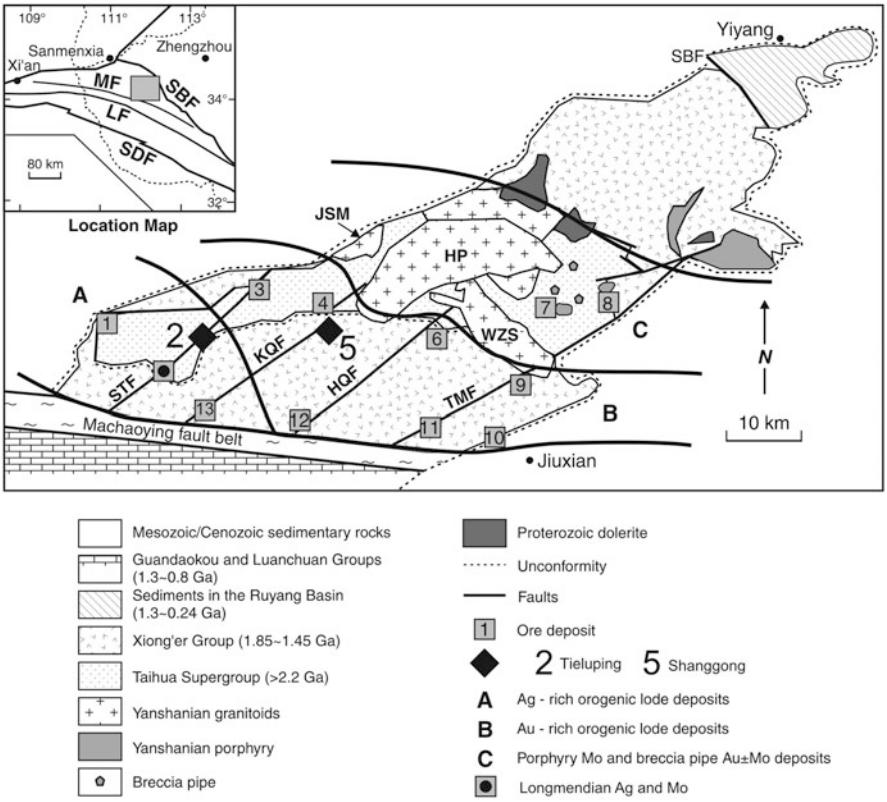

Fig. 5.8 Simplified geological map of the Xiong'er Terrane in the East Qinling and location and geological setting of the Tieluping and Shanggong deposits. Other hydrothermal ore deposits: *1* Haopinggou (Ag-Pb); *2* Tieluping Ag-Pb; *3* Xiaochigou(Au); *4* Hugou Au; *5* Shanggong Au; *6* Qinggangping (Au); *7* Leimengou (Mo-Au); *8* Qiyugou (Au-Mo); *9* Yaogou (Au); *10* Qianhe Au; *11* Tantou (Au); *12* Hongzhuang (Au); *13* Kangshan (Au-Ag-Pb); *A*, *B*, and *C* metallogenic districts, Ag-rich, Au-rich and Mo-rich, respectively; The Longmendian Ag and Mo deposit is discussed in Chap. 3; *JSM* Jinshanmiao granite; *HP* Haoping granite; *WZS* Wuzhangshan granite. Faults: *STF* Sanmen-Tieluping; *KQF* Kangshan-Qiliping; *HQF* Hongzhuang-Qinggangping; *TMF* Taochun-Mayuan. Location inset: *LF* Luanchuan fault, *MF* Machaoying fault, *SBF* San-Baofault, *SDF* Shang-Danfault. (After Chen et al. 2004a)

rocks is controversial. Kusky and Li (2003), suggested that the Xiong'er volcanic rocks are a bimodal succession formed in a northeast- trending rift system related to the opening of the Qinling ocean. Peng et al. (2005, 2008), on the other hand, showed that the Xiong'er volcanic rocks and dyke swarms are part of a 1.78 Ga large igneous province emplaced in a north-south-trending rift system developed across the NCC (see Fig. 5.8 and Chap. 7). The Guandaokou and Luanchuan Groups, south of the Machaoying fault (Fig. 5.8) contain carbonaceous carbonate rocks, quartz sandstones, shales and cherts (CSC sequence). The CSC rocks were largely sourced from the Taihua Group and the Xiong'er Group and deposited in a forearc basin between 1.3 and 0.8 Ga.

The lithostratigraphic units discussed above were intruded by Jurassic to Cretaceous (ca. 160 Ma to ca. 110 Ma) granites, including the 200 km^2 Haoping batholith, the Huashan Complex and a number of mineralised porphyry intrusions, diatremes and the Qiyugou Au-bearing breccia pipes, described in the sections that follow.

Tieluping Ag-Pb

The Tieluping Ag-Pb ± Au deposit is controlled by the northeast-trending sinistral Tieluping fault (Fig. 5.8) and hosted by plagioclase-amphibole gneisses, amphibolites and biotite-plagioclase gneisses of the Taihua Group (Chen et al. 2004a). The ore bodies are associated with a group of subsidiary, parallel fractures on the west side of the Tieluping fault that dips 50–80° west-northwest.

The two largest orebodies are 730 m long and 390 m deep, with average thickness of 4.6 m and an average grade of 347 g/t Ag; and 780 m long and 310 m deep, with average thickness of 4.7 m and an average grade of 303 g/t Ag. Although vertical zonation in alteration assemblages is not observed, lateral zoning is pronounced (Fig. 5.9). This zoning is gradational and is characterized by silicification proximal to the ore, through a zone of sericite-quartz grading into a distal chlorite-sericite zone. Orebodies are usually within multistage silicified zones that only locally form coarse-grained quartz veins. These veins commonly have cataclastic, banded, stockworks, or massive structures. Ore textures are highly variable. For example, brecciated quartz grains are replaced by galena and chalcopyrite; tetrahedrite is replaced by digenite; early formed pyrite and galena are usually brecciated, and replaced by galena or tetrahedrite; locally, embayed sphalerite and chalcopyrite are replaced by galena.

Three paragenetic stages, from early (E), middle (M) to late (L), are recognized on the basis of crosscutting relationships. They are: (1) E-stage fault-controlled pyrite-quartz veins, locally containing some galena, and pyrite-sericite-quartz assemblage in the wall rocks; (2) M-stage, with the assemblage quartz + sericite + galena + chalcopyrite + sphalerite + tetrahedrite + pyrite, is present in veinlets that cut the E stage assemblages; (3) L-stage veinlets of calcite ± quartz ± sericite ± chlorite ± digenite ± galena ± pyrite, with comb textures, crosscuts the E- and M-stage minerals and wall rocks. These paragenetic stages are in broad agreement with the results of fluid inclusion studies, in which homogenisation temperatures (uncorrected for pressure) fall into three groups: ca. 370 °C (E stage), ca. 250–165 °C (M stage) and ca. 135–203 °C (L stage). Microscope and electron microprobe studies indicate that Ag is present as native metal and within tetrahedrite, freibergite, polybasite, and galena. These minerals mostly formed during the M-stage. The E-stage massive galena and L-stage disseminated galena do not contain significant silver.

The results of C, S and Pb isotope systematics of ores and minerals from Tieluping enabled important constrains for understanding the genesis of this lode system. Depleted $\delta^{13}C$ values of CO_2 gas and carbonate minerals in hydrothermal ore deposits generally suggest a deep-seated juvenile source for the carbon (Faure 1986), however fluids from the Tieluping deposit have much higher $\delta^{13}C_{CO_2}$ values, which

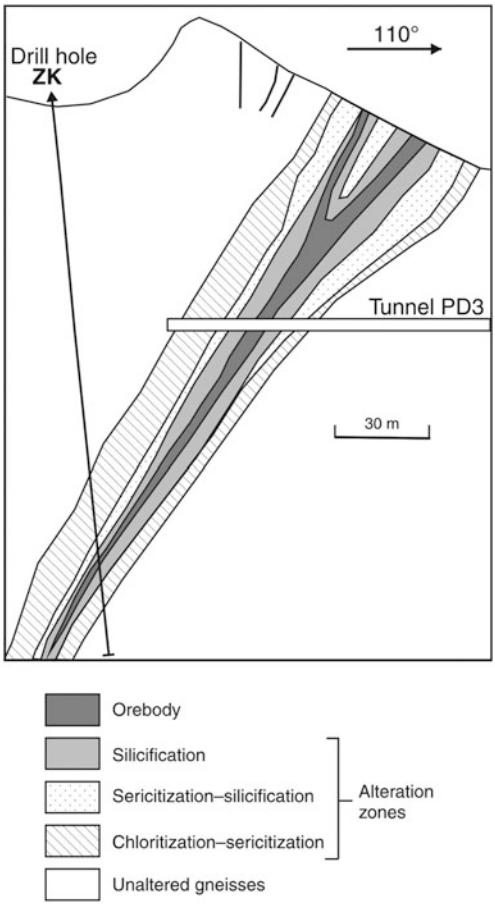

Fig. 5.9 Cross-section through the Tieluping orebody and wall-rock alteration zones. (After Chen et al. 2004a)

decrease with time, indicating a significant difference in fluid nature and source. In the E-stage, $\delta^{13}C_{CO_2}$ values range from 0.3 to 4.0 ‰, and averages 2.0 ‰, higher than those of organic matter (av. −27 ‰), CO_2 in fresh water (−9 to −20 ‰), igneous rocks (−3 to −30 ‰), continental crust (−7 ‰), and mantle (−5, −7 ‰) (Faure 1986; Hoefs 2004). This indicates that, whereas at Tieluping the CO_2 in the E-stage fluids could not be sourced from one or a mixture of the above-mentioned materials, they could be dominantly sourced from marine carbonates by metamorphic devolatilisation processes. $\delta^{13}C_{CO_2}$ values of L-stage fluid range from −0.3 to −2.0 ‰ (av. −1.3 ‰), lower than that of E-stage. Therefore, L-stage $\delta^{13}C$ values imply an atmospheric CO_2 component, which may have entered the crust with meteoric water and probably mixed with hydrothermal fluids of the Tieluping ore-fluid system. This may have led to the $\delta^{13}C$ values to decrease from E-stage to L-stage. One $\delta^{13}C_{CO_2}$ value for the M-stage sample, overprinted by L-stage, is 0.1 ‰, which

is between those of E-and L-stages. This suggests the M-stage fluid is a mix of meteoric and metamorphic fluids, or marks the transition from the E-stage metamorphic fluid to the L-stage meteoric fluid. Chen et al. (2004a) concluded that the carbon isotope compositions suggest that the E-stage fluid originated from metamorphic devolatilisation of marine carbonates, the L-stage fluid mainly from meteoric water containing atmospheric CO_2, and the M-stage fluid, although based only on one value, would suggest a mix of metamorphic and meteoric fluids or the transition from early metamorphic to late meteoric fluids.

The $\delta^{34}S$ ratios of galena separates and ores range from −8.8 to −0.6 ‰ and average −4.3 ‰. As no sulphate minerals have been observed in the Tieluping deposit, a reduced system can be inferred for the deposition of sulphides. The histogram of the $\delta^{34}S$ values for Tieluping, the Xiong'er Group and the granitic rocks of the Huashan Complex, shown in Fig. 5.10, indicates that the sulphur in the ore-forming fluid could not have been sourced from the Huashan Complex. The data also preclude a mantle source, because such a source would have $\delta^{34}S$ between 0 and 2 ‰ (Hoefs 2004).

Lead isotope analyses of the ores from the Tieluping deposit show that the ores have higher ratios of $^{207}Pb/^{204}Pb$, $^{206}Pb/^{204}Pb$ and $^{208}Pb/^{204}Pb$ than the Huashan granite, Xiong'er Group and Taihua Group. The Taihua Group, the Xiong'er Group and the Huashan Complex, as well as the lower crust and mantle beneath the Xiong'er Terrane have previously been considered as the sources of ore-forming fluids and metals. However, the lower crust and mantle should possess even lower contents of U, Th and lower lead isotope ratios than the upper crust (Taylor and McLennan 1995). Chen et al. (2004a) ruled out the possibility of the lower crust and/or mantle as a source of the ore lead, pointing out that together with the evidence of carbon and sulphur isotopic systems, the radiogenic lead characteristic of the Tieluping deposit may have been derived from the above-mentioned CSC sequence.

Shanggong Au

The Shanggong Au deposit, discovered in 1982, is hosted in volcanic rocks of the ca. 1.8 Ga Xiong'er Group, with a reported resource of about 30 t of Au metal with ore grades averaging 6.9 g/t Au (Chen et al. 2008a). Since its discovery, more than 10 large (>20 t) and medium (10–20 t) Au deposits and one large Ag deposit (>1,000 t Ag) have been found in the region (Fig. 5.8).

The Shanggong deposit, contains 30 orebodies within a horsetail-like dilational jog (Fig. 5.11), all located in high strain zones and distributed in a northeast-trending array, about 2,200 m long and 600 m wide (Fig. 5.11). The ore zones have irregular and gradational borders, depending on cut-off grades, but are commonly more or less lenticular or tabular, both in plan and section views. Orebodies are usually within silicified zones that contain thin (mostly >1 mm) quartz veins. These veins have brecciated, mylonitic and banded structures and form stockworks, disseminated veinlets and locally massive veins. The Shanggong orebodies are laterally zoned, from the centre outward: a Au-bearing sulphide-quartz-ankerite-sericite zone (usually 1–3 m

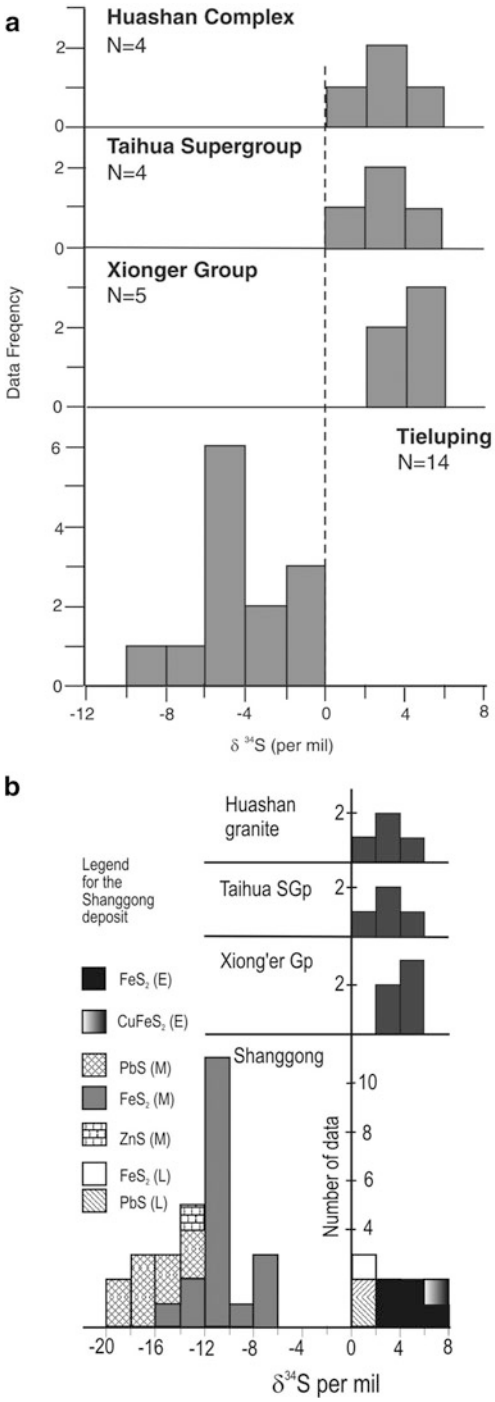

Fig. 5.10 $\delta^{34}S$ histogram for (**a**) Tieluping Ag deposit and associated rocks; (**b**) Shanggong Au deposit and associated lithologies, the Taihua Supergroup, Xiong'er Group and Huashan Complex have similar $\delta^{34}S$ values; the $\delta^{34}S$ values of E-and L-stages sulphides of the ores are similar to those of the wall rocks, the Xiong'er Group, whereas M-stage sulphides have negative $\delta^{34}S$ values suggesting a source characteristic of biogenic sulphur. (After Chen et al. 2004, 2008a)

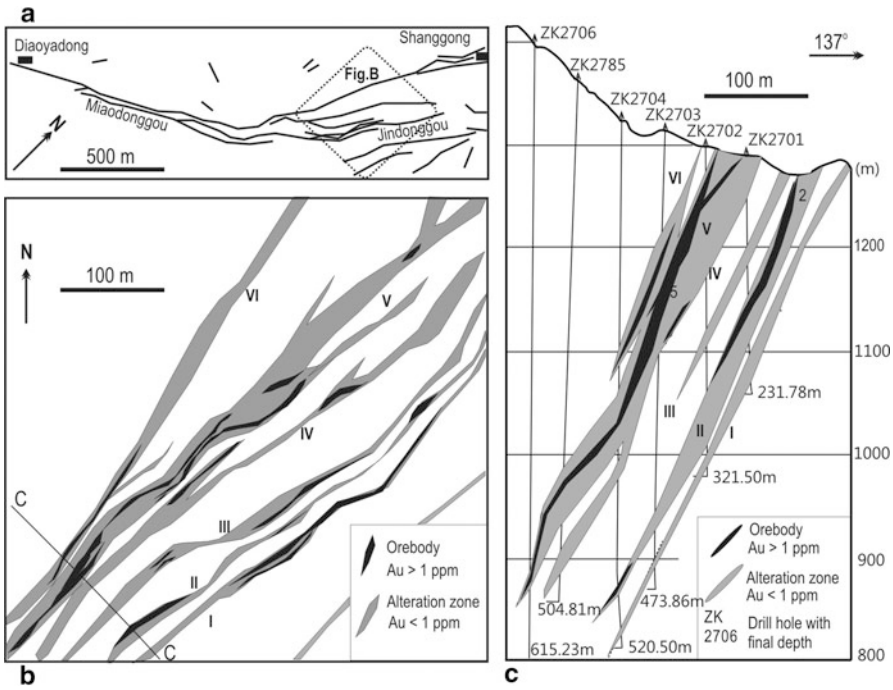

Fig. 5.11 Structurally-controlled Au orebodies and associated alteration zones. **a** The Shanggong Au deposit is located in a horsetail-like dilational jog of the Kangshan-Qiliping fault system. **b** At the 1,111 m level, the dilational fracture splays control the alteration and ore occurrence. **c** A profile along No. 27 exploration line, showing the vertical geometry of the orebodies and surrounding altered wall rocks. *Roman numerals* in **b** and **c** indicate the six main ore-hosting tectonite zones. (After Chen et al. 2006, 2008a)

wide; >3 g/t Au); a 1–20-m wide, pervasively altered, pyrite-carbonate-sericite-chlorite-epidote zone (0.5–3 g/t Au), grading outward to; a 50 m-wide of weakly altered pyrite-carbonate-sericite-chlorite-epidote zone (<1 g/t Au); and finally unaltered country rock of the Xiong'er Group (averaging 0.7 ppb Au). No vertical zoning is observed. Gangue minerals comprise quartz, ankerite and sericite, chlorite, epidote and fluorite, with lesser calcite, kaolinite, smectite, albite, apatite and tourmaline. Major ore minerals are pyrite and galena. Other ore minerals include magnetite, hematite, chalcopyrite, sphalerite, wolframite, scheelite, chalcocite, tetrahedrite, argentite, bornite, pyrrhotite, molybdenite, native Au, electrum, calaverite, hessite, petzite, altaite, melonite and siderite. In addition, limonite, jarosite, cerusite, anglesite, covellite, malachite, azurite and hydrocerussite are present in the weathering zone.

As is the case for the Tieluping lode deposit, field data, petrographic observations and textural relationships, show that the mineralisation and alteration can be divided into: an early (E), middle (M) and late (L) stages. The E-stage is further subdivided into an older substage characterized by sericite, albite, quartz, ankerite, chlorite,

epidote, pyrite and minor tourmaline, which form infills or replaces fine-grained (<2 mm) minerals, and a younger substage, of coarse-grained, milky quartz veins that contain ankerite, coarse-grained cubic pyrite, and locally, fluorite, scheelite, wolframite and molybdenite. The alteration assemblages and veins of E-stage are locally mylonitized with development of corona-like textures. The M-stage is characterized by stockworks of pyrite, galena, sphalerite, chalcopyrite, tetrahedrite and minor tellurides and native elements (Au, Ag, Cu and Te). M-stage gangue minerals include quartz, chlorite, sericite, epidote and ankerite, which also filled the brecciated E-stage coarse-grained milky quartz veins. The M-stage minerals are fine-grained, including fine-grained pentagonal dodecahedron pyrite and quartz and do not show any deformation. The L-stage is dominated by quartz-carbonate veinlets (1–30 mm), locally associated with chlorite, sericite and fluorite. These L-stage veinlets penetrate fracture zones in the country rocks, and quartz crystals typically grew from both walls towards the center, which is filled with calcite crystals. It is pertinent to note that E-stage anhedral quartz with undulose extinction, was replaced by L-stage euhedral unstrained quartz.

Stable isotope systematics and the geochemistry of ore fluids from the Shanggong Au deposits, published by Chen et al. (2006, 2008a), are summarized here. $\delta^{13}C$ values for ankerite range from −2.2 to 1.5 ‰, (average −0.8 ‰), whereas $\delta^{13}C_{CO_2}$ values for inclusion fluids released from M-stage quartz, range from −1.2 to 0.5 ‰ (average −0.2 ‰). The range of the high $\delta^{13}C$ values of the Shanggong ankerite are interpreted to reflect decarbonation of the marine carbonates of the underthrust Guandaokou and Luanchuan Groups (CSC sequence referred to above). Qi et al. (2005a) reported $\delta^{13}C_{Carbonate}$ values for these rocks, which range from −2.8 to 0.8 ‰ (average −0.9 ‰). According to calculations of fractionation factors for dolomite-CO_2 and calcite-CO_2 the $\delta^{13}C_{CO_2}$ values of metamorphic fluids equilibrated with the CSC sequence at 400 °C, would be in the range of −1 to 2.7 ‰, similar to the measured $\delta^{13}C$ of ankerite in the Shanggong ore system.

The E-stage sulphides have positive $\delta^{34}S$ values (average 4.3 ‰), which are similar to the rocks of the Xiong'er Group (average 4.1 ‰) (Fig. 5.10). Therefore, it is interpreted that the Xiong'er Group contributed much of the sulphur to the E-stage sulphides during fluid-rock interaction. This interpretation is also consistent with the observations that the E-stage sulphides are disseminated in the altered andesites and in lenticular quartz-veins. The $\delta^{34}S$ values of M-stage pyrite, galena and sphalerite range from −19.2 to −6.3 ‰ and are quite different from the $\delta^{34}S$ values of both the E- and L-stage sulphides (Fig. 5.10). This $\delta^{34}S$ variation shows that the S-isotope fractionations, among coexisting pyrite, galena and sphalerite, were not equilibrated, possibly due to rapid precipitation of the M-stage minerals. The M-stage mineral assemblage, which also contains native metallic elements, indicates that the M-stage sulphides were formed in a reducing environment, relative to the E- and L-stage fluids. In the Xiong'er terrane, only the CSC sequence contains organic material, which can be considered as a possible source of the biogenic sulphur of the Shanggong hydrothermal system. The average $\delta^{34}S$ value of sulphides of the L-stage is 1.1 ‰, suggests that this sulphur may have been sourced either from igneous rocks or from the immediate host rocks by meteoric water circulation.

Chen et al. (2006) found that the $\delta^{18}O$ values of ore fluids, extracted from fluid inclusions, systematically increase from unaltered volcanic rocks (6.7–8.0 ‰), through altered volcanic rocks (8.5–8.9 ‰) to ores (12.7 ‰). These values show that ^{18}O was added to the wall rocks during fluid-rock interaction. Calculated $^{18}O_W$ values for E-stage fluids average 8.1 ‰, which is in the range of metamorphic water. δD values for inclusion fluids of E-stage mineral separates range from −66 to −88 ‰, which plot in the magmatic box and below the metamorphic water box. Chen et al. (2006) concluded that the E-stage fluids show characteristics of magmatic and/or metamorphic fluids. Calculated values of $\delta^{18}O_w$ of L-stage fluids range from −2.4 to −1.1 ‰. These low values show that the L-stage fluids had a large meteoric water component. In addition, the δD_{H_2O} value of the L-stage fluid, extracted from fluid inclusions in fluorite, is −56 ‰, which together with the $\delta^{18}O_w$ value, would plot towards the meteoric water line. $\delta^{18}O_W$ values for M-stage fluids range from 1.9 to 4.5 ‰, are intermediate between those for E-stage (8.1 ‰) and L-stage (−2.4 to −1.1 ‰). These trends may be interpreted to indicate a mixing of deep-sourced metamorphic fluids with meteoric water.

5.3.3.2 Porphyries, Breccia Pipes and Skarns

The porphyry-skarn systems on the northern margin of the NCC, the South China Block and Qinling-Dabie orogenic belt are mostly of Yanshanian age, again demonstrating the vast impact that this tectono-thermal event has had in the formation of several types of ore systems. These porphyry systems share common features, such as hydrothermal alteration patterns and element associations, that also set them apart from the typical subduction-related and continental margin porphyry systems (Seedorff et al. 2005). For example, these deposits are characterised by H_2O-poor wall rock alteration, generally dominated by K-feldspar, epidote, carbonates and fluorite and rather weak H_2O-rich alteration minerals, such as sericite and chlorite. Fluid inclusion studies by Chen and Li (2009) have shown that K/Na, CO_2/H_2O and F/Cl ratios are especially high in these intracontinental porphyry systems. Fluorine has been recognised as being preferentially linked to intracontinental settings and having an important role in transport and concentration of lithophile elements (see Agangi et al. 2010).

Many of these porphyry systems have been dated using the Re-Os system (Mao et al. 2008a; Dai et al. 2009). Re-Os age data show that most ages group between 150 and 100 Ma. In the East and North Qinling, a porphyry Mo belt, south of the Luachun Fault, extends for more than 500 km, in a westerly trending metallogenic province. In the East Qinling orogen two peaks of mineralisation are noted at about 230–220 Ma and 145 Ma with a cluster of ages at 148–135 and 131–112 Ma (Mao et al. 2008a). The 230–220 Ma peak corresponds to the Indosinian tectono-thermal event that was also responsible for the development of porphyry-style mineral systems. One of these is the Wenquan Mo deposit in the West Qinling, for which a Re-Os age on molybdenite yielded 214.4 ± 7.1 Ma (Zhu et al. 2011b). The Wenquan porphyry Mo

deposit is considered to be related to the Triassic collision between the South Qinling and the Yangtze Craton, along the Mian-Lue suture (Fig. 5.7; Zhu et al. 2011b).

The Haoping pluton of the Huashan granitic complex has zircon SHRIMP ages of 130.7 ± 1.4 and 132.0 ± 1.6 Ma (Li et al. 2004). Other granites on the southern margin of the NCC were dated using the SHRIMP U-Pb zircon method (Mao et al. 2005). The results indicate that the Wenyu and Niangniangshan granitic plutons in the Xiaoqinling region were emplaced at 138.4 ± 2.5 and 141.7 ± 2.5 Ma, respectively, whereas granitic porphyries in the Xiong'ershan region yielded 136.2 ± 1.5 Ma for Leimengou, 158.2 ± 3.1 Ma for Nannihu and 157.6 ± 2.7 Ma for Shangfanggou (Mao et al. 2005). According to Han et al. (2007) the emplacement of these granites in three stages is a reflection of the geodynamic evolution of the Qinling orogen. More specifically, these stages would represent a tectonic transition from post-collisional to intraplate anorogenic geodynamics in the southern margin of the NCC.

The distribution of the East Qinling porphyry systems is shown in Fig. 5.12, where they have a total resource of Mo metal of about 2.7 Mt (Mao et al. 2008a). The following is abridged from Mao et al. (2008a). The Sandaozhuang, Shangfanggou, and Nannihu deposits contain 672,510 tonnes with an average grade of 0.110 % Mo, 715,800 tonnes at 0.134 % Mo, and 1,337,000 tonnes at 0.09 % Mo, respectively. In addition, the Sandaozhuang deposit also contains 502,465 tonnes of W metal, grading from 0.09 to 0.13 %. The rocks exposed in the Nannihu ore district belong to the Neoproterozoic Luanchuan Group comprising dolomitic marble of Meiyaogou Formation, marble and schist of Nannihu Formation, metasandstone and biotite-bearing marble of Sanchuan Formation, quartzite, schist intercalated with dolomitic marble, and quartzite of the Mesoproterozoic Guandaokou Group. All the granitic rocks that host the Mo(W) mineralisation in the Nannihu ore district are shallow-level, small stocks, consisting of granodiorite, monzogranite and granite porphyry. Both the Nannihu and Sandaozhuang Mo(W) deposits occur within and along the northwestern edge of the Nannihu granite porphyry. The Nannihu granite porphyry has a surface area of about 1.2 km^2 and contains low-grade Mo(W) mineralisation, accompanied by stockworks of K-feldspar or quartz-K-feldspar, and quartz. Common calc-silicate skarn minerals include garnet, salite, vesuvianite and wollastonite. Retrograde alteration minerals comprise amphibole, chlorite and epidote. Ore minerals are magnetite, scheelite, molybdenite, pyrite and minor chalcopyrite, galena, and sphalerite. The late stage quartz-molybdenite, and quartz-scheelite stockworks overprint the massive skarn.

Shangfanggou porphyry-skarn

The Shangfanggou porphyry–skarn deposit is located in and around the Shangfang granite, which intruded Neopreterozoic dolomitic marble. Due to the nature of the country rock, the skarn in the mine sequence is magnesian with the main minerals comprising garnet, diopside, forsterite, and humite, and associated retrograde alteration assemblages of phlogopite, tremolite, actinolite, serpentine, talc and

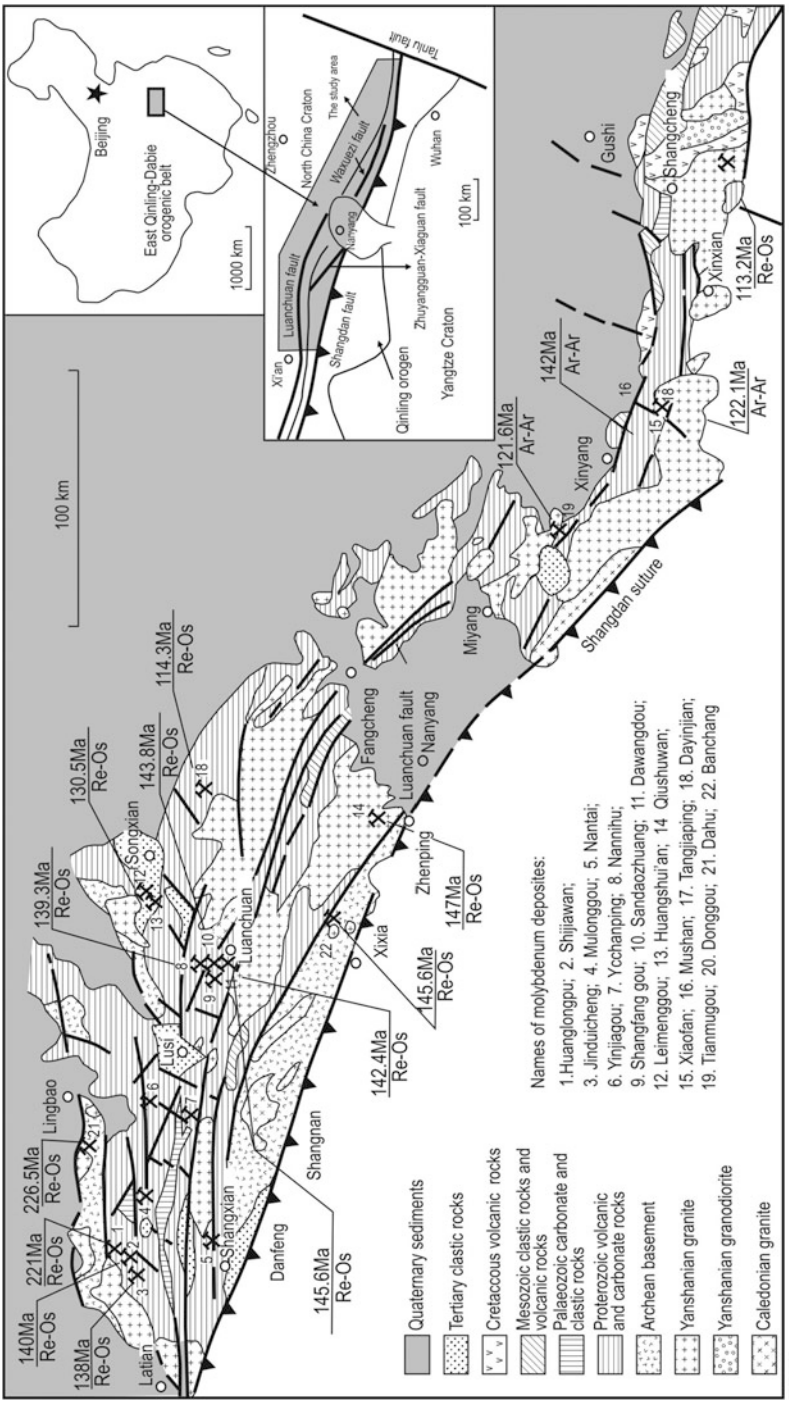

Fig. 5.12 Sketch map of the geology of the East Qinling—Dabie orogenic belt and distribution of porphyry Mo deposits. (After Mao et al. 2008a, based on Luo et al. 1991)

magnetite. The retrograde alteration shows clear zoning which, from the contact outwards, consist of phlogopite-actinolite, tremolite-actinolite tremolite-serpentine, with stockworks of potash feldspar and/or quartz overprinting the granite porphyry. The Mo orebodies are hosted in the magnesian skarn and altered granite.

Dawanggou porphyry-skarn, Leimengou, Shijiawan and Qiushuwan porphyry Mo and Cu-Mo

The recently discovered Dawanggou porphyry-skarn Mo deposit, is located at the contact of the Shibaogou granite pluton with Neoproterozoic clastic rocks and carbonate rocks interbedded with minor trachyte. The deposit is about 4 km southeast of the Nannihu district. The Dawangzhuang Mo deposit is a typical porphyry-skarn system, with disseminated and quartz vein/stockwork-hosted molybdenite quartz, chalcopyrite and pyrite hosted in the granite and associated garnet-pyroxene skarn in the host marble rocks. The mineralisation is generally associated with retrograde alteration in the skarn consisting of amphibole and chlorite.

The Leimengou porphyry Mo deposit is situated about 2 km west of Qiyugou (Fig. 5.12). This deposit, since its discovery in 1979, was reported as a porphyry style deposit with reserves of 340,110 tonnes Mo metal at a cut-off grade of 0.075 % Mo. The Leimengou porphyry deposit is associated with a number of breccia pipes and this porphyry-breccia pipes system is discussed in some detail in Section "Lemeingou-Qiyugou Mo-Au Porphyry-breccia Pipe System".

The Shijiawan porphyry Mo deposit is located between the Jinduicheng and the Huanglongpu Mo mines. Although it is a large-scale Mo deposit with a reserve of 100,000 tonnes Mo metal, little data are available for this deposit. The open pit mine was closed in the 1990s, but underground mining was started in 2007. The disseminated and stockwork molybdenite, pyrite, fluorite, K-feldspar and strong silicification in the apical zone of the Shijiawan granite porphyry and host rocks of the Mesoproterozoic basaltic rocks of the Xiong'er Group can still be observed.

The Qiushuwan porphyry–skarn Cu-Mo deposit in the North Qinling orogenic belt has a proven reserve of 500,000 tonnes Cu, averaging 0.8 % and 100,000 tonnes Mo, averaging 0.12 %. Like the Mo deposits along the southern margin of the NCC, the Qiushuwan Cu-Mo deposit area is cut by several northeast-trending faults. A group of Mesozoic biotite granodiorite stocks were emplaced along the intersection of these northeast-trending faults and west-northwest-trending thrust faults. The biotite granodiorite stock hosting the mineralisation has an ellipsoidal shape and intruded Early Proterozoic biotite gneissic rocks, biotite quartz schist, and marble. The Cu-Mo mineralisation occurs in two styles: (1) a Mo-dominant skarn type along the southern contact of the Qiushuwan granodiorite stock, and (2) a Cu-dominant style within a breccia about 1,000 m to the northeast. Alteration within the granodiorite stock is characterized by quartz, K-feldspar-quartz, and sericite-quartz, with skarn and phyllic alteration developed in the country-rocks. Ore minerals are chalcopyrite, molybdenite, pyrite, sphalerite, galena, with gangue minerals comprising quartz, potash-feldspar, sericite, calcite, epidote, garnet, and diopside.

Banchang

The Banchang polymetallic deposit is situated 50 km northwest to the Qiushuwan Cu-Mo deposit in the North Qinling orogenic belt. It is a polymetallic (Cu-Ag-Pb-Zn-Mo) porphyry-skarn-vein type deposit with 150,000 tonnes Cu averaging 0.66 %, Ag reserves of 2,000 tonnes grading 200 g/t, 300,000 tonnes Pb and Zn with a combined grade of 0.61 %. Although there is abundant Mo as molybdenite in the ores, the contained reserves for this deposit have not been calculated. This porphyry-related polymetallic mineralisation is developed in a west-northwest-trending granite porphyry dykes, with the ore characterized by breccias and silicified marble, and hosted by Proterozoic marble intercalated with plagioclase amphibolite. There are three types of ores: porphyry, skarn and veins. Both porphyry and skarn ores occur in the endo-contact of the granite porphyry dykes. The porphyry ore comprises molybdenite, quartz, pyrite, K-feldspar, fluorite, chalcopyrite, whereas both endo- and exoskarn ores contain grossularite–andradite, diopside-hedenbergite, vesuvianite, amphibole, retrograde alteration assemblages of actinolite, epidote, chlorite, fluorite, and ore minerals of chalcopyrite, pyrite, molybdenite, magnetite, galena and sphalerite. In the skarn ores, the mineralisation is closely associated with retrograde alteration consisting of chlorite, amphibole, epidote, and quartz. To the south, the west-northwest-trending and steeply dipping ore vein-type consist of pyrite, chalcopyrite, chalcocite, native silver, argentite, galena, sphalerite, molybdenite, and gangue minerals comprising quartz, K-feldspar, chlorite, sericite, and calcite.

Donggou porphyry Mo

The Donggou Mo deposit at the eastern end of the East Qinling Mo district has a proven reserve of 625,000 tonnes of Mo metal, averaging 0.11 %. The fine-grained Donggou granite porphyry is composed of phenocrysts of perthite and quartz, in a groundmass of perthite, quartz, plagioclase, biotite, and accessory minerals of magnetite, sphene, zircon and rutile. The Donggou porphyry was dated at 112 ± 1 Ma, which coincides with the age of the Taishanmiao alkaline granite intrusion to the south of the deposit. The Donggou porphyry deposit is surrounded by Pb-Zn-bearing hydrothermal veins, which may represent distal ore facies of the porphyry system. The host rocks for the Donggou granite porphyry and related mineralisation are Mesoproterozoic rhyolite, andesite intercalated with basalt, and tuffaceous siltstone of the Xiong'er Group. Mineralisation developed both within the Donggou granite porphyry and its contacts with the Xiong'er volcanic rocks. The orebodies have a tabular shape centered on the granite porphyry, and consist of stockworks and disseminations of molybdenite, and minor pyrite, chalcopyrite, sphalerite, and scheelite. The gangue minerals are quartz, K-feldspar, plagioclase, amphibole, diopside, biotite, chlorite, epidote, sericite, and fluorite. Major alteration minerals include quartz, K-feldspar, and biotite, accompanied by varying amounts of sericite, chlorite, fluorite, and carbonate. Four mineralisation stages in the Donggou deposit are recognised: (1) an early (barren) quartz-K-feldspar; (2) a quartz-K-feldspar-molybdenite; (3) quartz-molybdenite sulphide, and (4) post-ore carbonate.

Tangjianping porphyry Mo

The Tangjiaping porphyry Mo deposit is located in the easternmost part of the Qinling orogenic belt and is hosted by the Proterozoic Tongbai–Dabie metamorphic core complex. The deposit has a proven reserve of 130,000 tonnes Mo metal at 0.09 %. Although there are several Mo deposits in the Dabieshan area, Tangjiaping is the largest known deposit. A granite porphyry hosts most of the mineralisation and intruded into Proterozoic biotite plagioclase gneiss and amphibole plagioclase gneiss. The granite porphyry consists of potash-feldspar, plagioclase, quartz and accessory minerals of magnetite, rutile, zircon and pyrite. Mineralisation within the porphyry forms a tabular 1.0 km-long orebody, with a thickness of 200 m. The mineralisation is characterised by dense stockwork of quartz-sericite-molybdenite-pyrite and quartz-potash feldspar-molybdenite hosted by the granite porphyry.

Dajiashan and Tianmugou

The recently discovered Dajiashan and Tianmugou Mo occurrences are located 80 km and 200 km northwest of the Tiangjiaping Mo deposits. The Dayinjian Mo occurrence is a porphyry-skarn with predominantly disseminated and stockwork-style mineralisation hosted by the Dayinjian granite porphyry and minor skarn ore at the contact with the host marble, which belongs to the Proterozoic Tongbai-Dabieshan metamorphic complex. The ore minerals comprise molybdenite, scheelite, pyrite, chalcopyrite, with quartz, fluorite, and sericite as gangue and garnet, salite (Ca-Fe pyroxene), vesuvianite, amphibole, chlorite, and quartz, as skarn minerals. The average Mo grade is about 0.1 %. The Tianmushan Mo ore occurrence is near the roof zone of the Tianmushan–Lanmashan alkaline granite intrusion. The mineralisation consists of quartz-molydenite veins, within subparallel west-northwest-trending fractures, steeply dipping to either north-northeast or south-southwest. It is interesting to note that molybdenite flakes in this occurrence are unusually large, up to 0.5–1.5 cm, forming flower-like or radiating aggregates. The average grade of the ores is about 0.6 % Mo.

Dahu Au-Mo

The Dahu Au-Mo deposit is located on the northern margin of the Xiaoqinling area, and hosted by migmatitic granite and minor migmatitic gneiss and biotite-plagioclase gneiss of the Lujiayu Formation of the Archaean Taihua Group. The deposit, with a reserve of 100,000 tonnes, grading 0.24 % Mo, is associated with east-west-, northwest- and northeast-striking fractures, that are filled by dolerite and granite porphyry dykes. These fractures show multiple phases of ductile deformation, and have been overprinted by a series of extensional detachment faults that are filled with mylonite and cataclasite. Although fine-grained quartz-molybdenite stockwork had been known for long time, the Dahu deposit is considered as a quartz vein type Au ore system that was not recognized as a Mo deposit until 2003, because of the

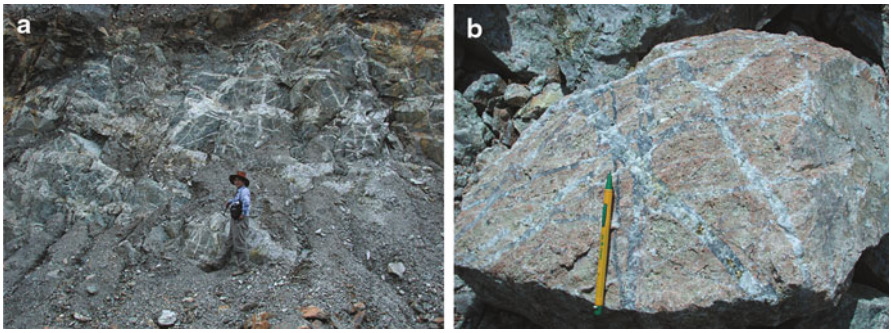

Fig. 5.13 **a** ca. 138 Ma Jinduicheng porphyry Mo in the Qinling orogen, Shanxi Province (central China), stockwork veining in hornfelsed country rocks; **b** Jinduicheng porphyry Mo, fine stockworks in host granite cutting through earlier potassic alteration (*pink-brown* patches)

low price of molybdenum metal at the time. Field observations show that the Au ore veins overprint the fine-grained stockwork quartz-molybdenite. The ores consist of quartz, pyrite, molybdenite and minor sericite, magnetite, chalcopyrite, sphalerite, galena, bornite, hematite and bismuthinite.

In a recent publication, Li et al. (2011) reported Re-Os ages of molybdenite and SHRIMP U-Th-Pb dating of hydrothermal monazite from this deposit. This latest age data indicated that the molybdenite mineralisation is older than the Au metallogeny, contradicting the above stating the opposite. This is based on the fact that the new geochronology shows two generations of monazite. One is associated with the molybdenite and is of Indosinian age (ca. 216 Ma), whereas a younger monazite, revealed by a mixing array of the Pb-Th-U data, is inferred to have an age of ca. 125 Ma. Li et al. (2011), concluded that the Mo mineralisation was first formed in Indosinian time and later overprinted by Yanshanian magmatism.

Jinduicheng Porphyry Mo

The Jinduicheng porphyry Mo deposit was first reported by Nie (1994) and Stein et al. (1997) and more recently by Zhu et al. (2010). The Jinduicheng deposit has resources of 907 Mt grading 0.1 % Mo. Stein et al. (1997) using the Re-Os isotopic system, determined the age of the mineralisation at ca. 138 Ma. The mineralisation is associated with a stock of porphyritic granite that protrudes from the Laoneushan biotite monzogranite batholith, intruded into the Archaean Taihua Group and the Palaeoproterozoic Xiong'er Group. The Jinduicheng porphyritic granite is 1.8 km long and about 400 m wide and consists of orthoclase, perthite, plagioclase, quartz and biotite with accessory ilmenite, pyrite, magnetite, apatite and fluorite.

The Mo mineralisation is contained in vein stockworks both within the porphyrytic granite stock and the country rocks (Fig. 5.13) and consist of quartz + K-feldspar ± pyrite ± fluorite. The veins also contain minor quantities of magnetite, chalcopyrite, sphalerite, galena, cassiterite, bismuthinite, sericite, biotite, beryl, topaz, calcite and apatite. Hydrothermal alteration is well zoned with silicification

and K-feldspar in a core zone, followed by phyllic and propylitic alteration with increasing distance from the intrusion. Phyllic and propylitic assemblages in the basaltic country rocks consist of epidote-albite-chlorite-calcite and montmorillonite-kaolinite-pyrophyllite, respectively. The Jinduicheng porphyry Mo deposit shares some similarities with the Climax Mo deposit in Colorado (Stein et al. 1997). Stein et al. (1997) suggested, on the basis of fluid inclusion and sulphur isotopic data ($\delta^{34}S$ ranging from 3.7 to 5.5 ‰), a magmatic origin for both the S and Mo at Jinduicheng, whereas the Sr isotopipc signature for the granite porphyry (initial $^{87}Sr/^{86}Sr = 0.7087 - 0.7095$) is indicative of a crustal source for the granite. This is supported by Pb isotope systematics ($^{206}Pb/^{204}Pb = 17.410$; $^{207}Pb/^{204}Pb = 15.428$; $^{208}Pb/^{204}Pb = 37.702$), which Stein et al. (1997) explained as due to melting of lower crust. Stable isotope studies of the Jinduicheng altered rocks by Nie (1994), show that the $\delta^{18}O$ ‰ values for quartz in the potassic alteration zone ranges from +5.0 to +9 ‰, which is similar to that of magmatic water. The $\delta^{18}O$ ‰ and $\delta^{34}S$ values of potassic-altered rocks suggest that the ore fluids were mainly of magmatic origin during the early stages. The $\delta^{18}O$ ‰ values from the zones of hydrolytic alteration have a range of +10.5 to +3.4 ‰ (mean +11.6 ‰); the $\delta^{34}S$ values for pyrite in the same zone range from −5.5 to −2.4 ‰ (mean −3.6 ‰). The isotopic composition of the hydrolytic zone indicates that meteoric waters predominated over the magmatic fluids (Nie 1994). The Jinduicheng granite porphyry is enriched in F, Rb, K and HREE and depleted in LREE, Ba and Sr. The chondrite-normalised REE patterns show a distinct negative Eu anomaly.

As noted above, the Juiduicheng and other companion systems in the Qinling molybdenum belt have similarities with the porphyry systems of the Colorado belt (Climax type). Stable isotope systematics (O, D and S) indicate oxidising magmas and transfer of magmatic sulphur. Stein et al. (1997) pointed out that the REE patterns of the East Qinling granitic intrusions bear striking similarities to the contrasting REE patterns of the quartz-monzonites and Climax-type granites in Colorado. In the Colorado mineral belt, the Neogene monzonites have distinct REE patterns from the Climax-type granites, which have marked negative Eu anomalies as do the Jinduicheng granitic rocks, whereas the granitic rocks of the Laoneushan batholith show REE patterns similar to the Colorado monzonites. These differences are attributed to a change from subduction-related magmas to extension-related crustal melting. The highly evolved Climax-type granites in Colorado and the Qinling granites are comparable, suggesting similar tectonic regimes. I return to this topic when discussing the Leimengou-Qiyugou ore system in the next section.

Lemeingou-Qiyugou Mo-Au Porphyry-breccia Pipe System

In the Xiong'ershan region, a porphyry Mo deposit and cluster of breccia pipes are present in the Qiyugou and Leimengou area near the eastern margin of the Mesozoic Huashani granite pluton (Han et al. 2007). The Leimengou-Qiyugou area is located 100 km south of the historic city of Luoyang. The Leimengou porphyry Mo deposit is a porphyry style deposit with reserves of 0.34 Mt tonnes of Mo metal at a cut-off grade of 0.075 % Mo, and with sulphur as byproduct at an average grade of 2.07 %

(No. 1 Geological Team of Henan 1983, unpublished data). There are no published detailed studies on this deposit, except for Luo et al. (2000), Mao et al. (2010, 2011) and a PhD study by Zhang (2006b) that focused on the Leimengou-Qiyugou district. The ore bodies are lensoid in shape and subhorizontal and are developed along the contact zone between the porphyry granite and the gneissic rocks of Taihua Group. The mineralised stocks are characterized by porphyritic fine-grained biotite granite and hornblende monzonite. The chemistry of the porphyry granite indicates that it is an A-type alkaline granite. Some breccia pipes are developed along the margins or around the granite stock. Quartz fluid inclusions from the breccia cement show second boiling temperature and salinity in the range from about 500–600 °C, and 5–35 wt % NaCl eq., respectively (Luo et al. 2000).

The quartz sericitic stage is associated with the mineralisation. The ore bodies are lensoid in shape and subhorrizonal and are developed along the contact zone between the porphyry granite and the gneissic rocks of Taihua Group. The mineralised stocks are porphyritic fine-grained biotite granite and hornblende monzonite. The porphyritic granite has a SHRIMP U-Pb age of 137 ± 2 Ma (Li 2005). The Leimengou porphyry Mo deposit, neighbouring the Qiyugou breccia pipe Au deposit, yielded two molybdenite Re-Os model ages of 131.6 ± 2.0 Ma and 133.1 ± 1.9 Ma (Mao et al. 2008a).

Based on field visits, the deposit has typical stockworks developed in granitic rocks with abundant molybdenite and pervasive hydrothermal alteration. The K-feldspar, quartz-sericitic and minor chlorite + argillic alteration zones are recognized from the center of the intrusion stock towards the margins. The quartz sericitic stage is related to mineralisation. Vein, stockwork and minor replacement ores occur above the intrusion. Ore minerals are pyrite, molybdenite, and minor chalcopyrite, sphalerite, and galena. Quartz-sericite-pyrite and potassic alteration can be recognised in outcrops and material in the dumps outside portals. Three stages of mineralisation and temperature are recognized (Luo et al. 2000): (1) K-feldspar-quartz, 380–420 °C for quartz; (2) Sulphide-quartz, 350–410 °C for quartz and pyrite; (3) Fluorite-sulphide and potassic-quartz, 290–385 °C for K-feldspar and fluorite. The isotopic composition of sulphur ranges from −2.8 to +3.72 ‰, average about +2.08 ‰.

Qiyugou Auriferous Breccia Pipes

In the Xiong'ershan region, a cluster of at least 35 breccia pipes occurs in the Qiyugou area, east of the Leimengou porphyry Mo deposit (Figs. 5.12 and 5.14). The mineral deposits are controlled by northeast-trending normal faults, near the eastern margin of the Mesozoic Huashani granite pluton. On the basis of isotopic dating (Mao et al. 2002a) suggested that the formation of the Qiyugou Au-bearing breccia pipes is not directly related to the porphyry systems that are present in the area. In the Xiong'ershan region, Mesozoic (Jurassic-Cretaceous) igneous rocks are mainly granites, including several plutons, such as the Huashani monzogranite, the Wuzhangshan pluton, referred to in Sect. 5.3.1, quartz-feldspar porphyry intrusions, dacite sills and dykes, diatremes and the Qiyugou breccia pipes. The Mesozoic intrusions have isotopic ages ranging from ca. 183 to 100 Ma. More specifically, these intrusions are

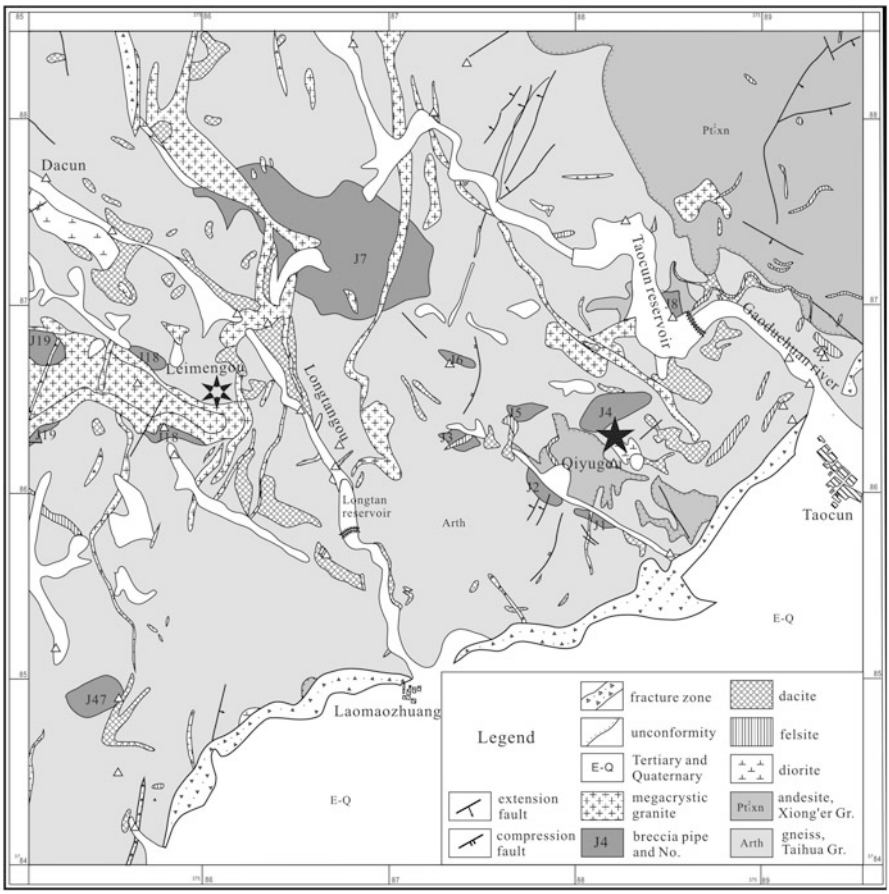

Fig. 5.14 Simplified geological map of the Qiyugou-Leimengou area and position of selected breccia pipes. (After Zhang et al. 2005; Zhang 2006b)

post-orogenic and associated with orogenic collapse and extensional tectonics (Chen et al. 2004a).

In the Qiyugou area at least seven breccia pipes are auriferous, with No. 2 and No. 4 as the main producers, with total reserves of about 40 t (Mao et al. 2002b). Ore grades range from 3 to 5 g/t and can reach values of up to 7 g/t (Mine staff, pers. comm. 2004). Higher gold grades are present in zones of complex alteration and of greater clast population. Gold has been mined in the region since ancient times, reaching a peak during the Han dynasty about 2,200 years ago (Gernet 1999). These breccia pipes and contained Au deposits are hosted in the Taihua Group. The pipes have a spindle or elliptical shape in plan with long axes ranging from less than 40 m to over a kilometre and have been traced vertically for more than 300 m. The breccia clasts consist of Archaean basement rocks (migmatite, gneiss and amphibolite), Palaeoproterozoic Xiong'er volcanic rocks and Mesozoic granitic rocks. The clasts range in size from a few centimetres to metres and have angular shapes with jigsaw-

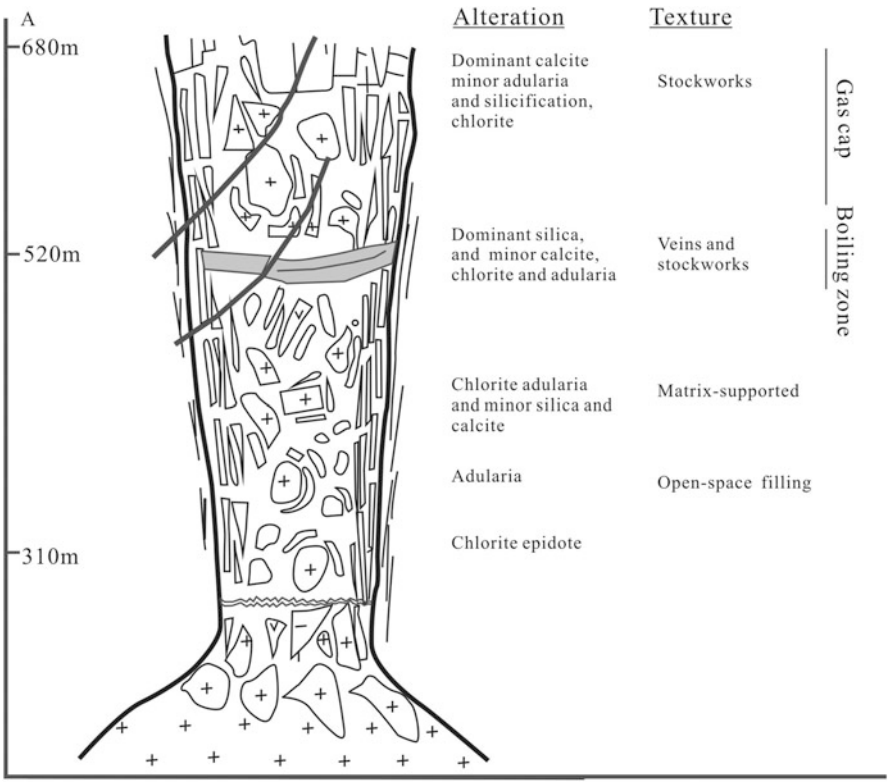

Fig. 5.15 Breccia pipe model. (After Zhang et al. 2007b, modified from Kirwin 1985)

fit type breccia to round shapes, suggesting multiple phases of volatile activity from hydraulic fracturing (jigsaw fit) to features typical of fluidisation processes (Zhang et al. 2007b). The contact between breccia pipes and wallrock is abrupt. Proximal wallrocks of the breccia pipes are cracked, forming shatter rims several to tens of metres wide. Alteration and mineralisation can be divided into three stages: (1) K-feldspar-quartz-epidote-pyrite, with pyrite forming coarse-grained cubes; (2) native gold-bearing polymetallic sulphides-quartz, with fine-grained pyritohedron pyrite; and (3) quartz-calcite ± pyrite stockwork, with adularia as alteration mineral phase (Zhang et al. 2006). The mineralisation styles include vein, disseminations and stockworks and the ore zones form subparallel sheets that are nearly perpendicular to the walls of the pipes (Fig. 5.15). Most of the Au ore is associated with subhorizontal pyrite and quartz veins that contain adularia and pyrite. The principal ore minerals are pyrite, chalcopyrite, galena and native gold. Sphalerite, electrum, molybdenite, chalcocite and magnetite are present in lesser amounts. Shao and Li (1989) reported the presence of Bi sulphosalts and sulphides. These minerals infill open spaces between the breccia clasts. Gold is mainly found in fine-grained pyrite, as inclusions or as fissure filling. In the breccia pipe, alteration and gold mineralisation of the matrix are more prominent than in the breccia clasts. Potas

sic alteration (K-feldspar, adularia, biotite and sericite), silicification, and abundant sulphides (especially pyrite) are generally indicative of good gold grades (Chen and Fu 1992). Chen et al. (2009a) recognised two main styles of alteration. The first is potassic and pre-gold mineralisation, mainly affects gneisses and volcanic rocks and consists of K-feldspar and quartz. The second is exclusively confined to the pipes and comprises two substages: (1) pervasive; (2) vein and open space filling. The pervasive stage consists of chlorite, actinolite, green biotite, epidote, quartz, adularia, calcite and sericite. Field and textural evidence suggests that the paragenetic sequence of this alteration is from green biotite + actinolite to epidote + chlorite + pyrite. The second substage is represented by quartz, adularia with calcite and minor sericite. This alteration affects not only the breccia clasts, but also the matrix. Calcite is a late phase, and cuts quartz veins, clasts, and the cementing material. Adularia and calcite infill open spaces and/or fissures in pyrite, or form veins that cut altered clasts. Textural relationships indicate that gold mineralisation is paragenetically associated with adularia-calcite and pyrite.

Fluid inclusion studies revealed three types of inclusions in quartz and calcite associated with the ore (Chen et al. 2009a): (1) water-rich inclusions (W-type), which include two-phase aqueous inclusions, consisting of vapor and liquid water at room temperature, and can be divided into two subtypes, i.e. V- and L-subtypes, according to their vapor to liquid ratio; (2) daughter mineral-bearing inclusions (S-type) are round and with negative shape, and isolated, with size varying between 7 and 25 μm. Daughter minerals are dominantly cube-shaped halite; (3) CO_2-rich fluid inclusions (C-type), most of which are two- or three-phase at room temperature (L_{CO_2}-L_{H_2O} or V_{CO_2}-L_{CO_2}-L_{H_2O}) and show round or oval shape. The carbonic phase occupies 10–85 vol% of the inclusion.

Homogenisation temperatures of fluid inclusions, range from 460 to 351 °C, 349 to 265 °C, and 244 to 157 °C, defining three stages, early, middle and late, with the above temperatures decreasing from early to late stages. The early- and middle-stages quartz contain fluid inclusions of W-, S- and C-types; whereas the late-stage quartz only contains W-type fluid inclusions, including V- and L-subtypes, although the L-subtype dominates over the V-subtype. Salinities were estimated in the ranges of 10.5–19.8 wt % NaCl equiv, 4.2–10.7 wt % NaCl equiv. and 3.7–6.0 wt % NaCl equiv., for the early, middle and late stages respectively, suggesting a gradual dilution from early to late. Salinities of CO_2-rich fluid inclusions estimated according to CO_2 clathrate melting points range from 9.3 to 12.3 wt % NaCl equiv. for the early stage, and from 4.8 to 8.7 wt % NaCl equiv. for the middle stage, showing similar change to those shown by the S- and W-types fluid inclusions. The salinities of ore-fluids consistently also decrease from early to late stages.

Trapping pressure of CO_2-rich fluid inclusions of the early and middle stages was estimated to be 22–45 MPa, according to partial and total homogeneous temperatures and the phase-transformation diagram for H_2O-CO_2 system (Schwartz 1989). This estimate is similar to the pressure measured for porphyry systems (Seedorff et al. 2005; Williams-Jones and Heinrich 2005), and suggests that the mineralisation depth ranges from 2.2 to 4.5 km, under hydrostatic pressure.

Chen et al. (2009a) concluded that the initial ore-fluids are CO_2-rich, high-temperature, high-salinity and high-fO_2 and likely magmatic in origin. Fluid-boiling,

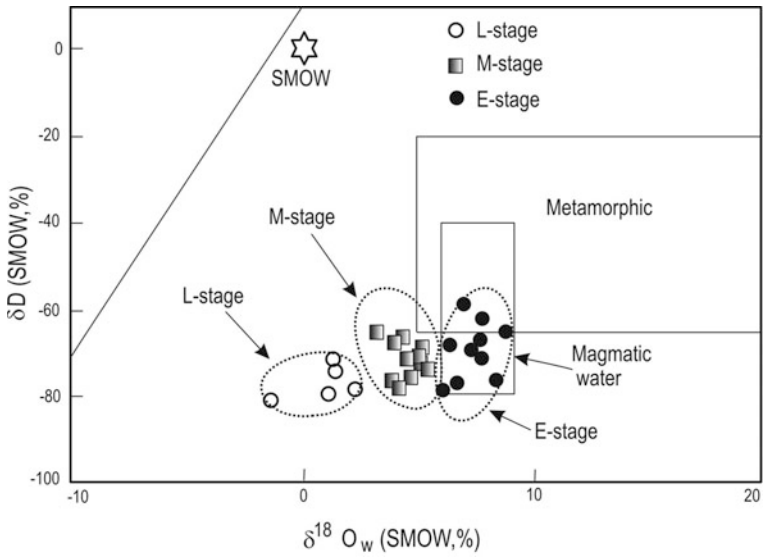

Fig. 5.16 δD *vs.* $\delta^{18}O$ diagram of ore-fluids from the Qiyugou gold deposit (after Guo et al. 2007; Chen et al. 2009a). Details in text

possibly due to CO_2 escape, resulted in decrease in temperature, salinity and fO_2, and rapid precipitation of ore-forming materials. Boiling-related hydrofractures were open and connected to the surface, leading to inflow of voluminous meteoric-water into and its mixing with the intrusion-related hypothermal fluid-system. The ore-fluid system became low-temperature, low-salinity and CO_2-poor. These conclusions are further supported by studies in stable and radiogenic isotopic compositions for ore materials, host rocks and associated granites. These are discussed below.

At Qiyugou, the $\delta^{18}O$ of early ore stages range between 6.0 and 8.9 ‰, with an average of 7.4 ‰; and the δD values vary between −58 and −78 ‰ and average −69 ‰. These values all plot in the magmatic water box (Fig. 5.16). The $\delta^{18}O_W$ of the middle stages range from 3.2 to 6.3 ‰ with an average of 4.7 ‰; δD values range from −65 to −78 ‰ with an average of −72 ‰, which are lower than those of the early stage, supporting the idea of input of and/or interaction with meteoric water (Fig. 5.16). The calculated $\delta^{18}O_W$ in equilibrium with late-stage quartz range between −2.7 and 2.9 ‰ with an average of 0.6 ‰; the calculated $\delta^{18}O_W$ in equilibrium with calcite vary between −5.1 and −1.4 ‰ with an average of −2.9 ‰. These values are typical of meteoric water. Data points from early to late stages shift from the magmatic water box towards the meteoric water line (Fig. 5.16).

Calcite samples of the late stage phase have $\delta^{13}C_{PDB}$ of −4.2 to −5.8 ‰ and average −5.0 ‰. Three calcite samples of late ore stage disseminated ores show $\delta^{13}C_{PDB}$ of −1.6 to −4.2 ‰, and average −2.4 ‰. Chen et al. (2009a) pointed out that these $\delta^{13}C$ values are significantly higher than carbon reservoirs, such as organic matter (−2.7 ‰), atmospheric CO_2 (−8 ‰), dissolved CO_2 in fresh water (−9 to −20 ‰; Hoefs 2004), continental crust (−7 ‰; Faure 1986), but are similar to or

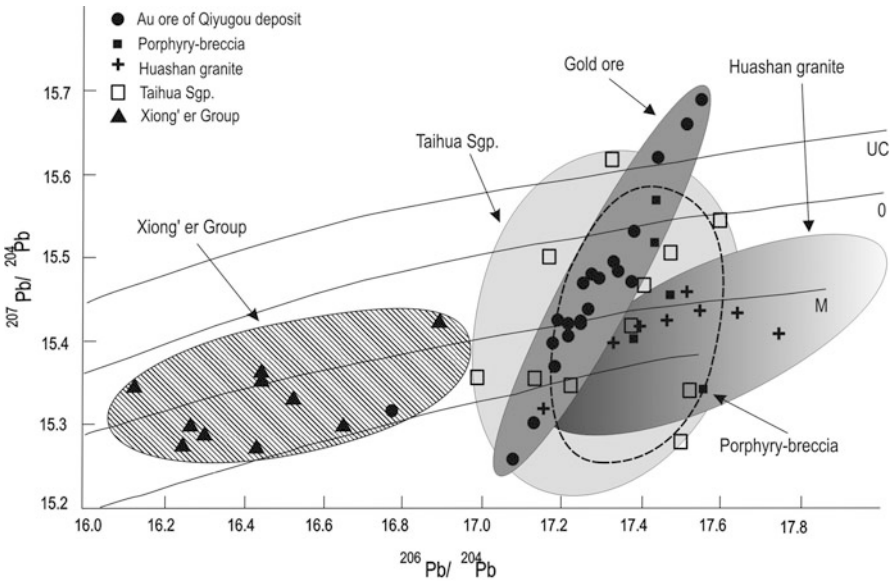

Fig. 5.17 Lead isotope diagram ($^{206}Pb/^{204}Pb$ *vs.* $^{207}Pb/^{204}Pb$) for the Qiyugou Au ores and associated lithologies. (After Chen et al. 2009a, b based on Zartman and Doe 1981)

slightly higher than those of mantle (−5 to −7 ‰) or igneous rocks (−3 to −30 ‰) (Hoefs 2004). This would indicate that CO_2 of ore fluids were probably sourced from a magmatic system, but perhaps with some input from metamorphic decarbonation of carbonate strata ($\delta^{13}C = 0.5$ ‰) (Chen et al. 2006). The $\delta^{34}S$ ratios of the ores range between −3.5 and 2.5 ‰, clustering between −1 and 1 ‰, and averaging −0.2 ‰, showing a pronounced normal distribution. The narrow range of sulphur isotopic values of the ores indicates that the sulphur was sourced from magmas. Compared with volcanic rocks of Xiong'er Group ($\delta^{34}S = 4.1$ ‰), metamorphic rocks of Taihua Group ($\delta^{34}S = 3.2$ ‰) and Huashan complex ($\delta^{34}S = 3.0$ ‰), the ores from Qiyugou tend to have lower $\delta^{34}S$ values. Considering that fractionation is caused by variations of physico-chemical conditions, the discrepancies of $\delta^{34}S$ cannot preclude these geologic bodies as possible sulphur sources. Compared with Shanggong Au deposit ($\delta^{34}S = -14.6$–6.3 ‰; Chen et al. 2006, 2008a), Tieluping silver deposit ($\delta^{34}S = -8.8$ to -0.6 ‰; Chen et al. 2004a), all in the Xiong'er terrane, the Qinyugou breccia pipe gold deposits have a narrower $\delta^{34}S$ range, mostly close to zero, implying a magmatic control on the mineralising event.

The Qiyugou ores have lead isotope ratios of $^{206}Pb/^{204}Pb$ from 16.771 to 18.530, with an average of 17.386; $^{207}Pb/^{204}Pb$ from 15.257 to 15.820, with an average of 15.535. The Qiyugou granite porphyries have $^{206}Pb/^{204}Pb$ ratios between 17.199 and 17.562, with an average of 17.379, and $^{207}Pb/^{204}Pb$ ratios between 15.278 and 15.570, with an average of 15.402. In Fig. 5.17, Pb isotope data plot across upper crust, orogen, mantle and lower crust lines (Zartman and Doe 1981), with most clustering near the mantle line, indicating complex lead sources. Pb isotopic data from the ores, porphyry, breccias and biotite granite largely fall in the data range

of the Taihua Group. Most Pb isotope data of K-feldspar in the Qiyugou granite fall in or close to the data range of the ores, indicating similar sources. In addition, lead isotopic compositions of the Qiyugou porphyry and the ores resemble those of Huashan Complex (Fig. 5.17), indicating similar sources.

Origin of Auriferous Breccia Pipes and Associated Porphyry Mo Deposit

The numerous breccia pipes in the Qiyugou area, the proximity of the Leimengou porphyry Mo deposit, together with the common presence of calcite and fluorite, are indicative of a large scale hydrothermal system that was driven by frequent volatiles exsolution. This would suggest interaction of magmas with a volatile-rich source. Chen et al. (2004a) working on the lode deposits of the Xiong'ershan (Tieluping and Shanggong, Sections "Tieluping Ag-Pb" and "Shanggong Au") proposed that the collision between the Yangtze and North China cratons that formed the Qinling orogen, between 240 and 140 Ma, resulted in subduction of a continental plate, crustal thickening and formation of a complex stack of north-verging thrust slabs (see Fig. 5.7). This underthrusting was accompanied by metamorphic devolatilisation of sedimentary rocks that included carbonate-shale-chert (CSC) successions of the Guandaokou and Luanchan Groups, south of the Maochaoying fault (Fig. 5.5). Northward underthrusting, crustal shortening and thickening was followed by extensional collapse and the emplacement of granitic magmas during the late Cretaceous phase of the Yanshanian tectonothermal events, as elaborated below. Based on robust isotopic and fluid inclusions evidence, Chen et al. (2004a) further proposed that metallogeny in the east Qinling area, which as previously mentioned, comprises precious metal lodes, porphyry and the breccia pipes, exhibit a zoning from the Maochaoying fault in the southwest to the northeast, from precious metal lodes to porphyry to the Qiyugou breccia pipes, respectively.

During the extensional collapse referred to above, it is envisaged that the magmas interacted with the volatile-rich sedimentary rocks thereby resulting in the emplacement of high level plutons from which a range of porphyry and intrusion-related ore systems developed between ca. 130 and ca. 110 Ma. From fluid inclusion data, Chen et al. (2009a) suggested that the Qiyugou deposits may have first formed in a hypothermal regime that subsequently evolved through mesothermal to epithermal. As such, the Qiyugou breccia pipe gold deposits may be considered as an intrusion-related ore system (e.g. Lang and Baker 2001). The volatile-rich nature of the hydrothermal fluids was conducive to the formation of the numerous breccia pipes in the region. The weakly negative $\delta^{34}S$ values for the Qiyugou sulphides could be derived from a "memory" of a sedimentary source, as postulated for similar values obtained from the precious metal lodes in the region (Chen et al. 2004a). The sub-horizontal (least compressive stress σ_3 perpendicular to the palaeosurface?) sheeted ore zones within the pipes are difficult to explain. It is possible that heated groundwater flow circulated in the pipe causing the redistribution of ore minerals and gold in shears or fractures that were formed during the solidification of the breccia pipes.

Release of magmatic fluids during second boiling and decompression is common in porphyry systems, in which a wide range of breccia types accompany the intrusions

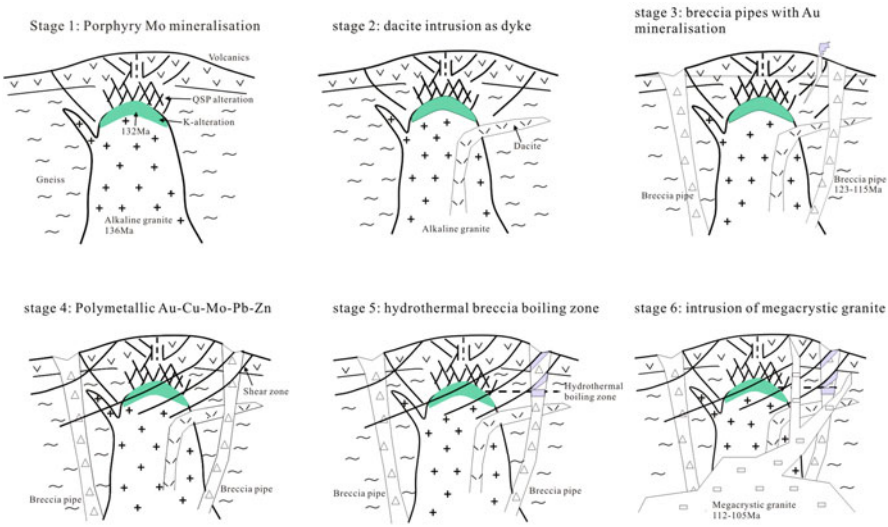

Fig. 5.18 Conceptual model showing a six stage emplacement of volatile-rich granitic magma and related development of a porphyry-breccia pipe magmatic-hydrothermal system; stage 1 emplacement of an alkali-rich granite at 136 Ma, porphyry Mo mineralisation forms at 132 Ma; stage 2 intrusion of dacite dykes; stages 3 and 4 breccia pipes are emplaced at about 120–115 Ma with Au and base metal mineralisation; stage 5 fluid evolution continues in the breccia pipes leading to boiling and the formation of a adularia-Au epithermal system; stage 6 intrusion of 112–105 Ma megacrystic granite (Based on Zhang 2006b; figure courtesy of Dr Zhang Yuanhou, Institute of Mineral Resources, Chinese Academy of Geological Sciences, Beijing)

(Sillitoe 1985). The mechanisms of breccia formation in the porphyry-epithermal environment are associated with the emplacement of hydrous melts near the surface. Exsolution of the aqueous phase during second boiling and subsequent decompression will cause expansion and the exsolution of more fluids leading to the formation of breccia pipes (Burnham 1985). Pulses of volatile release and gas streaming will result in the full range of jigsaw breccias and fluidisation breccias, where the gas/solid ratios are very high (McCallum 1985). Fluidisation results in the upward transport, mixing and milling of fragments and production of rock flour. Fluidisation is a term that describes a bed of particles or clasts with fluid-like properties due to the flow of interstitial gas, forming a gas-solid mixture (Walters et al. 2006). Breccia pipes develop due to the degassing of a volatile-rich intrusion, but it is possible that in some cases the development of a pipe does not run to completion due to local exhaustion of volatiles discharge. This may resume at a later stage, but the pipe develops along a different channel or pre-existing fracture or fault. A model of a breccia pipe is shown in Fig. 5.15. Considered together, the Leimengou porphyry Mo and the auriferous Qiyugou breccia pipes conform to an alkalic-type intrusion-related mineral system (Richards 1995).

A holistic model of a porphyry-breccia pipe system, proposed by Zhang (2006b) is shown in Fig. 5.18. In this model the breccia pipes formed after the emplacement

of the Leimengou porphyry Mo deposit. This is confirmed by the age data, which indicate that the porphyry intrusion has a SHRIMP U-Pb age of 137 ± 2 Ma, the Mo mineralisation has Re-Os ages ranging from 131.4 ± 1.4 to 116 ± 1.7 Ma (Mao et al. 2008a) and the breccia pipes have K-Ar ages ranging from 128 to 126 Ma. These age relationships find further confirmation in the No. 7 breccia pipe in which there are clasts of altered granite with stockworks and molybdenite. With reference to Fig. 5.18, the intrusion of an alkaline granite at 137 Ma was followed by degassing and development of magmatic-hydrothermal fluids, which resulted in the formation of a porphyry Mo deposit at about 131 Ma in the apical regions of the intrusion (Stages 1 and 2). With continuing degassing magmatic gases were channelled along conduits, fluidising material along the way and developing breccia pipes between 125 and 115 Ma (Stage 3). Shear zones and faults formed and channelled metalliferous hydrothermal fluids from the pipes to form polymetallic (Au-Cu-Mo-Pb-Zn) ores (Stage 4). Boiling occurred, perhaps due to partial unroofing and lowering of pressure, which resulted in the formation of subhorizontal ore zones with adularia and calcite (Stage 5). The last event is the intrusion of barren megacrystic granite at 112–105 Ma (Stage 6).

5.3.3.3 Carbonatite-related Mo-Pb Deposits

Apart from the Bayon Obo carbonatite complex, discussed in Chap. 3, so far not many carbonatites are known in China, except for those reported in the Himalayan orogen in Tibet (Hou et al. 2009). An overview of carbonatites in China can be found in Yang and Woolley (2006) and in Xu et al. (2010a). One of these is the Xuanglongpu carbonatite in the Qinling orogenic belt, represented by dykes with a U-Pb age on plumbodavidite of ca. 206 Ma intruded into rocks of the Xiong'er Group (Huang et al. 1984). Also in the Qinling orogenic belt are the Shaxiongdong carbonatite–syenite complexes emplaced at the southern margin of South Qinling, but these are not discussed here and the interested reader is referred to Xu et al. (2008a). The northeast-trending Xuanglongpu carbonatite dykes are from 10 to 500 m long and up to 20 m wide and are associated with biotite-syenite and aegirine-syenite.

Xu et al. (2010b) reported on the unusual Mo-Pb mineralisation that is associated with the Huanglongpu carbonatite dykes. The Huanglongpu carbonatite mineralisation is present in the Yuantoum, Dashigoum, Shijainwan II and Taoyuan ore fields, where the carbonatite dykes are composed of calcite (70–50 vol%), quartz, K-feldspar, barite, celestine, pyrite, galena, sphalerite and molybdenite, REE-fluorocarbonate, monazite, brannerite and locally fluorite. The molybdenite, which occurs as disseminated grains and films in fractures, was dated by the Re-Os method at 221 Ma (Huang et al. 1995). The dykes have alteration envelopes of biotite, epidote, pyrite and anhydrite. A somewhat unusual alteration type for carbonatites, which are generally associated with fenitic alteration haloes (alkali metasomatism with K-feldspar, alkali amphibole, sodic pyroxene and carbonate minerals; Pirajno 2009, in press). Yet, Xu et al. (2010a) confirmed the igneous and mantle-related origin of these carbonatites, based on their high REE, Sr and particularly the high Sr and Mn

abundances of the carbonate minerals (up to 1.3 wt % SrO and 2.5 wt % MnO), as observed in other carbonatites. REE-fluorocarbonate (bastaenesite and parasite mainly) and monazite occur as discrete pseudomorphs of unidentified silicates and as intergrowths with molybdenite and/or galena. The monazite has enhanced abundances of Th and S; whereas the fluorocarbonates are enriched in light REE (LREE).

The close paragenetic association of molybdenite and REE minerals support the concept that the Mo enrichment is primary and related to the carbonatite magma. Furthermore, the Huanglongpu carbonatites are characterised by very high heavy REE (HREE) and Mo contents (up to 1,130–1,000 ppm, respectively), which although not common in carbonatites (Woolley and Kemp 1989), according to Xu et al. (2010) cannot be attributed to secondary processes, such as interaction with hydrothermal fluids. In spite of the oddities shown by the Huanglongpu carbonatites, Xu and co-workers focused on the high Re content of the molybdenite to confirm their mantle source, based on a concept first proposed by Mao et al. (1999; see also Mao et al. 2008a). A low Re content in molybdenite (<10 ppm) samples indicate a crustal source of the ore, whereas a high Re content (>100 ppm) reflects a mantle source. Mafic underplating and mantle metasomatism would provide enrichment of Re in molybdenite relative to crustal levels. The Huanglongpu molybdenite has Re/Mo values (0.005) that are close to those of primitive mantle (0.006) leading Xu et al. (2010) to suggest that the host carbonatite did not significantly degass during emplacement. If this view is correct, it would explain the lack of fenititisation. The Mo enrichment of the Huanglongpu carbonatite dykes can be explained by the fact that the basement rocks of the Qinling orogneic belt in the region (Taihua Group, Xiong'er and Luanchan groups) and have higher Mo contents (2–15 ppm) than any other lithostratigrahoc units in eastern China (Gao et al. 1998) and the average crustal value of 0.6 ppm (Wedepohl 1995). The regional Mo anomaly in the Qinling could have been sourced either from the subcontinental lithospheric mantle, perhaps as a result of fluid overprint associated with the subduction system beneath the NCC in the Late Permian (Xu et al. 2010).

Resources, as reported by Xu et al. (2010), are as follows: at Yuantou 1,700 tonnes of Mo, grading 0.07–0.144 %; Dashigou contains 8,900 tonnes of Mo with grades ranging from 0.075 to 0.103 %; Shijiawan II (and I, which is not hosted by a carbonatite, but by a 121 Ma granite porphyry) total 6,000 tonnes, grading 0.041–0.104 % Mo; Taoyuan has 3,800 tonnes at grades ranging from 0.041 to 0.096 %.

Another carbonatite occurrence, studied by Xu et al. (2010c) is that associated with the Miaoya REE deposit in the Wudang Terrane of the South Qinling belt, on the northern margin of the Yangtze Craton. The Miaoya carbonatites are associated with a syenite intrusion, emplaced in Mesoproterozoic quartz-keratophyre and Early Palaeozoic shale rocks. The carbonatites form lenses, stocks and dykes that intrude the syenite and are composed of fine- to medium-grained calcite (ca. 85 vol%). The age of the carbonatite is poorly constrained by a biotite Ar-Ar date of ca. 278 Ma. The REE minerals of the Miaoya carbonatites are fluorapatite, monazite, bastanaesite and synchysite. The fluorapatite makes up 1–5 vol% of the rock and together with monazite, is an early phase formed before calcite. Other accessory minerals are magnetite, ilmenite, provskite, ferrocolumbite and Nb-rich rutile. It is of interest

to note that Xu et al. (2010c) on the basis of trace element data, suggested that since the primary calcite contains low REE, the REE must have been fractionated from the parental carbonatite liquid prior to the formation of the primary calcite. The parental liquid would have been enriched in P and F, as indicated by the early fractionation of fluorapatite and monazite, resulting in the subsequent depletion of REE in the residual liquid from which the carbonatite was formed. These authors then pointed out that the REE economic potential of carbonatite is influenced by crystal fractionation processes of specific minerals, such as phosphate, calcite and fluorocarbonates, which will result in changes in the availability of $(PO_4)^{-3}$, F- and $(CO_3)^{2-}$ as complexing ligands.

5.3.3.4 Carlin-style Deposits

Sedimentary-rock-hosted Au deposits, including Carlin-style are present in the southwestern part of the Yangtze Craton (Guizhou province, described in Chap. 4), in the Lower Yangzte River Valley and in the Qinling-Dabie orogenic belt (Fig. 5.19). In the Qinling-Dabie orogenic belt, Carlin-style mineral systems tend to occur in a foreland fold-and-thrust belt south of the Shangzhou-Danfeng (Mian-Lue) suture (Fig. 5.20). A comprehensive text documenting sediment-hosted (mostly including Carlin style) in China is the USGS Open-File report edited by Peters (2002). Peters (2002) subdivided these sediment-hosted Au deposits into those that occur in the West Qinling (inclusive of the Songpan-Ganzi terrane; discussed in Chap. 6) and East Qinling. Hofstra and Cline (2000) defined Carlin-type Au deposits as "*epigenetic, disseminated auriferous pyrite (marcasite or arsenopyrite) deposits characterised by carbonate dissolution, argillic alteration, sulfidation, and silicification of typically calcareous sedimentary rocks*". Bagby and Berger (1985) defined two subsets: (1) jasperoidal and (2) Carlin sensu stricto. There is a complete gradation between the two, and both have a strong correlation of Au with Hg, As, Tl and Sb. The jasperoidal subset includes deposits hosted in jasperoid, quartz veins and silicified wall rocks. The term jasperoid refers to an epigenetic body that consists of fine-grained ferruginous chert, which has replaced a pre-existing rock. Most jasperoid bodies are structurally controlled or located at contacts between carbonate rocks and shale. The Carlin subset is characterised by evenly disseminated Au and Ag in rocks that are not obviously silicified. The ore zones are tabular or pod-like and extend several tens of metres from the controlling structures. The association of gold with organic carbon, and locally with hydrocarbons, is typical of most Carlin-type deposits. This organic carbon consists of veinlets, seams and particles of amorphous carbon. The precise relationship between gold and carbon is unknown, although the reducing power of the carbon may have been the catalyst for the precipitation of the gold. Organic carbon was probably introduced with the main-stage hydrothermal fluids, but in terms of ore genesis the role of the carbonaceous and carbonate sedimentary rocks is of greater importance. The role of organic matter was recently examined and emphasised for the genesis of Carlin-type Au by Large et al. (2011). The removal of calcite and its replacement by silica-rich gold-bearing ore fluids was a key factor in the formation of the orebodies. Thus, the main stage of hydrothermal activity consisted of decalcification, argillisation, silicification and pyritisation.

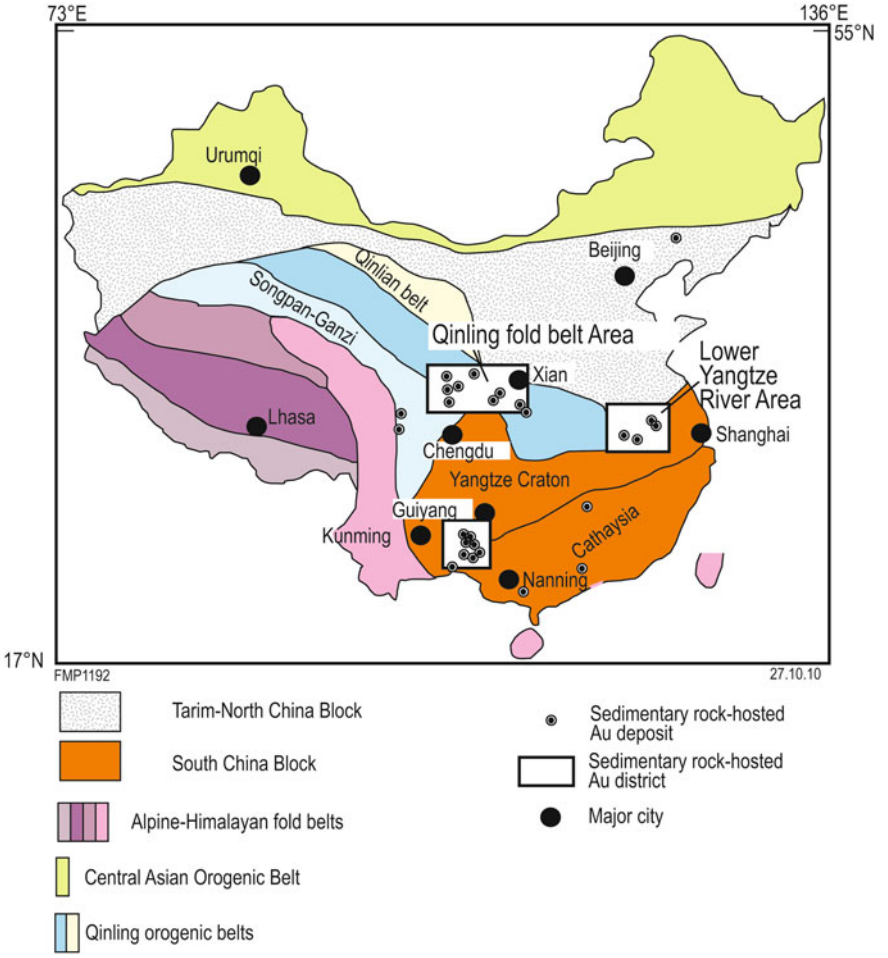

Fig. 5.19 Distribution of sedimentary-rock-hosted (Carlin-style) mineral systems in China. (After Peters 2002)

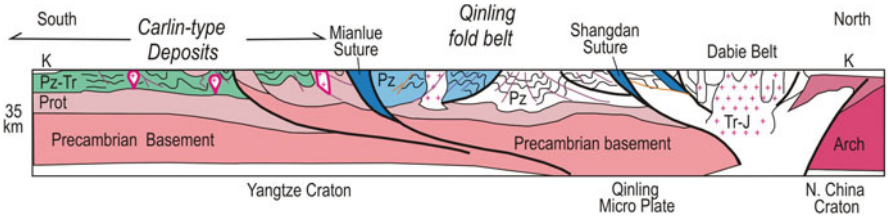

Fig. 5.20 Idealised north-south cross-section through the northern part of the Yangtze Craton, the southern margin of the North China Craton and the Qinling-Dabie orogenic belt. (Modified from Peters 2002)

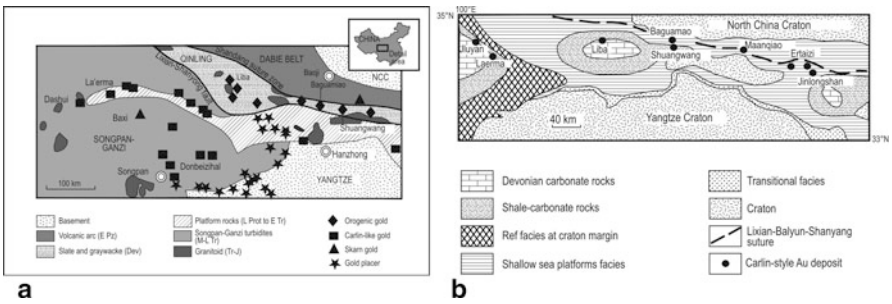

Fig. 5.21 (**a**) Schematic map of the West-East-Qinling and Songpan-Ganzi tectonic domains and distribution of selected Carlin-style Au deposits (**b**) Simplified geological map of Devonian lithofacies and distribution of Carlin-style Au deposits in parts of the Qinling-Dabie orogenic belt. (After Peters 2002)

Chen et al. (2004b) suggested that Carlin-style deposits in China were formed during the transition from compression to extension between the Yangtze and North China cratons. Collision resulted in the formation of imbricate north-dipping thrusts and subduction of continental crust. This caused intense crustal thickening and uplift and perhaps slab breakoff or delamination, which allowed asthenopsheric upwelling and partial melting of the lower crust and strong metamorphic devolitilisation. These processes would have generated melts and ore fluids from which Carlin-style and lode deposits developed, as described in the preceding sections.

The key lithologies for the formation of Carlin-style deposits are sedimentary carbonates, particularly carbonaceous rocks. In the Qinling orogenic belt Early to Mid-Palaeozoic sedimentation consisted of limestone, carbonaceous shales, sandstone and volcanic rocks, which were folded and metamorphosed between 570 and 405 Ma (Caledonian orogeny). This was followed in the Devonian by new sedimentation, largely consisting of flysch and limestone intercalated with volcanic rocks. These Devonian sedimentary units host the majority of Carlin-style deposits in the Qinling fold belt. More specifically, the Devonian succession consists of, from top to bottom, limestone beds overlying interbedded calcareous sandstone, limestone, argillaceous limestone and bioclastic limestone. These units are overlain by Carboniferous sandstone, carbonaceous shale and limestone. During the Permian there was deposition of more limestone, argillaceous limestone, shale and siltstone. These successions were subjected to folding from west to east, culminating with the deposition of Triassic shale and limestone (Peters 2002 and references therein). This sedimentation ceased by the end of the Indosinian period (230–195 Ma), when the entire sedimentary sequence was affected by deformation, metamorphism and magmatism associated with the collision of the Yangtze Craton with the NCC, as detailed above. This was followed by the Yanshanian tectono-thermal event in the Jurassic and Cretaceous, extensional tectonics, block faulting and basin formation.

The following overview on the distribution and metallogenic aspects of Carlin-style Au deposits in the Qinling orogenic belt is abridged and adjourned from Peters et al. (2002 and references provided therein). Carlin-style Au deposits in the Qinling fold belt are hosted in specific horizons of middle and late Devonian to Carboniferous

rocks in the east, and in early Triassic rocks in the western part of the fold belt (Fig. 5.21). Some Au deposits, such as the Laerma Au deposit, are hosted in early Palaeozoic sedimentary rocks, or in Middle to Lower Jurassic volcanic rocks, such as the Jiuyuan Au deposit. Anomalous concentrations of Au, Hg, Sb, and Ag and lesser concentrations of Tl, U, and W are associated with these deposits. Other Carlin-style Au deposits are spatially associated with some Pb and Zn deposits (e.g. Xiahe-Chengxian, Fengxian-Taibe, Yuexi and Xitonggou) along the Ding-Ma fold belt area in the East Qinling fold belt. The features and characteristics of the Carlin-style Au deposits along the Qinling-Dabie orogenic belt are not necessarily diagnostic of their origin. Alteration, ore mineralogy and geochemistry of these deposits have many characteristics, but in most cases Sb and As are ubiquitous. The age of the deposits is not clear and may range from the depositional age of the host sedimentary beds to ages related to orogenic events. The youngest ages (ca. 49.5 to ca. 12.7 Ma) of Au mineralisation recorded in the Qinling region is from both whole rock and ore minerals in the Laerma Au deposit (Li and Li 1994), whereas the oldest ages reported are ca. 337.5 to ca. 234.3 Ma from the Pingding Au deposit by isotope analysis of realgar and orpiment associated with Au mineralisation, using the U-Th-Pb method. Other ages are ca. 168 Ma (pyrite, U-Th-Pb), ca. 183 Ma (pyrite, $^{40}Ar/^{39}Ar$) in the Shuangwang Au deposit (Fan and Jin 1994), and ca. 210 Ma (whole rock and ore, U-Th-Pb) in the Baguamiao Au deposit (Wei and Chao 1994). This wide range of ages is compatible with multiple metallogenic events along the Qinling orogenic belt. Shear zone-hosted, syndeformational, sedimentary rock-hosted Au deposits, such as the Maanqiao, Shuangwang, and Baguamiao Au deposits along the Lixian-Baiyun-Shanyang fault zone in the East Qinling fold belt are in similar host rocks and have similar trace element geochemistry to the Carlin-type sedimentary rock-hosted Au deposits. These syndeformational deposits locally also contain quartz veining and native Au that are similar to features in orogenic vein- or shear zone hosted-type deposits. The geochemistry, mineralogy, and host rock types of the syndeformational sedimentary rock-hosted Au deposits lie along the same Devonian lithotectonic belt as the Jinlongshan Au deposits in the Ding-Ma Au belt to the east (Fig. 5.21) and may be deeper expressions of these deposits.

Stratabound Au mineralisation styles in many of these syndeformational Au deposits may have predated by Au mineralisation that developed along the shear zone (Peters 2002). Growth rim zoning of some pyrite grains in the syndeformational Au deposits is similar to sulphide textures contained in Carlin-type deposits (e.g. Zhang 1996). Ores in these syndeformational sedimentary rock-hosted Au deposits and in Carlin-type deposits both contain similar ore minerals, such as arsenopyrite, stibnite, and trace complex sulphide grains composed of As, Ni, As, Pb, Zn and Cu (e.g., Wang 1992). The geochemical signature of the Maanqiao Au ores, consisting of elevated As, Sb, also is similar to Carlin-type deposits. These Carlin-style Au deposits therefore contain some features that represent processes that are common to both orogenic Au lodes and to Carlin-type Au models types (Goldfarb et al. 1998, 2001; Groves et al. 1998).

Many sedimentary rock-hosted Au deposits in the West Qinling have high organic C content, such as the Songpangou, Qiaoqiaoshang, Dongbeizhai, Pingding, Jiuyuan, and Heidousi Au deposits. The organic C content in many of these deposits ranges

from 0.20 to 14.63 wt % (Li and Li 1994; Mao and Li 1994). Stratigraphic Palaeozoic and early Triassic horizons that host these deposits also contain high Au background concentrations 10–15 times higher than the regional background Au concentration and therefore, these organic-rich horizons have been considered as source-beds for both petroleum and for Au deposits. Mao and Li (1994) suggested that organic carbon was an important factor in enrichment of Au, because of the reducing environment favourable for Au precipitation. Alteration styles and mineralogy of gangue minerals and ores in the Qinling fold belt Carlin-style Au deposits have many similarities. These include illite-quartz, decarbonatisation and many common sulphide mineral assemblages, such as pyrite, arsenical pyrite, As-bearing sulphide minerals, and stibnite. Realgar and orpiment are abundant in many of the deposits, such as the Songpangou and Qiaoqiaoshang Au deposits in the West Qinling fold belt. High–As ores in the Qinling fold belt have many textural and mineralogical similarities to high As ores in Carlin-type deposits in Nevada (Hofstra and Cline 2000; Cline et al. 2005).

The West Qinling Carlin-style Au deposits are hosted in clastic and carbonate sedimentary rocks of Palaeozoic, Devonian and Triassic age (Zhou et al. 2002a). The country rocks are fine-grained carbonaceous calcareous sandstones, silty carbonates, shales and cherts, deposited in shallow sea environments. They have distinct geochemical signatures that are characterised by a metal association of $Au + As + Sb + Hg + Ag \pm Ba \pm Te \pm Pb\text{-}Zn \pm U$. Antimony, Hg, Ag, Pb, Zn, U and barite are locally recovered as by-products (Chen et al. 2004b). Hydrothermal alteration typically consists of zones of pervasive silicification. A study of these deposits by Chen et al. (2004b) revealed temperature of ore fluids ranging from 300 to 160 °C, fluid salinities from 4 to 10 % NaCl eq, pressures of 5–50 MPa and depths of ore formation of 0.5–5 km. The fluids were mainly derived from metamorphic and meteoric sources, although a magmatic component could not be excluded. The high content of C_2H_6, recorded in inclusion fluids, is indicative of organic sources. Radiometric ages range from about 220 to 120 Ma, with a peak at about 170 Ma. These deposits formed in the same time span as the lode (orogenic) and skarn deposits and for this reason these Carlin-style deposits may, after all, be related to intrusions, or associated with circulation of meteoric fluids powered by heat energy released by the intrusions. Recent views on the origin of Carlin-type Au deposits maintain that the element association that is characteristic of these mineral system, namely Au, As, Hg, Tl, Te, Cu, Sb are derived and transported by magmatic aqueous vapours that act on dominant carbonate lithologies during extensional tectonics (Muntean et al. 2010).

In the sections that follow, I describe selected Carlin-style Au deposits from the East Qinling (Jinlongshan, Maanqiao, Baguamiao, Shangwang) and deposits in the West Qinling fold belt (Songpangan, Qiaoqiaoshang, Dongbeizhai, Liba, Lianhencun, Laerma, Manaoke), abridged and adapted from Peters et al. (2002), to whom the interested reader is referred for more details.

East Qinling Carlin-style Au Deposits

The *Jinlongshan (Zhenan)* Au deposit is located in Zhenan County (Shaanxi Province) south of the historical city of Xi'an. The Au orebodies are 5–16 m wide,

grading 2.17–9.05 g/t Au and form stratabound, saddle reefs, veins, pods that pinch and swell and locally cut across bedding planes. The Jinlongshan deposit was discovered in 1993 and by 1999 was producing 300 tonnes of Au ore per day. The main feature of the orebodies in the Jinlongshan (Zhenan) Au deposit is the clustering of more than 10 orebodies, at cut off grades of 1 g/t Au, along a zone of 100 to several 100s of metres in length. The host sedimentary sequence in the Zhenan area consists of upper Palaeozoic (Carboniferous and Devonian) argillaceous and arenaceous sedimentary rocks. The host horizon for the Au deposit is a turbiditic sequence of fine-grained sandstone, siltstone-silty shale, calcareous siltstone, and limestone of the Upper Devonian Nanyangshan Formation, containing about 90 % of the Au resource. Another horizon, representing about 10 % of the Au resources, is in the Lower Carboniferous Yuanjiagou Formation and consists of cherty, banded limestone that is intercalated with silty shale, silty sandstone, argillaceous limestone, and calcareous shale. Structures in the Jinlongshan (Zhenan) mining area and along the greater Ding-Ma Au belt are, anticlinal, recumbent folds and faults. Ore is present along east-trending anticlines and commonly is hosted in east-striking, brittle-ductile shear zones that contain breccia, fault gouge, and fracture networks. A main conjugate fracture set strikes northeast and north and is closely related to Sb ores, which are associated with silicification and jasperoid alteration. Gold grades are highest at intersections of strong compressional, ductile and ductile-brittle deformation zones and are most intense along northeast-striking fractures. Microstructural textures do not cross cut the stratabound ore layers, which suggests that cleavage post-dates sulphide microlayering along bedding. This observation is compatible with syngenetic, stratiform gold deposition prior to brittle-ductile shearing. Hydrothermal alteration associated with Au occurrences in the Jinlongshan Au deposit area include silicification and calcite as replacements and veinlets with lesser veinlets of pyrite, arsenopyrite, barite, and kaolinite. In addition, dickite and fluorite are present. Gold mineralisation is associated with silica and pyrite. The ore minerals of the Jinlongshan Au deposit are pyrite, arsenical pyrite, arsenopyrite, stibnite, sphalerite, and chalcopyrite. Quartz, calcite, sericite, barite, and clay minerals are the main gangue minerals. Pyrite-bearing Au is disseminated in euhedral to subhedral crystals along bedding planes and in dissolution replacement zones and commonly has a growth-zoned As-rich pyrite rims texture. The Au is present as very fine microspheres (0.375–0.08 μm) along the margins of As-bearing pyrite and arsenopyrite and in micro-fractures in these minerals. A post-Au ore quartz vein event produced a series of ductile veins and veinlets and tabular quartz matrix breccia pods, which locally were synchronous with late Sb enriched zones and ores. The Jinlongshan Au deposit also contain anomalous concentrations of As, F, Cu, Pb, Co, and Ni, which is a geochemical suite generally compatible with other Carlin-type deposits in the West Qinling fold belt. Studies of ore minerals in the Jinlongshan Au deposit indicate that the temperature of formation ranges from 250 to 187 °C, with ore fluid salinities of 7.85–5.7 wt % NaCl equivalent. Fluid-inclusion CO_2 densities suggest formation depths of 1.5–1.9 km.

The *Maanqiao* Au deposit is located in the Qinling Mountains, west-southwest of the city of Xi'an (Fig. 5.21b). Twenty seven mineralized zones were identified during exploration work, of which 12 have economic potential (Fig. 5.22). Resources

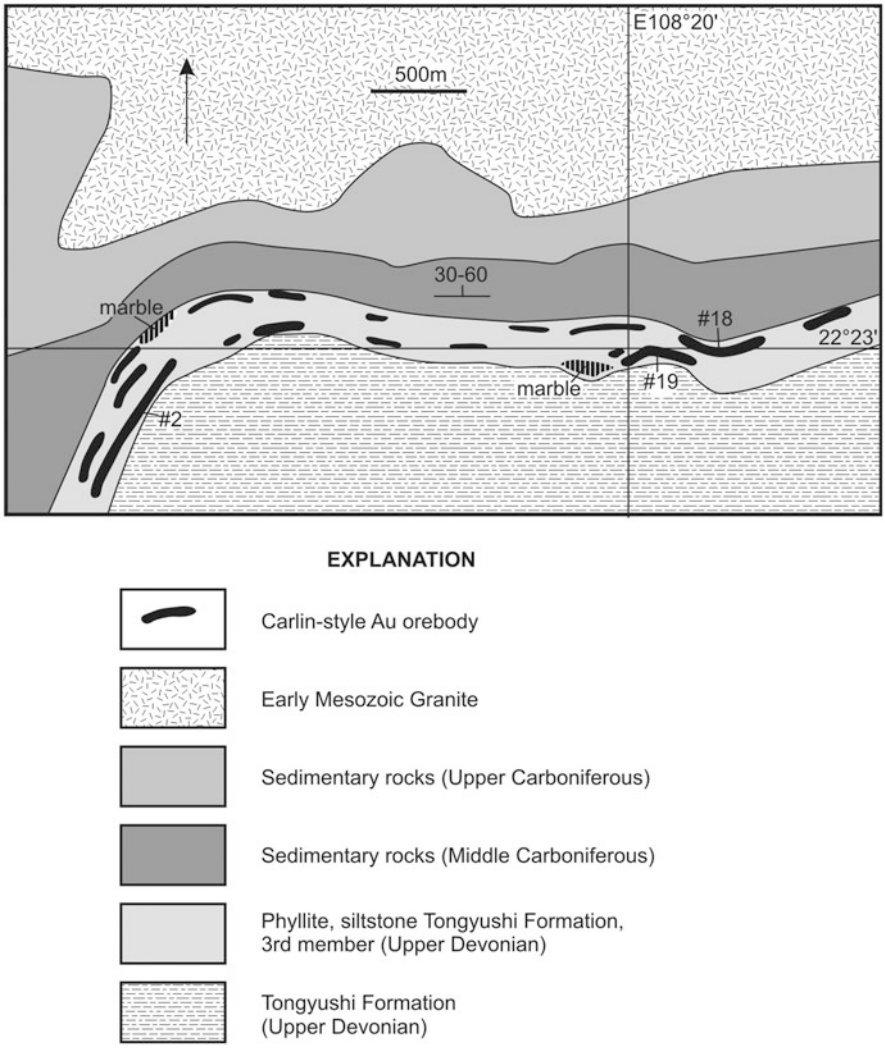

Fig. 5.22 Sketch geological map of the Maanqiao Au deposit, showing the stratabound nature of the ore zones. (After Peters et al. 2001)

of economic orebodies, at ≥4 g/t Au cut off grade, are 1 Mt along a 3-km long strike length in the 4-km-long and 1- to 3-km-wide mine area. Three economically important stratabound orebodies, are from 400 to 550 m long and 2.5–3 m thick, and have been traced to depths of 150–320 m by drilling. The total Au ore reserve is 7.6 tonnes grading 4.95 g/t. Au. The Maanqiao Au deposit area is characterised by an east-west-striking sequence of moderately, north-dipping, late Devonian to late Carboniferous fine-grained clastic, carbonaceous slate and limestone rocks, the upper

parts of which are in contact with an early Mesozoic granite to the north. The Upper Devonian Tongyushi Formation, consisting of phyllite and silty sandstone, is the main ore horizon. Contact metamorphism locally has converted the limestone in the ore-bearing horizon to marble (Fig. 5.22). Structures in the Maanqiao mine area are dominated by a south-dipping isocline and by the east-west-striking Wangjiashan-Zhengnangou (F1) and Maanqiao (F2) compressional faults that bound a 4,400 m long and 150 m wide, ductile shear zone that hosts and controls the orebodies. The stratabound, shear zone-hosted ore zones are surrounded by haloes of disseminated gold and sulphide minerals in the undeformed strata around the shear zones and these halos generally are thicker than the shear zones and grade between <3 and 0.3 g/t Au, whereas the main oreshoots in the shear zones usually grade between >3.0 and 5.0 g/t Au. Alteration consists of intense quartz-sericite-pyrite along the shear zones, accompanied by biotite, plagioclase, ankerite, dolomite, apatite, and calcite. Ore grades generally increase with the amount of quartz veinlets. The ore is black to dark gray and contains foliation-parallel quartz veinlets in a mylonitic fabric. Ore minerals at the Maanqiao Au deposit include pyrrhotite, pyrite, with lesser magnetite, arsenopyrite, chalcopyrite, sphalerite, galena, native Au, local stibnite, and Ni–Sb, Pb–Cu–Zn, and Pb–Sb sulphide minerals. Gold mainly is present as grains of native Au (about 81 vol%) and locally is present in the alteration matrix of the shear zone. Ore minerals typically are present as disseminations, veinlets, and locally in massive clusters of sulphide minerals along the shear zone fabric. The geochemical signature of the Maanqiao Au ores is characterised by anomalous concentrations of As and Sb, similar to other Carlin-style Au deposits in the Qinling fold belt. Elevated geochemical values of Cu, Pb, Zn, Ni and Co in the Maanqiao Au ores are compatible with Carlin-type deposits, but are also similar to those found in some orogenic quartz-vein deposits. Local values of Bi and Ag are higher in the Maanqiao Au deposit than in most other Qinling fold belt Carlin-style ores, but could reflect the proximity of the Mesozoic intrusions to the north. Thus, the Maanqiao deposit has some similarities to shear zone-hosted Au quartz vein deposits, such as native Au, quartz-sericite alteration, and local quartz veining along the host shear zone. Dolomite-ankerite alteration at the Maanqiao Au deposit may be products of thermal alteration and shear zone remobilisation from the dolomitic host rock, rather than products of hydrothermal carbonate alteration that commonly is associated with shear zone-hosted Au deposits. The genesis of the Maanqiao Au deposit, and the similar Baguamiao Au deposit (see below) to the west, is associated with processes that formed the host ductile shear zones. Sulphide minerals and Au appear to have grown simultaneous with deformation along the shear fabric of the shear zone, as suggested by strain shadows adjacent to sulphide mineral grains, by alignment of ore minerals in the shear zones, as well as growth of muscovite across some sulphide grains. This suggests that stratabound Au mineralisation predated the shear zone and was later concentrated by a deformation fluid processes during shear zone formation. The Maanqiao Au deposit may be a syndeformational-style deposit of the Carlin-type family of deposits, rather than part of the orogenic-type quartz vein deposits, but contains features suggesting redistribution of the ore minerals during later deformation.

The *Baguamiao* Au deposit, in Fengxian County (Shaanxi Province) (Fig. 5.21b) is about 40 km from Fengxian County town, southwest of the city of Xi'an in the East Qinling fold belt area. The deposit is included here for comparison with the Maanqiao Au deposit with which it shares many similarities. The deposit is a large-size (>50 tonnes Au), syndeformational, sedimentary rock-hosted Au deposit that lies northwest of the Shuangwang Au deposit (Fig. 5.21). The deposit is proximal to the Lixian-Baiyun-Shanyang suture and is hosted in Devonian marine sedimentary rocks, similar to the Maanqiao deposit and other Au deposits along the Ding-Ma Au belt. The Baguamiao ore zones are 1.7 km long, 50–160 m wide and extend to a depth of 500 m. It contains a measured resource of 80 tonnes Au. The largest, No. 14 orebody, is 500 m long and 4.8 m thick, and 220 m deep, grading 5.17 g/t Au, using a cut-off grade of 1 g/t Au. The orebodies are stratabound layers or lenses that branch, merge, swell, and pinch along sheared bedding layers. The host sedimentary rocks were deposited in a shelf-tidal flat environment.

The deposit lies within the Baguamiao syncline, which is a fold at the west end and north limb of west-northwest-trending Sujiagou-Kongguangou synclinorium. Flow cleavage, flow folds, sheath folds and recumbent folds are characteristic structural features in the Baguamiao syncline. The two main faults in the Baguamiao Au mine area are the west-northwest-striking F1 fault, near the contact between the Gudaoling and Xinghongpu Formations and the F2 fault in the northern part of the district. These two faults merge in the southeast part of the district and their intersection defines a several kilometres long, 10–20 m-wide cataclastic zone. Limestone and phyllite in this zone are brecciated and are locally converted to mylonite. Gold ores in the Baguamiao Au deposit are located along a northwest-striking ductile shear zone and are present as small stockworks and veinlets within this shear zone. The ore textures are brecciated or disseminated, but also are present as layers and massive accumulations of ore and gangue minerals. Alteration minerals form a broad, bleached zone that surrounds the host shear zone, similar to the Maanqiao Au deposit to the east. The main ore minerals in the Baguamiao Au deposit are pyrite, pyrrhotite, and marcasite with lesser chalcopyrite, ilmenite, molybdenite, rutile, native Au and Ag, and rare arsenopyrite, galena, sphalerite, Te and Bi minerals, and Au. Sericite, quartz, ankerite, chlorite, biotite, hydro-mica and tourmaline are the main gangue minerals. The ores exhibit a granoblastic texture. Gold is present as inclusions in minerals or at crystal boundaries and partings of minerals, or as intergrown particles. Visible Au (0.01 mm) is about 35 vol% and microscopic Au (0.01 ~ 0.05 μm) is about 45 vol%, and submicroscopic gold (0.01 μm) is about 20 vol%. The average fineness of Au is 878 (range from 836 to 931) and the average content of Ag is 11.53 wt %. PGE minerals are present and associated with silicification and dolomitisation. The concentration of PGE minerals is correlated with Au. PGE minerals are very fine (ca. 0.5 μm) and are present in joints of quartz and along contacts between quartz and sericite. The composition of the PGE minerals is Ru = 66.8 wt %, W = 23.63 wt %, Co = 7.189 wt % and Fe = 2.32 wt %.

The *Shuangwang* Au deposit is a large breccia-hosted sedimentary rock-hosted Au deposit (Fig. 5.21b) also located along the regional-scale Lixian-Baiyun-Shanyang

suture that lies north of Shuangwang and the Baguamiao Au deposit. The Shuangwang Au deposit, however, does not exhibit a strong shear fabric or mylonitic foliation, such as those at Baguamiao and Maanqiao. Economically significant (using a 1 g/t Au cut-off) Au-bearing breccia bodies are present in an extensional, 11.5 km long, 700–500 m wide, east-west to west-northwest-trending breccia zone. The No. 8 orebody is the largest, approximately 680 m long, 28 m wide, and 348 m deep. Platinum and Pd are enriched in pyrite and ferruginous dolomite in the Shuangwang Au deposit, as found at Baguamiao. The host breccia bodies locally crosscut Devonian Xinhongpu Formation rocks, which consist of silty slate, interbedded argillaceous silty limestone, micritic limestone, argillaceous limestone, and interbedded slate. Middle Devonian Gudaolong Formation rocks, which also host mineraliastion in breccia bodies, comprise calcareous sandstone and siltstone interlayered with limestone and calcareous slates. The breccia bodies are conformable or crosscut stratigraphy at low-angles. Breccia clasts, range in size from 10 cm to several metres, are composed of altered slate, siltstone, marble, and micritic limestone. The breccia matrix is made up of albite, ankerite and calcite, as well as local quartz and pyrite that were formed by multiple stages of hydrothermal activity. A light-colored alteration zone associated with the breccia bodies contains early albite and sericite and late ankerite that extends beyond the steep-dipping Au-bearing breccia bodies. This alteration assemblage, along with dolomite, calcite, quartz, rutile, and apatite constitute an important prospecting tool for the Au deposits in this area. Although Au is inversely related to areas of intense albitisation in most deposits, at Shuangwang albitisation is associated directly with Au in two occurrences. Albite generally is considered to be formed at an early paragenetic stage of hydrothermal activity, and is most likely pre-gold ore.

West Qinling Carlin-style Au Deposits

The West Qinling fold belt area constitutes much of the "*northern golden triangle*" area of Sichuan, Gansu, and Shaanxi Provinces and contains clusters of Carlin-style Au deposits on the north side of the Qinling fold belt in Gansu Province, on the south side of the fold belt in northern Sichuan Province, and also to the west along the north-northwest-trending Luhuo-Daofu fault zone in west-central Sichuan Province (Fig. 5.23). The deposits lie in the Bayankala fold belt and along the northwest-striking Ganzi-Litang suture. The West Qinling Au deposits are part of a large Au-(As)–Hg–(Sb) metallogenic zone that extends from Nima in Maqu County, Gansu Province to Manaoke, Nanping County, Sichuan Province, where Permian and Triassic carbonate and clastic rocks also host Hg-bearing sedimentary rock-hosted Au deposits. The salient points of the lithostratigraphic sequence in the West Qinling fold belt are also summarized from the comprehensive work of Peters et al. (2002), based on detailed work by the Bureau of Geology and Mineral Resources of Gansu Province (1989). Here, it will suffice to say that the West Qinling is divided into three north to south lithotectonic units or terranes, with the southern unit further

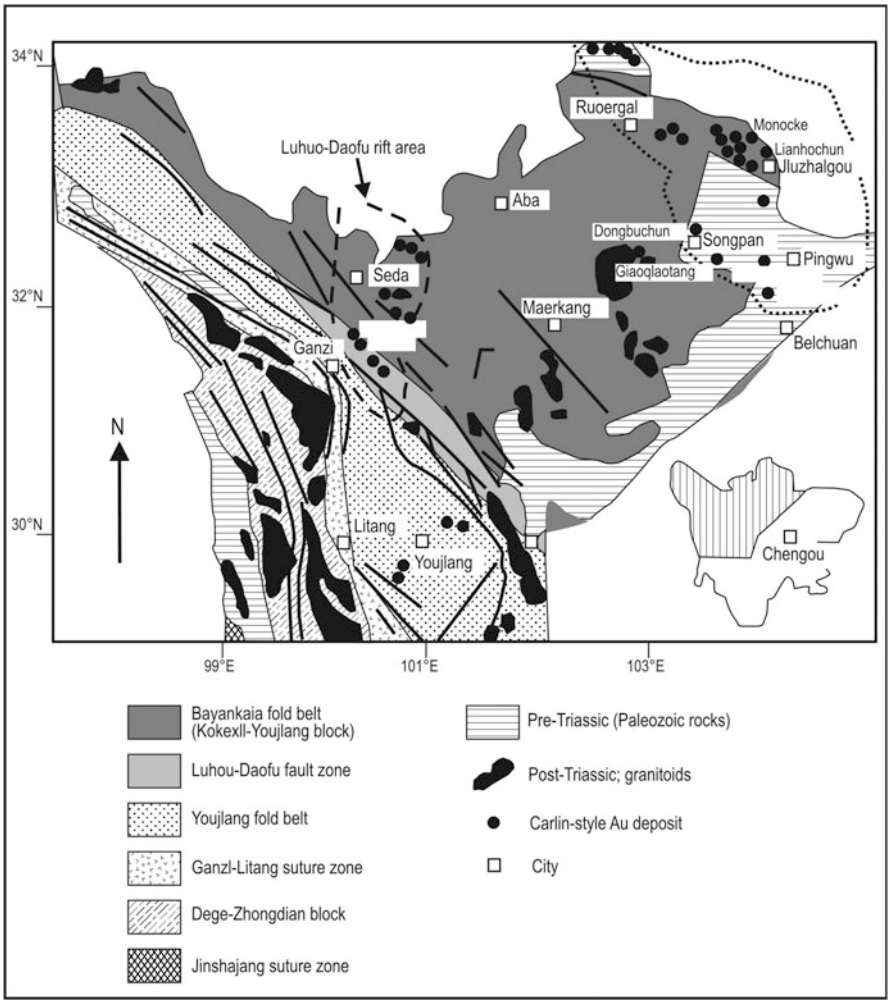

Fig. 5.23 Simplified geology of the West Qinling fold belt and distribution of Carli-style Au deposits. (After Peters et al. 2001)

divided into western and eastern parts. The lithostratigraphic sequences are from the Cambrian to the Triassic, with the Devonian rocks being the most common host of Carlin-style Au, Hg and Sb deposits. Below, I describe the Songpangou, Qiaoqiaoshang, Dongbeizhai. Liba, Yinchanggou, Lianhechun and Laerma deposits (again the reader is referred to Peters et al. 2001, for details). Most of these deposits share similar characteristics, except for the Laerma, Liba, and Manaoke Au deposits, which have some different features, such as an association with igneous rocks, or with deposits of Hg, W, or U.

The *Songpangou* Au deposit is in a remote, mountainous area (elevation about 3,000 m, a.s.l.) of Sichuan Province, 83 km from the Pingwu County town (Fig. 5.23). The ore consists of sheared, stratabound, and layered bodies, locally exhibiting pinch-and-swell structures. The mine area contains two main clusters of orebodies. One of these cluster (eastern) contains three 400–100 m long, and from 7.5 to 2.6 m thick orebodies that grade 0.41–2.1 g/t Au. The main regional-scale ore controlling structure is the Snow Mountain Fault that cuts through the main part of the Songpangou deposit area. Orebodies are controlled by northeast-striking, bedding-parallel fracture zones. Host rocks are the upper member of the Middle Devonian Shanhe Formation, consisting of thin-bedded carbonaceous, argillaceous, silty slate, medium- to fine-grained psammitic sandstone, quartz sandstone, banded and lenticular limestone, and dolomite. Early Mesozoic granitic and dioritic dykes occur along the shear zones that host the Songpangou ore. Ore minerals are similar to those found in most Carlin-type deposits and include pyrite, arseniferous pyrite, realgar, orpiment, siderite, stibnite, cinnabar, arsenopyrite, rutile, sphalerite, and magnetite. Pyrite displays intense and intricate growth zoning of As-rich cores and As-poor rims or viceversa. Oxidation penetrates to a depth of 10–20 m. Supergene minerals include goethite, limonite, scorodite, and orpiment, as well as clay minerals. Botryoidal scorodite is present along oxidized fractures at the hypogene-supergene interface. The Songpangou Au deposit has anomalous abundances of As, Hg, Pb, Zn, Ni and Tl, an association considered typical of other Carlin type deposits in the west Qinling fold belt and in the Din-Qian-Gui (Guizhou) area (see Chap. 4). The host rock, ore textures and mineralogy of the Songpangou deposit have many similarities to the Au deposits in north central Nevada, USA, where intense brittle-ductile, carbonaceous deformation fabrics locally dominate in realgar- and orpiment-rich ore zones (Berger 1986; Hofstra and Cline 2000).

The *Qiaoqiaoshang* Au deposit is in the mountainous northeast part of Songpan County, Sichuan Province. The orebody is one of several Carlin-type deposits located along the east-striking Snow Mountains Fault. Orebodies are east striking, forming multi-layered, stratabound, lenses, veins, envelopes and columnar shaped. The ore zones, as defined by cut-off grades of 1 g/t Au, are north dipping 35° to 45°, from about 140–1,000 m long and 25–1.5 m wide. Maximum grades are about 3 g/t Au and average grade is 2.0 g/t Au. Mining is conducted on oxidised ore in the southern part of the area at lower elevations and in hypogene ores in the higher, northern part of the area. The Qiaoqiaoshang ore is hosted in the Upper Devonian Xindu Qiao Formation, which consists of an east-striking, north-dipping calcareous slate interlayered with psammitic quartz sandstone. The second most important ore horizon consists of thick sandstone interlayered with thin-bedded slate and silty sandstone. Ore shoots are present at intersections of fractures with north—and northeast-striking fractures and folds. Dykes of Yanshanian (185–67 Ma) granite are locally present in the host lithostratigraphy; however, pluton-related features, such as hornfelsing, calc-silicate development, and veining are not present near the orebodies. Oxidized ore is present from the surface to a depth of 30–50 m in the south orebodies, in which Au is associated with limonite. Primary ore lies below about 30–50 m, except in the northern parts of the mine area where it is within 5 m of the surface. Hypogene Au ore has a

cataclastic texture and is consists of disseminations, bedding parallel veinlets bands and networks. This cataclastic ore consists of pyrite, marcasite, realgar, cinnabar, arsenopyrite, stibnite, and chalcopyrite in a gangue of quartz, clay, sericite, calcite, dolomite, chlorite, carbonaceous material, rare alunite, and gypsum. Pyrite is the main Au carrier. Brecciated ore also contains realgar and orpiment and consists of fragments of sandstone, slate, and quartz vein material cemented by an argillaceous matrix. Gangue minerals are calcite, white mica, chlorite, sericite, calcareous material, and locally kaolinite, pyrophyllite, biotite, anhydrite, and calcanthite. The geochemical signature of the Qiaoqiaoshang deposit hypogene ores reflects the high-As sulphide mineralogy and also contains anomalous concentrations of Hg, Cu, Pb, Zn, Ni, and Co.

The *Dongbeizhai* Au deposit also in Songpan County, Sichuan Province, is about 17 km from the Songpan town. This deposit lies at 3,000 m a. s. l. in the mountains of northwest Sichuan Province in the West Qinling fold belt (Fig. 5.23). The Dongbeizhai deposit consists of 30 layered, tabular, and lens-shaped orebodies in the foot wall of a controlling fault. The ore layers and lenses generally pinch and swell, or branch, and merge. The orebodies are from about 1,520 m to 160 long, 4 m thick and 813–90 m deep, trend north-south, dip west at angles of 16° to 30°, and steepen to dips of 60° to 80° at depth. At the end of 1997, the deposit had a reserve of 52.8 tonne Au, with an average grade of 5.54 g/t Au.

The Liba Au deposit, in Lixian County, Gansu Province, is 32 km from the Lixian County town and is one of several that lie in a regional-scale cluster of other Carlin-style Au deposits in Gansu Province in the west Qinling area (Fig. 5.21). The deposit differs from other deposits in the region because it is hosted in low-grade metamorphic Devonian and Triassic meta-siltstone, phyllite and slate in the contact aureole of the Zhongchwan granite intrusion, about 2 km northeast from the granite contact. The Liba deposit contains more than 20 complex lenses along steep-dipping faults that crosscut sedimentary bedding. The No. 5 and No. 6 are the main orebodies accounting for 80 % of the total proven reserves of the deposit. The No. 5 orebody is 2,000 m long, 6–7 m thick and 250 m deep; the No. 6 orebody is 600 m long, 5–6 m thick and 250 m deep, with average grades of 5 g/t and 4 g/t Au, respectively. The west-northwest-striking, southwest dipping main fault is interpreted as a reverse fault that is characterized by multistage movements that favoured the flow of ore fluids. The main orebody is thickened and higher grade where northwest-striking faults intersect west-northwest-striking faults, with the intersection zone being characterised by densely spaced fractures. The sedimentary rocks in the Liba Au deposit area are Middle-Upper Devonian, Carboniferous and Permian in age. The Upper Devonian Dachaotan and Xihanshui, and the Middle Devonian Sujiaba formations consist of coarse-grained, alternating marine and continental sediments. The Liba orebodies are hosted in the 1,106 m thick Sujiaba Formation, mainly in layers dominated by silty phyllite and metasandstone. Carboniferous rocks consist of carbonaceous, clastic rock interlayered with limestone, conglomerate, and siliceous rocks. Lower Permian and lower Triassic sedimentary rocks are composed of shallow marine argillite, and clastic rock with interlayers of carbonate rock, especially at the top. The 210 km^2 Zhongchuan granite (Fig. 5.21) intrudes the Middle Devonian

to Middle Carboniferous sedimentary rocks south of the deposit. The nature of this granite and its age are not well constrained, but it is inferred to be a series of intrusions spanning the Hercynian (405–230 Ma), Indosinian (230–195 Ma), and early Yanshanian periods. The intrusions comprise six large late Mesozoic granitic bodies, several small Middle Palaeozoic mafic stocks and local andesitic porphyritic-dacite subvolcanic rocks, as well as Cenozoic alkalic to ultramafic volcanic rocks. Spessartite, diorite, oligoclase aplite, and granodiorite dykes also are present. Zones of contact metamorphism around the granite consist of: (1) chlorite-sericite, (2) biotite, and (3) andalusite + cordierite. Gold orebodies are in the biotite zone. The Mesozoic granitic intrusions have anomalous abundances of Sn, W, Mo, and Bi. Typical Carlin-type ore minerals (stibnite, cinnabar, realgar, and orpiment) do not occur in the Liba deposit. Instead the deposit contains a mineral assemblage of pyrite, arsenopyrite, pyrrhotite, chalcopyrite, sphalerite, galena, pyrrhotite, rutile, native Au, minor bornite, magnetite, marcasite, and electrum which indicates ore minerals reached temperatures higher than in most Carlin-style Au deposits. Sericitisation is closely associated with Au, where the alteration pattern is observed from inner to the outer zones of the orebodies from pyrite-sericite, to sericite, to chlorite. The intrusive rocks in the Liba area may have provided a heat source for the ore-forming system and may account for this different mineralogy. Most ores are disseminated, but also are present in stockworks and bands. Muscovite, sericite, and quartz are the main gangue minerals with lesser amounts of feldspar, chlorite, biotite, carbonate minerals, graphite, organic carbon, minor tourmaline, zircon, apatite, zeolite, and clay minerals. Pyrite and arsenopyrite are the main Au carriers. Gold lies mainly along the boundaries between pyrite, quartz, sericite and limonite. Limonite, hematite, and jarosite carry Au in the oxide zone. Fluid inclusion studies of ore minerals from the Liba Au deposit indicate salinities of between 6.9 and 11.6 wt % NaCl equivalent, and densities of 0.65–0.86 g/cm^3, which are compatible with igneous related ore processes, but also are consistent with thermally metamorphosed stratabound ore. Peters et al. (2001) pointed out that although the Liba Au deposit was included in the Carlin-type family, the deposit may be intrusion-related, or possibly a modified Carlin-type deposit.

The medium-sized (20–50 tonne Au) *Lianhechun* Au deposit is located along the border of northern Sichuan and southern Gansu Province (Fig. 5.23). The deposit consists of east- and northeast-striking, lenticular ore zones, grading about 3 g/t Au. Locally, the orebodies are spatially associated with Mesozoic granite porphyry dykes (Fig. 5.25). The Lianhechun deposit area is characterised by the east-striking Middle Triassic Zagunao Formation to the north and Carboniferous and Middle Devonian sedimentary rocks to the south. The Zagunao Formation is conformable on top of Carboniferous sedimentary rocks (Fig. 5.25). The main host rocks are Devonian and Carboniferous slate and limestone, as well as northeast-striking Mesozoic granite porphyry dykes. A 150–50 m wide fault zone (F2) at the contact between the Devonian and Carboniferous sedimentary rocks, may have exerted some structural control for the mineralised zones (Fig. 5.25). Fractures parallel to and within granite porphyry dykes may also be important controls. Hydrothermal alteration consists of quartz, calcite, sericite, barite, kaolinite, and fluorite. Main ore minerals are pyrite,

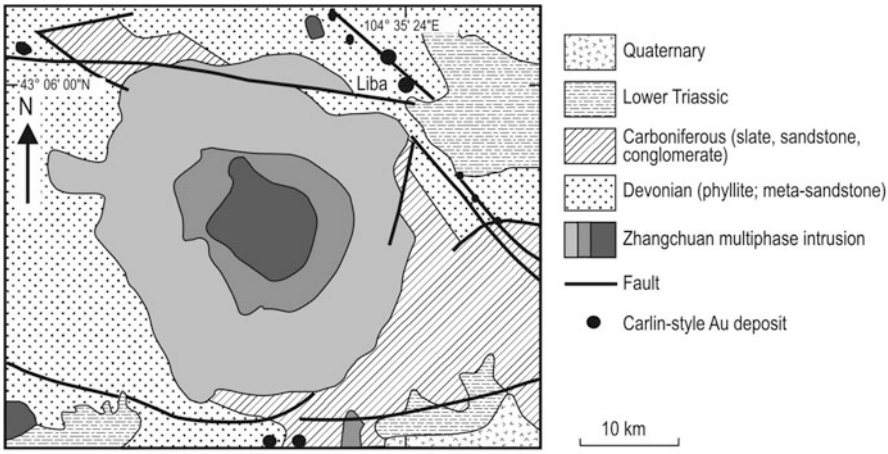

Fig. 5.24 Simplified geological map of the Liba Au deposit area. (After Peters et al. 2001)

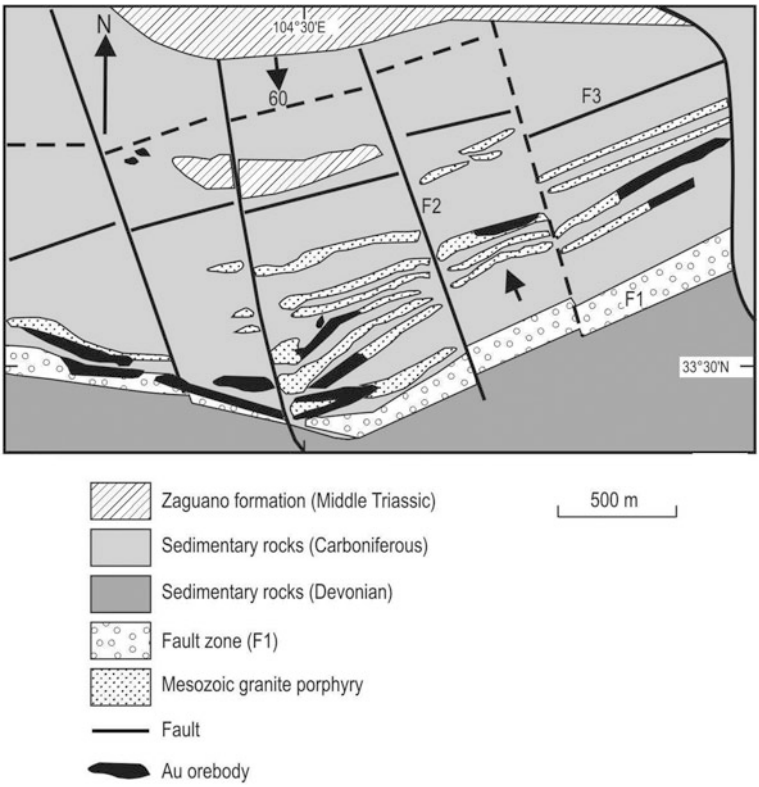

Fig. 5.25 Sketch cross-section of the Lianhechun Au deposit. (After Peters et al. 2001)

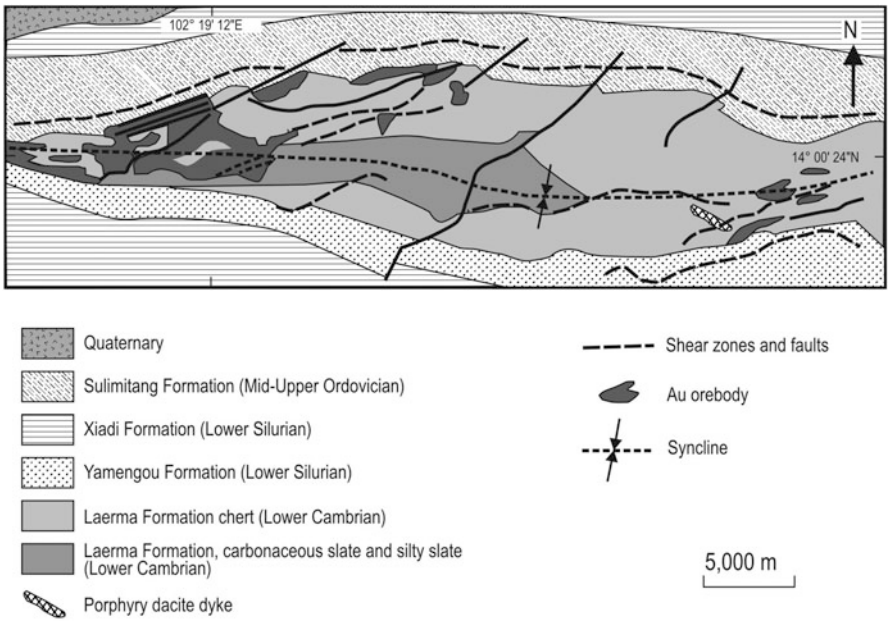

Fig. 5.26 Simplified geological map of the Laerma Au deposit area. (After Peters et al. 2001)

stibnite, arsenopyrite, pyrrhotite, cinnabar, and realgar. The ore zones are anomalous in Tl, Ba, Hg, Sb, and As.

The *Laerma* Au–U deposit, Gansu Province, (Figs. 5.21 and 5.26) is approximately 100 km north of the city of Ruoergai. The Laerma deposit mainly consists of a large number (>100) of ore zones, mostly lenticular in shape and up to 1,350 m long, grading between 1.0 and 24.7 g/t Au;. These orebodies cluster around a central pod-shaped zone, 200–100 m wide by 1,000 m long, with grades ≥3 g/t Au. Ages of the Au mineralisation in the Laerma deposit range from 49.5 to 12.7 Ma (Li and Li 1994). Uranium content of altered rocks ranges from 17 to 53 ppm U, with an average of 28 ppm. Faults in the mining district mainly trend east-west and fractures and other small structures trend northeast, northwest, and north-south (Fig. 5.26). Structural control at the Laerma Au–U deposit is related to these faults, particularly at their intersections. The deposit is hosted in rocks of the Lower Cambrian Taiyangding Group and Laerma Formations at the core of an east-plunging syncline. Three ore hosting horizons are present: (1) carbonaceous siliciclastics, carbonaceous siliceous slate, silty slate and carbonaceous slate; (2) carbonaceous slates, silty slate with layers of sericitic slate and phyllite; and (3) carbonaceous slate, sericitic slate and carbonaceous siltstone. Late Mesozoic to Early Cenozoic granite porphyry dykes locally are present and host some Au ore. There are more than 80 ore minerals associated with the deposit. Dominant ore minerals are: (1) pyrite, sphalerite, galena, chalcopyrite, chalcocite, pyrrhotite, marcasite, tetrahedrite, molybdenite, arsenopyrite, chalcomiclite, copper mica, gersdorffite, cinnabar, stibnite, realgar, orpiment,

and stibnite; (2) selenide minerals, tiemannite, clausthalite, stibioselenium; (3) Au–Ag minerals, native Au, kustelite, electrum; and (4) uraninite. Common gangue minerals are quartz, sericite, dickite, hydromica, chlorite, montmorillonite, kaolinite, illite, barite, gypsum, zeolite, chalcedonite, and dolomite. Barite, together with quartz, is present in veinlets and veins, which lie in alteration zones on the flanks of orebodies. Gold mainly is contained in pyrite, marcasite, quartz, barite, stibnite, and tiemannite, but also in realgar, orpiment, sphalerite, chalcopyrite, and siderite. Two types of pyrite, As-poor, and As-rich, are present in quartz-veinlets and in the host rock as disseminations. Pyrite with very low As has a corresponding low Au content, suggesting that the ability of pyrite to host sub-micron Au depends on its As content. Quartz also is a common host mineral of Au in the Laerma, containing 1–28 ppm Au, 13 ppm Hg, and elevated concentrations of As and Sb. Gold-bearing quartz can be distinguished from barren quartz by its high Al_2O_3 contents (>0.20 wt %); (2) high Hg content; and (3) high correlation of Au to high thermoluminescence values of quartz. Barite contains between 1 and 98 ppm Au, and also has elevated values of Ag, Sb, Se, and Hg. Alteration at the Laerma deposit consists of early pervasive silica with chlorite followed by fracture filling with quartz–calcite, sericite, and barite. These fracture-fill minerals are accompanied by decarbonatisation and the growth of dickite and allophane. The ores are anomalous in As, Sb, Hg, Ba, Se, U, and PGE. Organic C is enriched in the host rocks with a range from 0.66 to 14.63 wt % and an average of 3.24 wt % C. Gold concentration is closely related to organic C, such that Au content is much higher in carbonaceous silty slate than in silty slate. PGEs are enriched in the ore and in cataclastic carbonaceous siliceous slate. On the basis of analysis of 20 ore samples: Pt content ranges from 0.01 to 0.02 ppm, Pd content ranges from 0.001 to 0.024 ppm; Os content ranges from 0.001 to 0.005 ppm. PGEs locally are concentrated to form economic orebodies. The presence of the several base-metal minerals, uranium and PGE minerals may indicate either an evolved Carlin-type system, access of the mineralizing system to additional minerals at depth, overprinting of two separate hydrothermal systems, or a hydrothermal process similar to but distinct from those which form Carlin-type deposits.

The large-sized (>50 tonne Au) Manaoke Au–W deposit is in northern Sichuan Province approximately 60 km northwest of the city of Jiushigou along the Sichuan-Gansu Province boundary (Fig. 5.21). Ore minerals are pyrite, scheelite, tungstite, realgar, arsenopyrite, stibnite, and native Au, with euhedral, subeuhedral, and anhedral textures. The ore can be massive, disseminated, vein-network, cataclastic and as breccia bodies. Native Au is sub-micron- to micron size within arsenopyrite, pyrite, clay mineral grains and surrounding quartz grains. Locally, visible gold is present and is associated with quartz-stibnite intergrowth, where it commonly fills the boundary between the two minerals and generally is 0.05–0.2 mm in size. The geochemical signature of the Manaoke Au–W ores is characterised by anomalous concentrations of As, W, Sb, and Hg. Mineralogy of the ores is similar to most Carlin-type deposits, but this deposit too is unusual because of the W-bearing horizons, which may have developed separately. Tungsten-bearing minerals associated with quartz-pyrite veining have been recorded in the large Carlin-type Betze Au deposit in Nevada (Peters

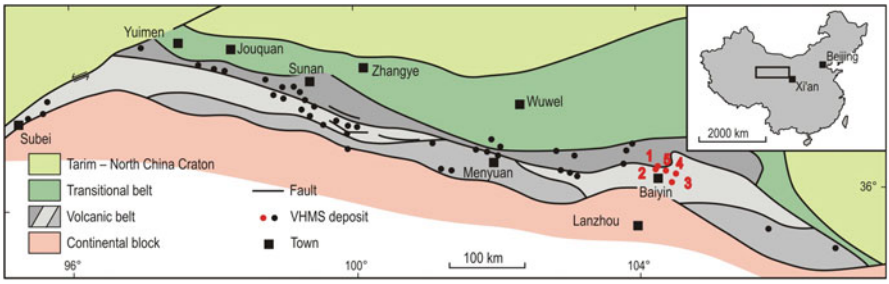

Fig. 5.27 Distribution of VMS deposits in the North Qilian orogen in NW China; deposits shown in *red* are *1* Zheyaoshan, *2* Huoyanshan, *3* Xiaotieshan, *4* Tongchangou, *5* Sigequan. (After Hou et al. 2008)

et al. 1998). Therefore, is possible that the W mineralisation may possibly also be related to the Au mineralizing event in some Carlin-type deposits.

5.3.3.5 Qilian Orogen and VMS Deposits in Gansu Province

The Qilian orogen (fold belt) can be considered as the western extension of the Qinling-Dabie orogenic belt (Figs. 2.3 and 5.19), striking west-northwest from Gansu Province, to Qinghai, Shaanxi and Henan provinces. The orogen is bound to the south by the Qaidam and the Songpan-Ganzi terranes (Chap. 6), whereas to the northwest by the Altyn-Tagh fault zone. Surprisingly little is published, at least in English-language papers, specifically addressing the geology of the Qilian orogen. Yang et al. (2001) described some of principal tectonic units of the Qilian belt. These authors recognised a volcanic arc (North Qilian arc), an ophiolite mélange complex and a central Qilian Block. In the geodynamic model proposed by Yang et al. (2001), during Early Palaeozoic northward-subduction of north Qilian ocean, resulted in the development of the North Qilian volcanic arc and a back-arc basin. In the latter, bimodal volcanism was responsible for the formation of three volcanic belts at about 480–460 Ma. Closure of the north Qilian ocean and back-arc basin took place between 460 and 420 Ma, resulting in the Qilian orogen or fold belt.

In southeastern Gansu Province, the Qilian orogen hosts at least 22 VMS deposits (Fig. 5.27), associated with felsic volcanic domes in the above-mentioned three major volcanic belts. The VMS deposits are in a submarine volcanic belt, about 1,200 km long and 50 km wide, at the southeast margin of the Tarim Craton, consisting of bimodal volcanic rocks ranging in age from 606 to 522 Ma (Sm-Nd isotopic system; Hou et al. 2008 and references therein). This volcanic belt was subjected to intense tectonic activity that culminated with rifting processes in the Proterozoic basement. Hou et al. (2008) studied in some detail the Baiyinchang VMS system and the following is summarised from these authors.

Five deposits at the eastern end of the ore belt (Fig. 5.27) have different metal assemblages: Zheyaoshan Cu, Huoyanshan Cu, Xiaotieshan Zn-Pb-Cu, Tongchangou

Cu-Zn and Sigequan Zn-Pb-Cu, each characterised by alteration pipes, zoned from chlorite in the core to quartz-sericite at the periphery. The five deposits are hosted by the 7 km-long, 5.6 km wide, Baiyin volcanic dome, which consist of a sequence of felsic volcanic rocks about 700 m thick, overlain by basaltic volcanic rocks. Two mines, Zheyashan and Huoyanshan, constitute the Baiyinchang VMS system studied by Hou and co-workers (Fig. 5.27). Zheyashan had 51 Mt of Cu ore (0.9 Mt remaining), whereas the Huoyanshan mine had 15 Mt of Cu ore. Grades range from 0.4 to 4.6 % Cu equivalent, averaging 1.17 %. The Baiyinchang VMS system consists of massive sulphides, disseminated sulphides and stringer ores. The orebodies can be stratabound with distal exhalites, probably deposited on the sea floor, and discordant massive sulphides hosted in felsic volcanic rocks. The Zheyaoshan orebody is a stratabound massive sulphide lens, underlain by stringer sulphide veins, enveloped in an alteration pipe, which is larger than the overlying sulphide lens and for this reason, Hou et al. (2008) consider Zheyaoshan as a pipe-style deposit. Massive sulphides contain 90 % of the Cu ore, are discordant to local bedding and are enclosed in felsic pyroclastic and lavas. The massive sulphide zone of the Zheyaoshan deposit is about 600 m long and 50 m wide, forming a series of steeply dipping lenses and consisting of a massive pyrrhotite-pyrite pipe, massive sulphide lenses surrounded by a halo of disseminated sulphides and a footwall stringer zone. The massive pyrrhotite pipe is elliptical and 50×30 m in plan view and extends to a depth of at least 150 m. The mineralogy is simple with pyrrhotite, pyrite, chalcopyrite, minor magnetite, galena and sphalerite. The pipe is concentrically zoned with a marginal zone of honeycomb, porous pyrite, a middle zone of massibe pyrrhotite-pyrite and an inner zone of stringer veinlets of chalcopyrite. The series of sulphide lenses range in length from 100 to 600 m, extending downdip for about 50–200 m and consist of three types of ores: pyrite-chalcopyrite, sphalerite-rich pyrite ore and chalcopyrite-rich pyrite ore. The sulphide ores are associated with Fe-Mn exhalites that form mound-shaped lenses from 30 to 50 m thick, unconformably overlain by black shale and limestone. One exhalite unit is more than 80 m thick and consist of hematite chert, Fe-Mn chert and Mn-Fe nodules.

Hou et al. (2008) carried out fluid inclusion and stable isotope studies for the host rocks and sulphide ores. They found four types of primary, pseudosecondary and secondary fluid inclusions: Type I two-phase fluid inclusions in massive sulphides, subdivided into Ia, Ib and Ic; type II multiphase inclusions with daughter minerals (mostly halite); type III CO_2-rich monophase and liquid CO_2-vapour CO_2 inclusions; type IV CH_4-rich inclusions. Microthermometric measurements for type I inclusions of massive sulphides showed variable homogenisation temperatures and salinities, from 405 to 90 °C and 3.1–19.8 wt % NaCl equiv., respectively for type Ia; 435–235 °C and 5.5–10.5 wt % NaCl equiv., respectively for type Ib inclusions in the stringer zone; and 485–378 °C and 16.1–11.1 wt % NaCl equiv., respectively for vapour-rich type Ic inclusions. Type Ia inclusions of wallrocks gave homogenisation temperatures of 175–75 °C and salinities of 20.8–4.5 wt % NaCl equiv. Type II inclusions in the stringer zone and in quartz recorded homogenisation temperatures of 400–350 °C and salinities of 38–31 wt % NaCl equiv. Type III, also in quartz and stringer zone, recorded homogenisation temperatures ranging from 348 to 226 °C and

salinities from 2.3 to 8.1 wt % NaCl equiv. The $\delta^{18}O$ from quartz show a limited range from 11.1 to 8.8 ‰, similar but slightly higher than the Kuroko deposits in Japan. Calculated $\delta^{18}O$ of ore fluids that precipitated quartz have a range of values from −0.16 to 3.91 ‰ for the massive ores and from −5.27 to 3.10 ‰ for the stringer zone. Fluid inclusions and stable isotopes support a sea water origin for the hydrothermal fluids, as is the case for VMS deposits, world-wide. The genetic model for the Baiyinchang VMS system, proposed by Hou et al. (2008), on the basis of their data, suggests that the emplacement of a felsic stock acted as a heat source that allowed the convective circulation of sea water. Hydrothermal fluids discharged on the sea floor as saline brines through a pipe-like zone and the discordant sulphide lenses formed by interaction of these brines with cold sea water, while lateral movement of hydrothermal fluids resulted in a halo of disseminated sulphides. Stratabound ore zones formed through the venting of the fluids on the sea floor.

5.4 Hinggan (Hing'an, Xing'an) Orogenic Belt, Northeast China

The closure of the Palaeo-Asian Ocean separating the NCC from the Siberian plate resulted in the formation of the Altai and Tianshan-Yishan-Great Xing'an orogenic belts (also called Tianshan-Hinggan fold belts or Xing'an-Mongolian Orogenic belt; hereinafter referred to as Hinggan), which is part of the Central Asian Orogenic Belt (CAOB, see Chap. 6). The CAOB is comprehensively described by Şengör and Natal'in (1996), Yakubchuk (2004) and Windley et al. (2007). To the west are the Altai (also spelt Altay) and the Tianshan fold belts, separated by the Junggar and Turpan blocks (basins). These units are discussed in some detail in Chap. 6, whereas in this section I focus on the Hinggan orogenic belt.

The Hinggan orogenic belt located between the northern margin of the NCC, the Jiamusi Block and the Erguna Block to the northeast, experienced a complex and protracted geodynamic evolution. From late Palaeozoic to early Mesozoic, closures of the Palaeo-Asian Ocean and the Mongol-Okhotsk Ocean and the final collision between the NCC and the Siberian Platform took place (Guo et al. 2001). Late Palaeozoic arc magmas are spread out along the east-west-trending faults (e.g. Datong-Chengde) as well as zoned mafic-ultramafic intrusions, in the northern margin of the NCC (Fig. 3.7). The Jiamusi and Erguna Blocks (also referred to as massifs or terranes, but probably best termed inliers) are microcontinental fragments located at the eastern end of the CAOB (Wu et al. 2012). The Erguna and Jiamusi inliers contain granulite facies metamorphic rocks, including sillimanite- and garnet-gneiss, biotite-plagioclase gneiss, hornblende-plagioclase gneiss, granitic orthogneiss and carbonate rocks (called khondalites; see Chap. 3), which are part of the ca. 496 Ma Mohe Complex and Mashan Complex, respectively (Zhou et al. 2011). About 1,000 km to the southeast is the ca. 490 Ma Hutou Complex with similar rocks.

The youngest rocks with typical subduction-related characteristics are of late Carboniferous to Permian age, recording ridge-trench and forearc collisions, followed

by slab break-off (Jian et al. 2010), whereas the oldest post-collision and intra-plate igneous rocks are of middle to late Mesozoic age (Davis et al. 2001). This relationship indicates that the Palaeo-Asian Ocean closed sometime during the very late Palaeozoic to early Mesozoic (Natal'in and Şengör 2005). The presence of mixed biota in Middle Permian lithologies marks the beginning of the collision between the NCC and the Siberian Platform. The end of the collision is marked by the molasse in the Early-Middle Triassic and the magmatic activity during the Middle Triassic. The area then entered into a post-collision intra-plate tectonic regime, characterized by intense volcanic activity and basin-and-range style tectonics in the Jurassic and Cretaceous (Fan et al. 2003; Davis et al. 2004). Shao et al. (2001) proposed that the lithosphere in northeast China was continuously in extension from Late Jurassic to early Cretaceous, on the basis of a mafic dyke swarms and the frequent magmatic activity, which evolved from calc-alkaline, to alkali-calcic, to alkaline series. Zhai et al. (2004) also suggested that northeast China had entered a stage of transition from compressional to extensional tectonics, starting at about 150 Ma, with a peak of activity at 120–110 Ma. The basin-and-range structures changed from east-west-trending to northeast-north-northeast-trending. Widespread metallogeny occurred due to the intensive tectonic-magmatic activity in the Mesozoic with three main pulses: ca. 190–160 Ma, ca. 140 Ma and ca. 120 Ma, which correspond with collisional orogeny, transition from compression to extension and delamination of lithosphere, respectively (Chen et al. 1998; Zhai et al. 2001; Mao et al. 2010).

The Hinggan Orogen in northeastern China is in the eastern part of the Altaids (Şengör and Natal'in 1996), and is bound by the Solonker suture and the Kangbao-Chifeng fault that separates the terranes of the Altaids from the Sino-Korean craton in the south (see Figs. 2.1, 2.4 and 6.3). The position of the final suturing between these plates and its timing are still debated. One group of researchers suggested that the Hegenshan ophiolite zone represents the final suture, with closure disputed as late Devonian-early Carboniferous, Permian or early Triassic (Robinson et al. 1999). Another group argues that the Wenduermiao-Yanji suture, which separates significantly different biotas (Şengör and Natal'in 1996) and stratigraphic assemblages, represents the final closure of the Palaeo-Asian Ocean in late Permian. According to Şengör and Natal'in (1996), Xiao et al. (2003, 2004) these two sutures represent the closure of the Palaeo-Asian Ocean with associated island arcs. Widespread development of the Permo-Triassic marine successions, as observed in the Lesser Hinggan Range areas, suggests that the final closure of the Palaeo-Asian Ocean could not predate the early Triassic. Northeastern China was involved in subduction and closure of the Mongolia-Okhotsk oceanic plate and also affected by subduction of the Palaeo-Pacific plate during Triassic-early Cretaceous time.

During the Mesozoic this part of the Altaids orogenic belt (CAOB) probably completed its compressive history related to the closure of Palaeo-Asian Ocean during the late Triassic to early Jurassic, indicated by widespread A-type granites (220–190 Ma) (Wu et al. 2002), when the Mongolia-Okhotsk oceanic plate was subducted beneath the Mongolia-North China continent (Zorin 1999). Mesozoic granites, porphyries, breccia-pipes and volcanic rocks were widely developed as part of the Yanshanian

tectono-thermal event, which was also characterized by the formation of the porphyry, epithermal precious and base metal deposits, discussed in this section.

At the early/middle Jurassic boundary, the Mongolia-Okhotsk Ocean was closed, involving thrusting, folding and magmatism, which lasted through middle and late Jurassic (Zorin 1999; Zorin et al. 2001). In the early Cretaceous, rifting, rotation, strike-slip, thrusting, crustal thickening and uplift occurred, which were caused by both post-collision following the closure of the Mongolia-Okhotsk Ocean and northward subduction of Palaeo-Pacific oceanic plate, and reached peak activity at 121–130 Ma, indicated by Ar-Ar dating of syn-tectonic muscovite and biotite of left-lateral strike-slip faults of northern Great Hinggan Range (Zorin 1999). During this time, the Palaeo-Pacific oceanic plate moved northward rapidly, resulting in strike-slip movement of main faults and orogenic collapse (Li et al. 2007).

In Inner Mongolia, the Solonker suture and adjacent areas have been investigated by Robinson et al. (1999), Miao et al. (2008) and Xiao et al. (2003). The Solonker suture is also known by several other names (a common problem with Chinese lithostratigraphic and tectonic nomenclatures), such as Solon Obo, Suloshan-Hegenshan, Hegenshan-Nenjiang-Heihe etc. As mentioned above and according to Şengör and Natal'in (1996), the suture separates the CAOB from the Manchurides fold belt, which was formed by collision and accretion of a subduction complex between the Siberian (Angara) craton and the North China Craton (Figs. 5.28 and 5.29). The Solonker suture is a belt of mélange, blueschist and ophiolitic rocks, about 700 km long and 60 km wide (Xiao et al. 2003). The mélange contains blocks of carbonate rocks, mafic and ultramafic rocks and marble, set in two major accretionary complexes, namely the Ondor Sum subduction-accretion complex and the Erdaojing accretion complex, squeezed between sections of the Bainiaomiao arc (see below). The Hegenshan ophiolite complex consists of blocks of serpentinised harzburgite and dunite, with lesser cumulate gabbro, mafic lavas and dykes, with ages of 295–298 Ma and intruded by 244 Ma granodiorite dykes (Miao et al. 2008). On the basis of high Nd isotopic signatures ($\varepsilon Nd(t) = +8.1$ to $+10$), Miao et al. (2008) suggested that the Hegenshan ophiolite was derived from oceanic crust of the Palaeo-Asian Ocean, formed in a supra-subduction zone setting.

The tectonic belts and the Solonker suture in Inner Mongolia are the result of collision and accretion of volcanic island and continental arcs, described by Xiao et al. (2003) and summarised here. The area investigated by Xiao et al. (2003) is shown in Fig. 5.29. The accretionary complexes made up of volcanic arcs occur both north and south of the Solonker suture. The southern accretionary zone contains the Mid-Ordovician-Early Silurian Ulan and Bainiamiao island arcs and the Ondor-Sum subduction-accretion complex. The entire southern zone then evolved into an Andean-type magmatic arc above a south-dipping subduction zone. The zone north of the suture contains the Hegenshan ophiolite-arc complex and the Late Carboniferous Baolidao Arc, together with remnants of Precambrian blocks. The northern zone also developed into an Andean-type magmatic arc, with a north-dipping subduction zone. Thus, the end result by the end of the Permian there were two opposing Andean-type continental margins, which collided to form the Solonker suture.

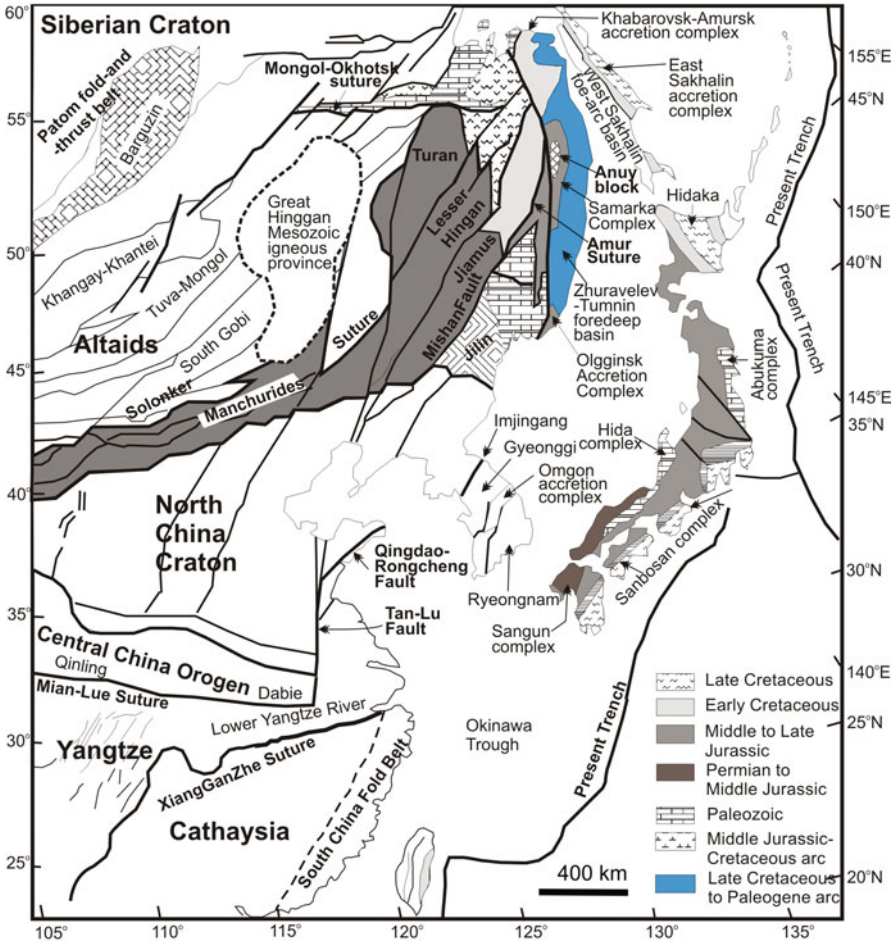

Fig. 5.28 Fold belts of the Central Asian Orogenic Belt (Altaids), the Hinggan fold belts (or Manchurides) and sutures that separate the North China Craton from the Siberian (Angara) Craton. (Modified after Şengör and Natal'in 1996)

The Bainiamiao Arc is bound to the south by the Chifeng-Bayan Obo Fault forming the northern boundary of the NCC (Fig. 5.29). This ancient island arc contains calc-alkaline tholeiitic basalts, felsic volcanics, alkaline basalts, pyroclastic rocks, granites and granodiorites with a Sm-Nd age of ca. 429 Ma. Furthermore, Andean-style porphyry Cu-Mo and lode Au deposits are present in rocks of this magmatic arc, but later affected by deformation and metamorphism during collision tectonics (Li et al. in press). To the north is the Ondor Sum subduction-accretion complex, which consists of an ophiolitic mélange, the deformed remnants of the island arc and a mylonite zone, which is interpreted to represent a high-pressure subduction complex. The mylonite also contains quartzite-chert, marble, quartz-pyrite-hematite,

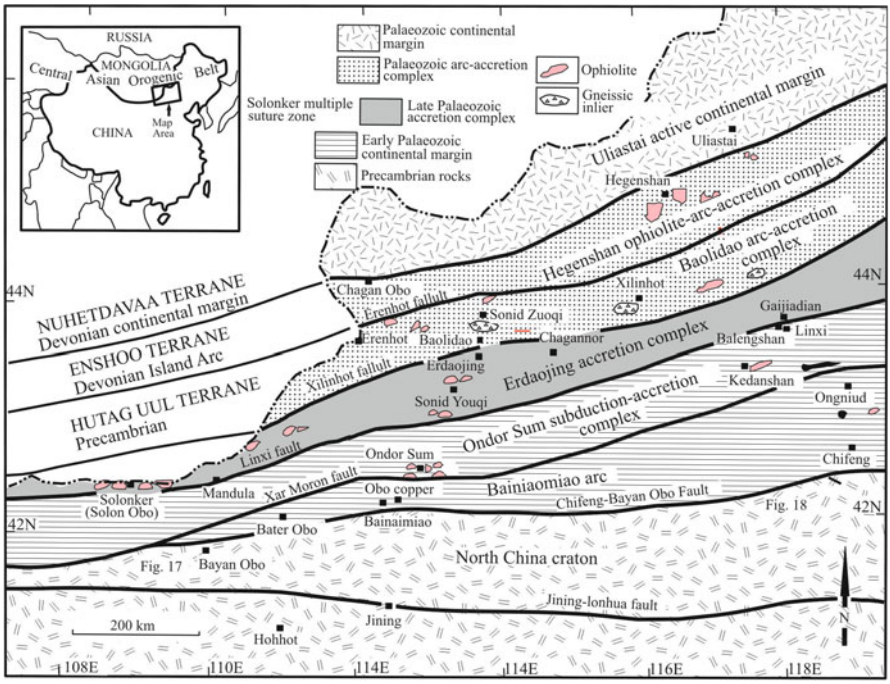

Fig. 5.29 Simplified geological map of central Inner Mongolia, showing east-west and east-northeast-trending tectonic belts, accreted island arcs and suture zones marked by ophiolitic rocks, just south of the Ondor Sum town are the Obo Copper sites, where porphyry systems related to the Mid-Palaeozoic Bainaimiao Arc (details in text). (After Xiao et al. 2003)

magnetite-pyrolusite, quartz-sericite schist, chlorite schist and chlorite-magnetite-epidote schist. Some of these rocks have been interpreted to represent fragments of ocean floor chert enriched in Fe and Mn tectonically interleaved with slices of basalt and gabbro (Xiao et al. 2003). The Baolidao Arc and the Ondor Sum subduction complex now forming a north-dipping thrust belt, also contain lenses of ophiolitic rocks. The Baolidao Arc consists of deformed gabbro, diorite, tonalite and granodiorite rocks with U-Pb zircon ages of ca. 310 Ma.

The Uliastai passive and active continental margins lie north of the Hegenshan ophiolite belt (Xiao et al. 2003). The passive margin sequence is represented by Cambrian limestone and siltstone, about 100 m thick, deposited on a basement of Proterozoic gneissic rocks. The change from passive to active margin occurred in the Ordovician with the deposition of about 2 km-thick succession of calc-alkaline andesite, tuffs and tuffaceous sandstone. In Mid-Late Devonian, andesite, basalt, porphyries and pyroclastic rocks define another major continental arc. These rocks are associated with shallow marine to continental limestone, siltstone, sandstone and arkosic sediments (Xiao et al. 2003 and references therein). In the lower Permian, another continental volcanic arc was formed with calc-alkaline volcanic and pyroclastic rocks. All these volcanic rocks (Devonian and Permian, with intervening

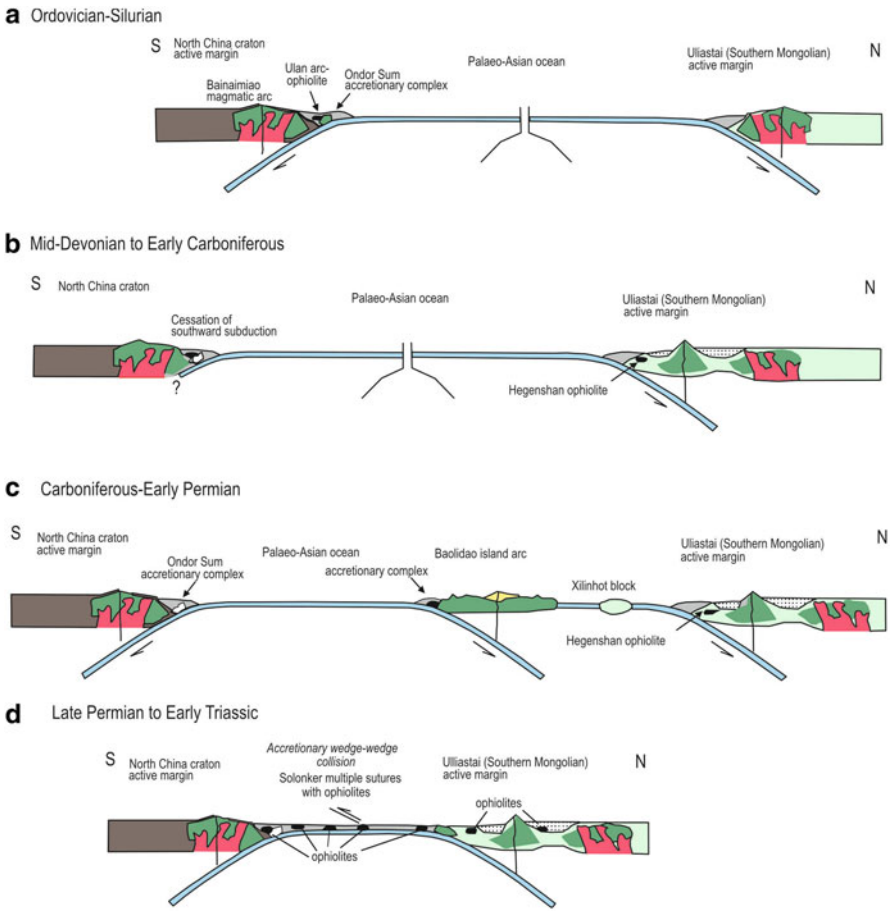

Fig. 5.30 Schematic representation of the geodynamic evolution of the terranes north and south of the Palaeo-Asian Ocean. (After Xiao et al. 2003)

Carboniferous sediments) were intruded by calc-alkaline Andean-type granitic plutons. The Uliastai arcs continue westward into Mongolia, where they are part of the Nuhetdavaa terrane.

In the final analysis, the Solonker suture zones and adjacent terranes north of the Chifeng-Bayan Obo Fault, would represent an ancient Palaeo-Asian Ocean, north of the Tarim-North China Cratons with north and south dipping subduction zones, volcanic arcs and back-arc basins. Further north was the Mongol-Okhotsk Ocean and a south-dipping subduction zone. The closure of these palaeooceans led to the complex array of accreted arc-back-arc-continental margin-ophiolitic terranes. The evolution of this part of the CAOB, as envisaged by Xiao et al. (2003) is shown in Fig. 5.30.

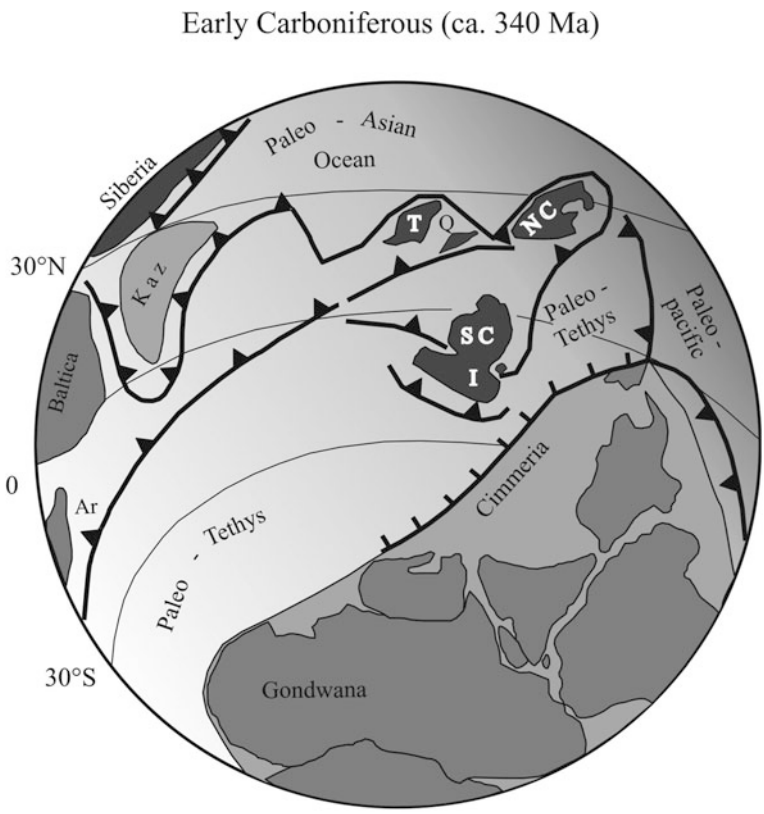

Fig. 5.31 Reconstruction of microcontinents on the northern margin of Gondwana in the Early Carboniferous (ca. 340 Ma); *T* Tarim, *Q* Qaidam, *NC* North China Crtaon, *SC* South China Block, *I* Indochina, *Kaz* Kazakhstan. (After de Jong et al. 2006)

De Jong et al. (2006), on the basis of new Ar-Ar data from blue schist rocks in the Ondor Sum subduction-accretion complex, argued that this complex developed along the northeastern margin of the Gondwana continent, which in the early Palaeozoic consisted of a number of microcontinents, fringed by subduction-accretion complexes, Andean-type continental margins and island arcs. These microcontinents included the South China Block, Tarim, the Alshan and Qaidam terranes (see Figs. 2.2 and 2.3), thereby forming a vast orogenic systems, or, as aptly put by de Jong et al. (2006), an archipelago of microcontinents and island arcs. This model of archipelago orogenesis was also proposed by Hsü et al. (1995) for the amalgamation of Tibet and Cathaysia on the northern margin of Gondwana. A reconstruction of lithospheric plates and position of microcontinents bordered and encircled by subduction zones is shown in Fig. 5.31.

5.4.1 Indosinian and Yanshanian Magmatism

Indosinian to Yanshanian intraplate magmatism overprinted the Hinggan fold belt and is associated with mineral systems. Magmatism during late Jurassic to early Cretaceous includes calc-alkaline to high-K calc-alkaline volcanic rocks and subvolcanic intrusions. Late Mesozoic volcanic rocks in northeastern China can be divided into two volcanic belts, separated by the Songliao basin. West of the Basin is the Great Hinggan Range volcanic province (Fig. 5.28) and an eastern volcanic belt on the other side. In the north of the Great Hinggan Range volcanic belt, late Mesozoic volcanic rocks mainly consist of three formations, which from lower to upper include: Tamulangou, Shangkuli and Yidelieke formations. The Tamulangou formation comprises olivine basalt, basalt, basaltic andesite, trachyandesite and welded tuff. Recent geochronological results indicate that this formation formed during the early Cretaceous (147–122 Ma, U-Pb, Ar-Ar methods), and to a lesser extent in late Jurassic (163–160 Ma, U-Pb, Ar-Ar) (Fan et al. 2003; Zhang et al. 2006). The Shangkuli formation is composed of a felsic volcanic sequence including rhyolite, rhyolite dacite, dacite, rhyolitic welded tuff, which was formed mainly between 135–111 Ma and to a lesser extent between 148–138 Ma (Fan et al. 2003; Wang et al. 2006). The Yidelieke formation, consisting of intermediate-mafic volcanic rocks, primarily include olivine basalt, trachyandesite, and trachybasalt, with ages between 126–101 Ma (Fan et al. 2003; Wang et al. 2006). In the south of the Great Hinggan Range, Mesozoic volcanic rocks mainly comprise a bimodal assemblage composed of basaltic andesite and dacite-rhyolite with isotopic ages of between 173–122 Ma (U-Pb). The Manitu and Baiyingaolao formations are intermediate-felsic assemblages, including andesite, dacite, and rhyolite, and has ages ranging from 134 to 124 Ma (U-Pb; Zhang 2006a). These studies demonstrate that the late Mesozoic volcanic rocks in the Great Hinggan Range were formed during late Jurassic to early Cretaceous. Late Mesozoic volcanic rocks in the Great Hinggan Range generally have calc-alkaline to high-K calc-alkaline characteristics, with minor alkaline basaltic series. Lin et al. (2003) proposed that these volcanic rocks constitute bimodal assemblages, in which low-Sr rhyolites and alkaline basaltic rocks in north Great Hinggan Range are typical of continental rift settings. However, high-Sr rhyolites and subalkaline basaltic rocks in south Great Hinggan Range show a range of geochemical variations, typical of calc-alkaline suites. Compared to bimodal basalt-rhyolite associations of the Great Basin in the USA (John 2001), the volcanic sequences in northeastern China show higher K_2O and $K_2O + Na_2O$ contents, lack low-SiO_2 basalts, and comprise many intermediate components. In the eastern volcanic belt, Mesozoic volcanic sequences mainly include intermediate-felsic volcanic rocks with ages between 118 and 106 Ma (Li et al. 2007). Different interpretations on the origins of late Jurassic to early Cretaceous volcanic rocks in northeastern China have been proposed. These include: (1) westward subduction of Palaeo-Pacific Ocean (Zhao et al. 1998); (2) mantle plume (Lin et al. 1998); (3) post-orogenic extension related to the closure of Palaeo-Asian and/or Mongolia-Okhotsk Ocean (Fan et al. 2003; Li et al. 2007); (4) removal

of subcontinental lithospheric mantle and upwelling asthenopsheric mantle (Zhang et al. 2006; Wang et al. 2006).

5.4.2 *Hydrothermal Mineral Systems*

The Hinggan orogenic belt is host to a large number of hydrothermal mineral systems, whose resources, nature and origin are not clearly established. In this section, I draw in part from unpublished data by Qi JP (Guanzhou Institute of Geochemistry), Chen YJ (Peking University) as well as earlier publications (Qi et al. 2005b, c; Pirajno 2006) with some modifications, based on my own field work in the region. The mineral systems of the Hinggan region include porphyry, skarns, epithermal and intrusion-related veins. Stable isotopic data (see below) suggest that the mineral systems of the Great Hinggan Range are closely associated with magmas and that the ore fluids were generated from these magmas and later modified by interaction with meteoric waters. A selection of these deposits is listed in Table 5.3 their distribution shown in Fig. 5.32.

The mineral systems of the Hinggan orogen are associated with superimposed Yanshanian volcanic rocks and volcano-sedimentary basins. The Hinggan mineral deposits can be grouped into: porphyry Mo, low-sulphide Au-Ag, high sulphide Au-Cu-Zn, and Ag-enriched polymetallic deposits. These occur in four districts or provinces: namely the northern Great Hinggan Range, the southern Great Hinggan Range, the Lesser Hinggan Range and Changbaishan (Fig. 5.32a). These deposits are hosted in late Jurassic to Early Cretaceous volcanic rocks, which were erupted during transitional regimes from uplift to basin formation. In general the deposits are sited: (1) along the margin of Mesozoic volcanic basins; for example, the Siwu Meadow Au deposit at the western margin of the Hailaer basin; (2) in volcanic depressions superimposed on uplifted basement; for example, the Moerdaoga Au and Xijinuo Pb-Zn deposits, in the volcanic depressions of the Erguna Massif; and (3) in the uplifted parts of volcanic basins; for example the Dong'an Au deposit located in a north-trending range, within the Mesozoic-Cenozoic Xunke basin (Fig. 5.32). In the Northern Great Hinggan Range metallogenic district (A in Fig. 5.32) there are at least 20 deposits, including low-sulphide Au, high sulphide Au-Cu-Zn and Ag-rich polymetallic occurrences. The Wunugetushan porphyry Cu-Mo system (see below) is located in this district. In the Lesser Hinggan Range district (C in Fig. 5.32), is the important Tuanjiegou deposit with Au reserves of about 80 tonnes, consisting of ore lenses in the apical portions of a granite porphyry, associated with a breccia pipe, intruding volcanic rocks and (Fig. 5.32a). In the northern part of the Songneng terrane (C in Fig. 5.32) is the Naoniushan Cu-Au mineralisation, hosted in a granite porphyry characterised by silica and K-feldspar alteration, suggesting the presence of a porphyry system at depth. Examples of mineral deposits in the Great Hinggan Range are shown in Fig. 5.32. Placer gold is common in northern Heilongjiang province. The large-scale mining of placer Au deposits has lasted more than 100 years since the Qing Dynasty. At least 60 placers Au deposits are distributed in Mohe, Heihe

Table 5.3 Principal geological characteristics of epithermal and intrusion-related vein deposits in northeastern China. (Compiled from Qi JP, Chen YJ and Pirajno unpublished data); see also Fig. 5.32

No. in Fig. 5.31	Deposit/county/province	Metal	Resource where known (Au Ag t/Cu PbZn Mt)	Grade, where known (g/t Au, %Pb, Zn)	Ore minerals	Main hydrothermal alteration minerals	Wall-rock and its age	Ore style	Ref.
1	Shabaosi/Mohe/Heilongjiang	Au			Py, apy, sp, cp, ga, mo, mag, li, Au, el	Q, cal, chl, ba, bi, mica, ep, graphite	Middle Jurassic sandstones and Proterozoic marbles	Lenticular or, stratiform	22
2	Ergenhe/Mohe/Heilongjiang	Au	Occurrence		Py, sb, Au	Q, cd, Ser, Chl, Kao	Middle Jurassic to Early Cretaceous sandstone, dacites	Vein, breccia	38
3	Yesuoku/Mohe/Heilongjiang	Au	Occurrence		Py, Au	Argillic, Q, carb	Early Cretaceous rhyolite and tuff	Vein	36
4	Mada'er/Mohe/Heilongjiang	Au	Occurrence		Py, mar, cp, pyrolusite, Au, Ag	Q, carb, ser, chl	Late Jurassic volcanic rocks	Vein	2, 3
5	Aolaqi/Mohe/Heilongjiang	Au	Occurrence		Py, cp, ga, sph, Au, el	Q, ser, kao, montmoril-lonite, carb	Early Cretaceous rhyolitic volcanic rocks	Vein	2, 36
6	Xijinuo Shan/Huzhong/Heilongjiang	Pb, Zn, Cu	Occurrence		Ga, cp, sph, py, Au; lesser co, ilmenite	Q, chl, ep, carb	Late Jurassic andesite-trachyandesite	Vein, lenticular	25, 36
7	Moerdaoga/Erguna/Inner Mongolia	Au	1.7		Py	Ser, Q, cal, adu	Early Cretaceous rhyolite	Vein	23, 32

Table 5.3 (continued)

No. in Fig. 5.31	Deposit/county/province	Metal	Resource where known (Au Ag t/Cu PbZn Mt)	Grade, where known (g/t Au, %Pb, Zn)	Ore minerals	Main hydrothermal alteration minerals	Wall-rock and its age	Ore style	Ref.
8	Deerbuer (or Sanhe)/ Genhe/Inner Mongolia	Pb, Zn, Ag	0.205; 0.1573	1.97 %; 1.60 %	Ga, sph, py, cp	Q, Ser, chl, ab, carb, kao, alu	Late Jurassic intermediate volcanic rocks and Early Cretaceous felsic volcanic rocks	Vein	35, 36
9	Erdaohezi/ Genhe/ Inner Mongolia	Pb + Zn Ag	1.03	8 %	Ga, sph, py, cp, ar;	Q, Ser, kao, carb, chl, ba	Early Cretaceous volcanic rocks	Vein	35, 36
10	Daba/ Manzhouli/ Inner Mongolia	Au, Cu	Occurrence		Py, cp, en, Au, el, malachite, az	Q, Ser, alu, pp, dic, kao, Ser, zeolite, carb	Early Cretaceous rhyolitic lava and tuff	Vein	32, 33
11	Jiawula/ Manzhouli/ Inner mongolia	Pb, Zn, Ag	16.71; 28.47 636	130.27; 3.43 %; 5.83 %	Ga, sph, py, mar, pyr, cp; lesser mag, hem, bn, apy, hessite and Ag	Ser, Q, illite, chl, hydromica, cc, flu, ba	Triassic andesite, basaltic andesite and basalt; sandstone, siltstone and Yanshanian volcanics-Subvolcanics	Vein	12, 16
12	Chaganbulagen/ Manzhouli/ Inner Mongolia	Ag, Pb + Zn 5 Au	3,000; 0.5;	288.18	Ag, el, fr, ar, ag, ga, sph, py, cp, apy, pyr	Q, il, hydro-muscovite, carb, kao, chl, ep	Early Cretaceous sedimentary rocks and rhyolitic lava and pyroclastic rocks	Vein	16, 27

Table 5.3 (continued)

No. in Fig. 5.31	Deposit/county/province	Metal	Resource where known (Au Ag t/Cu PbZn Mt)	Grade, where known (g/t Au, %Pb, Zn)	Ore minerals	Main hydrothermal alteration minerals	Wall-rock and its age	Ore style	Ref.
13	E'rentaolegai/ Manzhouli/ Inner mongolia	Ag, Mn Au	>1,006; 56,000 t; 2.8		Py, ga, cr, ps, ag, cryptomelane, fr, io, Ag, Au	Ser, Q, adu, rod, cc, cd, chl, zeolite, flu, ba	Early Cretaceous andesite and rhyolite	Vein	16, 36
14	Bayanhaolei/ Manzhouli/ Inner Mongolia	Au	Occurrence		Cpy, cov, py, en	Q, alu	Early Cretaceous felsic volcanic rocks	Vein	32, 36
15	Siwu Meadow/ Hailaer/Inner Mongolia	Au	Occurrence		Py, cp, ga, en, Au, Cu, Ag, iodyrite, ag, co, aco	Q, Ser, carb, kao, dic, alu	Late Jurassic trachyandesitic, lava and pyroclastic rocks???	Breccia, vein	6, 36
16	Tayuan/Tayuan/ Heilongjiang	Au, Ag, Cu	<1; 346; 4,317		Py, cp, ga, sph, tet, en, Au, ag, co <5 % or >5 %	Q, adu, Ser, carb, pp, chl, ep, ba	Late Jurassic rhyolitic lava and tuff, and andesite	Vein, stock-work	1, 30
17	Guliku/Songling/ Heilongjiang	Au, Ag	<1	1.23 ~ 3.27	Py, cp, ga, ag, tet, Mo, mag, st, el, kus, Cu, cov, malachite, li	Ser, Q, cd, ank, cc, adu, ep, chl, pp, clays, mica	Early Cretaceous andesitic-dacite and pre-Ordovician metamorphic rocks	Vein, stock-work, disseminated	29
18	Pangkaimen/ Tayuan/ Heilongjiang	Au, Ag	5.971; 132.39	4.34; 96.3	Py, pyr, mar, ga, sph, cp, Au, el, ag, calaverite	Q, carb, chl, ep, Ser, kao, smectite, flu	Early Cretaceous volcanic-clastic sequence???	Vein, breccia	31

Table 5.3 (continued)

No. in Fig. 5.31	Deposit/county/province	Metal	Resource where known (Au Ag t/Cu PbZn Mt)	Grade, where known (g/t Au, %Pb, Zn)	Ore minerals	Main hydrothermal alteration minerals	Wall-rock and its age	Ore style	Ref.
19	Zhengguang/ Nengjiang/ Heilongjiang	Au (Zn)	>20		Py, cp, ga, Au, sph, li, tet; lesser ag, hem, mag, pyr, cov	Q, Ser, chl, ep, cc	Ordovician andesitic tuff, andesite, chlorite sericite slate, and early Yanshanian diorite, diorite porphyrite	Vein, stock-work	26, 34
20	Sandaowanzi/ Heihe/ Heilongjiang	Au (and placer)	8.87	7.47	Py, pyr, he; trace cp, sph, ga, apy, el, kus, ag, Au (1.79 %)	Q, kao, ser, chl, ep, cc	Middle-Late Jurassic andesite and andesitic breccia	Vein	42
21	Naoniushan/ Suniteyouqi/ Inner Mongolia	Cu, Au Ag	26,500; 0.2	0.13 ~ 3.45 %	Py, cp, apy, pyr	Q, Ser chl, carb	Early Cretaceous andesite volcanic rocks	Breccia, Vein	14
22	Erbahuo/ Wenniuteqi/ Inner Mongolia	Ag	Occurrence	227.23	Py, ga, sph, cp	Ser, Q, chl, pp, carb, flu, kao	Early Cretaceous andesitic-rhyolitic lava and pyroclastic rocks	Lenticular, vein	15
23	Huanghuagou/ Wenniuteqi/ Inner Mongolia	Pb, Zn, Ag			Ga, sph, py	Ser, Q, feldspar, kao	Early Cretaceous subvolcanic rocks	Vein	14
24	Nailingou/ Chifeng/ Inner Mongolia	Au	Occurrence		Py, sb, Au, el, ag	Cd, Ser, kao, adu, cc, chl, ep	Early Cretaceous andesitic breccia and lava	Vein, pipe/ cone-like	20, 21

Table 5.3 (continued)

No. in Fig. 5.31	Deposit/county/province	Metal	Resource where known (Au Ag t/Cu PbZn Mt)	Grade, where known (g/t Au, %Pb, Zn)	Ore minerals	Main hydrothermal alteration minerals	Wall-rock and its age	Ore style	Ref.
25	Xiaokouhuaying/ Weichang/ Hebei	Mn, Ag	211.7		Ga, sph, ag, tet	Q, rod, ba	Early Cretaceous crystal tuff and ignimbrite	Vein	7, 9
26	Dong'an/Xunke/ Heilongjiang	Au Ag	24.3 208	9.05	Py; trace apy, co, ga, cp, sph, li, el, Au, kus, Ag, ag (<2.8 %)	Q, adu, chl, Ser, flu, kao, damourite	Early Cretaceous andesitic-rhyolitic volcanic rocks	Vein, lenticular	8, 13, 28, 39
27	Gaosongshan/ Xunke/ Heilongjiang	Au			Py, hem, cp, mag, ga, sph (low sulphide)	Q, mica, kao, cc, feldspar	Early Cretaceous andesite, rhyolite	Vein, breccia,	40
28	Tuanjiegou/ Jiayin/ Heilongjiang	Au	79.8	4.01	Mar, py, cp, sb, Au, el, ga, sph, cin, rea, Hg, or, li	Q, opal, cc, ank, adu, siderite, gypsum	Early Cretaceous felsic subvolcanic rocks and Proterozoic crystalline schists	Small vein, stockwork, disseminated, breccia	5, 18
29	Xinmin	Au			Py, pyr, apy; (1.5 ~ 4.5 %)	Q, ser, cd, chl, kao	Early Cretaceous volcanic rocks and clastic rocks	Vein, lenticular	41
30	Jinchang/ Dongning/ Heilongjiang	Au	51.3	8.32	Py; minor cp, ga, sph, apy, pyr, mo, co, sb, mag, li, hem, specularite, Au, el, kus, Ag (5–90 %)	Q, Ser, kao, cc, chl, ep, adu	Indosinian granodiorite, Yanshanian granitic porphyry and granite	Vertical pipe shaped, cone-like, lenticular	19, 37

Table 5.3 (continued)

No. in Fig. 5.31	Deposit/county/province	Metal	Resource where known (Au Ag t/Cu PbZn Mt)	Grade, where known (g/t Au, %Pb, Zn)	Ore minerals	Main hydrothermal alteration minerals	Wall-rock and its age	Ore style	Ref.
31	Ciweigou/Yanbian/Jilin	Au	6.08	4.94	Py, cp, tet, sph, ga, el, ag, Au, aurotellurite (0.5 ~ 5 %)	Q, cal, adu, cd, alu, ba	Middle Jurassic andesitic breccia and tuff	Vein	10, 11
32	Naozhi/Yanbian/Jilin	Au, Cu	4.66	6.4	Py, cp, ga, sph, el, kus, Au, malachite, cov	Q, Ser, chl, ep, ab, carb, flu, kao	Variscan granodiorite, and early cretaceous, middle Jurassic volcanicrocks	Lenticular	10, 17
33	Wufeng-Wuxingshan/Yanbian/Jilin	Au			Py, cp, ga, sph, li, Au, Ag, el, ag, cinnabar, calaverite, tet	Q, Ser, chl, ep, ab, carb, adu	Middle Jurassic andesitic, pyroclastic rock, trachyandesitic-trachytic subvolcanic rocks	Vein, lenticular, stock-work	4, 10

1 Cao (1994); 2 Chen et al. (2002); 3 Cong et al. (1999); 4 Feng (1998); 5 GHCPAPF (1995); 6 Guan and Chai (2004); 7 Guo and Wang (1998); 8 Guo et al. (2004); 9 Guo (2001); 10 Jiang et al. (2002); 11 Jin and Hao (2000); 12 Li and Qin (1999); 13 Liu (2006); 14 Liu et al. (2004a); 15 Luo (1997); 16 Pan et al. (1996); 17 Rui et al. (1995); 18 Sun et al. (1996); 19 Tian (1999); 20 Wang et al. (1994); 21 Wang et al. (1996); 22 Wang et al. (2003); 23 Wang et al. (2004); 24 Wu and Quan (2000); 25 Wu et al. (2001); Wu et al. (2005b); 26 Wu et al. (2006b); 27 Xie and Liu (2001); 28 Yu et al. (2005); 29 Yang et al. (2000); 30 Yang et al. (2002); 31 Yuan et al. (1998); 32 Zhao and Wu (2002); 33 Zhao and Zhang (1997); 34 Zhao et al. (2006); 35 Zhu et al. (1999); 36 Zhu et al. (2001); 37 Zhu et al. (2003); 38 Fu et al. (2001); 39 Zhang et al. (2010); 40 Liu et al. (2006); 41 Li et al. (2006); 42 Wu et al. (2005c)

ab albite; *aco* chalcocite; *adu* adularia; *ag* argentite; *alu* alunite; *ank* ankerite; *apy* arsenopyrite; *ar* aerosite; *az* azurite; *ba* barite; *bi* biotite; *bn* bornite; *cb* carbonate, *cc* calcite; *cd* chalcedony; *cin* cinnabar; *co* chalcocite; *cov* covellite; *cp* chalcopyrite; *cr* cerargyrite; *dic* dickite; *el* electrum; *en* enargite; *ep* epidote; *flu* fluorite; *fr* freibergite; *ga* galena; *hem* hematite; *il* illites; *io* iodyrite; *kao* kaolinite; *kus* kustelite; *li* limonite; *mag* magnetite; *mar*, marcasite; *mo* molybdenite; *or* orpiment; *ps* psilomelane; *pp* pyrophyllite; *py* pyrite; *pyr* pyrrhotite; *q* quartz; *rea* realgar; *rod* rhodochrosite; *sb* stibnite; *sp* sphalertie; *st* stephanite; *tet* tetrahedrite

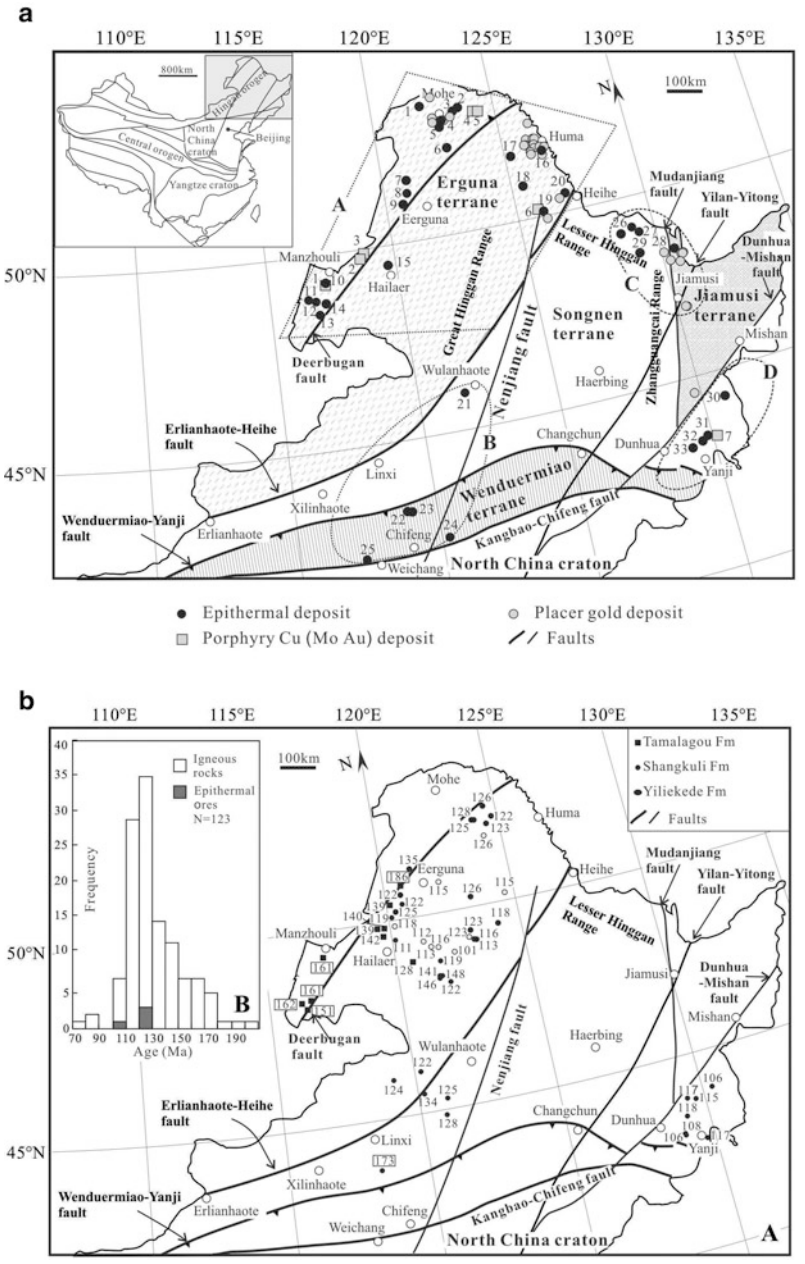

Fig. 5.32 **a** Distribution of porphyry, epithermal and intrusion-related vein systems in northeast China and metallogenic provinces; letters in figure: *A*, northern Great Hinggan Range; *B*, southern Great Hinggan Range; *C*, Lesser Hinggan Range; *D*, Changbaishan; **b** age data (U-Pb and Ar-Ar) and histogram from selected mineral systems (after Qi et al. 2005b, c and modified after Ren et al. 1999; Ye et al. 1994; Wu et al. 2002); Epithermal deposits (see also Table 5.2): *1* Shabaosi,

and Huma districts of the Northern Great Hinggan Range province (Zhao and Zhang 1997). Placer Au can help in tracing the source to hydrothermal Au deposits, as is the case for the discovery of Shabaosi, Xiaoyinuogaigou, and Laogou.

The Great Hinggan Range low-sulphide Au (Ag) epithermal systems are characterised by quartz veins, with low contents of sulphides (<5 % by vol), as exemplified by the Shabaosi, Sandaowanzi, Dong'an, Ciweigou and Tuanjiegou deposits (Table 5.3). Ore minerals are pyrite, native gold, with minor galena, sphalerite, chalcopyrite, electrum, and minor Ag-bearing sulphides; gangue minerals are mainly quartz (or/and chalcedony), sericite, (adularia), chlorite, carbonates, and kaolinite. The presence of adularia suggests that these deposits may be of the low-sulphidation epithermal type. High-sulphide Au (Cu, Zn) systems, are less common and exemplified by Jinchang Au deposit, Daba Au (Cu), Naozhi Au (Cu) and Naoniushan Cu (Au) deposits. Ore minerals are characterised by high contents of sulphides, including chalcopyrite, pyrite, sphalerite and galena. The Jinchang Au deposit is characterized by high pyrite (minor chalcopyrite) content (30–90 %) in quartz-pyrite veins and lower (5–20 %) in breccia and disseminated ores. It was reported as epithermal type (Zhu et al. 2003), however it is probably a porphyry-epithermal system as evidenced from deposit geology and fluid inclusion studies (Li et al. 2003a). Ar-Ar dating of ore minerals from Jinchang show that mineralisation was formed between 123 and 119 Ma.

The Ag-rich polymetallic deposits and occurrences are mainly found in the Manzhouli Basin and Erguna Massif (Fig. 5.32). These are characterized by high content of sulphides and Ag-bearing sulphides, halides, and sulphosalts. Several of these occurrences, exhibit similar features, such as bladed quartz (indicative of boiling fluids), colloform banded quartz and are associated with rhyolitic domes. Hydrothermal minerals include quartz, chalcedony, sericite, adularia, calcite, chlorite, fluorite, kaolinite, and barite, as exemplified by the Jiawula, Chaganbulagen and E'rentaolegai deposits. The Jiwula, Chaganbulagen, Xijinuo Shan and Erdaohezi deposits show atypical epithermal characteristics, because they are richer in base metal, lacking diagnostic minerals (adularia or enargite), and are considered as hydrothermal vein deposits (Wu et al. 2006a, 2006b). They are probably transitional to mesothermal conditions or to deeper levels of epithermal systems, as evidenced by the presence of three-phase CO_2-bearing fluid inclusions in Jiawula-Chaganbulagen ore field (Wu et al. 2006a, 2006b). The E'rentaolegai deposit, which is relatively Ag richer, could be considered as a low sulphidation Ag-rich base metal deposit for the presence of sericite-adularia assemblage, probably indicating a shallower formation depth.

2 Ergenhe, *3* Yesuoku, *4* Mada'er, *5* Aolaqi, *6* Xijinuo Shan, *7* Moerdaoga, *8* Deerbuer, *9* Erdaohezi, *10* Daba, *11* Jiawula, *12* Chaganbulagen, *13* E'rentaolegai, *14* Bayanhaolei, *15* Siwu Meadow, *16* Tayuan, *17* Guliku, *18* Pangkaimen, *19* Zhengguang, *20* Sandaowanzi, *21* Naoniushan, *22* Erbahuo, *23* Huanghuagou, *24* Nailingou, *25* Xiaokouhuaying, *26* Dongan, *27* Gaosongshan, *28* Tuanjiegou, *29* Xinmin, *30* Jinchang, *31* Ciweigou, *32* Naozhi, *33* Wufeng–Wuxingshan; Porphyry deposits: *1* Wunugetushan (Cu, Mo), *2* Babayi (Cu), *3* Badaguan (Cu, Mo), *4* Qiulibachi (Cu), *5* Ershiyizhan (Cu, Au), *6* Duobaoshan (Cu, Mo), *7* Xiaoxinancha

The Jiawula Zn-Pb-Ag district extends for about 10 km in a general northwest direction. Here Neoproterozoic basement is overlain by Cambrian marbles, dolomite and quartzites, intruded by felsic stocks and volcanic rocks that include basalt and andesite lavas, pyroclastics, rhyolite domes and stocks emplaced in narrow grabens on west side of Lake Hulun Nur. The Jiawula deposit has a mineral zonation from a core of quartz-sericite-pyrite- to actinolite-sericite-epidote, to epidote-carbonate-chlorite at the margins. Massive galena-sphalerite veins with pyrite and pyrrhotite are cut by late quartz-carbonate veinlets. Mineralisation is hosted by basalt, agglomerate, and breccia.

In the southern Manzhouli basin is a porphyry-epithermal district, where porphyry Cu-Mo mineralisation is associated with skarns and high-level epithermal systems. The Wunugetushan porphyry Cu-Mo has a drilling-inferred resource of 274 Mt grading 0.47 % Cu and 0.055 % Mo (Pirajno, unpublished data). Several base metal skarns are developed that are spatially associated with the Wunugetushan granitic batholith. Alteration zones are from outer propylitic (epidote-carbonate-chlorite), to phyllic (sericite-quartz-pyrite) to a core zone of potassic alteration (quartz-K-feldspar-sericite). Chalcopyrite and molybdenite occur in stockwork zones and the Mo mineralisation is restricted to the potassic zone, whereas Cu is associated with the phyllic zone.

5.4.2.1 Stable Isotope Systematics and Fluid Inclusions

Published $\delta^{18}O$, δD, $\delta^{34}S$ and fluid inclusion data from a number of Au deposits in the Great Hinggan Range have been used to construct the $\delta^{18}O$, δD of Fig. 5.33a and $\delta^{34}S$ in Fig. 5.33b (Zhang et al. 2001a; Wu et al. 2006b; Guo 2001; Liang et al. 2007; Chen and Rui 1993).

Most $\delta^{18}O$-δD data for fluids plot near the meteoric line, except for the Shabaosi, Jinchang and Jiawula systems, indicating that in most cases the ore fluids are of meteoric origin. The $\delta^{18}O_W$ values for Shabaosi and Jiawula fall in the range of magmatic water, but the δD_W data are lower than those of magmatic water. The high $\delta^{18}O_W$ data of these ore fluids can be interpreted as the result of water-rock interaction between meteoric water and volcanic rocks with high $\delta^{18}O_W$ values. In the Jiawula Pb-Zn-Ag deposits, the δD_W and $\delta^{18}O_W$ values range from -160 to -110 ‰ and -12 to 13 ‰, respectively. These low δD values and wide range of values imply a high-latitude meteoric origin and a variable W/R (water/rock) ratio. The high $\delta^{18}O_W$ values, up to 13 ‰, suggest an input of magmatic water. The data for the Jinchang Au deposit plot near the magmatic box, implying that the fluids were mainly derived from magmas, with some contribution from meteoric water circulation.

The histogram of $\delta^{34}S$ values of sulphides from a number of Au mineral systems in the Great Hinggan Range, shown in Fig. 5.33b, indicates that the largest number of observations cluster between -5 and $+5$ ‰, with lesser number of observations between -15 and $+10$ ‰. In general, two groups of deposits can be distinguished on the basis of the $\delta^{34}S$ values. One group, including most of the deposits, except for Shabaosi, Xijinuo Shan, Siwu Meadow, Tayuan, and Tuanjiegou, have narrow

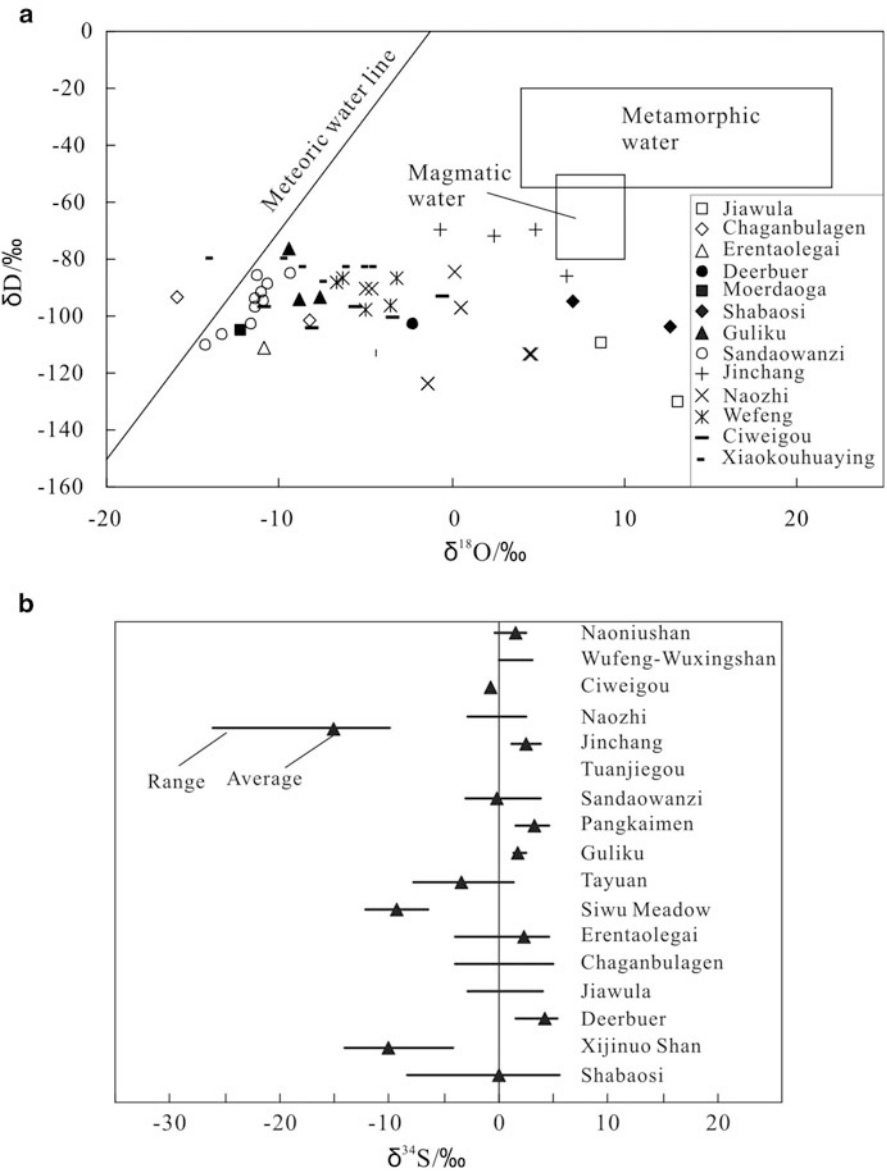

Fig. 5.33 **a** δD vs $\delta^{18}O$ plot of ore fluids calculated from inclusion fluids; **b** Histogram of $\delta^{34}S$ values of sulphides from Au deposits in the Great Hinggan Range; references cited in text and Table 5.2

$\delta^{34}S$ range from −4.0 to 5.4 ‰. The Ag-rich base metal deposits, such as the Jiawula, Chaganbulagen, E'rentaolegai and Deerbuer in the Northern Great Hinggan Range province, have most small positive $\delta^{34}S$ values, and show minor difference between various sulphides. For example, the $\delta^{34}S$ values for Chaganbulagen and Jiawula deposits, estimated from $\delta^{34}S$ of sulphide pairs is 2.3 ‰ and 1.1–3.3 ‰ respectively. Since these deposits are hosted by Early Cretaceous volcanic rocks and were associated with subvolcanic activity, the sulphur was probably sourced from the volcanic host rocks or from magmatic sources. The high-sulphidation Au (Cu) deposits, such as Jinchang Au deposit, Naoniushan Cu (Au) and Naozhi Au (Cu) have a narrow $\delta^{34}S$ range (0.3–2.4 ‰), suggesting a magmatic sulphur source. In the Changbaishan province, previous studies (Rui et al. 1995; Liang et al. 2003) revealed that Xiaoxinancha porphyry Au (Cu) deposit, Naozhi Au (Cu), Wufeng-Wuxingshan Au, and Ciweigou Au deposits, have a wide scatter of $\delta^{34}S$ values with increasing meteoric water, as revealed by D-O isotopes (Rui et al. 1995; Liang et al. 2003). These studies probably indicate that from porphyry Au (Cu) deposit, through high-sulphide Au to low-sulphide Au epithermal deposit, the sulphur (and probably ore metals as well) was initially sourced from magmas or volcanic rocks, increasingly diluted by meteoric water.

The second group of deposits have $\delta^{34}S$ values varying between 8.3 and 5.6 ‰ (Shabaosi), −12.2 to −6.4 ‰ (Siwu Meadow), −14.4 to −4.2 ‰ (Xijinuo Shan), −7.8 to 4 ‰ (Tayuan), and −33.6 to −0.4 ‰ (Tuanjiegou). The Shabaosi deposit shows different $\delta^{34}S$ values between vein and disseminated ores, with the former having negative $\delta^{34}S$ values. The low $\delta^{34}S$ values of the vein ores may suggest a significant contribution of sulphur from sedimentary host rocks (Qi et al. 2000). Pyrite and enargite of the Siwu Meadow deposit have low $\delta^{34}S$ values, with a gypsum sample showing a $\delta^{34}S$ value of 16.2 ‰, suggesting a sedimentary sulphur source from a rift basin (Guan and Chai 2004). The Tuanjiegou deposit has a wide scatter of $\delta^{34}S$ values of sulphides, with a general decrease from early to late. For example, the $\delta^{34}S$ is around −1 ‰ for pyrites separated from early-formed pyrite-sericite-quartz assemblage, −11 ‰ for pyrite and −30 ‰ for late stage framboidal marcasite. The near zero $\delta^{34}S$ values in earlier stage indicate an igneous sulphur source; the low $\delta^{34}S$ values in later stages may be due to a biogenic source from Heilongjiang Group, as evidenced by the discovery of pyritized algae in the ores (Chen and Rui 1993).

Three-phase CO_2-H_2O inclusions were observed in the Jinchang Au (Zhu et al. 2003), Shabaosi Au deposits and Jiawula Pb-Zn deposit (Wu et al. 2006b). In general, homogenisation temperatures of fluid inclusions range from 350 to 100 °C. Fluid inclusions from the E'rentaolegai deposit have a homogenisation temperature range of between 383 and 199 °C, with relatively high trapping pressures of fluid inclusions up to 68 MPa. Homogenisation temperatures and pressures of the Jinchang Au deposit range from 445 to 67 °C and 97–65 MPa, respectively, covering a range from near-surface hot springs to a porphyry system. Low CO_2/H_2O ratios (<0.6) and low salinities (≤10 wt % NaCl equivalent) of the fluid-systems, except for Shabaosi, Jiawula and Jinchang, also indicate that meteoric fluids dominate these hydrothermal systems in northeastern China, consistent with the results of H-O isotope. Low-sulphide deposits show generally lower salinities than high-sulphide deposits. High

salinities can be explained by the high contents of base metals in these deposits because chloride complexes are the most important for transport of base metal at medium to high temperatures (see Pirajno 2009 for an overview). In the Jiawula deposit, daughter minerals can be observed in fluid inclusions whose salinities reach 33–45 wt % NaCl eq, which can be interpreted as representing magmatic fluids. The salinities of the Jinchang deposit range largely from 0.33 to 70.33 wt % NaCl equivalent (Li et al. 2003a; Wang et al. 2007b). In the Jinchang Au deposit Wang et al. (2007b) reported the presence of halite-bearing inclusions, various daughter minerals, melting inclusions, coexisting with boiling phenomena containing a few three-phase CO_2-H_2O inclusions.

5.4.2.2 Dong'an Epithermal System, Lesser Hinggan Range

Dong'an is a low-sulphidation (adularia-sericite) epithermal Au deposit located in the Xunke county (near the Russian border), about 500 km north of the city of Harbin, Heilongjiang province, northeast China (Fig. 5.34; Table 5.2). The gold mineralisation at Dong'an was discovered in 2000 by Heilongjiang Academy of Geological Exploration for Nonferrous Metals, during a follow up of gold geochemical anomalies in soils. Total (measured, indicated, and inferred) resources for the Dong'an deposit are 14 Mt of ore grading 5.04 g/t Au and 82.74 g/t Ag (Zhang et al. 2010). Dong'an is the first gold deposit recognized in eastern China that contains a large quantity of adularia, although many other epithermal gold deposits in the region have been classified as adularia-sericite type (Mao et al. 2007). Published works on the geology and geochemistry of the Dong'an gold deposit (fluid inclusions, H and O isotope geochemistry as well as S and Pb isotope composition of sulphides), include Guo et al. (2004), Su et al. (2006), Yang (2008). More recently, Zhang et al. (2010) provided a comprehensive overview of the deposit, combined with new geochronological (SHRIMP U-Pb zircon and $^{40}Ar/^{39}Ar$) and whole rock geochemical data of the host subvolcanic and volcanic rocks. The following is condensed from Zhang et al. (2010).

The Dong'an gold deposit is located in the Lesser Hinggan Range in northeast China, south of the suture between the NCC and the Siberia craton and north of the Solonker-Xilinhot-Hegenshan fault system (Fig. 5.34a). The latter, as mentioned above, is a major and complex suture zone between the northern margin of the NCC and the Mongolian plate, characterised by Mid-Ordovician-Early Silurian subduction-accretion complexes, ophiolite belts and Andean-type magmatic arcs (Xiao et al. 2003; de Jong et al. 2006). The Hinggan fold belt was uplifted at the end of the late Carboniferous due to extensive emplacement of Hercynian granitic plutons. Since the Mid-Jurassic, oblique subduction of the Izanagi–Pacific plate under the eastern margin of Eastern China continent has led to the formation of the north-northeast-trending magmatic belts, north-northeast-strike-slip faults, and a basin and range style tectonics (Zhou et al. 2002a). The lithostratigraphic sequence in the Lesser Hinggan Range comprises four lithofacies units (Fig. 5.34b): (1) Precambrian metamorphic basement, (2) Cambrian and Permian submarine sedimentary cover,

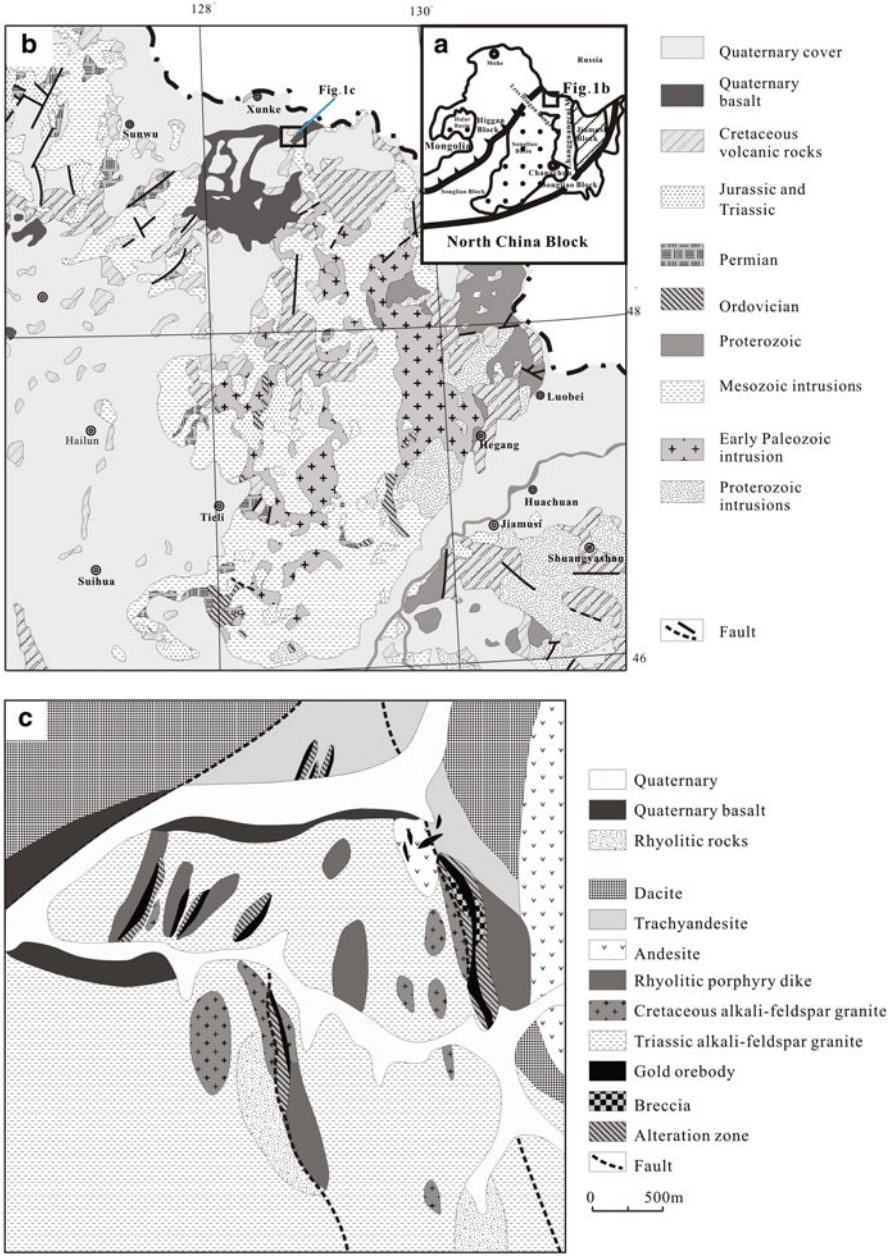

Fig. 5.34 **a** Simplified tectonic map of northeast China; **b** distribution of late Mesozoic volcanic rocks in the Lesser Hing'an Range and adjacent areas; **c** sketch geological map of the Dong'an district. (Modified after Zhang et al. 2010 and references therein)

(3) Jurassic to Cretaceous terrigenous clastic and volcanic rocks, and (4) Cenozoic coarse clastic and continental basaltic rocks. The Precambrian metamorphic rocks consist of schist, phyllite, and meta-felsic rocks. Cambrian strata, include dolomitic marble, phyllite and carbonaceous slate, discordantly overlying the Precambrian metamorphic rocks. Permian clastic rocks (e.g., sandstone, conglomerate and shale) discordantly overlie the Cambrian strata. The Permian lithologies, in turn, are discordantly overlain by Early Jurassic terrigenous clastic rocks, consisting of granitic conglomerate, sandstone, siltstone, and tuff sandstone intercalated with coal seams. Early Cretaceous volcanic rocks, are widespread throughout the whole belt, comprise a wide spectrum of rock types, including basaltic, trachyandesitic, and rhyolitic lava flows and rhyolitic tuff intercalated with rhyolitic perlite. Oligocene-Pliocene sandstone and conglomerate are also extensively distributed and cover all the Pre-Cenozoic strata. Quaternary alkaline basalts, which are a part of rift-related Cenozoic volcanic rock belt in eastern China, mainly outcrop along valleys.

The Early Cretaceous volcanic sequence can be divided into two formations: Fuminhe and Ganhe. The Fuminhe is composed predominantly of a 120–300 m-thick succession of rhyolitic and dacitic lava flows and welded tuff intercalated with breccia-bearing tuff and perlite, minor andesite and trachyandesite. The Ganhe Formation is 75–380 m thick and consists mainly of pyroxene-phyric basalt, basaltic andesite, trachyandesite and andesite with rhyolitic breccias at the bottom, conformably overlying Fuminhe. However, a gap in volcanic activity exists as indicated by a 1–2 m thick weathering crust developed on the rhyolites.

The Dong'an region is underlain by Fuminhe Formation Early Cretaceous volcanic rocks and Oligocene-Pliocene sandstone and conglomerate, almost all of which covered by Quaternary sediments. In the Dong'an area, the Fuminhe Formation consists predominantly of rhyolitic lava and rhyolitic tuff with minor dacite, overlying a Late Triassic coarse-grained alkali-feldspar granitic intrusion, which is also intruded by Cretaceous fine-grained alkali-feldspar granite stock. Rhyolitic porphyry dykes intruded the volcanic sequence and the Triassic granitic intrusion (Fig. 5.34c). The area is characterized by a series of tensile-shear, north-south-, northeast- and north-northeast-trending faults.

Fourteen Au orebodies, associated with quartz- and sericite-dominated alteration zones, are controlled by the north-south and northeast-striking faults. Eight of the orebodies are hosted in rhyolitic lavas, five in rhyolitic porphyry dykes, and one is hosted in Triassic alkali- feldspar granite. In general, the country rocks and Au orebodies have distinct boundaries which are characterized by alteration zones along faults. The size of ore veins vary considerably, from 50 to 800 m, 1 to 7 m in thickness, and extending to less than 400 m of depth (Fig. 5.35), with Au grades of 3–10 g/t. The largest vein is 770 m long, 6.70 m thick in average, and 358 m vertical extent, with an average Au grade of 9.05 g/t and Ag grade of 75.8 g/t.

Apart from native gold, native silver and electrum, there are lesser quantities (ca. 4 vol%) of pyrite, galena, chalcopyrite, sphalerite, arsenopyrite, magnetite and chalcocite. Most ore minerals form anhedral grains, although some have euhedral and subhedral textures. The gangue minerals include quartz, adularia, sericite and

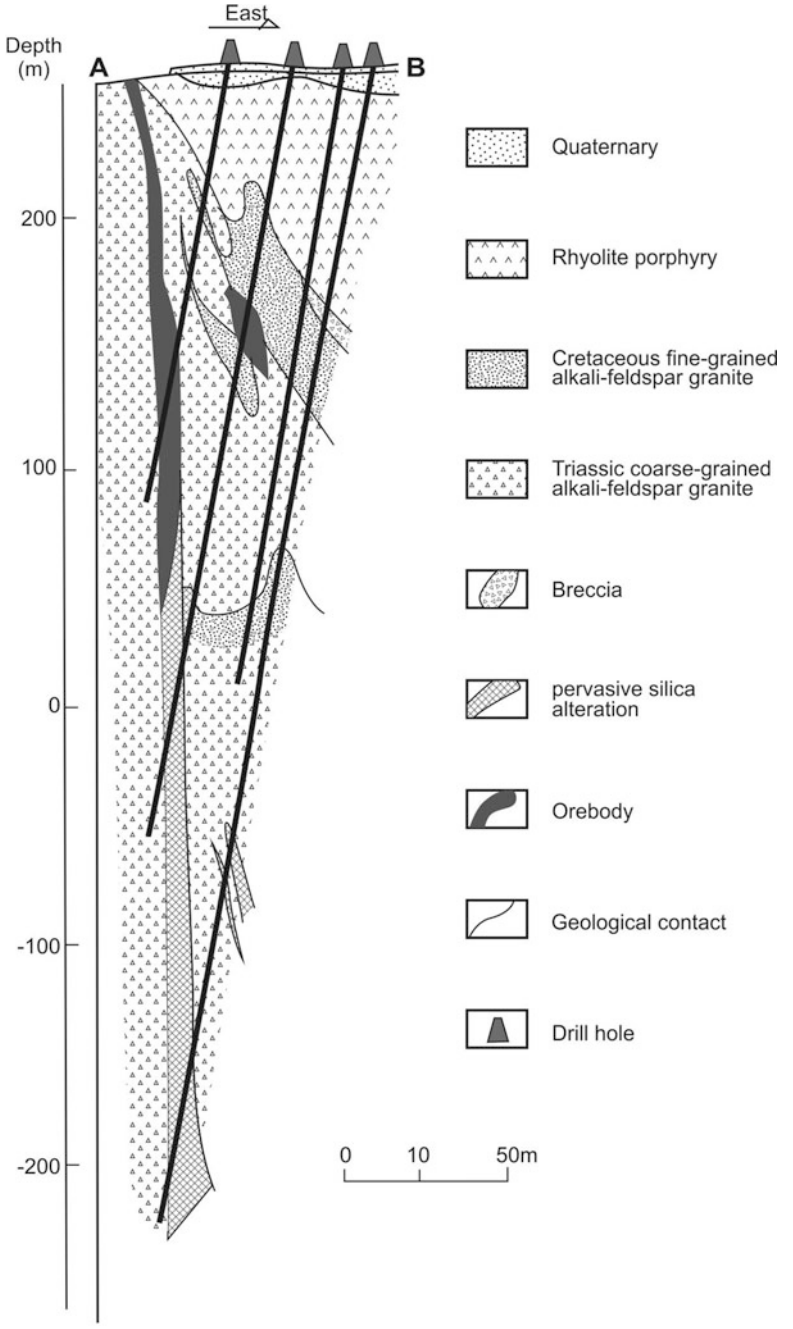

Fig. 5.35 Cross-section of the Dong'an epithermal Au deposit. (After Zhang et al. 2010)

fluorite, generally occurring as fine-grained assemblages. The ore minerals are predominantly distributed as sparse disseminations, locally as dense disseminations, or as veinlets and stockwork veins. In contrast, the gangue minerals occur as massive, banded, brecciated, vuggy structures, in places with comb and bladed textures, suggesting boiling fluids. Chemical analyses of pyrite indicate that the Au and Ag contents range from 12.8 to 295.2 ppm and 2.6 to 233.3 ppm, respectively. Electron microprobe analyses indicate that the gold percentage in electrum grains ranges from 50.1 to 65.1 % (Guo et al. 2004).

Three stages of Au mineralisation have been proposed (Guo et al. 2004), as follows. Stage 1 is represented by weakly auriferous (0.2–0.4 g/t Au) pervasive quartz with weak chlorite-sericite-pyrite alteration; during this stage, rhyolite and Triassic granite were locally replaced by disseminated low-temperature quartz and chalcedonic quartz. Stage 2 is characterized by white massive quartz veins, stockwork veins, and hydrothermal breccia, containing variable amounts of quartz, adularia and sericite. Cryptocrystalline chalcedonic quartz is present near the surface, whereas subhedral and anhedral quartz crystals developed at deeper levels. Some mineralisation was formed (3–5 g/t Au) during this stage. However, stage 3 is the most important for Au mineralisation. It is characterized by extensive grey-white veins, stockwork veins, veinlets with quartz-, adularia- and sericite-dominated, which overprint the previously emplaced stockwork of stage 2. Pyrite, chalcopyrite, galena and specularite are commonly associated with quartz, sericite, adularia and chlorite veins. The gold grade of this stage is generally >5 g/t. The mineral paragenetic assemblages are shown in Fig. 5.36. Wallrock alteration in the Dong'an Au deposit is dominated by quartz, adularia, sericite and fluorite, accompanied by lesser amounts of pyrite, chlorite and carbonate. The quartz, adularia, sericite and pyrite alteration is spatially and temporally closely associated with Au mineralisation. This hydrothermal alteration is mainly developed along faults and in breccias, and exhibits a clear concentric zoning pattern, from a central zone with a mineral assemblage of quartz, chalcedonic quartz, sericite, adularia, chlorite and pyrite, to envelopes of veining and stockworks containing a mineral assemblage of quartz, kaolinite, sericite, adularia and fluorite.

Adularia is the most important feature in the Dong'an epithermal system. Adularia occurs widely in the form of a distinctive pink 0.5–1.5 m wide-veins and is commonly closely associated with quartz and sericite. Fluorite is also a common mineral, developed extensively as veins. There are three stages of fluorite development. In the first, fluorite is in subhedral aggregates, associated with grey quartz, adularia and chlorite. The second stage fluorite is purple in color, associated with white quartz, adularia and chlorite. The third stage fluorite is green in color, associated with stockworks and veinlet of quartz, adularia and chlorite. In addition, cubic drusy fluorites are commonly found in cavities.

Zhang et al. (2010) reported on the geochemical, isotope systematics and geochronology of the volcanic and subvolcanic rocks in the Dong'an area. The Fuminhe and Ganhe lithostratigraphic units have distinct major element compositions. For example, SiO_2 contents of the Fuminhe rocks range from 60.3 to 80.7 wt % with MgO of 0.02–2.5 wt % (samples with very high SiO_2 contents show pervasive silica alteration), whereas the rocks from the Ganhe Formation exhibit relative low

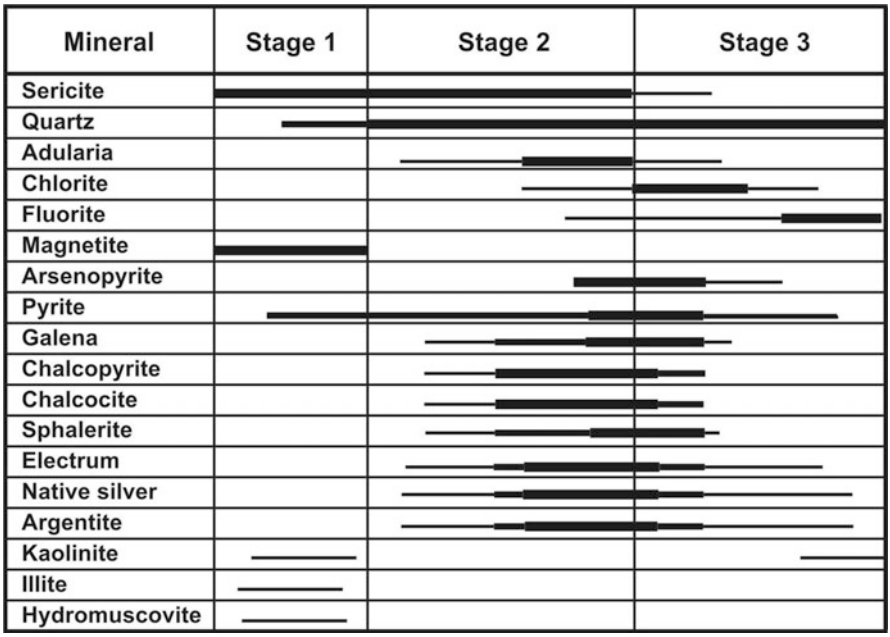

Fig. 5.36 Mineral paragenetic sequence of the Dong'an epithermal Au deposit. (Modified after Zhang et al. 2010)

SiO_2 contents, from 47.5 to 58.5 %, and high MgO contents, from 1.9 to 7.0 %. In a TAS diagram, rocks of the Fuminhe Formation plot as andesite, dacite, trachyte and rhyolite, and show high-K calc-alkaline to shoshonitic character, whereas those from the Ganhe Formation plot in the basalt, basaltic andesite, andesite and trachyandesite fields, and show calc-alkaline to high K calc-alkaline character. All rocks from Fuminhe and Ganhe units are subalkaline. Most rocks from these two Formations (Fuminhe and Ganhe) have similar chondrite-normalized rare earth element (REE) patterns, i.e., moderate light REE enrichment relative to heavy REE, with $(La/Yb)_n$ ratios of 5.4–12.8 (10.8 in average) and 2.3–15.6 (9.5 average) for Fuminhe and Ganhe, respectively. The Fuminhe samples display slightly to significantly negative Eu anomalies ($Eu^* = 0.12 - 0.92$) whereas the Ganhe samples has slightly negative Eu anomalies ($\delta Eu^* = 0.73 - 0.98$).

Rocks of the Fuminhe and Ganhe formations exhibit distinct Sr and Nd isotopic compositions. The Fuminhe rocks has a narrow age-corrected $^{87}Sr/^{86}Sr$ range of 0.707253–0.707373, and $\varepsilon_{Nd}(t)$ from −2.78 to −3.05 (t = 108 Ma), and exhibits much higher ($^{87}Sr/^{86}Sr$) and lower $\varepsilon_{Nd}(t)$ values in comparison with those from the Great Hinggan Range (Fan et al. 2003), Heilongjiang province. In contrast, the Ganhe Formation displays slightly lower $^{87}Sr/^{86}Sr$ range of 0.705434–0.705763 and $\varepsilon_{Nd}(t)$ from +0.76 to +1.83, which overlap those from the Great Hinggan Range. A mean age of 108.1 ± 2.4 Ma (SHRIMP U-Pb zircon) was obtained for rhyolite porphyry, whereas Ar-Ar dating on sericite, separated from auriferous quartz veins,

yielded and a plateau age of 107.2 ± 0.6 Ma, which is consistent with its isochron age (106.3 ± 5.4 Ma). The $^{40}Ar/^{39}Ar$ plateau age for sericite postdates the rhyolite porphyry, and as the sericite samples were separated from an ore vein, the 107.2 ± 0.6 Ma age would represent the timing of Au mineralisation. Zhang et al. (2010) drew attention to the fact that apart from the Dong'an Au deposit, there is no other 107 Ma-gold deposit in northeast China and therefore it is likely that ca. 107 Ma could represent an important pulse of Au mineralisation in the Lesser Hinggan Range, and possibly in northeast China, because volcanic rocks dated at 106–108 Ma are common throughout the region.

Tectonic Setting

Zhang et al. (2010) used their new age and geochemical data to propose a tectonic setting that would explain the origin of the Dong'an epithermal system, as follows. In northeast China, two pulses of epithermal mineral systems: 145 Ma (Tuanjiegou gold deposit in Heilongjiang province) and 122–127 Ma (Erdaogou in Liaoning province and Jinchanggouliang in Inner Mongolia), have been previously recognized (Mao et al. 2007), although a SHRIMP age of 111.5 Ma of zircon grains from the granite in the Jinchang Au ore field has been interpreted to represent a separate magmatic-hydrothermal event (Lu et al. 2009), and younger K-Ar ages (<120 Ma) were also reported (Qi et al. 2005c; Chen et al. 2007). Three major viewpoints have been proposed to interpret the tectonic setting of the Mesozoic volcanic rocks in northeast China: (1) mantle plume (Shao et al. 2001; Lin et al. 1998; Ge et al. 1999); (2) subduction of the Mongol–Okhotsk Ocean and subsequent post-orogenic extension (Fan et al. 2003; Guo et al. 2001; Wang et al. 2002b; Meng 2003); and (3) subduction of the Palaeo-Pacific plate beneath eastern China (Hilde et al. 1977; Wang et al. 2006; Zhang et al. 2008).

There are several lines of evidence to suggest that the mantle plume model is unlikely. Firstly, the linear distribution of the Mesozoic volcanic rocks along the whole northeast China, and volcanism migration from west to east during the Late Mesozoic (Wang et al. 2006; Zhang et al. 2008), do not support this interpretation. Secondly, magmatic activities extended from 185 to 105 Ma (Zhang et al. 2008), much longer than the period normally associated with intracontinental volcanism related to a mantle plume. Thirdly, the apparent lack of updoming of lithosphere and high-temperature picrites are inconsistent with the plume model.

Seismic tomography studies (Van der Voo et al. 1999) suggest that the Mongol–Okhotsk Ocean subducted northward beneath Siberia. Thus, the Mesozoic volcanic rocks in northeast China could not have formed by subduction of the Mongol–Okhotsk Ocean. Alternatively, the Mesozoic volcanic rocks in northeast China and surrounding areas are distributed in a north-northeast direction, parallel to the north-northeast-oriented Asian continental margin, suggesting that these volcanic rocks may be related to subduction of the Palaeo-Pacific plate.

Wang et al. (2006) proposed a delamination mechanism for the geodynamic setting beneath northeast Asia in the Late Mesozoic. The westward subduction of the

Palaeo-Pacific plate, caused a rise of strain in the lithosphere and finally resulted in a shear-like lithospheric delamination starting from the west of the Great Hinggan Range around 160 Ma and then gradually extended eastwards. This led to asthenospheric mantle upwelling and underplating, resulting in magmatic activity in the western Great Hinggan Range in the Late Jurassic and then in Lesser Hing'an Range in the late stages of Early Cretaceous. The age data of Zhang and co-authors are consistent with this viewpoint (see discussion in Chap. 7). Asthenospheric upwelling resulted in partial melting of mafic lower crust, producing the parental andesitic magmas, which experienced a different degree of fractionation to form the wide spectrum of rock types of the Fuminhe Formation (andesitic, dacitic and rhyolitic rocks). In contrast, the parental basaltic melts of the Ganhe Formation could be attributed to partial melting of a mixture of an incompatible element depleted anhydrous lherzolite asthenospheric mantle source and a hydrous lower enriched lithospheric mantle source.

Previous works have shown that the mineralogy, alteration, and two-phase (vapor and aqueous solutions) fluid inclusion characteristics of the Dong'an gold deposit (Yang 2008) are similar to those of other adularia-sericite-type or low-sulfidation epithermal systems. The Au orebodies are generally spatially associated with the rhyolite porphyries of the Fuminhe Formation (Fig. 5.34), although some orebodies are not hosted by these porphyries, but occupy fracture zones or faults, not far from rhyolite porphyries. The new $^{40}Ar/^{39}Ar$ and SHRIMP U-Pb zircon age data further provide evidence for a genetic link between rhyolite porphyry and Au mineralisation. because of the nearly synchronous ages within errors (108.1 ± 2.4 and 107.2 ± 0.6 Ma respectively) Therefore, the rhyolite porphyries are inferred to have supplied heat that drove the convective hydrothermal activity responsible for the development of the Dong'an epithermal deposit.

5.4.2.3 Geochronology and Timing of Epithermal Systems in Northeast China

Uranium-Pb zircon (LA-ICPMS) and Ar-Ar isotopic age determinations of the volcanic and subvolcanic rocks that host the epithermal systems range from 231 to 79 Ma, clustering in the range of 130–110 Ma and with a peak at about 130–120 Ma (Fig. 5.32b). These ages show that the northeastern China epithermal systems are intimately associated with Jurassic-Early Cretaceous magmatism. In the northern Hinggan province, the most common host rocks of epithermal deposits are the late Jurassic to early Cretaceous (Tamulangou and Shangkuli formations). Almost all the epithermal deposits in this province are partly or wholly hosted by the early Cretaceous Shangkuli formation (148–111 Ma). Similarly, deposits in the southern Hinggan province are mostly hosted by Early Cretaceous volcanic rocks (Zhang 2006a; Zhang et al. 2006). In the Lesser Hinggan Range province, the above-described Dong'an and the Xinmin Au (Table 5.2) deposits are hosted by Early Cretaceous volcanic rocks. The Tuanjiegou deposit is hosted by Cretaceous plagiogranite porphyry (Sun et al. 1996), covered by early Cretaceous sedimentary

rocks revealed by fossil spores and pollen (GHCPAPF 1995). These demonstrate that the timing of epithermal mineralisation cannot be earlier than the beginning of early Cretaceous, and were more likely formed during middle to late early Cretaceous, considering the common gaps between epithermal deposits and associated volcanic host rocks. A few ages of alteration minerals indicate that epithermal metallogeny occurred in early Cretaceous, for example, the K-Ar age of sericite in ores of Jiawula is 121 Ma (Qin et al. 1998). In the Changbaishan province, the Jingouling formation, one of the host rocks, has ages of latest Early Cretaceous (Li et al. 2007). In conclusion, the age data indicate that most epithermal deposits in northeastern China were probably mostly formed in the early Cretaceous and some in the late Cretaceous and as such these mineral systems can be linked to the Great Hinggan large igneous province (Fig. 5.28), reviewed in Chap. 7.

5.4.2.4 Xilamulun Metallogenic Belt: The Jiguanshan Mo Deposit

The approximately east-west-trending Xilamunum metallologenic belt, is within an accretionary orogen on the northern margin of the North China Craton (NCC) that is part of the Hinggan fold belt, bound to the south by the Chifeng fault and to the north by the Xilamulun fault (Fig. 5.37). The Xilamulun metallogenic belt is known to contain at least 20 porphyry Mo deposits as well as vein-type and epithermal deposits, of which some of the economically most important, at the time of writing are: Chehugou, Kulitou, Daiheshan, Xiaodonggou and Jiguanshan porphyry Mo, Nianzigou and Xinjing vein-type Mo and Hongshanzi Mo-U epithermal deposit (Zhang et al. 2010). The host rocks of these deposits are mostly Triassic to Lower Cretaceous porphyritic granite, syenite, diorite, monzogranite, rhyolite, dacite and associated pyroclastic rocks and lamprophyre dykes. Age determinations, using whole-rock Rb-Sr isochron, SHRIMP zircon U-Pb and Re-Os on molybdenite, range from ca. 258 Ma to ca. 130 Ma (Zhang et al. 2010). On the basis of these age data, Zhang et al. (2010) suggested three stages of tectonic, igneous and mineralising events, as follows. A post-collisional-extension stage 1 between ca. 258 and 210 Ma (Indosinian) with a number of porphyry Mo deposits being formed (e.g. Kulitou); stage 2 occurred between ca. 185 and 150 Ma with Nianzigou and Daheishan vein and porphyry systems, which is also a common ore-forming time in the Great Hinggan Range (see above); stage 3 spans the time between ca. 140 and 110 Ma when the Liutiagou Mo-U deposit was formed. Stages 2 and 3 are probably linked to the geodynamics involving closure of the Mongol- Okhotsk ocean between the Siberia-Mongolia block and the NCC and the subsequent change to subduction of the Izanagi plate (Palaeo-Pacific plate) beneath the eastern Asian continental margin (Fig. 5.28) Lithospheric delamination and basaltic underplating have been invoked, with partial melting of the lower crust during late-orogenic and/or post-collisional regimes. Zeng et al. (2008) listed four types of Mo mineralisation in the Xilamulun belt, with ages from ca. 261–257 Ma, 183 Ma, 150–138 Ma. They are: (1) porphyry type (e.g. Xiandonggou, Jigaunshan, Chehugou); (2) quartz vein (e.g. Nianzigou); (3) intrusion-related (e.g. Gangzi); (4) epithermal (e.g. Liutiaogou). Again and as

suggested by Zhang et al. (2010), magmatic and associated mineral systems are linked to stages of post-collisional extension, following the amalgamation of the NCC and the Siberia-Mongolian plates in the Triassic and the lithospheric thinning associated with the Mesozoc Yanshanian events that affected east China.

The Jiguanshan Mo deposit was studied and described by Wu et al. (2011) and the following is extracted from this work. The Jiguanshan Mo deposit, located about 35 km north of Chifeng, Inner Mongolia (Fig. 5.37a). The Mo resources for this deposit are estimated at more than 10 Mt with grades ranging from 0.8 to 0.11 %. The local lithostratigraphic sequence consists of Permian volcanic and sedimentary rocks, unconformably overlain by the felsic volcanic and pyroclastic rocks of Mesozoic age (Yanshanian event) (Fig. 5.37b). The Mesozoic volcanic and pyroclastic rocks, grouped under the Manketouebo Formation, comprise lithic and crystal-vitric tuffs, dacite, rhyolite and subvolcanic rhyolite porphyry. The lithic and crystal-vitric tuffs are located in the centre and south of the mining district, are characterised by flow structures and devitrification textures and are intruded by the Jiguanshan granite porphyry. The rhyolite, also characterised by flow banding, occurs in the southern part of the mining district. The subvolcanic rhyolite porphyry is also exposed in the southern area of the mining district and emplaced as a volcanic dome. The Jiguanshan deposit is situated in a Mesozoic rift basin, where annular and radial fault structures strike predominantly east-northeast, northeast, northwest and north-northwest, which provided the channelways for hydrothermal fluids and Mo mineralisation The north-northwest-fault is filled by late fluorite veins cutting through the porphyry and pyroclastic rocks.

Igneous activity was most intensive in Late Jurassic, resulting in the emplacement of the host porphyry, post-ore mafic and quartz porphyry dykes. The Mo orebody is roughly spindle shaped and east-northeast-striking and cut by post-ore northeast-trending dolerite and northwest-trending quartz porphyry (Fig. 5.37b). More than 80 % of the Mo mineralisation is contained in the east-northeast-trending granite porphyry, with some of the mineralisation hosted in the tuff and rhyolitic rocks. Ore minerals are molybdenite and pyrite, with minor amounts of chalcopyrite, sphalerite and magnetite. The gangue minerals are predominately quartz, feldspar and sericite with minor amounts of calcite, fluorite and muscovite. Mineralisation styles include disseminations and stockworks. In the mine area there is widespread, potassic, sericitic, silica, fluorite, kaolinitic, pyritic, chloritic and carbonate hydrothermal alteration. Based on the mineral assemblages and crosscutting relationships, four hydrothermal stages have been identified. Silicification began in the earliest stage and continued throughout the entire hydrothermal alteration event. The second stage is dominated by K-feldspar-sericite alteration mainly localized in the upper parts of the granite porphyry. The main mineralisation episode is closely related to this K-feldspar-sericite alteration. The third stage is quartz-sericite and is widely distributed in the interior of the granite porphyry and in the fractures of the pyroclastic and rhyolitic rocks. Quartz-sericite alteration is associated with a subsequent mineralisation event. In the fourth stage, silicification, fluoritic, chloritic, carbonate and kaolinitic alteration are associated with minor molybdeite and sphalerite mineralisation.

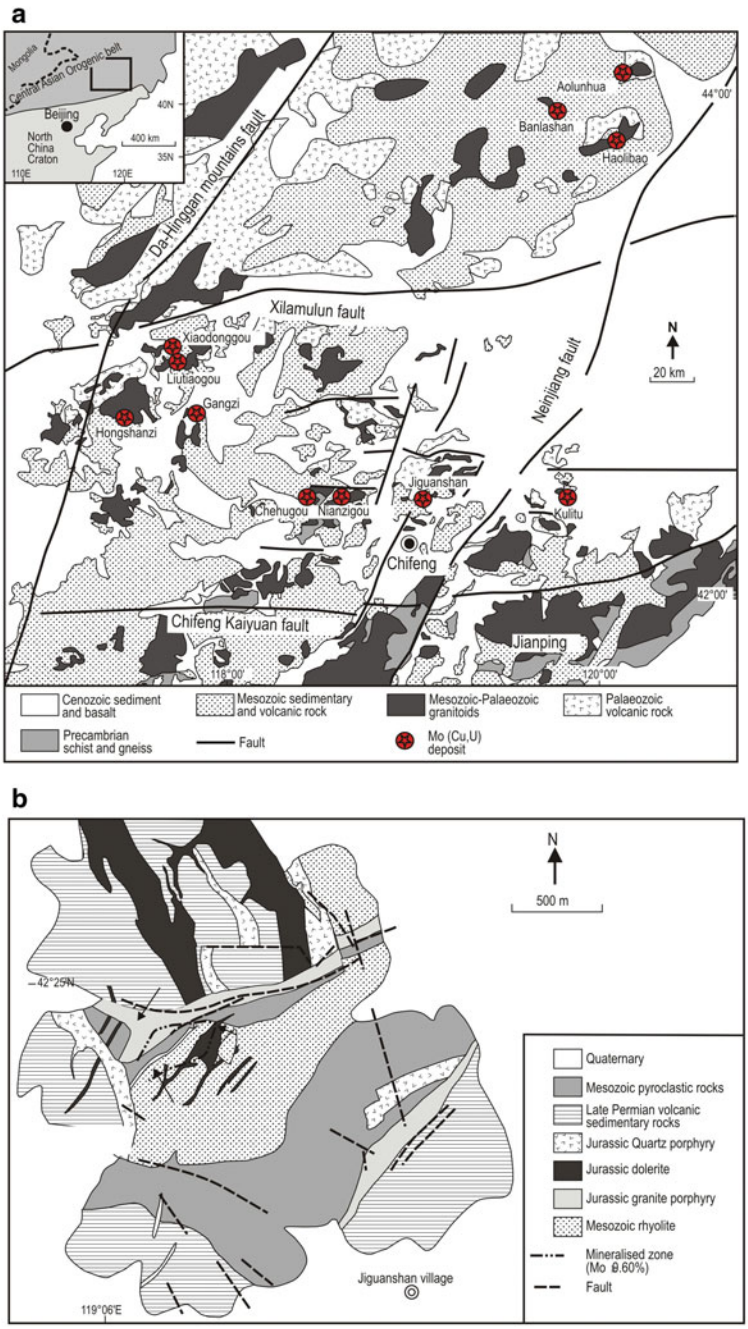

Fig. 5.37 Simplified geology of (**a**) Xilamulun metallogenic belt and distribution of porphyry systems and (**b**) Jiguanshan porphyry Mo deposit area. (After Wu et al. 2011)

Wu et al. (2011) reported on the results of Re-Os and Ar-Ar dating of molybdenite and whole rock, respectively. Molybdenite samples yield model ages ranging from 154.3 ± 2.5 to 156.2 ± 2.5 Ma, with a well-constrained $^{187}Re/^{187}Os$ isochron age of 155.4 ± 1.3 Ma and an average age of (155.3 ± 0.9 Ma). Six veinlet-type molybdenite samples yield relatively narrow ranges of Re–Os model ages from 151.7 ± 2.3 to 154.2 ± 2.3 Ma, with a well-constrained ^{187}Re–^{187}Os isochron age of 154.2 ± 3.1 Ma and an average of 153.0 ± 0.9 Ma. $^{40}Ar/^{39}Ar$ analytical results for the whole rock groundmass of host granite porphyry, post-ore dolerite and quartz porphyry. A well-defined plateau age of 155.2 ± 1.8 Ma was obtained for the host porphyry, whereas the post-ore mafic and quartz porphyry dykes show well-defined plateau ages of 149.8 ± 1.0 and 147.6 ± 0.9 Ma, respectively. These data restrict the time of the Mo mineralisation and host porphyry rocks between 156 and 154 Ma.

As mentioned above, the Xilamulun metallogenic belt in northeast China along the northern margin of the NCC, comprises several Mo deposits. These deposits have only recently been studied (Chen et al. 2008b; Qin et al. 2008; Wu et al. 2008, 2010; Zhang et al. 2009). The Jiguanshan porphyry Mo deposit, formed at about 155–160 Ma, is not the only mineralisation event at ca. 155 Ma in the Xilamulun metallogenic belt. In the Nianzigou Mo deposit, about 40 km west of the Jiguanshan Mo deposit (Fig. 5.37), the mineralisation was dated at 153–154 Ma (Zhang et al. 2009). Geochemical studies indicate that the host granite in the Nianzigou Mo deposit is an A-type granite, formed in an extensional setting (Chen et al. 2008b). The regional geology and geochronology results suggest that the Mo mineralisation in the Xilamulun belt developed in an extensional regime, as substantiated by the presence of post-mineralisation dykes in the Jiguanshan area. Regional extension occurred at around 155 Ma, in northeast China, providing additional time constraints for the inception of lithospheric extension in northeast China. Geochronology data for the Jiguanshan and the Nianzigou Mo deposits identify a mineralisation event at ca. 150–160 Ma in northeast China, which supports the series of metallogenic pulses in North China, namely 190–160 Ma, ca. 140 Ma and ca. 120 Ma, recognized by Mao et al. (2010).

5.4.3 Magmatic Mineral Systems

In this last section Palaeozoic to early Mesozoic orthomagmatic mineral Ni-Cu in late Triassic mafic-ultramafic rocks and Cr deposits are briefly introduced.

In northeast China and within the Hinggan fold belt there are about 1,000 mafic-ultramafic complexes (Wu et al. 2004). Close to the northeastern edge of the NCC, in the Hongqiling area, Jilin district, there is a series of northwest-trending mafic-ultramafic lens-shaped (zoned) intrusions and dykes, some of which host orthomagmatic disseminated and massive Ni-Cu sulphide mineralisation (Zhou et al. 2002b; Wu et al. 2004). Figure 5.38 shows the northwest-trending mafic-ultramafic intrusions in the Hongqiling district (see also Fig. 6.35). In the Hongqiling district at least five intrusions are known to have Ni-Cu sulphide mineralisation, of which

the No. 1 and No. 7 have been variably studied and commonly referred to in the literature as Hongqiling complex even though they are two separate intrusions. Lü et al. (2011) have made the distinction and called the No. 1 intrusion Dali and the No. 7 Fujia (Fig. 5.38). Indicated ore reserves for the No. 7 Fujia intrusion, reported by Zhou et al. (2002b; citing Chen and Li 1996) were 88.9 Mt grading 2.3 % Nim 0.63 % Cu and 0.05 % Co, starting production in 1971 at a rate of 108,000 tonnes of ore per year. Some details of the mineralogy of intrusion No. 7 and of its contained sulphides, can be found in Tang et al. (1992).

Zircon U-Pb SHRIMP dating of zircons from the Hongqiling mafic-ultramafic rocks yielded 216 ± 5 and 217 ± 3 Ma (Wu et al. 2004), whereas Re-Os dating of pyrrhotite from Ni-Cu sulphide ore in the Fuja intrusion, gave an age of 208 ± 21 Ma (Lü et al. 2011). These ages are more or less coincident with abundant A-type post-orogenic granitic magmatism in northeast China, suggesting widespread extensional tectonics in the region (Wu et al. 2004). Lü et al. (2011) noted an eastward younging trend for the mafic-ultramafic complexes and associated Ni-Cu deposits in the CAOB, from Late Caledonian (ca. 440 Ma), through Late Hercynian (300–265 Ma) in northwest China (Xinjiang province) to Late Indosinian (Triassic, 225–200 Ma) in northeast China. These authors suggested that this age trend may relate to gradual closure, from west to east, of the oceanic branch (Mongol-Okhotsk ocean), between the NCC and the Siberian Craton.

The No. 1 or Dali intrusion was emplaced into biotite gneiss and marble rocks of the Hulan Group. The intrusion is 980 m long, 280–150 m wide and is known to a depth of 560 m The intrusion is a zoned mafic-ultramafic complex made up of lherzolite and olivine websterite in the lower parts and pyroxenite (bronzitite) and gabbro in the upper parts (Wu et al. 2004). The orebody is at the base of the ultramafic section, as shown in a cross-section shown by Zhou et al. (2002b). The No. 7 intrusion (Fujia) at the southern end of the Hongqiling district (Fig. 5.38) is effectively a dyke, about 700 m long and 35 m average width and a maximum depth extent of 533 m, with similar rock types as the Dali intrusion, hosting the most significant Ni-Cu sulphide mineralisation. Wu et al. (2004) pointed out that almost the entire intrusion is effectively an orebody, characterised by disseminated sulphides in the bronzitite and massive sulphides in the ultramafic units. Ore minerals are mainly pyrrhotite, pentlandite and chalcopyrite mainly.

Although the topic of crustal contamination is taken up again in Chap. 7, when discussing the Jinchuan Ni-Cu deposit, Wu et al. (2004) do not consider that crustal contamination played a significant role in causing the development of Ni-Cu sulphides in the Hongqiling intrusions. It is generally assumed that mantle-derived magmas are sulphide-undersaturated and therefore sulphide saturation and immiscible sulphide ores must be a consequence of sulphur contamination of the parental magma. This contamination would be provided by crustal materials, as advocated by many authors (see Naldrett 2004 and references therein). However, there are some doubts if this is valid in all cases (Seat et al. 2009). Wu et al. (2004) proposed that in the case of the Hongqiling orthomagmatic sulphide deposits, the magma was saturated in sulphides after crystal fractional crystallisation, followed by immiscibility and precipitation of the Ni-Cu sulphides.

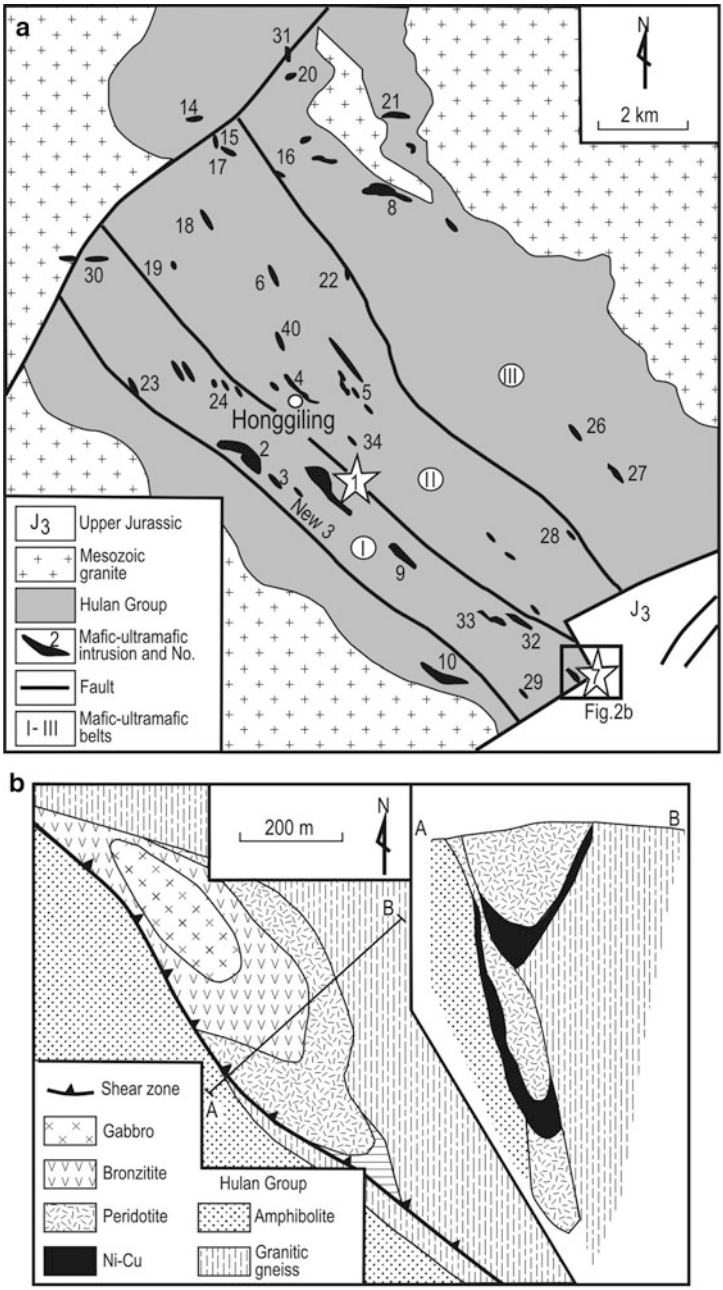

Fig. 5.38 **a** Hongqiling northwest-trending mafic-ultramafic intrusions (after Wu et al. 2004); **b** simplified geology and cross-section of the No. 1 intrusion and orebody. (After Zhou et al. 2002b)

5.4.3.1 Chromitite in Zoned Mafic-ultramafic Intrusions (Alaskan Type)

The Gaosi (Gaositai) complex intruded into granitic gneisses of Archaean age (Zhou and Bai 1992) and has recently been recognised as an Alaskan-type intrusion, emplaced along the east-west-trending Datong-Chengde Fault (Solonker suture) (Chen et al. 2009b; Tian et al. 2011). The Gaosi (or Gaositai) chromite deposit is hosted in a 9 km-long and 1–1.5 km wide zoned intrusion that consists mainly of dunite and pyroxenite (diopside), with pegmatoidal (or coarse-grained dunite) and fine-grained dunite in the central parts of the intrusive body, surrounded by envelopes of peridotite and pyroxenite (diopsidite) (Zhou and Bai 1992; Fig. 3.7). Furthermore, and again highlighting some of the uncertainties inherent to assumptions that some mafic-ultramafic rocks were originally part of the NCC, Tian et al. (2011), recorded a Re-Os age of 280 Ma for the Gaosi complex. In this case the Alaskan-type Gaosi (Gaositai) intrusion, and several others of the same type and presumably of the same age, would have been emplaced during southward subduction of the Palaeo-Asian oceanic slab, beneath the northern margin of the NCC, which acted as an Andean-type continental margin (Fig. 5.30c). The Gaosi (Gaositai) complex contains chromite mineralisation hosted in the pegmatoidal dunite, forming veins, disseminated, massive and layered ores, as well as breccia ores consisting of dunite clasts cemented by chromite. Zhou and Bai (1992) reported that similar chromite ores are present in other zoned intrusions, such as Pinding, Maojia, Zhuling and Fongma (Fig. 3.7). The 40 km^2 Xiaosong zoned intrusion consist of dunite, pyroxenite and gabbro. Disseminated, massive and banded chromite mineralisation is hosted by dunite at the base of the intrusion, whereas Cu-Ni sulphides are present in the gabbro units.

5.5 Concluding Remarks

The orogenic belts of South China, Central China, Qinling and Hinggan have all been extensively affected by the large-scale Mesozoic (Indosinian and Yanshanian) tectono-thermal events. Northeastern China was also involved in subduction and closure of Mongolia-Okhosk oceanic plate as well as subduction of Palaeo-Pacific Plate during Triassic-early Cretaceous time.

The abundance and variety of mineral systems that are present in these orogenic fold belts are mostly a consequence, directly or indirectly of this event. However, it must be pointed out that a number of mineral deposits of Indosinian age (>200 Ma), as is the case for the Xilamulun metallogenic belt, were later reworked or overprinted by Yanshanian magmatism. This is confirmed by the dating of monazite and molybdenite from a Mo-mineralised quartz vein in the Xiaoqiling terrane, recently reported (Li et al. 2011). In this work, the authors showed the presence of two hydrothermal monazites, one of the same age as the molybdenite (Re-Os; ca. 216 Ma) and the other at ca. 125 Ma, indicated by a mixing array. The Yanshanian tectono-thermal event of eastern China has been attributed to removal of subcontinental mantle lithosphere

and upwelling of asthenospheric mantle, as evidenced by seismic tomography studies (Griffin et al. 1998; Wu et al. 2005a; Zhao et al. 2010; Santosh et al. 2010). Yanshanian magmatism and its causes are discussed in more detail in Chap. 7. The Mesozoic igneous intrusions are accompanied by metamorphic core complexes and basin-and-range type structures, indicating crustal uplift and extension. Geochronological studies show that this Mesozoic magmatism occurred from the Triassic to Cretaceous, with peaks of activity at 233–210, 180–150 and 135–115 Ma. Triassic to Jurassic magmas were mostly derived from partial melting of ancient crust, whereas the Cretaceous magmas show juvenile signatures, indicating stronger mantle-derived components, leading to alkali basaltic magmatism that continues to the present day (Yang et al. 2008; Xu et al. 2005). These processes of fragmentation of lithospheric roots, crustal and lithospheric thinning, extension and rifting were probably first triggered by the Triassic collision between the NCC and the Yangtze Craton, followed by and/or associated with slab break-off of the subducting Pacific (Izanagi) plate (Yang et al. 2008). It is within these evolving geodynamic regimes that widespread and younger metallogeny was superimposed on the orogenic belts described in this chapter. Another issue worthy of mention in this concluding section is the unusual setting and characteristics of the porphryry deposits in the Qinling orogen and indeed along the northern margin of the NCC (see Chap. 3). These porphyry systems are intracontinental and cannot be directly linked to a subduction setting on a continental margin, such as those of the Andean belt. These intracontinental porphyry systems (and allied skarn and Fe deposits, largely due to granitic intrusions interacting with carbonate lithologies), typically have low-H_2O alteration mineral assemblages (K-feldspar, epidote), in addition to fluorite (in some cases quite abundant). Chen and Li (2009) were the first to recognise these differences. Fluid inclusion studies by these researchers indicate high ratios of K/Na, F/Cl and CO_2/H_2O, supporting the idea that these intracontinental porphyry are not subduction-related.

References

Agangi A, Kamenetsky VS, McPhie J (2010) The role of fluorine in the concentration and transport of lithophile trace elements in felsic magmas: insights from the Gawler Range Volcanics, South Australia. Chem Geol 273:314–325

Bagby WC, Berger BR (1985) Geologic characteristics of sediment-hosted, disseminated precious-metal deposits in the western United States. Rev Econ Geol 2:169–202

Berger BR (1986) Descriptive model of carbonate-hosted Au–Ag. In: Cox DP, Singer DA (eds) Mineral deposit models. U.S. Geological Survey Bulletin 1693, p 175

Bi SJ, Li JW, Zhou MF, Li ZK (2011) Gold distribution in As-deficient pyrite and telluride mineralogy of the Yangzhayu gold deposit, Xiaoqinling district, southern North China craton. Miner Depos 46:925–941

Bureau of Geology and Mineral Resources of Gansu Province (1989) Regional geology of Gansu Province. Geological Publishing House, Beijing, pp 70–292

Burnham CW (1985) Energy release in subvolcanic environments: implications for breccia formation. Econ Geol 80:1515–1522

Cao SE (1994) Geologic characteristics and prospecting directions of gold deposits in Heilongjiang province. Gold Geol Technol 39(1):31–35 (in Chinese with English abstract)

Chappell BW, White AJR (1974) Two contrasting granite type. Pac Geol 8:173–174
Chen YJ, Fu SG (1992) Gold mineralisation in West Henan, China. China Seismological Press, Beijing, p 234 (in Chinese)
Chen HC, Li JH (1996) The discovery history of mineral deposits of China, The Jiling Volume. Geological Publishing House, Beijing, pp 45–49
Chen YJ, Chen HY, Zaw K, Pirajno F, Zhang ZJ (2007) Geodynamic settings and tectonic model of skarn gold deposits in China: an overview. Ore Geol Rev 31:139–169
Chen YJ, Li N (2009) Nature of ore fluids of intracontinental intrusion-related hypothermal deposits and its difference from those in island arcs. Acta Petrol Sin 25:2477–2508 (in Chinese with English abstract)
Chen RY, Rui ZY (1993) Geological characteristics and metallogenic mechanism of the Wufeng epithermal gold deposit, Jilin province. Miner Depos 12(1):20–28 (in Chinese with English abstract)
Chen H, Xu B (1997) Isotope tracing and prospecting assessment of gold-silver deposits in Zhejiang Province. Acta Geol Sin 71(3):293–304
Chen YJ, Guo GJ, Li X (1998) Geodynamical setting of mineralization for the Cenozoic gold mines in the greenstone terrain of North China Craton. Sci China Ser D 28:35–40
Chen YJ, Li C, Zhang J, Li Z, Wang H (2000a) Sr and O isotopic characteristics of porphyries in the Qinling molybdenum deposit belt and their implication to genetic mechanism and type. Sci China D 43(Suppl):82–94 (in Chinese)
Chen CH, Lin W, Lu HY, Lee CY, Tien JL, Lai YH (2000b) Cretaceous fractionated I-type granitoids and metaluminous A-type granites in SE China: the Late Yanshanian post-orogenic magmatism. Trans Royal Soc Edinb Earth Sci 91:195–205
Chen M, Nie ZH, Wang XZ, Liang HJ, Song BJ (2002) Features of volcanic rocks and the prospecting direction of rock gold in the upper Heilongjiang. Gold Geol 8(4):37–42 (in Chinese with English abstract)
Chen YJ, Pirajno F, Sui YH (2004a) Isotope geochemistry of the Tieluping silver-lead deposit, Henan, China: a case study of orogenic silver-dominated deposits and related tectonic setting. Miner Depos 39:560–575
Chen YJ, Zhang J, Zhang FX, Pirajno F, Li C (2004b) Carlin and Carlin-like gold deposits in western Qinling mountains and their metallogenic time, tectonic setting and model. Geol Rev 50:134–152
Chen YJ, Pirajno F, Qi JP, Li J, Wang HH (2006) Ore geology, fluid geochemistry and genesis of the Shanggong gold deposit, eastern Qinling Orogen, China. Res Geol 56:99–116
Chen YJ, Pirajno F, Qi JP (2008a) The Shanggong gold deposit, Eastern Qinling Orogen, China: isotope geochemistry and implications for ore genesis. Asian J Earth Sci 33:252–266
Chen ZG, Zhang LC, Wu HY, Wan B, Zeng QD (2008b) Geochemistry study and tectonic background of A style host granite in Nianzigou Mo deposit in Xilamulun Mo metallogenic belt, Inner Mongolia. Acta Pet Sin 24:879–889 (in Chinese with English abstract)
Chen YJ, Pirajno F, Li N, Qi JP, Guo DS, Lai L (2009a) Isotope systematics and fluid inclusion studies of the Qiyugou breccia pipe-hosted gold deposit, Qinling Orogen, Henan province, China: implications for ore genesis. Ore Geol Rev 35:245–261
Chen B, Suzuki K, Tian W, Jahn B-M, Ireland T (2009b) Geochemistry and Os-Nd-Sr isotopes of the Gaositai Alaskan-type ultramafic complex from northern North China Craton: implications for mantle-crust interaction. Contrib Miner Pet 158:683–702
Cline JS, Hofstra AH, Muntean JL, Tosdal RM, Hickey KA (2005) Carlin-type gold deposits in Nevada: critical geologic characteristics and viable models. Econ Geol 100th Ann Iss:451–484
Cong RX, Yuan JH, Zhang X (1999) The features of volcanic rocks and gold mineralization in Mohe, Heilongjiang. Gold Geol 5(3):37–40 (in Chinese with English abstract)
Dai JZ, Mao JW, Xie GQ, Yang FQ, Wang YT, Zhao CS (2009) U-Pb, Re-Os dating and geodynamic setting of the Xiaojiayingzi Mo (Fe) deposit, western Liaoning province, China. Ore Geol Rev 35:235–244

Davis GA, Zheng YD, Wang C, Darby JD, Zhang CH, Gehrels G (2001) Mesozoic tectonic evolution of the Yanshan fold and thrust belt, with emphasis on Hebei and Liaoning provinces, northern China. Geol Soc Am Mem 194:171–197

Davis GA, Xu B, Zheng YD, Zhang WJ (2004) Indosinian extension in the Solonker suture zone: the Sonid Zuoqi metamorphic core complex, Inner Mongolia, China. Earth Sci Front 11:135–144 (in Chinese with English abstract)

de Jong K, Xiao WJ, Windley BF, Masago H, Lo CH (2006) Ordovician $^{40}Ar/^{39}Ar$ phengite ages from the blueschist-facies Ondor Sum subduction-accretion complex (Inner Mongolia) and implications for the early Paleozoic history of continental blocks in China and adjacent areas. Am J Sci 306:799–845

Deng JF, Mo XX, Zhao HL, Wu ZX, Luo ZH, Su SG (2004) A new model for the dynamic evolution of Chinese lithosphere: 'continental roots—plume tectonics'. Earth Sci Rev 65:223–275

Deng JF, Zhou MF, Flower MF I, Su SG, Zhai MG, Liu C, Zhao GC, Zhou S, Wu ZW (2007) A mechanism for transforming buoyant North Chinese cratonic lithosphere to a denser equivalent for delamination. Geol Soc, London, Sp Publ 280:317–330

Dong YP, Zhang GW, Hauzenberger C, Neubauer F, Yang Z, Liu XM (2010) Paleozoic tectonics and evolutionary history of the Qinling orogen: evidence from geochemistry and geochronology of ophiolite and related volcanic rocks. Lithos 122(1–2):39–56

Eby GN (1992) Chemical subdivision of the A-type granitoids: petrogenetic and tectonic implications. Geology 20:641–644

Fan SH, Jin QH (1994) The model of Shuanghwang gold deposit, Shannxi province. In: Liu DS, Tan YJ, Wang JY, Jiang SF (eds) Chinese Carlin-type gold deposits. Nanjing University Press, Nanjing, pp 254–285 (in Chinese)

Fan WM, Guo F, Wang YJ, Lin G (2003) Late Mesozoic calc-alkaline volcanism of post-orogenic extension in the northern Da Hinggan Mountains, northeastern China. J Volcanol Geotherm Res 121:115–135

Faure G (1986) Principles of isotope geology, 2nd edn. Wiley, New York, p 589

Feng SZ (1998) Metallogenetic and geological features of Wufeng-Wuxingshan gold deposit in Jilin province. Volcanol Miner Res 19(2):113–118 (in Chinese with English abstract)

Fowler MB, Henney PJ, Darbushire DPF, Greenwood PB (2001) Petrogenesis of high Ba-Sr granites: the Rogart pluton, Sutherland. J Geol Soc Lond 158:521–534

Fu ZC, Jin LC, Wang WL (2001) Metallogenic regularity of the Ergenhe gold deposit. Heilongjiang Geol 12(3):23–26 (in Chinese with English abstract)

Gao S, Luo TC, Zhang BR, Zhang HF, Han YW, Zhao ZD, Hu YK (1998) Chemical composition of the continental crust as revealed by studies in East China. Geochim Cosmochim Acta 62:1959–1975

Gao S, Rudnick RL, Carlson RW, Mcdonough WF, Liu YS (2002) Re–Os evidence for replacement of ancient mantle lithosphere beneath the North China craton. Earth Planet Sci Lett 198:307–322

Gao S, Rudnick RL, Yuan HL, Liu XM, Liu YS, Xu WL, Ling WL, Ayers J, Wang XC, Wang QH (2004) Recycling lower continental crust in the North China craton. Nature 432:892–897

Ge WC, Lin Q, Sun DY, Wu FY, Won CK, Lee MW, Jin MS, Yun SH (1999) Geochemical characteristics of the Mesozoic basalts in Da Hing'an Ling: evidence of the mantlecrust interaction. Acta Pet Sin 15:397–407 (in Chinese with English abstract)

Gernet J (1999) A history of Chinese civilization. Cambridge University Press, Cambridge, p 801

Gold Headquarters of the Chinese People's Armed Police Force (GHCPAPF) (1995) Geology of Tuanjiegou porphyry gold deposit in Heilongjiang. Seismic Press, Beijing, p 134 (in Chinese with English abstract)

Goldfarb RJ, Phillips GN, Nokleberg WJ (1998) Tectonic setting of synorogenic gold deposits of the Pacific Rim. Ore Geol Rev 13:185–218

Goldfarb RJ, Groves DI, Gardoll S (2001) Orogenic gold and geologic time: a global synthesis. Ore Geol Rev 18:1–75

Goldfarb RJ, Hart G, Davis G, Groves DI (2007) East Asian gold: deciphering the anomaly of Phenorozoic gold in Precambrian Cratons. Econ Geol 102:341–345

Griffin WL, Zhang A, O'Reilly SY, Ryan CG (1998) Phanerozoic evolution of the lithosphere beneath the Sino-Korean craton. In: Flower MFJ, Chung SL, Lo CH, Lee TY (eds) Mantle dynamics and plate interaction in East Asia. American Geophysical Union, Geodynamics Ser 27, pp 107–126

Groves DI, Goldfarb RJ, Gebre-Mariam M, Hagemann SG, Robert F (1998) Orogenic gold deposits: a proposed classification in the context of their crustal distribution and relationship to other gold deposit types. Ore Geol Rev 13:7–27

Guan JD, Chai XH (2004) Geological characteristics and genesis of the Siwumuchang epithermal gold deposit, eastern Inner Mongolia. Geol Prospect 40(2):36–40 (in Chinese with English abstract)

Guo GJ (2001) Characteristics of ore fluids and genesis of Xiaokouhuaying silver deposit in Yan-Liao area. In: Chen YJ, Zhang J, Lai Y (eds) Continental geodynamics and metallogeny. Seismic Press, Beijing, pp 148–153 (in Chinese)

Guo GJ, Wang SQ (1998) REE geochemistry of Xiaokouhuaying silver-manganese deposit in Heibei province. Acta Sci Nat Univ Pekin 34(4):510–518 (in Chinese with English abstract)

Guo F, Fan WM, Wang YJ, Lin G (2001) Petrogenesis of the late Mesozoic bimodal volcanic rocks in the southern Da Hinggan Mts, China. Acta Pet Sin 17:161–168 (in Chinese with English abstract)

Guo JH, Wang CS, Shi YJ (2004) Geological and geochemical features of the Dong'an gold deposit in Heilongjiang. Geol Prospect 40(4):37–41 (in Chinese with English abstract)

Guo DS, Chen YJ, Qi JP (2007) Isotope geochemistry and ore genesis of the Qiyugou gold deposit, Henan: a synthesis. Geol Rev 53:217–228 (in Chinese with English abstract)

Hacker BR, Wang X, Eide EA, Ratschbacher L (1996) The Qinling-Dabie ultra-high pressure collisional orogen. In: Yin A, Harrison TM (eds) The Tectonic evolution of Asia. Cambridge University Press, Cambridge, pp 345–370

Han YG, Zhang SH, Pirajno F, Zhang YH (2007) Evolution of the Mesozoic granites in the Xiong'ershan-Waifangshan region, western Henan province, China, and its tectonic implications. Acta Geol Sin 81(2):253–265

Han YG, Zhang SH, Pirajno F, Wang Y, Zhang YH (2009) New $^{40}Ar/^{39}Ar$ age constraints on the deformation along the Machaoying fault zone: implications for Early Cambrian tectonism in the North China Craton. Gondwana Res 16:255–263

He ZY, Xu XS (2011) Petrogenesis of the Late Yanshanian mantle-derived intrusions in south-eastern China: response to the geodynamics of paleo-Pacific plate subduction. Chem Geol. doi:10.1016/j/chemgeo.2011.09.014

He YH, Zhao GC, Sun M, Wilde SA (2008) Geochemistry, isotope systematics and petrogenesis of the volcanic rocks in the Zhongtiao Mountain: an alternative interpretation for the evolution of the southern margin of the North China Craton. Lithos 102:158–178

Hedenquist JW, Lowenstern JB (1994) The role of magmas in the formation of hydrothermal ore deposits. Nature 370:519–527

Hilde TWC, Uyeda S, Kroenke L (1977) Evolution of the western Pacific and its margin. Tectonophysics 38:145–165

Ho CS (1986) A synthesis of the geological evolution of Taiwan. Tectonophysics 125:1–16

Hoefs J (2004) Stable Isotope Geochemistry, 5th edn. Springer, Berlin

Hofstra AH, Cline JS (2000) Characteristics and models for Carlin-type gold deposits. Rev Econ Geol 13:163–221

Hou ZQ, Zaw K, Rona P, Li YQ, Qu XM, Song SM, Peng L, Huang JJ (2008) Geology, fluid inclusions and oxygen isotope geochemistry of the Baiyinchang pipe-style volcanic-hosted massive sulfide Cu deposit in Gansu province, northwestern China. Econ Geol 103:269–292

Hou ZQ, Tian SH, Xie YL, Yang ZS, Yuan ZX, Yin SP, Yi LS, Fei HC, Bai G, Li XY (2009) The Himalayan Mianning-Dechang REE belt associated with carbonatite-alkaline complexes, eastern Indo-Asian collision zone, SW China. Ore Geol Rev 36:65–89

Hou ZQ, Zhang HR, Pan XF, Yang ZM (2011) Porphyry Cu (-Mo-Au) deposits related to melting of thickened mafic lower crust: examples from the eastern Tethyan metallogenic domain. Ore Geol Rev 39:21–45

Hsü KJ, Guitang P, Şengör AMC, Ueli B, Chen H, Chen C, Harris N, Hsu P, Li J, Luo J, Lee T, Li ZX, Lu C, Powell C, Wang Q, Winterer EL (1995) Tectonic evolution of the Tibetan Plateau: a working hypothesis based on the Archipelago model of orogenesis. Int Geol Rev 37:473–508

Huang TK, Hsu KC (1936) Mesozoic orogenic movements in the Pinghsiang coalfield, Kiangsi. Bull Geol Soc China 16:177–194

Huang DH, Wang Y, Nie F, Jiang X (1984) Isotopic composition of sulphur, carbon and oxygen and source material of the Huanglongpu carbonatite vein-type of molybdenum (lead) deposits. Acta Geol Sin 3:252–264 (in Chinese with English abstract)

Huang DH, Wu CY, Du AD, He HL (1995) Re-Os isotope ages of moybdnemum deposits in East Qinling and their significance. Chin J Geochem 14:313–322

Jahn BM, Zhou XH, Li JL (1990) Formation and tectonic evolution of southeastern China and Taiwan: isotopic and geochemical constraints. Tectonophysics 183:145–160

Jian P, Liu DY, Kröner A, Windley BF, Shi YR, Zhang W, Zhang FQ, Miao LC, Zhang LQ, Tomurhuu D (2010) Evolution of a Permian intraoceanic arc-trench system in the Solonker suture zone, Central Asian orogenic Belt, China and Mongolia. Lithos 118:169–190

Jiang ZY, Wang XY, Liang HJ, Wang XZ (2002) Study on the geological characteristics and fluid inclusion of volcanic gold deposits in the east of Jilin. Gold Geol 8(2):26–30 (in Chinese with English abstract)

Jin LY, Hao XY (2000) The genetic feature of Ciweigou gold deposit. Gold 21(10):8–11 (in Chinese with English abstract)

John DA (2001) Miocene and early Pliocene epithermal gold-silver deposits in the northern Great Basin, western United States: characteristics, distribution, and relationship to magmatism. Econ Geol 96:1827–1853

Kirwin DJ (1985) Tourmaline breccia pipes. Msc thesis, James Cook University, North Queensland, p 139 (unpublished)

Kusky TM, Li JH (2003) Paleoproterozoic tectonic evolution of the North China Craton. J Asian Earth Sci 22:383–397

Kwon S, Sajeev K, Mitra G, Park Y, Kim SW, Ryu IC (2009) Evidence for Permo-Triassic collision in Far East Asia: the Korean collisional orogen. Earth Planet Sci Lett 279:340–349

Lai SC, Zhang GW, Yang RY (2000) Identification of the island-arc magmatic zone in the Lianghe-Raofeng-Wuliba area, south Qinling and its tectonic significance. Sci China 43:69–81

Lang JR, Baker T (2001) Intrusion-related gold systems: the present level of understanding. Miner Depos 36:477–489

Large RR, Bull SW, Maslennikov VV (2011) A carbonaceous sedimentary source-rock model for Carlin-type and orogenic gold deposits. Econ Geol 106:331–358

Li ZX (1998) Tectonic history of the major East Asian lithospheric blocks since the mid-Proterozoic—a synthesis, Mantle Dynamics and plate interactions in East Asia. American Geophysical Union, Washington, DC, pp 221–243

Li YF (2005) The temporal-spatial evolution of Mesozoic granitoids in Xiong'ershan area and their relationships to molybdenite–gold mineralisation. PhD thesis, China University of Geosciences, Beijing, p 135 (unpublished)

Li YD, Li YT (1994) Geological characteristics and genesis model of Laerma disseminated-type gold deposits, Gansu province. In: Liu DS, Tan YJ, Wang JY, Jiang SF (eds) Chinese Carlin-type gold deposits. Nanjing University Press, Nanjing, pp 226–253 (in Chinese)

Li ZX, Li XH (2007) Formation of the 1,300-km-wide intracontinental orogen and postorogenic magmatic province in Mesozoic South China: a flat-slab subduction model. Geology 35:179–182

Li XC, Qin KZ (1999) Distribution pattern of major ore-forming elements and its significance in the Jiawula-Chagan Ag-Pb-Zn-Cu orefield, Inner Mongolia. Geol Explor Non Ferr Met 8(6):512–516 (in Chinese with English abstract)

Li TD, Xiao XC (1996) Terrane structural analysis of the Tibet Plateau. The Lithospheric architecture and the development of the Tibet Plateau. Geological Publishing House, Beijing, pp 6–20

Li SG, Xiao Y, Liou D, Chen Y, Ge N, Zhang Z, Sun SS, Cong B, Zhang R, Hart SR, Wang S (1993) Collision of the North China and Yangtze blocks and formation of coesite-bearing eclogites: Timing and processes. Chem Geol 109:89–111

Li GS, Chen JR, Wang YZ, Jin BY, Wu YH, Yu WQ (2003a) Study on the main mineralization type and the inclusion features of the Jinchang gold deposit, Heilongjiang. Gold Geol 9(1):32–37 (in Chinese with English abstract)

Li YJ, Ding S, Chen YB, Liu ZW, Dong JG (2003b) New knowledge on the Wenquan granite in western Qinling. Geol Miner Resour South China 3:1–8 (in Chinese with English abstract)

Li YF, Mao JW, Guo BJ, Shao YJ, Fei HC, Hu HB (2004) Re-Os dating of Molybdenite from the Nannihu Mo (-W) orefield in the East Qinling and its geodynamic significance. Acta Geol Sin 78:463–470

Li Q, Liu HP, Kong HQ, Li YS, Jiang SJ (2006) Geologic features and genesis of Xinmin gold deposit, north Xiaoxin'anling Mountain. Gold 3(27):14–17 (in Chinese with English abstract)

Li CW, Guo F, Fan WM, Gao XF (2007) Ar-Ar geochronology of Late Mesozoic volcanic rocks from the Yanji area, NE China and tectonic implications. Sci China Ser D Earth Sci 50(4):505–518

Li N, Chen YJ, Fletcher IR, Zeng QT (2011) Triassic mineralization with Cretaceous overprint in the Dahu Au-Mo deposit, Xiaoqinling gold province: constraints from SHRIMP monazite U-Th-Pb geochronology. Gondwana Res 20:543–552

Li WB, Zhong R, Xu C, Song B, Qu WJ (in press) U-Pb, Re-Os geochronology of the Bainaimiao Cu-Mo-Au deposit in the North China Craton, Central Asia Orogenic Belt: implications for ore genesis and geodynamic setting. Ore Geol Rev

Liang JH, Jin CZ, Wang JG (2003) The hydrogen and oxygen isotope characteristics of epithermal-porphyry gold series in Yanbian region. Contrib Geol Miner Resour Res 18(2):108–112 (in Chinese)

Lin Q, Ge WC, Sun DY, Wu FY, Chong KW (1998) Tectonic significance of Mesozoic volcanic rocks in northeastern China. Sci Geol Sin 33(2):129–139 (in Chinese with English abstract)

Lin Q, Ge WC, Cao L, Sun DY, Lim KG (2003) Geochemistry of Mesozoic volcanic rocks in Da Hinggan Ling: the bimodal volcanic rocks. Geochimica 32(3):208–222 (in Chinese with English abstract)

Liou JG, Zhang RY, Wang X, Eide EA, Ernst WG, Maruyama S (1996) Metamorphism and tectonics of high-pressure and ultra-high-pressure belts in the Dabie-Sulu region, China. In: Yin A, Harrison TM (eds) The Tectonic evolution of Asia. Cambridge University Press, Cambridge, pp 281–299

Liu BS, Lu J (2006) Geological, geochemical and genetic study of the Sandaowanzi quartz vein-type gold deposit in Heihe city, Heilongjiang province. Geotecton Metallog 30(4):481–485 (in Chinese with English abstract)

Liu JM, Zhang R, Zhang QZ (2004) The regional metallogeny of Da Hinganling, China. Earth Sci Front 11(1):269–277 (in Chinese with English abstract)

Liu GG, Wang ED, Chang CJ, Jin BY, Yu WQ (2006) Discussion on metallogeny of Gaosongshan gold deposit, Xunke County, Heilongjiang province. Non Ferr Min Metall 22(4):1–4 (in Chinese with English abstract)

Lü LS, Mao JW, Li HB, Pirajno F, Zhang ZH, Zhou ZH (2011) Pyrrhotite Re-Os and SHRIMP zircon U-Pb dating of the Hongqiling Ni-Cu sulfide deposits in NE China. Ore Geol Rev 43(1):106–119

Luo ZW (1997) Geological characteristics of mineralization and ore prospecting indicators in the Erbahuo silver deposit. Miner Res Geol 11(58):87–90 (in Chinese with English abstract)

Luo MJ, Zhang FM, Dong QY, Xu YR, Li SM, Li KH (1991) Molybdenum deposits in China. Henan Press Sci Tech, Zhengzhou, p 452 (in Chinese)

Luo MJ, Li SM, Lu XX (2000) Major metallogenic series of ore deposits in Henan Province. Geological Publishing House, Beijing, p 136

Ma CQ, Yang KG, Ming HL, Lin CC (2004) The timing of tectonic transition from compression to extension in Dabieshan: evidence from Meszoic granites. Sci China D 47(5):453–462

Mao YN, Li XZ (1994) The main geological characteristics of Dongbeizhai gold deposit in joint area of Sichuan, Gansu and Shannxi provinces. In: Liu DS, Tan YJ, Wang JY, Jiang SF (eds) Chinese Carlin-type gold deposits. Nanjing University Press, Nanjing, pp 317–342 (in Chinese)
Mao JW, Zhang ZC, Zhang ZH, Du AD (1999) Re-Os isotopic dating of molybdenites in the Xiaoliugou W-(-Mo) deposit in the northern Qulian Mountains and its geological significance. Geochim Cosmochim Acta 63:1815–1818
Mao JW, Qiu YM, Goldfarb RJ, Zhang ZC, Garwin S, Fengshou R (2002a) Geology, distribution, and classification of gold deposits in the western Qinling belt, central China. Miner Depos 37:352–377
Mao JW, Godlfarb RJ, Zhang ZW, Xu WY, Qiu YM, Deng J (2002b) Gold deposits in the Xiaoqinling-Xiong'ershan region, Qinling Mountains, central China. Miner Depos 37:306–325
Mao JW, Xie GQ, Zhang ZH, Li XF, Wang YT, Zhang CQ, Li YF (2005) Mesozoic large-scale metallogenic pulses in North China and corresponding geodynamic settings. Acta Pet Sin 21(1):169–188 (in Chinese with English abstract)
Mao JR, Hu Q, Xu NZ, Chen R, Ye HM, Zhao XL (2006) Mesozoic magmatism and copper polymetallic mineralization processes in the Shanghang-Datian region, Fujan Province, southeast China. Chin J Geochem 25:266–278
Mao JW, Li XF, White NC, Zhao CS, Zhang ZH, Wang YT, Hu HB (2007) Types, characteristics, and geodynamic settings of Mesozoic epithermal gold deposits in Eastern China. Resour Geol 57:435–454
Mao JW, Xie QG, Bierlein FP, Qu WJ, Du AD, Ye HS, Pirajno F, Li HM, Guo BJ, Li YF, Yang ZQ (2008a) Tectonic implications from Re-Os dating of Mesozoic molybdenum deposits in the East Qinling-Dabie orogenic belt. Geochim Cosmochim Acta 72:4607–4626
Mao JW, Xie GQ, Guo CL, Yuan SD, Cheng YB, Chen YC (2008b) Spatial-temporal distribution of Mesozoic ore deposits in South China and their metallogenic settings. Geol J China Univ 14:510–526 (in Chinese with English abstract)
Mao JW, Xie GQ, Pirajno F, Ye HS, Wang YB, Li YF, Xiang JF, Zhao HJ (2010) Late Jurassic-Early Cretaceous granitoid magmatism in Eastern Qinling, central-eastern China: SHRIMP zircon U-Pb ages and tectonic implications. Aust J Earth Sci 57:51–78
Mao JW, Pirajno F, Xiang JF, Gao JJ, Ye HS, Li YF, Guo BJ (2011) Mesozoic molybdenum deposits in the East Qinling-Dabie orogenic belt: characteristics and tectonic settings. Ore Geol Rev 43(1):264–293
Maruyama S, Isozaki Y, Kimura G, Terabayashi M (1997) Paleogeographic maps of the Japanese Islands: Plate tectonic synthesis from 750 Ma to the present. Isl Arc 6:121–142
McCallum ME (1985) Fluidization processes in breccia formation. Econ Geol 80:1523–1543
Meng QR (2003) What drove late Mesozoic extension of the northern China–Mongolia tract? Tectonophysics 369:155–174
Meng QR, Zhang GW (2000) Geologic framework and tectonic evolution of the Qinling orogen, central China. Tectonophysics 323:183–196
Meng LF, Li ZX, Chen HL, Li XH, Wang XC (2012) Geochronological and geochemical results from Mesozoic basalts in southern South China Block support the flat-slab subduction model. Lithos 132/133:127–140
Menzies MA, Xu YG (1998) Geodynamics of the North China craton. In: Flower MFJ, Chung SL, Lo CH, Lee TY (eds) Mantle dynamics and plate interactions in East Asia. American Geophysical Union, Geodynamics Ser 100, pp 155–165
Miao LC, Fan WM, Liu DY, Zhang FQ, Shi Y, Guo F (2008) Geochronology and geochemistry of the Hegenshan ophiolitic complex: Implications for late-stage tectonic evolution of the Inner Mongolia-Daxinganling orogenic belt, China. J Asian Earth Sci 32:348–370
Miller LD, Goldfarb RJ, Nie FJ, Hart CJR, Miller ML, Yang YQ, Liu YQ (1998) North China gold—a product of multiple orogens. Soc Econ Geol Newsl 33:1–12
Muntean JL, Cline JS, Simon A, Longo AA (2010) The origin of Carlin-type gold deposits. Geol Soc Am Abstracts with Programs 42(5):45
Naldrett AJ (2004) Magmatic sulfide deposits. Springer, Berlin, p 727

Natal'in BA, Şengör AMC (2005) Late Palaeozoic to Triassic evolution of the Turan and Scythian platforms: the pre-history of the Palaeo-Tethyan closure. Tectonophysics 404:175–202

Nie FJ (1994) Rare earth element geochemistry of the molybdenite-bearing granitoids in the Jinduicheng-Huanglongpu district, Shanxi Province, northwest China. Miner Depos 29:488–498

Nie FJ (1997) An overview of the gold resources of China. Int Geol Rev 39:55–81

Pan LJ, Fu JD, Sun ES, Li ZA (1996) Geologic characteristics of large-scale deposits in Manzhouli-Xinyouqi copper, silver polymetal metallogenic belt. Non-ferrous metal Geologic Library of China, p 144 (in Chinese)

Pei R, Hong D (1995) The granites of South China and their metallogeny. Episodes 18:77–86

Peng P, Zai MG, Zhang HF, Guo JH (2005) Geochronological constraints on the Paleoproterozoic evolution of the North China Craton: SHRIMP zircon ages of different types of mafic dikes. Int Geol Rev 47: 492–508

Peng P, Zhai MG, Ernst RE, Guo JG, Liu F, Hu B (2008) A 1.78 Ga large igneous province in the North China Craton: The Xiong'er volcanic province and the North China dike swarm. Lithos 101:260–280

Peters SG (2001) Use of structural geology in mining of and exploration for sedimentary rock-hosted Au deposits. U.S. Geol Surv Open-File Report 01-151. http://geopubs.wr.usgs.gov/open-file/of01-151/

Peters SG (2002) Geology, geochemistry and geophysics of sedimentary-hosted Au deposits in P. R. China, Open-File Report 02-131, vol 1.0, U.S. Geol Surv, p 403

Peters SG, Ferdock GC, Woitsekhowskaya MB, Leonardson R, Rahn J (1998) Oreshoot zoning in the Carlin-type Betze orebody, Goldstrike Mine, EurekaCounty, Nevada: U.S. Geological Survey Open-File Report 98-620, p 49

Peters SG, Huang JZ, Jing CG (2002) Geology and geochemistry of sedimentary-rock-hosted Au deposits of the Qinling fold belt (Chuan-Shan-Gan) area, Shaanxi, Sichuan and Gansu provinces, P. R. China. Chapter 4 in Open-File Report 02-131, vol 1.0, U.S. Geol Surv, pp 173–254

Pirajno F (2006) Mantle dynamics and intraplate tectonics, magmatism and ore systems. IAVCEI 2006 Meeting, Guanzhou, China, Abstracts and Program, p. 176

Pirajno F (2009) Hydrothermal processes and mineral systems. Springer, Berlin, p 1256

Pirajno F (in press) Effects of metasomatism on mineral systems and their host rocks: alkali metasomatism, skarns, greisens, tourmalinites, rodingites, black-wall alteration, and listvenites. In: Harlov DE, Austrheim H (eds) Metasomatism and metamorphism: the role of fluids in crustal and upper mantle processes. Lecture Series in Earth Science, Springer

Pirajno F, Bagas L (2002) Gold and silver metallogeny of the South China Fold Belt: a consequence of multiple mineralising events? Ore Geol Rev 20:109–126

Pirajno F, Bagas L, Hickman AH, Gold Research Team (1997) Gold mineralisation of the Chencai-Suichang Uplift and tectonic evolution of Zhejiang Province, southeast China. Ore Geol Rev 12:35–55

Qi JZ, Liu HY, Jiang YH (2000) Yanshanian subduction and strike–slipping regime of East China, and its control of ore location. Volcanol Miner Res 21:244–265 (in Chinese with English abstract)

Qi JP, Zhang J, Tang GJ (2005a) Carbon and oxygen isotope composition of the Meso-Neoproterozoic strata south of the Xiong'er Terrane: evidences of the CMF model. Acta Pet Sin 21:1365–1372 (in Chinese with English abstract)

Qi JP, Chen YJ, Pirajno F (2005b) Geological characteristics and tectonic setting of the epithermal deposits in the northeast China. J Miner Pet 25:47–59

Qi JP, Chen YJ, Pirajno F (2005c) Tectonic setting of epithermal deposits in Mainland China. In: Mao JW, Bierlein FP (eds) Mineral deposit research: meeting the global challenge. Proceedings SGA 2005, Beijing, pp 577–580

Qin KZ, Tanka R, Li WS, Ishihara S (1998) The discovery of Indo-Sinian granites in Manzhouli Area: evidence from Rb-Sr isochrons. Acta Pet Miner 17(3):235–240 (in Chinese with English Abstract)

Qin F, Liu JM, Zeng QD, Zhang RB (2008) The metallogenic epoch and source of ore-forming materials of the Xiaodonggou porphyry molybdenum deposit, Inner Mongolia. Geoscience 22:173–180 (in Chinese with English abstract)

Ratschbacher L, Hacker BR, Calvert A, Webb LE, Grimmer JC, McWilliams MO, Ireland T, Dong S, Hu J (2003) Tectonics of the Qinling (Central China): tectonostratigraphy, geochronology and deformation history. Tectonophysics 366:1–53

Ren JS, Wang ZX, Chen BW, Jiang CF, Niu BG, Li JY, Xie GL, He ZJ, Liu ZG (1999) Geotectonic map of China and neighbouring area and its simple explanatory. Geological Publishing House, Beijing, p 50 (in Chinese with English Abstract)

Richards JP (1995) Alkalic-type epithermal gold deposits—a review. Mineral Assoc Can Short Course 23:367–400

Robinson PT, Zhou MF, Hu XF, Reynolds P, Bai WJ, Yang JS (1999) Geochemical constraints on the origin of the Hegenshan ophiolite, Inner Mongolia, China. J Asian Earth Sci 17:423–442

Rui ZY, Zhang HT, Wang LS, Chen RY, Jin BL, Jin FZ, Wan YS, Zhou YC, Meng QL (1995) Porphyry-epithermal Au-Cu deposits in Yanbian, Jilin. Miner Depos 14(2):99–113 (in Chinese with English Abstract)

Santosh M, Zhao DP, Kusky T (2010) Mantle dynamics of the Paleoproterozoic North China Craton: a perspective based on seismic tomography. J Geodyn 49:39–53

Schwartz MO (1989) Determining phase volumes of missed CO_2-H_2O inclusions using microthermometric measurements. Miner Depos 24:43–47

Seat Z, Beresford SW, Grguric BA, Gee MMA, Grassineau NV (2009) Reevaluation of the role of external sulfur addition in the genesis of Ni-Cu-PGE deposits: evidence from the Nebo-Babel Ni-Cu-PGE deposit: West Musgrave, Western Australia. Econ Geol 104:521–538

Seedorff E, Dilles JH, Proffett JM, Einaudi MT, Zurcher L, Stavast WJA, Johnson DA, Barton MD (2005) Porphyry deposits: characteristics and origin of hypogene features. Econ Geol 100th Ann Vol:251–298

Şengör AMC, Natal'in B (1996) Paleotectonics of Asia: fragments of a synthesis. In: Yin A, Harrison M (eds) The tectonic evolution of Asia. Cambridge University Press, Cambridge, pp 486–640

Şengör AMC, Cin A, Bowley DB, Nie S (1993) Space-time patterns of magmatism along the Tethysides: a preliminary study. J Geol 101:51–84

Shao KZ, Li SR (1989) Significance of quartz thermoluminescence in the study of Qiyugou (type) gold deposits. J Hebei Coll Geol 12(2):127–133 (in Chinese with English abstract)

Shao JA, Liu FT, Chen H, Han QJ (2001) Relationship between Mesozoic Magmatism and Subduction in the Da Hinggan–Yanshan Area. Acta Geol Sin 75:56–63 (in Chinese with English abstract)

Sheppard SMF (1986) Characterization and isotopic variations in natural waters. Rev Miner Min Soc Am 16:165–183

Sillitoe RH (1985) Ore-related breccias in volcanoplutonic arcs. Econ Geol 80:1467–1514

So CS, Zhang DQ, Yun ST, Li DX (1998) Alteration-mineralization zoning and fluid inclusions of the high sulfidation epithermal Cu-Au mineralization at Zijinshan, Fujian province, China. Econ Geol 93:961–980

Stein HJ, Markey RJ, Morgan JW (1997) Highly precise and accurate Re-Os ages for molybdenite from the East Qinling molybdenum belt, Shaanxi Province, China. Econ Geol 92:827–835

Su RK, Yu JB, Chu YJ, Song CB (2006) Geological characteristics and prospecting potential of Dong An gold ore field in Heilongjiang. Gold Sci Technol 14:9–13 (in Chinese with English abstract)

Sun FX, Wu GX, Yang P (1996) Geological feature and metallogenic model from Tuanjegou gold deposit, Heilongjiang Province, China. Jilin Geol 15(2):52–60 (in Chinese with English Abstract)

Sun XM, Liu YJ, Sun QC, Han GQ, Wang SQ, Wang YD (2008) $^{40}Ar/^{39}Ar$ geochronology evidence of strike-slip movement in Dunhua-Mishan Fault Zone. J Jilin Univ Earth Sci Edition 38:965–972 (in Chinese with English abstract)

Tan LP (1991) The Chinquashih gold-copper deposits, Taiwan. SEG Newsl 7:22–24

Tang ZL, Ren DJ, Xue ZR, Mu YK (1992) Nickel deposits of China, in mineral deposits of China, Editorial Committee of Mineral Deposits, China, vol. 2. Geological Publishing House, Beijing, pp 59–99

Taylor SR, McLennan SM (1995) The geochemical evolution of the continental crust. Rev Geophys 33:241–265

Tian YC (1999) Geological background, gold ore-forming condition and prospecting direction in the southeastern margin of Jiamusi uplift. J Guilin Inst Technol 19(4):303–309 (in Chinese with English Abstract)

Tian W, Chen B, Ireland TR, Green DH, Suzuki K, Chu Z (2011) Petrology and geochemistry of dunites, chromitites and mineral inclusions from the Gaositai Alaskan-type complex, North China Craton: implications for mantle source characteristics. Lithos 127:165–175

Van Der Voo R, Spakman W, Bijwaard H (1999) Mesozoic subducted slabs under Siberia. Nature 397:246–249

Walters A, Phillips J, Brown R, Field M, Sparks RSJ (2006) The role of fluidisation processes in the formation of volcaniclastic kimberlite: gran size observations and experimental investigation. J Volcanol Geotherm Res 155:119–137

Wan TF (2004) Rotation of the Jurassic crust and transformation of the lithosphere in eastern China. Geol Bull China 23:966–972 (in Chinese with English abstract)

Wang XC (1992) Indicator significance of As, Sb, Hg, Tl and Ba for the fine disseminated type of gold deposits. Miner Res Geol 6(4):307–312 (in Chinese)

Wang YS (2010) Physical and chemical characteristics of the host rocks in controlling the mineralization of the Chinkuashih high-sulfidation gold-copper deposits, northeastern Taiwan. J Geochem Explor 104:61–68

Wang SQ, Sun CY, Cui WY, Wu CY, Yu FZ, Yu JA, Zhao BL, Wang YF (1994) Geology of gold deposits in Chifeng region, Inner Mongolia, China. Inner Mongolia People Press, Huhhot, p 375 (in Chinese with English Abstract)

Wang YL, Zhang WX, Zhan KL (1996) Types and geological characteristics of gold deposits in Chifeng region. Miner Resour Geol 10(56):395–399 (in Chinese with English abstract)

Wang H, Chen J, Ji JF, Qu XM (1997) Geological and geochemical characteristics of the Hetai Gold deposit, South China: gold mineralisation in an auriferous shear zones. Int Geol Rev 39:181–190

Wang YS, Sasaki M, Sasada M, Chen C-H (1999) Fluid inclusion studies of the Chinquashih high-sulfidation gold-copper deposits in Taiwan. Chem Geol 154:155–167

Wang YJ, Fan WM, Guo F (2002a) K-Ar dating of Late Mesozoic volcanism and geochemistry of volcanic gravels in the North Huaiyang belt, Dabie Orogen: constraints on the stratigraphic framework and exhumation of the northern Dabie orthogneiss complex. Chin Sci Bull 47:1668–1695

Wang PJ, Liu ZJ, Wang SX, Song WH (2002b) $^{40}Ar/^{39}Ar$ and K/Ar dating of the volcanic rocks in the Songliao basin, NE China: constraints on stratigraphy and basin dynamics. Int J Earth Sci 91:331–340

Wang XZ, Shu BY, Liang HJ, Chen M (2003) Ore control factors and genesis of the Shabaosi gold deposit, North Daxing'anling. Gold Geol 9(3):45–48 (in Chinese with English abstract)

Wang XY, Zhao CR, Wang ZY, Li XW, Cui XW (2004) Industrial types and geological features of the northern Daxing'anling gold deposits. Gold Geol 10(2):50–54 (in Chinese with English abstract)

Wang YJ, Fan WM, Peng TP, Zhang HF, Guo F (2005a) Nature of the Mesozoic lithospheric mantle and tectonic decoupling beneath the Dabie Orogen, Central China: Evidence from $^{40}Ar/^{39}Ar$ geochronology, elemental and Sr-Nd-Pb isotopic compositions of Early Cretaceous mafic igneous rocks. Chem Geol 220:165–189

Wang H, Zhang SH, He H (2005b) China and Mongolia. In: Selley RC, Robin I, Cocks M, Plimer IR (eds) Encyclopedia of geology, vol 1. Elsevier, Oxford, pp 345–358

Wang F, Zhou XH, Zhang LC, Ying JF, Zhang YT, Wu FY, Zhu RX (2006) Late Mesozoic volcanism in the Great Xing'an Range (NE China): timing and implications for the dynamic setting of NE Asia. Earth Planet Sci Lett 251:179–198

Wang XX, Wang T, Jahn BM, Hu NG, Chen W (2007a) Tectonic significance of Late Triassic post-collisional lamprophyre dikes from the Qinling Mountains, China. Geol Mag 144:1–12
Wang Y, Xi BB, Zhang DH, Zhang WH (2007b) Geochemical characteristics of fluid inclusions in Jinchang gold deposit, Heilongjiang Province. Miner Depos 26(2):184–194 (in Chinese with English abstract)
Wang TH, Mao JW, Wang YB (2008) Research on SHRIMP zircon U-Pb chronology in Xiaoqinling—Xion'ershan area: the evidence of delamination of lithosphere in Qinling orogenic belt. Acta Pet Sin 24:1273–1287
Wang Q, Wyman DA, Li ZX, Bao ZW, Zhao ZH, Wang YX, Jian P, Yang YH, Chen LL (2010) Petrology, geochronology and geochemistry of ca. 780 Ma A-type granites in South China: petrogenesis and implications for crustal growth during the breakup of the supercontinent Rodinia. Precambr Res 178:185–208
Wang X, Chen WL, Griffin WL, O'Reilly SY, Huang PY, Li X (2011a) Two stages of crystallisation in the Jingshan monzogranite, Bengbu Uplift: implications for the syn-collisional granites of the dabie-Sulu UHP orogenic eblt and the climax of movement on the Tan-Lu fault. Lithos 122:201–213
Wang FY, Ling MX, Ding X, Huy YH, Zhou JB, Yang XY, Liang HY, Fan WM, Sun WD (2011b) Mesozoic large magmatic events and mineralization in SE China: oblique subduction of the Pacific plate. Int Geol Rev 53:704–726
Wedepohl KH (1995) The composition of the continental crust. Geochim Cosmochim Acta 59:1217–1232
Wei LM, Chao YG (1994) Geological characteristics and genesis analysis of Baguamiao gold deposits, Shannxi province. In: Liu DS, Tan YJ, Wang JY, Jiang SF (eds) Chinese Carlin-type gold deposits. Nanjing University Press, Nanjing, pp 286–305 (in Chinese)
Whalen JB, Currie KL, Chappell BW (1987) A-type granites: geochemical characteristics, discrimination and petrogenesis. Contrib Miner Pet 95:407–419
White NC, Leake MJ, McCaughey SN, Parris BW (1995) Epithermal gold deposits of the southwest Pacific. J Geochem Explor 54:87–136
William-Jones AE, Heinrich CA (2005) Vapor transport of metals and the formation of magmatic-hydrothermal ore deposits. Econ Geol 100:1287–1312
Windley BF, Alexeiev D, Xiao WJ, Kröner A, Badarch G (2007) Tectonic models for accretion of the Central Asian Orogenic Belt. J Geol Soc London 64:31–47
Woolley AR, Kempe DRC (1989) Carbonatites: nomenclature, average chemical composition. In: Bell K (ed) Carbonatites: genesis and evolution. Unwin Hyman, London, pp 1–14
Wu G, Quan H (2000) Geology and prospect of 'New-type' gold deposits in Shangheilongjiang depression. In: Geological Society of China (ed) Symposium of important achievements in geological science and technology during the Ninth Five-year Plan. Geological Publishing House, Beijing, pp 336–339 (in Chinese with English abstract)
Wu CY, Bai G, Xu LM (1993) Types and distribution of silver ore deposits in China. Miner Depos 28:223–239
Wu G, Yano T, Inomata M (1998) Yanshanian orogenies in south China: a relation to Neotethyan evolution. Sci Geol Sin 7:1–10
Wu G, Quan H, Li GY (2001) Geological characteristics of the Xijinuoshan polymetal ore field in Heilongjiang province. Geol Resour 10(4):226–234 (in Chinese with English abstract)
Wu FY, Sun DY, Li HM, Jahn BM, Wilde S (2002) A-type granites in northeastern China: age and geochemical constraints on their petrogenesis. Chem Geol 187:143–173
Wu FY, Wilde SA, Zhang GL, Sun DY (2004) Geochronology and petrogenesis of the post-orogenic Cu-Ni sulfide-bearing mafic-ultramafic complexes in Jilian Province, NE China. J Asian Earth Sci 23:781–797
Wu FY, Lin JQ, Wilde SA, Zhang XO, Yang JH (2005a) Nature and significance of the Early Cretaceous giant igneous event in eastern China. Earth Planet Sci Lett 233:103–119
Wu G, Sun FY, Zhao CS, Li ZT, Zhao AL, Pang QB, Li GY (2005b) Discovery of the Early Paleozoic post-collisional granites in northern margin of the Erguna massif and its geological significance. Chin Sci Bull 50(23):2733–2743

Wu ZY, Wang HB, Xu DH, Zhou YC (2005c) Geological and geochemical studies of the Sandaowanzi gold deposit, Heihe County, Heilongjiang province. Geol Rev 51(3):264–267 (in Chinese with English abstract)

Wu ZY, Sun YC, Wang BQ (2006a) Geology and geochemistry of Zhengguang gold deposit, Heilongjiang province. Geol Prospect 42(1):38–42 (in Chinese with English abstract)

Wu G, Sun FY, Zhu Q, Li ZT, Ding QF, Li GY, Pang QB, Wang HB (2006b) Geological characteristics and genesis of gold deposits in Upper Heilongjiang Basin. Miner Depos 25(3):215–230 (in Chinese with English abstract)

Wu HY, Zhang LC, Chen ZG, Wan B (2008) Geochemistries, tectonic setting and mineralization potentiality of the ore-bearing monzogranite in the Kulitu molybdenum (copper) deposit of Xar moron metallogenic belt, Inner Mongolia. Acta Pet Sin 24:867–878 (in Chinese with English abstract)

Wu HY, Zhang LC, Wan B, Chen ZG, Xiang P, Pirajno F, Du AD, Qu WJ (2011) Re-Os and $^{40}Ar/^{39}Ar$ ages of the Jiguanshan porphyry Mo deposit, Xilamulun metallogenic belt, NE China, and constraints on mineralization events. Miner Depos 46:171–186

Wu G, Chen YC, Chen YJ, Zeng QT (2012) Zircon U-Pb ages of the metamorphic supracrustal rocks of the Xinghuadukou Group and granitic complexes in the Argun Massif of the northern Great Hinggan Range, NE China, and their tectonic implications. J Asian Earth Sci 49:214–233

Xiang JX (2009) Petrogenesis of Zhangshiying intrusive complex in Central Henan Province, China. MSc thesis, China University of Geosciences, Beijing, pp 1–74 (in Chinese with English abstract) (unpublished)

Xiao WJ, Windley BF, Hao J, Zhai MG (2003) Accretion leading to collision and the Permian Solonker suture, Inner Mongolia, China: termination of the central Asian orogenic belt. Tectonics 22(6):8–20, 1069

Xiao WJ, Zhang LC, Qin KZ, Sun S, Li JL (2004) Paleozoic accretionary and collisional tectonic of the eastern Tianshan (China): implication for the continental growth of central Asia. Am J Sci 304:370–395

Xie CB, Liu M (2001) Geological features and genetic type of Chaganbulagen Ag, Pb, Zn (Au) deposit. World Geol 20(l):25–29 (in Chinese with English abstract)

Xie GQ, Mao JW, Li LR, Ye HS, Wan YS, Li HM, Gao JJ, Zheng RF (2007a) SHRIMP zircon U-Pb dating for the volcanic rocks of the Dayingzi Formation in the Baofeng basin in the East Qinling and its significance. Acta Pet Sin 23:2387–2396 (in Chinese with English abstract)

Xie GQ, Mao JW, Li RL, Qu WJ, Pirajno F, Du AD (2007b) Re–Os molybdenite and Ar–Ar phlogopite dating of Cu–Fe–Au–Mo (W) deposits in southeastern Hubei, China. Miner Pet 90:249–270

Xu B (1988) Stable isotope geochemistry of gold deposits in the Shaoxing-Longquan ore forming zone, Zhejiang province. Mineral Deposits 3:53–61 (in Chinese with English abstract)

Xu ZG (1990) Mesozoic volcanism and volcanogenic iron-ore deposits in eastern China. Geological Society of America, Boulder, Spec Paper 237, pp 1–46

Xu B, Li C, Chen H (1994a) Mineralization chronology and isotopic geochemistry of the Haoshi silver deposit in Zhejiang Province. Miner Depos 13:271–281 (in Chinese with English abstract)

Xu G, Niu H, Wang Y, Fu H (1994b) Tectonic framework and evolution of Precambrian on the southeastern margin of the Yangtze plate. Sci Geol Sin 3:255–264

Xu B, Li C, Chen H (1995a) Isotope geochemistry of the Xinchang-Yongjia silver (lead-zinc) ore belt in eastern Zhejiang Province. Acta Geol Sin 8:69–83 (in Chinese with English abstract)

Xu G, Yao S, Zhang C, Wang P (1995b) A case study of the Zhilingtou gold-silver deposit, Zhejiang, China. PACIFIC RIM '95, Abstracts Volume, Aust Inst Min Metall pp 645–649

Xu YG, Ma JL, Frey FA, Feigenson MD, Liu JF (2005) Role of lithosphere-astenosphere interaction in the genesis of Quaternary alkali and tholeiitic basalts from Datong, western North China Craton. Chem Geol 224:247–271

Xu C, Campbell IH, Allen CM, Chen YJ, Huang ZL, Qi L, Zhang GS, Yan ZF (2008a) U-Pb zircon age, geochemical and isotopic characteristics of carbonatite and syenite complexes from the Shaxiaongdong, China. Lithos 105:118–128

Xu JF, Zhang BR, Han YW (2008b) Geochemistry of the Mian-Lue ophiolites in the Qinling Mountains, Central China: constraints on the evolution of the Qinling orogenic belt and collision of the North and South China Cratons. Asian J Earth Sci 32:336–347

Xu C, Wang LJ, Song WL, Wu M (2010a) Carbonatites in China: a review for genesis and mineralization. Geosci Front 1:105–114

Xu C, Kynicky J, Chakhmouradian AR, Qi L, Song WL (2010b) A unique Mo deposit associated with carbonatites in the Qinling Orogenic belt, central China. Lithos 118:50–60

Xu C, Kynicky J, Chakhmouradian AR, Campbell IH, Allen CM (2010c) Trace-element modeling of the magmatic evolution of rare-earth-rich carbonatite from the Miaoya deposit, Central China. Lithos 118:145–155

Yakubchuk A (2004) Architecture and mineral deposit settings of the Altaid orogenic collage: a revised model. J Asian Earth Sci 23:761–779

Yang TZ (2008) Geology and geochemistry of the Mesozoic volcanic rocks and Dong'an gold deposit in Heilongjiang province. Master Degree thesis, China University of Geosciences, Beijing (unpublished)

Yang ZM, Woolley A (2006) Carbonatites in China: a review. J Asian Earth Sci 27:559–575

Yang FL, Zhu Q, Li ZT, Wu ZW (2000) Geology and genesis of Guliku gold (-silver) deposit. J Precious Met Geol 9(1):7–14 (in Chinese with English abstract)

Yang JS, Xu ZQ, Zhang JX, Chu CY, Zhang RY, Liou JG (2001) Tectonic significance of early Paleozoic high-pressure rocks in Altun-Qaidam-Qilian mountains, northwest China. Geol Soc Am Mem 194:151–170

Yang YQ, Li, Y, Fan JZ (2002) Metallogenic system in gold-silver-copper deposits, Tayuan district, Heilongjiang province. J Jilin Univ Earth Sci Edition 32(3):229–232 (in Chinese with English abstract)

Yang JS, Liu FL, Wu CL, Xu ZQ, Shi RD, Chen SY, Deloule E, Wooden J (2005) Two ultrahigh-pressure metamorphic events recognised in the central orogenic belt of China: evidence from the U-Pb dating of coesite-bearing zircons. Int Geol Rev 47:327–343

Yang JH, Wu FY, Wilde SA, Belousova E, Griffin WL (2008) Mesozoic decratonization of the North China block. Geology 36:467–470

Ye HS (2006) The Mesozoic tectonic evolution and Pb-Zn-Ag metallogeny in the south margin of North China Craton. PhD thesis, Chinese Academy of Geological Sciences, Beijing, p 217 (in Chinese with English abstract) (unpublished)

Ye M, Zhang SH, Wu FT (1994) The classification of the Paleozoic tectonic units in the area crossed by M-S GGT. J Chang Univ Earth Sci 24:241–245 (in Chinese with English abstract)

Ye Y, Shimakazi H, Simizu M, Hu S (1998) Tectono-magmatic evolution and metallogenesis along the Northeast Jiangxi Deep Fault, China. Resour Geol 48:43–50

Ye HS, Mao JW, Li YF, Guo BJ, Zhang CQ, Liu J, Yan QR, Liu GY (2006) SHRIMP zircon U-Pb and molybdenite Re-Os dating for the superlarge Donggou porphyry Mo deposit in East Qinling, China, and its geological implications. Acta Geol Sin (Chinese edn) 80(7):1078–1088 (in Chinese with English abstract)

Yin A, Nie SY (1996) A Phanerozoic palinspastic reconstruction of China and its neighboring regions. In: Yin A, Harrison TM (eds) The Tectonic evolution of Asia. Cambridge University Press, Cambridge, pp 442–485

Yu JB, Su RK, Liu ZM (2005) Ore-controlled facter and ore-forming material origin of the Dong'an gold deposit, Heilongjiang province. Gold Sci Technol 13(6):8–11 (in Chinese with English abstract)

Yuan JH (1998) Metallogenic conditions and metallogenic regularity of gold deposits in western Huma, Heilongjiang. Gold Geol 4(l):68–73 (in Chinese with English abstract)

Zartman RE, Doe BR (1981) Plumbotectonics-the model. Tectonophysics 75:135–162

Zeng QD, Liu JM, Qin F, Zhang ZI, Chen WJ, Zhang RB, Ye J, Yu CM (2008) Preliminary research on Mesozoic four-stage Mo mineralization in DaHinggan mountains, China. Gondwana 13, Extended Abs: 251–252

Zhai MG, Yang JH, Liu WJ (2001) Large clusters of gold deposits and large-scale metallogenesis in the Jiaodong peninsula, eastern China. Sci China 44:758–768

Zhai MG, Meng QR, Liu JM, Hou QL, Hu SB, Li Z, Zhang HF, Liu W, Shao JA, Zhu RX (2004) Geological features of Mesozoic tectonic regime inversion in Eastern North China and implication for geodynamics. Earth Sci Front 11:285–298 (in Chinese with English abstract)

Zhang FX (1996) Mode of occurrence of submicron gold in Qinling micron-dissemianetd stratabound antimony-gold deposits. Geol Rev 42(6):541–549 (in Chinese)

Zhang JH (2006a) Geochronological Framework of the Mesozoic Volcanic Rocks in the Great Xing'an Range, NE China. MSc thesis. Jilin University, Jilin, p 97 (in Chinese with English Abstract)

Zhang YH (2006b) The Qiyugou auriferous breccia pipes: an adularia-sericite epithermal system, associated with porphyry Mo in the Xiong'ershan, Henan Province, China. PhD thesis, China University of Geosciences, Beijing (unpublished)

Zhang GW, Xiang LW, Meng QR (1995) The Qinling Orogen and intracontinental orogen mechanism. Episodes 18:36–39

Zhang GW, Meng QR, Yu ZP, Sun Y, Zhou DW, Guo AL (1996) Orogenesis and dynamics of the Qinling orogen. Sci China 39:225–234

Zhang JF, Wang XZ, Quan H, Wu G, Zhu HC (2001a) The forming conditions of nonferrous and precious metal deposits in the north of Derbugan metallogenic province. Geol Resour 10(4):220–225 (in Chinese)

Zhang GW, Zhang BR, Yuan XC, Xiao QH (2001b) Qinling orogenic belt and continental dynamics. Science Press, Beijing, pp 1–885 (in Chinese with English abstract)

Zhang YH, Zhang SH, Han YG, Pirajno F (2005) Low-sulphidation epithermal gold-bearing Qiyugou breccia pipes, Xiong'ershan mountains, China. In: Mao JW, Bierlein FP (eds) Mineral deposit research: meeting the global challenge, vol 2. Springer, Berlin, pp 1111–1113

Zhang JH, Ge WC, Wu FY, Liu XM (2006) Mesozoic bimodal volcanic suite in Zhalantun of the Da Hinggan Range and its geological significance: zircon U-Pb age and Hf isotopic constraints. Acta Geol Sin 80(1):58–69

Zhang HF, Jin LL, Zhang L, Harris N (2007a) Geochemical and Pb–Sr–Nd isotopic compositions of granitoids from western Qinling belt: constraints on basement nature and tectonic affinity. Sci China Ser D Earth Sci 50:184–196

Zhang YH, Zhang SH, Pirajno F (2007b) Fluidization: an important process in the formation of the Qiyugou Au-bearing breccia pipes in Central China. Acta Geol Sin 81:226–238

Zhang LC, Zhou XH, Ying JF, Wang F, Guo F, Wan B, Chen ZG (2008) Geochemistry and Sr–Nd–Pb–Hf isotopes of Early Cretaceous basalts from the Great Xinggan Range, NE China: implications for their origin and mantle source characteristics. Chem Geol 256:12–23

Zhang LC, Wu HY, Wan B, Chen ZG (2009) Ages and geodynamic settings of Xilamulun Mo-Cu metallogenic belt in the northern part of the North China Craton. Gondwana Res 16:243–254

Zhang ZC, Mao JW, Wang YB, Pirajno F, Liu JL, Zhao Z (2010) Geochemistry and geochronology of the volcanic rocks associated with the Dong'an adularia-sericite epithermal gold deposit in the Lesser Hing'an Range, Hellongjiang province. NE China: constraints on the metallogenesis. Ore Geol Rev 37:158–174

Zhao ZP (1986) Review of the 50th anniversary of the Indosinian Movement. Sci Geol Sin 1:7–15

Zhao CS, Wu G (2002) Epithermal deposits in Manzhouli area, Inner Mongolia. Geol Resour 11(2):96–103 (in Chinese with English abstract)

Zhao YM, Zhang DQ (1997) Metallogeny and prospective evaluation of copper-polymetallic deposits in the Da Hinggan mountains and its adjacent regions. Seismological Press, Beijing, p 318 (in Chinese with English abstract)

Zhao HL, Deng JF, Chen FJ, Hu Q, Zhao SK (1998) Petrology of the Mesozoic volcanic rocks and the basin formation in the northeast China. Geoscience 12(1):56–62 (in Chinese with English abstract)

Zhao TP, Zhou MF, Zhai MG, Xia B (2002) Paleoproterozoic rift-related volcanism of the Xiong'er Group, North China Craton: implications for the breakup of Columbia. Int Geol Rev 44:336–351

Zhao GJ, Huo YS, Wang BQ (2006) Geological characteristics and genesis of Zhengguang gold deposit in Heilongjiang province. Non Ferr Min Metall 22(3):3–6 (in Chinese with English abstract)

Zhao DP, Pirajno F, Dobretsov NL, Liu L (2010) Mantle structure and dynamics under East Russia and adjacent regions. Russ Geol Geophys 51:901–914

Zhao HX, Jiang SY, Frimmel HE, Dai BZ, Ma L (2012) Geochemistry, geochronology and Sr-Nd-Hf isotopes of two Mesozoic granitoids in the Xiaoqinling gold district: implications for large-scale lithospheric thinning in the North China Craton. Chem Geol 294/295:173–189

Zheng M, Liu JM (1987) Physico-chemical conditions and ore-forming process of the Zhilingtou Au-Ag deposit, Zhejiang, China. Acta Geol Sin 3:253–266 (in Chinese with English abstract)

Zhou MF, Bai WJ (1992) Chromite deposits in China and their origin. Miner Depos 27:192–199

Zhou D, Graham SA (1996) The Songpan-Ganzi complex of the West Qingling Shan as a Triassic remnant ocean basin. In: Yin A, Harrison TM (eds) The Tectonic evolution of Asia. Cambridge University Press, Cambridge, pp 281–299

Zhou XM, Li WX (2000) Origin of Late Mesozoic igneous rocks in Southeastern China: implications for lithosphere subduction and underplating of mafic magmas. Tectonophysics 326:269–287

Zhou TH, Goldfarb RJ, Phillips GN (2002a) Tectonics and distribution of gold deposits in China—an overview. Miner Depos 37:249–282

Zhou MF, Yang ZX, Song XY, Keays RR, Lesher C M (2002b) Magmatic Ni-Cu-(PGE) sulphide deposits in China. In: Cabri LJ (ed) The geology, geochemistry, mineralogy and mineral beneficiation of platinum-group elements. pp 619–636

Zhou XM, Sun T, Shen WZ, Shu LS, Niu YL (2006) Petrogenesis of Mesozoic granitoids and volcanic rocks in South China: a response to tectonic evolution. Episodes 29:26–33

Zhou JB, Wilde SA, Zhang XZ, Ren SM, Zheng CQ (2011) Early Paleozoic metamorphic rocks of the Erguna Block in the Great Xing'an Range, NE China: evidence for the timing of magmatic and metamorphic events and their tectonic implications. Tectonophysics 499:105–117

Zhu HC, Zhang JF, Quan H, Zhang H (1999) Metallogenic characteristics of nonferrous and noble metals in Ergun region. J Precious Met Geol 8(4):193–198 (in Chinese with English abstract)

Zhu Q, Wu G, Zhang JF (2001) Development in division of Deerbugan metallogenic belt and prospecting technology. Chin Geol 28(7):19–27 (in Chinese with English abstract)

Zhu CW, Chen JR, Li TG, Cui B, Jin BY, Wang KQ (2003) Geology and ore genesis of Jinchang gold deposit, Heilongjiang province. Miner Depos 22(1):56–64 (in Chinese with English abstract)

Zhu G, Wang YS, Liu GS, Niu LM, Xie CL, Li CC (2005) $^{40}Ar/^{39}Ar$ dating of strike-slip motion on the Tan–Lu fault zone, East China. J Struct Geol 27:1379–1398

Zhu LM, Zhang GW, Guo B, Lee B, Gong HJ, Wang F (2010) Geochemistry of the Jinduicheng Mo-bearing porphyry and deposit, an dits implications for the geodynamic setting in East Qinling, P. R. China. Chem Erde 70:159–174

Zhu XY, Chen F, Li SQ, Yang YZ, Nie H, Siebel W, Zhai MG (2011a) Crustal evolution of the North Qinling terrain of the Qinling Orogen, China: evidence from detrital zircon U-Pb ages and Hf isotopic composition. Gondwana Res 20:194–204

Zhu LM, Zhang GW, Chen YJ, Ding ZJ, Guo B, Wang F, Lee B (2011b) Zircon U-Pb ages and geochemistry of the Wenquan Mo-bearing granitoids in West Qinling, China: constraints on the geodynamic setting for the newly discovered Wenquan Mo deposit. Ore Geol Rev 39:46–62

Zi F, Wang Q, Dai SQ, Xu W, Xu JF, Qiu HN, Liang XR, Tu XL, Liu Y (2007) Geochronology and geochemistry of Chuzhou and Shangyaopu adakitic intrusive rocks in the eastern area of Anhui province: Implication for petrogenesis and mineralisation. Acta Pet Sin 23:1485–1500 (in Chinese with English abstract)

Zorin Y (1999) Geodynamics of the western part of the Mongolia-Okhotsk collisional belt, Trans-Baikal region (Russia) and Mongolia. Tectonophysics 306:33–56

Zorin YA, Zorina LD, Spiridinov AM, Rutshtein IG (2001) Geodynamic setting of gold deposits in Eastern and Central Trans-Baikal (Chita Region, Russia). Ore Geol Rev 17:215–232

Chapter 6
Tianshan, Junggar and Altay Orogens (NW China), the Alpine-Himalayan Fold Belts (Tethyan Orogens), Kunlun and Songpan-Ganzi Terranes

Abstract The Tianshan, Junggar and Altay orogenic belts in northwest China (Xinjiang) are part of the huge Central Asian Orogenic Belt (CAOB), which extends from the Uralides in the west to the Pacific Ocean margin of eastern Asia. The CAOB is a complex collage of fragments of ancient microcontinents and subduction-related island arc terranes, fragments of oceanic crust volcanic islands and plateaux and successions formed at passive continental margins. The amalgamation of these terranes occurred at various times from the Neoproterozoic to the Mesozoic and was accompanied by several episodes of magmatism. The CAOB is endowed with a large variety and number of mineral deposits, including: epithermal, porphyry and skarn systems, volcanogenic massive sulphides (VMS), lode style Au deposits, orthomagmatic Ni-Cu-PGE, rare metals in pegmatites and sandstone-hosted U deposits. There is abundant literature on various aspects of the geodynamic evolution of the Tianshan, Altay and Junggra belts and selected mineral deposits, both in Chinese and English. A review of the Tuwu, Baogutu porphyry deposits and those of the western Tianshan is provided. Epithermal precious metal deposits of high-sulphidation and low-sulphidation type are numerous in NW China and examples presented are Kuoerzhenkuola, Jinxi-Yelmand, Axi, Kuruer, Shuanffengshan, Jinshangou, Shiyingtan and Mazhaungshan. Similarly, precious metal lodes are abundant in the Tianshan, Junggar and Altay orogenic belts. Typically these lode deposits, commonly labeled as orogenic, occur within high strain zones in brittle (lower greenschist facies), brittle-ductile structures (mid-upper greenschist facies) to ductile (amphibolite facies). Many of the orogenic deposits have a spatial relationship to igneous rocks, while for others there is no clear connection with igneous activity. Therefore, these mineral systems are referred to as Au lodes, avoiding the orogenic or intrusion-related qualifiers.

In the southern Altay fold belt, Au lodes are distributed along second order faults within 5–10 km of the crustal scale Irtyish fault zone. Similarly, in the West Junggar fold belt, more than 300 lode deposits and occurrences are distributed along the Dalabute fault zone. In the East Junggar, lode deposits follow the Karamay fault for about 400 km. In the Tianshan, lode Au deposits abound, and for many the spatial links with granitic intrusions are well displayed, as is the case for the Kanggurtag deposit.

Skarn deposits are present in both the East Tianshan and Altay orogenic belts. In the East Tianshan the skarn deposits are Fe-Cu and Cu-Ag-Pb-Zn types. Iron-rich skarns in the East Tianshan include: Yamansu, Weiquan, Bailingshan, Heijianshan,

F. Pirajno, *The Geology and Tectonic Settings of China's Mineral Deposits,*
DOI 10.1007/978-94-007-4444-8_6,

Chilongfeng, Hongyuntan, Aqishan, Heilogfeng, Shuangfengshan and Shaquanzi. In the Altay belt, Mengku and Qiaoxiahala Fe deposits are economically important, as well as somewhat controversial in their origin. The Abagong Fe-P deposit also in the Altay, still being mined at the time of writing, is considered as a Kiruna-type ore system.

Volcanogenic massive sulphide (VMS) ore systems are present in both the Tianshan and Altay orogenic belts. They include the Qiaorequanzi Cu-Zn (in the Tianshan), Keketele Pb-Zn, Ashele Cu-Zn, Koktal Pb-Zn, Abagong Cu-Pb-Zn and Tiemuert Pb-Zn-Cu in the Altay orogen. For the latter, it has also been suggested that the deposit is not a VMS, but a base metal orogenic system. The Altay VMS deposits were formed in Devonian, fault-bound volcano-sedimentary basins, namely: Maize, Kelang and Qongut (or Chonghuer), containing mafic-felsic (bimodal) volcanic successions, possibly related to continental rifting. These Devonian volcano-sedimentary basins are strongly deformed and folded and their bimodal sequences metamorphosed from greenschist to upper amphibolite and granulite facies.

Ni-Cu sulphides in zoned and layered intrusions are present in the East Tianshan, Altay and in the West Junggar. Podiform chromite in ophiolitic rocks occurs in the West Junggar. On the southern margin of the Altay orogen the Kalatongke belt of mafic-ultramafic intrusions is distributed along the Irtysh fault zone. In the eastern Tianshan region there are two major belts of mafic-ultramafic rocks: the Huangshan-Jing'eruquan and Baishiquan belts, whereas in the western Tianshan is the Qingbulake belt. The Altay and Tianshan magmatic Ni-Cu deposits are genetically associated with and hosted in funnel-shaped, differentiated layered and/or zoned mafic-ultramafic intrusions. Several of these intrusions were originally emplaced in intracontinental rifts and are spatially and temporally associated with flood basalts and A-type granitic rocks. The Altay and Tianshan mafic-ultramafic intrusions have features that are similar to Alaskan-type complexes.

Sandstone-hosted roll-front type uranium deposits in Xinjiang include Wuyer, Wuyisan and Wuyiyi, located near the Kazakhstan border in the Yili basin and a fourth, called Shihongtan, in the Tuha Basin, about 200 km southeast of Urumqi. The U deposits in the Yili basin are considered to be an extension of a large U province in Kazakhstan and Uzbekistan. Both the Yili and Tuha basins also host oil and gas reservoirs and coalfields.

A belt of about 1,000 pegmatite veins extends for more than 450 km, in the Central Altaishan terrane. Here more than 150 pegmatite-hosted rare metal deposits and occurrences are within high-grade metamorphic rocks and granitic intrusions. The Keketuohai No. 3 zoned pegmatite is one of the largest rare metal producers in China containing Be-, Li, Nb-Ta-, Cs-, Zr-, Hf-, U- and Bi-bearing minerals.

The Alpine-Himalayan orogenic belts or Tethysides extend from the Alpine orogen in Europe, to the Himalaya proper, Tibet and to southeast Asia. In this chapter, I discuss the Chinese portion of the Tethysides, more specifically Tibet, southwest China and the Kunlun region on the northern margin of the Tibetan Plateau. The Chinese Tethysides are also referred to as Himalayan-Tibetan orogen, an orogenic collage of magmatic arcs with a complex geodynamic evolution extending from Cambrian to Late Triassic. Recent published special issues have highlighted the

number and variety of mineral deposits in the Tibetan orogen, which is after all not as well geological explored as other parts of China. Several porphyry copper and gold deposits in the eastern Qiantang terrane are located along the Jinshajiang and Red River fault systems. These ore deposits are associated with alkaline intrusions emplaced at 40–30 Ma. Porphyry copper and gold deposits associated with 18–10 Ma shoshonitic and potassic calc-alkaline (adakitic) intrusions are located along the Gangdese thrust in the Lhasa terrane.

The 270 km long and 15 km wide Cenozoic Mianning-Dechang (MD) belt in eastern Tibet and western Sichuan is located in on the western margin of the Yangtze Craton and is characterised by numerous syenite and carbonatite intrusions, spatially associated with the prominent strike-slip faults in the region (Red River, Ailaoshan, Xiaojiang faults) and within the prominent north-trending Panxi rift. The MD belt is endowed with a total of 3 Mt of REE ore in the Maoniuping and Dalucao deposits, plus a number of other occurrences. These deposits are related to magmatic activity (40–24 Ma, with a peak of activity at 35 Ma) in the region forms a nearly continuous potassic igneous province. The carbonatite–alkaline complexes in western Sichuan intrude Proterozoic crystalline basement and overlying Palaeozoic–Mesozoic volcano-sedimentary sequence, forming a narrow, north-trending REE mineralised corridor (Panxi rift). Finally, the sandstone- and limestone-hosted Jinding Zn-Pb deposit in western Yunnan, is considered to be the largest in China, with estimated resources of about 200 Mt (total Pb + Zn). The host rocks are of Cretaceous and Cenozoic age, making Jinding the youngest sedimentary-rock hosted Pb-Zn deposit in the world.

The Kunlu and Songpan-Ganzi terranes, separated by sutures from the Qiangtang (Tibetan plateau) in the south, South China Block to the east and Tarim-North China cratonic blocks to the north. The Ordovician to Triassic western Kunlun subduction-accretionary complex was developed between the southern margin of the Tarim block and the northern margin of the Tibetan Plataeu. The western Kunlun orogen, forming a 1,000 km long mountain range, consisting of magmatic arc-type terranes, ranging in age from Proterozoic to Lower Palaeozoic. The Kunlun orogen contains several types of ore systems, reflecting the complexity of its tectonic assemblages, from magmatic arc, to oceanic lithosphere, to back-arc settings. Porphyry Cu deposits, volcanogenic massive sulphides (VMS), sedimentary Fe deposits and MVT Pb-Zn deposits and orogenic Au lodes are present. The Yunwuling porphyry Cu deposit occurs in a metallogenic belt along the Kunlun fault, whereas orogenic Au lodes are found in the eastern Kunlun and have an age of ca. 239 Ma. A newly discovered and unusual Co-Au deposit, called Tuolugou, within the Kunlun orogenic belt has resources estimated at greater than 20,000 t of Co and 4 t of Au.

6.1 Introduction

The Mesozoic-Cenozoic Tarim, Junggar and Turpan Basins (described in Chap. 8), are surrounded by the Palaeozoic Tianshan, Kunlun, Altay, West and East Junggar fold belts, which are all part of the Central Asian Orogenic Belt (CAOB). These

fold belts were affected by tectonic deformation relating to events resulting from the closure of the Palaeo-Asian, Palaeo- and Neo-Tethys oceans (see Fig. 2.1a, b). The northward India-Asia collision resulted in their rejuvenation and uplift, which continues today. The fold belts that are situated between the Arabian and Indian blocks to the south and east and the Tarim, Kazakhstan and East European blocks to north and the South China block to the east, form the huge Alpine-Himalayan fold belts or Tethyan orogens. The Songpan-Ganzi terrane (orogen) is situated between the Alpine-Himalayan fold belts and the Qinling Orogen. It is very difficult to do justice to the complexities of these tectonic domains in a few pages, but for a comprehensive and excellent overview, the interested reader is directed to the work of Sengör and Natal'in (1996). In this chapter, I briefly describe the western sector of the Chinese CAOB (Altay and Tianshan, West and East Junggar) in northern Xinjiang Province (NW China), the Kunlun and the Songpan-Ganzi terranes and their associated mineral systems.

6.2 Central Asian Orogenic Belt; Tianshan and Altay Orogenic Belts in Northern Xinjiang (NW China)

The NW China region mostly encompasses the Xinjiang Uygur Autonomous Region (Xinjiang Province), with its capital city in Urumqi, covering about 1,660,000 km^2, one-sixth of China's total territory, bordering Mongolia, Kazakhstan, Kyrgyzstan, Tajikistan, Afghanistan and Pakistan. The physiography of Xinjiang is dominated by three economically important basins, the Tarim, Turpan and Junggar, rich in coal and hydrocarbon resources (Chap. 8). These basins are surrounded by mountain chains, with breathtaking scenery; the Altay in the north, the Tianshan in the centre and the Kunlun-Karakorum in the south (Fig. 6.1a). The Tianshan (Tian = heaven, Shan = mountains; with peaks reaching in excess of 5,000 m a.s.l., Bogdashan, and up to 7,439 m a.s.l. in the Pobedy Peak), extends across the centre, geographically separating the Province into two regions, southern and northern Xinjiang, whereas the Aiden Lake depression in the Turpan (also called Turpan-Hami, or Tuha in Chinese literature) Basin, at 154 m below sea level is the second lowest land on Earth (Fig. 6.1a). The Tarim Basin is covered by the Taklimakan and Kurutag deserts. Rivers draining the Kunlun mountains discharge into the Taklimakan desert. A major river system, Yakant and Tarim, flows along the western and northern margins of the Tarim Basin (Fig. 6.1a). The Tianshan, Kunlun, Altay, West and East Junggar fold belts were affected by a series of tectonic and magmatic events culminating with the accretion of the huge Central Asian Orogenic Belt (CAOB). Between the Tianshan and the Junggar is the Yili Block, considered by some workers as a remnant of a microcontinent. Pirajno et al. (2011) reviewed the general geology and selected mineral systems of the Tianshan, Altay, West and East Junggar fold belts. Parts of what follows are taken from this work.

The CAOB (Jahn 2004) or Altaid orogenic collage; (Sengör et al. 1993), or Central Asian Orogenic Supercollage (Yakubchuk 2004, 2009; Yakubchuk et al. 2005), was

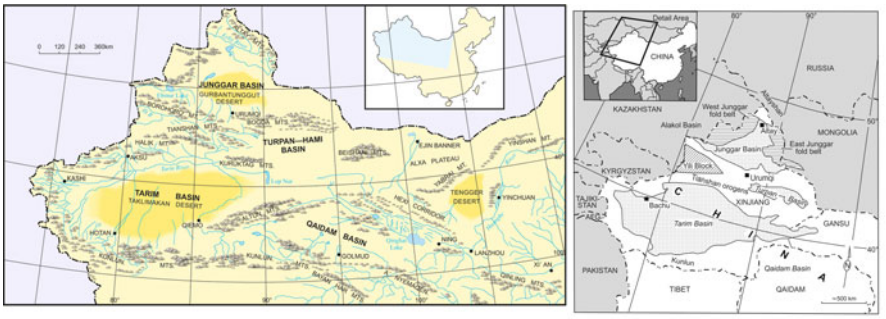

Fig. 6.1 **a** A sketch map of NW China (re-designed and modified by Murray C. Jones (Geological Survey of Western Australia) from Zhou and Dean 1996); **b** Xinjiang Uigur Autonomous Region in NW China and its principal tectonic units. (After Rui et al. 2002)

described in some detail by Windley et al. (2007). The CAOB extends from the Uralides in the west to the Pacific Ocean margin of eastern Asia and is bounded to the north by the Siberian Craton and to the south by the Tarim-North China cratonic blocks (Fig. 6.2). Overviews can be found in Sengör and Natal'in (1996), Rui et al. (2002) and Mao et al. (2003), whereas more recently Xiao and Kusky (2009) and Xiao et al. (2008a, 2009) edited special issues devoted to the geodynamic evolution and associated metallogenesis of Central Asia. In September 2011, the CAOB was the focus of the Penrose conference, held in Urumqi (Schulmann and Paterson 2011). The geodynamic evolution of the CAOB involved almost continuous convergence by subduction-related accretion and continental collision, followed by post-collision extension. The CAOB has been considered as the "fossil" equivalent of the island arcs of the southeast Asia (Indonesia, Philippines) and Japan islands (archipelago model; Xiao 2004a, b). This possibility was discussed at the Penrose conference and a new tectonic model introduced namely that the Lachlan Orogen of eastern Australia and its southwest Pacific extension may be a more suitable analogue for the CAOB (Schulmann and Paterson 2011).

The CAOB is a complex collage of fragments of ancient microcontinents and arc terranes, fragments of oceanic volcanic islands (e.g. seamounts), perhaps also volcanic plateaux (e.g. Junggar block), oceanic crust (ophiolites), and successions formed at passive continental margins. The amalgamation of these terranes occurred at various times from the Neoproterozoic (ca. 1,250 Ma) to the Mesozoic and was accompanied by several episodes of magmatism. Geochronologically well constrained magmatic events range in age from Ordovician (ca. 450 Ma) to Triassic-Cretaceous (ca. 220–120 Ma), resulting in the emplacement of large volumes of granitic intrusions (Jahn 2004) and mafic volcanic rocks (Zhu et al. 2005), accompanied by lesser volumes of mafic-ultramafic material. A-type granitic and peralkaline intrusions in the CAOB are common and are associated with post-collisional tectonism. In northeast China and Mongolia, A-type granites are associated with extensive Mesozoic and Cenozoic volcanism (Jahn 2004). Nd-Sr isotope studies indicate that

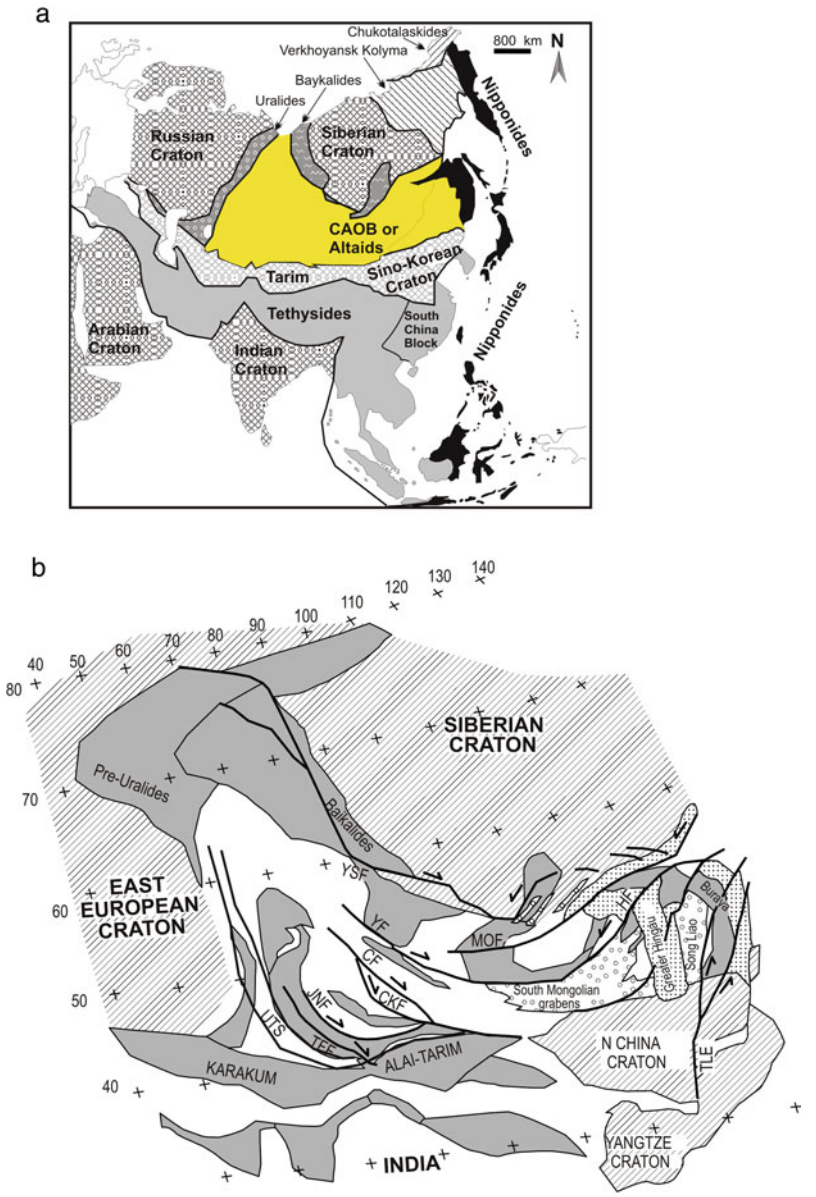

Fig. 6.2 **a** Position of the Central Asian Orogenic Belt (CAOB) in Asia and its relationship to other tectonic units (after Sengör and Natal'in 1996); **b** Central Asian Orogenic Belt (CAOB), microcontinental blocks and major strike-slip faults (after Yakubchuk 2004); *YF* Irtysh Fault, *HF* Hinggan Fault, *MOF* Mongol-Okhotsk Fault, *CF* Chingiz Fault, *TFF* Talas-Ferghana Fault

these A-type and peralkaline granites are juvenile and of mantle origin (Jahn 2004). It is more likely that the granites of the region include arc-related syn- to post-orogenic, as well as anorogenic types, as shown in the published geological maps of Xingjiang (BGMRX, Bureau of Geology and Mineral Resources of Xingjiang Uygur Autonomous Province 1993). Radiometric dating of these granites indicates that they were emplaced during the Carboniferous to the Triassic (ages range approximately from 330 to 230 Ma; Jahn 2004). The extent of the CAOB terranes, fold belts and associated igneous lithologies in China is shown in Fig. 6.3. The boundary between the CAOB and the Tarim-North China cratonic blocks is determined by suture zones, characterized by ophiolitic mélanges, marking the closure of the Palaeo-Asian ocean. In the western sector (NW China), ophiolite mélanges form the Southern Tianshan suture, which in the Beishan orogen also include accreted magmatic arcs (Xiao et al. 2010). The Southern Tianshan suture zone connects to the east with the Solonker suture. In the eastern sectors, the boundary between the North China Craton and the CAOB was referred to as Manchurides by Sengör and Natal'in (1996), where ophiolitic rocks constitute the Solonker suture (Fig. 5.27), bordering the Great Hinggan volcanic province, superimposed on the Hinggan Orogen (Chap. 5 and 7). The eastern end of the CAOB in China is represented by the Erguna Block and Jiamusi Block (also referred to as massifs/inliers), microcontinental fragments in the Hinggan fold belt (Chap. 5).

As explained in the pages ahead, the CAOB was overprinted by strike-slip and extensional tectonics between the Permian and the Mesozoic, followed by Cenozoic intracontinental shortening (see Yin 2010).

In NW China, the Altay Orogen, West- and East Junggar fold belts and the Tianshan orogenic belt, are characterised by accreted terranes that were later affected by rifting processes and post-collision intraplate rift magmatism with granitic, mafic-ultramafic intrusions and continental flood basalts, between the Carboniferous-Permian and the Late Cretaceous (Xia et al. 2003, 2004; Pirajno et al. 2008). The history of convergence and assembly of the microcontinental blocks and subduction-accretion complexes in NW China has been investigated by Coleman (1989), Mossakovsky et al. (1994), Carroll et al. (1995), Xiao et al. (2004a, 2004a, 2008b), Wang et al. (2011, 2012), Yang et al. (2012b), Han et al. (2011). The simplified geology of NW China is shown in Fig. 6.4.

6.2.1 Tianshan and Yili Block

The Tianshan range extends 2,500 km, approximately east-west, from northern China to the central Asian republics of Kazakhstan, Kyrgyzstan, Tajikistan and Uzbekistan. GPS measurements and apatite fission track records (Abdrakhmatov et al. 1996; Zhou et al. 2001; Glorie et al. 2010) demonstrate the ongoing uplift of the Tianshan, which is due to the far-field effect of the India-Asia collision. The Tianshan is essentially a collage of subduction-accretion complexes that have been added between the Tarim Craton, the Junggar Basin and the Siberian Craton. Rui et al. (2002) divided the

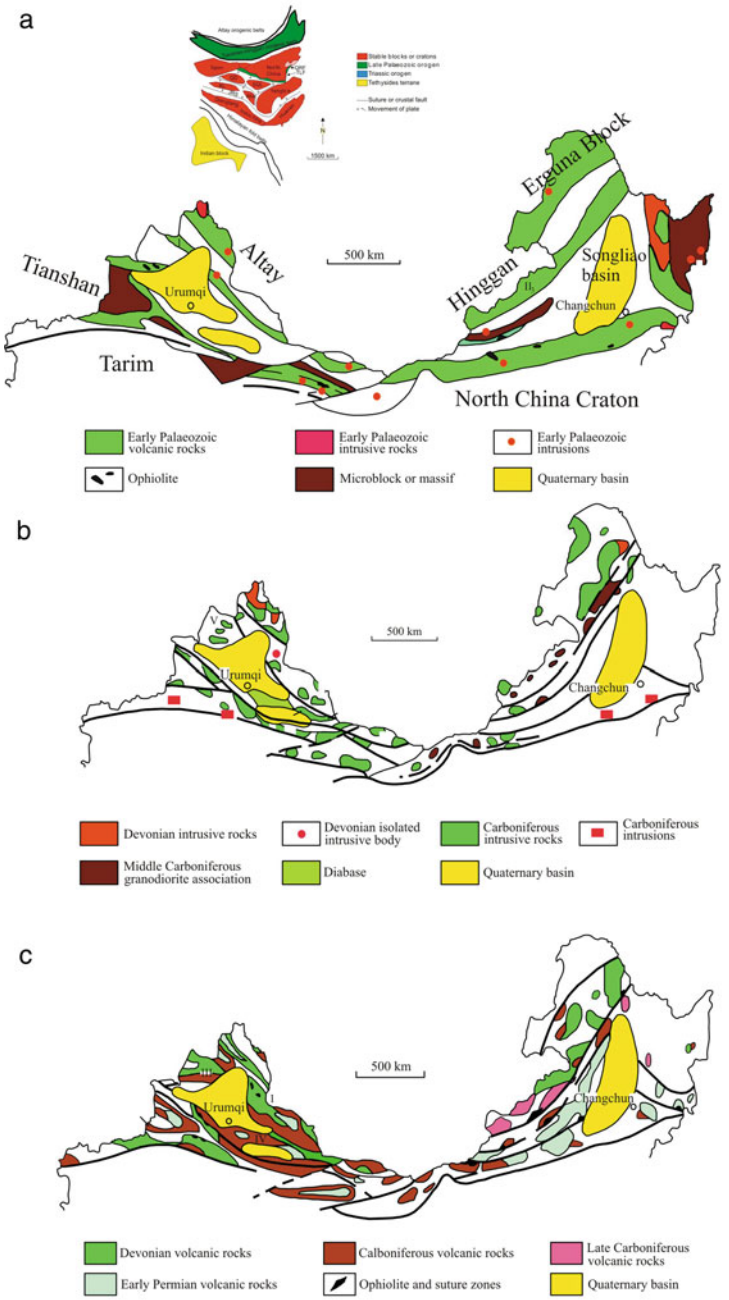

Fig. 6.3 Extent of the Altay, Tianshan and Hinggan fold belts and associated igneous lithologies in China; **a** Early Palaeozoic, **b** Devonian-Mid Carboniferous, **c** Carboniferous-Permian; *inset* above shows the relationship with other tectonic domains of China. (Modified after Cheng 2000)

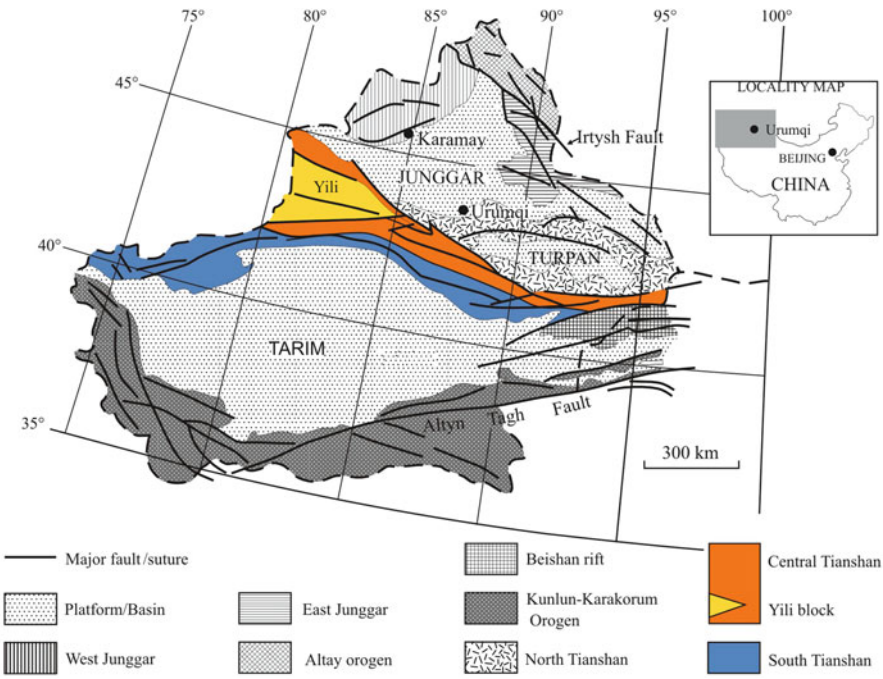

Fig. 6.4 Simplified geology of NW China (Xinjiang province). (After Pirajno et al. 2008)

Tianshan belt into Northern, Southern and Central (including the Yili Block; see below) Tianshan (Fig. 6.4). The same subdivisions are used in the western part of the orogenic belt in Uzbekistan and Kyrgyzstan, but these do not exactly correspond with the Chinese sector of the Tianshan (Chiaradia et al. 2006). Gao et al. (2009) attempted to bridge the "rift" between the western Tianshan (Kazakh, Kyrgyz, Uzbek and Tajiki) on the one hand, and the Chinese Tianshan on the other. They proposed three tectonic domains: Kazakhstan (North Tianshan)-Yili plate, Central Tianshan Terrane and the Tarim Plate. In this scheme, the Kazakhstan-Yili plate is separated from the Central Tianshan by the Nikolaev Line (Kyrgystan and Kazakhstan) and the North Nalati Fault in NW China, both marked by ophiolites, interpreted as relics of a palaeoocean, which were thrust over the island arc complexes of the North Tianshan. The Central Tianshan is separated from the northern margin of the Tarim Plate by the Southern Central Tianshan Suture (SCTS; Gao et al. 2009), or sutures (Wang et al. 2011). The northern margin of the Tarim Plate is overlain by rift-type intraplate volcanic rocks and intruded by syenite, nepheline syenite, aegirine syenite and A-type rapakivi granites (Gao et al. 2009). For the sake of completeness it must be pointed out that many researchers, when discussing specific areas and/or topics, prefer to geographically consider the Tianshan into western and eastern sectors (e.g. Wang et al. 2007a; Shu et al. 2004).

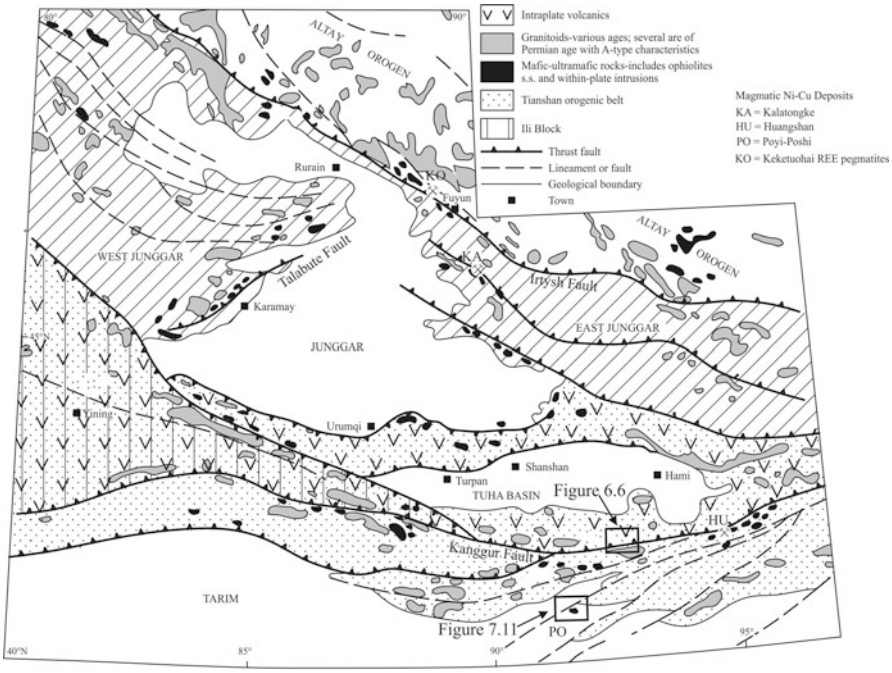

Fig. 6.5 Simplified geology of parts of the Tianshan and Altai orogenic belts in northern Xinjiang and distribution of mafic-ultramafic and granitic rocks, intraplate volcanics and selected mineral deposits; *boxes* show areas of Figs. 6.6 and 7.11. (After Pirajno et al. 2008 and references therein)

In this book, I retain the divisions of North, Central (with Yili block) and South Tianshan, which are still adopted by most workers (e.g. de Jong et al. 2009 and references therein). The boundaries between these divisions are typically marked by strike-slip shear zones that post-date the amalgamation of the CAOB, with both dextral and sinistral movements linked to rotation of the Siberian (anticlockwise) and Tarim (clockwise) cratonic units (Van der Voo et al. 2006). Movements along the major strike-slip faults and uplift of the orogens are continuing today due to far field effects of the India-Eurasia collision (e.g. Yang and Liu 2002; Fang et al. 2007; Metelkin et al. 2010 and references therein). The rotational movements of the Siberian and Tarim blocks were accommodated by these large-scale strike-slip shear zones and accompanied by the formation of pull-apart basins, which are typically filled with molasse (continental) type sediments and alkali basalts (shoshonitic).

The *North Tianshan* (Fig. 6.4), best represented in the Bogdashan range east of Xinjiang's capital city, Urumqi, consists of Carboniferous calc-alkaline volcanic and sedimentary rocks, intruded by mafic and intermediate-felsic plutons (Charvet et al. 2007; Fig. 6.5). The Bogdashan, together with the Kanggur terrane (also called Jueluotage belt or terrane), are interpreted as volcanic arcs, which could have formed

either as north-directed or as a south-directed subduction of oceanic crust and separated by an ocean from other island arcs, such as the Aqishan-Yamansu arc and the Dananhu-Tousuquan arc. The Aqishan-Yamansu and the Dananhu-Tousuquan arcs, host a series of porphyry systems, namely Yandong, Tuwu, Linglong and Chihu (see below). The *Central Tianshan* (Fig. 6.4) is a wedge-shaped zone comprising, from north to south, a forearc mélange, a Carboniferous volcanic arc and a Silurian-Devonian volcanic arc. The Central Tianshan also contains basement inliers of Late Proterozoic age, which may have been part of an earlier microcontinent (i.e. Yili block or microcontinent) (Zhang et al. 1984). The Central Tianshan Ordovician-Silurian arc system is interpreted by Xiao et al. (2004b) as a composite Andean type volcanic arc with volcanic rocks of calc-alkaline affinity and I-type granitic intrusions, on a Precambrian basement that comprises 1,400 Ma gneiss, schist, migmatite and marble. The *South Tianshan* belt (Fig. 6.4) consists of Carboniferous felsic to intermediate volcanic and volcaniclastic rocks attributed to volcanic arcs, and Silurian volcanogenic sedimentary rocks, deposited in a back arc setting (Charvet et al. 2007). These rocks are separated from the North Tianshan by the Kanggur Fault, a major east-west-trending suture and strike-slip fault (Fig. 6.5). The South Tianshan belt also contains fragments of oceanic crust material in fault contact with a sequence of sandstone, shale, chert and limestone of Mid-Silurian to Mid-Carboniferous age, which were possibly deposited on a passive margin on the north side of the Tarim block (Carroll et al. 1995).

According to Carroll et al. (1995, 2001), the Central Tianshan collided with a north-facing passive margin on the north side of the Tarim during Late Devonian-Early Carboniferous. In this way, the South and Central Tianshan were amalgamated with the Tarim Block. Between the Late Carboniferous and Early Permian, the intervening ocean between the North Tianshan arcs and the amalgamated Tarim-South-Central Tianshan tectonic unit closed and the North Tianshan arc was accreted to the Central Tianshan orogen (Windley et al. 1990; Charvet et al. 2007). Granitic rocks intrude the island arc successions and consist of a number of batholiths that include granodiorite, diorite and monzonitic granite. U-Pb dating of these granitic intrusions yielded ages ranging from 333 to 389 Ma (Han et al. 2006a and references therein).

The Yili Block or terrane is a fragment of a microcontinent that consists of a series of Precambrian terranes that were amalgamated in the Early Palaeozoic (Rui et al. 2002). The Late Devonian-Carboniferous volcanic rocks in west Tianshan (and Yili Block) were formed in a continental arc environment (Wang et al. 2007a; Zhu et al. 2009). Su et al. (2010) supported the Yili-Tarim collision model and, on the basis of U-Pb geochronology of eclogites, suggested that this event occurred at about 320 Ma. More recently, Wang et al. (2012), envisaged a separate Kazakhstan-Yili magmatic arc that moved southward towards the Central Tianshan. The central parts of the Yili Block are dominated by Carboniferous sedimentary rocks intercalated with basaltic volcanic rocks. The nature of these volcanic rocks (calc-alkaline arc-related versus intraplate rift-related) is pivotal in the understanding not only of the Yili Block but also the surrounding region. Xia et al. (2003, 2004) considered these volcanic rocks as mantle-plume related and part of a large igneous province, whereas Wang et al.

(2007a, 2011, 2012) considered the sedimentary-basalt package as being part of a south-directed subduction-related volcanic arc. According to Xiao et al. (2004b, 2008), the Yili microplate and Central Tianshan are bound by suture zones against the Kokshaal-South Tianshan accretionary complex on the south side and the North Tianshan accretionary complex with the Harlik-Dananhu volcanic arc on the north side. The Harlik-Dananhu arc was separated from the East Junggar by the Karamay (Karamai) Ocean. Xiao and co-workers suggested that the Harlik-Dananhu magmatic arc and Xiaopu-Bogda back-arc system of the North Tianshan belt, may have been formed by a south-dipping subduction zone. Along the southern edge of the Turpan Basin, this arc system is composed of Ordovician and Devonian-Carboniferous Dananhu arc, including the Devonian Kalatag, Dananhu, Tousuquan and Kanggurtag Formations, comprising mafic lavas, pyroclastic rocks, clastic sedimentary rocks and felsic volcanic lavas and tuffs (a bimodal sequence?). The Carboniferous includes the Xiaorequanzi Formation, Qiatekaertag Group, Dikaner Formation comprising tholeiitic lavas, pyroclastic rocks, greywacke and carbonates (Xiao et al. 2004b). SHRIMP zircon ages ranging from ca. 383 to 334 Ma have been obtained from arc granitic rocks (Xiao et al. 2004b). To the north of the Dananhu arc and in fault contact is the Kanggurtag forearc accretionary complex, which consists of a sequence of volcano-sedimentary rocks of Lower to Mid-Carboniferous age. Other mélange rocks of the accretionary complex include Devonian-Carboniferous basaltic and spilitic lavas, keratophyre (felsic volcanics), pyroclastics, chert and deep-sea turbidites, imbricated in a 5-km thick sequence (Xiao et al. 2004b). Part of this accretionary complex are ophiolitic rocks that comprise pillow basalts, serpentinite, metagabbro, plagiogranite (low-K granitic rock formed at mid-ocean ridges), keratophyre, chert, structurally juxtaposed onto greywacke, phyllite, quartz-sericite schist and meta-tuff in the Kanggur (Kanggurtag) area.

The Kanggur (Kanggurtag) area is close to the major tectonic boundary separating the North Tianshan from the South Tianshan terranes. The main structural elements in the area are the east-west trending Kanggurtag Fault (or Kanggur Shear Zone) in the north and the west-northwest-trending Kulungetag Fault in the south. The Kanggurtag and Kulungetag faults enclose rocks of the Juluotag volcanic arc, which are in fault contact (along the Yamansu Fault) with a sequence of sedimentary and volcaniclastic rocks (mainly siltstone, sandstone and tuffs that were possibly trench sediments). The rocks of the Juluotag arc include intermediate to felsic volcanics of Carboniferous age. South of the Juluotag arc are mafic volcanics interpreted to represent a back-arc basin setting. The contact between these and the arc volcanics is intruded by a large granite pluton. A K-Ar age of 293 Ma is reported for one of these granites (BGMRX 1993). Thus, the overall tectonic setting is that of a trench, volcanic arc, and a back arc basin, with subduction polarity towards the south, as indeed envisaged by Xiao et al. (2004b).

The description of these rocks by Xiao et al. (2004a, b, 2008) together with personal field observations, suggest that these rocks may be part of oceanic crust and associated volcanic islands. Strong deformation and thrust belts in the region actually hamper an accurate assessment of the true nature of these rocks. Xiao et al. (2004b, 2008) included in the Dananhu arc system zoned mafic-ultramafic complexes, some

containing Ni-Cu magmatic sulphides (see Sect. 6.3.6). These authors recognised the affinity of these zoned intrusions to the Alaskan zoned mafic-ultramafic complexes, as independently did Pirajno et al. (2008). However, SHRIMP zircon dating shows that the age of these complexes is Permian (280–270 Ma; see references in Xiao et al. 2008; Pirajno et al. 2008), suggesting that the zoned intrusions belong to the widespread intraplate magmatism that affected central Asia in this period (Pirajno et al. 2009). In this light, these rocks cannot be linked to subduction systems and therefore the interpretations of Xiao and co-workers must be taken with caution and re-assessed in the light of field observations. I return to this issue in Sect. 6.3.6. To the south of the Kanggurtag forearc belt is the Yamansu forearc-arc belt, which consists of Devonian-Carboniferous basaltic and andesitic lavas, dacite, rhyolite intercalated with clastic and carbonate rocks and radiolarian chert. Isotopic ages of the volcanic rocks range from 340 to 290 Ma. The Yamansu arc hosts VMS deposits. Ophiolitic and mélange rocks characterise the Aqqikudug-Shaquanzi fault zone, with harzburgite, dunite and gabbro. Basaltic lavas and chert units (Gangou and Mishigou ophiolites), enclosing fault-bounded mafic granulite blocks (Xiao et al. 2004b). Figure 6.6 shows parts of the Kanggurtag, Yamansu and Dananhu arc systems.

The geodynamic history of the Tianshan orogenic belts remains controversial and plagued by several unresolved issues, largely on subduction polarities, the role and nature of ophiolitic rocks and location of suture zones (Fig. 6.5; Wang et al. 2011). Figures 6.7 and 6.8, present two models of the tectonic evolution of the Tianshan and northern margin of the Tarim. In Fig. 6.7 (Xiao et al. 2004b) the northern part of the Tarim is interpreted as a passive margin, with double-subduction polarities, responsible for the inception of island arcs (Harlink-Danhahu) (Fig. 6.7a). The central Tianshan is a magmatic arc formed by north-directed subduction and separated by an oceanic arm (Kumishi) from the northern Tarim (Fig. 6.7b). In Early-Mid Carboniferous, an inter-arc basin developed between the Harlik island arc and the Yamansu arc, while the Karamay oceanic seaway started to close (Fig. 6.7c). In the Late Carboniferous, the Dananhu-Yamansu-Harlik arc system collided with the Altay orogen (Siberian plate), with the collision line marked by the ophiolites of the Karamay suture zone, while north-directed subduction continued under the Central Tianshan and the Yamansu arc. In the latest Carboniferous and Permian (Fig. 6.7e), complete amalgamation of all tectonic domains occurred, eventually leading to the overprinting by strike-slip faults and related pull-apart basins in the Late Permian-Mesozoic. In my view, it is in this environment that zoned mafic-ultramafic complexes and associated magmatic Ni-Cu sulphide deposits, were formed, as explained in more detail in Sect. 6.3.6.

Wang et al. (2011), citing *interalia* Biske and Seltmann (2010), opposed a dominant north-dipping subduction polarity of the South Tianshan. Instead, these authors suggested south-directed subduction systems (Fig. 6.8), based on their interpretation of northern Tarim was not a passive margin, but a subduction-related arc, whereas the nature of ophiolitic mélange within the southern Chinese Tianshan, comprises N-MORB type mafic and ultramafic rocks, as well as alkali basalts with a OIB signature. The former are tectonically juxtaposed with chert, limestone, associated with

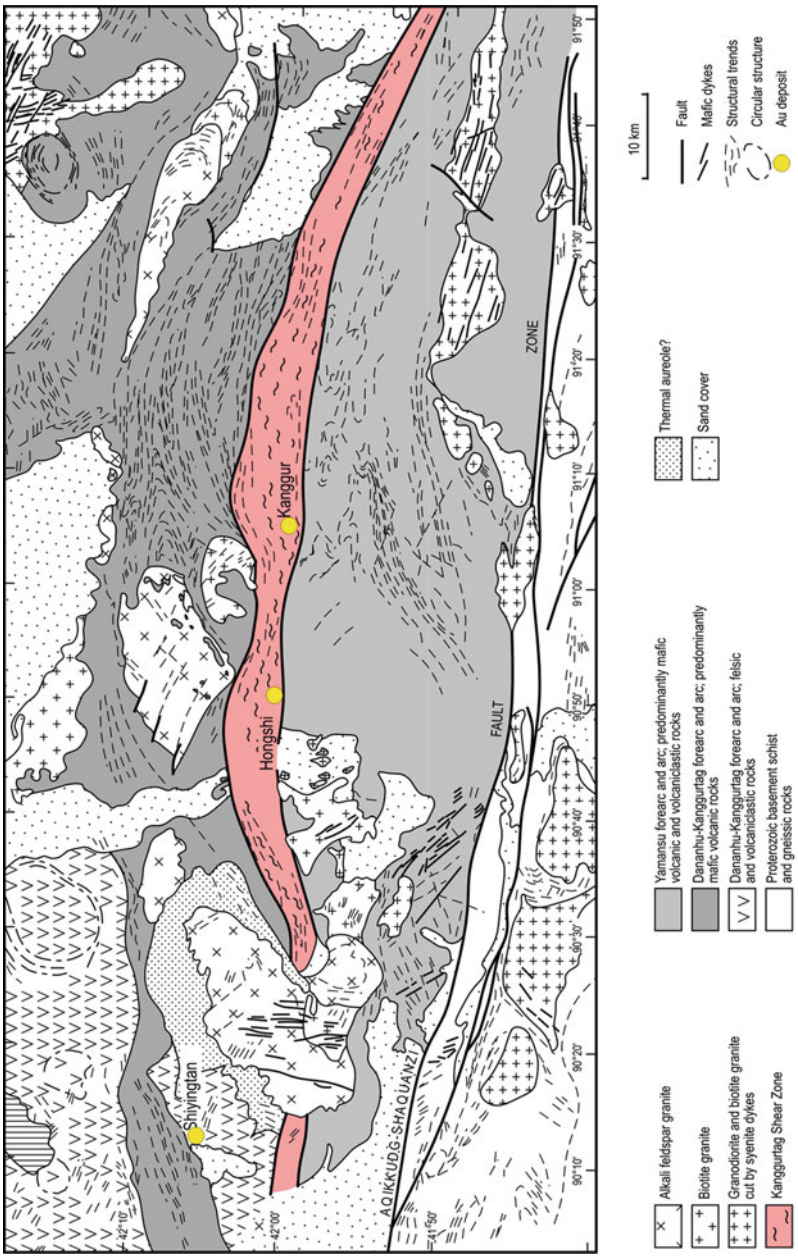

Fig. 6.6 Simplified geology of the Kanggurtag (or Kanggur) shear zone, Yamansu and Dananhu volcanic arcs and distribution of key mineral deposits; based on field mapping (Pirajno unpublished), see also Figs. 6.5 and 6.26. (After Pirajno CR142)

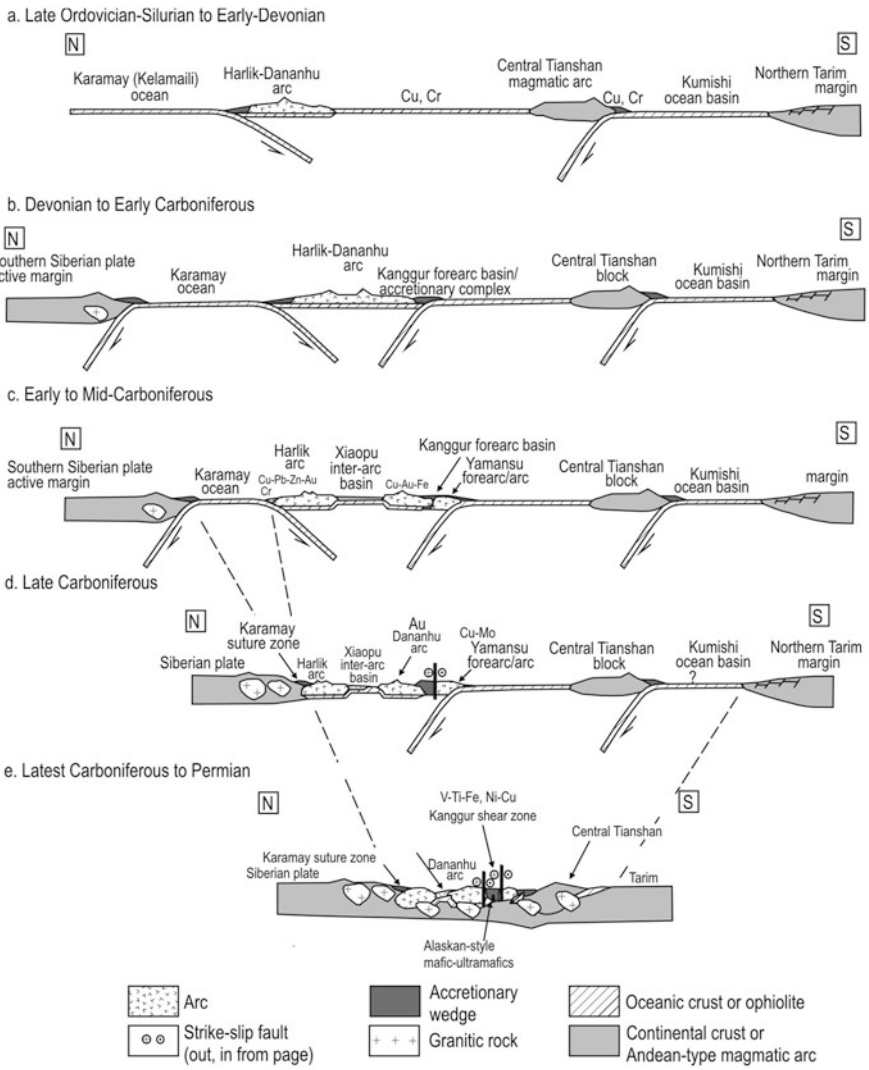

Fig. 6.7 Model of the geodynamic evolution of the Tianshan orogen and associated metallogeny, between the late Ordovician and the Permian; see text for details. (Slightly modified after Xiao et al. 2004b)

tholeiitic basalts showing trace element geochemical signatures, likely representing oceanic crust (e.g. Zr/Nb ranging from 24 to 46; Zr/Hf from 29–31; Nb/Ta 13–14, similar to N-MORB), which led to Wang et al. (2011) to envisage for the South Tianshan oceanic crust developed in the early stages of a continental back-arc basin (Fig. 6.8b). In contrast, alkali basalts and andesites have OIB-like geochemical sig-

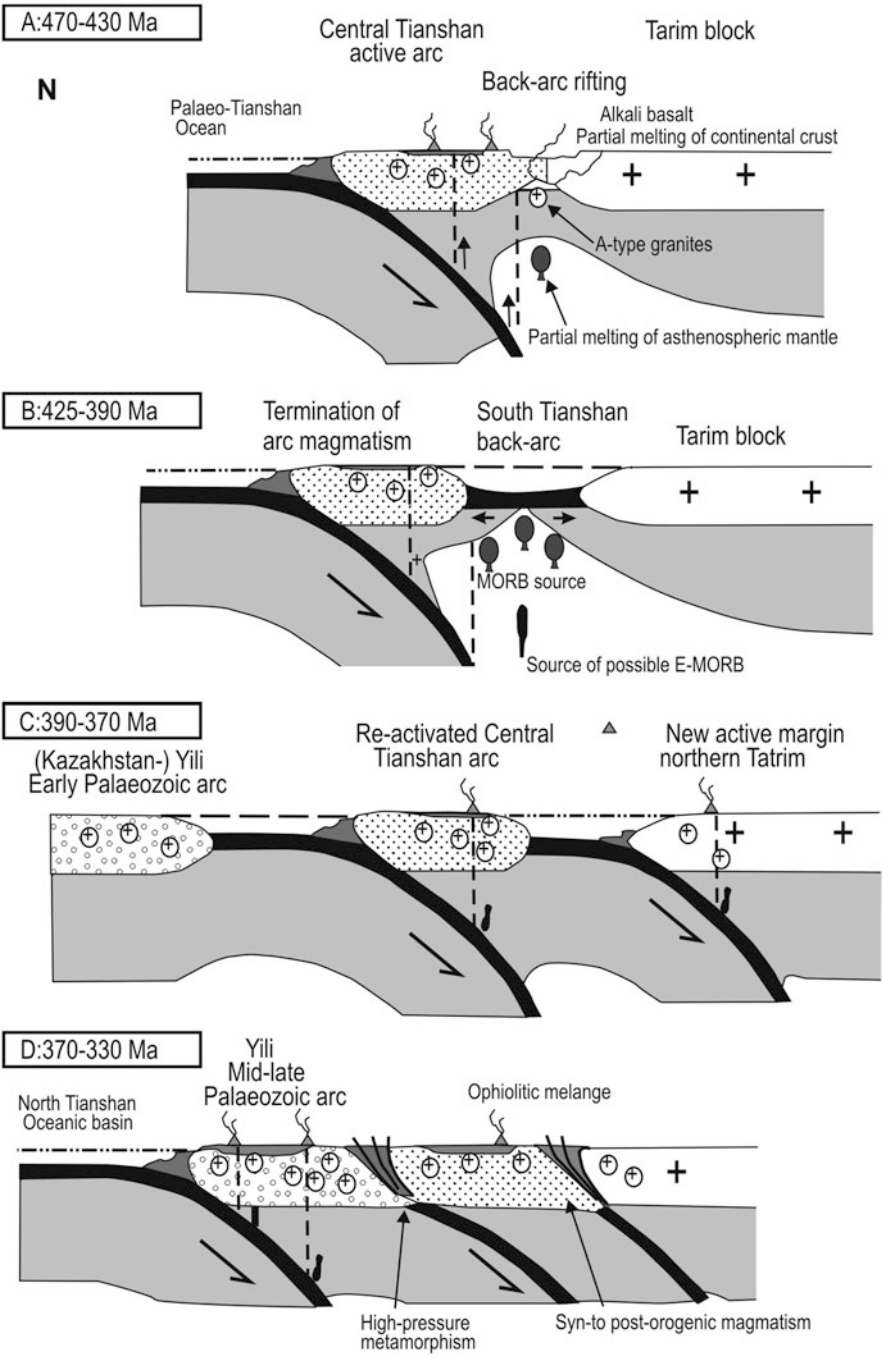

Fig. 6.8 Tectonic evolution of the Central Tianshan, Yili terrane and northern part of the Tarim Craton, between the Ordovician and Carboniferous; see text for details. (After Wang et al. 2011)

nature (e.g. negative εNd(t) values), produced in an intraplate setting. Furthermore, the Wang et al.'s model proposes two suture zones, a Central Tianshan suture and a South Tianshan suture, deriving from the closure of two subduction zones (Fig. 6.8c, 6.8d). The northern Tarim Craton was part of an active continental margin (Fig. 6.8c), developed as follows (Wang et al. 2011). Calc-alkaline volcanic rocks of Ordovician-Silurian (490–427 Ma) and Devonian (ca. 396 Ma) ages occur between the Central and South Tianshan sutures and are associated with arc-type granitic rocks (447–423 and 395 Ma). These calc-alkaline igneous rocks are interpreted to have formed in an early Palaeozoic Central Tianshan magmatic arc, developed on Neoproterzoic basement. This magmatic arc, developed on the northern part of the Tarim Craton, was later rifted in the Silurian-Early Devonian, due to the opening of the South Tianshan bac-arc basin. Finally, the Central Tianshan arc collided with the northern Tarim, leading to the development of two suture zones, in which key structural element are typically top-to-the-north (Fig. 6.8d), while a north Tianshan oceanic plate subducted under the Yili terrane to form a mid-late Palaeozoic magmatic arc.

6.2.2 Altay (Altai) Orogen

The Altay (Altai) orogen extends for more than 2,500 km from Kazakhastan, across northeastern Xinjiang province to western Mongolia (Figs. 6.2 and 6.5). Sengör and Natal'in (1996) described two main tectonic units for the Altay: the Kolyvan-Rudny Altay and the Gorny Altay, both consisting of Early Palaeozoic accretionary wedges and Mid-Late Palaeozoic magmatic arcs. The Altay orogen was formed through a complex series of events that include accretion, subduction and opening and closing of small basins (Windley et al. 2002; Goldfarb et al. 2003). The Chinese part of the Altay orogen was divided by Windley et al. (2002) into five fault-bound terranes. These are briefly described below. (1) The Altayshan terrane consisting of Late Devonian-Early Carboniferous metasedimentary rocks, overlain by shale, siltstone, greywackes and limestone (Kumasu Group). These rocks are in fault contact with sedimentary and intermediate-felsic volcanic rocks. All are intruded by granitic plutons. The terrane is interpreted to represent the remnants of two island arcs. (2) The northwest Altayshan terrane contains sedimentary and volcanic rocks of Neoproterozoic to Early Devonian age forming a sequence of metasedimentary rocks up to 6,000 m thick (Habahe Group), interpreted as continental-derived turbidites. These rocks are unconformably overlain by shale, limestone, andesite and porphyry volcanic rocks (Baihaba Group), associated with tonalite, granodiorite and hornblende granite plutons. One of these granites has a Sm/Nd isochron age of 390 Ma. The entire succession is interpreted as a continental volcanic arc. (3) The Central Altayshan terrane forms the central part of the Chinese Altay orogen and contains high-grade metamorphic rocks and granites ranging in age from Neoproterozoic to Silurian. In one area (west of the Fuyun Fault) is a belt of gneiss, migmatites, quartzite and fossiliferous marble (Habahe Group), overlain by a succession of a continental

turbidites, approximately 8,000 m thick. In the Keketuohai area are major pegmatite fields, including one of the largest pegmatites in the world, mined for rare metals (see Sect. 6.3.8) and associated with post-tectonic granites. Undeformed granites in the Keketuohai area have U-Pb SHRIMP and Sm-Nd ages of ca. 248 Ma (Zhu et al. 2005). (4) The Qiongkuer-Abagong terrane consists of upper Silurian to lower Devonian arc andesitic volcanic and volcanic clastic rocks with lesser basaltic rocks with a Rb-Sr isochron ages ranging from 307 to 285 Ma. These rocks are overlain by the Altay Formation which consists of a turbiditic sandstone-shale succession, associated with basaltic pillow lavas. (5) The Erqis terrane is wedged in between terrane 4 and the Irtysh fault (see below). This terrane consists of a high-grade metamorphic Precambrian basement (gneiss and schist) with Pb model ages ranging from 1,849 and 1,791 Ma. This basement is overlain by Devonian and Carboniferous fossiliferous sedimentary rocks, intruded by post-orogenic granites. Chai et al. 2009) suggested the presence of northwest-trending Early Devonian (ca. 412 Ma) fault-bound volcano-sedimentary basins, aligned along the Abagong and Irtysh fault zones, but ill-defined due to subsequent and multiphase strike-slip deformation. One of these is the Kelang Basin. containing felsic, mafic and clastic sedimentary rocks (Kangbutiehao Formation) metamorphosed to greenschist and amphibolite facies and associated with mineral deposits, such as Abagong Fe-P, discussed below. The Kangbutiehao Formation, according to Chai et al. (2009), was formed in an active continental margin, developed in the Mid-Late Palaeozoic in the southern Altay orogenic belt. The felsic metavolcanic units of the Kangbutiehao Formation are temporally associated with deformed syn-orogenic granites in the southern Altay, such as the Mengku pluton (Yang et al. 2010; Fig. 6.9). Yang et al. (2011) examined the U-Pb ages and Hf isotopic composition of a section of the Altay orogen, consisting of Middle to Upper Cambrian turbiditic (flysch) rocks intercalated with bimodal volcanics and Devonian arc volcanics (termed by the authors Altai-Qinghe tectonic slice and Fuyun tectonic slice), which could be part of the Kangbutiehao Formation. On the basis of the isotopic data and REE geochemistry, Yang et al. (2011) proposed that the Cambrian rocks may represent a rifted margin of Gondwana and a seaway of the Palaeo-Asian ocean, whereas the Devonian arc volcanics would have formed in an Andean-type margin by north-directed subduction. A somewhat similar conclusion (north-directed subduction system) was reached by Long et al. (2011), who studied Nd isotopic composition of these turbiditic succession.

An important structural element of the Altay orogen is the Irtysh (also spelt Erqis or Yrtys) transcurrent fault zone (Fig. 6.2), which extends for more than 1,000 km into Mongolia and Kazakhstan and can reach widths of up to 50 km. Both sinistral and dextral strike slip movements occurred along the Irtysh fault zone. South of the Irtysh fault is a Devonian-Carboniferous terrane that is interpreted as an island arc (felsic-intermediate volcanic rocks and calc-alkaline plutons) that is accreted onto the eastern margin of the Junggar Basin (Windley et al. 2002).

A critical phase of the geodynamic evolution of the Altay orogen took place at the Permian-Triassic transition, when oblique collision occurred between the Tarim block and the Altay collage and the North China craton (Yakubchuk et al. 2005).

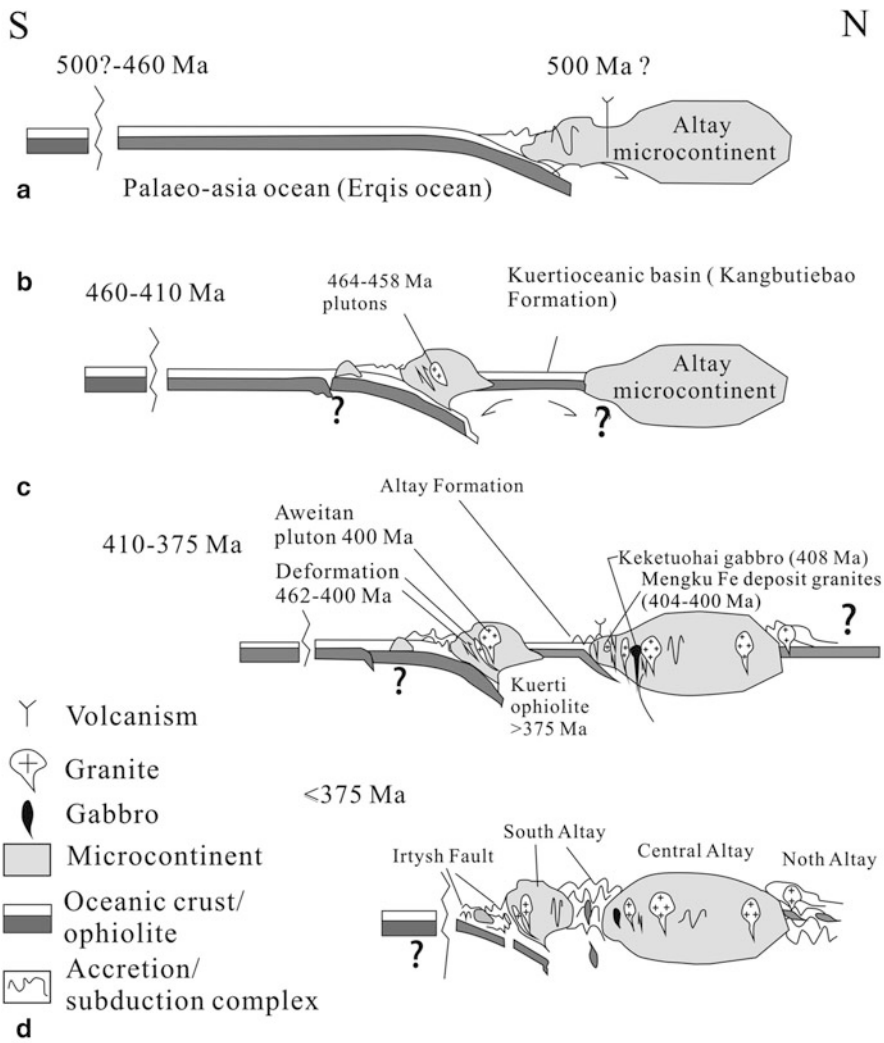

Fig. 6.9 Model for the geodynamic evolution of the Altay Orogen, between Late Cambrian and Late Devonian, and the formation of mineral systems. (After Wang et al. 2006a; Yang et al. 2010)

The zoned mafic-ultramafic plutons of the Kalatongke belt (Fig. 6.5), locally hosting magmatic Ni-Cu ores (see below), are temporally and spatially associated with Permian A-type granites and were emplaced along a zone within the Irtyish Fault. The Kalatongke mafic rocks have been dated using the Rb-Sr method (285 and 298 Ma), and by Sm-Nd isochron (298 Ma with ε_{Nd} (T) = +6.0; Han et al. 1997 and references therein). Han et al. (1997) pointed out that the Ulungur A-type granites and the mafic rocks in the region, considered to be ophiolites, have a similar range of ε_{Nd}

(T) values and therefore these granites and the mafic rocks may both originate from the same long-lived depleted upper mantle source. These authors go on to state that these A-type granites, and by inference the associated mafic rocks, are anorogenic, mantle-derived and emplaced in rift settings.

Based on zircon U–Pb SHRIMP ages and geochemistry of the granites from the Mengku Fe deposit and the work of Wang et al. (2006a) and Yang et al. 2010, a model of the geodynamic evolution of the Altay orogen is shown in Fig. 6.9. During the Early–Middle Ordovician (500–460 Ma), the Palaeo-Asia ocean was subducted northward beneath the original Altay microcontinent, forming arc volcanic rocks (Fig. 6.9a; Windley et al. 2002). Between 460 and 410 Ma, a continental arc was developed in which the Qiemuerqieke granitic pluton (462 Ma), Abagong–Tiemiert (Tiemurt) granites, Kuerti granite (416 Ma) and Chonghuer granite (413 Ma) were emplaced (Fig. 6.9b). Subduction of the Palaeo-Asian oceanic plate at 413 Ma, resulted in a series of continental-margin fault basins on the southern margin of the Altay microcontinent, including the Maizi, Kelan and Chonghuer basins, and Kuerti backarc basin. During the period 413–400 Ma (Late Silurian–Early Devonian), a bimodal succession of rhyolite–basalt volcanic rocks and sedimentary rock of the Kangbutiebao Formation formed in a back-arc extensional setting, resulting in a series of volcano-sedimentary rift basins. It is suggested that at this time, the VMS and Fe deposits were developed in the basins, as exemplified by Ashele and Keketale Pb–Zn deposits and Abagong Fe–P deposit (Sect. 6.3.4 and 6.3.5). At ca. 400 Ma, magmatism and orogeny culminated, as exemplified by the Mengku granite (400 Ma) and the Qiongkuer granite (399 Ma) in the Mengku Fe deposit area (Sect. 6.3.4) intruded into the Kangbutiebao Formation (Fig. 6.9c). Related to the intrusion of these granitic plutons, skarn mineral systems formed near and along the contacts of the plutons, apophysis and dykes with the Kangbutiebao Formation volcanic rocks and limestone. Deformation of these plutons and the associated Fe-skarns also took place during this time. At ca. 375 Ma, a small number of granites (e.g. the Wuliqi granites, Jianggusitale granite) were formed by crustal melting in the late stage of syncollisional setting (Fig. 6.9d). Subsequently, all the tectonic units were accreted on the Altay microcontinent.

6.2.3 West- and East Junggar Fold Belts

The West and East Junggar fold belts (also referred to as terranes; Fig. 6.11) border the northwestern and northeastern margins of the Junggar Basin, respectively and both are characterised by dismembered Palaeozoic ophiolites and post-collisional granitic intrusions (Chen and Jahn 2004; Xiao et al. 2008b; Figs. 6.1 and 6.5). Both fold belts are interpreted as having formed by the accretion of island arcs and intervening seaways (ophiolites), between the Cambrian and the Carboniferous. The West Junggar terranes, such as Tangbale, Kekesayi, Ebinur, Laba, Karamay and Malyia (Cambrian-Silurian) are all intra-oceanic and were docked in a series of subduction systems (Buckman and Aitchison 2004). The Sartuohai terrane is largely ophiolitic and was

emplaced as a mélange in the late Carboniferous. Post-collision events included the intrusion in the Permian of A-type granites and mafic dykes, clearly indicative of widespread extension and mantle upwelling (Jahn 2004; Buckman and Aitchison 2004), as corroborated by the Sm/Nd isotopic system ($\varepsilon Nd_{(T)}$ values ranging from ca. +5.2 to +7.1; Chen and Jahn 2004). Indeed, and as pointed out by Buckman and Aitchison (2004), the Permian extension and intraplate magmatic activity affected the whole of central Asia (Pirajno et al. 2009). This event is of considerable importance for metallogeny, particularly for magmatic ore systems (Sect. 6.3.6). Granites in the West Junggar include coarse-grained alkali-feldspar granite, associated with diorite and monzodiorite stocks and northeast-trending dioritic dykes. West and north of Karamay, anorogenic alkali-feldspar granite plutons, with isotopic ages ranging from 321 to 280 Ma (Zhao 1992) intrude rocks of the ophiolitic mélange zone. A K-Ar age of 279 Ma and a U-Pb zircon age of 305 Ma are reported for two alkali feldspar granite plutons near the Saourtuhai Cr deposit (BGMRX 1993).

In the West Junggar, the Dalabute (Talabute) Fault is a major sinistral northeasterly to easterly trending fault zone. Associated with the Dalabute Fault is a mélange zone, the Tangbale Ophiolite Melange, containing mafic-ultramafic, sedimentary and volcanic rocks. All rocks in this region are extensively tectonised, but with no dominant tectonite fabric. Rocks of the Tangable Melange comprise radiolarian chert, pillow lava, gabbro, serpentinite, harzburgite and lherzolite. These rocks are thought to represent Early Palaeozoic oceanic crust formed in a back arc basin setting (Zhao 1992). Radiometric dating of leucogabbro (U-Pb), olivine cumulates and basalts (Sm-Nd), gives ages of 523, 489 and 447 Ma, with a collision age based on Ar-Ar dating of amphibolite of 356 Ma (Zhao 1992). In the Saourtuhai Cr mining area (see Sect. 6.3.6), the Dalabute fault separates a sedimentary package from an ophiolitic mélange containing a chaotic assemblage of blocks of diverse size (cm to tens of m) and rock types including serpentinite, chert and volcanics.

The eastern end of the West Junggar, known as Sawuer region, is characterised by volcanic caldera complexes that host epithermal systems (Shen et al. 2007, 2008). Late-Palaeozoic volcanic rocks of the Sawuer region include the Middle Devonian Sawurshan Formation and the Lower Carboniferous Heishantou Formation (Shen et al. 2008). The Sawurshan Formation consists of intermediate-felsic volcanic rocks (rhyolites, dacites and andesites), volcaniclastic rocks and basaltic lavas. The Heishantou Formation was erupted in the Early Carboniferous and consists of a succession of mafic volcanic rocks and volcaniclastics with intercalations of siltstone and limestone. Rb/Sr isochron ages of ca. 343 Ma for andesites in the Kuoerzhenkuola area, where the Eastern Sawuer caldera complex is located and hosts epithermal systems (I return to discuss this caldera and Kuoerzhenkuola epithermal deposits in Sect. 6.3.2).

The East Junggar terranes comprise a number of accretionary and subduction complexes, and at least two important ophiolite belts. Xiao et al. (2008b) list the following tectonic units for the East Junggar, from north to south: Dulate-Baytag arc, Yamaquan arc and the Armantai and Kalamaili ophiolitic belts. The Dulate-Baytag arc consists of boninite, pillowed basalt, adakite, andesitic basalt, chert and gabbroic rocks, variably imbricated with radioalarian chert, turbidites and Devonian-

Carboniferous Yamaquan arc volcanic. These arc systems are, according to Xiao et al. (2008) of mature (Andean?) settings, based on the presence of andesite and porphyry Cu deposits. The Armantai ophiolite belt trends northwest and contains peridotite, pyroxenite, gabbro, troctolite, dolerite, basalt, serpentinite and chert structurally interlayered with Devonian-Carboniferous sedimentary rocks. The Karamay (also spelled Karamai, Kalamaili) ophiolite trends west-northwest and is distributed along the fault of the same name, and contains the same rocks as the Armentai ophiolite. This ophiolite is thought to be similar to the classic Cyprus Troodos Igneous Complex and as such of a supra-subduction zone origin in a fore-arc setting (Xiao et al. 2008b). As for the Armantai ophiolite, the Kalamaili rocks are also structurally interlayered with Devonian-Carboniferous volcanic and pyroclastic rocks.

Finally, in the East Junggar and southeast of the Armantai ophiolite, are volcanic rocks of Permian age have been interpreted as being part of an island arc, but I doubt this interpretation because evidence shows that magmatism in the Permian, throughout most of Central Asia, is intraplate and related to upwelling mantle (see Pirajno et al. 2009 and references therein). The interpretation of Permian volcanic rocks being of subduction-related setting is based in geochemical data that includes early Carboniferous andesite to late-Permian basalt from imbricated areas of the East Junggar fold belt (Zhao et al. 2006c, d). Zhou et al. (2008) in their study of granitic magmatism (Sawuer Granites) in the West Junggar, where they recognised 337–302 Ma I-type and 297–290 Ma A-type granites, suggested that they were emplaced during compressional (I-type) and extensional (A-type) settings. Geng et al. (2009) and Tang et al. (2010), on the other hand, classified the West Junggar granites as diorite, charnockite and alkali-feldspar, or granodiorite-diorite and considered their origin as being the result of upwelling asthenospheric mantle through a break in a ridge subduction setting (slab window model). Zhou et al. (2008) proposed a more practical model of geodynamic evolution for the Tianshan and Junggar terranes, shown in Fig. 6.10, and explained below.

In the pre-collisional period (Fig. 6.10a), the Tarim plate moved northward and a subduction zone from the Palaeo-Asian Ocean formed the Dananhu-Tousuqan volcanic arc, against the Junggar plate. This was followed by back-arc rifting, which evolved to form the Bogda rift (Fig. 6.10b). At the same time, southward subduction beneath the Tarim began and the Aqishan-Yamansu volcanic arc was established. Collision between the Tarim and Junggar plates began in the Carboniferous (Fig. 6.10b), which consumed the Palaeo-Asian Ocean, resulting in the development of the Kanggur shear zone. Collision between the Siberian and Junggar plates occurred with the West Junggar ophiolite belts marking the resulting suture zones. The post-collisional period (Fig. 6.10c) began in the Lower Carboniferous, transitional to extension, resulted in the emplacement of I-type granites in the West Junggar, probably due to asthenospheric mantle upwelling. Finally, in the Early Permian, an extensional regime associated with lithospheric thinning and rifting occurred. Melting of the crust by heat from the upwelling of asthenospheric mantle, produced the alkaline A-type granites and eruption of bimodal volcanic rocks.

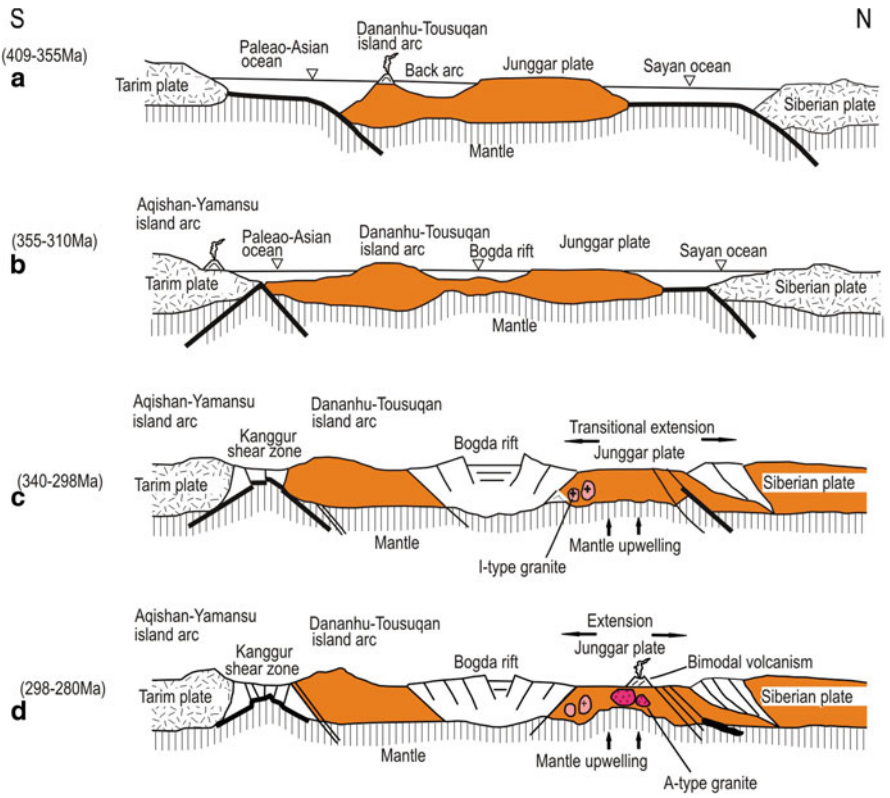

Fig. 6.10 Geodynamic evolution of the Tianshan-Junggar terranes, based on a study of granitic magmatism (Sawuer Granites) in the West Jungga, from pre-collisional and collisional (**a** and **b**) to post-collisional and extension (**c** and **d**). (After Zhao et al. 2008a)

6.3 Mineral Systems of Tianshan, and Altay Orogens and Yili Block in NW China

Economically significant mineral systems in Xinjiang include: epithermal, porphyry and skarns, volcanogenic massive sulphides (VMS), lode style Au deposits, orthomagmatic Ni-Cu-PGE, rare metals in pegmatites and sandstone-hosted U deposits. West of the Chinese border, the Tianshan range is well endowed with giant lode gold deposits and low-sulphidation epithermal gold deposits in a convergent margin magmatic arc setting. These well known gold deposits include Kochbulak, Muruntau, Zarmitan, Kokpatas (Seltmann and Porter 2005), Taldybulak Levoberezhnyi and Kumtor (Seltmann and Jenchuraeva 2001).

There is abundant literature on selected mineral deposits of Xinjiang, both in Chinese and English. Zhao et al. (2006) published a monograph on mineral deposits

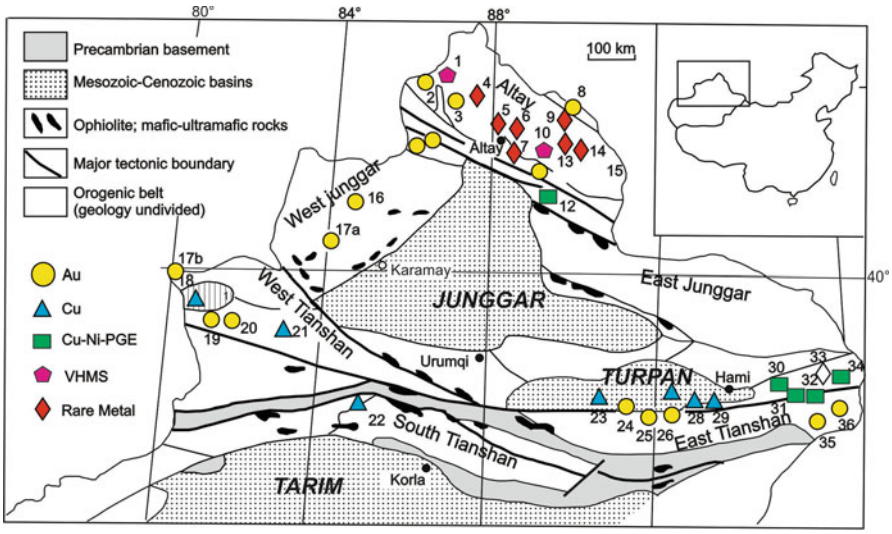

Fig. 6.11 Distribution (approximate positions) of selected mineral deposits in northern Xinjiang (modified after Mao et al. 2003; Qin et al. 2003; Zhang et al. 2011); *1* Ashele Cu-Zn, *2* Duolonasayi Au, *3* Saisu Au, rare metals deposits in pegmatites at *4*, *5*, *6*, *7*, *8*, *9*, *13*, *14*, *15* and *33*, *10* Keketale Cu-Zn, *11* Saebulake Au, *12* Kalatongke Cu-Ni-PGE, *16* Hatu Au, *17a* Sartuhoi Au, *17b* Sawayaerdun, *18* Lamasu Cu, *19* Jinxi-Yelmand (also called Yiermand), *20* Axi Au, *21* Lailisigao'er Cu-Mo and Kendenggaor Cu, *22* Shengli Cu, *23* Xiaorequanzi Cu, *24* Xitan (Shiyingtan) Au, *25* Kanggur Au, *26* Matoutan Au, *27* Kalatage Au, *28* Yandong Cu, *29* Tuwu Cu, *30* Xiangshan Cu-Ni, *31* Huangshan Cu-Ni, *32* Huangshandong Cu-Ni, *34* Hulu Cu-Ni, *35* Jinwozi (Jinouzhi), *36* Mazhuangshan Au; the distribution of the Altay orogenic belt skarn deposits are shown in Fig. 6.27

related to alkaline rocks in Xinjiang. A book on the mineral resources of Xinjiang province is by Zhang et al. (1990; all in Chinese). Important publications in English include Rui et al. (2002) and the collection of papers in Mao et al. (2003). The mineral systems of Xinjiang commonly constitute well defined metallogenic belts, such as the Kanggurtag or East Tianshan belt that extends in an east-west direction for about 600 km, is 100 km wide, and contains epithermal Au, porphyry Cu deposits, lode Au and Cu-Ni-PGE magmatic deposits (Mao et al. 2005); the Altayshan metallogenic belt with rare metal pegmatites, intrusion-related and lode Au, VMS, skarns and magmatic deposits (Goldfarb et al. 2003); the West Junggar (including the Hatu-Saertuohai Au belt) belt with its orogenic Au deposits (Wang et al. 2004) and the East Junggar lode style and epithermal Au deposits (Rui et al. 2002). In the sections ahead, a selection of mineral systems according to type: porphyry, epithermal, skarns, lode style Au, VMS, magmatic and sandstone-hosted roll-type U are described. An overview of the distribution of mineral deposits in the Xinjiang region is given in Fig. 6.11.

6.3.1 Porphyry Systems

A number of porphyry systems are present in the Junggar terranes, the eastern Tianshan (Kanggur belt and Yamansu-Dananhu arcs) and the western Tianshan. In the Junggar terranes is the Baogutu porphyry Cu belt, about 30–50 km west of the town of Kelamayi (Shen et al. 2009, 2010a, b, 2012), those in the eastern Tianshan include the Yandong, Linglong, Chihu and Tuwu porphyry systems (Fig. 6.11; Han et al. 2006a, b; see also Fig. 6.26). Of these the Tuwu porphyry deposit is perhaps the best known in the literature (Seltmann and Porter 2005). In the western Tianshan, porphyry Cu, Cu-Mo and Cu-Zn deposits occur in the late Palaeozoic Korkinqin island arc (Zhang et al. 2010c). A review of porphyry deposits in the Junggar was recently published in Yang et al. (2012a), who identified four metallogenic belts as follows: (1) Late Silurian-Early Devonian Cu-Mo deposits in the Qiongheba district; (2) Late Devonian Cu deposits in Kalaxiane'er belt; (3) Early Carboniferous porphyry-skarn Cu-Mo in the Xilekuduke-Suoekuduke belt; (4) Late Carboniferous Baogutu porphyry Cu-Mo.

In the following I describe the Tuwu, Baogutu porphyry Cu systems and the porphyry deposits of the western Tianshan.

6.3.1.1 Tuwu

The Tuwu porphyry is hosted in Carboniferous rocks of the Qi'eshan Group of the Dananhu-Tousuquan arc, which mainly contains basaltic, andesitic and rhyolitic lavas and clastic sedimentary rocks. A total resource of 2.04 Mt of Cu metal was estimated for this deposit, discovered in 1997 and briefly exploited between 1998 and 2002, with a new mining operation beginning in 2003. The ore-hosting granitic porphyry and diorite porphyry were emplaced into the volcano-sedimentary succession and at least 23 stocks and plugs have been identified in the area. Re-Os dating of molybdenite yielded an age of 323 Ma (Rui et al. 2002), whereas U-Pb ages of the granitic porphyry range from 333 to 334 Ma (Han et al. 2006a). The granitic porphyry is characterised by strongly fractionated chondrite-normalised REE patterns (ΣREE from 45 to 75 ppm), with LREE enrichment and HREE depletion, with slight positive Eu anomalies. MORB-normalised trace element patterns show depletions in Nb and Y. These patterns have been interpreted as being similar to those of subduction-related calc-alkaline magmatic arcs.

The Tuwu deposit contains two ore zones; Tuwu and Eastern Tuwu. The former is elongated in the east-west direction and wedge shaped in cross-section is and using a 0.50 % Cu cutoff grade it has a length of 900 m and an average width of 25 m. The Eastern Tuwu ore zone is about 1,300 m long, with widths varying from 30 to 85 m. The style of the mineralisation includes disseminations and stockworks. Ore minerals are dominantly chalcopyrite and pyrite with lesser bornite, digenite, sphalerite, magnetite, hematite and rickardite (Cu_4Te_3). The ores have large amounts of hematite and magnetite. The ore zones are hosted in lithic sandstone and conglomeratic tuffs in contact with the granite porphyry. From the core outwards alteration zones are:

quartz, chlorite-biotite, phyllic, argillic and propylitic. The chlorite-biotite zone occurs as pods and veins and is associated with pyrite and chalcopyrite; the biotite is Mg-rich. The phyllic zone is mainly represented by the quartz-sericite assemblage and is associated with the bulk of the sulphide mineralisation. The propylitic zone is widespread and composed of chlorite, epidote and albite.

Six stages of alteration-mineralisation have been recognised, as follows: (1) Mg-rich biotite is accompanied by albite and K-feldspar (alkali metasomatism) with the sulphide assemblage of chalcopyrite-pyrite-bornite; (2) phyllic alteration (quartz-sericite, epidote-chlorite) and veins of chalcopyrite-pyrite-bornite; (3) quartz-molybdenite veins as well as chalcopyrite-pyrite-bornite; (4) gypsum and anhydrite and calcite-laumontite follow, with lesser sulphide veinlets; (5) continuing calcite-laumontite alteration with sulphide precipitation waning; (6) supergene alteration with malachite and limonite mainly.

Fluid inclusion data (Han et al. 2006a) show homogenisation temperatures (Th) ranging from 101 to 409 °C, with peaks at 125, 175 and 225 °C, salinities range from 0.35 to 16.4 wt % NaCl equivalent, with a peak at 7.5 wt % equivalent. However, Han et al. (2006a) did not specify the type of fluid inclusions and they may be pseudosecondary and as such not representative of primary porphyry-related fluids. Oxygen and deuterium isotopic compositions show $\delta^{18}O$ values ranging from 7.70 to 9.70 ‰ in quartz and chlorite. The $\delta^{18}O_{H_2O}$ values for the fluid are between −5.37 and 6.62 ‰, using quartz-water and chlorite-water fractionation equations. δD values of quartz and chlorite range from −45 to −63 ‰. Sulphur isotopic compositions measured on chalcopyrite and pyrite have, a narrow range from −0.9–1.3 ‰, suggesting magmatic and mantle sources for the sulphur. The ore-bearing porphyry rocks have initial $^{87}Sr/^{86}Sr$ ratios in the range of 0.7039–0.7067. The above isotopic data suggest that ore material was derived from the upper mantle.

Han et al. (2006a, b) interpreted the formation of the Tuwu, and other porphyry systems in the region, as being related to one of the calc-alkaline island arcs that developed between the Junggar and the Tarim plates. The Dananhu-Tousuquan island arc was formed by north-dipping subduction with some characteristics of adakites (high-Mg andesites), which are melts were derived from a subducted slab. Han et al. (2006a, b) suggested slab roll back and break off with multiple new pulses of granitic magmatism, due to asthenospheric upwelling, promoting partial melting of crustal material, resulting in the intrusion of granitic plutons, one of which produced the Tuwu porphyry system.

6.3.1.2 Baogutu Porphyry Cu-Mo-Au Deposit

In the western Junggar a belt of porphyry systems, west of the town of Karamay, has been identified and named Baogutu porphyry copper belt, in which the mineralisation is hosted in dioritic rocks. In the Baogutu deposit in situ metal resources of 111 tonnes at 0.28 % Cu, >0.01 % Mo and 0.25 ppm Au have been reported (Shen et al. 2009 and references therein). The following is summarised from the work of Shen et al. (2009, 2010a, b, 2012).

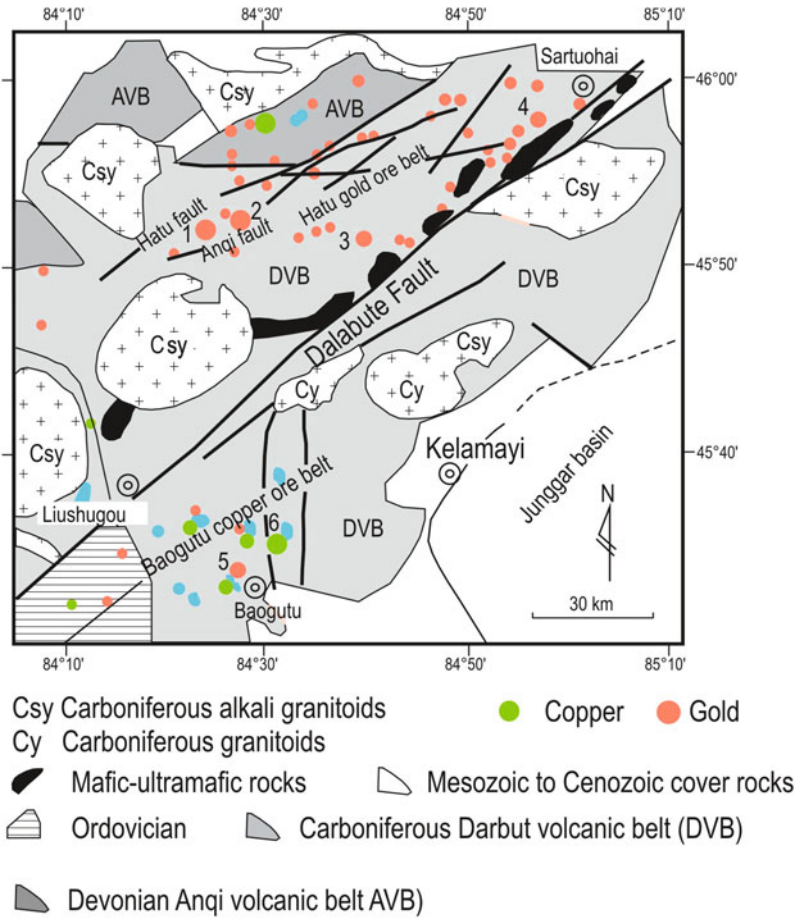

Fig. 6.12 Schematic geology of the area around the Dalabute Fault (also called Darbut), western Junggar, showing distribution of porphyry systems (Baogutu Cu-Mo) and lode gold deposits (*1* Hatu, *2* Qiqiu, *3* Baobei, *4* Sartuohai, *5* Baogutu). (After Shen et al. 2009)

More than 20 stocks (numbered with Roman numerals I to XX in Fig. 3 of Shen et al. 2009) of dioritic composition occur in the porphyry copper belt (Fig. 6.12). The dioritic stocks intruded Devonian to Carboniferous volcanic rocks at about 322 Ma and are included into a poorly exposed Baogutu intrusive complex, variably described in previous works due to extensive hydrothermal alteration, which tends to mask the original composition of the rocks. The mineralisation seems confined to stocks I, II, III, IV, V and VIII, which together define the Baogutu mineral belt (Fig. 6.12). Shen et al. (2010a) recognised two intrusive phases: (1) equigranular porphyritic diorite and quartz-diorite; (2) diorite porphyry. Hydrothermal breccias are also recognised. The alteration and mineralisation are associated with the main phase diorites and the hydrothermal breccias. The main stage intrusive phase is characterised by an

inner equigranular diorite, which forms the centre of the complex located 500 m below the surface and is overlain and/or flanked by porphyritic diorite and quartz-diorite (Fig. 6.12a). Zircons from this stage, dated using the U-Pb method, yielded a weighted mean age of 325.1 ± 4.2 Ma. The diorite porphyries of the second phase occur at the margins of the main phase intrusions. Breccia bodies, referred to by Shen et al. (2010a, b) as hydrothermally cemented breccias and matrix-rich breccias, form bodies or zones with thickness and widths of about 300–400 m, overprint both equigranular diorite and porphyritic diorite (phase 1). These breccias, containing angular, rounded to subrounded clasts, as well as silt-size matrix, have gradational contacts with the host intrusives. The hydrothermal breccias are confined to zones of potassic alteration that are not overprinted by later phyllic alteration, whereas the opposite is observed for the matrix-rich breccias. It is possible that these breccias are the result of multiphase of volatile exsolution and fluidisation processes that occurred in the magmatic stage (potassic alteration, hydrothermal breccia) and later during influx of H_2O-rich fluids (phyllic alteration, matrix breccias). The mineralisation consists of two zones: Cu-Au and Mo. The first occupies the main part of the intrusive complex and extends into the adjacent country rocks, whereas the second occurs at depth within the complex and its outer contacts. Molybdenite from the Mo ores was dated by the Re-Os method, yielding ages of about 310 Ma (Song et al. 2007) and more recently by Shen et al. (2012), who obtained a weighted mean age of 312.4 ± 1.8 Ma (Fig. 6.13).

A paragenetic sequence of alteration and mineralisation can be summarised as follows (Fig. 6.13b). Stage 1 began with the emplacement of the equigranular diorite with local actinolite-magnetite-albite alteration (substage 1A), followed by substage 1B pervasive potassic and phyllic alteration, comprising pervasive biotite-quartz-magnetite-rutile-chlorite alteration accompanied by disseminated chalcopyrite, pyrite, pyrrhotite and chalcopyrite-pyrite veinlets in the dioritic rocks. Substage 1B alteration-mineralisation in the dioritic rocks is associated with the formation of the hydrothermal breccias and constitutes the main phase of Cu mineralisation with the highest grades (>0.4 %). Potassic and propylitic alteration of substage 1B extend into the wall rocks. Substage 1C comprises pervasive sericite-quartz-pyrite-chlorite-calcite alteration with minor quartz-molybdenite-chalcopyrite-pyrite veins and quartz-pyrite-chalcopyrite veins. This alteration extends to the wall rocks, but is not pervasive and is only accompanied by weak Cu mineralisation. Ore grades of substage 1C range from 0.2 to 0.4 % Cu and up to 0.002 % Mo. Stage 2 (not shown in Fig. 6.13b) began with the emplacement of the porphyritic diorite, accompanied by selectively pervasive biotite-quartz-magnetite-chlorite alteration and weak Cu mineralisation (substage 2A). Substage 2B is associated with the formation of the matrix-rich breccias and consists of minor but pervasive gypsum and biotite-quartz alteration in both intrusives and adjacent wall rocks.

Microthermometric measurements revealed five types of fluid inclusions (Shen et al. 2010b): (1) two-phase liquid-rich (L1); (2) two-phase liquid-vapour (L2); (3) two-phase vapour-rich (V1); (4) monophase vapour (V2); and (5) multiphase solid (halite). Methane, CO_2 and H_2O were detected in most inclusions and the oxidisation of the CH_4 to CO_2, interpreted to represent the transition from stage

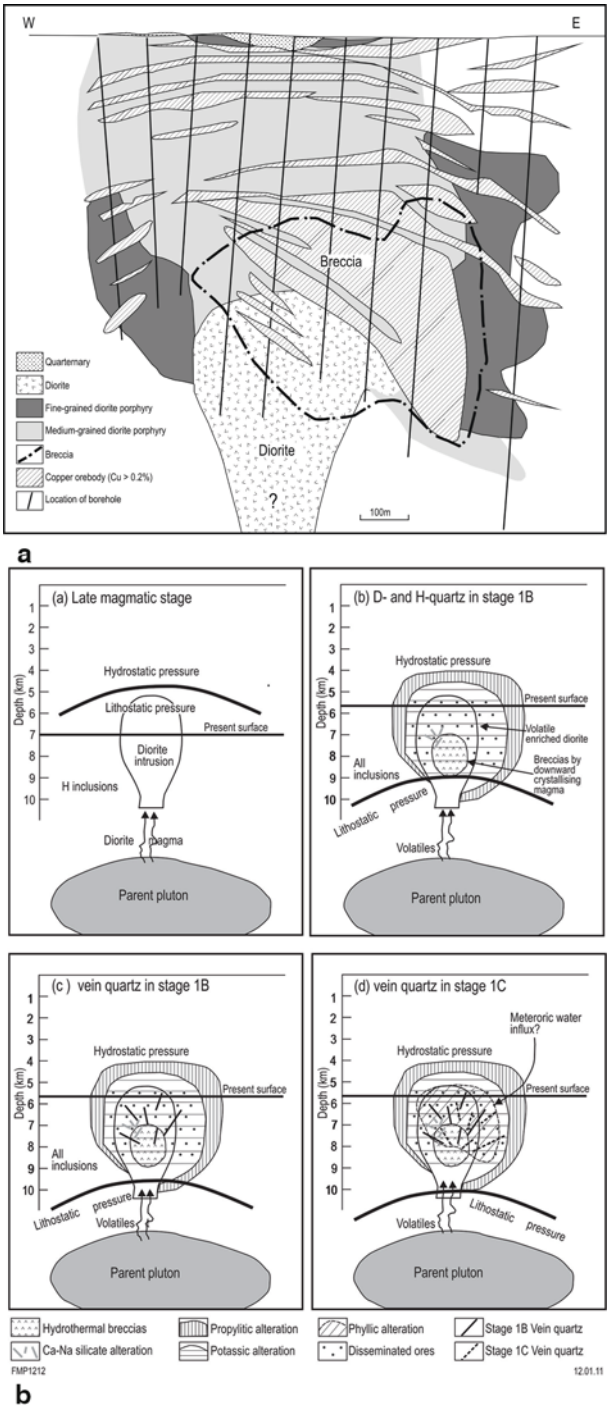

Fig. 6.13 **a** Schematic cross-section of the Baogutu Cu-Mo-Au porphyry deposit; **b** alteration-mineralisation stages (1A to 1C; see text for details), shown on idealised cross-sections; both **a** and **b**. (After Shen et al. 2010a, b)

1B (potassic alteration) to stage 1C (phyllic alteration). Fluid inclusions in vein quartz from hydrothermal stage 1B have homogenisation temperatures (Th) ranging from 180 to 420 °C, with a bimodal distribution of 180–260 °C and 260–420 °C. This bimodality is interpreted by Shen et al. (2010b) to indicate that the ore-forming fluids at Baogutu may have derived from two different sources, namely: magmatic with an influx of an external low-salinity fluid. Fluid inclusions in quartz from stage 1C, have Th of between 170 and 270 °C for L1 type inclusions; L2 inclusion homogenise between 170 and 390 °C; whereas V1 inclusions have the highest apparent Th (180–460 °C), concentrating between 250 and 390 °C.

Shen et al. (2010a) concluded that the Baogutu intrusions were derived from multiple sources, such as oceanic crust and subduction modified mantle wedge, during convergence between the Junggar plate and the Darbut (or Dalabute) volcanic arc.

6.3.1.3 Porphyry Deposits of the Western Tianshan

The work of Zhang et al. (2010c) is used in this section to provide an overview of porphyry systems in the Chinese western Tianshan, more specifically in the Lailisigao'er-Lamasu region (Nos. 21a and 18, respectively in Fig. 6.11). Although referred to as Chinese western Tianshan, this region is in the northwestern part of the Central Tianshan (see Fig. 6.4). Other porphyry style deposits in the same region listed by these authors are: Mosizaote Cu, Dabate Cu, Dongtujing Cu, Kenderggao Cu (No. 21b in Fig. 6.11), 3571Cu, Tawuerbieke, Kesibukale, 109 and Qunji (no metal endowment provided). The porphyry systems of the Lailisigao'er-Lamasu region are part of a Late Palaeozoic Andean-style magmatic arc, called by Zhang et al. (2010c) Bigiintaw-Kokirqin. The general area comprises microcontinental fragments of Precambrian age and Palaeozoic magmatic arc rocks, amalgamated during the collision of the Kazakhstan and Tarim plates (see Fig. 6.8). Lower to Middle Palaeozoic rocks in the region consist of chert and carbonates, flysch units, intercalated with calc-alkaline volcanic rocks, intruded by Late Palaeozoic granites. Rocks of Devonian age comprise conglomerate, sandstone, siltstone, shale and limestone. Granites of Carbonifeorus age intrude the basement and overlying rocks and are considered by the authors as the most important igneous events responsible for the Cu-Mo porphryry systems in the Chinese western Tianshan (again refer to Fig. 6.8). These porphyry systems are poorly known in Western literature, with only few studies, apart from Zhang and co-authors, reported in Chinese publications.

In the Lailisigao'er-Lamasu region, more than 10 porphyry stocks have been recognised, with outcrop areas of about 0.1 km^2 or less and about half of these stocks are mineralised, with total resources of 4,600 tonnes of combined Mo + Cu metal, with grades ranging from 0.062 to 0.32 % Mo and 0.1–0.2 % Cu (Wan et al. 2008, cited by Zhang et al. 2010c). The ore zones are characterised by disseminated sulphides in the exocontact of the porphyry stocks and in breccias, Ore minerals are molybdenite, chalcopyrite, pyrite, bornite, sphalerite, scheelite and pyrrhotite.

Hydrothermal alteration minerals typically include K-feldspar, albite, quartz, carbonate, chlorite, sericite and epidote. Alteration is reported as being pervasive in the porphyry stocks and with distinct zonation from potassic in the central parts of the stock, with silicification, sericitic and propylitic alteration outward. One of the porphyry deposit is Lamasu (No. 18 in Fig. 6.11), which is related to a stock with an area of 0.60 km^2, contains Cu and Zn and is best defined as a combined porphyry-skarn system. The Lamasu stock (or stocks, not clear from Zhang et al. 2010c), are apophyses and veins (again, not quite clear what the authors refer to a stock or stocks) that intrude carbonate rocks of the Mesoproterozoic Kuximuqieke Group. Along the contacts with the stock(s), the carbonates are altered to calc-silicate skarns. The Lamasu Cu-Zn deposit contains more than 1 Mt Cu + Zn, grading 0.3–3.7 % Cu and 0.6–0.7 % Zn. The porphyry stock(s) hosts 25 % of the ore and the skarns about 75 %. Given the poor knowledge on these deposits in the region, there is controversy as to their genesis. For example, Zhang et al. (2010c) quoting various sources, mentioned the following: hydrothermal (unspecified), skarn and porphyry-skarn. The porphyry-skarn type would apply to the Lamasu Cu-Zn deposit, whereas the Lailisigao'er and the 3571 Cu deposits conform to the porphyry type. The Lamasu deposit is related to tonalitic and granodioritic intrusions, in addition to porphyry style potassic, propylitic and phyllic alteration has also skarn-type alteration and contains chalcopyrite, sphalerite, pyrite, pyrrhotite, galena and molybdenite as ore minerals. The age of the granitic rocks, determined by LA-ICPMS U-Pb, is 390.5 ± 7 Ma, whereas εNd(t) values range from −0.3 to −0.2 and I_{Sr} from 0.70722 to 0.70757 (Zhang et al. 2010c). The Lailisigao'er and 3571 deposits are hosted by granodiorite and monzogranite stocks, with pyrite, chalcopyrite and molybdenite as the main ore minerals. The age of the Lailisigao'er granitic rocks, also determined by LA-ICPMS U-Pb, is 346.5 ± 1.2 Ma, εNd(t) values range from −2.9 to −0.6 and I_{Sr} from 0.70786 to 0.70941 (Zhang et al. 2010c). The LA-ICPMS U-Pb age of the 3571 granitic rocks, is 354 ± 0.68 Ma, εNd(t) values range from −3.7 to −2.3 and I_{Sr} from 0.708496 to 0.71028 (Zhang et al. 2010c). These authors presented good evidence of geochemical signatures of the ore-hosting porphyries, considered typical of calc-alkaline igneous suites of subduction-related arc magmatism. For example all of the above deposits have similar MORB-normalised patterns and fractionated REE patterns, are enriched in LILE and depleted in HSFE, relative to MORB, as well as negative Nb, Ta and Ti anomalies. Further confirmation of the significance of these geochemical signatures is found in the The/Yb vs Nb/Yb diagram, in which the Lailisigao'er and Lamasu samples all plot in the field of Andean-style continental magmatic arc (Fig. 10 in Zhang and co-authors' paper). Similarly the I_{Sr} values compare well with those of western North America continental arc granites (0.70722–0.71028).

According to Zhang et al. (2010c), the tectonic setting of the western Tianshan porphyry systems is one of a double-polarity subduction of oceanic crust beneath the Yili microcontinent, between the Junggar and Tarim during Late Devonian-Early Carbonifeorus (ca. 390–340 Ma), with magmas originated by partial melting of a subcontinental mantle lithosphere, enriched by the subduction plate fluids. At a later stage (Late Carboniferous-Permian; ca. 300–250 Ma), and following collision between the Junggar-Yili-Tarim, associated with transtensional settings along the

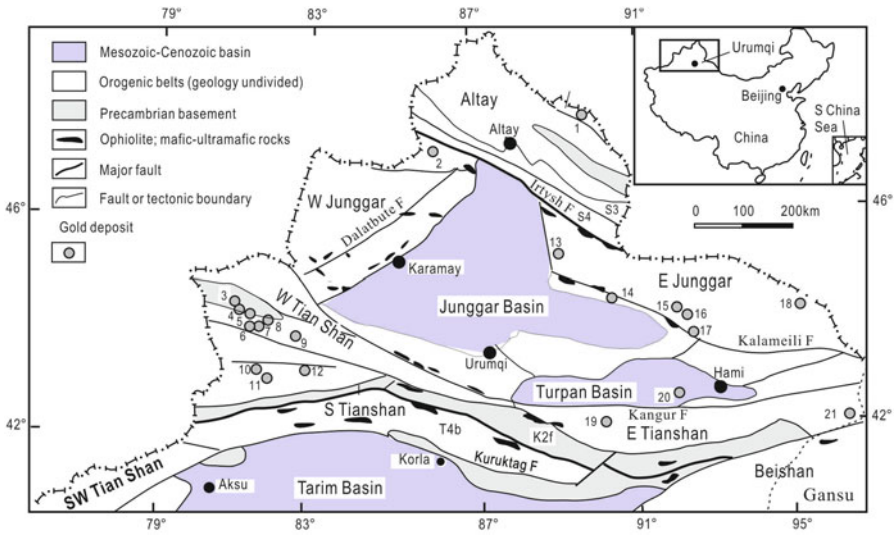

Fig. 6.14 Distribution (approximate positions) of epithermal systems in northern Xinjiang (after Chen et al. 2012b); *1* Aketishikan, *2* Kuorzhenkuola, *3* Jinxi-Yelmand, *4* Jingxibulake, *5* Axi, *6* Abiyindi, *7* Tawuerbieke, *8* Qabukanzuota, *9* Xiaoyuzan, *10* Tieliekesayi, *11* Kuruer, *12* Tuola, *13* Qingshui, *14* Jinshangou, *15* Peak 1583 or Shuangfengshan II, *16* Shuangfengshan, *17* Suorbasitao, *18* Beishan, *19* Shiyingtan (Xitan), *20* Hongshan (Kelatage), *21* Mazhuangshan

collision boundaries, with emplacement of granitic magmas along the suture and formation of Mo-Cu deposits of Permian age (Fig. 9 in Zhang et al. 2010c). Again, this is in stark contrast to the models of the Tianshan geodynamic evolution, shown in Figs. 6.7 and 6.8 (Xiao et al. 2004; Wang et al. 2011, respectively).

6.3.2 Epithermal Systems

A selection of epithermal Au deposits is described in the pages ahead, mostly based on data from Chen et al. (2012b) and Yang et al. (2009), as well as other authors as cited in the appropriate sections. The distribution of epithermal deposits in Xinjiang is shown in Fig. 6.14 (see also Figs. 6.11 and 6.26) and a list provided in Table 6.1

6.3.2.1 Kuoerzhenkuola

The Kuoerzhenkuola (also spelt Kurzhenkula) epithermal Au deposit (No. 2 in Fig. 6.14) is hosted and formed in Early Carboniferous in a pre-collisional volcanic arc setting. The Kurzhenkula deposit is located in the eastern Sawuer mountains and is a medium-sized Au deposit with proven resources of 11.7 t of gold at an average grade of 6.02 g/t (Shen et al. 2008).

Table 6.1 List of epithermal gold deposits in Northern Xinjiang, numbers correspond to those shown in Fig. 6.14 (from Chen et al. 2012b); note that grades in this table are approximate and/or averaged, for more accurate details refer to individual deposits, described in text and references cited

No.	Deposit/ County	Latitude/ Longitude	Grade (g/t)	Ore minerals	Gangue minerals	Major alteration minerals	Type	Lithology and age of host rock	Tectonic unit	Data source
01	Aketishikan/ Fuyun	47°05′07″/ 89°50′14″	1.1–3.9	Apy, Py, Po	Q, ser, adl, mm, agl, clc	si, py, ser, adl, agl, carb, pro, mm	LS	Early Carboniferous dacitic to rhyolitic tuff, lava and ignimbrite; Hongshanzui Fm	Nurte back-arc continental volcanic basin, Altay	Wang and Zhao 2006; Zhao et al. 2000
02	Kurzhenkuola/ Jimunai	47°05′38″/ 86°26′20″	5.1–11.2 (av 9.2)	Au, Py, Po, Cp	Q, kao, ser, chl, epi, mm, aln	si, py, ser, chl, mm, ill, aln, kao	HS	Early Carboniferous andesite and pyroclastic rocks, Heishantou Fm	Sawur island arc, W Junggar	Shen et al. 2007, 2008; Wang et al. 2005c
03	Jinxi-Yelmand/ Yining	44°19′57″/ 81°31′00″	1.0–3.0	Au, Py, Apy, Lm, Hem, Mr	Q, clc, ser, chl	si, clc, bar, kao, ser, chl, epi, fl, bio	HS?	Early Carboniferous felsic tuff; Dahalajunshan Fm	Tulasu intra-arc basin, W Tianshan	Feng and Wang 2005; Xiao et al. 2005a
04	Jingxibulake/ Yining	44°19′21″/ 81°31′39″	1.0–3.0	Au, Py, Apy, Jr, Le	Q, clc, ser, chl	si, *ser, clc*, chl	LS	Early Carboniferous felsic tuff, Dahalajunshan Fm	Tulasu intra-arc basin, W Tianshan	Xiao et al. 2002a, b
05	Axi/ Yining	44°13′45″/ 81°36′30″	2.0–13.8 (av 5.6)	Py, Apy, Cp, Mr, El, Au	Q, chd, adl, clc, ser, chl, ill	si, py, chl, adl, agl, carb, ill, ser	LS	Early Carboniferous intermediate-felsic volcanic-subvolcanic rocks, Dahalajunshan Fm	Tulasu intra-arc basin, W Tianshan	Hart et al. 2003; Zhai et al. 2009

Table 6.1 (continued)

No.	Deposit/ County	Latitude/ Longitude	Grade (g/t)	Ore minerals	Gangue minerals	Major alteration minerals	Type	Lithology and age of host rock	Tectonic unit	Data source
06	Abiyindi/ Yining	44°12′00″/ 81°36′00″	2.0–6.0	Py, Au, El, Lm	Q, chl, clc, dol, ser, mus, bar	si, ser, chl, carb, bar	LS	Early Carboniferous andesite, dacite, breccia and tuff, Dahalajunshan Fm	Tulasu intra-arc basin, W Tianshan	Jia et al. 2001a
07	Tawuerbieke/ Yining	44°12′10″/ 81°37′00″	3.0–10.0 (∼ 176)	Au, El, Py, Cp	Q, ser, chl, clc	si, ser, chl, mu, py, carb	LS?	Early Carboniferous volcanic rocks, Dahalajunshan Fm	Tulasu intra-arc basin, W Tianshan	Jia et al. 2001a; Wang et al. 2004a
08	Qabukanzuota/ Yining	44°12′26″/ 81°41′29″	1.0–3.0	Au, Py, Apy	Q, clc, ser, chl	si, py, kao	LS?	Early Carboniferous tuffaceous conglomerate and felsic tuff, Dahalajunshan Fm	Tulasu intra-arc basin, W Tianshan	Dong and Sha 2005
09	Xiaoyuzan/ Nileke	43°58′20″/ 82°37′13″	1.8–7.0	Py	Q, chd, ser, kao	si, py, ser, agl, carb, pro	?	Early Carboniferous intermediate-acidic volcanic rocks, Dahalajunshan Fm	Yelimodun intra-arc basin, W Tianshan	Xu 1998
10	Tieliekesayi/ Yining	44°10′59″/ 81°34′06″	1.0–10.0	Py, Lm	Q, clc, chl	si, agl, py, pro, jr	LS?	Early Carboniferous andesitic breccia and tuff, Dahalajunshan Fm	Yishijilike arc on Ili block, W Tianshan	Xie and Zeng 2001
11	Kuruer/ Tekesi	43°19′00″/ 82°00′23″	1.2–14.5	Py, Cp, Bn, Au, Cc, Cpt	Q, bar, fl, clc	si, agl, chl, carb, pro	HS	Early Carboniferous volcanic rocks, Dahalajunshan Fm	Yishijilike arc on Ili block, W Tianshan	Xie and Zeng 2001

Table 6.1 (continued)

No.	Deposit/ County	Latitude/ Longitude	Grade (g/t)	Ore minerals	Gangue minerals	Major alteration minerals	Type	Lithology and age of host rock	Tectonic unit	Data source
12	Tuola/ Gongliu	44°12′00″/ 82°02′00″	1.0–10.0	Py, Au, Cp, Gn, Sp, Cv, Lm	Q, clc, ser, chd, chl	si, agl, py, ser, pro	LS?	Early Carboniferous tuff and andesite, Dahalajunshan Fm	Yishijilike arc on Ili block, W Tianshan	Xie and Zeng 2001
13	Qingshui/ Fuyun	45°08′00″/ 89°22′30″	4.0–13.0 (-43.0)	Au, El, Py, Cp, Gn	Q, clc, albite, ser, chl	si, py, ser, carb, chl	LS	Early Carboniferous tuffaceous siltstone and basaltic andesite, Nalinkala Fm	Kulankazigan arc north of Kalameili geosuture, E Junggar	Zhang et al. 1992
14	Jinshangou/ Qitai	44°32′13″/ 90°28′51″	1.0–9.0	Py, Cp, Gn, Sp, Apy, Au, El, Ag	Q, flp, clc, chl, bar, aln, pyl	si, py, ser, chl, kao, mm, aln	HS	Early Carboniferous basalt, andesite and tuff, Batamayineishan Fm	Island arc south of Kalameili geosuture, E Junggar	Zhang et al. 1992; Yang et al. 1999
15	Peak 1583 or Shuangfeng-shan II/ Balikun	44°13′34″/ 92°09′15″	1.1–5.9 (-12.6)	Py, Ci, Au	Q, clc, chl, pyl	si, kao, chl, py, pyl, carb	HS	Early Carboniferous basalt and tuff, Batamayineishan Fm	Kulankazigan arc north of Kalameili geosuture, E Junggar	Zhang et al. 1992
16	Shuangfeng-shan/ Balikun	44°11′54″/ 92°15′45″	2.0–8.6 (∼ 33.8)	Py, Apy, Au	Q, chd, adl, mm, clc, ser, chl, epi	si, py, mm, ser, chl, carb, adl	LS	Early Carboniferous andesite, rhyolite and pyroclastic rocks, Batamayineishan Fm	Kulankazigan arc north of Kalameili geosuture, E Junggar	Peng et al. 2004
17	Suorbasitao/ Balikun	43°38′45″/ 92°17′16″	1.7–10.8	Py	Q, ser, adl	si, ser, adl	LS	Early Carboniferous basalt and andesite, Batamayineishan Fm	Kulankazigan arc north of Kalameili geosuture, E Junggar	Li et al. 2001b

Table 6.1 (continued)

No.	Deposit/ County	Latitude/ Longitude	Grade (g/t)	Ore minerals	Gangue minerals	Major alteration minerals	Type	Lithology and age of host rock	Tectonic unit	Data source
18	Beishan/ Yiwu	44°05′00″/ 95°05′00″	1.1–7.0	Au, Py, Cp, Gn, Sp, Apy, Tth	Q, ser, clc, bio, kao, chl	py, si, ser, carb, aln, bar, kao, chl	HS?	Devonian tuff and volcanic rocks, Zhoumubasitao Fm	Santanghu arc north of Kalameili geosuture, E Junggar	Liu 2003
19	Shiyingtan (Xitan)/ Shanshan	42°04′55″/ 90°11′54″	5–10 (av 7.2)	Py, Cp, Apy, Au, El	Q, chd, clc, ser, adl	si, py, ser, chl, carb, adl, kao	LS	Permian andesite, dacite and tuff, Arbashayi Fm	Yamansu-Jueluotag arc-basin system, E Tianshan	Li et al. 1998; Rui et al. 2002
20	Hongshan (Kelatage)/ Hami	42°37′00″/ 91°29′00″	4.0–5.0 Au; 2.0 % Cu	Au, Cp, Py, Bn, Cc	Q, flp, ser, ill, chl, pyl, aln	si, ill, ser, lm	HS	Triassic dacitic volcanic-subvolcanic rocks	Dananhu island arc, E Tianshan	Xu et al. 2006
21	Mazhuang-shan/Hami	41°57′29″/ 95°49′28″	1.0–30.0 (av 7.9)	Au, El, Py, Cp, Gn, Sp, Apy	Q, clc, kao, flp, pyl	si, ser, pyl, carb, kao	HS	Early Carboniferous andesitic-rhyolitic lava, tuff and breccia, Hongliuyuan Fm	Yamansu-Jueluotag arc-basin system, E Tianshan	Li et al. 1999; Li and Liu 2002

Size abbreviations: Gold deposit: *S* small (< 5 t Au); *M* medium (5–20 t Au); *L* large (20–100 t Au).
Ore minerals: *Ag* native silver; *Apy* arsenopyrite; *Au* native gold; *Bn* bornite; *Cc* chalcocite; *Ci* cinnabar; *Cp* chalcopyrite; *Cpt* cuprite; *El* electrum; *Gn* galena; *Hem* hematite; *Jr* jarosite; *Le* leucoxene; *Lm* limonite; *Mr* marcasite; *Po* pyrrhotite; *Py* pyrite; *Sp* sphalerite; *Tth* tetrahedrite
Gangue mineral and/or alteration: *adl* adularia; *agl* argillite; *aln* alunite; *bar* barite; *bio* biotite; *carb* carbonate; *chd* chalcedony; *clc* calcite; *chl* chlorite; *dol* dolomite; *epi* epidote; *fl* fluorite; *flp* feldspar; *gp* gypsum; *ill* illite; *jr* jarosite; *ka* K-alteration; *kao* kaolinite; *lam* laumontite; *lm* limonite; *mm* montmorillonite; *mu* muscovite; *pro* propylitization; *py* pyrite; *pyl* pyrophyllite; *ser* sericite; *si* silicification
Type: *HS* high-sulfidation; *LS* low-sulfidation

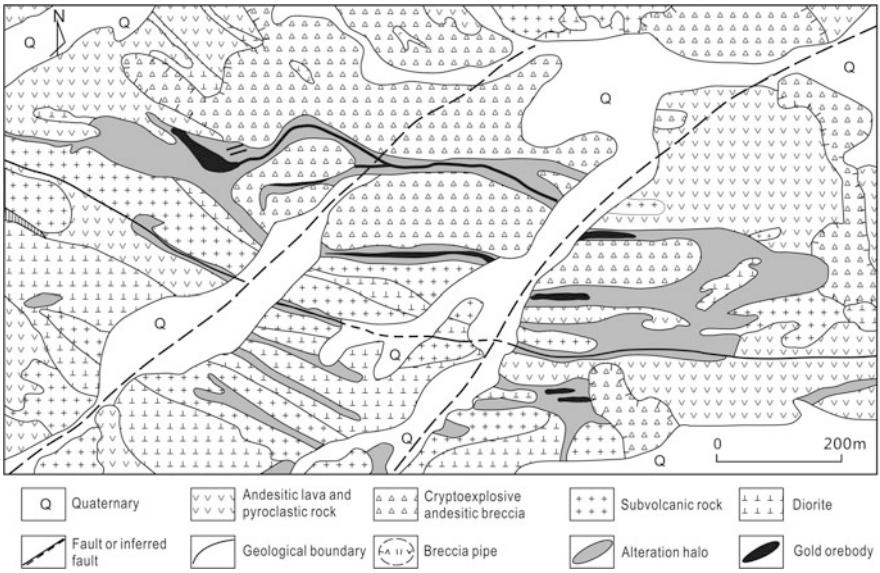

Fig. 6.15 Ore zones of the Kuoerzhenkuola Au deposit. (After Yin et al. 1996)

The deposit, studied and described by Shen et al. (2007, 2008) is located in the eastern end of the Zharma-Sawur Palaeozoic arc, which was possibly related to oceanic plate subduction along the Jeson-Armantai ophiolite belt (Li 1999). The regional lithostratigraphy includes the Sawur and Heishantou Formations consisting of Early Carboniferous andesite, andesite porphyry, sandstone, siltstone, mudstone and limestone. In the region, Late Palaeozoic granodiorites, granites, diorite porphyries, albite-porphyry dykes and breccia pipes are widespread. Main structures are east-northeast-trending folds and major east-west-trending and minor northeast- and northwest-trending faults.

The Kuoerzhenkuola ore field contains two epithermal systems located along the rims of an elliptical caldera complex, Kuoerzhenkuola on the southern rim and Buerkesidai on the northern rim. The caldera complex is associated with an Early Carboniferous felsic and andesitic rocks and breccia pipes that crop out in the center of the orefield. The breccia pipes are mainly composed of andesitic porphyry and basaltic andesitic lava. The caldera complex was intruded by subvolcanic stocks and dykes and, according to Shen et al. (2008) was formed in three magmatic cycles. The first cycle with the eruption of andesite, basalt and dacite, formed an elliptical caldera structure with an east-west 9 km long axis and a north-south 4 km short axis. The second cycle is characterised by both explosive and effusive activity, resulting in the formation of smaller nested calderas within the larger one of the first cycle. A breccia pipe was formed in the second cycle. The third cycle is characterised by the emplacement of diorite necks, granite porphyry and albitite dykes.

Gold mineralisation is developed along the rims of the breccia pipes. Six Au-bearing alteration zones are controlled by west-northwest-trending faults and are hundreds to thousands metres long and 10–30 m wide (Fig. 6.15). Hydrothermal

alteration includes kaolinitisation, silicification, sericitisation, chloritisation, epidotisation, alunitisation and flouritisation. Because of the strong kaolinitisation and alunitisation the deposit is attributed to be HS-style epithermal system (Shen et al. 2007, 2008; Zeng et al. 2007). All the gold orebodies are contained within these alteration zones. The largest orebody is 1,700 m long and 1.6–10 m wide, with albite porphyry dykes commonly in both hanging and footwalls. Ore grades range from 2.6 to 79 g/t (average 7.3 g/t). There are two types of ore: (1) sulphide-quartz stockworks, disseminations and breccias; (2) massive sulphide-quartz veins. Ore minerals are mainly pyrite, chalcopyrite, pyrrhotite, native gold; whereas gangue minerals include quartz, montmorillonite, kaolinite, chlorite, epidote, calcite and alunite. Two generations of gold deposition have been recognized by Shen et al. (2008). Stage I is represented by a pyrite-quartz assemblage, with minor pyrrhotite, chalcopyrite and quartz filling fractures. This constitutes low-grade ores. The sulphides of the older generation and host rocks are brecciated and cemented by quartz and sulphides as a result of later successive hydrothermal stages. Stage II is the main and high-grade ore-forming phase with fine-grained polymetallic sulphide-quartz stockworks, disseminated fine-grained polymetallic sulphide-quartz ores and brecciated quartz-sulphides.

The temperatures of the ore fluids vary between 119 and 276 °C, with salinities between 2.7–7.9 wt % NaCl equiv., calculated ore forming depths between 200 and 300 m, with the fluids having Na^{+}-HS^{-}-Cl^{-}-H_2O composition (Shen et al. 2007, 2008). These authors also inferred that gold was transported as Au-S complex and precipitated under reducing condition.

Zeng et al. (2007) reported, $\delta^{34}S$ values ranging from 1.5 to 3.5 ‰, and averaging 1.9 ‰, suggesting that the ore-forming sulfur were sourced from magmas that fed subvolcanic intrusions and surface volcanism. The estimated $\delta^{18}O_{water}$ values vary from 1.8 to 3.2 ‰, with corresponding δD values of from −84 to −89 ‰, indicative that the ore-forming fluid-system is a mixture of magmatic and meteoric waters. On the basis of the stable isotopic data Liao et al. (2000), Feng et al. (2000) and Wang et al. (2005c) argued that fluid-mixing and water-rock interactions resulted in gold-precipitation. The volcanic-subvolcanic rocks hosting the mineralisation have an age of 343 ± 22 Ma (Liu et al. 2003b), suggesting the mineralisation could not be earlier than 343 Ma. This interpretation is supported by a Rb-Sr isochron age of 341 ± 30 Ma obtained from gold-bearing quartz-vein (Cai et al. 2000) and two ^{40}Ar-^{39}Ar ages of 332 ± 22 Ma from fluid inclusions also from auriferous quartz-vein (Shen et al. 2007, 2008; Table 6.1).

The Kuoerzhenkuola Au deposit is a high-sulphidation (HS) epithermal system hosted in Early Carboniferous volcanic-subvolcanic rocks, formed in an island arc related to oceanic plate subduction. The caldera activity in the Eastern Sawuer mountains provided both ore-forming fluids and conduits for the transportation of the mineralising fluids and the structural locales for the deposition of gold. These features are consistent with typical epithermal systems such as those of the SW Pacific margin.

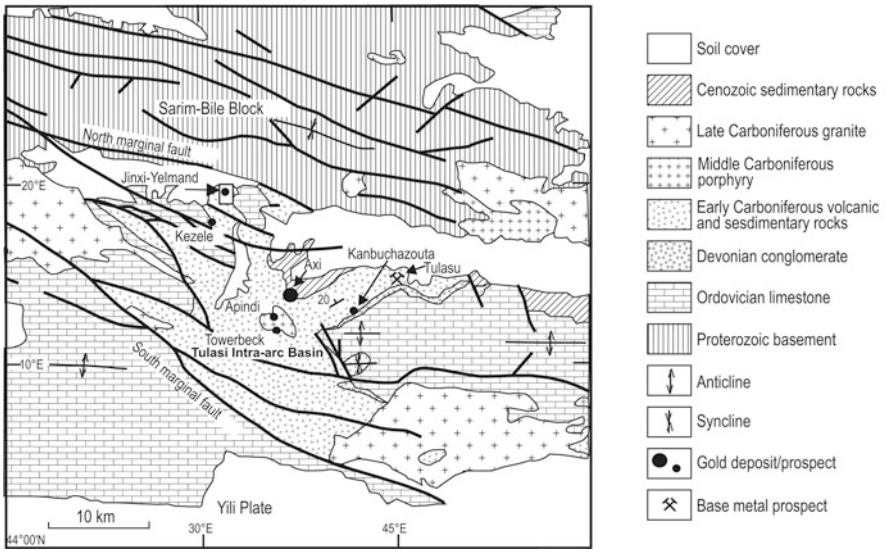

Fig. 6.16 Jinxi-Yelmand and Axi region in the Yili Block; details in text. (After Xiao et al. 2005a)

6.3.2.2 Jinxi-Yelmand

The Jinxi-Yelmand high-sulphidation epithermal Au deposit (No. 3 in Fig. 6.14), together with a number of other deposits including Axi (Sect. 6.3.2.3), is hosted in the Tulasi Basin of the Borohoroshan magmatic arc (Fig. 6.16). West-northwest-trending faults define the boundaries of the Tulasi Basin, which is segmented by northeast-northnortheast-trending faults, forming a series of horst and graben structures. The Tulasi Basin contains volcanic and sedimentary rocks, with a total thickness probably greater than 9 km, overlying the Proterozoic basement of the Yili Block. The Tulasi succession began in the Ordovician with a variety of limestone rocks, followed in the Devonian by clastic sediments and in the Carboniferous by felsic volcanic rocks, including ignimbrites and tuffs, and minor basalt. The volcanic rocks are interbedded with sedimentary rocks, recording a transition from platform sedimentation to littoral and fluvial subearial environments. The Jinxi-Yelmand Au mineralisation is hosted by the Early Carboniferous Dahalajunshan Formation, which consists of five units, from conglomeratic and feldspathic sandstone rocks at the base, which are the principal host of the mineralisation, followed by ignimbrite, crystal vitric tuffs in the overlying units. The Dahalajunshan sequence is interpreted to have been erupted in a sub-aerial environment. Andesitic stocks intrude the Dahalajunshan Formation and have an emplacement U-Pb age of ca. 347 Ma (Li et al. 1998).

The Jinxi-Yelmand epithermal Au deposit was studied by Xiao et al. (2005a), based on diamond drill core and field mapping, and the following is summarized from these authors.

Jinxi-Yelmand is a low-grade deposit, with the highest Au grades obtained from an adit, where a zone 27 m wide averaged +1.0 g/t, with a maximum grade of 4.54 g/t. The SEG Newsletter (No. 73, April 2008) reported combined measured, indicated and inferred resources at Gold Mountain (which includes Jinxi-Yelmand) totalling 95 Mt @ 0.9 g/t Au. It should be pointed out that the double name of Jinxi and Yelmand is because, although these deposits outcrop separately at the surface, they are in fact connected at depth into a single and larger mineralised zone.

The Jinxi-Yelmand mineralisation is controlled by a north-south fault zone, interpreted to be the main feeder of the hydrothermal fluids. Hydrothermal alteration extends over an area of about 4 km^2 and is more intensely developed in Unit 1 of the Dahalajunshan Formation, with less intense alteration in the underlying carbonate rocks. Xiao et al. (2005a), using a variety of methods, including the use of a PIMA instrument (Portable Infrared Mineral Analyser) and XRD analyses, as well as conventional petrographic techniques, recognised three zones of alteration. From core to periphery they comprise: a zone 1 of dominantly silicic alteration, associated with vuggy quartz, minor dickite and diaspore; a zone 2 of advanced argillic alteration consisting of dickite, quartz and kaolinite; and a zone 3 of argillic alteration with smectite, kaolinite and dickite. Zone 1 grades laterally and vertically into the advanced argillic alteration of zone 2. The alteration zoning reflects three stages of the hydrothermal process. The first stage was silicification and advanced argilllic alteration, followed by a second stage characterised by hydraulic brecciation with more silicification and formation of late barite and anhydrite veins. The last stage was supergene kaolinite and oxidation of sulphides.

Microthermometric measurements of primary and pseudosecondary fluid inclusions, show a range of homogenisation temperatures from 275 to 198 °C with a mean of 240 °C; calculated salinities range from 0.7 to 5.0 wt % NaCl equiv. with salinity and homogenisation temperatures exhibiting a negative correlation. Late stage fluid inclusions (type 2) in barite and hydrothermal quartz, show a range from 108 to 85 °C (mean 95 °C) with salinities ranging from 0.3 to 2.0 wt % NaCl equiv. Stable isotope systematics (O-D and S) of samples taken from the alteration zones show a range of $\delta^{18}O_{qtz}$ values from 17.2 to 21.6 ‰ and calculated $\delta^{18}O_{H_2O}$ values ranging from 4.1 to 5.8 ‰. The δD values of inclusion fluids show a range from −68 to −93 ‰. The O-D isotopic data of the Jinxi-Yelmand hydrothermal fluids plot close to the box of magmatic water, compared with Axi and Shiyingtan (Fig. 6.17).

Sulphur isotopic data calculated from aqueous H_2S, estimated from fluid inclusions, show a range of $\delta^{34}S$ values from 5.05 to 8.09 ‰ in sulphides, 3.77–13.23 ‰ in altered sandstone and 5.63–15.84 ‰ in unaltered sandstone. The range of $\delta^{34}S$ values from Jinxi-Yelmand, compared with those of Shiyingtan and Axi is shown in Fig. 6.18. The $\delta^{34}S$ values of Jinxi-Yelmand are not especially diagnostic of HS epithermal systems, but the more restricted range of sulphur isotopic values of pyrite were interpreted by Xiao et al. (2005a) to be close to magmatic sulphur, but with contributions from the sedimentary rocks.

The Jinxi-Yelmand deposit is the first reported HS epithermal system and appears to be one of several large low-grade gold deposits potentially amenable to bulk mining in the Tulasi basin. High-sulfidation gold deposits are characterized by well-

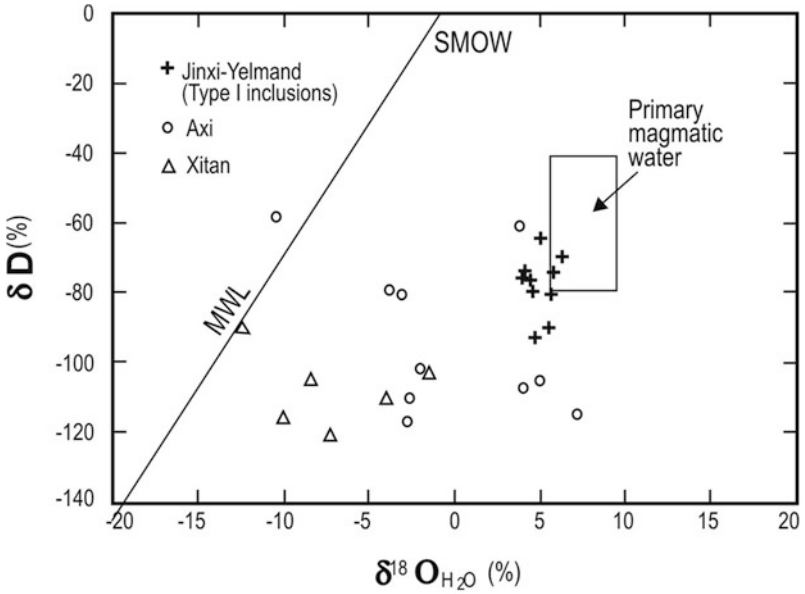

Fig. 6.17 $\delta^{18}O$ vs δD plot, comparing data from Jinxi-Yelmand, Axi and Shiyingtan epithermal systems; note the proximity of the isotopic composition of fluids from Jinxi-Yelmand to the magmatic box. (After Xiao et al. 2005a)

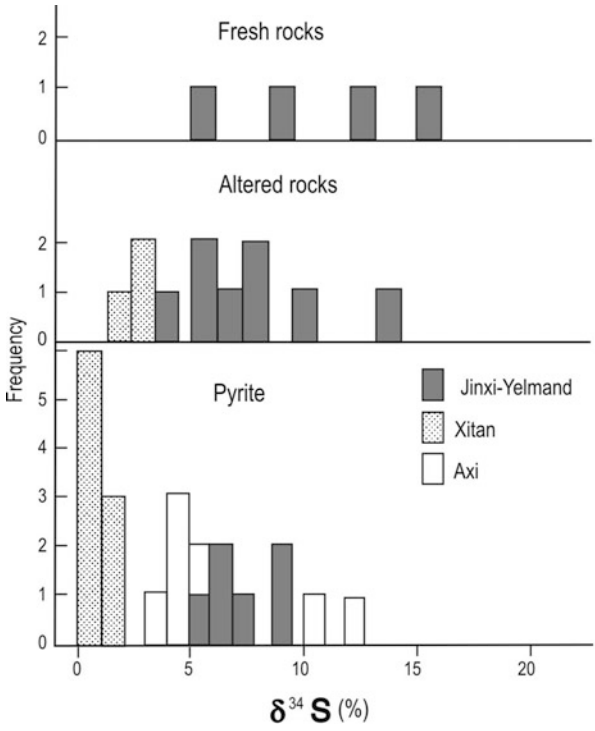

Fig. 6.18 Frequency histogram of $\delta^{34}S$ values from Jinxi-Yelmand, Axi and Shiyingtan. (After Xiao et al. 2005a)

zoned hydrothermal alteration patterns, as observed at Jinxi-Yelmand, where a zone of vuggy quartz is surrounded by advanced argillic alteration, followed outward by argillic alteration. Diagnostic alteration minerals of advanced argillic alteration commonly include quartz, alunite, kaolinite, less commonly pyrophyllite, diaspore and anhydrite, as well as barite as late vein minerals.

There are, however, some differences between the Jinxi-Yelmand deposit and other high sulphidation epithermal Au deposits. Jinxi-Yelmand has only minor vuggy quartz, little base-metal mineralisation, and no alunite. These differences suggest either that these features were developed but not preserved or overlooked within the limits of current exposures, or that the ore fluids were perhaps not as acidic as those associated with more typical high-sulfidation deposits. Reduced acidity could be explained by partial neutralisation of acidic fluids upon interaction with the thick underlying Ordovician limestone units, which might have occurred along the fluid conduits, but the presence of vuggy quartz shows that this did not occur. Furthermore, acid neutralisation by this mechanism would have produced increased CO_2 levels, but again this is not consistent with the observations that the measured CO_2 contents in the fluids are not unusually high; this is supported by the absence of clathrate in fluid inclusions, and of carbonate minerals at the margins of the hydrothermal alteration zone. The second possible explanation is that late pervasive silicification may have largely obliterated more widespread early vuggy quartz. This latter explanation is preferred because the central parts of the pervasive silicification (Zone 1) preserve ghost textures and advanced argillic alteration mineral assemblages, such as dickite, kaolinite and diaspore.

A generalized alteration and ore genesis model of the Jinxi-Yelmand high-sulfidation epithermal deposit is shown in Fig. 6.19.

The model proposed by Xiao et al. (2005a) for Jinxi-Yelmand is as follows: emplacement of a shallow-level intermediate porphyry stock occurred in the Middle Carboniferous, from which SO_2-rich volatiles and a residual brine exsolved. Volatile phases ascended along normal faults and interacted with meteoric fluids to generate highly acidic hydrothermal fluids with temperatures ranging from 198 to 275 °C and salinities less than 5.0 wt % NaCl equiv. These fluids flowed laterally along the highly permeable rocks of the Dahalajunshan Formation where initial acid leaching enhanced the secondary porosity of the host conglomerate formation by the development of vuggy quartz. Increased permeability caused greater mixing with meteoric fluids from the basin, leading in turn, to more rapid cooling and dilution of the hot acidic fluids. Meteoric water dominated hydrothermal fluid activity occurred in the late stages at a lower temperature of around 100 °C and with lower salinities that are less than 1.6 wt % NaCl equiv. With decreasing temperature, silica-rich fluids deposited and sealed most of the pore spaces within the hosting rocks, overprinted early vuggy quartz and possibly destroyed any alunite that might have been present, replacing it with kaolinite. Continued fluid injection caused hydrofracturing of the brittle, silicified rocks and formed breccias and intermediate to advanced argillic alteration. Gold was probably carried by bisulphide complexes and deposited in both intensely silicified parts and marginal argillic alteration zone, due to a combination of decreasing pressure and temperature, culminating in boiling and increasing

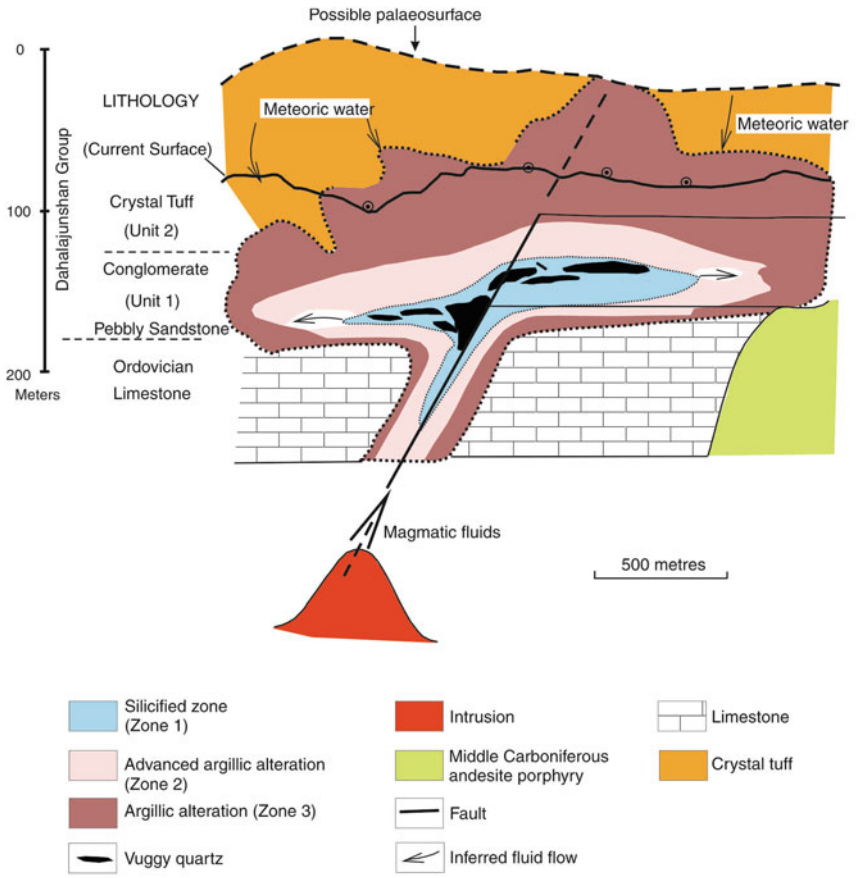

Fig. 6.19 Idealised reconstruction of the Jinxi-Yelmand epithermal system; details in text. (After Xiao et al. 2005a)

pH. This is perhaps the most important gold mineralisation stage. Continuing hydrothermal activity caused local brecciation that overprinted silicification. During this stage, barite veins were formed, filling the opening fractures. Supergene gold enrichment resulted from post-mineralisation fracturing/jointing and accompanying Cenozoic weathering and oxidisation. On the basis of its alteration zoning and the unusual overprinting by silica-rich fluids of advanced argillic alteration assemblages, Xiao et al. (2005a) proposed that the Jinxi-Yelmand Au deposit is a modified high-sulphidation epithermal system.

6.3.2.3 Axi

The Axi deposit (Fig. 6.16 and No. 5 in Fig. 6.14), is located 30 km northwest of Yining County, and is probably the largest epithermal Au system in North Xinjiang.

A good account of the Axi low-sulphidation epithermal system can be found in Hart et al. (2003). A more recent publication on this deposit is by Zhai et al. (2009), who provided details of fluid inclusions, their composition and isotope systematics. The Axi gold deposit is in the Yili Block within the Tulasu Early Carboniferous volcanic basin on the southern slopes of Kerguqinshan of the Boluohuluo accretionary arc (Sha et al. 2003) and is one of a cluster of epithermal systems in the Tulasu district that includes Jinxi-Yelmand, Abiyndi, Tulasu, Tuhulasu, Qiabukanzauota, Tawuerbieke (Hart et al. 2003). About 70 km to the east is the Yelimodun district with more Au deposits (Jiamante, Langbula, Tieliekete, Xiaoyuzan; see Hart et al. 2003 for description of these deposits). The Tulasu basin is 30 km long and 8 km wide, and hosts several other important epithermal Au deposits (No. 3–8 in Fig. 6.14). All epithermal systems in the Tulasu basin are hosted by the Early Carboniferous volcanic rocks of the Dahalajunshan Formation, which overlies a pre-Devonian metamorphic basement comprising of Mesoproterozoic-Silurian carbonate, flysch and felsic-intermediate volcanic rocks. The Dahalajunshan Formation is a 1,500 m thick andesite-dacite-rhyolite sequence (including lava, breccia, tuff and ignimbrite), with minor basalt intercalations, unconformably overlain by the Lower Carboniferous Aqialehe Formation, which comprises conglomerate, sandstone, shale and limestone. The rocks of the Dahalajunshan Formation belong to a calc-alkaline series volcanic succession, formed in an arc setting in the West Tianshan. A caldera structure (or pipe?), 2–3 km in diameter with ring and radial faults is present in the Axi orefield.

Nine orebodies are represented by veins and lenses in a 1,000 m long and 200 m wide belt in the hanging wall of a fault zone. The largest and economically most important is the No. 1 orebody, which is 940 m long, up to 41 m wide (average ca. 19.5 m), and >450 m deep (Fig. 6.20). The average ore grades are 5.57 g/t Au and 11.02 g/t Ag (see also Table 6.1). The No. 1 orebody constitutes 90 % of the total Au reserves of the Axi deposit (about 70 t Au; Rui et al. 2002).

The Axi deposit include oxidized and primary ores. The oxidized ores extend to a depth of about 70 m, with high grades, but only representing about 5–10 % of the total. The primary ore accounts for 90–95 % of the total and are subdivided into three types: (1) quartz vein, composed of smoky gray quartz, chalcedony and auriferous sulphides, representing 20 % of the total; (2) altered rock, also with 20 % of the total; and (3) breccia ore, with 60 % of the total, formed by multiple phases of brecciation and represented by replacement and filling of the other two types.

In the Axi orefield wall-rock hydrothermal alteration consists of several stages of silica (mainly quartz or chalcedony), sericite, pyrite, chlorite, albite, carbonate, laumontite, adularia, with local kaolinite (Chen et al. 2003). The pre-ore alteration is characterized by propylitic assemblages, including chlorite, carbonate, albite and sericite. This propylitic alteration is pervasive and coeval with volcanic eruptions, showing no obvious relationship to gold mineralisation and is possibly related to greenschist facies regional metamorphism. At least four generations of wall-rock alteration assemblages have been identified (Chen et al. 2003), namely: (1) pyrite-sericite-quartz, locally cavitary; (2) quartz-chalcedony; (3) polymetallic sulphides-carbonate-quartz vein; and (4) carbonate-laumontite veinlets. The characteristic ore textures are breccia, banded and crustiform, as well as drusy cavities.

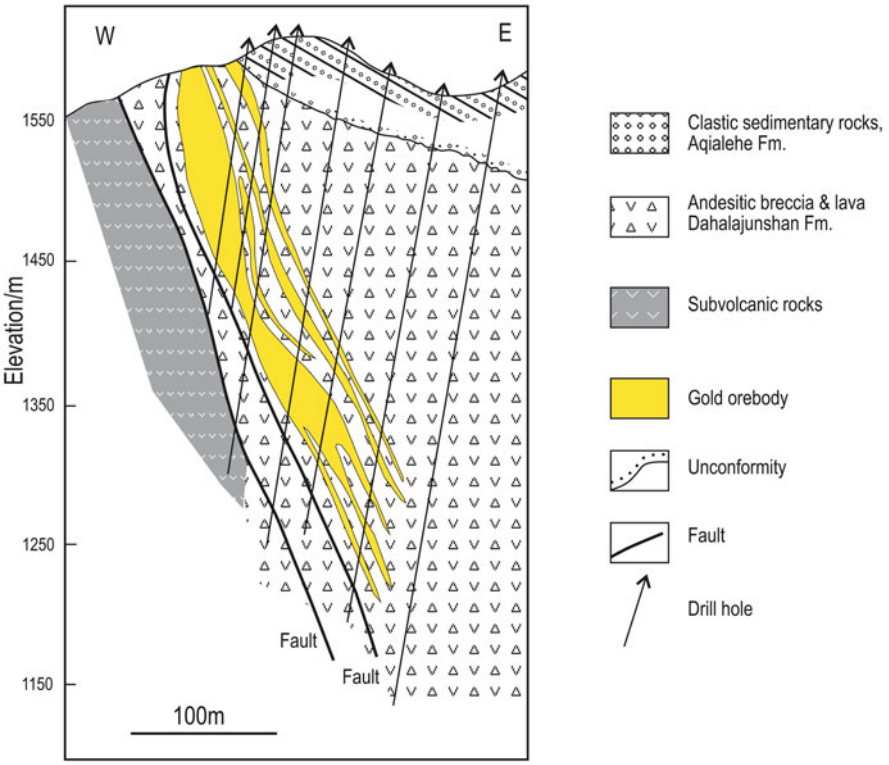

Fig. 6.20 Cross-section of Axi deposit. (After Zhai et al. 2009)

Ore minerals include more than 40 mineral species, with the dominant minerals being pyrite, marcasite, arsenopyrite and electrum, followed by chalcopyrite, galena, sphalerite and native gold (Sha et al. 2003, 2005). Sulphides are relatively low in contents and base metal minerals can be observed only in the medium to deep parts of orebodies. The gold minerals include electrum and native gold with low fineness (average 761).

According to Bao (2001), fluid inclusions in quartz are small and rare. Fluid inclusions in the auriferous quartz-veins are compositionally two-phase H_2O-NaCl, with homogenisation temperatures ranging from 80 to 294 °C, averaging 150 °C. Calculated depths of the fluid system vary from 300 to 900 m. Salinity ranges from 0.48 % to 5.16 wt % NaCl equiv. Rb-Sr age dating of fluid inclusions shows a range from 339 to 301 Ma and a 275 Ma age for illite, suggesting that the epithermal mineralisation was modified or overprinted by a late hydrothermal event.

The $\delta^{34}S$ values of pyrites in ores range from 0.95 to 10.5 ‰, and averages 4.9 ‰ (Sha 1998; Jia et al. 2001b; Wang and Zhao 2006), suggesting that an important component of sulphur source was magmatic. The $\delta^{18}O_{water}$ values range from −10.0

to 6.7 ‰, which calculated from the $\delta^{18}O_Q$ values of between 5.9 and 13.2 ‰, with corresponding δD values from −59 to −115 ‰, suggesting that the ore-forming fluids were mainly sourced from meteoric water (Bao 2001; Jia et al. 2001b).

The Axi gold deposit is a low-sulphidation (LS)-type epithermal ore system originally formed in pre-collisional volcanic arc setting and then superimposed by syn- to post-collisional magmatism-related hydrothermal event.

6.3.2.4 Kuruer

The Kuruer Au-Cu deposit (No. 11 in Fig. 6.14) is located 25 km north of Tekesi County. The deposit, together with two other epithermal gold deposits (Nos. 10 and 12; Fig. 6.14), is in the Early Carboniferous volcanic arc and hosted by the Dahalajunshand Formation, unconformably overlain by the Early Carboniferous Akeshake Formation. In the Kuruer orefield, the main structures are northwest-trending faults, and post-ore north-northeast-trending faults. The northwest-trending faults (F2) have a 310–330°, strike and are traceable for more than 5 km, dipping 55–75° south (Xie and Zeng 2001). Subsidiary structures control the location of orebodies and related alteration. The ore-hosting F2 fault is crosscut by quartz-albite porphyry and diorite porphyry dykes. The quartz-albite dykes are locally altered and in places may become part of orebodies. The orebodies are distributed along the F2 fault zone as discontinuous veins, with local swelling, thinning and bifurcation or combinations thereof, both in the vertical and horizontal sense. Orebody I at the surface it extends for more than 500 m with average width of about 10 m, with grades ranging from 2.45 to 11.4 g/t. Orebody II is 150 m long and 8.2 m wide at the surface, with grades ranging from 1.30 to 2.88 g/t. The overall grade, as reported by Xie and Zeng (2001) range from 1.2 to 14.5 g/t (see Table 6.1)

Ore styles are characterized by veinlets, stockworks, disseminations and banding. Wallrocks are gray-purple rhyolitic ignimbrite and purple-grayish rhyolite and exhibit hydrothermal alteration dominated by silica, sericite, argillic and pyrite-bearing phyllic type. Beside native gold, other metallic minerals are pyrite, chalcopyrite, hematite, magnetite, galena, sphalerite, bornite, and chalcocite. Gangue minerals include quartz, K-feldspar, albite, biotite and amphibolite, as well as kaolinite, sericite, chlorite, calcite, fluorite and barite.

Inclusion fluids in quartz and calcite consist mainly of a pure liquid phase and a minor gas phase (Qi JP, unpublished data; and Chen et al. 2012). The pure liquid inclusions form planar and linear arrays and are less than 4 μm in size. The gas inclusions have mostly irregular shapes, with a few being round or square, commonly from 2 to 5 μm in size. The fluids are mainly composed of H_2O, accounting for about 53 %. Major cations are K^+, Ca^{2+} and Mg^{2+}, followed by Na^+. SO_4^{2-} is the dominant anion. The composition of gas is dominated by H_2O and CO_2. Gold was possibly transported in the fluids as Au-S complexes. Decrepitation temperatures of fluid inclusions in pyrite range from 270 to 300 °C, which are at the high end of epithermal system temperatures (Pirajno 2009).

Stable isotope analyses on quartz separates from ores yields δD_W and $\delta^{18}O_W$ values of −65.1 and −5.74 ‰ (relative to SMOW), respectively. This indicates that the ore-forming fluid-system was a mixture of magmatic and meteoric waters, but dominated by meteoric water. The $\delta^{34}S$ values of pyrites range from 3.7 to 4.5 ‰, and average 4.2 ‰, showing that most of the ore-forming sulphur was sourced mainly from igneous rocks. Dong and Sha (2005) suggested that the timing of the ore formation was Early Carboniferous because the ore is hosted in Early Carboniferous volcanic rocks. Xie and Zeng (2001), however, suggested a Permian-Triassic age for the deposit on the basis of Pb-isotope model ages, range from 214 to 273 Ma.

6.3.2.5 Shuangfengshan

The Shuangfengshan gold deposit, located 95 km northwest of Balikun County (No. 16 in Fig. 6.14). The deposit is situated in the East Junggar accretionary complex on the north side of the Kalameili fault belt. In the period of Devonian-Early Carboniferous, the northward and southward subductions of the Junggar oceanic plate resulted in the development of the East Junggar accretionary-arc complex and the Bogda-Harlike-Dananhu island arc on the north and south sides of the Karamay (Kalameili) geosuture, respectively (Ma et al. 1997).

The Shuangfengshan orefield is in Early Carboniferous andesitic and rhyolitic lavas, breccias and tuffs (Fig. 6.21a), which form a north-west-trending anticline with andesitic rocks in the core. The anticline is cut by the north-west- and east-west-trending thrusts, and by northeast- and eastnortheast-trending strike-slip faults. A syenite porphyry dyke can be observed near the axis of the anticline (Fig. 6.21b). Gold orebodies form vein-like lodes or lenses along the contacts between the andesitic and rhyolitic rocks and/or within faults (Fig. 6.21a). The orebodies are 360–550 m long, 0.6–12.5 m thick and more than 113 m deep, dipping to northeast or north-northeast.

Mineralisation styles include breccias, quartz veinlets and disseminated stockworks. Gold grades range from 2 to 8 g/t and can reach up to 33.8 g/t (Table 6.1). Ore minerals are manly pyrite and arsenopyrite, with minor native gold. Gangue minerals are quartz and chalcedony, with lesser adularia, montmorillonite, sericite, fluorite, calcite, chlorite and epidote. Wallrock alteration is characterized by silica, pyrite, arsenopyrite, montmorillonite, adularia, sericite, chlorite and carbonate. These alteration minerals are indicative of a low sulphidation (LS) epithermal system. Alteration zoning is present and consist, from ore to wallrocks, of silicified breccia, quartz (adularia), stockworks (orebody), pyrite, montmorillonite and propylitic alteration (Peng et al. 2004). The mineralisation can be divided into two stages: (1) volcanic hot-spring, and (2) hydrothermal system related to subvolcanic intrusion, forming auriferous quartz (adularia) stockworks, filling in the fractures of the altered volcanic rocks.

The REE distribution patterns of ores are similar to those of andesite, rhyolite, dacitic porphyry and quartz porphyry, showing that the ore system is genetically related to these volcanic-subvolcanic rocks (Lin et al. 1999). The $\delta^{34}S$ values of ore

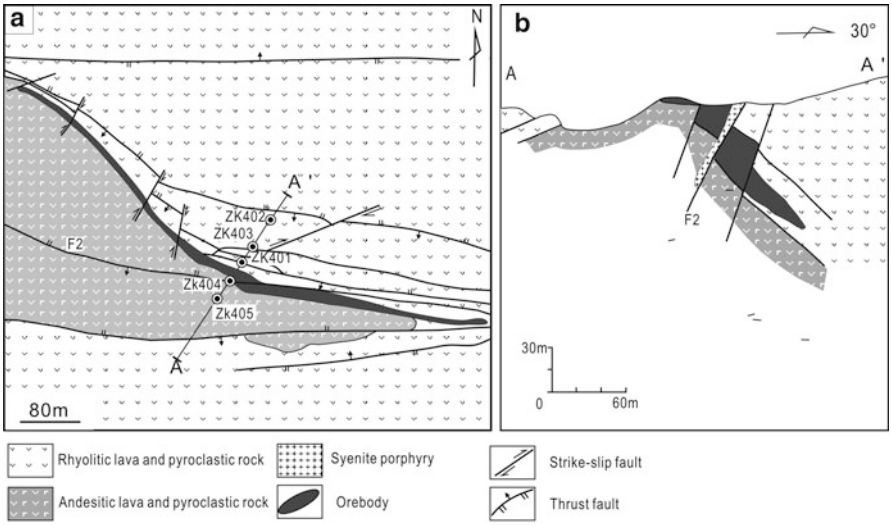

Fig. 6.21 Shuangfengshan ore field and cross-section. (After Peng et al. 2004)

sulphides, range from −9.7 to 1.6 ‰ (Xi 1999), again suggesting a dominant magmatic source. Two Rb-Sr isochron ages of 226 ± 21 and 226 ± 44 Ma were obtained from altered quartz-albite porphyries and Au-bearing quartz veins, respectively (Li et al. 2005). Hence the deposit is a post-collisional LS-style epithermal ore system.

6.3.2.6 Jinshangou

The Jinshangou Au deposit is located 130 km northeast of Qitai County (No. 14 in Fig. 6.14). The deposit is situated immediately south of the Kelameili suture. Its host rocks, like for the Shuangfengshan deposit, are part of the Early Carboniferous Batamayineishan Formation, a volcanic-sedimentary sequence formed in an arc setting. Rock types in the deposit area are basalt, andesitic basalt, pyroxene andesite, dacite, trachyandesite and rhyolite, and associated breccias, tuffs and ignimbrites, together making up a calc-alkaline series (Yang et al. 1999). Granitic, rhyolitic, dacitic and andesitic porphyries and dolerite dykes are also present. Ignimbritic rocks yield a whole-rock K-Ar age of 309.6 Ma (Zhang et al. 1992). The mineralisation is developed within volcanic domes and calderas and associated ring and radial fractures, which are structurally overprinted by the regional northeast- and north-northeast-trending faults.

Five mineralized zones have been delineated, containing 10 orebodies and 6 mineralized veins. The ores form veins and lenses (80–480 m long; 2–4 m thick), controlled by ring and radial faults and their intersections, with grades ranging from 1.0 to 8.8 g/t (Table 6.1).

The ores contain only from 1 to 2 % of sulphides (Zhang et al. 1992), Ore minerals include pyrite, chalcopyrite, galena, sphalerite, arsenopyrite, tetrahedrite, bornite, magnetite, hematite, ilmenite, native gold, electrum and native silver. Gangue minerals are quartz, feldspar, calcite, sericite, kaolinite, barite, fluorite, chlorite, epidote, tourmaline, monazite, alunite, pyrophyllite and montmorillonite. The ore paragenesis consists of early pyrite-sphalerite-quartz, polymetallic sulphides, pyrite-quartz-gold, and late carbonate veinlets. The hydrothermal alteration minerals indicate that the Jinshangou deposit is a high sulphidation-style epithermal (HS), although the sulphide content in the ores is very low.

Homogenisation temperatures of fluid inclusions in mineralized quartz range from 242 to 310 °C and average 272 °C. The fluid salinities range from 1.2–10.5 wt % NaCl equiv. The depth is estimated to be 500–600 m (Zhang et al. 1992). The cations in the fluids are mainly Ca^{2+}, Na^{+} and K^{+}, with minor Mg^{2+}. Anions are mainly $SO_4{}^{2-}$ and Na^{-}, with minor F^{-}. The gas composition is mainly H_2O, followed by CO_2, CO, N_2 and CH_4.

The δD value of inclusion fluids in quartz ranges from −105.8 to −121.2 ‰, together with $\delta^{18}O_{water}$ values of between −3.8 and −7.5 ‰ calculated from $\delta^{18}O_Q$ value of 4.3–13.5 ‰, showing that the ore-forming fluid-system is a mixture of magmatic and meteoric waters (Liu et al. 2002). The $\delta^{13}C_{V-PDB}$ and $\delta^{18}O_{V-SMOW}$ values of calcites range from −3.2 to 0.1 ‰ and 4.1–7.7 ‰, respectively, suggesting that calcite crystallized from a low-temperature fluid-system dominated by meteoric water. The $\delta^{34}S$ values of pyrite, galena and ores are from −0.7 to 3.8 ‰, with peak value of 2.5 ‰, supporting a magmatic source of sulphur.

6.3.2.7 Shiyingtan

The Shiyingtan (also called Xitan) Au deposit is located 90 km southwest of Shanshan County (No. 19 in Fig. 6.14) and has resources estimated at about 6.4 t Au, with grades ranging from 5 to 10 g/t (Rui et al. 2002). Pirajno et al. (1997) reported that the deposit contained about 5.5×10^6 t of ore, grading 7 g/t Au (using a cut-off value of 1 g/t). The Shiyingtan orefield, extends for about 1.8 km along strike and is 1.2 km wide, situated in a Permian continental facies volcanic basin, which was superimposed on the Yamansu-Jueluotag Palaeozoic arc-back-arc system in East Tianshan (see Figs. 6.4 and 6.9). The basin was filled by continental facies volcanic rocks of the Arbashayi Formation of Early Permian age, consisting of purple-colored andesitic to dacitic lavas, breccias and tuffs, yielding two Rb-Sr isochron ages of 281 ± 10 and 285 ± 7 Ma (Li et al. 1998). The basin's basement consists of Early Carboniferous basalt, andesite and dacite that belong to the Xiaorequanzi Formation.

The Early Permian volcanic sequence (Aqikebulake Formation) can be locally observed in small basins formed during syn- to post-collisional orogenesis. This Early Permian stratigraphic unit was also folded and faulted. In addition to the development of volcanic rocks, Carboniferous and Permian intermediate-to-felsic stocks were emplaced in the Yamansu-Jueluotag tectonic unit.

The Shiyingtan Au deposit is situated on the northwest margin of a caldera structure, with a diameter of approximately 20 km and infilled with felsic volcanic and associated pyroclastic rocks. The Au mineralisation is hosted in a breccia pipe-like structure that is undeformed and unmetamorphosed, suggesting that it was emplaced during a post-tectonic volcanic episode and possibly during a subsequent rifting event. The fragmented material is pervasively silicified and laced by multidirectional veins. This central zone of silicification is associated with pyrophyllite and chlorite and is surrounded by an envelope of pyrite + sericite. This is, in turn followed by a zone containing calcite, dolomite, chlorite and ankerite. The ore minerals include free gold (usually found interstitial to grain boundaries), pyrite, various sulphosalts of Ag and As, some selenides (Ag_2Se) and chlorides (Ag_2Cl). The breccia is composed of lithic clasts now pervasively replaced by alteration phases, which include chalcedonic quartz, quartz and pyrophyllite. Spaces between clasts and microfractures are filled with euhedral quartz and sericite. Vein material is composed of coarse-grained calcite + quartz, with zones of bladed calcite crystals, due to precipitation from CO_2-rich boiling solutions, with pyrophyllite ± quartz at the vein margins. Late veinlets of gypsum are also present.

Eighteen orebodies have been recognized in veins, lenses and tear-shaped zones (Fig. 6.22). Four ore zones are economically important and numbered as L1, L2-1, L2-4 and L3. Orebody L1 is 340 m long and 0.89–8.92 m thick (average 3.8 m), and hosted in a fracture zone dipping north at angles ranging from 34° to 51°. The average grade of orebody L1 is 12.5 g/t Au. Orebody L2-1 is 106 m long and 0.86 m thick, with an average grade of 3.5 g/t Au. Orebody L2-4 is 86 m long and 0.5–2.5 m thick (average 1.6 m), with a gold grade of 1.71 g/t. The L3 orebody is 220 m long, 1.9–17.6 m thick (average 12 m), dipping north at angles of 50–75°, with gold grades ranging from 3.73 to 25.6 g/t, averaging 15.6 g/t, reaching a maximum of up to 111 g/t.

The ores exhibit granular and brecciated textures. Common ore styles include disseminations, stockworks and veinlets. The ores are sulphide-poor, with pyrite being the main sulphide mineral, followed by marcasite, arsenopyrite, chalcopyrite, calaverite, galena and sphalerite. The gangue minerals are mainly quartz and chalcedony, with minor sericite, albite and calcite. The ore assemblages include electrum-pyrite-quartz, electrum-native gold-quartz-sericite and electrum-native gold-quartz-calcite. Proximal hydrothermal alteration is characterized by silica, sericite, carbonate, limonite and laumontite with occasional adularia. Distal alteration includes kaolinite, propylitisation and carbonates.

Electrum, native gold and calaverite, tend to form very small grains, flakes or dendritic shapes. The fineness of gold minerals is generally between 565 and 746. Gold occurs as intergranular, inclusions and in fissures, of which the intergranular accounts for 97 %. Microgranular gold is less than 0.01 mm in size and accounts for 95 % of the ore and is mainly distributed in between quartz or/and pyrite crystals. Fissure gold occupies microcracks in quartz, whereas gold inclusions are mostly contained in pyrite.

Feng et al. (2000) and Wang et al. (2005c) carried out fluid inclusion studies and reported that homogenisation temperatures in quartz range from 191 to 109 °C, with

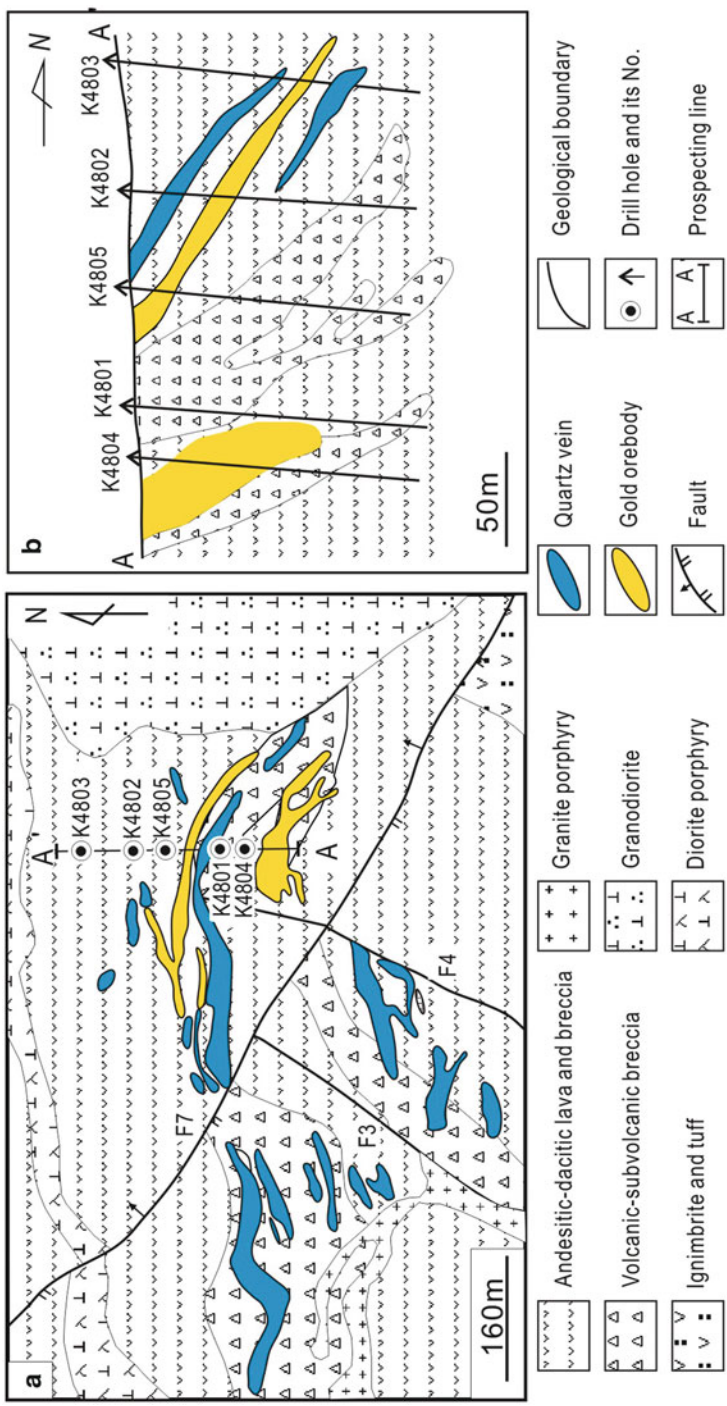

Fig. 6.22 Shiyngtan ore field and cross-section; see text for details. (After Ji et al. 1999)

an average of 150 °C. Ore fluid pressure estimated by Feng and co-authors range from 1 to 3.5 MPa, corresponding to depths of 100–350 m. The δD_{water} and $\delta^{18}O_{water}$ values are from −81 to −95 ‰ and −2.5 to −10.4 ‰, respectively, showing the fluid-system is dominated by meteoric water. The $\delta^{34}S$ value of pyrite in ore ranges from 0.6 to 1.3 ‰, and averages 1.0 ‰, implying that it was sourced from igneous rocks or mantle material. Based on the above, the Shiyingtan deposit was formed at low-temperature, shallow-depth, by a meteoric water-dominated fluid-system, which continuously leached ore-forming elements from the volcanic-subvolcanic rocks and precipitated Au into favorable loci, such as fault zones.

The timing of the Shiyingtan mineralizing event has been determinded using different isotopic systems, such as Rb-Sr isochron and U-Pb (Li et al. 1998, 2005; Ji et al. 1996). Isotopic ages of host rocks and related intrusions in the orefield range from ca. 293 and ca. 255 Ma (Early Permian), whereas ages for metallogenesis are between ca. 288 and ca. 237 Ma (Early Permian-Early Triassic). This shows that the metallogenesis slightly postdated the magmatic activity and that both occurred in the post-subduction tectonic setting. The Shiyingtan deposit can be classified as a low-sulphidation (LS) epithermal system and the breccia pipe could be the remnant of a hydrothermal explosion crater, similar to those that occur in the Taupo Volcanic Zone in New Zealand (e.g. Cole and Spinks 2009).

6.3.2.8 Mazhuangshan

The Mazhuangshan Au deposit (No. 21 in Fig. 6.14) is located near the border between Xinjiang and Gansu province, about 250 km southeast of Hami City. With reserves of 21.5 t Au, it is ranked as a large gold deposit in China. Like for the Shiyingtan deposit, Mazhuangshan is situated in the Yamansu-Jueluotag arc-back-arc system (Jing and Xu 1997), but hosted in volcanic rocks of Early Carboniferous rather than Permian.

The host volcanic rocks belong to the Lower Carboniferous Hongliuyun (or Baiyushan) Formation, subdivided into three members. The lower member is composed of sandstone, slate, andesite and basalt with tuff, volcanic breccia, limestone and marble. The middle member hosts most of the gold deposits and consists mainly of andesite, dacitic breccia, tuff, rhyolite and slate. The upper member includes limestone, andesite and dacitic pyroclastic rocks. Fossils found in the tuffaceous sediments and limestone show that the Hongliuyuan Formation was mainly formed in a marine basin or in a volcanic island. The rocks of the Hongliuyuan Formation are tightly folded and structures are dominated by northwest-, northeast-, and east-west-trending faults, which are the main locus of the orebodies and quartz veins. Porphyry rhyolitic and dacitic subvolcanic intrusions are present in the orefield with their emplacement resulting in a dome-like structure. These subvolcanic felsic porphyries are spatially related to the orebodies and quartz veins, and yield whole-rock Rb-Sr isochron ages of 301 ± 21 and 303 ± 26 Ma (Li et al. 1999).

The orebodies occur in silicified zones, represented by a total of 11 ore veins, arranged in three ore belts or zones (Fig. 6.23). The south ore belt is the most

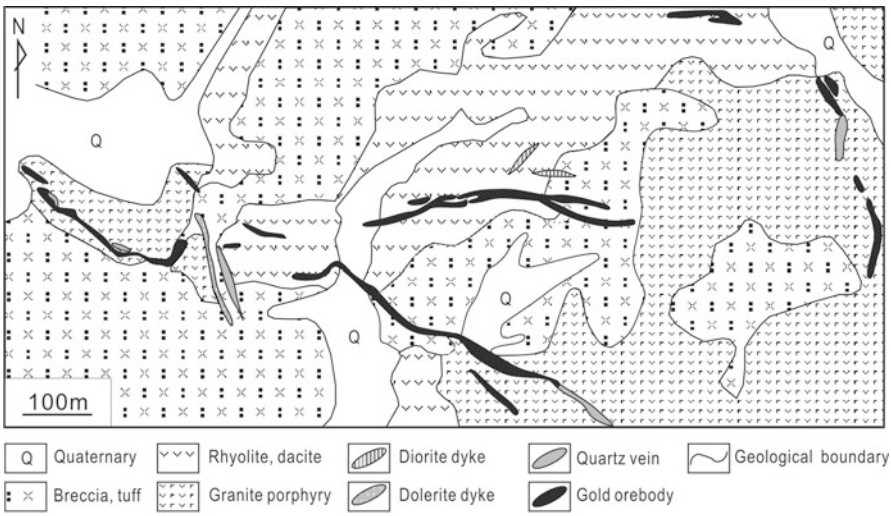

Fig. 6.23 Simplified geology and ore zones of the Mazhuangshan Au deposit, see text for details. (After Li et al. 1999)

important, with orebodies occurring near and within the rhyolitic porphyry. The largest ore zone is 530 m long, 5–6.5 m thick (up to 14 m) and 350 m deep, dipping NE with angles of 35–75°, and an average gold grade of 7.9 g/t. The north ore belt is 300 m long, 22.5 m thick and 150 m deep, with a Au grade of 7.9 g/t, a Ag grade of 20–50 g/t, up to 287 g/t. The west ore belt is 370 m long, comprising small orebodies tens to >100 m long, 1–3 m thick and less than 150 m deep.

Ore minerals are mainly native gold, electrum, pyrite, chalcopyrite, arsenopyrite, galena and sphalerite (Jing and Xu 1997). The content of sulphides in the ores is generally less than 3 %. Gangue minerals are quartz, sericite, calcite, kaolinite, feldspar and pyrophyllite. Main wallrock alteration minerals include silica, sericite, pyrite, kaolinite, pyrophyllite and chlorite. Gold minerals are mainly native gold, followed by electrum, as irregular grains (up to 0.05–0.1 mm) or as arborescent filaments. Most of the gold grains are intergranular, followed by gold deposited in microfissures or cracks.

Homogenisation temperatures of fluid inclusions in quartz range from 250 to 180 °C, with salinity of 16.2–7.5 wt % NaCl equiv, and average 9.6 wt % NaCl eqv. The ore-forming fluid is rich in Na^+, K^+ and Cl^-; whereas volatiles in the fluids are mainly H_2O, followed by CO_2 (Jing and Xu 1997).

Jing and Xu (1997), Chen et al. (2000), and Li and Liu (2002) studied the stable isotopic composition of the fluids. These authors reported that the $\delta^{18}O_{water}$ values are from 1.1 to 2.4 ‰, with δD values of between −93 and −106 ‰, suggesting that the ore-forming fluids are mixture of magmatic and meteoric waters. The $\delta^{34}S$ values of pyrite in the ores range from 4.5 to 8.0 ‰, and average 6.0 ‰, suggesting that the sulphur may have been sourced from a mix of igneous rocks and sulphate-bearing

rocks. The Rb-Sr isochron age of fluid inclusions in quartz from No. 2 orebody is 298 ± 28 Ma (Li et al. 1999), slightly younger than those of the granitic porphyries.

The Mazhuangshan gold ore-system is spatially and genetically associated with subvolcanic felsic porphyries. It was formed by low temperature-medium salinity magmatic and meteoric waters fluids. The presence of kaolinite and pyrophyllite is an indication that it is a high-sulphidation (HS) epithermal system and not a LS-type as suggested by in previous researchers (e.g. Qin et al. 2002).

6.3.3 Gold Lodes

Gold lodes are particularly common in the Tianshan, Junggar and Altay fold belts. Many of these lodes have been classified as orogenic (Rui et al. 2002), defined by Groves et al. (1998) as "*coherent group of deposits*" consistently found in collisional orogens with the mineralisation hosted in a variety of lithologies metamorphosed to lower-upper greenschist facies, and less commonly to lower amphibolite facies. The deposits occur within high strain zones in brittle (lower greenschist facies), brittle-ductile structures (mid-upper greenschist facies) to ductile (amphibolite facies). Many of the orogenic deposits have a spatial relationship to igneous rocks, while for others there is no clear connection with igneous activity. This is certainly the case for the CAOB fold belts of NW China, where for several Au lodes the relationship with igneous rocks is either not clear or unknown for lack of adequate investigations, whereas for others a spatial link with granitic intrusion is well established, but a genetic connection remains elusive. Thus, the difference between orogenic lodes and intrusion-related lodes in areas of deformation (e.g. strike-slip zones; see Pirajno 2010) remains conjectural, at best. Henceforth, these mineral systems are referred to as gold lodes, avoiding the orogenic or intrusion-related qualifiers.

In the southern Altay fold belt, Au lodes are distributed along second order faults within 5–10 km of the crustal scale Irtyish fault zone. Similarly, in the West Junggar fold belt, more than 300 lode deposits and occurrences are distributed along the Dalabute fault zone, where they have been mined since the Ming dynasty in the mid thirteenth century. In the East Junggar, lode deposits follow the Karamay fault for about 400 km, where they are generally worked by local people. In the Tianshan, lode Au deposits abound, and for many the spatial links with granitic intrusions are well displayed, as is the case for the Kanggurtag deposit. Below, a selection of the better known and economically more important Au lode deposits in NW China are described.

6.3.3.1 Western and Eastern Tianshan (Kanggurtag Ore Belt)

In the Western Tianshan, about 100 km southwest of Urumqi, a gold lode district called Wangfeng-Tianger-Saridale, is structurally controlled by east-west and

northwest-trending shear zones that parallel the east-west-trending crustal scale North Tianshan Fault. Rui et al. (2002) reported that the Wangfeng deposit contains at least 19 ore zones, consisting of quartz veins and stockwork veinlets in footwall rocks, with a gold resource estimated at ca. 2.4 tonnes, and the ores are in silicified, ductile shear zones, typically with 1–2 % pyrite, with grades that decrease with depth, from 18 g/t in the upper levels to 1.4 g/t in the lowest levels. According to a more recent work (Zhu et al. 2007), the part of the North Tianshan Fault hosting the Wangfeng-Tianger-Saridale district, is referred to as Tianger (Bingdaban) shear zone, with about 20 orebodies (or deposits), totalling proven Au reserves of 15 tonnes, is most likely the same one mentioned in Rui et al. (2002), as Wangfeng deposit. Other auriferous quartz vein lodes in the Tianger (Bingdaban) shear zone include Sawayaerdun, Bulong and Dashankou. Rb-Sr isochron ages have been determined for Sawayaerdun (342–246 Ma) and Dashankou (354–344 Ma) (Chen and Li 2003). The Tianger (Bingdaban) shear zone strikes east-west for about 100 km, dips to the north at about 80° and is from 500 to 2,000 m wide. Zhu et al. (2007) consider this shear zone as part of thrust that separates a Silurian (442 Ma) gneissic granite from Carboniferous sedimentary rocks, with the latter on the north side of the thrust. The shear zone typically displays mylonitic fabrics and hosts disseminated sulphides. The auriferous quartz veins too exhibit mylonitic fabrics. A brittle fault zone is located within the Tianger (Bingdaban) shear zone, characterised by brecciated mylonitised granite and sulphide-bearing quartz veins. The Tianger lode Au deposit contains eight orebodies with an estimated total resource of about 8 tonnes, with Au tenors averaging 7 g/t. The Tianger Au lode deposit is oriented parallel to the stretching and lineation fabrics of the host shear zone. Zhu et al. (2007) identified two ore types: gold- and pyrite-bearing mylonitised granite and gold-bearing sulphide-quartz veins that cut the former. These researchers also identified a paragenetic sequence, from unmineralised pre-shear and mylonitic stages, to ore-formation stage, to post-ore stage. The ore-formation stage is characterised by two substages. The first stage is represented by the ductile fabrics containing auriferous sulphides as well as sheared pyrite-bearing quartz vein. Thus, the Au mineralisation is associated with sulphides and varying degrees of pyritic alteration. Pyrite is the main sulphide phase at Tianger, associated with minor amounts of pyrrhotite and chalcopyrite. Gold grains (up to 40 μm across) occur as inclusions and in microfractures in pyrite, pyrrhotite and quartz. The second stage is characterised by pyrite-biotite veinlets cross-cutting the mineral phases of the first stage. Zhu et al. (2007), in addition to detailed mineral chemistry of the shear zone alteration minerals (amphibole, muscovite, biotite), also carried out Ar-Ar and Rb-Sr age determinations of muscovite and wall rocks, respectively. The Ar-Ar isotopic data yielded weighted mean ages ranging from 220.6 ± 0.6 to 220.3 ± 0.6 Ma, whereas Rb-Sr isotopic system yielded an isochron ages on muscovite of ranging from 222 ± 1.2 to 220.9 ± 0.8 Ma, with high initial $^{87}Sr/^{86}Sr$ ratio of 0.7309 and 0.7294. Sulphur isotope systematics performed on auriferous pyrite returned $\delta^{34}S$ values from +16.5 to 11.2 ‰, averaging +14.01 ‰. Integrating field observations with geochemical and isotopic data, Zhu et al. (2007), developed an interesting model of the P-T path for the Tianger shear zone and related formation of Au lodes, shown in Fig. 6.24. Gold deposition in the shear zone occurred during the

latest stage (Stage III), an observation consistent with other shear-zone-hosted lode deposits (see Pirajno 2010, 2009), which typically follows the change or transition from ductile to brittle deformation regimes. The latter, again typically, is associated with greenschist facies metamorphism (400–350 °C), a favourable temperature range for the deposition of Au from hydrothermal solutions. Ore genesis for the Tianger Au lode system, as proposed by Zhu et al. (2007) is as follows. Hydrothermal fluids were probably sourced from depth and channelled along the shear fabrics during ductile and brittle deformation phases. This is shown by two generations of pyrite veins: an earlier stage (pyrite-quartz) is associated with ductile fabrics, whereas the late stage pyrite-biotite veins are not deformed and are likely part of the brittle deformation phase. Shearing and deformation post-date the granitic rocks in the area and age data show that ore-formation must have taken place at about 224 Ma. Similarly, other lode systems in the same region, such as the above-mentioned Dashankou and Sawayaerdun, have Ar-Ar ages from 210 to 207 Ma. This ore-forming time for lode deposits as well as rare metal pegmatites (Sect. 6.3.8) is common in the northern Xinjiang area (Fig. 6.11; Pirajno et al. 2009). Textural features of quartz grains in ore-bearing quartz veins suggest that the activity of silica-saturated fluids, probably generated during metamorphism and/or deformation. On the other hand, geochemical differences (Au contents and REE patterns) between pyrite in mylonitised granitic rocks and pyrite from wall rocks, led Zhu et al. (2007) to conclude that there was multi-stage hydrothermal activity (Fig. 6.24).

The Sawayaerdun lode deposit, hosted in turbidite facies rocks metamorphosed to greenschist facies, consists of 24 orebodies, distributed into four ore zones (Liu et al. 2007; Chen et al. 2012a). Ore zone No. IV is the largest extending for about 4,200 m along strike, between 15 and 48 m wide, with reserves estimated at about 62 t of Au. Ore grades range from 2 to 3 g/t, but locally can reach up to 27 g/t. Furthermore, high grades of Ag (20–70 ppm), Sb (up to 13 %) and W (150 ppm) are also recorded (Liu et al. 2007). The ore minerals include pyrite, arsenopyrite, native Au, stibnite, pyrrhotite, distributed within five alteration assemblages. There are four ore styles: quartz veinlets, quartz stockworks, altered carbonaceous phyllite and silicified siltstone. Fluid inclusion studies carried out by Chen et al. (2012a), revealed three main types of fluid inclusions, all of liquid-vapour (L + V): $H_2O + NaCl$, $H_2O + NaCl + CO_2$ and CO_2. Homogenisation temperatures range from 111 to 415 °C and salinities (wt % NaCl equiv) from 0.7 to 17.5. Three paragenetic stages have been recognized (Chen et al. 2012a): early barren and high temperature stage with pyrrhotite-bearing quartz veins, a middle stage with quartz-polymetallic sulphides as veinlets and stockworks and a late barren and low-temperature stage with carbonate-quartz veins. Gold is mostly associated with the middle stage and temperatures from about 270 to 220 °C and at depths of 4–8 km.

In the Eastern Tianshan, the Kanggurtag ore belt, within the Kanggurtag Shear Zone, contains a series of mineralised zones and lodes, about 60 km east of the Shiyingtan epithermal system (Figs. 6.6 and 6.26). The Kanggurtag belt also contains replacement-type Fe-Cu and Au deposits, hosted in volcanic rocks of the Yamansu and Aqishan Formations. Igneous intrusive rocks in the ore belt include syn- to late-orogenic monzonite and granite and post-orogenic alkali granite and syenite. Lode

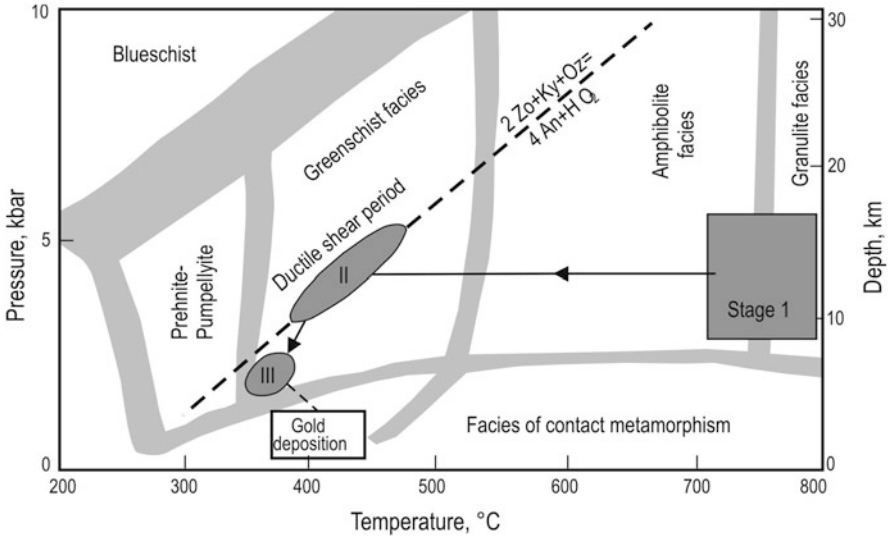

Fig. 6.24 Possible P–T path for the evolution of the Tianger shear zone and associated lode Au deposit. Stage I occurs at depth greater than 10 km, at amphibolite facies, Stage II is represented by zoisite amphibolites in mylonitized granite; P–T conditions were constrained by metamorphic facies and the reaction of 1 albite + 4 anorthite + $2H_2O$ = 1 pargasite + 2 zoisite + 2 quartz; Stage III represents the brittle deformation following the ductile shear period. *An* anorthite, *Ky* kyanite, *Qz* quartz, *Zo* zoisite. (After Zhu et al. 2007 and references therein)

Au deposits are localised in ductile shear zones. One of these lodes is the Kanggurtag (Kangguer) Au deposit, with base metal credits (Cu, Pb and Zn) and hosted in volcanic rocks of the Aqishan Formation. Nearby deposits include Matoutan, Dadongou and Yuanbaoshan. The Kanggurtag deposit consists of a 1–2 m-wide quartz vein extending approximately to a depth of 500 with a strike length of 1,000 m. The mineralisation is distinctly zoned, with the upper 100–150 m being essentially Au-rich (tenors range from 5 to 7 g/t), grading downward through an Au + Cu zone below 150 m to a Pb + Zn zone in the deeper levels (>300 m), with grades that may reach up to 5 % Pb, 10 % Cu and 10 % Zn (Rui et al. 2002). The mineralised vein is surrounded by a 20-m-wide alteration envelope, in which Au grades of between 0.5 and 1.5 g/t, and locally up to 5 g/t occur from 1 to 3 m from the vein margins into the altered wall rocks. The ore minerals comprise pyrite, chalcopyrite, magnetite and lesser amounts of sphalerite, galena, Ag sulphosalts and barite (Ruit et al. 2002). Li et al. (1998) used the Rb-Sr system to date the host rocks and a nearby tonalite stock. Ages range from 300 to 280 Ma; whereas a U-Pb date of the tonalite yielded an age of 275 Ma. Li et al. (1998) suggested that mineralising events may have occurred some 20–30 Myrs later that the tonalite intrusion. Stable isotope measurements, reported in Rui et al. (2002), show $\delta^{18}O$ values ranging from 11.3 to 17.7 ‰ and δD values of fluid inclusions from −53 to −61 ‰. Sulphur isotope of sulphides yielded $\delta^{34}S$

values of −0.9–3.3 ‰. Rui et al. (2002), pointed out that results these stable isotopic compositions cannot distinguish between magmatic and metamorphic fluids.

Pirajno et al. (1997), on the basis of field observations, suggested that the Kanggurtag mineralised event was followed by tectonic activity, during which deformation and new mineral phases may have been introduced, or pre-existing phases redistributed. Wall-rock alteration and metal zoning (from Au near the surface to base metals at depth) suggest that the deposit was originally a vein-type low-sulphidation epithermal system.

6.3.3.2 West Junggar

More than 300 Au lode deposits as well as placer deposits, with a total resource of about 75 tonnes have been reported in the West Junggar area (Rui et al. 2002). Gold lodes are present in the Baogutu district, on the southeastern side of the Dalabute Fault (No. 5 in Fig. 6.12), where An and Zhu (2009, 2010) in a recent work on the Baogutu Au lode deposit, detected the presence of Sb minerals, including stibnite, ullmannite, tetrahedrite, as well as native As and Sb and, co-existing with chalcopyrite and pyrrhotite, or as isolated grains enclosed in calcite veins. Most of the lode deposits are in the Hatu district within a zone about 70 km long and 20 km wide, on the northwest side of and along the Dalabute fault and associated splays (Fig. 6.12). The Hatu district alone contains approximately 200 Au occurrences and deposits, within a 60-km radius of the Hatu mine. The Hatu district includes the Hatu, Qiqiu No. 1, Qinyiqiu No. 2 and Saourtuhai No. 1 deposits. The mineralisation is structurally controlled and spatially associated with the east-northeast-trending Anqi and Hatu faults. The Hatu Au occurrences and deposits are distributed within five zones. The No. 1 Zone is along the Anqi Fault and includes the Hatu mine proper; the No. 2 Zone includes the Saourtuhai No. 1 deposit; the No. 3 Zone contains a number of occurrences (e.g. Huang, Gezhitoug) that are spatially associated with granitic rocks; the No. 4 Zone is some 60 km to the west and includes a deposit called Bozate; the No. 5 Zone includes 6 or 7 occurrences south of Hatu.

The Hatu Au mineralisation is hosted in quartz veins emplaced within Carboniferous basaltic (lavas and tuffs) and sedimentary (siltstone and sandstone) rocks. The veins extend for about 100 along strike, are up to 5 m thick, have grades of between 5 and 10 g/t Au, have a NW trend and are spatially associated with the east-northeast-trending Anqi Fault. Other veins sets are present in the area, trending east-west, northeast and north-south, but these are either not mineralised or contain uneconomic mineralisation. The average grade of the Hatu deposit is approximately 3 g/t (cut-off grade is 1.5 g/t), with a remaining resource of about 600,000 t of ore. Gold is free-milling; minor quantities of sulphides are present and include arsenopyrite and pyrite. Hydrothermal alteration haloes are not well-developed, but where present they contain chlorite, sericite, Fe-carbonate and sulphides. Samples collected from the ore zone (−320 level), reveal a pervasively altered volcanic rock (texture still recognisable), with several generations of quartz + carbonate material as bands and veinlets, and disseminated pyrite euhedra and anhedral chalcopyrite. Fluid inclusion studies

by Wang et al. (2005c) conducted on quartz vein material, yielded homogenisation temperatures ranging from 358 to 210 °C, whereas fluid inclusions in pyrite gave temperatures ranging from 385 to 179 °C. Wang et al. (2005c) observed two main temperature ranges for both pyrite and quartz fluid inclusions: 390–340 and 287–179 °C, possibly showing two stages of Au metallogenesis, with one high-temperature fluid, probably of magmatic origin, overprinted by a second, lower-temperature fluid. This is reflected in the mineral assemblages of quartz-pyrite in white quartz veins with low Au grades (high T stage) and quartz-pyrite-arsenopyrite in grey-white quartz veins with high Au grades (low T, overprinting fluid).

The Saourtuhai (or Sartuohai) district (Fig. 6.12) is within ophiolitic and metavolcanic rocks along the Dalabute Fault, which provide favourable source rocks for gold. Saourtuhai No. 1 is a small, but rich (30 g/t) deposit and has been exploited by artisanal workers. Details of grades and resources were not available at the time of the field visit (2003). Samples collected from an alteration zone show that the host rocks contain carbonate, quartz, chalcedonic quartz and a white mica (fuchsite probably; Pirajno unpublished data). These minerals form an irregular assemblage of interlocking grains. No texture is discernable and it is likely that this rock is the product of pervasive hydrothermal alteration of an unknown protolith.

6.3.3.3 Altay and East Junggar

The Altay and Eastern Junggar are well endowed with lode and placer Au deposits, but not well documented in the English literature. In the Altay belt, Au lodes are distributed along the crustal scale Irtysh Fault (Figs. 6.5 and 6.11), which was likely a first-order control for mineralising fluids. Lode Au deposits include Duolanasayi, Saidu, Taerde, and Kabenkulke, associated with felsic granitic rocks, sedimentary and volcaniclastic rocks. Duolanasayi is the largest of these, hosted in Mid-Devonian clastic rocks at contact with limestones, and comprising a number of ore lenses distributed along a 20 km long and 10 km wide zone. Hydrothermal alteration of wall rocks consists of assemblages of quartz, pyrite, sericite, carbonate and chlorite. Skarn calc-silicate minerals are present where the lodes cut the limestone rocks. In fact, hornfels are associated with a 290 Ma tonalite intrusion, cut by granodiorite and granite dykes (Rui et al. 2002). In the Eastern Junggar there are many small Au lodes, mostly distributed along the Karamay Fault, and generally exploited by artisanal workers. Of these, worthy of note are Qingshui, Nanmingshui, Jinshan and Adake, all hosted in metasedimentary rocks (Rui et al. 2002).

6.3.3.4 Intrusion-related Au Lodes in Gansu Province

This mining area is located in Gansu Province, only a few kilometres from the border with Xinjiang, about 1 km north of the highway linking the towns of Hami and Liuyuan (Gansu). The area is underlain by sedimentary rocks (shale with thin limestone beds and sandstone) of Permian and Cambrian-Silurian ages, intruded by

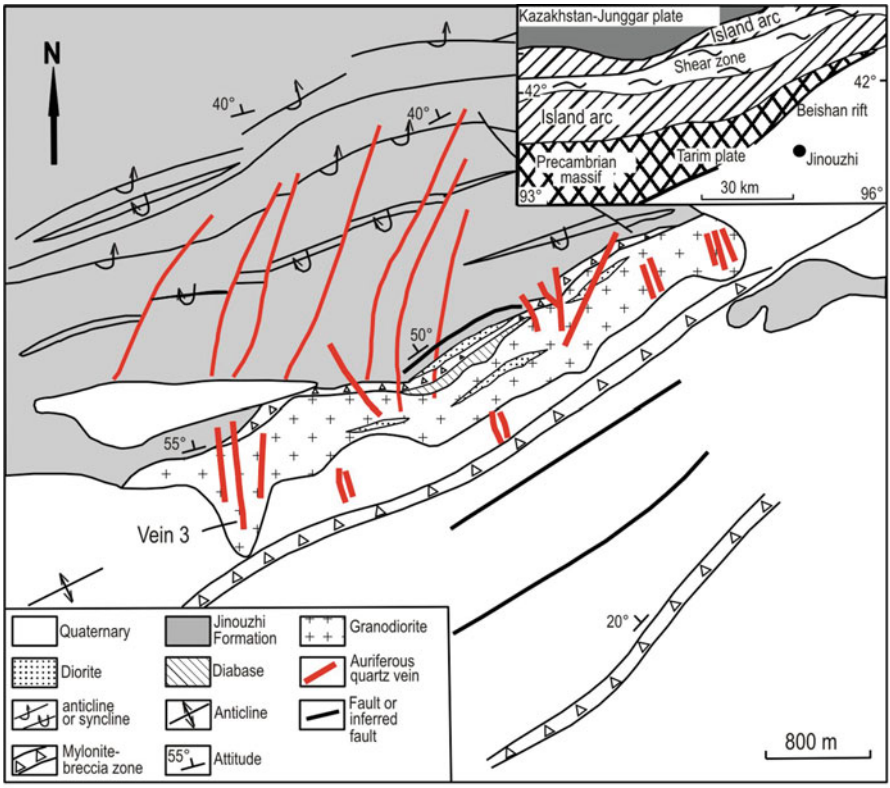

Fig. 6.25 Simplified geology of the Jinhouzi area and distribution of auriferous quartz veins. (After Liu et al. 2003a)

granodiorite and monzogranite plutons of Devonian age. A simplified geological map of the area is shown in Fig. 6.25. The general structural grain of the country rocks is northeast.

The Jinouzhi (also spelt Jinwozi) Au deposit (Pirajno unpublished data; Liu et al. 2003a) is hosted in granitic rocks (quartz-diorite, granodiorite and monzogranite) of Permian age that have intruded Upper Devonian sedimentary rocks of the South Tianshan Terrane. The deposit consists of north-trending vein systems, which occur in a zone approximately 5 km long. A single vein may be up to 1.5 km long. The No. 3 orebody contains a number of veins extending over a zone of about 400 m. The veins are steeply dipping towards the west and extend to depths of approximately 200 m; other veins are rootless and blind (do not outcrop). Vein widths range from a few cm to 5–6 m. The minimum mining width is 1 m, with grades of between 6 and 8 g/t Au. Assays on single intersections may range from 5.12 to 26 g/t Au over widths of 25 cm to 1.2 m respectively. Underground the veins exhibit a laminated structure (ribbon quartz), between which are narrow septa of country rocks (evidence of crack-seal

mechanism of infilling). Fluid inclusions studies by Liu et al. (2003a) from two veins (Nos. 3 and 210), gave homogenisation temperatures ranging from 320 to 240 °C and from 300 to 220 °C, peaking around 300–260 and 280–240 °C, respectively, with salinities ranging from 3 to 6 and 8–14 NaCl wt % equiv., respectively. Rb-Sr dating of fluid inclusions in quartz yielded ages of 230–228 Ma. Sulphur isotopic composition of sulphide separates yielded $\delta^{34}S$ values from 3.1 to 6.3 ‰ in galena and 5.6–7.9 ‰ in pyrite (Liu et al. 2003a). These data, together with $\delta^{18}O$ and δD, also reported by Liu et al. (2003a), suggest that the fluids may have originated from degassing felsic magmas, but mixed with meteoric fluids.

Alteration haloes may or may not be present. Where present, this alteration does not extend for more than 2–3 m from the vein margins. Hydrothermal alteration phases include quartz, sericite and pyrite. The ore minerals are native gold, electrum, pyrite, chalcopyrite and galena. The last two tend to infill late microfractures and contain inclusions of native gold particles, ranging in size from 40 to 700 µm. There is no apparent vertical zonation, but some veins have Ag-rich zones (possibly associated with galena). The sulphides occur as stringers in the vein quartz material.

The vein material of Zinouzhi is characterised by an assemblage of coarse, interlocking and highly strained quartz crystals, clouded by numerous fluid inclusions.

6.3.4 Iron Skarns

Iron skarn deposits are present in both the East Tianshan and Altay orogenic belts. For the East Tianshan, Mao et al. (2005) divided the skarn deposits into Fe-Cu and Cu-Ag-Pb-Zn types, emphasising that the latter are not VMS type. Iron-rich skarns in the East Tianshan include the following: Yamansu, Weiquan, Bailingshan, Heijianshan, Chilongfeng, Hongyuntan, Aqishan, Heilogfeng, Shuangfengshan and Shaquanzi (Fig. 6.26). Most are small, but Yamansu has been economically mined for many years. In the Altay orogenic belt, Mengku and Qiaoxiahala Fe deposits are economically important, as well as somewhat controversial in their origin. The Abagong Fe-P deposit also in the Altay, still being mined at the time of writing, is considered as a Kiruna-type ore system and is briefly described here. The distribution of skarn-type and Kiruna-style mineral deposits is presented in Fig. 6.27.

6.3.4.1 Yamansu and Weiquan

The Yamansu Fe-Cu skarn deposit is one of the largest in NW China, with 32 Mt at 51 % Fe and 20,000 t at 0.06 % Cu (Mao et al. 2005). The mineralisation is hosted by Lower Carboniferous bimodal volcanic, clastic and calcareous rocks of the Yamansu Formation. Around the Yamansu open pit (Fig. 6.28), the Yamansu Formation comprises andesitic pyroclastic rocks, limestone, keratophyre and other felsic rocks. Skarns are developed in limestone rocks that are intercalated with felsic and intermediate volcanic. About 500 m southwest of the orebodies, a subvolcanic

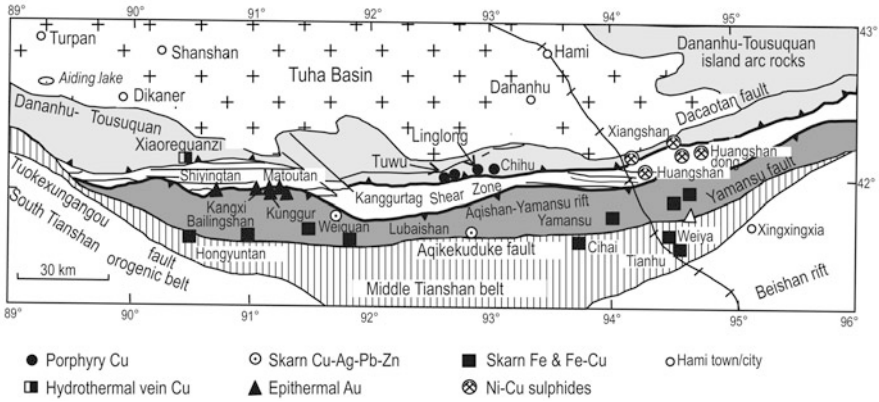

Fig. 6.26 Simplified geology of the East Tianshan region, showing distribution of mineral systems (porphyry, skarns, epithermal, magmatic); details for these deposits in text, see also Fig. 6.6. (Modified after Mao et al. 2005)

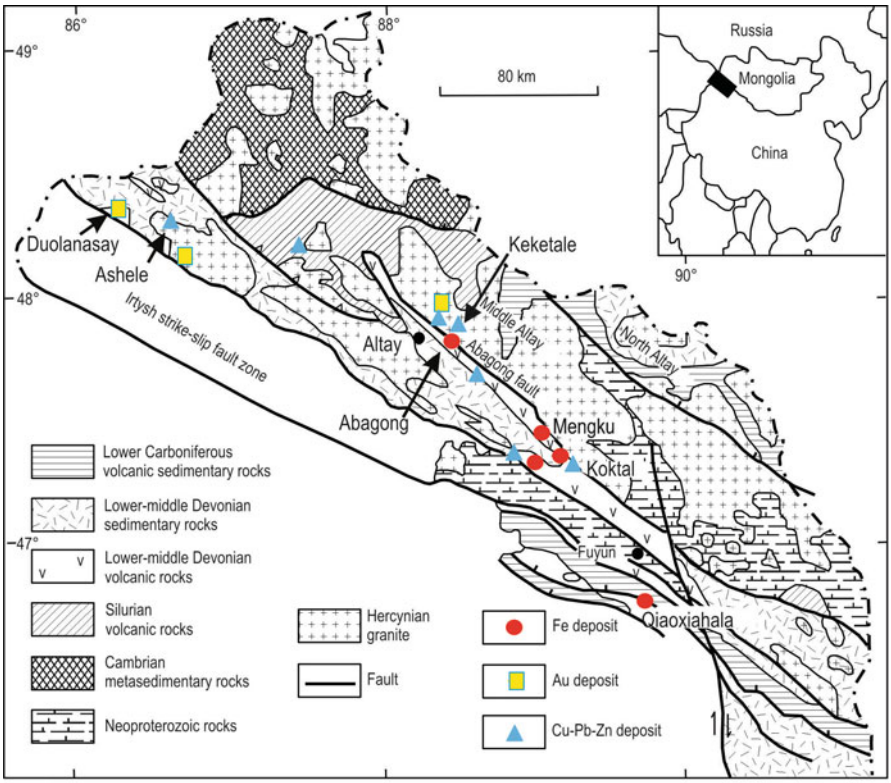

Fig. 6.27 Regional geology of the southern Altay, distribution of selected lode Au, VMS deposits and Fe deposits (positions are approximate). (Modified from Xu et al. 2010 and references therein)

Fig. 6.28 Yamansu open pit: remnant blocks of marmorised carbonate rocks (*white*) embedded in magnetite skarns (*dark rocks*)

pyroxene-diorite porphyry intrusion is present and gravity data suggest that other plutonic rocks may exist at depth (Mao et al. 2005). The Yamansu ore minerals include magnetite, hematite, pyrite and chalcopyrite, forming disseminated and massive orebodies. Prograde skarn minerals are grossularite-andradite, diopside-hedenbergite, epidote, vesuvianite and wollastonite, whereas retrograde skarn assemblages consist of actinolite, chlorite, sericite and calcite. Fluid inclusion studies show homogenisation temperatures of around 340–330 °C for magnetite and 220–150 °C for pyrite, with salinities of between 12.9 and 2.7 wt % NaCl equiv. (Mao et al. 2005 and references therein). Whole rock K-Ar ages have a range from ca. 360 and 190 Ma, whereas a Rb-Sr isochron age of ca. 286 Ma was obtained from mineralised quartz veins from a similar skarn deposit (Bailingshan), also in the Aqishan-Yamansu rift belt (Mao et al. 2005).

The Aqishan-Yamansu belt in the East Tianshan, contains several other skarn systems with a different metal association than that at Yamansu. These are polymetallic skarns, exemplified by the Weiquan Cu-Ag-Pb-Zn deposit, hosted in felsic and carbonate rocks of the Mid-Carboniferous Tugutubulake Formation (Fig. 6.26). The carbonate rocks occur as lenses intercalated with the felsic volcanic rocks and are pervasively altered to calc-silicate skarns, within which are the polymetallic ores. Diorite dykes and a biotite granite intrusion of Late Carboniferous to Early Permian age are present near the skarns. Minerals that compose the skarns include andradite, diopside, vesuvianite, and epidote (prograde assemblage) and actinolite, fluorite and chlorite (retrograde minerals).

At surface the Weiquan deposit is 250 m long and up to 24 m wide, with a distinct metal zoning from Ag-Pb-Zn to Cu-rich at depth. Near the surface is a supergene ore with malachite, covellite and jarosite. Copper grades in the oxidised ore range from 0.2 to 36.7 % and in the primary ore from 0.2 to 4.1 %, with an average Ag grade of 466 g/t and 2.7 % combined Pb + Zn (Mao et al. 2005). The ore-forming age is fairly well constrained by a U-Pb SHRIMP age of ca. 290–280 Ma and a $^{39}Ar/^{49}Ar$ age of ca. 277 Ma determined on skarn amphiboles.

6.3.4.2 Mengku

The Mengku Fe skarn deposit is located in the Altay mountains, within a metallogenic province that includes VMS deposits (see below) and the above-described Au lodes (Fig. 6.29). The Mengku Fe deposit had resources estimated at about 110 Mt of ore with grades ranging from 24 to 57.6 % (Wang et al. 2003), but more recent data indicate a total resource of 200 Mt (Yang et al. 2010), with one orebody (No. 1) containing 35 Mt grading 41 % Fe (Xu et al. 2010). Wang et al. (2003b), Yang et al. (2010) and Xu et al. (2010) reported on this deposit and the following is taken from these authors.

The Mengku deposit is on the nortwestern limb of anticline of Upper Silurian rocks of the Kulumuti Group and Lower Devonian rocks of the Kangbutiebao Formation. The Kulumuti Group is 6,000 m thick and comprises metasandstone, phyllite, slate, biotite schist, two-mica schist, gneiss and migmatite. In the area, the Kangbutiebao Formation totals 1,300 m in thickness and comprises brown marble, banded impure marble (Lower Member), hornblende granulite, leptite, hornblende gneiss, amphibolite (Middle Member) and the main host of the Fe ore (Upper Member), which consists of hornblende-biotite-quartz schist, marble, hornblende-albite granulite and hornblende gneiss (Chai et al. 2009). Also in the host sequence is a Na-rich metarhyolite (Wang pers. comm., 2003b). The upper units of the Kangbutiebao Formation consist of a 700 m-thick sequence of metasandstone, biotite-quartz schist, hornblende-garnet schist, marble and felsic metavolcanic rocks. Granitic rocks of assumed Hercynian age are exposed in the deposit area, comprising gneissic granite, alkali-feldspar granite, biotite granite, two-mica granite and quartz diorite. One of the local granites is the Mengku pluton, with U-Pb zircon ages of ca. 404–400 Ma (Yang et al. 2010). The Mengku deposit comprise 29 orebodies, ranging in shape from podiform to lenticular to irregular and striking 120–110°. The Fe ore is arranged in a synclinal structure within the northeastern limb of the above-mentioned regional anticline (Fig. 6.29), where it forms at least 20 stratiform lenticular orebodies. The Fe mineralisation is characterised by banded, massive, disseminated, brecciated and veins styles, with the following recognised ore types: diopside-magnetite, garnet-magnetite, diopside-amphibole-magnetite, quartz-albite-magnetite-hematite, apatite-magnetite and quartz-pyrite-magnetite. The main ore minerals are magnetite, pyrite, chalcopyrite and pyrrhotite. The wallrocks exhibit skarn assemblages, such as garnet, diopside, actinolite, tremolite, scapolite, epidote and chlorite. At least

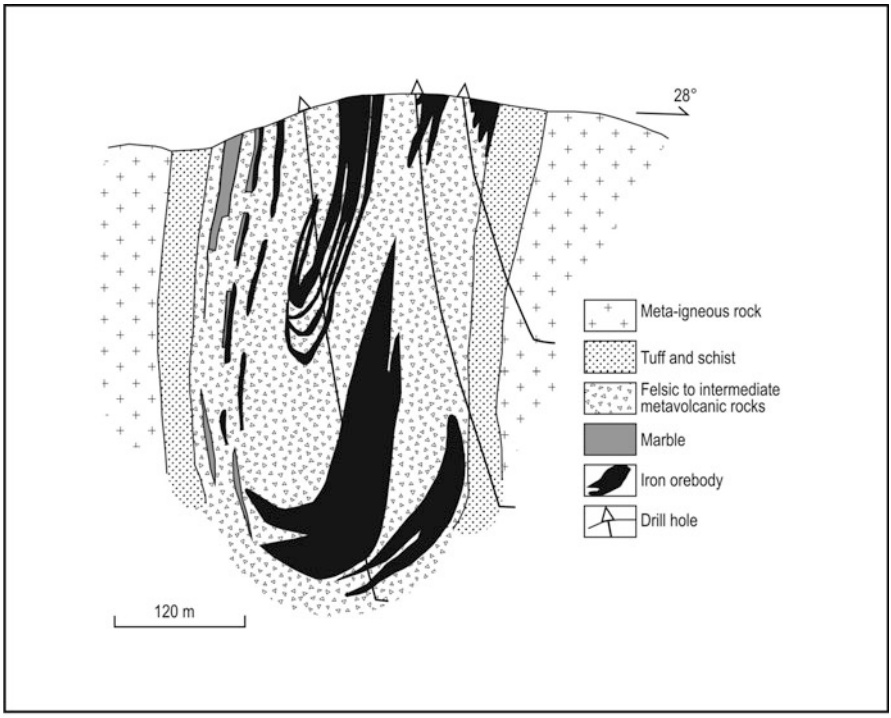

Fig. 6.29 Cross-section of the Mengku Fe orebody. (After Wang et al. 2003b)

four stages of skarn have been recognised (Xu et al. 2010), namely: (1) prograde stage with clinopyroxene-garnet-albite-scapolite-apatite; (2) retrograde stage with magnetite-clinopyroxene-garnet-amphibole-scapolite-apatite-epidote-chlorite-quartz; (3) sulphide stage with pyrite-chalcopyrite-pyrrhotite-garnet-chlorite-quartz-calcite; (4) supergene stage with hematite-goethite-malachite-quartz-calcite. Sulphur isotopic compositions show $\delta^{34}S$ values in the range of 1.9–14.0 ‰. Fluid inclusion data, as reported by Wang et al. (2003b and references therein) indicate trapping temperatures of about 426–362 °C. Further work on fluid inclusions by Xu et al. (2010), revealed three types of inclusions in garnet: liquid-rich, vapour-rich and vapour only. Homogenisation temperatures of fluid inclusions in garnet range from 500 to 348 °C, with salinities ranging from 12.9 to 9.6 wt % NaCl equiv; in clinopyroxene range from 490 to 241 °C, with salinities of 13.0–10.7 wt % NaCl equiv. Liquid-vapour fluid inclusions in quartz gave homogenisation temperatures ranging from 382 to 166 °C, with corresponding salinities of 13.0–9.6 wt % NaCl equiv. In summary, fluid inclusion studies indicate a fluid evolution from high temperature and moderate salinity of prograde skarn, to moderate temperature and high salinity in the retrograde stage, to finally low temperature and salinity in the sulphide stage. Stable isotopic data (O-D) obtained from quartz and calcite of the sulphide stage, plot half way

between the magmatic water box and the meteoric water line (Xu et al. 2010). On the basis of fluid inclusion data and isotope systematics, the Mengku skarn is likely to have originated from fluids of magmatic origin, derived from granitic intrusions, although abundant meteoric water was involved in the ore fluids of the retrograde and sulphide stages.

The Mengku iron skarn, and probably other skarns in the same metallogenic belt (Fig. 6.27), were formed in a continental margin setting, during Early-Mid Palaeozoic subduction under the Altay microcontinent (Yang et al. 2010). The intrusion of the Mengku granite (400 Ma), north of orebody No. 1 (404 Ma) and the Qiongkuer granite (399 Ma) in the Mengku area into the Kangbutiebao Formation (Yang et al. 2010), resulted in the development of skarns near and along the contacts of the plutons, apophysis and dykes with the Kangbutiebao Formation volcanic rocks and limestone. Following the development of these skarns, iron oxides (mostly magnetite) precipitated from the hydrothermal fluids to form the Mengku skarn-type iron deposit.

6.3.4.3 Qiaoxiahala

The Qiaoxiahala Fe-Cu-Au mineralisation is located along the Irtysh Fault zone, about 100 km southeast of the Mengku Fe deposit and about 137 km southeast of Abalong deposit (see below and Fig. 6.27). The nature and origin of this deposit have been controversial and poorly understood for many years. Wang et al. (1999) labelled Qiaoxiahala as a massive sulphide deposit, Chen et al. (2005a), proposed that the deposit is associated with picritic basalt and should be considered as new type of mineral system, Ying et al. (2006) suggested that it is an IOCG (Fe-Cu-Au deposit), whereas Chen et al. (2007), listed it as a skarn (No. 64 in Table 4.5 and Fig. 4.16). The account that follows is based on the work of the above-cited authors and my own field observations in the Altay region. The Qiaoxiahala mineralisation may have had a multistage genesis, in which the last stage may have resulted in the formation of a skarn system, as outlined below.

The host rocks are a suite of Middle Devonian mafic volcanic and volcaniclastic rocks of the Beitashan Formation. The orebodies comprise magnetite, Cu-bearing magnetite and chalcopyrite as the main ore minerals. Other, but minor, ore minerals are bornite and pyrite. Gold occurs as inclusions in these sulphides, up to 230 ppm in chalcopyrite, 395 ppm in bornite and 158 ppm in pyrite (Chen et al. 2005a). Ore grades, as reported in Chen et al. (2005a) are: 30–40 % Fe and up to 57.8 % Fe in the magnetite ores, 0.2–2.97 % Cu and 0.03–0.65 ppm Au.

The $^{40}Ar/^{39}Ar$ plateau age of hornblende from diorite in the western Qiaoxiahala area is 378.1 ± 3.6 Ma and its $^{39}Ar/^{40}Ar$-$^{36}Ar/^{40}Ar$ by stepwise heating inverse isochron age is 382 ± 17 Ma. Based on the field observation that diorite dykes cross-cut the Fe ore lenses, it is likely that the Fe ore is older than 380 Ma. The Qiaoxiahala deposit is subdivided into the western, middle and eastern sectors (Fig. 6.30). Magnetite orebodies are dominant in the western sector and are called Fe1, Fe2 etc. together with several small Cu orebodies, referred to as Cu1, Cu2 etc. In the eastern sector, Cu orebodies are relatively dominant and are numbered as I, II, III etc.

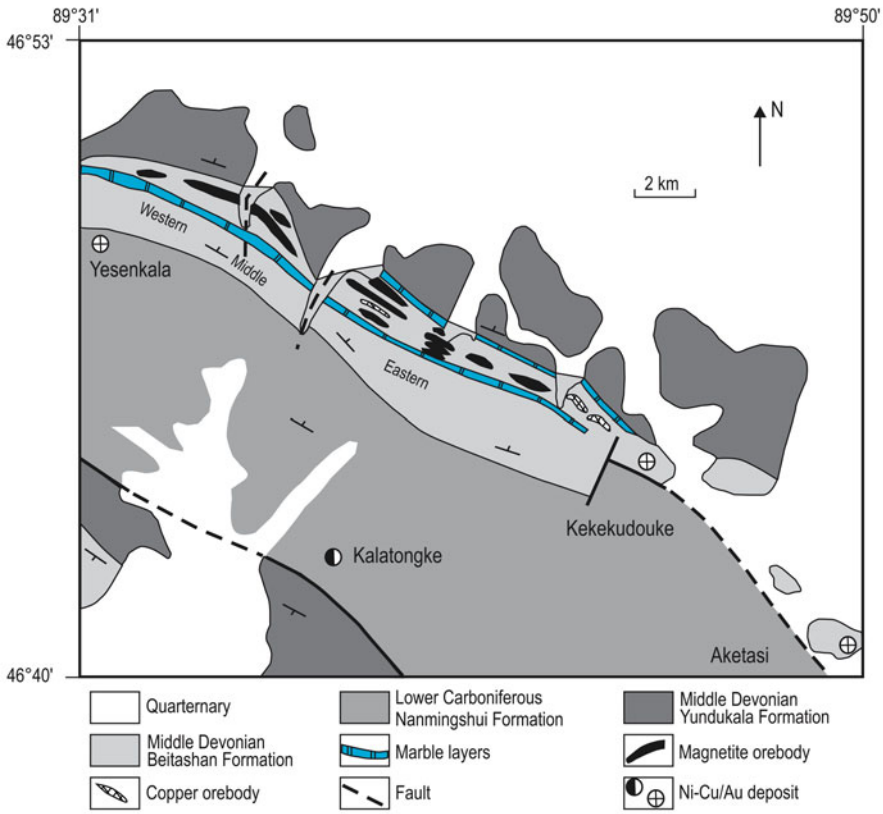

Fig. 6.30 Distribution of the Qiaoxiahala ore lenses. (Modified from Ying 2007, unpublished data; Pirajno field observations 2009)

The Fe oxide orebodies are stratiform and/or lenticular in shape and are associated with the mafic volcanic rocks. The size of the Qiaoxiahala magnetite orebodies range from 10 to 50 m in strike length, 0.5–30 m in thickness and 20–300 m in width. The dip of the orebodies is about 40–80° to the northeast. The host mafic rocks are extensively deformed and are best described as mafic schist, although from geochemical and petrographic data, picrite, olivine basalt, tholeiite basalt, and tuff have been recognised. In the mining area diorite, porphyritic diorite and porphyritic pyroxene diorite intruded the metavolcanic rocks. These intrusive rocks usually form dykes crosscutting the orebodies and therefore, as mentioned above, postdated the main phase of magnetite mineralisation. The rocks hosting the Fe-Cu-Au mineralisation show skarn style hydrothermal alteration. The alteration minerals are pyroxene, garnet, epidote, calcite, quartz, sericite and chlorite. Epidote alteration is widespread, and forms banded epidote-magnetite in the western sector. Ore styles include massive magnetite ore and massive chalcopyrite ore, banded magnetite ore and disseminated chalcopyrite ore. Textural evidence shows that the magnetite

and Cu-bearing magnetite are locally overprinted by a later phase of mineralisation, which is mainly represented by chalcopyrite. The hydrothermal alteration and mineralisation are associated with epidote-magnetite skarn, with the chalcopyrite mineralisation overprinting the stratiform Fe oxides.

Sulphur isotope systematics (Ying unpublished data 2007; Zhang et al. 1987), show a range of $\delta^{34}S$ for pyrite from +0.1 to +2.92 ‰, with an average of +1.22 ‰; $\delta^{34}S$ values for chalcopyrite range from −1.1 to +2.72 ‰, with +1.18 ‰ on average. $\delta^{34}S$ values of sulphides from Qiaoxiahala range from −1.1 to +2.92 ‰, with an average of +1.21 ‰. Compared to other sulphur isotopes from other deposits in the Altay region, Qiaoxiahala sulphur was possibly sourced from a deep-seated magma. $\delta^{34}S$ values of sulphides from Ashele (see below) change between −2.77 and 8.17 ‰, most in the range of 4–6 ‰, higher than that of Qiaoxiahala. The $\delta^{34}S$ values of sulphides from Abagong (next section) are 1.0 ‰ and those of Tiemurt are between 1.7 and +3.4 ‰, similar to Qiaoxiahala. The range of $\delta^{34}S$ of pyrite and chalcopyrite from rocks and ores in Qiaoxiahala is quite narrow, indicating a similar sulphur source for volcaniclastic rocks, skarns, veins and ores. Since sulphur in Qiaoxiahala has a magmatic source, the $\delta^{34}S$ values can indicate that the ore-bearing hydrothermal fluids were derived from the magmas that produced the volcanic and intrusive rocks. The genesis of the Qiaoxiahala Fe-Cu-Au deposit may well be related to at least two hydrothermal events. First, submarine volcanic exhalations supplying Fe and minor Cu, resulted in the deposition of chemical sediments forming layers and lenses of Fe oxides and Cu sulphides. This volcanic hydrothermal event was later overprinted by hydrothermal activity related to the dioritic intrusions, which formed skarn magnetite and chalcopyrite associated with the diorite intrusions. Again, additional mineralising stages may have affected the metavolcanic rocks and the temporal relationship to the magmetite and skarn stages is at the time of writing not known. However, it is of interest to note that locally mafic schist (picritic basalt?), exhibit pervasive alteration to Fe carbonates carrying fuchsite (Cr-bearing mica), typical of a rock known as listvenite (fuchsite-quartz-carbonate (ankerite, magnesite) rock, derived from metasomatic alteration of ultramafic rocks). Listvenites are in some cases associated with lode Au mineralisation and less commonly with Au-Sb, Co, Sb, Cu (Pirajno in press). Furthermore, the putative listvenites in the Qiaoxiahala area are locally cut by quartz stockworks with chalcopyrite and bornite sulphides, exploited by the local people for their gold content (Pirajno unpublished field data 2009; Fig. 6.31).

6.3.4.4 Abagong; A Kiruna-style Fe-P Deposit?

The Abagong magnetite-apatite deposit (Fig. 6.27) is one of several Au and Cu-Pb-Zn mineral systems (including Abagong VMS, see below) that are aligned along the northwest-trending Abagong (or Abagong-Kurti) fault zone. These deposits are hosted in the metamorphosed felsic igneous and sedimentary rocks of the Kangbutiebao Formation which, according to Chai et al. (2009), was deposited in the folded

Fig. 6.31 Qiaoxiahala mine area; **a** quartz stockwork veining in carbonated ultramafic rock (*listvenite*); **b** massive skarn ore consisting of bands of magnetite and epidote (*greenish*); **c** mafic schist replaced by Fe carbonate; **d** mine shaft

and strongly deformed Kelang volcano-sedimentary basin (see below). The Kangbutiebao Formation rocks, comprising rhyolitic lavas and pyroclastics, mafic rocks (amphibolites), sandstone and carbonate rocks, are metamorphosed to greenschist-lower amphibolite facies (see below and Fig. 6.33), However, the metamorphic grade of these rocks is probably higher, reaching upper amphibolite to granulite facies and locally reaching stages of partial melting, as shown by the presence of migmatites (Pirajno field notes 2009).

The Abagong Fe-P mineralisation at the time of a field visit (2009) was being mined underground and by open cuts. The ores discontinuously extend along an east-west strike for approximately 1.5 km. The nature of the Abagong mineralisation is poorly known, with only conference abstracts, specifically addressing this deposit (e.g. Liu et al. 2009a, b) or simply reporting on associated lithogies (e.g. Li and Chen 2004; Liu et al. 2008; Chai et al. 2009). From these authors it can be surmised that the Abagong mineralisation occurs primarily as structurally-controlled lenses and veins. Liu et al. (2009a), on the basis of REE composition (LREE-enriched, marked negative Eu anomalies) of the apatites as well as the magnetite-apatite ore association, classified Abagong as a Kiruna-style mineral system, similar to those that occur in the Ningwu volcano-sedimentary basin in the Yangtze River Valley metallogenic

belt, described in Chap. 4. The host rocks of the Kangbutiebao Formation have been studied in some detail by Chai et al. (2009), who performed SHRIMP U-Pb analyses of zircons from the metarhyolites, yielding ages ranging from 412.6 ± 3.5 to 406.7 ± 4.3 Ma. Liu et al. (b), on the other hand, reported SHRIMP U-Pb zircon ages of 462 ± 3.6 and 457.8 ± 3.1 Ma for gneissic granites, considered to be part of a large granitic batholith in the region.

The following observations are from the field visit to the Abagong area in 2009 and subsequent petrographic analysis of ore and wall rock samples. The main host rocks are indeed metarhyolites, typically with a polygonal granoblastic texture (felsitic, high-temperature static recrystallisation), but locally overprinted by regional planar fabrics, probably associated with multiphase strike-slip movements of the Abagong Fault. Other rocks in the mine area include fine-grained biotite-granite, biotite schist, gneissic granite and cross-cutting pegmatite. In one place a lamprophyre dyke can be seen intruding the magnetite ore at the contact between gneissic granite and metarhyolite rocks. The Abagong ores occur as lenses, veins and breccias; the ore minerals are magnetite, apatite (?fluoroapatite), fluorite and lesser pyrite. Ore lenses, commonly consist of magnetite-dominant and apatite-dominant bands (Fig. 6.32). The felsitic host rocks have undergone degrees of metasomatic alteration with the formation of quartz, calcite, muscovite, phlogopite and epidote. These minerals are also present in the Fe-P ores of the Kiruna district, where they were considered part of a skarn association (e.g. Frietsch 1978; Nyström and Henríquez 1994). However, at Abagong no skarn was noted. There are at least two generations of both magnetite and apatite. Magnetite (1) shows well-developed hematite exsolution lamellae and is along the edges altered to martite; a platy magnetite (2) does not exhibit exsolution lamellae and may be a later (hydrothermal?) phase. Similarly, two generations of apatite comprise a euhedral to subhedral mosaic with interstitial magnetite and fluorite and a later poikiloblastic apatite that overprints magnetite (Fig. 6.32).

Strike-slip deformation along the northwest-trending major structures in the Altay orogenic belt, such as the Irtysh and Abagong fault zones (Figs. 6.4 and 6.27), renders the interpretation of tectonic, igneous and ore-forming events difficult, in spite of geochronological data. One important conclusion reached by Chai et al. (2009) is that the magnetite-apatite ores postdate the rocks of the Kangbutiebao Formation, which they suggested may have formed in a subduction-related setting. The Early Devonian silicic magmatism, now represented by metarhyolites, would have been formed by partial melting of continental crust, whereas mafic rocks resulted from a heat source related to mafic underplating, which then caused partial melting of the overlying continental crust. No explanation was offered for the magnetite-apatite ores, except that they resemble Kiruna-style mineral systems, such as those seen in the previously mentioned Yangtze River Valley metallogenic belt (Chap. 4). The Kiruna-type label is probably correct, but it must be borne in mind that the origin of Kiruna-type Fe-P ores is controversial, although a magmatic origin is perhaps undisputed, but details have remained conjectural since their first discovery in Sweden, some 300 years ago (Geijer 1931). Genetic models include: (1) related to subvolcanic alkaline plutons and late magmatic fluids (Hildebrand 1986); (2) related to cooling of felsic-intermediate lavas (Nyström and Henríquez 1994); (3) intrusive-magmatic (Frietsch 1978); (4)

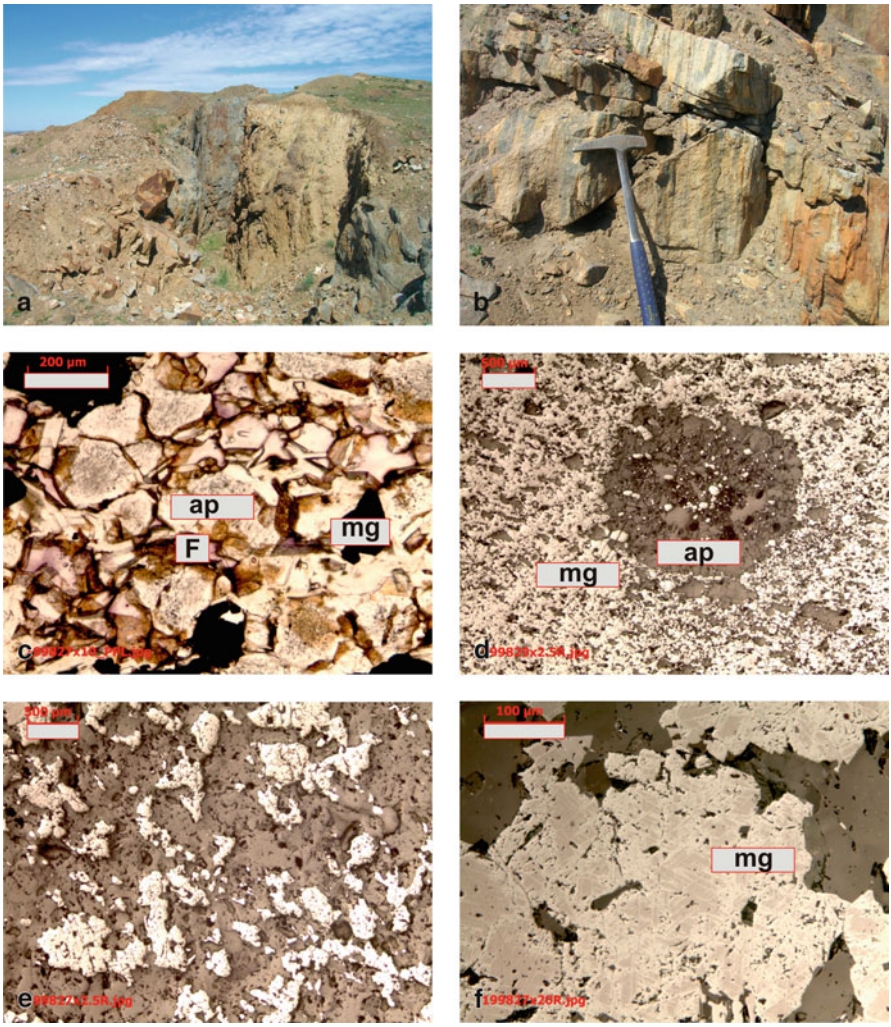

Fig. 6.32 Abalong Fe-P deposit; **a** magnetite ore and felsitic (metarhyolite) host rocks; **b** banded magnetite (*dark*) and apatite (*brown*) ore; **c** plane polarised photomicrograph showing apatite-fluorite polygonal aggregate and magnetite; **d** reflected light photomicrograph showing fine-grained magnetite ore and apatite porphyroblast; **e** reflected light photomicrograph showing primary (magmatic) magnetite disseminations; **f** detail of magnetite grain showing exsolution lamellae of hematite; *ap* apatite, *mg* magnetite, *F* fluorite

associated with porphyry and skarn systems, as discussed in Chap. 4; (5) they are part of the iron oxide copper gold (IOCG) class, but associated with volcanic diatremes and related pyroclastic (see Pirajno 2009 and references therein); (6) formed by magmatic processes related to Fe-rich magmas, later modified by hydrothermal

activity (Nylström et al. 2008). The Abagong Fe-P mineralisation is intimately associated with felsites (metarhyolite), derived from high-temperature metamorphism of subvolcanic rhyolite porphyries. The magnetite-apatite mineralisation could have formed first during the magmagtic evolution of the rhyolite porphyries, then remobilised in a second stage during strike-slip movements along the Abagong and Irtysh faults. On the basis of field, petrographic observation and published work the following sequence of events is tentatively suggested: emplacement of subvolcanic rhyolites → formation of magnetite-apatite from cooling magma → strong deformation due to shearing, forming laminated and brecciated ores → hydrothermal phase with a second generation of magnetite-apatite ore. The door to the Abagong Fe-P mineralisation remains open and further work is needed to unravel its origin and ore system classification.

6.3.5 Volcanogenic Massive Sulphides (VMS)

Volcanogenic massive sulphide (VMS) ore systems are present in both the Tianshan and Altay orogenic belts. They include the Qiaorequanzi Cu-Zn (about 60 km northeast of Shiyingtan; see Fig. 6.26), Keketele Pb-Zn, Ashele Cu-Zn, Koktal Pb-Zn, Abagong Cu-Pb-Zn and Tiemurt Pb-Zn-Cu in the Altay orogenic belt. For the latter deposit, it must be pointed out that recent research by Zhang et al. (2012), on fluid inclusions and field observations has led these authors to suggest that the Tiemurt deposit is structurally controlled and that the ore-forming process can be resolved into three stages and that last stage consists of undeformed veinlets that infill open spaces. Zhang et al. (2012) proposed that the Tiemurt Pb-Zn-Cu deposit is not a VMS, but may be considered an orogenic base metal deposit.

In this section, I provide a brief description of the Keketale, Ashele and Koktal deposits (Fig. 6.26). Wang et al. (1999) provided a review of VMS deposits in the Altay belt, in which iron skarn types (Mengku) and other deposits were included in the VMS family. Wang et al. (1999, (2003c) suggested that the Altay VMS deposits were formed in Devonian, volcano-sedimentary basins, namely: Maize, Kelang and Qongut (or Chonghuer), containing mafic-felsic (bimodal) volcanic successions, possibly related to continental rifting (Wan et al. 2010). These Devonian volcano-sedimentary basins in the Altay orogen are strongly deformed and folded and their bimodal sequences metamorphosed from greenschist to upper amphibolite and granulite facies, hampering a clear assessment of their nature and tectonic setting. Here I adopt the rift basin model advocated by researchers working on the Altay orogen.

6.3.5.1 Keketale

The Keketale VMS deposit, with estimated reserves of 0.89 Mt Pb, grading 1.5 % and 1.94 Mt Zn, grading 3.16 %, was studied by Wan et al. (2010) and the following

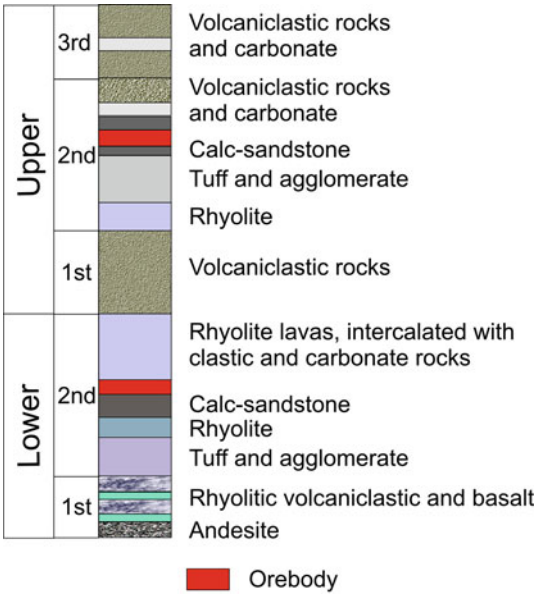

Fig. 6.33 Lithostratigraphy of the Kangbutiebao Formation and position of VMS orebodies; the rocks in the lithostratigraphic column are interpreted protoliths (see text for details), the second column (1st, 2nd etc), are volcanic-sedimentary cycles in each Group. (Modified from Chai et al. 2009; Wan et al. 2010)

is summarised from these authors. The deposit is located in the Maizi volcano-sedimentary basin, in which rocks of the Kangbutiebao Formation (Fig. 6.33) form an overturned syncline with a northeast dip and with the orebodies hosted in the overturned limb (Fig. 6.34). In this area, the Kangbutiebao Formation is divided into Lower and Upper lithostratigraphic units (members?), difficult to unravel due to deformation and high-grade metamorphism, leading to contradicting results by researchers. The Lower unit is estimated to be from 1,500 to 500 m thick and consists of metarhyolitic rocks, quartz-mica schist, amphibolite, hornblende granulite, leucoleptite and metasandstone. The protoliths of these rocks have been suggested to be rhyolitic lavas and volcaniclastic, sandstone, carbonate rocks, basalt and andesite (Wan et al. 2010). The Upper unit is estimated to be from 3,000 to 185 m thick and contains felsite, metarhyolitic crystal tuff and volcaniclastic, schist, marble, hornblende granulite, interpreted as various pyroclastic units, sandstone and rhyolite lavas. Age determinations by SHRIMP U-Pb on zircons from metarhyolitic rocks, yielded 408.7 ± 5.3 (Lower unit), 412.6 ± 3.5 and 406.7 ± 4.3 Ma, both from the Upper unit (Chai et al. 2009).

Wan et al. (2010), in their Fig. 3, show two sulphide orebodies, one in each of the Lower and Upper units (Fig. 6.33). The No. 7 orebody is the largest and consists of several deformed lenses, with variable sizes, up to 700 m long, 80 m thick and down-dip extent of 500 m (Fig. 6.34). The main No. 7 ore lens consists of massive sulphides, banded and laminated sulphide ore and disseminated ore, mostly along the margins of the massive ore, but disseminated and vein sulphides are structurally above the main ore and are interpreted to represent the overturned(?) feeder zone of the sub-seafloor hydrothermal system. Ore minerals are pyrite, sphalerite, galena,

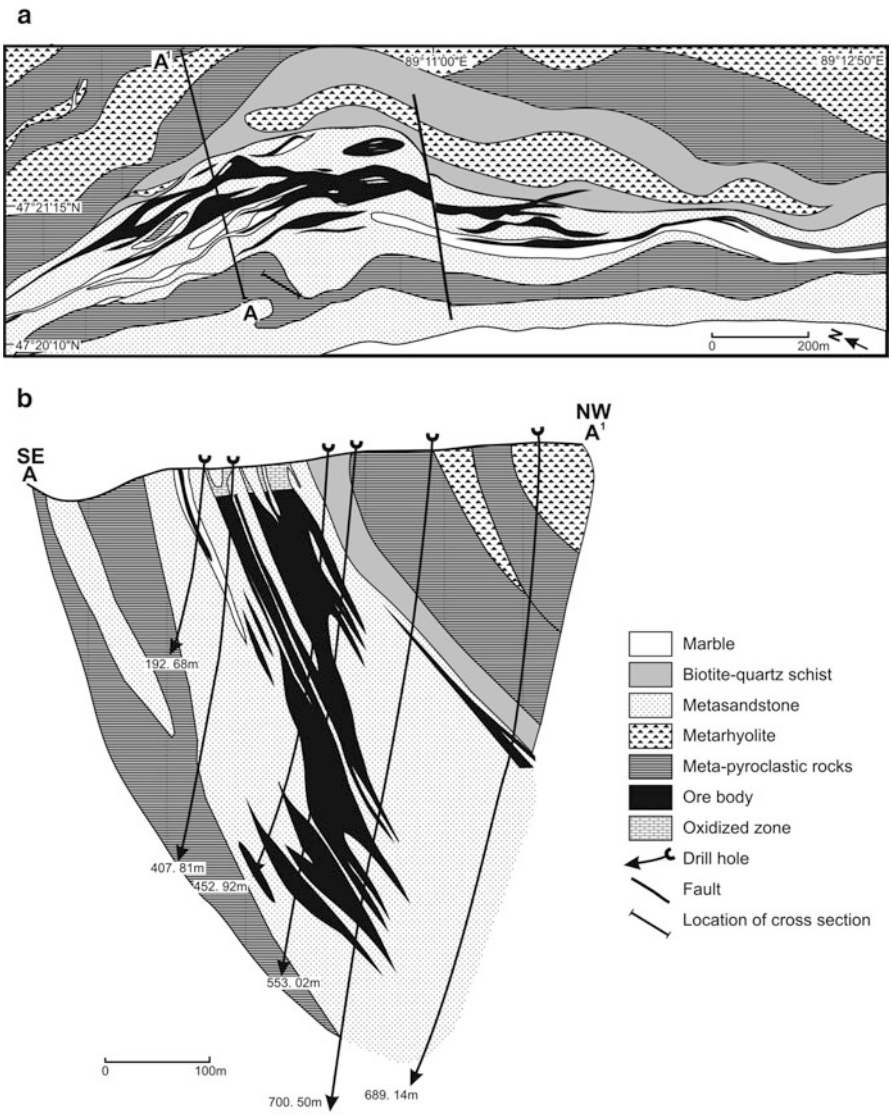

Fig. 6.34 Simplified geological map of the Keketale Pb-Zn VMS deposit area and position of the orebodies (**a**) and cross-section showing orebodies in the overturned syncline (**b**). (After Wan et al. 2010)

pyrrhotite and chalcopyrite with gangue minerals including quartz, calcite, biotite and feldspar. Pyrrhotite and chalcopyrite, typically with xenomorphic textures, tend to be more abundant in the upper parts of the ore lens. Sphalerite, commonly occurs interstitial to pyrite grains. Galena mainly forms idiomorphic grains and also as interstitial to other sulphides, in the middle and lower parts of the orebody. Wan et al.

(2010) suggested a metal zonation from Fe-Cu in the upper parts of the No. 7 orebody, to Fe-Zn-Pb (Zn > Pb) in the central parts, to Fe-Pb-Zn (Pb > Zn) in the lower parts. In spite of the presence of chalcopyrite in the orebody, Cu is not economically important at Keketale. The ore lenses are associated with zones of hydrothermal alteration, including an inner chlorite-dominant zone (± pyrite ± quartz ± carbonate), enveloped by a sericite-dominant zone (±chlorite ± carbonate), carbonate, pyrite and skarn minerals. Skarn minerals form narrow stratiform sheet below the ore lens. The ore lenses are capped by an oxidised zone to depths of about 20 m (Fig. 6.34).

Sulphur isotopic compositions of sulphides from disseminated, massive and banded ore show $\delta^{34}S$ values ranging from 0.2 to −11.1 ‰, which Wan et al. (2010) separated in two groups: (1) feeder zone sulphides with $\delta^{34}S$ values close to 0 ‰, and (2) main ore lens sulphides with $\delta^{34}S$ values ranging from −11.1 to −8.8 ‰. Wan et al. (2010), on the basis of the sulphur isotopic data, suggested that the S may have been derived from bacterial reduction of seawater sulphate, or leached from the underlying rocks, or a mix of the two, whereas the S isotopic signature from the feeder zone is probably magmatic (near 0 ‰ values). Rb–Sr and Sm–Nd isotopic compositions of sulphide ores with a model age of 400 Ma the initial $^{87}Sr/^{86}Sr$ ratios of the ores range from 0.70351 to 0.70951 and the εNd(t) values range from −3.6 to −0.4. The initial $^{87}Sr/^{86}Sr$ ratios and εNd(t) values of the metasedimentary rocks are 0.70774–0.70938 and −3.6 to −0.4, respectively, whereas values in the underlying volcanic rocks are 0.70444–0.74987 and −1.7 to +0.4, respectively (Wan et al. 2010).

The origin of the Keketale VMS deposit has been controversial, with models ranging from Iberian Pyrite Belt type (e.g. Tornos 2006), to a transitional SEDEX-VMS type (Wang et al. 1999), due to the previously-mentioned difficulty of assessing field relationships and rock types along strike-slip fault zones in the region and metamorphic overprints. However, Wan et al. (2010), on the basis of geochemical and isotope systematics, helped in shedding light on Keketale (and by inference to other VMS deposits in the region). The Keketale VMS fits in the model of classic VMS deposits, generated at and below the seafloor by hydrothermal fluids associated with felsic-mafic bimodal volcanism in a back-arc tectonic setting (Kuroko-style; e.g. Franklin et al. 2005; Fig. 6.9).

6.3.5.2 Ashele

The Ashele VMS, discovered in 1994, has been the subject of a limited number of studies (Wang 1999, 2003; Wang et al. 1998). The following is taken from the above cited works, intergrated with field observations (Pirajno, unpublished). The Ashele deposit is hosted by Mid-Devonian bimodal volcanic rocks, interbedded with cherts and reef limestones and has resources of about 1 Mt metal, with 2 % combined Cu + Zn grades, but with significant Au grades of about 0.5–1.7 g/t. Sm-Nd isochron ages of the volcanic rocks range from ca. 368 to 352 Ma (Li et al. 1998). The volcanic rocks comprise spilitic basalt, tuff, keratophyre and dacite of the Ashele Formation, intruded by Late Devonian dacite and mafic porphyry (lamprophyre?), overlain by

basalt and dacite of the Qiye Formation. The VMS deposit contains at least 10 ore zones, but only the No. 1 orebody, a north-south-trending lens of massive sulphides, was economic and being mined at the time of a mine visit in 2003. The No. 2 ore zone is a polymetallic-barite lens, whereas the No. 3 ore zone consists of massive Cu-rich sulphides, hosted in pyroclastic rocks.

The No. 1 orebody is near the contact between spilitic and dacitic rocks and footwall alteration is represented by various combinations of sericite, chlorite and carbonate minerals and disseminated chalcopyrite. In the hangingwall, the dominant alteration minerals are pyrite and chlorite. The massive sulphides have a geochemical signature characterised by a sodium depletion halo, both in the hangingwall and footwall. The Ashele ore can be subdivided into three types: (1) veinlets and stringers in brecciated volcanic rocks; (2) massive sulphides; and (3) quartz veins in shear zones. Veinlets and stringers are part of the hydrothermal conduit and as such these underlie the massive sulphide lens, whereas the quartz veins are the result of later re-working associated with tectonic movements. The main ore minerals are pyrite, chalcopyrite, sphalerite, galena and tetrahedrite; lesser amounts of other ore minerals include bornite, chalcocite, covellite, arsenopyrite, argentite, native gold, electrum, hessite and marcasite. Also present are magnetite, hematite and psilomelane. Gangue minerals include quartz, sericite, chlorite and calcite. Barite is abundant in other ore zones, but not in the No. 1 orebody. Pyrite and chalcopyrite are the dominant ore minerals in the syngenetic VMS ore, but are also present in remobilised veins. The ore mineral assemblages are distinctly zoned. In the No. 1 orebody the chalcopyrite-galena-sphalerite-barite assemblage is at the top, followed downward by galena-sphalerite-chalcopyrite, sphalerite-chalcopyrite-pyrite and chalcopyrite-pyrite at the bottom. The stringer ore, which underlies the massive sulphide lenses, consists of chalcopyrite-pyrite-quartz and minor sphalerite-tetrahedrite. Fluid inclusions in quartz yield homogenisation temperatures ranging from 313 to 296 °C, in sphalerite from 239 to 168 °C. Sulphur isotopic compositions were determined from about 100 samples of sulphide, barite and wallrocks. The $\delta^{34}S$ values from the No. 1 orebody have a fairly narrow range from −2.77 to 8.17 ‰. Barite from the No. 2 orebody has $\delta^{34}S$ values from 18.89 to 23.54 ‰. Wang (2003) suggested that the Ashele VMS was formed in an oceanic island or seamount environment near a continental margin and that the host volcanic sequence may be related to a hotspot.

6.3.5.3 Koktal

The Koktal Pb-Zn massive sulphide deposit, discovered in 1986, with resources of about 3 Mt grading 1.5 % Pb, 3.16 % Zn and 0.08 % Cu (Wang et al. 1999, 2003c). The deposit is located in the same Devonian volcanic belt as the Mengku Fe deposit (Sect. 6.3.4.2). The deposit geology was described in Wang et al. (2003c) and is summarised here.

The Koktal VMS system consists of a series of stratiform sulphide lenses, typically underlain by uneconomic zones of stringer/stockwork mineralisation. The rocks

in the region are mafic and felsic metamorphosed rocks of the Devonian Kangbutiebao Formation (Chai et al. 2009). The orebodies are hosted in rhyolitic flows and pyroclastic rocks, have a northwest strike and are from 1,700 to 100 m long and 40–7 m wide and extend downdip for up to 700 m. The stratiform sulphide lenses are characterised by disseminated and banded semi-massive to massive sulphide ores, underlain by a feeder pipe. The ore minerals include mainly sphalerite, galena and pyrite with lesser amounts of chalcopyrite. Other ore minerals are pyrrhotite, marcasite, arsenopyrite, tetrahedrite, bornite, magnetite and barite. Pyrrhotite is more abundant near a granitic intrusion. Fluorite and tourmaline are also present in the ores. The presence of these two minerals, hints at hydrothermal fluids associated with granitic intrusions (pers. observation). The primary textures of the ore minerals have been obliterated by recrystallisation due to subsequent deformation events. Wang et al. (2003c) recognised three types of alteration in the footwall rocks. A "white zone" distal alteration that consists of sericite-K-feldspar; a proximal "green zone", represented by chlorite, actinolite and biotite; and the above-mentioned feeder pipe is characterised by quartz, chlorite and lesser epidote alteration associated with the stringer and veinlet sulphides.

Fluid inclusions in quartz revealed three groups of homogenisation temperatures: (1) 390–244 °C in the stringer/stockwork zone, 330–222 °C in the massive ores and 330–300 °C in the semi-massive ores. Salinities in all inclusions vary from 11 to 7 % NaCl equiv. Sulphur isotope compositions show that the $\delta^{34}S$ of sulphides range from −15.8 to 5.1 ‰, with an average of −10.5 ‰. There are differences between the ore zones. The stratiform ores all have negative $\delta^{34}S$ values, namely: −7.2 ‰ for disseminated sulphides, −10.8 ‰ for semimassive sulphides and −13.2 ‰ for massive sulphides. The underlying stringer/stockwork sulphides have $\delta^{34}S$ values of 5.1–1.0 ‰, which are close to magmatic values. Wang et al. (2003c) compared the Koktal $\delta^{34}S$ values with those of other VMS deposits and concluded that the Koktal sulphur isotopic compositions are close to those of the massive sulphides in the Iberian Pyrite Belt (see Tornos 2006; Pirajno 2009 for an overview of the Iberian Belt).

6.3.6 Magmatic Ni-Cu-(PGE) and Ophiolite-hosted Cr Deposits

Several magmatic sulphide and oxide deposits are present in the East Tianshan, in the Altay orogenic belt and in the West Junggar (Figs. 6.5). These include Ni-Cu sulphides in zoned and layered intrusions and podiform chromite in ophiolitic rocks. Further to the east, in Gansu Province but still in NW China is the world-class Jinchuan deposit, described in Chap. 7. In this section, following a brief note on podiform chromite, magmatic Ni-Cu sulphide deposits in the mafic-ultramafic intrusions of northern Xinjiang are described.

The mafic-ultramafic intrusions of northern Xinjiang are discontinuously distributed along major faults (Fig. 6.5). On the southern margin of the Altay orogen are the Kalatongke and Keketuohai belts of mafic-ultramafic intrusions. In the

eastern Tianshan region there are two major belts of mafic-ultramafic rocks: the Huangshan-Jing'eruquan and Baishiquan belts, whereas in the western Tianshan is the Qingbulake belt. Along the northern margin of the Tarim basin and bordering the Tianshan orogen are the Xingditage and Pobei mafic-ultramafic intrusions. The distribution of these mafic-ultramafic complexes and associated Ni-Cu deposits and occurrences are shown in Fig. 6.35. The mafic-ultramafic intrusions of northern Xinjiang, span ages from ca. 434 (Silurian) to ca. 251 Ma (Permian-Triassic). In the West Tianshan, the Qingbulake belt is known to contain at least 10 mafic-ultramafic intrusions, one of which is the recently discovered ca. 434 Ma Qingbulake (also spelled Jingbulake) complex hosting Ni-Cu sulphide mineralisation investigated by Zhang et al. (2010b) and Yang et al. (2012c). The important point here is that many of these intrusions are part of dismembered ophiolite belts, marking sutures between major tectonic units of the CAOB (Figs. 6.5 and 6.35), as is the case for the Qingbulake belt and the Dalabute ophiolite, briefly introduced in the next section, whereas other mafic-ultramafic complexes also distributed along strike-slip faults and suture zones, are funnel-shaped and zoned, but emplaced in a post-collisional extensional environment and as such are not part of ophiolite belts, which represent fragments of obducted oceanic crust. Discriminating ophiolitic rocks from other types of mafic-ultramafic complexes in NW China, is a difficult task. This issue has been on the forefront for the understanding of the geodynamic evolution of the tectonic terranes and fold belts of the Tianshan and Altay orogens. More recently, precise geochronological studies (Re-Os, U-Pb) provided better constraints in separating ophiolitic rocks from post-collisional mafic-ultramafic systems, as exemplified in the above mentioned work by Zhang et al. (2010b).

6.3.6.1 Podiform Chromite

Chromium mineralisation occurs along the northeast-trending Dalabute Ophiolite Melange, within which is the Saourtuhai (also Sartuohai and Sartokai) chromite deposit, located approximately 60 km east of the Saourtuhai lode Au deposit (Fig. 6.12). The chromite mineralisation is of the podiform type hosted in ultramafic rocks of the Tangabale Ophiolite Belt (Fig. 6.12). The ultramafic rocks include peridotite, harzburgite, dunite and troctolite, all in various stages of serpentinisation. The ore is hand-sorted with a production of about 60 t/day (2003, field visit). The chromite contains about 10 % Fe oxides, traces of PGE, Ni and Co. Samples collected from this area of serpentinite material and chromite ore show that the former contains serpentine minerals, calcite and opaque euhedral crystals (possibly magnetite); calcite occurs as late porphyroblastic growths. The chromite is massive, with a cataclastic texture and has interstitial pyrrhotite, associated with carbonate material. In the West Junggar terrane two types of podiform chromite deposits have been recognised (Bai et al. 1995). One type is characterised by high Cr and is associated with dunite and orthopyroxene-poor harzburgite. The other, to which the Saourtuhai deposit belongs, has lower Cr contents (high Al) and is associated with lherzolite, minor dunite and harzburgite.

6.3.6.2 Magmatic Ni-Cu Deposits of Eastern Tianshan and Altay

The Altay and Tianshan magmatic Ni-Cu deposits are genetically associated with and hosted in funnel-shaped, differentiated layered and/or zoned mafic-ultramafic intrusions (Fig. 6.35). Several of these intrusions occur in intracontinental rifts and are spatially and temporally associated with flood basalts and A-type granitic rocks (Pirajno et al. 2008). The Altay and Tianshan mafic-ultramafic intrusions have features that are similar to the concentrically zoned and funnel-shaped Alaskan-type complexes (Xiao et al. 2008b; Pirajno et al. 2008). Typically, Alaskan complexes consist of an ultramafic core surrounded by an envelope of earlier gabbroic rocks and are usually of small size ranging from 12 to 40 km^2 and are known to be related to subduction systems (see Johan 2002, for an overview of Alaskan-type intrusions and related mineralisation). The general zoning of Alaskan-type complexes passes from a dunite core, through successive zones of olivine-clinopyroxenite, biotite and hornblende-bearing clinopyroxenite, then hornblendite and finally to an outer zone of monzonite-gabbro. A similar pattern, albeit with variations between various intrusions, characterises the intrusions in the Altay and Tianshan orogenic belts. In the Urals, Alaskan-type complexes are spatially and temporally linked with subduction-related calc-alkaline magmatism and accretionary terranes (Zoneshain et al. 1990). I suggest that this is not the case for the northern Xinjiang zoned mafic-ultramafic complexes, which were emplaced in a post-collisional extensional setting in the Permo-Triassic. However, Li et al. (2012) presented a new model for the magmatism and formation of the Ni-Cu orthomagmatic deposits. These researchers suggested that following subduction, a slab window related to ridge subduction or slab breakoff during a transitional stage of arc-arc or arc-continent collision resulted in the emplacement of the mafic-ultramafic intrusions. Slab window magmatism and associated asthenospheric upwelling is considered characteristic for the emplacement of zoned mafic-ultramafic intrusion (Alaskan-type; Johan 2002). To be sure, an Alaskan-type intrusion is located in Inner Mongolia, west of the Hohhot city (Fig. 6.35). This is the Wengeqi mafic-ultramafic complex consisting of pyroxenites, amphibolite, gabbro and websterite dykes. Su and Lesher (2012) determined a 399 ± 4 Ma age for the pyroxenite, using the U-Pb SHRIMP method on zircon and reported the presence of magmatic sulphides (pyrite, chalcopyrite, pyrrhotite and pentlandite) and PGE minerals in the websterite dykes. Grades range from 1 to 3 ppm (Pd + Pt).

The origin of these mafic-ultramafic intrusions and associated magmatic sulphides is still controversial. Zhou et al. (2004) proposed a mantle plume model to explain the emplacement of the mafic-ultramafic intrusions and associated A-type granites in northwest China. The timing of the Huangshan magmas is post-orogenic and within-plate, as are many of the A-type granitic rocks in the region, and the zoned intrusions are of Alaskan-style, but related to mantle plume activity, possibly the ca. 280 Ma Tarim event (Pirajno et al. 2009). Han et al. (2010), working on the Xiangshan Ni-Cu-Co deposit, instead suggested that the mafic-ultramafic complexes are typically Alaskan type and as such related to subduction zone-arc setting, as in the Cenozoic orogen of Alaska. In yet another model, Zhang et al. (2011), referring

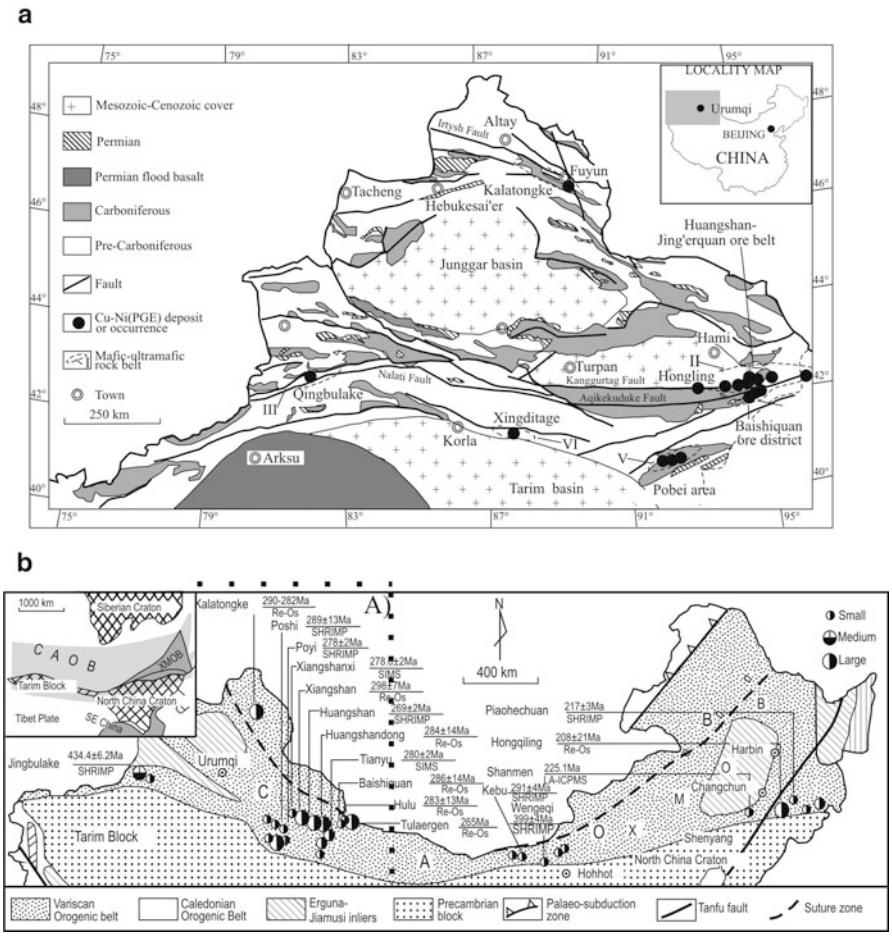

Fig. 6.35 **a** Distribution of magmatic Ni-Cu sulphide deposits in northern Xinjiang; mafic-ultramafic belts: *I* Kalatongke, *II* Huangshan-Jing'ershan, *III* Qingbulake, *IV* Baishiquan, *V* Pobei, *VI* Kurutag (after Zhang et al. 2008; Wang et al. 2006b); **b** CAOB (Central Asian Orogenic Belt) and the XMOB (Xing'an-Mongolia Orogenic Belt or Hinggan; see Chap. 5), northern China, showing the temporal-spatial distribution of magmatic Ni-Cu deposits, size of deposits, based on Ni resources: large—Ni ≥ 100,000 tonnes; medium—Ni 100,000–20,000 tonnes; small—Ni < 20,000 tonnes. (After Lü et al. 2011; Su and Lesher 2012)

to the Huangshanxi Ni-Cu deposit and using geochemical and Sm-Nd systematics, suggested that the mafic-ultramafic intrusions of the Huangshan belt correlate with within-plate tholeiitic basalts in the Turpan-Hami (Tuha) Basin (Fig. 6.35; see also Chap. 7). Pirajno et al. (2008) suggested that these zoned complexes were emplaced by the diapiric uprise of small mantle plumes (or plumelets), arising from a plume head. Pirajno (2010) further suggested that the zoned mafic-ultramafic intrusions were emplaced from mantle plume lateral flow towards pull-apart basins created

in stike-slip shear zones. A similar conclusion was proposed by Qin et al. (2011) and Su et al. (2011), who suggested that these magmatic events occurred during an extensional regime, possibly related to a mantle superplume event that affected much of central Asia in the Permian, of which the 250 Ma Greater Siberian large igneous province (LIP), the (260 Ma) Emeishan LIP and the Tarim (280 Ma) event, are part. Branquet et al. (2012), on the other hand, doubted that these zoned intrusions are of the Alaskan-type. They suggested that true Alaskan intrusions have dominant PGE ores, unlike the NW China mafic-ultramafic complexes, which are PGE-poor (see also Gao et al. 2012).

Taking into consideration the spatial-temporal relationship of these mafic, mafic-ultramafic complexes with coeval A-type granites, I concur with Zhang et al. (2008), Qi et al. (2011) and Su et al. (2011) that these magmatic events occurred during an extensional regime, possibly related to a mantle superplume event that affected much of central Asia in the Permian, of which the 250 Ma Greater Siberian large igneous province (LIP), the (260 Ma) Emeishan LIP and the Tarim (280 Ma) event, are part (Borisenko et al. 2006; Pirajno et al. 2009; Dobretsov 2011). The plume model is by no means universally accepted, as further discussed below for the Tianyu intrusion.

The outcrop area of the mafic-ultramafic intrusions in northern Xinjiang, range from 0.1 km^2 (Kalatongke) to about 3 km^2 (Huangshandong). These mafic-ultramafic rocks have mineralogical evidence to show that their liquidus temperatures decrease outwards through the successive zones, as in a fractional crystallisation sequence, with hornblende being a late product in the outer zones (Zhou et al. 2004). A possible model for the origin of these complexes is that of intrusions of a tholeiitic magma, which gives rise to gabbro or gabbronorite, followed at a later stage by ultramafic magmas that are emplaced at localised centres as multiple intrusions in order of increasing liquidus temperature, from pyroxenite, then wehrlite to dunite. The mineralisation styles include massive sulphide, sulphide-matrix breccias, interstitial sulphide networks, and disseminated sulphide. Sulphide veins and dissemination locally penetrate footwall rocks. The environment of emplacement of the multiple ore-bearing intrusions of ultramafic magma (probably mantle-derived) is the upper crust in tensional environments associated with rifting. Contamination of the magma was an important factor for sulphur saturation and formation of a sulphide phase (Naldrett 2004).

Another feature of the NW China mafic-ultramafic intrusions is their common and similar hydrothermal alteration. This alteration is locally pervasive to fracture-controlled and includes talc-carbonate, biotite-chlorite, sericite-muscovite-chlorite, actinolite-tremolite assemblages. The reasons for this alteration are not clear. One possibility is that these intrusions act as a powerful heat source that can generate hydrothermal convection cells within and around the intrusive body, once it is emplaced. The convective fluids then cause varying degrees of hydrothermal alteration in the rocks through which they circulate. It may be that the strong hydrothermal alteration observed in the ore-bearing Huangshan mafic-ultramafic rocks may be due to post-emplacement hydrothermal activity. Zhou et al. (2004), on the other hand, considered that this alteration may be due to water added to the source magmas prior to their emplacement. In this respect, the NW China intrusions are more like

Table 6.2 Selected magmatic Ni-Cu sulphide deposits in the East Tianshan. (After Mao et al. 2005)

Name	Length × width (km)	Size/grade	Rock types
Xiangshan	10 × 3.5	Cu 20,000 t/0.3 % Ni 40,000 t/0.5 %	Hornblende-peridotite, peridotite, pyroxenite, diorite, gabbro
Huangshan	3.8 × 8	Cu 0.21 Mt/0.31 % Ni 0.32 Mt/0.49 %	Gabbro-diorite, hornblende gabbro, gabbro-norite, lherzolite, websterite
Huangshandong	5.3 × 1.12	Cu 0.18 Mt/0.27 % Ni 0.36 Mt/0.53 %	Hornblende-olivine gabbro, pyroxene-hornblende gabbro, gabbro-diorite, gabbronorite, hornblende-peridotite
Huangshannan	5.2 × 1.3	Cu 1,300 t/0.3 % Ni 10,000 t/0.4 %	Hornblende-peridotite, hornblende pyroxenite, peridotite, lherzolite, hornblende-gabbro, norite
Huangshanbei	10 × 0.9	Cu 2,000 t/0.2 % Ni 12,000 t/0.4 %	Gabbro, pyroxenite, peridotite, diorite
Erhongwa	3.33 × 2.56 and 1.72 × 1.14	Cu 4,000 t/0.2 % Ni 18,000 t/0.2 %	Lherzolite, gabbro-norite, olivine-gabbro, pyroxene-diorite, quartz-diorite
Tudun	1.4 × 0.7	Cu 3,000 t/0.2 % Ni 15,000 t/0.3 %	Gabbro, pyroxene-hornblende peridotite, olivine-hornblende pyroxenite

the ultramafic pipes of the Ivrea Zone in Italy, for which a mantle plume origin is advocated (Garuti et al. 2001).

In the East Tianshan these zoned mafic-ultramafic intrusion are numerous and tend to be located near the contact between the northern part of the Kanggurtag shear zone and the Dananhu arc. Mao et al. (2005) listed the following: Tudui, M102, Erhonwa, Xiangshan, Huangshannan, Huangshan, Huangshandong, Hongshigang, Heishiliang, Huludong, Chuanzu and Madi. Of these the Huangshan, Huangshandong, Huangshannan, Xiangshan, Tudun and Hulu host economic Ni-Cu sulphides and some of the essential details are given Table 6.2.

Huangshan-Jingerquan District

Gu et al. (1995), Zhou et al. (2004), Zhang et al. (2008) and Zhang et al. (2011) have described the geology and mineralisation of the mafic-ultramafic intrusions in the Huangshan-Jingerquan district in the eastern Tianshan. A summary of their observation follows. The Huangshan-Jingerquan district, about 140 km southeast of the town of Hami, contains more than 25 mafic-ultramafic complexes, some of which have subeconomic and economic magmatic Ni-Cu-(PGE) mineralisation. The Xianshan, Huangshandong, Huangshanxi and Tianyu are part of a series of mafic-ultramafic complexes along the Aqishan-Yamansu suture zone (Fig. 6.35). These complexes are spatially associated with the east-northeast-trending Kanggur-Gandun faults and the main rock types are: peridotite, olivine pyroxenite, websterite, gabbronorite,

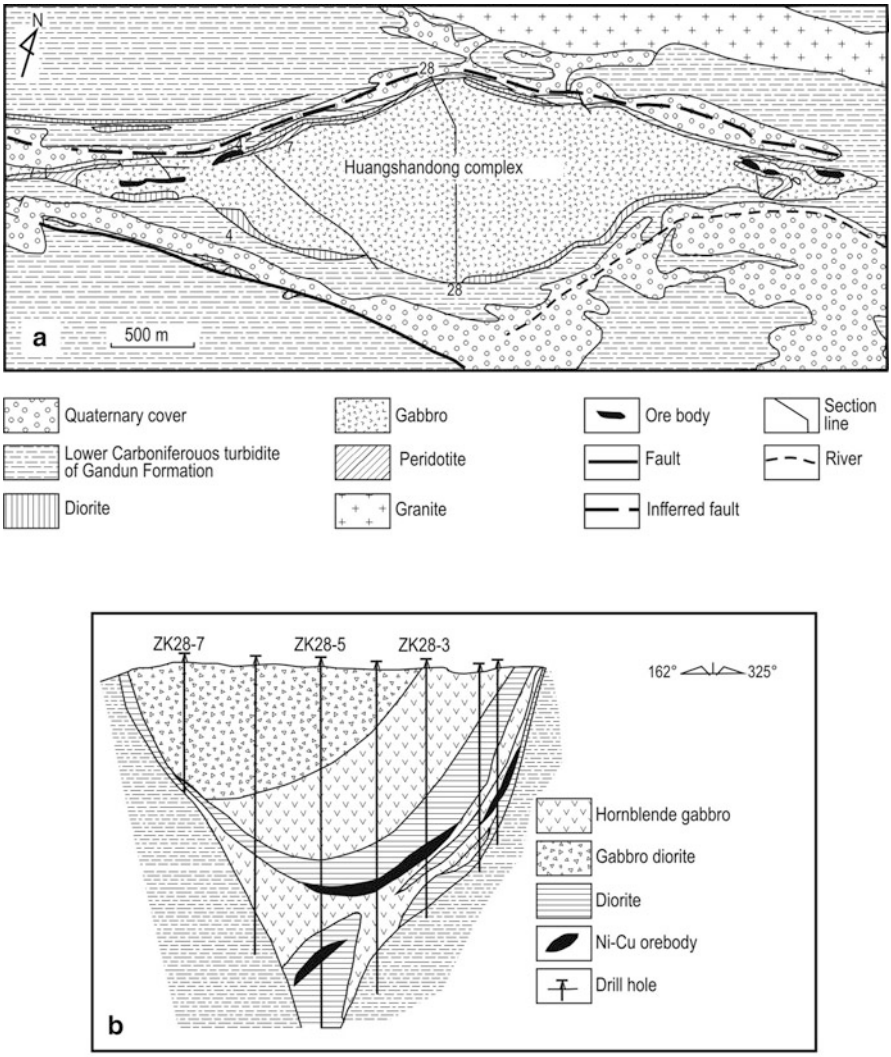

Fig. 6.36 Simplified geology of the Huangshandong zoned intrusion (**a**) and cross-section (**b**). (After Mao et al. 2008)

troctolite, gabbro and diorite. These mafic-ultramafic rocks intrude flysch-type sedimentary rocks of the mid-Carboniferous Gangdun (or Gandu) Group and basaltic lavas and pyroclastic rocks of the Wutongwozi Group.

The funnel-shaped Huangshanxi intrusion is about 3.8 km long and 800 m wide, but with a smaller surface exposure about 2.5 km long and 50–400 m wide. The Huangshanxi intrusion is composed of an early ultramafic unit, intruded by a layered ultramafic-mafic unit and a late mafic unit (Fig. 6.36). The rock type of the first unit is

peridotite, the second unit comprises, from base to top, wehrlite (ca. 150 m), olivine websterite (ca. 570 m), plagioclase websterite (ca. 350 m), gabbro and noritic gabbro (ca. 200 m) and finally diorite (ca. 150 m). The last unit forms the lower margin of the intrusion and is a fine-grained gabbronorite. A crystallisation sequence, according to Zhou et al. (2004), is as follows: cpx ± ol → cpx-opx ± ol → cpx-opx ± pl → cpx-opx-pl → pl-qtz-bt. At least 40 ore zones have been identified in the Huangshanxi intrusion with resources of about 80 Mt grading 0.54 % Ni and 0.30 % Cu. The ore minerals are pyrrhotite, pentlandite and lesser chalcopyrite. The Huangshandong intrusion is lozenge-shaped in cross-section and lens-shaped on the surface, 3.5 km long and 1.2 km wide, and like the Huangshanxi intrusion is composed by a sequence of intrusive phases. From the base to top, rock types of the first phase are olivine gabbro, hornblende gabbro and diorite. The second phase consists of gabbronorite dykes that intrude phase one rocks; the third phase comprises hornblende lherzolite, troctolite and gabbro. Twenty ore zones are present in the Huangshandong intrusion with reserves of approximately 135 Mt grading 0.30 % Ni and 0.16 % Cu. The ore minerals are pyrrhotite, pentlandite, chalcopyrite and pyrite.

SHRIMP U-Pb dating of zircons from the more evolved rocks of the Huangshanxi intrusion by Zhou et al. (2004) yielded a mean $^{206}Pb/^{238}U$ age of 269 ± 2 Ma. In addition, the same investigators carried out Rb-Sr and Sm-Nd analyses and obtained $^{87}Sr/^{86}Sr$ ratio of 0.71023 ± 4 and $^{143}Nd/^{144}Nd$ ratio of 0.511845 and positive εNd(t) values ranging from +6.7 to +9.3. Zhang et al. (2008) carried out Re-Os dating of sulphide ore from Huangshandong and obtained an age of 284 ± 14 Ma. A Rb-Sr isochron age of ca. 260 Ma from a muscovite granite that intrudes the mafic-ultramafic rocks was reported by Gu et al. (1995).

Zhou et al. (2004) proposed that the Huangshan intrusions are typical of continental settings and, on the basis of geochemical data, that the parental magmas were high-Mg tholeiitic basaltic magmas. The Huangshan Ni-Cu mineralisation is of magmatic origin as shown by cumulus-intercumulus textures and its stratiform-stratabound style. The timing of the Huangshan magmas is post-orogenic and within-plate, as are many of the A-type granitic rocks in the region. Zhou et al. (2004) further proposed a mantle plume model to explain the emplacement of the mafic-ultramafic intrusions and associated A-type granites.

The Tianyu intrusion dated at 280 ± 2 Ma (U-Pb on zircon) is a dyke-like body outcropping for about 2,000 m along strike, 100 m wide and traced to depths of 250–350 m (Tang et al. 2011, 2012). The Tianyu intrusion consists of lherzolite, olivine webesterite, gabbro and diorite. The ultramafic rocks host disseminated and net-textured sulphides (pyrrhotite, pentlandite and chalcopyrite). Interestingly, the Tianyu intrusion is also hydrothermally altered with serpentine + magnetite after olivine, actinolite-tremolite replace the clinopyroxene and sericite, epidote and albite replace the plagioclase. Tang et al. (2011) pointed out that the presence of a negative Pt anomaly in the massive sulphides, but not in sulphide-poor samples is consistent with post-magmatic hydrothermal alteration. These authors, contrary to the mantle plume hypothesis, proposed a model of upwelling asthenospheric mantle through a slab breakoff during a transitional regime from subduction to arc-arc collision in the Permian. Decompression melting and mixing with granitic magmas and

contamination with upper crustal material would have formed the parental magma of the Tianyu intrusion.

Kalatongke

The Kalatongke region (Fuyun district) in the Altay orogen is characterised by a 200 km long and 20 km wide zone containing a series of mafic-ultramafic intrusions, along the Irtysh fault and intruded into sedimentary and volcanic rocks of Lower Carboniferous age (Figs. 6.5 and 6.35). In the last 10 years or so, the Kalatongke Cu-Ni deposit enjoyed considerable popularity amongst researchers, resulting in several papers. of which those published in English, include Yan et al. (2003), Han et al. (2004), Wang et al. (2004b), Han et al. (2007), Zhang et al. (2009), Song and Li (2009) and Li et al. (2012). The geology, geochemistry and isotope systematics of the Kalatongke ores and their host rocks have been studied by Yan et al. (2003), Song and Li (2009), Zhang et al. (2008) and Zhang et al. (2009) and the following is summarised from these authors. Also in the Fuyun area, a number of mafic-ultramafic intrusions of Early Devonian age (ca. 409 Ma) have been reported. One of these is the Keketuohai complex (not to be confused with the Keketuohai rare metal pegmatite), which is zoned and as such also considered as Alaskan type, with a dunite core surrounded by olivine gabbro, hornblende gabbro and pyroxene diorite (Cai et al. 2012). No sulphide mineralisation has been yet reported from this intrusion (Min Su written comm. 2012).

In the area of the Kalatongke Cu-Ni deposit at least 11 zoned and differentiated mafic-ultramafic complexes have been identified. In the Kalatongke ore district, these 11 intrusions are located on the south side of, and approximately 10 km from the Irtysh fault zone, and arranged along two corridors, one to the northeast and one to the southwest (Fig. 6.37a). The southwestern corridor is 4,000 m long and 100–300 m wide and contains the No. 1, 2, 3, 10 and 11 intrusions (also referred to as Y1, Y2, Y3 etc), whereas the northeastern corridor is 2,200 m long and 50–250 m wide and contains the No. 5, 6, 7, 8 and 9 intrusions (Fig. 6.37a). The No. 1, No. 2 and No. 3 intrusions are well differentiated, showing well-defined lithological zones. As mentioned previously, Nos.1 and 2, which are in the southwestern belt, constitute the host of the Cu-Ni sulphide ores, with the largest ore zone being in the No.1 intrusion. The No. 1 intrusion has an outcrop area of about 0.1 km^2, is 695 m long, is funnel-shaped and consists of biotite-diorite and gabbro enclosing hornblende norite and olivine norite (Fig. 6.37b). The No. 2 intrusion is >1,440 m long and, like the No. 1, it consists of shells of biotite diorite and gabbro enclosing noritic rocks. The No. 4 to No. 9 intrusions in the northeastern belt are smaller in size, are poorly differentiated and have comparatively weak sulfide mineralisation. The No. 6, No. 7 and No. 8 intrusions strike approximately northeast and as such deviate from the regional northwest trend of the other mafic-ultramafic bodies. The No. 1 intrusion is estimated to have reserves of 18 Mt of ore, grading 1.4 % Cu and 0.88 % Ni; the No. 2 intrusion contains 10 Mt of ore, grading 1.1 % Cu and 0.6 % Ni (Song and Li 2009; Li et al. 2012).

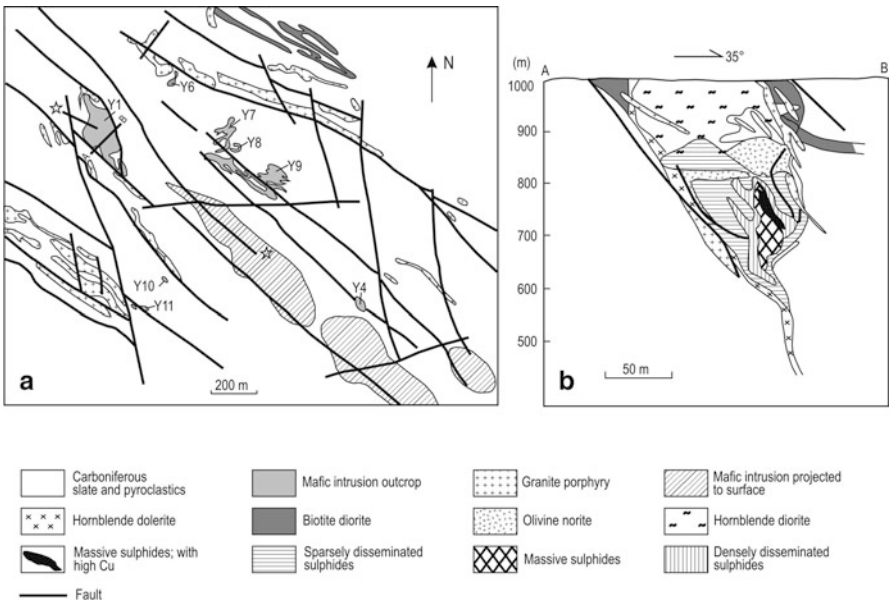

Fig. 6.37 Simplified geology of the Kalatongke area and distribution of mafic and mafic-ultramafic intrusions (**a**); cross-section of the Y1 intrusion and position of sulphide orebody (**b**). (After Zhang et al. 2008)

The Cu-Ni sulphide orebodies are located in the middle and lower parts of the intrusions (Fig. 6.37b). Mineralisation styles include massive sulphides, densely disseminated, and sparsely disseminated sulphides. The boundary between massive and disseminated sulphides is well defined, but there are gradational boundaries between the disseminated sulphides and their wall rocks. Dominant ore fabrics are droplet-like, disseminated and banded structures and net-textured, reflecting deposition from sulphide liquids. In addition, vein-stockworks are locally present and these probably indicate that they were the result of sulphide redistribution during hydrothermal processes.

Economic magmatic Cu-Ni sulphide deposits occur in three of the above mentioned 11 zoned mafic intrusions, constituting the Kalangtoke deposit, which is the second largest in China after Jinchuan (discussed in Chap. 7). The main Kalatongke intrusion (No. 1) hosting the sulphide ores is funnel-shaped and characterised by a fine-grained biotite-hornblende gabbro shell enclosing biotite-hornblende diorite, biotite-hornblende norite and olivine norite (Fig. 6.37b). More than 50 ore minerals are recognised in the different types of ore, including sulphides, arsenides, tellurides, oxides, and native metals. The dominant ore minerals are pyrrhotite, chalcopyrite and pentlandite, with subordinate magnetite, pyrite, violarite and ilmenite and minor sphalerite, galena, alabandite, valleriite, bornite and skutterudite and noble metals, such as native gold, native silver, electrum, hessite, teniplapalladite, merenskyite, niteplatinite, and sperrylite.

These mafic rocks have total alkali contents of up to 7 %, suggesting an alkaline affinity. Geochemical data published by Yan et al. (2003) show that these intrusions contain less MgO and more silica and alkalies suggesting some degree of differentiation. In addition, these authors also report increases in ore-forming elements (S, Cu, Ni, Co) with increases in the MgO contents of the rocks (i. e. from diorite to norite).

Sulphur isotope analyses carried out by Yan et al. (2003) on 96 samples from an ore-bearing Kalatongke intrusion give a range of $\delta^{34}S$ from −3.5 to +3.0 ‰, with an average of 0.2 ‰. These values are consistent with mantle-derived sulphur. Lead isotopic compositions of sulphide minerals reported by the same authors indicate that the lead was derived from the subcontinental mantle. Zhang et al. (2008) showed that the Kalatongke intrusions have initial $^{87}Sr/^{86}Sr$ ratios ranging from 0.70375 to 0.7054 and εNd(T) from +6.3 to +8.2, implying that the magmas originated from depleted asthenospheric mantle, but with strong crustal contamination as revealed by Re-Os isotope systematics. In addition, precise Re-Os dating on sulphide ores yielded isochron ages ranging from ca. 282 to 284 Ma (Zhang et al. 2008). These authors pointed out that these ages are, within errors, close to those of A-type granites in the Altay orogen and also of related Cu and Au deposits.

6.3.7 Sandstone-hosted (roll-front) Uranium

Min et al. (2005a, b) studied and reported on sandstone-hosted roll-front type uranium deposits in Xinjiang. Three of these deposits, Wuyer, Wuyisan and Wuyiyi, are located near the Kazakhstan border in what the authors refer to as YL Basin (Yili; Fig. 6.38) and a fourth, called Shihongtan, in the Tuha Basin, about 200 km southeast of Urumqi (details are given in Chap. 8). The U deposits in the YL basin are considered to be an extension of a large U province in Kazakhstan and Uzbekistan. Both the YL and Tuha basins also host oil and gas reservoirs and coalfields, and both have a basement of Proterozoic and Palaeozoic sedimentary and volcanic rocks, unconformably overlain by successions of Triassic sandstone and shale, Jurassic conglomerate, sandstone, shale and coal beds (Shuixigou Group), Cenozoic red conglomerate, sandstone and shale. The U deposits are hosted in sandstone units of the Shuixigou Group (note that this lithostratigraphic unit is the same for both Yili and Tuha basins; see Min et al. 2005b; and not listed in Zhang 2009), divided into three formations, from base to top: Badaowan Formation with conglomerate, sandstone and coal; the Sangonghe Formation with conglomerate, sandstone, pelitic rocks and coal, overlain by the Xishanyao Formation with pelite, coal, sandstone and conglomerate (Fig. 6.39). The ore-bearing sandstone units are overlain and underlain by impermeable shales and are interpreted to be of alluvial fan and braided river facies. For the Tuha Basin the coal measures, hosting the U mineralisation, comprise low-stand system tract, lacustring system tract and highstand system tract, well studied by Wu et al. (2009). The host sandstone is composed of quartz, feldspar, carbonaceous debris and lithic fragments in a matrix of clay and silt. The orebodies

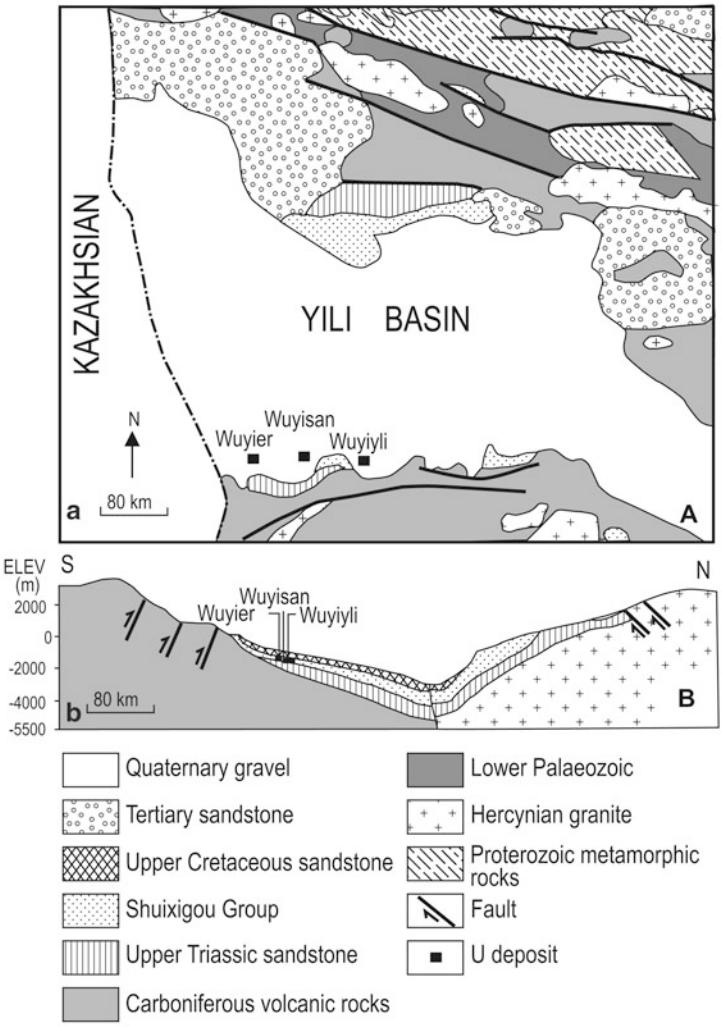

Fig. 6.38 (**a**) Distribution of sandstone-hosted (roll-front) U deposits in the YL (Yili) basin; (**b**) cross-section. (After Min et al. 2005a, b)

have a classic single or double C-shape (roll-front) at the interface between oxidised and reduced rocks (Fig. 6.39). The ore minerals are uraninite, coffinite, pyrite, marcasite, galena and not precisely identified cryptocrystalline urano-organic complexes. Min et al. (2005b) also reported that plant material in the ore zones contains U, Se, Mo and Re. The mineralisation has U-Pb ages of ca. 17–11 Ma.

Dahlkamp (2009) lists more sandstone-hosted U deposits in the southern part of the Yili Basin, as well as various U occurrences on the northern margin. The

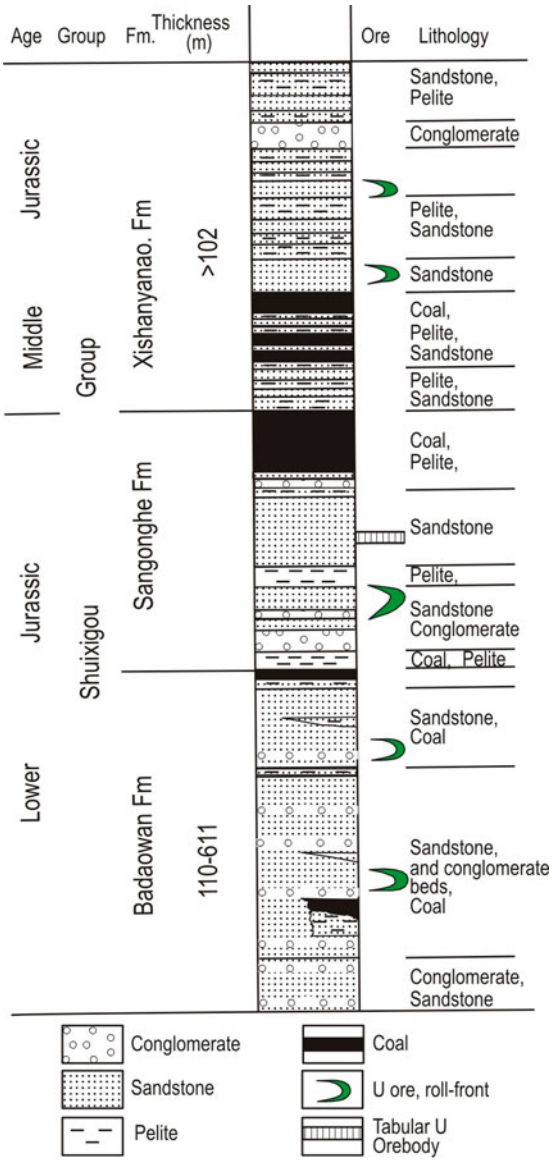

Fig. 6.39 Stratigraphy of the Shuixingou Group and position of roll-front U deposits. (After Min et al. 2005a, b)

sandstone-hosted U deposits listed by Dahlkamp include, Kujieertai, Wulkuqi, Thajistan, Mengqiguer, Daladi, none of which seem to correspond to those reported by Min (2005a, b). However, the reader has to bear in mind the problem of different spellings for the same name, as outlined in Chap. 1. Based on their position on locality figures shown in Min et al. (2005a, b) and Dahlkamp (2009), it can be

surmised that Daladi may correspond to Min et al.'s Wuyiyi and Kujieertai could be Wuyier. According to Dahlkamp (2009), the U deposits of the Yili Basin occur in braided delta sedimentary systems, in clastic sequences containing organic carbon. The host rocks are sandstone, feldspathic (kaolinised) sandstone, volcanic debris and sandy conglomerate of fluvial and/or deltaic facies. Alteration is shown by yellow to yellow-brown colouration of the sandstone beds with high hydrogoethite.

6.3.8 Rare Metal Pegmatites

There are more than 150 pegmatite-hosted rare metal deposits and occurrences in the Chinese Altay mountains (northern Xinjiang), located within the Central Altaishan terrane, which consists of high-grade metamorphic rocks and granitic intrusions. These pegmatites form a belt that extends for more than 450 km, with Altay City approximately in the middle of the belt (Figs. 6.5 and 6.11). Rare metal pegmatites have been studied and reported by Wang et al. (2003d) and Zhu et al. (2006). These authors' publications provided the information for this section. A selection of rare metal pegmatite deposits is given in Table 6.3.

Wang et al. (2003d) classified the pegmatite-hosted rare metal deposits of the Chinese Altay into three types (for a comprehensive classification of pegmatites see Černý and Ercit 2005), based on metal and mineral associations: (1) mineralogically complex deposits, enriched in Be, Li, Nb, ta, Zr, Rb, Cs, Hf and U; (2) pegmatites enriched in Be, Nb, Ta and gem-quality Be; and (3) rare metal bearing muscovite deposits hosted in gneissic rocks and Palaeozoic granitic rocks. In the first group belong the Keketuohai No. 3 pegmatite vein and the Kulumutu No. 112 pegmatite vein. In this section, I limit my discussion to the Keketuohai deposit.

6.3.8.1 Keketuohai

The Keketuohai No. 3 pegmatite is one of about 1,000 pegmatite veins in the region. The No. 3 vein was mined out by 1999, but it constituted one of the largest rare metal producers in China with more than 3 Mt of ore extracted. However, according to Zhu et al. (2006), more than 60 % of the pegmatite body was left unmined, due to unfavourable market conditions at that time. The No. 3 pegmatite when last visited in 2009 was in full operation (Fig. 6.40). In the deposit area, are deformed (gneissic) and undeformed granitic rocks (Zhu et al. 2006; Wang et al. 2007b). The undeformed granites occur as small plutons of biotite granites and two-mica granites that are part of the Aral Batholith and intrude Carboniferous volcano-sedimentary rocks, Ordovician metamorphic rocks and gneissic granite. Importantly, the gneissic granite yielded K-Ar ages of 390–330 Ma, whereas biotite from the biotite granite plutons yielded a K-Ar age of ca. 251 Ma (Zhu et al. 2006 and references therein).

Table 6.3 Selected pegmatite-hosted rare metal deposits in the Altay region. (After Wang et al. 2003d)

Deposit	Ore metals	Host rocks	Intrusions	Mineral assemblage
Yelaman	Be	Qtz-mica (schist, gneiss)	Two-mica granite (ys^2)	Ms, Be, Spod, Ab, Qtz
Akekungeyiti	Be	Qtz-Bi schist		Ber, Qtz, Col
Shangkelan	Be	Phyllite, Meta-sandstone	Ms-granite (y_4^{2a}), lamprophyre	Ber
XiaoKalasu	Nb, Ta, Be, Li	Bi-Sta schist, Sta-And-Bi-Qtz schist, gneiss	Granititc porphyry (y_4^{3a}), fine-grained granite (y_4^{3b}), gneissic granite (y_4^{2a})	Qtz, Ms, A, Mic; Cle, Cota
Bazhai		Schist	Porphyrytic granite	Ber
Kukalagai	Li, Be, Nb, Ta	Sil-Cord-Bi-Qtz schist, And-Bi-Qtz schist, Sta-Bi-Qtz schist	Two-mica granite (y_4^{3b}), Bi-granite and Bi-granite (y_4^{2a})	Qtz, Ab, Spod, Mic, Lep, Ber, Cota
Azubai	Be	Schist	Gneissic granite	Ber, Ms, Ab, Qtz
Abagong	Nb, Ta	Meta-volcanic rocks	Granite	Qtz, Ms, Ab, Cota
Hulugong	Nb, Ta, Be	Meta-volcanic rocks	Ms-granite, two-mica granite	Cota, Ber, Qtz, Ab
Husiter	Be	Gneiss	Granite	Ber, Qtz, Ab
Qiongku	Be	Gneiss	Granite	Ber, Qtz, Ab
Dakalasu	Nb, Ta	Gneiss, Meta-volcanic rocks	Bi-granite, two-mica granite	Qtz, Ab, Col, Tan, Cota
Kujierte	Be	Gneiss, schist	Amphibolite	Mic, Qtz, Ms, Gar, Tou, Ap, Zr, Ber, Cota, Spod, Lep
Keketuohai	Be, Li, Nb, Ta, Cs, Zr, Hf	GneissicBi-Qtz schist, And-Ky-Bi-Qtz schist	Gneissic Bi-granite, basic rocks, evjite, gabbro	Qtz, Ab, Mic, Ms, Lep, Spod, Tou, Ap, Gar, Be, Zr
Asdaoqia	Be	Migmatite, granulite, gneiss, schist	Migmatitic granite, two-mica granite, diorite	Mic, Qtz, Ab, Ms, Ber, Zr, Ap, Cota, Tou, Gar, on
Aershate	Be, Ga, Rb	Qtz, schist, granulite, gneiss	Granite, diorite, granodiorite	Qtz, Ms-Ber, Mol, Py, Gar
Kulumutu	Li, Be, Nb, Ta	Qtz-Ms Schist, gneiss	Bi-migmatitic granite, Gneissic two-mica granite	Ab, Mic, Qtz, Ms, Spod (max: $5 \times 60 \times 240$ mm), Ber, Cota
Alasan	Be, Nb, Ta, Rb	Gneiss, Bi-Qtz schist, migmatite	Bi-migmatitic granite, two-mica granite	Mic, Ab, Qtz, Ms, Gar, Tou, Ber, Ap, Col, Xe, Spi
Wukuang	Be, Nb, Ta	Qtz-Bi schist, migmatite, gneiss	Granite	Qtz, Ms, Mic, Ab, Ber, Col, Hf-Zr
Taerqiate	Be, Nb, Ta	Gneiss, schist, magmatite	Gabbro-norite, two-mica granite	Qtz, Ms, Mic, Ab, Spod, Cota, Zr

Annotations: *qtz* quartz; *kfs* K-feldspar; *Ms* muscovite; *Ber* beryl; *Spod* spodumene; *Ab* albite; *Col* columbite; *Sta* staurolite; *And* andalusite; *Mic* microcline; *Cle* clevelandite; *Cota* columbotantalite; *Tan* tantalite; *Lep* lepidolite; *Phe* phenakite; *Mol* molybdenite; *Py* pyrite; *Cp* chalcopyrite; *Fl* fluorite; *Chry* chrysoberyl; *Gar* garnet; *Tou* tourmaline; *Ap* apatite; *Zr* zircon; *Ky* kyanite; *Mon* monazite; *Xe* xenotime; *Spi* spinel

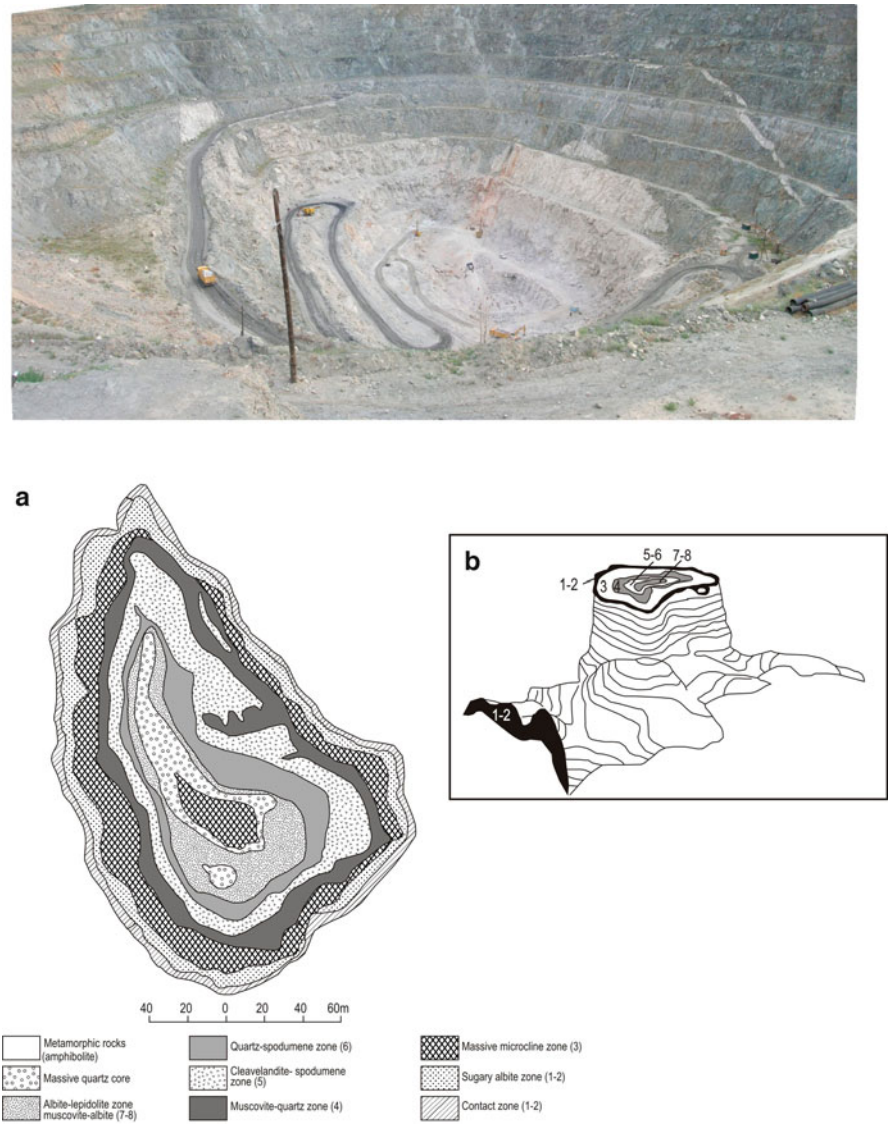

Fig. 6.40 No. 3 pegmatite open pit; **a** Geological map of the No. 3 pegmatite; **b** 3D view and zonation of the pegmatite (not-to-scale), below surface and not shown is a quartz-pollucite zone. (Modified from Wang et al. 2003d; Zhu et al. 2006)

The undeformed biotite granite plutons are associated with the pegmatite veins. The No. 3 vein is a zoned pegmatite that contained Be-, Li, Nb-Ta-, Cs-, Zr-, Hf-, U- and Bi-bearing minerals, this vein and 25 others in the deposit area are mostly hosted in mafic rocks, with a few in granitic or schist rocks. The No. 3 pegmatite vein has a peculiar cupola shape, about 2.16 km long along a north-south trend and 1.66 km wide,

that flattens to an almost subhorizontal sheet at its base. The cupola is divided into the following zones that from the margins to the centre are: (1) graphic and sub-graphic contact zone; (2) Be-enriched nested zone of sugary albite; (3) massive microcline; (4) Be-enriched muscovite and quartz; (5) Nb-Ta cleavelandite and spodumene; (6) Nb-Ta quartz-spodumene; (7) Nb-Ta lamellar albite; (8) albite-lepidolite; and (9) Cs-enriched massive microcline and quartz. Zhu et al. (2006) recognised 10 zones, which from rim to centre, are the same as 1–6 above, with a slightly different zone 7 (muscovite-albite), an 8th zone with albite and lepidolite, a 9th zone with quartz and pollucite and a 10th zone of highly differentiated massive microcline-quartz. The No. 3 pegmatite had some of the largest crystals ever found, such as an 8 m-long spodumene crystal, weighing 8 tonnes (Zhu et al. 2006). Alteration of the country rocks around the pegmatite consists of biotite, chlorite and tourmaline in mafic rocks and albite, sericite and greisen in more felsic rocks. The mineralogy of the pegmatite is dominated by microcline, albite and quartz with accessory minerals of tourmaline, garnet, apatite and muscovite. The main ore minerals comprise spodumene, lepidolite, beryl, tantalite, microlite, Cs-garnet, Li-vivianite, variscite, gahnite, bismutite, Hf-enriched zircon, pyrite, galena, sphalerite, petalite and fluorite.

The age of the No. 3 pegmatite vein was first determined using the $^{40}Ar/^{39}Ar$ isotopic system on muscovite and feldspar, yielding ages ranging from ca. 178 to 148 Ma (Wang et al. 2003d). Zhu et al. (2006) reported apatite and muscovite Rb-Sr isochron ages of 218.4 ± 5.8 Ma and an initial $^{87}Sr/^{86}Sr$ ratio of 0.708. On the other hand, SHRIMP U-Pb zircon dating by Wang et al. (2007b), yielded weighted mean ages of 220 ± 9, 213 ± 6 and 198 ± 7 Ma; with the last two ages probably representing stages of hydrothermal alteration (Wang et al. 2007b). The U-Pb age data indicate that the 220 Ma is the age of emplacement.

Helium isotopes ($^3He/^4He$ ratios) show values ranging from 1.795 to 2.540, interpreted to represent a mantle source (Wang et al. 2003d). Zhu et al. (2006) discussed the genesis of the Keketuohai pegmatites and convincingly showed that both partial melting of continental crust and upper mantle material were the main source of the magmas that produced the pegmatites. Various lines of evidence also show that A-type magmatism in the region with juvenile compositions was comparatively common in the Permian and Triassic. The pegmatites have εNd(T) values of between −0.76 and −3.04 with model ages ranging from 1.47 to 1.45 Ga, indicating that old continental crust was indeed involved in magma generation, or a mixture of old continental crust and volcanic arc material (Zhu et al. 2006). The εNd(T) values of whole rocks (apatite in pegmatite −2.75 to −3.04; biotite from granites −2.75 to −3.15; pegmatite whole rock −277 to −3.21), suggest that the granites and pegmatite have a common source. However, Zhu et al. (2006) pointed out that the genetic relationship between granites and pegmatites may be more complicated, because apatite samples separated from granites have higher εNd(T) values (−0.76 to −1.05) than those of the pegmatites. The explanation may lie in prolonged fractional crystallisation processes that have produced the well developed internal zoning. This is confirmed by the different ages of the pegmatite zones, from 246 Ma for the external zones to 120–115 Ma for the internal zones. Given the Triassic age range of the No. 3 pegmatite and the involvement of anatexis of old continental crust and upper mantle

(Zhu et al. 2006), it is possible that the Altay pegmatite field were formed during the widespread intraplate thermal event that affected large areas of Central Asia, where rare metal mineralisation in pegmatites and alkaline intrusions is widely recognised (see Pavlova et al. 2004; Borisenko et al. 2006).

6.4 Alpine-Himalayan Orogenic Belts (Tethysides)

The Alpine-Himalayan orogenic belts extend for thousands of kilometres from the Alpine orogen in Europe, to the Himalaya proper, Tibet and to southeast Asia, where they link with the Indian and Pacific Oceans volcanic arcs. The Alpine-Himalayan orogenic system, from Turkey to southeast Asia is the end result of the closure of the Palaeo- and Neo-Tethys Oceans that separated Gondwana from Laurasia in the Mesozoic and Cenozoic, respectively, hence also known as Tethysides (Sengör and Natal'in 1996). In this section, I discuss the Chinese part of the Tethysides, more specifically Tibet, southwest China and the Kunlun region on the northern margin of the Tibetan Plateau (Figs. 2.1–2.3). The Chinese Tethysides is also referred to as Himalayan-Tibetan orogen, an orogenic collage of magmatic arcs that developed in a complex geodynamic evolution extending from Cambrian to Late Triassic (Yin and Harrison 2000). The Himalayan-Tibetan orogen was later involved in the greater India-Eurasia collision, which was (and still is) affected by compressional, strike-slip and extensional movements due to the on-going collisional tectonics. The subduction of the India plate underneath Tibet, is now well documented by seismic reflection data and seismic tomography images (e.g. Zhao et al. 1993; Shapiro et al. 2004; Kind and Yuan 2010; Zhang et al. 2011; Zhao et al. 2011 and by the INDEPTH seismic project, Nelson et al. 1996; Brown et al. 1996), all supporting the original concepts that arose from a fascinating history of geological research, spanning more than a century, which focused on this equally fascinating region of the globe: Tibet and the Himalaya. Indeed, it is difficult to do justice in a few pages to those geologists who contributed to what I consider one of the best and most enduring continental geotectonic model: Suess (1904, 1906, 1908), Argand (1924), Molnar and Tapponier (1978), Dewey et al. (1988). All these works are brilliantly reviewed in an essay by Şengör and Natal'in (2007), whereas for a geophysical overview of the India-Tibet (Eurasia) collision zone, the reader is referred to Fowler (2009). Figure 6.41 illustrates models of the India-Eurasia collision, lithospheric thickening and uplift. The profile of Fig. 6.41b indicate the presence of a partially molten layer in the middle crust, which caused partial melting and the formation of granitic magmas. Normal faulting and K-rich basaltic volcanism began 8–12 Ma, probably related to extension and melting of the subcontinental lithosphere due to removal of the lower part of the lithosphere, which is then replaced by asthenospheric mantle. All these tectonic and magmatic features played a major role in the development of mineral systems in the region, as further elaborated below.

These processes of plate convergence formed the Tibetan plateau and activated major east-west, northwest-southeast and northerly-trending strike-slip fault sys-

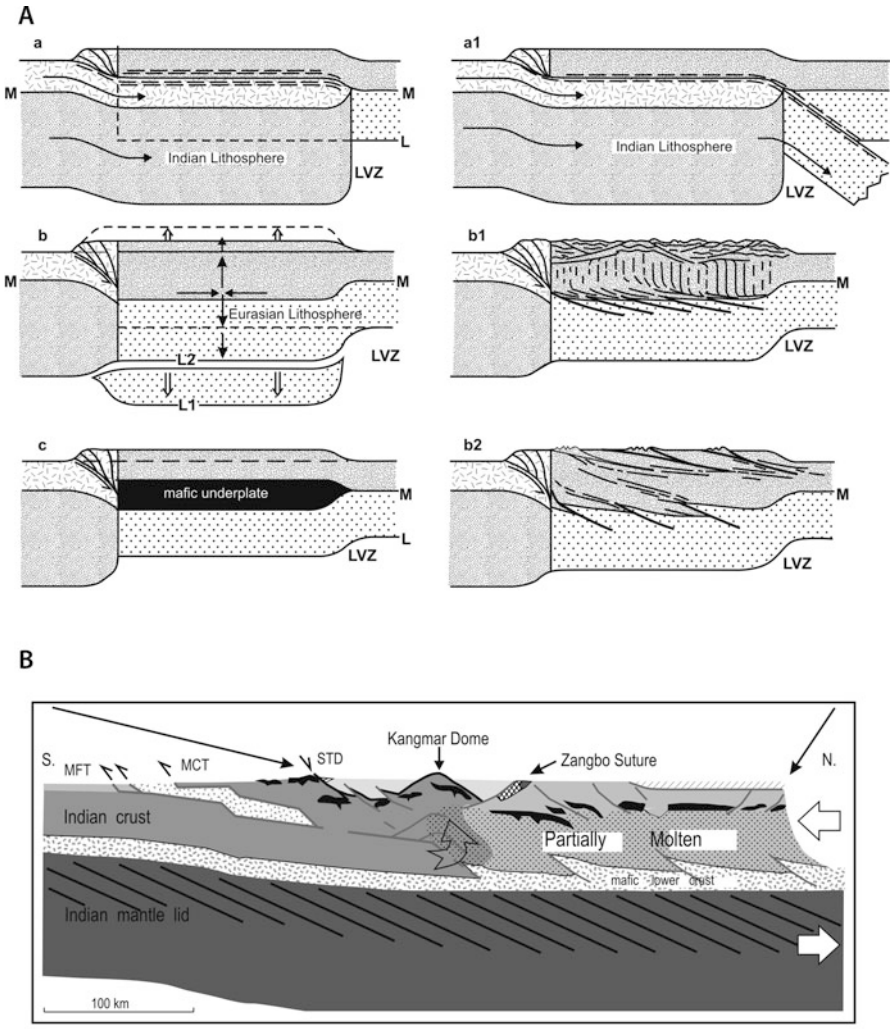

Fig. 6.41 Models of the India-Tibet collision tectonics; **A** three models from Dewey et al. (1988), (**a**) underthrusting of Indian lithosphere beneath Eurasia and delamination of the Eurasian lithospheric mantle, (**b**) north-south shortenting and thickening of the Eurasian lithosphere, **b1** and **b2** are interpreted structures of b, (**c**) thickening of the Tibetan crust and magmatic underplating, *M* Moho discontinuity, *L* base of thermal lithopsphere, *L1* base of thermal lithopsphere at end of thickening phase, *L2* base of thermal lithopsphere after delamination, *LVZ* low velocity zone; **B** Profile reconstructed from the INDEPTH seismic program, this section is across the Yadong-Gulu rift in southern Tibet modified after Nelson et al. (1996); *MFT* main frontal thrust, *STD* South Tibetan detachment system

tems, such as the Altyn Tagh and the Jinshajiang-Red River, as well as re-activating and uplifting pre-existing orogenic belts, such as the Tianshan, some 2,000 km to the north of the collision front (Figs. 2.1–2.3). These Centozoic tectonic movements reflect changes in deformation regimes from eastward-extrusion-dominated indentation tectonics to crustal thickening tectonics (Windley 1995), favoured by a low-viscosity (partially molten lower crustal layer) channel flow beneath the Tibetan plateau (Shapiro et al. 2004 and *topographic ooze* of Clark and Royden 2000). The low-viscosity channel model has recently been disputed by 3-D mechanical modelling, based on GPS measurements across the plateau, which show different patterns of faulting from extensional in the south margin to strike-slip in the north margin of Tibet (see Clark and Royden 2000; Qi et al. 2001; Copley et al. 2011; Freymuller 2011 and references therein). Nevertheless, numerical models will have to compete with the constraints provided by seismic anisotropy and seismic reflection profiles beneath southern Tibet, as well as seismic tomography (see Schulte-Pelkum et al. 2005; Shapiro et al. 2004; Zhou and Murphy 2005). In this respect, a recent re-evaluation o seismic profiles shows that in central Tibet a thin Tibetan lithosphere is underthrust by the Asian lithosphere from the north, whereas continental subduction of the Indian plate underrides the Tibetan plateau (Zhao et al. 2011).

Tibet and southwest China are an amalgamation of terranes that were accreted to the southern margin of Eurasia between the Mesozoic and the Cenozoic. The Tibet-southwest China region is therefore characterised by several suture zones that link the Qilian, Kunlun-Qaidam, Songpan-Ganzi, Qiangtang and Lhasa terranes, related to the birth and closure of the Tethys oceans, associated with the assembly and breakup of Gondwana (Yin 2010; Zhu et al. 2011, 2012). It has been pointed out that these terranes, particularly Lhasa and Tethyan Himalayan, and associated sutures, effectively record and complex history of continental break-up, subduction, collision and associated magmatism from Neoproterozoic to Cenozoic (Zhu et al. 2011, 2012).

Reviews on the tectonics and stress patterns of the Indo-Asian collision can be found in Yin and Harrison (1996, 2000), Yin (2000, 2010) and Chung et al. (2000, 2010) and Chung et al. (2005). The main sutures are: Nujiang (also called Bangong-Nujiang; Zhao et al. 2008b), Yarlung-Zangbo, Garze-Litang, Jinshajiang and Lancanjiang (Yang 1998; Hou et al. 2011; Figs. 6.42 and 6.43). The Nujiang suture extends for about 1,200 km in central Tibet and comprises ophiolites, mélange, flysch and volcanic rocks (Yin and Harrison 2000). The Yarlung-Zangbo suture zone comprises fragments of oceanic lithosphere, whereas the Lhasa terrane consists of a gneissic basement overlain by Ordovician to Permian sedimentary rocks of shallow marine facies, locally overlain by Cenozoic volcanic sequences (Yin and Harrison 2000). In the western part of the of the Yarlung-Zangbo suture is the Zhongba ophiolite, which mainly consists of harburgite and dunite (Dai et al. 2011). The ophiolites along the Yarlung-Zangbo suture have been interpreted as originally being part of a 2,500 km long intra-oceanic subduction system, comprising island arcs and marginal seas, within the Neo-Tethys ocean, whose closure in the Late Cretaceous resulted in the formation of the ophiolites in the Yarlung-Zangbo suture. Dai et al. (2011)

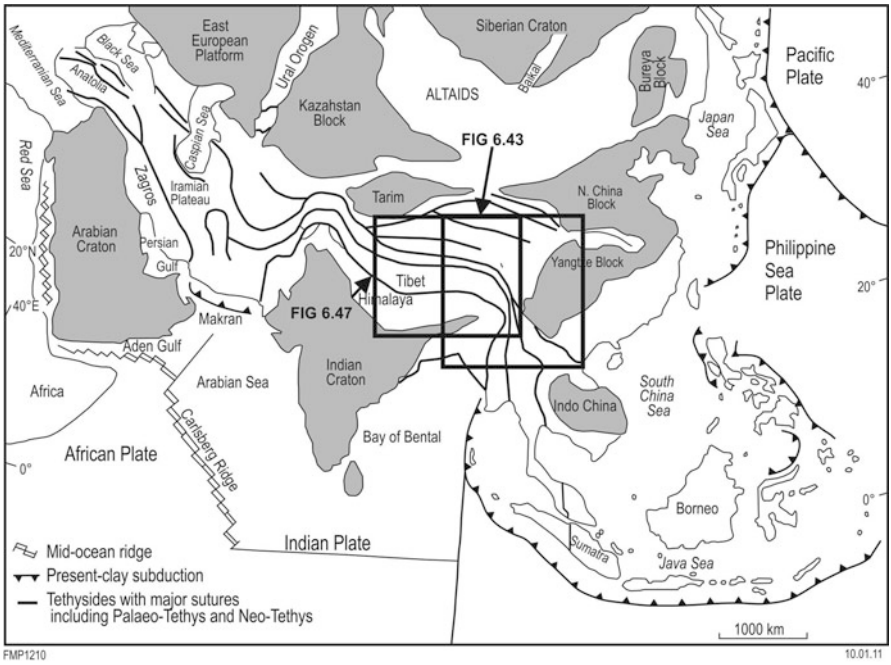

Fig. 6.42 Simplified tectonic framework of the Tethysides (slightly modified from Hou et al. 2011); *squares* indicate approximate position of Figs. 6.43 and 6.47

compared this subduction system in the Neo-Tethys to the present-day intra-oceanic subduction zones and island arcs of the western Pacific ocean.

Zhu et al. (2011) investigated the U-Pb and Hf isotopic systematics of detrital zircons from Lower Permian sandstones of the Lhasa terrane and found ages of about 1,170 Ma, which are not recorded in the Qiangtang and other Himalayan terranes. Zhu DC and co-authors concluded that before the Permian the Lhasa terrane was probably geographically adjacent to northwest Australia and more specifically the detritus that makes up the sandstones in the Lhasa terrane were derived from the Albany-Fraser belt in southwest Australia. This conclusion is supported by studies of U-Pb and Hf isotopic analyses and palaeocurrent directions in western Australia (Zhu et al. 2011; Veevers et al. 2005). Zhu et al. (2011; their Fig. 4) further proposed that the Palaeo-Tethys oceanic crust was subducted beneath the east Gondwana continental margin, resulting in the back-arc rifting of the Lhasa terrane from western Australia and at the same time separation of the Qiangtang terrane from northern India. A detailed account of the Tibetan Plateau geodynamic evolution, associated magmatism between 530 and 80 Ma and the link between the Lhasa terrane and Gondwana Australia is provided by Zhu et al. (2012).

The Garze-Litang suture marks the western margin of the Yangtze Craton and contains ophiolitic rocks and volcanic arcs (Fig. 6.43). The ophiolitic belt comprises

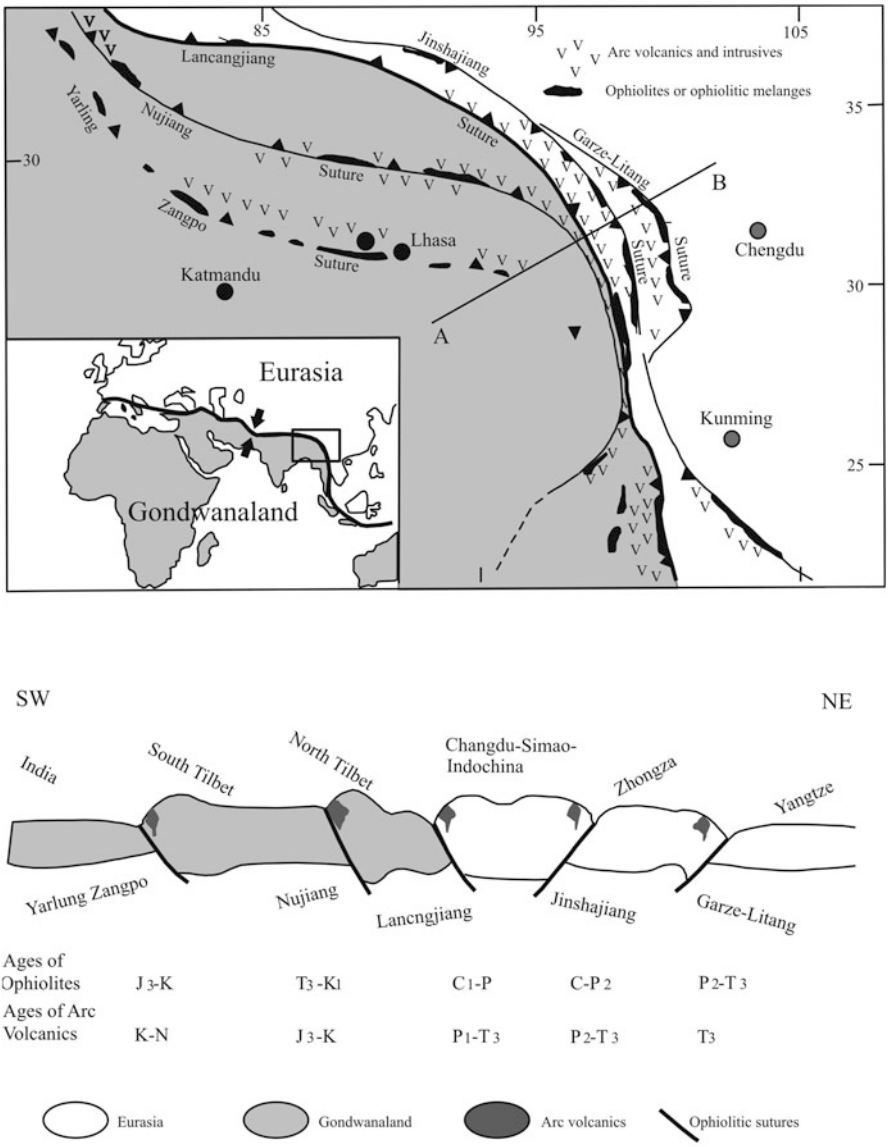

Fig. 6.43 Tectonic divisions, ophiolite belts and arc volcanics of the eastern Tethyan or Himalayan orogen in southwestern China (*top*), *line A-B* refers to the sketch in the bottom panel, which depicts a schematic geological section across the Tethyan orogen, showing principal sutures and arc volcanics. (After Yang 1998)

Late Permian-Triassic limestone, radiolarian chert, pillow lavas and fragments of mafic and ultramafic rocks. The Garze-Litang suture connects with the Jinshanjiang suture (Fig. 6.43), which separates the western margin of the Yangtze Craton from the North Tibet terrane, extending for about 2,000 km from Tibet to the Ailoshan region (Yunnan province). The Garze-Litang ophiolite is typically represented by ultramafic

rocks (serpentinite, peridotite) and gabbroic intrusions. Finally, the Lancanjiang suture zone is characterised by a sequence of dismembered ophiolites extending along more than 3,000 km. The Garze-Litang and Jinshajiang sutures are flanked by abundant volcanic rocks, such as the above mentioned volcanic arcs (Fig. 6.43). Most of the mafic rocks associated with these suture have been considered as having sourced from mid-oceanic ridges and as such they are a remnant of a sector of the Palaeo-Tethys Ocean. Xiao et al. (2008c) examined the geochemistry and isotopic signatures of the Jinshanjiang suture and flanking volcanic rocks and its ophiolitic mélange and proposed a model of geodynamic evolution, which is especially interesting because it links the geodynamic evolution of the region with the Emeishan mantle plume (Chap. 7). The geochemical and isotopic signature of mafic rocks in the suture, are the same as those of the Emeishan flood basalt. Xiao et al. (2008c) suggested that the Jinshanjiang mafic rocks can be interpreted as being the remnant of a volcanic rifted margin and that the opening of the Palaeo-Tethys Ocean was caused by the Emeishan mantle plume that was active on the western margin of the Yangtze Craton between 300 and 260 Ma, resulting in the eruption of the Emeishan basalts at 260 Ma. Closure of the Jingshnajiang Ocean followed in the mid Permian, leading to westward subduction and the formation of a volcanic arc west of the Jingshnajiang suture. The subduction complex was partially destroyed together with the volcanic rifted margin, resulting in the discontinuous and highly deformed mélange that is observed today. The model proposed by Xiao et al. (2008c) is shown in Fig. 6.44.

It is important to note that a series of north-south trending rifts are present in Tibet due to the active east-west extension of the plateau. These rifts may record delamination of mantle lithosphere beneath the region in the Late Miocene and Pliocene, removal of dense lithosphere may have caused uplift, as sinking cold lithosphere is replaced by hot and buoyant asthenosphere. This upwelling of hot asthenosphere may have induced crustal melting and be responsible for the intrusion-related mineral systems in the Tibet and southwest China regions. An alternative view was proposed by Xiao et al. (2007) who, on the basis of geophysical and structural data, suggested that the underthrust Indian lithosphere split in two slabs, a northward moving high-angle western slab underlying the western sector of the plateau and a northeastward moving low-angle eastern slab penetrating the eastern sector. The boundary between the two sectors is the Yadong-Anduo-Golmud (YAG) tectonic corridor (Fig. 6.45). Studies of Cenozoic syn- and post-collisional igneous rocks emplaced in the Tibetan crust shows that the YAG corridor separates significant geographic variations in both the ages and types of magmatism. Miocene and Quaternary potassic volcanism predominate west of the YAG corridor in the Qiangtang terrane, whereas Eocene-Oligocene volcanism predominates east of the YAG. Within the Lhasa terrane, voluminous Palaeogene volcanic rocks and minor Cretaceous and Eocene granites occur west of the YAG corridor. In contrast, Cretaceous and Eocene granites, with only minor Palaeocene volcanic rocks, are more abundant in the eastern sector of the terrane. In addition, the western sector of the Lhasa terrane also contains earlier Miocene potassic and ultra-potassic volcanic rocks, whereas only sparse younger Miocene ($<$17 Ma) volcanic rocks occur in its eastern sector (Williams et al. 1999; Nomade et al. 2004). High-K and shoshonitic volcanic and intrusive rocks dominate in the

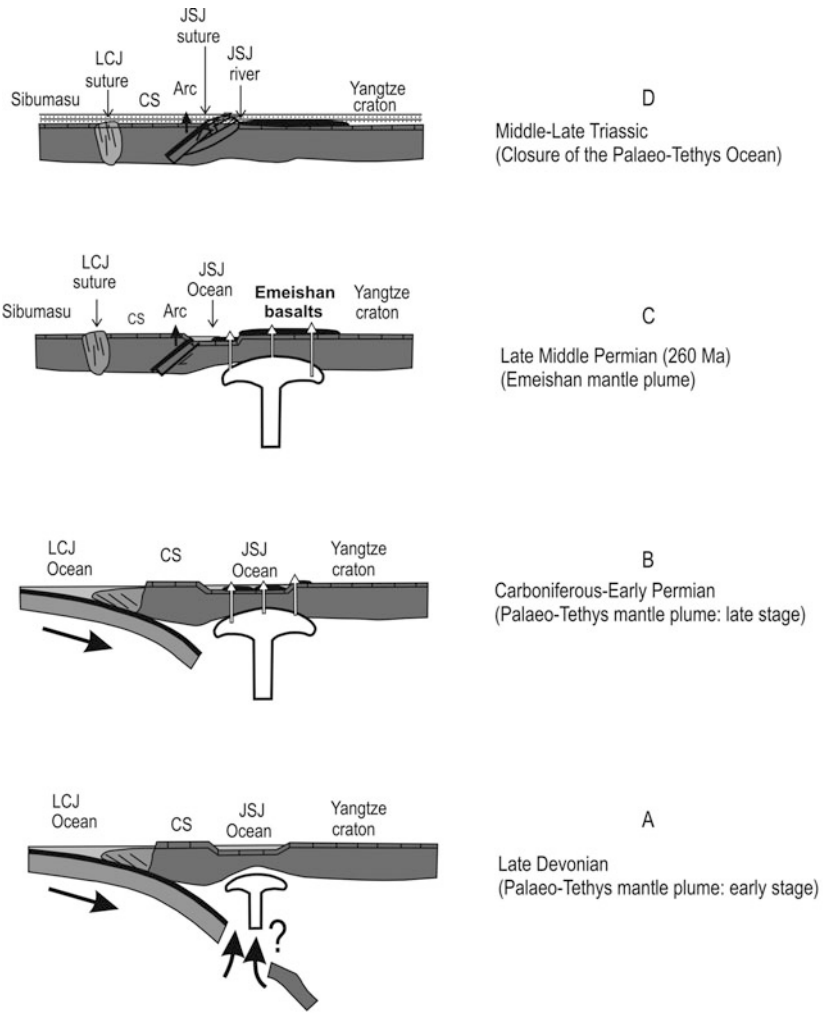

Fig. 6.44 Geodynamic evolution of the Jingshanjiang suture and Palaeotethys Ocean. (As envisaged by Xiao et al. 2008c)

western sector, whereas the eastern sector contains mostly potassic and calc-alkaline rocks (Chung et al. 2005). The volcanic rocks that outcrop on the islands of Hainan and the western side of Taiwan are of Eocene and Pleistocene age, and belong to the Himalayan Orogeny (<90 Ma).

More recently, Hou and Cook (2009) in their introduction to a special issue on the metallogenesis of the Tibetan sector of the Tethysides (Tibetan Orogen), considered a three stage tectono-magmatic evolution and associated metallogenic events (Fig. 6.46): (1) main continental collision and underthrusting (65–41 Ma); (2) late

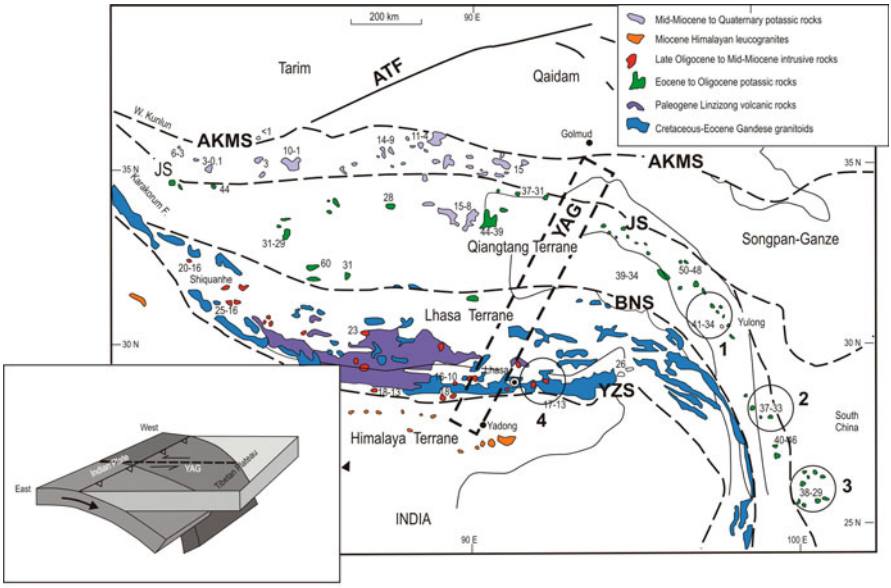

Fig. 6.45 Simplified geological map of the Tibetan Plateau and surrounding areas (modified from Chung et al. 2005; Xiao et al. 2007). Ages of post-collision potassic magmas are shown (Chung et al. 2005). Elevations of the Plateau are after Fielding (1996). *Inset* shows the Xiao et al.'s model of split subducting plate in the Tibetan plateau as the Yadong-Anduo-Golmud (YAG) tectonic corridor shown as a *rectangle*. *AKMS* is the Ayimaqin-Kunlun-Muztagh suture or Longmu Tso-Shuanghu Suture, *YZS* Indus-Yarlung Zangbo suture, *JS* Jinshanjiang or Jinsha suture, *BNS* Bangong-Nujiang suture. *Circles* indicate belts and/or clusters of porphyry systems in the Jinshajiang-Red River fault zone, *1* Yulong; *2* Tongchan; *3* Machangqing; *4* Gangdese belt

collision (40–26 Ma); and (3) post-collision to present (25 Ma to present). The following is abridged from Hou and Cook (2009). The timing of the main collisional period remains controversial with dates ranging from 65 to 41 Ma, 55 to 50 or 55 to 52 Ma, with the first considered more reliable. During this phase tectonism and deformation evolved from early compressional to late stress-relaxation. This is the time of the development of the Tethyan Himalayan thrust belt in south Tibet, the Gangdese range in the Lhasa terrane and Cenozoic contractional systems in central Tibet. The Tethyan Himalayan thrust belt, estimated to have shortened by 130–140 km, consists of fold and imbricate thrusts involving the passive continental margin sequence of the Tethyan Himalaya. The Gangdese range, formed by emplacement of Paleocene syn-collisional granites, is a high but narrow mountain range. In central Tibet the Shiquanhe–Gaize–Amdo thrust system, the Fenghuoshan–Nangqian fold-thrust belt, and the Qimen–Tagh thrust system are important for their association with igneous events and mineral systems (Fig. 6.46). Four principal magma suites have been recognized in the Gangdese range, forming a >1,000 km-long, east-west-trending tectono-magmatic belt (Fig. 6.47): (1) a ca. 5 km-thick, early-Cenozoic (65–58 Ma) Linzizong volcanic succession, geochemically, the suite is calc-alkaline

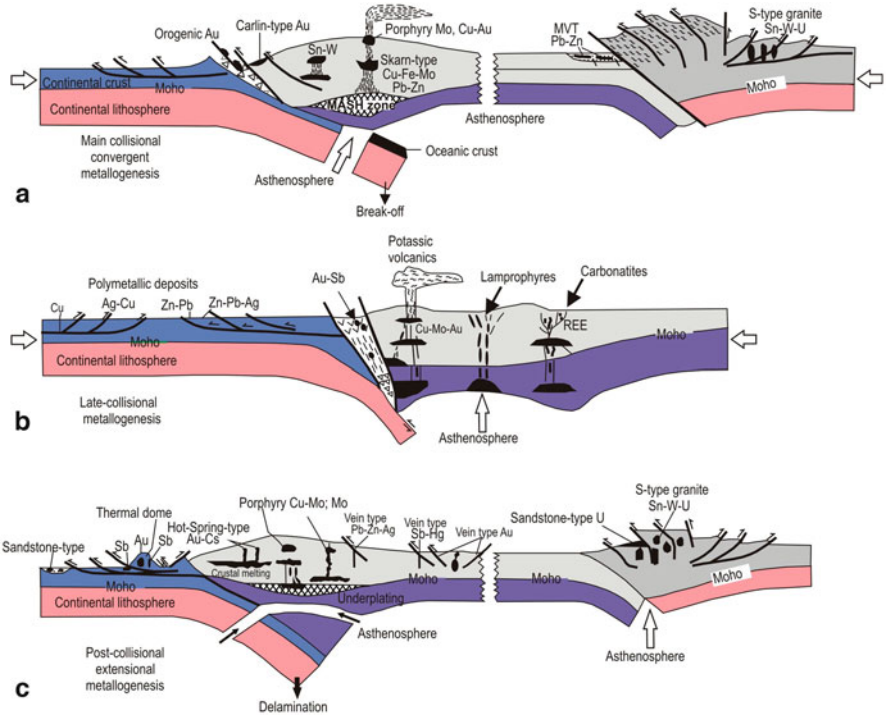

Fig. 6.46 Tectonic, magmatic and metallogenic evolution of the Tibetan orogen, according to Hou and Cook (2009); **a** collisional period with slab underthrusting resulted, crustal shortening, and thickening, which resulted in low-f_{O2} crustal anatexis and CO_2-fluids due to metamorphic devolatilisation, with the formation of Au lodes, porphyry systems and Sn–W–U. Breakoff of the subducted slab induced upwelling of the asthenosphere, mantle,/crust melting and stress relaxation, creating hydrous, high-f_{O2} felsic melts and formation of magmatic-hydrothermal polymetallic systems and MVT deposits in the foreland; **b** late collision setting and large-scale strike-slip faulting, shearing and thrusting, where translithospheric upwelling of the asthenosphere, probably resulted in lamprophyric and carbonatite-alkalic magma systems, with the development of porphyry Cu–Mo–Au and REE deposits. Thrust and nappe systems at shallow structural levels controlled sediment-hosted base metallic deposits formed by migration of basinal brines; **c** post-collisional regime promoting lithospheric delamination at depth, crustal extension and partial melting of the thickened crust. Anatexis of the middle-upper crust generated leucogranites and associated Sn–W–U mineralization in the central axial zone and Au mineralization in the foreland. Potassic felsic magmas with porphyry Cu–Mo mineralization are related to melting of a thickened, newly-formed lower-crust in the collisional zone. The detachment fault systems related to extension and high-level emplacement of felsic magmas result in convective geothermal systems and associated Au, Au–Sb, Sb, and Cs mineralization in the rift zone and in the exhumed core complex or domes; terrigenous sediments in rift basins, within the orogenic belt, are linked with sandstone-type U deposits

and high-K calc-alkaline with minor shoshonitic character, and shows LREE enrichment; (2) Palaeocene (52–47 Ma) syn-collisional muscovite granites, potassic calc-alkaline granites, monzonite and syenitic rocks, locally associated with Sn mineralisation; (3) Eocene (52–42 Ma) gabbros and granitic intrusions, developed along the southern margin of the Lhasa terrane; these granites usually have mafic enclaves and are associated with polymetallic mineralisation; and (4) basaltic subvolcanic rocks. These events have been correlated with variations in the Indo-Asia continental rate of convergence.

The late-collisional period is marked by potassic magmatism in transpressional tectonic regimes. In east Tibet southeastern extrusion of the Indochina block, block rotation and internal shortening, culminated with three styles of deformations considered important for the generation of collision related mineralisation in strike-slip fault zones. The first is large-scale Cenozoic strike-slip fault systems, striking both east-west and north-south, forming the Gali–Gaoligong fault system, the Mangkang–Lijiang fault belt, which controls the Yulong porphyry Cu belt and the Xianshuihe–Xiaojiang fault system, which controls the Mianning-Dechang REE belt (Fig. 6.46). Magmatism associated with the late-collision period extends for about 2,000 km from the Qiandang terrane eastward to the western Yangtze region. Three main magmatic provinces are controlled by Cenozoic strike-slip faults (Hou and Cook 2009). These provinces from west to east are: (1) potassic igneous intrusions hosting Cu-Mo-Au deposits; (2) potassic, calc-alkaline and lamprophyre province; and (3) north-south trending zone of carbonatites and alkaline complexes, with REE mienralisation. The post-collisional period, continues to present day and is associated with crustal shortening at deep crustal levels, continuing underthrusting of the Indian plate under Eurasia and importantly lateral flow and southward extrusion of hot and ductile Tibetan lower crust. Magmatism that can be related to post-collision tectonics occurred at 25–13 and 13–0.5 Ma, the younger event is mostly restricted to north Tibet. In southern Tibet, the first period of magmatism resulted in the formation of leucogranite belts (Himalayan granites) and 17.6–9.5 Ma granitic plutons, hosting Au-Sb mineralisation (see below). In the Lhasa terrane between 23 and 13 Ma a potassic and ultrapotassic igneous belt was formed, extending for 1,500 km.

6.4.1 Mineral Systems; Overview

Figures 6.46 and 6.47 illustrate the distribution and tectonic settings of the Himalayan-Tibetan orogen's mineral systems. In southwest China (eastern part of the Himalayna-Tibetan orogenic belt), is the Sanjiang Tethyan Metallogenic Domain (STMD; Hou et al. 2007a), where volcanogenic massive sulphides, Ag-polymetallic, Sn greisen and porphyry systems are present. Hou et al. (2007a) provided a comprehensive listing of the mineral deposits in the STMD (Table 6.4), whereas Hou and Cook (2009) listed a number of giant or large-size deposits in the Tibetan orogen (Table 6.5 and Fig. 6.47). These two tables demonstrate the number and variety of mineral deposits in a region, which is after all not as well geological explored as other parts of China (e.g. Qinling or Yangtze River Valley). Several porphyry copper and

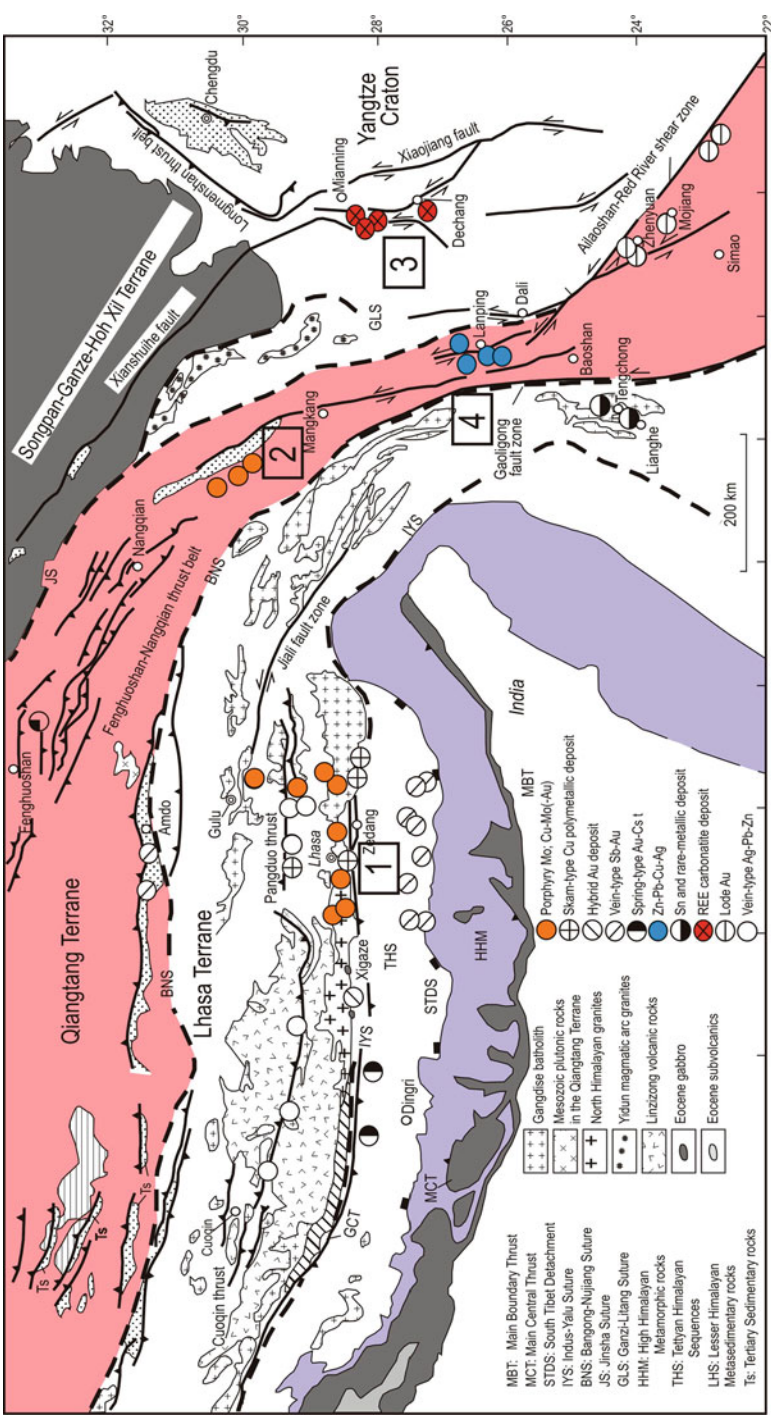

Fig. 6.47 Simplified geology (from Yin and Harrson 2000) of the Chinese Tethyan terranes (Tibetan orogen) and distribution of mineral deposits (see also Fig. 6.45 and Tables 6.2 and 6.3, for details of individual deposits); deposits discussed in this Chapter are shown by the coloured symbols Gangdese (*1*) and Jinshanjain-Red River (*2*) porphyry systems, Miannig-Dechang REE belt (*3*) and Jinding base metal deposits (*4*). (After Hou and Cook 2009)

Table 6.4 Listing of 54 mineral deposits in the Sanjiang Tethyan metallogenic domain (STMD). (Modified after Hou et al. 2007a and references therein)

Name/number in Fig. 1 of Hou et al. (2007a)	County/ province	Longitude/ latitude	Metals	Tonnage	Grade	Host rock	Dominant alteration/ mineral phases	Ore minerals (in order of abundance)	Genetic type
Yulong	Yamda, Tibet	97°44′ 31°24′	Cu-Mo	Cu: 6.5 Mt	Cu: 0.99 % Mo: 0.028 %	Monzonitic granite porphyry, quartz monzonitic porphyry, Triassic sandstone and mudstone	Outwards from centre: potassic alteration → quartz sericite zone → argillic → propylitic	Chalcopyrite, molybdenite, pyrite, bornite, tetrahedrite, cubanite, sphalerite, galena, native gold, native silver	Porphyry Cu-Mo
Mangzong	Jamda, Tibet	97°45′ 31°20′	Cu-Mo	Cu: 0.25 Mt	Cu: 0.34 % Mo: 0.03 %	Monzonitic granite porphyry	Outwards from centre: potassic alteration → quartz sericite zone → propylitic	Chalcopyrite, pyrite, molybdenite, galena, sphalerite, tennantite, chalcocite	Porphyry Cu-Mo
Zhanaga	Jamda, Ribet	97°43′ 31°20′	Cu-Mo	Cu: 0.3 Mt	Cu: 0.36 % Mo: 0.03 %	Monzonitic granite porphyry; syenitic granite porphyry	From south to north: tourmalinization (quartz, sericite zone) → argillic → propylitic	Chalcopyrite, molybdenite, pyrite, magnetite, chalcocite, bismuthinite	Porphyry Cu-Mo

Table 6.4 (continued)

Name/number in Fig. 1 of Hou et al. (2007a)	County/ province	Longitude/ latitude	Metals	Tonnage	Grade	Host rock	Dominant alteration/ mineral phases	Ore minerals (in order of abundance)	Genetic type
Duoxiasongduo	Jamda, Tibet	97°55 31°10′	Cu-Mo	Cu: 0.5 Mt	Cu: 0.38 % Mo: 0.04 %	Alkali-feldspar granite porphyry; Monzonitic granite porphyry	Outwards from centre: potassic alteration → quartz sericite zone → propylitic	Chalcopyrite, pyrite, molybdenite; magnetite, galena; sphalerite, bornite	Porphyry Cu-Mo
Malasongduo	Jamda, Tibet	98°00′ 31°00′	Cu-Mo	Cu: 2.3 Mt	Cu: 0.44 % Mo: 0.14 %	Monzonitic granite porphyry; syenitic granite porphyry	Outwards from centre: potassic alteration → quartz sericite zone -argillic → propylitic	Chalcopyrite, pyrite molybdenite, galena, sphalerite, bornite, tetrahedrite	Porphyry Cu-Mo
Mamupu	Mangkang, Tibet	98°30′ 30°00′	Cu-Au	No data	Cu: 0.12–0.32 % Au: 6.4–131.1 g/t	Syenitic porphyry	No zoning	Chalcopyrite, pyrite, molybdenite, galena, sphalerite, native gold	Porphyry Cu-Au
Zhaokalong	Yushu, Qing-hai	97°21′ 32°38′	Fe-Pb-Zn-Ag	Fe: 11 Mt	Total Fe: 31.8–47.1 % Pb: 0.001–4.12 % Zn: 0.05–1.02 % Ag: 6.5–191.5 g/t	Siltstone, slate, dolomite; limestone and andesite	Barite sericitic, chloritisa-tion	Siderite, magnetite, galena, sphalerite, chalcopyrite, pyrite, bornite	VHMS

Table 6.4 (continued)

Name/number in Fig. 1 of Hou et al. (2007a)	County/ province	Longitude/ latitude	Metals	Tonnage	Grade	Host rock	Dominant alteration/ mineral phases	Ore minerals (in order of abundance)	Genetic type
Jiaduoling	Jamda, Tibet	98°05′ 31°50′	Fe	No data	No data	Triassic dioritic porphyry	Albitisation, sericitisation, chloritisation	No data	Porphyry Fe? it
Luchun	Deqin, Yunnan	98°42′ 28°05′	Cu-Zn-Pb	Cu: 0.3 Mt Pb + Zn: 0.4 Mt	Cu: 0.65 % Pb: 0.76–1.67 % Zn: 0.98–4.49 %	Bimodal suite: felsic volcanic rock	Silicification, sericitisation, chloritisation	Chalcopyrite, pyrite, galena, magnetite, pyrrhotite, sphalerite	VHMS
Yargla	Deqin, Yunnan	99°10′ 29°20′	Cu-Zn	Cu: 1 Mt Pb_Zn: 3 Mt	Cu: 0.6 %	Calc-alkaline andesitic-dacitic volcanic rocks	Chloritisation, skarn	Chalcopyrite, pyrite, magntite, galena, sphalerite	VHMS
Gala	Garze, Sichuan	99°15′ 31°50′	Au	Au: < 20 t	Au: 3.3–8.0 g/t	Ophiolitic suite: Triassic basaltic rocks	Silicification, sericitisation, carbonatisation, pyrite	Pyrite, arsenopyrite, stibnite, native gold	Shear-zone
Erze	Muli, Sichuan	110°28′ 28°18′	Au-Ag-Cu	Au: 10.8 t	Au: 4.7–7.8 g/t Ag Ag: 10–50 g/t Cu: 0.5–2.5 %	Upper Permian marble, dolomitic limestone, phyllite and mica schist	Sericitisation, pyrite, carbonate	Pyrite, chalcopyrite, arsenopyrite, tetrahedrite, siderite	Vein-type

Table 6.4 (continued)

Name/number in Fig. 1 of Hou et al. (2007a)	County/ province	Longitude/ latitude	Metals	Tonnage	Grade	Host rock	Dominant alteration/ mineral phases	Ore minerals (in order of abundance)	Genetic type
Gayiqiong	Baiyu, Sichuan	99°18′ 31°34′	Zn-Pb-Cu-Ag	Zn + Pb + Cu: 0.5 Mt	Pb: 3.2 % Zn: 3.49 %	Bimodal suite; dacitic volcaniclastic pile, and associated siderite and jasper	Potassic, silicification, sericitisation	Pyrite, sphalerite, galena, tetrahedrite, chalcopyrite, arsenopyrite	Kuroko-type VHMS
Gacun	Baiyu, Sichuan	99°32′ 31°11′	Zn-Pb-Cu-Ag	Zn + Pb + + Cu: 4 Mt Ag: 3,800 t	Zn: 5.4 % Pb: 3.7 % Cu: 0.44 % Ag: 160 g/t	Bimodal suite; rhyolitic volcaniclastic pile and associated jasper, barite, and dolomite	Silicification, sericitisation, chloritisation, epidotisation	Pyrite, sphalerite, galena, tetrahedrite, chalcopyrite, arsenopyrite, bornite	Kuroko-type VHMS
Kongmasi	Baiyu, Sichuan	99°10′ 31°30′	Hg	Ha: 1,879 t	Hg: 0.1 %	High-K rhyolitic volcanic rocks and limestone	Silicification, sericitisation, carbonate, pyrite	Metacinnabar, pyrite, sphalerite, galena, orpiment, psilomelane, pyrolusite, rhodochrosite	Vein-type
Nongduke	Baiytu, Sichuan	99°24′ 30°56′	Ag-Au	Ag: 1,300 t Au: 1.3 t	Ag: 200 g/t Au: 2–10 g/t	Late Triassic high-K rhyolitic rocks	Silicification, sericitisation, pyrite	Stibnite, tennanite, pyrite, sphalerite, orpiment, realgar, native gold	Epithermal vein-type

Table 6.4 (continued)

Name/number in Fig. 1 of Hou et al. (2007a)	County/ province	Longitude/ latitude	Metals	Tonnage	Grade	Host rock	Dominant alteration/ mineral phases	Ore minerals (in order of abundance)	Genetic type
Xuejiping	Zhongdian, Yunnan	99°50′ 28°02′	Cu	Cu: 0.30 Mt	Cu: 0.60 %	Dioritic porphyry and monzonitic porphyry	Silicification, chloritisation, actinolite	Chalcopyrite, pyrite, magnetite	Porphyry Cu deposit
Hongshan	Zhongdian Yunnan	99°53′ 28°07′	Cu-Pb-Zn-Ag	Cu: 0.29 Mt	Cu: 1.1 %	Layered skarn between Triassic slate and felsic intrusion	Skarn	Chalcopyrite, pyrite, magnetite, galena, sphalerite	Skarn-type deposit
Cuomolong	Batang, Sichuan	99°22′ 30°30′	Sn-Pb-Zn	Sn: 11,511 t	Sn: 0.22–1.38 % Pb: 0.3–0.5 % Zn: 0.5–2.5 %	Skarn between granite and Triassic sandstone	Skarn	Pyrite, magnetite, cassiterite, galena, sphalerite	Skarn-type ?deposit
Xiasai	Batang, Sichuan	99°36′ 30°27′	Ag-Pb-Zn	Ag: 5,600 t	Ag: 300 g/t Pb: 8 % Zn: 2 %	Upper Triassic sandstone and slate sequence	Silicification, sericitisation	Galena, sphalerite, pyrite, native silver	Vein-type
Najiaoxi	Batang, Sichuan	99°21′ 29°22′	Pb-Zn	Pb: 0.24 Mt Zn: 0.26 Mt	Zn: 36 % Pb: 3.4 %	Cambrian crystalline limestone and dolomite	Silicification, sericitisation, carbonate	Pyrite, sphalerite, magnetite, galena	Skarn-type

Table 6.4 (continued)

Name/number in Fig. 1 of Hou et al. (2007a)	County/ province	Longitude/ latitude	Metals	Tonnage	Grade	Host rock	Dominant alteration/ mineral phases	Ore minerals (in order of abundance)	Genetic type
Baiyangping	Batang, Sichuan	99°21′ 29°22′	Cu-Co-Ag	In exploring	Cu: 0.93–2.5 % Co: 0.10–0.27 %	Cretaceous transitional zone between porous sandstone and low-permeability carbonaceous bargillite	Silicification, carbonate, chlorite, epidote	Tetrahedrite, pyrite, chalcopyrite, galena, freibergite	Vein-type polymetallic
Fulongchang	Lanping, Yunnan	99°14′ 26°49′	Cu-Ag-Pb	In exploring	Cu: 1.4–9.5 % Ag: 51.502 g/t Pb: 4.2 %	Cretaceous transitional zone between porous sandstone and low-permeability carbonaceous argillite	Silicification; carbonate	Tetrahedrite, pyrite, chalcopyrite, galena, freibergite	Vein-type polymetallic
Yanzidong	Lanping, Yunnan	99°18′ 26°45′	Pb-Zn-Cu-Ag	In exploring	No data	Upper Triassic dolomitic limestone, limestone breccia, sandstone and conglomerate	Carbonate chloritisation, barite, celestite	Bornite, tennantite, tetrahedrite, pyrite, chalcopyrite, galena, siderite, freibergite	Sedex

Table 6.4 (continued)

Name/number in Fig. 1 of Hou et al. (2007a)	County/ province	Longitude/ latitude	Metals	Tonnage	Grade	Host rock	Dominant alteration/ mineral phases	Ore minerals (in order of abundance)	Genetic type
Huishan	Lanping, Yunnan	99°17′ 26°43′	Pb-Zn-Cu-Ag	In exploring	No data	Upper Triassic siliceous rocks, dolomitic limestone and limestone breccia	Carbonate, chloritisation, barite, celestite	Galena, sphalerite, pyrite, chalcopyrite, bornite	Sedex
Jinding	Lanping, Yunnan	99°25′ 26°24′	Zn-Pb-Ag	Zn: 12.84 Mt Pb: 2.64 Mt	Zn: 8.32–10.52 % Pb: 1.16–2.42 % Ag: 12.5–12.6 g/t	Cenozoic argillaceous dolomite, argillaceous siltstone, sandstone and siltstone	Pyrite, marcasite, calcite, dolomite, hematite, silica, barite, celestite	Galena, Sphalerite, pyrite, pyrrhotite, marcasite, chalcopyrite, native silver	Sedex?
Baiyangchang	Yunlong, Yunnan	99°24′ 26°07′	Ag-Cu-Pb-Zn	Exploring	Ag: 110–245 g/t Cu: 0.36–1.61 % Pb: 0.22–3.24 % Zn 1.11 %	Jurassic-Cretaceous high-porous limestone and the overlying low-porous carbargillite	Barite, carbonate, discolouration	Tennantite, chalcopyrite, bornite, freibergite, pyrite, argentite, sphalerite, galena, native silver	Sedex
Diatan	Tengchong, Yunnan	98°26′ 25°39′	Sn	No data	No data	Mesozoic biotite granite, dolomitic limestone, arenaceous mudstone and sandstone	Skarn, silicification, sericitisation, chloritisation	Pyrite, cassiterite, galena, sphalerite, magnetite, pyrrhotite	Skarn-type Sn

Table 6.4 (continued)

Name/number in Fig. 1 of Hou et al. (2007a)	County/ province	Longitude/ latitude	Metals	Tonnage	Grade	Host rock	Dominant alteration/ mineral phases	Ore minerals (in order of abundance)	Genetic type
Dantongchang	Tengchong, Yunnan	98°44′ 25°32′	Sn	Sn: < 10,000 t	Sn: 0.016–0.26 % Pb: 0.67–15.7 % Zn: 1–35 % Cu: 0.38–1.08 % Ag: 1–326.8 g/t	Mesozoic biotite granite, dolomitic limestone, arenaceous mudstone and sandstone	Skarn, silicification, tremolite, sericitisation, chloritisation, fluorite	Pyrite, cassiterite, galena, sphalerite, magnetite, pyrrhotite	Sn-bearing sulphide type
Xiaolonghe	Tengchong, Yunnan	98°26′ 25°27′	Sn	Sn: 26,200 t	Sn: 0.18–0.42 %	Mesozoic biotite granite, sandy slate	Greisenisation, sericitisation, silicification, chloritisation	Pyrite, topaz, cassiterite, magnetite	Cassiterite-sulphide type
Gudong	Tengchong, Yunnan	98°30′ 25°20′	Sn	No data	No data	Mesozoic biotite granite, sandy slate	Greisenisation, sericitisation, silicification, chloritisation	Pyrite, topaz, cassiterite, magnetite	Cassiterite-sulphide type
Tieyaoshan	Tengchong Yunnan	98°24′ 25°15′	Sn	No data	No data	Mesozoic biotite granite, sandy slate	Greisenisation sericitisation, silicification, chloritisation	Pyrite, topaz, cassiterite, magnetite	Cassiterite-sulphide type
Laopingshan	Tengchong, Yunnan	98°22′ 25°00′	Sn	No data	No data	Mesozoic biotite granite, sandy slate	Greisenisation, sericitisation, silicification, chloritisation	Pyrite, topaz, cassiterite, magnetite	Cassiterite-sulphide type

Table 6.4 (continued)

Name/number in Fig. 1 of Hou et al. (2007a)	County/ province	Longitude/ latitude	Metals	Tonnage	Grade	Host rock	Dominant alteration/ mineral phases	Ore minerals (in order of abundance)	Genetic type
Lailishan	Lianghe, Yunnan	98°167′ 24°55′	Sn	Sn: 42,600 t	Sn: 0.63–1.58 %	Himalayan K-feldspar granite; metamorphosed feldspathic sandstone, argillaceous siltstone, dolomite	Potassic, kaolinite, sericitisation, silicification, pyrite chloritisation	Pyrite, topaz, pyrrhotite, cassiterite	Cassiterite-sulphide type
Shuiyinchang	Baoshan, Yunnan	98°57′ 25°20′	Hg	No data	No data	Devonian-Carboniferous limestone formation	Silicification, pyrite, dolomitisation	Pyrite, cinnabar, sphalerite, galena	Vein-type Hg
Maocaopo	Baoshan, Yunnan	98°54′ 24°22′	Hag	No data	No data	Devonian-Carboniferous limestone formation	Silicification, pyrite, dolomitisation	Pyrite, cinnabar, sphalerite, galena	Vein-type Hg
Dongshan	Baoshan, Yunnan	99°11′ 24°26′	Pb-Zn	No data	No data	Early-Palaeozoic limestone formation	Silicification, pyrite, chloritisation, dolomitisation	Pyrite, sphalerite, galena, pyrrhotite	Massive sulphide
Mengxing	Baoshan, Yunnan	99°11′ 23°52′	Pb-Zn	No data	No data	Early-Palaeozoic limestone formation	Silicification, pyrite, chloritisation, dolomitisation	Pyrite, sphalerite, galena, pyrrhotite	Massive sulphide

Table 6.4 (continued)

Name/number in Fig. 1 of Hou et al. (2007a)	County/ province	Longitude/ latitude	Metals	Tonnage	Grade	Host rock	Dominant alteration/ mineral phases	Ore minerals (in order of abundance)	Genetic type
Shiluang-chang	Nanjian, Yun-nan	100°09′ 25°19′	Au-Sb-As	No data	No data	Upper Triassic limestone and sandy-slate	Silicification, sericitisation, pyrite, dolomitisation	Pyrite, realgar, orpiment, sphalerite, galena	Vein-type Au-Sb-As
Manshan	Nanjian, Yun-nan	100°03′ 25°15′	Hg:	Hg: <1,000 t	Hg: 0.05–0.2 %	Upper Triassic slate and limestone	Pyrite, dolomite, silicification, calcite	Pyrite, cinnabar, sphalerite, galena	Vein-type Hg
Zhacun	Nanjian, Yun-nan	100°10′ 25°07′	Au	Au: <10 t	Au: 2.16–3.55 g/t	Feldsapthic sandstone, carbonaceous argillite, siltstone, shale	Pyrite, dolomitisation, silicification, calcite, barite	Pyrite, ankerite, galena, sphalerite, native gold	Vein-type Au
Bijiashan	Nanjian, Yun-nan	100°00′ 25°00′	Au	No data	No data	Feldspathic sandstone, argillite, siltstone, shale	Pyrite, dolomitisation, silicification, calcite	Pyrite, ankerite, galena, sphalerite, native gold	Vein-type Au
Tongchangije	Yunxian, Yun-nan	99°45′ 24°20′	Cu	Cu: 0.2 Mt	Cu: 154 %	Permo-Carboniferous mafic volcanic sequence	Silicification, sericitisation, chloritisation, carbonate	Pyrrhotite, pyrite, chalcopyrite, sphalerite, galena, hematite, magnetite	VHMS t

Table 6.4 (continued)

Name/number in Fig. 1 of Hou et al. (2007a)	County/ province	Longitude/ latitude	Metals	Tonnage	Grade	Host rock	Dominant alteration/ mineral phases	Ore minerals (in order of abundance)	Genetic type
Laochang	Lanchang, Yunnan	99°44′ 22°45′	Pb-Zn-Ag	Pb: 0.51 Mt Zn: 016 Mt Ag: < 500 t	Pb: 1.21–8.90 % Zn: 2.89–5.09 % Ag: 57.5–195 g/t	Trachybasaltic-andesitic lava and associated volcaniclastics; and metamorphosed basaltic volcaniclastics intercalated with jasper	Silicification, sericitisation, tremolite, epidote, chloritisation, carbonate	Pyrrhotite, sphalerite, pyrite, galena, chalcopyrite, magnetite	VHMS
Denghaishan	Simao, Yunnan	100°52′ 23°40′	Cu	No data	No data	Jurassic-Cenozoic sandstone formation	No data	Chalcocite, bornite, covellite, chalcopyrite, malachite, pyrite, cuprite	Sandstone-type Cu
Bailong	Simao, Yunnan	100°55′ 23°05′	Cu	No data	No data	Jurassic-Cenozoic sandstone formation	No data	Chalcocite, bornite, covellite, chalcopyrite, malachite, pyrite, cuprite	Sandstone-type Cu
Yaojiashan	Simao, Yunnan	101°43′ 22°23′	Cu	No data	No data	Jurassic-Cenozoic sandstone formation	No data	Chalcocite, bornite, covellite, chalcopyrite, malachite, pyrite, cuprite	Sandstone-type Cu

Table 6.4 (continued)

Name/number in Fig. 1 of Hou et al. (2007a)	County/ province	Longitude/ latitude	Metals	Tonnage	Grade	Host rock	Dominant alteration/ mineral phases	Ore minerals (in order of abundance)	Genetic type
Laownagzhai	Qingyuan Yun-nan	101°27′ 23°54′	Au	Au: 106 t	Au: 3.7–7.7 g/t	Palaeozoic greywacke, mafic tuff and basaltic lava	Silicification, sericitisation, carbonate, pyrite, chloritisation	Pyrite, arsenopyrite, sibnite, native gold, sphalerite, chalcopyrite, tetrahedrite	Shear zone-type
Donggualin	Zhenyuan, Yun-nan	101°26′ 23°53′	Au	Au: 50 t	Au: 5.2 g/t	Palaeozoic siliceous slat, meta-quartzite, sandstone, and lamprophyre	Silicification, sericitisation, carbonate, pyrite, chloritisation	Pyrite, arsenopyrite, stibnite, native gold, sphalerite, chalcopyrite, tetrahedrite	Shear zone-type
Lannitang	Zhenyuan, Yun-nan	101°25′ 23°52′	Au	No data	Au: 5.0 g/t	Palaeozoic ultramafic rock, basaltic lavas, greywacke and lamprophyre	Silicification, sericitisation, carbonate, pyrite, chloritisation	Pyrite, arsenopyrite, sibnite, native gold, sphalerite, chalcopyrite, tetrahedrite	Shear zone-type
Jinchang	Mojiang, Yun-nan	101°45′ 23°30′	Au	Au: 27 t	Au: 1–55.45 g/t	Palaeozoic tuffaceous sandstone, siltstone, basaltic rocks, augite peridotite	Silicification, pyrite, sericitisation, serpentinisation, chloritisation, carbonate	Pyrite, tetrahedrite, chalcopyrite, gersdorffite, milerite	Shear zone-type

Table 6.4 (continued)

Name/number in Fig. 1 of Hou et al. (2007a)	County/ province	Longitude/ latitude	Metals	Tonnage	Grade	Host rock	Dominant alteration/ mineral phases	Ore minerals (in order of abundance)	Genetic type
Daping	Yuanyang, Yunnan	102°59′ 22°51′	Au	Au: >20 t	Au: 1–32.5 g/t	Diorite, granite, porphyry, lamprophyre, siliceous shale, sandstone, limestone	Sericitisation, carbonate, chloritisation, silicification, tremolite, epidote, pyrite	Sphalerite, pyrite, galena, chalcopyrite, tetrahedrite, pyrrhotite, chalcocite	Shear zone-type
Dapingzhang	Simao, Yunnan	100°31′ 22°47′	Cu-Pb-Zn	Cu: 0.3 Mt Pb: 0.15 Mt Zn: 0.15 Mt	Cu: 1.93–6.1 % Pb: 0.2–1.1 % Zn: 0.4–1.8 %	Quartz keratophyre, arc spillite-keratophyre sequence	Silicification, sericitisation, chloritisation	Sphalerite, pyrite, chalcopyrite, pyrrhotite,	VHMS
Sandashan	Jinghong, Yunnan	100°50′ 22°02′	Cu	Cu: 0.2 Mt	Cu: 0.5 %	Bimodal suite; felsic volcanic rocks	Silicification, sericitisation, chloritisation	Chalcopyrite, pyrite, pyrrhotite	VHMS

gold deposits in the eastern Qiantang terrane are located along the Jinshajiang and Red River fault systems (Wang et al. 2005a). These ore deposits are associated with alkaline intrusions emplaced at 40–30 Ma. Porphyry copper and gold deposits associated with 18–10 Ma shoshonitic and potassic calc-alkaline (adakitic) intrusions, are located along the Gangdese thrust in the Lhasa terrane, with most occurrences within the Yadong-Anduo-Golmud (YAG) tectonic corridor, referred to above, and the western sector of the Plateau, between Lhasa and Xigate (Xiao et al. 2007). Geothermal fields tend to cluster within the YAG corridor and in the eastern sector (Blisniuk et al. 2001). High-temperature geothermal fields and hot springs caused by exceptionally high heat flows are also located within the YAG corridor. This suggests that the corridor hosts a thermal anomaly as well as a seismic discontinuity. This thermal anomaly could be the result of upwelling of buoyant and hot asthenosphere into the gap provided by the split subducting continental slab. This asthenopsheric mantle could also flow laterally along major lithospheric breaks, represented by the fault systems (Gangdese, Jinshanjiang-Red River, Kunlun), where partial melting of crustal material occurs producing the magmatic-hydrothermal mineral systems discussed in this section. A selection of these mineral systems is discussed below and include: (1) the Gangdese porphyry Cu belt (Hou et al. 2004a, b; Hou et al. 2011); (2) the Jinshanjian-Red River alkaline intrusion-associated Au and porphyry Cu belt (Yulong, Tongchang, Machangqing; Wang et al. 2005a, 2005b; Hu et al. 2004; Hou et al. 2007b, 2009a, 2011); (3) carbonatite related REE mineralisation (Hou et al. 2009b) and the Jinding SEDEX type Zn-Pb deposit in SW China (Xue et al. 2007). The geodynamic settings and distribution of these mineral systems are shown in Figs. 6.45–6.47.

6.4.1.1 Tethyan Porphyry Systems in Tibet (Qinghai-Xizang) and Southwest China

Cenozoic tectonic movements in Tibet and southwest China regions reflect changes in deformation regimes from eastward-extrusion indentation tectonics to crustal thickening tectonics (Windley 1995). As mentioned above, the Tibet and southwest China regions are a collage of accreted terranes, from south to north: Lhasa, Qiantang, Songpan-Ganze and Qaidam, separated by major faults and/or sutures (Figs. 6.42 and 6.43). These are bound by the Himalayan orogen in the south, the Tarim Block in the north and the Yangtze and South China blocks to the east. A good overview of the geology of the Tibet (Qinghai-Xizang) and southwest China regions can be found in the 1:1,500,000 geological map and guide book published by the China Geological Survey and Chengdu Institute of Geology and Mineral Resources (Wang and Hu 2004).

The eastern part of the great Himalayn-Tibetan orogen is host to numerous hydrothermal ore systems. In southwest China, the Sanjiang Tethyan Metallogenic Domain (STMD, Hou et al. 2007a), is endowed with volcanogenic massive sulphides, Ag-polymetallic, Sn greisen and porphyry systems (Tables 6.2 and 6.3).

Table 6.5 Selected giant mineral deposits in the Tibetan orogenic belt. (Modified after Hou and Cook 2009 and references therein)

Deposits	Longitude/ latitude	Metal commodity	Tonnage	Grade	Tectonic setting and environment	Host rock	Genetic type
Sanshan-Yangzidong	99°18′ 26°45 - 43′	Zn-Pb Cu-A	Zn + Pb: >0 5 Mt; Ag: >3,000 t Cu: ~ 0.3 Mt	Pb: 1.27–33.5 % Zn: 1.6–3.39 % Cu: 0.38–1.8 % Ag: 16–189 g/t	Fracture zones within hanging-wall of Huachangshan thrust fault; front zone in the eastern thrust-nappe system	Upper Triassic dolomitic limestone, breccia limestone, breccia limestone, sandstone and conglomerate	Sediment-hosted vein-type Zn-Pb-Cu-Ag
Yaguila	92°40′ 30°20′	Pb-Zn-Cu	Pb + Zn: 4 Mt	Pb + Zn: 15 %	Northern contact zones between Eocene granites and Carboniferous limestone; collisional zone	Eocene granite with $+e_{Nd}$ value; Carboniferous limestone and tuffaceous mudstone	Skarn-type Pb-Zn-Cu
Mengya'a	92°10′ 30°20′	Pb-Zn-Cu	Pb + Zn: >0 45 Mt	Pb + Zn: 8.2 %	Northern contact zones between Eocene granites and Carboniferous limestone; collisional zone	Eocene granite with $+e_{Nd}$ value; Carboniferous limestone and tuffaceous mudstone	Skarn-type Pb-Zn-Cu
Xiongcun	88°26′ 29°23′	Cu-Au	Cu: 0.82 Mt Au: 113 T	Cu: 0.45 Au: 0.62	NW-striking fault fractural zone; the collisional zone	Mesozoic granitoids and pyroclastic rocks, intruded by Eocene granitic dykes	Hybrid-type Cu-Au

Table 6.5 (continued)

Deposits	Longitude/ latitude	Metal commodity	Tonnage	Grade	Tectonic setting and environment	Host rock	Genetic type
Jiama	91°40′ 29°39′	Cu-Pb-Zn	Cu: ≤ 5 Mt	Cu: 1.1 T Pb: 3.48 % Zn: 1.04 % Au: 0.5 ppm	Orogen-transverse normal fault and its intersection with thrust fault; collisional zone with post-collisional crustal extension	Mid-Miocene monzogranite	Porphyry Cu-Pb-Zn
Qulong	91°38′ 29°41′	Cu-Mo	Cu: 8 Mt	Cu: 0.45 % Mo: 0.03–0.06 %	Orogen-transverse normal fault and its intersection with thrust fault; collisional zone with post-collisional crustal extension	Mi-Miocene monzogranite and granite	Porphyry Cu-Mo
Tinggong	90°02′ 29°35′	Cu-Mo	Cu: >1 Mt	Cu: 0.5 %	Orogen-transverse normal fault and its intersection with thrust fault; collisional zone with post-collisional crustal extension	Mid-Miocene quartz monzogranite, granite	Porphyry Cu-Mo
Chongjiang	89°58′ 29°37′	Cu-Mo	Cu: 1.5 Mt	Cu: >0.45 %	Orogen-transverse normal fault; the collisional zone with post-collisional crustal extension	Mid-Miocene monzogranite	Porphyry Cu-Mo

Table 6.5 (continued)

Deposits	Longitude/ latitude	Metal commodity	Tonnage	Grade	Tectonic setting and environment	Host rock	Genetic type
Bairong	89°56′ 29°37′	Cu-Mo	Cu: >0.5 Mt	Cu: 0.73 %	Orogen-transverse normal fault; collisional zone with post-collisional crustal extension	Mid-Miocene monzogranite	Porphyry Cu-Mo
Narusongduo	88°48′ 29°57′	Pb-Zn-Ag	Pb + Zn: >0.5 Mt	Pb + Zn: >20 %	Orogen-transverse normal fault and its intersection with thrust fault in a collisional zone	Palaeozoic and Mesozoic clastic sequences	Vein-type Pb-Zn-Ag
Targejia	85°44′ 29°36′	Cs(-Au)	Cs: 14, 459 T	Cs: 0.10–0.26 %	Modern geothermal field within orogen-transverse rift zones; collisional zone with post-collisional crustal extension	Quaternary silica sinters near the vents	Sinter-hosted Cs deposit
Mazhala	91°49′ 28°27′	Sb-Au	>10,000 T Sb	Sb: 35 Au: 3.8 8 g/t	STDs and their intersection with orogen-transverse normal faults in the Tethyan Himalaya	Lower-Middle Jurassic clastics and Cenozoic diorite porphyry	Vein-type Sb-Au
Shalagang	89°54′ 28°51′	Sb	≤0.1 Mt Sb	Sb: 31.5 %	STDs and their intersection with orogen-transverse normal fault in the Tethyan Himalaya	Early Cretaceous clastics, siliceous rock, sandstone and Cenozoic diorite	Vein-type Sb
Langkazi	90°22′ 29°01′	Au	No data	Au: 2.0 g/t	Detachment faults and their intersection with orogen-transverse normal fault in the Tethyan Himalaya	Metamorphic core-complex and central-intruded granites	Vein-type Au

Several porphyry copper and gold deposits in the eastern Qiantang terrane are located along the Jinshajiang and Red River fault systems (Hou et al. 2004a, b; Wang et al. 2005a). These ore deposits are associated with 40–30 Ma alkaline intrusions. Porphyry copper and gold deposits associated with 18–10 Ma shoshonitic and potassic calc-alkaline (adakitic) intrusions are located along the Gangdese thrust in the Lhasa terrane, with most occurrences within the Yadong-Anduo-Golmud corridor and the western sector of the Plateau, between Lhasa and Xigate (Hou et al. 2004a). The above-mentioned high-temperature geothermal fields and hot springs located within the Yadong-Anduo-Golmud corridor (Fig. 6.45), produce unusual Cs-bearing sinter deposits (Table 6.2; Zhao et al. 2006a, 2006b). Upwelling of buoyant and hot asthenosphere along major lithospheric breaks, represented by the fault systems (Gangdese, Jinshanjiang-Red River, Kunlun), where partial melting of crustal material occurs producing the intrusion-related magmatic-hydrothermal mineral systems discussed in this section.

The Miocene Gangdese Porphyry Belt

The Gangdese (also spelt Gangdise) Cu porphyry belt of Miocene age is 350 km long and lies in the Lhasa terrane (Figs. 6.45 and 6.47). The Lhasa terrane is characterised by Ordovician to Triassic shallow marine clastic rocks and the Gangdese magmatic province that consists of Late Palaeocene to Early Eocene calc-alkaline volcanic rocks and is intruded by granite batholiths rocks of Cretaceous to Neogene age, with peak ages around 55–45 and 30–24 Ma, conciding with the timing of the India-Asia collision and Gangdese thrusting, respectively. East-west extension followed with the development of north-south-trending rifts across the Gangdese belt. It is at this time (18–10 Ma) that potassic calc-alkaline volcanism and shallow level emplacement of granite porphyry occurred within the north-south-trending rift structures. These granitic rocks intruded the earlier batholiths and are associated with the porphyry systems in the Gangdese belt, which is characterised by a regional metal zoning. From west to east, the belt contains porphyry Cu-Au, Cu-Mo and Cu. In addition, lithogeochemical surveys have shown several areas of strongly anomalous Au (Li et al. 2001a).

The ore-bearing porphyries consist of monzonite and quartz-monzonite composed of quartz, andesine-oligoclase, K-feldspar and minor biotite and hornblende. Re-Os dating of molybenite from the Gangdese belt gives model ages of about 14 Ma (Hou et al. 2004a, b). The porphyry have silica contents >56 wt % and a range of K_2O from 2.6 to 8.7 wt % with an overall shoshonitic and/or potassic calc-alkaline composition, quite different from syn-collisional granites in the same belt. Furthermore, the porphyry also have adakitic affinities as indicated by high Sr/Y ratios, lack of Eu anomalies and negative anomalies of Nb, Ta, P and Ti. Initial $^{87}Sr/^{86}Sr$ vary from 0.7047 to 0.7069 and $^{143}Nd/^{144}Nd$ values from 0.51230 to 0.51290; these compositions lie within the mantle array (Gao et al. 2003). The adakitic composition is thought to derive from hot subducted lithosphere.

The Gangdese Cu porphyries were controlled by the north-south-trending rifts, associated with regional uplift and extensional tectonics, following the underthrusting of the Lhasa terrane beneath the Qiangtang terrane at 24–30 Ma. This post-collision extensional regime provided the conduits for the emplacement of the porphyry stocks and associated mineralisation (Fig. 6.46). The porphyry intrusions resulted from partial melting of the lower crust and lithospheric mantle, related to upwelling of asthenopheric material, whether by delamination or slab breakoff or, as outlined above, by flowing into the gap of split subducting slab and along fault and fracture systems.

The Gangdese porphyry Cu belt has been extensively reviewed by Hou et al. (2009a, 2011). The belt contains the Qulong Cu-Mo deposit (ca. 8 Mt of Cu metal resource), the Tinggong, Jiama and Chongjiang porphyry deposits (ca. >1 Mt Cu metal resource) and a number of Cu-Mo deposits in smaller porphyry stocks. In addition to porphyry systems the Gangdese belt is also host to a number of skarn-type Cu-Pb-Zn deposits. The Qulong and Tinggong deposits are briefly described below.

The Qulong Cu-Mo deposit is located at the intersection of east-west-trending thrusts and north-northeast-trending faults. The mineralisation is hosted by a small monzogranite stock with a U-Pb age of ca. 17.6 Ma, which intruded older multiphase intrusions, mainly consisting of granodiorite and monzogranite. As in many other porphyry systems, Cu and Mo mineralisation is associated with potassic alteration and three ore styles. One style is characterised by stockworks of pyrite + chalcopyrite + molybdenite + bornite, forming a pipe-like body in the porphyry intrusion and with pockets of high grade Cu mineralisation (1.79 %). In the zone of potassic alteration, the hydrothermal biotite is associated with sulphide-magnetite-quartz-anhydrite veinlets, whereas the K-feldspar is associated with quartz-sulphide veinlets. The second style of mineralisation consists of quartz-molybdenite veinlets and chalcopyrite + bornite + sphalerite + galena stockworks, generally within the quartz-sericite alteration zone and associated with an assemblage of fluorite + quartz + sericite. Supergene mineralisation represents the third style and consists of malachite, covellite and lesser chalcocite, grading downward into a 160 m-thick transitional sulphide zone, overlying the hypogene sulphides of styles 1 and 2. The supergene zone is not enriched with respect to the hypogene mineralisation. Hydrothermal alteration is zoned around the causative stock and typically comprises a potassic zone, surrounded by quartz-sericite-argillic and propylitic haloes. The potassic alteration is characterised by biotite, K-feldspar and anhydrite, whereas the quartz-sericite zone is dominated by granular quartz, sericite and pyrite, as in most porphyry systems, world-wide. The quartz-sericite zone is locally overprinted by structurally controlled argillic alteration, with minerals of the kaolinite group. The propylitic alteration zone is extensive and affecting rocks other than the mineralised stock and dominated by chlorite, epidote and calcite.

The Tinggong Cu-Mo deposit has a resource of about 1 Mt Cu equivalent, with an average Cu grade of 0.5 %. As for the Qulong porphyry, the deposit is located at the intersection of major thrusts and northeast-trending faults, and is related to a multiphase intrusion consisting of early monzogranite and late granitic porphyries that

intruded granite batholiths of Palaeocene age and a Palaeocene-Oligocene volcano-sedimentary sequence (Linzizong Volcanics). The main and steeply dipping orebody, although discontinuous near the surface, is continuous at depth and is >1,500-m long, 500-m wide and >200-m deep. Similar with the Qulong deposit, a supergene zone is transitional to the primary sulphide zone in the stock and contains malachite, covellite and limonite. The ore minerals of the primary porphyry mineralisation, reported by Hou et al. (2009a) comprise chalcopyrite, chalcocite, molybdenite and minor bornite and galena. However, the presence of chalcocite and bornite, would suggest a certain degree of supergene alteration. Hou et al. (2009a) also suggested that the hypogene sulphide mineralisation was formed in two stages, namely: an early intense veinlets and disseminated Cu-Mo sulphides associated with potassic alteration and characterised by high chalcopyrite/pyrite ratios (2:1) and a late, less intense, fine veinlet disseminations containing chalcopyrite, pyrite, galena and associated with the quartz-sericite alteration zone. No mineralisation has been detected in the argillic zone. Haloes of concentric hydrothermal alteration consist of a core of K-silicate, surrounded by quartz-sericite and an outer propylitic zone, with patches of argillic alteration. The potassic zone is typically formed by K-feldspar, Mg-rich biotite and fine-grained quartz, where hydrothermal feldspar replaces the igneous feldspars and groundmass and is associated with Cu-Mo veinlets. By contrast the hydrothermal biotite is interstitial to the igneous crystals and developed around the Cu-Mo mineralisation. Quartz and sericite replace most silicate minerals and partly overprint the early-formed K-silicate zone. Pervasive sericitic alteration and synchronous silicification resulted in sericite and fine veinlets containing pyrite + chalcopyrite + molybdenite + galena assemblages that infill microfractures in the alteration zone. Argillic alteration is fracture-controlled and is represented by kaolinite and clay minerals that overprint the quartz–sericite zone. The propylitic alteration forms a wide halo around the porphyry and is mainly developed in the northern parts of the stock and surrounding volcano-sedimentary sequence.

Hou et al. (2009a) concluded that the mineral systems of the Gangdese belt (porphyry and skarns) are ultimately linked with the Miocene magmatism that followed the exhumation of the Palaeocene granitic batholiths and are associated with east-west extension and the inception of north-south-trending rifts. Importantly, the sequence of magmatic and metallogenic events is related to a change in the tectonic regime from crustal-thickening-compressional to extensional, a feature that seems to be universal in the development of magmatic-hydrothermal mineral systems (see Chen et al. 2004, 2005b). Various lines of evidence, suggest that continental collision, crustal thickening and underplating of mafic magmas, rather than subduction, are the essential elements for the generation of Cu- and Mo-bearing adakitic magmas (Fig. 6.46).

The Jinshanjian-Red River Fault Porphyry Systems

The eastern margin of the Tibetan Plateau is marked by major strike-slip faults that bound several terranes, such as the Songpan-Ganzi, Qiantang and Lhasa terranes

(Figs. 6.42 and 6.43). These terranes were first juxtaposed in the Mesozoic, but following the India-Asia collision and eastward extrusion or escape tectonics (Tapponier and Molnar 1976), a complex array of strike-slip faults developed along the terrane boundary zones. One of these fault systems is the northwest-westnorthwest-trending left-lateral Jinshanjian-Red River fault (Figs. 6.43, 6.45 and 6.47) or Ailao Shan-Red River fault (Tapponier et al. 1990), extending for well over 2,000 km into the South China Sea. Along this fault zone, is a 1,000 km-long and 50–80 km wide magmatic belt of alkaline igneous rocks, with ages ranging from about 29 to 41 Ma, and spatially associated with rift and/or strike-slip pull-apart basins in the Qiangtang terrane (Hu et al. 2004). The basin contain up to 4,000 m of gypsum-bearing clastic sediments intercalated with alkaline volcanic rocks. The igneous rocks, both extrusive and intrusive, range in composition from basaltic to rhyolitic and with an ultrapotassic or shoshonitic character, highly enriched large-ion lithophile elements (LILE) and LREE and depleted high-field strength elements (HFSE) (Hu et al. 2004). These alkaline rocks cluster into five groups of which at least three, Machangqing, Tonchang and Yulong, are associated with Cu and Au mineralisation (Figs. 6.45 and 6.47). The Yulong district alone contains over 100 porphyry intrusions. Their geochemical composition, together with Sr and Nd isotopic systematics, support a source from a metasomatised lithospheric mantle, contaminated by a subducted oceanic slab (Hou et al. 2003). Furthermore, the presence of rift basins indicates that these alkaline rocks were emplaced in a post-collisional extensional tectonic setting. The $^{3}He/^{4}He$ ratios of pyrite from Yulong and the Machanqing, range from 0.3 to 2.5 Ra (where Ra represents the ratio of $^{3}He/^{4}He$ in air) and $^{40}Ar/^{36}Ar$ ratios of 316–1,736. Thus, He and Ar isotope systematics confirm a mantle source for both magmas and ore fluids. Wang et al. (2005b) determined ages of 34.4 ± 1.6 and 33.9 ± 0.5 Ma for the mineralisation, using the Re-Os system in molybdenite.

The Machanqing ore field comprises three Cu-Au $\pm$ Mo deposits: Machanqing, Yao'an and Beiya, where the alkaline intrusions mainly consist of syenite porphyry with alteration zoning, outward, from K silicate, quartz-sericite, argillic to propylitic. The mineralisation style is stockwork veins containing chalcopyrite, molybdenite, bornite, pyrite and galena. Average copper grades are about 0.8 %, with 4–6 g/t Au in 0.25 Mt Cu metal (Hu et al. 2004 and references therein). Temperatures of the ore fluids range from 120 to 430 °C (Hu et al. 2004). Local gold mining takes place in Silurian carbonaceous limestones intruded by the syenites and in bauxitic material developed in karst cavities (my field observations 2003).

The Yulong ore belt is about 300 km long and 15–30 km wide, with more than 20 mineralised porphyry intrusions. A series of papers by Hou et al. (2003, 2007a, b, 2011) provides up-to-date information of this ore belt, which is summarised as follows. These porphyry intrusions are emplaced into Triassic volcanic and sedimentary rocks and were emplaced within 1–3 km from the palaeosurface. The porphyry bodies are near-vertical pipe-like, with small individual outcrop (<1 km^2), with breccia pipes along their margins, associated with quartz-tourmaline veins and sulphides. The breccia pipes suggest intensive degassing of a magmatic-hydrothermal system. The Yulong ore belt contains a number of polymetallic deposits, but always with Cu as the main economic metal. These deposits are listed in Table 6.2.

Below I briefly discuss the two largest deposits of the Yulong belt: Yulong and Malasongduo. Other deposits in the Yulong porphyry Cu belt include Duoxiasongduo, Zhanage and Mangzong (Table 6.3), in addition to several minor prospects and occurrences. Liang et al. (2006) using U-Th-Pb laser ICPMS spectrometry were able to determine an age progression from Yulong (oldest at 41.2 Ma), Zhanaga (38.5 Ma), Mangzong (37.6 Ma), Duoxiaosongduo (37.5 Ma) to Malasongduo (36.9 Ma) and suggested separate pulses of magmatism along the Jinshanjian-Red River fault. This age progression, is reasonably supported by precise molybdenite Re-Os age data which also indicate a range of mineralisation episodes from 40 to 32 Ma, with peaks at 40 ± 1 Ma for Yulong, 36 ± 1 Ma for Duoxiaosongduo and 32 ± 1 Ma for Xifanping (Hou et al. 2011).

Liang et al. (2006) suggested that left-lateral transcurrent movements had a significant vertical component, which pushed one side of a continental block deep into the lithospheric mantle causing partial melting. However, the model does not clearly explain the age progression, which is thought to be related to the southeastwards movement of one plate along the fault over a local melting zone. Liang et al. (2006) also used the Ce^{4+}/Ce^{3+} ratios of zircons to distinguish ore-bearing intrusions from barren ones. The Ce^{4+}/Ce^{3+} ratio is largely controlled by oxygen fugacity and temperature of crystallisation. Ore-bearing granitic rocks have $Ce^{4+}>/Ce^{3+}$ ratios measurably higher than those from barren granites, suggesting that the former derive from more oxidised melts. The oxygen fugacity of a melt controls the oxidation state of sulphur, so that high-oxygen fugacity melts will have SO and SO_2 sulphur species, whereas sulphur in low-oxygen fugacity melts occurs as S^{2-}. The transition from S^{2-} to SO and SO_2 impedes the formation of a immiscible sulphide phase, making this metal available for enrichment during differentiation and partition into a hydrothermal fluid. The porphyry rocks of the Yulong area all have Ce^{4+}/Ce^{3+} ratios higher than barren shoshonites from the same region (Liang et al. 2006).

The Yulong Cu-Mo-Au deposit is the largest in the region, with a resource of 6.3 Mt Cu metal (Table 6.3). The Yulong intrusion is multiphase, but dominantly consisting of monzogranite porphyry. Hydrothermal alteration is well zoned comprising an inner K-feldspar zone, followed by quartz-sericite grading to argillic and propylitic envelopes. The sedimentary wall rocks are hornfelsed, with skarns developed in limestone units. From fluid inclusion studies, three main stages of alteration-mineralisation are recognised (Li et al. 1981): (1) early K-silicate stage with temperatures of 440–700 °C, associated with a main phase of Cu-Mo mineralisation; (2) quartz-sericite with temperatures of 200–500 °C, associated with Cu-Mo-Fe; (3) a final stage of argillic and propylitic alteration at a temperature of about 230 °C and associated with high sulphidation Cu-Au mineralisation (Hou et al. 2007b). The ore zones include a pipe-like porphyry Cu-Mo orebody, surrounded and overlain by a ring-shaped high-grade Cu-Au zone. The Cu-Au high sulphidation ore is a hydrothermal breccia zone formed as a result of fluid boiling near the roof of the porphyry stock. The alteration associated with the Cu-Au orebody is texture-destructive advanced argillic, consisting of quartz, kaolinite, dickite, montmorillonite and some alunite. Sulphides include chalcocite, tennantite, covellite, bornite and pyrite. This orebody is overlain by a blanket of supergene chalcocite-malachite (Hou et al. 2007b).

The second largest deposit is Malasongduo with a resource of 2.3 Mt Cu metal (Hou et al. 2011; Table 6.2). The Malasongduo monzogranite porphyry is also a multistage intrusion which was emplaced in Early Triasic rhyolitic lavas and pyroclastics. The alteration pattern is similar to that of the Yulong porphyry system. The mineralisation is laterally and vertically zoned. Laterally an inner Cu zone, grades to a Cu-Mo zone and an outer Ag-Pb-Zn zone; vertically a disseminated veinlet ore zone grades upward to a fine veinlet Cu zone to a supergene enriched zone. In this deposit, four generations of ore-bearing veinlets are recognised: (1) quartz-sulphide, mainly quartz-pyrite-chalcopyrite, quartz-pyrite-bornite, quartz-chalcocite; (2) biotite-chalcopyrite; (3) calcite-quartz-pyrite-chalcopyrite; and (4) tourmaline-quartz-chalcopyrite-pyrite-molybdenite.

Geochemical studies by Hou et al. (2003) show that the Yulong intrusions are characterised by high K_2O, Rb and Ba contents. In the monzogranite porphyry, initial $^{87}Sr/^{86}Sr$ ratios range from 0.7065 to 0.7077, $^{143}Nd/^{144}Nd$ values of 0.512451–0.512495 and with $^{206}Pb/^{204}Pb$ values of 18.75–18.89, $^{207}Pb/^{204}Pb$ 15.49–15.68, $^{208}Pb/^{204}Pb$ 38.53–39.12. These Sr-Nd-Pb isotopic compositions fall in the type II enriched mantle (high radiogenic Sr and low non-radiogenic Nd) space and transitional type II enriched mantle and MORB space, leading Hou et al. (2003) to conclude that the Yulong porphyries derived from a mantle source metasomatised by hydrous fluids sourced from a wet subducted oceanic slab. However, the Yulong porphyry system has not a primary relationship to a subduction margin, as have the porphyry Cu-Au of the western Pacific region or the those of the Andean belt in South America. The Yulong porphyries (and those in the Gangdese belt) are in a intracontinental setting and were formed during post-collision extensional tectonics and, quite possibly, as a result of asthenospheric upwellings into lithospheric windows created by slab splitting or breakoff or delamination, followed by partial melting of lower crustal and/or metasomatised lithospheric materials (Fig. 6.48).

6.4.1.2 Rare-earths and Carbonatites in the Mianning-Dechang Belt

The 270 km long and 15 km wide Cenozoic Mianning-Dechang (MD) belt in eastern Tibet and western Sichuan (also referred to as Himalayan MD belt) is located in on the western margin of the Yangtze Craton and is characterised by numerous syenite and carbonatite intrusions, spatially associated with the prominent strike-slip faults in the region (Red River, Ailaoshan, Xiaojiang faults) and within the prominent north-trending Panxi rift (Fig. 6.49). The Himalayan MD REE belt has been studied by Yang et al. (2000, 2001), Hou et al. (2009b) and Xie et al. (2006, 2009). The synopsis given below is taken from these authors. The main characteristics of the REE deposits in the belt are shown in Table 6.6.

The MD belt is estimated to contain a total of 3 Mt of REE ore in the Maoniuping and Dalucao deposits, plus a number of other occurrences. Himalayan magmatic activity (40–24 Ma, with a peak of activity at 35 Ma) in the region forms a nearly continuous potassic igneous province, including from west to east: (1) a 1,000-km-long belt, of potassic igneous rocks, associated with early-middle Cenozoic pull-apart

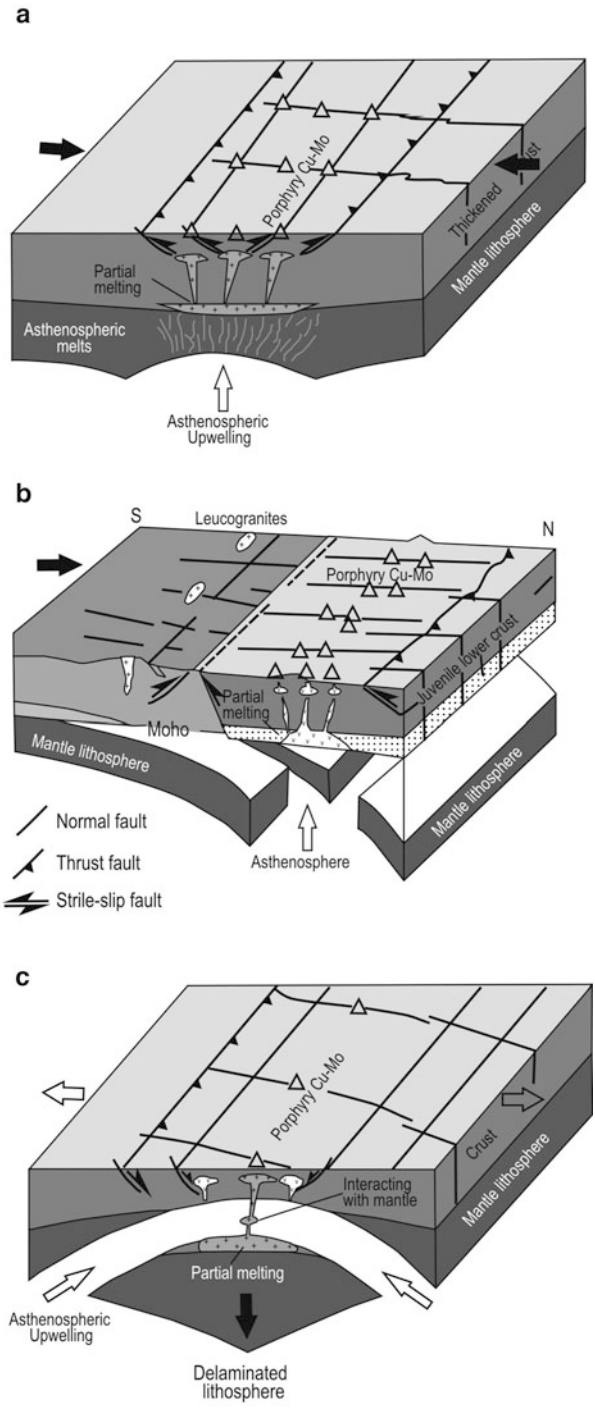

Fig. 6.48 Tectonic and magmatic models as envisaged by Hou et al. (2010), slightly modified, to explain the development of porphyry Cu-Mo deposits in settings other than subduction-related magmatic arcs and applicable to the porphyry belts of the Tibetan orogen; **a** partial melting of lower crust tiggered by upwelling asthenosphere channelled along strike-slip faults; **b** slab breakoff and asthenospheric mantle rising through the space of the broken slab leading to partial melting of the lower crust; **c** delamination of subcontinental lithospheric mantle and subsequent asthenopheric upwelling, leading to the formation of prinitive adakitic magmas from crust-mantle interaction, in **b** and **c** magmas are emplaced in an anorogenic post-collisional setting

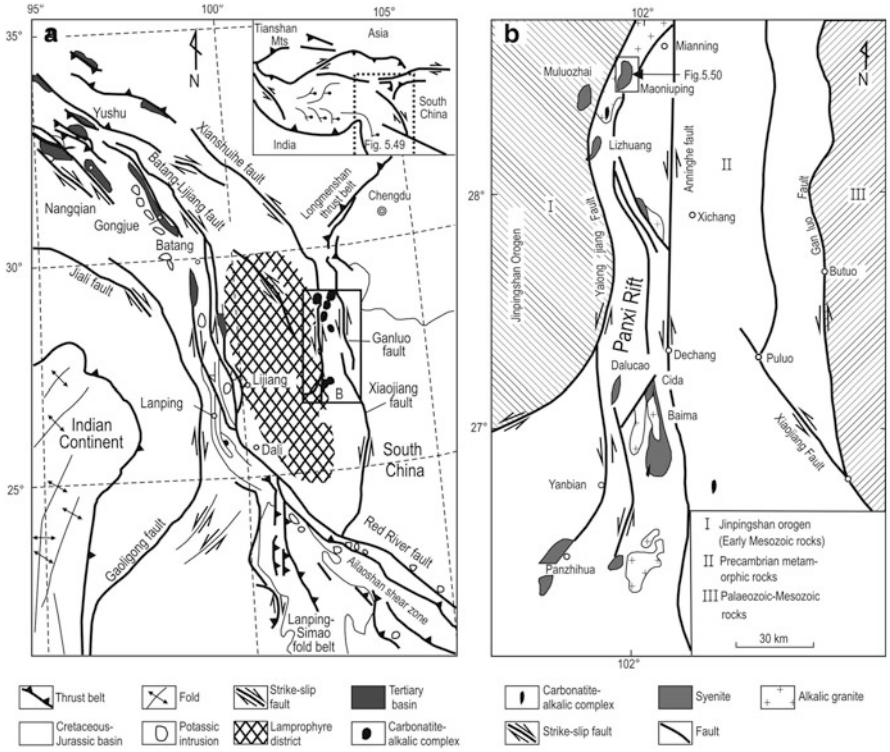

Fig. 6.49 Distribution of strike-slip fault-controlled Cenozoic Mianning-Dechang (MD) belt of alkakine intrusions and carbonatites in eastern Tibet and the north-trending Panxi rift (**a**), detailed map of the area of REE mineralised carbonatites (**b**); *inset* in **a** shows regional position of the MD region (after Hou et al. 2009b); see also Fig. 7.12

basins and developed along the Nanqian thrust, the Batang–Lijiang fault and the Red River shear zone; (2) a 50,000 km^2 shoshonitic (calc-alkaline) lamprophyre district (Fig. 6.49); and (3) the MD belt of carbonatite–alkaline complexes (Fig. 6.49). The carbonatite–alkaline complexes in western Sichuan intrude Proterozoic crystalline basement and overlying Palaeozoic–Mesozoic volcano-sedimentary sequence, forming a narrow, north-trending REE mineralised corridor (Panxi rift; see also Chap. 7 and Fig. 7.12), bordered by north-south strike-slip faults (Fig. 6.49). There are two districts of carbonatite–alkaline complexes: (1) a northern district, which comprises Maoniuping, Lizhuang and Muluozhai; (2) a southern district controlled by the Dalucao strike-slip fault (Fig. 6.49b). The northern district has 40–30 Ma syenitic intrusions with carbonatite dykes and sills, whereas the southern area consists of syenite stocks, carbonatite sills, and REE-bearing breccia-pipes, with SHRIMP U-Pb zircon ages for carbonatite and nordmarkite of 12.99 ± 0.94 and 14.53 ± 0.31 Ma, respectively.

Table 6.6 Main features of the Himalayan MD REE belt of eastern Tibet and western Sichuan. (After Hou et al. 2009b)

Deposit	Structure	Wall rock	Host rock	Mineral assemblage	Alteration	Grade and tonnage	Ore type
Maoniuping	Haha strike-slip fault	Granite, basalt, rhyolite, nordmarkite, carbonatite	Nordmarkite	Microcline, quartz, biotite, aegirine, aegirine-augite, arfvedonite, chevkinite; calcite + fluorite + barite + celestine + bastnaesite; fluorite + barite + quartz + bastnaesite; Fe-Mn oxides and calcite; cerussite + witherite + strontianite + wulfenite	Fenitisation; carbonatisation;	About 1.2 Mt of REO; grading on average of 2/90 % REO	Pegmatitic, carbonatitic, breccia, and stringer (stockwork)
Dalucao	Dulcao Strike-slip fault	Quartz diorite, nordmarkite, carbonatite	Nordmarkite	Microcline, quartz, biotite, aegirine, aegirine-augite, arfvedonite, chevkinite; calcite + fluorite + barite + celestine + bastnaesite; fluorite + barite + quartz + bastnaesite; Fe-Mn oxides and calcite; cerussite + witherite + strontianite + wulfenite	Fenitisation; carbonatisation	About 0.76 Mt of REO; grading on average of 5.0 % REO 1.05–6.69 % REO	Breccia ore; barite + fluorite + bastnaesite ores; celestine + fluorite + bastnaesite; stringer ore; massive, block-like disseminated ore
Lizhuang	Intersections of NE-striking with NW-striking strike-slip faults	Granite, nordmarkite, carbonatite	Nordmarkite	The mineral associations at Lizhuang are relatively simple	Fenitisation	1.05–6.69 % REO	Brown disseminated ore; yellow banded ore; stockwork ore; black powder-like ore
Muluozhai	Yalongjiang strike-slip fault	Nordmarkite, carbonatite	Nordmarkite	The mineral associations at Muluozhai are relatively simple	Fenitisation; carbonatisation; aegirine or aegirine-augite alteration	About 0.45 Mt of REO, grading on average of 3.97 % REO	Massive fluorite-bastnaesite, impregnated, banded ores

Hou et al. (2009b) classified the Maoniuping REE deposit as world-class, after Bayan Obo (Chap. 3) and Mountain Pass in the western USA (see Castor 2008), containing a resource of 1.2 Mt REO at an average grade of 2.89 % REO. The REE mineralisation is temporally and genetically associated with the Maoniuping complex, which consists of syenitic and carbonatite intrusions, porphyritic alkaline aegirine-augite-bearing granitic dykes and alkaline pegmatite dyke swarms. The carbonatites form dykes and sills, which at depth merge into a 90 m-wide carbonatite intrusion. The granitic dykes are a late phase in the evolution of the alkaline-carbonatite complex, as they cut all other units. The Maoniuping carbonatite-alkaline complex is controlled by a strike-slip fault, is about 1.4 km long and 260–350 m wide and is intruded into Mesozoic granitic and rhyolitic rocks. The Maoniuping complex is surrounded by a 1,800 m long and up to 600 m wide halo of fenitic alteration, mainly represented by albite, aegirine-augite, arfvedsonite and Mg-rich biotite replacing country rocks. This fenitic halo is characterised by REE-bearing albite veins cutting through the Mesozoic country rock and a zone of aegirine and aegirine-augite developed within the carbonatite and pegmatitic rocks. The fenitised rocks contain disseminated bastanaesite, but the bulk of the REE mineralisation is related to late stages of fenitisation, typically associated with veins containing calcite, fluorite, barite, celestite, aegirine-augite and bastnaesite. The Maoniuping vein system has a north-northeast strike and is about 2.65 km long and is made up of 1–30 cm-thick veinlets, stockworks and stringers, forming a well-defined swarm in the centre of the complex. Stockworks generally occur at the margins of the vein zones and consists of bastnaesite-bearing barite + aegirine-augite, fluorite + orthoclase and calcite + fluorite. In the north of the complex large (15–50 cm long) bastnasite crystals are present within a fluorite–quartz–barite–bastnaesite zone in the centre of the system to an outer barite–aegirine-augite zone. In addition, microscopy studies by Xie et al. (2006), revealed the presence of unusual minerals including zinccooperite (Cu_2Zn) and Sn-bearing native copper. Hou et al. (2009b) reported that at the time of their study, 71 orebodies had been defined by drilling programs. These orebodies form bands and lenses that dip 65–80° to the northwest, vary from 10 to more than 1.1 km in strike extent and from 1 to >32 m thick, averaging 1–9.05 % REO. Four main ore type are recognised, as follows. (1) Pegmatitic ore forming thick ore veinlets or pockets, in the northern part of the complex and divided into pegmatitic barite + fluorite + aegirine-augite + bastnaesite and orthoclase + aegirineaugite + fluorite + bastnaesite ores. Where bastnaesite occurs as bands on both sides of a veinlet, an inner zone is recognised with aegirine-augite, a transitional zone of barite and aegirine-augite, and an outer zone of alternating barite–aegirine-augite and bastnaesite–fluorite bands. Where the bastnaesite bands are in the centre of the ore veinlets, the zonation is in the opposite sense. Pegmatitic ores comprising orthoclase, aegirineaugite, fluorite and bastnaesite show a lateral zonation varying from a quartz core through a microcline or barite–microcline–aegirine-augite–bastnaesite transitional zone to an aegirine-augite outer zone. (2) Carbonatitic ore occurs as disseminations in dykes and/or sills, and form thick lenses in the northern parts of the deposit. The carbonatite ore contains coarse-grained calcite, barite (10–20 %), fluorite (5–10 %) minor bastnaesite (0.5–5 %), locally with varying

amounts of pyrite, sphalerite and galena. (3) Brecciated ore occurs in the southern and middle segments of the deposit, grading laterally into stringer and parallel vein zones; the breccia is clast-supported, with the clasts consisting largely of angular fragments of nordmarkite, in a matrix of f fluorite + barite + calcite + bastnaesite assemblages. (4) Stringer ores form stockwork zones between the main orebody and surrounding wall-rocks (nordmarkite and fenitised granite pluton). A paragenetic sequence comprising five stages has been proposed: (1) an early high-T stage (up to 700 °C), in which carbonatite–alkaline complex underwent strong fenitisation; (2) a medium-T stage (up to 350 °C) with associated LREE mineralisation, in which a coarse-grained assemblage of calcite + fluorite + barite + celestine + bastnaesite was formed; (3) a medium- and low-T sulphide stage (100–200 °C), associated with fine-grained fluorite + barite + quartz + bastnaesite; and (4) a waning stage dominated by REE-bearing Fe–Mn Fe–Mn oxides and calcite, and (5) a supergene stage, characterized by secondary cerussite, witherite, strontianite and wulfenite. The age of the Maoniuping REE deposit reported by Yuan et al. (1995) and determined by K–Ar dating of biotite and magnesio-arfvedonite, yielded an age range of 31.8 ± 0.7–40.3 ± 0.7 Ma, whereas magnesio-arfvedonite yielded an age of 31.7 ± 0.7 Ma and biotite from the stringer zone gave an age of 27.8 ± 0.5 Ma.

Melt inclusions (M), melt/fluid inclusions (ML) and fluid inclusions (L) have been recognised in mineral phases of the Maoniuping and Dalucao REE deposits. Fluid inclusions (Hou et al. 2009b) include aqueous–vapor (L-I), aqueous–liquid CO_2 (L-II), aqueous–liquid CO_2–daughter mineral (L-III), aqueous–vapor CO_2–daughter mineral (L-IV) and pure-CO_2 inclusions (L-V). Melt inclusions (Xie et al. 2009) are found mainly in calcite and fluorite from the carbonatites, and lesser amounts in gangue quartz. They are composed mostly of melt-glass, daughter minerals, some with a small amount of volatiles. Melt/fluid inclusions are abundantly present in gangue fluorite and contain several solids, occupying 60–95 vol% of the inclusion. Raman spectroscopy and SEM/EDS analyses show that these solids mainly consist of bastnasite, gypsum, barite and fluorite in bastnaesite-hosted inclusions; fluorite and celestine in fluorite-hosted inclusions; quartz, calcite and gypsum in quartz-hosted inclusions; and barite, celestine and strontianite in calcite-hosted inclusions (Yang et al. 2001). Thermometric measurements of fluid inclusions revealed the complexity of carbonatite and REE mineral fluids, containing K_2SO_4–Na_2SO_4–CO_2–H_2O, instead of the more common NaCl–H_2O–CO_2 (Hou et al. 2009b). Homogenisation temperatures (Th) measured from fluid inclusions in quartz, calcite, fluorite, barite and bastaenasite indicate average values ranging from ca. 410–142 °C. Stable isotope systematic (O-D and C) show variable values that are difficult to interpret, but suggesting mixing of high-T hydrothermal fluids with crust-derived fluids, as well as meteoric fluids introduced in the final stages in the evolution of the carbonatite-REE mineral system.

Origin of Carbonatites, a Genetic Model for the Carbonatite-syenite Complexes and Associated Mineralisation in the MD REE Belt and Geotectonic Setting

The increasing importance of rare earth elements in modern technology (e.g. solar panels, wind turbines, fibre optics, television screens, light bulbs etc.), makes it

appropriate to briefly examine how magmas that commonly contain these elements, namely carbonatites, form. Bayan Obo, the largest repository of economically viable REE in the world, is described discussed in Chap. 3. The MD REE belt in eastern Tibet and western Sichuan are typically associated with carbonatite magmas. The origin of carbonatite magma is controversial, and at the heart of the controversy is the relationship between carbonatites and the silica-undersaturated rocks with which they are commonly associated. Theories that attempt to explain the origin of carbonatite are summarised below:

- carbonatites evolve via crystal fractionation, at crustal pressures, of a mantle-derived alkali-rich silicate melt (Watkinson and Wyllie 1971). Silica-undersaturated extrusive mafic rocks are considered to represent primary mantle–derived liquids and their formation at mantle depths requires significant amounts of CO_2. These silica-undersaturated liquids are thought to be the parental magmas for ultramafic-alkaline-carbonatite complexes. Extensive fractionation would lead to the crystallisation of silicates, while carbonates (calcite, dolomite) would crystallize from the residual liquids after removal of alkalies by fenitisation processes. The origin of carbonatite liquids by partial melting of a carbonated lithospheric mantle or mantle source is supported by experimental data, which indicate that carbonate melts can be generated from carbonated peridotites at depths greater than 70 km (Gudfinnson and Presnall 2005; Veksler and Lentz 2006), with near-solidus liquids dominated by calcite and magnesite (dolomitic), with the concentration of other components being related to the bulk composition of the mantle source.
- carbonatites are a direct result of melting of dolomite-peridotite within the mantle, which may form from anatectic melting of crustal carbonate rocks (Lentz 1999).
- carbonatites are derived via immiscible separation of a liquid from an originally homogeneous carbonated silicate melt, the stage of separation determining the composition of both magmas (e.g. Le Bas 1987). Silicate-carbonate liquid immiscibility may occur from peralkaline nephelinitic magmas. This liquid immiscibility has been investigated in several experiments, although it has to be cautioned that experimental systems may not be totally applicable to natural magmatic systems. Nevertheless, liquid immiscibility has been detected in melt inclusions, providing evidence that carbonatite genesis my be linked to silicate-carbonate unmixing (Veksler and Lentz 2006).
- A two-stage process, as envisaged by Nielsen and Veksler (2002), whereby Na-rich minerals are formed within a nephelinitic-phonolitic volcanic plumbing system by the activity of magmatic-hydrothermal fluids. Subsequently the consolidated fluids are re-melted and re-mobilised by the heat energy provided by a following pulse of ascending silicate magma. This model links the origin of natrocarbonatite with fenitising fluids, which would exsolve from carbonatitic liquids.

For a comprehensive work on carbonatites the reader is referred to Bell (1989) and Bell et al. (1998). On the basis of isotopic and trace element analyses of peridotite xenolihs from the ocean islands of Western Samoa and Austral Islands, Hauri et al. (1993) suggested that carbonatitic melts may well be present in the source region of plume-related basalts. A study by Bell and Simonetti (1996), based on Nd, Pb and Sr

isotopic systematics from Oldoinyo Lengai, a 2,200 m high nephelinite-phonolite-carbonatite volcano in the East African Rift (northern Tanzania) support a mantle plume source. They envisaged that carbonatites and associated nephelinitic magmas are derived from a two-stage process, linked to a mantle plume. In the first stage, melts are generated directly from an upwelling mantle plume. Volatiles released from the plume itself cause intense metasomatism of the overlying lithosphere. In the second stage, low degrees of partial melting in the metasomatised subcontinental lithosphere produce the carbonatite-nephelinite volcanic activity that characterises the Gregory Rift in the East African Rift System (Pirajno 2000, 2009).

In most cases, the recognition of true carbonatites can be ascertained by the presence of key silicate minerals, such as phlogopite, acmite-diopside, forsteritic olivine, nepheline and monticellite, or accessory phases such as apatite, pyrochlore, perovskite, in addition to dominant carbonate minerals (ankerite, calcite, dolomite). Six igneous series are generally associated with carbonatites (Woolley 2003; Woolley and Kempe 1989): (1) melilite-nephelinite-phonolite-trachyte; (2) nephelinite-phonolite-trachyte (ijolite); (3) basanite-trachyte-alkali gabbro; (4) phonolite-trachyte-nepheline, sodalite, cancrinite syenites; (5) trachyte, syenite; (6) kimberlite.

In the MD REE belt a liquid immiscibility origin for carbonatite–syenite suite is advocated by Hou et al. (2009b), who cited the following points to reinforce their view: (1) the close temporal and spatial relationship between carbonatites and alkalic syenites; (2) low contents of MgO (<0.73 %) and FeO (<1.20 %) in the carbonatites, distinguishing them from primary magnesiocarbonatites derived directly from partial melting of a mantle source; (3) similar REE patterns of syenites and carbonatites with higher total REE amount and lower Ce/Yb ratios, which coincide with experimental results on REE partitioning between immiscible carbonatitic and silicate melts. In addition, F- and REE-rich fluids can be separated from carbonatite magma by liquid immiscibility. The MD REE belt deposits always occur within the carbonatite–alkaline complexes, and mineralisation appears related to the highly evolved CO_2-rich silicate magma. Fluid inclusion data indicate that gangue minerals such as fluorite, quartz and barite from the MD REE belt deposits host abundant melt and melt/fluid inclusions with abnormally high homogenisation temperatures (up to 750 °C) and enriched in $BaSO_4$, K_2SO_4, $CaSO_4$, $CaCO_3$, CaF_2 and CO_2 (Xie et al. 2009). Xu et al. (2003) determined C, O and Sr isotopic compositions for the Maoniuping REE deposit; showing that the $\delta^{13}C_{PDB}$ and $\delta^{18}O_{SMOW}$ values range from −6.6 to −7.0 ‰ and 6.4–7.4 ‰, respectively, are well within the range of primary igneous carbonatites. Similarly, the initial Sr and Nd isotopic compositions (e.g. $^{87}Sr/^{86}Sr = 0.706074–0.706149$; $\varepsilon Nd = -4.2$ to -3.7) fall within the range of both carbonatites and syenitic rocks (Xu et al. 2003). All these features are typical of carbonatites and peralkaline magmas.

The model put forward by Hou et al. (2009b) is shown in Fig. 6.50, in which the authors envisage three levels (probably end-members) in which REE mineralisation can be formed. At the lower level (ca. 2.5–3 km), are high-T, REE- and sulphate-bearing NaCl–KCl–$CaCl_2$ fluids, derived from the carbonatitic–syenitic magmas and no interaction with external fluids. Filling and replacement of carbonatite by calcite + fluorite + barite + bastnaesite assemblages represent mineralisation along

fractures and as dissemination within and above the carbonatite-syenite complex (panel C of Fig. 6.50). At intermediate levels, multi-phase hydrothermal activity results in the formation of pegmatitic and complex vein systems developed along a mesh of fractures containing developed in a transpressional regime and characterised by bastnaesite-bearing assemblages (e.g., Maoniuping, panel B in Fig. 6.50 and geology and cross-section of the Maoniuping REE deposit). At high levels, extensive boiling of the ore forming fluids, resulting in hydrothermal breccia pipes. accompanied by REE minerals precipitation (e.g., Dalucao; panel A in Fig. 6.50). Introduction of meteoric waters into the hydrothermal system caused precipitation of lesser amounts of fine-grained bastnasite, quartz and Fe oxides.

Most carbonatite–alkalic complexes and associated REE mineralisation occur in continental rifts generated by mantle plumes, such as the East African Rift System (Pirajno 2000). Typically, Sr–Nd–Pb isotopic systematics are interpreted to involve interaction between HIMU-like mantle plumes and EMI-like lithospheric-mantle (Bell and Simonetti 1996). The Himalayan MD REE belt, is associated with the Indian-Asian continental collision at 65–55 Ma and a series of Cenozoic strike-slip faults, reactivated fault systems (Guo et al. 2005) and large-scale shear zones, such as the Red River Shear zone (i.e., RRSZ, Figs. 6.45 and 6.47; Tapponnier et al. 1990), along the eastern margin of the Tibetan plateau and Eocene-Oligocene pull-apart basins and alkaline igneous rocks formed by these strike-slip faults at about 35 Ma (Hou et al. 2003).

6.4.1.3 Jinding Zn-Pb Deposit

The sandstone- and limestone-hosted Jinding Zn-Pb deposit in western Yunnan, is considered to be the largest in China, with estimated resources of about 200 Mt (Table 6.2); total Pb + Zn metal of ca. 15 Mt (Xue et al. 2007; Liu et al. 2010). The host rocks are of Cretaceous and Cenozoic age, making Jinding the youngest sedimentary-rock hosted Pb-Zn deposit in the world (Xue et al. 2007). The following is summarised from the work of Xue et al. (2007 and references cited therein).

The Jinding deposit, located in the Hengduanshan Mountains in South China, in the northern part of the Meso–Cenozoic intracontinental Lanping–Simao Basin, which formed on the Changdu–Lanping–Simao micro-plate between the Yangtze Craton to the east and the Tibet–Yunnan Plate to the west, separated by the Lancangjiang and Jinshajiang–Ailaoshan faults (Fig. 6.51). The Lanping–Simao Basin evolved from a remnant marine and marine-continental basin during the Triassic, through a continental depression during the Jurassic–Cretaceous, to a pull-apart continental basin during the Cenozoic. The Cenozoic tectonic events, are particularly important for the formation of the Jinding Zn–Pb deposit and consist of westward thrusting that led to the formation of the Jinding nappe, a local continental crust with uplifting that produced the Jinding dome, associated with alkaline magmatism between 68 and 23 Ma. This magmatism resulted in the emplacement of quartz-syenite, granite porphyry, essexite, alkaline basalt and trachyte, mostly distributed along the Lanping-Simao fault and the western margin of the Yangtze plate (Fig. 6.51a).

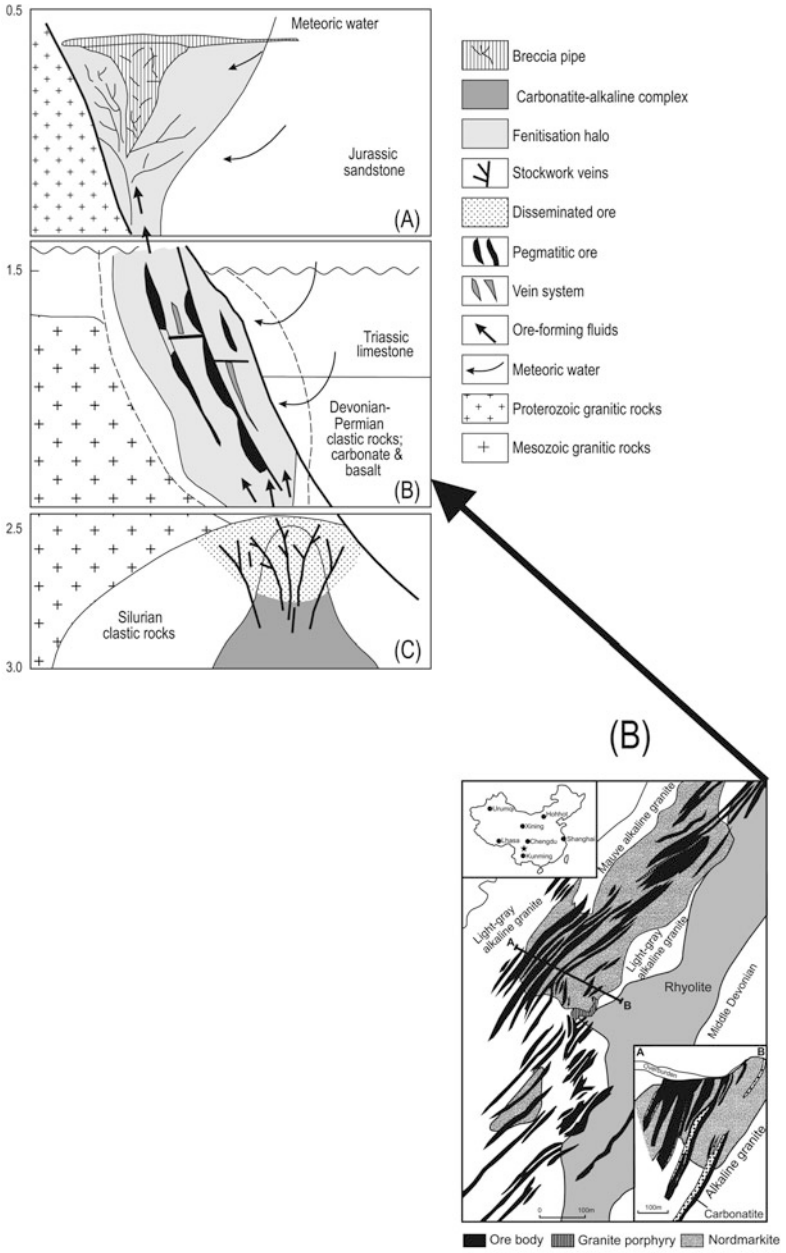

Fig. 6.50 Genetic model of REE mienralisation associated with carbonatite-alkaline intrusion in the Tibetan orogenic belt (details in text). (After Hou et al. 2009b)

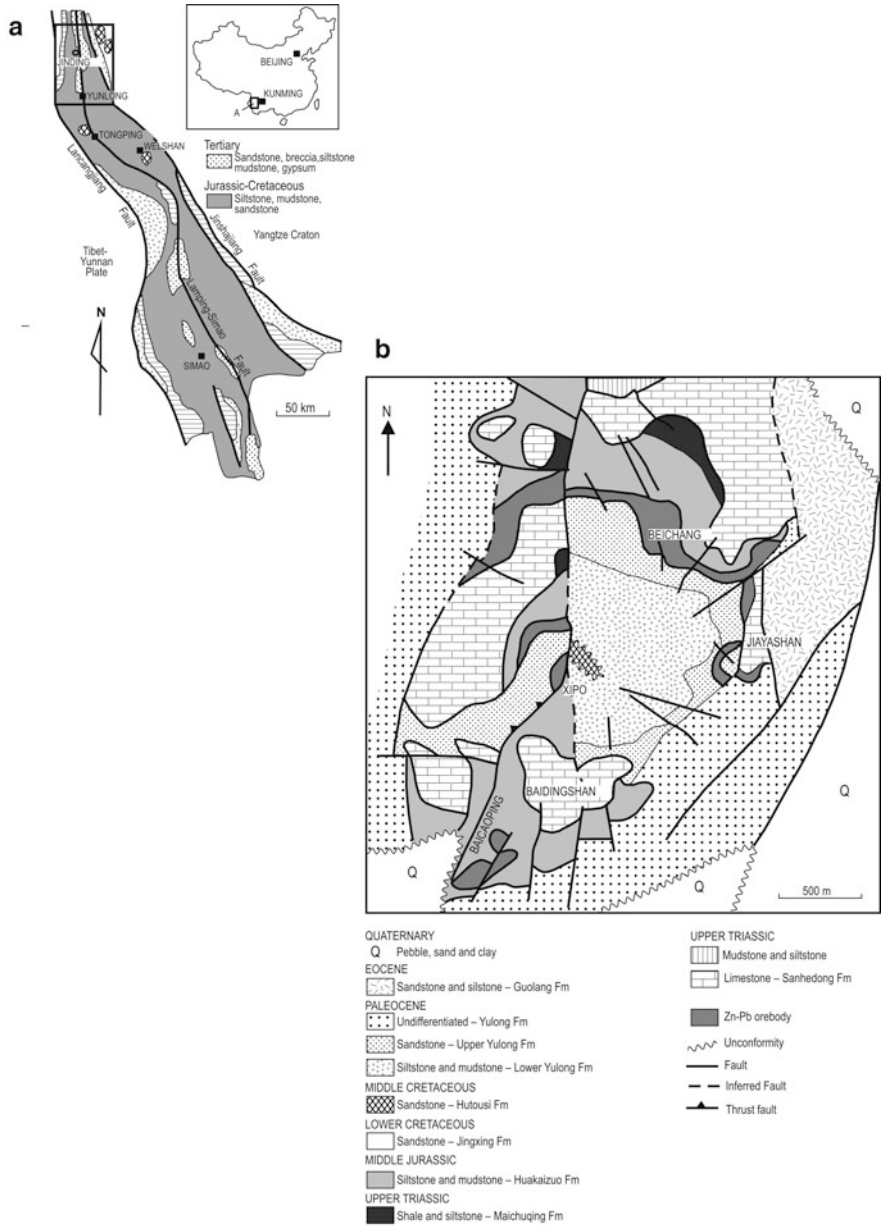

Fig. 6.51 **a** Simplified geology of the Lanping-Simao Basin and position of the Jinding Zn-Pb deposit; **b** distribution of radial fault-controlled Jinding orebodies. (After Xue et al. 2007)

The Jinding mineral district comprises more than 100 orebodies, distributed around the Jinding dome and divided into six ore blocks, representing fragments of original ore lenses subsequently cut and/disrupted by faults radiating from the dome (Fig. 6.51b). Of these, the Beichang ore block accounts for 75 % of the total resources. The Jinding orebodies occur in the hangingwall and footwall of the F_2 thrust fault, defined as Upper Ore Zone in Lower Cretaceous sandstone of the Jingxing Formation and as Lower Ore Zone in the Palaeocene Yunlong Formation clastic succession, respectively. The Upper Ore Zone (UOZ) mineralisation is stratabound within a sandstone layer and contains disseminated sulphides, with ore boundaries that are gradational with the host sandstone and therefore defined only by assay values. The No. 1 orebody of the Beichang block is the largest, accounting for 60 % of the ore in the UOZ. The rocks that lie above the UOZ (actual hangingwall) comprise red beds of the Middle Jurassic Huakaizuo Formation, show a zone of bleaching and silicification extending no more than 1 m wide. The orebodies in the Lower Ore Zone (LOZ) form lenses, veins and irregular zones. Sulphide filling joints and fissures are also common. The ore in the LOZ is hosted in breccias of the Yunlong Formation. Breccia clasts are subrounded and poorly sorted and consist of limestone associated with bitumen, mudstone and siltstone. Ore minerals in both UOZ and LOZ mainly comprise sphalerite, galena pyrite and minor chalcopyrite, argentite, wurtzite and tetrahedrite, occurring as disseminations in the breccia matrix. Xue et al. (2007) reported the occurrence of more than 30 primary minerals, which apart from sulphides, also include oxides, carbonates (calcite), sulphates (celestine, gypsum, anhydrite, barite) and native metals. Locally, pyrite exhibits colloform textures, whereas in other cases pyrite is associated with celestine, calcite and gypsum in late-stage veins and/or nodules. Galena and sphalerite tend to have high contents of Ag, Tl and Cd, as solid solutions or fine inclusions. It is also of interest to note that some sulphates, such as gypsum and celestine, were derived from two sources: hydrothermal fluids and evaporites of the Yunlong Formation. As mentioned above, hydrocarbons (bitumen) occurs in veins and disseminations in both ore zones and the matrix of the host clastic rocks. This highlights the importance of evaporite sequences and hydrocarbons for a range of ore forming fluids, as envisaged by several researchers for the genesis of SEDEX ore systems (see Warren 2000). Paragenetic studies and intergrowth relationships of the primary ore minerals at Jinding suggest three stages, namely: (1) quartz + sphalerite + galena; (2) sphalerite + galena + celestine; and (3) galena + calcite + celestine + gypsum. The disseminated bitumen formed before the sulphide mineralisation was hydrothermally matured and remobilised, forming part of the third stage. The mineral assemblages of the Jinding deposit exhibit vertical and horizontal (east to west) zoning from the feeder Pijiang Fault (Fig. 6.52), as follows: celestine–gypsum–barite → pyrite–marcasite → sphalerite → sphalerite → galena → galena. Furthermore, the Jinding deposit is also characterised by a zone of oxidised ore that extends to a depth of more than 100 m. This oxidised ore is characterised by higher metal grades than the primary ore and also accounts for >40 % of the total ore reservet. Supergene ore minerals comprise smithsonite, hydrozincite, cerussite, strontianite, calamine, plumbojarosite, limonite, celestine, barite, and calcite. Generally the ore in this zone has a higher grade than the primary ore.

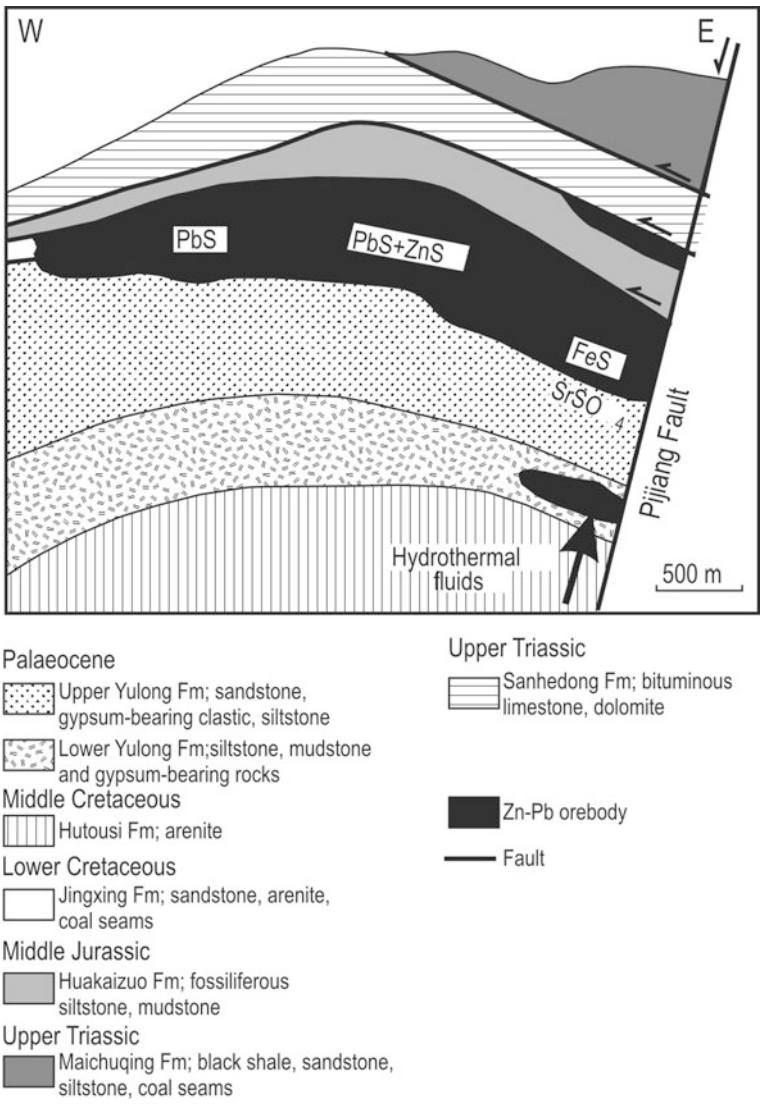

Fig. 6.52 Schematic cross-section of the Jinding Pb-Zn ore deposit, showing ore mineral zoning from the Pijiang feeder fault and the local lithostratigraphy. (After Xue et al. 2007)

Detailed fluid inclusions microthermometry and isotopic (He, Ne, Xe, Pb, S) studies on ore and gangue minerals were carried out by Xue et al. (2007). Below, are briefly discussed some key aspects of these studies. Three types of primary and pseudosecondary fluid inclusions were identified at room temperature: single-phase (L_{H_2O}), two-phase (L_{H_2O} and V_{H_2O}) and three-phase (L_{H_2O}, V_{CO_2}, V_{H_2O}). The homogenisation temperatures (Th) range from 54 to 309 °C, averaging 182 °C in

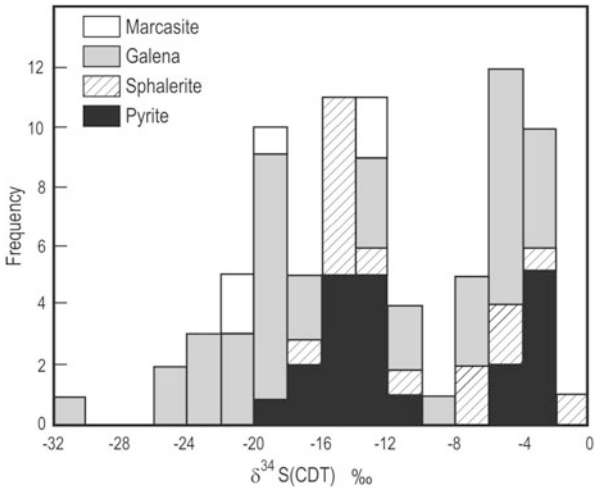

Fig. 6.53 Histogram of δ^{34}S(CDT) of sulphides from the Jinding Zn-Pb deposit (details in text). (After Xue et al. 2007)

quartz, 154 °C in sphalerite, 140 °C in celestine, 126 °C in calcite and 98 °C in gypsum. The measured Th cluster in three peaks: 170–190, 110–140 and 80–100 °C, interpreted by the authors to correspond to the three hydrothermal stages, mentioned above. Salinity values (NaCl eq.) range from 1.6 to 18 wt %, averaging 8.7 wt % in quartz, 5.2 wt % in calcite and 3.6 wt % in gypsum. Xue et al. (2007) also noted an increase in salinity values from east (av. 5.8 wt %) to west (9.6 wt %), in other words, away from the feeder fault. Helium, Ne and Xe isotopic compositions were also determined using fluid inclusions in pyrite, sphalerite, celestine and barite. These measurements show 2.0–15.6 % mantle He (He^3), some 53 % mantle Ne and a considerable amount of mantle Xe in the ore-forming fluids. The Pb-isotope composition of galena, pyrite and sphalerite also suggests that this metal is mainly of mantle origin, mixed with a lesser amount of crustal lead. The δ^{34}S(CDT) values of sulphides show a wide range from −1.7 to −30.4 ‰, with a general progressive trend δ^{34}S values from sphalerite to pyrite to galena to marcasite (Fig. 6.53), implying multiple S sources, but with predominating organic and evaporite sulphate sources. The wide range and dominantly negative δ^{34}S values of the Jinding sulphide minerals suggest that organic or bacterial sulphate reduction provided the reduced sulphur to enable precipitation of sulphides in the Jinding system.

Ore genesis

The Jinding mineralisation is hosted in terrigenous clastic rocks and carbonate beds of the Lanping-Simao Basin, probably a pull-apart structure formed during multi-phase movements of the Ailoishan-Red River Shear Zone and the Chongshan Shear Zone (locally Jinshnajiang and Lancanjiang faults; see Figs. 6.47 and 6.51). The ore

genesis for Jinding remains somewhat controversial with both syngenetic and epigenetic models being proposed. Xue et al. (2007) pointed out that since the ore bodies are located in hanging- and footwall of the Pijiang thrust fault (F2) is good evidence for an epigenetic origin, supported by replacement and open-space filling textures and vein-type mineralisation. The age of the mineralisation is poorly constrained, in spite of dating attempts of sulphide minerals using the Re-Os system. Nevertheless, the age of the Jinding mineralisation is likely to be slightly younger than the end of the sedimentation of the Yunlong Formation (57 Ma), which practically coincides with the above-mentioned Himalayan alkaline magmatism. In addition, isotope systematics of noble gases and lead all support mantle-derived fluids and metals for the Jinding ores. Thus given the genetic uncertainties, the Jinding Zn-Pb mineral systems is different from other sedimentary-hosted (SEDEX) base metal deposits because, Xue et al. (2007) concluded, Jinding was formed in an active tectonic setting and is structurally controlled and that SEDEX mineral systems form in marine basins during phases of thermal subsidence. As such, these researchers proposed that Jinding is a new type of sedimentary-hosted base metal deposit (Jinding-type).

But with the mineralisation also being hosted by rocks of the Palaeocene Yunlong Formation, which is chronologically associated with the Himalayan alkaline intrusions and considering that hydrothermal fluids were channelled along a fault (feeder), from which they migrated along permeable lithologies (Fig. 6.52), suggests that both epigenetic and syngenetic systems were active, either over a long period of time or perhaps only during the Himalayan magmatic event. If this is correct, then the Jinding Zn-Pb deposit would compare well with other SEDEX deposits, such as those in Australia and South Africa (see overview in Pirajno 2009).

6.5 Kunlun and Songpan-Ganzi Terranes

The northern margin of the Tibetan plateau and the southern margin of the Tarim Block are marked by suture zones, east-west-trending thrusts and strike-slip faults, effectively forming mountain ranges north of, and on the opposite side of the Himalaya. Thus, the Kunlu and Songpan-Ganzi terranes are separated by sutures from the Qiangtang (Tibetan plateau) in the south, South China Block to the east and Tarim-North China cratonic blocks to the north (Figs. 2.3 and 6.54). The Kunlun is divided into an eastern and western Kunlun, at the juncture Altyn Tagh fault zone, bordering the Songpan-Ganzi and Qiantang terranes (Fig. 6.54).

The Ordovician to Triassic western Kunlun subduction-accretionary complex was developed between the southern margin of the Tarim block and the northern margin of the Tibetan Plataeu and has been extensively studied by Xiao et al. (2002c, 2002d, 2005b). The western Kunlun is divided into North Kunlun, South Kunlun and Mazar terranes and is also called Western Kunlun orogen, forming a 1,000 km long mountain range. The North and South Kunlun consist of magmatic arc-type terranes, ranging in age from Proterozoic to Lower Palaeozoic. One of these magmatic arcs is the 211 Ma Sailiyak continental arc comprising granodiorite, monzogranite,

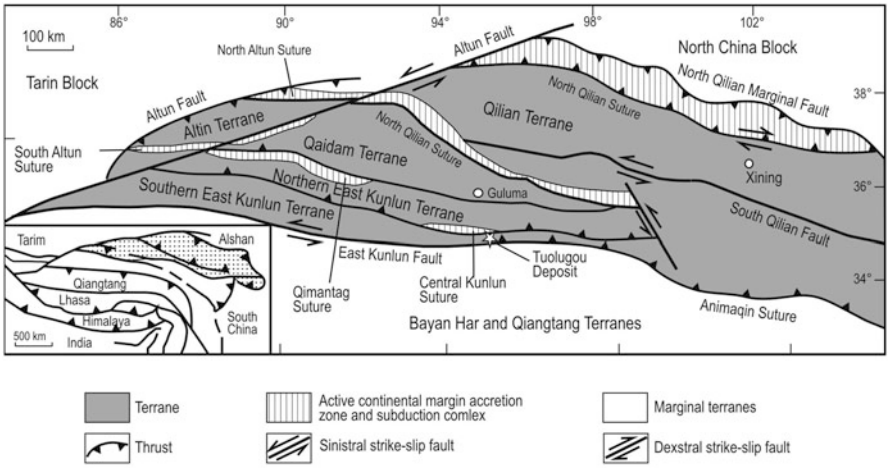

Fig. 6.54 Simplified map showing the accretionary and composite terranes developed on the northern margin of the Tibetan plateau (see *inset* and also Fig. 2.3 and 6.42). (After Feng et al. 2009)

tonalite, monzodiorite, intermediate volcanic and pyroclastic rocks. The Sailiyak arc was formed by northward subduction of the Palaeo-Tethys Ocean, during the Carboniferous to Early Permian. The Mazar terrane is made up of three tectonic assemblages (Xiao et al. 2002c, 2002d): (1) Bazar Dara subduction-accretion complex; (2) the Hewitan subduction complex; and (3) Qitai fore arc basins. These together with the Sailiyak arc, were accreted to form a 500 × 250 km collage during closure of the Palaeo-Tethys Ocean. The subduction-accretion complex also includes remnants of oceanic volcanic seamounts (Xiao et al. 2002c). In a subsequent paper, Xiao et al. (2005b), re-interpreted and expanded their model back in time to the Late Cambrian. In this model southward subduction in the Late Cambrian to Early Ordovician formed an arc complex (Yixiede). Subduction changed direction to the north, beneath the southern margin of the Tarim block in the Middle Ordovician to Late Devonian, resulting in complex tectonic assemblages, associated with granitic intrusions and lamprophyre dykes, with ages ranging from 408 to 405 Ma. Final accretion saw the development of an Andean type mountain belt and the emplacement of an ophiolite (Kudi ophiolite). Subduction of oceanic crust occurred both beneath the Andeantye margin and southward beneath the Qiantang northern margin, between the Late Carboniferous-Permian and Early Mesozoic (Xiao et al. 2005b).

6.5.1 Kunlun Terranes and Qaidam Terrane

The Kunlun terranes frame the southern margin of the Tarim Basin with the Altyn Tagh Fault as the major structure in the region (Fig. 6.4), representing a series of

orogenic collages between the southern margin of the Tarim and the northern margin of the Tibetan Plateau (Fig. 6.54). These terranes record the Palaeozoic and Mesozoic history of the Eurasian continent and the Tethyside orogens (Dewey et al. 1988, Yin and Harrson 2000). The oldest terrane is the 1,760 Ma metamorphic Kunlun Terrane *sensu stricto*, separated from the Tarim by the Kudi thrust (also called Tamkaral faut), which marks the underthrusting, in the Silurian, of the Tarim beneath the Kunlun Terrane. This underthrusting was followed by syn to post-collision granitic magmatism between 460 and 380 Ma (Rui et al. 2002). Important strike-slip movements took place in the Cenozoic along the Alty Tagh and Karakash fault system, resulting in the eastward displacement of a Caledonian volcanic arc and the Precambrian terranes by hundreds of kilometres to form the East Kunlun orogen (Fig. 6.54). To the north of the East Kunlun is the Qaidam block, which is considered a fragment of the Tarim that was also offset, eastward by the Cenozoic India-Asia collision. The Palaeo-Tethys oceanic crust was thrust northward beneath the amalgamated Tarim-Qaidam-Kunlun Terrane, leading to the accretion of the Qiangtang, Tianshuihai and the Lhasa terranes between the Jurassic and Late Triassic (Rui et al. 2002). The Tianshuihai terrane contains flysch units that were subducted and accreted to the southern margin of the Kunlun block along the Altyn Tagh Fault and anatectic granites were intruded between 210 and 180 Ma on both sides of the Fault (Rui et al. 2002). In the southeast of Xinjiang province are tectonic units that were laterally offset and surround the Qaidam Basin (Chap. 8). Palaeozoic flysch and island arc rocks are part of the Altyn Tagh Shan that is part of a complex orogenic belt. South of the East Kunlun-Qaidan block is the Mesozoic flysch succession of the Songpan-Ganzi terrane, interpreted as a sea arm trapped between the colliding cratonic blocks of China (Sengör et al. 1993; and see below).

Geodynamic models that attempt to explain the evolution of the Kunlun terranes, as summarised by Xiao et al. (2006 and references therein) include: multiple terrane amalgamation as a series of accretionary complexes; a forearc accretion model, which emphasizes the role that accretionary prisms and magmatic fronts played in Palaeozoic orogenesis; a backarc collapse model that utilises SE Asia as a modern analogue and assigns all orogenesis to back-arc collapse (archipelago model of Hsu et al. 1995). Xiao et al. (2006) suggested that the above models fail to explain the nature and age of some key collage components and the time of their final amalgamation.

On the basis of new geochemical, stratigraphic, structural and tectonic data a more up-to-date geodynamic model is the multiple accretion model (Xiao et al. 2006 and references therein). From north to south, the general geology of the Tibetan northern plateau and associated Kunlun terranes can be summarised as follows (1) an early Palaeozoic south-dipping (present-day coordinates) subduction system that became accreted to the southern margin of Tarim, on a new north-dipping subduction zone beneath its southern margin; and (2) a mid-Ordovician to early Mesozoic south-facing Andean-type margin. The southward accretionary tectonic history was interrupted by the incorporation of possible old continental fragments (Kudi, Qaidam, and Central Qilian) or composite blocks amalgamated from these fragments. An archipelago

palaeogeography was created in the eastern Tethyan Ocean in which the continental fragments were accreted to the southern Eurasian continent. New geochronological data, tectonic interpretations, and preliminary metallogenic data suggest that in the Palaeozoic to early Mesozoic the Northern Tibetan Plateau was a long-lasting, complex accretionary orogen and in the early Mesozoic an Andean-type active continental margin that developed on the Palaeozoic-accreted margin of the Tarim block. In the late Palaeozoic to early Mesozoic the continuous active margin extended for some 10,000 km in southern Eurasia north of the Palaeo-Tethys Ocean (Heubeck 2001).

6.5.2 Songpan-Ganzi

The Triassic Songpan-Ganzi terrane (also referred to as Complex or Basin), approximately with an area of 200,000 km^2, contains turbiditic sediments from 5 to 15 km thick, representing the largest volume of flysch-facies in the world (Wang et al. 2008b). For this reason the Songpan-Ganzi is best known for the study of provenance of turbiditic sediments, rather than mineral systems. The Songpan-Ganzi, studied and described by Zhou and Graham (1996), Yin and Harrison (2000), Chang (2000), Enkelmann et al. (2007) and Wang et al. (2008b), is interpreted as the metamorphosed remnant of a Triassic ocean basin, located at the eastern end of the Qinling orogen, between the North China Craton and Yangzte Craton (Fig. 6.55, see also Figs. 2.3 and 5.19). The Songpan-Ganzi oceanic basin was closed during a scissor-style and therefore diachronous collision between the North China and Yangtze cratonic blocks between the Late Carboniferous and Late Triasic. The lithostratigraphy of this Songpan-Ganzi terrane (basin) comprises mostly Triassic deep marine sedimentary deposits (micritic limestone, calcareous shale, sandstone, siltstone and turbiditic clastic rocks). Except for some Triassic granites, Na-rich and peraluminous rhyolites and high MgO andesites in the northern Songpan-Ganzi terrane near the suture between the Songpan-Ganzi and Kunlun terranes are the only known coeval volcanic rocks (Wang et al. 2008b). Wang et al. (2008b) reported new age data (Late Triassic 210–212 Ma) and geochemical and isotopic characteritics for these volcanics. The peraluminous rhyolites have high Sr/Y and La/Yb ratios, low Y and Yb contents and negligible to positive Eu and Sr anormalies, comparable to slab derived adakites, whereas the andesites are characterized by high MgO, Cr and Ni contents, comparable to sanukitoids (so named from the Setouchi volcanic arc of Japan; see examples in Windley 1995). In addition, both the rhyolites and andesites have low εNd(t) values ranging from −7.57 to −9.59 and high $(^{86}Sr/^{87}Sr)I$ from 0.7086–0.7106. These authors suggested that the Songpan-Ganzi rhyolites were derived by partial melting of sediments from northward-subducted Songpan-Ganzi ocean during the Triassic, and the high-Mg andesites were derived from the interaction between sediment-derived melts and mantle peridotites.

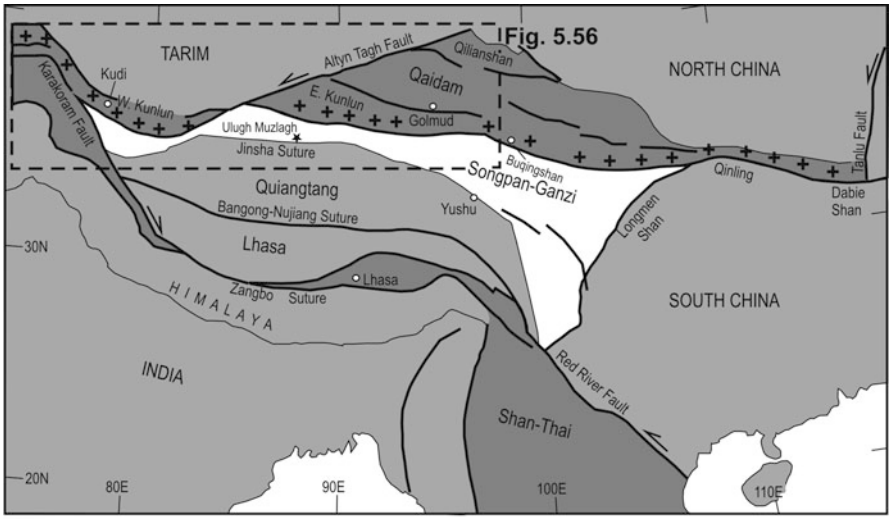

Fig. 6.55 Simplified map of the Kunlun-Qaidam and the Songpan-Ganzi terranes developed on the northern margin of the Tibetan plateau and to the south of the Tarim; see also Figs. 2.3 and 6.42. (After Xiao et al. 2005b)

6.5.3 Mineral Systems in Kunlun and Songpan-Ganzi Terranes

The Kunlun orogen contains a variety of ore systems, briefly mentioned here, which reflect the complexity of its tectonic assemblages, from magmatic arc, to oceanic lithosphere, to back-arc settings. Porphyry Cu deposits, volcanogenic massive sulphides (VMS), sedimentary Fe deposits and MVT Pb-Zn deposits and orogenic Au lodes are present in the Kunlun (Fig. 6.42; Xiao et al. 2006), but not much is known about these deposits, at least not in the English literature. The VMS and MVT deposits were probably formed in back-arc or rifted marginal basins. The Yunwuling porphyry Cu deposit occurs in a metallogenic belt along the Kunlun fault, whereas orogenic Au lodes are found in the eastern Kunlun and have an age of ca. 239 Ma (Xiao et al. 2006). The orogenic lodes are probably related to accretion tectonics of the Kunlun terranes.

A newly discovered, rather intriguing and unusual Co-Au deposit, called Tuolugou, was reported and described in some detail by Feng et al. (2009). The Tuologou Co-Au is within the Kunlun orogenic belt, about 60 km south of the town of Golmud. The resources are estimated at greater than 20,000 t of Co and 4 t of Au, grading 0.06 % Co and 0.45–1.05 g/t Au. The Tuolugou mineralisation is hosted by a metamorphosed volcano-sedimentary succession, affected by Caledonian, Indosinian and Yanshanian tectono-thermal events. In the deposit area, the succession consists of, from base to top, black shale, tuff, sandstone, chlorite-sericite slate, quartz-sericite schist intercalated with graphitic argillite and a quartz-albitite rock.

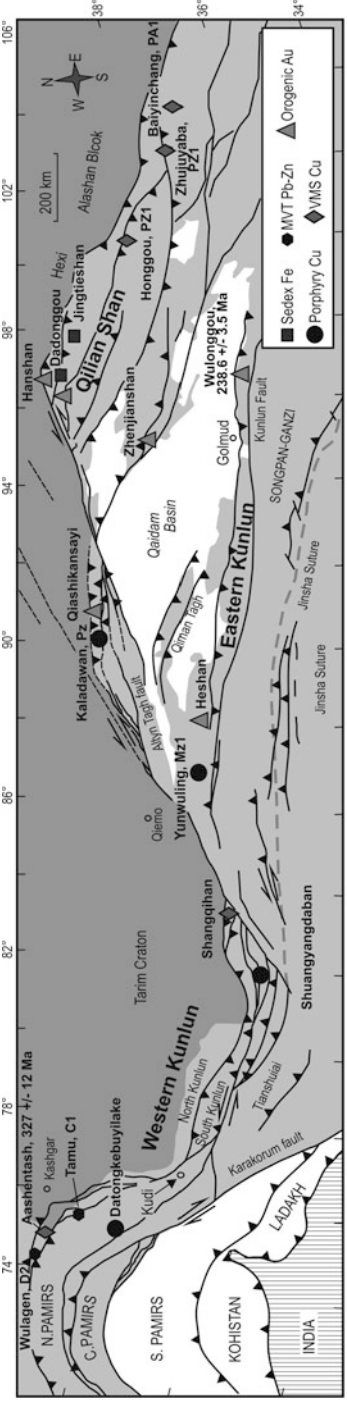

Fig. 6.56 Simplified geology map of the Kunlun terranes on the northern margin of the Tibetan Plateau and distribution of ore deposits. (After Xiao et al. 2006 and references therein)

The quartz-albitite, which hosts the mineralisation, is characterised by thin rhythmic laminations within quartz-sericite schist and chlorite-sericite schist. The texture and appearance of the quartz-albitite is interpreted by Feng and co-workers to be of chemical-sedimentary (exhalative?) origin. The mineralised zone is 7 km long and 15–50 m thick, with single orebodies having dimensions in the order of 500–50 long and 1 to about 8 m thick. The ores consist of massive, banded and disseminated pyrite in quartz-albitite and quartz-sericite schist. Ore minerals are pyrite, minor arsenopyrite, chalcopyrite, bornite and sphalerite. Rare ore minerals are cobaltiferous pentlandite, cobaltiferous pyrite, native Au, native Cu and Co minerals, such as linnaeite and carrollite. The Co mineralisation is generally associated with pyrite, of which two generations are recognised: an early fine-grained xenomorphic and cataclastic cobaltiferous pyrite and a late-stage euhedral coarse pyrite. Native Au is found in fissures in the cataclastic pyrite. Re-Os dating of pyrite from the deposit yielded an isochron age of 429 ± 29 Ma. The early pyrite is interpreted as predating regional deformation and metamorphic events. Wallrock alteration consists of silica, pyrite, sericite and carbonate. Feng et al. (2009) determined $\delta^{34}S$ values for pyrite ranging from -1.8 to -0.2 ‰, suggesting a magmatic source for the sulphur in the ore system, whereas fluid inclusions show low temperatures in the range of 200–180 °C with low salinities of between 9.0 and 0.4 wt % NaCl equiv. Feng et al. (2009), compared the Tuolugou Co-Au deposit with the stratabound Co-Cu-Au deposits in Idaho (USA) and similar occurrences in Norway and Canada. The Tuolugou Co-Au deposit is thought to have formed by syngenetic exhalative processes, but modified during later orogenic events.

Carlin-style Au deposits are present in the Songpan-Ganzi terrane in northern Sichuan Province, characterised by thick flysch successions consisting of shale and sandstone intercalated with carbonate beds (Mao et al. 2002). Here the largest of these deposits is Dongbeizhai, located in a mountainous area, with reserves of about 52 t Au, grading 5.5 g/t (Mao et al. 2002). Other deposits in this area with significant resources include Zheboshan and Qiaoqiaoshang. The deposits of the Songpan-Ganzi terrane have a Au-As + Sb + Hg + W metal association. Peters (2002) included the Songpan-Ganzi and contained Carlin-style Au deposits in the West Qinling fold belt (Chap. 5 and Fig. 5.20). However, it is preferable to have the Songpan-Ganzi separate from the Qinling-Dabie orogenic belt.

6.6 Concluding Remarks

In this chapter I have discussed mineral systems in tectonic domains of the western part of China, from the CAOB to the Himalayan orogenic belts, north of the Himalayan front and bordering the western margin of the South China Block. These tectonic domains continue for thousands of kilometres outside the borders of the P. R. China and therefore have been and are being studied by several national and international groups. A period of open scientific endevours in the earlier part of the twentieth century, was unfortunately followed by poor communications due to new

political orders, till about the 1980s, but now finally brought together by global scientific interest, thereby uncovering fascinating aspects of *sans-frontier* geology of this part of planet Earth.

The Tianshan and Altay orogenic belts in northern Xinijang are well endowed with a range of mineral systems, from porphyry, epithermal to shear zone-hosted lode Au deposits and Ni-Cu sulphides in mafic-ultramafic complexes. Some epithermal systems, shear zone-hosted Au and magmatic Ni-Cu deposits were formed between 290 and 240 Ma. In particular, the development of Au mineralisation reached a peak between 290–270 Ma and is thought to have resulted from extensive convective circulation of ore fluids, associated with granitic intrusions, controlled by strike-slip faults (de Jong et al. 2009).

The geodynamic evolution of the Tianshan and Altay orogenic belts has been investigated by several researchers (e.g. Allen et al. 1992; Biske and Seltmann 2010; Seltmann et al. 2011; Windley et al. 1990, 2002, 2007; Zhao et al. 2008a; Xiao et al. 2004a, b, 2008a, Gao et al. 2009). Scenarios that attempt to explain the geodynamics of the Altay and Tianshan orogenic belts, abound in the literature of the last 5 years or so (e.g. Wang et al. 2008a, 2010; Dong et al. 2011; Xiao et al. 2011; Cai et al. 2010; Geng et al. 2011; Gao et al. 2011; Zhu et al. 2010).

The mineral systems in the CAOB of NW China region were formed in distinct tectonic settings. Subduction-related (active continental margins and island arcs) systems, were largely responsible for the formation of porphyry, epithermal, VMS and skarn mineral deposits. There is evidence, particularly in the Kanggur shear zone that some of the Au lodes may have been re-worked from pre-existing subduction-related intrusion-related and/or epithermal systems. Recent Ar-Ar geochronology of shear-zone-hosted Au deposits in the eastern Tianshan (Kanggur, Hongshi and Hongshan), has shown that the Au mineralisation is temporally related to late stages of the shear zone activity in the region. Chen et al. (2009) showed that the main ductile shear deformation time was between 262.9 and 248.8 Ma, whereas the timing of the mineralisation was between 261.0 and 246.5 Ma. Furthermore, the mineralising event may have started after the rapid uplift in the middle-western part of the shear zone. It can then be speculated that the uplift was conducive to the influx of meteoric waters, which may have enhanced and redistributed pre-existing Au mineralisation.

The skarn Fe-dominated deposits in the Altay orogenic belt, are associated with extensive metamorphism, that locally reaches amphibolite grade and even partial melting (migmatites), suggesting a combination of high-temperature and high-pressure metamorphism, possibly related to strike-slip movements along the Irtysh shear zone. The Irtysh shear zone was affected by multiphase deformation and associated metamorphism, which could have not only modified pre-existing mineral deposits, but also formed new ones, such as the Ni-Cu sulphides of the funnel-shaped mafic-ultramafic intrusions. I consider it possible that the high-temperature skarns, A-type granites and the mafic-ultramafic intrusions, may all be associated with upwelling asthenospheric mantle or lateral flow from a mantle plume. The nature of Alaskan-style mafic-ultramafic intrusions and associated Cu-Ni magmatic

ore deposits, and their spatial-temporal relationship with coeval A-type granites, ultimately support the role of a mantle superplume event that affected much of central Asia in the Permian.

The Tethysides (part of the Alpine-Himalayan orogens), present a particularly interesting aspect of intraplate tectono-magmatic processes and associated mineral systems. The papers by Hou et al. (2007a, b, 2009a, b, 2011) nicely highlighted the important features of the Tethysides in China, namely the Tibetan orogenic belts, north of the Himalaya, with major sutures reactivated as strike-slip faults that extend southeast to form the well-know Jinshannjan-Red River Fault zone, where important clusters or metallogenic belts host porphyry type and carbonatite REE deposits. Hou ZQ and co-workers suggested that adakitic melts formed from partial melting of thickened lower crust, were followed by a series of tectonic and asthenospheric upwelling processes. Uplift of the Tibetan Plataeu, thought to be caused by delamination and subsequent asthenopsheric upwelling, resulted in the development of ore-bearing magmas forming more porphyry, skarns and other mineral systems, in a regime of crustal extension and collapse.

The carbonatite and alkaline complexes in eastern Tibet (Mianning-Dechang REE belt) are all spatially associated with Cenozoic intracontinental strike-slip faults, activated during the India-Eurasia collision. Hou et al. (2009b) pointed out the unique setting of the alkaline and carbonatite complexes in the Tibetan region. Carbonatite- and alkaline intrusion-related REE deposits normally occur in rift settings, linked with large igneous provinces and mantle plume events (e.g. Bayan Obo; Chap. 3).The host rocks and REE mineralisation in the Tibetan orogenic belts are dominated by nordmarkite (quartz-bearing syenite), characterised by variable K_2O contents suggesting a lower alkalinity of alkaline magmas. Carbonatites in rift zones, such as those in the East African Rift System are associated with mantle plumes, whereas those in the collisional and strike-slip fault zones of the Tibetan domains were derived from partial melting of metasomatised, enriched, subcontinental lithospheric mantle (Hou et al. 2009b). The carbonatite-related REE deposits from rift zones are usually enriched in Nb, P, and Fe, locally forming economically significant Nb and Fe orebodies, such as Bayan Obo. The carbonatite and REE deposits of Tibet are not significantly enriched in Nb, Ta, P, Zr, Hf, Ti and Fe. The possible presence of magma chambers at depths of 15–20 km have been deduced from seismic profiles across the Lanping-Simao Basin. Again, one must stress the importance of strike-slip fault systems in the upwelling of magmas and hydrothermal fluids, producing regional high-temperature metamorphic effects, as also observed along the Irtysh Fault in the Altay Orogen (Sect. 6.2.2). A link between strike-slip faults, magmas and mineralisation is difficult to dispute.

The Kunlun and Songpan-Ganzi terranes are still poorly known from the point of view of mineralisation and more work is required in order to assess their mineral potential, within the regional tectonic framework.

References

Abdrakhmatov KY, Aldazhanov SA, Hager BH, Hamburger MW, Herring TA, Kalabaev KB, Makarov VI, Molnar P, Panasyuk SV, Prilepin MT, Reilinger RE, Sadybakasov IS, Souter BJ, Trapeznikov YuA, Tsurkov VYe, Zubovich AV (1996) Relatively recent construction of the Tien Shan inferred from GPS measurements of present-day crustal deformation rates. Nature 384:450–453

Allen MB, Windley BF, Chi Z (1992) Paleozoic collision tectonics and magmatism of the Chinese Tien Shan, Central Asia. Tectonophysics 220:89–115

An F, Zhu YF (2009) Native arsenic found in Baogutu gold deposit. Chin Sci Bull 54(10):1744–1749

An F, Zhu YF (2010) Native antimony in the Baogutu gold deposit (west Junggar, NW China): its occurrence and origin. Ore Geol Rev 37:214–223

Argand E (1924) La tectonique de l'Asie: In: Vaillant-Carmanne H (ed) Congres Geologique International. Liege, pp 171–372

Bai WJ, Wang BX, Liang RX, Yang FY (1995) Chromite deposits of China, in mineral deposits of China, Editorial Committee of mineral deposits, China, vol 2. Geological Publishing House, Beijing, pp 189–225

Bao JX (2001) Metallogenesis of the Axi and Aiken epithermal Au/Cu deposits. PhD Dissertation, Peking University, p 108 (unpublished)

Bell K (ed) (1989) Carbonatites; genesis and evolution. Unwin Hyman, London, p 618

Bell K, Kjarsgaard BA, Simonetti A (eds) (1998) Carbonatites—into the twenty-first century, a volume in honour of John Gittins. J Pet 39(11&12)

BGMRX (Bureau of Geology and Mineral Resources, Xinjiang) (1993) Regional geology of Xingjiang Uygur Autonomous region, Ministry of Geology and Mineral Resources

Biske YS, Seltmann R (2010) Paleozoic Tian-Shan as a transitional region between the Rheic and Urals-Turkestan oceans. Gondwana Res 17:602–613

Blisniuk PM, Hacker BR, Glodny J, Ratschbacher L, Bi SW, Wu ZH, McWilliams MO, Calvert A (2001) Normal faulting in central Tibet since at least 13.5 Myr ago. Nature 412:628–632

Borisenko AS, Sotnikov VI, Izokh AE, Polyakov GV, Obolensky AA (2006) Permo-Triassic mineralization in Asia and its relation to plume magmatism. Russ Geol Geophys 47:166–182

Branquet Y, Gumiaux C, Sizaret S, Barbanson L, Wang B, Cluzel D, Li GR, De Launay A (2012) Synkinematic mafic/ultramafic sheeted intrusions: emplacement mechanism and strain restoration of the Permian Huangshan Ni-Cu ore belt (Eastern Tianshan, NW China). J Asian Earth Sci do: 10.1016/j.jseaes.2012.05.021

Brown LD, Zhao WJ, Nelson KD, Hauck M, Alsdorf D, Ross A, Cogan M, Clark M, Liu XW, Che JK (1996) Bright spots, structure and magmatism in southern Tibet from INDEPTH seismic reflection profiling. Science 274:1688–1690

Buckman S, Aitchison JC (2004) Tectonic evolution of Palaeozoic terranes in West Junggar, Xinjiang, NW China. Geological Society, London, Sp Publ 226, pp 101–129

Cai H, Li HQ, Chen FW (2000) Study on chronology and origin of the Kuzhenkula gold deposit in northwestern margin of the Junggar Basin. Geol Miner Res South China 4:19–22

Cai K, Sun M, Yuan C, Zhao GC, Xiao WJ, Long XP, Wu FY (2010) Geochronological and geochemical study of mafic dykes from the northwest Chinese Altai: implications for petrogenesis and tectonic evolution. Gondwana Res 18:638–652

Cai K, Sun M, Yuan C, Zhao GC, Xiao WJ, Long XP (2012) Keketuohai mafic-ultramafic complex in the Chinese Altai, NW China: petrogenesis and geodynamic significance. Chem Geol 294–295:26–41

Carroll AR, Graham SA, Hendrix MS, Ying D, Zhou D (1995) Late Paleozoic tectonic amalgamation of northwestern China: sedimentary record of the northern Tarim, northwestern Turpan, and southern Junggar Basins. Geol Soc Am Bull 107:571–594

Carroll AR, Graham SA, Chang E, McKnight CL (2001) Sinian through Permian tectonostratigraphic evolution of the northwestern Tarim Basin, China. Geol Soc Am Mem 194:47–68

Castor SB (2008) The Mountain Pass rare-earth carbonatite and associated ultrapotassic rocks, California. Can Mineral 46:779–806

Černý P, Ercit TS (2005) The classification of granitic pegmatites. Can Mineral 43:2005–2026

Chai FM, Mao JW, Dong LH, Yang FQ, Liu F, Geng XX, Zhang ZX (2009) Geochronology of metarhyolites from the Kangbutiebao Formation in the Kelanf Basin, Altay mountains, Xinjiang: implications for the tectonic evolution and metallogeny. Gondwana Res 16:189–200

Chang EZ (2000) Geology and tectonics of the Songpan-Ganzi fold belt, southwestern China. Int Geol Rev 42:813–831

Charvet J, Shu SL, Laurent-Charvet S (2007) Paleozoic structural and geodynamic evolution of eastern Tianshan (NW China): welding of the Tarim and Junggar plates. Episodes 30:162–186

Chen B, Jahn BM (2004) Genesis of post-collisional granitoids and basement nature of the Junggar Terrane, NW China. Nd-Sr isotopic and trace element evidence. J Asian Earth Sci 23:691–703

Chen FW, Li HQ (2003) Metallogenic chronology of the Sawaya'erdun gold-antimony deposit in Xinjiang. Acta Geosinica Sin 24:563–567 (in Chinese with English abstract)

Chen SZ, Zhou JY, Gu LX, Cui BF, Xiao HL (2000) Genesis of ore-forming fluids and precipitation mechanism of gold in the Mazhuangshan gold deposit, Hami, Xinjiang. Miner Depos 19:193–200 (in Chinese with English abstract)

Chen YJ, Bao JX, Zhang ZJ, Chen HY, Liu YL (2003) Laumontitization as an exploration Indicator of epithermal gold deposits: a case study of the Axi and other epithermal systems in West Tianshan. Chin J Geochem 22:289–301

Chen YJ, Pirajno F, Sui YH (2004) Isotope geochemistry of the Tieluping silve-rlead deposit, Henan, China: a case study of orogenic silver-dominated deposits and related tectonic setting. Miner Depos 39:560–575

Chen YC, Liu DQ, Zhou RH, Tang YL, Wang DH, Ying LJ, Liang T (2005a) Discovery of picrite and related iron-copper-gold mineralization in North Junggar, Xinjiang, China. In: Mao JW, Bierlein FP (eds) Mineral deposit research: meeting the global challenge. Springer, Berlin, pp 1297–1300

Chen YJ, Pirajno F, Qi JP (2005b) Origin of gold metallogeny and sources of ore-forming fluids, Jiadong Province, eastern China. Int Geol Rev 47:530–549

Chen YJ, Chen HY, Zaw K, Pirajno F, Zhang ZJ (2007) Geodynamic settings and tectonic model of skarn gold deposits in China: an overview. Ore Geol Rev 31:139–169

Chen W, Zhang Y, Yong Y, Liu XY (2009) The Ar-Ar geochronological study of the shear zone type deposit of East Tianshan, Xinjiang, NW China, Goldschmidt Conf, pp. A214.

Chen HY, Chen YJ, Baker MJ (2012a) Evolution of ore-forming fluids in the Sawayaerdun gold deposit in the southwestern Chinese Tianshan metallogenic belt, northwest China. J Asian Earth Sci 49:131–144

Chen YJ, Pirajno F, Wu G, Qi JP, Xiong XL (2012b) Epithermal deposits in North Xinjiang, NW China. Int J Earth Sci Geol Rundsch 101(4):889–947

Cheng YQ (ed) (2000) Concise regional geology of China. Geological Publishing House, Beijing, p 430

Chung SL, Chua MF, Zhang YQ, Xie YG, Lo CH, Lee TY, Lan CY, Li XH, Zhang Q, Wang YZ (2005) Tibetan tectonic evolution inferred from spatial and temporal variations in post-collisional magmatism. Earth Sci Rev 68:173–196

Chiaradia M, Konopelko D, Seltmann R, Cliff RA (2006) Lead isotope variations across terrane boundaries of the Tien Shan and Chinese Altay. Mineral Deposita 41:411–428

Clark MK, Royden LH (2000) Topographic ooze: building the eastern margin of Tibet by lower crustal flow. Geology 28:703–706

Cole JW, Spinks KD (2009) Caldera volcanism and rift structure in the Taupo Volcanic Zone, New Zealand. Geological Society, London, Sp Publ 327, pp 9–30

Coleman RG (1989) Continental growth of Northwest China. Tectonics 8:621–635

Copley A, Avouac JP, Wernicke BP (2011) Evidence for mechanical coupling and strong Indian lower crust beneath southern Tibet. Nature 472:79–81

Dai J, Wang C, Hebert R, Santosh M, Li Y, Xu J (2011) Petrology and Geochemistry of periodites in the Zhongba ophiolite, Yarlung Zangbo Suture Zone: implications for the Early Cretaceous intra-oceanic subduction zone within the Neo-Tethys. Chem Geol 288:133–148

Dahlkamp FJ (2009) Uranium deposits of the world, Chap. 1, China, Peoples Republic of. Springer, Berlin, p 156

de Jong K, Wang B, Faure M, Shu LS, Cluzel D, Charvet J, Ruffet G, Chen Y (2009) New $^{40}Ar/^{39}Ar$ age constraints on the Late Palaeozoic tectonic evolution of the western Tianshan (Xinjiang, northwestern China), with emphasis on Permian fluid ingress. Int J Earth Sci Geol Rundsch 98(6):1239–1258

Dewey JF, Shackleton FR, Chang CF, Sun Y (1988) The tectonic evolution of the TIbetan Plateau. Phil Trans Royal Soc Lond A327:379–413

Dobretsov NL (2011) Early paleozoic tectoncs and geodynamics of Central Asia. Russ Geol Geophys 52:1539–1552

Dong LH, Sha DM (2005) Late paleozoic epithermal gold deposits in West Tian Shan. Geological Publishing House, Beijing, p 154 (in Chinese)

Dong YP, Zhang GW, Neubauer F, Liu SM, Hauzenberger C, Zhou DW, Li W (2011) Syn- and post-collisional granitoids in the Central Tianshan orogen: geochemistry, geochronology and implications for tectonic evolution. Gondwana Res 20:568–581

Enkelmann E, Weislogel A, Ratschbacher L, Eide E, Renno A, Wooden J (2007) How was the Triassic Songpan-Ganzi basin filled? A provenance study. Tectonics 26:1–24 TC4007

Fang SH, Yan S, Jia CZ, Guo ZJ, Zhang ZC, Liu LJ (2007) Timing of Cenozoic intense deformation at the north margin of Tianshan an its implications for petroleum accumulation. Earth Sci Front 14(2):205–214 (in Chinese with English abstract)

Feng JP, Wang JL (2005) Study on fluid inclusions and discussion on gold mineralization styles of Axi, Jingxi-Yelmend gold deposits in western Tianshan, Xinjiang. Northwest Geol 38:31–36 (in Chinese with English abstract)

Feng CY, Xue CJ, Ji JS, Zhang LC, Li HQ (2000) Geochemistry of the Xitan epithermal gold-silver deposit, East Tianshan Mountains. Miner Depos 19:322–329

Feng CY, Qu WJ, Zhang DQ, Dang XY, Du A, Li DX, She HQ (2009) Re-Os dating of pyrite from the Tuolugou stratabound Co(Au) deposit, eastern Kunlun orogenic belt, nortwestern China. Ore Geol Rev 36:213–220

Fielding EJ (1996) Tibet uplift and erosion. Tectonophysics 260:55–84

Fowler CMR (2009) The solid earth—an introduction to global geophysics, 2nd edn. Cambridge University Press, Cambridge, p 685

Franklin JM, Gibson HL, Jonasson IR, Galley AG (2005) Volcanogenic massive sulfide deposits. Econ Geol 100th Ann Vol:523–560

Freymueller JT (2011) A new mechanichal model for Tibet. Nature 472:48–49

Frietsch R (1978) On the magmatic origin of iron ores of the Kiruna type. Econ Geol 73:476–485

Gao YF, Hou ZQ, Wei RH, Zhao RS (2003) Post-collisional adakitic porphyries in Tibet: geochemical and Sr-Nd-Pb isotopic constraints on partila melting of oceanic lithosphere and crust-mantle interaction. Acta Geol Sin 77:194–203

Gao J, Long LL, Klemd R, Qian Q, Liu DY, Xiong XM, Su W, Liu W, Wang YT, Yang FQ (2009) Tectonic evolution of the South Tianshan Orogen, NW China: geochemical and age constraints of granitoid rocks. Int J Earth Sci 98(6):1221–1238

Gao J, Klemd R, Qian Q, Zhang X, Li J, Tuo J (2011) The collision between the Yili and Tarim blocks of the southwestern Altaids: geochemical and age constraints of a leucogranite dike crosscutting the HP-LT metamorphic belt in the Chinese Tianshan orogen. Tectonophysics 499:118–131

Gao JF, Zhou MF, Lightfoot PC, Wang CY, Qi L (2012) Origin of PGE-poor and Cu-rich magmatic sulfides from the Kalatongke deposit, Xinjiang, northwest China. Econ Geol 107:481–506

Garuti G, Bea F, Zaccarini F, Montero P (2001) Age, geochemistry and petrogenesis of the ultramafic pipes in the Ivrea Zone, NW Italy. J Petrol 42:433–457

Geijer P (1931) The iron ores of the Kiruna type. Sver Geol Unders C624;1–32

Geng HY, Sun M, Yuan C, Xiao WJ, Xian WS, Zhao GC, Zhang LF, Wong K, Wu FY (2009) Geochemical, Sr-Nd and zircon U-Pb-Hf isotopic studies of Late carboniferous magmatism in the West Junggar, Xinjiang: implications for ridge subduction? Chem Geol 266:364–389

Geng HY, Sun M, Yuan C, Zhao GC, Xiao WJ (2011) Geochemical and geochronological study of early Carboniferous volcanic rocks from the West Junggar: petrogenesis and tectonic implications. J Asian Earth Sci 42:854–866

Glorie S, De Grave J, Buslov MM, Elburg MA, Stockli DF, Gerdes A, Van Den Haute P (2010) Multi-method chronometric constraints on the evolution of the Northern Kyrgyz Tien Shan granitoids (Central Asian Orogenic Belt): from emplacement to exhumation. J Asian Earth Sci 38:131–146

Goldfarb RJ, Mao JW, Hart C, Wang D, Anderson E, Wang Z (2003) Tectonic and metallogenic evolution of the Altay Shan, Northern Xinjiang Uygur Autonomous Region, northwestern China. In: Mao J-W, Godlfarb RJ, Seltmann R, Wang DH, Xiao WJ, Hart C (eds) Tectonic evolution and metallogeny of the Chinese Altay and Tianshan. International Association on the Genesis of Ore Deposits, Centre for Russian and Central Asian Mineral Studies, Natural History Museum, London, pp 17–30

Groves DI, Goldfarb RJ, Gebre-Mariam M, Hagemann SG, Robert F (1998) Orogenic gold deposits: a proposed classification in the context of their crustal distribution and relationship to other gold deposit types. Ore Geol Rev 13:7–27

Gu LX, Zhu JL, Guo JC, Liao JJ, Yan ZF, Yang H (1995) Geology and genesis of the mafic-ultramafic complexes in the Huangshan-Jingerquan (HJ) belt, East Xinjiang: Chin J Geochem 14:98–116

Gudfinnson GH, Presnall DC (2005) Continuous gradations among primary carbonatitic, kimberlitic, melilitic, basaltic, picritic and komatiititc melts in equilibrium with garnet lherzolite at 3–8 GPa. J Pet 46:1645–1659

Guo ZF, Hertogen J, Liu JQ, Pasteels P, Boven A, Punzalan L, He HY, Luo XJ, Zhang WH (2005) Potassic magmatism in western Sichuan and Yunnan provinces, SE Tibet, China: petrological and geochemical constraints. J Pet 46:33–78

Han BF, Wang SH, Jahn BM, Hong DW, Kagami H, Sun YL (1997) Depleted-mantle source for the Ulungur River A-type granites from North Xinjiang, China: geochemistry and Nd-Sr isotoppic evidence, and implications for Phanerozoic crustal growth. Chem Geol 138:135–159

Han BJ, Song B, Chen L, Li Z (2004) SHRIMP zircon U-Pb ages of Kalatongke No. 1 and Huangshandong Cu-Ni-bearing mafic-ultramafic complexes, North Xinjiang and geological implications. Chin Sci Bull 49:2424–2429

Han CM, Xiao WJ, Zhao GC, Mao JW, Li SZ, Yan Z, Mao QG (2006a) Major types, characteristics and geodynamic mechanism of Upper Paleozoic copper deposits in northern Xinjiang, northwestern China. Ore Geol Rev 28:308–328

Han CM, Xiao WJ, Zhao GC, Mao JW, Li SZ, Yan Z, Mao QG (2006b) Geological characteristics and genesis of the Tuwu porphyry copper deposit, Hami, Xinjiang, Central Asia. Ore Geol Rev 29:77–94

Han CM, Xiao WJ, Zhao GC, Qu WJ, Du A (2007) Re-Os dating of the Kalatongke Cu-Ni deposit, Altay Shan, NW China, and resulting geodynamic implications. Ore Geol Rev 32:452–468

Han CM, Xiao WJ, Zhao GC, Ao SJ, Zhang J, Qu WJ, Du AD (2010) In-situ U-Pb, Hf and Re-Os isotopic analyses of the Xiangshan Ni-Cu-Co deposit in eastern Tianshan (Xinjiang), Central Asia Orogenic Belt: constraints on the timing and genesis of the mineralization. Lithos 120:547–562

Han BF, He GQ, Wang XC, Guo ZJ (2011) Late Carboniferous collision between the Tarim and Kazakhastan-Yili terranes in the western segment of the South Tian Shan Orogen, Central Asia, and implications for the North Xinjiang, western China. Earth Sci Rev 109(3–4):74–93

Hart CJR, Wang Y, Goldfarb R, Begg G, Mao JW, Dong L (2003) Axi and associated epithermal gold deposits in western Tianshan, Xinjiang. Tectonic evolution and metallogeny of the Chinese Altay and Tianshan. In: Mao JW, Goldfarb RJ, Seltmann R, Wang DH, Xiao WJ, Hart C (eds) IAGOD and CERCAMS. IGCP-473 Project Field Excursion, Xinjiang, pp 209–226

Hauri EH, Shimuzu N, Dieu JJ, Hart SR (1993) Evidence for hotspot-related carbonatite metasomatism in the oceanic upper mantle. Nature 365:221–227

Heubeck C (2001) Assembly of central Asia during the middle and late Paleozoic. In: Hendrix MS, Davis GA (eds) Paleozoic and Mesozoic tectonic evolution of Central and Eastern Asia. Geol Soc Am Mem 194:1–22

Hildebrand RS (1986) Kiruna-type deposits: their origin and relationship to intermediate subvolcanic plutons in the Great Bear Magmatic zone, northwest Canada. Econ Geol 81:640–649

Hou ZQ, Cook NJ (2009) Metallogenesis of the Tibetan collisional orogen: a review and introduction to the special issue. Ore Geol Rev 36:2–24

Hou ZQ, Ma HW, Zaw K, Zhang YQ, Wang MJ, Wang Z, Guitang P, Renli T (2003) The Himalayan Yulong porphyry copper belt: product of large scale strike-slip faulting in eastern Tibet. Econ Geol 98:125–146

Hou ZQ, Gao YF, Qu XM, Rui ZY, Mo XX (2004a) Origin of adakitic intrusives generated during mid-Miocene east-west extension. Earth Planet Sci Lett 220:139–155

Hou ZQ, Qu XM, Wang SX, Du A, Gao YF, Huang W (2004b) Re-Os age for molybdenite from the Gangdese porphyry copper belt on Tibetan plateau: implication for geodynamic setting and duration of the Cu mineralization. Sci China Ser D 47:221–231

Hou ZQ, Zaw K, Pan GT, Mo XX, Xu Q, Hu YH, Li XZ (2007a) Sanjiang Tethyan metallogenesis in S. W. China: tectonic setting, metallogenic epochs and deposit types. Ore Geol Rev 31:48–87

Hou ZQ, Xie YL, Xu WJ, Li YQ, Zhu XK, Zaw K, Beaudoin G, Rui ZY, Wei H, Ciren LB (2007b) Yulong deposit, eastern Tibet: a high-sulfidation Cu-Au porphyry deposit in the Eastern Indo-Asian collision zone. Int Geol Rev 49:235–258

Hou ZQ, Yang ZM, Qu XM, Meng XJ, Li ZQ, Beaudoin G, Rui ZY, Gao YF, Zaw K (2009a) The Miocene Gangdese porphyry copper belt generated during post-collisional extension in the Tibetan Orogen. Ore Geol Rev 36:25–51

Hou ZQ, Tian SH, Xie YL, Yang ZS, Yuan ZX, Yin SP, Yi LS, Fei HC, Bai G, Li XY (2009b) The Himalayan Mianning-Dechang REE belt associated with carbonatite-alkaline complexes, eastern Indo-Asian collision zone, SW China. Ore Geol Rev 36:65–89

Hou ZQ, Zhang HR, Pan XF, Yang ZM (2011) Porphyry Cu (-Mo-Au) deposits related to melting of thickened mafic lower crust: examples from the eastern Tethyan metallogenic domain. Ore Geol Rev 39:21–45

Hsu KJ, Guitang P, Sengör AMC, Ueli B, Chen H, Chen C, Harris N, Hsu P, Li J, Luo J, Lee T, Li ZX, Lu C, Powerll C, Wang Q, Winterer EL (1995) Tectonic evolution of the Tibetan Plateau: a working hypothesis based on the archipelago model of orogenesis. Int Geol Rev 37:473–508

Hu RZ, Burnard PG, Bi XW, Zhou MF, Pen JT, Su WC, Wu KX (2004) Helium and argon isotope geochemistry of alkaline intrusion-associated gold and copper deposits along the Red River-Jinshajaing fault belt, SW China. Chem Geol 203:305–317

Jahn BM (2004) The Central Asian Orogenic Belt and growth of the continental crust in the Phanerozoic. In: Malpas J, Fletcher CJN, Ali JR, Aitchison JC (eds), Aspects of the tectonic evolution of China. Geol Soc London Sp Publ, pp. 73–100

Ji JS, Zhang LC, Zeng ZR, Lu DR, Yang XK, Yang ZG (1996) Chronology study of Kanggultage gold metallogenic belt, East Tianshan. Sci Geol Sin 31:80–89

Ji JS, Xue CJ, Feng CY (1999) Xitan gold deposit of epithermal type in Xinjiang. J Xi'an Eng Univ 21:1–5

Jia B, Mu RS, Tian CL, Sha DM, Yang S (2001a) The characteristics of the Tawuerbieke-Abiyindi porphyry gold deposits. Geol Resour 10:139–145 (in Chinese with English abstract)

Jia B, Mu RS, Tian CL, Sha DM (2001b) The characters of the mineralization fluid of Axi gold deposit in Xinjiang. Gold Geol 7:39–46

Jing J, Xu B (1997) Mazhuangshan gold deposit and its metallogenic geochemical conditions. Xinjiang Geol 15:327–341 (in Chinese with English abstract)

Johan Z (2002) Alaskan-type complexes and their platinum-group element mineralization. In: Cabri LJ (ed) The geology, geochemistry, mineralogy and mineral beneficiation of platinum-group elements. Can Inst Min Metall (CIM) Sp Vol 54:669–720

Kind R, Yuan XH (2010) Seismic images of the biggest crash on earth. Science 329:1479–1480
Le Bas MJ (1987) Nephelinites and carbonatites. In: Fitton JG, Upton BGJ (eds) Alkaline igneous rocks. Geological Society, London, Sp Publ 30, pp 53–86
Lentz DR (1999) Carbonatite genesis: a re-examination of the role of intrusion-related pneumatolitic skarn processes in limestone melting. Geology 27:335–338
Li ZC (1999) Two tectono-metallogenic types of gold deposits and their metallogenic models in the southern Altay Mountain. Geotecton Metallog 23:16–28 (in Chinese with English abstract)
Li HQ, Chen FW (2004) Isotopic, geochronology of regional mineralization in Xinjiang, China. Geological Publishing House, Beijing, p 361 (in Chinese with English abstract)
Li XJ, Liu W (2002) Fluid inclusion and stable isotope constraints on the genesis of the Mazhuangshan gold deposit, eastern Tianshan Mountains of China. Acta Pet Sin 18:551–558 (in Chinese with English abstract)
Li YQ, Rui ZY, Cheng LX (1981) Fluid inclusions and mineralization of the Yulong porphyry copper (Mo) deposit. Acta Geol Sin 55:18–23 (in Chinese with English abstract)
Li HQ, Xie CF, Chang HL, Cai H, Zhu JP, Zhou S (1998) Study on metallogenetic chronology of nonferrous and precious metallic ore deposits in North Xinjiang, China. Geological Publishing House, Beijing, p 264 (in Chinese with English abstract)
Li HQ, Chen FW, Cai H, Liu HQ (1999) Study on isotopic chronology of the Mazhuangshan gold mineralization, eastern Xinjiang. Sci Geol Sin 34:215–256 (in Chinese with English abstract)
Li S, Deng J, Hou ZQ, Xiao R, Yuan WM, Feng XL, Zhao Z, Shen JF, Zhou S (2001a) Regional fractures and denudation of gold ore deposits in Gangdise block, Tibet: evidence of Ag/Au values. Sci China Ser D 44:121–127
Li JA, Mo JP, Peng XM (2001b) Metallogenic and geological conditions of gold deposits in the north of eastern Tianshan. Xinjiang Geol 19:268–275 (in Chinese with English abstract)
Li HQ, Chen FW, Lu YF, Yang HM, Guo J, Mei YP (2005) New chronological evidence for Indosinian diagenetic mineralization in Eastern Xinjiang, NW China. Acta Geol Sin 79:264–275 (English Edition)
Li C, Zhang MJ, Fu PE, Qian ZH, Hu PQ, Ripley EM (2012) The Kalatongke magmagtic Ni-Cu deposits in the Central Asian Orogenic Belt, NW China: product of slab window magmatism? Miner Depos 47:51–67
Liang HY, Campbell IH, Allen C, Sun WD, Liu CQ, Yu HX, Xie YW, Zhang YQ (2006) Zircon $Ce4^{+}/Ce3^{+}$ ratios and ages for Yulong ore-bearing pophyries in eastern Tibet. Miner Depos 41:152–159
Liao QL, Dai TG, Liu WH (2000) A preliminary study on mineralization and mineralizing model for the Kuoerzhankuola epithermal gold deposit. Geotecton Metallog 24:57–64
Lin JF, Xie QL, Xi XP, Hu CQ, Liu JY (1999) Geological features of the volcanic-hosted Shuangfengshan gold deposit in Xingjiang. Geol Rev 45:1099–1104
Liu JY (2003) Main characters of the gold ore deposits and prospect in Beishan gold mine area, Yiwu County, Xinjiang, China. J Guilin Inst Technol 23:252–257 (in Chinese with English abstract)
Liu JY, Qian JP, Cheng ZP, Shan NL (2002) Continental volcanic action and metallogenesis for gold and copper deposit of east Junggar, Xinjiang. Geological Publishing House, Beijing, p 218
Liu W, Li XJ, Deng J (2003a) Sources of ore-forming fluids and metallic materials in the Jinwozi lode gold deposit, eastern Tianshan mountains of China. Sci China Ser D 46(Suppl):136–153
Liu GR, Long ZN, Chen QZ, Zhou G (2003b) The formation age and geochemical characteristics of the volcanic rock of Kuoerzhenkuola gold mine in Xinjiang. Xinjiang Geol 21:177–180
Liu JJ, Zheng MH, Cook NJ, Long XR, Deng J, Zhai YS (2007) Geological and geochemical characteristics of the Sawaya'erdun gold deposit, southwestern Tianshan. Ore Geol Rev 32(1–2):125–156
Liu F, Li YH, Mao JW, Yanf FQ, Chai FM, Geng XX, Yang XX (2008) The SHRIMP U-Pb ages of Abagong granites in the Altaid orogen and its geologic implications. Acta Geosci Sin 29:795–804
Liu F, Yang FQ, Li YH, Chai FM, Geng XX (2009a) The indication of metallogeny for iron deposit in Abagong area in the southern margin of Altay, Xinjiang, China. In: Podosek FA (ed) 19th Goldschmidt Conference, Geochimica et Cosmochimica Acta, p A776

Liu F, Mao JW, Yang FQ (2009b) The geologic implication of the SHRIMP U-Pb ages of two granites near Abagong iron deposit, Altay, Xinjiang, NW China. In: Podosek FA (ed) 19th Goldschmidt Conference, Geochimica et Cosmochimica Acta, p A556

Liu JL, Wang AJ, Xia HR, Zhai YF, Gao L, Xiu QY, Zhang ZC, Zhao ZD, Cao DH (2010) Cracking mechanisms during galena mineralization in a sandstone-hosted lead-zinc- ore deposit: case study of the Jinding giant sulfide deposit, Yunnan, SW China. Miner Depos 45:567–582

Long XP, Yuan C, Sun M, Xiao WJ, Wang YJ, Cai K, Jiang YD (2011) Geochemistry and Nd isotopic composition of the early Paleozoic flysch sequence in the Chinese Altai, Central Asia: evidence for a northward-derived mafic source and insights into Nd model ages in accretionary orogen. Gondwana Res 211:637–653

Lü LS, Mao JW, Li HB, Pirajno F, Zhang ZH, Zhou ZH (2011) Pyrrhotite Re-Os and SHRIMP zircon U-Pb dating of the Hongqiling Ni-Cu sulfide deposits in Northeast China. Ore Geol Rev 43(1):106–119

Ma RS, Shu LS, Sun JQ (1997) Tectonic framework and crust evolution of eastern Tianshan Mountains. Geological Publishing House, Beijing, p 202 (in Chinese)

Mao JW, Qiu YM, Goldfarb RJ, Zhang ZC, Garwin S, Fengshou R (2002) Geology, distribution, and classification of gold deposits in the western Qinling belt, central China. Miner Depos 37:352–377

Mao JW, Godlfarb RJ, Seltmann R, Wang DH, Xiao WJ, Hart C (eds) (2003) Tectonic evolution and metallogeny of the Chinese Altay and Tianshan. International Association on the Genesis of Ore Deposits, Centre for Russian and Central Asian Mineral Studies, Natural History Museum, London, p 282

Mao JW, Goldfarb RJ, Wang YT, Hart CJ, Wang ZL, Yang JM (2005) Late Paleozoic base and precious metal deposits, East Tianshan, Xinjiang, China: characteristics and geodynamic setting. Episodes 28:23–36

Mao JW, Pirajno F, Zhang ZH, Chai FM, Wu H, Chen LS, Yang JM, Zhang CQ (2008) A review of the Cu-Ni sulphide deposits in the Chinese Tianshan and Altay orogens (Xinjiang Autonomous Region, NW China): principal characteristics and ore-forming processes. J Asian Earth Sci 32(2–4):184–203

Metelkin DV, Vernikovsky VA, Kazansky AYu, Wingate MTD (2010) Late Mesozoic tectonics of Central Asia based on paleomagnetic evidence. Gondwana Res 18:400–419

Min MZ, Chen J, Wang JP, Wei GH, Fayek M (2005a) Mineral paragenesis and textures associated with sandstone-hosted roll-front uranium deposits, NW China. Ore Geol Rev 26:51–69

Min MZ, Xu HF, Chen J, Fayek M (2005b) Evidence of uranium biomineralization in sandstone-hosted roll-front uranium deposits, northwestern China. Ore Geol Rev 26:198–206

Molnar P, Tapponnier P (1978) Active tectonics of Tibet. J Geophys Res 85:5361–5375

Mossakovsky AA, Ruzhentsev SV, Samygin SG, Kheraskova TN (1994) Central Asian fold belt: geodynamic evolution and formation history. Geotectonics 27:445–474

Naldrett AJ (2004) Magmatic sulfide deposits. Springer, Berlin, p 727

Nelson KD, Zhao WJ, Brown LD, Kuo J, Che JK, Liu XW, Klemperer SL, Makovsky Y, Meissner R, Mechie J, Kind R, Wenzel F, Nabelek J, Chen LS, Tan HD, Wei WB, Jones AG, Booker J, Unsworth M, Kidd WSF, Hauck M, Aksdorf D, Ross A, Cogan M, Wu CD, Sandvoi E, Edwards M (1996) Partially molten middle crust beneath southern Tibet: synthesis of project INDEPTH results. Science 274:1684–1687

Nielsen TFD, Veksler IV (2002) Is natrocarbonatite a cognate fluid condensate? Contrib Miner Pet 142:425–435

Nyström JO, Henríquez F (1994) Magmatic features of iron ores of the Kiruna type in Chile and Sweden: ore textures and magnetite geochemistry. Econ Geol 89:820–839

Nyström JO, Billstrom K, Henríquez F, Fallick AE, Naslund HR (2008) Oxygen isotope composition of magnetite in iron ores of the Kiruna type in Chile and Sweden. GFF (J Geol Soc Swed) 130:177–188

Pavlova G, Gushchina L, Borovikov A, Borisenko A, Obolensky AA (2004) Silver and antimony in hydrothermal solutions of Ag-Sb deposits. Russ Geol Geophys 45:1186–1197

Peng XM, Mo JP, Li JA, Xi XP, San JZ (2004) Geological characteristics and metallogenic model of Shuangfengshan epithermal gold deposit in eastern Junggar, Xinjiang. Miner Depos 23:101–106 (in Chinese with English abstract)

Peters SG (2002) Geology, geochemistry and geophysics of sedimentary-hosted Au deposits in P. R. China, Open-File Report 02-131, vol 1.0, U. S. Geol Surv, p 403

Pirajno F (2000) Ore deposits and mantle plumes. Kluwer Academic, Dordrecht, p 556

Pirajno F (2009) Hydrothermal processes and mineral systems. Springer, Berlin, p 1250

Pirajno F (2010) Intracontinental strike-slip faults, associated magmatism, mineral systems and mantle dynamics; examples from NW China and Altay-Sayan (Siberia). J Geodyn 50:325–346

Pirajno F (in press) Effects of metasomatism on mineral systems and their host rocks: alkali metasomatism, skarns, greisens, tourmalinites, rodingites, black-wall alteration, and listvenites. In: Harlov DE, Austrheim H (eds) Metasomatism and metamorphism: the role of fluids in crustal and upper mantle processes, Lecture Series in Earth Science. Springer, Berlin, pp XXXX

Pirajno F, Luo ZQ, Liu SF, Dong L (1997) Gold deposits of the Eastern Tianshan, Northwestern China. Int Geol Rev 39:391–904

Pirajno F, Mao JW, Zhang ZC, Zhang ZH, Chai FM (2008) The association of mafic-ultramafic intrusions and A-type magmatism in the Tianshan and Altay orogens, NW China: implications for geodynamic evolution and potential for the discovery of new ore deposits. J Asian Earth Sci 32:165–183

Pirajno F, Ernst RE, Borisenko AS, Fedoseev G, Naumov EA (2009) Intraplate magmatism in central Asia and China and associated metallogeny. Ore Geol Rev 35:114–136

Pirajno F, Seltmann R, Yang YQ (2011) A review of mineral systems and associated tectonic settings of northern Xinjiang, NW China. Geosci Front 2:157–185

Qi W, Pei-Zhen Z, Freymueller JT, Bilham R, Larson KM, Xi'an L, You XZ, Niu ZJ, Wu JC, Li YX, Liu JN, Yang ZQ, Chen QH (2001) Present-day crustal deformation in China constrained by global positioning system measurements. Science 294:574–577

Qin KZ, Sun S, Li JL, Fang TH, Wang SL, Liu W (2002) Paleozoic epithermal Au and porphyry Cu deposits in North Xinjiang, China: epochs, features, tectonic linkage and exploration significance. Resour Geol 52:291–300

Qin KZ, Zhang LC, Xiao WJ, Xu XW, Yan Z, Mao JW (2003) Overview of major Au, Cu, Ni, and Fe deposits and metallogenic evolution of the eastern Tianshan mountains, northwestern China. In: Mao J-W, Godlfarb RJ, Seltmann R, Wang DH, Xiao WJ, Hart C (eds) Tectonic evolution and metallogeny of the Chinese Altay and Tianshan. International Association on the Genesis of Ore Deposits, Centre for Russian and Central Asian Mineral Studies. Natural History Museum, London, pp 227–248

Qin KZ, Su BX, Sakyi PA, Tang DM, Li XH, Sun H, Xiao QH, Liu PP (2011) SMS Zircon U-Pb Geochronology and Sr-Nd Isotopes of Ni-Cu-bearing mafic-ultramafic intrusions in Eastern Tianshan and Beishan in correlation with flood Basalts in Tarim Basin (NW-China): contraints on a Ca. 280 Ma Mantle Plume. Am J Sci 311:237–260

Rui ZY, Goldfarb RJ, Qiu YM, Zhou TH, Chen RY, Pirajno F, Yun G (2002) Paleozoic-early Mesozoic gold deposits of the Xinjiang Autonomous Region, Northwestern China. Miner Depos 37:393–418

Schulmann K, Paterson S (2011) Asian continental growth. Nat Geosci 4:827–829

Schulte-Pelkum V, Monsalve G, Sheehan A, Pandey MR, Sapkota S, Bilham R, Wu F (2005) Imagining the Indian subcontinent beneath the Himalaya. Nature 435:1222–1225

Seltmann R, Jenchuraeva R (eds) (2001) Paleozoic geodynamics and gold deposits in the Kyrgyz Tien Shan. IGCP-373 Excursion guidebook. International Association on the Genesis of Ore Deposits (IAGOD), London, p 182

Seltmann R, Porter TM (2005) The porphyry Cu–Au/Mo deposits of Central Eurasia: 1. Tectonic, geologic and metallogenic setting and significant deposits. In: Porter TM (ed) Super Porphyry Copper and gold deposits: a global perspective. 2. PGC Publishing, Adelaide, pp 467–512

Seltmann R, Konopelko D, Biske G, Divaev F, Sergeev S (2011) Hercynian post-collisional magmatism in the context of Paleozoic magmatic evolution of the Tien Shan orogenic belt. J Asian Earth Sci 42(5):821–838

Sengör AMC, Natal'in BA (1996) Paleotectonics of Asia: fragments of synthesis. In: Yin A, Harrison TM (eds) The tectonic evolution of Asia. Cambridge University Press, Cambridge, pp 486–640

Şengör AMC, Natal'in BA (2007) Eduard Suess and the Altaids: what is in a name? In: Seltmann R, Borisenko AS, Fedoseev G (eds) Magmatism and metallogeny of the Altai and adjacent large igneous provinces with an introductory essay on the Altaids. International Association Genesis of Ore Deposits (IAGOD), IAGOD Guidebook Series 16, CERCAMS/NHM, London, pp 188–294

Sengör AMC, Natal'in BN, Burtman VS (1993) Evolution of the Altai tectonic collage and Palaeozoic crustal growth in Eurasia. Nature 364:299–307

Sha DM (1998) The fluid inclusion of Axi gold deposit in West Tianshan Mountains. J Precious Metall Geol 7:180–188 (in Chinese with English abstract)

Sha DM, Dong LH, Bao QZ, Wang H, Hu XJ, Zhang JD, Sun JP (2003) The genetic types of gold deposits and their prospecting in West Tianshan Mountains. Xinjiang Geol 21:419–425

Sha DM, Jing CZ, Dong LH, Wu RS, Tian CL, Jia B (2005) Study on the metallogenic geochemistry of Axi gold deposit in western Tianshan Mountains. Geol Resour 14:118–125

Shapiro NM, Ritzwoller MH, Molnar P, Levin V (2004) Thinning and flow of Tibetan crust constrained by seismic anisotropy. Science 305:233–235

Shen P, Shen Y, Liu T, Li G, Zeng Q (2007) Genesis of volcanic-hosted gold deposits in the Sawur gold belt, northern Xinjiang, China: evidence from REE, stable isotopes and noble gas isotopes. Ore Geol Rev 32:207–226

Shen P, Shen YC, Liu TB, Li GM, Zeng QD (2008) Geology and geochemistry of the Early Carboniferous eastern Sawur caldera complex and associated gold epithermal mineralization, Sawur mountains, Xinjiang, China. J Asian Earth Sci 32:259–279

Shen P, Shen YC, Liu TB, Meng L, Dai HW, Yang YH (2009) Geochemical signatures of porphyries in the Baogutu porphyry copper belt, western Junggar, NW China. Gondwana Res 16:227–242

Shen P, Shen YC, Pan HD, Wang JB, Zhang R, Zhang YX (2010a) Baogutu porphyry Cu-Mo-Au deposit, west Junggar, northwest China: petrology, alteration and mineralization. Econ Geol 105:947–970

Shen P, Shen YC, Wang JB, Zhu HP, Wang LJ, Meng L (2010b) Methane-rich fluid evolution of the Baogutu porphyry Cu-Mo-Au deposit, Xinjiang, NW China. Chem Geol 275:78–98

Shen P, Shen YC, Pan HD, Li XH, Wang JB, Zhu HP, Dai HW, Guan W (2012) Geochronology and isotope geochemistry of the Baogutu porphyry copper deposit in the West Junggar region, Xinjiang, China. J Asian Earth Sci 48:99–145

Shu LS, Yu JH, Charvet J, Laurent-Charvet S, Sang HQ, Zhang R (2004) Geological, geochronological and geochemical features of granulites in the Eastern Tianshan, NW China. J Asian Earth Sci 24:25–41

Song XY, Li XR (2009) Geochemistry of the Kalatongke Ni-Cu-(PGE) sulfide deposit, NW China: implications for the formation of magmatic sulfide mineralization in a post-collisional environment. Miner Depos 44:303–328

Song HX, Liu YL, Qu WJ, Song B, Zhang R, Cheng Y (2007) Geological characters of Baogutu porphyry copper deposit in Xinjiang, NW China. Acta Pet Sin 23:1891–1988 (in Chinese with English abstract)

Su SG, Lesher CM (2012) Genesis of PGE mineralization in the Wengeqi mafic-ultramafic complex, Guyang County, Inner Mongolia, China. Miner Depos 47:197–207

Su W, Gao J, Klemd R, Li JL, Zhang X, Li XH, Chen NS, Zhang L (2010) U-Pb zircon geochronology of Tianshan eclogites in NW China: implications for the collision between the Yili and Tarim blocks of the southwestern Altaids. Eur J Miner 22:473–478

Su BX, Qin KZ, Sakyi PA, Li XH, Yang YH, Sun H, Tang DM, Liu PP, Xiao QH, Malaviarachchi SPK (2011) U-Pb ages and Hf-O of zircons from Late Paleozoic mafic-ultramafic units in the southern Central Asian Orogenic Belt: tectonic implications and evidence for an Early-Permian mantle plume. Gondwana Res 20:516–531

Suess E (1904) The face of the earth. Clarendon, Oxford, p 604
Suess E (1906) The face of the earth. Clarendon, Oxford, p 566
Suess E (1908) The face of the earth. Clarendon, Oxford, p 400
Tang GJ, Wang Q, Wyman DA, Li ZX, Zhao ZH, Jia XH, Jiang ZQ (2010) Ridge subduction and crustal growth in the Central Asian Orogenic Belt: evidence from Late Carboniferous adakites and high-Mg diorites in the western Junggar region, northern Xinjiang (west China). Chem Geol 277:281–300
Tang DM, Qin KZ, Li CS, Qi L, Su BX, Qu WJ (2011) Zircon dating, Hf-Sr-Nd-Os isotopes and PGE geochemistry of the Tianyu sulfide-bearing mafic-ultramafic intrusion in the Central Asian Orogenic Belt, NW China. Lithos 126:84–94
Tang DM, Qin KZ, Sun H, Xiao QH (2012) The role of crustal contamination in the formation of Ni-Cu sulfide deposits in Eastern Tianshan, Xinjiang, northwest China: evidence from trace element geochemistry, Re-Os, Sr-Nd, zircon Hf-O and sulfur isotopes. J Asian Earth Sci 49:145–160
Tapponier P, Molnar P (1976) Slip-line field theory and large-scale continental tectonics. Nature 264:319–324
Tapponier P, Lacassin R, Leloup PH, Scharer U, Zhong DL, Wsu HW, Liu XH, Ji SC, Zhang LS, Zhong JY (1990) The Ailao Shan/Red River metamorphic belt: tertiary left-lateral shear between Indochina and South China. Nature 343:431–437
Tornos F (2006) Environment of formation and styles of volcanogenic massive sulfides: the Iberian Pyrite Belt. Ore Geol Rev 28(3):259–307
van der Voo R, Levashova NM, Skrinnik LI, Kara TV, Bazhenov ML (2006) Late orogenic, large-scale rotations in the Tian Shan and adjacent mobile belts in Kyrgyzstan and Kazakhstan. Tetonophysics 426:335–360
Veevers JJ, Saeed A, Belousova EA, Griffin WL (2005) U-Pb ages and source composition by Hf-isotope and trace-element analysis of detrital zircons in Permian sandstone and modern sand from southwestern Australia and a review of the palaeogeographical and denudational history of the Yilgarn Craton. Earth Sci Rev 68:245–279
Veksler IV, Lentz D (2006) Parental magmas of plutonic carbonatites, carbonate-silicate immiscibility and decarbonation reactions: evidence from melt and fluid inclusions: Miner Assoc Can Short Course 36:123–149
Wan Y, Wu QB, Zhang ZX, Zeng YF, Tian R (2008) Geological survey report of copper-molybdenum-polymetallic deposit in the in the Lailisigao'er region, Inghe County, Xinjiang. Bur Geol Miner Resour (in Chinese, unpublished)
Wan B, Zhang LC, Xiao WJ (2010) Geological and geochemical characteristics and ore genesis of the Keketale VMS Pb-Zn deposit, southern Altai metallogenic belt, NW China. Ore Geol Rev 37:114–126
Wang DH (1999) Geological setting and features of the Ashele Cu-Zn deposit, Xinjiang, China. Explor Min Geol 8:197–210
Wang DH (2003) Geology, geochemistry and geodynamics of the Ashele VHMS Cu-Zn deposit, northwestern Xinjiang. In: Mao JW, Goldfarb RJ, Seltmann R, Wang DH, Xiao WJ, Hart C (eds) Tectonic evolution and metallogeny of the Chinese Altay and Tianshan. International Association on the Genesis of Ore Deposits, Centre for Russian and Central Asian Mineral Studies, Natural History Museum, London, pp 153–168
Wang CS, Hu KD (eds) (2004) Geological map of the Qinghai-Xizang (Tibet) and adjacent areas. Chengdu Institute of Geology and Mineral Resources, Chengdu Publishing House, Chengdu
Wang YB, Zhao DJ (2006) Gold deposits in Xinjiang, China. Geological Publishing House, Beijing, pp 11–36 (in Chinese with English abstract)
Wang DH, Chen YC, Mao JW (1998) The Ashele deposit: a recently discovered volcanogenic massive sulfide Cu-Zn deposit in Xinjiang, China. Resour Geol 48:31–42
Wang JB, Deng JI, Zhang JH, Qin KZ (1999) Massive sulphide deposits related to the volcano-passive continental margin in the Altay Region. Acta Geol Sin 73:253–263
Wang ZL, Mao JW, Wu GG, Yang JM, Ma TL, Han CM (2003a) Geochemistry of fluid inclusions from the Shiyingtan gold deposit in eastern Tianshan, Xinjiang. Geol Prospect 39:6–10 (in Chinese with English abstract)

Wang YW, Wang JB, Wang SL, Ding RF, Wang LJ (2003b) Geology of the Mengku iron deposit, Xinjiang, China—a metamorphosed VMS? In: Mao JW, Godlfarb RJ, Seltmann R, Wang DH, Xiao WJ, Hart C (eds) Tectonic evolution and metallogeny of the Chinese Altay and Tianshan. International Association on the Genesis of Ore Deposits, Centre for Russian and Central Asian Mineral Studies, Natural History Museum, London, pp 181–200

Wang JB, Wang YW, Wang SL, Rufu D (2003c) The Koktal Pb-Zn massive sulfide deposit. In: Mao JW, Godlfarb RJ, Seltmann R, Wang DH, Xiao WJ, Hart C (eds) Tectonic evolution and metallogeny of the Chinese Altay and Tianshan. International Association on the Genesis of Ore Deposits, Centre for Russian and Central Asian Mineral Studies, Natural History Museum, London, pp 169–180

Wang DH, Xu ZG, Zou TR, Chen YC, Wang LS (2003d) Major types and regional metallogeny of rare metal deposits in the Altay mountains, Xinjiang. In: Mao J-W, Godlfarb RJ, Seltmann R, Wang DH, Xiao WJ, Hart C (eds) Tectonic evolution and metallogeny of the Chinese Altay and Tianshan. International Association on the Genesis of Ore Deposits, Centre for Russian and Central Asian Mineral Studies, Natural History Museum, London, pp 117–130

Wang ZL, Mao JW, Zhang ZH, Zuo GC, Wang LS (2004a) Types, characteristics and metallogenic geodynamic evolution of the Paleozoic polymetallic copper-gold deposits in the West Tianshan Mountains. Acta Geol Sin 78:836–847 (in Chinese with English abstract)

Wang YW, Wang JB, Wang LJ, Wang Y, Tu CN (2004b) REE characteristics of the Kalatongke Cu-Ni deposit, Xinjiang, China. Acta Geol Sin 78:396–403

Wang DH, Mao JW, Yan SH, Yang JM, Xu J, Chen YC, Xue CJ (2005a) Episodes of Cenozoic gold mineralisation on the eastern margin of the Qingai-Tibet plateau: $^{40}Ar/^{39}Ar$ dating and implication for geodynamic events. Acta Geol Sin 79:233–253

Wang DH, Qu WJ, Li ZW, Yin HL, Chen YC (2005b) Mineralization episode of porphyry copper deposits in the Jinshajiang-Red River mineralization belt: Re-Os dating. Sci China Ser D 48:192–198

Wang LJ, Wang JB, Wang YW, Zhu HP, Qu LL (2005c) The study of ore-fluid and C-S-Pb isopope of S-rich and S-poor types epithermal gold deposits, Junggar area, Xinjiang. Acta Pet Sin 21:1382–1388 (in Chinese with English abstract)

Wang T, Hong DW, Jahn BM, Tong Y, Wang YB, Han BF, Wang XX (2006a) Timing, petrogenesis and setting of Paleaozoic synorogenic intrusions from the Altai mountains, northwest China: implications for the tectonic evolution of an accretionary orogen. J Geol 114:735–751

Wang YW, Wang JB, Wang LJ, Peng XM, Hui WD, Qin QX (2006b) An intermediate type of Cu-Ni Sulfide and V-Ti magnetite deposit: Xiangshanxi deposit, Hami, Xinjiang, China. Acta Geol Sin 80(1):61–73

Wang B, Shu LS, Cluzel D, Faure M, Charvet J (2007a) Geochemical constraints on Carboniferous volcanic rocks of the Yili Block (Xinjiang, NW China): implication for the tectonic evolution of Western Tianshan. J Asian Earth Sci 29:148–159

Wang T, Tong Y, Jahn BM, Zou TR, Wang YB, Hong DW, Han BF (2007b) SHRIMP U-Pb zircon geochronology of the Altai No. 3 pegmatite, NW China, and its implications for the origin and tectonic setting of the pegmatite. Ore Geol Rev 32:325–336

Wang B, Faure M, Shu LS, Cluzel D, Charvet J, de Jong K, Chen Y (2008a) Paleozoic tectonic evolution of the Yili Block, western Chinese Tianshan. Bull Soc Geol Franc 179:483–490

Wang Q, Wyman DA, Zhu YT, Zhao ZH (2008b) Late Triassic rhyolites and high-Mg andesites in the northern Hohxil area, Songpan-Ganzi terrane Goldschmidt Conference Abs, p A999

Wang QC, Shu LS, Charvet J, Faure M, Ma HD, Natal'in B, Gao J, Kroner A, Xiao WJ, Li JY, Windley B, Chen Y, Glen R, Jian P, Zhang W, Seltmann R, Wilde S, Chouler F, Wan B, Quinn C, Rojas-Agramonte Y, Shang QH, Zhang W, Wang B, Lin W (2010) Understandign and study perspectives on tectonic evolution and crustal structure of the Paleozoic Chinese Tianshan. Episodes 33:242–265

Wang B, Shu LS, Faure M, Jahn BM, Clazel D, Charvet J, Chung SL, Meffre S (2011) Paleozoic tectonics of the southern Chinese Tianshan: insights from structural, chronological and geochemical studies of the Heiyingshan ophiolitic melange (NW China). Tectonophysics 497:85–104

Wang B, Jahn BM, Shu L, Li K, Chung SL, Liu D (2012) Middle-Late Ordovician arc-type plutonism in the NW Chinese Tianshan: implications for the accretion of the Kazakhstan continent in Central Asia. J Asian Earth Sci 49:40–53

Warren JK (2000) Evaporites, brines and base metals: low-temperature ore emplacement controlled by evaporite diagenesis. Aust J Earth Sci 47:179–208

Watkinson DH, Wyllie PJ (1971) Experimental study of the join $NaAlSiO_4$-$CaCO_3$-H_2O and the genesis of alkali rock-carbonatite complexes. J Pet 12:357–378

Williams H, Turner S, Kelley S, Harris N (2001) Age and composition of dikes in Southern Tibet: New constraints on the timing of east-west extension and its relationship to postcollisional volcanism. Geology 29:339–342

Windley BF (1995) The evolving continents, 3rd edn. Wiley, Chichester, p 526

Windley BF, Allen MB, Zhang C, Zhao Z, Wang C (1990) Paleozoic accretion and Cenozoic redeformation of the Chinese Tian Shan range, Central Asia. Geology 18:128–131

Windley BF, Kröner A, Guo JH, Qu GS, Li YY, Zhang C (2002) Neoproterozoic to palaeozoic geology of the Altai orogen, NW China: new zircon age data and tectonic evolution. J Geol 110:719–737

Windley BF, Alexeiev D, Xiao WJ, Kröner A, Badarch G (2007) Tectonic models for accretion of the Central Asian Orogenic Belt. J Geol Soc Lond 64:31–47

Woolley AR (2003) Igneous silicate rocks associated with carbonatites: their diversity, relative abundances and implications for carbonatite genesis. Period Miner 72:9–17

Woolley AR, Kempe DRC (1989) Carbonatites: nomenclature, average chemical compositions, and element distribution. In: Bell K (ed) 1989, Carbonatites, genesis and evolution. Unwin Hyman, Boston, pp 1–14

Wu LQ, Jiao YQ, Roger M, Yang SK (2009) Sedimentological setting of sandstone-type uranium deposits in coal measures on the southwestern margin of the Turpan-Hami Basin, China. J Asian Earth Sci 36:223–237

Xi XP (1999) Geological features and genetic study of Shuangfengshan gold deposit. Miner Resour Geol 13:28–33 (in Chinese with English abstract)

Xia LQ, Xu XY, Xia ZC, Li XM, Ma ZP, Wang LS (2003) Carboniferous Post-collisional Rift Volcanism of the Tianshan Mountains, Northwestern China. Acta Geol Sin 77:338–360

Xia LQ, Xu XY, Xia ZC, Li XM, Ma ZP, Wang LS (2004) Petrogenesis of Carboniferous rift-related volcanic rocks in the Tianshan, northwestern China. Geol Soc Am Bull 116:419–433

Xiao WJ, Kusky T (eds) (2009) Geodynamic processes and metallogenesis of the Central Asia and related orogenic belts. Gondwana Res 16:167–169

Xiao L, Wang FZ, Begg G, Fu ML (2002a) Gold mineralization styles of Jingxi-Yelmend deposit, Xinjiang: evidence from hydrothermal alteration and fluid inclusion data. Miner Depos 21:58–64 (in Chinese with English abstract)

Xiao L, Wang FZ, Zhang GL, Fu ML, Begg G, Hayward N (2002b) Identifying criteria and implications of high-sulphidation epithermal Jinxi-Yelmend gold deposit in western Tianshan, Xinjiang. Geol Sci Technol Inf 21:74–78 (in Chinese with English abstract)

Xiao WJ, Windley BF, Chen HL, Zhang GC, Li JL (2002c) Carboniferous-Triassic subduction and accretion in the western Kunlun, China: implications for the collisional and accretionary tectonics of the northern Tibetan Plateau. Geology 30:295–298

Xiao WJ, Windley BF, Hao J, Li JL (2002d) Arc-ophiolite obduction in the Western Kunlun Range (China): implications for the Palaeozoic evolution of Central Asia. J Geol Soc Lond 159:517–528

Xiao WJ, Windley BF, Hao J, Zhai MG (2003) Accretion leading to collision and the Permian Solonker suture, Inner Mongolia, China: termination of the central Asian orogenic belt. Tectonics 22:8–20, 1069

Xiao WJ, Windley BF, Badarch G, Sun S, Li J, Qin K, Wang Z (2004a) Palaeozoic accretionary and convergent tectonics of the southern Altaids: implications for the growth of Central Asia. J Geol Soc Lond 161:339–342

Xiao WJ, Zhang LC, Qin KZ, Sun S, Li JL (2004b) Paleozoic accretionary and collisional tectonic of the eastern Tianshan (China): implications for the continental growth of central Asia. Am J Sci 304:370–395

Xiao L, Hayward N, Begg G, Fu ML, Wang FZ, Pirajno F (2005a) The Jinxi-Yelmand high-sulfidation epithermal deposit, Western Tianshan, Xinjiang Province, P. R. China. Ore Geol Rev 26:17–37

Xiao WJ, Windley BF, Liu DY, Jian P, Liu CZ, Yuan C, Sun M (2005b) Accretionary tectonics of the Western Kunlun orogen, China: a Paleozoic-Early Mesozoic, long-lived active continental margin with implications for the growth of southern Eurasia. J Geol 113:687–705

Xiao WJ, Pirajno F, Windley BF, Han CM (2006) Paleozoic-early Mesozoic accretionary tectonics and metallogeny of the northern Tibetan Plateau Extended Abs, IAGOD meeting, Moscow

Xiao L, Wang X, Pirajno F (2007) Is the Underthrust Indian Lithosphere Split beneath the Tibetan Plateau? Int Geol Rev 49:90–98

Xiao WJ, Pirajno F, Seltmann R (2008a) Geodynamics and metallogeny of the Altaid orogen; Editorial. Asian J Earth Sci 32:77–81

Xiao WJ, Han CM, Yuan C, Sun M, Lin SF, Chen H, Li ZL, Li JL, Sun S (2008b) Middle Cambrian to Permian subduction-related accretionary orogenesis of Northern Xinjiang, NW China: implications for the tectonic evolution of Central Asia. J Asian Earth Sci 32:102–117

Xiao L, He Q, Pirajno F, Ni PZ, Du JX, Wei QR (2008c) Possible correlation between a mantle plume and the evolution of Paleo-Tethys Jinshajiang Ocean: evidence from a volcanic rifted margin in the Xiaru-Tuoding area, Yunnan, SW China. Lithos 100:112–126

Xiao WJ, Kröner A, Windley B (2009) Geodynamic evolution of Central Asia in the Paleozoc and Mesozoic. Int J Earth Sci Geol Rundsch 98:1185–1188

Xiao WJ, Mao QG, Windley B, Han CM, Qu JF, Zhang JE, Ao SJ, Guo QQ, Cleven NR, Lin SF, Shan YH, Li JL (2010) Paleozoic multiple accretionary and collisional processes of the Beishan orogenic collage. Am J Sci 310:1553–1594

Xiao Y, Zhang HF, Shi JA, Su BX, Sakyi PA, LU XC, Hu Y, Zhang Z (2011) Late Paleozoic magmatic record of East Junggar, NW China and its significance: implications from zircon U-Pb dating and Hf isotope. Gondwana Res 20:532–542

Xie CH, Zeng XJ (2001) The types and geological characters of gold deposits in Yishijilike ore belt, Xinjiang. Miner Res Geol 15(Suppl):464–468 (in Chinese with English abstract)

Xie YL, Hou ZQ, Xu WY, Yuan ZX, Bai G, Li XY (2006) Discovery of Cu-Zn, Cu-Sn intermetallic minerals and its significance for genesis of the Mianning-Dechang REE metallogenic belt, Sichuan Province, China. Sci China Ser D 49:597–603

Xie YL, Hou ZQ, Yin SP, Dominy SC, Xu JH, Tian SH, Xu WY (2009) Continuous carbonatitic melt-flid evolution of a REE mineralization system: evidence from inclusions in the Maoniuping REE deposit, western Sichuan, China. Ore Geol Rev 36:90–105

Xu GD (1998) Geology and geochemistry of Xiaoyuzan epithermal gold deposit in Yeliemodun area, Xinjiang. Miner Res Geol 12:14–19 (in Chinese with English abstract)

Xu C, Huang ZL, Liu CQ, Qi L, Li WB, Guan T (2003) Geochemistry of carbonatites in Maoniuping REE deposit, Sichuan Province, China. Sci China Ser D 46:246–256

Xu YX, Ding KS, Qin KZ, Miao Y, Fang TH, Xu XW, Sun H (2006) Krausite, rhomboclase and parabutlerite found for the first time in the Hongshan high-S epithermal Cu-Au deposit, Xinjiang, and their significance. Geol China 33:598–605 (in Chinese with English abstract)

Xu LG, Mao JW, Yang FQ, Hennig D, Zheng JM (2010) Geology, geochemistry and age constraints on the Mengku skarn iron deposit in Xinjiang Altai, NW China. J Asian Earth Sci 39:423–440

Xue CJ, Zeng R, Liu SW, Chi GX, Qing HR, Chen YC, Yang JM, Wang DH (2007) Geologic, fluid inclusion and isotopic characteristics of the Jinding Zn-Pb deposit, western Yunnan, South China: a review. Ore Geol Rev 31:337–359

Yakubchuk A (2004) Architecture and mineral deposit settings of the Altaid orogenic collage: a revised model. J Asian Earth Sci 23:761–779

Yakubchuk AS (2009) Revised Mesozoic-Cenozoic orogenic architecture and gold metallogeny in the northern Circum-Pacific. Ore Geol Rev 35:447–454

Yakubchuk AS, Shatov VV, Kirwin D, Edwards A, Tomurtogoo O, Badarch G, Buryak VA (2005) Gold and base metal metallogeny of the Central Asian Orogenic Supercollage. Econ Geol 100th Anniv Vol:1035–1068

Yan SH, Zhang ZC, Wang DH, Chen BL, He LX, Zhou G (2003) Kalatongke magmatic copper-nickel sulphide deposit. In: Mao JW, Goldfarb R, Seltmann R, Wang DH, Xiao WJ, Hart C (eds) Tectonic evolution and metallogeny of the Chinese Altay and Tianshan. Centre for Russian and Central Asian Mineral Studies (CERCAMS), London, pp 131–151

Yang KH (1998) A plate reconstruction of the eastern Tethyan orogeny in southwestern China. American Geophysical Union, Geodynamic Ser 27, Washington, DC, pp 269–287

Yang YQ, Liu M (2002) Cenozoic deformation of the Tarim plate and the implications for mountain building in the Tibetan Plateau and the Tian Shan. Tectonics 21:1–17

Yang FQ, Wu H, Zhang YR (1999) Geological characteristics and genesis of the Jinshangou gold deposit, Xinjiang. J Precious Met Geol 8:76–80 (in Chinese with English abstract)

Yang ZX, William-Jones AE, Pu GP (2000) Geological features of Maoniuping REE deposit, Sichuanm China. J Miner Petrol 20:28–34 (in Chinese with English abstract)

Yang ZX, William-Jones AE, Pu GP (2001) A fluid inclusion study of Maoniuping REE deposit, Sichuan, China. J Miner Petrol 21:26–33 (in Chinese with English abstract)

Yang FQ, Mao JW, Bierlein FP, Pirajno F, Zhao CS, Ye HH, Liu F (2009) A review of the geological characteristics and geodynamic mechanisms of Late Paleozoic epithermal gold deposits in North Xinjiang, China. Ore Geol Rev 35:217–234

Yang FQ, Mao JW, Liu F, Chai FM, Guo Z, Geng X, Gao J (2010) Geochronology and geochemistry of the granites from the Mengku iron deposit, Altay Mountains, northwest China: implications for its tectonic setting and metallogenesis. Aust J Earth Sci 57:803–818

Yang TN, Li J, Zhang J, Hou K (2011) The Altai-Mongolia terrane in the Central Asian Orogenic Belt (CAOB): a peri-Gondwana one? evidence from zirocn U-Pb isotopes and REE abundances. Precambrian Res 187:79–98

Yang FQ, Mao JW, Pirajno F, Yan SH, Liu GR, Zhou G, Zhang ZX, Liu F, Geng XX, Guo CL (2012a) A review of the geological characteristics and geodynamic setting of Late Paleozoic porphyry copper deposits in the Junggar region, Xinjiang Uygur Autonomous Region, Northwest China. J Asian Earth Sci 49:69–79

Yang WB, Niu HC, Shan Q, Luo Y, Sun WD, Li CY, Li NB, Yu XY (2012b) Late Paleozoic calc-alkaline to shoshonitic magmatism and its geodynamic implications, Yuximolegai area, western Tianshan, Xinjiang. Godwana Res 49:80–98

Yang SH, Zhou MF, Lightfoot PC, MalpasJ, Qu WJ, Zhou JB, Kong DY (2012c) Seelective crustal contamination and decoupling of lithophile and chalcophile element isotopes in sulfide-bearing mafic intrusions: an example from the Jingbulake intrusion, Xinjiang, NW China. Chem Geol 302–303:106–118

Yin A (2000) Mode of Cenozoic east-west extension in Tibet suggesting a common origin of rifts in Asia during the Indo-Asian collision. J Geophys Res 105:21745–21759

Yin A (2010) Cenozoic tectonic evolution of Asia: a preliminary synthesis. Tectonophysics 488:293–325

Yin A, Harrison M (ed) (1996) The tectonic evolution of Asia. Cambridge University Press, Cambridge, p 666

Yin A, Harrison M (2000) Geologic evolution of the Himalayan-Tibetan Orogen. Annu Rev Earth Planet Sci 28:211–280

Yin YQ, Chen DJ, An YC, Li JX, Fan Y, You ZF, Yang JR (1996) Characteristics of the Kuo-erzhenkuola epithermal gold deposit in Sawuershan, Xinjiang. Geol Explor Non Ferr Met 5:278–283 (in Chinese with English abstract)

Ying LJ, Wang DH, Liang T, Zhou RH, Ma J, Qu WJ, Chen ZY (2006) Chemical composition and typomorphic characteristics of magnetite and its geological significance in Qiaoxiahala iron-copper-gold deposit of Latai, Xinjiang. Acta Miner Sin 26:59–68

Yuan ZX, Shi ZM, Bai G, Wu CY, Chi RA, Li XY (1995) The Maoniuping Rare Earth Ore Deposit. Seismological Press, Beijing, p 150 (in Chinese)

Zeng QD, Liu JM, Liu TB, Shen YC, Shen P, Li GM (2007) Geology and Geochemistry of the Buerkesidai and Kuoerzhenkuola Gold Deposits in the Sawuershan Region, Xinjiang Uigur Autonomous Region, Northwest China. Resour Geol 57:313–324

Zhai W, Sun XM, Sun WD, Su LW, He XP, Wu YL (2009) Geology, geochemistry and genesis of Axi: a Paleozoic low-sulfidation type epithermal gold deposit in Xinjiang, China. Ore Geol Rev 36:265–281

Zhang SX (ed) (2009) Geological formation names of China (1866–2000). Springer, Dordrecht, p 1537

Zhang ZH, Liou JG, Coleman RG (1984) An outline of the plate tectonics of China. Geol Soc Am Bull 95:295–312

Zhang JZ, Feng BH, Jin HJ, Liu B, Luo YP, Jin ZM, Zhu MZ, Chen SZ (1987) The genetic relationship between marine volcanic rocks and iron deposits at Abagong-Mengku area, Altay district, Xinjiang and ore-forming geological features. Bull Xi'an Inst Geol Miner Resour, Chin Acad Geol Sci 20:89–180 (in Chinese)

Zhang LC, Liu DG, Tang YL (1990) Mineral resources in Xinjiang. Hong Kong Educational and Cultural Press ltd, Hong Kong, p 328 (in Chinese)

Zhang YR, Zhu MY, Ming KH, Liu XQ, Shen XY, Ma WY (1992) Geology, and gold and tin deposits of East Junggar. Seismological Press, Beijing, p 266 (in Chinese with English abstract)

Zhang ZH, Mao JW, Du AD, Pirajno F, Yang JM, Wang ZL, Chai FM, Zhang ZC (2008) Re-Os dating of the two largest Cu-Ni sulfide deposits in northern Xinjiang, and its geological significance. Asian J Earth Sci 32:204–217

Zhang ZC, Mao JW, Chai FM, Yan SG, Chen BL, Pirajno F (2009) Geochemistry of the Permian Kalatongke mafic intrusions, northern Xinjiang, northwest China: implications for the genesis of magmatic Ni-Cu sulfide deposits. Econ Geol 104:185–203

Zhang MJ, Li C, Fu P, Hu PQ, Ripley EM (2010a) The Permian Huangshanxi Cu-Ni deposit in western China: intrusive-extrusive association, ore genesis and exploration implications. Miner Depos 46:153–170

Zhang ZH, Mao JW, Wang ZL, Pirajno F, Wang YB (2010b) Geochemical and SHRIMP U-Pb age constraints on the origin of the Qingbulake mafic-ultramafic complex in the West Tianshan Mountains. Aust J Earth Sci 57:819–837

Zhang DY, Zhang ZC, Xue CJ, Zhao ZD, Liu JL (2010c) Geochronology and geochemistry of the ore-forming porphyries in the Lailisigao'er-Lamasu region of the Western Tianshan Mountains, Xinjiang, NW China: implications for petrogenesis, metallogenesis, and tectonic setting. J Geol 118:543–563

Zhang Q, Sandvol E, Ni J, Yang YJ, Chen YSJ (2011) Rayleigh wave tomography of the northeastern margin of the Tibetan Plateau. Earth Planet Sci Lett 304:103–112

Zhang L, Zheng Y, Chen YJ (2012) Ore geology and fluid inclusion geochemistry of the Tiemurt Pb-Zn-Cu deposit, Altay, Xinjiang, China: a case study of orogenic-type Pb-Zn systems. J Asian Earth Sci 49:69–79

Zhao Z (1992) Paleozoic tectonic evolution of West Junggar region, Xingjiang, China. Mem Lithospheric. Tecton Evol Res 1:128–133

Zhao W, Nelson KD, Project INDEPTH Team (1993) Deep seismic reflection evidence for continental underthrusting beneath southern Tibet. Nature 366:557–559

Zhao YY, Nie FJ, Hou ZK, Li ZQ, Zhao XW, Ma ZB (2006a) Geological characteristics and age of the Targeja hot spring Cs deposit in Tibet. Miner Depos 25:281–291 (in Chinese with English abstract)

Zhao YY, Nie FJ, Hou ZK, Li ZQ, Zhao XW, Ma ZB (2006b) Isotopic characteristics and formation process of hot-spring type cesium deposit in Targeja, Tibet. Miner Depos 25:613–619 (in Chinese with English abstract)

Zhao ZH, Bai ZH, Xiong XL (2006c) The alkali-rich igneous rocks and related mineralization in North Xinjiang, China. Geological Publishing House, Beijing, p 302 (in Chinese with English abstract)

Zhao ZH, Guo ZJ, Han BF, Wang Y (2006d) The geochemical characteristics and tectono-magmatic implications of the latest Palaeozoic volcanic rocks from the Santagu basin, eastern Xinjiang, northwest China. Acta Pet Sin 22:199–214

Zhao TF, Feng Y, Yu F, Zhang D, Cooke D, Zhao GC (2008a) Granites in the Sauwer region of the west Junggar province, China: geochronological and geochemical characteristics and geodynamic significance. Lithos 115:177–189

Zhao TP, Zhou MF, Zhao JH, Zhang KJ, Chen W (2008b) Geochronology and geochemistry of the c. 80 Ma Rutog granitic pluton, northwestern Tibet: implications for the tectonic evolution of the Lhasa terrane. Geol Mag 145:845–857

Zhao WJ, Kumar P, Mechie J, Kind R, Meissner R, Wu ZH, Shi D, Su HP, Xue GQ, Karplus M, Tilmann F (2011) Tibetan plate overriding the Asian plate in central and northern Tibet. Nat Geosci 4:870–873

Zhou Z, Dean WT (ed) (1996) Phanerozoic geology of NW China. Science Press, Beijing, p 307

Zhou D, Graham SA (1996) The Songpan-Ganzi complex of the West Qingling Shan as a Triassic remnant ocean basin. In: Yin A, Harrison TM (eds) The tectonic evolution of Asia. Cambridge University Press, Cambridge, pp 281–299

Zhou HW, Murphy MA (2005) Tomographic evidence for wholesale underthrusting of India beneath the entire Tibetan plateau. J Asian Earth Sci 25:445–457

Zhou TF, Yuan F, Yue SC, Yuan XY (2000) Magmatism and Mineralization in Nurte area, Xinjiang. Geological Publishing House, Beijing, p 127 (in Chinese)

Zhou D, Graham SA, Chang EZ, Wang BY, Hacker B (2001) Paleozoic tectonic amalgamation of the Chinese Tian Shan: evidence from a transect along the Dushanzi-Kuqa Highway. Geol Soc Am Mem 194:23–46

Zhou MF, Lesher CM, Yang ZX, Li JW, Sun M (2004) Geochemistry and petrogenesis of 270 Ma Ni-Cu-(PGE) sulphide-bearing mafic intrusions in the Huangshan district, eastern Xinjiang, northwest China: implications for the tectonic evolution of the Central Asian orogenic belt. Chem Geol 209:233–257

Zhou TF, Yuan F, Fan Y, Zhang DY, Cooke D (2008) Granites in the Sawuer region of the west Junggar, Xinjiang Province, China: geochronological and geochemical characteristics and their geodynamic significance. Lithos 106:191–206

Zhu Y, Zhang L, Gu L, Guo X, Zhou J (2005) The zircon SHRIMP chronology and trace element geochemistry of the Carboniferous volcanic rocks in western Tianshan Mountains. Chinese Sci Bull 50(19):2201–2212

Zhu YF, Zeng YS, Gu LB (2006) Geochemistry of the rare metal-bearing pegmatite No. 3 vein and related granites in the Keketuohai region, Altay Mountains, northwest China. J Asian Earth Sci 27:61–77

Zhu YF, Zhou J, Zeng YS (2007) The Tianger (Bingdaban) shear zone hosted gold deposit, west Tianshan, NW China: petrographic and geochemical characteristics. Ore Geol Rev 32:337–365

Zhu YF, Xuan G, Song B, Zhang LF, Gu LB (2009) Petrology, Sr–Nd–Hf isotopic geochemistry and zircon chronology of the Late Palaeozoic volcanic rocks in the southwestern Tianshan Mountains, Xinjiang, NW China. J Geol Soc Lond 166:1085–1099

Zhu WB, Zheng BH, Shu LS, Ma DS, Wan JL, Zheng DW, Zhang ZY, Zhu XQ (2010) Geochemistry and SHRIMP U-Pb zircon geochronology of the Korla mafic dykes: constrains on the Neoproterozoic continental breakup in the Tarim Block, southwest China. J Asian Earth Sci 42(5):791–804

Zhu DC, Zhao ZD, Niu YL, Dilek Y, Mo XX (2011) Lhasa terrane in southern Tibet came from Australia. Geology 39:727–730

Zhu DC, Zhao ZD, Niu YL, Dilek Y, Hou ZQ, Mo XX (2012) The origin and pre-Cenozoic evolution of the Tibetan Plateau. Gondwana Res. doi:10.1016/j.gr.2012.02.002

Zoneshain LP, Kuzmin MI, Natapov LM (1990) Geology of the USSR: a plate tectonic synthesis. In: Page BM (ed) Geology of the USSR: a plate tectonic synthesis. American Geophysical Union, Washington, DC, pp 27–54

Chapter 7
Large Igneous Provinces (Xiong'er, Dashigou, 827 Ma Event, Tarim, Emeishan) and the Yanshanian Tectono-thermal Event of Eastern China

Abstract In this chapter the Large Igneous Provinces (LIPs) of China and the widespread Yanshanian (Mesozoic) tectono-thermal event are reviewed. Confirmed LIPs of China cover a long span of geological history, beginning in the Palaeoproteozoic with the 1.78 Ga Xiong'er volcanic province, the recently discovered 925 Ma Dashigou dyke swarm emplaced in the North China Craton; the 850–825 Guibei large igneous province in South China; the 291–272 Ma Tarim LIP; and the 260 Ma Emeishan LIP in southwest China.

The 1.78 Ga Xiong'er LIP consists of volcanic rocks at the southern edge of the North China Craton, A-type granites and a number of coeval dyke swarms within the northerly trending Trans North China Orogen. The volcanic rocks comprise a suite of basaltic andesite, andesite, trachyandesite, dacite, rhyodacite and rhyolite, with continental sedimentary intercalations and pyroclastic units. The Xiong'er LIP is interpreted to have been deposited in a three-arm rift system with its three branches trending approximately west-southwest, southeast and a northeast branch within the Trans North China Orogen. The Xiong'er LIP is approximately coeval with other LIPs, such as the Uruguayan, Espinhaço in Brazil, Dubois-Cochetopa in Colorado, and the Hart-Carson event in the Kimberley Basin of Western Australia. No mineralisation of significance that can be related to the Xiong'er LIP has yet been discovered, but clearly the door remains open for new discoveries, which may include magmatic Ni-Cu sulphides in mafic-ultramafic rocks and perhaps IOCG mineral systems associated with A-type granites.

The Dashigou dyke swarm in the North China Craton, with ages ranging from ca. 926 to 920 Ma, was recently discovered by researchers of the Chinese Academy of Sciences, using systematic dating of baddeleyite grains in mafic intrusions. The interpretation that the Dashigou dykes are part of a possible radiating swarm with a central focus on the southeastern margin of the North China Craton is of considerable importance in terms of mineral targeting, because focal points of a mantle plume head may be associated with layered intrusions and related magmatic ore deposits.

A mantle plume or superplume event(s), was one of the main causes for the breakup of the Rodinia supercontinent. In China, this thermal event is represented by the 850–825 Ma dykes and sills that constitute the Guibei LIP in South China. The large ca. 825 Ma Jinchuan intrusion. The latter hosts the giant Ni-Cu-PGE deposit in Gansu Province on the southwest margin of the North China Craton is part of the same thermal event. It is of considerable interest to note that within the Rodinia

F. Pirajno, *The Geology and Tectonic Settings of China's Mineral Deposits,*
DOI 10.1007/978-94-007-4444-8_7, © Springer Science+Business Media Dordrecht 2013

context the age of this LIP (and the Jinchuan intrusion) corresponds to that of the Gairdner dyke swarm in Australia. The Jinchuan Ni-Cu-PGE deposit is the third largest deposit in the world after Noril'sk and Sudbury. The sulphide mineralisation is hosted in the Jinchuan mafic-ultramafic a northwest-trending dyke-like intrusion that resembles the Great Dyke of Zimbabwe.

The 291–272 Ma Tarim thermal event remains controversial as to whether it can be considered as a LIP or the result of asthenopsheric upwellings due to post-collision delamination of the lithosphere. The Tarim LIP, which mostly occur under the cover of Tarim platform, is largely represented by Early Permian alkaline and tholeiite basalts, dolerite, gabbro, syenite, ultramafic rocks and perhaps kimberlites. As pointed out in this chapter the Tarim LIP has enormous economic potential. Orthomagmatic Ni-Cu deposits that can be confidently assigned to this event include the world-class Kalatongke deposit in the Altay, the Huangshan-Huangshanxi-Jing'erquan ore belt in the eastern Tianshan (both described in Chap. 6), the Beishiquan and Pobei deposits in the Tianshan orogen. The clustering of several zoned mafic-ultramafic intrusions in the east Tianshan suggests that this region must have been a focus for the uprising of mantle material. These zoned mafic-ultramafic intrusions have some features that are comparable with Alaskan-type complexes. Taking into consideration the spatial-temporal relationship of these mafic, mafic-ultramafic complexes with coeval A-type granites, these magmatic events must have occurred during an extensional regime, possibly related to a mantle superplume that affected much of central Asia in the Permian.

The 260 Ma Emeishan LIP, one of the best studied large igneous provinces of the planet, covers areas of southwest China and northwest Vietnam. The western boundary of the ELIP is the Ailao Shan-Red River Fault zone, a major crustal structure separating the Yangtze Craton from the Gandese and Yunnan fold belts. The near contemporaneity of the Emeishan, Siberian and Tarim LIPs led some authors to suggest a possible Ni-Cu-PGE enriched superplume activity or a flare-up of mantle plume (superplume) activity in the age brackets of 250–280 Ma. The Emeishan LIP is well endowed with magmatic ore deposits such as the Ni-Cu-PGE sulphides at Baimazhai, Niulanchong, Yangliuping and Limahe, PGE-dominated Lufangqing, Bading, Dayanzi and Jimbaoshan the Hongge Fe-V-Ti oxide ores and the Fe-V-Ti-(PGE) ores of Panzihua and REE mineralisation in carbonatites, both in the Panxi district.

The Yanshanian (Mesozoic-Cenozoic) tectono-thermal events affected large areas of eastern margin of mainland Asia, extending from Far East Russia, through the Baikal and Mongolia regions, to north-eastern and eastern China. Yanshanian rifting, basin formation and magmatism played an all important role for the development of mineral systems, as separately discussed in the chapters of this book. These rifts, basins and mineral systems are superimposed on Archaean, Proterozoic and Palaeozoic terranes, occasionally resulting in uncertainty in some areas, unless well-constrained age data are available. This chapter focuses on the Yanshanian volcanic province of the Great Hinggan Range, which although does not qualify as a conventional LIP (scattered alkali basalt-dominated volcanism), is considered

as a giant igneous event. The Great Hinggan Range magmatism is mainly associated with porphyry, skarn and epithermal systems, described in the preceding chapters.

7.1 Introduction

In the last couple of decades intraplate and anorogenic thermal events and their relationship to mantle dynamics have somewhat polarised the geoscience community. The mantle plume paradigm, since its first introduction by J. Tuzo Wilson (1963), subsequently elaborated by Morgan (1971, 1972) for oceanic islands and extended to continents by Burke and Dewey (1973), has been "hotly" debated, leading to a large number of publications, as papers, special issues in international journals and books. The details of the mantle plume theory and alternative hypotheses are beyond the scope of this book, and the interested reader is referred to the following selection of publications and references therein: Condie (2001), Schubert et al. (2001), Ernst and Buchan (2001, 2003), Ernst et al. (2005), Foulger and Jurdy (2007), Yuen et al. (2007), Sheth (2007), Ritter and Christensen (2007), Bryan and Ernst (2008), Foulger (2010) and the interesting discussion by Cañón-Tapia (2010). However, it should be pointed out that the presence of conduits of hot mantle, arising from the core-mantle boundary (CMB), at or from below the 660-km discontinuity (upper-lower mantle boundary) ending up at the surface of our planet with volcanoes and volcanic provinces, or hot spots, is effectively supported by an increasing number of field, geochemical and isotopic data as well as improving resolutions of seismic tomography (e.g. Zhao 2009). Key works on seismic tomography, which provide excellent confirmation for the existence of corridors of hotter mantle (negative seismic velocities), include Montelli et al. (2004, 2006) and Zhao (2009). Furthermore, exciting new insights with supporting data on the nature of the inner (solid) and outer (liquid) core are coming to light (e.g. van der Hilst et al. 2007; Waszek et al. 2011; Gubbins et al. 2011), all of which support the hypothesis of mantle plumes originating by thermal instability at the CMB.

The mantle plume paradigm postulates that they are narrow upwelling currents or narrow cylindrical conduits of hot, low-density material originating either from the core-mantle boundary and rising through the lower and upper mantle, or from the 670 km discontinuity at the base of the upper mantle (e.g. Campbell and Griffiths 1990, 1992). En route, these upwelling currents may entrain pieces of upper mantle and/or metasomatised lithospheric and subducted slab material. Mantle plumes eventually impinge on either continental or oceanic lithospheric plates, resulting in the eruption of great volumes of mafic melts. These eruptions form vast fields of lava flows and associated igneous complexes, cover extensive areas (see below), or form lines of oceanic islands, such as the Emperor-Hawaian chain, thousands of kilometres long. In the ocean these vast lava fields are known as oceanic plateaux,

such as the Ontong Java and Kerguelen plateaux. Plumes may also intersect a mid-ocean ridge forming large islands such as Iceland. Where mantle plumes impinge onto subcontinental lithosphere, rifting may occur and may be accompanied by the eruption of continental flood basalts (CFB), such as the Karoo, Siberian Traps or the Deccan Traps. These enormous fields of lava flows and associated intrusions are popularly known in the geological community as Large Igneous Provinces, or by the acronym LIP (Coffin and Eldhom 1993).

Definitions of what is a LIP are varied and generally depend on which particular feature is taken into account. By and large an accepted definition of LIP is that proposed by Bryan and Ernst (2008), who stated that LIPs are "*magmatic provinces with areal extents >0.1 Mkm^2, igneous volumes >0.1 Mkm^3 and maximum lifespans of ca. 50 Myr that have intraplate tectonic settings or geochemical affinities, and are characterised by igneous pulse(s) of short duration (ca 1–5 Myr), during which a large proportion (>75%) of the total igneous volume has been emplaced*." Included in this definition are giant continental dyke warms, sills and mafic-ultramafic intrusions, felsic or silicic provinces and tholeiite-komatiite associations (Archaean LIPs). In addition, a mafic LIP may also contain silicic volcanic rocks. Several types of magmatic and magmatic-hydrothermal mineral systems are commonly related to the emplacement of LIPs, whether continental or oceanic. Details and overviews of ore deposits that are associated with LIPs (and where appropriate with mantle plumes) can be found in Pirajno (2000, 2004, 2007).

In China, the following LIPs have been recognised (Fig. 7.1): ca. 1.8 Ga Xiong'er province, a ca. 925 Ma dyke swarm, the ca. 827 Ma event, the ca. 280 Ma Tarim (Bachu) event and the ca. 260 Ma Emeishan LIP in southwest China, which is probably part of the Siberian superplume event. In addition, the eastern margin of Asia is typically characterised by widespread intraplate magmatism, for which various lines of evidence show that it can be attributed to tectono-thermal events beginning in the Early Mesozoic (ca. 208 Ma) and probably continuing to present day (Pirajno et al. 2009). This Mesozoic-Cenozoic intraplate magmatism and extensional tectonics, extend from north-eastern and eastern China, through the Baikal and Mongolia regions to Far East Russia. These phenomena are broadly linked with a complex series of tectonic events, involving subduction, plate collisions, crustal thickening, post-collision collapse and rifting. The Mesozoic and Cenozoic extensional tectonics of mainland China and the rest of eastern Asia are ultimately the surface expressions of shallow mantle dynamics in the region, linked to the oblique subduction of the Pacific plate under the Eurasian plate, affecting the continental margin of eastern Asia (Sengör et al. 1993). This magmatism extends well inboard of the east Asian plate margin and many of the intrusion complexes, commonly alkaline, and bimodal volcanic successions are within rift settings (e.g. Shanxi and Baikal rift systems, Fig. 7.1), suggesting that intraplate mantle processes and underplating were the primary cause for the emplacement of plutonic and volcanic rocks. Furthermore, the presence of CO_2 gas pools in a rift basin filled with alkaline basalts in northeastern China and He isotope systematics support the argument of mantle upwellings in the region (Zheng et al. 2001). Other recognised, but less known and investigated, thermal events mostly

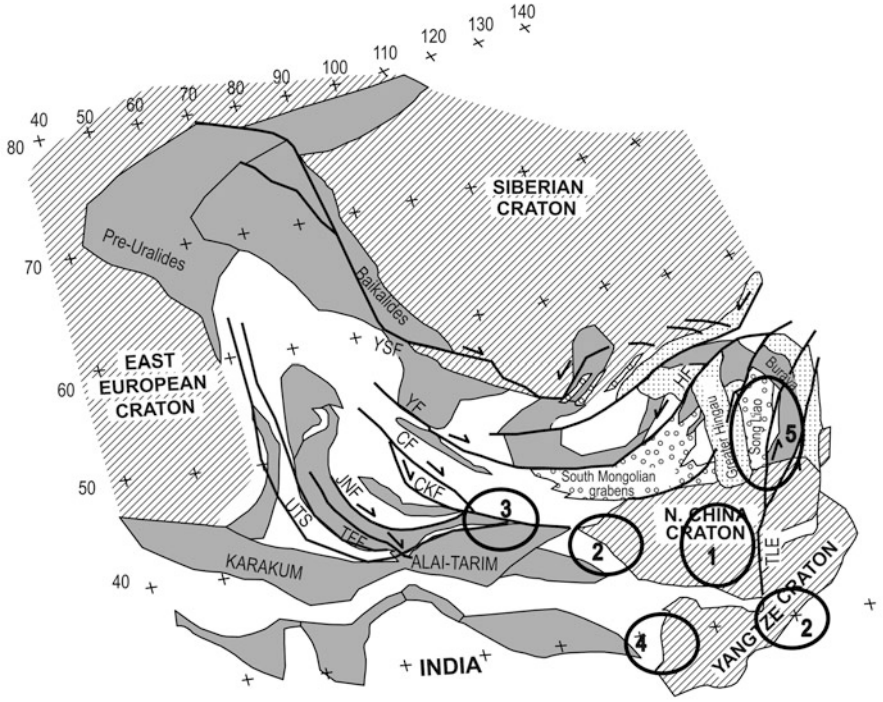

Fig. 7.1 Distribution of large igneous provinces (LIPs) in Eurasia and supposed mantle plume centres; *1* Xiong'er, *2* 825 Ma, *3* Tarim, *4* Emeishan, *5* NE China and Great Hinggan; Central Asian Orogenic Belt (CAOB), microcontinental blocks and major strike-slip faults; *YF* Irtysh Fault, *HF* Hinggan Fault, *MOF* Mongol-Okhotsk Fault, *CF* Chingiz Fault, *TFF* Talas-Ferghana Fault. (Map of Eurasia is after Yakubchuk 2004)

represented by ultramafic-mafic dykes and alkaline intrusions, include: ca. 2,500 Ma Eastern Hebei (Li et al. 2010b), the 1,980–1,970 Ma Xiwangshan-Liaohe and the 2,147 Ma Hengling (Peng et al. 2005; Table 7.1).

Most of the metallogeny and mineral deposits, which can be associated with thermal events responsible for the emplacement of mafic-ultramafic intrusions, dyke swarms and flood basalts and granitic intrusions and other volcanic products, a selection of which have been described in the preceding chapter in accordance with the tectonic settings in which the deposits in question occur. For other mineral systems, such as those for example that are formed as a result of a LIP and that may overlap boundaries between tectonic domains, are treated in this chapter. These include the Ni-Cu and Ti-V magmatic deposits related to the Emeishan LIP and the Tarim event. In this chapter, I briefly describe the above-mentioned igneous provinces and related metallogeny (Table 7.1).

Table 7.1 Major intraplate magmatic events in China. (Pirajno et al. 2009; see also references in individual sections)

Event	Approximate age (Ma)	Where	Main lithologies	Metallogeny
Yanshanian	208-present day	Eastern China	Basalts, mafic-ultramafic intrusions, granitoids, alkaline complexes, dykes, carbonatites	Ni-Cu-PGE, porphyry Cu-Mo, skarns, polymetallic vein systems
Emeishan	260	SW China; Vietnam	Flood basalts, mafic-ultramafic intrusions	Ni-Cu-(PGE); Fe-Ti-V, Au-Hg
Tarim	ca. 290–272	Tarim, NW China	Flood basalts, rhyolites, syenite, mafic-ultramafic intrusions	Cu-Ni Cu-Mo, Au-As
South China (Guibei, Suxiong-Xiaofeng, Kangding events)	850–825	South China and western margin of North China Craton	Mafic-ultramafic intrusions, dyke swarms	Ni-Cu-(PGE)
(Tarim-1) Qiganbulake, Aksu, Kudi events	825–780	Tarim block	Bimodal volcanism, mafic-ultramafic and felsic intrusions	Unknown
Dashigou	925	North China Craton	Dyke swarm and sills	Unknown
Xiong'er	1,780–1,770	North China Craton	Basaltic andesite, rhyolite, N-NW (fanning) dykes	Unknown
Xiwangshan (-Liaohe)	1,970–1,980	North China Craton	Dykes & volcanics	Unknown
Hengling (-Hutuo)	2,147 (−2,180)	North China Craton	Dykes	Unknown

7.2 The Xiong'er Volcanic Province and Coeval Dyke Swarms in the Central North China Craton: A 1.78 Ga Large Igneous Province

The Palaeoproterozoic Xiong'er volcanic province (Xiong'er Group), lies at border between Shaanxi, Shanxi and Henan provinces, with Sanmenxia city, approximately in the middle and the historical ancient capital of Xi'an in the west (Fig. 7.2). The Xiong'er Group, with thicknesses ranging from 3 to 7.6 km and an inferred

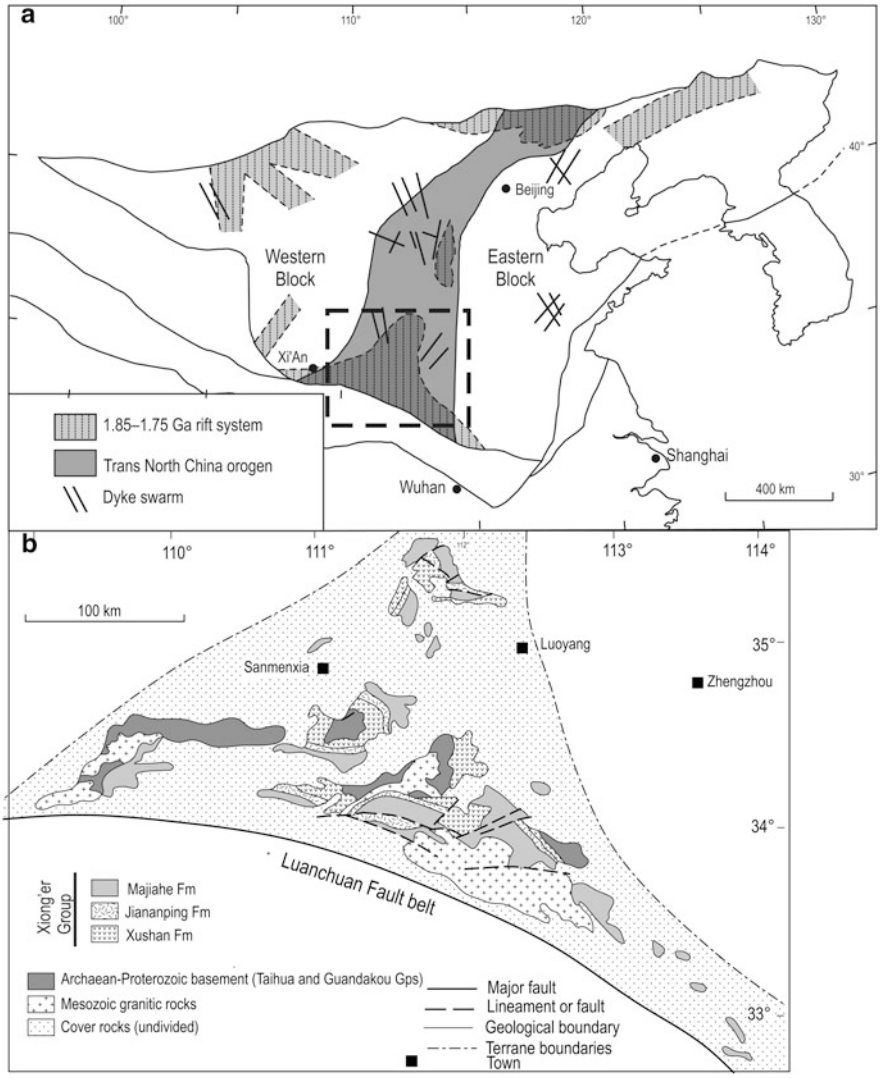

Fig. 7.2 **a** Sketch map of North China Craton, Trans North China Orogen (TNCO), rift systems and dyke swarms of approximately 1.8 Ga (after Peng et al. 2005); **b** geological map of the Xiong'er volcanic province at the southern margin of the North China Craton. (Modified from Zhao et al. 2002b)

present day areal extent of about 60,000 km^2 (Zhao et al. 2002b), is a well-preserved unmetamorphosed, only locally deformed, predominantly volcanic sequence that unconformably overlies the metamorphic basement (Taihua Group) and is overlain by Mesoproterozoic clastic and carbonate rocks of the Ruyang Group and Guandakou

Group (see Chap. 5 for details). The Xiong'er volcanic province is bounded to the south by the Luanchuan fault and a simplified geological map of the province is shown in Fig. 7.2b.

The Xiong'er volcanic rocks include a variety of types such as basaltic andesite, andesite, trachyandesite, dacite, rhyodacite and rhyolite, with minor sedimentary intercalations (mostly continental river- and lake-facies sediments) and pyroclastic units. The Xiong'er Group is divided into four formations, which from bottom to top are: Dagushi, Xushan, Jidanping and Majiahe (HBGMR 1989) (Fig. 7.3). The Dagushi Formation is a basal terrigenous clastic sedimentary unit. The Xushan Formation contains lava flows of basaltic andesite, andesite, trachyandesite; the Jidanping Formation has predominantly felsic units (dacite-rhyodacite-rhyolite) at the base followed by basaltic andesite, overlain by more felsic rocks; the Majiahe Formation comprises basaltic andesite with intercalations of sedimentary rocks. Zhao et al. (2002b) recognised two main cycles of volcanism. The first cycle is from mafic to felsic and represented by the Xushan and Jidanping formations; the second cycle, represented by the Majaihe Formation is early basaltic to late andesitic. However, it is not clear if and how much of the topmost Majiahe Formation has been lost to erosion. Also, as shown in Fig. 7.3, the cycles of the volcanic succession could be reinterpreted as a series of mafic-felsic couplets. This is supported by field observations from the area (Pirajno, unpublished). On this basis, the Xiong'er volcanic succession could be redefined as at least three mafic-felsic cycles, as follows: first cycle basaltic andesite-felsic rocks (Xushan Fm), second cycle basaltic andesite-felsic rocks (Jidanping Fm), third cycle basaltic andesite and intercalated sedimentary rocks (Majiahe Fm) (Fig. 7.3). The topmost Majahe Formation is probably erosion-truncated because it is unconformably overlain by clastic sedimentary rocks of the Ruyang Group.

Andesitic and basaltic andesite, usually occur as massive well-jointed flows, commonly porphyritic and with amygdales filled with chlorite, quartz, epidote and calcite. Felsic volcanic rocks, which include dacite, rhyodacite and rhyolites, are porphyritic to aphanitic, massive and locally featureless, but locally exhibit well-developed flow banding and lithophysae. The lava flows have no sedimentary intercalations, except for the topmost formations. The contact between lava flows is marked by amygdaloidal tops. Basaltic andesitic rocks of the Xushan Formation typically contain plagioclase and pyroxene phenocrysts in a fine-grained intersertal matrix composed of plagioclase microlites and pyroxene granules. Notably the phenocrysts are selectively altered to chlorite and epidote. The felsic rocks of the Jidanping Formation are characterised by glomeroporphyritic textures with bunches of plagioclase crystals up to 5–6 mm across, and embayed quartz in a felsitic groundmass of quartz and feldspar. The phenocrysts are commonly altered to chlorite, calcite, sericite and probably celadonite. In the basaltic rocks of the Jindaping formation, quench textures are observed and are especially evident as skeletal plagioclase crystals. The mafic lavas of the Majiahe Formation have a microporhyritic texture with chlorite-replaced pyroxene phenocrysts set in an intersertal to intergranular matrix of plagioclase microlites and pyroxenes. Plagioclase and pyroxene are usually replaced by chlorite,

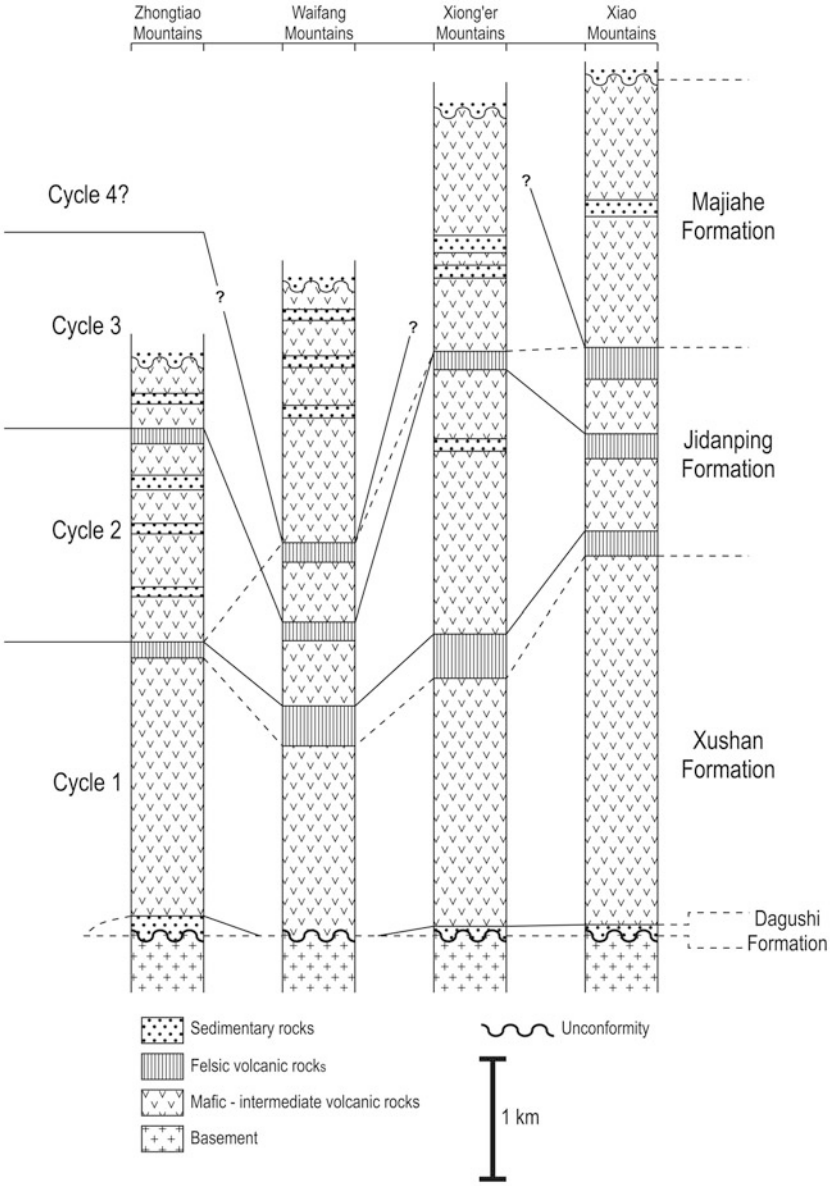

Fig. 7.3 Stratigraphy of the Xiong'er Group, from four localities (after Zhao et al. 2002b) and possible subdivisions based on mafic-felsic couplets to form four cycles

epidote and calcite. Lamprophyre and granitic dykes, dioritic and gabbroic rocks intrude the lavas, but their absolute ages are not known and many of these intrusions could belong to later events (e.g. Mesozoic Yanshanian). However, Cui et al. (2011) recently reported a diorite intrusion coeval with the age of the Xiong'er volcanic rocks (see below).

The age of the Xiong'er Group is reasonably well constrained. Volcanic rocks of the Xiong'er Group yielded SHRIMP U-Pb zircon ages of 1,789 ± 20, 1,779 ± 20 and 1,761 ± 16 Ma (Zhao et al. 2004; Peng et al. 2008). Single and multigrain zircon populations (Sun et al. 1990, 1991), including SHRIMP U-Pb ages obtained from rhyolitic rocks yielded: 1,826 ± 32 Ma from a single zircon, 1,840 ± 14 Ma from 16 zircon grains. Zhao et al. (2002b) calculated an age of 1.76 Ga from Sm/Nd isotopic data. These authors reported εNd (t = 1.76 Ga) values from −4.5 to −9.3, reflecting a primary magma source. More recently, Cui et al. (2008) provided precise U-Pb zircon and baddeleyite ages from the Shizhaigou Diorite, intruded into the upper part of the Majiahe Formation. Mean U-Pb ages this diorite intrusion are 1,789 ± 3.5 Ma (baddeleyite) and 1,780 ± 11 Ma (zircon). Cui et al. (2011), on the basis of major and trace element geochemical data, interpreted the Shizhaigou Diorite as having originated by partial melting of the Xiong'er volcanic rocks, during a late stage of the Xiong'er thermal event. Indeed, there may well be more intrusions that are coeval with the Xiong'er volcanic rocks and as such part of the same thermal event.

7.2.1 Tectonic Setting and the Mantle Plume Debate

The origin and tectonic setting of the Xiong'er Group volcanic rocks have been and remain controversial. Jia (1987), Sun et al. (1990) and He et al. (2008) suggested that the Xiong'er Group was part of an Andean type continental arc system that developed along the southern margin of the North China Craton, by the north-dipping subduction of oceanic lithosphere. Kusky and Li (2003), on the other hand, suggested that the Xiong'er volcanic rocks are a bimodal succession formed in a north-east-trending rift system related to the opening of the Qinling Ocean. Based on comprehensive geochemical and petrographic data, Zhao et al. (2002b) concluded that the Xiong'er Group volcanics are continental flood basalts, derived from an enriched mantle source and modified by crustal contamination. Peng et al. (2005, 2007) working on the geochronology of dyke swarms in the North China Craton, identified four dyke suites with SHRIMP U-Pb ages of 2,147 ± 5, 1,929 ± 8, 1,973 ± 4 and 1,778 ± 3 Ma. On the basis of this geochronology, Peng et al. (2005, 2007) suggested that the older group of dyke suites could relate to the amalgamation of the North China Craton to the Columbia supercontinent, whereas the younger suites (e.g. Taihang Mountains dyke swarm) may be related to the breakup of Columbia and a mantle plume event at 1,780–1,750 Ma. This mantle plume would have been implicated in a triple-junction rifting at the southern margin of the North China Craton at ca. 1.78 Ga, leading to its breakup from the Dharwar Craton in India (Peng et al. 2005). Swarms of mafic dykes, which are thought to be part of a mantle plume event at 1,780–1,750 Ma, could

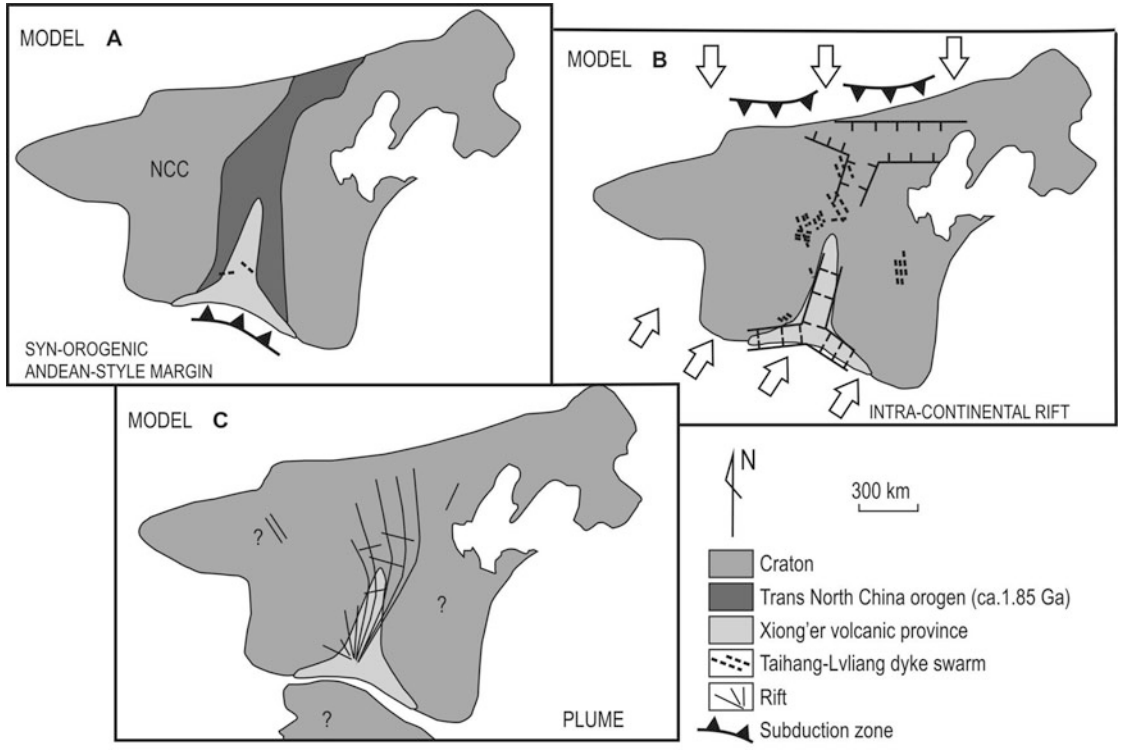

Fig. 7.4 Models proposed to explain the emplacement of the Xiong'er Group volcanic province and associated mafic dyke swarms; **a** subduction-related Andean-style margin; **b** intracontinental rift; **c** mantle plume and radiating dyke swarm (after Peng 2010), see text for details

conceivably be the feeders to the Xiong'er lava flows (Peng et al. 2005; Wang et al. 2004a). A comprehensive palaeomagnetic study of ca. 1.78 Ga mafic dykes in the North China Craton has recently been conducted by Piper et al. (2011), who presented a supercontinent reconstruction (Palaeopangea ca. 1,780–1,750 Ma), with a different arrangement between India and the North China Craton, from the one discussed below (see Fig. 7.5). These interpretations are supported by field observations, as well as the regional tectonic setting and the age of associated intrusive rocks, as briefly discussed below.

The tectonic setting of the Xiong'er Group has been, in my opinion, misinterpreted by a number of researchers, who based their models on whole-rock geochemical data applied to some specific areas (e.g. Zhongtiaoshan) of the Xiong'er volcanic province (He et al. 2008, 2010c; Zhao et al. 2009). The Xiong'er volcanic rocks are largely distributed in an area with an approximately triangular shape in the southern part of the Trans North China Orogen (TNCO), with the southern part along the Luanchan Fault belt (Fig. 7.2b). On the basis of the geochemical data presented by He et al. (2008, 2010c), there is a good case for suggesting a subduction setting for the Xiong'er volcanism. However, geochemistry alone can be quite misleading, unless examined in the light of field observations, well-constrained age data and the widespread presence in the TNCO of coeval dyke swarms, as repeatedly reported by Peng et al. (2005, 2007, 2008) and Peng (2010), and ignored by researchers advocating an Andean style magmatic arc for the Xiong'er volcanic rocks. In addition, Zhao and Zhou (2009) reported the presence of A-type granites of similar age as the Xiong'er volcanics and dykes in the Songshan region, in the TNCO. Furthermore, volcanic rocks from recognised large igneous provinces, may have geochemical signatures (calc-alkaline) of subduction settings, inherited in the mantle source of intraplate magmas. Pirajno and Chen (2005) used geochemical data from Zhao et al. (2002b) on the Xiong'er Group volcanic rocks, as well as data from the Taihang Mountains mafic dyke swarm from Wang et al. (2004a) to construct a series of geochemical plots. In silica versus alkalies diagrams, the Xiong'er volcanic rocks and the Taihang dykes plot in the subalkaline field and have a distinct bimodal trend. Plots of rare earth elements (REE) normalised to chondrite and multielements normalised to primitive mantle of the Xiong'er volcanics were compared with the Emeishan continental flood basalts (Xiao et al. 2003) and the East China-Mongolia alkali basalts (Barry and Kent 1998). The REE pattern of the Xiong'er volcanic rocks is almost identical to that of the Emeishan and North East China basalts, all exhibiting a moderate LREE enrichment. In addition a multielement spider diagram is suggestive of a subduction modified mantle source for the Xiong'er volcanics, the Emeishan and North East China basalts. As such, it is seems clear that the geochemical signature of these volcanic rocks represent an inherited subduction-modified component. Geochemical parameters for anorogenic or orogenic magmas are numerous and sometimes ambiguous. The presence of andesites in the Xiong'er Group does not preclude a rift-related, mantle plume associated origin. Andesites or basaltic andesites are by no means an exception in rift-related rocks. Furthermore as there are no "basalts" in the Xiong'er rocks, a full calc-alkaline succession (basalt-

andesite-dacite-rhyolite) does not appear to be present. He et al. (2008), citing Zhao et al. (2002a) mentioned that amygdales in basaltic andesites of the Xiong'er Group have mantle-sourced CH_4 and H_2, supporting a petrogenesis involving H_2O-rich fluids.

The research works by Zhao et al. (2002b), Wang et al. (2004a), Peng et al. (2005, 2007, 2008) and Peng (2010) demonstrated, on the basis of geochronological, isotopic and geochemical data as well as age correlations with dyke swarms further north, that the Xiong'er Group represents the remnants of an ancient large igneous province (LIP) emplaced at a triple junction that was developed along the southern margin of the North China Craton at about 1.8 Ga. Recognition of the Xiong'er volcanic province as a LIP warranted a place on the website http://www.largeigneousprovinces.org as the June 2005 LIP of the month (Pirajno and Chen 2005).

A number of extensional structures (aulacogens and rift basins) were formed along the margins and in the central parts of the North China Craton between 1.85 and 1.7 Ga (Lu et al. 2002; Kusky and Li 2003). One of these could have been a three-arm Xiong'er rift, with its northeast-trending branch being an aulacogen, a failed rift arm of a triple junction that was formed along the weak zone of the TNCO. Mafic dyke swarms of the same age range, trending northwest and north-northeast (Fig. 7.2a), were emplaced in the North China Craton (Qian et al. 1987). $^{40}Ar/^{39}Ar$ geochronology of mafic dykes in the Taihang region, within the TNCO, and just north of the Xiong'er terrane yielded plateau ages of 1,780, 1,765 and 1,774 Ma (Wang et al. 2004a; also listed as no. 141 event by Ernst and Buchan 2001). These ages are within experimental error of the 1.76 Ga Sm/Nd age reported for the Xiong'er volcanic rocks by Zhao et al. (2002b). Anorthosite and rapakivi granites of the same age have also been reported from the region (Lu et al. 2002). Some mafic and ultramafic intrusions elsewhere in the North China Craton also have ages of around 1.75 Ga (e.g. Damiao complex with Cu-Ni and V-Ti deposits, see Chap. 3).

Thus, it is considered likely that the Xiong'er Group (Xiong'er volcanic province) was deposited in a three-arm rift system with its three branches trending approximately west-southwest, southeast on the southern margin of the North China Craton and a northeast branch (Fig. 7.2a). The two southern branches (west-southwest and southeast) are within the Huaxiong terrane that was interpreted to be the northernmost tectonic unit of the Qinling mountains of central China, or the southernmost unit of the North China craton (Chen et al. 2004). The northeast branch, usually referred to as Xiyanghe Group, is along the boundary between the Songji and Zhongtiao blocks and is the third failed arm of the rift system. This third arm is thought to be extended far into the interior of the North China Craton, e.g., the Lvliang Mts. (Peng et al. 2008 and reference therein) (Fig. 7.4c).

Models of the tectonic setting that could explain the emplacement of the Xiong'er volcanic province and associated dyke swarms have been reviewed by Peng (2010), who concluded that a mantle plume model best explains the Xiong'er event (Fig. 7.4). Peng (2010) discounted the Andean-style margin model which, as explained above, is solely based on geochemical data that can be equally interpreted by continental rift

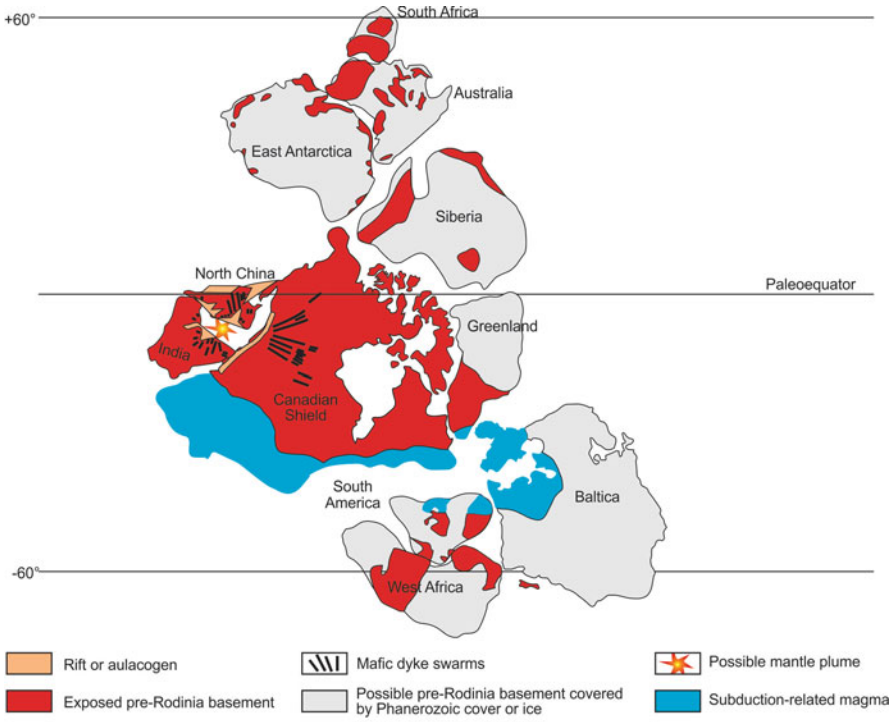

Fig. 7.5 Giant radiating dyke swarms at ca. 1.8 Ga emanating from a mantle plume located between India, the North China Craton and the Canadian shield in a reconstruction of the Columbia supercontinent. (After Hou et al. 2008)

and mantle plume models. Peng (2010) favoured the mantle plume model (Fig. 7.4c) with magma originating from a rifting centre, satisfying four out of five criteria for plume-related intralate igneous activity, as suggested by Campbell (2001, 2007): (1) uplift prior to volcanism (recorded by the 1.80–1.78 Ga regional P–T–t paths and extensional deformation; e.g. Zhao et al. 2005; Guo et al. 2005a); (2) a radiating dyke swarm; (3) massive volcanic flows correlated over a large area (>90,000 km^2) and a long distance (>500 km); (4) plume-associated chemistry (an enriched magma source followed shortly by a depleted source with OIB affinity: Peng et al. 2007).

The real extent of the Xiong'er LIP is not known with certainty, mainly because (1) the region is mountainous and heavily vegetated and (2) uplift and erosion may have eliminated a substantial part of the succession. There are limited data on the volcanics and much remains to be done to map and study associated intrusives, some of which may be prospective for magmatic and/or hydrothermal ore deposits. The study of the Xiong'er Group as a LIP would provide further insights on world-wide ca. 1.76–1.8 Ga thermal events (e.g. Uruguayan, Espinhaço in Brazil, Dubois-Cochetopa in Colorado, and the Hart-Carson event in the Kimberley Basin of Western Australia; see http://www.largeigneousprovinces.org August 2006 LIP of the Month and Ernst

and Buchan 2001, for listing and references) and their possible link to mantle plumes or superplume and their role in the breakup of the Columbia supercontinent.

Correlations that may enable a Columbia supercontinent reconstruction have been proposed by Hou et al. (2008), as summarised below and shown in Fig. 7.5. Ages of mafic dyke swarms in the North China Craton, Southern Indian Craton and Canadian Shield range from 1,850 and 1,650 Ma, suggesting that Late Paleoproterozoic dyke swarms were intruded during a long-lived extension event in all three continents. The undeformed and unmetamorphosed mafic dyke swarms in the North China Craton, Southern Indian Craton and Canadian Shield also indicate that extension and dyke swarm emplacement began at ca. 1.85 Ga in these three continents. If the North China Craton, Southern Indian Craton and Canadian Shield are joined together, the overall pattern of the mafic dyke swarms appears to constitute a giant radiating swarm, with the Xiong'er rift (aulacogen) as a piercing point. In which case, Hou et al. (2008) reasoned that the North China Craton, South Indian Craton and Canadian Shield may have been fragmented from the same landmass, i.e. the Paleoproterozoic supercontinent Columbia (Fig. 7.5). The ca. 1.8 Ga mafic dyke swarms in the North China Craton are centered off the Xiong'er three-arm rift system. The above also fit well with the geometry of two Late Paleoproterozoic continental rift-related Cuddapah and Singhbhum basins containing thick volcaniclastic successions, perpendicular to the eastern coast of the Indian Peninsula (Fig. 7.5). These basins contain 10 km-thick bimodal volcaniclastic successions, which cover a total of about 30,000 km^2 in both basins. Hou et al. (2008) further contended that these thick volcaniclastic successions can be regarded as a part of Late Paleoproterozoic LIPs, that include the Xiong'er Group in the southern margin of the North China Craton and the eastern coast of southern India. The total areas are ca. 400,000 km^2 covered by volcanics in aulacogens and basins, 200,000 km^2 of mafic dykes in the North China Craton and 125,000 km^2 of mafic dykes in the South Indian Block (French et al. 2008).

There is little doubt, given the evidence, that a mantle plume impacted the base of the Palaeoproterozoic lithosphere, created a triple junction rift system in the overlying crust and formed the Xiong'er LIP.

7.3 A Newly Discovered LIP: ca. 925 Ma Dashigou Dyke Swarm in the North China Craton: Implications for Mineral Deposit Targeting

A newly discovered LIP, represented by a ca. 925 Ma dyke swarm in the North China Craton (NCC) was identified and reported by Peng et al. (2011a). The general trend of the swarm is shown in Fig. 7.6, together with other swarms, one of which is also shown in Fig. 7.5c and which defines the Xiong'er LIP event. Peng et al. (2011a) using new precise U-Pb data on baddeleyite grains (ID-TIMS; isotope dilution thermal ionisation mass spectrometry) recognised that a number of dykes with ages ranging from ca. 926 to 920 Ma, which they named Dashigou swarm and trending northwest and north. The Dashigou dykes are coarse-grained and mostly composed

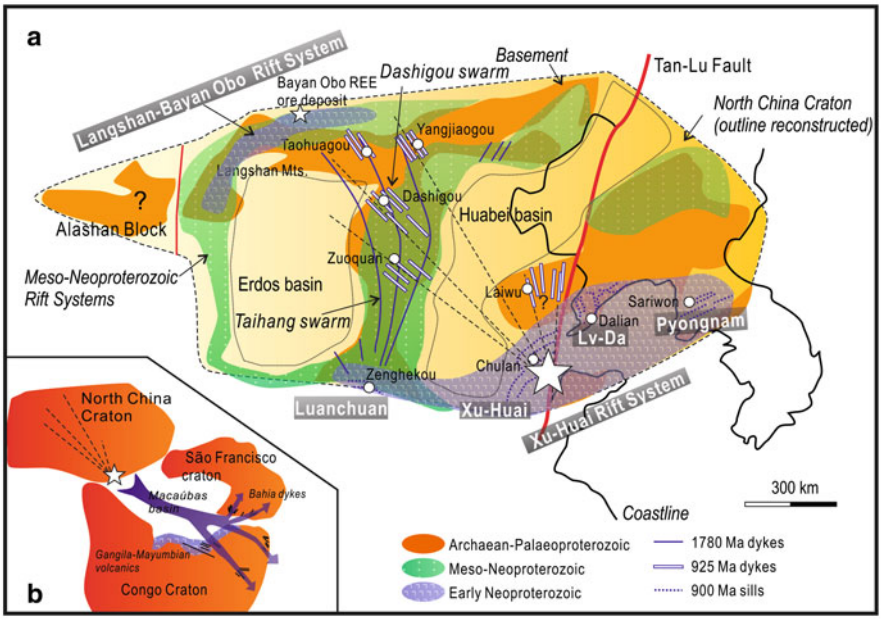

Fig. 7.6 North China Craton (NCC) and general trend of radiating dyke swarms, the Xiong'er dykes and LIP (see Fig. 7.5c) and the newly discovered 920–925 Ma Dashigou dyke swarm, radiating from the southern margin of the NCC and possibly defining an ancient triple junction that led to the break-off of the NCC from other cratonic blocks. (Figure reproduced unchanged by courtesy of Dr Peng P, Institute of Geology and Geophysics, Chinese Academy of Sciences, Beijing)

of clinopyroxene, feldspar with or without olivine. Individual dykes have widths of 10–100 m and extend along strike for up to 10 km. The Dashigou dykes have OIB-like geochemical and isotopic signature (εNdt) ranging from +1.8 to +3.1 and $^{87}Sr/^{86}Sr$ (t = 920) values ranging from 0.7019–0.7047. The Dashigou dykes have comparable ages, petrographic, geochemical features and trend to dykes in the Zuoquan and Taishan areas, all cutting across the Craton and, defining an overall radiating swarm, converging to a focal point in the southeastern margin of the Craton and assumed to be the source from a Neoproterozoic mantle plume head. This focal point, Peng and co-workers show that it coincides with sills of approximately the same age (ca. 900 Ma) called Chulan-Dalian-Sariwon sill complex, of which the Sariwon sills are located in the Pyongnan basin in the Korean peninsula, in the eastern extension of the NCC (Peng et al. 2011b). This sill complex and the approximately coeval radiating dyke swarms (Fig. 7.6) could define an ancient rift system and triple junction, similar to those shown in Figs. 7.5c and 7.6, in respect of the Xiong'er event, initiated at cratonic margins (see Begg et al. 2010). This triple junction may have been instrumental to the break-off of the NCC from adjacent cratonic blocks (the authors suggested São Francisco-Congo cratonic blocks), based on nearly coeval ages of the Bahia dyke swarms and Gangila-Mayubian volcanism, respectively (see Ernst and Buchan 2001 for details and references). Furthermore, as Peng and co-authors pointed out, the sub-

continental lithospheric mantle of the NCC was metasomatised at least twice during the 1,780–1,750 Ma Xiong'er and ca. 925 (925–900 Ma) Dashigou LIP events, before being partly consumed during the Yanshanian tectono-thermal event (see Sect. 7.6).

The new LIP reported by Peng et al. (2011a) and interpretation of a possible radiating swarm with a central focus on the southeastern margin of the NCC is of considerable importance in terms of mineral targeting, because focal points of mantle plume head may be associated with layered intrusions and related magmatic sulphide and oxide mineral systems.

7.4 850–825 Ma Event and the Rodinia Connection

Several authors proposed that a widespread thermal event at 850–825 Ma, perhaps as early as 900 Ma, was related to a mantle plume or superplume event(s), which was a major cause for the breakup of the Rodinia supercontinent (e.g. Li et al. 1999, 2003, 2008; Wang et al. 2008a, 2009, 2010a, b; Dong et al. 2011). In China, this thermal event is represented by the Guibei large igneous province in South China, K-rich calc-alkaline and tonalite-trondhjemite-granite (TTG) intrusions, ascribed to crustal melting above a mantle plume, alkaline rocks and associated mafic dykes (Li et al. 2003, 2010a), as well as the ca. 825 Ma Jinchuan intrusion. The latter hosts the giant Ni-Cu-PGE deposit described in the next section, in the Alashan block on the southwest margin of the North China Craton (Gansu Province). The Jinchuan intrusion is located in the Lonshoushan uplift and linked to the mantle plume event in South China (Li et al. 2005b). Other mafic-ultramafic complexes with similar ages in China include Lengshuiqin (ca. 821 Ma; Zhu et al. 2007) and Baotan (ca. 828 Ma, Li et al. 1999). Li et al. (1999) determined a U-Pb zircon age of 828 ± 7 Ma for mafic and ultramafic dykes and sills from South China and correlated them with the Gairdner dyke swarm and other mafic-ultramafic units in South Australia, together forming the Willouran basic province (Zhao et al. 1994; Wingate et al. 1998; Wang et al. 2010a, b). Li et al. (1999) suggested that the impact of a mantle plume caused rifting, emplacement of mafic dykes and sills and crustal anatexis in South China. This mantle plume would have rifted the Cathaysia from the Yangtze Craton, forming the Nanhua Rift (see also Chap. 4), between 840 (early doming of the crust) and 820–800 Ma (onset of rifting and mafic intrusions). Li et al. (1999) placed the South China block between Laurentia and eastern Australia in an early Proterozoic Rodinia configuration, with a mantle plume focus being located east of the Adelaidean Fold Belt, approximately at the southern end of the Gairdner dyke swarm. Wang et al. (2010a) correlated the Guibei LIP with the Willouran basic province which, as mentioned above, includes the Gairdner dyke swarm, of South and Central Australia and regarded the mantle plume that produced these two Neoproterozoic LIPs, as an important tectono-thermal event that peaked at about 825 Ma (see also http://www.largeigneousprovinces.org); August 2010 LIP of the month (Wang et al. 2010b) and, as mentioned above, responsible for the formation of rift systems (Adelaide Rift in South Australia and the Nanhua Rift in South China),

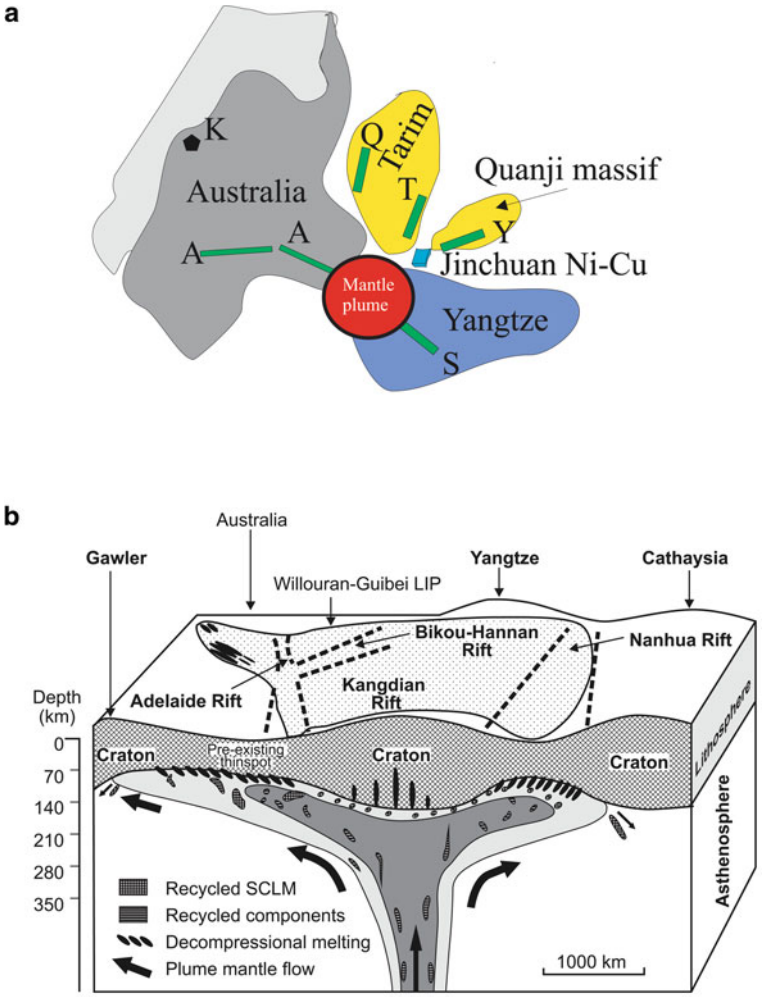

Fig. 7.7 **a** Schematic distribution of ca. 825 Ma dyke swarms linked to a Neoproterozoic mantle plume in a partial reconstruction of Rodinia continents (modified after Li et al. 2008), approximate position of the Jinchuan intrusion (see Fig. 7.8) also shown; **b** cartoon showing the impingement of the Neoproterozoic mantle plume that may have caused a series of rift systems and eventually the breakup of the Rodinia supercontinent at that point (after Wang et al. 2010)

at the margins of stable cratonic blocks (Fig. 7.7). In addition, Neoproterozoic mafic intrusions along the northwestern margin of the Yangzte Craton (Hannan rift), at a (triple?) junction between the Songpan and Qinling belts have ages of around 900 Ma and have also been attributed to a mantle plume (Dong et al. 2011; see below and Figs. 7.7 and 7.8). Whether accurate or not and subject to further testing, these cross-continental reconstructions are important for providing insights into the geodynamic

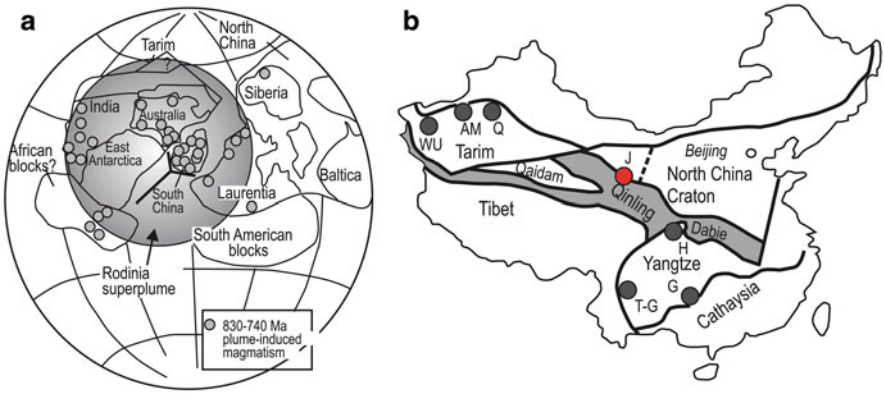

Fig. 7.8 Distribution of mantle plume magmatism in the Rodinia supercontinent (**a**) and distribution of igneous complexes in China that are assigned to the ca. 825 thermal event (**b**) WU Bachu layered complex, *AM* Aksu mafic dykes, *Q* Qiganbulake, *J* Jinchuan *T-G* Tongke-Gaojiacun complex, *H* Hannan complex, *G* Guangxi mafic dykes and sills. (After Zhang et al. 2007)

environment of ore formation and, importantly, allows a degree of predictability that can assist in exploration targeting for mineral deposits. The mantle plume hypothesis is reinforced by the discovery of the 825 Ma Yiyang komatiitic basalts in South China, formed by melting of a mantle source with temperatures greater than 1,500 °C (Wang et al. 2007)

The Qiganbulake mafic–ultramafic-carbonatite ring complex and associated Xingdi granodiorite and the Taiyangdao granite in the northeast margin of the Tarim Block have ages ranging from ca. 820 to 795 Ma, comparable with the ca. 800 Ma Aksu mafic dykes, the ca. 830 Ma Bachu layered mafic intrusive complex and 790–750 Ma alkaline diorites in central Tarim and the above-mentioned ca. 780 Ma alkaline bimodal intrusive complex in southwest Tarim, as well as the Jinchuan mafic-ultramafic complex (Zhang et al. 2007). The 820–750 Ma bimodal intrusives in the Tarim, studied by Zhang et al. (2007), have been correlated with plume events responsible for the 820–800 Ma lamprophyre and kimberlite fields in the Kimberley Block of Western Australia and the 755 Ma Mundine dyke swarm, also in Western Australia (Li et al. 2008 and references therein), within a Rodinia supercontinent reconstruction (Fig. 7.8).

7.4.1 Mineral Systems

The best known and economically important magmatic sulphide deposits hosted in mafic-ultramafic intrusions related to the 850–825 Ma thermal event in China, is undoubtedly the Jinchuan Ni-Cu-PGE deposit, described below. Some of the mafic intrusions of the Hannan Complex (Massif) in at the northwestern margin of the Yangtze Craton (South China block) have a similar age as Jinchuan (ca. 820 Ma) and

hosts V-Ti mineralisation (Li et al. 2005b and references therein). The position of these complexes in China is shown in Fig. 7.8.

7.4.1.1 Jinchuan

The Jinchuan Ni-Cu-PGE deposit is the third largest magmatic deposit in the world after Noril'sk and Sudbury and has been mined since 1964 (Naldrett 2004). Studies on the Jinchuan deposit proposing various interpretations for the origin of the intrusion and related sulphides include those of Li et al. (2005b), Lehmann et al. (2007), Yang et al. (2008), Tang et al. (2009), Li, Ripley (2011) and Song et al. (2012). The age of the Jinchuan intrusion is well constrained by U-Pb SHRIMP dating of magmatic zircon and baddeleyite, which yielded ages of 827 ± 8 and 812 ± 25 Ma, respectively (Li et al. 2005b). However, Re-Os isochron ages of sulphides reported by Yang et al. (2008), yielded apparent ages of $1{,}117 \pm 67$, $1{,}074 \pm 120$ and 867 ± 75 Ma, with initial $^{187}Os/^{188}Os$ ratios of 0.120 ± 0.0012 and 0.162 ± 0.017 and 0.235 ± 0.027, for disseminated, net-textured and massive sulphide ores of the Jinchuan deposit. Yang et al. (2008) concluded that these age discrepancies reflect degrees of Os post-segregation diffusion according to different ore textures during cooling, resulting in the observed trends of apparent Re-Os ages from massive to net-textured to disseminated. The Re-Os age data from the massive sulphides is consistent with the U-Pb age of the Jinchuan intrusion, because diffusion of Os and re-equilibration occurred during cooling from about 850 to 400 °C.

The mineralisation is hosted in the Jinchuan mafic-ultramafic a northwest-trending dyke-like intrusion that resembles the Great Dyke of Zimbabwe (see Wilson 1996). Another interpretation suggests that the Jinchuan intrusion was originally emplaced as a sill and subsequently rotated to vertical (Lehmann et al. 2007). Like the Great Dyke, the Jinchuan intrusion is subdivided into an East sub-chamber, West-central sub-chamber and a West sub-chamber (Fig. 7.9; Lehmann et al. 2007). The intrusion is deeply eroded and consists of dunite, troctolite, lherzolite, plagioclase lherzolite and olivine pyroxenite (Naldrett 2004; Li et al. 2005b). Chai and Naldrett (1992) noted a lateral zonation in the west and horizontal layering in the eastern parts, suggesting that the two parts formed by flow differentiation processes. The ultramafic rocks have high MgO and low TiO_2, Al_2O_3, CaO, Na_2O and K_2O contents (Li et al. 2005b) and it was suggested that the parental magma was a high-Mg tholeiite derived from high degrees of melting of the mantle (Chai and Naldrett 1992), although εNd(t) negative values (−8.9 to −12.0) suggest contamination by crustal material (Li et al. 2005b). The Jinchuan intrusion contains more than 100 sulphide orebodies, of which three main orebodies, one in each sub-chamber: orebody-24, orebody-1 and orebody-2, contain more than 85 % of the total reserves (Su et al. 2008; Song et al. 2009). The Jinchuan deposit had an estimated 500 Mt of ore, grading 1.2 % Ni and 0.7 % Cu (Lehmann et al. 2007). The orebodies are tabular in shape and consist of massive lenticular sulphide bodies, net-textured sulphides and disseminations of pyrrhotite, pentlandite and chalcopyrite. Pyrrhotite is the dominant sulphide and other ore minerals are cubanite, mackinawite and pyrite. PGE concentrations are

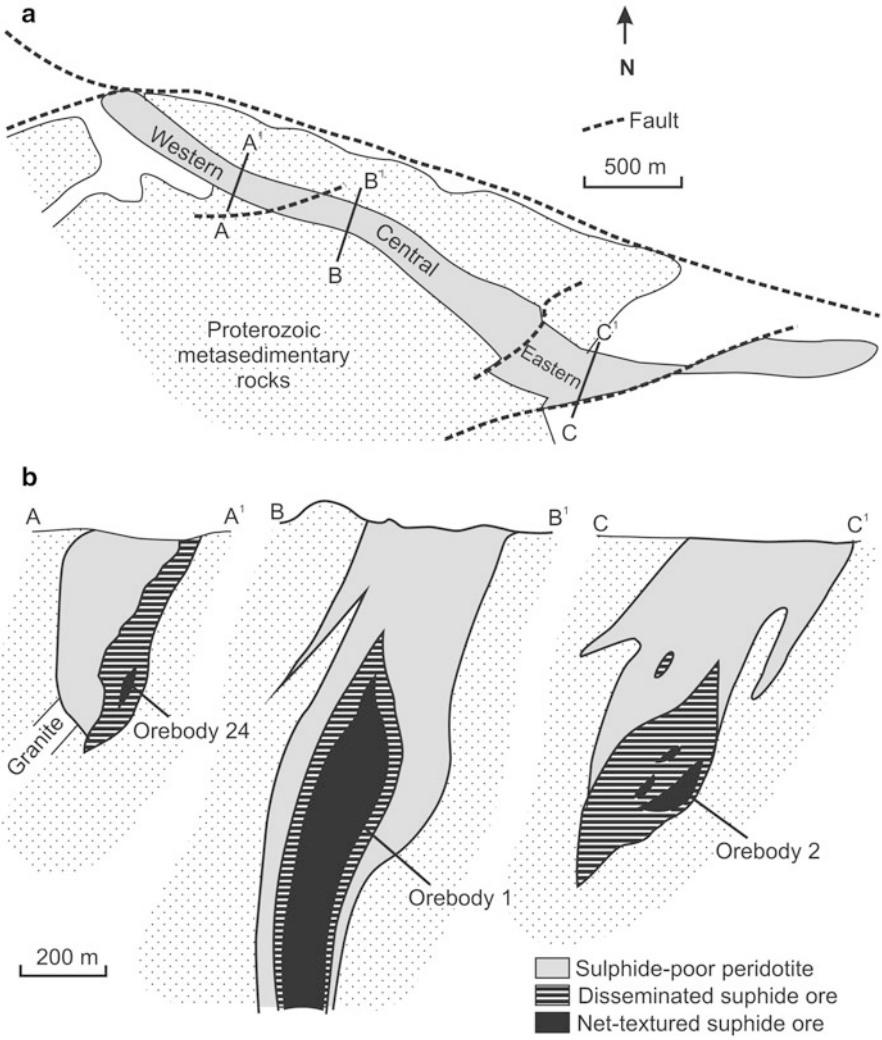

Fig. 7.9 **a** Geology of the Jinchuan Ni-Cu deposit; **b** cross-section of orebodies, 1, 2, and 24 (after Lehmann et al. 2007); see Fig. 7.7 for position of Jinchuan

low with values of around 1 ppm (Naldrett 2004). The genetic model, as envisaged by Naldrett (2004), is that a high Mg tholeiitic magma was advected along a rift fault. The magma, containing chromite, olivine and sulphide droplets, was emplaced in a series of funnel-shaped intrusions. Magma continuously flowed along the central parts of the conduits, giving rise to layered rocks. This continuing flow allowed fresh magma to come into contact with sulphides already present enriching them in chalcophile elements. This resulted in the central parts of the funnels to be the richest, whereas the sulphides along the walls, which cooled more rapidly, are less

enriched. The mechanism of continuing and fresh magma flow is the same as that envisaged for Noril'sk and Sudbury (Naldrett 2004). Lehmann et al. (2007) advanced a model in which precipitation of sulphides may have been caused by interaction of the magma with marble rocks. This would have resulted in the release of CO_2-rich fluids, due to decarbonation of the floor rocks, these fluids reacted with the olivine cumulates increasing the oxygen fugacity, causing the segregation of a sulphide liquid. In contrast, de Waal et al. (2004) proposed multiple pulses of magmas with emplacement of sulphide-bearing and sulphide-free from a deep layered magma chamber.

Su et al. (2008) examined the effects of post-magmatic hydrothermal alteration at Jinchuan. The alteration minerals are serpentine, magnetite, chlorite, actinolite that principally affect the olivines, and chlorite, epidote, tremolite and Na plagioclase, affecting magmatic pyroxene and plagioclase (Su et al. 2008 and references therein). Contact zones are extensively sheared and altered (tremolite-chlorite). Quite commonly the sulphide assemblages are replaced by silicates and oxide minerals by up to 30 vol%. Su et al. (2008) found that this post-magmatic hydrothermal alteration results in some remobilisation of platinum-group elements (PGE). A similar situation has been found for the Jinbaoshan Pt-Pd deposit in the Emeishan large igneous province (see below).

It was proposed that the Jinchuan intrusion was emplaced during the initial breakup of the Rodinia supercontinent at about 830 Ma as a result of a mantle plume that impinged beneath the Yangtze Craton (Li et al. 1999). However, in the latest publication on the Jinchuan deposit, Li and Ripley (2011) suggested that on the basis of regional stratigraphic correlations the Jinchuan intrusion is located at the western margin of the North China Craton and therefore could not have been in the Yangtze Craton. Nevertheless and notwithstanding the position of the mafic-ultramafic intrusion at the edge of the North China Craton, following the model proposed by Begg et al. (2010), it can be surmised that a mantle plume flowed laterally towards the thinner lithosphere at cratonic margins.

7.5 Tarim Event (291–272 Ma)

The Tarim intraplate magmatic event formed a LIP that consists of tholeiitic volcanic rocks, mafic dykes, mafic-ultramafic rocks and syenites covering an area in excess of 300,000 km^2 and with a thickness variably estimated to range from 600 to 800 m or from 1,200 to 3,000 m, in the western and southwestern parts of the Tarim basin, largely on the basis of oil well data and a network of seismic profiles (Fig. 7.10; Jiang et al. 2006; Yang et al. 2007; Zhang et al. 2008, 2010b; Zhou et al. 2009; Yu et al. 2011; Tian et al. 2010). Individual outcropping lava flows reach thickness in excess of 30 m (Tian W, pers. comm. 2011). The Tarim event in the wider Asian context was discussed in Borisenko et al. (2006) and Pirajno et al. (2009).

The Tarim LIP is mainly represented by Early Permian alkaline and tholeiite basalts with ages ranging from 246 to 291 Ma, which mostly occur under the cover

of Tarim platform, associated with igneous intrusions that include dolerite, gabbro, syenite, ultramafic rocks and perhaps kimberlites near the Wajitage complex (Zhang et al. 2010b; Tian et al. 2010). One of the intrusive rocks is a quartz-syenite with an A-type geochemical affinity (Li et al. 2006), but according to more recent literature other A-type intrusions occur to the northwest of the Tarim Block with ages ranging from 273 to 269 Ma (Zhang et al. 2010b). The Bachu ultramafic-mafic-syenite layered complex, called Wajitage complex, in the western Tarim Block consists of four main lithofacies (Zhang et al. 2008) magnetite-olivine-pyroxenite, olivine-pyroxenite, gabbro and syenitic rocks, with some transitional rock types such as diorites and pyroxene and/or nepheline-bearing syenite. No mineralisation has been reported from the Bachu Complex, but clearly the possibility needs to be assessed, particularly in the ultramafic parts of the Complex. K-Ar dating yields a range of ages from 277 ± 4 to 288 ± 10 Ma, whereas Ar-Ar dating shows a plateau age of 278.5 ± 1.4 Ma. Other igneous complexes in the Bachu area include bimodal (dolerite-syenite) dyke swarms in the Mazaertage area are associated with a gabbro-syenite complex called Xiaohaizi (Zhang et al. 2010b) as well as a suite of picrite-basalt-rhyolite in the northern edge of the Tarim (Northern Tarim Uplift) in which the rhyolites were derived through fractional crystallisation of the basalts (Tian et al. 2010; Fig. 7.10). According to Tian et al. (2010; pers. comm. 2011), the Tarim LIP was formed in two major pulses: one between 291–285 Ma and the other, which includes the Bachu dykes and the rhyolitic rocks between 287–272 Ma.

Although not yet well defined, this magmatic province may have a huge extension, from the western margin of the Tarim block to the Qilian Mountains in the east, a distance of at least 1,800 km (Tian et al. 2010). This widespread magmatism may have been linked with a mantle superplume and the evolution of the Palaeo-Tethys Ocean (Yang et al. 2006, 2007). The Tarim LIP covers parts of the Tarim Platform (Fig. 7.10), almost the entire length of the Chinese Tianshan (eastern and western), central Asian parts of the Tianshan and rift structures in the Altai. The Turpan (Tuha or Turpan-Hami) Basin, within the Tianshan Orogen and located between the Junggar Basin and the Tarim (see Chap. 8 for details) contains tholeiitic basalts that are coeval (ca. 270–280 Ma) with the Huangshan-Huanshanxi and Tianyu mafic-ultramafic intrusions (described in Chap. 6) in the eastern Tianshan and correlated by Zhang et al. (2011a) with the Tarim LIP. Similarly, the numerous mafic-ultramafic intrusions that outcrop at the southwestern end of the Beishan Rift (Fig. 7.10b), have U-Pb ages of ca. 280 Ma and positive values of $\varepsilon Nd(t)$, are coeval with felsic rocks, suggesting a bimodal magmatic system related to the Tarim LIP (Su et al. 2011a, b).

The Tarim plume event may have in its final stages temporally overlapped with the initial stages of the Siberian and Emeishan mantle plumes at the Permo-Triassic boundary and, as mentioned above, these three events, temporally associated with voluminous A-type granitic magmatism, isotopically characterised by positive $\varepsilon Nd(t)$ values and spanning 30–40 Myrs, may have been linked either to a series of plume activity, or to ramifications from a single superplume that could have impinged beneath the Asian continent (Siberian traps region), with plume material flowing along major lithospheric breaks, orogenic belts and rift faults (Borisenko et al. 2006; Pirajno et al. 2009; Pirajno 2010).

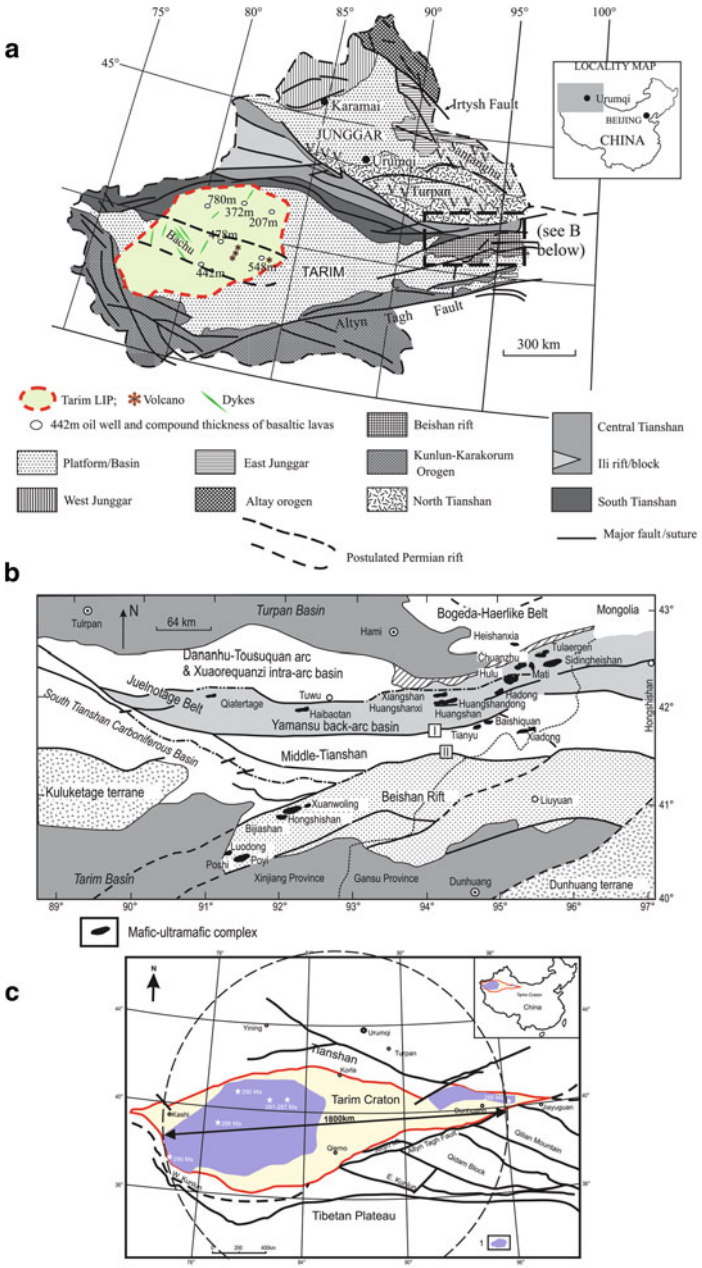

Fig. 7.10 **a** Extent of the ca. 291–272 Ma LIP in the Tarim Basin, estimated from oil wells and seismic profiles (Zhou et al. 2009; Tian et al. 2010), the position and compound thickness of basaltic lavas from drillholes are approximate; **b** mafic-ultramafic complexes in the Beishan rift and in the eastern Tianshan, where the Huangshan and Huangshanxi Ni-Cu deposits are located, I Aqikuduke-Shaquanzi Fault, II Hongliuhe Fault (this figure is modified after Su et al. 2011b); **c** inferred total extent of the Tarim LIP; mafic-ultramafic complexes, dykes, tholeiitic volcanic rocks, as well as rhyolites and A-type granites in the same age range, tholeiitic rocks also occur in the Turpan and Santanghu basins and on the southwestern margin of the Junggar basin. (Tian et al. 2010)

A question remains about the Tarim LIP, which does not seem to have been addressed by the above mentioned researchers. If it is accepted that a mantle plume was responsible for the emplacement of flood basalt in the Tarim, a feeder or feeders must have been present to channel mafic melts through to the surface. The occurrence of poorly exposed dyke swarms, such as the Bachu dykes, and of volcanic edifices as revealed by seismic profiling (Tian et al. 2010) suggest the possibility of a rift system, extending at least for 600 km in the central parts of the Tarim craton (Fig. 7.10a). Indeed, and as shown in Fig. 8.5, a rift basin of Permian age was postulated by Li et al. (1996), largely on the basis of the Tarim basin sedimentary successions and tectonic evolution. Therefore it can be hypothesised that this rift system may have been formed by a mantle plume impacting to the base of the subcontinental lithospheric mantle, followed by the emplacement of layered mafic-ultramafic intrusions, dyke swarms and flood basalts. The association of rift systems with plume-related intraplate igneous provinces is widely recognised, as shown by the East African Rift System, the Siberian rifts and East Antarctic rifts (e.g. Borisenko et al. 2006; Pirajno 2011; Ferraccioli et al. 2011).

It is worth mentioning that rift-related continental basalt flood volcanism and mafic dyke swarms occurred at about 284–280 Ma in Tethyan Himalaya of South Tibet (Nar-Tsum, Bhote Kosi and Selong basalts), which are coeval with the Panjal Traps and Permian granites in the High Himalaya (Garzanti et al. 1999). Following on from Garzanti et al. (1999), Zhu et al. (2012) interpreted this continental magmatism as being related to mantle plume activity that resuled in the formation of a 2,000 km long rift, leading to the breakup of northern Gondwana and opening of the Neo-Tethys ocean. The almost identical age of the Panjal-South Tibet continental magmatism with the Tarim event, could be interpreted that they are part of the same mantle plume (or superplume?). If this interpretation is valid, then the prospectivity for orthomagmatic Cu-Ni deposits that characterise the Tarim event could be extended to South Tibet.

7.5.1 Mineral Systems

The Tarim LIP has considerable economic potential. Known orthomagmatic Ni-Cu ore deposits that belong to this event are (Fig. 6.35):

- Kalatongke Ni-Cu sulphide deposit in the Altay orogen (Chap. 6)
- Huangshan-Huangshanxi-Jing'erquan Ni-Cu ore belt in eastern Tianshan (Chap. 6)
- The Pobei (Poyi, Poshi, Luodong) Ni-Cu sulphide deposits in Beishan rift (this section)
- Beishiquan Ni-Cu deposit (this section)

Pirajno et al. (2008) examined the nature of mafic-ultramafic intrusions and associated Ni-Cu magmatic ore deposits in NW China. Most of these intrusions are funnel-shaped and concentrically zoned with lenses of ultramafic rocks enclosed in

an envelope of gabbroic composition. These zoned mafic-ultramafic intrusions have some features that are comparable with Alaskan-type complexes. Taking into consideration the spatial-temporal relationship of these mafic, mafic-ultramafic complexes with coeval A-type granites, I concur with Zhang et al. (2007, 2008, 2010b) that these magmatic events occurred during an extensional regime, possibly related to a mantle superplume event that affected much of central Asia in the Permian, of which the 250 Ma Greater Siberian LIP, and the (260 Ma) Emeishan LIP, together with the 291–272 Ma Tarim event, are part. Apart from the orthomagmatic Ni-Cu in the eastern Tianshan and the Altay orogenic belt, briefly described in Chap. 6, not much is really known at this point in time about mineral deposits that can be ascribed to the Tarim LIP in China. These igneous systems and associated Ni-Cu sulphide mineralisation cannot be related to subduction tectonics, but are attributed to post-collisional Permo-Triassic intraplate magmatic activity that is ultimately linked either with the activity of a mantle plume, or with upwelling asthenospheric melts. These funnel-shaped zoned mafic-ultramafic intrusions are spatially associated with networks of orogen-scale strike-slip faults, up to several hundred kilometres long and tens of kilometres wide, common in central and south Asia. More specifically, these intrusions are emplaced during post-collision extensional processes leading to the formation of pull-apart basins in the strike-slip shear zones. Pirajno (2010) proposed a model of lateral flow from the plume head, towards regions of lower pressure, which are provided by transcrustal and/or translithospheric structures and shear bounded crustal-lithospheric blocks. Alternatively, translithospheric strike-slip faulting channel magmas derived from partial melting of thickened juvenile mafic lower crust or delaminated mafic lower crust, triggered by upwelling asthenospheric material. This mantle flow and subsequent upwelling may be the "root" cause of magmatism and the generation and re-activation of pre-existing mineral systems. Begg et al. (2010), on the other hand, hypothesised that cratonic margins are particularly suitable to channel mantle plume flow towards thinner lithosphere (see Fig. 2 of Begg et al. 2010 and note in Concluding remarks).

7.5.1.1 Pobei (Poyi-Poshi)

The Pobei area in the southwest of the Beishan rift (Fig. 7.10b, see also Fig. 6.35), is underlain by Proterozoic metamorphic basement rocks and Carboniferous lavas, pyroclastic rocks and marble beds. The U-Pb ages of zircons from mafic and felsic rocks in the Beishan rift (Figs. 7.10b and 7.11) range from ca. 284 to 251 Ma, with zircons from the Pobei gabbro yielding U-Pb ages from 284.0 ± 2.2 to 274.0 ± 4.0 Ma (Su et al. 2011a, b), well within the range of the Tarim thermal event. The Pobei intrusions were emplaced within a major transtentional northeast-trending strike-slip shear zone (Fig. 7.11).

There are at least three ultramafic intrusions, enclosed in the Pobei gabbro body, namely: Poyi, Poshi and Luodong (Fig. 7.11; Mao et al. 2008; Pirajno et al. 2008). The following is summarised from Mao et al. (2008).

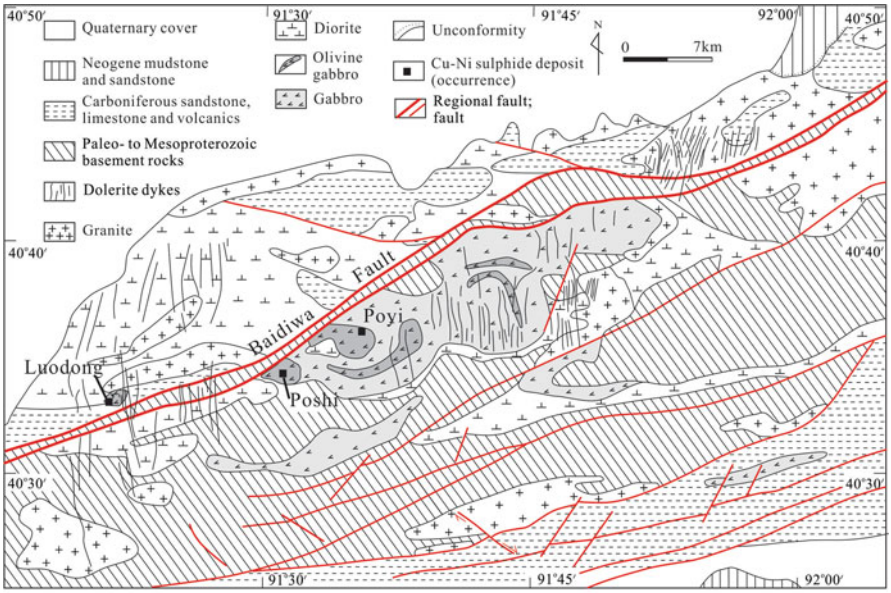

a

b

Fig. 7.11 **a** Simplified geology of the Pobei area and distribution of the Poyi, Poshi and Luodong ultramafic intrusions, locally containing Ni-Cu sulphide mineralisation (after Mao et al. 2008a); **b** field photograph of the Poshi ultramafic zone (eroded and forming a low-lying area), surrounded by massive Pobei gabbro rocks

The Ni-Cu mineralisation in Poyi and in Poshi was discovered in 1989 by the No. 6 Geological Party of the Xinjiang Bureau of Geology and Mineral Exploration and Development. At a later stage, Yang et al. (2003) found the Luodong intrusion, on the north side of the Baidiwa fault (Fig. 7.11), by using remote sensing image interpretation and field follow-up, which led to the discovery of Cu-Ni sulphide mineralisation. As mentioned above, these intrusions typically consist of ultramafic zones, enclosed by a larger east-northeast-trending gabbroic body, along the Baidiwa Fault (Fig. 7.11). The ultramafic rocks probably post-date the gabbro. The Poyi ultramafic intrusion, has a trapezoidal shape in plan view, is up to 3.2 km long from east to west and ca. 1.08 km wide from north to south, with an outcrop area of 3.6 km^2. The Poshi ultramafic intrusion has an elliptical shape and is located west of Poyi (Fig. 7.11) and is about 2 km long from east to west and 1.6 km wide from north to south, with an outcrop area of 3.2 km^2 (Fig. 7.12). To the west and on the north side of the Baidiwa fault is the 370 m long and 210 m wide Luodong complex (Fig. 7.11), which consists of gabbro, olivine gabbro, peridotite, harzburgite, and pyroxenite. Although the surface geochemical Ni and Cu anomalies over the Poyi ultramafic body are pronounced, most Ni is contained in the olivine and no sulphide zones have been identified.

In the Poshi ultramafic rocks, exploration drilling has outlined four outcropping sulphide zones and five below the surface. The outcropping mineralisation has a semi-circular shape (Fig. 7.12a). The sulphide mineralisation forms lensoid bodies, which approximately follow the shape of the lithological zones (Fig. 7.12b). Grades range from 0.3 to 0.6 % Ni with maximum values of up to 0.96 %. Copper and Co contents are generally low but tend to increase in ore zones where the Ni content is greater than 0.6 %. The Ni resources in the Poshi complex are 147,000 tonnes, but exploration is ongoing. The dominant ore minerals are pentlandite, chalcopyrite, pyrrhotite, magnetite, and chrome-spinel with very small amounts of vallerite, bornite, and millerite. The sulphides have euhedral-subhedral granular textures and locally form net-textured ore zones, but usually occur as sparse disseminations, locally densely disseminated and massive ores.

7.5.1.2 Beishiquan

The Beishiquan (Baishiquan) mafic-ultramafic intrusion occurs within the Aqikuduke-Shaquanzi fault zone in the Middle Tianshan, south of the world-class Huangshan Ni-Cu ore belt (Fig. 7.10). The U-Pb age of the gabbro component in the Beishiquan intrusion is reported as ca. 282 Ma (Mao et al. 2006) and ca. 284 Ma (Wu et al. 2005). The Beishiquan intrusion and associated sulphide mineralisation was studied by Chai et al. (2008), who focused their work on the petrography, major and trace element geochemistry and radiogenic isotope systematics. The Beishiquan intrusions are composed mainly of olivine pyroxenite, pyroxene peridotite, troctolite, hornblendite, diorite, norite and gabbro. These were emplaced in two stages. The first stage comprises 90 % of the complex and consists of diorite, gabbro and norite. The contacts between these rocks are gradational. The second stage is represented

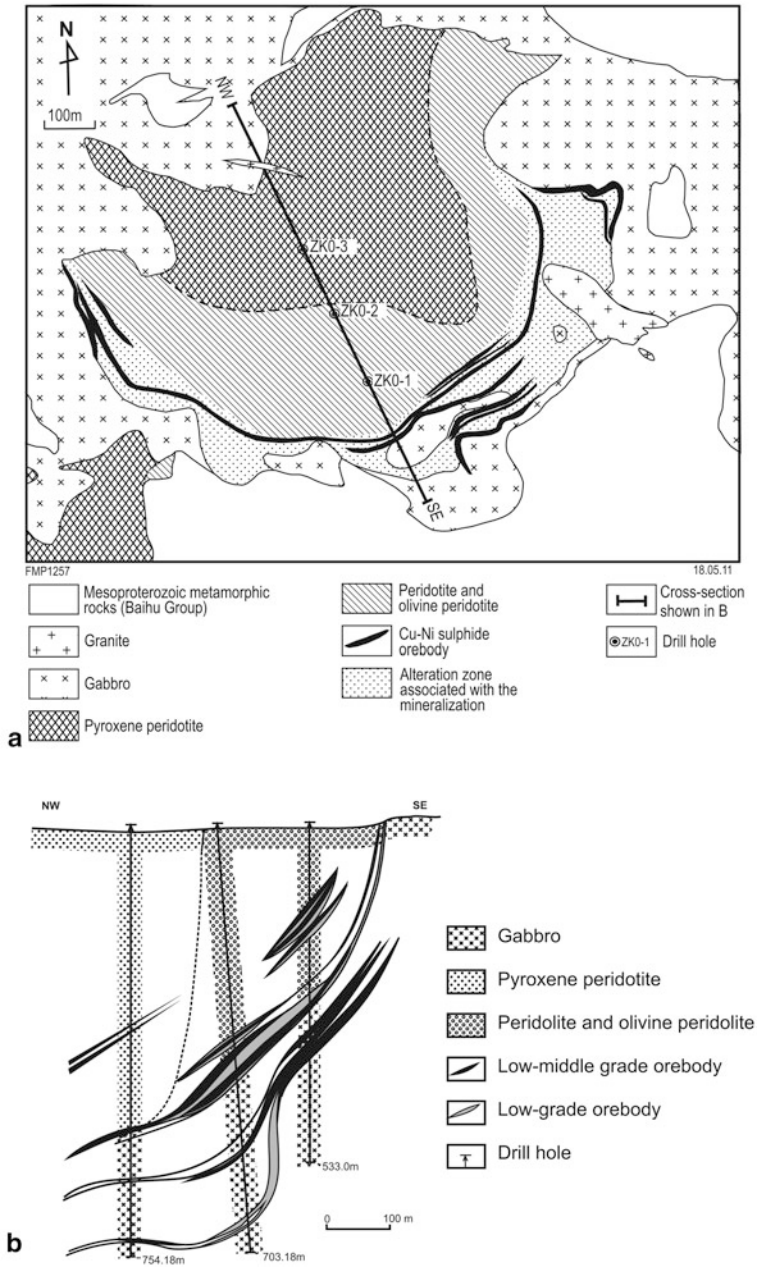

Fig. 7.12 **a** Geological map of the Poshi intrusion and Ni-Cu sulphide zones; **b** cross-section. (After Mao et al. 2009)

by dykes and elliptical bodies of hornblendite, peridotite, troctolite and pyroxenite, which in contrast to the first stage intrusions, have sharp contacts. As generally seen in the mafic-ultramafic intrusions within strike-slip shear zones, the ultramafic rocks are commonly altered to talc and serpentine. Peridotite and olivine-pyroxenite host Cu–Ni sulphides, which form small lenses near the base of these lithologies. Ore minerals comprise chalcopyrite, pyrite and pyrrhotite, forming disseminations and veins. A field examination and petrographic analysis of samples collected in 2005, revealed features not recognised or reported in the recent literature, such as the presence of anorthosite. The Beishiquan intrusion remains to be fully evaluated.

7.6 Emeishan Large Igneous Province

The Emeishan Large Igneous province (ELIP) covers an area of at least 250,000 km^2 (Chung and Jahn 1995; Chung et al. 1998) in southwest China (Yunnan, Sichuan and Guizhou provinces), and in northwest Vietnam (Figs. 7.1 and 7.13). The western boundary of the ELIP is the Ailao Shan-Red River Fault zone, a major crustal structure separating the Yangtze Craton from the Gandese and Yunnan fold belts (Fig. 7.13). The ELIP is one of the best studied large igneous provinces of the planet. In the last 15 years or so, perhaps more papers have been published in both Chinese and English language than in any other large igneous province in the rest of the world. Indeed, research on the ELIP continues vigourously, covering a wide range of important issues, such as mass extinctions (Wignall et al. 2009), arguments for and against domal uplift due to the impact of a mantle plume (He et al. 2003; Peate and Bryan 2008), petrogenesis of low- and high-Ti basalts and mantle plume-lithosphere interactions (Xiao et al. 2004b; He et al. 2010a) and of course magmatic sulphide and oxide mineral systems that were formed in the ELIP (see below). Some of the key works perused for this section, include: Xu et al. (2001, 2004a), Xiao et al. (2003, 2004a, b), Ali et al. (2002, 2004, 2005, 2010), Shellnutt and Zhou (2007), Shellnutt and Jahn (2009), the collection of papers in Shellnutt et al. (2010), practically covering most of the above-mentioned topics.

The ELIP consists of a succession of predominantly tholeiites, with minor picritic and rhyolitic lava flows and associated pyroclastic rocks. In addition to lava flows, mafic-ultramafic layered complexes, dykes and sills, syenite and other alkaline intrusions (A-type granites), are part of the ELIP. The maximum thickness of the lava flows is estimated at about 5,400 m in the Panxi (or Pan-Xi, abbreviated from Panzhihua and Xichang regions) rift, decreasing to less than 500 m eastward from the rift (Xiao et al. 2003, 2004a, b; Xu et al. 2004a). In the Binchuan area (Panxi rift) the volcanic stratigraphy (Xiao et al. 2003, 2004a, b) consists of six units from amygdaloidal basalts (Unit 1 at the base), hyaloclastites, aphyric basalts (Unit 2), porphyritic and aphyric basalts, hyaloclastites (Units 3, 4 and 5) to trachytic lavas (Unit 6) at the top (Fig. 7.14). At Jinping, the volcanic succession is about 4,000 m, comprising basaltic hyaloclastites, amygdaloidal basalts, aphyric and plagioclase-phyric basalts (Fig. 7.14b). The ELIP volcanic successions overlie limestones of the

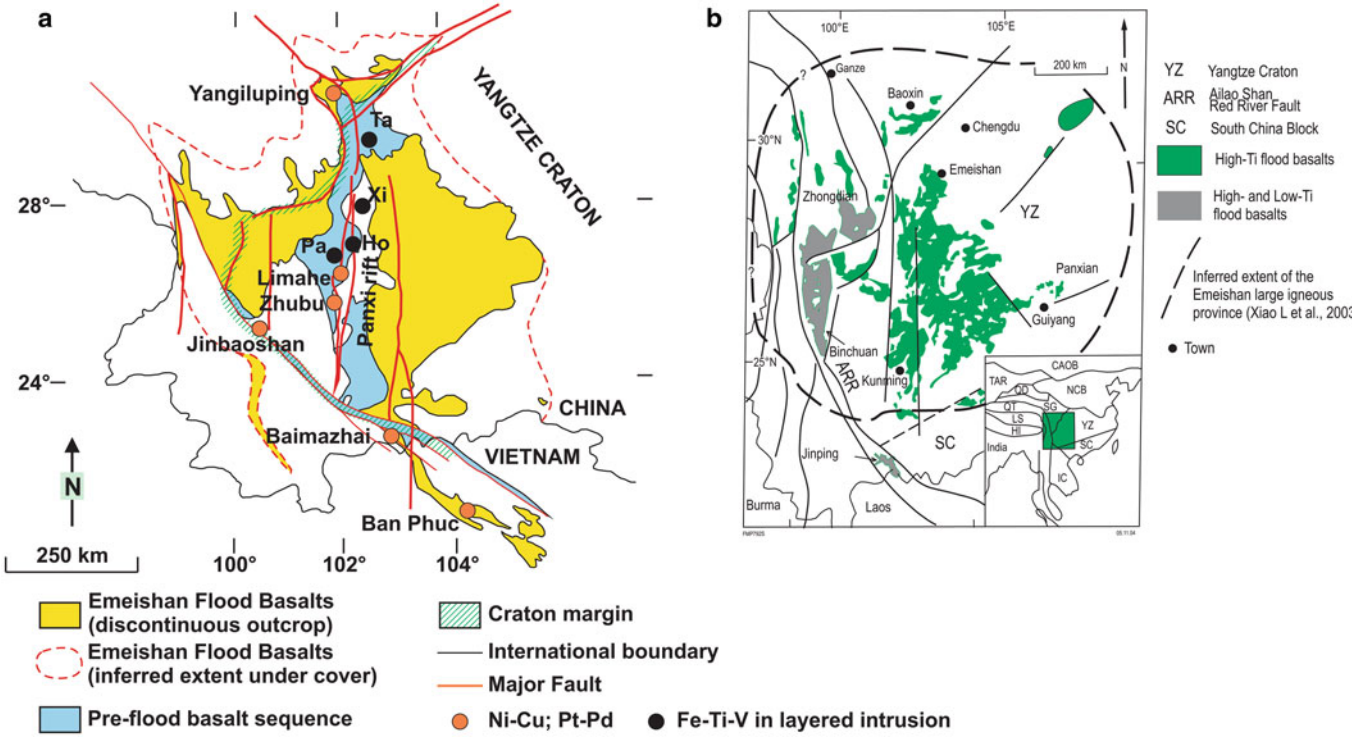

Fig. 7.13 **a** Inferred extent of the Emeishan large igneous province and approximate distribution of Ni-Cu sulphide and PGE-dominated deposits (names of deposits in full; Zhang et al. 2006c) and Fe-Ti-V deposits in layered intrusions (names of deposits abbreviated to avoid cluttering, Ho Hongge, Pa Panzhihua, Ta Tahe Xi Xinjie); **b** one of several versions representing the distribution of the Emeishan flood basalts in southwest China (this is based and modified from Chung and Jahn 1995; Chung et al. 1998); *inset* shows position of the ELIP in the context of adjacent tectonic domains; *CAOB* Central Asian Orogenic Belt, *TAR* Tarim, *NCC* North China Craton, *QD* Qaidam, *QT* Qunlun, *HI* Himalayan orogenic belt, *LS* Lhasa Block, *IC* Indochina, *SC* South China, *YZ* Yangtze Craton *SG* Songpan-Ganzi

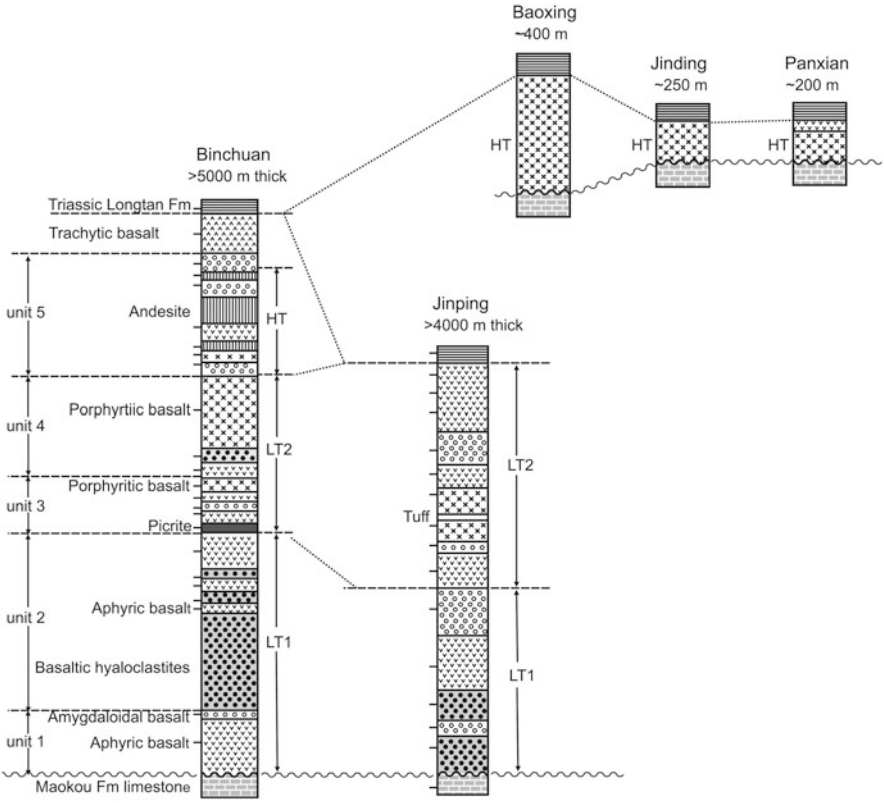

Fig. 7.14 Lithostratigraphy of the Emeishan volcanic rocks in the Binchuan, Jinping, Baoxing, Jinding and Panxian areas (see Fig. 7.12 for positions of these localities). (Adapted from Xiao et al. 2003)

Mid-Permian Maokou Formation and are overlain by Triassic clastic sedimentary rocks (Longtan Formation).

Xu et al. (2001) distinguished two main magma types that produced the lava flows, low-Ti (Ti/Y < 500; Mg# 51–63; εNd(t) −1.8- +1.4) and high-Ti (Ti/Y > 500; Mg# 30–45; εNd(t) +1.1- +4.8), with the latter (high-Ti type) further subdivided into three subtypes, HT1, HT2 and HT3. The HT1 is characterized by significant high TiO_2 (3.65–4.7 wt%) and Nb/La (0.75–1.1) and low SiO_2 (45–51 wt%); HT2 lavas are geochemically similar to HT1 except that they are depleted in U and Th with respect to HT1; HT3 lavas have higher Mg# (0.51–0.61). Based on geochemistry, Xiao et al. (2003, 2004a, b) distinguished two types of low-Ti magmas, LT1 and LT2. LT1 lavas exhibit higher Mg# (51–67) and ($^{87}Sr/^{86}Sr$)I ratios (0.706–0.707) than the LT2 lavas. The lithostratigraphy of the Emeishan volcanic rocks at Binchuan (Fig. 7.14), shows that LT1 and LT2 are overlain by the HT lavas. The results of these studies suggest mantle-lithosphere interactions that have been interpreted in

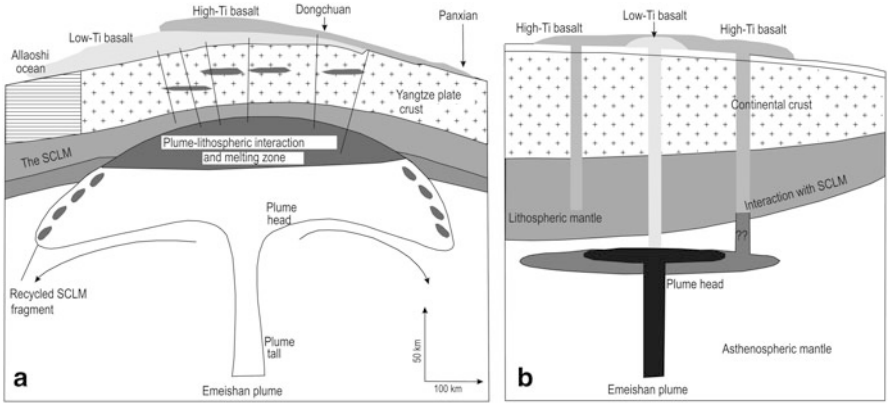

Fig. 7.15 Models that attempt to explain the source of high-Ti and low-Ti basalts in the Emeishan large igneous province; **a** from Xiao et al. (2004b) and **b** from Xu et al. (2007); more details in text

different ways. One view is that the ELIP low-Ti melts were derived from enriched subcontinental mantle lithosphere (SCLM) (Fig. 7.15a), with a trend from shallower (LT1) to deeper lithospheric mantle (LT2). The HT magmas, on the other hand, apparently may have formed directly from the melting zone of the mantle plume head (Fig. 7.15a; Xiao et al. 2004b; Chen et al. 2010). In another view, Xu et al. (2007) suggested that low-Ti basalts originated from the plume head, whereas high-Ti basalts from melting of the SCLM and/or plume melts interacting with SCLM (Fig. 7.15b). On the other hand, He et al. (2010a) proposed that the petrogenesis of high-Ti and low-Ti basalts is related to thermal zonations within the melting column of the mantle plume. More specifically, these authors suggested on geochemical and isotopic grounds, that the high-Ti were produced from deep melting plume zones and have a geochemical signature similar to ocean island basalt (OIB), whereas the low-Ti are generated by melting of the plume head at shallower levels (Fig. 7.16). In their work, He et al. (2010a) used Gd/Yb values to estimate depth of melting and La/Yb values to estimate the degree of partial melting.

SHRIMP zircon U-Pb dating of ELIP mafic and ultramafic intrusions yielded ages ranging from 259 ± 3 to 263 ± 3 Ma (Guo et al. 2004; Zhang et al. 2009), and volcanism is inferred to have taken place over a similar short interval of 257–263 (He et al. 2007). Additional $^{40}Ar/^{39}Ar$ ages (Ali et al. 2004) yielded younger ages, ranging from 147 to 42 Ma, which they attributed to thermal resetting due to tectonic events that affected the western Yangtze Craton between the Jurassic-Cretaceous (Yanshanian orogeny) and the Eocene (Himalayan-Alpine orogeny). This has important implications, because one or both of these thermal resets may have affected and modified the host rocks and magmatic sulphide ores at Baimazhai and at the Niulanchong Ni prospect, to be discussed in the mineral systems section.

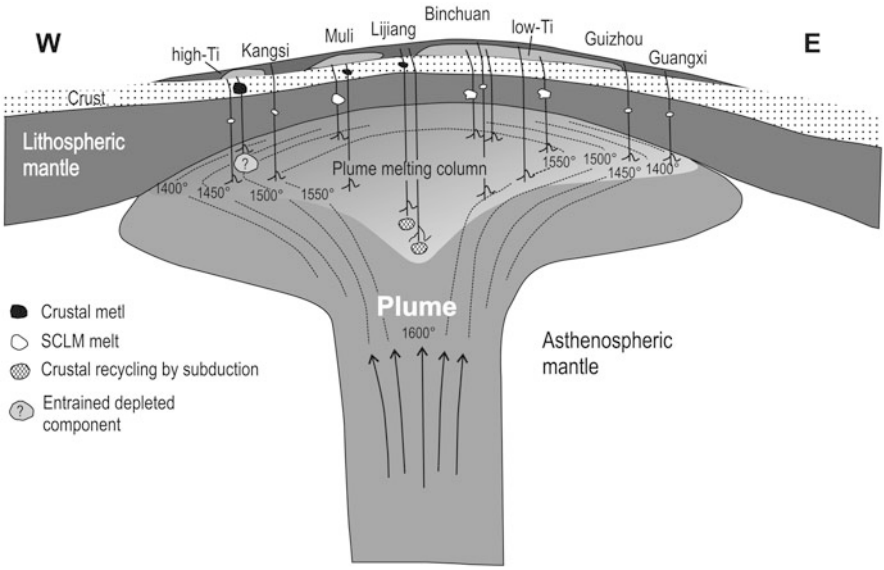

Fig. 7.16 Latest model to explain the spatial range of Emeishan basaltic lavas from deep plume melting to plume-lithosphere interaction. (After He et al. 2010a)

7.6.1 The Emeishan Mantle Plume

The emplacement age of the ELIP indicates that it is close (10 Myr older) with the Siberian LIP (Siberian Traps; Dobretsov 2005), which hosts the world-class Noril'sk Cu-Ni-PGE deposits (Naldrett 2004; Lightfoot and Keays 2005). The near contemporaneity of the Emeishan, Siberian and Tarim events (see below) also led to proposals of a possible Ni-Cu-PGE enriched superplume activity (Yakubchuk and Nikishin 2004) or to a flare-up of mantle plume (superplume) activity in the age brackets of 280–250 Ma (Dobretsov 2005; Borisenko et al. 2006). Magma underplating is inferred from seismic reflection and refraction studies, which revealed high-velocity layers (P-wave velocity) in the upper and lower crust (Vp of 6.0–6.6 km/s and 7.1–7.8 km/s, respectively), as well as upper mantle (8.4–8.6 km/s), where the high Vp zone forms a well-defined lens about 200 km long and 40 km thick (Xu and He 2007; Chen et al. 2010). Furthermore, Xu and He (2007) pointed out that these high velocity layers are confined within the inner zone of a domal structure, which was probably part of a crustal uplift caused by the impingement of the Emeishan mantle plume. The actual extent of the ELIP is difficult to gauge due to the fact that parts of the ELIP were deformed and/or dismembered during Triassic and Cenozoic tectonic movements (e.g. strike-slip along the Ailaoshan-Red River Fault), as well tectonic events related to the closure of the Palaeo-Tethys Ocean (Xiao et al. 2008). The geometry and manifestations of the Emeishan mantle plume are illustrated in Figs. 7.15

and 7.16. The geodynamic evolution of the region in the context of the mantle plume model for the ELIP is shown in Fig. 7.17.

The case of crustal doming associated with the Emeishan flood volcanism and by inference with other large igneous provinces, was elegantly proven by detailed sedimentological studies conducted on the Maokou Formation by He et al. (2003, 2006). The thickness variations of the Maokou Formation shows spatial variations from west to east and an unconformity with the overlying Emeishan basalts, marked by a basla conglomerate along the contact. In addition, palaeosols and karst features are preserved in the outer zones from the uplift and these areas of palaeo-weathering also endowed with regolith-style mineralisation, such as industrial clays, Mn oxides and bauxite. However, this model was disputed by Peate and Bryan (2008). These authors interpreted the alluvial fan sediments, considered by He et al. (2003) as having been deposited along the flanks of a pre-volcanic domal uplift, as submarine hydromagmatic (volcaniclastic) deposits, thereby discounting a domal uplift entirely. But, Ali et al. (2010) and He et al. (2010b) provided further arguments to support the crustal uplift model, largely based on the undisputable evidence of the presence of sinkholes, palaeokarsts and palaeosols at the top of the Maokou Formation, spatially arranged from the domal uplift outward towards the palaeosealevel (see Fig. 8 in He et al. 2010b). A mantle plume impacting the lithosphere does not need, and most probably will not have a symmetrical geometry, as depicted in many simple experimental laboratory models. Tomographic images show that most plumes are not simple vertical structures. Rather, lithosphere heterogeneities and deep fracture systems all contribute to what could be a very uneven uplift, with local subsidences, not to mention later far-field tectonic events. All these features need to be taken into consideration, resulting in a range of possible structures and igneous systems, as exemplified by the 1,070 Ma Warakurna province in Western Australia (Pirajno and Hoatson 2012), manifested by layered mafic-ultramafic complexes and felsic igneous rocks, rapidly uplifted at the eastern end during later tectonics, through to sedimentary basins, sill complexes, dykes and basaltic lavas at the central and western end of the province. The mantle plume model, especially when considered in conjuction with the Siberian and Tarim thermal events, best explains the ELIP and surrounding features. The north-south-trending faults, within which mafic-ultramafic complexes are located, are near and at the inferred domal uplift, resulting in the exposure of Precambrian basement and the Emeishan mafic-ultramafic complexes from the lower levels of the ELIP (Fig. 7.13).

7.6.2 Mineral Systems

In the ELIP magmatic ore deposits include the Ni-Cu-PGE sulphides at Baimazhai, Niulanchong, Yangliuping and Limahe (Tang et al. 1992; Song et al. 2003, 2005; Zhou et al. 2002b; Zhang et al. 2006c), the PGE-dominated Lufangqing, Bading, Dayanzi and Jinbaoshan deposits (Yao et al. 2001; Wang et al. 2005), the Hongge Fe-V-Ti oxide ores (Zhong et al. 2002, 2003) and the Fe-V-Ti-(PGE) ores in the Panxi

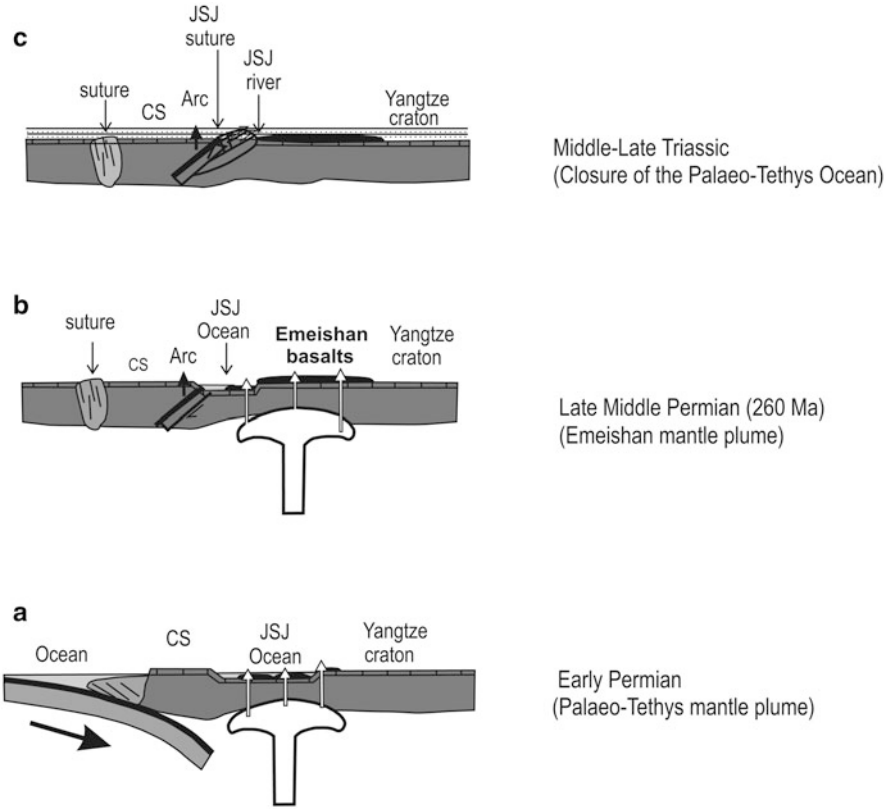

Fig. 7.17 Permian-Triassic geodynamic evolution of the western margin of Yangtze Craton associated with the Emeishan mantle plume and the closure of the Palaeotethys ocean, now marked by the Jinshajiang suture (JSJ); this oceanic arm formed in a rift created by crustal uplift, due to the mantle impingement, resulting in the eruption of volcanic rocks and of volcanic rifted margins (**a**), the Emeishan mantle plume was active to the east along the western margin of the Yangtze Craton at about 260 Ma that produced Emeishan flood basalts (**b**), the impingement of the Emeishan plume resulted in uplift and rifting that formed the Panzhihua- Xichang Rift in western Sichuan, followed by extension and rifting along the Ganze-Litang suture, which separated the Zhongza terrane from the western Yangtze craton margin. In the late Permian, the Jinshajiang ocean ceased its spreading and began its subduction stage, directed westward beneath the Changdu-Simao (CS) block. The time frame (**c**) illustrates the final closure of the Jinshajiang Ocean, while westward subduction generated arc-type volcanic and intrusive rocks of the Jiangda-Weixi arc to the west of the Jinshajiang suture. This subduction also partly destroyed and/or tectonically sliced the volcanic rifted margin, resulting in a complex mélange system with ophiolite-like rocks now strung out along the Jinshajiang-Ailaoshan suture zone, illustrating the challenge facing geoscientists in attempting to unravel the complexities of the ELIP in terms of deformation and dismembering along the western margin of the Yangtze Craton. (After Xiao et al. 2008)

district (e.g. Panzhihua and Xinjie; Zhou et al. 2005; Zhu et al. 2010). The gabbroic intrusions that host Fe-Ti-V oxide deposits are also somewhat enriched in PGE (Yao et al. 2001). The Panzhihua, Hongge, Baima and Taihe intrusions (Fig. 7.13) have been estimated to contain total resources of oxide ores of about 7.54 billion tonnes, averaging 36 % Fe, 0.28 % V_2O_5 and 12.6 % TiO_2 (Ma et al. 2003; Zhou et al. 2005). Detailed descriptions of Limahe and Baimazhai as Ni deposits can be found in Tang et al. (1992), and of Panzhihua Fe-V-Ti deposit in Zhou et al. (2005). Rare earth (REE) mineralisation was reported in a number of quartz-syenite-carbonatite intrusions within the Panxi rift (Niu et al. 2003). Exposures of the ELIP are present in northwestern Vietnam, where a komatiite-basalt complex hosts the Ban Phuc Ni-Cu-PGE deposit (Glotov et al. 2001). In addition, Keeweenawan-type deposits (native Cu in amygdaloidal basaltic lavas and associated sedimentary rocks) have been reported along the border area between Yunnan and Guizhou provinces (Zhu et al. 2003b; Mao et al. 2003; Li et al. 2005a). Native gold was detected in picritic lavas (Zhang et al. 2006b).

Below, I describe a selection of mineral deposits, including: Baimazhai Ni-Cu, Limahe Ni-Cu, Panzhihua and Hongge Fe-Ti-V, Jinbaoshan Pt-Pd and briefly the REE deposits associated with alkaline complexes. SHRIMP zircon U-Pb dating of the Baimazhai intrusion yielded an age of 258.5 ± 3.5 Ma (Wang et al. 2004b); ages of 263 ± 3 and 262 ± 2 Ma were obtained for the Panzhihua and Baima gabbroic rocks hosting Fe-Ti-V deposits, respectively and 263 ± 3 Ma for the Limahe Ni-Cu sulphide deposit (Zhou et al. 2005). SHRIMP U-Pb dating of zircons from mineralised gabbro of the Hongge intrusion yielded a concordia age of 259 ± 1.3 Ma (Zhong and Zhu 2006). All these deposits are coeval with the Emeishan flood basalts, with which the mafic-ultramafic rocks hosting the magmatic sulphides and oxides deposits are intimately associated.

7.6.2.1 Baimazhai Ni-Cu

The Baimazhai Ni-Cu deposit is located near the town of Jinping, on the southwest margin of the Yangtze Craton, and within the Jinping-Song Da rift, in southeast Yunnan Province (Fig. 7.13). The geology, geochemistry and origin of the Baimazhai deposit have been reported by Tang et al. (1992), Wang et al. (2004b), Wang and Zhou (2006) and Zhang et al. (2006c). Other publications that deal with various aspects of the Baimazhai deposit include Song et al. (2003, 2005) and Zhang et al. (2004, 2005). The following is extracted from Zhang et al. (2006c and references therein).

The area around Jinping is underlain by Lower Ordovician clastic sedimentary rocks, Silurian and Devonian siltstone, shale and limestone. These sedimentary rocks are intruded by northwest-trending mafic and ultramafic layered sill-like bodies extending along a strike of about 20 km. To the west of this mafic-ultramafic sill zone and separated by a northwest-trending fault, is a thick (about 4.5 km) succession of basaltic rocks (Fig. 7.14b). Syenite porphyry and lamprophyre dykes crosscut the

sedimentary, volcanic rocks and the sills. To the east of the zone of sills are elongate intrusions of biotite granite, quartz monzonite and nepheline-acmite syenite.

The Baimazhai Ni-Cu sulphides deposit is hosted by three mafic-ultramafic intrusions (No. 1, 2, 3; Fig. 7.18) emplaced into Lower Ordovician sedimentary rocks of the Baimazhai Formation (locally also known as Xiangyang Formation). The No. 2 and 3 intrusions contain massive sulphides, but only No. 3 has economically viable grades (Ni and Cu up to 3.5 and 2.3 %, respectively; Wang and Zhou 2005). The deposit in No. 3 intrusion has reserves of 50,000 t of Ni metal, with a total resource of about 100,000 t of Ni metal (unpublished data from mine staff, 2003). The No. 3 intrusion is banana-shaped, approximately 500 m long, 190 m wide and up to 64 m thick (Tang et al. 1992; Wang and Zhou 2005), and consists of a mafic shell enclosing a core of ultramafic rocks, which host the massive sulphides (Fig. 7.18a, b). From the margins to the core, rock types are: gabbro, pyroxenite, olivine-pyroxenite, and peridotite. These rock types, all show near-pervasive to pervasive alteration to assemblages containing varying amounts of amphibole, chlorite, quartz, talc and carbonate. The cross-cutting lamprophyre dykes are not affected by this hydrothermal alteration. Gabbro and pyroxenite have sharp contacts. Pyroxenite has fine-grained marginal or border facies suggesting that it was formed later.

The gabbro is from 2 to 55 m thick and forms the outer shell of the No. 3 intrusion. The gabbro is thinner at the base of the intrusion and thicker along the edges and tends to become richer in Fe-Mg silicate minerals towards the centre. The gabbro is fine-grained with a hypidiomorphic-granular texture and is composed mainly of plagioclase, pyroxene, brown hornblende, with accessory quartz, ilmenite, magnetite and sulphides. Plagioclase is generally replaced by prehnite, penninite and calcite and in most instances only the original outline of the crystals remained. Brown hornblende forms subhedral grains and is commonly replaced by tremolite-actinolite and more rarely talc and penninite (Tang et al. 1992). The mineral assemblage of the least altered rock consists of plagioclase (about 40–60 vol%), clinopyroxene (up to 30 vol%), tremolite (up to 50 vol% in places) which tends to replace the pyroxene. Ilmenite and apatite (3–5 vol%) are accessory minerals. Where present, alteration is pervasive and includes assemblages containing various proportions of epidote, carbonate, biotite, quartz, chlorite and tremolite-actinolite and talc. Pyroxenite, from 2 to 9.5 m thick, is situated between the gabbro and olivine-pyroxenite, but in the northern parts is in direct contact with peridotite. Locally, there is a transitional zone to the olivine-pyroxenite, with increasing olivine content, but elsewhere the contacts are sharp. Pyroxenite is also strongly altered with chlorite, talc and tremolite and with minor alteration phases including serpentine, actinolite, and clinochlore. Although most or all primary rock-forming minerals have been completely altered, the original minerals can be recognised by the crystal shapes. On this basis this rock type is composed of short prismatic pyroxene crystals (0.2–1.2 mm in size), long prismatic brown hornblende (0.3–1.6 mm in size), some olivine and accessory ilmenite, magnetite, chrome spinel and sulphides (Tang et al. 1992). Olivine-pyroxenite, from 0.5 to 13 m thick, surrounds the peridotite unit, with sharp contacts near the surface and subsurface, but with transitional contacts at depth. All primary minerals are altered to talc (40–55 vol%), tremolite (20–40 vol %), serpentine olivine pseudomorphs

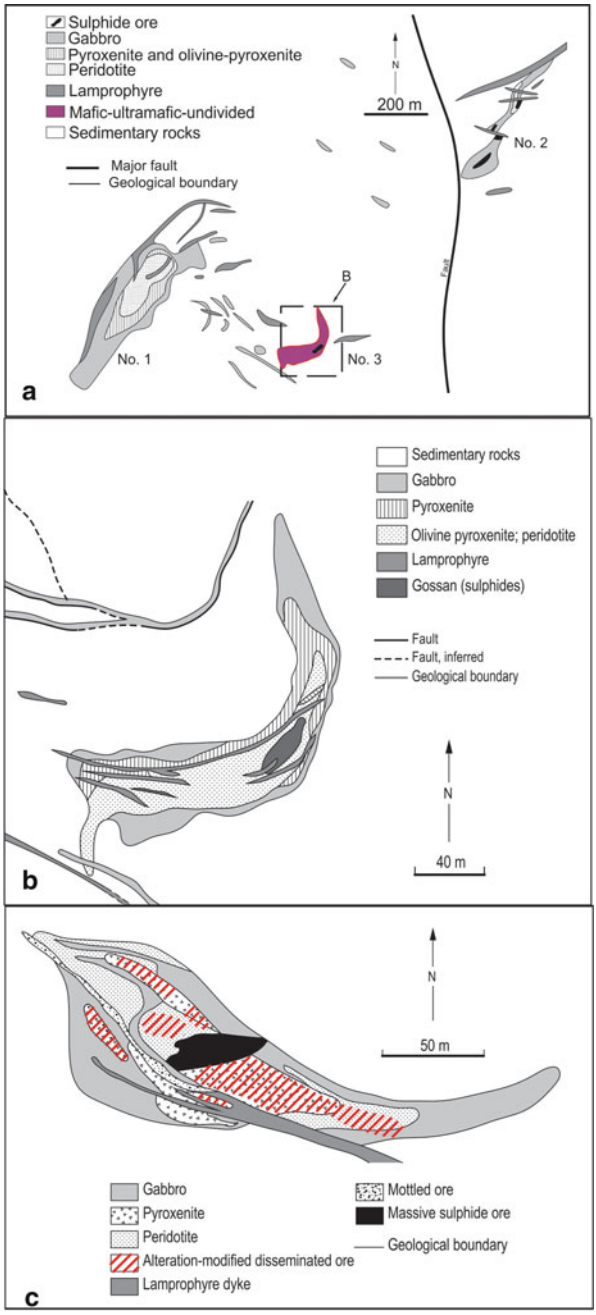

Fig. 7.18 **a** Baimazhai No. 1, 2 and 3 mafic-ultramafic intrusions; **b** geology of the No. 3 intrusion and **c** Level 11 Ni-Cu orebody. (After Zhang et al. 2006c)

(10–30 vol%) and lesser quantities of carbonate (dolomite), quartz, chlorite, mica phlogopite, sphene and apatite. In the lower parts this rock is entirely altered to talc-carbonate, and locally with biotite alteration. Peridotite, is 9 m-thick and is at the core of the intrusion and generally forms a ring around the sulphide ores. The peridotite has a hypidiomorphic granular texture or a cumulus-intercumulus texture where sulphides are present. Peridotite too is strongly altered, but retains the original shape of its component crystals (pseudomorphs). Primary minerals include olivine, clino- and orthopyroxene, and brown hornblende with accessory ilmenite, magnetite, chrome spinel and sulphides. Olivine pseudomorphs make up about 30–60 vol%. This olivine is present as euhedral crystals from 0.2 to 1 mm in size, and entirely replaced by antigorite, tremolite and talc. Likewise, orthopyroxene is replaced serpentine and talc, whereas clinopyroxene is replaced by tremolite, clinochlore and penninite. Brown hornblende is replaced by tremolite and penninite. Other alteration minerals are carbonate, phlogopite, actinolite-tremolite and biotite.

At Baimazhai the styles of sulphide mineralisation are: disseminated, alteration-modified disseminated, net-textured and massive ores (Fig. 7.18b, c). Disseminated sulphides are present in gabbro and pyroxenite and are generally distributed around the margins of massive sulphides, effectively forming a shell. The ore minerals include pyrrhotite, pentlandite, pyrite, marcasite, chalcopyrite and violarite with trace amounts of magnetite, ilmenite and chrome spinel. In the gabbro host the sulphides are finer-grained than in the pyroxenite host. The distribution of alteration-modified disseminated ores is shown in Fig. 7.18c. These form tabular bodies within the zones of disseminated sulphides. The content of alteration-modified disseminated sulphides is from 15 to 30 vol% and the sulphides have irregular or ovoid shapes and locally occur as abundant, veinlets. Ore minerals comprise pyrrhotite, pentlandite, chalcopyrite, magnetite, chrome spinel and ilmenite with trace amounts of galena, Ni-cobaltite and parkerite ($Ni_3(Bi, Pb)_2S_2$). Sulphides in these ores characteristically fill microfractures of alteration minerals and are commonly associated with a brown biotite, actinolite-tremolite and chlorite, which not only form the host groundmass, but also tend to be intergrown with the margins of the sulphide grains, imparting a peculiar barbed texture.

Net-textured and massive sulphides form flat, tabular bodies in the centre of the host rock and are locally transgressive across the igneous layers (Fig. 7.18b, c). The transgressive structure could be either an original feature that resulted from the emplacement of the sulphide liquid, or due to later tectonic deformation. The content of net-textured sulphides is from 15 to 30 vol%; whereas in the massive ore the sulphide content reaches 90–99 vol%. Both net-textured and massive ore minerals include pyrrhotite, pentlandite, chalcopyrite and magnetite with minor galena, parkerite, argentopentlandite, Ni-colbaltite, mackinawite, altaite and electrum (Tang et al. 1992). Mackinawite is present in very small amounts, and is less than 0.05 mm in size. It occurs in flame form within chalcopyrite or at the contact between magnetite and chalcopyrite and penetrates into chalcopyrite. It is probably a product of exsolution, but occasionally it is also noted to occur within fine-grained pentlandite. Argentopentlandite ($Ag_{0.619-0.748}$, $Ni_{3.394-2.826}$, $Fe_{4.331-4.147}$, $Cu_{0.009})_{8.344-7.730}S_8$ is fine grained, less than 0.05 mm in size, and displays a light reddish brown reflection

color, which is similar to that of bornite and djerfisherite but slightly brighter; it forms graphic intergrowths with fine-grained seriate-textured pentlandite and is replaced by late stage chalcopyrite. Ni-cobaltite is euhedral, less than 0.05 mm across, and mainly occurs within pyrrhotite. Altaite occurs as small grains, 0.01 mm across, only within chalcopyrite. Electrum is found in fissures in pyrrhotite. Textural relationships indicate that pentlandite and pyrrhotite crystallized first, followed by Ni-cobaltite, chalcopyrite, argentopentlandite and parkerite, whereas galena, mackinawite, altaite and electrum formed in the latest stages. An unusual features of the massive ores is the relatively high content of Ag and In (in argentopentlandite and electrum; Tang et al. 1992). In addition to disseminated, alteration-modified disseminated and massive ores there are also brecciated and "mottled" (local term for irregular patches of pyrrhotite and chalcopyrite aggregates) ores (Fig. 7.18c).

Breccias are present in sandstone and gabbro, where the component clasts are cemented by sulphides. Breccia ores contain the same sulphides as in the massive ores but with relatively higher content of chalcopyrite. The ore minerals include pyrrhotite, pentlandite and chalcopyrite. The Cu content is generally higher than that in massive ores. Some quartz and carbonate are present. The "mottled" ore is hosted by gabbro, with the sulphides forming pisolitic-like or droplet-like aggregates with grain size ranging from 5 to 15 mm across.

The Baimazhai Ni-Cu sulphides and hydrothermally altered host rock are crosscut by unaltered lamprophyre dykes. While the age of these dykes in the Jinping area is unknown, a belt of alkaline rocks, including lamprophyres and syenites, is present along the Ailaoshan-Red River fault zone (ARR; Fig. 7.13) with ages ranging from 40 to 30 Ma (Wang et al. 2001; Hu et al. 2004; Guo et al. 2005a). Post-Permian tectono-thermal events in China occurred in the Late Indosinian (260–208 Ma), Yanshanian (190–90 Ma; see below) and the Himalayan (65–0 Ma; Chap. 6). If the lamprophyre dykes at Baimazhai are of Himalayan age (40–30 Ma), then the hydrothermal event at Baimazhai is bracketed between the Late Indosinian and Yanshanian events (260–90 Ma). The age of the Baimazhai deposit, using the $^{40}Ar/^{39}Ar$ method on selected whole rocks (peridotite, pyroxenite and gabbro), yielded ages ranging from 170.02 ± 3.4 to 160.48 ± 3.32 Ma (Mid-Jurassic). These ages are in marked contrast with the Permo-Triassic boundary age of the ELIP. The 160–170 Ma age range is consistent with the $^{40}Ar/^{39}Ar$ age clusters ($\pm$ 175 Ma) reported by Ali et al. (2004) and ascribed to resetting due to a 177–135 Ma collision event (Ali et al. 2004), that brought together the Lhasa Block and the Qiantang-Indochina Block (see inset of Fig. 7.13b and Chap. 2). This tectonic event, which was accompanied by the intrusion of granodiorite plutons (Wang et al. 2002a), falls within the age range of the Yanshanian tectono-thermal event (see below).

Genetic Model

A generally accepted model of ore genesis for mafic-ultramafic hosted massive and disseminated Ni-Cu sulphides calls on liquid immiscibility between a silicate melt and a sulphide liquid. The magmatic segregations of the Ni-Cu sulfides is probably

facilitated by introduction of crustal sulphur into an originally sulphur undersaturated silicate melt (e.g. Naldrett 2004). The Baimazhai sulphides have an orthomagmatic origin and are considered to have been the result of multiple melt injections along the same conduit (Tang et al. 1992). Wang et al. (2004b) suggested that the Baimazhai sulphide deposit was formed by the emplacement of an olivine- and sulphide-rich crystal mush. The sulphide liquids due to their immiscibility were subsequently concentrated in the center of the intrusion (Wang and Zhou 2006). Wang and Zhou (2005, 2006) reported εNd values ranging from −3.3 to −8.4 for the Baimazhai rocks and suggested that these low εNd values are consistent with crustal contamination and subsequent S oversaturation, which induced precipitation of sulphides. These authors further suggested that the Baimazhai intrusion was derived from a staging magma chamber that was lodged in the crust. At Baimazhai, petrographic and textural evidence shows hydrothermal alteration of the intrusive rocks, whereby the silicate minerals were pervasively replaced by hydrous phases. Evidence of hydrothermal activity has been reported from other areas within the ELIP. For example, Li et al. (2005a) discussed the epigenetic-hydrothermal features of Keewenawan type Cu mineralisation in the basaltic lavas, mentioned earlier (Zhu et al. 2003a). Dating of hydrothermal minerals such as laumontite, actinolite and heulandite in the Cu-bearing basalts by the $^{40}Ar/^{39}Ar$ method yielded ages ranging from 238 to 134 Ma (Li et al. 2005a, citing Zhu et al. 2004). Li et al. (2005a) commented that these ages are from 30 to 120 Ma younger than the Emeishan basalts and therefore the Cu mineralisation must be later than the ELIP magmatic event and of hydrothermal origin. The hydrothermal fluids may not have modified the entire body of massive sulphides, but it is possible that tectonic movements have affected its margins, forming zones of disrupted or brecciated sulphides. This would have facilitated the introduction of hydrothermal fluids resulting in disseminated and interstitial sulphide ores. The "alteration-modified" sulphides are interpreted as an example of this tectonic and hydrothermal activity. This is also indicated by the presence of sulphide phases, other than the normal pyrrhotite-pentlandite-chalcopyrite assemblage, in which metal redistribution of certain trace elements such as Bi and Pb occurred to precipitate exotic sulphides (e.g. parkerite). Post-crystallisation alteration of primary Ni-Cu sulphides results in the formation of Cu-rich ores, accompanied by mineral phases such as Pt- and Pd-rich arsenides, tellurides and Bi-bearing minerals (Farrow and Watkinson 1999). These minerals are also associated with hydrous silicates (e.g. chlorite and sericite) and, importantly, with enrichment in Au and Ag, as in fact observed at Baimazhai. Therefore, these modified ores tend to be enriched in Cu, Au and Pd.

The model proposed by Zhang et al. (2006c) for Baimazhai is schematically illustrated in Fig. 7.19. In this model two possible cases are envisaged: (1) a massive sulphide body (Fig. 7.19a; Case 1) was deformed and its margins, which became disrupted and brecciated forming a shell of disseminated sulphides around the massive ores (Fig. 7.19b; Case 1). This shell or envelope allowed the access of hydrothermal fluids, which texturally and perhaps compositionally modified the sulphides and the host rock (Fig. 7.19c, D; Case 1); (2) alternatively, a magmatic massive sulphide body was originally associated with a zone of magmatic disseminated sulphides (Fig. 7.19a; Case 2); upon deformation of the massive-disseminated sulphide

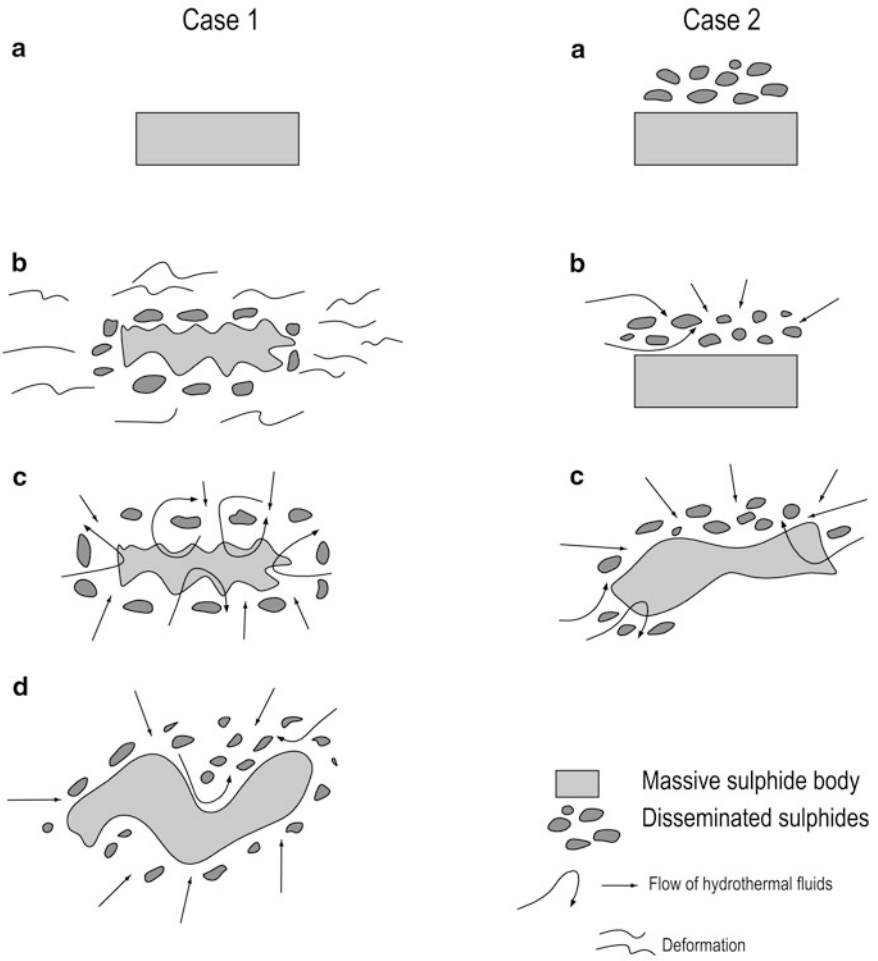

Fig. 7.19 Models for the hydrothermally modified magmatic sulphides at Baimazhai (after Zhang et al. 2006c); *Case 1* a magmatic massive sulfide zone (**a**) is subjected to deformation, resulting in the disruption of the sulfide zone along its margins, forming an envelope of disseminated sulfides (**b**); this is followed by an influx of hydrothermal fluids (**c**), which texturally and compositionally modify the envelope of sulfide disseminations (**d**). *Case 2* the original magmatic ore zone consists of massive and disseminated sulfides (**a**), during deformation hydrothermal fluids penetrate the easily accessible zone of disseminated sulfides (**b**), resulting in the observed textural modifications (**c**)

system, hydrothermal fluids penetrated the most permeable zones represented by the disseminated sulphides (Fig. 7.19b, c; Case 2). In both cases the contact between sulphides and wall rock is a zone of highest geochemical gradient as well as a favourable structural locale and the fluids are expected to be focussed within this zone. Hydrothermal remobilisation at Baimazhai is probably linked to post-magmatic

tectono-thermal events in the region. These events produced hydrothermal fluids that were focused into suitable structures and the same fluids also modified existing mafic-ultramafic sulphide systems. Field observations show that mylonites are present in the ASRR (Ailoishan-Red River) fault zone and an overturned anticline affects the sedimentary rocks that are intruded by the Baimazhai intrusions. Wang and Zhou (2005) suggested that the Baimazhai magma was tectonically emplaced into the Ordovician sedimentary rocks in a convergent margin setting, at the boundary between the South China Block and the Indosinian Block. Moreover, quartz veins can be seen to cut through the sulphide ores (Wang, pers. comm. 2005), further confirming the activity of hydrothermal fluids.

The Emeishan flood basalts were erupted at about 260 Ma marking the impingement of a mantle plume beneath the western margin of the Yangtze Craton, as discussed in Sect. 7.5.1 (Fig. 7.17; Xiao et al. 2008). The closure of the Palaeo-Tethys ocean and the collision between the Indo-China Block and the Yangtze Craton took place in Mid-Triassic times, forming the major ASRR fault zone and leading to the final amalgamation of the Indo-China terranes with the Yangtze Craton and South China Block. The ASRR and adjacent sutures were reactivated during the 55–50 Ma collision of the Indian plate with Eurasia (Chap. 6). This reactivation of the ASRR is estimated at about 300 km of left-lateral strike slip movement (Tapponier et al. 1990). The movements along the ASRR was coincident with regional prograde metamorphism (up to amphibolite facies) and a predominantly alkaline magmatic activity during the Eocene-Oligocene (Guo et al. 2005a).

As previously mentioned, Ali et al. (2004) used Ar-Ar dating to chronologically define the post-Permian tectono-thermal events in the Indo-China-western Yangtze region, affected by the Emeishan flood volcanism. These events cluster at ca. 175, 142, 98 and 42 Ma, which Ali et al. (2004) ascribed to strike-slip and collision tectonic movements along the complex major sutures that separate the Indian block in the west from the Indo-China and the South China blocks to the east and the Songpan-Ganze basin to the northwest. Zhang et al. (2006c) suggested that the ca. 170 Ma Ar-Ar ages reported in their work, most likely indicate a thermal resetting in the Mid-Jurassic. It is also possible that the hydrothermal modification of the Baimazhai sulphide system was the result of tectonic movements along the ASRR fault zone during phases of the Himalayan orogeny, which also resulted in the emplacement of alkaline igneous rocks (lamprophyre and syenites; Chap. 6) in the zone. The age of this magmatism in southeastern Tibet and Yunnan Province is constrained by Ar-Ar at between 32 and 34 Ma (Guo et al. 2005a). Zhang et al. (2006c) argued that the whole rock Ar-Ar ages for the Baimazhai deposit could represent a "mixed" resetting between the 260 Ma of the Emeishan flood basalts and the Himalayan tectonothermal events (65–0 Ma).

7.6.2.2 Limahe Ni-Cu

The Limahe Ni-Cu deposit (Sichuan Province) was described by Tang et al. (1992), Zhou et al. (2002b); dated and studied by Tao et al. (2008, 2010). The Limahe sulphide ores are hosted in a mafic-ultramafic subvolcanic sill-like intrusion, about

800 m long up to 180 m wide, but in cross-section to a depth of about 200 m the intrusion is a funnel-shaped body (Fig. 7.20a). The rock types of the Limahe intrusion as described in Tang et al. (1992) are diorite, gabbro and peridotite rocks, with the latter hosting most of the Ni-Cu sulphides. The diorite is flanked by gabbro and a narrow peridotite lens, largely controlled by a north-trending fault. The gabbro and diorite have gradational boundaries. The Limahe gabbro is medium to coarse-grained and consists of clinopyroxene and plagioclase, with minor hornblende, biotite, ilmenite and magnetite. The diorite consists of plagioclase, amphibole and lesser clinopyroxene. The ore-bearing ultramafic rocks, previously referred to as peridotite, intrude the gabbro-diorite body and surrounding country rocks. The Limahe ultramafic rocks comprise olivine-websterite (30–20 vol% olivine and 60–50 vol% pyroxenes) and wehrlite (50–40 vol% olivine and 40–30 vol% augite), mostly made up of cumulus olivine, with minor orthopyroxene and interstitial clinopyroxene, magnetite and sulphides (Tao et al. 2008; Zhang et al. 2009). It must be noted that here too the ore-bearing ultramafic rocks are strongly altered, with olivine replaced by serpentine and calcite. The olivine-websterite and wherlite rocks have gradational contacts and show igneous layering, form a dyke-like intrusion, about 700 m long and 28–30 m wide and vertically dipping against the above mentioned fault. Disseminated, net-textured and massive Ni-Cu sulphides occur exclusively within the ultramafic rocks and occur as lenses subparallel to the orientation of the dyke-like intrusion. The orebody is 500 m long and has thicknesses of between 29 and 2 m. The ore minerals comprise pentlandite, pyrrhotite and chalcopyrite, with lesser quantities of pyrite, magnetite and galena (Zhou et al. 2002b). Nickel reserves estimated during the production years (1958–1985) were 2.49 Mt grading 1.11 % Ni and ca. 0.6 % Cu (Zhou et al. 2002b).

Petrogenetic studies based on major, trace elements and isotopic data (Zhang et al. 2009) show that unlike other intrusions in the region, such as Panzhihua and Xinjie (Fig. 7.13) in which rhythmic layering is observed suggesting multiple injections of new magma in a staging magma chamber, the Limahe intrusion was formed by a single pulse of magma. Zhang et al. (2009) showed that the peridotite and gabbro in the Limahe intrusion, exhibit sharp contacts and that distinct compositional gaps (e.g. 13–21 wt% MgO) between these rock types in the intrusion cannot be explained by fractional crystallisation from the same parental magma, even though they are spatially associated. The sharp contacts and geochemical compositional gaps, demonstrate that the peridotite was emplaced later than gabbro. The Limahe peridotite has pronounced negative Nb–Ta and Ti anomalies and negative εNd(t), indicating low-εNd(t) in the source mantle or variable contamination of magmas with low-εNd(t) crustal materials. Zhang and co-authors concluded that the Limahe ultramafic units were formed by mixing between two components a mantle end-member probably an Emeishan picrite, and the other granitic crust. Furthermore, the Limahe ultramafic units occur as a dyke, indicating that it was not formed in situ, but ascended to the present site from a deeper crustal magma chamber, where the picritic magma assimilated granitic rocks. On the other hand, Tao et al. (2010), using Re-Os and εNd(t = 260 Ma) data, showing marked differences between sulphide-bearing and sulphide-barren ultramafic magmas, postulated multiple pulses of magma, with

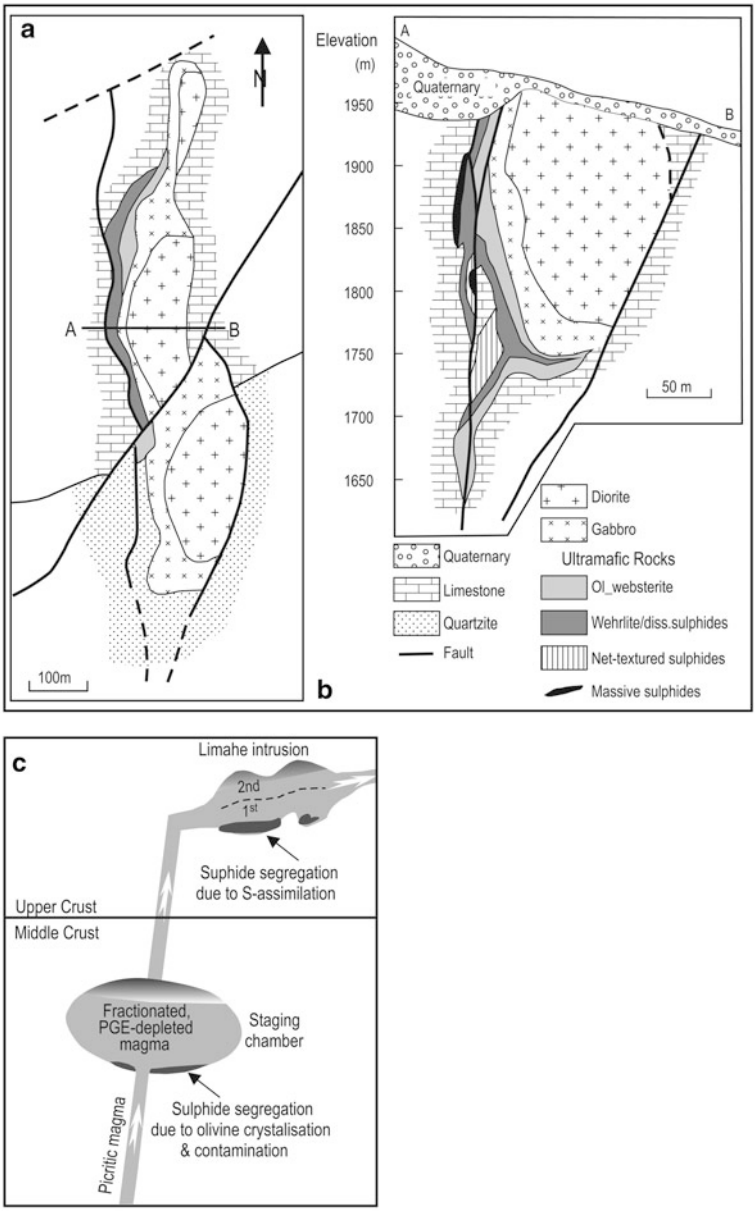

Fig. 7.20 **a** Schematic geology of the Limahe intrusion; **b** cross-section showing the funnel-shaped and zoned Limahe intrusion and associated Ni-Cu sulphide ores (after Tao et al. 2008, 2010); **c** genetic model for the formation of the Ni-Cu sulphides in the Limahe ultramafic rocks (after Tao et al. 2008); details in the text

at least two stages of crustal contamination and resulting sulphide segregation. Thus the genetic model for the Limahe deposit proposed by Tao et al. (2010) involves a series of steps, namely: (1) olivine cumulates derived from a hypothetical mantle plume-derived picritic magma; (2) this magma rises, fractionates and undergoes contamination with lower crust, sulphide segregations take place; (3) early sulphide segregation could have formed the Jinbaoshan Pt-Pd deposit (see Sect. 7.6.2.4); (4) daughter magma, depleted in PGE due to more segregation of sulphides; (5) olivine cumulates from daughter magma; (6) contamination of this daughter magma with upper crust, followed by a second-stage of sulphide segregation; (7) these second-stage sulphides constitute the Limahe Ni-Cu ores. This model is schematically illustrated in Fig. 7.20c.

7.6.2.3 Panzhihua and Hongge Fe-Ti-V

The Panxi rift (Fig. 7.13, see also Fig. 6.49) is defined by major north-trending faults, within which are pre-Emeishan basement rocks and several mafic intrusions, such as the V-Ti-bearing-magnetite Taihe, Baima, Panzhihua and Honggu. The Panxi rift is an important structure on the western margin of the Yangzte Craton and characterised by uplifted Precambrian metamorphic complexes, overlain by Palaeozoic and Mesozoic sedimentary rocks. The bounding deep-seated faults of the Panxi rift are in the west the Jinhe-Qinghe Fault and in the east Xiaojiang Fault, other faults trend north-south, northwest, north-northeast and northeast. The Panxi rift, in my interpretation, may have been reactivated during the crustal uplift related to the impingement of the Emeishan mantle plume, resulting in subsequent rifting, erosion and exposure of differentiated gabbroic intrusive bodies below the flood basalts. This view finds confirmation in the work of Zhou et al. (2005), who reported on several stages of tectonic deformation and final exhumation and the Panxi rift at about 170 Ma. The Panzhihua and Hongge intrusions and contained Fe-Ti-V mineralisation are discussed in this section.

Panzhihua

The Panzhihua mafic intrusion is a 19 km long and 2 km thick sill-like gabbroic body, trending northeast, dipping 60–50° to the northwest and containing layers, pods and veins of Ti-V-rich magnetite in the lower parts (Ganino et al. 2008). The Panzhihua deposit contains 1,333 Mt of ore grading about 33 % Fe, 12 % TiO_2 and 0.3 % V_2O_5 (Ma et al. 2003; Ganino et al. 2008; Pang et al. 2010 and references therein). The deposit was discovered and explored in 1936–1940, mining was commenced in 1967 and still active today (Pang et al. 2010). Published works on the Panzhihua Fe-Ti-V deposit that I have perused for this section are: Zhou et al. (2005), Ganino et al. (2008), Zhang et al. (2009), Pang et al. (2010), Shellnutt and Jahn (2009).

A simplified geological map of the Panzhihua intrusion is shown in Fig. 7.21, together with lithostratigraphic columns. The intrusion, offset by north-trending faults,

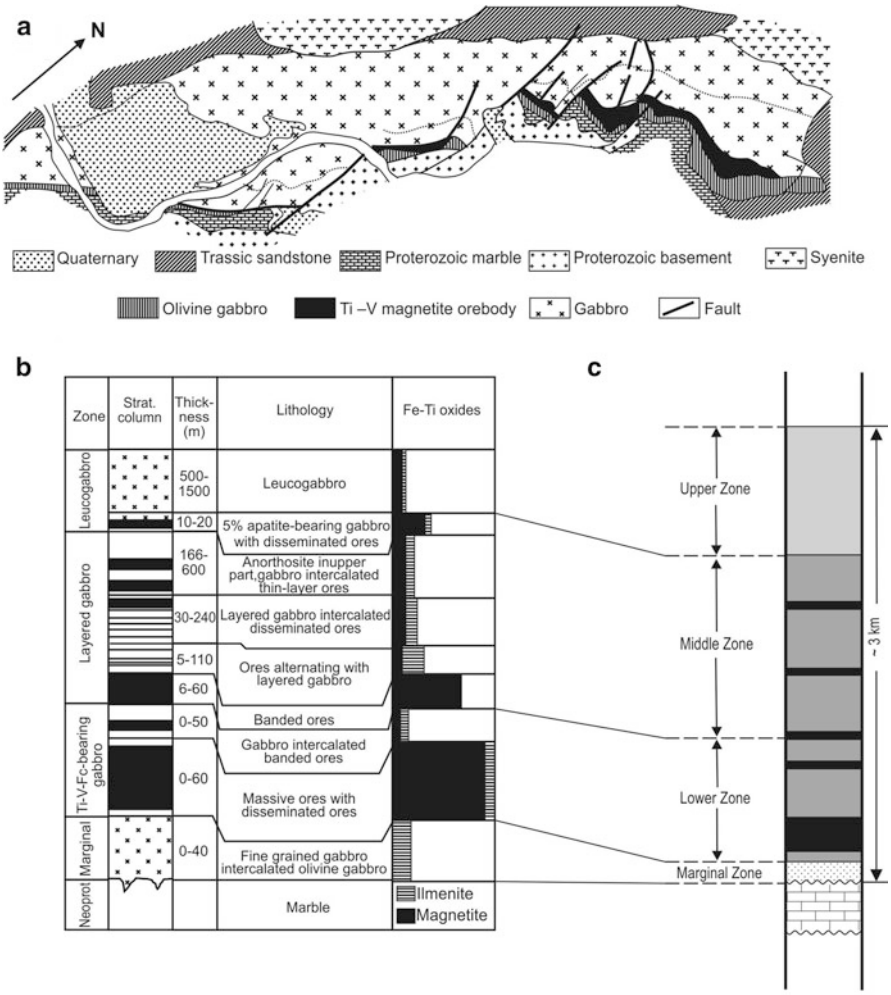

Fig. 7.21 **a** Geological map of the Panzhihua intrusion (according to Zhang et al. 2009 and reference therein); **b** lithostratigraphy of the intrusion and distribution of the Fe-Ti-V oxide mineralisation (Zhang et al. 2009); **c** simplified lithostratigraphy and oxide ore zones. (After Zhou et al. 2005)

but otherwise unmetamorphosed and undeformed, is emplaced in Neoproterozoic carbonate rocks of the Dengying Formation. The intrusion was divided into four zones: (1) a 0–40 m thick marginal zone of olivine- and hornblende-gabbro at the base of the intrusion and containing xenoliths derived from the footwall rocks; (2) a 0–110 m thick lower zone of layered melanocratic gabbro, which contains the titanomagnetite ore layers that are up to 60 m thick; (3) a middle zone up to 800 m thick of weakly mineralised layered gabbro; and (4) a 500–1,500 m thick upper zone of

unmineralised upper leucogabbro zone (Fig. 7.21c); SHRIMP U-Pb zircon ages from the leucogabbro yielded 263 ± 3 and 265 ± 4 Ma (Zhou et al. 2009). A more detailed igneous stratigraphy, showing the corresponding abundance of the oxides (ilmenite and magnetite) with the various units (Zhang et al. 2009) is shown in Fig. 7.21b. As shown in these figures the oxide layers and their thickness decrease upward in accordance with increasing degrees of fractionation. The oxide mineralisation, both with massive and disseminated styles, forms tabular or lensoid orebodies, with the major ore located at the base of the lower zone (Fig. 7.21b, c), extending for about 15 km along strike and with a depth of at least 850 m. The size and distribution of the orebodies varies considerably: for example at one locality (Nalanching) there are 14 ore lenses, up to 160 m long and 30 m wide. According to Zhou et al. (2005) small ore lenses are hosted in the footwall marble rocks, which do not show the presence of skarn alteration, but Pang et al. (2010) have recorded that the footwall rocks are characterised by a 300-m-thick thermal aureole of marble and skarns. Massive oxide ores consist of >80 % titanomagnetite, with the remaining minerals represented by clinopyroxene, plagioclase and olivine. Disseminated oxide ore zones are coarse-grained and comprise about 50 % titanomagnetite, 20 % clinopyroxene, 20 % plagioclase and 10 % ilmenite. The rock-forming silicates (olivine, plagioclase etc) are surrounded and/or overprinted by the oxide minerals. Minor amounts (1–5 %) of sulphides (pyrrhotite and pentlandite) are also present in both massive and disseminated ores.

The Panzhihua intrusion was considered to be derived from fractionation crystallisation of highly evolved parental magmas, which are Fe-rich residual liquids. Su et al. (2008) suggested that the oxide ores were formed as a result of oxidising conditions due to release of CO_2-rich fluids, from the reaction of carbonate country rocks with the intruding magmas. These oxidising conditions induced early crystallisation of magnetite, which by density segregation accumulated in the lower parts of the intrusion. The mafic intrusions in the Panxi rift are spatially and temporally associated with peralkaline A-type granitic plutons, including granite, syenite and syenodiorite and associated trachytes (Shellnutt and Jahn 2009). Coeval I-type granites are also present, but they are interpreted as having derived from melting of basement rocks (Zhong et al. 2011; see below). These felsic and peralkaline complexes are stratigraphically above the mafic layered intrusion and can be up to 10 km long, 2 km thick and wide, and are mineralogically composed of microcline, pyroxene, hornblende, quartz, biotite and minor apatite. Geochemical and isotopic data indicate that a genetic relationship between the peralkaline rocks, as shown for example by εNd(t) overlapping values of clinopyroxenes (+1.1 to +3.2) in the layered gabbros and those of whole-rock peralkaline rocks (+2.1 to +2.9). Field observations combined with trace element modelling led Shellnutt and Jahn (2009) to propose a petrogenetic model that combines intrusion of the mafic magma, its fractional crystallisation to felsic and peralkaline magmas (granite and syenodiorite), which intruded the overlying Emeishan flood basalts and erupted as trachytes at the top of the flood basalt sequence. The model, simple and viable, is shown in Fig. 7.22.

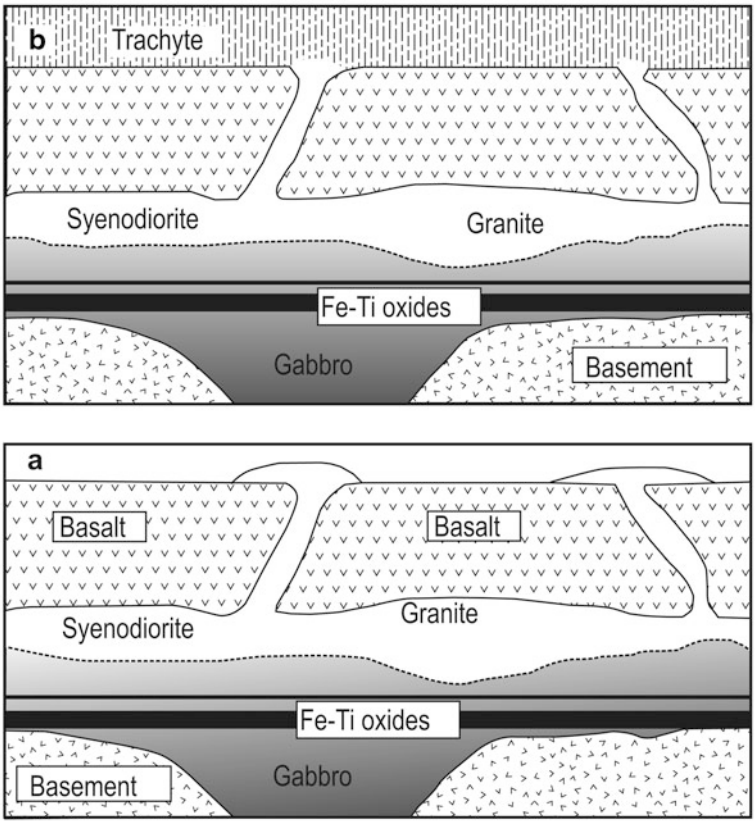

Fig. 7.22 Petrogenetic model suggested by Shellnutt and Jahn (2009); **a** intrusion of parental mafic magma, fractional crystallisation, producing Fe-Ti oxides cumulates (ore bodies) and alkaline rocks (syenodiorite and alkali granite), locally venting to the surface as trachyitic lavas; **b** columnar jointing due to cooling forms in the trachyte lavas; more details in text

Hongge

The Hongge Fe-Ti-V deposit had reserves of 183 Mt FeOt (Fe oxides total), grading 27 %, 19.6 Mt Ti grading 10.57 % TiO_2 and 1.45 Mt V ore, grading 0.24 % V_2O_5 with PGE enrichment (Zhong et al. 2002). The Hongge layered intrusion from the base upward, consists of olivine clinopyroxenite (Lower Zone), clinopyroxenite (Middle Zone) and gabbro (Upper Zone) (Zhong et al. 2003, 2011; Fig. 7.23). These zones are characterised by cyclic units (Cycle 1 in the Lower Zone, Cycles 2 and 3 in the Middle Zone and Cycle 4 in the upper Zone), from cumulus olivine in the first cycle to plagioclase and apatite in the last cycle. These cycles are associated with marked reversal of major and trace elements at boundary of each cyclic unit, suggesting that pulses of primitive magmas were injected into the

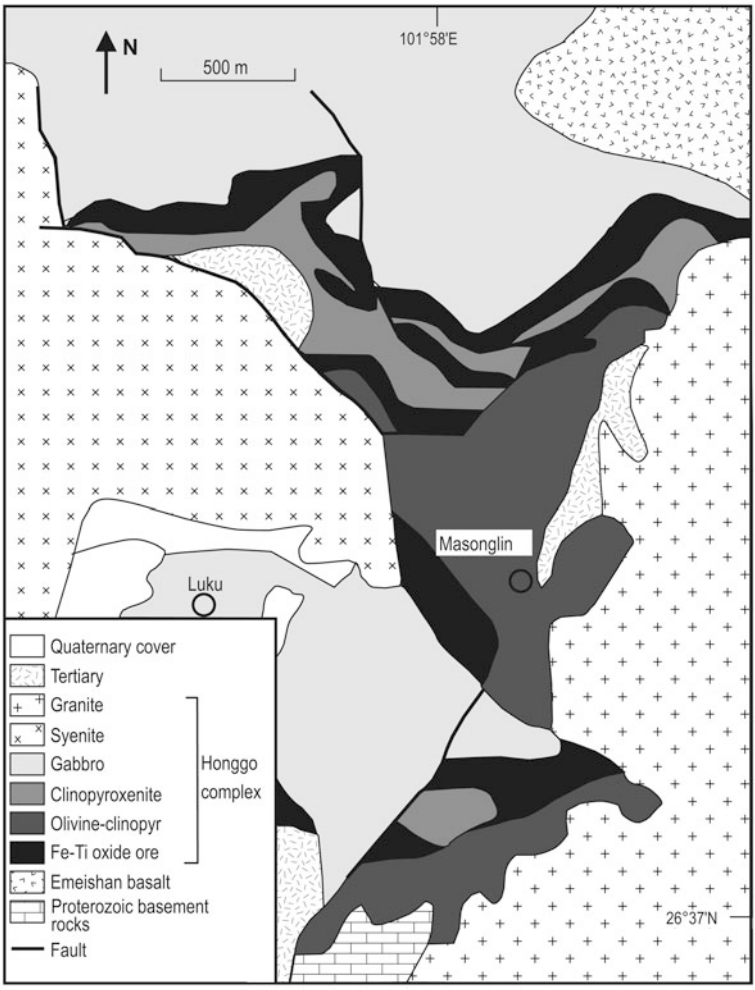

Fig. 7.23 Simplified geological map of the Hongge layered complex. (After Zhong et al. 2011)

resident liquids (Zhong et al. 2003), a common feature of many layered mafic-ultramafic intrusions, as exemplified by the well-studied giant Bushveld Igneous Complex in South Africa (e.g. Eales and Cawthorn 1996). The Lower Zone (Cycle 1, 342 m thick) has cumulus olivine (30–15 vol%), intercumulus clinopyroxene and hornblende (40–50 vol%), Fe-Ti oxides (mostly titanomagnetite, 5–10 vol%), sulphides and chromite. The titanomagnetite is euhedral and rounded olivine are enclosed in titaniferous clinopyroxene. The upper part of the Lower Zone has cumulus olivine and clinopyroxene, with intercumulus titanomagnetite and ilmenite, minor hornblende and plagioclase. The Middle Zone (Cycles 2, 63 m thick and Cycle 3, 87 m thick) comprises olivine clinopyroxenite (60–70 vol% clinopyroxene,

Table 7.2 Abundances of PGE and sulphide enriched magnetite horizons. (After Zhong et al. 2002)

Zone	Cycle	PGE ppm	Ni %	Cr %	Cu %	Co %
Lower	1	0.354	0.89	1.60	1.07	0.36
Middle	2	0.533	5.49	1.95	1.70	2.37

5–10 vol% olivine) at the base and clinopyroxenite at the top, with more abundant interstitial magnetite and ilmenite (15–20 vol%) than the Lower Zone. The Fe-Ti oxide minerals are associated with lesser sulphides and occur at the base of each cyclic unit. The Upper Zone (Cycle 4, >750 m thick) consists of banded gabbro, leucogabbro, pegmatoidal clinopyroxenite and minor lherzolite and anorthosite. In the Upper Zone gabbroic rocks consist of plagioclase (40–50 vol%), clinopyroxene (30–40 vol%), Fe-Ti oxides (5–10 vol%) with the amount of plagioclase increasing towards the top, gradually changing to a leucogabbro rock. Zhong et al. (2002 and references therein) recognised a crystallisation sequence for the Lower and Middle Zones as follows: olivine → olivine + magnetite + chromite → clinopyroxene + magnetite ± orthopyroxene + olivine → clinopyroxene + magnetite → clinopyroxene + plagioclase. The magnetite horizons at the base of Lower and Middle zones (olivine-clinopyroxenite) are PGE and sulphide enriched (Table 7.2; Zhong et al. 2002). Sulphide minerals are pyrrhotite, pentlandite, pyrite, chalcopyrite and cubanite. The most common PGE minerals, which are enclosed in the sulphides, include sperrylite and vincentite and a $(Ru,Os)S_2$ mineral (probably Os-bearing laurite). The Upper Zone has the following sequence of cumulus minerals: plagioclase + clinopyroxene + apatite ± orthopyroxene ± magnetite in the lower section, followed by olivine + magnetite + clinopyroxene → plagioclase + clinopyroxene + apatite in the upper section. Both the Middle and Upper zones host layers of disseminated vanadiferous titanomagnetite, from 15 to 85 m thick and up to 1,700 m long.

As recorded for other intrusions in the Panxi rift, such as the above-discussed Panzhihua, the Hongge layered complex is spatially associated with granitic intrusions. This aspect of bimodality (mafic-ultramafic and felsic rocks) in the ELIP has been investigated by a number of researchers (e.g. Shellnutt and Jahn 2009; Niu et al. 2003), as well as Zhong et al. (2011) who specifically referred to the Hongge intrusion, as discussed below from the latter authors. The spatially associated I-type Ailanghe granitic batholith, with an outcrop area of $>100\,km^2$, intruded the Hongge mafic–ultramafic intrusion and the Emeishan basalts. The Ailanghe granite batholith is composed of coarse- to medium-grained biotite, K–feldspar granite and medium- to fine-grained monzonitic granite. Zircon grains from the Ailanghe batholith yielded SHRIMP U-Pb ages of 256.8 ± 2.8 and 256.2 ± 3.0 Ma, with a xenocrystic zircon giving a discordant age of 792 Ma. The latter age, combined with Hf isotopic data, indicate that these Permian-age granitic rocks were formed by partuial melting of continental crust (Zhong and Zhu 2006; Zhong et al. 2011) and not by fractional crystallisation of mafic-ultramafic magmas, as was the case of the Panzhihua intrusion (see above).

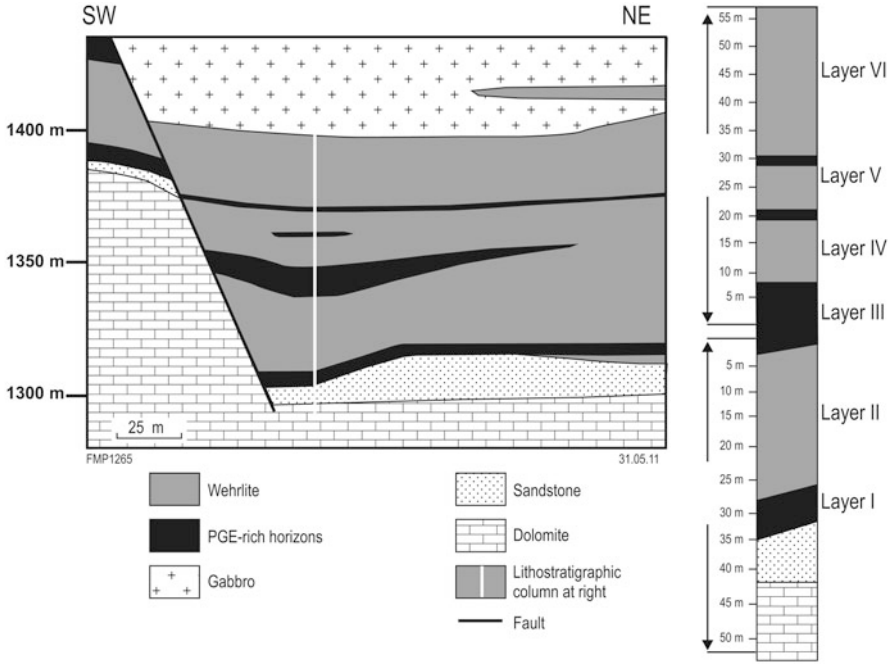

Fig. 7.24 Cross-section of the Jinbaoshan sill-like intrusion and contained PGE-rich horizons and subdivisions of Layers I to VI. (Modified after Wang et al. 2010)

7.6.2.4 Jinbaoshan Pt-Pd

Wang et al. (2005, 2008b, 2010) studied the Jinbaoshan Pt-Pd deposit in Yunnan province (Fig. 7.13), hosted in a sill-like ultramafic intrusion, over 4.7 km long that belongs to the ELIP. The age of the Jinbaoshan intrusion is 259.2 ± 4.5 Ma (SHRIMP U-Pb zircon dating; Tao et al. 2009). This deposit contains 1 Mt of ore, grading 3.0 g/t Pt + Pd, in at least three horizons, defined by a cutoff value of 0.5 ppm Pt + Pd. The largest PGE-bearing horizon contains 44 % of the total reserves, is at the base of the ultramafic sill and is 2,100 m long, 400–600 m wide and up to 16 m thick. Two other PGE mineralized horizons (>0.5 ppm Pt + Pd) occur in the middle and upper parts of the intrusion, whereas one smaller and lower grades PGE-bearing horizon lies just above the middle one. The PGE-bearing Jinbaoshan intrusion is made up of wehrlite, with lenses of olivine-clinopyroxenite, overlain by a gabbro unit. The orebodies are offset by a southeast-dipping fault. Although the boundaries between the PGE-bearing horizons and the host wehrlite rocks are gradational, Wang et al. (2010) subdivided the intrusion into six layers (I to VI), with Layer I being the basal PGE-rich horizon (Fig. 7.24). The PGE minerals (PGM) are moncheite ($PtTe_2$), sperrylite ($PtAs_2$), cooperite (PtS), sudburyte (PdSb), irarsite (IrAsS), kotulkisite (PdTe) and atokite (Pd_3Sn). Chromite is also present as euhedral grains in olivine or

as zoned grains interstitial between rock-forming silicates (see below) and usually less than 10 vol%, but locally chromite can reach 20 vol%. Sulphides, although not readily detectable by the naked eye, do occur in amounts of 3–10 % as shown under the microscope and include pyrrhotite, pyrite, pentlandite, chalcopyrite and violarite, mostly associated with the above-listed Sn-, Te- and As-bearing platinoids. Wang et al. (2010) determined that the PGE-rich layers in the intrusion have the same rock-forming silicate mineralogy as the non-mineralised layers. These rock-forming minerals consist of anhedral to subhedral olivine and clinopyroxene with granular to poikilitic textures, locally hydrothermally altered to serpentine, actinolite-tremolite and biotite. The chromite-rich layer is at the base of the intrusion and overlain by the sulphide-rich layer, but in other places chromite and sulphides occur together and are interstitial to the hydrothermally altered olivine and clinopyroxene crystals. Therefore, Wang and co-authors surmised that the chromite and sulphides must post-date the rock-forming silicate minerals.

The Jinbaoshan deposit is an unusual magmatic mineral system, which Wang et al. (2008b), on the basis of detailed petrographic studies, suggested that it was originally formed by magmatic processes and later modified by hydrothermal fluids. These fluids leached platinum-group elements (PGE) from net-textured magmatic sulphides and produced intense alteration of the mafic-ultramafic rocks. However, in later and more detailed geochemical studies Wang et al. (2010) proposed a model based on the special relationship between the chromite and sulphides in the Jinbaoshan intrusion, and that the sulphides precipitated not as a result of crustal contamination of the parental magma, but following the precipitation of chromite. These authors used the Pd/Cr and Pt/Y ratios to examine the chromite-sulphide relationship, because chromite precipitation under S-undersaturated conditions results in higher Pd/Cr ratios and constant Pt/Y ratios in the fractionated magma, whereas immiscible sulphide segregation results in decrease of these ratios in the fractionated magma (Fig. 7.25a). Furthermore, all the Jinbaoshan rocks have very low Cu/Pd ratios (20–2,000). Usually magma that experienced the removal of sulphide would be highly depleted in PGE due to high partition of these elements in the sulphide liquid resulting in extremely high Cu/Pd ratio of the residual magma. However, at Jinbaoshan the low Cu/Pd ratios are due to the relatively high Pd concentrations, and as such it is unlikely that the magmas from which the Jinbaoshan sill formed experienced sulphide removal. The high PGE and low Cu/Pd ratios are similar to those of the Critical Zone of the Bushveld Igneous Complex (Naldrett et al. 2009). According to Wang et al. (2010 and references therein) an open-system and multistage-dissolution for the formation of high PGE concentrations could be the result of a multistage upgrading process with dissolution of pre-existing sulphides. A likely model to interpret the PGE enrichment of the rocks at Jinbaoshan is that they formed from PGE-rich magma, as envisaged by Kerr and Leitch (2005), prompting Wang et al. (2010) to propose that strong chromite segregation will trigger sulphide saturation of the magma. The heavier chromite will settle at the base of the magma chamber, with the sulphides forming the overlying layer. In other words, the genetic model for the Cr- and PGE-rich layers of the Jinbaoshan intrusion, shown in Fig. 7.26a, involved an open system of magma conduits, in which pulses of S-undersaturated magma reached sulphide saturation

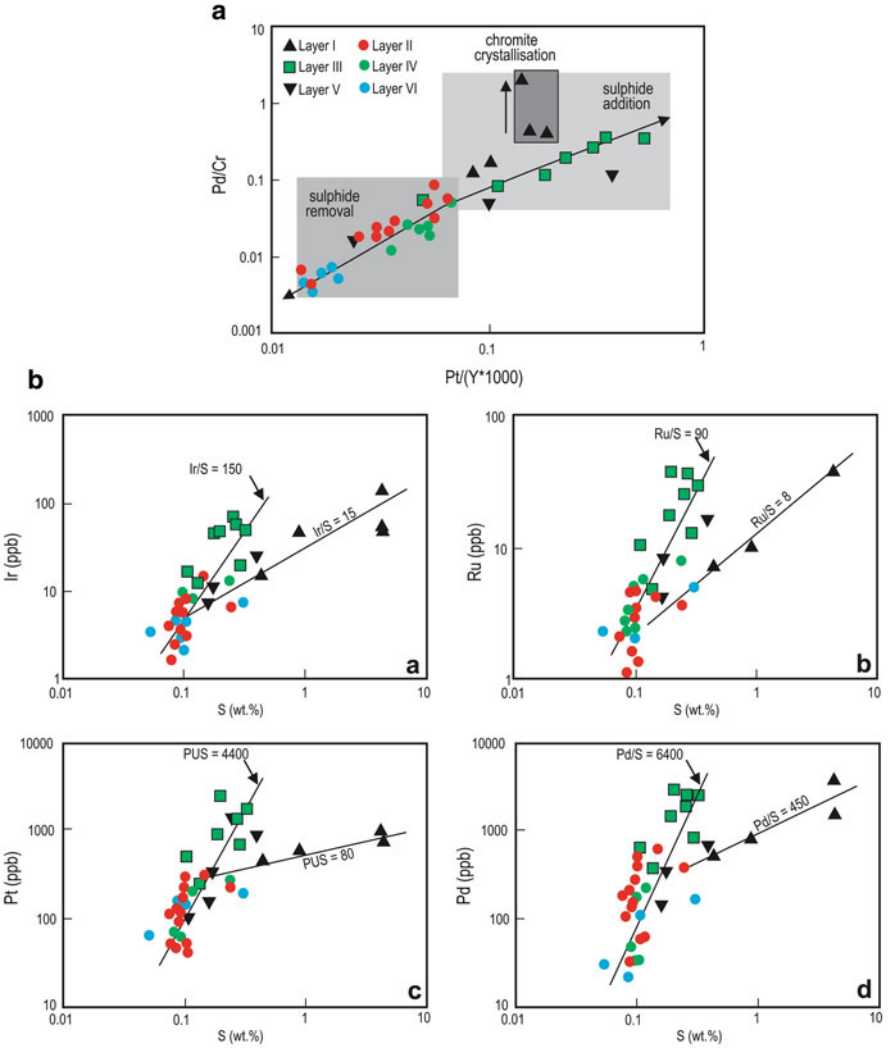

Fig. 7.25 Plots of (**a**) Pd/Cr vs Pt/Y ratios and (**b**) examples of distinct trends of PGE (Pt and Pd, Ir and Ru) vs S, showing the difference between PGE-rich and PGE-poor rocks in the Jinbaoshan intrusion (after Wang et al. 2010); details in text

due to fractionation of olivine and chromite and producing an immiscible sulphide liquid segregated in a deep-seated staging magma chamber. In the staging magmas, sulphide saturation was likely triggered by crustal contamination, as generally accepted for the formation of Ni-Cu sulphide deposits (Naldrett 2004). Successive pulses of S-undersaturated magma were injected into the staging magma chamber, resulting in the enrichment of the sulphide liquid in PGE, followed by later magma

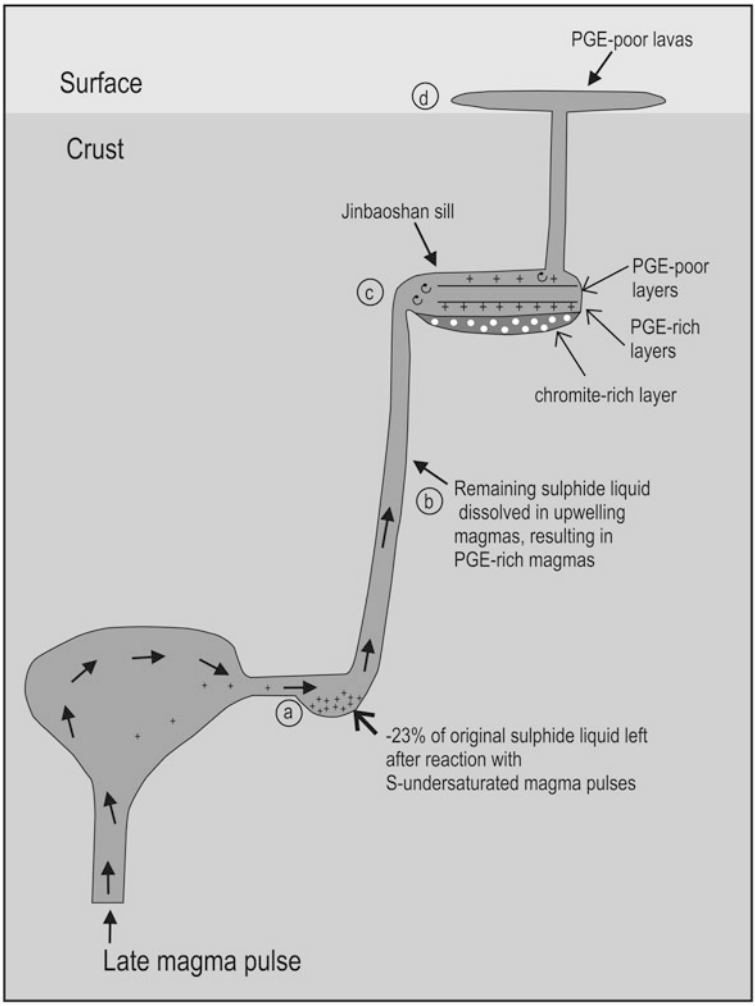

Fig. 7.26 The genetic model for the Jinbaoshan Pt-Pd-rich intrusion (as proposed by Wang et al. 2010); details in text

injections along the same conduit, forming a PGE-rich magma (Fig. 7.26b). The next stage is the formation of an upper magma chamber in the crust, where chromite crystallisation would have enhanced sulphide saturation of the melt, leading to chromite, sulphides and olivine segregation which, due to density contrast, settle towards the base of the new intrusion (Fig. 7.26c). The chromite settles at the bottom of the chamber due to their higher density relative to sulphides and the magma, resulting in chromite-rich sulphide-poor layer at the bottom, overlain by PGE-rich sulphide-rich

layers (Fig. 7.26c). Wang et al. (2010) noted different trends recorded in plots of S versus metals, such as Cu, Ni and PGE, an example of which is shown in Fig. 7.25b. From this these researchers suggested that the two trends exhibited by the S versus ore metals are possibly due to turbulence and/or convection of new melt pulses in the magma chamber, which may also allow the suspending sulphide liquid access to more silicate liquid, thereby reaching the highest PGE concentrations. This process would account for the variable sulphide contents of the Jinbaoshan igneous layers.

The rocks of the Jinbaoshan sill have MgO contents ranging from 40 to 20 wt% and this together with the textural feature of chromite and sulphides interstitial to olivine cumulates, would indicate that these rocks are more fractionated than a parental magma and that the sill may have formed from a melt emplaced in the upper chamber (Fig. 7.26). An interesting alternative, also proposed by Wang et al. (2010), speculates that fractionated silicate melts may have been injected after magma was emplaced, perhaps during tectonic movements. The injected fractionated magma can also erupt to the surface as lavas inheriting the PGE-rich to PGE-depleted characteristics of the source layers of the magma chamber (Fig. 7.26d).

7.6.2.5 REE Deposits in the Panxi Rift

The Panxi rift is well endowed with several REE deposits related to carbonatite-syenitic complexes, which are part of the Cenozoic Mianning-Dechang (MD) belt in eastern Tibet and western Sichuan, discussed in Chap. 6. The Cenozoic age of these complexes and associated REE mineralisation indicate that they are not part of the ELIP event, although to what extent some or all of these deposits were modified by later tectonic events (Himalayan orogens), is not known at this stage. Niu et al. (2003) in a short paper reported on light rare earth deposits associated with syenite-carbonatite complexes in the Panxi rift. According to these authors, REE-bearing alkaline and peralkaline and carbonatites rocks are spatially associated with the mafic and ultramafic intrusion, described in the preceding sections (e.g. Panzhihua). Other researchers who carried out studies of isotope systematics on other REE deposits hosted in carbonatite-syenite complexes (e.g. Tian et al. 2005; see also references in Chap. 6), did not report on the age of the REE mineralisation and hosting alkaline rocks. He (pers. comm. 2011; see also He et al. 2006) believe that north-trending faults probably formed in Neoproterozoic (820–750 Ma) and the boundaries of Nanhua rift (Fig. 7.6 and Chap. 4). Those faults might have been reactivated in response to the uplift caused by the Emeishan mantle plume, but definitively reactivated in Cenozoic, forming a very deep rift or basin (Panxi rift). However, as shown in Fig. 7.27 and discussed above, some alkaline intrusions are spatially and temporally associated with the Panzhihua, Baima, Hongge and Taihe mafic-ultramafic intrusions of the Emeishan event (Hou et al. 2011, quoting Cong 1988).

Fig. 7.27 Distribution of alkaline rocks temporally and genetically associated with the mafic-ultramafic intrusions in the Panxi rift. (After Hou et al. 2011)

7.7 The Yanshanian Tectono-thermal Events in Eastern China

Pirajno et al. (2009) reviewed the Mesozoic-Cenozoic intraplate tectonism and magmatism that affected much of the eastern margin of mainland Asia, extending from Far East Russia, through the Baikal and Mongolia regions, to north-eastern and eastern China. These phenomena are broadly linked with a complex series of tectonic events, involving subduction, plate collisions, crustal thickening, post-collision collapse and rifting. The Mesozoic and Cenozoic extensional tectonics of mainland China and the rest of eastern Asia are ultimately the surface expressions of shallow mantle dynamics in the region, linked to the oblique subduction of the Pacific plate under the Eurasian plate, affecting the continental margin of eastern Asia (Sengör et al. 1993).

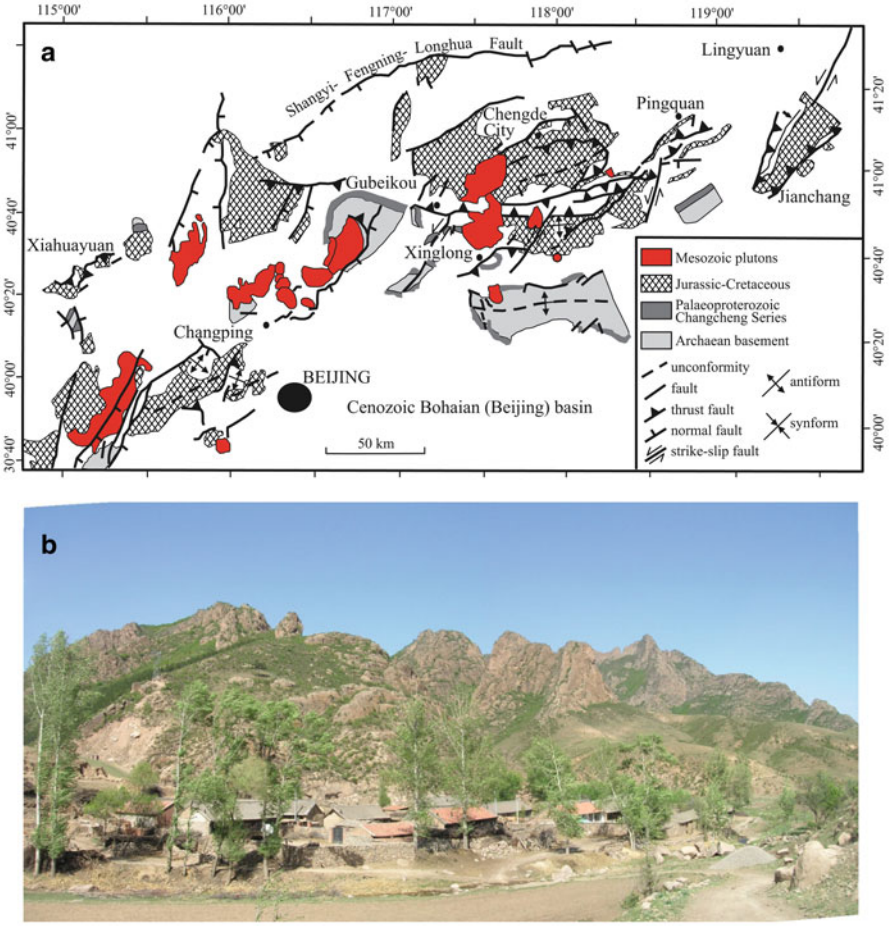

Fig. 7.28 **a** Yanshan region, the type area of the Mesozoic Yanshanian magmatism (after Kusky et al. 2007); **b** granitic rocks in the Yanshan mountains, northern Hebei

Wong (1927) was the first to recognise a "Yanshan mobilisation" (cited in Deng et al. 2007), which was later referred to as Yanshanian, which comprises a series of fairly well constrained tectono-thermal events that began in the Early Mesozoic at ca. 216–208 Ma and assumed to have terminated ca. 90 Ma (Zhou et al. 2002a). The type area is the Yanshan belt, north of Beijing (Fig. 7.28). The record of Yanshanian magmatism in eastern and northeastern China is generally bimodal and dominantly comprises I-, A-type and alkaline granites intrusions, breccia pipes, felsic and alkali basaltic lavas. The alkali ring complexes in the Luxi area, and a SHRIMP zircon U-Pb age of ca. 177 Ma recorded for the granodiorite in the alkaline complexes (Hu et al. 2005), suggest that mantle activity and/or lithospheric thinning began in the Mid-Jurassic. Volcanic eruptions migrated from the circum-Bohai basins to the Luxi

uplift, with ages ranging from 136–135 to 124–115 Ma for the volcanic rocks in the Luxi area (Mao et al. 2008a and references therein). Several carbonatite dykes in Badou and Xueye, Luxi area, with K-Ar ages of ca. 123 Ma, have also been recorded and are coeval with lamprophyre and felsic dykes (Mao et al. 2008a). Other alkaline complexes and associated carbonatites that have Yanshanian ages include Zijinshan and Huanyangchuan (134 and 181 Ma, respectively; Shaanxi province), Weishan and Yangdun (ca. 110 and 122 Ma, respectively; Shandong province) (for comprehensive listings of carbonatites in China see Xu et al. 2010; for carbonatites and alkaline complexes associated with rare earths deposits, see Wu et al. 1996). It is of interest to note that alkaline ring complexes and carbonatites of the same age (130–125 Ma) occur further north in Siberia in the Aldan region and Transbaikalia (Ripp et al. 2011; Borisenko et al. 2011), effectively extending the belt of Cretaceous intraplate alkaline magmatism by 2,000–3,000 km beyond China's borders to the north (see also Seltmann et al. 2010).

Therefore the period from 135 to 115 Ma is important and appears to mark a series of intracontinental thermal events, which are temporally associated with porphyry deposits, skarn and epithermal systems as well as lode Au mineralisation in eastern and northeastern China, mostly but not all being superimposed on older geotectonic domains or terranes, as described in the Chapters of this book. The Yanshanian events affected regions extending for up to 1,000 km westward, inland from the coastal areas, along major zones of crustal weakness, such as the boundaries and sutures between the North and Yangtze Cratons and the North China and Siberian Cratons, and the crustal-scale north-northeast-trending Tanlu Fault.

The distribution of the Meso-Cenozoic magmatism in eastern and southern China is shown in Fig. 7.29. Post-orogenic A-, I-type granites and rift-related syenites, show a coastward younging trend, as discussed in more detail below. The main phases of Yanshanian tectono-magmatic activity peaked with extensive I- and A-type plutonism in the Cretaceous between ca. 130 and 90 Ma (Jahn et al. 1990; Chen et al. 2000; Zhou and Li 2000). Chen et al. (2000) and Zhou and Li (2000) noted the presence of Cretaceous A-type plutonic rocks and widespread high-level I-type plutonic rocks. They related this plutonism to a geothermal gradient greater than 40 °C/km, large-scale underplating of basaltic magma, and a high exhumation rate.

Zhou and Li (2000) further suggested that the slab-dip angle of the early Pacific oceanic plate subduction beneath southeastern China increased from a low angle to a moderate angle between 180 and 80 Ma. The consequence of this change in angle was that magmatic activity migrated some 800 km southeast towards the coastal regions of the Zhejiang and Fujian provinces (southeast China). According to Li and Li (2007), the uplift of the coastal region in southeast China is associated with the Mid-Permian North China-South China collision. Li and Li (2007) interpreted the anorogenic I- and A-type magmatism to reflect slab breakoff and asthenospheric upwelling, resulting in a Basin-and-Range topography. The younging of this magmatism towards the coast is interpreted as due to successive phases of slab roll-back that produced a combination of arc-related and bimodal rift-related volcanism. A similar model was proposed by Wang et al. (2006) for the Yanshanian volcanism in the Great Xing'an

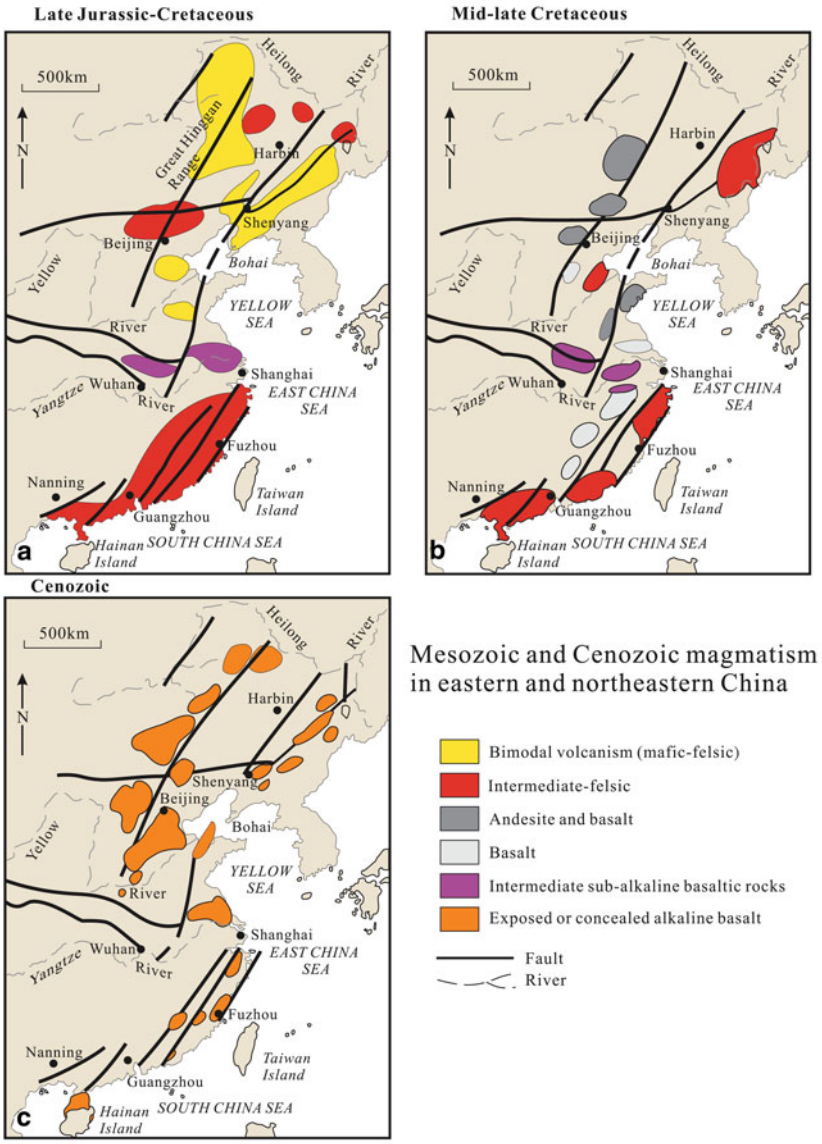

Fig. 7.29 Mesozoic-Cenozoic intracontinental volcanism in eastern China (modified after Yi et al. 1992; Qi et al. 2005a, b; Pirajno et al. 2009). These volcanic rocks were emplaced in extensional settings (graben style rift basins) and are associated with dyke swarms, I- and A-type granites. Collision of continental plates, North China Craton with the Yangzte craton in the south and the Siberian craton in the north, followed later by the westward subduction of the west Pacific, all contributed to a succession of post-collisional collapses due to lithospheric delamination and pulses of asthenospheric mantle upwellings. The effects of this type of mantle dynamics may result in partial destruction of lithosphere and lower crust (de-cratonisation, details in text)

Range with age peaks at 163–160, 147–140, 125–120 and 116–113 Ma, as detailed below in Sect. 7.6.2.

A generally accepted view is that the thermo-tectonic evolution of the lithospheric mantle beneath eastern China that led to the Yanshanian events resulted from extension, lower crust and lithospheric keel delamination, followed by asthenospheric upwelling (Griffin et al. 1998; O'Reilly et al. 2001; Xu et al. 1998a; Xu 2001), with the possibility of deep mantle plumes being ruled out, given the scattered nature of the volcanism in the region and the lack of evidence of mantle-source $^{3}He/^{4}He$ values in igneous rocks (Barry et al. 2007). The loss of lithospheric root beneath the Eastern Block of the North China Craton is deduced by mantle xenoliths brought up by Palaeozoic kimberlites and Cenozoic basalts (for details see Griffin et al. 1998; Xu et al. 1998a, b, 2004b; O'Reilly et al. 2001). Pressure-temperature data from these xenoliths show that in the Ordovician the lithosphere-asthenosphere boundary was at about 180 km, whereas in the Cenozoic this boundary rose to about 80 km depth. Delamination of subcontinental lithospheric mantle beneath isostatically compensated orogens results in an increase in gravitational potential energy and promotes uplift and horizontal extension (Wells and Hoisch 2008). Isostatic uplift and upwelling asthenopheric mantle induce decompression melting and at the same time heating of the crust leads to anatexis and production of felsic magmas and A-type granites. It is important to note that comparable geodynamic settings of the same age are present in eastern Australia (Johnson 1989), western North America (Wells and Hoisch 2008) and western Europe (Schmincke 2007; Wilson and Downes 1991). Wu et al. (2005) suggested that a superplume event at about 130–120 Ma, which was responsible for the Ontong Java-Manihiki-Hikurangi (Taylor 2006) and Kerguelen (Coffin et al. 2002) oceanic plateaux, may have been the far-field trigger to enhance subduction rates of the Palaeopacific east Asian continental margin. In turn, this would have led to or assisted delamination of the lithospheric mantle, resulting in magmatic underplating, crustal melting and the development of A- and I-type granitic magmas, volcanism along the east Asian margin and in associated rift structures.

The Yanshanian event resulted in the establishment of a broad magmatic zone, as much as 1,000-km wide and 3,000-km long, along the eastern margin of China. The main stages of Yanshanian tectonic and magmatic activity are outlined in Table 7.3. Similarly, Deng et al. (2007) described four main stages of the Yanshanian event, as follows: (1) pre-orogenic extension in the Early Jurassic, characterised by mafic volcanism and deposition of coal-bearing sedimentary formations, start of compressional movements and high-P low-T metamorphism; (2) Mid- and Late Jurassic compressional deformation episodes, accompanied by felsic magmatism, molasse type sedimentation; (3) Early Cretaceous mafic magmatism and intrusion of alkaline granitic rocks, and deposition of lacustrine sediments; (4) Mid-Late Cretaceous characterised by normal faulting, bimodal dyke swarms, A-type alkali granites, metamorphic core complexes and deposition of coal-bearing strata.

As also pointed out in Chap. 5, in southeastern China (Fig. 5.1), the Yanshanian magmatic zone is subparallel to and overlaps with magmatic belts of Caledonian-Variscan and Indosinian ages, which are attributed to successive phases of oceanic

Table 7.3 Main Yanshanian events. (Slightly modified after Shao et al. 2007)

Episode	Formation	Volcano-sedimentary sequence	Magma	Age (Ma)	Tectonism
Mesozoic sedimentary formation, and volcanic and tectonic activity in the Yanshan area					
Dabeigou cycle, end of Early Cretaceous	Nandian	River-lake facies, oil shale or coal			Activity diminishing, fault basin changing into downwarped basin
	Qingshilazi Huajiying	Intermediate basic volcanic-sedimentary rocks, basalts at bottom		119–123 (K-Ar)	
	Xiguayuan Dabeigou				
Uplift, formation of metamorphic core complex, and instrusion of mafic dyke swarms and granites (130–120 Ma)					
Zhangjiakou cycle, start of Early Cretaceous	Zhangjiakou	High-K rhyolitic and trachytic magmatism	High-K felsic magmas from partially melted lower crust with initial $^{87}Sr/^{86}Sr$ ratios of 0.7064–0.7073	130–132 (zircon U-Pb)	Uplift and metamorphic core complexes
	Baiqi	Pyroclastic volcanic rocks and intermediate lava		136 (zircon U-Pb) 138–139 (WR Rb-Sr)	
Differential elevation, interruption and denundation of sediments, thrust-nappe structure (to 140 Ma)					
Tiaojishan cycle, Late Jurassic	Houcheng	Fluvial-lacustrine facies formation with interbedded bimodal volcanic rocks	Mixture of two magmas from upper mantle and lower crust with ($^{87}Sr/^{86}Sr$); of 0.7065–0.7073	145–140 (K-Ar)	Volcanic rift basin changing into downwarped basin
	Tiaojishan	K-rich trachyandesite basalatic volcanism		157 (U-Pb) 148 (Ar-Ar)	
Interruption of sedimentation, local angular discordance, differential elevation (ca. 160 Ma)					
Nandaling cycle	Jiulongshan	River-lake facies			Rift basin evolving to coal-bearing downwarped basin
	Xiahuayuan	Fluvial-lacustrine facies bearing coal	Primary magma produced by partial melting of upper mantle	177–198 (K-Ar)	
Middle-Early Jurassic	Nandaling	Continental alkali basalts			
Late Triassic	Xingshikou	Fluvial-lacustrine facies	Granulite, alkaline rocks	230 (zircon U-Pb) 228–220 (Ar-Ar)	Large-scale surface uplift and sedimentation in rift basins

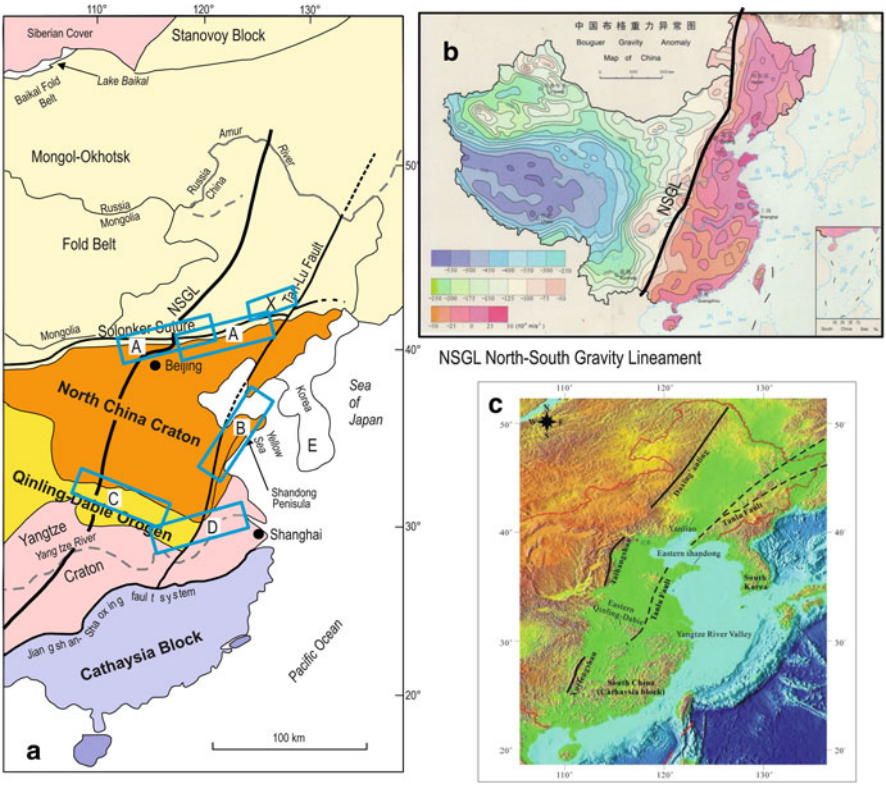

Fig. 7.30 **a** Approximate position of Mesozoic metallogenic provinces in eastern China, located along zones of structural weakness at cratonic margins and east of a pronounced gravity lineament (NSGL); labelled metallogenic provinces and corresponding Chapter in this book, where applicable: *A* Yanshan-East Liaoning-Solonker (Chap. 3), *B* Shandong and Tan-Lu (Chap. 4), *C* Qinling-Dabie orogenic belt (Chap. 5), *D* Middle Lower Yangtze River Valley (Chap. 4), *X* Xilamulun Mo belt (Chap. 3 and 5) (after Mao et al. 2010); **b** Bouguer gravity map of China showing remarkable contrast in gravity signature east and west of the NSGL (courtesy of Prof Zhang of Chinese Academy of Sciences, Beijing); **c** relief map of eastern China and adjacent regions, note low topography east of the NSGL; details in text. (After Mao et al. 2010)

crust subduction beneath an active continental margin (Jahn et al. 1990), or to the flat subduction of Li and Li (2007).

Kusky et al. (2007) discussed the "de-cratonisation" of the North China Craton, pointing out the prominent north-south gravity lineament (NSGL), as defined in the Bouguer gravity map of China (Fig. 7.30), marks the boundary between thick lithosphere to the west and thin lithosphere to the east (Figs. 3.1, 3.6 and 7.30). Furthermore, this gravity lineament is approximately parallel to the Pacific subduction margin. To the east of the NSGL, the crust and lithosphere are thinner and there is high heat flow and the Bouguer anomalies are from zero to slightly positive (Fig. 7.30b). This region is also seismically active and beneath the source areas of earthquakes, there are low-velocity and high-conductivity anomalies, which have

been interpreted to be associated with fluids (Kusky et al. 2007). Gravity changes by 100 mgals from west to east in the NSGL across a width of 250–200 km. To the west of the NGSL, there are high negative gravity anomalies, low heat flow and high seismic velocities (8.3–8.1 km/s), 200–150 km thick lithospheric mantle, coupled to a 45–40 km thick crust with elevated topography. Areas to the east of the NSGL, have high heat flow, lower seismic velocities of 7.7–7.6 km/s, the lithosphere is only 90–60 km thick and the overlying crust thins from 42 to 28 km and a low-relief surface topography. The latter feature has been explained by thermal subsidence following lithospheric delamination, allowing a surface lowering of at least 1.3 km over a period of 100 Myrs (Windley et al. 2010). The gravity lineament (NSGL) referred to above, more or less coincides with the tectonic boundary (Trans-North-China orogen that separates the Western Block and Eastern Block of the NCC), and along the eastern part of the Great Hinggan and Taihang Mountains. The Tanlu fault, is approximately parallel to the NSGL. As already mentioned, the NSGL, parallels the western Pacific subduction margin, suggesting a causative relationship with the magmatism east of the gravity lineament. Mesozoic igneous activity in the Eastern Block of the NCC, range from gabbro through monzonite, monzogranite to syenite, with geochemical signatures ranging from high K-calc-alkaline to shoshonite, high Sr-Ba and Sr/Y, La/Yb and highly enriched Sr-Nd isotopic compositions and εNd(t) from −20 to −8 and Sr*i* from 0.7053 to 0.710 (Windley et al. 2010). U-Pb zircon ages range from 180 to 120, with peak activity between 135 and 127 Ma. Mao et al. (2011a, b), on the basis of extensive geochronological data from the Yangtze River Valley, suggested that calc-alkaline magmatism was predominant before 135 Ma and that shoshonitic magmatism after 135 Ma, corresponding to different styles of mineralisation, namely porphyry-skarns-stratabound Cu-Au-Mo-Fe and Kiruna-style Fe-P (magnetite-apatite) deposits, respectively.

Other models that attempt to explain the igneous activity and its association with lithosphere thinning, extensional tectonics and the formation of volcano-sedimentary basins include: Pacific back-arc extension, hospot-mantle plume, intraplate rifting and mantle delamination resulting from thickening due to Triassic collision between the Yangtze and North China Craton. Back-arc extension is favoured by Ratschbacher et al. (2000), on the basis of the calc-alkaline geochemistry of some of the volcanic fields. The hotspot-mantle plume model (Wilde et al. 2003) argues that a mantle avalanche was induced by the closure of the Palaeo-Tethys Ocean at 180 Ma, followed by the rise of mantle plumes. The magmatic activity continued, however, through to the Early Neogene along the entire continental margin of eastern Asia (Sengör et al. 1993). A genetic link between Yanshanian magmatism and mineralisation in eastern China is well documented (Mao et al. 2011a, b).

7.7.1 Mechanisms of Lithosphere Thinning and Mantle Dynamics Under Eastern China

Mechanisms that are suggested for lithospheric thinning can be grouped into: (1) delamination model; and (2) thermal erosion model (Zhang 2007). The delami-

nation models propose that mafic lower crust and underlying lithospheric mantle collapse by their negative buoyancy, as a result of thickening due to collision tectonics. Delamination results in rapid upwelling of asthenospheric mantle, followed by decompression melting and eruption of basaltic lavas, mafic underplating and partial melting of lower crust materials. The thermal erosion model proposes that a large heat supply causes a thermal anomaly. As mentioned previously, in the case of eastern China, this thermal anomaly may have been caused by the far-field forcing of the Ontong-Java mantle plume at 130–120 Ma (Zhang 2007 and references therein). Interesting to note that also Windley et al. (2010) suggested that the Kula-Pacific plate subduction may have been enhanced by superplume activity in the Pacific Ocean (Ontong-Java oceanic plateaux, which would have pushed the plate to subduction; equivalent to ridge push, but much stronger). Lithosphere extension is also associated with stress relaxation following collision events. This may have been the case for the North China Craton collision with the Yangtze Craton and the Siberian-Mongolian plates. In other words, lithosphere thinning and extension relate to a combination of processes, as outlined above, resulting in the generation of core complexes, rifts and basins. Regional extension was most active between 140 and 100 Ma, with the formation of rift basins and metamorphic core complexes (Kusky et al. 2007; Zhang 2007; Windley et al. 2010).

Huang et al. (2007) examined the nature of Yanshanian mafic rocks in the North China Craton. These rocks have ages ranging from ca. 155 to 98 Ma and include gabbro, diorite, dolerite, pyroxenite, alkaline basalt, lamprophyre, olivine basalt-shoshonite. Chemically these rocks have signatures of an enriched sublithospheric mantle, with two models being proposed. In one model, the subcontinental lithospheric mantle is enriched by several episodes of metasomatism linked to Archaean and Proterozoic subduction-related processes, during assembly of the North China Craton. Partial melting of this enriched lithospheric material at different depths would explain the geochemical characteristics of the mafic rocks. The second model proposes that the subcontinental lithospheric mantle was modified by subducted material from the South China Block and the Pacific plate (Huang et al. 2007). The second model, according to Huang et al. (2007), seems to explain the EMII-type signatures of the mafic rocks and the carbonatites in the western Shandong and Luxi-Jiaodong area, but it cannot explain the EMI-type signatures of mafic rocks in the central parts of the North China Craton. A lithospheric thinning model and delamination are proposed to explain the geochemical features of these mafic rocks and carbonatites. Hot asthenospheric mantle occupies the space of the detached mafic crust and lithospheric mantle and by decompression melting would produce a basaltic melt with a depleted isotopic signature.

The model envisaged by Huang et al. (2007) shows stages of the evolution of the lower crust and lithosphere of the North China Craton, from the Palaeozoic to the Cenozoic. In the top panel (Fig. 7.31a) two subduction zones are active, one towards the north from the Yangtze craton (South China Block) and the other towards the south from the Mongolian oceanic plate. Hydrous fluids are released from the subducting slabs, which metasomatise the overlying mantle wedge; kimberlite pipes carrying peridotite xenoliths are emplaced. During the Triassic to Early Jurassic

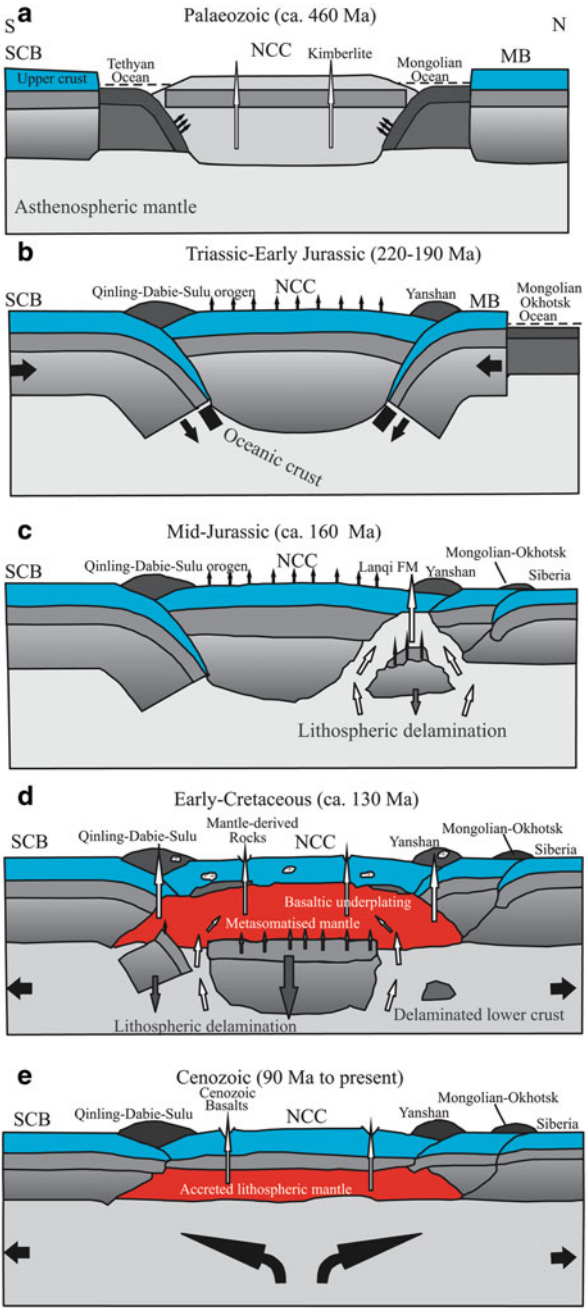

Fig. 7.31 Stages in the geodynamic evolution of the cratonic keel and subcontinental lithospheric mantle of the North China Craton (details in text). (After Huang et al. 2007)

(Fig. 7.31b), the North China Craton collided with the South China Block along the Qinling-Dabie-Sulu zone and the Mongolian plate along the Yanshan belt, resulting in uplift and thickened lithosphere. In the Mid Jurassic (ca. 160 Ma; Fig. 7.31c), the Mongol-Okhotsk Ocean closed and the Siberian plate collided with the North China Craton; the collision zone is marked by belts of ophiolites (Solonker suture and see Chap. 3 and Fig. 5.29). Some delamination occurred with upwelling of asthenopsheric mantle, volcanism and granitic magmatism with which porphyry mineral systems are associated, as exemplified by the porphyry Mo and vein deposits in northern Hebei (Fig. 5.37), discussed in Chap. 5. Large scale lithospheric delamination occurred in the Early Cretaceous (ca. 130 Ma), beneath the North China Craton and the Qinling-Dabie-Sulu orogenic belt (Fig. 7.31d). Partial melting of metasomatised lithospheric mantle took place in an extensional regime, resulting in the development of mafic melts and granitic rocks derived from crustal partial melting and basaltic underplating. Post-collisional magmatism occurred in both the Qinling-Dabie-Sulu and Yanshan orogenic belts. Finally, in the Cenozoic to Present (Fig. 7.31e), north-northeast extension along the eastern margin of Asia resulted in further thinning of the mantle lithosphere, accompanied by alkaline basaltic magmatism erupted in rift basins (Bohai and Songliao; Chap. 8).

Windley et al. (2010) proposed an interesting model to account for lithospheric thinning in eastern China, based on the role of mantle water derived from dehydration of subduction slabs and introduced in the upper mantle transition zone between 410 and 660 km depth. The following is summarised from these authors.

7.7.1.1 Hydration of Sub-oceanic Lithosphere and Double Subduction

Lithospheric thinning in the Cenozoic also affected areas north of the NCC (Fig. 1 of Windley et al. 2010). This has been ascribed to the subducting Pacific plate and perhaps the flat (stagnant) slab model, as suggested by seismic tomography (Zhao 2004, 2009). The tomographic images produced by Zhao and co-workers since about 2004 and published in several papers, exhibit exceptionally well a flat or stagnant subduction slab at the 600–410 km transition zone. The stagnant slab is related to westward subduction of the Pacific plate, with Datong, Wudalianchi and Changbai active volcanoes being related to the Pacific subduction processes. Asthenospheric flow above the Pacific subduction plate and the stagnant slab played an important role in the lithospheric erosion (thermal or otherwise), because it provided H_2O to underlying mantle, triggering partial melting of a fertile SCML and the rise of new asthenospheric melts. Zhao et al.'s model is shown in Fig. 7.32.

The subduction of either young, hot slabs or old, cold oceanic lithosphere such that of the western Pacific, release and/or transport abundant water into the overlying mantle wedge and to the 410–660 km transition zone, respectively.

The Pacific plate (old and present day), subducts westward at the same time as the Indo-Australian plate subducts northeast. The north- and northeast-directed Indo-Australian subduction has been active since the break-up of Gondwana. Tomographic images confirm the presence of flat-lying fast seismic wave anomalies, interpreted as

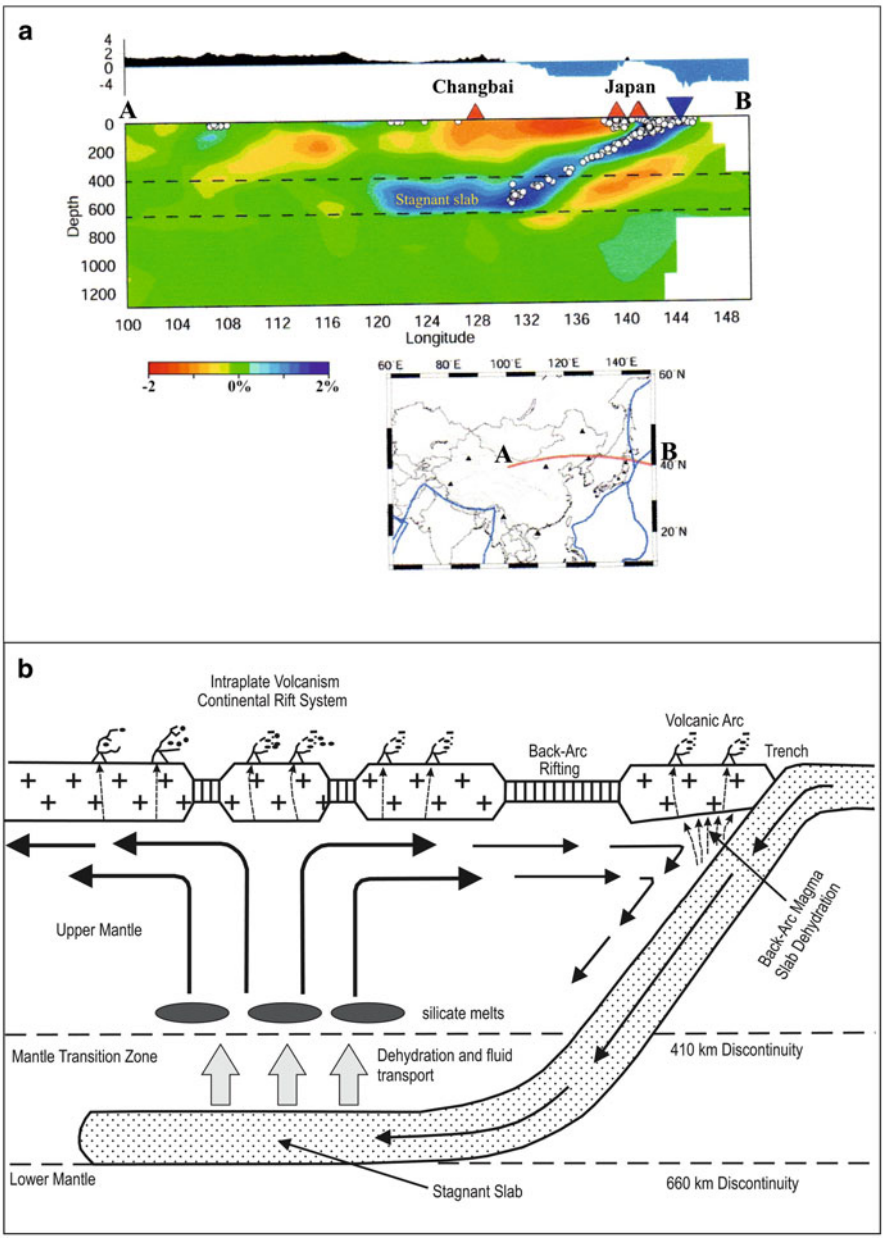

Fig. 7.32 **a** Vertical cross section of P-wave tomography from the surface down to 1,300 km depth along a profile shown on the insert map (Huang and Zhao 2006). *Red* and *blue* colors denote slow and fast velocity perturbations (in %), respectively. The velocity perturbation scale is shown below the cross sections. *White dots* denote earthquakes within 100-km width of the profile. The two *dashed lines* show the 410 and 660 km discontinuities. *Solid triangles* show the active volcanoes. The *reverse triangle* shows the location of the Japan Trench; reproduced unchanged by courtesy of

ancient stagnant slabs, not related to present-day subduction slabs. The implication here is that these flat slabs at the 410–660 km transition zone, survives for tens of million years and gradually would have released water, due to heating from the upper mantle (below the 660 km boundary), thereby creating hydrous plumes.

Water in the transition zone is stored in what Windley and co-authors called "nominally" anhydrous minerals in "hydrogen-related point defects". Olivine, for example, in the upper 400 km of the mantle is calculated to store up to 2,000 ppm by weight water at 13 GPa and 1,100 °C, clinopyroxene up to 3,000 ppm and so on. These calculations lead to the conclusion that if saturated a transition zone with 70 % wadsleyite (β-Mg_2SiO_4), would contain four times the amount of water in the Earth's hydrosphere and thus constitute the largest reservoir of hydrogen on Earth. But besides oceanic crust, continental crust too can transport abundant water into the mantle, as experimentally shown by Wu et al. (2009). Phengite and lawsonite can carry 5 % by weight water at 9 GPa (200 km depth), while beyond 9 GPa clinopyroxene, stishovite and K-hollandite also contain water. The 410-km discontinuity represents the phase transformation of olivine to β spinel and can store up to 3.1 wt% water at 15.5 GPa. This, brings to mind the issue of dehydrating continental slabs (A-subduction), where for example evaporites would release abundant water (as well as S and CO_2), inducing partial melting of continental crust (Chen et al. 2004) and discussed in Chap. 5. Water released from a stagnant, flat slab can also enhance electrical conductivity. Stored water in "hydrous" phases at 410–660 km depth would become unstable with time due to conductive heating from the underlying mantle, and eventually dehydrate into anhydrous phases, releasing free water at the 410 km boundary.

These multiple subductions from the Pacific plate, Indo-Australian plate, Solonker, Mongol-Okhotsk and Qinling-Dabie, operated for a considerable cumulative geological time, probably since at least 550 Ma (see also Collins et al. 2011). The effects of multiple subduction of hydrated oceanic crust must have resulted in equally considerable multi-hydration and what Windley and co-authors refer to as hydro-weakening of the sub-continental lithosphere. Windley et al. (2010) proposed that it is this situation that led to lithospheric thinning and delamination. This lithospheric thinning and delamination would have been further enhanced by post-collisional thrusting to the north (Solonker orogenic belt) and south (Qinling-Dabie orogenic belt) of the NCC. Post-collisional tectonics triggered collapse and/or delamination in the Early Cretaceous of the hydro-weakened crustal roots of the NCC, between these two orogenic belts. The replacement of the SCLM by fertile asthenospheric mantle in the Cenozoic produced the widespread alkali basaltic magmatism

---

Prof Zhao Dapeng; **b** flat stagnant slab at the 660 km discontinuity, dehydration and degassing of the slab producing fluids that move upward, lowering the melting point and forming pools of dense hydrous magma; upwelling of these melts induces localised rifting, melting of the lithosphere and lower crustal and alkaline volcanism (after Ohtani and Zhao 2009), the age progression of the magmatism from west to east, can be explained by successive slab breaks or retreats in the same direction, which would allow mantle material to upwell through the breaks

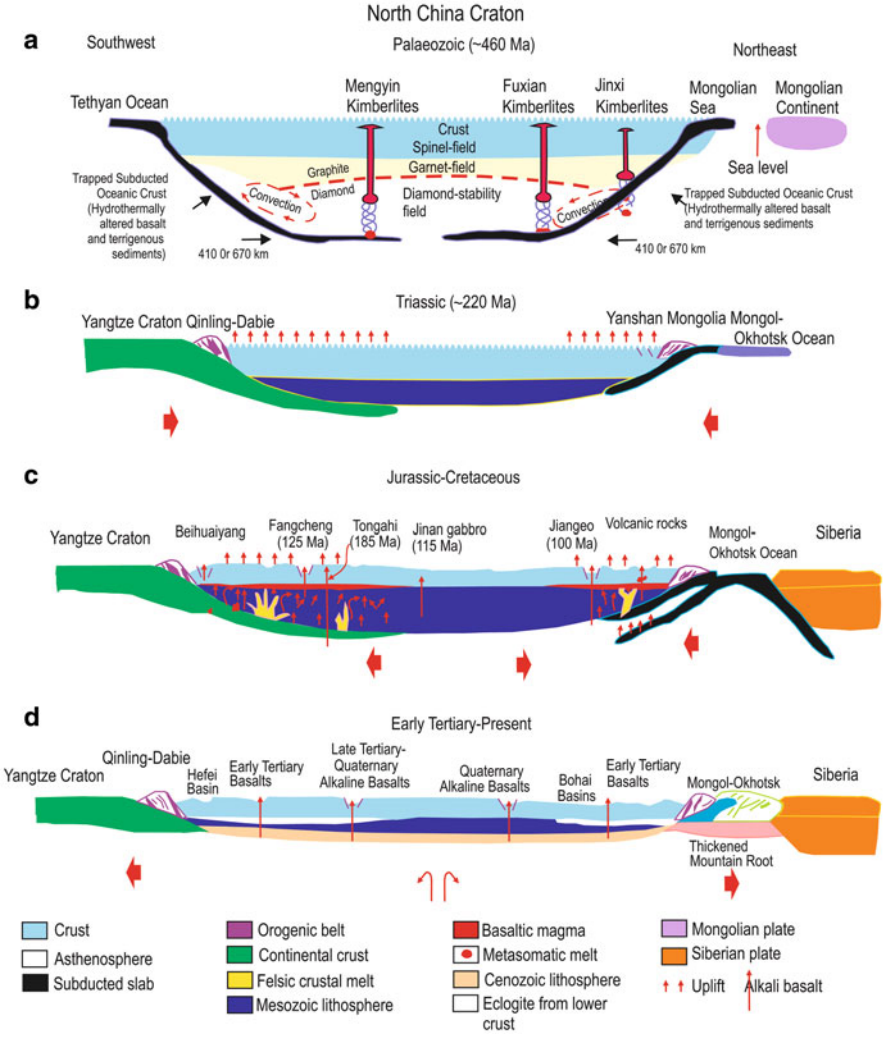

Fig. 7.33 Geodynamic evolution and mantle-lithosphere-crustal interaction of the North China Craton and adjacent areas (details in text). (After Zhang 2007; Windley et al. 2010 and references therein)

east of the NSGL (Eastern block of the NCC) (Barry and Kent 1998). A model proposed by Zhang (2007) and Windley et al. (2010), illustrating the tectono-magmatic processes, double subduction and lithospheric thinning is shown in Fig. 7.33. Double subduction during the Palaeozoic from the Palaeo-Tethys ocean northeastward and the Mongolian ocean southwestward, beneath the NCC, resulted in dehydration melting of the subducted oceanic crust producing partial melting of the lithosphere and the formation of kimberlites (Fig. 7.33a). In the Permo-Triassic collision of the

Yangzte Craton with the NCC and Mongolian microcontinent took place, forming the Qinling-Dabie-Sulu and Yanshan orogenic belts and parts of the Central Asian Orogenic Belt (CAOB, Chap. 6), resulting in tectonic uplift along the cratonic margins (Fig. 7.33b). In the Jurassic-Cretaceous time frame (Fig. 7.33c), subduction of continental crust (A-type subduction) produced felsic crustal melts, basaltic underplating and small rift volcano-sedimentary basins. Late Cretaceous to Cenozoic (Cenozoic-Quaternary) time frame (Fig. 7.33d) and the hydrous alteration from a westward flat subduction of the Pacific plate, induced lithospheric and lower crust delamination, with extensional basins and metamorphic core complexes in the NCC and a new Cenozoic lithosphere.

7.7.2 Great Hinggan (Xing'an) Range: A Yanshanian Giant Igneous Event in Northeast China

The Great Hinggan Range is characterised by Mesozoic volcanic rocks (basalt, andesite, dacite and rhyolite), erupted mainly in the early Cretaceous at about 125 Ma, and coincident with the timing of the lithospheric thinning of the Eastern Block of the NCC. Wu et al. (2005) and Wang et al. (2006) described in detail the Late Mesozoic volcanism in the Great Xinggan Range (also spelt Xing'an and Da Hinggan). Wu et al. (2005) referred to this Late Mesozoic volcanism as a giant igneous event. This Great Hinggan volcanic and associated intrusive activity affected large areas of northeast China, southern Mongolia and Korea (Fig. 7.34). The following is taken from Wang et al. (2006 December LIP of the month, posted on http://www.largeigneousprovinces.org and references therein, based on the published paper by Wang et al. 2006) and from Pirajno (unpublished data).

The Great Hinggan Range has the steepest altitude gradient that coincides with the steepest gravity gradient, which is where lithosphere thickness changes from about $<$100–60 km and high heat flow east of the NGSL to a crust 150–200 km thick and low heat flow thick west of the lineament (Figs. 7.30 and 7.34). In other words, reflecting an abrupt change from hot and seismically slow asthenosphere east of the NGSL to cold and seismically fast lithosphere to the west. As elaborated in Chap. 8, extensional structures developed into a series of volcano-sedimentary basins (e.g. Songliao), as far as the eastern Gobi Desert in Mongolia. $^{40}Ar/^{39}Ar$ dating of volcanic rocks at the base of the successions in these basins, yielded ages ranging from 155 to about 158 Ma, heralding the start of extensional tectonics. This volcanism was coeval with the emplacement of A-type granites, alkaline rocks and dyke swarms, which together with the development of core complexes attest to widespread extensional tectonism. In the Great Hinggan Range volcanic rocks cover about 100,000 km^2, with volcanic successions attaining a cumulative thickness of about 4.5 km. As shown in Fig. 7.34, these volcanic rocks extend beyond the Great Hinggan Range to the Songliao Basin, eastern Mongolia, Jiadong peninsula and the Yanshan region.

In the northern Great Hinggan Range volcanic belt, late Mesozoic volcanic rocks mainly comprise three lithostratigraphic units, which from lower to upper include:

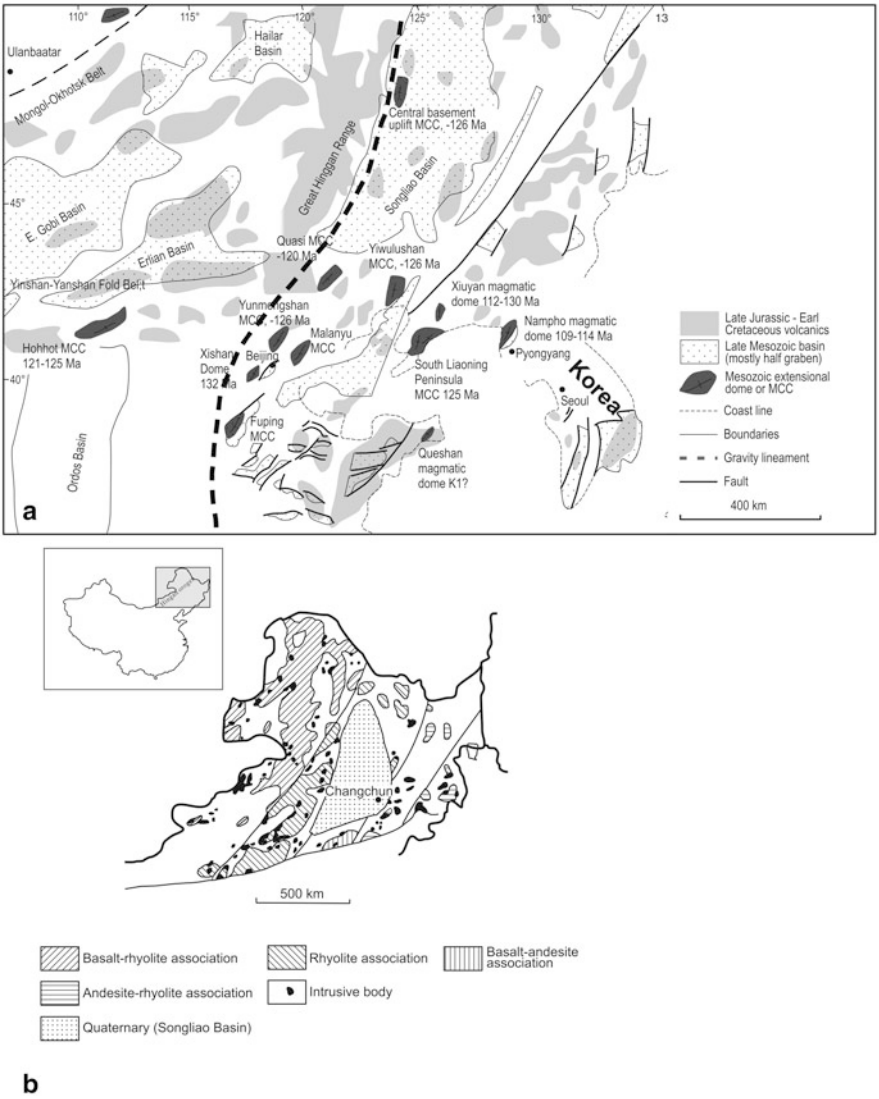

Fig. 7.34 Great Hinggan Range volcanic province; **a** distribution of Late-Jurassic volcanic rocks in north-eastern China, rift basins and core complexes, resulting from extensional tectonics linked to lithospheric thinning (modified after Windley et al. 2010), see also Fig. 8.2; **b** schematic distribution and nature of volcanic suites and associated intrusions of the Great Higgan Range province

Tamulangou, Shangkuli and Yidelieke formations (Bureau of Geology and Mineral Resources of Nei Mongol Autonomous Region, BGMRNM 1991), with a general bimodal compositional trend (Fig. 7.34). The Tamulangou formation comprises olivine basalt, basaltic andesite, trachyandesite, and welded tuff. Recent precise chronological results indicate that this formation formed during early Cretaceous (147–122 Ma,

U-Pb, Ar-Ar methods), and to a lesser extent in late Jurassic (163–160, U-Pb, Ar-Ar) (Ge et al. 2001; Fan et al. 2003; Wu et al. 2005; Wang et al. 2006; Zhang et al. 2006a). The Shangkuli formation is composed of a felsic volcanic sequence including rhyolite, dacite and rhyolitic welded tuff, erupted mainly between 135–111 Ma and to a lesser extent between 148–138 Ma (Fan et al. 2003; Zhang 2006; Wang et al. 2006). The Yidelieke formation, consisting of intermediate-mafic volcanic rocks, primarily include olivine basalt, trachyandesite, and trachybasalt, with ages between 126–101 Ma (Fan et al. 2003; Zhang 2006; Wang et al. 2006). In the southern Great Hinggan Range, Mesozoic volcanic rocks mainly comprise Manketouebo, Manitu, Baiyingaolao, and Meiletu formations. The Manketouebo formation is a bimodal assemblage composed of basaltic andesite and dacite-rhyolite. Isotopic ages of the formation are between 173 and 122 Ma (U-Pb) (Zhang 2006). The Manitu and Baiyingaolao formations are intermediate-felsic in composition, including andesite, dacite, and rhyolite, with ages ranging between 134 and 124 Ma (Zhang 2006). These studies demonstrate that the late Mesozoic volcanism in the Great Hinggan Range occurred during late Jurassic to early Cretaceous. Wang et al.'s (2006) age data revealed four groupings: 160–163, 147–140, 125–120 and 105–115 Ma. Histograms of age data compiled from the literature (including Wang et al. 2006 and references therein), show fairly well defined peaks at 135 Ma with most data clustering between 100–110 and 160 Ma (Fig. 7.35). This indicates that the main surge of igneous activity was during the Early Cretaceous, continuing with less intensity into the beginning of the Late Cretaceous and progressively decreasing through to the Late Cretaceous. Wang et al. (2006), using their age data and those from Wu et al. (2005) and Wang et al. (2002b) proposed a model in which igneous activity would have migrated from west to east during the Late Mesozoic, as shown in Fig. 7.36. A similar scenario by Zhang et al. (2011b), who used the flat-subduction (stagnant slab) model to envisage the formation of a combination of volcanic back arc-extension and subduction volcanism migrating from west to east.

This migration from the Mongol-Okhotsk suture to the Japanese islands (Fig. 7.36), is attributed to successive episodes of slab breakoff and delamination from the subduction of the Izanagi plate and the Pacific. Wang et al.'s (2006) model suggests that during the Late Mesozoic (ca. 160–140 Ma) the closure of the Mongol-Okthosk Ocean and resulting collision of the North China Craton-Mongolia Block with the Siberian Craton at ca. 160 Ma (Zorin 1999) acted as a "door stop" to the northwestward movement of the North China Craton-Mongolia block, due to the westward subduction of the Izanagi plate. This caused thicknening of the lithosphere followed by delamination and rising asthenopheric melts that induced underplating and magmatism at ca. 130–120 Ma. As crustal shears opened eastward, alkali granitic magmatism became dominant, suggesting ponding of mafic melts in the lower crust and partial melting of upper crust. The generation of alkaline plutonic activity was associated with rift-basin formation and metamorphic core complexes. It is this activity that was largely responsible for the development of hydrothermal mineral systems in the region.

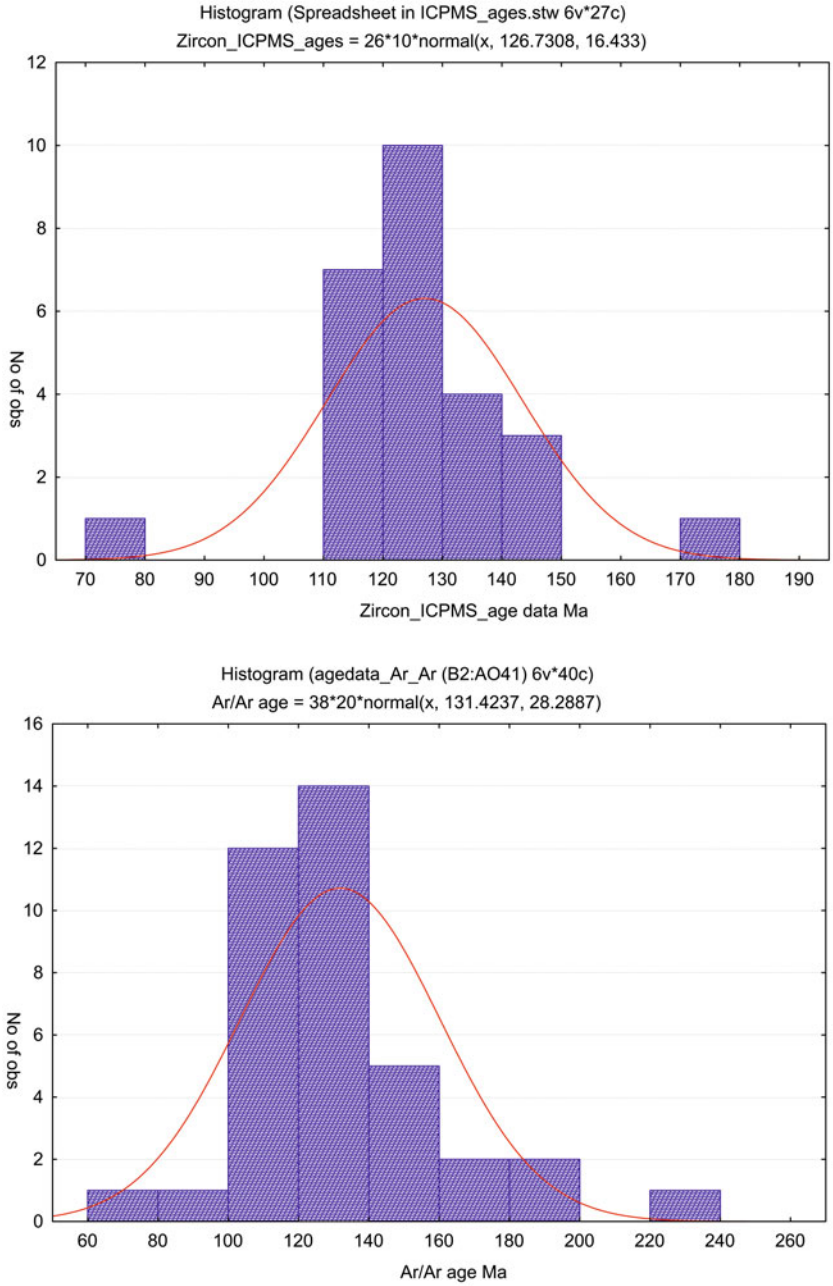

Fig. 7.35 Histograms of whole rock and single mineral isotopic ages (Ar-Ar, K-Ar, U-Pb and Rb-Sr, zircon LA-ICPMS, TIMS) of volcanic and subvolcanic rocks in the Great Hinggan Range, using data compiled by Qi et al. (2005a, b), Qi et al. (unpublished) from the following: Cong et al. (1999), Fan et al. (2003), Ge et al. (2001), Guo (2001), Jia et al. (2008), Jiang and Quan (1988), Jin (1993), Liu et al. (2002), Meng and Zhou (1996), Qin et al. (1998), Sun et al. (1996), Wu et al. (2001), Zhang et al. (2001), Zhang et al. (2006a), Zhu et al. (2003a)

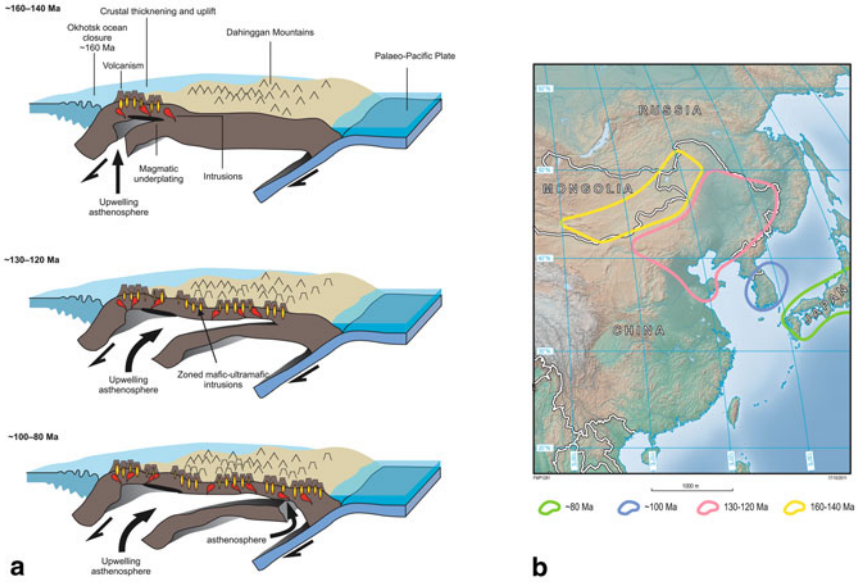

Fig. 7.36 **a** Wang et al.'s (2006) model to explain the Mesozoic magmatism in northeastern China, showing sequential delamination and slab breakoff of the Palaeopacific (Izanagi) plate, due to inboard obstruction from colliding pates and closure of the Mongol-Okhotsk Ocean; the delamination progresses eastward as does the resulting magmatism. This model may explain the type of diffuse magmatism, localized rifting and perhaps the zoned mafic-ultramafic intrusions (see Chap. 6); **b** sketch map showing the spatial and temporal trends of peak magmatism in NE Asia, showing an eastwards migration from southeastern Mongolia-Great Xin'an Range to southwestern Japan. (Data from the age compilations of Wang et al. 2006; figure also shown on http://www.largeigneousprovinces.org)

The post-Palaeozoic tectonic evolution of the Great Hinggan Range region of northeastern China can be summarized as follows. During Triassic to middle Jurassic, closure of Mongolia-Ohotsk Ocean and collision between the Siberian craton and the amalgamated Mongolia-Sino-Korea(-North China) blocks occurred at the early-middle Jurassic boundary (Zorin 1999), with subsequent thrusting, folding and magmatism until the latest Jurassic. This was followed by Early Cretaceous post-collisional extension and lithosphere delamination and late Cretaceous to present-day intraplate tectonic evolution affected by westward subduction of the Pacific plate. The last two events were closely associated with intraplate magmatism and associated mineralisation in northeastern China.

7.7.3 Mineral Systems

More than 1,000 mafic-ultramafic intrusions have been identified in northeastern China (Wu et al. 2004). Some of these intrusions, such as Hongqiling, host magmatic

Ni-Cu sulphide deposits (Wu et al. 2004; Zhou et al. 2002b; Lü et al. 2011). A wide range of hydrothermal mineral systems associated with the Yanshanian magmatism include porphyry, porphyry-skarn, Kiruna-style Fe deposits, precious metal lodes, hosted in orogenic or fold belts developed at the margins of stable cratonic blocks (e.g. North China, Yangtze), many of which have been discussed in the preceding chapters.

7.8 Concluding Remarks

In central Asia and mainland China intraplate magmatism is widespread and occurred several times between the Palaeoproterozoic and Cenozoic. This intraplate magmatism is anorogenic in nature and characterised by geochemical and isotopic signatures indicative of mantle sources. Degree of partial melting, volatile contents, nature of mantle material (enriched, depleted, entraining fragments of subducted slabs) control the products of intraplate and anorogenic magmatism, which is variably manifested by the emplacement of continental flood basalts, layered mafic-ultramafic intrusions, dyke swarms, bimodal or alkaline igneous rocks, I- and A-type granitic intrusions. Kimberlites, lamproites and carbonatites are included in this anorogenic magmatism (Ernst and Bell 2010). The impingement of mantle plumes leads to mafic underplating, which provides a source of thermal energy, resulting in widespread magmatic breakouts and consequently the formation of many different types and style of magmatic and hydrothermal ore deposits (Pirajno 2000, 2007). It is also important to bear in mind that mantle plumes impinging on the lithosphere cause uplifts of the continental crust and emplacement of LIPs, which are later dissected by rifting, affected by erosion and weathering. The rifted segments may also be involved in collision tectonics. All these phenomena result in complex terranes, where the interpretation of geodynamics is rendered difficult to recognise, leading to controversial interpretations and models.

The mineral systems of central Asia and China linked to various forms of intraplate and anorogenic magmatism include: (1) orthomagmatic Ni-Cu-PGE in mafic-ultramafic layered intrusions (e.g. Jinchuan) and in zoned mafic-ultramafic intrusions (e.g. Kalatongke); (2) hydrothermal mineral systems that include polymetallic veins, REE and rare metals associated with alkaline complexes and carbonatites, breccia pipes, porphyry and skarn deposits, intrusion-related Au lodes, generally associated with I- and A-type granites; and (3) diamondiferous kimberlites. The potential exists for iron oxide copper gold (IOCG), but this as yet remains to be tested.

Intraplate magmatism can be derived from two principal mantle sources: (1) deep mantle plumes that originate from the core-mantle boundary; and (2) shallow mantle plumes associated with asthenospheric upwellings that follow lower crustal and subcontinental lithospheric delamination. The first may be associated with a combination of effects resulting from supercontinent assembly, subduction along its external margins and subducted slab cascading or mantle avalanches, which cause instability at the core-mantle boundary, resulting in the rise of mantle plumes (Pirajno

2000 and references therein; Li et al. 2008). Large igneous provinces (LIPs), characterised by flood volcanism, dyke swarms, layered intrusions, are the manifestation of decompression melting of these deep plumes. Intracontinental rifting processes, triple junction tectonics and basin formation accompany the impingement of these mantle plumes, which are the cause of alkaline magmatism in rift settings. These alkaline magmatic systems host polymetallic veins, REE and rare metal deposits. Carbonatites and kimberlites may also be part of mantle plume activity, resulting from modification of lithospheric mantle, as documented by Griffin et al. (2005). Increasing and significant precise ages of mafic and ultramafic rocks, combined with isotope systematics more and more reveal the role of deep mantle plume or superplume events. A good example is the recently reported ca. 925 Ma LIP and correlative dyke swarms in the NCC.

PGE and Ni-Cr-bearing magnetite horizons in the layered intrusions of the ELIP host large amounts of vanadiferous magnetite, comparable to those of the Bushveld Igneous Complex. The origin of the magnetite orebodies in these layered intrusions suggests that Fe- and Ti-rich parental magmas could originate from plume melts that interact with subcontinetal lithospheric mantle enriched in those elements (Zhang et al. 2009). In the case of the Panzhihua, Hongge and other Emeishan mafic-ultramafic intrusions it is possible that progressive magnetite and ilmenite crystallisation ends up with Fe-poor and silica- and alkali-rich granitic magmas (e.g. syenites). Jakobsen et al. (2005) investigated liquid immiscibility of Fe- and silica-rich melts for the Skaergaard intrusion in eastern Greenland, where fractional crystallisation is proposed for the formation of Fe-rich (32–25 wt%) and silica-rich (70–60 wt%; granophyre) melts. Jakobsen et al. (2005) proposed that the segregation of Fe-rich and silica-rich liquids and their immiscibility, occurs in slowly cooled melts and in the case of the Skaergaard intrusion, which may well be comparable with those of the ELIP. The onset of immiscibility leads to the segregation of a dense Fe-rich melt, which sinks to the base of the magma chamber, whereas towards the top of the intrusion pods and layers of silica-rich and Fe-poor rocks are formed. As mentioned above, in the ELIP intrusions (e.g. Panzhihua, Hongge), layers of Fe-Ti oxides are segregated by liquid immiscibility, followed upward by silica-rich alkaline rocks (Fig. 7.21). Thus, there must be a distinction between alkaline rocks associated with ELIP mafic-ultramafic intrusions and younger carbonatite-alkaline complexes in the Panxi rift. This is not always clear cut in Chinese literature. It is also important to note that continental rifting caused by mantle plumes may be followed by seafloor spreading and eventually to subduction during closure of the intervening sea. This is well exemplified by the southwestern margin of the South China Block, after the emplacement of the Emeishan LIP (see Fig. 7.17). This was also shown by Dong et al. (2011), in relation to the northwestern margin of the Yangtze Craton (Hannan rift), where after the impingement of a mantle plume at ca. 900 Ma, subduction occurred between 799 and 750 Ma, resulting in what must have been significant overprinting of intraplate mineral systems by subduction-related mineral systems.

Shallow mantle plumes, or more specifically asthenospheric mantle upwellings, tend to rise from above the 660 km discontinuity and are related to continental and microcontinental collisions, crustal and lithopsheric thickening and collapse,

resulting in Basin-and-Range style rifting. Magmatic activity is manifested by scattered volcanism, dominated by alkali basalts, I- and A-type granitic intrusions and perhaps zoned Alaskan-type mafic-ultramafic intrusions at depth. Mineral systems that are associated with this geodynamic setting would include orthomagmatic Ni-Cu sulphides in the zoned intrusions, plus a wide range of hydrothermal mineral deposits, including auriferous intrusion-related vein systems and breccia pipes, porphyry Cu-Mo and skarns. A possible geodynamic scenario that can be considered for this type of intraplate magmatism, involves the previously mentioned delamination of lower crust and subcontinental lithospheric mantle, causing asthenospheric upwellings. The flat-stagnant slab model of Zhao and co-workers has also been invoked to explain the scattered alkali volcanism in continental interiors and the commonly spatially associated graben-style rift structures (see Chap. 8 for more details on rift basins). The complexity of the eastern China and Eurasian seaboard, along which extensive intraplate magmatism occurred during the Mesozoic is essentially linked to the destruction of cratonic keels and of the subcontinental lithospheric mantle by upwelling asthenopsheric mantle. This resulted in a dichotomy of crustal thickness delimited by a north-trending gravity anomaly; east of the anomaly the crust and lithosphere have normal thickness, whereas to the east the crust and lithosphere are thinned. The latter is largely associated with the emplacement of Mesozoic intraplate intrusions and volcanism, locally generating a large variety of mineral systems. This is certainly the case for many world-class mineral systems in eastern China, unrelated to convergent margins, located in intracontinental settings and associated with potassic calc-alkaline, shoshonitic and felsic magmas. These mineral systems were emplaced during a major tectono-thermal event, known as Yanshanian, which occurred during the Mesozoic and affected much of the eastern margin of mainland Asia, as far inland as Lake Baikal, Mongolia and eastern China. In eastern China, Yanshanian intracontinental mineral deposits are largely controlled by extensional structures, translithospheric strike-slip faults and fold belts, along cratonic margins of the North China Craton (NCC) and South China Craton (SCC). Furthermore, geochronological, structural, and isotope systematics, all support the concept that these intracontinental mineral systems are related to Jurassic-Early Cretaceous granites emplaced in a tectonic regimes transitional from compression to extension, associated with lithospheric thinning and delamination. The polymetallic mineral systems of eastern China were formed as a result of the unique set of geodynamic conditions and mantle dynamics discussed in this Chapter.

References

Ali JR, Thompson GM, Song XY, Wang YL (2002) Emeishan basalts (SW China) and the "end-Guadalupian" crisis: magnetobiostratigraphic constraints. J Geol Soc Lond 159:21–29

Ali JR, Lo CH, Thompson GM, Song XY (2004) Emeishan basalt Ar-Ar overprint ages define several tectonic events that affected the western Yangtze platform in the Mesozoic and Cenozoic. J Asian Earth Sci 23:163–178

Ali JR, Thompson GM, Zhou MF, Song XY (2005) Emeishan large igneous province, SW China. Lithos 79:475–489

Ali JR, Fitton JG, Herzberg C (2010) Emeishan large igneous province (SW China) and the mantle-plume up-doming hypothesis. J Geol Soc Lond 167:953–959

Barry TL, Kent RW (1998) Cenozoic magmatism in Mongolia and the origin of Central and East Asian Basalts. Geodynamics 27:347–364

Barry TL, Saunders AD, Kempton PD, Windley BF, Pringle MS, Dorjnamjaa D, Saandar S (2003) Petrogenesis of Cenozoic basalts from Mongolia: evidence for the role of asthenospheric versus metasomatised lithospheric mantle sources. J Pet 44(1):55–92

Barry TL, Ivanov AV, Rasskazov SV, Dementerova EI, Dunai TJ, Davies GR, Harrison D (2007) Helium isotopes provide no evidence for deep mantle involvement in widespread Cenozoic volcanism across Central Asia. Lithos 95:415–424

Begg GC, Hronsky JAM, Arndt NT, Griffin WL, O'Reilly SY, Hayward N (2010) Lithospheric, cratonic and geodynamic setting of Ni-Cu-PGE sulfide deposits. Econ Geol 105:1057–1070

Borisenko AS, Sotnikov VI, Izokh AE, Polyakov GV, Obolensky AA (2006) Permo-Triassic mineralization in Asia and its relation to plume magmatism. Russ Geol Geophys 47:166–182

Borisenko AS, Gas'kov IN, Dashkevich EG, Okrugin AM, Pnomarchuk AV, Travin AV (2011) Geochronology of magmatic processes and ore-formation in the central Aldan gold-ore region. Int Symp on Large Igneous Provinces of Asia; mantle plumes and metallogeny, Irkutsk, Russia 2011, Abs Vol: 38–39

Bryan S, Ernst RE (2008) Revised definition of Large Igneous Provinces (LIPs). Earth Sci Rev 86:175–202

Bureau of Geology and Mineral Resources of Nei Mongol autonomous region BGMRNM (1991) Regional geology of Nei Mongol autonomous region. Geological Publishing House, Beijing, p 725

Burke K, Dewey JF (1973) Plume-generated triple junctions: key indicators in applying plate tectonics to old rocks. J Geol 81:406–433

Campbell IH (2001) Identification of ancient mantle plumes. Geol Soc Am Sp Paper 352:5–21

Campbell IH (2007) Testing the plume theory. Chem Geol 241:153–176

Campbell IH, Griffiths RW (1990) Implications of mantle plume structure for the evolution of flood basalts. Earth Planet Sci Lett 99:79–93

Campbell IH, Griffiths RW (1992) The changing nature of mantle hotspots through time: implications for the chemical evolution of the mantle. J Geol 92:497–523

Cañón-Tapia E (2010) Origin of Large Igneous Provinces: the importance of a definition. Geol Soc Am Sp Paper 470:77–101

Cawthorn RG (2010) Origin of magnetitite layers and plugs, Bushveld Complex. Giant Ore Deposits Down-Under, 13th IAGOD Symp Proceed, pp 306–307

Chai G, Naldrett AJ (1992) Characteristics of Ni-Cu-PGE mineralization and genesis of the Jinchuan deposit, northwest China. Econ Geol 87:1475–1495

Chai FM, Zhang ZC, Mao JW, Dong LH, Zhang ZH, Wu H (2008) Geology, petrology and geochemistry of the Baishiquan Ni-Cu-bearing mafic-ultramafic intrusions in Xinjiang, NW China: implications for tectonics and genesis of ores. J Asian Earth Sci 32:218–235

Chen CH, Lin W, Lu HY, Lee CY, Tien JL, Lai YH (2000) Cretaceous fractionated I-type granitoids and metaluminous A-type granites in SE China: the late Yanshanian post-orogenic magmatism. Trans R Soc Edinb Earth Sci 91:195–205

Chen YJ, Pirajno F, Sui YH (2004) Isotope geochemistry of the Tieluping silver-lead deposit, Henan, China: a case study of orogenic silver-dominated deposits and related tectonic setting. Miner Depos 39:560–575

Chen JY, Yang XS, Xiao L, He Q (2010) Coupling of basaltic magma evolution and lithospheric seismic structure in the Emeishan large igneous province: MELTS modelling constraints. Lithos 119:61–74

Chung SL, Jahn BM (1995) Plume-lithosphere interaction in generation of the Emeishan flood basalts at the Permian-Triassic boundary. Geology 23:889–892

Chung SL, Jahn BM, Wu GY, Lo CH, Bolin C (1998) The Emeishan flood basalts in SW China: a mantle plume initiation model and its connection with continental breakup and mass extinction at the Permian-Triassic boundary. In: Flower FJM, Chung SL, Lo CH, Lee TY (eds) Mantle dynamics and plate interactions in East Asia. American Geophysical Union, Washington, DC, pp 47–58

Coffin MF, Eldhom O (1993) Scratching the surface: estimating dimensions of large igneous provinces. Geology 21:515–518

Coffin MF, Pringle MS, Duncan RA, Gladczenko TP, Storey M, Muller RD, Gahagan LA (2002) Kerguelen hotspot magma output since 130 Ma. J Pet 43(7):1121–1139

Collins WJ, Belousova EA, Kemp AIS, Murphy JB (2011) Two contrasting Phanerozoic orogenic systems revealed by hafnium isotope data. Nat Geosci 4:333–337

Condie KC (2001) Mantle plumes and their record in Earth history. Cambridge University Press, Cambridge, p 306

Cong BL (1988) Formation of the Pan-Xi paleorift. Science Press (in Chinese), Beijing, p 424

Cong RX, Yuan JH, Zhang X (1999) The features of volcanic rocks and gold minerlization in Mohe, Heilongjiang. Gold Geol 5:37–40

Cui ML, Zhang BL, Zhang LC (2011) U-Pb dating of baddeleyite and zircon from the Shizhaigou diorite in the southern margin of North China Craton: constraints on the timing and tectonic setting of the Paleoproterozoic Xiong'er Group. Gondwana Res 20:184–193

de Waal SA, Xu ZH, Li C, Mouri H (2004) Emplacement of viscous mushes in the Jinchuan ultramafic intrusion, western China. Can Miner 42:317–392

Deng JF, Zhou MF, Flower MFI, Su SG, Zhai MG, Liu C, Zhao GC, Zhou S, Wu ZW (2007) A mechanism for transforming buoyant North Chinese cratonic lithosphere to a denser equivalent for delamination. Geological Society, London, Sp Publ 280, pp 317–330

Dobretsov NL (2005) 250 Ma large igneous province of Asia: Siberian and Emeishan traps (plateau basalts) and associated granitoids. Russ Geol Geophys 46:879–890

Dong YP, Liu XM, Santosh M, Zhang XN, Chen Q, Yang C, Yang Z (2011) Neoproterozoic subduction tectonics of the northwestern Yangtze Block in South China: constraints from zircon U-Pb geochronology and geochemistry of mafic intrusions in the Hannan Massif. Precambrian Res 189:66–90

Eales HV, Cawthorn RG (1996) The Bushveld Complex. In: Cawthorne RG (ed) Layered intrusions. Elsevier, Amsterdam, Dev Geol 15:181–230

Ernst RE, Bell K (2010) Large igneous provinces (LIPs) and carbonatites. Miner Pet 98:55–76

Ernst RE, Buchan KL (eds) (2001) Mantle plumes; their identification through time. Geol Soc Am Sp Pap 352:591

Ernst RE, Buchan KL (2003) Recognising mantle plumes in the geological record. Annu Rev Earth Planet Sci 31:469–523

Ernst RE, Buchan KL, Campbell IH (2005) Frontiers in large igneous province research. Lithos 79:271–297

Fan WM, Guo F, Wang YJ, Lin G (2003) Late Mesozoic calc-alkaline volcanism of post-orogenic extension in the northern Da Hinggan Mountains, northeastern China. J Volcanol Geotherm Res 121:115–135

Farrow CEG, Watkinson DH (1999) An evaluation of the role of fluids in NI-Cu-PGE-bearing mafic ultramafic systems. Geol Assoc Can Short Course Notes 13:31–67

Ferraccioli F, Finn CA, Jordan TA, Bell RE, Anderson LM, Damaske D (2011) East Antarctic rifting triggers uplift of the Gamburtsev Mountains. Nature 479:388–392

Foulger GR (2010) Plates vs Plumes—a geological controversy. Wiley-Blackwell, Chichester, p 328

Foulger GR, Jurdy DM (eds) (2007) Plates, plumes and planetary processes. Geol Soc Am Sp Pap 430:997

French JE, Heaman LM, Chacko T, Srivastava RK (2008) 1891–1883 Ma Southern Bastar-Cuddapah mafic igneous events, India: a newly recognized large igneous province. Precambrian Res 160:308–322

Ganino C, Arndt NT, Zhou MF, Gaillard F, Chauvel C (2008) Interaction of magma with sedimentary wall rock and magnetite ore genesis in the Panzhihua mafic intrusion, SW China. Miner Depos 43:677–694

Garzanti E, Le Fort P, Sciunnach D (1999) First report of Lower Permian basalts in South Tibet: tholeiitic magmatism during break-up and incipient opening of Neotethys. J Asian Earth Sci 17:533–546

Ge WC, Li XH, Lin Q, Sun DY, Wu FY, Yun SH (2001) Geochemistry of early Cretaceous alkaline rhyolites from Hulun lake, Daxing'anling and its tectonic implications. Chin J Geol 36:176–183

Glotov AI, Ployakov GV, Hoa TT, Balykin PA, Akimtsev VA, Krivenko AP, Tolstykh ND, Phuong NT, Thanh HH, Hung TQ, Petrova TE (2001) The Ban-Phuc Ni-Cu-PGE deposit related to the Phanerozoic komatiite-basalt association in the Song Da rift, northwestern Vietnam. Can Miner 39:573–589

Griffin WL, Andi Z, O'Reilly SY, Ryan CG (1998) Phanerozoic evolution of the lithosphere beneath the Sino-Korean Craton. In: Flower M, Chung SL, Lo CH, Lee TY (eds) Mantle dynamics and plate interactions in East Asia. American Geophysical Union, Washington, DC, pp 107–126

Griffin WL, Natapov LM, O'Reilly SY, Achterbergh E van, Cherenkova AF, Cherenkov VG (2005) The Kharamai kimberlite field, Siberia: modification of the lithospheric mantle by the Siberian trap event. Lithos 81:167–187

Gubbins D, Streenivasan B, Mound J, Rost S (2011) Melting of the Earth's inner core. Nature 473:361–364

Guo GJ (2001) Characteristics of ore fluids and genesis of Xiaokouhuaying silver deposit in Yan-Liao area. In: Chen YJ, Zhang J, Lai Y (eds) Continental geodynamics and metallogeny. Seismic Press, Beijing, pp 148–153

Guo F, Fan WM, Wang YJ, Li CW (2004) When did the Emeishan plume activity start? Geochronological evidence from mafic-ultramafic dikes in southwestern China. Int Geol Rev 46:226–234

Guo ZF, Hartogen J, Liu JQ, Pasteels P, Boven A, Punzalan L, He HY, Luo XJ, Zhang WH (2005a) Potassic magmatism in Western Sichuan and Yunnan Provinces, SE Tibet, China: petrological and geochemical constraints on petrogenesis. J Pet 46:33–78

Guo JH, Sun M, Chen FK, Zhai MG (2005b) Sm–Nd and SHRIMP U–Pb zircon geochronology of high-pressure granulites in the Sanggan area, North China Craton: timing of Palaeoproterozoic continental collision. J Asian Earth Sci 24:629–642

He B, Xu YG, Chung SL, Xiao L, Wang Y (2003) Sedimentary evidence for a rapid, kilometre scale crustal doming prior to the eruption of the Emeishan flood basalts. Earth Planet Sci Lett 213:391–405

He B, Xu YG, Wang YM, Luo ZY (2006) Sedimentation and lithofacies paleogeography in south-western China, before and after the Emeishan Flood Volcanism: new insights into surface response to mantle plume activity. J Geol 114:117–132

He B, Xu YG, Huang XL, Luo ZY, Shi YR, Yang QJ, Yu SY (2007) Age and duration of the Emeishan flood volcanism, SW China: geochemistry and SHRIMP zircon U-Pb dating of silicic ignimbrites, post-volcanic Xuanwei Formation and clay tuff at the Chaotian section. Earth Planet Sci Lett 255:306–323

He YH, Zhao GC, Sun M, Wilde SA (2008) Geochemistry, isotope systematics and petrogenesis of the volcanic rocks in the Zhongtiao Mountain: an alternative interpretation for the evolution of the southern margin of the North China Craton. Lithos 102:157–178

He Q, Xiao L, Balta B, Gao R, Chen JY (2010a) Variety and complexity of the Late-Permian Emeishan basalts: Reappraisal of plume-lithosphere interaction processes. Lithos 119:91–107

He B, Xu YG, Guan JP, Zhong YT (2010b) Paleokarst on the top of the Maokou formation: further evidence for domal crustal uplift prior to the Emeishan flood volcanism. Lithos 119:1–9

He YH, Zhao GC, Sun M, Han YG (2010c) Petrogenesis and tectonic setting of volcanic rocks in the Xiaoshan and Waifangshan areas along the southern margin of the North China Craton: constraints from bulk-rock geochemistry and Sr-Nd isotopic composition. Lithos 114:186–199

Henan Bureau of Geology and Mineral Resources (HBGMR) (1989) Regional Geology of Henan province. Geological Publishing House, Beijing, p 780 (in Chinese with English Abstract)
Hou GT, Santosh M, Qian XL, Lister GS, Li JH (2008) Configuration of the late Palaeoproterozoic supercontinent Columbia: insights from radiating mafic dyke swarms. Gondwana Res 14:355–409
Hou T, Zhang ZC, Ye XR, Encarnacion J, Liu JL, Zhao ZD (2011) Noble gas isotope systematics of Fe-Ti-V oxide ore-related mafic-ultramafic layered intrusions in the Panxi area, China: the role of recycled oceanic crust in their petrogenesis. Geochim Cosmochim Acta 75(22):6727–6741
Hu RZ, Burnard PG, Bi XW, Zhou MF, Pen JT, Su WC, Wu KX (2004) Helium and argon isotope geochemistry of alkaline intrusion-associated gold and copper deposits along the Red River-Jinshajaing fault belt, SW China. Chem Geol 203:305–317
Hu HB, Mao JW, Liu DY, Niu SY, Wang YB, Li YF, Shi RR (2005) SHRIMP zircon U-Pb dating of the Tongshi magmatic complex in western Shandong and its implication. Acta Geol Sin 79:401–406
Huang J, Zhao D (2006) High-resolution mantle tomography of China and surrounding regions. J Geophys Res 111:B09305
Huang F, Li SG, Yang W (2007) Contributions of the lower crust to Mesozoic mantle-derived mafic rocks from the North China Craton: implications for lithospheric thinning. Geological Society, London, Sp Publ 280, pp 55–75
Jahn BM, Zhou XH, Li JL (1990) Formation and tectonic evolution of southeastern China and Taiwan: isotopic and geochemical constraints. Tectonophysics 183:145–160
Jakobsen JK, Veksler IV, Tegner C, Brooks CK (2005) Immiscible iron- and silica-rich melts in basalt petrogenesis documented in the Skaergaard intrusion. Geology 33:885–888
Jia CZ (1987) Geochemistry and tectonics of the Xiong'er group in the eastern Qinling mountains of China—a mid-Proterozoic volcanic arc related to plate subduction. Geological Society, London, Sp Publ 33, pp 437–448
Jia GZ, Chen JR, Yang ZG, Bian, HY, Wang YZ, Liang HJ, Jin TH, Li ZH (2008) Geology and genesis of the superlarge Jinchang gold deposit. Acta Geol Sinica 82(4):750–761
Jiang GY, Quan H (1988) Mesozoic volcanic rocks of Genhe and Hailar basins in Da Hinggan Mountains. J Shenyang Inst Geol Miner Source Chin Acad Geol Sci 3:23–100
Jiang CY, Li YZ, Zhang PB, Ye SF (2006) Petrogenesis of Permian basalts on the western margin of the Tarim Basin, China. Russ Geol Geophys 47:232–241
Jin PL (1993) Geological characteristics and genesis on gold deposits of Mesozoic volcanic type in Yanbian, Jilin province. In: Li ZN, Wang BX (eds) Collection of paper of 2nd all-China Conference for volcanic rocks. Geological Publishing House, Beijing, pp 231–236 (in Chinese)
Johnson RW (ed) (1989) Intraplate alkaline volcanism in eastern Australia and New Zealand. Cambridge University Press, Sydney, p 408
Kerr A, Leitch AM (2005) Self-destructive sulfide segregation systems and the formation of high-grade magmatic ore deposits. Econ Geol 100:311–332
Kusky TM, Li JH (2003) Paleoproterozoic tectonic evolution of the North China Craton. J Asian Earth Sci 22:383–397
Kusky TM, Windley BF, Zhai MG (2007) Tectonic evolution of the North China Block: from orogen to craton to orogen. Geological Society, London, Sp Publ 280, pp 1–34
Lehmann J, Arndt N, Windley B, Zhou MF, Wang CY, Harris C (2007) Field relationships and geochemical constraints on the emplacement of the Jinchuan intrusion and its Ni-Cu-PGE sulphide deposit, Gansu, China. Econ Geol 102:75–94
Li ZX, Li XH (2007) Formation of the 1300-km-wide intracontinental orogen and postorogenic magmatic province in Mesozoic South China: a flat-slab subduction model. Geology 35:179–182
Li C, Ripley EM (2011) The giant Jinchuan Ni-Cu-(PGE) deposit: tectonic setting, magma evolution, ore genesis, and exploration implications. In: Li C, Ripley EM (eds) Magmatic Ni-Cu and PGE deposits: geology, geochemistry and genesis. Rev Econ Geol 17:163–180
Li DS, Liang DG, Jia CZ, Wang G, Wu QH, He DF (1996) Hydrocarbon accumulations in the Tarim Basin, China. AAPG Bull 80(10):1587–1603

Li ZX, Li ZH, Kinny PD, Wang J (1999) The breakup of Rodinia: did it start with a mantle plume beneath South China? Earth Planet Sci Lett 173:171–181

Li ZX, Li XH, Kinny PD, Wang J, Zhang S, Zhou H (2003) Geochronology of Neoproterozoic syn-rift magmatism in the Yangtze Craton, South China and correlation with other continents: evidence for a mantle superplume that broke up Rodinia. Precambrian Res 122:85–109

Li HM, Mao JW, Chen YC, Wang DH, Zhang CQ, Xu H (2005a) Epigenetic hydrothermal features of the Emeishan basalt copper mineralization in NE Yunnan, SW China. Mineral deposits research: meeting the global challenge. In: Mao JW, Bierlein F (eds) Proceedings 8th Biennial SGA Meeting, Beijing, vol. 1, pp 149–152

Li XH, Su L, Chung SL, Li ZX, Liu Y, Song B, Liu DY (2005b) Formation of the Jinchuan ultramafic intrusion and the world's third largest Ni-Cu sulfide deposit: associated with the ~825 Ma south China mantle plume? Geochem Geophys Geosyst 6-Q11004. doi:10.1029/2005GC001006

Li ZL, Yang, SF, Chen HL, Yu X (2006) Discovery of a Permian quartz-syenite dyke and bimodal dyke from the Tarim Basin and its tectonic implications. International Conference on Continental Volcanism, IAVCEI 2006, Guangzhou, China. Abstracts and Program, p 64

Li ZX, Bogdanova SV, Collins AS, Davidson A, De Waele B, Ernst RE, Fitzsimons ICW, Fuck RA, Gladkochub DP, Jacobs J, Karlstrom KE, Lu SN, Natapov LM, Pease V, Pisarevsky SA, Thrane K, Vernikovskiy V (2008) Assembly, configuration, and break-up history of Rodinia: a synthesis. Precambrian Res 160:179–210

Li XH, Li WX, Li QL, Wang XC, Liu Y, Yang YH (2010a) Petrogenesis and tectonic significance of the ~ 850 Ma Gangbian alkaline complex in South China: evidence from in situ U-Pb dating, Hf-O isotopes and whole-rock geochemistry. Lithos 114:1–15

Li TS, Zhai MG, Peng P, Chen L, Guo JH (2010b) Ca. 2.5 billion year old coeval ultramafic-mafic and syenitic dykes in Eastern hebei: Implications for cratonization of the North China Craton. Precambrian Res 180:143–155

Lightfoot PC, Keays RR (2005) Siderophile and chalcophile metal variations in flood basalts from the Siberian trap, Noril'sk region: implications for the origin of the Ni-Cu-PGE sulfide ores. Econ Geol 100:439–462

Liu W, Zheng ZD, Cai JH, Yu Y (2002) Discussion of geology character and origin of Dongan gold deposit in Xunke country Heilongjiang province. Miner Res Geol 16(6):332–336 (in Chinese with English Abstract)

Lu SN, Yang CL, Li HK, Li H (2002) A group of rifting events in the terminal Paleoproterozoic in the North China Craton. Gondwana Res 5:123–131

Lü LS, Mao JW, Li HB, Pirajno F, Zhang ZH, Zhou ZH (2011) Pyrrhotite Re-Os and SHRIMP zircon U-Pb dating of the Hongqiling Ni-Cu sulfide deposits in Northeast China. Ore Geol Rev 43(1):106–119

Ma Y, Ji X-T, Li J-C, Huang M, Kan Z-Z (2003) Mineral resources of the Panzhihua region. Sichuan Science and Technology Press, Chengdu, p 275 (in Chinese)

Mao JW, Wang ZL, Li HM, Wang CY, Chen YC (2003) Carbon and isotope components in the Permian basalt-hosted copper deposit in the Ludian area, Yunnan: implication for the mineralization process. Geol Rev 49:610–615 (in Chinese)

Mao QG, Xiao WJ, Han CM, Sun M, Yuan C, Yan Z, Li JL, Yong Y, Zhang JE (2006) Zircon U-Pb age and geochemistry of the Baishiquan mafic-ultramafic complex in the eastern Tianshan, Xinjiang: constraints on the closure of the Paleo-Asia Ocean. Acta Geol Sin 22:153–162 (in Chinese with English abstract)

Mao JW, Pirajno F, Zhang ZH, Chai FM, Wu H, Chen SP, Cheng LS, Yang JM, Zhang CQ (2008a) A review of the Cu-Ni sulphide deposits in the Chinese Tianshan and Altay orogens (Xinjiang Autonomous Region, NW China): principal characteristics and ore-forming processes. J Asian Earth Sci 32(2–4):184–203

Mao JW, Xie GQ, Bierlein F, Qü WJ, Du AD, Ye HS, Pirajno F, Li HM, Guo BJ, Li YF, Yang ZQ (2008b) Tectonic implications from Re-Os Dating of Mesozoic Molybdenum Deposits in the East Qinling—Dabie Orogenic Belt. Geochim Cosmochim Acta 72:4607–4626

Mao JW, Xie GQ, Pirajno F, Ye HS, Wang YB, Li YF, Xiang JF, Zhao HJ (2010) Late Jurassic-Early Cretaceous granitoid magmatism in Eastern Qinling, central-eastern China: SHRIMP zircon U-Pb ages and tectonic implications. Aust J Earth Sci 57:51–78

Mao JW, Pirajno F, Cook N (eds) (2011a) Mesozoic metallogeny in East China and corresponding geodynamic settings—an introduction to the special issue. Ore Geol Rev 43(1):1–7

Mao JW, Xie GQ, Duan C, Pirajno F, Ishiyama D, Chen YC (2011b) A tectono-genetic model for porphyry-skarn-stratabound Cu-Au-Mo-Fe and magnetite-apatite deposits along the Middle-Yangtze River Valley, eastern China. Ore Geol Rev 43(1):203–216

Meng QL, Zhou YC (1996) The formation and evolution of Magma for J2-K1 volcanic-intrusive complex in Eastern Yanbian, Jilin province. Acta Pet Miner 15(1):30–39

Montelli R, Nolet G, Dahlen FA, Masters G, Engdahl ER, Hung SH (2004) Finite-frequency tomography reveals a variety of plumes in the mantle. Science 303:338–343

Montelli R, Nolet G, Dahlen FA, Masters G (2006) A catalogue of deep mantle plumes: new results from finite-frequency tomography. Geochem Geophys Geosyst 7-Q1107. doi:10.1029/2006GC001248

Morgan JW (1971) Convection plumes in the lower mantle. Nature 230:42–43

Morgan WJ (1972) Deep mantle convection plumes and plate motions. Bull Am Assoc Pet Geol 56:202–213

Naldrett AJ (2004) Magmatic sulphide deposits. Springer, Berlin, p 727

Naldrett AJ, Wilson A, Kinnaird J, Chunnett G (2009) PGE tenor and metal ratios within and below the Merensky Reef, Bushveld Complex: implications for its genesis. J Pet 50:625–659

Niu HC, Shan Q, Chen XM, Zhang HX (2003) Relationship between light rare earth deposits and mantle processes in Panxi rift, China. Sci China Ser D 46(Suppl):41–49

Ohtani E, Zhao D (2009) The role of water in the deep upper mantle and the transition zone: dehydration of stagnant slabs and its effects on the big mantle wedge. Russ Geol Geophys 50:1073–1078

O'Reilly SY, Griffin WL, Djomani YHP, Morgan P (2001) Are lithospheres forever? Tracking changes in subcontinental lithospheric mantle through time. GSA Today 11:4–10

Pang KN, Zhou MF, Qi L, Shellnutt G, Wang CY, Zhao DG (2010) Flood basalt-related Fe-Ti oxide deposits in the Emeishan large igneous province, SW China. Lithos 119:123–136

Peate IU, Bryan SE (2008) Re-evaluating plume-induced uplift in the Emeishan large igneous province. Nat Geosci 1:625–629

Peng P (2010) Reconstrution and interpretation of giant mafic dyke swarms: a case study of 1.78 Ga magmatism in the North China Craton. Geological Society, London, Sp Publ 338, pp 163–178

Peng P, Zai MG, Zhang HF, Guo JH (2005) Geochronological constraints on the Paleoproterozoic evolution of the North China Craton: SHRIMP zircon ages of different types of mafic dikes. Int Geol Rev 47:492–508

Peng P, Zhai M, Guo JH, Kusky T, Zhao TP (2007) Nature of mantle source contributions and crystal differentiation in the petrogenesis of the 1.78 Ga mafic dykes in the central North China Craton. Gondwana Res 12:29–46

Peng P, Zhai MG, Ernst RE, Guo JG, Liu F, Hu B (2008) A 1.78 Ga large igneous province in the North China Craton: the Xiong'er Volcanic Province and the North China Dyke Swarm. Lithos 101:260–280

Peng P, Bleeker W, Ernst RE, Söderlund U, McNicoll V (2011a) U-Pb baddeleyite ages, distribution and geochemistry of 925 Ma mafic dykes and 900 Ma sills in the North China Craton: evidence for a Neoproterozoic mantle plume. Lithos 127:210–221

Peng P, Zhai M, Li Q, Wu F, Hou Q, Li Z, Li T, Zhang Y (2011b) Neoproterozoic (~ 900 Ma) Sariwon sills in North Korea: geochronology, geochemistry and implications for the evolution of the south-eastern margin of the North China Craton. Gondwana Res 20:243–254

Piper JDA, Zhang JS, Huang BC, Roberts AP (2011) Palaeomagnetism of Precambrian dyke swarms in the North China Shield: the ~ 1.8 Ga LIP event and crustal consolidation in late Palaeoproterozoic times. J Asian Earth Sci 41:504–524

Pirajno F (2000) Ore deposits and mantle plumes. Kluwer Academic, Dordrecht, p 556

Pirajno F (2004) Hotspots and mantle plumes: global intraplate tectonics, magmatism and ore deposits. Miner Pet 82:183–216

Pirajno F (2007) Mantle plumes, associated intraplate tectono-magmatic processes and ore systems. Episodes 30:6–19

Pirajno F (2010) Intracontinental strike-slip faults, associated magmatism, mineral systems and mantle dynamics: examples from NW China and Altay-Sayan (Siberia). J Geodyn 50:325–346

Pirajno F (2011) Giant continental rift systems, "ore-making factories" and mantle plumes: examples from southern Africa, southwest-southern central Africa and Australia. Large Igneous Provinces of Asia; Mantle plumes and metallogeny, Irkutsk, Russia, Abstract Vol, p 183–186

Pirajno F, Chen YJ (2005) The Xiong'er Group: a 1.76 Ga large igneous province in east-central China? http://www.largeigneousprovinces.org/ June LIP of the Month

Pirajno F, Hoatson DM (2012) A review of Australia's Large Igneous Provinces and associated mineral systems: implications for mantle dynamics through geological time. Ore Geol Rev doi: 10.1016/j.oregeorev.2012.04.007

Pirajno F, Mao JW, Zhang ZC, Zhang ZH, Chai FM (2008) The association of mafic-ultramafic intrusions and A-type magmatism in the Tian Shan and Altay orogens, NW China: Implications for geodynamic evolution and potential for the discovery of new ore deposits. J Asian Earth Sci 32(2-4):165–183

Pirajno F, Ernst RE, Borisenko AS, Fedoseev G, Naumov EA (2009) Intraplate magmatism in central Asia and China and associated metallogeny. Ore Geol Rev 35:114–136

Qi JP, Chen YJ, Pirajno F (2005a) Geological characteristics and tectonic setting of the epithermal deposits in the northeast China. J Miner Pet 25:47–59 (in Chinese with English abstract)

Qi JP, Chen YJ, Pirajno F (2005b) Tectonic setting of epithermal deposits in Mainland China. In: Mao JW, Bierlein FP (eds) Mineral Deposit Research: Meeting the Global Challenge, vol 1. pp 577–580

Qian XL, Chen YP (1987) Late Precambrian mafic dyke swarms of the North China craton. In: Halls HC, Fahrig WF (eds) Mafic dykes swarms. Geol Assoc Can Spec Pap 34:385–391

Qin KZ, Tanka R, Li WS, Ishihara S (1998) The discovery of Indo-Sinian granites in Manzhouli Area: evidence from Rb-Sr isochrons. Acta Pet Miner 17(3):235–240 (in Chinese with English abstract)

Ratschbacher L, Hacker BR, Webb LE, McWilliams M, Ireland T, Dong S, Calvert A, Cateigner D, Wenk HR (2000) Exhumation of the ultrahigh-pressure continental crust in east central China: Cretaceous and Cenozoic unroofing and the Tan-Lu fault. J Geophys Res 105:13303–13338

Ripp GS, Doroshkevich AG, Posokhov VF, Izbrodin IA, Konopel'ko DL, Sergeev SA (2011) The age of carbonatites and mafic rocks (SHRIMP II and Rb-Sr dating) from the Oshurkovo apatite-bearing pluton (western Transabaikalia). Russ Geol Geophys 52:517–525

Ritter RR, Christensen UR (eds) (2007) Mantle plumes—a multidisciplinary approach. Springer, Berlin, p 501

Schmincke HU (2007) The Quaternary volcanic fields of the East and West Eifel (Germany). In: Ritter RR, Christensen UR (eds) Mantle plumes—a multidisciplinary approach. Springer, Berlin, pp 241–322

Schubert G, Turcotte DL, Olson P (2001) Mantle convection in the Earth and planets Cambridge University Press, Cambridge, p 940

Seltmann R, Soloviev S, Shatov V, Pirajno F, Naumov E, Cherkasov S (2010) Metallogeny of Siberia: tectonic, geologic and metallogenic settings of selected significant deposits. Aust J Earth Sci 57:655–706

Sengör AMC, Natal'in BA, Burtman VS (1993) Evolution of the Altayd tectonic collage and Paleozoic crustal growth in Eurasia. Nature 364:299–307

Shao J, He G, Zhang L (2007) Deep crustal structures of the Yanshan intracontinental orogeny: a comparison with pericontinental and intracontinental orogenies. Geological Society, London, Sp Publ 280, pp 189–200

Shellnutt JG, Jahn BM (2010) Formation of the Late Permian Panzhihua plutonic-hypabyssal-volcanic igneous complex: implications for the genesis of Fe-Ti oxide deposits and A-type granites of SW China. Earth Planet Sci Lett 289:509–519

Shellnutt JG, Zhou MF (2007) Permian peralkaline, peraluminous and metaluminous A-type granites in the Panxi district, SW China: their relationship to the Emeishan plume. Chem Geol 243(3–4):286–316

Shellnut JG, Zhou MF, Chung SL (eds) (2010) The Emeishan large igneous province: advances in the strattigraphic correlations and petrogenetic and metallogenic models. Lithos 119:Special Issue, p 161

Sheth HC (2007) 'Large Igneous Provinces (LIPs)': definition, recommended terminology and a hierarchical classification. Earth Sci Rev 85:117–124

Song XY, Zhou MF, Cao ZM, Sun M, Wang YL (2003) Ni-Cu-PGE magmatic sulphide deposits in the Yangliuping area, Permian Emeishan igneous province, SW China. Miner Depos 38:831–843

Song XY, Zhong H, Tao Y, Zhou MF (2005) Magmatic sulfide deposits in the Permian Emeishan large igneous province, SW China. In: Mao JW, Bierlein FP (eds) Mineral deposit research: meeting the global challenge, vol 1. Proceedings of the 8th Biennial SGA Meeting, Beijing, pp 465–467

Song XY, Keays RR, Zhou MF, Qi L, Ihelnfield C, Xiao JF (2009) Siderophile and chalcophile constraints on the origin of the Jinchuan Ni-Cu(PGE) sulfide deposit, NW China. Geochim Cosmochim Acta 73:404–424

Song XY, Danyushevsky LV, Keays RR, Chen LM, Wang YS, Tian YL, Xiao JF (2012) Structural, lithological and geochemical constraints on the dynamic magma plumbing system of the Jinchuan Ni-Cu sulfide deposit, NW China. Mineralium Depos 47(3):277–298

Su SG, Li C, Zhou MF, Ripley EM, Qi L (2008) Controls on variations of platinum-group element concentrations in the sulfide ores of the Jinchuan Ni-Cu deposit, western China. Miner Depos 43:609–622

Su BX, Qin KZ, Sakyi PA, Li XH, Yang YH, Sun H, Tang DM, Liu PP, Xiao QH, Malaviarachchi SPK (2011a) U-Pb ages and Hf-O isotopes from Late Paleozoic mafic-ultramafic units in the southern Central Asian Orogenic Belt: tectonic implications and evidence for an Early-Permian mantle plume. Gondwana Res 16:516–531

Su BX, Qin KZ, Sakyi PA, Liu PP, Tang DM, Malaviarachchi SPK, Xiao QH, Sun H, Dai YC, Hu Y (2011b) Geochemistry and geochronology of acidic rocks in the Beishan region, NW China: petrogenesis and tectonic implications. J Asian Earth Sci 41(1):31–43

Sun DZ, Hu WX, Min T, Zhao HF, Condie KC (1990) Origin of Late Archean and Early Proterozoic rocks and associated mineral deposits from the Zhongtiao mountains, east-central China. Precambrian Res 47:287–306

Sun DZ, Li HM, Zhou HF, Zhao FQ, Tang M (1991) Precambrian geochronology, chronotectonic framework and model of chronostructural structure of the Zhontiao mountains. Acta Geol Sin 65:216–231 (in Chinese with English abstract)

Sun FX, Wu GX, Yang P (1996) Geological feature and metallogenic model from Tuanjegou gold deposit, Heilongjiang Province, China. Jilin Geol 15:52–60

Taylor B (2006) The single largest oceanic plateau: Ontong-Java-Manihiki-Hikurangi. Earth Planet Sci Lett 241:372–380

Tang ZL, Ren DJ, Xue ZR, Mu YK (1992) Nickel deposits of China, in mineral deposits of China, Editorial Committee of mineral deposits, China, vol 2. Geological Publishing House, Beijing, pp 59–99

Tang ZL, Song XY, Su SG (2009) Ni-Cu deposits related to high-Mg basaltic magma, Jinchuan, Western China. In: Li C, Ripley EM (eds) New developments in magmatic Ni-Cu and PGE deposits. Geological Publishing House, Beijing, pp 121–140

Tao Y, Li C, Song XY, Ripley EM (2008) Mineralogical, petrological and geochemical studies of the Limahe mafic-ultramafic intrusion and associated Ni-Cu sulfide ores, SW China. Miner Depos 43:849–872

Tao Y, Ma YS, Miao LC, Zhu FL (2009) SHRIMP U–Pb zircon age of the Jinbaoshan ultramafic intrusion, Yunnan province, SW China. Chin Sci Bull 54:168–172

Tao Y, Li C, Hu RZ, Qi L, Qu WJ, Du AD (2010) Re-Os isotopic constraints on the genesis of the Limahe Ni-Cu deposit in the Emeishan large igneous province, SW China. Lithos 119:137–146

Tapponier P, Lacassin R, Leloup PH, Scharer U, Zhong DL, Wu HW, Liu XH, Ji SC, Zhang LS, Zhong JY (1990) The Ailao Shan/Red River metamorphic belt: tertiary left-lateral shear between Indochina and South China. Nature 343:431–437

Tian SH, Hou ZQ, Ding T, Xie YL, Yuan ZX, Bai G, Zou TR (2005) Muluozhai REE deposit in Sichuan province, China: stable isotope data and their implications on the dynamics of mineralization, mineral deposits research: meeting the global challenge. In: Mao JW, Bierlein F (eds) Proceedings of the 8th Biennial SGA Meeting, Beijing, vol 1, pp 845–847

Tian W, Campbell IH, Allen CM, Guan P, Pan WQ, Chen M, Yu HJ, Zhu WP (2010) The Tarim picrite-basalt-rhyolite suite, a Permian flood basalt from northwest China with contrasting rhyolites produced by fractional crystallization and anatexis. Contrib Miner Petrol 160;407–425

van der Hilst RD, de Hoop MV, Wang P, Shim SH, Ma P, Tenorio L (2007) Seismostratigraphy and thermal structure of Earth's core-mantle boundary region. Science 315:1813–1817

Wang CY, Zhou MF (2005) Origin of the Permian Baimazhai Ni-Cu-PGE sulfide deposit, Jinping, Southern Yunnan Province, SW China. 10th Platinum Int Symp, Oulu, Finland, Extended Abs Part 5, pp 606–609

Wang CY, Zhou MF (2006) Genesis of the Permian Baimazhai magmatic Ni-Cu-(PGE) sulfide deposit, Yunnan, SW China. Miner Depos 41:771–784

Wang JH, Qi L, Yin A, Xie GH (2001) Emplacement age and PGE geochemistry of lamprophyres in the Laowangzhai gold deposit, Yunnan, SW China. Sci China Ser. D 44(Supp):146–154

Wang YJ, Fan WM, Guo F, Li HM, Liang XQ (2002a) U-Pb dating of early Mesozoic granodioritic intrusions in southeastern Hunan Province, South China and its petrogenetic implications. Sci China Ser D 45:280–288

Wang PJ, Liu WZ, Wang SX, Song WH (2002b) 40Ar/39Ar and K/Ar dating on the volcanic rocks in the Songliao Basin, NE China: constraints on stratigraphy and basin dynamics. Int J Earth Sci Geol Rundsch 91:331–340

Wang YJ, Fan WM, Zhang YH, Guo F, Zhang HF, Peng TP (2004a) Geochemical, 40Ar/39Ar geochronological and Sr-Nd isotopic constraints on the origin of Paleoproterozoic mafic dikes from the southern Taihang Mountains and implications for the ca. 1800 Ma event of the North China Craton. Precambrian Res 135:55–47

Wang CY, Zhou MF, Keays RR (2004b) Origin of the Permian Baimazhai Ni-Cu-PGE sulfide deposit, Jinping, southern Yunnan Province, SW China. Proceedings of the IGCP 479, Hong Kong, Abstracts, pp 76–78

Wang CY, Zhou MF, Zhao DG (2005) Mineral chemistry of chromite from the Permian Jinbaoshan Pt-Pd-sulphide-bearing ultramafic intrusion in SW China with petrogenetic implications. Lithos 83:47–66

Wang F, Zhou XH, Zhang LC, Ying JF, Zhang YT, Wu FY, Zhu RX (2006) Late Mesozoic volcanism in the Great Xing'an Range (NE China): timing and implications for the dynamic setting of NE Asia. Earth Planet Sci Lett 251:179–198

Wang XC, Li XH, Li WX, Li ZX (2007) Ca. 825 Ma komatiitic basalts in South China: first evidence for >1,500 °C mantle melts by a Rodinian plume. Geology 35:1103–1106

Wang XC, Li XH, Li ZX, Liu Y, Yang YH, Liang XR, Tu XL (2008a) The Bikou basalts in northwestern Yangzte Block, South China: remains of 820–810 Ma continental flood basalts? Geol Soc Am Bull 120:1478–1492

Wang CY, Prichard HM, Zhou MF, Fisher PC (2008b) Platinum-group minerals from the Jinbaoshan Pd-Pt deposit, SW China: evidence for magmatic origin and hydothermal alteration. Miner Depos 43:791–803

Wang XC, Li XH, Li WX, Li ZX (2009) Variable involvement of mantle plumes in the genesis of mid-Proterozoic basaltic rocks in South China: a review. Gondwana Res 15:381–395

Wang CY, Zhou MF, Qi L (2010) Origin of extremely PGE-rich mafic magma system: an example from the Jinbaoshan ultramafic sill, Emeishan large igneous province, SW China. Lithos 119:147–161

Wang XC, Li XH, Li ZX, Liu Y, Yang YH (2010a) The Willouran basic province of South Australia: its relation to the Guibei large igneous province in South China and the breakup of Rodinia. Lithos 119:569–584

Wang XC, Li ZX, Li XH (2010b) The Willouran-Guibei large igneous province (LIP): dismembered during the breakup of the supercontinent Rodinia? August 2010 LIP of the Month. http://www.largeigneousprovinces.org/

Waszek L, Irving J, Deuss A (2011) Reconciling the hemispherical structure of Earth's inner core with its super-rotation. Nat Geosci 4:264–267

Wells ML, Hoisch TD (2008) The role of mantle delamination in widespread Late Cretaceous extension and magmatism in the Cordilleran Oroge, western United States. GSA Bull 120:515–530

Wignall PB, Sun YD, Bond DPG, Izon G, Newton RJ, Vedrine S, Widdowson M, Ali JR, Lai XL, Jiang HS, Cope H, Bottrell SH (2009) Volcanism, mass extinction and carbon isotope fluctuations in the Middle Permian of China. Science 324:1179–1182

Wilde SA, Zhou XH, Nemchin AA, Sun M (2003) Mesozoic crust-mantle interaction beneath the North China craton: a consequence of the dispersal of Gondwanaland and accretion of Asia. Geology 31:817–820

Wilson JT (1963) A possible origin for the Hawaiian islands. Can J Phys 41:863–870

Wilson AH (1996) The Great Dyke of Zimbabwe. In: Cawthorn RG (ed) Layered intrusions.Elsevier, Amsterdam, Dev Geol 15:365–402

Wilson M, Downes H (1991) Tertiary-Quaternary extension-related alkaline magmatism in Western and Central Europe. J Pet 32:811–849

Windley BF, Maruyama, S, Xiao WJ (2010) Delamination/thinning of subcontinental lithospheric mantle under eastern China: the role of water and multiple subduction. Am J Sci 310:1250–1293

Wingate MTD, Campbell IH, Compston W, Gibson GM (1998) Ion microprobe U-Pb ages for Neoproterozoic basaltic magmatism in south-central Australia and implications for the breakup of Rodinia. Precambr Res 87:135–159

Wong WH (1927) Crustal movements and igneous activities in eastern China, since Mesozoic time. Bull Geol Soc China 6:9–37

Wu C, Yuan Z, Bai G (1996) Rare earth deposits in China. In: Jones AP, Wall F, Williams CT (eds) Rare earth minerals: chemistry origin and ore deposits, Mineral Soc Ser 7. Chapman & Hall, London, pp 281–310

Wu G, Quan H, Li GY (2001) Geological characteristics of the Xijinuoshan polymetal ore field in Heilongjiang province. Geol Resour 10(4):226–234 (in Chinese with English abstract)

Wu FY, Wilde SA, Zhang GL, Sun DY (2004) Geochronology and petrogenesis of the post-orogenic Cu-Ni sulfide-bearing mafic-ultramafic complexes in Jilin Province, NE China. J Asian Earth Sci 23:781–797

Wu FY, Lin JQ, Wilde SA, Zhang X'O, Yang JH (2005) Nature and significance of the Early Cretaceous giant igneous event in eastern China. Earth Planet Sci Lett 233:103–119

Wu Y, Fei Y, Jin Z, Liu X (2009) The fate of subducted upper continental crust: an experimental study. Earth Planet Sci Lett 233:103–119

Xiao L, Xu YG, Chung SL, He B, Mei HJ (2003) Chemostratigraphic correlation of Upper Permian lavas from Yunnan Province, China: extent of the Emeishan large igneous province. Int Geol Rev 45:753–766

Xiao L, Xu YG, Xu JF, He B, Pirajno F (2004a) Chemostratigraphy of flood basalts in the Garze-Litang region and Zongza Block: implications for western extension of the Emeishan Large Igneous Province, SW China. Acta Geol Sin 78:61–67

Xiao L, Xu YG, Mei HJ, Zheng YF, He B, Pirajno F (2004b) Distinct mantle sources of low-Ti and high Ti basalts from the western Emeishan large igneous province, SW China: implications for plume-lithosphere interaction. Earth Planet Sci Lett 228:525–546

Xiao L, He Q, Pirajno F, Ni PZ, Du JX, Wei QR (2008) Possible correlation between a mantle plume and the evolution of Paleo-Tethys Jinshajiang Ocean: evidence from a volcanic rifted margin in the Xiaru-Tuoding area, Yunnan, SW China. Lithos 100:112–126

Xu YG (2001) Thermo-tectonic destruction of the Archaean lithospheric keel beneath the Sino-Korean Craton in China: evidence, timing and mechanism. Phys Chem Earth 26:747–757

Xu YG, He B (2007) Thick, high-velocity crust in the Emeishan large igneous province, southwestern China: evidence for crustal growth by magmatic underplating or intraplating. In: Foulger GR, Jurdy DM (eds) Plates, plumes, and planetary processes. Geol Soc Am Sp Pap 430:841–858

Xu YG, Menzies MA, Vroon P, Mercier JC, Lin C (1998a) Texture-temperature-geochemistry relationship in the upper mantle as revealed from spinel peridotite xenoliths from Wangping, N.E. China. J Pet 39:469–493

Xu S, Nagao K, Uto K, Wakita H, Nakai S, Liu C (1998b) He, Sr and Nd isotopes of mantle-derived xenoliths in volcanic rocks in NE China. J Asian Earth Sci 16:547–556

Xu YG, He B, Chung SL, Jahn BM, Wu GY (2001) Petrologic and geochemical constraints on the petrogenesis of Permian-Triassic Emeishan flood basalts in southwestern China. Lithos 58:145–168

Xu YG, He B, Chung SL, Menzies MA, Frey FA (2004a) Geologic, geochemical and geophysical consequence of plume involvement in the Emeishan flood-basalt province. Geology 32:917–920

Xu YG, Chung SL, Ma JL, Shi LB (2004b) Contrasting Cenozoic lithospheric evolution and architecture in the western and eastern Sino-Koren craton: constraints from geochemistry of basalts and mantle xenoliths. J Geol 112:593–605

Xu JF, Katsushiko S, Xu YG, Mei HJ, Li J (2007) Os, Pb, and Nd isotope geochemistry of the Permian Emeishan continental flood basalts: insights into the source of a large igneous province. Geochim Cosmochim Acta 71:2104–2119

Xu C, Wang LJ, Song WL, Wu M (2010) Carbonatites in China: a review for genesis and mineralization. Geosci Front 1:105–114

Yakubchuk A (2004) Architecture and mineral deposit settings of the Altaid orogenic collage: a revised model. J Asian Earth Sci 23:761–779

Yakubchuk A, Nikishin A (2004) Noril'sk-Talnakh Cu-Ni-PGE deposits: a revised tectonic model. Miner Depos 39:125–142

Yang JM, Zhang YJ, Chen W, Wang ZL, Jiang LF, Ji HG, Han CM (2003) Application of ETM^{TM} remote sensing alteration anomaly extraction technique to Gobi area, East Tianshan mountains. Miner Depos 22(3):278–286 (in Chinese)

Yang SF, Chen HL, Li ZL, Dong CW, Jia CZ, Wei GQ (2006) Early to Middle Permian magmatism in the Tarim Basin. IAVCEI, Int Conf Continental Volcanism Abstracts and Program 54

Yang SF, Li ZL, Chen HL, Santosh M, Dong CW, Yu X (2007) Permian bimodal dyke of Tarim Basin, NW China: geochemical characteristics and tectonic implications. Gondwana Res 12:113–120

Yang SH, Qu WJ, Tian Y, Chen JF, Yang G, Du A (2008) Origin of the inconsistent apparent Re-Os ages of the Jinchuan Ni-Cu sulfide ore deposit, China: post-segregation diffusion of Os. Chem Geol 247:401–418

Yao Y, Viljoen MJ, Wilson AH, Zhong H, Liu BG, Ying HL, Tu GZ, Luo N (2001) Geological characteristics of PGE-bearing layered intrusions in southwest Sichuan Province, China. Univ Witwatersrand Econ Geol Res Unit Inf Circ 358:1–17

Yi TZ, Ping H, Xu KD (1992) The Mesozoic-Cenozoic east China rift system. Tectonophysics 208:341–363

Yu X, Yang SF, Chen HL, Chen ZQ, Li ZL, Batt GE, Li YQ (2011) Permian flood basalts from the Tarim Basin, northwest China: SHRIMP zircon U-Pb dating and geochemical characteristics. Gondwana Res 20:485–497

Yuen DA, Maruyama S, Karato S, Windley BF (eds) (2007) Superplumes: beyond plate tectonics. Springer, Berlin, p 567

Zhang JH (2006) Geochronological Framework of the Mesozoic Volcanic Rocks in the Great Xing'an Range, NE China. MSc Thesis, Jilin University, p 97 (in Chinese with English abstract)

Zhang HF (2007) Temporal and spatial distribution of Mesozoic mafic magmatism in the North China Craton and implications for secular lithospheric evolution. Geological Society, London, Sp Publ 280, pp 35–54

Zhang JF, Wang XZ, Quan H, Wu G, Zhu HC (2001) The forming conditions of nonferrous and precious metal deposits in the north of Derbugan metallogenic province. Geol Resour 10(4):220–225 (in Chinese)

Zhang XS, Qin DX, Fan ZG, Nian H, Liu GL (2004) Genetic relation between Permian flood basalts and nickel-copper deposits in the Jinping area. Geol Prospect 40(5):49–56 (in Chinese with English abstract)

Zhang XS, Qin DX, Fan ZG, Nian H, Liu GL (2005) Geochemical characters of mafic-ultramafic swarms in the Baimazhai nickel and copper deposit, Jinping, Yunnan. Geol Prospect 41(4):51–56 (in Chinese with English abstract)

Zhang JH, Ge WC, Wu FY, Liu XM (2006a) Mesozoic bimodal volcanic suite in Zhalantun of the Da Hinggan Range and its geological significance: zircon U-Pb age and Hf isotopic constraints. Acta Geol Sin 80:58–69

Zhang ZC, Mao JW, Wang FS, Pirajno F (2006b) Native gold and native copper grains enclosed in olivine phenocrysts in a pricrite lava of the Emeishan large igneous province. Am Miner 91:1178–1183

Zhang XS, Pirajno F, Qin DX, Fan ZG, Liu GL, Nian H (2006c) Baimazhai, Yunnan province, China: a hydrothermally modified magmatic nickel-copper-PGE sulfide deposit. Int Geol Rev 48:725–741

Zhang CL, Li XH, Li ZX, Lu SN, Ye HM, Li HM (2007) Neoproterozoic ultramafic-mafic-carbonatite complex and granitoids in Quruqtagh of northeastern Tarim Block, western China: geochronology, geochemistry and tectonic implications. Precambrian Res 152:149–169

Zhang CL, Li XH, Li ZX, Ye HM, Li CN (2008) A Permian layered intrusive complex in the western Tarim Block, northwestern China: product of a ca. 275-Ma mantle plume. J Geol 116:269–287

Zhang ZC, Mao JW, Saunders AD, Ai Y, Li Y, Zhao L (2009) Petrogenetic modeling of three mafic-ultramafic layered intrusions in the Emeishan large igneous province, SW China, based on isotopic and bulk chemical constraints. Lithos 113:369–392

Zhang YT, Liu JQ, Guo ZF (2010a) Permian basaltic rocks in the Tarim basin, NW China: implications for plume-lithosphere interaction. Gondwana Res 18:596–610

Zhang CL, Xu YG, Li ZX, Wang HY, Ye HM (2010b) Diverse magmatism in the Tarim Block, NW China: genetically linked to the Permian Tarim mantle plume? Lithos 119:537–552

Zhang MJ, Li C, Fu P, Hu P, Ripley EM (2011a) The Permian Huangshanxi Cu-Ni deposit in western China: intrusive-extrusive association, ore genesis, and exploration implications. Miner Depos 46:153–170

Zhang C, Ma CQ, Liao QA, Zhang JY, She ZB (2011b) Implications of subduction and subduction zone migration of the Paleo-Pacific Plate beneath North China, based on distribution, geochronology and geochemistry of Late Mesozoic volcanic rocks. Int J Earth Sci Geol Rundsch 100:1665–1684

Zhao DP (2004) Global tomographic images of mantle plumes and subducting slabs: insights into deep Earth dynamics. Phys Earth Planet Int 146:3–34

Zhao DP (2009) Multiscale seismic tomography and mantle dynamics. Gondwana Res 15:297–323

Zhao JX, McCulloch MT, Korsch RJ (1994) Characterisation of a plume-related ~800 Ma magmatic event and its implications for basin formation in central-southern Australia. Earth Planet Sci Lett 121:349–367

Zhao TP, Zhou MF (2009) Geochemicall constraints on the tectonic setting of Paleoproterozoic A-type granites in the southern margin of the North China Craton. J Asian Earth Sci 36:183–195

Zhao JN, Ren FG, Li SB (2002a) Characters and significance of amygdaloidal fabric copper ore in Dasheping Copper Mine, Ruyang, Henan Province. Program Precambrian Res 25:97–104 (in Chinese)

Zhao TP, Zhou MF, Zhai MG, Xia B (2002b) Paleoproterozoic rift-related volcanism of the Xiong'er Group, North China Craton: implications for the breakup of Columbia. Int Geol Rev 44:336–351

Zhao TP, Zhai MG, Xia B, Li HM, Zhang YX, Wang YS (2004) Zircon U-Pb SHRIMP dating for the volcanic rocks of the Xiong'er Group: constraints on the initial formation age of the cover of the North China Craton. Chinese Sci Bull 40(23):2495–2502

Zhao GC, Min S, Wilde SA, Li SZ (2005) Late Archean to Paleoproterozoic evolution of the North China Craton: key issues revisited. Precambrian Res 136:177–202

Zhao GC, He YH, Sun M (2009) The Xiong'er volcanic belts at the southern margin of the North China Craton: Petrographic and geochemical evidence for its outboard position in the Paleo-Mesoproterozoic Columbia Supercontinent. Gondwana Res 16:170–181

Zheng L, Wang S, Liao YS Feng Z (2001) CO2 gas pools in Jiyang sag, China. Appl Geochem 16:1033–1039

Zhong H, Zhu WG (2006) Geochronology of layered mafic intrusions from the Pan-Xi area in the Emeishan large igneous province, SW China. Miner Depos 41:599–607

Zhong H, Zhou, XH, Zhou MF, Sun M, Liu BG (2002) Platinum-group element geochemistry of the Hongge Fe-Ti-V deposit in the Pan-xi area, southwestern China. Miner Depos 37:226–239

Zhong H, Yao Y, Hu SF, Zhou XH, Liu BG, Sun M, Zhou MF, Viljoen MJ (2003) Trace-element and Sr-Nd isotopic geochemistry of the PGE-bearing Hongge layered intrusion, southwestern China. Int Geol Rev 45:317–382

Zhong H, Campbell IH, Zhu WG, Allen CM, Hu RZ, Xie LW, He DF (2011) Timing and source constraints on the relationship between mafic and felsic intrusions in the Emeishan large igneous province. Geochim Cosmochim Acta 75:1374–1395

Zhou MF, Li WX (2000) Origin of Late Mesozoic igneous rocks in southeastern China: implications for lithosphere subduction and underplating of mafic magmas. Tectonophysics 326:269–287

Zhou TH, Goldfarb RJ, Phillips GN (2002a) Tectonics and distribution of gold deposits in China—an overview. Miner Depos 37:249–282

Zhou MF, Yang ZX, Song XY, Keays RR, Lesher CM (2002b) Magmatic Ni-Cu-PGE sulphide deposits in China. Chem Geol 209:233–257

Zhou MF, Robinson PT, Lesher CM, Keays RR, Zhang CJ, Malpas J (2005) Geochemistry, petrogenesis and metallogenesis of the Panzhihua gabbroic layered intrusion and associated Fe-Ti-V oxide deposits, Sichuan Province, SW China. J Pet 46:2253–2280

Zhou MF, Zhao JH, Jiang CY, Gao JF, Wang W, Yang SH (2009) OIB-like, heterogeneous mantle sources of Permian basaltic magmatism in the western Tarim Basin, NW China: Implications for a possible Permian large igneous province. Lithos 113:583–594

Zhu CW, Chen JR, Li TG, Cui B, Jin BY, Wang KQ (2003a) Geology and ore genesis of Jinchang gold deposit, Heilongjiang province. Miner Depos 22:56–64

Zhu BQ, Hu YG, Zhang ZW, Chang XY (2003b) Discovery of the copper deposits with features of the Keeweenawan type in the border area of Yunnan and Guizhou provinces. Sci China Ser D 46:60–72

Zhu BQ, Dai TM, Hu YG, Zhang ZW, Chen GH, Peng XY (2004) The isotopic dating evidence of two periods of hydrothermal mineralization in the large igneous province of Emeishan basalts in northeast Yunnan, China. Bull Mineral Pet Geochem 23(Suppl):108 (in Chinese)

Zhu WG, Zhong H, Li XH, Liu BG, Deng HL, Qin Y (2007) ^{40}Ar-^{39}Ar age, geochemistry and Sr-Nd-Pb isotopes of the Neoproterozoic Lengshuiqing Cu-Ni sulphide-bearing mafic-ultramafic complex, SW China. Precambrian Res 155:98–124

Zhu WG, Zhong H, Hu RZ, Liu BG, He DF, Song XY, Deng HL (2010) Platinum-group minerals and tellurides from the PGE-bearing Xinjie layered intrusion in the Emeishan large igneous province, SW China. Miner Pet 98:167–180

Zhu DC, Zhao ZD, Niu YL, Dilek Y, Hou ZQ, Mo XX (2012) The origin and pre-Cenozoic evolution of the Tibetan Plateau. Gondwana Res. doi:10.1016/j.gr.2012.02.002

Zorin Y (1999) Geodynamics of the western part of the Mongolia-Okhotsk collisional belt, Trans-Baikal region (Russia) and Mongolia. Tectonophysics 306:33–56

Chapter 8
Volcano-sedimentary and Sedimentary Basins in China: Junggar, Tarim, Tuha, Qaidam-Hoh Xil, Ordos; Basins in Eastern China Associated with Lithospheric Thinning (Songliao, Bohai)

Abstract Volcano-sedimentary, sedimentary basins and grabens cover much of China. The basins briefly introduced in this chapter include the Junggar, Tarim and Tuha in NW China, Qaidam, Ordos basins in central China and the Songliao and Bohai basins in eastern China. These basins are economically important mainly because of their hydrocarbon resources and sandstone-hosted U deposits.

The Tarim, Junggar and Tuha basins have been mentioned several times in the preceding chapters. These basins are covered by thousands of metres of Mesozoic to Cenozoic and Quaternary successions (e.g. up to 15 km thick in the Tarim Basin). Thanks to oil wells, the Mesozoic and Cenozoic lithostratigraphy is fairly well known and has allowed geologists to understand the depositional palaeo-environments. Oil wells have also intersected mafic and felsic lavas, thereby revealing and constraining associated thermal events, many of which are important for magmatic mineral systems in the region. Furthermore, recent exploration has also shown that the NW China basins host roll-front (sandstone-hosted) U deposits. Sandstone-hosted U deposits and occurrences have also been found in the Ordos basin. The U mineralisation in the Ordos basin is hosted in sandstone rocks of braided river channels facies.

The Mesozoic-Cenozoic rift systems of eastern China extend for more than 4,000 km in a north-northeast direction and between 400 and 1,000 km along an east-west direction. These rift systems cover an area of about 2×10^6 km^2 with about 300 half-grabens, forming basins from 50 to 150 km long and 10–50 km wide. Many of these rifts are still seismically active, have high heat flow and present-day hot springs. The initial subsidence and formation of half-grabens was followed by inversion during compressional and strike-slip movements and stress relaxation, followed again by renewed rifting in the Eocene, which continues to present day.

8.1 Introduction

The inception of grabens, rift basins with associated diffuse volcanism, as well the generation of coal seams and hydrocarbons in the sedimentary rocks of Junggar, Tarim, Tuha, Qaidam-Hoh-Qil and Ordos basins, are briefly introduced in this Chapter. The word "introduced" is here emphasised, mainly because the topic of coal seams and hydrocarbon resources are beyond the scope of this book. Nevertheless, the interconnection of geoscientific arguments cannot and should not be avoided. For this reason, this chapter aims to raise the awareness of the importance of "soft rock"

F. Pirajno, *The Geology and Tectonic Settings of China's Mineral Deposits,*
DOI 10.1007/978-94-007-4444-8_8,

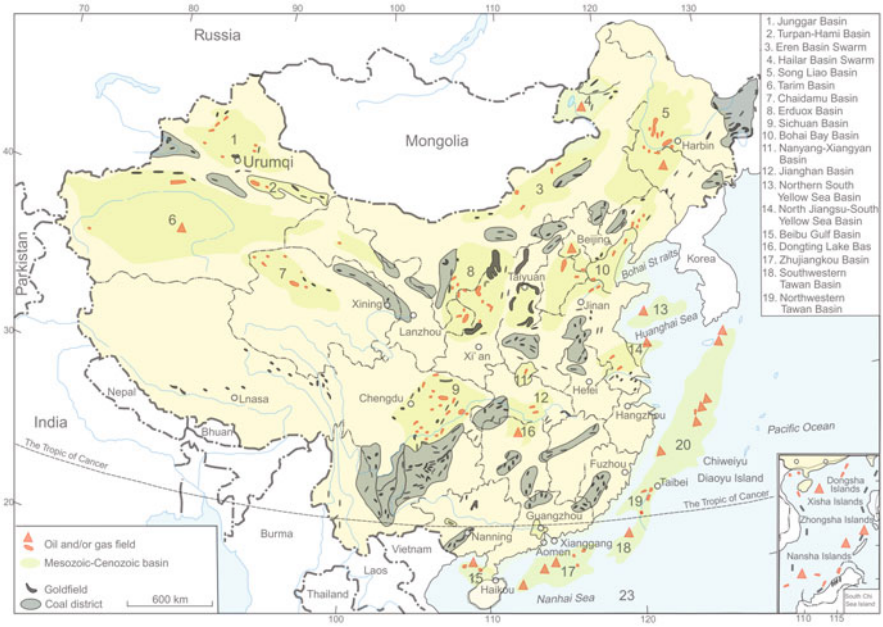

Fig. 8.1 Distribution of Mesozoic to Cenozoic sedimentary and volcano-sedimentary basins in China and associated oil, gas and coal fields. (After Zhu 2007)

geology in the overall understanding for "hard rock" geologists (and viceversa). The distribution of sedimentary, volcano-sedimentary basins and hydrocarbon fields in China are schematically shown in Fig. 8.1.

Ma and Wu (1987), Watson et al. (1987), Li (1996), Gilder et al. (1991), Tian et al. (1992), Jin et al. (1999), Ren and Xiao (2002), Ren et al. (2002), Meng (2003), Meng et al. (2003), Shu et al. (2009) discussed the formation of rift structures and associated basins in mainland China. Gilder et al. (1991) and Yi et al. (1992) provided an overview of the temporal and spatial distribution of rift systems in China and Ren et al. (2002) gave an excellent account of the evolution of the Mesozoic to Cenozoic rift systems in eastern China. Figure 8.2 shows the distribution of the main rifts in eastern and southeastern China that were formed in the Mesozoic and Cenozoic, which are also mentioned in this chapter, due to the importance that these rift systems have in the understanding of the geodynamic evolution of this economically, from the mineral resources viewpoint, important part of China.

The Mesozoic-Cenozoic rift systems of eastern China extend for more than 4,000 km in a north-northeast direction and between 400 and 1,000 km along an east-west direction. These rifts, which extend from China across to Far East Russia, cover an area of about 2×10^6 km^2 with about 300 half-grabens, forming basins from 50 to 150 km long and 10–50 km wide (Ren et al. 2002), roughly paralelling the Lake Baikal rift system to the west (Zorin et al. 2003). Many of these rifts are still seismically active, have high heat flow and present-day hot springs.

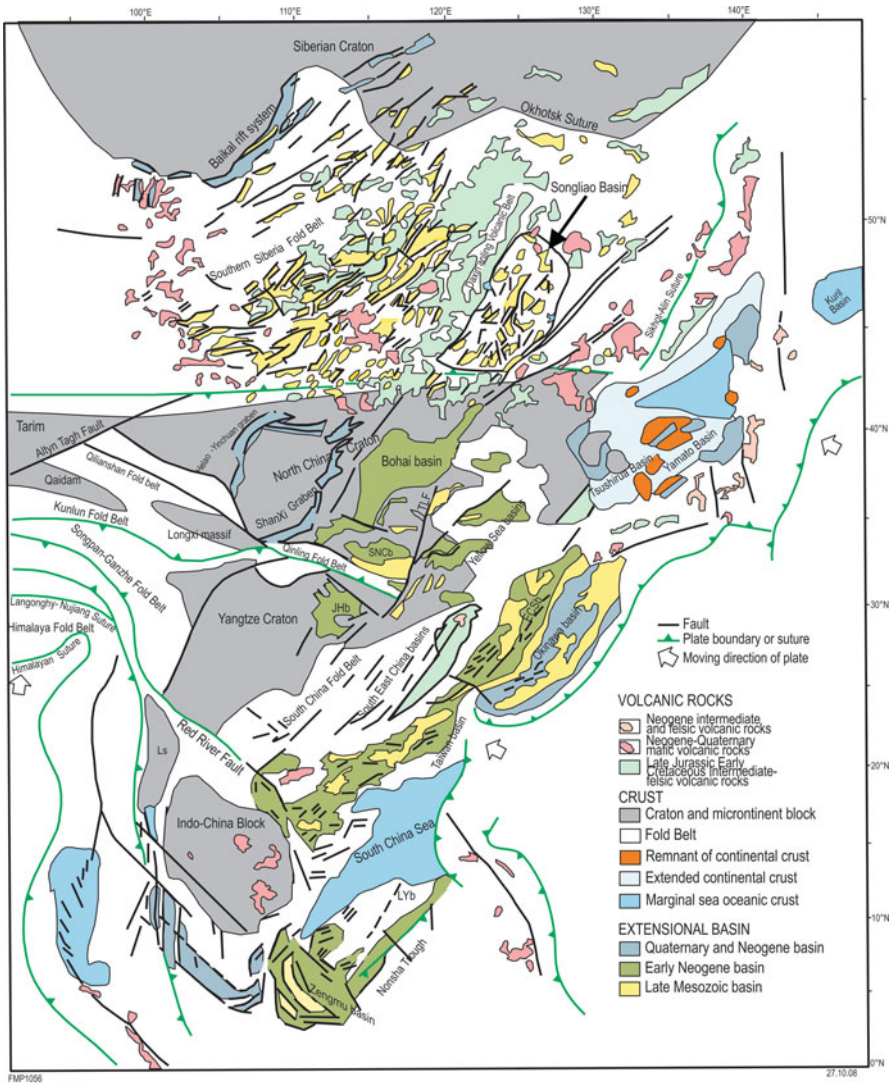

Fig. 8.2 Distribution of Mesozoic and Cenozoic rift systems and basins in eastern, southern China and adjacent regions. (After Ren et al. 2002)

Late Jurassic-Early Cretaceous and Eocene-Neogene rifting cycles are recognised, based on sedimentological and volcanological studies. These rift systems were initiated and superimposed on pre-existing north-northeast and west-northwest trending structures. The initial subsidence and formation of half-grabens was followed by inversion during compressional and strike-slip movements and stress relaxation, followed again by renewed rifting in the Eocene, which continues to present day (Yi et al. 1992). An interesting observation made by Ren et al. (2002) is that the

structural style of the rift basins depends on the rheology and architecture of the substrate. Thus, block-faulting and half-grabens with little folding seem to predominate in volcano-sedimentary rift basins covering the North China and Yangtze cratons, whereas those that formed on orogenic belts exhibit considerable compressional deformation. Most rift basins of eastern China contain syn-rift and post-rift lithological successions. Many large and small Mesozoic and Cenozoic rift basins cover parts of the North China Craton and beyond (Meng et al. 2003). These rift basins were formed between the Jurassic and Cretaceous and from the Cretaceous to Quaternary. The north-northeast trending Shanxi graben system in the centre of the North China Craton (Figs. 8.2 and 8.3), the Hebuai Basin, in the south at the boundary with the Yangtze Craton, the Bohai and Songliao basins are good examples. There is general agreement that the formation of these basins is related to extensional stress fields associated with lithospheric thinning and asthenospheric upwelling, detailed in Chap. 7. Some researchers contend that lithospheric thinning and extensional tectonics are related to subduction processes of the Kula and Pacific plates beneath the eastern margin of Asia (e.g. Griffin et al. 1998). Geophysical data show that the thinner lithosphere corresponds to the deepest Cenozoic basins, such as the Songliao Basin (see below). The Shanxi and the Yinchuang-Hetao graben systems surrounding the Ordos Block in the western North China Craton were initiated in the Cenozoic with the Shanxi grabens being the youngest at ca. 6 Ma, its opening occurring with northward propagation (Xu and Ma 1992; Kusky et al. 2007). Basins in southeast China (Cathaysia) and associated mineral systems are briefly discussed in Chap. 4 and therefore not included in this Chapter.

Watson et al. (1987) classified the basins as flexural basins and rift basins. The former are formed by subsidence due to downwarping of the lithosphere in response to compressional tectonics. Rift basins are formed as a result of extensional thinning of the lithosphere, followed by thermal subsidence. Rift basins in eastern China are generally of the Basin-and-Range style of the western USA and are commonly associated with metamorphic core complexes (Cope and Graham 2007). Yanshanian core complexes are especially common in the eastern Liaoning Peninsula and are described by Lin et al. (2007).

The distribution of China's major basins is shown in Figs. 2.7 and 8.1. In the northwest, southwest and central regions of China large basins were formed as a result of tectonic processes unrelated to the Yanshanian movements. Instead, the inception of these basin is linked to the India-Eurasian collision, which resulted in foreland extension (foreland basins). Economically important for hydrocarbon resources and sandstone-hosted U deposits are the Junggar and Tarim basins in the Xinjiang Province, the Qaidam Basin to the southeast of Tarim, Ordos and Sichuan basins in central China and the Songliao and Bohai basins in eastern China (Figs. 2.7 and 8.1). The Junggar, Tarim and the Turpan basins, may have been connected, but were later separated by thrusting along the Bogdashan in the Tianshan Orogen (Greene et al. 2001). In the pages that follow, I discuss the Junggar, Turpan-Hami and Tarim basins in northwest China, the Qaidam and Ordos basins in central China and the Bohai and Songliao basins in eastern China and, where warranted, respective uranium mineral systems.

Fig. 8.3 Major faults, strike-slip faults and associated rift basins and extent of Mesozoic-Cenozoic volcanics in the eastern interior and seaboard of Asia (note that size of polygons is approximate and in places only depicts concealed or inferred extent). Volcanic products are characterised by plateau basalts, lava shields, cinder cones and maars, associated with graben structures. (After Pirajno et al. 2009 and references therein)

8.2 Junggar Basin

The sedimentary successions of the Junggar Basin are about 11 km thick (Carroll et al. 1990) overlying a poorly known basement that possibly formed as a remnant oceanic basin, a Mid-Carboniferous back-arc basin, or a Permian foreland basin (Vincent and Allen 2001), originating from the Palaeo-Tethys Ocean. The sedimentary successions of the Junggar Basin comprise Upper Carboniferous deposits and non-marine strata of Mesozoic age. The former is at least 7 km thick and consists from the base upward of volcaniclastic turbidites succession, pyroclastic units and pillow basaltic rocks of the Carboniferous Liushugou Formation, overlain by turbiditic sandstone, mudstone and shale (Carroll et al. 1995). This is followed by the Lower Permian Shirenzigou and Tashikula formations consisting of slope deposits, shelf sandstone, carbonate with algal stromatolites and fluvial cross-bedded sandstone. The Upper Permian includes six formations, with lacustrine mudstone, siltstone, fluvial sandstone and conglomerates, organic-rich lacustrine mudstone, nodular dolomite and, finally, fluvial conglomerates with minor coals (Carroll et al. 1995). The organic-rich Lucagou and Hongaynchi formations in the Upper Permian sequence are referred to as oil shales and are thought to constitute the main source rocks of petroleum in the Junggar Basin. The Mesozoic to Cenozoic and Quaternary stratigraphy is described in detail by Vincent and Allen (2001). Typically these sedimentary sequences are separated by unconformity surfaces characterised by fluvial conglomerates. The deposition of the Mesozoic strata is linked to pulses of sedimentation related to continent-continent and arc-continent collisions and uplifts. A 1.8 km thick Triassic to Early Cretaceous succession in the eastern part of the Junggar Basin. This succession consists of alluvial fans, fluvial to shallow lacustrine sediments and aeolian deposits. In the Dingshan area in the northern part of the Junggar Basin Cenozoic successions were studied by Chen et al. (2005, 2011). These authors listed three formations, which from oldest to youngest are: the Palaeocene-Eocene Honglishan, the Eocene-Oligocene Wulunghu, the Miocene Suosuoquan formations, covered by Quaternary conglomeratic sediments. The Honglishan Formation consists of conglomerate, sandstone, mudstone of fluvial and alluvial fan facies, unconformably overlying a Palaeozoic-Mesozoic basement. The lower units of the Ulunguhe (previously called Wulunghu) Formation consist of conglomerate and plant-bearing mudstone, the middle units include conglomerate, sandstone, and laminated mudstone, whereas the uppermost units were deposited in a fluvial-lacustrine environment and comprise sandstone and mudstone. The Suosuoquan Formation contains mudstone and siltstone with calcite cement, deposited in shallow water fluvial-lacustrine to swamp environments. Chen et al. (2005, 2011) used the term "billabong" (Australian Aboriginal word referring to a dry river bed) to describe a blind river channel, formed at the intersection of north-northwest and east-west faults, where sandstone-type U mineralisation is hosted. Chen et al. (2011) pointed out that the late Cenozoic activity in the Junggar basin may have played an important role in the evolution of landforms, which control the formation of sandstone-type U deposits. Details of the lithostratigraphy in the northern Junggar Basin are shown in Table 8.1

Table 8.1 Cenozoic lithostratigraphy of the northern Junggar basin. (Modified after Chen et al. 2011)

Series/Epoch	Formation	Rock types	Facies	Contact relationships, with unit below
Holocene		Fluvial sediment, aeolian sand	Active river; desert sands	Unconformity
Upper Pleistocene	Xinjiang conglomerate	Conglomerate, sand, clay	Alluvial fans	Unconformity
Miocene	Suosuoquan	Brown-reddish mudstone, interbedded with fine-grained sandstone, mudstone and siltstone	Swamp and shallow-water lacustrine	Unconformity
Eocene-Oligocene	Upper Ulunguhe	Red mudstone, siltstone, sandstone Pebbly sandstone, mudstone and siltstone at base	Meandering fluvial, shallow-water-fluvial lacustrine	
	Middle Ulunguhe	Conglomerates, sandstone, mudstone Pebbly sandstone, conglomerate and siltstone at base	Braided fluvial and debris flow	
	Lower Ulunguhe	Plant-bearing massive grey mudstone, conglomerate, sandstone, siltstone Grey sandstone and conglomerate at base	Distal fan swamp Alluvial fan	Unconformity
Palaeocene-Eocene	Honglishan	Red mudstone Conglomerate and sandstone Sandstone and mudstone Laminated grey mudtstone, red and grey conglomerate	Fluvial Braided fluvial Alluvial fans	Unconformity
Pre-Cenozoic basement				

Fig. 8.4 Typical landscape of the desert in the Tuha Basin; Jurassic sedimentary rocks (sandstone, mudstone and coal measures)

8.2.1 Mineral Systems

Apart from hydrocarbons, so far the only mineralisation reported in the Cenozoic sedimentary successions of the northern Junggar Basin is sandstone-hosted (roll-front type) U (Chen et al. 2011). More specifically roll-front U is present in the lower Ulunguhe Formation (Table 8.1) in a unit labelled as interlayer oxidation zone, which extends for about 20 km east-west and 17 km in the north-south direction and is intercalated between impermeable mudstone beds. The interlayer oxidation zone conforms to a series of anticlines and synclines with the U-bearing roll-front at the front, where a reducing environment (plants and pyrite) causes precipitation of U minerals. The roll-front was intersected at depths of 155–214 m and its thickness varies from about 4 to 12 m, averaging 9 m. The U content is reported as being 0.016 % over 3 m; the highest value is 0.126 % over 2 m. Chen ZL and co-authors, on the basis of gamma rays logs, suggested that the U mineralisation is considerably younger than the host rocks. The source of the U is thought to be Palaeozoic granites and volcanic rocks in the surrounding Junggar fold belts.

8.3 Tuha (Turpan-Hami)

The Tuha Basin (also called Tu-Ha, from the towns of Turpan and Hami) is positioned between the Junggar Basin, with which it may have once been connected, and the northeast side of the Tarim Basin. Most of the Tuha Basin is extremely arid and desert (Fig. 8.4).

In the southwestern part of the Tuha Basin and just south of the town of Turpan is Aiding Lake, which is the second lowest land surface on Earth (150 m below sea level). Allen et al. (1991) and Windley et al. (1990) have studied the evolution of

the Tuha Basin and proposed that it was formed as a foreland basin during the collision events that formed the Tianshan Orogen. Carroll et al. (1995) and Greene et al. (2001) described the stratigraphy and sedimentology of the Carboniferous-Permian to Triassic-Jurassic sedimentary successions of the basin. Palaeocurrent directions indicate sediment derivation from the Tianshan range in the south. The Tuha succession consists of Upper Carboniferous to Lower Permian volcano-sedimentary units, mainly shallow marine limestone and sandstone, interbedded with andesitic and dacitic volcanic rocks. The marine sequence is overlain by non-marine deposits, which are composed of interbedded siltstone, sandstone, conglomerate and again andesitic and dacitic volcanic rocks. The interebedded volcanic units tend to increase up-stratigraphy.

8.3.1 Mineral Systems

The general geology of Shihongtan sandstone-hosted (roll-front) U deposit in the southwestern margin of the Tuha Basin, as described in Dahlkamp (2009), is summarised here (see also Sect. 6.3.7 in Chap. 6). The first hint that an important U occurrence may have been present in the region, was the discovery of radioactive anomalies in coal measures. As mentioned above, the U mineralisation is hosted in the Lower-Middle Jurassic Shuixigou Group (Fig. 6.38), The ores extend for about 20 km along the axis of the basin and along a crescent-shaped redox front. The mineralisation is primarily hosted in unconsolidated, carbonaceous arkose, lithic and argillaceous sandstone, containing varying amounts of pyrite and carbonate. These ore-hosting beds are altered to Fe oxides and hydroxides updip from the redox front. Uranium ore minerals include pitchblende, coffinite and uraniferous leucoxene, which is an alteration product of Fe-Ti oxides. Other elements that are present in anomalous abundances are Mo, Se, Re, Ga and Sc. Kaolinite, chlorite and illite are present as alteration minerals. Some U occurs adsorbed to clay minerals and carbonaceous debris, with ore grades averaging 0.03 % U.

Recent works in the Aiding Lake area (Shihogtan) focussed on sedimentological work and sequence stratigraphy (Wu et al. 2009). Wang et al. (2011) investigated U and Mo soil anomalies resulting from a basin-wide geochemical survey. Apart from the Shihongtan sandstone-hosted U occurrence, large and well-defined U-Mo soil anomalies were delineated near the town of Dananhu, south of the Hami. Exploration drilling at Dananhu has identified sandstone-hosted U mineralisation at a depth of 300 m.

8.4 Tarim Basin

The Tarim Basin is the largest of the Chinese basins with a 15 km thick sedimentary succession covering an area of about 560,000 km^2 that overlies the ancient rocks of the Tarim Craton. The basement rocks that constitute the Tarim Craton are described

in Chap. 3. The Tarim Basin is bound by the Tianshan orogenic belts in the north and the Tibetan plateau and Kunlun fold belt in the south (see Fig. 2.5) and therefore is a continental foreland basin (overthrust by both fold belts to the north and to the south). The Tarim is dominated by fluvial and lacustrine sediments of Triassic and Jurassic age. Oil and gas fields are present in marine sedimentary rocks (Li et al. 1996). It is interesting to follow the history of the name Tarim in Sengör and Natal'in (1996, p. 639), allegedly meaning agriculture or agricultural land in Turkish idiom and first named as such by Huang (1945).

The Tarim Basin was subjected to a complex geodynamic history extending from the Cambro-Ordovician to the Quaternary. Li et al. (1996) proposed the following evolutionary stages: (1) Aulacogen stage in the Cambro-Ordovician; (2) intracratonic depression in the Silurian-Devonian; (3) a marginal sea stage in the Carboniferous; (4) rifting in the Permian; (5) foreland basin stage in Triassic-Jurassic; and (6) uplift (Bachu) and inland basin stage in the Palaeogene through to the Quaternary. Thus, the sequence of tectonic events, from the Cambrian through to the Quaternary, including at least two rifting events, one in the Cambrian-Ordovician and one in the Permian is shown in Fig. 8.5.

The lithostratigraphy of the Tarim Basin as recently established following extensive hydrocarbon and coal exploration is shown in Fig. 8.6 (Zeng et al. 2010). The sedimentology and stratigraphy of the basin have been reported by Carroll et al. (1995), who considered the following geographic regions: western part of the Tarim Basin, Northwestern Tarim-Bachu Uplift, Northwestern Tarim-Wusi, Yingan-Sishigan and Northern Tarim-Kuqa/Baicheng.

The western part of the Tarim Basin includes Upper Palaeozoic marine beds thrust over Cretaceous continental red beds. Lower Permian rocks include carbonate rocks, turbidite successions, conglomerate and siliciclastic strata. The northwestern Tarim-Bachu Uplift consists of a conformable succession of Silurian to Lower Permian shallow marine to non-marine carbonate and siliciclastic rocks, including Devonian red sandstone and mudstone, and Ordovician limestones units are present in small fault blocks. The Lower Carboniferous section contains interbedded mudstone, micrite and evaporitic beds. Evaporite beds are also present in the northern Tarim Basin, where they reach a thickness of 200–300 m (Carroll et al. 1995). The Tarim-Bachu Uplift succession is also intruded and cut by gabbroic sills and dykes with Ar-Ar ages of ca. 275 Ma, which are part of the Tarim 290–271 Ma event, discussed in Chap. 7. The Northwestern Tarim-Wusi section includes about 2,000 m of Lower to Mid-Carboniferous shallow marine and conglomeratic rocks, outcropping near the town of Wusi. Non-marine conglomerate beds are overlain by interbedded mudstone, micrite and siliciclastic turbidite units. The Yingan-Sishichang section is characterised by Upper Carboniferous rocks that are unconformable on Devonian red beds. The Upper Carboniferous Sishichang Formation consists of conglomerate, sandstone, mudstone and limestone. Lower Permian rocks of the Kangekelin Formation overlie the Sishichang Formation and consist of limestone grading upward to rocks of the Kukupuziman Formation, which include variegated non-marine mudstone, sandstone, conglomerates and coal seams. The coal seams are of high

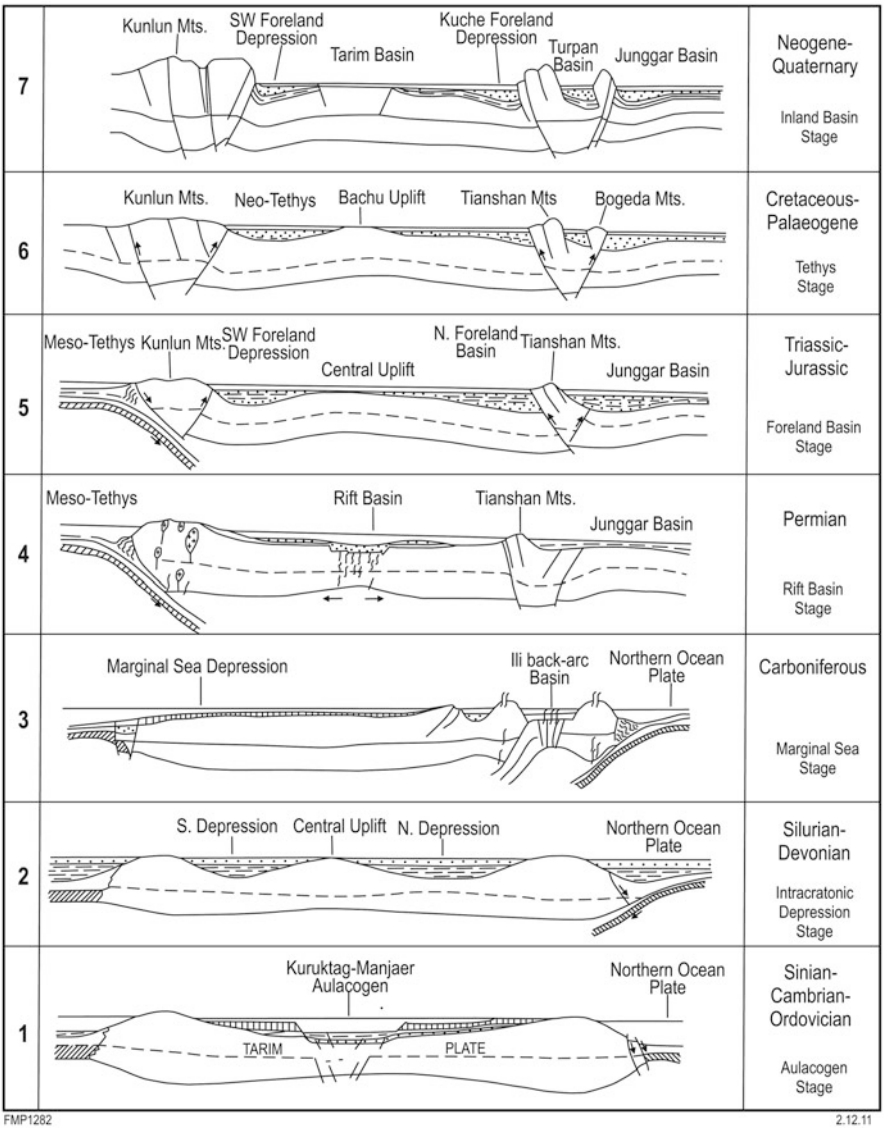

Fig. 8.5 Geodynamic evolution of the Tarim Basin from the Cambrian-Ordovician to Neogene-Quaternary. (After Li et al. 1996)

quality near Sishichang and have vitrinite reflectances ranging from 0.54 to 0.59 %, suggesting burial depths of several kilometres. Basaltic lava flows are intercalated with mudstone and sandstone of the Kukupuziman Formation and attain thicknesses of 150–200 m, forming columnar, vesicular flows. These basaltic rocks are part of continental flood basalts that cover wide areas in the northwest of the Tarim Basin

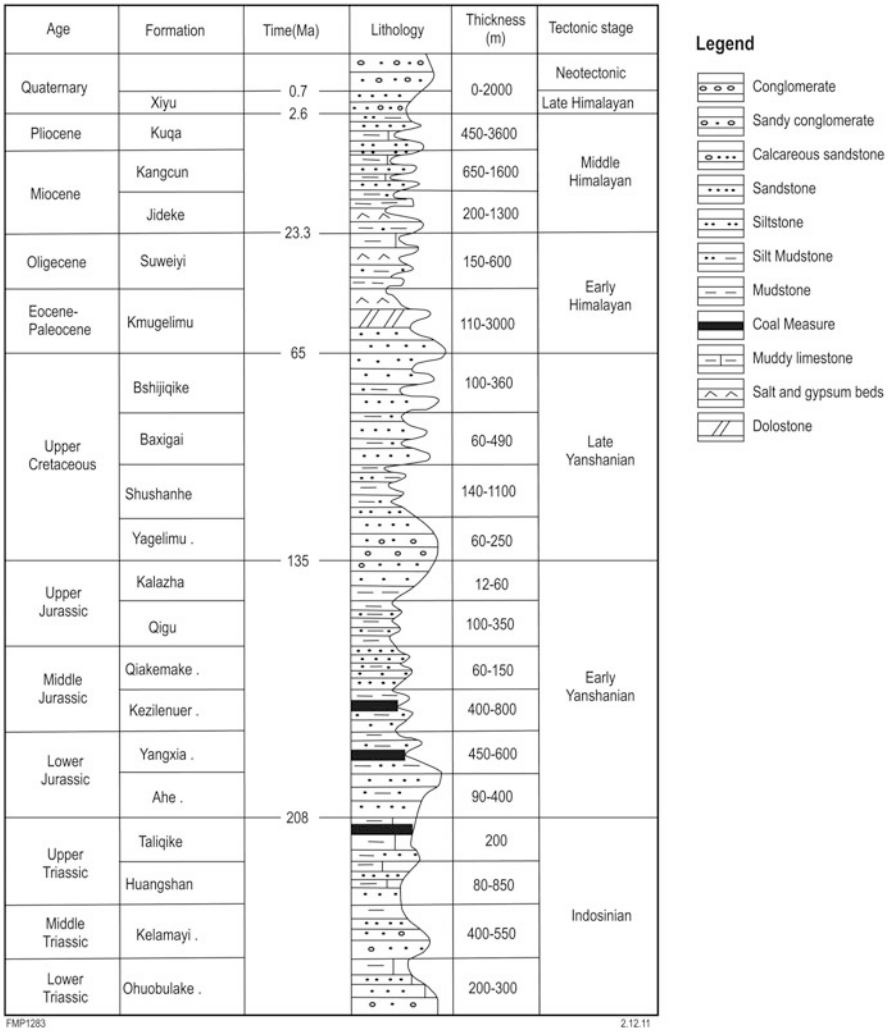

Fig. 8.6 Triassic to Quaternary lithostratigraphic succession in the northern part of the Tarim Basin. (Kuqa depression; modified after Zeng et al. 2011)

and again these are part of the Tarim (Bachu) intraplate magmatic event (Pirajno et al. 2009). The Northern Tarin-Kuqa/Baicheng section is interpreted by Carroll et al. (1995) as being a Carboniferous siliciclastic turbidite succession, overthrust from the north by Lower Permian intermediate to felsic volcanic rocks. These volcanic rocks attain several km in thickness and consist of a mix of pyroclastic units, lavas and rhyolite breccia, which have Ar-Ar ages ranging from ca. 289 to 267 Ma and are therefore coeval with the mafic rocks of the Bachu Uplift and the Sishichang basaltic lavas.

Sediment-hosted Cu deposits of possible Cretaceous age have been reported from northwest margin of the Tarim, in the Xikeer district, but very little is known and all in Chinese language (Bai and Shi 2008; Zhao 2009). The Dishui Au-Cu mine project in Baicheng county is said to come into production (Zhaojin Mining, December 2011; 256,000 t of Cu metal, the ore grading 1.06 % Cu and a Au content of 2,757 kg with ore grade of 0.41 g/t) (information downloaded from http:/en.zhaojin.com.cn/data/upload/LTN20111230639_vl9ugy.pdf).

8.5 Qaidam and Hoh Xil Basins

The Qaidam Basin, together with the adjacent Hoh Xil Basin to the south, were part of a larger depression in the Palaeogene known as the Palaeo-Qaidam Basin, between the south-verging Fenghuoshan and a north-verging thrust belt bordering the Qilianshan (Fig. 8.7). The Palaeo-Qaidam Basin, was separated into the Qaidam and Hoh Xil basins, due to the uplift of the Eastern Qunlun Range in the Neogene. According to the Yin et al. (2008b), a similar Cenozoic geodynamic evolution separated the Tarim Basin from the Junggar Basin, as a result of the uplift of the Tianshan range.

The Qaidam Basin located on the southeastern margin of the Tarim Basin, extends east-southeast for 700 km and is up to 300 km wide (Figs. 6.1b and 6.55), has an average elevation of 2,800 m above sea level and is one of the driest deserts on Earth with a precipitation of less than 50 mm/year, in the western part (Kapp et al. 2011). Much of our geological knowledge of the basin comes from researchers working on petroleum and coal geology (e.g. Cao et al. 2008, 2012; Pan et al. 2010). Yin et al. (2007, 2008a, b) combined field data with reflection seismic profiles to reconstruct the Cenozoic history of the region, related to the India-Asia collision. The following is taken from Yin A and co-workers.

The Cenozoic lithostratigraphy of the Qaidam and Hoh Xil basins is shown in Table 8.2. Alluvial and fluvial-lacustrine are the principal lithofacies in both basins. The Qaidam-Hoh Xil structural depression began to form at the onset of the India-Eurasian collision during the Palaeocene. The Qaidam Basin has a triangular shape, bounded by the Altyn Tagh fault in the northwest, the eastern Kunlun thrust belt in the south and the north Qaidam Thrust in the northeast (Ritts and Biffi 2001). Seismic profiles show that the crustal thickness of the basin is about 10–25 km thinner than the surrounding thrust belts that form mountain ranges, which provided the fluvial and fluvial-lacustrine sediments that accumulated in the basin. The sedimentary fill of the basin is deformed in a broad synclinorium, with amplitudes of 16 and 4 km in the west and east, respectively. The Cenozoic sedimentary rocks, which have been extensively prospected for hydrocarbons, unconformably overlie a basement of Precambrian-Silurian metamorphic rocks, generally exposed along the margins of the basin. The Cenozoic sedimentary strata reach a thickness of more than 15 km.

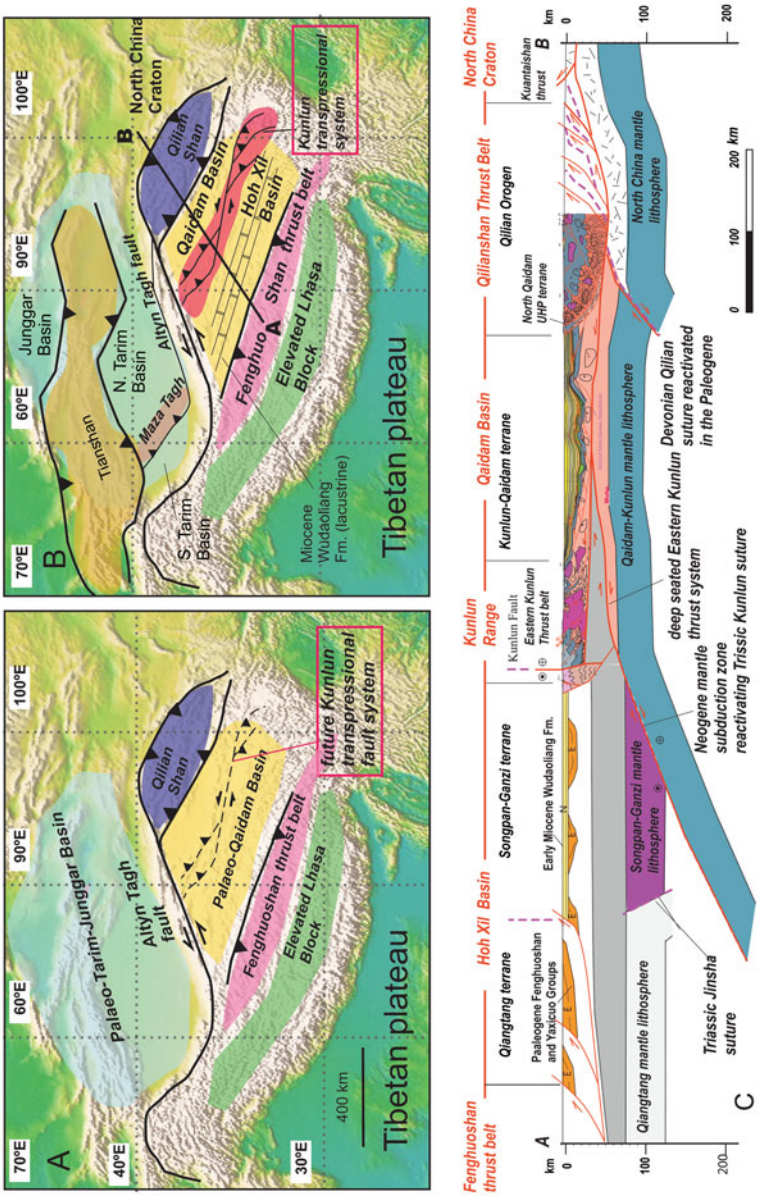
A
70°E
60°E
90°E
100°E
40°E
30°E
Palaeo-Tarim-Junggar Basin
Altyn Tagh fault
Qilian Shan
Palaeo-Qaidam Basin
Fenghuoshan thrust belt
Elevated Lhasa Block
future Kunlun transpressional fault system
400 km
Tibetan plateau
B
70°E
60°E
90°E
100°E
Junggar Basin
Tianshan
N. Tarim Basin
Maza Tagh
Altyn Tagh fault
S. Tarim Basin
North China Craton
Qilian Shan
Qaidam Basin
Hoh Xil Basin
Fenghuo Shan thrust belt
Elevated Lhasa Block
Kunlun transpressional system
Miocene Wudaoliang Fm. (lacustrine)
Tibetan plateau
C
Fenghuoshan thrust belt
Hoh Xil Basin
Kunlun Range
Qaidam Basin
Qilianshan Thrust Belt
North China Craton
Qiangtang terrane
Songpan-Ganzi terrane
Kunlun Fault
Eastern Kunlun Thrust belt
Kunlun-Qaidam terrane
Qilian Orogen
Kuantaishan thrust
Paaleogene Fenghuoshan and Yaxicuo Groups
Early Miocene Wudaoliang Fm.
North Qaidam UHP terrane
km
A
B
0
100
200
Qiangtang mantle lithosphere
Songpan-Ganzi mantle lithosphere
Qaidam-Kunlun mantle lithosphere
North China mantle lithosphere
Triassic Jinsha suture
Neogene mantle subduction zone reactivating Trissic Kunlun suture
deep seated Eastern Kunlun thrust system
Devonian Qilian suture reactivated in the Paleogene
0
100
200 km

Fig. 8.7 **a** Palaeogene tectonic configuration of the Tibetan Plateau in present-day geographic coordinates. The Palaeo-Qaidam Basin lies between the elevated Lhasa Block and the Fenghuo Shan thrust belt in the south and the elevated Qilian Shan in the north. The region north of the Tibetan plateau was a large topographic depression that links Tarim and Junggar basins across the Tian Shan, as the Tian Shan was not uplifted until the early Miocene. **b** Neogene tectonic configuration of the Tibetan Plateau in present-day geographic coordinates. The initiation of the Eastern Kunlun left-slip transpressional system caused the uplift of the Eastern Kunlun Range, which has partitioned the Paleo-Qaidam Basin into the Hoh Xil Basin to the south and the Qaidam Basin to the north. The uplift of the Tian Shan range similarly partitioned the once-united Tarim-Junggar Basin into the Tarim Basin to the south and Junggar Basin to the north. The development of the Maza Tagh thrust zone in central Tarim Basin is currently partitioning the Tarim Basin into northern and southern subbasins. **c** Schematic cross section showing first-order crustal structures of the central and northern Tibetan Plateau. (This figure and its caption are reproduced unchanged by courtesy of Prof. Yin An of the University of California (Los Angeles), as published in An et al. 2008b)

Table 8.2 Cenozoic stratigraphy of the southern part of the Qaidam and Hoh Xil basins. (After Yin et al. 2008b and references therein)

Geologic time		*Age (Ma)*	*Southern Qaidam Basin*			*Hoh Xil Basin*		
			Units	*Thickness (m)*	*Facies*	*Units*	*Thickness (m)*	*Facies*
PLIO		10	Shizigou Formation	>1500	Lacustrine			
MIOCENE	Late		Shangyou-shashan Fm	>822	Lacustrine			
	Middle	20	Xiayousha-shan Fm	1243	Lacustrine/ fluvial			
	Early					Wudaoliang Group	370	Lacustrine
OLIGOCENE	Late	30	Shanggan-chaigou Fm	848	Fluvial/lacustrine	Missing or no depositional records		
	Early	40	Lower and Upper Xiangan-chaigou Fm	1011	Fluvial/lacutrine	Yaxicuo Group	670	Fluvial/ lacustrine
EOCENE	Late	50				Fenghuo Shan Group	4790	Fluvial/ lacustrine/fan-delta
	Middle							
PALEOCENE	Early	60	Lulehe Formation	1043	Alluvial/fluvial			
						Underlying Jurassic and Cretaceous strata		

8.6 Ordos Basin

The Ordos Basin overlies the western part of the North China Craton, is rich in coal resources (Li et al. 1995), oil and gas (Cai et al. 2007a) and covers about 320,000 km^2 (Fig. 8.1; see also Figs. 2.5 and 2.7). The basin is bordered by uplifted areas, forming the Luliang and Helan mountains.

At least six structural domains have been recognised in the Ordos Basin (Cai et al. 2007a, b): (1) western fold belt; (2) Tianhuan depression; (3) Shanbei slope; (4) Jinxi fold belt; (5) Weibei Uplift; and (6) Yimeng Uplift. The lithostratigraphic succession of the basin extends from the Cambrian-Ordovician to the Quaternary with thicknesses of sedimentary rocks ranging from 740 to 2,723 m, divided into 15 formations, including carbonates, evaporites, shallow marine to fluvial, lacustrine, swamp and Aeolian facies rocks (Table 8.3).

Ren and Xiao (2002) considered the Ordos Basin as a polyciclic superimposed remnant of an earlier basin with a Cambrian-Ordovician marine sedimentary units, followed by later Carboniferous-Permian coal measures. According to Ren and Xiao (2002), the basin was successively affected by Caledonian, Indosinian, Yanshanian and Himalayan orogenic movements (see Tables 1.2 and 1.4 in Chap. 1), resulting in folds and overthrusts along its margins. A series of grabens (known as Fenwei, Hetao and Yinchuan) encircle the basin on the northern, southern and northwestern margins.

Table 8.3 Lithostratigraphic column of the Ordos Basin. (After Cai et al. 2007a)

System/Period	Formation (mineralisation)	Thickness (m)	Lithology
Quaternary		0–80	Aeolian red clays and loess
Cretaceous	Zhidan	0–450	Fluvial facies (sandstone and mudstone); swamp facies (carbonaceous mudstone and coal)
Jurassic	Anding	80–150	
	Zhiluo (with Uranium deposits)	200–400	
	Yanan	250–300	
	Fuxian	0–150	
Triassic	Yanchang	790–1,415	Lacustrine facies (sandstone and mudstone)
	Zhifang	300–530	
	Heshangg	47–169	
	Liujiagou	202–422	
Permian	Shiqian	200–345	Alternating marine and terrestrial sandstone. mudstone, coal seams and limetsone
	Sshihezi	200–340	
	Xshihezi	80–200	
	Shanxi	37–125	
Carboniferous	Taiyuan	22–276	
	Benxi	15–58	
Cambro-Ordovician		300–2,000	Platform carbonates and evaporites

8.6.1 Mineral Systems

Sandstone-hosted U deposits and occurrences have been found in the Ordos Basin and reported by Cai et al. (2007a, b) and Xue et al. (2010, 2011). The distribution of the U occurrences in the Basin is shown in Fig. 8.8, which are hosted in sandstone rocks of braided river channels facies. In the Dongsheng area, known as the Yimeng Uplift, in the northern part of the basin, a number of sandstone roll-front U deposits are present along a redox front, several tens of kilometres long.

Various aspects of the Dongsheng U mineralisation have been studied by Cai et al. (2007a, b), Li and Li (2011), Xue et al. (2010, 2011) and reviewed by Dalhkamp (2009). Uranium resources in the area are estimated at 5,000 t of U metal, with an average grade of 0.2 % U. The Zhiluo Formation, which hosts the ore (Table 8.3), consists of three member units of meandering fluvial, flood plain and swamp facies. From top to bottom these are: a 60–100 m thick member of purple-reddish sediments, a 20–40 m thick member composed of grey-coloured point bar sandstone interfingered with mudstone and coal seams interbeds, and a 20–40 m thick lower member of north-northwest to south-southeast-oriented braided fluvial channels, interpreted as an alluvial fan shedding from the uplifted part of the basin. The rocks in the lower member of the Zhiluo Formation are dark-grey coarse- to medium-grained sandstone containing organic matter and sulphides. Channels in the member are also incised into sedimentary rocks of the underlying Yanan Formation, within which are curvilinear redox fronts that are between 10 and 20 m thick. The main U ore minerals are pitchblende, adsorbed on clay minerals and closely

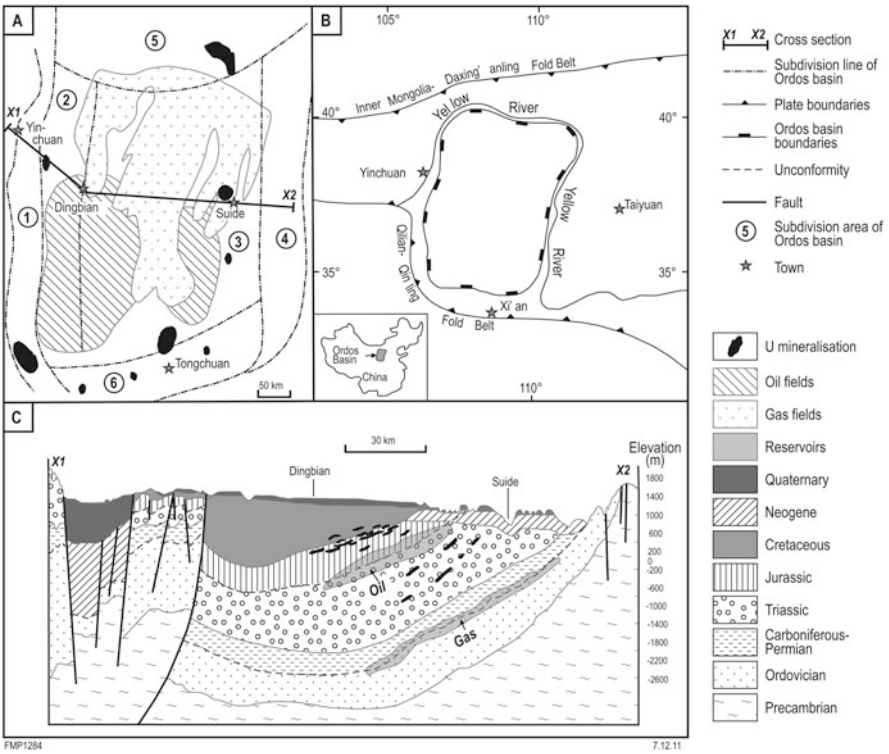

Fig. 8.8 **a** Simplified geology of the Ordos Basin and distribution of sandstone-hosted U mineralisation. **b** Setting of the Ordos Basin. **c** Cross-section showing distribution of U-bearing strata, oil and gas reservoirs. (After Xue et al. 2011)

associated with pyrite, and coffinite, which is thought to have replaced fossil microorganisms (Cai et al. 2007a, b). The U ore zones are roll-shaped or tabular in shape at depths of about 77–185 m, with productivity factors ranging from 1.72 kg U/m^2 to 10.67 kg/m^2 (Dalhkamp 2009). The deposits are characterised by lateral zoning of alteration minerals within and from the oxidation-reduction front. Reddish coloured sandstone units in the oxidation zone include carbonate, sericite, illite, kaolinite and limonite alteration minerals, whereas in the reduction zone grey to greenish grey sandstone units have albite, carbonate, chlorite, epidote and pyrite as the most common alteration minerals (Li and Li 2011).

The ore-forming processes for the U mineralisation in the Ordos basins have been investigated by Xue et al. (2010, 2011) and Cai et al. (2007a, b), who used geochemical, fluid inclusions, stable isotopic data and numerical modelling. Homogenisation temperatures from 180 to 60 °C of fluid inclusions, are interpreted by Xue et al. (2010) to be indicative of hydrothermal rather than diagenetic conditions. However, Cai et al. (2007a, b) argued that the microbial degradation of hydrocarbons occurs under low temperature conditions and therefore within a diagenetic regime. Stable

isotope systematics ($\delta^{13}C$ ranging from −14 to −2.7 ‰; δD from −130 to −94 ‰; $\delta^{18}O$ from −9.1 to +8.8 ‰—SMOW; $\delta^{34}S$ ranging from −34 to +17 ‰) on calcite, kaolinite and pyrite associated with the mineralisation, indicate the importance of the role of hydrocarbons and sulphate-reducing bacteria for the genesis of the mineralisation. Thus, the Ordos Basin's sandstone-hosted U mineralisation provides an interesting case of polyphase ore genesis, linked to interaction between tectonics, topographic relief and basinal fluids. Furthermore, the evidence shows that at least two fluids were involved. One was an upward moving low temperature hydrothermal fluid, driven by overpressure due to sediment compaction, from the basin central part towards the margins. Topographic relief at the margins of the basins was responsible for the gravitational flow of the second fluid system (meteoric in nature), which moved downward from the basin margins towards the centre. Xue et al. (2010) proposed that U was leached from the Cretaceous and Jurassic clastic rocks by the downward moving meteoric fluids. Reduction of the U^{6+} to U^{4+} was largely due to hydrocarbons carried by ascending hydrothermal fluids, followed by precipitation of U minerals at the redox boundary, which was situated in the Jurassic strata. The age interval of the U mineralisation is estimated to be from 120 to 95 Ma (Li and Li 2011).

8.7 Songliao and Bohai Volcano-sedimentary Basins

The Songliao and Bohai basins, which contain volcanic and sedimentary successions, are located in northeastern China (Figs. 2.7, 8.1 and 8.2), and were formed in the Late Jurassic to Early Cretaceous and Cenozoic (Fig. 8.9). These basins are close to the Sea of Japan, built on the North China Craton and are bound by Tanlu Fault in the east and are economically very important accounting for over 80 % of the oil and gas production in China (Li et al. 1997).

High geothermal anomalies are associated with the Songliao and Bohai basins. The central part of the Songliao basin has high heat flow (75–82 mw/m^2, Yuan 1996) and geothermal gradients (4–5 °C/100 m; Yi et al. 1992). Gravity data show two north-northeast trending uplift regions (see Fig. 7.30), which correspond to a shallow Moho and indicate significant lithosphere thinning. The Bohai Basin has higher geothermal gradients of 63.2–98.8 mw/m^2 than the surrounding areas (Liu et al. 1996). The highest heat flow (98.8 mw/m^2) is located at Bozhong in the center of the Bohai Bay, where the shallowest Moho at a depth of 29 km is recorded. Furthermore, the Songliao Basin contains Late-Jurassic to Early Cretaceous basalt-andesite volcanic rocks and has about 600 Cenozoic alkali basaltic volcanoes. Other features are radiating drainage systems for both basins and frequent earthquake activity. However, some of these earthquakes could be due to the Tanlu fault and other north-northeast-trending faults. The Songliao Basin has an approximately north-south elongation parallel to the western Pacific Plate subduction zone and it has been suggested that this is evidence that the current sub-continental lithospheric thinning

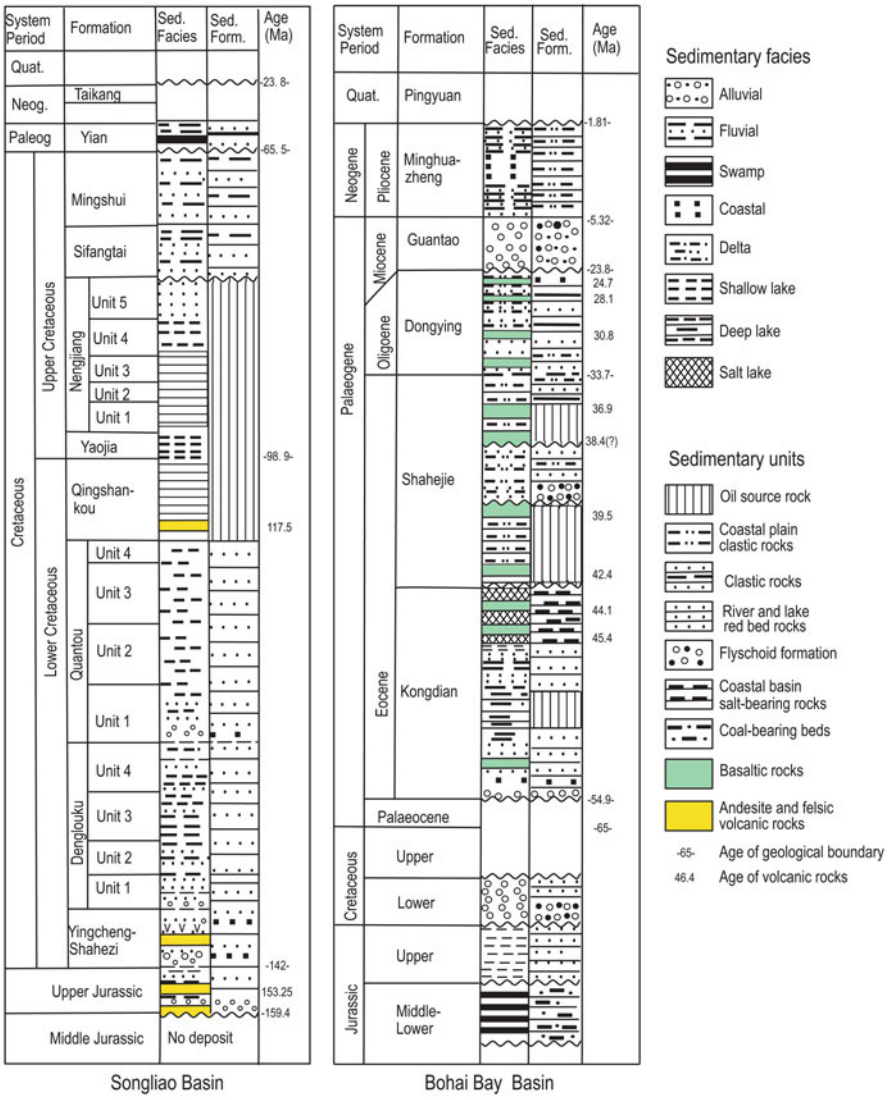

Fig. 8.9 Lithostratigraphy of the Songliao and Bohai basins. (After Wang et al. 2002; Xiao et al. 2004)

of less than 60 km explains the volcanic development of the basins from about 90 Ma to the Present (Windley et al. 2010).

Xiao et al. (2004) and Zhou et al. (2012) suggested that the formation of the Songliao and Bohai basins were controlled by shallow mantle plumes, arising from asthenospheric upwellings. Spatial and temporal relationship between these two basins can be traced through sedimentary and volcanic records, suggesting that the

plume(s) moved toward south-southeast during Middle Cretaceous and Miocene. Quaternary mafic volcanism in the region, with active volcanoes such as the Wudalianchi volcanic field in northeast China, suggest that the asthenospheric mantle upwelling is still active today.

8.7.1 Songliao Volcano-sedimentary Basin

The Songliao Basin covers an area of about 260,000 km^2 and is the largest oil and gas producing basin in China, yielding about 55 Mt of crude oil per year (Wang et al. 2002). Its basement includes pre-Mesozoic metamorphic rocks and Early to Middle Meosozoic sedimentary and volcanic rocks. The rifting of Songliao Basin began from the Late Jurassic (139 Ma) and ended in the Early Cretaceous around 115 Ma (Wu et al. 2001). The Songliao Basin is characterised by a syn-rift and a post-rift sequence, separated by an unconformity. The total thickness of the sedimentary rocks deposited during the rifting stage is over 3,000 m and the post-rift sequence was deposited during the Early Cretaceous in a series of sub-basins that alternate with uplifts. These sub-basins are filled by volcaniclastic and alluvial-lacustrine rocks and reached a depth of 10 km. The overlying post-rift sequence developed as a broad depression (sag phase?) filled with lacustrine facies rocks and alluvial fan and fluvial strata of Eocene and Neogene age. A recent tectonic assessment of the Songliao Basin was made by Li et al. (2012), using detrital zircon ages and Sr-Nd isotopes. These authors suggested that the Songliao Basin was first formed during the tectonic convergence of the Mongol-Okhotsk and Palaeopacific oceans.

Ren et al. (2002) proposed a three stage evolutionary history of the Songliao Basin. The first rifting phase was heralded by intense volcanic eruptions in the Late Jurassic, the second phase was characterised by the formation of fault-bounded sub-basins, and the third phase by the above mentioned broad depression, as well as tens of small-scale fault basins. Inversion of the basin took place after the deposition of the Sifangtai and Minshui formations (Fig. 8.9) in the Late Cretaceous. Zhang et al. (2010) confirmed the episodic nature and accompanying volcanism of rifting in the Songliao Basin. Their U-Pb age data on zircons indicate that this Cretaceous volcanism took place in the period from 115 to 109 Ma. The volcanic rocks of this period are dominated by rhyolites, but also include trachyandesite, basaltic trachyandesite, trachyte and dacite. Geochemical signatures, such as high-K calc-alkaline and enrichment in large ion lithophile elements (LILE), indicate a subduction-related system (Zhang et al. 2010). Zhang et al. (2010) also proposed a back-arc setting model for the formation of the Songliao Basin and accompanying volcanism, associated with subduction of the Palaeopacific Plate, known as Izanagi, lithospheric thinning and upwelling of asthenospheric mantle along the eastern continental margin of China in the Early Cretaceous, caused by subduction slab roll-back.

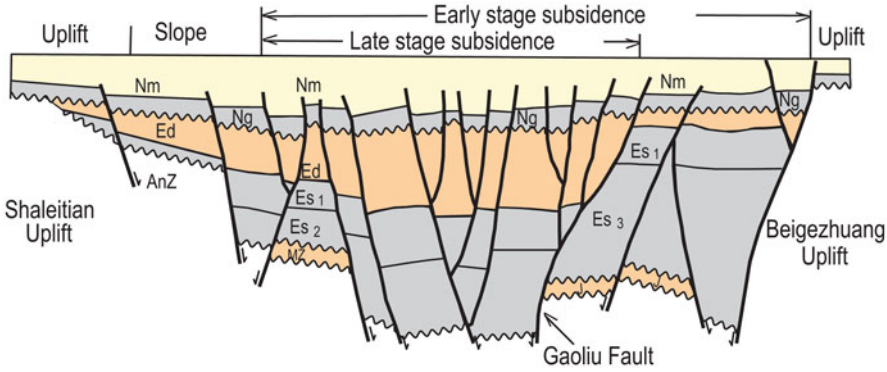

Fig. 8.10 Simplified cross-section of the Nanpu Sag sub-basin, illustrating the architecture and evolution of a rift basin in eastern China; Es Eocene Shaheje Formation (rifting stage: lacustrine and fluvio-lacustrine facies), Ng and Nm Neogene Guantao and Minghuazhen formations (intracontinental sag or depression stage: dominantly fluvial sand and mud). (After Dong et al. 2010)

8.7.2 Bohai Volcano-sedimentary Basin

The Bohai Basin contains a succession of extension and rifting stages sediments and volcanic rocks about 8,000 m thick formed during the Eocene (55 Ma) and early Oligocene (28 Ma). The basin (also called the Bohaiwan Basin by Ren et al. 2002) has a north-northeast elongate rhombic shape with a maximum width of about 450 km. Crustal extension during the Early Cretaceous and compressional movements caused uplift in the Late Cretaceous, resulting in a major regional unconformity during this period. Rifting resumed in the Palaeocene along a series of northeast and north-northeast-trending fault zones, resulting in rapid subsidence of fault sub-basins, in which up to 6 km of continental and lacustrine clastic sediments accumulated. These sub-basins are half-grabens, with the Nanpu Sag being an example, shown in Fig. 8.10 (Dong et al. 2010). Sedimentation along steeper flanks of the half-grabens was fault-controlled and dominated by deep-water lacustrine shale, mudstone and mass flow deposits, whereas sedimentation on the less steep flanks was dominated by fluvial and deltaic fans with bioclastic carbonate banks. Rifting was concluded at the end of Neogene and was followed by uplift and a period of erosion. Following erosion, thermal subsidence, resulting in the inception of a saucer-shaped basin in which Neogene and Quaternary sediments covered the uplifted blocks and sub-basins (Nm in Fig. 8.10).

Seismic profiles show electrically high-conductive layers in both basin areas (Yuan 1996). In the Songliao Basin, layers of low-velocity of the P-wave are situated at 20–40 km in the crust and 60–100 km within mantle (Yuan 1996). Similar low-velocity layers exist beneath the Bohai Basin, but some of these layers are interbedded with high-velocity layers. These low-velocity layers are normally interpreted as melt-contained layers or layered magma chambers. These geophysical features suggest

that deep mantle processes (i.e. upwelling, partial melting, magma underplating and emplacement) could have been important contributing factors for the formation of these two basins.

Volcanic rocks are an important component of the Bohai Basin. Cenozoic volcanic rocks provide valuable information to constrain basin evolution (Lu et al. 1997; Tao et al. 1999). Volcanic rocks in the basin were erupted during the Late Jurassic (157–147 Ma), early Cretaceous (136–113 Ma) and Eocene and Oligocene (56.3–24.7 Ma) (Liu 1992; Wang et al. 2002). In the Xialiaohe Sag, in the northern part of the basin, four stages of basaltic volcanism have been recognized during the early Eocene, Middle Eocene, early Oligocene and late Oligocene. These basaltic rocks have a total thickness of 2,000 m and are interbedded with sedimentary beds. In the southern part of the Bohai Basin, volcanism in the Jiyang Sag lasted until the Miocene. Their spatial, temporal and rock-type distribution are typically of a continental rift setting, in which early stage Eocene sub-alkaline basalts was followed by late stage Oligocene and Miocene alkaline basalts. Furthermore, depths and basaltic rock types show a spatial and temporal variation. The later stage basalt was from a shallower mantle source (Lu et al. 1997), suggesting that the melting depth of mantle was rising. Most of the Late Jurassic volcanic rocks include andesite, trachyandesite and sub-alkaline basalts. These rocks have lower TiO_2, P_2O_5, Nb, Ti and higher K_2O abundances than arc basalts. High field strength elements (HFSL), such as Nb and Ti have low concentrations, whereas K, Th, Ce and Sm have high concentrations in these rocks (Xiao et al. 2004). However, the Middle Cretaceous basalts that are enriched in HFSE, show positive Nb and Ta anomalies, interpreted as being similar to those of oceanic island basalt (OIB) by Xiao et al. (2004).

As mentioned above, basaltic rocks in the Bohai Basin show OIB-like patterns in primitive-normalized plots, although post-Eocene basaltic rocks show relatively higher incompatible elements than the Eocene ones, which suggests that they were originated from an enriched mantle source. The Sr-Nd-Pb isotope data also indicate that they were generated from enriched mantle sources (Liu 1992). Picritic tholeiite and alkaline picritic basalts were found in Huanghua Sag of the basin (Lu et al. 1997), confirming a mantle source and high degrees of partial melting.

Xiao et al. (2004) suggested that mantle upwelling may have been involved in the formation of the Songliao and Bohai basins. According to these authors, a starting (shallow?) mantle plume began to form the Songliao Basin in the Late Mesozoic. This process may have been linked to subduction of the Izanagi plate, which engendered asthenospheric upwelling in a kind of back-arc setting. Upwelling of asthenospheric mantle since the Middle Jurassic induced crustal uplift and then significant crustal extension and lithospheric thinning from the Late Jurassic. This lithosphere extension and crustal thinning lasted until the late Early Cretaceous and produced voluminous eruption of volcanic rocks. The Songliao Basin was then formed and filled with sediments and volcanic rocks. The hotspot moved south-southeast, when the North China Craton moved to north-northwest during the Middle Cretaceous (Ren and Huang 2002). The mantle plume relocated in the Bohai Bay area in the Eocene, when similar processes led to the formation of the Bohai Basin. Lithosphere extension and thinning, crustal rifting, decompression partial melting of enriched mantle and filling

of sediments in the Bohai Basin, eventually forming the largest oil and gas field of China.

The northward shift of subsidence probably can be related to the collision between the Indian and Eurasia plates, which resulted in the clockwise rotation of the combined North China and South China cratons, which allowed the plume head to move to the north, thereby causing the observed northward shift of subsidence. The Bohai Bay area is still geologically active. Continuing volcanism in the surrounding region and earthquake activity are indicative of active mantle dynamics in the region, melting of sublithospheric mantle and emplacement of magma. It is worth pointing out the mantle dynamics and associated tectonic and magmatic events in eastern China were coeval with and may have been due to far-field effects from the Pacific mantle superplume event that led to the formation of Cretaceous (ca. 120 Ma) the Ontong-Java oceanic plateau (Pirajno et al. 2009).

8.7.3 Mineral Systems

Although no "hard rock" mineral deposits of economic significance have been reported from the Songliao and Bohai basins, the possibility exists that hydrothermal vents may have been active during magmatic activity. In this respect, seismic reflection profiles may be used, not only for the detection of hydrocarbon traps, but also to identify signs of hydrothermal activity associated with the emplacement of laccoliths, stocks, sills and feeder dykes. In the northern South Yellow Sea Basin, half way between the Jiaodong Peninsula and Korea (Figs. 8.1 and 8.2), numerous seismic reflection profiles have revealed in remarkable clarity various igneous complexes (stocks, sills, laccoliths and dykes) intruding the sedimentary pile and interacting with hydrocarbons traps (Fig. 8.11; Lee et al. 2006). Indeed, Lee et al. (2006) pointed out that in basins in the Norwegian Sea some 20,000–30,000 hydrothermal vents have been identified along seismic lines alone. These hydrothermal vents are "vertical piercement structures", enhancing fluid migration and locally forming explosion-type breccia and mud volcanoes. Although speculative, it may be that similar hydrothermal vents may have been activated in the latest stages of basin formation, where subaqueous sedimentation took place.

8.8 Concluding Remarks

In this Chapter, selected sedimentary and volcano-sedimentary basins have been briefly examined. The Tarim, Tuha, Junggar basins located in the northwestern parts of China, the Ordos and Qaidam basins in central China, and the Songliao and Bohai basins located in the east. The economic significance of these basins is primarily for oil, gas and coal resources, although more and more exploration is also directed at the targeting of U mineral systems. In this respect, it is worthy of note that seismic

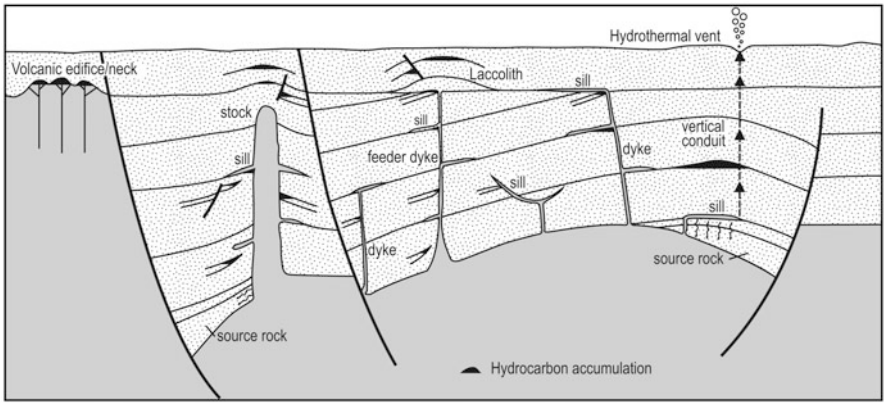

Fig. 8.11 Cross-section interpreted from seismic reflection data from the South Yellow Sea Basin (see Fig. 8.1); laccoliths, sills, small volcanic edifices and hydrothermal vent structure have been identified. It is speculated that similar hydrothermal vents may have been present in the inland basin, where subaqueous sedimentation occurred. (After Lee et al. 2006)

profiling conducted to define hydrocarbon traps and commonly followed by drilling programs, can be equally useful for the targeting of mineral resources, as well as for the general understanding of the geodynamics of the basins.

The basins of northwestern China contain thick sedimentary successions, which may have been largely related to foreland tectonics associated with the India-Eurasia collision (Himalayan Orogeny). On the other hand those of the eastern China seaboard were formed during complex processes of lithospheric thinning, extensional processes and felsic to alkaline mafic magmatism (described in Chap. 7).

The Cenozoic successions of the Tarim, Tuhua, Junggar and Ordos basin tend to be predominantly sedimentary, with volcanism and mafic to felsic intrusion confined to Permian post-collisional stages. Uranium deposits have been identified in the Tuha, Junggar and Ordos basins.

As mentioned in previous chapters (e.g. Chap. 7) the Late Jurassic to Early Cenozoic Songliao and Bohai basins in eastern China sit above the thinnest lithosphere. As Ren et al. (2002) pointed out, the association of thin crust and lithosphere, extensive volcanism, high heat flow and geothermal gradient indicates extensive upwelling of the asthenosphere. This interpretation is supported by 3D P-wave tomographic data that suggest large-scale lithospheric thinning and detachment (Windley et al. 2010, citing Huang and Zhao 2009).

Windley et al. (2010) pointed out that these sedimentary basins, including those along the Yangtze River Valley (Chap. 4) are filled with coarse, immature clastic sediments, probably derived from the erosion of uplifted or mountainous regions during the Mesozoic. The eastern China mountains were formed by crustal thickening, uplift, resulting in widespread erosion, crustal stretching and the formation metamorphic core complexes (MCC). This was followed by collapse (stress-relaxation) and extensional tectonics from the end of the Jurassic (ca. 145 Ma) and continued

to the Early Cretaceous. The association of active rifting, thin crust and lithosphere, high rates of volcanism, high heat flow and geothermal gradient points to extensive upwelling of the asthenosphere (Ren et al. 2002). This is confirmed by 3D P-wave tomographic models by Huang and Zhao (2009), which indicate that a high-velocity anomaly under the Bohai Basin extends from a depth of 150 km down to 300 km, suggestive of large-scale lithospheric thinning and detachment.

References

Allen MB, Windley BF, Zhang C, Zhao ZY, Wang GR (1991) Basin evolution within and adjacent to the Tien Shan Range, NW China. J Geol Soc 148:369–378

Bai HH, Shi YJ (2008) Geological characteristics and ore genesis of sandstone-hosted Cu deposits in the southwest Tianshan. Xinjiang Non Ferr Met 4:14–18 (in Chinese)

Cai CF, Dong HL, Li HT, Xiao XJ, Ou GX, Zhang CM (2007a) Mineralogical and geochemical evidence for coupled bacterial uranium mineralization and hydrocarbon oxidation in the Shashagetail deposit, NW China. Chem Geol 236:167–179

Cai CF, Li H, Qin M, Luo X, Wang F, Ou G (2007b) Biogenic and petroleum related ore-forming processes in Dongsheng uranium deposit, NW China. Ore Geol Rev 32(1–2):262–274

Cao J, Hu K, Wang K, Bian L-Z, Liu YT, Yang SY, Wang LQ, Chen Y (2008) Possible origin of 25-norhopanes in Jurassic organic-poor mudstone from the northern Qaidam Basin (NW China). Org Geochem 39:1058–1065

Cao J, Wu M, Chen Y, Hu K, Bian LZ, Wang LG, Zhang Y (2012) Trace and rare element geochemistry of Jurassic mudtsone in the northern Qaidam Basin, northwest China. Chem Erde. doi:10.1016/j.chemer.2011.12.002

Carroll AR, Liang Y, Graham SA, Xiao X, Hnedrix MS, Chu J, McKnight CL (1990) Junggar basin, northwest China: trapped Late Paleozoic ocean. Tectonophysics 181:1–14

Carroll AR, Graham SA, Hendrix MS, Ying D, Zhou D (1995) Late Paleozoic tectonic amalgamation of northwestern China: sedimentary record of the northern Tarim, northwestern Turpan, and southern Junggar Basins. GSA Bull 107(5):571–594

Chen ZL, Jiu J, Gong HL, Zheng EJ, Wang XH (2005) Cenozoic tectonic movement and its control on sandstone-type uranium deposits in the northern Junggar Basin. In: Mao JW, Bierlein FP (eds) Mineral deposit research: meeting the global challenge, vol 1. Springer, Berlin, pp 237–239

Chen ZL, Liu J, Gong HL, Hang FH, Briggs SM, Zheng EJ, Wang G (2011) Late Cenozoic tectonic activity and its significance in the northern Junggar basin, northwestern China. Tectonophysics 497:45–56

Cope TD, Graham SA (2007) Upper-crustal response to Mesozoic tectonism in Western Liaoning, North China, and implications for lithospheric delamination. Geological Society, London, Sp Publ 280, pp 201–222

Dahlkamp FJ (2009) Uranium deposits of the world, Chap. 1, China, Peoples Republic of. Springer, Berlin, p 156

Dong YX, Xiao L, Zhou HM, Wang CZ, Zheng JP, Zhang N, Xia WC, Ma Q, Du JX, Zhao ZX, Huang HX (2010) The Tertiary evolution of the prolific Nanpu Sag of Bohai Bay Basin, China: constraints from volcanic records and tectono-stratigraphic sequences. Bull Geol Soc Am 122(3/4):609–626

Gilder SA, Keller GR, Luo M, Goodell PC (1991) Timing and spatial distribution of rifting in China. Tectonophysics 197:225–243

Greene TJ, Carroll AR, Hendrix MS, Graham SA, Wartes MA, Abbink OA (2001) Sedimentary record of Mesozoic deformation and inception of the Turpan-Hami basin, northwest China. Geol Soc Am Sp Publ 194:317–340

Griffin WL, Andi Z, O'Reilly SY, Ryan CG (1998) Phanerozoic evolution of the lithosphere beneath the Sino-Korean Craton. In: Flower M, Chung SL, Lo C-H, Lee T-Y (ed) Mantle dynamics and plate interactions in East Asia, Monogr 27. American Geophysical Union, pp 107–126

Huang ZK (1945) On major tectonic forms of China. Geol Mem A20, National Geol Surv China, Pehpey

Huang J, Zhao DP (2009) Seismic imaging of the crust and upper mantle under Beijing and surrounding regions. Phys Earth Planet Int 173(3–4):330–348

Jin Q, Xiong SS, Lu P (1999) Catalysis and hydrogenation: volcanic activity and hydrocarbon generation in rift basins, eastern China. Appl Geochem 14:547–558

Kapp P, Pelletier JD, Rohrmann A, Heermance R, Russell J, Ding L (2011) Wind erosion in the Qaidam basin, central Asia: implications for tectonics, paleoclimate and the source of the Loess Plateau. GSA Today 21:4–10

Kusky TM, Li JH, Santosh M (2007) The Paleoproterozoic North Hebei Orogen: North China craton's collisional suture with the Columbia supercontinent. Gondwana Res 12:4–28

Lee GH, Kwon YI, Yoon CS, Kim HJ, Yoo HS (2006) Igneous complexes in the eastern Northern South Yellow Sea Basin and their implications for hydrocarbon systems. Mar Pet Geol 23:631–645

Li DS (1996) Basic characteristics of oil and gas basins in China. J SE Asian Earth Sci 13(3–5):299–304

Li RX, Li YZ (2011) The geologic features of mineralization at the Dongsheng uranium deposit in the northern Ordos Basin (Central China). Russ Geol Geophys 52:593–602

Li ST, Mao BZ, Lin CS (1995) Coal resources and coal geology in China. Episodes 18(1–2):26–30

Li DS, Liang DG, Jia CZ, Wang G, Wu QH, He DF (1996) Hydrocarbon accumulations in the Tarim basin, China. AAPG Bull 80(10):1587–1603

Li ST, Lu FX, Lin CS (1997) Evolution of Mesozoic and Cenozoic basins in eastern China and their geodynamic background. China University of Geoscience Press, Wuhan, p 239

Li SQ, Chen F, Siebel W, Wu JD, Zhu XY, Shan XL, Sun XM (2012) Late Mesozoic tectonic evolution of the Songliao basin, NE China: Evidence from detrital zircon ages and Sr-Nd isotopes. Gondwana Res doi: 10.1016/j.gr.2012.04.002

Lin W, Faure M, Monie P, Wang QC (2007) Polyphase Mesozoic tectonics in the eastern part of the North China Block: insights from the eastern Liaoning peninsula massif (NE China). Geological Society, London, Sp Publ 280, pp 153–170

Liu RX (ed) (1992) Cenozoic basalt in China: geochronology and geochemistry. Seismol Press, Beijing, p 427

Liu GX, Zhao WJ, LI ZX, Zhang X (1996) Geophysical analysis on the Tertiary rift valley Expanding of Bohai Sea. Northwest Seismol J 18(3):18–24 (in Chinese with English abstract)

Lu F, Zhu Q, Li S, Xie Y, Zheng J (1997) Mesozoic volcanism surrounding Songliao Basin, China: implications for the relationship with evolution of basin. J China Univ Geosci 8(1):72–77

Ma XY, Wu DN (1987) Cenozoic extensional tectonics in China. Tectonophysics 133:243–255

Meng QR (2003) What drove Late Mesozoic extension of the northern China-Mongolia tract? Tectonophysics 369:155–174

Meng QR, Hu JM, Jin JQ, Zhang Y, Xu DF (2003) Tectonics of the late Mesozoic wide extensional basin system in the China-Mongolia border region. Basin Res 16:397–415

Pan CC, Zhang M, Peng DH, Yu LP, Liu JZ, Sheng GY, Fu JM (2010) Confined pyrolysis of Tertiary lacustrine source rocks in the Western Qaidam Basin, Northwest China: implications for generative potential and oil maturity evaluation. Appl Geochem 25:276–287

Pirajno F, Ernst RE, Borisenko AS, Fedoseev G, Naumov EA (2009) Intraplate magmatism in central Asia and China and associated metallogeny. Ore Geol Rev 35(2):114–136

Ren JS, Xiao LW (2002) Tectonic settings of petroliferous basins in continental China. Episodes 25(4):227–235

Ren JY, Tamaki K, Li ST, Zhang JX (2002) Late Mesozoic and Cenozoic rifting and its dynamic setting in eastern China and adjacent areas. Tectonophysics 344:175–205

Ritts BD, Biffi U (2001) Mesozoic northeast Qaidam basin: response to contractional reactivation of the Qilian Shan, and implications for the extent of Mesozoic intracontinental deformation in central Asia. Geol Soc Am Mem 194:293–316

Sengör AMC, Natal'in BA (1996) Paleotectonics of Asia: fragments of synthesis. In: Yin A, Harrison TM (eds) The tectonic evolution of Asia. Cambridge University Press, Cambridge, pp 486–640

Shu LS, Zhou XM, Deng P, Wang B, Jiang JH, Yu JH, Zhao XX (2009) Mesozoic tectonic evolution of the Southeast China Block: new insights from basin analysis. J Asian Earth Sci 34:376–391

Tao KY, Mao JR, Xing GF, Yang ZL, Zhao Y (1999) Strong Yanshanian volcanic-magmatic explosion in east China. Miner Depos 18(4):316–322

Tian ZY, Han P, Xu KD (1992) The Mesozoic-Cenozoic East China rift system. Tectonophysics 208:341–363

Vincent SJ, Allen MB (2001) Sedimentary record of Mesozoic intracontinental deformation in the eastern Junggar Basin, northwest China: response to orogeny at the Asian margin. Geol Soc Am Sp Publ 194:314–360

Wang PJ, Liu WZ, Wang SX, Song WH (2002) 40Ar/39Ar and K/Ar dating on the volcanic rocks in the Songliao Basin, NE China: constarints on stratigraphy and basin dynamics. Int J Earth Sci Geol Rundsch 91:331–340

Wang XQ, Xu SF, Zhang BM, Zhao SD (2011) Deep-penetrating geochemistry for sandstone-type uranium deposits in the Turpan-Hami basin, north-western China. Appl Geochem 26:2238–2246

Watson MP, Hayward AB, Parkinson DN, Zhang ZM (1987) Plate tectonic history, basin development and petroleum source rock deposition onshore China. Mar Pet Geol 4:205–225

Windley BF, Allen MB, Zhang C, Zhao Z, Wang C (1990) Paleozoic accretion and Cenozoic redeformation of the Chinese Tian Shan range, Central Asia. Geology 18:128–131

Windley BF, Maruyama, S, Xiao WJ (2010) Delamination/thinning of subcontinental lithospheric mantle under eastern China: the role of water and multiple subduction. Am J Sci 310:1250–1293

Wu FY, Sun DY, Li HM, Wang XL (2001) The nature of basement beneath the Songliao basin in NE China: geochemical and isotopic constraints. Phys Chem Earth 26(9–10):793–803

Wu LQ, Jiao YQ, Roger M, Yang SK (2009) Sedimentological setting of sandstone-type uranium deposits in coal measures on the southwestern margin of the Turpan-Hami Basin, China. J Asian Earth Sci 36:223–237

Xiao L, Wang FZ, Wang H, Pirajno F (2004) Mantle Plume Tectonics constraints on the formation of Songliao and Bohaiwan Basins. Earth Sci J China Univ Geosci 29:284–292

Xu XW, Ma XY (1992) Geodynamics of the Shanxi rift system, China. Tectonophysics 208:325–340

Xue CJ, Chi GX, Xue W (2010) Interaction of two fluid systems in the formation of sandstone-hosted uranium deposits in the Ordos basin: geochemical and hydrodynamic modeling. J Geochem Explor 106:226–235

Xue CJ, Chi GX, Xue W (2011) Effects of hydrocarbon generation on fluid flow in the Ordos basin and its relationship to uranium mineralization. Geosci Front 2(3):439–447

Yi TZ, Ping H, Xu KD (1992) The Mesozoic-Cenozoic east China rift system. Tectonophysics 208:341–363

Yin A, Dang YW, Zhang M, McRivette MW, Burgess WP, Chen XH (2007) Cenozoic evolution of Qaidam basin and its surrounding regions (Part 2): Wedge tectonics in southern Qaidam basin and the eastern Kunlun Range. Geol Soc Am Sp Paper 433:369–390

Yin A, Dang YQ, Wang LC, Jiang WM, Chen XH, Gehrels GE, McRivette MW (2008a) Cenozoic tectonic evolution of Qaidam basin and its surrounding regions (Part 1): the southern Qilian Shan-Nan Shan thrust belt and northern Qaidam basin. GSA Bull 120(7/8):813–846

Yin A, Dang YW, Zhang M, Chen XH, McRivette MW (2008b) Cenozoic tectonic evolution of the Qaidam basin and its surrounding regions (Part 3): structural geology, sedimentation and regional tectonic reconstruction. GSA Bull 120:847–876

Yuan XC (1996) Velocity structure of the Qinling lithosphere and mushroom cloud model. Sci China Ser D 39(3):235–244

Zeng LB, Wang HJ, Lei G, Liu BM (2010) Impacts of the tectonic stress field on natural gas migration and accumulation: a case study of the Kuqa Depression in the Tarim Basin, China. Mar Pet Geol 27:1616–1627

Zhang FQ, Chen HL, Yu X, Dong CW, Yang SF, Pang YM, Batt GE (2010) Early Cretaceous volcanism in the northern Songliao Basin, NE China and its geodynamic implications. Gondwana Res 19(1):163–176

Zhao HL (2009) Ore deposit geology and modeling of the Dishui sandstone Cu deposit in Xinjiang. Xinjiang Non Ferr Met 5 (Suppl 1):43–45

Zhou J, Xu F, Wang T Cao A, Yin C (2006) Cenozoic deformation history of the Qaidam Basin, NW China: results from cross-section restoration and implications for Qinghai-Tibet Plateau tectonics. Earth Planet Sci Lett 243:195–210

Zhou LH, Fu LX, Lou D, Lu Y, Feng JY, Zhou SH, Santosh M, Li SZ (2012) Structural anatomy and dynamics of evolution of the Qikou Sag, Bohai Bay Basin: implications for the destruction of North China craton. J Asian Earth Sci 47:94–106

Zorin YA, Turutanov EK, Mordvinova VV, Kozhevnikov VM, Yanovskaya TB, Treussov AV (2003) The Baikal rift zone: the effect of mantle plumes on older structure. Tectonophysics 371:153–173

Epilogue

In this book I have undertaken to describe a selection of the most important mineral deposits of the Peoples Republic of China, in the context of the general geology with some emphasis on their geodynamic evolution in the wider tectonic framework of the Asian continent. The mineral systems discussed in this book are largely based on my understanding of China's geology and mineralisation, gained through personal experience in the field and a large amount of information and data derived from publications in national and international journals. Therefore the mineral deposits that I have chosen for this book are by no means all-inclusive, nor do they cover all tectonic settings. Nevertheless, I do believe that this book provides the first broad treatise in English of China's geology and mineral deposits, as brought together by a western author from the perspective of the latest geological concepts. As already stated, this book is based on first-hand knowledge of China's geology and mineral deposits gained during numerous field visits over the past 18 years, leading to several publications in international journals. In the writing of this book I was faced, time and again, with the challenge posed by the constant stream of publications (in English) by Chinese and non-Chinese researchers in all fields of geology and mineral deposit studies. In attempting to put together a reference book one is faced with the major task of having to sort out names of localities with different spellings, various other language difficulties, the inconsistent use of geological terms and lack of consensus of geological terminology, as pointed out in Chap. 1. However, the geological community in China is coming to grips with addressing these issues and there is no doubt in my mind that within a few years Chinese researchers will reach parity, if not surpass, the coordination and systemic approach of the West.

The study of the geology and tectonic setting of mineral deposits of the Peoples Republic of China, poses a constant challenge. This challenge is not confined to China alone, it probably applies to researchers world-wide in the last 20 years or so, largely because of the lack of adequate field constraints and good petrographic observations, prior to or in conjunction with undertaking laboratory studies, such as geochronological, isotopic and geochemical. Indeed, ground truth can only be provided by detailed field observations, as HH Read wrote: *the best geologist is, other things being equal, he who has seen most rocks. . . . . The best geologist of all, therefore, is one who has been able to keep his fieldwork going even though he has become elderly and more rotund* (Read HH, 1969, The geologist as historian, Proceed Geologists Assoc 81: 409–420).

F. Pirajno, *The Geology and Tectonic Settings of China's Mineral Deposits,*
DOI 10.1007/978-94-007-4444-8, © Springer Science+Business Media Dordrecht 2013

Index

F. Pirajno, *The Geology and Tectonic Settings of China's Mineral Deposits,*
DOI 10.1007/978-94-007-4444-8, © Springer Science+Business Media Dordrecht 2013